Frontiers in Earth Sciences

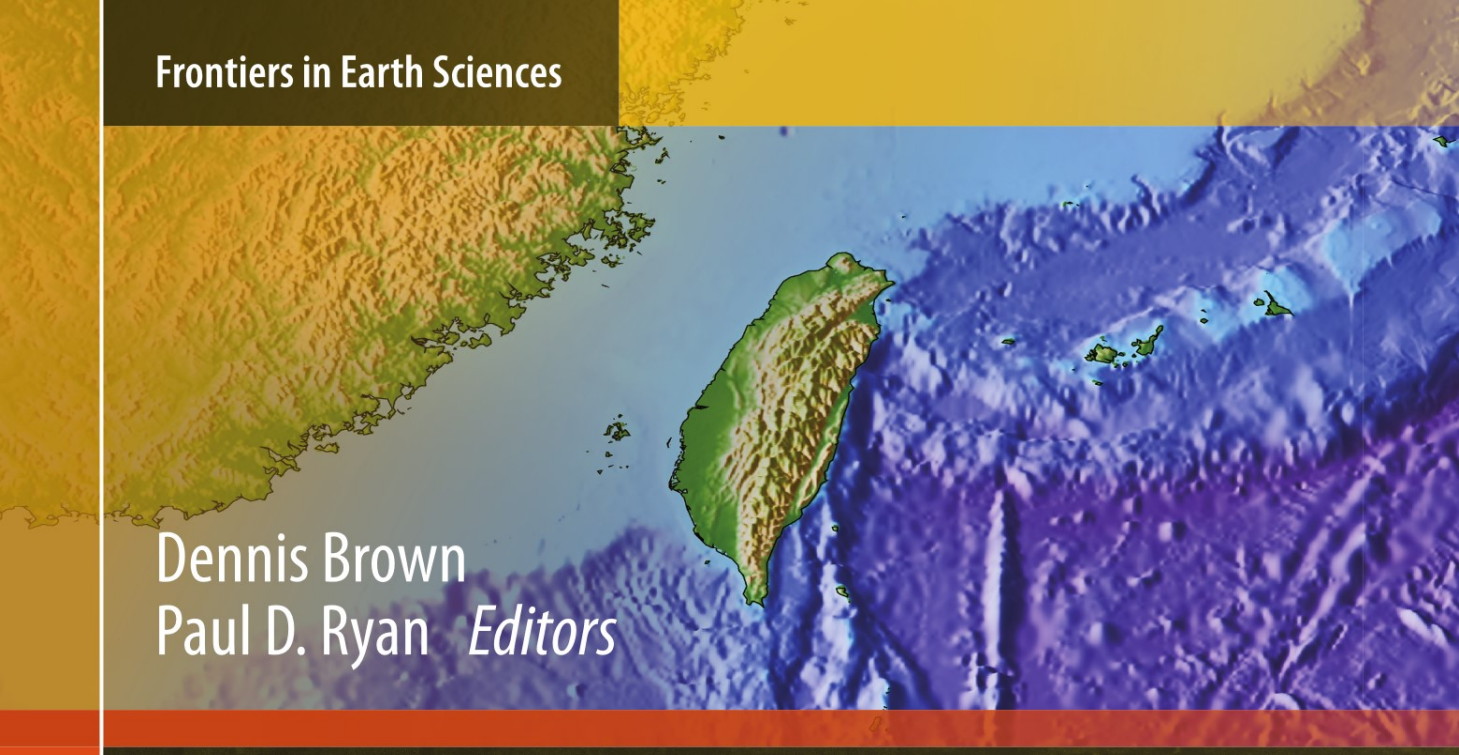

Dennis Brown
Paul D. Ryan *Editors*

Arc-Continent Collision

Springer

Frontiers in Earth Sciences

Dennis Brown • Paul D. Ryan
Editors

Arc-Continent Collision

Springer

Editors
Dr. Dennis Brown
Instituto de Ciencias de la Tierra
"Jaume Almera", CSIC
C/ Lluis Sole i Sabaris s/n
08028 Barcelona
Spain
dbrown@ija.csic.es

Dr. Paul D. Ryan
National University of Ireland, Galway
Dept. Earth & Ocean Sciences (EOS)
University Road
Galway
Ireland
paul.ryan@nuigalway.ie

This publication was grant-aided by the National University of Ireland, Galway

ISBN 978-3-540-88557-3 e-ISBN 978-3-540-88558-0
DOI 10.1007/978-3-540-88558-0
Springer Heidelberg Dordrecht London New York

Library of Congress Control Number: 2011931205

Cover design: deblik, Berlin

Printed on acid-free paper

Springer is part of Springer Science+Business Media (www.springer.com)

Preface

One of the key areas of research in the Earth Sciences are processes that occur along the boundaries of the tectonic plates that make up Earth's lithosphere. Of particular importance are the processes of tectonic accretion and erosion along convergent plate boundaries. One of the principal mechanisms of accretion occurs when intra-oceanic volcanic arcs collide with the margin of a continent in what is called arc–continent collision. Arc–continent collision has been one of the important tectonic processes in the formation of mountain belts throughout geological time and continues today along tectonically active plate boundaries such as those in the SW Pacific or the Caribbean. Well-constrained fossil arc–continent collision orogens supply the third and fourth dimension (depth and time) that are generally missing from currently active examples where tectonic processes such as subduction, uplift and erosion, and the formation of topography can be observed. Arc–continent collision is also thought to have been one of the most important processes involved in the growth of the continental crust over geological time, and may also play an important role in its recycling back into the mantle via subduction. The integration of research between active and fossil arc–continent orogens provide key data for the understanding of how plate tectonics works today, and how it might have worked in the past. Understanding the geological processes that take place during arc–continent collision is therefore of importance for our understanding of how collisional orogens evolve and how the continental crust grows or is destroyed. Furthermore, zones of arc–continent collision are producers of much of the worlds primary economic wealth in the form of minerals, so understanding the processes that take place during these tectonic events is of importance in modeling how this mineral wealth is formed and preserved.

Arc–continent collision orogeny is generally short-lived, lasting from c. 5 to 20 My, although much longer-lived regional events do occur. The duration of an arc–continent collision orogeny depends on a number of factors, among which the obliquity of the collision, the subduction velocity, and the structural architecture of the arc and the continental margin involved are of primary importance. In this book we define the onset of arc–continent collision as the arrival of the leading edge of the continental margin (continental crust to oceanic crust transition) at the subduction zone, something that is often difficult to identify in the geology of an orogen. Thinned, extended continental margins often reach 150–400 km in width and are highly structured. There is now widespread evidence that this thinned crust can be deeply subducted (>200 km) before being returned to the surface as high- and ultrahigh-pressure rocks. Dating these high-pressure rocks can provide important constraints on the timing of arrival of the continental margin at the subduction zone.

A further constraint can be supplied by the arc volcanics, whose geochemistry may record the entrance of continentally derived sediments, or the thinned continental crust itself, into the subduction zone. In currently active systems, imaging the subducted continental lithosphere with techniques such as seismic tomography can also provide key data for determining the timing of on-set of collision and the rates at which the continental crust is being subducted. With the arrival of thicker continental crust (c. 20–30 km thick) at the subduction zone the developing orogen is generally uplifted to above sea level where it begins to erode and provide sediment to a foreland basin and across the arc–continent suture zone and the forearc. As convergence continues, the active volcanic front generally shuts down shortly after the entry of the continental crust into the subduction zone, and volcanic activity can move away from the subduction zone to continue outboard of it for some time before stopping completely. During the final stage of collision, a change in the location of the subduction zone can take place, further marking the end of the arc–continent collision. The final result of the arc–continent collision is a significant change in the structural architecture, composition, and rheology of the continental margin.

The aim of this book is to bring together a series of papers that are dedicated to the investigation of the tectonic processes that take place during arc–continent collision. A further aim is to investigate how tectonic processes influence the large-scale geological characteristics of these accretionary orogens and their mineral wealth. Finally, specific examples of arc–continent collisions are investigated. These range in age from the Neoproterozoic to those that are currently active, covering a large portion of geological time. To advance these aims, a series of points are developed which we attempt to address where possible in each paper. These points are:

- The large-scale crust and mantle structure.
- The nature and role of the lithosphere and asthenospheric mantle in the dynamics and chemistry of the subduction and collision processes.
- Processes that take place deep within the subduction channel in pure intraoceanic subduction and during the subduction of the continental crust.
- The geochemical and petrological evolution of the arc both before and during collision.
- The nature of the continental margin and its response to the collision.
- The formation of topography and the erosion of the developing mountain belt to form a foreland and a suture forearc basin.
- Fore-arc subduction or accretion.
- The emplacement of ophiolites and ultramafic massifs.
- Metamorphism within the developing orogen.
- The possibility of changes in the location of the post-collision subduction zone.
- Place constraints on the duration of arc–continent collision orogeny.
- Recycling, or growth and destruction of the continental crust.

The book is organised in four sections. In the first section, numerical modeling and natural examples are used to look at the three main players involved in arc–continent collision; the continental margin, the volcanic arc, and the subduction zone. In the second section, natural examples of arc–continent collisions are described. In the third section, modeling of various aspects of arc–continent collision are presented. In the fourth section, we bring together the material presented in the previous sections addressing the series of points outlined above and, where possible, attempt to provide answers to them.

Finally, this publication was grant-aided by the Publications Fund of the National University of Ireland, Galway. Also, we would like to extend our thanks to those who kindly provided reviews of the papers. This is an IGCP 524 publication.

Barcelona, Spain — Dennis Brown
Galway, Ireland — Paul D. Ryan

Contents

Contributors

J.C. Afonso Department of Earth and Planetary Sciences, GEMOC ARC Key Centre for Geochemical Evolution and Metallogeny of Continents, Macquarie University, North Ryde, 2109 Sydney, NSW, Australia

J. Alvarez-Marron Instituto de Ciencias de la Tierra "Jaume Almera", CSIC, c/Lluís Solé i Sabarís s/n, 08028 Barcelona, Spain

D. Boutelier Helmholtz Zentrum Potsdam, Deutsches GeoForschunsZentrum, Telegrafenberg, 14471 Potsdam, Germany

D. Brown Instituto de Ciencias de la Tierra "Jaume Almera", CSIC, c/Lluís Solé i Sabarís s/n, 08028 Barcelona, Spain

J.P. Burg Department of Earth sciences, ETH- and University Zurich, Sonneggstrasse 5, CH 8092 Zurich, Switzerland

T. Byrne Center for Integrative Geosciences, University of Connecticut, Beach Hall, U-2045, 354 Mansfield Rd, Storrs, CT 06269, USA

A.J. Calvert Department of Earth Science, Simon Fraser University, 8888 University Drive, Burnaby, BC V5A 1S6, Canada

J.F. Casey Department of Geosciences, University of Houston, Houston, TX, USA

Y.-C. Chan Institute of Earth Sciences, Academia Sinica, 128, Sec. 2, Academia Road, Nangang, Taipei 11529, Taiwan

A. Chemenda Géoazur, Université de Nice-Sophia Antipolis, CNRS, 250 av. A. Einstein, 06560 Valbonne, France

F.A. Cook Department of Geoscience, University of Calgary, Calgary, AB T2N1N4, Canada

S.M. DeBari Geology Department, MS 9080, Western Washington University, Bellingham, WA 98225, USA

J.F. Dewey Department of Geology, UC Davis, One Shields Avenue, Davis, CA 95616, USA

T.V. Gerya Geophysical Fluid Dynamics Group, Institute of Geophysics, Department of Earth Sciences, Swiss Federal Institute of Technology (ETH-Zurich), Sonneggstrasse, 5, 8092 Zurich, Switzerland

A. Greene Department of Geology and Geophysics, SOEST, University of Hawaii, Honolulu, HI 96822, USA

R. Harris Brigham Young University, Provo, UT, USA

R.J. Herrington Department of Mineralogy, Natural History Museum, Cromwell Road, London SW7 5BD, England

M. Johnsen Department of Geology and Geophysics, SOEST, University of Hawaii, Honolulu, HI 96822, USA

E. Konstantinovskaya Institut national de la recherche scientifique, Centre Eau, Terre et Environnement (INRS-ETE), 490 de la Couronne, Quebec, QB G1K 9A9, Canada

Y.-H. Lee Earth and Environmental Sciences, National Chung Cheng University, 168 University Road, Chiayi 621, Taiwan

C.-Y. Lu Department of Geological Sciences, National Taiwan University, 1, Sec. 4, Roosevelt Road, Taipei 106, Taiwan

G. Manatschal IPGS-EOST, Université de Strasbourg, 67084 Strasbourg, France

R.-J. Rau Department of Earth Sciences, National Cheng Kung University, 1 University Road, Tainan 701, Taiwan

T. Reston Earth and Environmental Sciences, School of Geography, University of Birmingham, Birmingham, UK

P.D. Ryan Earth and Ocean Sciences, National University of Ireland Galway, Galway, Ireland

C. van Staal Geological Survey of Canada, 625 Robson St, Vancouver, BC V6B5J3, Canada

Y.-J. Wang Institute of Geophysics, National Central University, 300 Jhongda Road, Jhungli, Taiwan

A. Zagorevski Geological Survey of Canada, 601 Booth St, Ottawa, ON K1A 0E8, Canada

S. Zlotnik School of Geosciences/School of Mathematical Sciences, Monash University, Clayton Campus, 3800 Melbourne, VIC, Australia. Currently at LaCaN, Laboratori de Calcul Numeric, Applied Mathematics Department III, UPC-Barcelona Tech, Jordi Girona 1–3, E-08034 Barcelona, Spain

The Editors

Dr. Dennis Brown is a senior research scientist at the Institute of Earth Sciences "Jaume Almera", CSIC, in Barcelona, Spain. He obtained a Ph.D. in structural geology from Royal Holloway, University of London in 1994. His research interests lie in the general area of mountain building processes. Within this broad theme, he is especially interested in processes of arc–continent collision, the structure and kinematics of foreland thrust and fold belts, and the crustal-scale structure and geodynamics of collisional orogens. He is also active in petrophysical studies of the continental crust.

Dr. P.D. Ryan is Emeritus Professor of Geology at Earth and Ocean Sciences, National Univeristy of Ireland, Galway. He obtained a PhD in Geology from The University of Keele, North Staffordshire in 1974. His research interests include continental tectonics, finite element modelling of lithospheric scale processes, application of non-parametric statistics to geological problems, field geology in Western Europe and reform of geological higher education in the context of the Bologna Process. He has developed a special interest in the process of arc–continent collision during his 40 years of field experience in the Caledonides of western Ireland.

Part I
The Main Players

Chapter 1
Rifted Margins: Building Blocks of Later Collision

T. Reston and G. Manatschal

1.1 Introduction

The first order tectonic process of continental breakup initiates the plate tectonic cycle of plate creation and destruction. Rifted margins are the trailing edges of the continents that develop as the continents are rifted apart (Fig. 1.1) and are thus also the site of eventual continental or arc–continent collision and mountain building. In this paper, we describe the evolution of such rifted margins and the key structures created during the rifting process which may be exploited during subsequent subduction initiation, closure of the ocean basin and eventual arc–continent collision.

Continental breakup occurs through lithospheric extension, thinning and eventual rupture resulting in the formation of a new plate boundary. Lithospheric stretching and thinning allows the underlying asthenospheric mantle to well up towards the surface, undergoing decompression melting according to the amount and rate of upwelling, coupled with the temperature and fertility of the asthenosphere (Bown and White 1995). The thinning of the crust causes subsidence, which during and shortly after rifting, is offset either partly or under certain conditions fully by the thermal uplift provided by the thinning of the entire lithosphere (McKenzie 1978) and the compression of the lithospheric isotherms due to the upwelling of the asthenosphere. As a result, the distribution of subsidence in time and space provides constraints on the amount of extension and thinning of the different lithospheric levels. Extension of the brittle upper crust is accommodated by faulting and fracturing: summing the fault heaves provides an estimate of the amount of extension, but unless distributed deformation within the fault blocks is included the estimate will always be an underestimate. Other parts of the lithosphere may initially deform by other means (ductile flow or creep), although there is evidence that deformation in parts of the lower crust and uppermost mantle are localised into shear zones (Reston 1988, 1993). However the deformation mechanics of the lithosphere evolve during extension and thinning, as the initial rheological properties are modified by strain, by changes in temperature and pressure (Pérez-Gussinyé and Reston 2001), resulting in increased coupling between crust and mantle, culminating in complete crustal embrittlement. These processes are strongly controlled by inheritance, i.e., initial composition, thermal state and pre-rift structures.

In the past, rifted margins have been classified as volcanic or non-volcanic margins. These terms are a bit misleading as even non-volcanic margins exhibit magmatism, so in this paper we will prefer the term "magma-poor" and "magma-rich" rifted margins (Reston 2009), depending whether or not more magmatism is observed than might be expected during rifting above undepleted mantle with a potential temperature of 1,300°C (Tp – the temperature it would have if brought rapidly to the surface – Pérez-Gussinyé et al. 2006). During rifting, the upwelling of such mantle leads to decompression melting producing 6–7 km for very rapid rifting and hence upwelling, but perhaps 3–4 km for typical rift durations (Minshull et al. 2001). However, the distinction between magma-rich and magma-poor is complicated by the occurrence of hybrid margins, where the amount of magmatism

T. Reston
Earth and Environmental Sciences, School of Geography, University of Birmingham, Birmingham, UK
e-mail: t.j.reston@bham.ac.uk

G. Manatschal
IPGS-EOST, Université de Strasbourg, 67084 Strasbourg, France

D. Brown and P.D. Ryan (eds.), *Arc-Continent Collision*, Frontiers in Earth Sciences,
DOI 10.1007/978-3-540-88558-0_1,

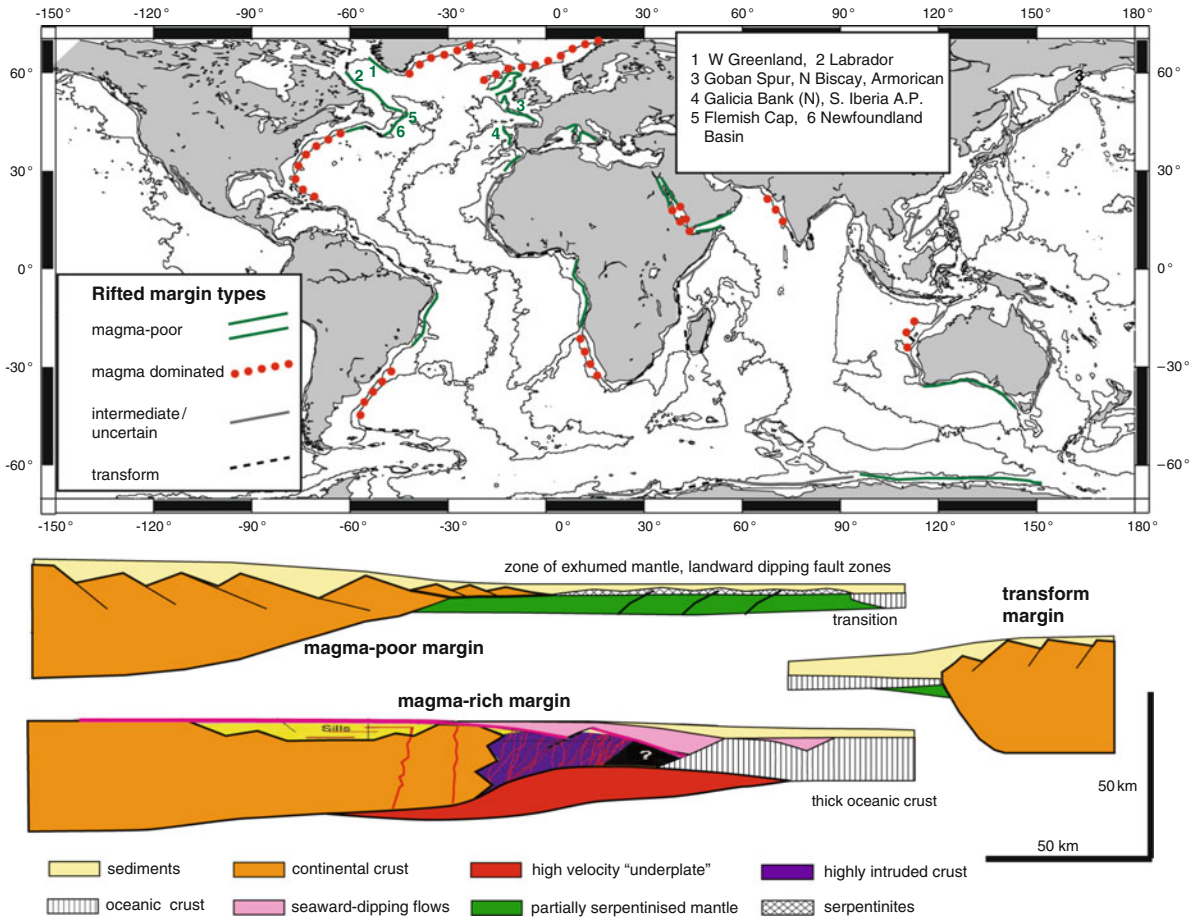

Fig. 1.1 *Top*: Worldwide distribution of different margin types (modified after Boillot and Coulon 1998) and the locations of the margins discussed in this paper (*bold*). Magma-poor, magma-dominated and transform are all approximately equally numerous. *Below*: Cartoon sections summarising the architecture of magma-poor (based on observations made in this paper), magma-rich (modified after Geoffroy 2005) and transform (based on Sage et al. 2000) margins.

varies along strike (e.g., West Greenland – Chalmers and Pulvertaft 2001) and margins where magma-poor rifting is followed by magma-rich breakup (e.g., Voring basin and margin – Osmundsen and Ebbing 2008; Rockall Trough – Reston 2009) or vice-versa (India-Seychelles – Armitage et al. 2010). These complication should be borne in mind as in the following sections we discuss end-member features of rifted margins and how these may affect their behaviour in subsequent orogenesis.

Transform margins (e.g., Sage et al. 2000) form a completely separate class of rifted margins formed during continental breakup, generally exhibiting little magmatism, but marked by abrupt changes in crustal thickness. The presence of deeply penetrating fracture zones along such transform margins leads to localised mantle serpentinization (Sage et al. 2000), providing some similarity with magma-poor rifted margins but showing extreme strain localization. However, discussion of these margins is beyond the scope of this paper.

1.2 Magma Rich Margins

Many rifted margins (e.g., East Greenland and Voring margins – Fig. 1.2) are characterised by thick sequences of mainly subaerially erupted basalts, expressed as seaward-dipping reflectors, the seismic signature of flexurally (and to a lesser extent thermally) rotated lava flows (Hinz 1981; Mutter et al. 1988), and thick intrusive sequences at or near the base of the crust, commonly termed underplate.

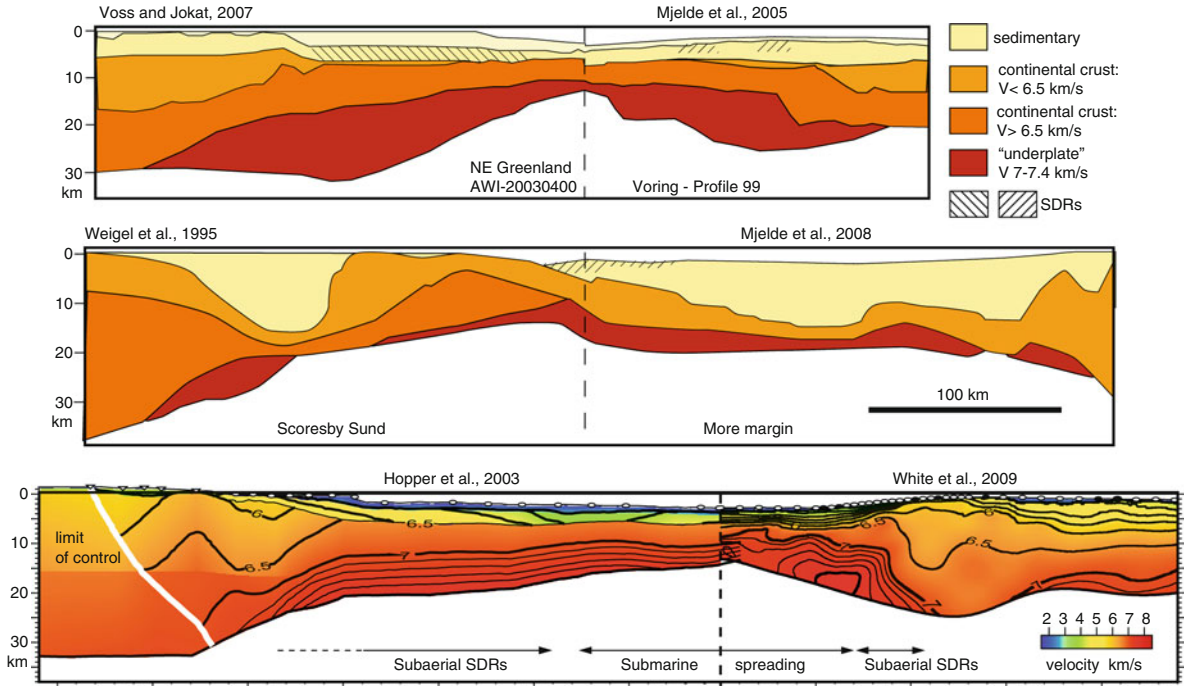

Fig. 1.2 Sections across conjugate pairs of magma-rich margins between East Greenland and Norway (*top* two – Mjelde et al. 2005, 2008; Voss and Jokat 2007; Weigel et al. 1995) and Scotland (Hopper et al. 2003; White and Smith 2009 – *bottom*). Note that the margins display variable thicknesses of "underplate", which may consist of both mafic intrusions and the lower most crust being intruded, variable widths of seaward-dipping reflectors (SDRs), interpreted as lava flows, and varying degrees of crustal thinning, generally reflecting the rift evolution prior to extensive magmatism and breakup. The margins are far from symmetric as commonly supposed.

The emplacement of the seaward-dipping lavas is in places accompanied by the development of large landward-dipping faults, accommodating both the margin flexure and extension. The "underplate" commonly occurs as the crust thins over a distance of up to 50 km from $\gg$20 km to $<$10 km (Fig. 1.1). The total thickness of igneous rocks emplaced during rifting and breakup at these margins is typically estimated at well over 10 km, i.e., considerably more than predicted by passive upwelling of "normal" asthenosphere beneath the thinning crust. It should be borne in mind that these estimates generally assume that the high velocity lenses beneath the margin consists entirely of igneous additions to the crust, whereas they may consist of original crust heavily intruded by igneous material. Past studies (e.g., White et al. 1987) suggested that the igneous additions were characterised by little internal reflectivity, relatively uniform velocities in the range of 7.2–7.4 km/s and low velocity gradients, well below 0.05 per second, all suggesting the presence of large bodies of intruded igneous rock rather than a volume of country rock intruded by many smaller intrusions. If so, the enormous thickness of the high velocity body (e.g., exceeding 15 km at the East Greenland margin – Voss and Jokat 2007) would indeed require that much more melt was generated than would be expected by passive upwelling of normal temperature mantle beneath the thinning lithosphere. However, more recent data have shown that the "underplate" is internally reflective, has downward increasing velocities and a velocity gradient close to 0.1 per second (White and Smith 2009). Together these led White and Smith (2009) to interpret the high velocity lower crust as a series of sill-like intrusions rather than a single large zone of underplate.

The exact cause of excess magmatism at magma-rich margins is disputed, but must explain both the volume of melt and the subaerial eruption of the lavas, requiring some mechanism to elevate the thinned crust above sea level. The simplest way of generating more than 6–7 km of melt is through rapid extension above undepleted mantle with a potential temperature (Tp) greater than ~1,300°C. Hot mantle has a lower density than "normal mantle" and so has been generally

associated with upwelling convection limbs, or mantle plumes (e.g., White and McKenzie 1989). Both the higher temperature and the rapid upwelling of a mantle plume could contribute to the production of more melt than expected from the passive upwelling of "normal" temperature mantle, leading to the formation of magma-rich rifted margins where rifting and continental breakup occurs above such plumes (White and McKenzie 1989). In contrast Anderson et al. (1992) suggested that thermal anomalies in the upper mantle need not be related to plumes rising from below, in which case the melting anomaly would be a consequence of the temperature anomaly alone and not any excess upwelling.

Increasing the volume of upwelling mantle without invoking a temperature anomaly may also allow the generation of excess melt. As the space into which the mantle can rise is limited by the amount of lithospheric extension and hence thinning, excess upwelling can only occur if the previously upwelled mantle can be removed somehow. Mutter et al. (1988) suggested that the presence of cold lithosphere beneath the adjacent rift flanks could cool the upwelling mantle, increase its density and lead to its sinking. Such "secondary convection" increases the volume of asthenosphere passing through the melting zone and thus increases the amount of melt produced. However, Nielson and Hopper (2002) show that the viscosity of the mantle is too great for significant secondary convection, especially once volatiles have been extracted with the melt, unless the asthenosphere is also at above average temperature, i.e., unless there was also a temperature anomaly.

A final way of increasing the amount of melt produced is by changing the chemistry of the mantle: instead of a pyrolitic composition, the upper mantle might be enriched in volatiles and incompatible elements, lowering the solidus and increasing the volume of melt that can be produced for a given amount of extension (Anderson et al. 1992). However, a local chemical anomaly is likely to be rapidly exhausted, implying that magma volumes should decrease toward standard with time.

The different methods of increasing the volume of melt predict a different chemistry of melt and thus different physical properties, including seismic velocity, as a function of the volume of melt produced (Holbrook et al. 2001). Thus mean seismic velocities together with estimated thicknesses of the igneous crust may be used to distinguish between different models of excess melt production. The results from the east Greenland margin (Holbrook et al. 2001) suggest that elevated mantle temperatures play a role, but that enhanced upwelling is a contributory factor, especially near the proposed "hotspot", suggesting plume-like activity.

At many magma-rich margins, the excess magmatism appears to be associated with final breakup following a longer phase of magma-poor rifting (e.g., Osmundsen and Ebbing 2008). For instance inboard of the Voring margin, the basement of the Voring basin thins to ~10 km or less (Osmundsen and Ebbing 2008) as a result of Late Jurassic to Early Cretaceous extension occurring prior to the voluminous magmatism in the Paleogene. The Rockall Trough inboard of the Rockall and Hatton margins have a layer with crustal basement velocity of ~6 km thickness and a width of up to 200 km. In both cases, the final breakup took place away from the line of earlier rifting.

Conversely, at other margins excessive magmatism appears to have preceded the rifting that led to breakup (Armitage et al. 2010). Magmatism in the Deccan Traps may have initiated the development of the magmatic Gop rift between India and the Laxmi Ridge, but preceded the late separation from the Seychelles. Armitage et al. (2010) suggest that melting beneath the Gop rift depleted the thermal anomaly associated with the Deccan Traps so that by the time the Seychelles split off, breakup largely occurred over normal temperature mantle and was thus not accompanied by excessive magmatism.

Although the exact cause of the excess magmatism is disputed and the relative contributions of high asthenospheric temperatures, secondary convection and an originally volatile enriched source is much debated, the net result (Figs. 1.1 and 1.2) is a margin quite different from the magma-poor margins.

1.3 Magma-Poor Rifted Margins of the North Atlantic and Neighbouring Areas

Magma-poor rifted margins are found in most oceans, but those in the North Atlantic, together with those exposed on land within mountain belts, especially the Alps in Western Europe, have been most intensively

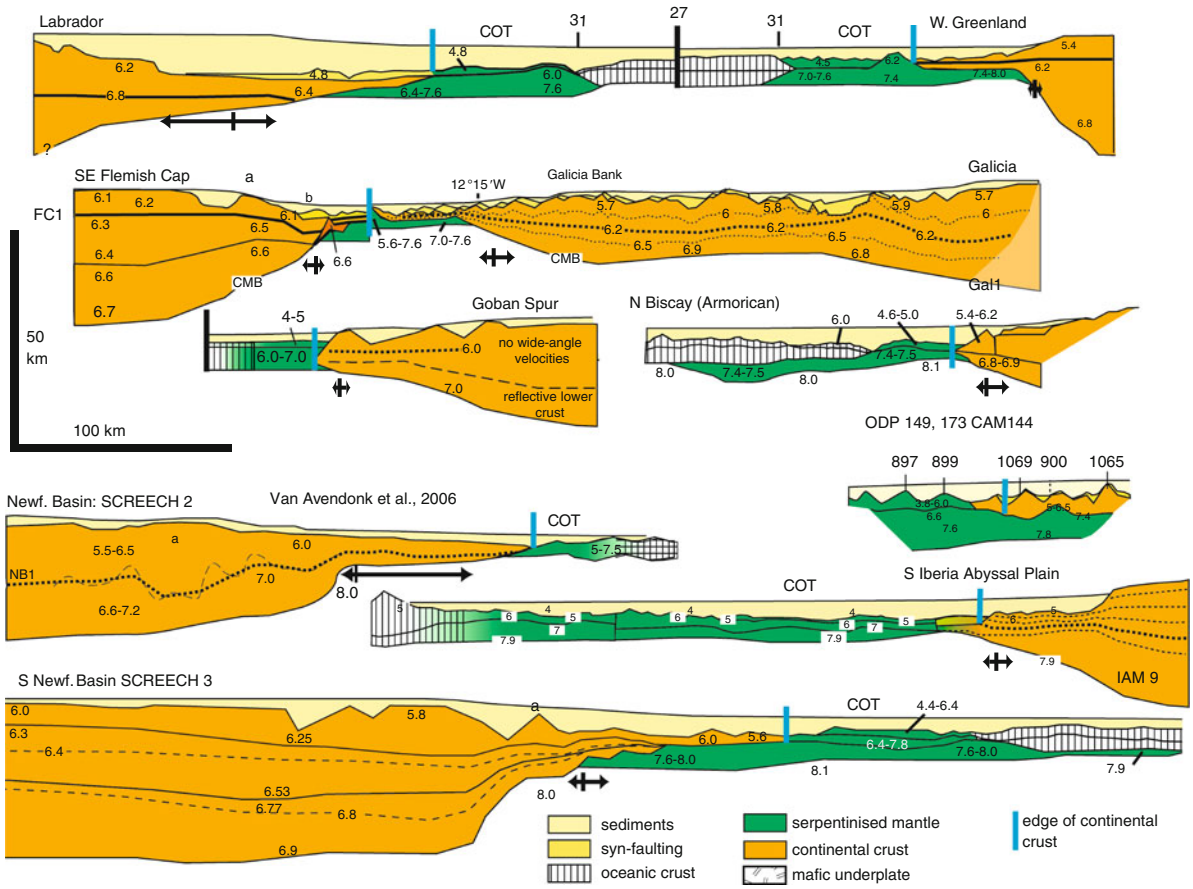

Fig. 1.3 Sections at the same scale with no vertical exaggeration, through ten magma-poor margins, including four conjugate or near-conjugate margin pairs, best constrained by combined seismic reflection and wide-angle data. Key velocity boundaries and contours are marked. Also marked is the point where the crust thins to the value at which it should have become brittle during rifting. These can be compared spatially to the landward limit of serpentinized mantle. The spatial correspondence is remarkable for the W Greenland, SE Flemish Cap (SCREECH 1), S Newfoundland Basin (SCREECH 3) margins and within a fault block for the Galicia south IAP (IAM9), within error but less good for the N. Newfoundland Basin (SCREECH 2) and Labrador margins.

studied (Fig. 1.3). Examples include parts of Labrador-West Greenland (Chian et al. 1995; Chalmers and Pulvertaft 2001), Flemish Cap – Goban Spur (Keen et al. 1989; Bullock and Minshull 2005), North Biscay (Thinon et al. 2003), Flemish Cap-Galicia Bank (Hopper et al. 2004; Funck et al. 2003; Zelt et al. 2003; Reston et al. 1996), Newfoundland Basin – South Iberia Abyssal Plain (Van Avendonk et al. 2006; Krawczyk et al. 1996; Pickup et al. 1996; Dean et al. 2001; Chian et al. 1999; Whitmarsh et al. 2001; Peron-Pinvidic and Manatschal 2009), and S Newfoundland Basin – Tagus (Lau et al. 2006). Other margins which appear very similar to the above either are not well enough characterized geophysically (South Australia) or have thick postrift sedimentary sequences that obscure the deeper structure so that it is not always totally clear whether they are magma-poor or not (e.g., Santos margin in the South Atlantic).

Focussing on the magma-poor Iberia-Newfoundland rifted margins which are well constrained by geophysical (both reflection and refraction) and ODP data and which show neither important magmatic additions nor salt, (Fig. 1.3), a number of common features can be observed that seem to be characteristic of magma-poor rifted margins (see also Fig. 1.1).

1. Extreme crustal thinning from 30 to 35 km to a few km in most cases over a distance of 100–200 km. Well-defined fault blocks are imaged on most margins, but the amount of extension associated with

these is generally less than required to explain the crustal thinning. This is the so-called extension discrepancy, discussed below. The thinning occurs most rapidly (in time or in space) in a necking zone between about 20 and 10 km: most margins are characterised by a broad shelf, a steep continental slope and an extensive continental rise of very thin crust. As discussed below the mechanics of crustal thinning in the necking zone are of fundamental importance to our understanding of the processes leading to breakup and margin formation.

The crustal thinning at such margins creates accommodation space in which thick sedimentary sequences can accumulate. The water-loaded total subsidence associated with thinning the crust to perhaps 5 km is in excess of 6 km, corresponding to perhaps 15 km of possible sediment accumulation. Such thick sedimentary piles are observed at some margins (Holbrook et al. 1994) and form the thick deforming pile in some orogens. For instance the cumulative thickness of the Dalradian reaches 25 km (Anderton 1982), although this represents in part the migration of the depocentre with time: the maximum thickness in any one place is perhaps closer to 10 km. As discussed more below the presence of a thick sedimentary sequence during rifting may have considerable influence on the mechanics of rifting and the structure of the resulting margin.

If crustal thinning is accompanied by lithospheric thinning, the highly stretched crust of magma poor margins should be accompanied by several km of magmatic additions. Where these are not observed, the lack of magmatism may be attributed to cool mantle temperatures (Reston and Phipps Morgan 2004), to a depth-dependent distribution of lithospheric strain (the crust locally thinned more than the entire lithosphere – Huismans and Beaumont 2008), to cooling effects of nearby unthinned lithosphere (Bown and White 1995) or to depleted mantle (Muntener and Manatschal 2006)

2. A zone of anomalous basement between the last identifiable continental crust and the first true oceanic crust. This unit typically has a moderate velocity gradient (~0.2 per second), passing down from 5 km/s to close to 8 km/s and weak magnetic anomalies. The unit has been sampled by dredging, by submersible (Boillot et al. 1989) and by drilling on the West Iberian margin (sites 637, 897, 899, 1068 and 1070 – Boillot and Winterer 1988; Whitmarsh et al. 2001), by drilling off the Newfoundland margin (Tucholke et al. 2007) Site 1277 and by dredging to the south of Australia (Nicholls et al. 1981), and has been found to be partially serpentinized peridotites. The anomalous crust is thus thought to be exhumed mantle, with downward decreasing degrees of serpentinization explaining the velocity gradient. Elsewhere, it has been identified by similar geophysical characteristics (velocity), a lack of a clear Moho reflection, a lack of the well defined oceanic spreading anomalies and rough, diffractive top basement expected for oceanic crust, and a lack of clear fault block structure, including the presence of prerift or at least pre-faulting sedimentary sequence atop the fault blocks, expected for thinned continental crust. Within the zone of exhumed mantle at the west Iberian margin, local ridges developed during rifting and onlapped by postrift sediments, are associated with later minor thrusting and the formation of monoclines in the overlying postrift sedimentary sequence: compressional stresses appear to have reactivated rift related structures within the exhumed mantle rather than in the thinned crust (Péron-Pinvidic et al. 2008).
3. Lenses with velocity intermediate between those of the crust and mantle, occurring beneath crust that had thinned during rifting to less than about 8 km. Typically they have a velocity of between 7 and 7.8 km/s, and a velocity gradient of close to 0.1 per second. In most cases, the bodies can be traced laterally into zones of unroofed mantle (see above) and so are interpreted as partially serpentinized peridotites, "undercrusting" (Boillot et al. 1989) the crust. Where they cannot be traced laterally, they might alternatively have been interpreted as mafic underplate or a zone of mantle intruded with mafic intrusions, if it were not for the paucity of magmatism at most of these margins. Although serpentinized mantle has not yet actually been sampled beneath the thinned continental crust of a present-day margin, it has been at magma-poor margins preserved within orogens, such as the Alps as is discussed below. As a result, it is generally accepted that the high velocity, high gradient zone beneath thinned crust at magma-poor margins is indeed largely serpentinized mantle. The upper limit on the velocity of these lenses is

perhaps marginally higher than the intruded zone at magma-rich margins, the velocity gradient perhaps somewhat better developed, and with less evidence for a Moho reflection from the base, but none of these are really diagnostic alone. Perhaps the most convincing way to distinguish between serpentinized "undercrust" and high velocity mafic intrusions are the association of the former with crust that had been thinned to <8 km (Reston 2009) and the association of the latter with SDRs.

4. At some margins, the boundary between highly thinned continental crust and the underlying zone interpreted as serpentinized mantle is marked by a sharp reflector, most clearly imaged on depth images produced by prestack depth migration. Examples include the S reflector west of Galicia (de Charpal et al. 1978; Reston et al. 1996), the H reflector in the Iberia Abyssal Plain (Krawczyk et al. 1996), and the P reflection beneath the Porcupine Basin (Reston et al. 2001). In each case, the reflector does not only appear to separate crustal rocks from the underlying serpentinized mantle, but also to act as a detachment onto which the overlying fault blocks ride. Analyses of the physical properties of the H and S reflections (Krawczyk 1995; Reston 1996) have shown that they are compatible with a relatively sharp boundary between fractured crustal rocks and partially serpentinized peridotites, perhaps supplemented by a thin zone of reduced velocity at the detachment itself (Leythaeuser et al. 2005).

In the following sections we examine the processes that may have led to the development of these characteristics at magma-poor rifted margins and derive a generic model for the formation of magma-poor margins.

1.3.1 Rheological and Tectonic Evolution of Magma-Poor Rifted Margins

This paper is concerned with aspects of the structure and tectonics of rifted margins that may affect future arc–continent or continent–continent collisions. As such, we suggest that the formation of magma-poor rifted margins is of particular interest as these may be the sites of subduction initiation and the obduction of "ophiolites" such as the Alpine peridotites (Lemoine et al. 1987; Whitmarsh et al. 1993; Manatschal and Muntener 2009; Beltrando et al. 2010). Furthermore, as discussed above, many magma-rich margins may have evolved initially as magma poor rifts and thus share many of the key structural elements present at magma poor margins (Osmundsen and Ebbing 2008). The lack of thick basalt sequences at magma poor margins allow better seismic imaging of the structures controlling crustal extension and thinning and also allow access to depth for the drill bit.

The structure of magma-poor rifted margins is controlled by the consequences of increasing amounts of extension. These consequences include the changing rheology of the crust and the development of complex cross-cutting structures. Downward increasing pressure increases the stress required to cause brittle failure, whereas downward increasing temperature reduces the viscosity of a given lithology, causing a downward transition from brittle to ductile behaviour. Superimposed on this, it is generally accepted that changes in the dominant mineralogy of the lithosphere from granitic (quartz-dominated rheology), through mafic-gabbroic (plagioclase dominated rheology) to ultramafic (olivine dominated rheology) produces a general rheological stratification of the lithosphere. At the onset of rifting, the portions of the crust dominated by low viscosity creep form weak zones, separating stronger zones where deformation is either brittle (including the seismogenic brittle upper crust which is perhaps 8–10 km thick – Kusznir and Park 1987; Jackson and White 1989) or of higher viscosity. These weak zones generally occur in the mid-crust and at the base of the crust, except where the latter is dominated by very mafic lithologies such as the Permian gabbros intruded into the lower crust prior to rifting in the Alpine domain, and separate stronger zones where deformation is either brittle (including the seismogenic brittle upper crust which is 8–10 km thick – Kusznir and Park 1987; Jackson and White 1989) or of higher viscosity. The net result is that the lithosphere behaves as a partially decoupled multilayer of strong beams separated by weak zones.

The extension of such a decoupled system promotes broadly symmetric lithospheric-scale extension (Huismans and Beaumont 2002), controlled by localised structures within the uppermost mantle (Reston 1993) as well as the upper crust. However, where the lower crust does not decouple the upper crust from the mantle, more asymmetric extension develops

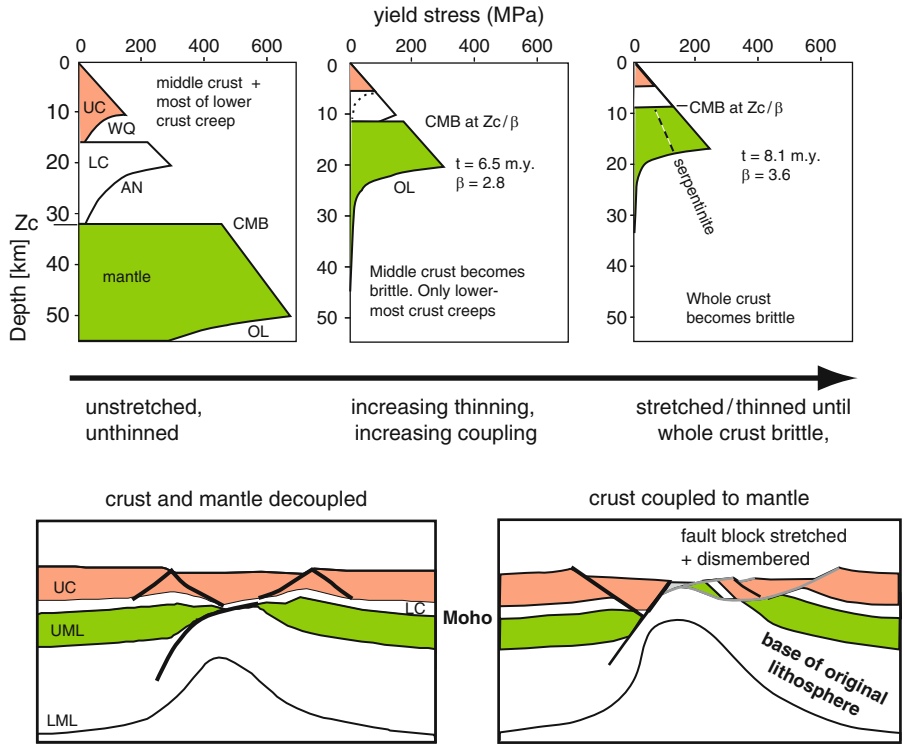

Fig. 1.4 Rheological evolution of the upper lithosphere during pure shear stretching. Initial weak zones within the midcrust and lowermost crust gradually disappear as the crust thins and creeping rocks become brittle (Pérez-Gussinyé and Reston 2001). Once the entire crust becomes brittle, water can reach the mantle, causing serpentinization. The gradual embrittlement of the crust leads to increased coupling between crust and mantle, leading to a transition from symmetric, decoupled extension to asymmetric coupled extension.

(Huismans and Beaumont 2002). Thus a change from decoupling to coupling changes the rift style. Just such a change occurs during progressive rifting: as the crust thins and cools, the reduction in overburden pressure and temperature means that rocks which originally deformed by plastic creep gradually become brittle and fracture. The result is that the initial weak zones in the middle crust and deep crust disappear and the entire crust becomes brittle. This is illustrated by a one-dimensional model (Fig. 1.4), in which the entire crust becomes brittle, not through the lateral displacement of any ductile layer (impossible in a 1-D model), but through originally ductile rocks becoming brittle. Although the real world is clearly not 1-D, this model illustrates that for the entire crust to become brittle a layer that was originally ductile may just become brittle rather than disappear as implied by analog modelling (e.g., Brun and Beslier 1995), which cannot easily replicate the changing rheology that occurs in real systems.

One consequence of the progressive embrittlement of originally ductile rocks during lithospheric extension is that lateral flow or displacement of particular layers within the crust should become progressively more difficult as rifting proceeds. A second consequence is that the upper crust becomes coupled to the mantle, allowing the development of a through-going fault zone, thus promoting increasing asymmetry as extension continues (Huismans and Beaumont 2002; Lavier and Manatschal 2006). Furthermore, the formation of crustal-scale brittle faults provides conduits for the transport of aqueous fluids from the surface into the mantle, allowing extensive mantle serpentinization. Except for extreme cases, complete crustal embrittlement occurs at stretching factors between 3 and 5, depending on the rift duration and the original lithospheric configuration (Perez-Gussinye et al. 2001 – Fig. 1.5); changing the mineralogy and rheology of the lower crust in particular (e.g., from aggregate to dry quartz or to anorthosite) results in

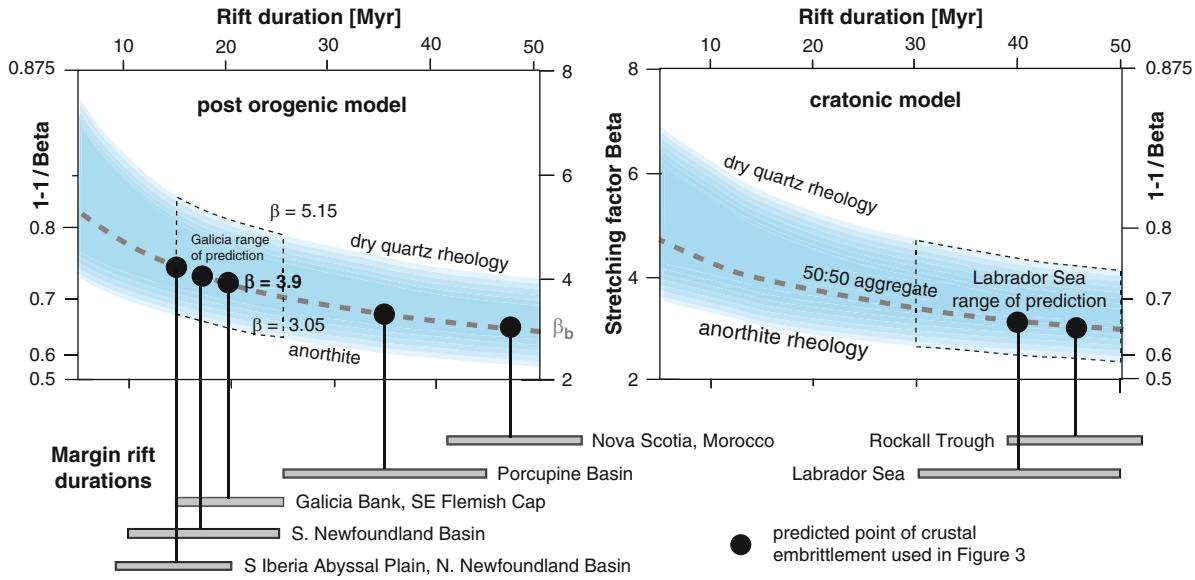

Fig. 1.5 Plot (modified from Reston 2009) for two different lithospheric models showing the stretching factor at which the entire crust is predicted to become brittle (β_b) (Pérez-Gussinyé et al. 2001) as a function of rift duration. *Broad blue band* – limits of predicted embrittlement depending on whether dry quartz (upper limit) or feldspar (lower limit) better approximates lower crustal rheology. *Grey dashed line* is for a 50:50 dry quartz/feldspar aggregate. Estimates of rift duration for margins shown [West Greenland, Labrador – Chalmers and Pulvertaft (2001); Reston and Pérez-Gussinyé (2007); Rockall Trough – Pérez-Gussinyé et al. (2001); Armorican – Thinon et al. (2003); Goban Spur – Bullock and Minshull (2005); Porcupine Basin – O'Reilly et al. (2006); South Newfoundland Basin – Reid (1994), Lau et al. (2006); SE Flemish Cap – Tucholke et al. (2007); Galicia Bank – Mauffret and Montadert (1987), Reston (2009); Iberia Abyssal Plain – Wilson et al. (2001); Minshull et al. (2001); Tucholke et al. (2007); Morocco – Maillard et al. (2006); Nova Scotia – Funck et al. (2004), Wu et al. (2006)]. β_b depends more on lower crustal rheology than with range of possible rift duration at any given margin, the former is used to give first estimate of β_b uncertainty (Galicia is illustrated) used to plot predicted embrittlement in Fig. 1.3.

embrittlement at lower stretching factors, as does increasing the strain rate. The predicted thickness of the crust at the point it becomes entirely brittle agrees well with the landward limit of mantle serpentinites (Fig. 1.3).

The embrittlement of the crust and the serpentinization of the underlying mantle have significant consequences for the structural and tectonic evolution of the evolving rifted margin, leading to a transition between different structural styles. Initial rifting, (see "stretching phase" described by Lavier and Manatschal 2006), may have occurred along an array of sub-parallel faults as in a rift basin such as the North Sea (White 1990): extension in such a setting is accommodated by displacements on the normal faults, by the back-rotation of a dominant set of faults, dipping in one direction, and by the internal deformation of the blocks. At depth the normal faults would decouple into a creeping middle and lower crust, perhaps separated by a strong lower crustal layer deforming by boudinage (Reston 1988; Lavier and Manatschal 2006). Some heterogeneous crustal extension is likely to occur, with the locus of extension in the lower crust being controlled by boudinage and in the upper crust by the brittle faults. The resulting shear between the upper and lower crust would thus produce strong strain fabrics, a possible cause of the lower crustal reflectivity observed in many terranes (Reston 1988, 1993). As the crust and mantle are most strongly decoupled during this initial phase, it is during this phase that heterogeneous or depth-dependent crustal stretching might be expected. However, most studies of rifts such as the North Sea do not show significant difference between the amount of thinning and the amount of measurable extension (White 1990; Kusznir and Karner 2007), implying that crustal extension although decoupled, remains largely uniform with depth.

Rifts such as the North Sea are characterised by stretching factors of up to 2, corresponding to 100% extension (e.g., White 1990). At rifted margins the degree of extension and thinning are much higher, with consequences for both the rheological evolution of the crust and for the complexity of structural geometries. When extension approaches 100%, normal faults will have rotated to ~30°, even allowing for some internal block deformation (Reston 2005). At such angles, even under optimum continuing stress orientations, it should be easier to form a new fault than to continue slip along an existing structure. Thus a second phase of faulting would be expected, most probably focusing into a narrow region (Cowie et al. 2005) as observed for instance in the Galicia Interior Basin (Reston 2005).

As extension increases, the combination of a reduction in the overburden pressure at depth (due to crustal thinning) and cooling causes originally low viscosity rocks forming the weak zones within the crust to become increasingly viscous and in places even brittle (Fig. 1.4). The result is a pronounced increase in the degree of coupling between the upper crust and the lower crust, so that second generation of faults are likely to cut from the surface down into the lowermost crust (Lavier and Manatschal 2006), and thus control the extension of virtually the entire crust. At this stage, crustal extension may still be somewhat decoupled from that in the mantle, which undergoes brittle boudinage, allowing focused infiltration of hotter mantle from below. As a result, as rifting focuses to a narrower zone during what Lavier and Manatschal term the "thinning phase", extension becomes controlled by just one or two main structures (e.g., Cowie et al. 2005). As extension focuses on these structures, others are abandoned, leading to a focussing of extension onto a few important structures (strain localization). The consequence would be both a strong thinning of the crust in these places and also the local overprinting of the early rift structures (Reston 2005), which would become progressively more difficult to recognise (Proffett 1977; Jackson and White 1989) The thinning may be accompanied by some limited heterogeneous crustal extension, but this would become increasingly difficult as only the lowermost crust remains ductile and capable of any degree of flow.

As coupling increases, eventually the entire crust becomes brittle when, for the magma-poor margins of the North Atlantic, the crust had thinned to between one third to one fifth of its original thickness (Fig. 1.5), depending on the rift duration, and on the initial composition and structure of the crust (Perez-Gussinye et al. 2001). Complete crustal embrittlement allows water to pass along brittle faults from the surface directly into the mantle, and thus the formation of hydrated minerals such as serpentine (below ~400°C) and talc. These minerals have friction coefficients that are far lower than normal crustal and mantle rocks (e.g., Escartin et al. 1997). However as the serpentinization is focussed along narrow faults zones, the crust is not decoupled from the mantle by the development of these serpentinites: instead, they provide a mechanism for the asymmetric unroofing of lower crustal and mantle rocks within the continent–ocean transition. The unroofing of mantle rocks in particular is a feature of magma-poor margins, (Figs. 1.3 and 1.6), the unroofed partially serpentinized peridotites within the continent–ocean transition (COT) appearing to be the geophysical continuation of the reduced velocity mantle undercrusting the feather edge of the continental crust. When the crust has become entirely brittle, the rheology of the thinned lithosphere becomes dominated by the mantle and by the formation of serpentine and talc along mantle faults, allowing the exhumation of mantle rocks. Until the onset of voluminous magmatism, the process continues through successive detachments, resulting in the exhumation of a large expanse of mantle within the continent–ocean transition, through the removal of overlying portions of the lithosphere (Fig. 1.7). As final exhumation to the surface must have occurred in the brittle regime, everywhere this unroofed mantle must be topped by faults which must locally predate the structures that offset the top of the mantle basement and which defines the fault block topography within the COT. The preponderance of landward-dipping shear zones within the exhumed mantle (Fig. 1.7) means that on reactivation as thrusts or reverse faults (e.g., Peron-Pinvidic et al. 2007), the wide expanses of exhumed mantle at magma-poor margin is likely to form the hanging wall to those reverse faults, i.e. the overriding plate if full-blown subduction begins.

The rifted margins produced by these processes are likely to show a broad region where extension is well below 100% (stretching factor below 2), a fairly narrow region where the crust thins dramatically from ~30 or 20 km to less than 10 km, a region of small

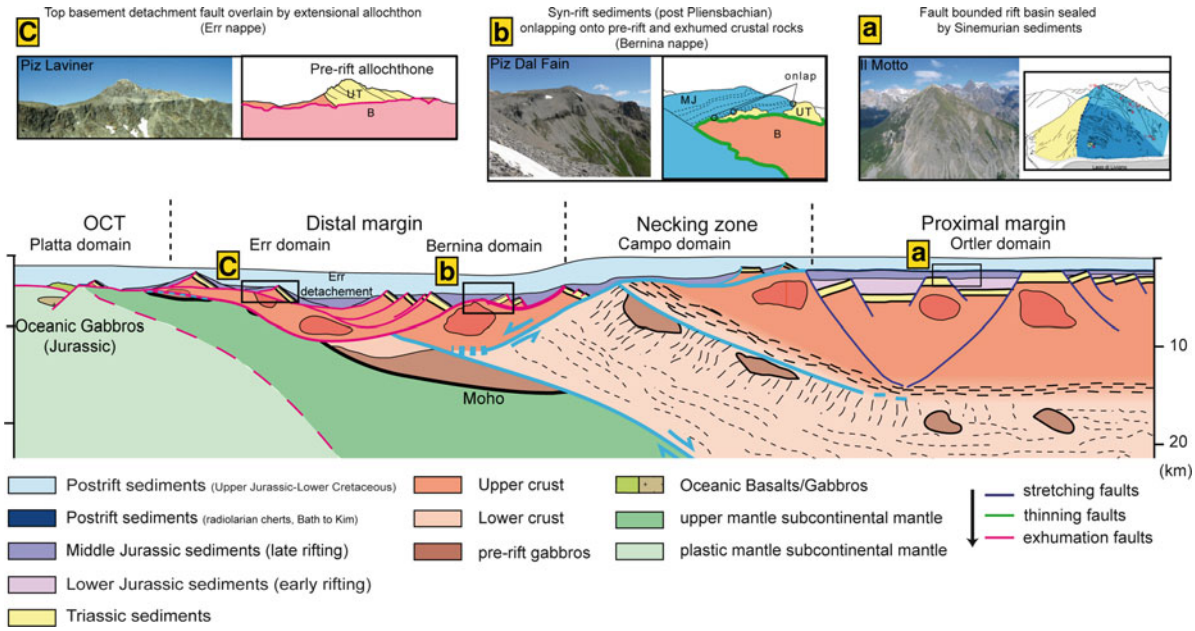

Fig. 1.6 Tentative palinspastic reconstruction of the Adriatic margin across the Austroalpine and South-Penninic units in Grisons (SE Switzerland) (modified after Mohn et al. 2010). The section shows the different type of extensional structures responsible for crustal extension. (**a**) Il Motto in the proximal margin shows the breakaway of a high-angle normal fault that is sealed by Upper Sinemurian sediments. (**b**) Piz dal Fain in the distal margin exposes a top basement detachment fault that is overlain by small allochthones of pre-rift sediments onlapped by Late Pliensbachian syn-rift sediments. (**c**) Piz Laviner shows a tilted block of pre-rift sediments and crystalline basement rocks truncated by a low-angle detachment fault.

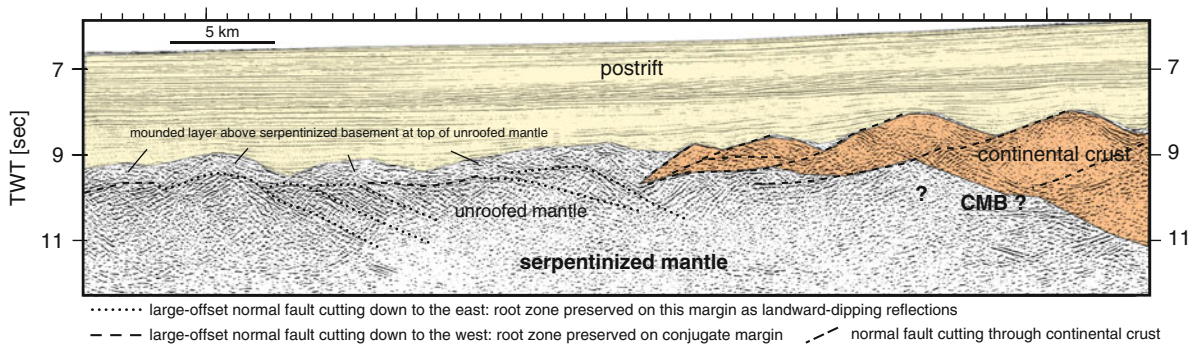

Fig. 1.7 Seismic image of the feather edge of continental crust and the start of a broad region of exhumed mantle at the south Iberian Abyssal Plain (after Pickup et al. 1996). West of the feather edge of continental crust, a broad expanse of mantle continues for ~150 km before true oceanic crust is formed. Note the presence of dominantly landward-dipping structures cutting to depth.

tilted blocks above a weak layer of serpentinized mantle and finally a broad region where exhumed mantle peridotites are overlain directly by the postrift sediments, and which grades into true oceanic crust as the amount of magmatism increases. This is precisely the pattern of thinning observed at many rifted margins (Reston 2009). In this section, we consider further the implications that this structural model has for the eventual incorporation of the rifted margins into collisional orogens.

The above discussion has been based to a large extent on the observations made at the sediment-starved West Iberia margin and the modelling of rifting at a cool margin (Reston and Phipps Morgan

2004) with little synrift sedimentation. Margins buried beneath a thick sequence of postrift sediments may have similar structure, albeit less well resolved and out of the reach of the drill bit. However, margins characterised by rapid and/or thick sedimentation during the rifting phase may be quite different as the sediment affects the rift process. In particular, the thermal effects of a thick sedimentary sequence mean that during rifting the crust cannot cool as efficiently and may indeed heat up beneath the insulating blanket of sediments, reducing the strength of the crust and lithosphere (Sandiford et al. 1998). Thus a well sedimented margin such as the South Atlantic margins and the Laurentian margin (the latter buried beneath the Dalradian supergroup) may have been rheologically much weaker than the West Iberia margin.

1.4 Margins Exposed in Orogenic Belts

The detailed geology of in situ margins is limited to information gleaned from sparse drill data and geophysical techniques, especially seismic profiling and wide-angle seismic. Complementary information can be obtained from fossil rifted margins sampled in collisional orogens. Here we consider the Dalradian of Scotland and Ireland (Leslie 2008) and the remnants of the former Tethys margins exposed in the Alps (Manatschal 2004; Manatschal et al. 2006). The Alpine Tethyan remnants represent spectacular outcrops that provide detailed, although sometimes incomplete and patchy observations, that are complementary to the largely geophysical study of the in situ magma-poor margins offshore. Detailed mapping and kinematic inversion of the Alpine structures enabled restoration of the architectures of the former Alpine Tethys margin from the most proximal to the most distal parts of the margin, including the zone of exhumed continental mantle (see Manatschal et al. 2006; Mohn et al. 2010 for a review and Fig. 1.6).

The Alpine margins show a change from fault-bounded North Sea type rift basins in the proximal margins (e.g., Bourg d'Oisans or Generoso, Lemoine et al. 1987 and Bernouilli 1984) to basins floored by detachment faults in the distal margin (e.g., Froitzheim and Eberli 1991). The most spectacular structures are top-basement detachment faults that can be mapped over tens of kilometres (Manatschal and Nievergelt 1997) and that are responsible for the final crustal thinning and mantle exhumation at the edges of the continents. This is best documented in the Tasna area, where a wedge of continental crust can be observed separated along a detachment fault from the underlying mantle and sealed by post-rift sediments (Florineth and Froitzheim 1994; Manatschal et al. 2006). These outcrops are important, because they show the importance of low-angle faults in accommodating extension in the most distal edges of the continents and represent "windows" in geological settings that are, at present-day margins, covered by several kilometres of sediments and water. Other important observations that can be made in the Alpine example are (1) the polyphase nature of rifting and its migration towards the area of future breakup (Manatschal 2004); (2) the oceanward increase in the volume of magma within the ocean continent transition (Desmurs et al. 2002), and (3) the occurrence of different types of mantle rocks including exhumed sub-continental mantle, infiltrated enriched mantle and oceanic mantle lithosphere (Muntener et al. 2010). Because the Alpine Tethys margins display the same general characteristics like those observed along the Iberia-Newfoundland rifted margins, it seems likely that they also share a common mode of formation.

The Dalradian, exposed in Scotland and in Ireland, was deposited on the future Laurentian margin prior to breakup and the opening of the Iapetus "Ocean". The cumulative thickness of the Dalradian succession totals ~25 km, but is considerably thinner in any one place. The oldest units, the Grampian and Appin Groups are thickest in the northwest, whereas the younger Argyll and Southern Highland Groups are thickest in the southeast, reflecting the migration of the depocentre with time. The duration of Dalradian deposition is poorly constrained, but the recent correlation of the Port Askaig formation (part of the Argyll Group) with the Sturtian glaciation (between 740 and 720 Ma – Prave 1999) and the expansion of the supergroup into the Ordovician (Tanner and Sutherland 2007) implies that depositional duration probably exceeds 300 Myr (Prave 1999), a duration greater than the Paleozoic (Prave 1999). Thus simple interpretations in terms of subsidence during a prolonged

period of rifting would appear unlikely. Instead, this period may include several phases of rifting and postrift/interrift interludes (Glover et al. 1995), or perhaps deposition under quite different tectonic controls: Prave (1999) suggests that deposition was in a foredeep and then on a shelf until rift initiation shortly after the deposition of the Port Askaig formation and the overlying Jura Quartzite (~700 Ma?), an interpretation supported by the identification of a major unconformity at the top of the Jura Quartzite equivalent in Ireland (Hutton and Alsop 2004). This is borne out by the relatively uniform thickness and lack of lateral facies variations in the lower Dalradian in contrast to the Argyll group where rapid changes in both thickness and facies appear to have been fault controlled (Prave 1999). Rifting may have culminated with the deposition of the Tayvallich formation, dated at 595 Ma, with subsequent deposition of the Southern Highland Group being controlled by thermal subsidence. These age constraints imply a duration of rifting corresponding to the deposition of most of the Argyll Group of just over 100 Myr, comparable for instance with the duration of Triassic-Cretaceous rifting west of Iberia and the main phase of rifting in the North Sea.

Voluminous magmatism is largely absent except for the occurrence in one part of the Argyll Group of the Tayvallich volcanics, a sequence up to 3,000 m thick of pillow lavas, airfall tuffs and hyaloclastics intercalated with deep water sedimentary sequences including turbidites (Halliday et al. 1989). The Tayvallich volcanics have been interpreted as being emplaced in a local pull-apart basin during or after continental breakup (Graham 1986), developed at a high angle to the earlier rift structures Thus rifting that created the Argyll group accommodation space may have been polyphase and with time-varying orientations and locations (Soper and England 1995), and largely magma-poor. In several respects the Dalradian may thus have been comparable with the west Iberia margins, where rifting was also polyphase, migrating oceanwards (Reston 2009) and magma poor. The analogy is strengthened by the similarity between the ophicarbonates, serpentinites and limited pillow basalts of the Highland Border Ophiolite (Tanner and Sutherland 2007; Leslie 2008) and the exhumed mantle and sparse basalts found within the continent–ocean transition west of Iberia. Some along strike variation, such as the Tayvallich volcanics and the proposed magmatic segment beneath South Mayo (Ryan 2008) might indicate along strike change from magma-poor to magma-rich, as observed west of Greenland (Chalmers and Pulvertaft 2001). However, a major difference between the Dalradian and the West Iberian margin is the thickness of the sedimentary cover: up to 10 km in the Dalradian whereas only a few km at most west of Iberia. As noted above, this might have led to a somewhat different thermomechanical evolution.

1.5 The Future of Margins: Emplacement or Subduction?

Whitmarsh et al. (1993) pointed out that the presence of serpentinized mantle within the continent–ocean transition might provide the weak zone necessary for the emplacement of Alpine peridotites. They identified the association of peridotite ridges with later small monoclines within the COT, proposing that these monoclines formed by incipient thrusting within the weak COT (see also Péron-Pinvidic et al. 2008). We take this argument further, suggesting that some of the extensional detachments that allow a broad zone of mantle to be unroofed in the COT (Fig. 1.7) may be reactivated during incipient collision as reverse faults and further suggest that such margins may be one site, along with old fracture zones similarly weakened by serpentinization, where subduction may initiate, as proposed for the Pyrenees (Jammes et al. 2009). Whereas subduction initiation at a fracture zone would promote the formation of an intra-oceanic subduction zone and thus an island arc, similar initiation at a serpentine rich rifted margin would lead to Cordilleran style orogenesis, with a magma poor margin trapped in the forearc waiting for eventual obduction when subduction gives way to continental collision. Thus the formation of magma poor serpentine margins may be of fundamental importance in the initiation of both an arc and its eventual collision with a continent. If subduction does initiate at magma poor margins, the preponderance of landward-dipping structures, probably faults or shear zones (Fig. 1.7), means that such margins are likely to end up in the overriding plate, explaining the successful emplacement of the more distal portions of such margins, such as the Briançonnais in the Alps over more proximal parts (Lemoine et al. 1987). The obduction of the distal portion of such margins (the Alpine peridotites) further implies that

failure does not necessarily occur close to the feather edge of the continental crust but further oceanward within the zone of exhumed mantle (see also Péron-Pinvidic et al. 2008).

The process of subduction initiation at a rifted margin leading to eventual incorporation into an orogen has been studied by Jammes et al. (2009) in the western Pyrenees, where inversion has exposed the rift architecture. Here, the eastern continuation of the south Biscay margin has been underthrust by the eastern continuation of the North Iberian margin. During the opening of the Bay of Biscay in the Early Cretaceous, extreme crustal thinning, partly transtensional, ahead of a propagating rift, culminated in the exhumation of mantle and lower crust along extensional detachments in the Aptian-Albian. These detachments were partly reactivated as thrust faults during subsequent shortening, although locally cutting down in the footwall; the landward-dipping extensional detachment at the northern margin becoming the locus of subduction initiation (Fig. 1.8).

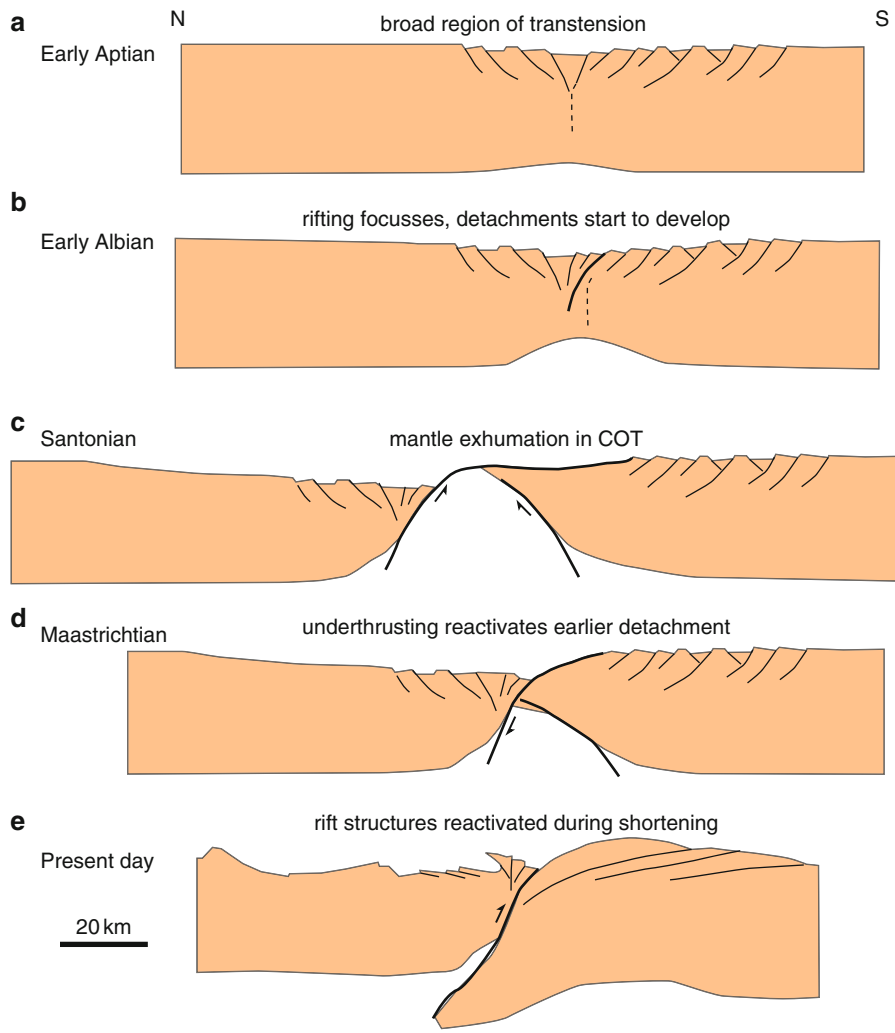

Fig. 1.8 Evolution of the western Pyrennees, simplified after Jammes et al. (2009), showing only major basement structures. Transtension in the Early Cretaceous (**a**) led to rifting and subsidence. As the crust thinned, detachments developed (**b**), which eventually unroofed the mantle within the continent–ocean transition (COT) along landward-dipping shears (**c**). These were reactivated during subsequent oblique convergence (**d**), culminating in the Pyrenneean orogeny (**e**).

1.6 Magma-Rich Margins During Collision

As discussed above, the formation of magma-rich margins may parallel that of magma-poor margins for much of their evolution, with substantive structural differences developing during final breakup. Nevertheless, although magma-poor margins are preserved in orogenic belts (Manatschal et al. 2001, 2006; Manatschal 2004), magma-rich margins are not generally recognised (although Ryan (2008) infers the remains of a volcanic margin at depth beneath the South Mayo Trough), implying that some fundamental property of magma-rich margins prevents their accretion in collisional orogens. The key processes that distinguish magma-rich margins from magma-poor margins are the intrusion of large igneous bodies at the base of and within the thinned crust and the eruption of large volumes of basalt at the surface.

Both these intrusions and the lava flows may affect the rheology and strength of the margin and provide a magmatic transition to the subsequent formation of oceanic lithosphere. Shallow level intrusion of a network of saucer-shaped diabase sills (e.g., Schofield et al. 2010) with or without feeder dikes may strengthen the uppermost crust and sedimentary sequences, as evidence by the undercompaction of sediment trapped within sills off Newfoundland (e.g., Karner and Shillington 2005). At depth, the intrusion of gabbros is similarly likely to increase the strength of the deep crust once the gabbros have cooled to ambient temperature: in the rifted margins preserved in the Alps, early gabbros not related to the rifting form a strong layer at the base of the crust, undergoing boudinage during subsequent extension (e.g., Ivrea lower crustal body). Overall, magma-rich rifted margins are unlikely to be considerably weaker than the unrifted crust and somewhat stronger if rifting occurs after the margin has cooled back to an unstretched geotherm. Thus in contrast to magma-poor margins, subduction is less likely to initiate along former magma-rich margins. Furthermore, the voluminous mafic igneous rocks at magma-rich margins may be converted to eclogite if such margins are partially subducted, allowing further subduction and the destruction of the margin. The parts of a magma-rich margin perhaps most likely to be preserved in orogenic belts may be any rift basins that developed before final magma-rich breakup occurred and which lie inboard of several magma-rich margins as noted above. These such as the Voring and More basins and Rockall Trough, unlike the later margin located outboard of these basins, may be significantly weaker than the original unextended continental crust and thus the focus for deformation during eventual collision. Subduction of the outboard magma-rich margin would leave only a magma-poor rift basin to be emplaced and preserved within the orogen.

Magma rich margins are thus likely to consist of a strong outer margin, resistant to deformation, and in places weaker earlier rift basins. As subduction is less likely to initiate at magma-rich than at magma-poor margins, the former are likely to form the downgoing plate during eventual convergence. As they enter the subduction zone, the collision of such rigid margins with the arc may be partly taken up by shortening in any weaker magma-poor basins, which may eventually be caught up in the orogen, but the mafic crust within the continent–ocean transition is likely to be subducted rather than emplaced in the orogen. The fluid-catalysed conversion of mafic rocks to eclogite is likely to contribute to the successful subduction of such margins to depth as eclogites can be as or even more dense than mantle rocks (Boutelier et al. 2003).

1.7 Conclusions

This paper has focussed on the large-scale structure and symmetry of rifted margins insofar as this is likely to affect their behaviour during eventual arc–continent or continent–continent collision.

The overall structure of magma-poor rifted margins is the logical result of progressive extension:

1. The extreme thinning of the crust (Fig. 1.6) is the result of multiple phases of extensional tectonics: that not all of these are recognised is to be expected. The focussing of extension results in the development of a few major structures responsible for much of the thinning of the crust.
2. The undercrusting of the crust by serpentinized mantle is the logical result of the complete embrittlement of the crust once a stretching factor of about 4 has been reached (Fig. 1.5). The passage of water into the mantle results in a volume increase and a reduction in both the density and

velocity of the uppermost mantle. The spatial onset of serpentinization inferred at magma-poor margins (i.e., the landward limit of serpentinized mantle) occurs where crustal thinning is very close to that where it is predicted that the entire crust became brittle during rifting.

3. The serpentinized mantle beneath the crust is laterally continuous with serpentinized mantle that forms the basement between the last continental crust and the first unambiguous oceanic crust (Figs. 1.3 and 1.7). Mantle unroofing is the logical result of continued extension once the entire crust has become brittle and deformation localizes in the weak mantle serpentinites. The unroofed mantle is weakened both by pervasive serpentinization and perhaps particularly by deeply penetrating mantle serpentinization along landward-dipping shear zones and faults: these may be reactivated during subsequent shortening, both allowing the initiation of subduction along such margins and the eventual obduction of the magma-poor rifted margin.

Magma-rich margins may follow a similar pattern of development with two key differences: the presence of voluminous melt during (and probably initiating) final crustal breakup prevents the unroofing of expanses of mantle rocks within the continent–ocean transition and the subsequent cooling of this melt (to form deep crustal gabbros and networks of sills and dikes at higher levels) increases the rigidity of the crust and its resistance to subsequent deformation. Furthermore, the largely mafic crust near the COT at magma-rich margins can readily convert to eclogite during convergence and collision and thus be lost through subduction.

References

Anderson DL, Zhang Y-S, Tanimoto T (1992) Plume heads, continental lithosphere, flood basalts and tomography. Geol Soc Lond Spec Publ 68:99–124

Anderton R (1982) Dalradian deposition and the late Precambrian–Cambrian history of the N Atlantic region: a review of the early evolution of the Iapetus Ocean. J Geol Soc 139: 421–431

Armitage JJ, Collier JS, Minshull TA (2010) The importance of rift history for volcanic margin formation. Nature 465: 913–917

Beltrando M, Rubatto D, Manatschal G (2010) From passive margins to orogens: the link between ocean-continent transition zones and (ultra)high pressure metamorphism. Geology 38(6):559–562

Bernouilli D (1984) The early history of the Atlantic-Tethyan system. Ann Geophys 2:133–136

Boillot G, Coulon C (1998) La déchirure continentale et l'ouverture océanique. Gordon and Breach Science publishers, Amsterdam, p 208

Boillot G, Winterer E (1988) Editors: ODP Leg 103, Scientific Results

Boillot G, Feraud G, Recq M, Girardeau J (1989) Undercrusting by serpentinite beneath rifted margins. Nature 341: 523–525

Boutelier D, Chemenda A, Burg J-P (2003) Subduction versus accretion of intra-oceanic volcanic arcs: insight from thermo-mechanical analogue experiments. Earth Planet Sci Lett 212:31–45

Bown JW, White RS (1995) Effect of finite extension rate on melt generation at rifted continental margins. J Geophys Res 100:18011–18029

Brun JP, Beslier MO (1995) Mantle exhumation at passive margins. Earth Planet Sci Lett 142:161–173

Bullock AD, Minshull TA (2005) From continental extension to seafloor spreading: crustal structure of the Goban Spur rifted margin, SW of the UK. GJI 163:527–546

Chalmers JA, Pulvertaft TCR (2001) Development of the continental margins of the Labrador Sea: a review. In: Wilson RCL, Whitmarsh RB, Taylor B, Froitzheim N (eds) Non-volcanic rifting of continental margins: a comparison of evidence from land and sea, vol 187. Geological Society of London, Special Publication, London, pp 77–105

Chian D, Louden K, Reid I (1995) Crustal structure of the Labrador Sea conjugate margin and implications for the formation of nonvolcanic continental margins. J Geophys Res 100:24239–24253

Chian D, Louden KE, Minshull TA, Whitmarsh RB (1999) Deep structure of the ocean-continent transition in the southern Iberia abyssal plain from seismic refraction profiles; Ocean Drilling Program (legs 149 and 173) transect. J Geophys Res 104:7443–7462

Cowie PA, Underhill JR, Behn MD, Lin J, Gill CE (2005) Spatio-temporal evolution of strain accumulation derived from multi-scale observations of Late Jurassic rifting in the northern North Sea: a critical test of models for lithospheric extension. Earth Planet Sci Lett 234:401–419

De Charpal O, Guennoc P, Montadert L, Roberts DG (1978) Rifting, crustal attenuation and subsidence in the Bay of Biscay. Nature 275:706–711

Dean SM, Minshull TA, Whitmarsh RB, Louden KE (2001) Deep structure of the ocean-continent transition in the southern Iberia abyssal plain from seismic refraction profiles; the IAM-9 transect at 40 degrees 20′N. J Geophys Res 105:5859–5885

Desmurs L, Muntener O, Manatschal G (2002) Onset of magmatic accretion within a magma-poor passive margin: a case study from the Err-Platta ocean-continent transition, Eastern Switzerland. Contrib Mineral Petrol 144:365–382

Escartin J, Hirth G, Evans B (1997) Effects of serpentinization on the lithospheric strength and the style of normal faulting at slow-spreading ridges. EPSL 151:181–189

Florineth D, Froitzheim N (1994) Transition from continental to oceanic basement in the Tasna Nappe (Engadine Window, Graubunden, Switzerland) – evidence for Early Cretacoues opening of the Valais Ocean. Schweizerische Mineralogische und Petrographische Mitteilungen 74: 437–448

Froitzheim N, Eberli GP (1991) Extensional detachment faulting in the evolution of a Tethys passive continental-margin, Eastern Alsp, Switzerland. Geol Soc Am Bull 102: 1297–1308

Funck T, Hopper JR, Larsen HC, Louden KE, Tucholke BE, Holbrook WS (2003) Crustal structure of the ocean-continent transition at Flemish Cap: seismic refraction results. J Geophys Res 108 (B11), Art No 2531

Funck T, Jackson HR, Louden KE, Dehler SA, WuY (2004) Crustal structure of the northern Nova Scotia rifted continental margin (Eastern Canada). J. Geophys. Res. 109: B09102, doi:10.1029/2004JB003008

Geoffroy L (2005) Volcanic passive margins. C R Geosci 337: 1395–1408

Glover BW, Key RM, May F, Clark GC, Phillips ER, Chacksfield BC (1995) A Neoproterozoic multi-phase rift sequence: the Grampian and Appin groups of the south-western Monadhliath Mountains of Scotland. J Geol Soc 152:391–406

Graham CM (1986) The role of the Cruachan Lineament during Dalradian evolution. Scot J Geol 22:257–270

Halliday AN, Graham CM, Aftalion M, Dymoke P (1989) The depositional age of the Dalradian Supergroup: U-Pb and Sm-Nd isotopic studies of the Tayvallich Volcanics, Scotland. J Geol Soc 146:3–6

Hinz K (1981) A hypothesis on terrestrial catastrophes: wedges of very thick oceanward dipping layers beneath passive margins – their origin and palaeoenvironement significance. Geol Jahrb 22(1981):345–363

Holbrook WS, Purdy GM, Sheridan RS, Glover L, Talwani M, Ewing J, Hutchinson D (1994) Seismic structure of the U.S. Mid-Atlantic continental margin. J Geophys Res 99: 17871–17891

Holbrook WS, Larsen HC, Korenaga J, Dahl-Jensen T, Reid ID, Kelemen PB, Hopper JR, Kent GM, Lizarralde D, Bernstein S, Detrick RS (2001) Mantle thermal structure and active upwelling during continental breakup in the North Atlantic. Earth Planet Sci Lett 190(2001):251–266

Hopper JR, Dahl-Jensen T, Holbrook WS, Larsen HC, Lizarralde D, Korenaga J, Kent GM, Kelemen PB (2003) Structure of the SE Greenland margin from seismic reflection and refraction data: implications for nascent spreading center subsidence and asymmetric crustal accretion during North Atlantic opening. J Geophys Res 108(B5):2269. doi:10.1029/2002JB001996

Hopper JR, Funck T, Tucholke BE, Larsen HC, Holbrook WS, Louden KE, Shillington D, Lau H (2004) Continental breakup and the onset of ultraslow seafloor spreading off Flemish Cap on the Newfoundland rifted margin. Geology 32:93–96

Huismans RS, Beaumont C (2002) Asymmetric lithospheric extension; the role of frictional plastic strain softening inferred from numerical experiments. Geology 30:211–214

Huismans R, Beaumont C (2008) Complex rifted continental margins explained by dynamical models of depth-dependent lithospheric extension. Geology 36:163–166

Hutton DHW, Alsop GI (2004) Evidence for a major Neoproterozoic orogenic unconformity within the Dalradian Supergroup of NW Ireland. J Geol Soc Lond 161:629–640

Jackson JA, White NJ (1989) Normal faulting in the upper continental crust – observations from regions of active extension. J Struct Geol 11(1–2):15–36

Jammes S, Manatschal G, Lavier L, Masini E (2009) Tectono-sedimentary evolution related to extreme crustal thinning ahead of a propagating ocean: example of the western Pyrenees. Tectonics 28:TC4012

Karner GD, Shillington DJ (2005) Basalt sills of the U reflector, Newfoundland Basin: a serendipitous dating technique. Geology 33:985–988

Keen C, Peddy C, de Voogd B, Matthews D (1989) Conjugate margins of Canada and Europe; results from deep reflection profiling. Geology 17:173–176

Krawczyk CM (1995) Detachment tectonics during continental rifting off the west Iberia margin: seismic reflection and drilling constraints. Dissertation, University of Kiel, p 127

Krawczyk CM, Reston TJ, Beslier MO, Boillot G (1996) Evidence for detachment tectonics on the Iberia Abyssal Plain margin. In: Whitmarsh R, Sawyer D, Klaus A (eds) Proc ODP, Scientific Results 149, Ocean Drilling Program, College Station, TX, pp 603–615

Kusznir N, Karner G (2007) Continental lithospheric thinning and breakup in response to upwelling divergent mantle flow: application to the Woodlark, Newfoundland and Iberia margins. Geol. Soc. London, Spec. Publ. 282:389–419

Kusznir N, Park RG (1987) The extensional strength of continental lithosphere: its dependence on geothermal gradient, and crustal composition and thickness. In: Coward MP, Dewey JF, Hancock PL (eds) Continental extensional tectonics, vol 28. Geological Society of London, Special Publication, London, pp 35–52

Lau KWH, Louden KE, Funck T, Tucholke BE, Holbrook WS, Hopper JR, Larsen HC (2006) Crustal structure across the Grand Banks–Newfoundland Basin continental margin (part I) – results from a seismic refraction profile. Geophys J Int 167:127–156

Lavier LL, Manatschal G (2006) A mechanism to thin the continental lithosphere at magma-poor margins. Nature 440: 324–328

Lemoine M, Tricart P, Boillot G (1987) Ultramafic and gabbroic ocean-floor of the Ligurian Tethys (Alps, Corsica, Appenines)- in search of a genetic model. Geology 15:622–625

Leslie G (2008) Are remnants of an ocean-continent-transition zone preserved at the Highland Border in Scotland? Geoscientist

Leythaeuser T, Reston TJ, Minshull TA (2005) Waveform inversion of the S reflector west of Spain; fine structure of a detachment fault. Geophys Res Lett 32:L22304. doi: 10.1029/2005GL024026

Maillard A, Malod J, Thiebot E, Klingelhoefer F, Rehault JP (2006) Imaging a lithospheric detachment at the continent-ocean transition off Morocco. Earth Planet. Sci. Lett. 241: 686-698

Manatschal G (2004) New models for evolution of magma-poor rifted margin based on a review of data and concepts from West Iberia and the Alps. Int J Earth Sci 93:432–466

Manatschal G, Muntener O (2009) A type sequence across an ancient magma-poor ocean-continent transition: the example of the western Alpine Tethys ophiolites. Tectonophysics 473: 4–19

Manatschal G, Nievergelt P (1997) A continent-ocean transition recorded in the Err and Platta nappes (eastern Switzerland). Eclogae Geol Helv 90:3–27

Manatschal G, Froitzheim N, Rubenach M, Turrin BD (2001) The role of detachment faulting in the formation of an ocean-continent transition: insights from the Iberia Abyssal Plain. In: Wilson RCL, Whitmarsh RB, Taylor B, Froitzheim N (eds) Non-volcanic rifting of continental margins: a comparison of evidence from land and sea, vol 187. Geological Society of London, Special Publication, London, pp 405–428

Manatschal G, Engstrom A, Desmurs L, Schaltegger U, Cosca M, Muntener O, Bernoulli D (2006) What is the tectono-metamorphic evolution of continental break-up: the example of the Tasna ocean-continent transition. J Struct Geol 28:1849–1869

Mauffret A, Montadert L (1987) Rift tectonics on the passive continental margin off Galicia (Spain), Mar. Pet. Geol. 40: 49–70

McKenzie DP (1978) Some remarks on the development of sedimentary basins. Earth Planet Sci Lett 40:25–32

Minshull TA, Dean SM, White RS, Whitmarsh RB (2001) Anomalous melt production after continental break-up in the southern Iberia Abyssal Plain. In: Wilson RCL et al (eds) Non-volcanic rifting of continental margins: a comparison of evidence from land and sea, vol 187. Geological Society of London, Special Publication, London, pp 537–550

Mjelde R, Raum T, Myhren B, Shimamura H, Murai Y, Takanami T, Karpuz R, Næss U (2005) Continent–ocean transition on the Vøring Plateau, NE Atlantic, derived from densely sampled ocean bottom seismometer data. J Geophys Res 110(B05101):1–19

Mjelde R, Raum T, Breivik AJ, Faleide JI (2008) Crustal transect across the North Atlantic. Mar Geophys Res 29:73–87

Mohn G, Manatschal G, Muntener O, Beltrando M, Masini E (2010) Unravelling the interaction between tectonic and sedimentary processes during lithospheric thinning in the Alpine Tethys margins. Int J Earth Sci 99(Suppl 1):S75–S101

Muntener O, Manatschal G, Desmurs L (2010) Plagioclase Peridotites in Ocean-Continent Transitions: Refertilized Mantle Domains Generated by Melt Stagnation in the Shallow Mantle Lithosphere, J. Petrology, 51:153–183

Muntener O, Manatschal G (2006) High degrees of melting recorded by spinel harzburgites of the Newfoundland margin: the role of inheritance and consequences for the evolution of the southern North Atlantic. Earth Planet Sci Lett 252:437–452

Mutter JM, Buck WR, Zehnder CM (1988) Convective partial melting 1: a model for the formation of thick basalt sequences during the initiation of spreading. J Geophys Res 93:1031–1048

Nicholls IA, Ferguson J, Jones H, Marks GP, Mutter JC (1981) Ultramafic blocks from the ocean-floor southwest of Australia. Earth Planet Sci Lett 56:362–374

Nielsen TK, Hopper JR (2002) Formation of volcanic rifted margins: are temperature anomalies required? Geophys Res Lett 29(21):2022. doi:10.1029/2002GL015681

Osmundsen PT, Ebbing J (2008) Styles of extension offshore mid-Norway and implications for mechanisms of crustal thinning at passive margins. Tectonics 27:TC6016

Pérez-Gussinyé M, Reston TJ (2001) Rheological evolution during extension at passive non-volcanic margins: onset of serpentinization and development of detachments to continental break-up. J Geophys Res 106:3691–3975

Perez-Gussinye M, Reston TJ, Phipps Morgan J (2001) Rheological and magmatic evolution during extension at passive non-volcanic margins: the effect of initial lithospheric structure. Geol Soc Lond Spec Publ 187:551–576

Pérez-Gussinyé M, Phipps Morgan J, Reston TJ, Ranero CR (2006) The rift to drift transition at non-volcanic margins: insights from numerical modelling. EPSL 244:458–473

Peron-Pinvidic G, Manatschal G (2009) The final rifting evolution at deep magma-poor passive margins from Iberia-Newfoundland: a new point of view. Int J Earth Sci 98:1581–1597

Peron-Pinvidic G, Manatschal G, Minshull TA, Sawyer DS (2007) Tectonosedimentary evolution of the deep Iberia-Newfoundland margins: evidence for a complex breakup history. Tectonics 26:TC2011. doi:10.1029/2006TC001970

Pickup S, Whitmarsh RB, Fowler CMR, Reston TJ (1996) Insight into the nature of the ocean-continent transition off West Iberia from a deep multichannel seismic reflection profile. Geology 24:1079–1082

Prave AR (1999) The Neoproterozoic Dalradian Supergroup of Scotland: an alternative hypothesis. Geol Mag 136(6): 609–617

Proffett JM (1977) Cenozoic geology of the Yerington district, Nevada, and implications for the nature of Basin and Range faulting. Bull Geol Soc Am 88:247–266

Reid ID (1994). Crustal structure of a nonvolcanic rifted margin east of Newfoundland. J. Geophys. Res. 99:15,161–15,180

Reston TJ (1988) Evidence for shear zones in the lower crust offshore Britain. Tectonics 7:929–945

Reston TJ (1993) Evidence for extensional shear zones in the mantle offshore Britain, and their implications for the extension of the continental lithosphere. Tectonics 12: 492–506

Reston TJ (1996) The S reflector west of Galicia: the seismic signature of a detachment fault. Geophys J Int 127:230–244

Reston TJ (2005) Polyphase faulting during the development of the west Galicia rifted margin. Earth Planet Sci Lett 237: 561–576

Reston TJ (2009) The structure, evolution and symmetry of the magma-poor rifted margins of the North and Central Atlantic: a synthesis. Tectonophysics 468:6–27

Reston TJ, Phipps Morgan J (2004) The continental geotherm and the evolution of rifted margins. Geology 32:133–136

Reston TJ, Pérez Gussinyé M (2007) Lithospheric extension from rifting to continental breakup at magma-poor margins: rheology, serpentinisation and symmetry. Int. J. Earth Sci. DOI 10.1007/s00531-006-0161-z

Reston TJ, Krawczyk CM, Klaeschen D (1996) The S reflector west of Galicia: evidence from prestack depth migration for detachment faulting during continental breakup. J Geophys Res 101:8075–8091

Reston TJ, Pennell J, Stubenrauch A, Walker I, Pérez-Gussinyé M (2001) Detachment faulting, mantle serpentinization and serpentinite mud volcanism beneath the Porcupine Basin SW Ireland. Geology 29:587–590

Ryan PD (2008) Preservation of forearc basins during island arc-continent collision: some insights from the Ordovician of western Ireland. Geol Soc Am Spec Pap 436:1–9

Sage F, Basile C, Mascle J, Pontoise B, Whitmarsh RB (2000) Crustal structure of the continent-ocean transition off the Cote d'Ivoire-Ghana transform margin: implications for thermal exchanges across the palaeotransform boundary. Geophys J Int 143:662–678

Sandiford M, Paul E, Flottmann T (1998) Sedimentary thickness variations and deformation intensity during basin inversion in the Flinders Ranges, South Australia. J Struct Geol 20(12): 1721–1731

Schofield N, Stevenson C, Reston T (2010) Magma fingers and host rock fluidization in the emplacement of sills. Geology 38(1):63–66. doi:10.1130/G30142.1

Soper NJ, England RW (1995) Vendian and Riphean rifting in NW Scotland. J Geol Soc Lond 152:11–14

Tanner PWG, Sutherland S (2007) The Highland Border Complex, Scotland: a paradox resolved. J Geol Soc 164: 111–116

Thinon I, Matias L, Rehault JP, Hirn A, Fidalgo-Gonzalez L, Avedik F (2003) Deep structure of the Armorican Basin (Bay of Biscay): a review of Norgasis seismic reflection and refraction data. J Geol Soc Lond 160:99–116

Tucholke BE, Sawyer DS, Sibuet J-C (2007) Breakup of the Newfoundland-Iberia Rift. Geol Soc Lond Spec Publ 282: 9–46

Van Avendonk HJA, Holbrook WS, Nunes GT, Shillington DJ, Tucholke BE, Louden KE, Larsen HC, Hopper JR (2006) Seismic velocity structure of the rifted margin of the eastern Grand Banks of Newfoundland, Canada. J Geophys Res 111: B11404. doi:10.1029/2005JB004156

Voss M, Jokat W (2007) Continent-ocean transition and voluminous magmatic underplating derived from P-wave velocity modelling of the East Greenland continental margin. Geophys J Int 170:58–604

Weigel W, Flueh ER, Miller H, Butzke A, Dehghani GA, Gebhardt V, Harder I, Hepper J, Jokat W, Klaeschen D, Kreymann S, Schueßler S, Zhao Z (1995) Investigations of the East Greenland continental margin between 70° and 72°N by deep seismic sounding and gravity studies. Mar Geophys Res 17:167–199

White N (1990) Does the uniform stretching model work in the North Sea? In: Blundell DJ, Gibbs AD (eds) Tectonic evolution of the North Sea rifts, vol 181. Oxford Science Publications (International Lithosphere Program), pp 217–239

White R, McKenzie D (1989) Magmatism at rift zones: the generation of volcanic continental margins and flood basalts. J Geophys Res 94:7685–7729

White RS, Smith LK (2009) Crustal structure of the Hatton and the conjugate east Greenland rifted volcanic continental margins, NE Atlantic. J Geophys Res 114:B02305. doi:10.1029/2008JB005856

White RS, Spence GD, Fowler SR, McKenzie DP, Westbrook GK, Bowen AN (1987) Magmatism at rifted continental margins. Nature 330:439–444

Whitmarsh RB, Pinheiro LM, Miles PR, Sibuet JC (1993) Thin crust at the western Iberia ocean-continent transition and ophiolites. Tectonics 12:1230–1239

Whitmarsh RB, Manatschal G, Minshull TA (2001) Evolution of magma-poor continental margins from rifting to seafloor spreading. Nature 413:150–154

Wilson RCL, Manatschal G, Wise S (2001) Rifting along non-volcanic passive margins: stratigraphic and seismic evidence from the Mesozoic of the Alps and Western Iberia, Geol. Soc. London Spec. Publ. 187:429–452

Wu Y, Louden KE, Funck T, Jackson HR, Dehler SA (2006) Crustal structure of the central Nova Scotia margin off Eastern Canada. Geophys. J. Int. 166:878–906

Zelt CA, Sain K, Naumenko JV, Sawyer DS (2003) Assessment of crustal velocity models using seismic refraction and reflection tomography. Geophys J Int 153:609–626

Chapter 2
Intra-oceanic Subduction Zones

T.V. Gerya

2.1 Introduction

According to the common definition, intra-oceanic subduction brings oceanic slabs under the overriding plates of oceanic origin. As a consequence oceanic magmatic arcs are formed worldwide (Fig. 2.1) with typical examples such as the Izu-Bonin-Mariana arc, the Tonga-Kermadec arc, the Vanuatu arc, the Solomon arc, the New Britain arc, the western part of the Aleutian arc, the South Sandwich arc and the Lesser Antilles arc (Leat and Larter 2003). Intra-oceanic subduction zones comprise around 17,000 km, or nearly 40%, of the subduction margins of the Earth (Leat and Larter 2003). Indeed, intra-oceanic arcs are less well studied than continental arcs since their major parts are often located below sea level, sometimes with only the tops of the largest volcanoes forming islands. Intra-oceanic subduction zones are sites of intense magmatic and seismic activities as well as metamorphic and tectonic processes shaping out arc compositions and structures. During an ocean closure (e.g., Collins 2003) such arcs may collide with continental margins creating distinct structural and compositional record in continental orogens (such as in Himalaya, Burg 2011) which makes them of particular interest for the present book.

Several years ago Leat and Larter (2003) published a comprehensive review on intra-oceanic subduction systems. The review focused on tectonic and magmatic processes in intra-oceanic arcs and was mainly based on observational constraints. In addition, Schellart et al. (2007) compiled detailed nomenclature and taxonomy of Subduction zones worldwide. The following major characteristics of intra-oceanic subduction zones can be summarized (Leat and Larter 2003; Schellart et al. 2007 and references therein)

- *Convergence rates* vary from ca 2 cm/yr in the Lesser Antilles arc to 24 cm/yr in the northern part of the Tonga arc, the highest subduction rates on Earth. Typical rates are in the range 5–13 cm/yr. Intra-arc variations are almost as large as inter-arc ones.
- *Ages of subducting slabs* range from ca 150 Ma (Pacific Plate subducting beneath the Mariana arc) to close to zero age (along part of the Solomon arc). Along-arc variations in slab ages are typically not large ($\pm$10 Ma). There are indeed large variations in the topography of the subducting plates (up to 5 km, Fig. 2.1): some are relatively smooth, some contain ridges and seamounts that affect subduction and arc tectonics.
- *Sediment thicknesses* are notably variable (from 70 m to >6 km, typically 150–650 m). Sediment cover is commonly thinner over basement highs. Variations in thickness and composition of subducted sediments are probably greatest where arcs are close to, or cut across, ocean–continent boundaries.
- *Accretion v. non-accretion*. Most modern intra-oceanic arcs are non-accreting, i.e. there is little or no net accumulation of off-scrapped sediment forming accretionary complexes. In other words, all the sediments arriving at the trenches are subducted (over a period) into the mantle. The two exceptions are the Lesser Antilles and Aleutian arcs, both of which have relatively high sediment inputs and where accretionary complexes have formed.

T.V. Gerya
Geophysical Fluid Dynamics Group, Department of Earth Sciences, Institute of Geophysics, Swiss Federal Institute of Technology (ETH-Zurich), Sonneggstrasse, 5, 8092 Zurich, Switzerland
e-mail: taras.gerya@erdw.ethz.ch

D. Brown and P.D. Ryan (eds.), *Arc-Continent Collision*, Frontiers in Earth Sciences,
DOI 10.1007/978-3-540-88558-0_2, © Springer-Verlag Berlin Heidelberg 2011

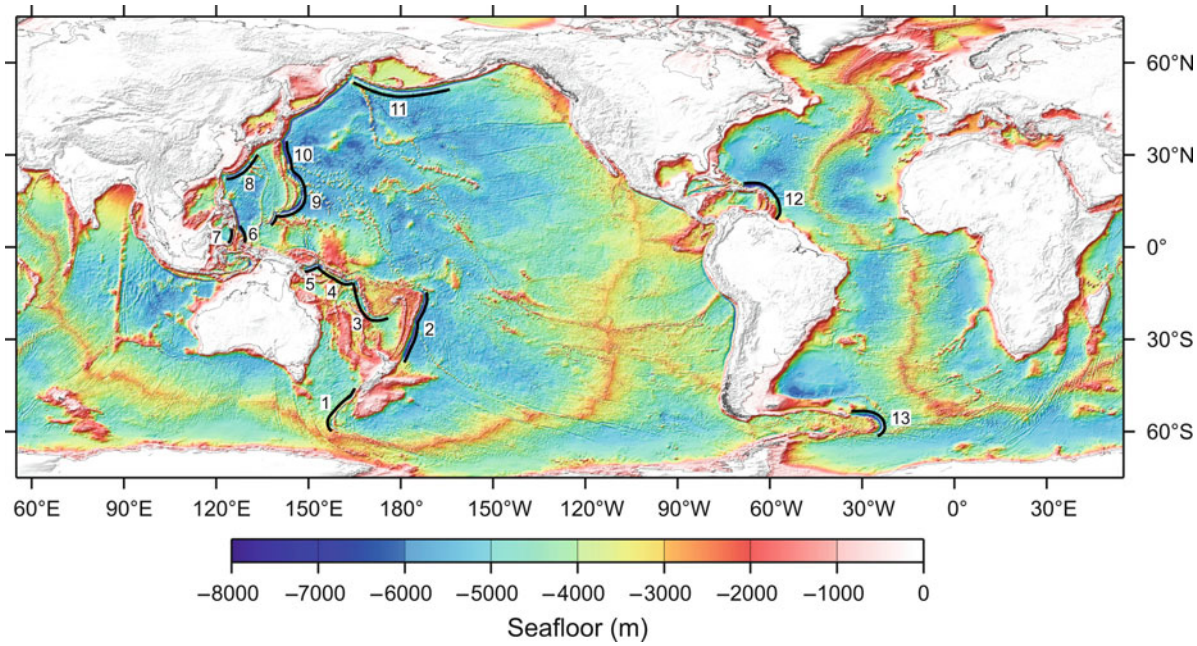

Fig. 2.1 Location of modern intra-oceanic subduction zones. The trenches of these subduction systems are indicated by heavy black lines, and identified by numbers that correspond to those of Leat and Larter (2003): 1 – MacQuarie; 2 – Tonga-Kermadec; 3 – Vanuatu (New Hebrides); 4 – Solomon; 5 – New Britain; 6 – Halmahara; 7 – Sangihe; 8 – Ryuku; 9 – Mariana; 10 – Izu-Bonin (Ogasawara); 11 – Aleutian; 12 – Lesser Antilles; 13 – South Sandwich.

- *Back-arc extension*. Most of the arcs have closely associated back-arc rifts. Only the Solomon and Aleutian arcs are exceptions in having no apparent back-arc extension. In most cases, the back-arc extension takes the form of well-organized seafloor spreading for at least part of the length of the back-arc. Such spreading appears to follow arc extension and rifting in at least some cases.
- *Arc thicknesses* depend on arc maturity, tectonic extension or shortening, and the thickness of pre-arc basement. Only approximately, therefore, is it true to say that the thin crusts (e.g. of the South Sandwich and Izu-Osgaswara) arcs represent arcs in the relatively early stages of development, whereas arcs with thicker crusts are more mature (e.g. the Lesser Antilles and Aleutian arcs).
- *Pre-arc basements* of the arcs are very variable. Only one intra-oceanic arc (the Aleutian arc) is built on normal ocean crust. The others are built on basements comprising a range of oceanic lithologies, including ocean crust formed at back-arc spreading centres, earlier intra-oceanic arcs, accretionary complexes and oceanic plateaux. This also points out toward complexity of intraoceanic subduction (re)initiation scenarios.

In the recent years significant new literature on intra-oceanic subduction appeared (in particular, on high-resolution seismic studies of arc structures and on numerical modeling of intra-oceanic subduction) that should be added to the state-of-the-art knowledge which is one of the reasons for writing this chapter. Also, taking into account that the present volume mainly concentrates on arc collision processes I will focus the review on relatively shallow portions of intraoceanic subduction-arc system from which the record can be preserved in the resulting collision zones (e.g. Burg 2011). The following major issues will be discussed in the review

- Initiation of intra-oceanic subduction
- Internal structure and composition of arcs
- Subduction channel processes
- Dynamics of crustal growth
- Geochemistry of intra-oceanic arcs

In order to keep a cross-disciplinary spirit of modern intra-oceanic subduction studies often combining

observational constrains with results of numerical geodynamic modelling the later will be used here for visualizing various subduction-related processes instead of more traditional hand-drawn cartoons.

2.2 Initiation of Intra-oceanic Subduction

It is yet not entirely clear how subduction in general and intraoceanic subduction in particular is initiated. The gravitational instability of an old oceanic plate is believed to be the main reason for subduction (Vlaar and Wortel 1976; Davies 1999). Oceanic lithosphere becomes denser than the underlying asthenosphere within 10–50 Ma after it forms in a mid-ocean ridge due to the cooling from the surface (Oxburg and Parmentier 1977; Cloos 1993; Afonso et al. 2007, 2008). However, despite the favourable gravitational instability and ridge-push, the bending and shear resistance of the lithosphere prevent subduction from arising spontaneously (McKenzie 1977). Consequently, the following question arises: what forces can trigger subduction (besides the negative buoyancy and ridge-push)? At least 12 hypotheses have been proposed to answer this question:

1. Plate rupture within an oceanic plate or at a passive margin (e.g. McKenzie 1977; Dickinson and Seely 1979; Mitchell 1984; Müeller and Phillips 1991).
2. Reversal of the polarity of an existing subduction zone (e.g. Mitchell 1984).
3. Change of transform faults into trenches (e.g. Uyeda and Ben-Avraham 1972; Hilde et al. 1976; Karson and Dewey 1978; Casey and Dewey 1984).
4. Sediment or other topographic loading at continental/arc margins (e.g. Dewey 1969; Fyfe and Leonardos 1977; Karig 1982; Cloetingh et al. 1982; Erickson 1993; Pascal and Cloetingh 2009).
5. Forced convergence at oceanic fracture zones (e.g. Müeller and Phillips 1991; Toth and Gurnis 1998; Doin and Henry 2001; Hall et al. 2003; Gurnis et al. 2004).
6. Spontaneous initiation of retreating subduction (Fig. 2.2) due to a lateral thermal buoyancy contrast at oceanic fracture zones separating oceanic plates of contrasting ages (e.g. Gerya et al. 2008; Nikolaeva et al. 2008; Zhu et al. 2009).
7. Tensile decoupling of the continental and oceanic lithosphere due to rifting (Kemp and Stevenson 1996).
8. Rayleigh-Taylor instability due to a lateral compositional buoyancy contrast within the lithosphere (Niu et al. 2003).
9. Addition of water into the lithosphere (Regenauer-Lieb et al. 2001; Van der Lee et al. 2008).
10. Spontaneous thrusting (Fig. 2.3) of the buoyant continental/arc crust over the oceanic plate (Mart et al. 2005; Nikolaeva et al. 2010; Goren et al. 2008).
11. Small-scale convection in the sub-lithospheric mantle (Solomatov 2004).
12. Interaction of thermal-chemical plumes with the lithosphere (Ueda et al. 2008).

In the recent review by Stern (2004 and references therein) two major types of subduction initiation scenarios applicable to intraoceanic subduction are proposed based on both theoretical considerations and natural data: induced and spontaneous. Induced subduction nucleation may follow continuation of plate convergence after jamming of a previously active subduction zone (e.g. due to arrival of a buoyant crust to the trench). This produces regional compression, uplift and underthrusting that may yield a new subduction zone in a different place. Two subtypes of induced initiation, transference and polarity reversal, are distinguished (Stern 2004 and references therein). Transference initiation moves the new subduction zone outboard of the failed one. The Mussau Trench and the continuing development of a plate boundary SW of India in response to Indo–Asian collision are the best Cenozoic examples of transference initiation processes (Stern 2004 and references therein). Polarity reversal initiation also follows collision, but continued convergence in this case results in a new subduction zone forming behind the magmatic arc; the response of the Solomon convergent margin following collision with the Ontong Java Plateau (Stern 2004 and references therein) and dramatic reorganization of the tectonic plate boundary in the New Hebrides region (Pysklywec et al. 2003 and references therein) are suggested to be the examples of this mode.

Spontaneous nucleation results from inherent gravitational instability of sufficiently old oceanic lithosphere

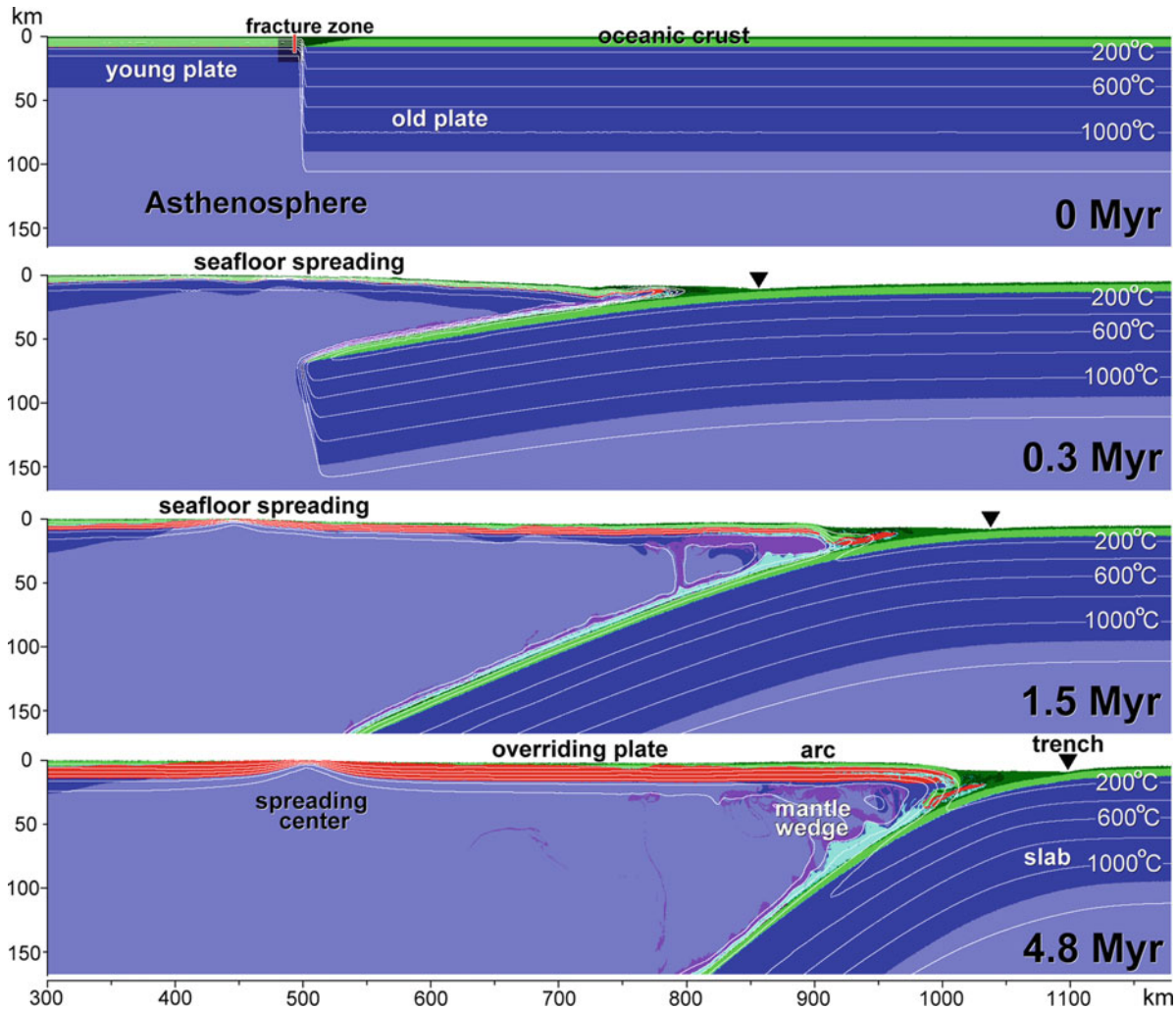

Fig. 2.2 Dynamics of spontaneous initiation of retreating subduction at a transform/fracture zone separating oceanic plates of contrasting ages. Results from 2D numerical experiments by Gerya et al. (2008).

compared to the underlying mantle, which is also the main reason for operating of the modern regime of plate tectonics. It is widely accepted (e.g. Stern 2004 and references therein) that intra-oceanic subduction can initiate spontaneously either at a transform/fracture zone (Fig. 2.2) or at a passive continental/arc margin (Fig. 2.3), in a fashion similar to lithospheric delamination. According to the theoretical prediction (e.g. Stern 2004) and numerical modeling results (e.g. Gerya et al. 2008; Nikolaeva et al. 2008; Zhu et al. 2009) spontaneous initiation across a fracture zone separating oceanic plates of contrasting ages associates with an intense seafloor spreading (Fig. 2.2, 0.3–1.5 Myr), as asthenosphere wells up to replace sunken lithosphere of the older plate. This is the presumable origin of most boninites and ophiolites (Stern 2004 and references therein). Such initiation process assumed to have produced new subduction zones along the western edge of the Pacific plate during the Eocene (Stern 2004 and references therein). Development of self-sustaining one-sided subduction is marked by the beginning of down-dip slab motion, formation of the mantle wedge and appearance of the magmatic arc at 100–200 km distance from the retreating trench (Fig. 2.2).

Passive continental/arc margin collapse (Fig. 2.3) is driven by the geometry of the margin, where relatively thick (20–35 km) low-density continental/arc crust is

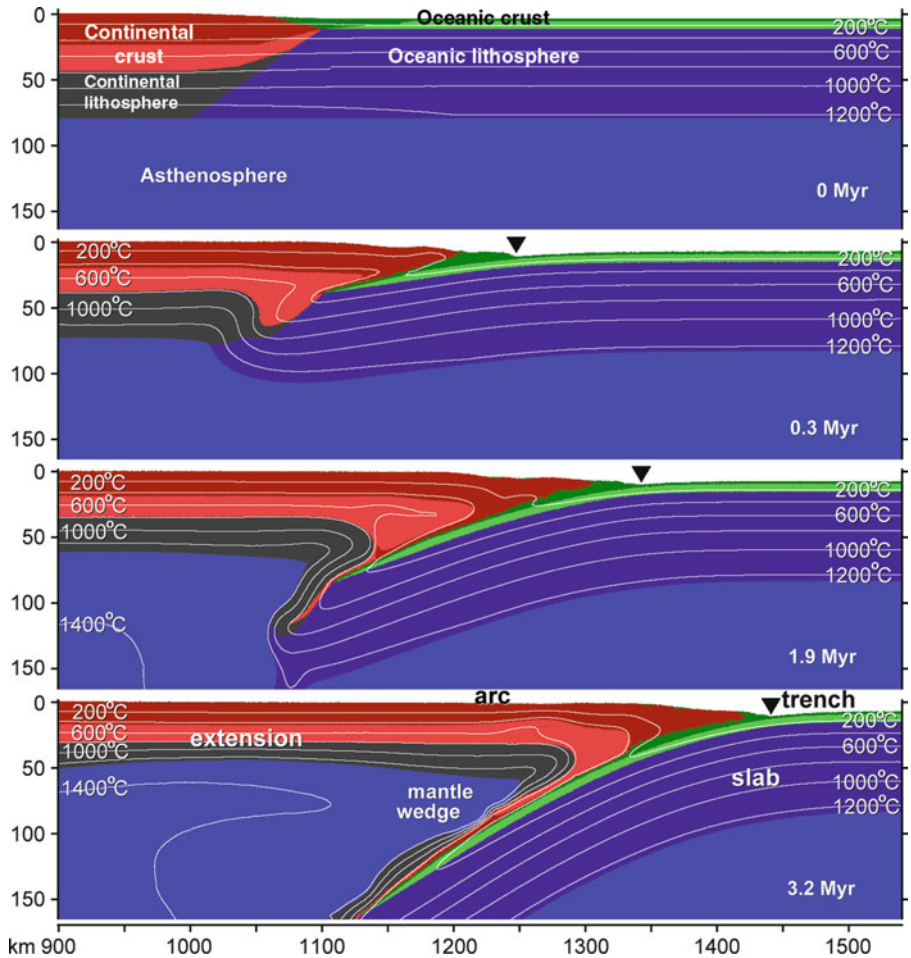

Fig. 2.3 Dynamics of spontaneous subduction initiation at a passive continental/arc margin. Results from 2D numerical experiments by Nikolaeva et al. (2010).

bounded laterally by significantly more dense oceanic lithosphere. When during the margin evolution forces generated from this lateral density contrast become big enough to overcome the continental/arc crust strength then this crust starts to creep over the oceanic one (Fig. 2.3, 0.3 Myr). This causes deflection of the oceanic lithosphere (Fig. 2.3, 0.3 Myr) and may actually lead to its delamination from the continental/arc lithosphere (Fig. 2.3, 0.3–1.9 Myr) thus triggering retreating subduction process (Fig. 2.3, 1.9–3.2 Myr). This type of subduction nucleation has been successfully modelled with both analogue (Mart et al. 2005; Goren et al. 2008) and numerical (Nikolaeva et al. 2010) techniques. No undeniable modern example of such ongoing subduction initiation is yet known: a possible recent exception is suggestion for subduction/overthrusting initiation at the eastern Brasilian margin (Marques et al. 2008). Indeed, Goren et al. (2008) speculated that such type of initiation was relevant in the past for two active intra-oceanic subduction systems in which Atlantic lithosphere is being subducted: the Lesser-Antilles and the South Sandwich subduction systems. Also, Masson et al. (1994) and Alvarez-Marron et al. (1996, 1997) argued that an arrested subduction zone nucleation can be distinguished in the North Iberian Margin based on structural and seismic data.

Both spontaneous and induced subduction initiation can be potentially distinguished by the record left on the upper plates: induced nucleation begins with strong compression and uplift, whereas spontaneous one begins with rifting and seafloor spreading (Stern 2004).

2.3 Internal Structure of Intra-oceanic Arcs

Internal structure and compositions of intra-oceanic arcs are strongly variable depending on both the pre-existing plate structure and on the dynamics of subduction and associated crustal growth (e.g. Leat and Larter 2003). In addition, deep parts of the arcs are mainly reconstructed based on seismic data and fragmentary records left in orogens after arc-continent collisions, which creates further uncertainties for interpretations of intra-oceanic arc structures. As was indicated by Tatsumi and Stern (2006) understanding how continental crust forms at intra-oceanic arcs requires knowledge of how intra-oceanic arcs form and mature with key questions being:

1. What is the nature of the crust and mantle in the region prior to the beginning of subduction?
2. How does subduction initiate and initial arc crust form?
3. How do the middle and lower arc crusts evolve?
4. What are the spatial changes of arc magma and crust compositions of the entire arc?

In this respect, in addition to robust natural data, realistic self-consistent numerical modelling of subduction and associated crustal growth (e.g., Nikolaeva et al. 2008; Kimura et al. 2009; Sizova et al. 2009; Gerya and Meilick 2011) can complement the interpretations of details and variability in arc structures. Figure 2.4 shows a schematic cross-section across a mature intra-oceanic arc corresponding to the retreating subduction regime. The cross-section is based on recent results of numerical petrological-thermomechanical modelling (Gerya and Meilick 2011). The following major structural components of the arc can be distinguished based on this scheme and natural data: (a) accretion prism (if present), (b) pre-arc basement (c) serpentinized fore-arc including subduction channel composed of tectonic melange, (d) magmatic crust, (e) sub-arc lithosphere (cumulates?, replacive rocks?, intercalation of crustal and mantle rocks and melts?), (f) back-arc region with new oceanic floor and a spreading center and (g) paleo-arc (in the rear part

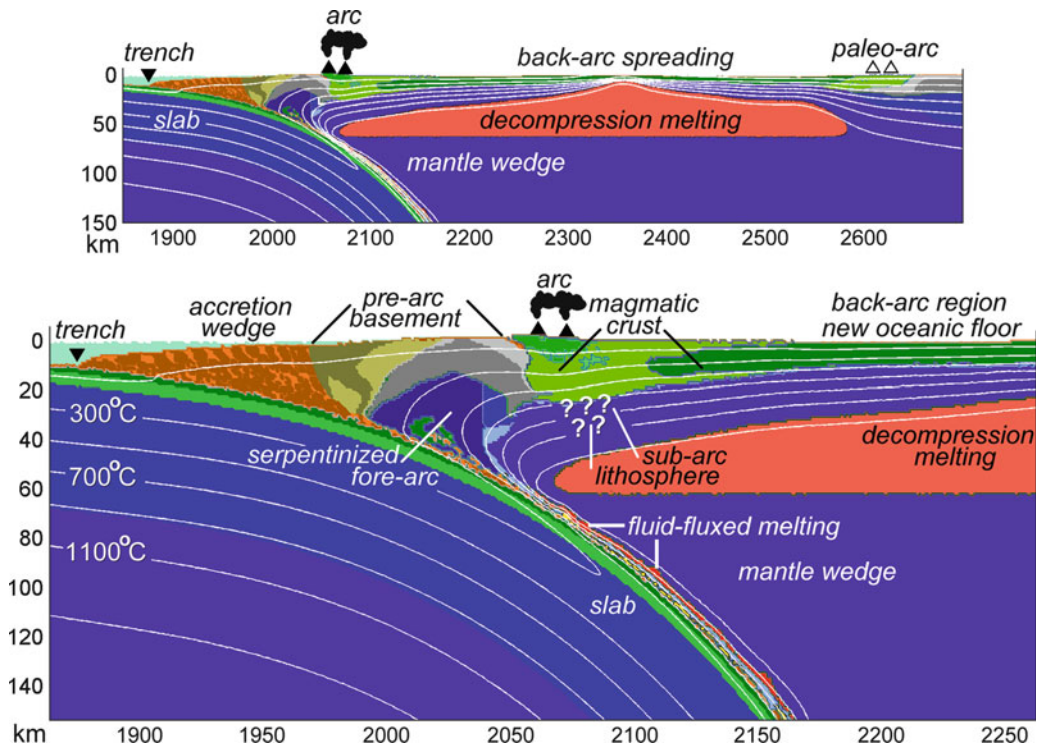

Fig. 2.4 Schematic cross-section of an intra-oceanic arc associated with retreating subduction. Results from 2D numerical experiments by Gerya and Meilick (2011).

of the back-arc spreading domain). Obviously this structure is non-unique and significant variations can be expected in both nature (e.g. Tatsumi and Stern 2006; Takahashi et al. 2007, 2009; Kodaira et al. 2006, 2007, 2008) and models (e.g. Nikolaeva et al. 2008; Sizova et al. 2009; Gerya and Meilick 2011), depending on arc history, subduction dynamics and sub-arc variations in melt production intensity, distribution and evolution (e.g. Tamura 1994; Tamura et al. 2002; Honda et al. 2007; Zhu et al. 2009).

Recently new high-resolution data (see Calvert 2011) were obtained concerning seismic structure of the arc crust in Izu-Bonin-Mariana system (e.g. Takahashi et al. 2007, 2009; Kodaira et al. 2006, 2007, 2008). These data suggest that lateral variations in crustal thickness, structure and composition occur both along and across intra-oceanic arcs (e.g. Figs. 4.1–4.7 in Calvert 2011; Kodaira et al. 2006; Takahashi et al. 2009). Such variations are interpreted as being the results of laterally and temporally variable magmatic addition and multiple episodes of fore-arc, intra-arc and back-arc extension (e.g. Takahashi et al. 2007, 2009; Kodaira et al. 2006, 2007, 2008). Seismic models demonstrate notable velocity variations (Fig. 4.1 in Calvert 2011) within the arc middle and lower crusts, which are interpreted to be respectively of intermediate to felsic and mafic compositions (e.g. Takahashi et al. 2007). In the regions of the maximal thickness (around 20 km, Fig. 4.1 in Calvert 2011) the oceanic-island-arc crust is composed of a volcanic-sedimentary upper crust with velocity of less than 6 km/s, a middle crust with velocity of ~6 km/s, laterally heterogeneous lower crust with velocities of ~7 km/s, and unusually low mantle velocities (Takahashi et al. 2009; also see crust–mantle transition layer in Fig. 4.1a, b in Calvert 2011). Petrologic modeling of Takahashi et al. (2007) suggests that the volume of the lower crust, presumably composed of restites and olivine cumulates remained after the extraction of the middle crust, should be significantly larger than is observed on the seismic cross-sections. Therefore, such mafic-ultramafic part of the lower crust (if at all present in the arcs, e.g. Jagoutz et al. 2006) should have seismic properties similar to the mantle ones and consequently look seismically as a part of the mantle lithosphere.

There are notable uncertainties in interpreting seismic structures of intra-oceanic arcs, which are related to current uncertainties in understanding melt differentiation processes under the arcs. As summarised by Leat and Larter (2003) the major element composition of magmas feeding arcs from the mantle has been and remain (e.g. Jagoutz et al. 2006) a subject of debate, particularly regarding the Mg and A1 contents of primary magmas. Mafic compositions in arcs have variable MgO content, but with a clear cut-off at about 8 wt% MgO or even less (in the case of mature arcs). High-MgO, primitive non-cumulate magmas have indeed been identified in many arcs, but they are always volumetrically very minor (Davidson 1996). One question is, therefore, whether the MgO cut-off point represents composition of the mantle-derived parental magmas, or whether the mantle-derived parental magmas are significantly more MgO-rich (>10% MgO), but are normally unable to reach the surface and erupt. It has been argued that they have difficulty in traversing the crust without encountering magma chambers because of their relatively high density (Smith et al. 1997; Leat et al. 2002). In addition, as argued by Pichavant and Macdonald (2003) only the most water-poor primitive magmas are able to traverse the crust without adiabatically freezing.

It should, however, be mentioned that the above explanations are not fully satisfactory in explaining the "MgO-paradox". First, as has recently been demonstrated numerically (Gerya and Burg 2007; Burg et al. 2009) local density contrast between rising dense magmas and surrounding crustal rocks plays only a secondary role compared the rheology of the crust. According to the numerical results, in case of relatively strong lower crust even very dense ultramafic magmas can easily reach the surface given that they are generated below a sufficiently dense and thick mantle lithosphere. Second, when differentiation of the parental high-MgO mantle-derived magma takes place inside the arc crust, significant volumes of high-MgO cumulates should be produced. Fractionation models indicate that 15–35% crystallization is necessary to lower the MgO content adequately (e.g., Conrad and Kay 1984). Such cumulates should either (1) form a major component below the seismic Moho (e.g. Kay and Kay 1985; Müntener et al. 2001; Takahashi et al. 2007) or (2) delaminate and sink back into the mantle (e.g., Kay and Kay 1991, 1993; Jull and Kelemen 2001). The delamination theory is presently favoured based on the lack of appropriate upper mantle rocks brought to the surface in continental regions

(e.g. Rudnick and Gao 2003), the absence of primitive cumulate rocks in the exposed Talkeetna paleo-island arc crust section (Kelemen et al. 2003) and evidence for active foundering of the lower continental crust below the southern Sierra Nevada, California (Zandt et al. 2004; Boyd et al. 2004).

An alternative explanation of magma differentiation processes in the arcs has recently been proposed by Jagoutz et al. (2006) based on geochemical data from the Kohistan paleo-arc in NW Pakistan. According to this hypothesis the melt rising through the Moho boundary of an arc has already a low-MgO basaltic–andesitic composition, while the primary magma generated in the mantle wedge is a high-MgO primitive basaltic liquid. Fractionation of the mantle-derived melt takes place in the mantle lithosphere within km-scaled isolated conduits (replacive channels). The dunitic ultramafic bodies found in the lowermost section of the Kohistan paleo-arc are interpreted as remnants of such melt channels through which the low-MgO (i.e. differentiated) lower-crustal intrusive mafic sequence was fed. As suggested by Jagoutz et al. (2007) such differentiation within the upper mantle is an important lower crust-forming process which can also explain the absence of high-MgO cumulates in the lower crust of exposed island arcs (e.g., Kelemen et al. 2003).

2.4 Subduction Channel Processes

Subduction channel development is an important component of intra-oceanic arc evolution (Fig. 2.4). Processes taking place in the subduction channel lives notable and directly accessible record at the surface in form of exhumed high- and ultrahigh-pressure rocks complexes (e.g., Ernst 1977; Cloos 1982; Shreve and Cloos 1986; Hermann et al. 2000; Abbott et al. 2006; Federico et al. 2007; Krebs et al. 2008). Subduction channel processes may also contribute to a magmatic record through deep subduction and melting of hydrated rock mélanges formed in the channel (e.g., Gerya and Yuen 2003; Gerya et al. 2006; Castro and Gerya 2008; Zhu et al. 2009).

It is widely accepted that the deep burial of high pressure metamorphic rocks in intra-oceanic settings is due to subduction of these rocks with the downgoing slab. However, the mechanisms of their exhumation remain subject of discussion and several models have been proposed (e.g., Cloos 1982; Platt 1993; Maruyama et al. 1996; Ring et al. 1999). According to the most popular corner flow model (Hsu 1971; Cloos 1982; Cloos and Shreve 1988a, b; Shreve and Cloos 1986; Gerya et al. 2002), exhumation of high-pressure metamorphic crustal slices at rates on the order of the plate velocity is driven by forced flow in a wedge-shaped subduction channel.

Gerya et al. (2002) investigated numerically the self-organizing evolution of the accretionary wedge and the subduction channel during intra-oceanic subduction (Fig. 2.5). In this model the geometry of the accretionary wedge and the subduction channel are neither prescribed nor assumed to represent a steady state. Instead, the system is free to evolve, starting from an imposed early stage of subduction, being controlled by the progressive modification of the thermal, petrological, and rheological structure of the subduction zone. In this evolution, upward migration of the aqueous fluid released from the subducting slab and progressive hydration of the mantle wedge play a dominant role. The following conclusions have been made based on numerical results (Gerya et al. 2002):

- Burial and exhumation of high-pressure metamorphic rocks in subduction zones are likely affected by progressive hydration (serpentinization) of the fore-arc mantle lithosphere (e.g. Schmidt and Poli 1998). This process controls the shape and internal circulation pattern of a subduction channel. Widening of the subduction channel due to hydration of the hanging wall mantle results in the onset of forced return flow in the channel. This may explain why the association of high- and/or ultrahigh-pressure metamorphic rocks with more or less hydrated (serpentinized) mantle material is often characteristic for high-pressure metamorphic complexes. Complicated non-steady geometry of weak hydrated subduction channels (Figs. 2.7, 2.9 and 2.11) was also predicted numerically (Gerya et al. 2006; Gorczyk et al. 2006, 2007a; Nikolaeva et al. 2008). This geometry forms in response to non-uniform water release from the slab that is controlled by metamorphic (dehydration) reactions in subducting rocks. Depleted mantle rocks from the base of the arc lithosphere and newly formed magmatic arc crust can be included into the channels

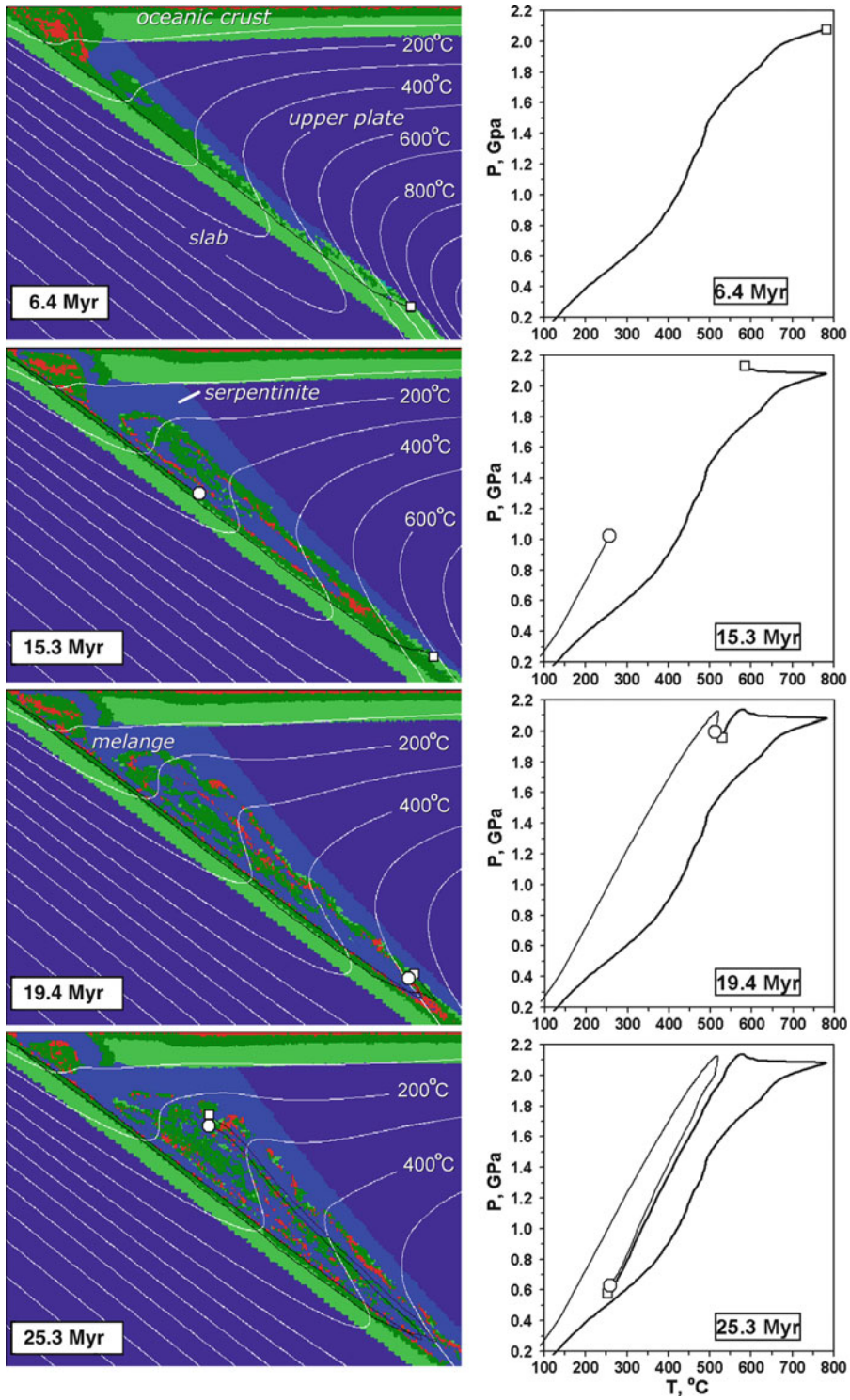

Fig. 2.5 Spontaneous development of weak serpentinized subduction channel during intra-oceanic subduction. Left column – development of the lithological field and isotherms (*white lines*, °C). Right column – development of P–T paths for two rock fragments (see *open circle* and *open rectangle* in the left column). Results from 2D numerical modelling by Gerya et al. (2002).

(Figs. 2.11 and 2.12) at a mature stage of subduction (Nikolaeva et al. 2008).

- The shape of the P–T path, and the maximum P–T conditions achieved by an individual high-pressure metamorphic rock, depend on the specific trajectory of circulation in the subduction channel (Fig. 2.5). Both clockwise and counterclockwise P–T paths are possible for fragments of oceanic crust that became involved in the circulation. Counterclockwise P–T paths are found for slices that are accreted to the hanging wall at an early stage of subduction, and set free by the progress of hydration and softening in a more evolved stage, returning towards the surface in a cooler environment. On the other hand, slices that were involved in continuous circulation, or that entered the subduction zone when a more stable thermal structure was already achieved, reveal exclusively clockwise trajectories. Model also indicates that P–T trajectories for the exhumation of high-pressure rocks in subduction channel fall into a P–T field of stability of antigorite in the mantle wedge (Fig. 2.6c).
- An array of diverse, though interrelated, P–T paths (Fig. 2.6c) rather than a single P–T trajectory is expected to be characteristic for subduction-related metamorphic complexes. The characteristic size and shape of the units with an individual history depend on the effective viscosity of the material in the subduction channel. Lower viscosities result in smaller characteristic length scales for coherent units and a marked contrasts between adjacent slices, a structure commonly termed melange, while higher viscosities favour the formation of extensive coherent nappe-like slices.

These conclusions based on relatively simple low-viscosity serpentinized subduction channel model (Figs. 2.5 and 2.6a) were recently supported by petrological studies (e.g. Federico et al. 2007; Krebs et al. 2008) of subduction-related serpentinite mélanges. For example, Federico et al. (2007) tested the serpentinized channel hypothesis by investigating a serpentinite mélange in the Western Alps, which contains exotic mafic and metasedimentary tectonic blocks, recording heterogeneous metamorphic evolutions and variable high-pressure ages. The peak metamorphic conditions range from eclogite- to garnet-blueschist-facies. The structural evidence and the pressure–temperature paths of the different blocks suggest coupling between blocks and matrix, at least in the blueschist facies. ^{39}Ar-^{40}Ar dating indicates eclogite-facies peak at ca. 43 Ma and blueschist-facies peak at ca. 43 and 40 Ma in different blocks, respectively. These data point to diachronous metamorphic paths resulting from independent tectonic evolutions of the different slices (compare with Figs. 2.5 and 2.6).

Krebs et al. (2008) presented coupled petrological and geochronological evidence from serpentinite melanges of the Rio San Juan Complex, Dominican Republic (Hispaniola) formed by intra-oceanic Caribbean subduction. It has been demonstrated that dispersed blocks of various types of metamorphic rocks in the mélanges provide fossil evidence for the dynamics of the subduction zone channel between 120 and 55 Ma. Based on three exemplary samples of eclogite and blueschist, a series of different but interrelated P–T–time paths was delineated. Eclogites indicate a low P/T gradient during subduction and record conditions in the nascent stages of the subduction zone with an anticlockwise P–T path (compare with Fig. 2.5, 6.4–15.3 Myr). Other blocks record the continuous cooling of the evolving subduction zone and show typical clockwise P–T-paths (compare with Fig. 2.5, 15.3–25.3 Myr). Omphacite blueschists correspond to the mature subduction zone recording very high ("cold") P/T gradients. Cooling rates and exhumation rates of the metamorphic blocks were estimated to be 9–20°C/Ma and 5–6 mm/a, respectively. The derived P–T–time array is compared with the serpentinized channel models (Gerya et al. 2002) with convergence rates of 10–40 mm/a resulting in an increasingly more funnel-shaped subduction channel system with time (Fig. 2.5). The numerically derived array of simulated P–T–time paths as well as the calculated rates of exhumation and cooling agree well with the P–T–time data derived from the metamorphic blocks of the Rio San Juan serpentinite mélanges when convergence rates of 15–25 mm/a are chosen (Krebs et al. 2008). This value is also in accord with available paleogeographic reconstructions calling for a long-term average of 22 mm/a of orthogonal convergence. On the basis of the comparison, the onset of subduction in the Rio San Juan segment of the Caribbean Great Arc can be constrained to approximately 120 Ma. This segment was thus obviously active for more than 65 Ma. An orthogonal convergence rate of 15–25 mm/a requires that a minimum amount of 975–1,625 km of oceanic crust must have been subducted. Both petrological/geochronological data and numerical

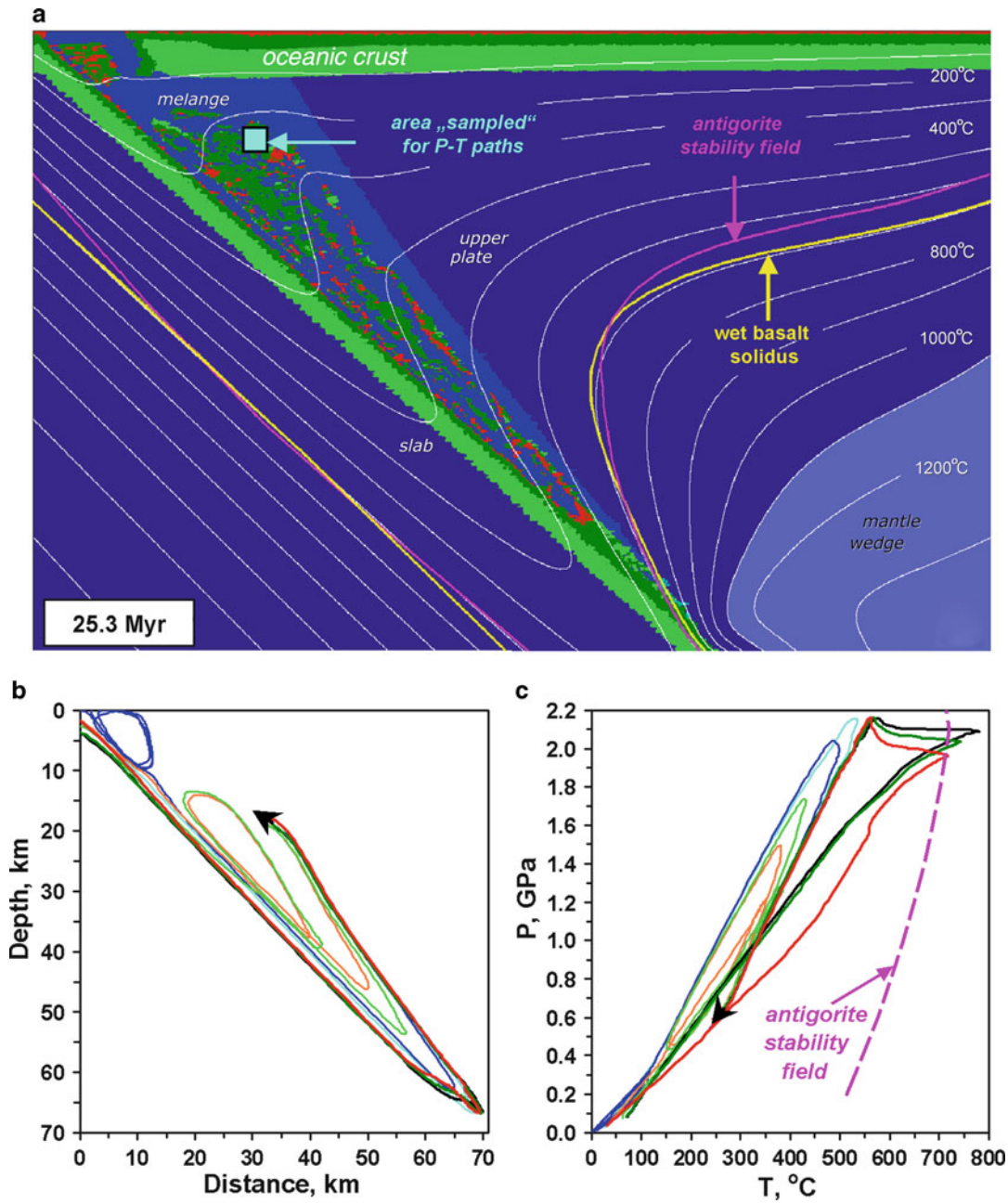

Fig. 2.6 Serpentinite melange (**a**) forming in the spontaneously evolving subduction channel (Fig. 2.6) and characteristic spatial trajectories (**b**) and P–T paths (**c**) of crustal rocks composing the melange. Results from 2D numerical modelling by Gerya et al. (2002).

simulation underscore the broad spectrum of different P–T–time paths and peak conditions recorded by material subducted at different periods of time as the subduction zone evolved and matured.

It has also been shown recently that not only high-pressure eclogites but also ultrahigh-pressure mantle rocks (garnet-bearing peridotites) can be present in intra-oceanic subduction melanges (e.g. in Greater Antilles in Hispaniola, Abbott et al. 2006). Gorczyk et al. (2007a) modelled this phenomenon numerically (Fig. 2.7) and concluded that exhumation of such garnet-bearing peridotites can be related to fore-arc

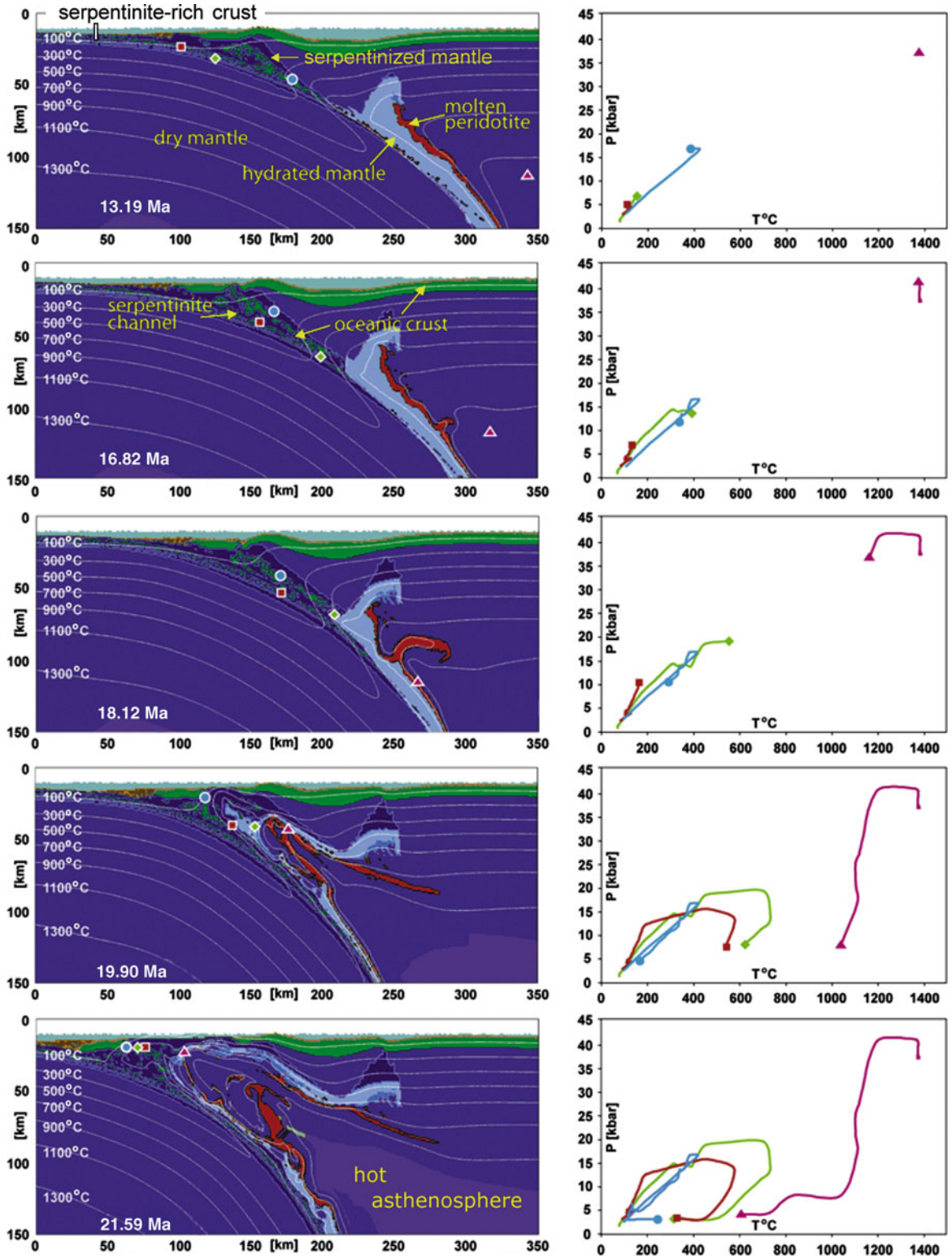

Fig. 2.7 Exhumation of high- and ultrahigh-pressure rocks during retreating intra-oceanic subduction of an oceanic plate originated at slow spreading ridge (left columns) and characteristic P–T paths of crustal and mantle rocks (right column). Results from 2D numerical modelling by Gorczyk et al. (2007a).

extension during subduction of an oceanic plate formed at a slow spreading ridge and characterized by serpentinite-rich crust. In this case subduction channel contains both serpentinites accreted from the subducting plate crust and progressively serpentinized fore-arc mantle. Intense rheological weakening of the mantle wedge takes place due to its strong hydration during subduction of water-rich crust formed at slow spreading ridge. This weakening triggers upwelling of the hydrated peridotites and partially molten peridotites followed by upwelling of hot asthenosphere and subsequent retreat of the subducting slab. According to numerical modelling of P–T paths this process can explain exhumation of UHP rocks in an intra-oceanic setting from depths of up to 120 km (4 GPa).

2.5 Magmatic Crust Growth and Thermal-Chemical Convection in the Mantle Wedge

Reymer and Schubert (1984) estimated rates of crustal generation during intra-oceanic subduction as 20–40 km^3/km/Myr for the western Pacific region based on the total arc crust volume divided by the oldest known igneous age. More recent estimates for the same area by Taira et al. (Izu-Bonin island arc, 1998), Holbrook et al. (Aleutian island arc, 1999) and Dimalanta et al. (Tonga, New Hebrides, Marianas, Southern and Northern Izu-Bonin, Aleutian island arcs, 2002) are somewhat higher, 40–95 km^3/km/Myr and are much higher, 120–180 km^3/km/Myr, according to the work of Stern and Bloomer (early stage of IBM development, 1992). In particular, the arc magmatic addition rate of the arc of the New Hebrides varies between 87 and 95 km^3/km/Myr as determined by Dimalanta et al. (2002). They also give values for addition rates of other island arcs, all of which vary between 30 and 70 km^3/km/Myr. These values are average rates of crust production, calculated by dividing the estimated total volume of produced crust by the time in which it was produced and by the length of the arc.

It is commonly accepted that dehydration of subducting slabs and hydration of the overlying mantle wedges are key processes controlling magmatic activity and consequently crustal growth above subduction zones (e.g., Stern 2002; van Keken et al. 2002; van Keken and King 2005). Mantle wedge processes have been investigated from geophysical (e.g. Zhao et al. 2002; Tamura et al. 2002), numerical (e.g. Davies and Stevenson 1992; Iwamori 1998; Kelemen et al. 2004a; Arcay et al. 2005; Gerya et al. 2006; Nikolaeva et al. 2008), experimental (e.g., Poli and Schmidt 2002; Schmidt and Poli 1998), and geochemical (e.g., Ito and Stern 1986; Sajona et al. 2000; Kelley et al. 2006) perspectives. Indeed, detailed thermal structure and melt production patterns above slabs are still puzzling. Particularly, the relative importance of slab melting (e.g. Kelemen et al. 2004a; Nikolaeva et al. 2008) versus melting induced by simple thermal convection (Honda et al. 2002, 2007; Honda and Saito 2003) and/or thermal-chemical plumes (diapirs) (e.g. Tamura 1994; Hall and Kincaid 2001; Obata and Takazawa 2004; Gerya and Yuen 2003; Manea et al. 2005; Gerya et al. 2006; Gorczyk et al. 2007b; Zhu et al. 2009) to melt production in volcanic arcs is not fully understood.

Several authors (e.g., Tamura et al. 2002; Honda et al. 2007; Zhu et al. 2009) analyzed the spatial distribution of volcanism in Japan and concluded that several clusters of volcanism can be distinguished in space and time (Fig. 2.8). The typical spatial periodicity of such volcanic clusters is 50–100 km (see the spacing between "cigars" in Fig. 2.8b) while their life extent corresponds to 2–7 Myr (see the lengths of "cigars" in time in Fig. 2.8b). Two trench-parallel lines of volcanic density maxima can also be distinguished for some periods of intra-oceanic arc evolution (Fig. 2.8a). Spatial and temporal clustering of volcanic activity also associates with strongly variable (Fig. 4.4 in Calvert 2011) distribution of crustal thickness along intra-oceanic arcs (e.g. Fig. 4.4 in Calvert 2011; Kodaira et al. 2006, 2007) and distribution of seismic velocity anomalies in the mantle wedges under the arcs (e.g. Zhao et al. 1992, 2002; Zhao 2001; Tamura et al. 2002). This further points toward the relations between the mantle wedge processes and crustal growth in intra-oceanic arcs.

Based on 3D numerical models Honda and co-workers (Honda et al. 2002, 2007; Honda and Saito 2003; Honda and Yoshida 2005) proposed the development of small-scale thermally driven convection in the uppermost corner of the mantle wedge with lowered viscosity (low viscosity wedge, LVW, Billen and Gurnis 2001; Conder and Wiens 2007; Honda and Saito 2003; Honda et al. 2002; Honda and Yoshida 2005; Arcay et al. 2005). These authors suggested that

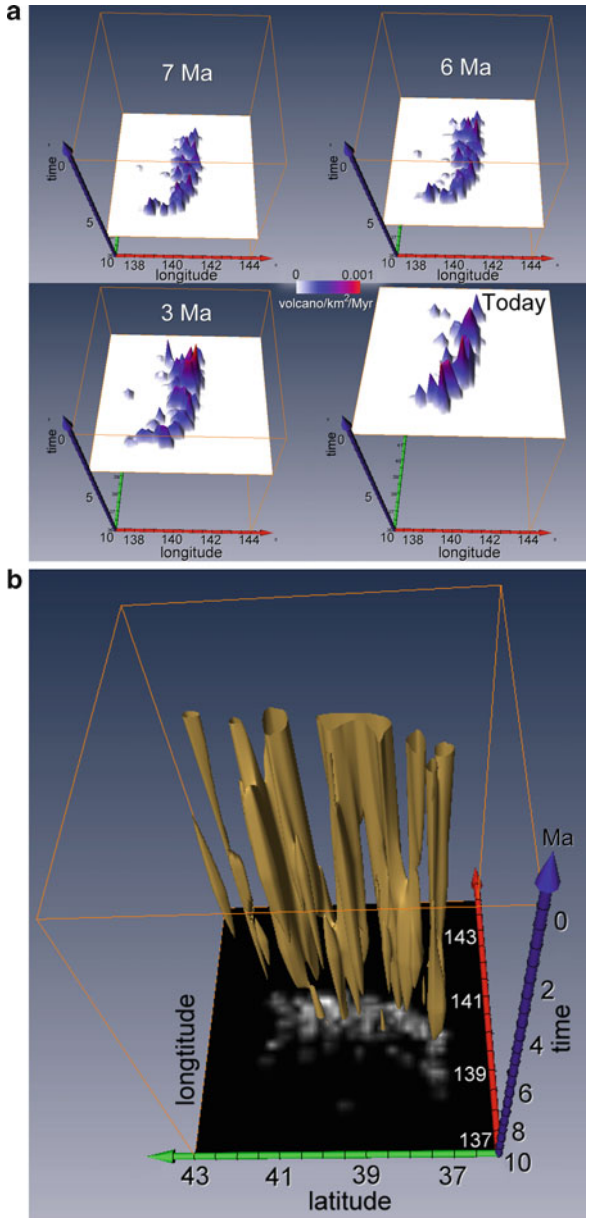

Fig. 2.8 Variations in volcanic activity in NE Japan (Honda and Yoshida 2005; Honda et al. 2007; Zhu et al. 2009). (**a**) variations in the spatial density of volcanoes with their age during the past 10 Myr. (**b**) the isosurface of 0.0003 volcano/km^2/Myr for the observed density of volcanoes in space and time. The density of volcanoes notably evolves showing formation of spatially confined clusters that remain active within certain period of time that could be possibly related to the activity of mantle wedge plumes (cf. Fig. 2.10).

a roll (finger)-like pattern of hot (upwellings) and cold (downwellings) thermal anomalies emerges in the mantle wedge above the subducting slab contributing to clustering of magmatic activity at the arc surface. These purely thermal mantle wedge convection models, however, neglected chemical buoyancy effects coming from hydration and melting atop the subducting slab and leading to thermal-chemical convection and diapirism phenomena (e.g. Tamura 1994; Hall and Kincaid 2001; Gerya and Yuen 2003). These aspects have been recently studied numerically based on petrological-thermomechanical models including water transport and melting. These models predict

1. Spontaneous formation of a low viscosity wedge by hydration of the mantle atop the slab (Arcay et al. 2005; Zhu et al. 2009)
2. Growth of diapiric structures ("cold plumes", Figs. 2.9 and 2.10) above the subducting slab (e.g., Gerya and Yuen 2003; Gorczyk et al. 2007b; Zhu et al. 2009)
3. Broad variation in seismic velocity beneath intraoceanic arcs due to hydration and melting (Gerya et al. 2006; Nakajima and Hasegawa 2003a, b; Gorczyk et al. 2006; Nikolaeva et al. 2008)
4. Variations in melt production and crustal growth processes caused by propagation of hydrated plumes in the mantle wedge (Gorczyk et al. 2007b; Nikolaeva et al. 2008; Zhu et al. 2009)

Nikolaeva et al. (2008) investigated crustal growth processes on the basis of a 2D coupled petrological–thermomechanical numerical model of retreating intraoceanic subduction (Figs. 2.11 and 2.12). The model included spontaneous slab retreat and bending, subducted crust dehydration, aqueous fluid transport, mantle wedge melting, and melt extraction resulting in crustal growth. As follows from the numerical experiments the rate of crust formation is strongly variable with time and positively correlates with subduction rate (Fig. 2.11, bottom diagram). Modelled average rates of crustal growth (30–50 km^3/km/Ma, without effects of dry decompression melting) are close to the lower edge of the observed range of rates for real intraoceanic arcs (40–180 km^3/km/Ma). The composition of new crust depends strongly on the evolution of subduction. Four major magmatic sources can contribute to the formation of the crust: (1) hydrated partially molten peridotite of the mantle wedge, (2) melted subducted sediments, (3) melted subducted basalts, (4) melted subducted gabbro. Crust produced from the first source is always predominant and typically comprise more than 95% of the growing arc crust

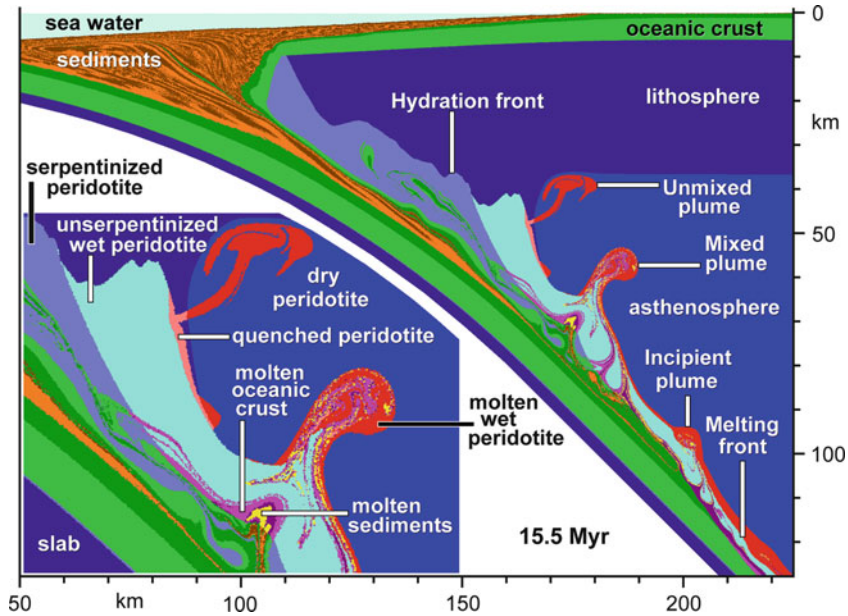

Fig. 2.9 Development of unmixed and mixed plumes due to hydration of the mantle wedge by fluids released from the slab. Plumes rising from the slab are colder then the surrounding mantle wedge (see Fig. 2.10a for 3D thermal structures around such plumes). The corrugations along the hydration front reflect dynamics of slab dehydration controlled by metamorphic reactions. Zoomed area shows lithological structures of mixed and unmixed plumes. Results from 2D numerical modelling by Gerya et al. (2006).

(Nikolaeva et al. 2008). In all studied cases, it appears shortly after beginning of subduction and is a persistent component so long as subduction remains active. Significant amount of crust produced from other three sources appear (1) in the beginning of subduction due to the melting of the slab "nose" and (2) at later stages when subduction velocity is low(<1 cm/a), which leads to the thermal relaxation of the slab. Both the intensity of melt extraction, and the age of subducted plate affect the volume of new crust. On a long time scale the greatest volume of magmatic arc crust is formed with an intermediate melt extraction threshold (2–6%) and medium subducted plate ages (70–100 Ma) (Nikolaeva et al. 2008).

Recently thermal-chemical mantle wedge convection and related melt production dynamics (Fig. 2.10) were also examined numerically in 3D (Zhu et al. 2009; Honda et al. 2010). Honda et al. (2010) analysed simple subduction model including moderately buoyant chemical agent (water) and found that the hydrated region tends to stay in the corner of the mantle wedge because of its low density and this results in the low temperature zone ("cold nose") there. Moderate chemical buoyancy present in the mantle wedge may either suppress or shift toward the back arc the thermally driven small-scale convection under the arc and make the dominant mantle flow velocity to be normal to the plate boundary. Zhu et al. (2009) examined more complex 3-D petrological-thermomechanical model of intra-oceanic subduction focussing on geometries and patterns of hydrous thermal-chemical upwellings ("cold plumes") formed above the slab (Figs. 2.9 and 2.10). These numerical simulations showed that three types of plumes occur above the slab: (a) finger-like plumes that form sheet-like structure parallel to the trench (Fig. 2.10a, b); (b) ridge-like structures perpendicular to the trench; (c) flattened wave-like instabilities propagating upwards along the upper surface of the slab and forming zig-zag patterns subparallel to the trench.

Zhu et al. (2009) also computed spatial and temporal pattern of melt generation (i.e. crust production) intensity above the slab, which appeared to be strongly controlled by the hydrous plume activities (Fig. 2.10c, d). Peaks of the melt production projected to the arc surface at different moments of time (Fig. 2.10c) always indicate individual thermal-chemical plumes growing at that time. Such peaks often form the linear

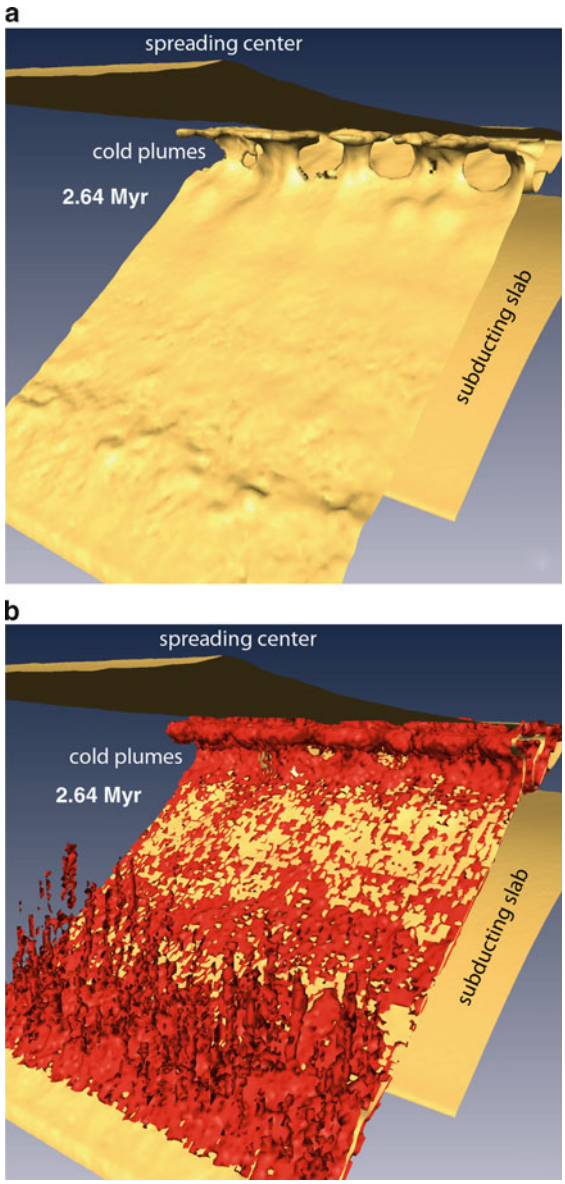

Fig. 2.10 (continued)

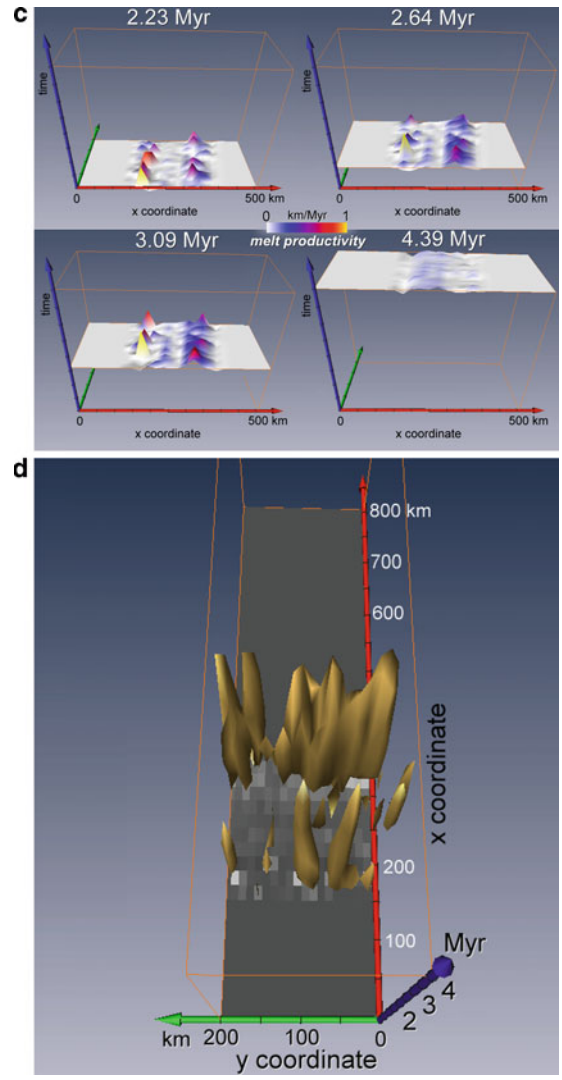

Fig. 2.10 Thermal-chemical plumes (**a**, **b**) growing in the mantle wedge during intra-oceanic subduction and corresponding variations of melt production (**c**, **d**). (**a**) the 1,350 K isosurface of temperature at 2.64 Myr, note that plumes rising from the slab are colder than the surrounding mantle wedge. (**b**) same temperature isosurface (*yellow*) with partially molten rocks, which are responsible for plume buoyancy, shown in *red*. (**c**) variations in the spatial intensity of melt production beneath the surface, peaks in the melt production correspond to individual thermal-chemical plumes shown in (**a**). (**d**) the isosurface of 0.6 $km^3/km^2/Myr$ for melt production, which implies crustal growth intensity of 600 m/Myr. Results from 3D numerical modelling by Zhu et al. (2009).

structure close to the trench, and another line of peaks in linear pattern, which is approximate 200 km away from the trench. The former ones are mainly from the depth of 50–70 km; the latter ones are mainly from the depth of 140–170 km. Figure 2.10d shows the melt productivity in time by visualizing the isosurface (0.6 $km^3/km^2/Myr$) of melt production intensity. The plume-like structures are reflected by distinct "cigar-like" features that are bounded in both time and space (Fig. 2.10d). Each "cigar" corresponds to the activity of a distinct plume that (1) increases the melt productivity during the early stage when the growing melt production is related to decompressing and heating of the rising plume material and (2)

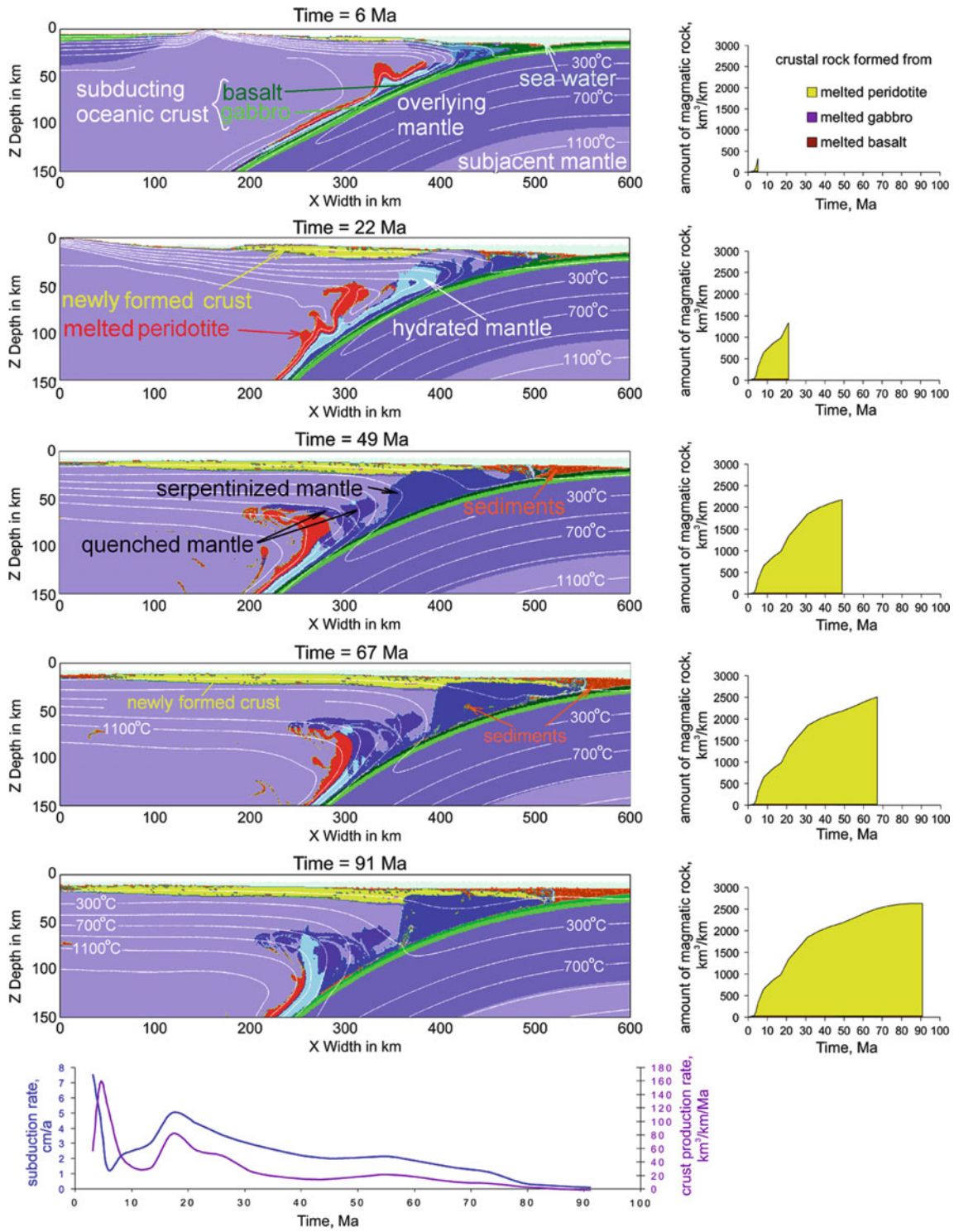

Fig. 2.11 Dynamics of a pure retreating intra-oceanic subduction (left column) and associated magmatic crust growth (right column). Spontaneous changes in subduction rate (for this model subduction rate and trench retreat rate are equal) and crust accumulation rate with time are depicted below. Time is dated from the beginning of subduction. Subduction results in a hydration and partial melting of mantle wedge rocks, which leads to the formation of volcanic arc rocks (*yellow*) above the area of melting. Results from 2D numerical modelling by Nikolaeva et al. (2008).

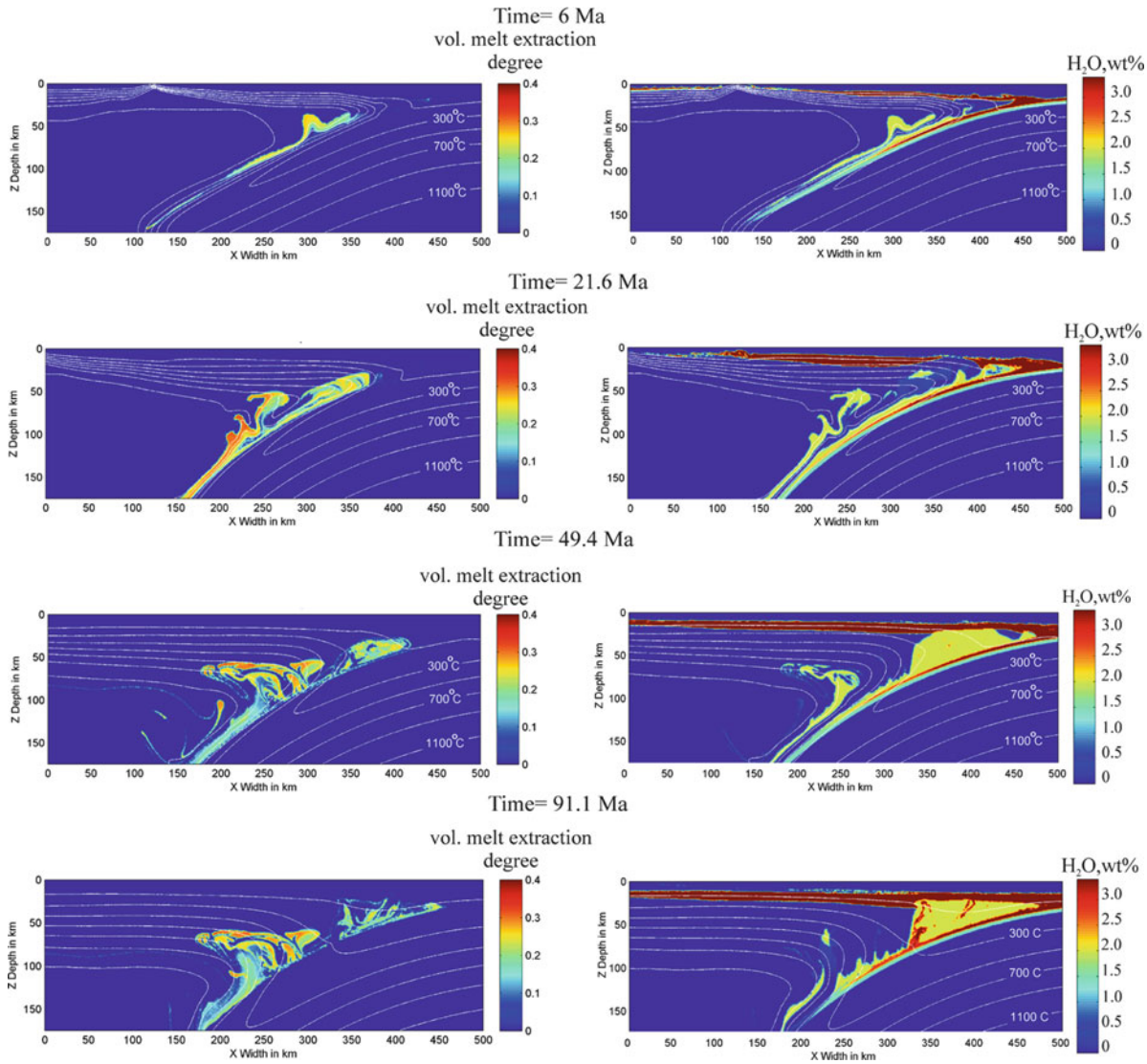

Fig. 2.12 Evolution of degree of melt extraction (left column) and water content (right column) in the mantle wedge and subducting oceanic crust. Corresponding lithological field is depicted on the Fig. 2.11. Results from 2D numerical modelling by Nikolaeva et al. (2008).

decreases the melt productivity during the later stage when the temperature, the pressure and the degree of melting stabilize inside the horizontally spreading and thermally relaxing plume.

The modelled wavelength (25–100 km) and the growth time (2–7 Myr, see the lengths of "cigars" in time in Fig. 2.10d) of the thermal-chemical plumes are comparable to spatial periodicity (50–100 km) and the life extent (2–7 Myr, see the lengths of "cigars" in time in Fig. 2.8b) of volcanic clusters and to spatial periodicity (50–100 km, Fig. 4.4b in Calvert 2011) of crustal thickness variations in intra-oceanic arcs. The existence of two contemporaneous trench-parallel lines of melt productivity (Fig. 2.10b) is also similar to the natural observations (see two trench-parallel lines of Quaternary volcanic density maxima in Fig. 2.8a, at 6 Ma). To explain such phenomena, Wyss et al. (2001) have proposed an additional source of fluids to be located at the top of the slab (at about 150 km depth). Their proposition is based on the velocity tomography

in the mantle wedge above the slab, and on the mapping of earthquake size distribution within the mantle wedge. Geochemical evidence (Kimura and Yoshida 2006) for Quaternary lavas from the NE Japan arc also shows the deeper mantle-derived rear-arc lava coming from 100–150 km depth.

2.6 Geochemistry of Intra-oceanic Arcs

The role of subduction zones in global geochemical dynamics is generally twofold: first, crustal materials are recycled back into the deep mantle, and second, new crust is produced in magmatic arcs above subduction zones (e.g. Bourdon et al. 2003). Because the physical and chemical changes within the subducting plate and mantle wedge are largely inaccessible to a direct observation, geochemical investigations concentrate on the input (rocks subducted atop the slabs) and output (magmatic products of island arcs) signals of subduction zones (e.g., Plank and Langmuir 1993; Hauff et al. 2003). For example, as discussed by Kimura and Yoshida (2006), Quaternary lavas from NE Japan arc show geochemical evidence of mixing between mantle-derived basalts and crustal melts at the magmatic front, whereas significant crustal signals are not detected in the rear-arc lavas.

Analyses of comprehensive geochemical data sets for the input and output rock-members (Hauff et al. 2003) from several arc systems such as Aleutian (Yogodzinski et al. 2001), Izu-Bonin-Mariana (Tatsumi et al. 2008), New Britain, Vanuatu (Arai and Ishimaru 2008), Kamchatka (Churikova et al. 2001; Dosseto et al. 2003; Yogodzinski et al. 2001) and Tonga-Kermadec arcs (Turner and Hawkesworth 1997) lead to the conclusion that subduction-related arc basalts (output signal) characteristically have elevated contents of large-ion lithophile element (LILEs) and light rare earth element (LREEs) with depleted heavy REE (HREE) and high field strength elements (HFSEs) compared to subducted crust (input signal) (McCulloch and Gamble 1991; Elliott et al. 1997; Elliott 2003; Plank and Langmuir 1993; Kimura et al. 2009). In relation to that, the following processes are believed to be responsible for the element partitioning in intra-oceanic arc magmas (e.g. Kimura et al. 2009 and reference therein):

- Extraction of fluids and/or melts from the subducted slab; combined slab fluid and melt fluxes may be responsible for geochemical variations along or across magmatic arcs (Eiler et al. 2005; Ishizuka et al. 2006); separate deep and shallow slab components have also been proposed (Kimura and Yoshida 2006; Pearce and Peate 1995; Pearce et al. 2005)
- Fluid fluxed melting of the mantle wedge responsible for generation of high-MgO primitive arc basalts (Arculus and Johnson 1981; Davidson 1996; Elliott et al. 1997; Hawkesworth et al. 1993; Kelemen et al. 1998; Kimura and Yoshida 2006; Plank and Langmuir 1993; Poli and Schmidt 1995; Stern 2002; Stolper and Newman 1994; Tatsumi and Eggins 1995; Turner et al. 1997)
- Slab melt–mantle reaction generating high-MgO primitive arc andesites (Kelemen et al. 2004b; Tatsumi and Hanyu 2003; Tsuchiya et al. 2005; Yogodzinski et al. 1994; Zack et al. 2002)
- Melting of mantle wedge metasomatized by slab-derived fluid or melt (Eiler et al. 2007; Sajona et al. 1996)
- Direct supply of felsic melt from eclogitic slab melting (Defant and Drummond 1990; Martin 1999; Martin et al. 2005)
- Melting of hydrated mantle and subducted tectonic melanges in respectively unmixed and mixed thermal-chemical plumes (Fig. 2.9) rising from the top of the slab (Tamura 1994; Gerya et al. 2006; Castro and Gerya 2008; Castro et al. 2010)

Despite the broad variability of involved geochemical mechanisms currently there is a consensus (e.g. Kimura et al. 2009) about the relative significance of various processes and it is widely believed that slab dehydration or melting combined with the interaction of this slab-derived flux with variously depleted mantle generates primary arc magmas with the observed geochemical characteristics. These primary magmas typically have radiogenic Sr and Pb isotopic composition, with less radiogenic Nd in lavas erupted from the volcanic front compared to rear-arc magmas apparently derived from more depleted upper mantle sources (Elliott et al. 1997; Ishizuka et al. 2003; Kelemen et al. 2004b; Kimura and Yoshida 2006; Manning 2004; Rapp and Watson 1995; Stolper and Newman 1994; Tatsumi and Eggins 1995).

Elliott (2003) and other authors (Hawkesworth et al. 1993; Leat and Larter 2003; McCulloch and Gamble 1991; Stern 2002) describe two distinct major slab components present in arc rocks with different sources and transport mechanisms: (1) melt of the down-going sediments, and (2) aqueous fluid derived from altered oceanic crust. Direct melting of the slab is also suggested as a possible mechanism for melts generation (e.g. Defant and Drummond 1990; Martin 1999; Martin et al. 2005; Kelemen et al. 2004a; Nikolaeva et al. 2008). Fluids and melts liberated from subducting oceanic crust produce melting above slabs and finally lead to efficient subduction-zone arc volcanism (Fig. 2.4). The exact composition of the mobile phases generated in the subducting slab have however, remained incompletely known (e.g. Kessel et al. 2005). In this respect the fundamental control appears to be (e.g. Kimura et al. 2009) the P–T paths of rocks in the subducting slab, which can be approximated by geodynamic modelling (e.g., Peacock and Wang 1999; Gerya and Yuen 2003; Castro and Gerya 2008). For example in the model of Peacock and Wang (1999), subduction of old and cold oceanic plate leads to low slab surface temperature. In contrast, subduction of young and hot oceanic crust typically results in higher slab surface temperatures (Stern et al. 2003).

Such contrasting thermomechanical behaviour can presumably be observed in the arcs of Japan (Peacock and Wang 1999), where the old Pacific Plate (>120 Ma, NE Japan) and the young Shikoku Basin (15–27 Ma, SW Japan) are subducting beneath the Eurasia plate (Kimura and Stern 2009; Kimura et al. 2005; Kimura and Yoshida 2006). Consequently, in NE Japan slab dehydration seems to dominate geochemical signal in the primary arc basalts (Kimura and Yoshida 2006; Moriguti et al. 2004; Shibata and Nakamura 1997), whereas in SW Japan slab melting is proposed to be responsible for generation of high-MgO andesites or adakitic dacites (Kimura and Stern 2009; Kimura et al. 2005; Shimoda and Nohda 1995; Tatsumi and Hanyu 2003). Recently Kimura et al. (2009) obtained similar results from simulations of geochemical variability of primitive magmas across an intra-oceanic arc based on partitioning of incompatible element and Sr-Nd-Pb isotopic composition in a slab-derived fluid and in arc basalt magma generated by an open system fluid-fluxed melting of mantle wedge peridotite (Fig. 2.4). Similar contrasting geochemical behaviour has been also shown (e.g. Kimura et al. 2009 and reference therein) between arcs along the western and eastern Pacific rims. Arc magmatism due to slab-derived fluids is proposed for the western Pacific arcs, including the Kurile, NE Japan, and the Izu-Bonin-Mariana arcs (Ishikawa and Nakamura 1994; Ishikawa and Tera 1999; Ishizuka et al. 2003; Kimura and Yoshida 2006; Moriguti et al. 2004; Pearce et al. 2005; Ryan et al. 1995; Straub and Layne 2003). High-MgO primary mafic magmas from these relatively cold subduction zones show geochemical signatures of extremely fluid mobile elements such as B, Li, or U (Ishikawa and Nakamura 1994; Ishikawa and Tera 1999; Moriguti et al. 2004; Ryan et al. 1995; Turner and Foden 2001). In contrast, slab melting better explains the origin of high-MgO intermediate lavas in the eastern Pacific (Kelemen et al. 2004b; Straub et al. 2008) although the role of slab fluid remains an important factor in some of the arcs (Grove et al. 2006).

Alternative ideas that explain broad variability of slab fluid and slab melt geochemical components in arc magmas were proposed recently based on petrological-thermomechanical numerical modeling of subduction zones (Gerya et al. 2006; Castro and Gerya 2008; Castro et al. 2010). Gerya et al. (2006) suggested that one possibility for transporting two distinct geochemical signatures through the mantle wedge can be related to generation and propagation of partially molten compositionally buoyant diapiric structures (cold plumes, Tamura 1994; Hall and Kincaid 2001; Gerya and Yuen 2003) forming atop the slab. Numerical experiments of Gerya et al. (2006) show that two distinct types of plumes can form in the mantle wedge (Fig. 2.9):

1. Mixed plumes form atop the slab and consist of partially molten mantle and recycled sediments mixed on length-scales of 1–100 m (i.e. subducted tectonic melange). Magma production from such compositionally heterogeneous plumes may produce a strong crustal melt signature in resulting magmas.
2. Unmixed plumes form above the slab and consist of hydrated partially molten mantle located at a distance from the slab, which is therefore not mechanically mixed with subducted crustal rocks. Magma production from such hydrated but compositionally homogeneous plumes may produce a pronounced slab fluid signature.

These distinct plume types can explain the presence of different magmas in volcanic arcs (e.g., Stern 2002): magmas with distinct crustal signatures (e.g., adakites) and primitive magmas from peridotitic source (e.g., arc tholeiites). Thermal zoning inside rapidly rising unmixed cold plumes can result in transient bimodal magmatism because of both the compositional and the thermal zoning of these structures (Fig. 2.10a, b), which would generate basalts from its water-depleted, hot rinds, and boninites from its water-enriched, cooler interiors (Tamura 1994). Rates of plume propagation vary between several centimeters to meters per year (Gerya and Yuen 2003; Gerya et al. 2004) corresponding to 0.1–3 Myr transfer time through the asthenospheric portion of the mantle wedge. This is consistent with U–Th isotope measurements from island arc magmas that suggest short transfer times for fluids (0.03–0.12 Myr) and slab-derived melts (several Myr) (Hawkesworth et al. 1997). It is noteworthy that the diapiric transport (e.g. Tamura 1994; Hall and Kincaid 2001) of various geochemical components in the mantle wedge does not require melting of subducted crust immediately at the slab surface (e.g. Kelemen et al. 2004a). Intense melting of subducted sediments and oceanic crust in the mixed plumes occurs in the temperature range of 900–1,400°C (Gerya and Yuen 2003; Gerya et al. 2006; Castro and Gerya 2008; Castro et al. 2010) after penetration of these structures into the hot portion of the mantle wedge. This behaviour agrees well with geochemical models suggesting notable sediment melting beneath the arc, behaviour which is otherwise not trivial to reconcile (e.g. Kelemen et al. 2004a) with low slab surface temperature inferred from thermal models for subduction zones as discussed by George et al. (2003).

Mixed cold plumes composed of tectonic melanges derived from subduction channels can transport the fertile subducted crustal materials towards hotter zones of the suprasubduction mantle wedge leading to the formation of silicic melts. Recently magmatic consequences of this plausible geodynamic scenario were evaluated by using an experimental approach (Castro and Gerya 2008; Castro et al. 2009, 2010). Melt compositions, fertility and reaction between silicic melts and the peridotite mantle (both hydrous and dry) were tested by means of piston–cylinder experiments at conditions of 1,000°C and pressures of 2.0 and 2.5GPa. The results indicate that silicic melts of trondhjemite and granodiorite compositions may be produced in the ascending mixed plume megastructures. Experiments show that the formation of an Opx-rich reaction band, developed at the contact between the silicic melts and the peridotite, protect silicic melts from further reaction in contrast to the classical view that silicic melts are completely consumed in the mantle. It has also been demonstrated experimentally (Castro et al. 2010) that the composition of melts formed after partial melting of sediment-MORB mélanges is buffered for broad range of sediment-to-MORB ratios (from 3:1 to 1:3), producing liquids along a cotectic of granodiorite to tonalite composition in lower-variance phase assemblage Melt+Grt+Cpx+Pl. The laboratory experiments, therefore, predict decoupling between major element and isotopic compositions: large variations in isotopic ratios can be inherited from a compositionally heterogeneous source but major element compositions can be dependent on the temperature of melting rather than on the composition of the source (Castro et al. 2010).

Important geochemical constrains concerns distribution and amount of water above subduction zones that impose strong controls on chemistry of magmatic arc rocks forming at the surface (e.g., Kelley et al. 2006 and references therein). Flux of water originating from the dehydrating, subducting slab lowers the mantle solidus (e.g., Kushiro et al. 1968) triggering melting of the mantle wedge beneath arcs and back-arc basins (Fig. 2.4). This is supported by a range of various widespread observations on subduction zone lavas (e.g., Kelley et al. 2006 and references therein), seismological data (e.g. Tamura et al. 2002; Jung and Karato 2001; Iwamori 2007) and numerical modelling constrains (Iwamori 1998; Arcay et al. 2005; Nikolaeva et al. 2008; Hebert et al. 2009).

Back-arc basins related to intra-oceanic subduction (Fig. 2.4) are natural places to investigate water-related processes in the mantle wedge because these settings can be treated, in many ways, like mid-ocean ridges (Kelley et al. 2006). Particularly, the driest back-arc basin melts (Fig. 2.13) are compositionally equivalent to mid-ocean ridge melts and can be interpreted as melts generated by decompression melting of ascending mantle (Fig. 2.4). Geochemical studies of back arcs related to intra-oceanic subduction (e.g. Stolper, and Newman 1994; Taylor and Martinez 2003; Kelley et al. 2006) demonstrated the hybrid nature of the back-arc basin melting process:

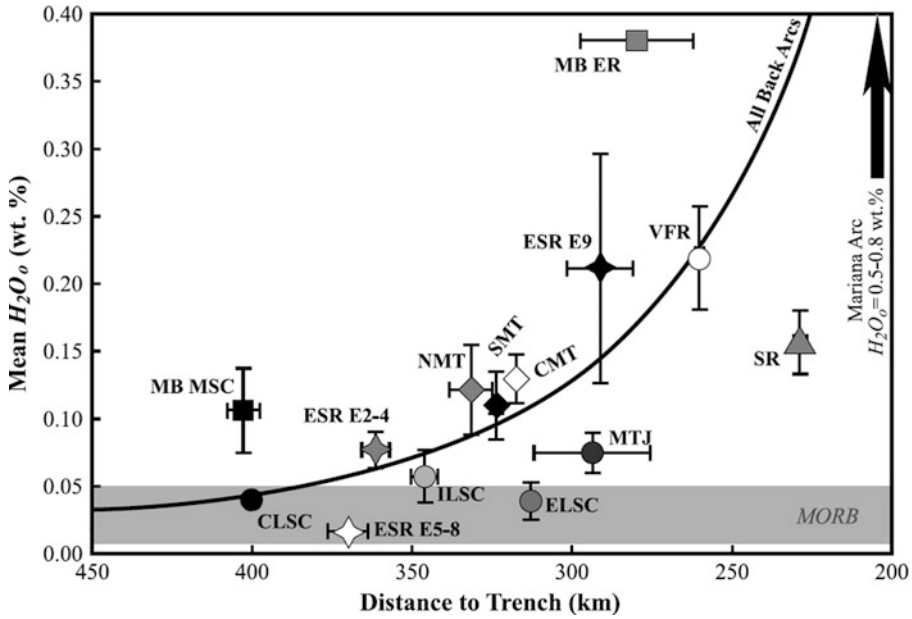

Fig. 2.13 Mean water content in the mantle source (H_2Oo) versus distance to the trench at back-arc basins (Kelley et al. 2006). The back-arc basin data are regional averages of the Manus basin Eastern Rifts (MB ER) and the Manus spreading center/eastern transform zone (MB MSC), the Lau basin central Lau spreading center (CLSC), the intermediate Lau spreading center (ILSC), the Mangatolu triple junction (MTJ), the eastern Lau spreading center (ELSC) and the Valu Fa ridge (VFR), the East Scotia ridge segments (ESR E2–E4, ESR E5–E8, ESR E9), and the Mariana trough northern third (NMT), central third (CMT) and southern third (SMT). The shaded field is the range of H_2Oo for MORB from the same study. The black arrow indicates the direction that volcanic arcs are predicted to plot (Kelley et al. 2006).

MORB-like geochemistry found in relatively dry back-arc melts is systematically perturbed in wetter samples affected by the addition of H_2O-rich material from the subducted slab (Fig. 2.13).

Recently Kelley et al. (2006) examined data compiled from six back-arc basins and three mid-ocean ridge regions and evaluated concentration of H_2O in the mantle source based on measured H_2O concentrations of submarine basalts collected at different distances from the trench (Fig. 2.13). This study clearly demonstrated that water concentrations in back-arc mantle sources increase toward the trench, and back-arc spreading segments with the highest water content are at anomalously shallow water depths, consistent with increases in crustal thickness and total melt production resulting from high H_2O. In contrast to mid ocean ridges, back-arc basin spreading combines ridge-like adiabatic decompression melting with nonadiabatic mantle melting paths that may be independent of the solid flow field and depend on the H_2O supply from the subducting plate (Kelley et al. 2006). This conclusion is also consistent with numerical modelling results (e.g. Iwamori 1998; Arcay et al. 2005; Nikolaeva et al. 2008; Honda et al. 2010) predicting that water-rich mantle sources should mainly concentrate at 100–250 km distances from the trench in proximity of water-rich, depleted and chemically buoyant "cold nose" of the mantle wedge (Figs. 2.11 and 2.12).

2.7 Conclusions

The following messages are "to take home" from this chapter:

- Modern intra-oceanic subduction zones comprise around 40%, of the convergent margins of the Earth and most of them are not accreting sediments and have back-arc extension.
- It is not yet entirely clear where and how intra-oceanic subduction initiates although two major types of subduction zone nucleation scenarios are proposed: induced and spontaneous.

- Internal structure and compositions of intra-oceanic arcs is strongly variable. Both along- and across-arc variation of crustal thickness and lithological structure are inferred based on seismological data and numerical modeling.
- Base of the arc includes crust–mantle transitional layer of partly enigmatic origin (cumulates?, replacive rocks?, intercalation of various rocks and melts?) and imprecisely known thickness.
- Major element composition of magmas feeding arcs from the mantle is debatable, particularly regarding the MgO content of erupted basaltic magmas which are too MgO-poor to represent the parental high-MgO mantle-derived magma. Magma fractionation and reactive flow models are suggested to explain this MgO-paradox.
- Exhumation of high- and ultrahigh-pressure crustal and mantle rocks during intra-oceanic subduction are strongly controlled by serpentinized subduction channels forming by hydration of the overriding plate and incorporation of subducted upper oceanic crust. Newly formed volcanic rocks and depleted mantle from the base of the arc lithosphere can be included into subduction channels at a mature stage of subduction.
- An array of diverse both clockwise and counter clockwise P–T–time paths rather than a single P–T trajectory is characteristic for high-pressure rock melanges forming in the serpentinized channels.
- Crustal growth intensity in intra-oceanic arcs (40–180 km^3/km/Myr) is variable in both space and time and should strongly depend on subduction rate as well as on intensity and character of thermal-chemical convection in the mantle wedge driven by slab dehydration and mantle melting. This convection can possibly include hydrated diapiric structures (cold plumes) rising from the slab and producing silicic magmatic rocks by melting of subducted rock melanges.
- Subduction-related arc basalts (output signal) characteristically have elevated contents of large-ion lithophile element (LILEs) and light rare earth element (LREEs) with depleted heavy REE (HREE) and high field strength elements (HFSEs) compared to subducted oceanic crust (input signal).
- The exact origin of geochemical variations in arc basalts is debatable and may involve a range of processes such as (a) extraction of fluids and/or melts from the subducted slab, (b) fluid fluxed and decompression melting of the mantle wedge, (c) slab melt–mantle reactions, (d) melting of mantle wedge metasomatized by slab-derived fluid or melt, (e) direct supply of felsic melt from eclogitic slab melting, (f) melting of hydrated mantle and subducted tectonic melanges in thermal-chemical plumes.
- Water concentrations in back-arc mantle sources increase toward the trench. Back-arc basin spreading combines mid-ocean-ridge-like adiabatic decompression melting with nonadiabatic fluid-fluxed mantle melting depending on the H_2O supply from the subducting plate. Numerical modeling results predict that water-rich mantle sources should mainly concentrate at 100–250 km distances from the trench in proximity of water-rich, depleted and chemically buoyant „cold nose„ of the mantle wedge.

In conclusion, despite recent progress in both observation and modelling many of the first-order features of intra-oceanic subduction remain only partly known and require further cross-disciplinary efforts.

Acknowledgements This work was supported by ETH Research Grants ETH-0807-2, ETH-0807-3, ETH-0609-2, SNF Research Grants 200020-126832, 200020-129487, SNF ProDoc program 4-D-Adamello and TopoEurope Program.

References

Abbott RN, Draper G, Broman BN (2006) P-T path for ultra-high-pressure garnet ultramafic rocks of the Cuaba Gneiss, Rio San Juan complex, Dominican Republic. Int Geol Rev 48:778–790

Afonso JC, Ranalli G, Fernandez M (2007) Density structure and buoyancy of the oceanic lithosphere revisited. Geophy Res Lett 34, Article Number: L10302

Afonso JC, Zlotnik S, Fernandez M (2008) Effects of compositional and rheological stratifications on small-scale convection under the oceans: implications for the thickness of oceanic lithosphere and seafloor flattening. Geophys Res Lett 35, Article Number: L20308

Alvarez-Marron J, Perez-Estaun A, Danobeitia JJ, Pulgar JA, Martinez Catalan JR, Marcos A, Bastida E, Ayarza Arribas R, Aller J, Gallart A, Gonzalez-Lodeiro E, Banda E, Comas MC, Cordoba D (1996) Seismic structure of the northern continental margin of Spain from ESCIN deep seismic profiles. Tectonophysics 264:153–174

Alvarez-Marron J, Rubio E, Torne M (1997) Subduction-related structures in the North Iberian Margin. J Geophys Res 102:22497–22511

Arai S, Ishimaru S (2008) Insights into petrological characteristics of the lithosphere of mantle wedge beneath arcs through peridotite xenoliths: a review. J Petrol 49:665–695

Arcay D, Tric E, Doin MP (2005) Numerical simulations of subduction zones: effect of slab dehydration on the mantle wedge dynamics. Phys Earth Planet Inter 149:133–153

Arculus RJ, Johnson RW (1981) Island-arc magma sources: a geochemical assessment of the roles of slab derived components and crustal contamination. Geochem J 15:109–133

Billen M, Gurnis M (2001) A low viscosity wedge in subduction zones. Earth Planet Sci Lett 193:227–236

Bourdon B, Turner S, Dosseto A (2003) Dehydration and partial melting in subduction zones: constraints from U-series disequilibria. J Geophys Res 108, Article Number: 2291

Boyd OS, Jones CH, Sheehan AF (2004) Foundering lithosphere imaged beneath the southern Sierra Nevada, California, USA. Science 305:660–662

Burg JP (2011) The Asia-Kohistan-India collision. Review and discussion. In: Brown D, Ryan P (eds) Arc-continent collision: the making of an orogen, Frontiers in earth sciences. Springer, Heidelberg

Burg J-P, Bodinier J-L, Gerya T, Bedini R-M, Boudier F, Dautria J-M, Prikhodko V, Efimov A, Pupier E, Balanec J-L (2009) Translithospheric mantle diapirism: geological evidence and numerical modelling of the Kondyor zoned ultramafic complex (Russian Far-East). J Petrol 50:289–321

Calvert AJ (2011) The seismic structure of island arc crust. In: Brown D, Ryan P (eds) Arc-continent collision: the making of an orogen, Frontiers in earth sciences. Springer, Heidelberg

Casey JF, Dewey JF (1984) Initiation of subduction zones along transforms and accreting plate boundaries, triple junction evolution, and forearc spreading centers: implications for ophiolitic geology and obduction. In: Gass IG, Lippard SJ, Shelton AW (eds) Ophiolites and oceanic lithosphere, vol 13. Geol Soc Spec Publ, London, pp 269–290

Castro A, Gerya TV (2008) Magmatic implications of mantle wedge plumes: experimental study. Lithos 103:138–148

Castro A, García-Casco A, Fernández C, Corretgé LG, Moreno-Ventas I, Gerya T, Löw I (2009) Ordovician ferrosilicic magmas: experimental evidence for ultrahigh temperatures affecting a metagreywacke source. Gondwana Res 16: 622–632

Castro A, Gerya T, Garcia-Casco A, Fernandez C, Diaz-Alvarado J, Moreno-Ventas I, Low I (2010) Melting relations of MORB-sediment melanges in underplated mantle wedge plumes; implications for the origin of Cordilleran-type batholiths. J Petrol 51:1267–1295

Churikova T, Dorendorf F, Worner G (2001) Sources and fluids in the mantle wedge below Kamchatka, evidence from across-arc geochemical variation. J Petrol 42:1567–1593

Cloetingh SAPL, Wortel MJR, Vlaar NJ (1982) Evolution of passive continental margins and initiation of subduction zones. Nature 297:139–142

Cloos M (1982) Flow melanges: numerical modelling and geologic constraints on their origin in the Fransiscan subduction complex, California. Geol Soc Am Bull 93:330–345

Cloos M (1993) Lithospheric buoyancy and collisional orogenesis: subduction of oceanic plateaus, continental margins, island arcs, spreading ridges, and seamounts. Geol Soc Am Bull 105:715–737

Cloos M, Shreve RL (1988a) Subduction-channel model of prism accretion, melange formation, sediment subduction, and subduction erosion at convergent plate margins, 1, Background and description. Pure Appl Geophys 128: 455–500

Cloos M, Shreve RL (1988b) Subduction-channel model of prism accretion, melange formation, sediment subduction, and subduction erosion at convergent plate margins, 2, Implications and discussion. Pure App Geophys 128:501–545

Collins WJ (2003) Slab pull, mantle convection, and Pangaean assembly and dispersal. Earth Planet Sci Lett 205:225–237

Conder JA, Wiens DA (2007) Rapid mantle flow beneath the Tonga volcanic arc. Earth Planet Sci Lett 264:299–307

Conrad WK, Kay RW (1984) Ultramafic and mafic inclusions from Adak Island; crystallization history, and implications for the nature of primary magmas and crustal evolution in the Aleutian arc. J Petrol 25:88–125

Davidson JP (1996) Deciphering mantle and crustal signatures in subduction zone magmatism. In: Bebout GE, Scholl DW, Kirby SH, Platt JR (eds) Subduction top to bottom. American Geophysical Union Monographs, vol 96., pp 251–262

Davies GF (1999) Dynamic Earth. Cambridge University Press, New York

Davies JH, Stevenson DJ (1992) Physical model of source region of subduction zone volcanics. J Geophys Res 97: 2037–2070

Defant MJ, Drummond MS (1990) Derivation of some modern arc magmas by melting of young subducted lithosphere. Nature 347:662–665

Dewey JF (1969) Continental margins: a model for conversion of Atlantic type to Andean type. Earth Planet Sci Lett 6: 189–197

Dickinson WR, Seely DR (1979) Structure and stratigraphy of fore-arc regions. Am Assoc Petrol Geol Bull 63:2–31

Dimalanta C, Taira A, Yumul GP, Tokuyama H, Mochizuki K (2002) New rates of western Pacific island arc magmatism from seismic and gravity data. Earth Planet Sci Lett 202: 105–115

Doin M-P, Henry P (2001) Subduction initiation and continental crust recycling: the roles of rheology and eclogitization. Tectonophysics 342:163–191

Dosseto A, Bourdon B, Joron J-L, Dupre B (2003) U-Th-Pa-Ra study of the Kamchatka arc: new constraints on the genesis of arc lavas. Geochem Cosmochem Acta 67:2857–2877

Eiler JM, Carr MJ, Reagan M, Stolper EM (2005) Oxygen isotope constraints on the sources of Central American arc lavas. Geochem Geophys Geosyst 6, Article Number: Q07007

Eiler JM, Schiano P, Valley JM, Kita NT, Stolper EM (2007) Oxygen-isotope and trace element constraints on the origins of silica-rich melts in the subarc mantle. Geochem Geophys Geosyst 8, Article Number: Q09012

Elliott T (2003) Tracers of the slab. In: Eiler J (ed) Inside the subduction factory. American Geophysical Union, Washington, DC, pp 23–46

Elliott T, Plank T, Zindler A, White W, Bourdon B (1997) Element transport from slab to volcanic front at the Mariana arc. J Geophys Res 102:14991–15019

Erickson SG (1993) Sedimentary loading, lithospheric flexure, and subduction initiation at passive margins. Geology 21: 125–128

Ernst WG (1977) Mineral parageneses and plate tectonic settings of relatively high-pressure metamorphic belts. Fortschr Miner 54:192–222

Federico L, Crispini L, Scambelluri M, Capponi G (2007) Ophiolite mélange zone records exhumation in a fossil subduction channel. Geology 35:499–502

Fyfe WS, Leonardos OH (1977) Speculations on causes of crustal rifting and subduction, with applications to Atlantic margin of Brazil. Tectonophysics 42(1):29–36

George R, Turner S, Hawkesworth C, Morris J, Nye C, Ryan J, Zheng S-H (2003) Melting processes and fluid and sediment transport rates along the Alaska-Aleutian arc from an integrated U-Th-Ra-Be isotope study. J Geophys Res 108, doi:10.1029/2002JB001916

Gerya TV, Burg J-P (2007) Intrusion of ultramafic magmatic bodies into the continental crust: numerical simulation. PEPI 160:124–142

Gerya TV, Meilick FI (2011) Geodynamic regimes of subduction under an active margin: effects of rheological weakening by fluids and melts. J Metamorphic Geol 29:7–31

Gerya TV, Yuen DA (2003) Rayleigh-Taylor instabilities from hydration and melting propel "cold plumes" at subduction zones. Earth Planet Sci Lett 212:47–62

Gerya TV, Stoeckhert B, Perchuk AL (2002) Exhumation of high-pressure metamorphic rocks in a subduction channel – a numerical simulation. Tectonics 21, Article Number: 1056

Gerya TV, Yuen DA, Sevre EOD (2004) Dynamical causes for incipient magma chambers above slabs. Geology 32:89–92

Gerya TV, Connolly JAD, Yuen DA, Gorczyk W, Capel AM (2006) Sesmic implications of mantle wedge plumes. Phys Earth Planet Inter 156:59–74

Gerya TV, Connolly JAD, Yuen DA (2008) Why is terrestrial subduction one-sided? Geology 36:43–46

Gorczyk W, Gerya TV, Connolly JAD, Yuen DA, Rudolph M (2006) Large-scale rigid-body rotation in the mantle wedge and its implications for seismic tomography. Geochem Geophys Geosyst 7, Article Number: Q05018

Gorczyk W, Guillot S, Gerya TV, Hattori K (2007a) Asthenospheric upwelling, oceanic slab retreat, and exhumation of UHP mantle rocks: insights from Greater Antilles. Geophys Res Lett 34, Article Number: L21309

Gorczyk W, Gerya TV, Connolly JAD, Yuen DA (2007b) Growth and mixing dynamics of mantle wedge plumes. Geology 35:587–590

Goren L, Aharonov E, Mulugeta G, Koyi HA, Mart Y (2008) Ductile deformation of passive margins: a new mechanism for subduction initiation. J Geophys Res 113, Article Number: B08411

Grove TL, Chatterjee N, Parman SW, Medard E (2006) The influence of H2O on mantle wedge melting. Earth Planet Sci Lett 249:74–89

Gurnis M, Hall C, Lavier L (2004) Evolving force balance during incipient subduction. Geochem Geophys Geosyst 5, Article Number Q07001

Hall PS, Kincaid C (2001) Diapiric flow at subduction zones: a recipe for rapid transport. Science 292:2472–2475

Hall C, Gurnis M, Sdrolias M, Lavier LL, Müller RD (2003) Catastrophic initiation of subduction following forced convergence across fracture zones, Earth Planet. Sci Lett 212: 15–30

Hauff F, Hoernle K, Schmidt A (2003) Sr-Nd-Pb composition of Mesozoic Pacific oceanic crust (Site 1149 and 801, ODP Leg 185): implications for alteration of ocean crust and the input into the Izu-Bonin-Mariana subduction system. Geochem Geophys Geosyst 4, Article Number: 8913

Hawkesworth CJ, Gallagher K, Hergt JM, McDermott F (1993) Trace element fractionation processes in the generation of island arc basalts. Philos Trans R Soc London Ser A 342: 179–191

Hawkesworth CJ, Turner SP, McDermott F, Peate DW, van Calsteren P (1997) U-Th isotopes in arc magmas: implications for element transfer from the subducted crust. Science 276:551–555

Hebert LB, Antoshechkina P, Asimow P, Gurnis M (2009) Emergence of a low-viscosity channel in subduction zones through the coupling of mantle flow and thermodynamics, Earth Planet. Sci Lett 278:243–256

Hermann J, Muntener O, Scambelluri M (2000) The importance of serpentinite mylonites for subduction and exhumation of oceanic crust. Tectonophysics 327:225–238

Hilde TWE, Uyeda S, Kroenke L (1976) Evolution of the western Pacific and its margin. Tectonophysics 38: 145–165

Holbrook WS, Lizarralde D, McGeary S, Bangs N, Diebold J (1999) Structure and composition of Aleutian island arc and implications for continental crustal growth. Geology 27: 31–34

Honda S, Saito M (2003) Small-scale convection under the back-arc occurring in the low viscosity wedge, Earth Planet. Sci Lett 216:703–715

Honda S, Yoshida T (2005) Application of the model of small-scale convection under the island arc to the NE Honshu subduction zone. Geochem Geophys Geosyst 6, Article Number: Q06004

Honda S, Saito M, Nakakuki T (2002) Possible existence of small-scale convection under the back arc. Geophys Res Lett 29:20–43

Honda S, Yoshida T, Aoike K (2007) Spatial and temporal evolution of arc volcanism in the northeast Honshu and Izu-Bonin arcs: evidence of small-scale convection under the island arc? Isl Arc 16:214–223

Honda S, Gerya T, Zhu G (2010) A simple three-dimensional model of thermo–chemical convection in the mantle wedge. Earth Planet Sci Lett 290:311–318

Hsu KJ (1971) Franciscan melange as a model for eugeosunclinal sedimentation and underthrusting tectonics. J Geophys Res 76:1162–1170

Ishikawa T, Nakamura E (1994) Origin of the slab component in arc lavas from across-arc variation of B and Pb isotopes. Nature 370:205–208

Ishikawa T, Tera F (1999) Two isotopically distinct fluid components involved in the Mariana Arc: evidence from Nb/B ratios and B, Sr, Nd, and Pb isotope systematic. Geology 27:83–86

Ishizuka O, Taylor RN, Milton JA, Nesbitt RW (2003) Fluid-mantle interaction in an intra-oceanic arc: constraints from high-precision Pb isotopes, Earth Planet. Sci Lett 211: 221–236

Ishizuka O, Taylor RN, Milton JA, Nesbitt RE, Yuasa M, Sakamoto I (2006) Variation in the mantle sources of the northern Izu arc with time and space – Constraints from

high-precision Pb isotopes. J Volcanol Geotherm Res 156: 266–290

Ito E, Stern RJ (1986) Oxygen-isotopic and strontium isotopic investigations of subduction zone volcanism – the case of the Volcano Arc and the Marianas Island-Arc. Earth Planet Sci Lett 76:312–320

Iwamori H (1998) Transportation of H2O and melting in subduction zones, Earth Planet. Sci Lett 160:65–80

Iwamori H (2007) Transportation of H2O beneath the Japan arcs and its implications for global water circulation. Chem Geol 239:182–198

Jagoutz O, Müntener O, Burg J-P, Ulmer P, Jagoutz E (2006) Lower continental crust formation through focused flow in km-scale melt conduits: the zoned ultramafic bodies of the Chilas Complex in the Kohistan island arc (NW Pakistan). Earth Planet Sci Lett 242:320–342

Jull M, Kelemen PB (2001) On the conditions for lower crustal convective instability, J. Geophys. Res., B. Solid Earth Planets 106:6423–6446

Jung H, Karato S (2001) Water-induced fabric transitions in olivine. Science 293:1460–1463

Karig DE (1982) Initiation of subduction zones: implications for arc evolution and ophiolite development. Geol Soc Lond Spec Pub 10:563–576

Karson J, Dewey JF (1978) Coastal Complex, western Newfoundland: an early Ordovician oceanic fracture zone. BullGeol Soc Amer 89:1037–1049

Kay SM, Kay RW (1985) Aleutian tholeiitic and calc-alkaline magma series: 1. The mafic phenocrysts. Contrib Mineral Petrol 90:276–290

Kay SM, Kay RW (1991) Creation and destruction of lower continental crust. In: Stoeckhert B, Wedepohl KH (eds) Crustal dynamics; pathways and records, International Journal of Earth Sciences, vol 80, 2, Springer, Berlin, pp 259–278

Kay SM, Kay RW (1993) Delamination and delamination magmatism. In: Green AG, Kroener A, Goetze HJ, Pavlenkova N (eds) New horizons in strong motion; seismic studies and engineering practice, Tectonophysics, vol 219, 1–3, Elsevier, Amsterdam, Netherlands, pp 177–189

Kelemen PB, Hart SR, Bernstein S (1998) Silica enrichment in the continental upper mantle via melt/rock reaction. Earth Planet Sci Lett 164:387–406

Kelemen P, Hanghoj K, Greene A (2003) One view of the geochemistry of subduction-related magmatic arcs, with an emphasis on primitive andesite and lower crust. In: Rudnick RL (ed) The crust, treatise on geochemistry, vol 3. Elsevier Pergamon, Oxford, pp 593–659

Kelemen PB, Rilling JL, Parmentier EM, Mehl L, Hacker BR (2004a) Thermal structure due to solid-state flow in the mantle wedge beneath arcs. In: Eiler JM (ed) Inside the subduction factory, vol 138, Geophys Monogr Ser. AGU, Washington, DC, pp 293–311

Kelemen PB, Yogodzinski GM, Scholl DW (2004b) Along-strike variation in the Aleutian island arc: genesis of high Mg# andesite and implications for continental crust. In: Eiler JM (ed) Inside the subduction factory, vol 138, Geophys Monogr Ser. AGU, Washington, DC, pp 223–276

Kelley KA, Plank T, Grove TL, Stolper EM, Newman S, Hauri E (2006) Mantle melting as a function of water content beneath back-arc basins. J Geophys Res 111, Article Number: B09208

Kemp DV, Stevenson DJ (1996) A tensile, flexural model for the initiation of subduction. Geophys J Int 125:73–94

Kessel R, Schmidt MW, Pettke T, Ulmer P (2005) The trace element signature of subduction zone fluids, melts, and supercritical liquids at 120–180 km depth. Nature 437:724–727

Kimura J-I, Stern RJ (2009) Neogene volcanism of the Japan island arc: the K-h relationship revisited. In: Circum pacific tectonics, geologic evolution, and ore deposits. Arizona Geological Society Digest, Arizona Geological Society, Tucson, vol 22, pp 187–202

Kimura J, Yoshida T (2006) Contributions of slab fluid, mantle wedge and crust to the origin of quaternary lavas in the NE Japan arc. J Petrol 47:2185–2232

Kimura J-I, Stern RJ, Yoshida T (2005) Re-initiation of subduction and magmatic responses in SW Japan during Neogene time. Geol Soc Am Bull 117:969–986

Kimura J-I, Hacker B.R, van Keken PE, Kawabata H,Yoshida T, Stern RJ (2009) Arc basalt simulator version 2, a simulation for slab dehydration and fluid-fluxed mantle melting for arc basalts: modeling scheme and application. Geochem Geophys Geosyst 10, Article Number: Q09004

Kodaira S, Sato T, Takahashi N, Ito A, Tamura Y, Tatsumi Y, Kaneda Y (2006) Seismological evidence for variable growth of crust along the Izu intraoceanic arc. J Geophys Res 112, Article Number: B05104

Kodaira S, Sato T, Takahashi N, Miura S, Tamura Y, Tatsumi Y, Kaneda Y (2007) New seismological constraints on growth of continental crust in the Izu-Bonin intra-oceanic arc. Geology 35:1031–1034

Kodaira S, Sato T, Takahashi N, Yamashita M, No T, Kaneda Y (2008) Seismic imaging of a possible paleoarc in the Izu-Bonin intraoceanic arc and its implications for arc evolution processes. Geochem Geophys Geosyst 9, Article Number: Q10X01

Krebs M, Maresch WV, Schertl H-P, Münker C, Baumann A, Draper G, Idleman B, Trapp E (2008) The dynamics of intra-oceanic subduction zones: a direct comparison between fossil petrological evidence (Rio San Juan Complex, Dominican Republic) and numerical simulation. Lithos 103:106–137

Kushiro I, Syono Y, Akimoto S (1968) Melting of a peridotite nodule at high pressures and high water pressures. J Geophys Res 73:6023–6029

Leat PT, Larter RD (2003) Intra-oceanic subduction systems: introduction. In: Larter RD, Leat PT (eds) Intra-oceanic subduction systems: tectonic and magmatic processes, vol 219. Geological Society of London, Special Publications, London, pp 1–17

Leat PT, Riley TR, Wareham CD, Millar IL, Kelley SP, Storey BC (2002) Tectonic setting of primitive magmas in volcanic arcs: an example from the Antarctic Peninsula. J Geol Soc Lond 159:31–44

Manea VC, Manea M, Kostoglodov V, Sewell G (2005) Thermo-mechanical model of the mantle wedge in Central Mexican subduction zone and a blob tracing approach for the magma transport. Phys Earth Planet Inter 149:165–186

Manning CE (2004) The chemistry of subduction-zone fluids. Earth Planet Sci Lett 223:1–16

Marques FO, Gerya T, Nikolaeva K (2008) Subduction initiation at a passive margin: a prototype candidate. 33rd IGC, Abstract Volume, Oslo, Norway

Mart Y, Aharonov E, Mulugeta G, Ryan W, Tentler T, Goren L (2005) Analogue modelling of the initiation of subduction. Geophys J Int 160:1081–1091

Martin H (1999) Adakitic magmas: modern analogues of Archaean granitoids. Lithos 46:411–429

Martin H, Smithies RH, Rapp R, Moyen J-F, Champion D (2005) An overview of adakite, tonalite-trondhjemite-granodiorite (TTG), and sanukitoid: relationships and some implications for crustal evolution. Lithos 79:1–24

Maruyama S, Liou JG, Terabayashi M (1996) Blueschists and eclogites in the world and their exhumation. Int Geol Rev 38:485–594

Masson DG, Cartwright JA, Pinheiro LM, Whitmarsh RB, Beslier M-O, Roeser H (1994) Compressional deformation at the ocean–continent transition in the NE Atlantic. J Geol Soc London 151:607–613

McCulloch MT, Gamble JA (1991) Geochemical and geodynamical constraints on subduction zone magmatism. Earth Planet Sci Lett 102:358–374

McKenzie DP (1977) The initiation of trenches: a finite amplitude instability. In: Talwani M, Pitman WC III (eds) Island arcs, deep sea trenches and back-arc basins, vol 1, Maurice Ewing Series. AGU, Washington, DC, pp 57–61

Mitchell AHG (1984) Initiation of subduction of post-collision foreland thrusting and back-thrusting. J Geodyn 1:103–120

Moriguti T, Shibata T, Nakamura E (2004) Lithium, boron and lead isotope and trace element systematics of Quaternary basaltic volcanic rocks in northeastern Japan: mineralogical controls on slab-derived fluid composition. Chem Geol 212:81–100

Müeller S, Phillips RJ (1991) On the initiation of subduction. J Geophys Res 96:651–665

Müntener O, Kelemen PB, Grove TL (2001) The role of H2O during crystallization of primitive arc magmas under uppermost mantle conditions and genesis of igneous pyroxenites; an experimental study. Contrib Mineral Petrol 141:643–658

Nakajima J, Hasegawa A (2003a) Estimation of thermal structure in the mantle wedge of northeastern Japan from seismic attenuation data. Geophys Res Lett 30, Article Number: 1760

Nakajima J, Hasegawa A (2003b) Tomographic imaging of seismic velocity structure in and around the Onikobe volcanic area, northeastern Japan: implications for fluid distribution. J Volcanol Geotherm Res 127:1–18

Nikolaeva K, Gerya TV, Connolly JAD (2008) Numerical modelling of crustal growth in intraoceanic volcanic arcs. Phys Earth Planet Inter 171:336–356

Nikolaeva K, Gerya TV, Marques FO (2010) Subduction initiation at passive margins: numerical modeling. J Geophys Res 115, Article Number: B03406

Niu Y, O'Hara MJ, Pearce JA (2003) Initiation of subduction zones as a consequence of lateral compositional buoyancy contrast within the lithosphere: a petrological perspective. J Petrol 44(5):851–866

Obata M, Takazawa E (2004) Compositional continuity and discontinuity in the Horoman peridotite, Japan, and its implication for melt extraction processes in partially molten upper mantle. J Petrol 45:223–234

Oxburg ER, Parmentier EM (1977) Compositional and density stratification in oceanic lithosphere – causes and consequences. J Geol Soc London 133:343–355

Pascal C, Cloetingh SAPL (2009) Gravitational potential stresses and stress field of passive continental margins: insights from the south-Norway shelf. Earth Planet Sci Lett 277:464–473

Peacock SM, Wang K (1999) Seismic consequence of warm versus cool subduction metamorphism: examples from southwest and northeast Japan. Science 286:937–939

Pearce JA, Peate DW (1995) Tectonic implications of the composition of volcanic arc magmas. Annu Rev Earth Planet Sci 23:251–285

Pearce JA, Stern RJ, Bloomer SH, Fryer P (2005) Geochemical mapping of the Mariana arc-basin system: implications for the nature and distribution of subduction components. Geochem Geophys Geosyst 6, Article Number: Q07006

Pichavant M, Macdonald R (2003) Mantle genesis and crustal evolution of primitive calc-alkaline basaltic liquids from the Lesser Antilles arc. In: Larter RD, Leat PT (eds) Intra-oceanic Subduction Systems: Tectonic and Magmatic Processes, vol 219. Geological Society of London, Special Publications, London, pp 239–254

Plank T, Langmuir CH (1993) Tracing trace-elements from sediment input to volcanic output at Subduction Zones. Nature 362:739–743

Platt JP (1993) Exhumation of high-pressure rocks: a review of concepts and processes. Terra Nova 5:119–133

Poli S, Schmidt MW (1995) H2O transport and release in subduction zones: experimental constraints on basaltic and andesitic systems. J Geophys Res 100:22299–22314

Poli S, Schmidt MW (2002) Petrology of subducted slabs. Annu Rev Earth Planet Sci 30:207–235

Pysklywec RN, Mitrovica JX, Ishii M (2003) Mantle avalanche as a driving force for tectonic reorganization in the southwest Pacific. Earth Planet Sci Lett 209:29–38

Rapp EP, Watson EB (1995) Dehydration melting of metabasalt at 8–32 kbar: implications for continental growth and crustal-mantle recycling. J Petrol 36:891–931

Regenauer-Lieb K, Yuen DA, Branlund J (2001) The initiation of subduction: critically by addition of water? Science 294: 578–580

Reymer A, Schubert G (1984) Phanerozoic addition rates to the continental crust and crustal growth. Tectonics 3:63–77

Ring U, Brandon MT, Willett SD, Lister GS (1999) Exhumation processes. In: Ring U, Brandon MT, Lister GS, Willett SD (eds) Exhumation processes: normal faulting, ductile flow, and erosion, Geological Society, London, Special Publications, 154, pp 1–27

Rudnick RL, Gao S (2003) The composition of the continental crust. In: Rudnick RL (ed) The crust, treatise on geochemistry, vol 3. Elsevier, Oxford, pp 1–64

Ryan JG, Morris J, Tera F, Leeman WP, Tsvetkov A (1995) Cross-arc geochemical variations in the Kurile Arc as a function of slab depth. Science 270:625–627

Sajona FG, Maury RC, Bellon H, Cotten J, Defant M (1996) High field strength element enrichment of Pliocene-Pleistocene island arc basalts, Zamboanga Peninsula, western Mindanao (Philippines). J Petrol 37:693–726

Sajona FG, Maury RC, Prouteau G, Cotten J, Schiano P, Bellon H, Fontaine L (2000) Slab melt as metasomatic

agent in island arc magma mantle sources, Negros and Batan (Philippines). Isl Arc 9:472–486
Schellart WP, Freeman J, Stegman DR, Moresi L, May D (2007) Evolution and diversity of subduction zones controlled by slab width. Nature 446:308
Schmidt MW, Poli S (1998) Experimentally based water budgets for dehydrating slabs and consequences for arc magma generation. Earth Planet Sci Lett 163:361–379
Shibata T, Nakamura E (1997) Across-arc variations of isotope and trace element compositions from Quaternary basaltic rocks in northeastern Japan: implications for interaction between subducted oceanic slab and mantle wedge. J Geophys Res 102:8051–8064
Shimoda G, Nohda S (1995) Lead isotope analyses: an application to GSJ standard rock samples. Human Environ Stud 4:29–36
Shreve RL, Cloos M (1986) Dynamics of sediment subduction, melange formation, and prism accretion. J Geophys Res 91:10229–10245
Sizova E, Gerya T, Brown M, Perchuk LL (2009) Subduction styles in the Precambrian: insight from numerical experiments. Lithos. doi:10.1016/j.lithos.2009.05.028
Smith IEM, Worthington TJ, Price RC, Gamble JA (1997) Primitive magmas in arc-type volcanic associations: examples from the southwest Pacific. Can Mineral 35:257–273
Solomatov VS (2004) Initiation of subduction by small-scale convection. J Geophys Res 109, Article Number: B05408
Stern RJ (2002) Subduction zones. Rev Geophys 40:3-1–3-38
Stern RJ (2004) Subduction initiation: spontaneous and induced. Earth Planet Sci Lett 226:275–292
Stern RJ, Bloomer SH (1992) Subduction zone infancy: examples from the Eocene Izu-Bonin-Mariana and Jurassic California arcs. Geol Soc Am Bull 104:1621–1636
Stern RJ, Fouch MJ, Klemperer SL (2003) An overview of the Izu-Bonin-Mariana subduction factory. In: Eiler J (ed) Inside the subduction factory, vol 138, Geophys Monogr Ser. AGU, Washington, DC, pp 175–222
Stolper E, Newman S (1994) The role of water in the petrogenesis of Mariana trough magmas, Earth Planet. Sci Lett 121:293–325
Straub SM, Layne GD (2003) The systematic of chlorine, fluorine, and water in Izu arc front volcanic rocks: implications for volatile recycling in subduction zones. Geochim Cosmochim Acta 67:4179–4203
Straub SM, LaGatta AB, Martin-DelPozzo AL, Langmuir CH (2008) Evidence from high-Ni olivines for a hybridized peridotite/pyroxenite source for orogenic andesites from the central Mexican Volcanic Belt. Geochem Geophys Geosyst 9, Article Number: Q03007
Taira A, Saito S, Aoike K, Morita S, Tokuyama H, Suyehiro K, Takahashi N, Shinohara M, Kiyokawa S, Naka J, Klaus A (1998) Nature and growth rate of the Northern Izu-Bonin (Ogasawara) arc crust and their implications for continental crust formation. Isl Arc 7:395–407
Takahashi N, Kodaira S, Klemperer SL, Tatsumi Y, Kaneda Y, Suyehiro K (2007) Crustal structure and evolution of the Mariana intra-oceanic island arc. Geology 35:203–206
Takahashi N, Kodaira S, Tatsumi Y, Yamashita M, Sato T, Kaiho Y, Miura S, No T, Takizawa K, Kaneda Y (2009) Structural variations of arc crusts and rifted margins in the southern Izu-Ogasawara arc-back arc system. Geochem Geophys Geosyst 10, Article Number: Q09X08
Tamura Y (1994) Genesis of island arc magmas by mantle derived bimodal magmatism: evidence from the Shirahama Group. Jpn: J Petrol 35:619–645
Tamura Y, Tatsumi Y, Zhao DP, Kido Y, Shukuno H (2002) Hot fingers in the mantle wedge: new insights into magma genesis in subduction zones. Earth Planet Sci Lett 197: 105–116
Tatsumi Y, Eggins S (1995) Subduction-zone magmatism. Blackwell Science, Cambridge, MA, 211 pp
Tatsumi Y, Hanyu T (2003) Geochemical modeling of dehydration and partial melting of subducting lithosphere: toward a comprehensive understanding of high-Mg andesite formation in the Setouchi volcanic belt, SW Japan. Geochem Geophys Geosyst 4, Article Number: 1081
Tatsumi Y, Stern RJ (2006) Manufacturing continental crust in the subduction factory. Oceanography 19:104–112
Tatsumi Y, Shukuno H, Tani K, Takahashi N, Kodaira S, Kogiso T (2008) Structure and growth of the Izu-Bonin-Mariana arc crust: 2. Role of crust-mantle transformation and the transparent Moho in arc crust evolution. J Geophys Res 113, Article Number: B02203
Taylor B, Martinez F (2003) Back-arc basin basalt systematic. Earth Planet Sci Lett 210:481–497
Toth J, Gurnis M (1998) Dynamics of subduction initiation at pre-existing fault zones. J Geophys Res 103:18053–18067
Tsuchiya N, Suzuki S, Kimura J-I, Kagami H (2005) Evidence for slabmelt/mantle reaction: petrogenesis of Early Cretaceous and Eocene high-Mg andesites from the Kitakami Mountains, Japan. Lithos 79:179–206
Turner S, Foden J (2001) U, Th and Ra disequilibria, Sr, Nd, and Pb isotope and trace element variations in Sunda arc lavas: predominance of a subducted sediment component. Contrib Mineral Petrol 142:43–57
Turner S, Hawkesworth C (1997) Constraints on flux rates and mantle dynamics beneath island arcs from Tonga-Kermadec lava geochemistry. Nature 389:568–573
Turner S, Hawkesworth CJ, Rogers N, Bartlett J, Worthington T, Hergt J, Pearce JA, Smith IME (1997) 238U-230Th disequilibria, magma petrogenesis, and flux rates beneath the depleted Tonga-Kermadec island arc. Geochim Cosmochim Acta 61:4855–4884
Ueda K, Gerya T, Sobolev SV (2008) Subduction initiation by thermal–chemical plumes. Phys Earth Planet Inter 171:296–312
Uyeda S, Ben-Avraham Z (1972) Origin and development of the Philippine Sea. Nature 240:176–178
Van der Lee S, Regenauer-Lieb K, Yuen DA (2008) The role of water in connecting past and future episodes of subduction. Earth planet Sci Lett 273:15–27
Van Keken PE, King SD (2005) Thermal structure and dynamics of subduction zones: insights from observations and modeling. Phys Earth Planet Inter 149:1–6
van Keken PE, Kiefer B, Peacock SM (2002) High resolution models of subduction zones: implications for mineral dehydration reactions and the transport of water into the deep mantle. Geochem Geophys Geosyst 3, Article Number: 1056
Vlaar NJ, Wortel MJR (1976) Lithospheric aging, instability and subduction. Tectonophysics 32:331–351
Wyss M, Hasegawa A, Nakajima J (2001) Source and path of magma for volcanoes in the subduction zone of northeastern Japan. Geophys Res Lett 28:1819–1822

Yogodzinski GM, Volynets ON, Koloskov AV, Seliverstov NI, Matvenkov VV (1994) Magnesian andesites and the subduction component in a strongly calcalkaline series at the Piip volcano, far Western Aleutian. J Petrol 35:163–204

Yogodzinski GM, Lees JM, Churikova TG, Dorendorf F, Woerner G, Volynets ON (2001) Geochemical evidence for the melting of subducting oceanic lithosphere at plate edges. Nature 409:500–504

Zack T, Foley SF, Rivers T (2002) Equilibrium and disequilibrium trace element partitioning in hydrous eclogites (Trescolmen, central Alps). J Petrol 43:1947–1974

Zandt G, Gilbert H, Owens TJ, Ducea M, Saleeby J, Jones CH (2004) Active foundering of a continental arc root beneath the southern Sierra Nevada in California. Nature (Lond) 431:41–46

Zhao DP (2001) Seismological structure of subduction zones and its implications for arc magmatism and dynamics. Phys Earth Planet Inter 127:197–214

Zhao DP, Hasegawa A, Horiuchi S (1992) Tomographic imaging of P and S wave velocity structure beneath north-eastern Japan. J Geophys Res 97:19909–19928

Zhao DP, Mishra OP, Sanda R (2002) Influence of fluids and magma on earthquakes: seismological evidence. Phys Earth Planet Inter 132:249–267

Zhu G, Gerya TV, Yuen DA, Honda S, Yoshida T, Connolly JAD (2009) 3-D Dynamics of hydrous thermalchemical plumes in oceanic subduction zones. Geochem Geophys Geosyst 10, Article Number Q11006

Chapter 3
The Subductability of Continental Lithosphere: The Before and After Story

J.C. Afonso and S. Zlotnik

What I cannot create, I do not understand
R. Feynman

3.1 Introduction

Although once believed that continental crust could not be subducted to significant depths due to its relative buoyancy, it is now accepted that relatively large sections of continental crust were subducted to depths >100 km and exhumed at numerous locations worldwide (cf. Chopin 2003). The discovery of metamorphic diamonds (e.g. Kokchetav massif) and especially of pyroxene exsolution in garnets (e.g., Otrøy Island, Sulu metamorphic belt) further demonstrated the possibility of ultra-deep subduction of continental crust to depths >250 km (cf. Chopin 2003; Ernst and Liou 2008, and references therein). Detailed thermobarometry and chronologic studies, and the fact that these ultra-high pressure (UHP) belts outcrop today, reflect the viability of effective exhumation mechanisms acting during the evolution of orogens. Analog experiments and numerical simulations of continental collision have demonstrated that both subduction of continental crust to depths of ~100–150 km and rapid exhumation are an integral part of an orogenic cycle (Gerya et al. 2006; Warren et al. 2008; Yamato et al. 2008; Beaumont et al. 2009; Li and Gerya 2009). These studies have also shown that the final depth that continental material can reach and the style of exhumation are dependent on a number of factors, foremost among these are the convergence rate and the assumed rheology of both crust and mantle. The thermal structure of the incoming plate and erosion rates can also play a secondary role (Yamato et al. 2008; Li and Gerya 2009). The style of exhumation predicted by these studies include: pulse-like buoyant exhumation (dominated by either one or more pulses), syncollisional exhumation with two or more stages with distinct velocity, and continuous circulation in the critical wedge of an accretional prism. Of these, only the first two have been successful in reproducing HP-UHP P-T-paths and crustal structures compatible with observations (Beaumont et al. 2009; Li and Gerya 2009).

In all studies of continental subduction, the relative buoyancy of the continental material with respect to the surrounding mantle (or crust) is a key factor. It ultimately controls the fate of the different subducted continental rocks (e.g. sedimentary, volcanic, igneous, etc.) and therefore the recycling of important chemical species such as large-ion lithophile elements (LILEs) and water (e.g., Ono 1998; Rapp et al. 2008). The way in which this positively buoyant material affects the dynamics of the collision depends strongly on the mechanical behavior (i.e., rheology) of the crustal units and on their bulk composition. If the crust is felsic and strong enough to maintain its mechanical coherence during subduction, it will effectively and continuously increase the positive buoyancy of the slab. Eventually, after a critical volume of continental crust has subducted, the slab reaches the state of "neutral buoyancy" and subduction stops (e.g., Ranalli et al. 2000). In contrast, if this felsic crust is relatively soft, it will be delaminated during subduction and thicken

J.C. Afonso
Department of Earth and Planetary Sciences, GEMOC ARC Key Centre for Geochemical Evolution and Metallogeny of Continents, Macquarie University, North Ryde, Sydney, NSW 2109, Australia
e-mail: juan.afonso@mq.edu.au

S. Zlotnik
School of Geosciences/School of Mathematical Sciences, Monash University, Clayton Campus, Melbourne, VIC 3800, Australia

D. Brown and P.D. Ryan (eds.), *Arc-Continent Collision*, Frontiers in Earth Sciences,
DOI 10.1007/978-3-540-88558-0_3,

at shallow levels (e.g., Faccenda et al. 2009), making its contribution to increasing the positive buoyancy of the slab negligible. On the other hand, if more mafic crustal components are considered, as suggested for the lower crust by field and xenolith evidence (e.g., Rudnick and Gao 2003), eventual eclogitization of these components could increase the negative buoyancy of the slab, promoting subduction of crustal material. Similarly, the geometry and nature (volcanic vs non-volcanic) of the colliding passive margin should exert a non-negligible influence. It is evident therefore that the final configuration and evolution of the collision will depend on the interplay between these factors.

The possibility of continental material being subducted to depths pertaining to the transition zone, and perhaps even to the lower mantle, is supported by geochemical isotopic signatures in magmas erupted in island arcs presumably from source regions at depth >300 km (Workman et al. 2004). Another set of evidence for deep subduction is provided by experimental data at extremely high pressures (e.g., Irifune et al. 1994; Dobrzhinetskaya and Green 2007; Rapp et al. 2008; Zhai and Ito 2008; Wu et al. 2009). These studies indicate that a "depth of no return" for continental derived materials may exist at around 8.5–9 GPa, where dense silicates start to form (e.g., Irifune et al. 1994; Dobrzhinetskaya and Green 2007; Rapp et al. 2008; Zhai and Ito 2008). Irifune et al. (1994) hypothesized about the settings in which subduction of continental derived materials would occur. These authors proposed active ocean–ocean and ocean–continent subduction zones as one potential environment, where significant amounts of sediments are being subducted into the mantle (e.g., Clift and Vannucchi 2004). The other, arguably more important, is along zones of continental collision (arc–continent and continent–continent), where large pieces of continental crust could be subducted. However, the actual amount of continental material that can be subducted below the point of no return and its final fate has never been assessed with coupled thermomechanical-thermodynamic numerical models.

This paper attempts to provide new insights into the large-scale evolution of an arc–continent collision from the subduction of normal oceanic lithosphere to the cease of subduction. We use 2D fully dynamic thermomechanical-thermodynamic numerical simulations and a new thermodynamic database that includes all major phases relevant to deep subduction of continental material. Particular emphasis is put on the self-consistent evolution of convergence velocities (i.e., no velocity boundary conditions imposed) and on the roles of compositional heterogeneities, rheological properties, and thermal structures of the subducting plate.

3.2 Methods and Numerical Setup

In the following three sections we briefly describe the methodology and numerical setup used in this study. The interested reader in these topics should refer to the appendices, where we provide a detailed explanation of all the numerical strategies and their implementations into our code.

3.2.1 Bulk Properties of Rocks

When direct comparisons with geological, geochemical, and geophysical evidence are sought, numerical simulations need to include realistic thermophysical properties for all the materials composing the model. In recent years, particular attention has been given to the self-consistent combination of mineral physics and thermodynamic calculations into fluid dynamical simulations of the Earth (e.g., Gerya et al. 2006; Li and Gerya 2009; Tirone et al. 2009; Nakagawa et al. 2009; Yamato et al. 2007). This approach has two important advantages over other standard methods. One is that it maximizes the internal consistency of the system by "tightening" together all physical parameters and governing equations through a thermodynamic model. Therefore, a given change in density due for instance to a change in P-T conditions is also reflected in appropriate (thermodynamically consistent) changes in all other parameters (e.g., heat capacity, compressibility, etc.). The other advantage is that it allows realistic modelling of metamorphic reactions driven by the dynamics of the system. These include not only solid state reactions but also hydration/dehydration reactions, partial melting, and melt-solid interactions. This in turn is essential when comparing real petrological and geophysical observables with simulation results (Gerya et al. 2006; Beaumont et al. 2009; Li and Gerya 2009).

Following previous pioneering works (e.g., Sobolev and Babeyko 2005; Gerya et al. 2006) we couple our thermo-mechanical solvers with thermodynamic data sets that account for all metamorphic reactions and phase changes (see Appendix A). Relevant bulk properties (e.g., density, thermal expansion coefficient, etc.) are calculated a priori for different compositions, water contents, and P-T range of interest, and saved in "look-up" tables that are read by the thermo-mechanical solver during execution. One of the main differences with previous models is that while they make use of thermodynamic databases strictly suitable at pressures $\lesssim$ 3 Gpa, we use an augmented-modified version of the Holland and Powell (1998) database (revised in 2002) valid up to ~25 GPa that includes all major phases obtained in UHP experiments on compositions relevant to the continental crust (e.g., Irifune et al. 1994; Wu et al. 2009; Ono 1998; Zhai and Ito 2008; Rapp et al. 2008). Since it has been suggested that some dense silicates such as K-hollandite ($KAlSi_3O_8$) and CAS ($CaAl_4Si_2O_{11}$) could be responsible for the recycling of continental material and important trace elements into the transition zone or lower mantle (Zhai and Ito 2008; Rapp et al. 2008; Wu et al. 2009), using a database that correctly predicts phase relations at such conditions is of particular relevance. See Appendix A.6 for details on the thermodynamic formalism and database used in this study.

3.2.2 Starting Materials

Our reference starting model is shown in Fig. 3.1. It is composed of five main domains, namely the continent *sensu stricto*, the passive margin, the oceanic domain, the arc domain, and the sublithospheric mantle. Each of these domains is characterized by a compositional and thermal structure based on real case examples. In the case of the continental, oceanic, and passive margins domains, our reference model is based on the integrated geophysical-petrological model of Fernàndez et al. (2010) across the Namibian volcanic margin. In the case of the 2D arc crustal structure, we use the present-day structure of the Mariana arc as a proxy (Takahashi et al. 2008). The continental domain is made of a granodioritic upper crust, a mafic granulitic lower crust, a depleted shallow lithospheric mantle, and a deep (less depleted) lithospheric mantle. The oceanic domain is composed of a thin layer of pelagic sediments, a basaltic upper crust, a gabbroic lower crust, a depleted shallow lithospheric mantle, and a deep (less depleted) lithospheric mantle. The reference passive margin includes some layers from the continental and oceanic domains plus two additional layers: a silicoclastic sedimentary wedge (miogeoclinal prism) and a gabbroic underplating body. The arc structure includes a tonalitic upper/middle crust, a gabbroic lower crust, a depleted shallow lithospheric mantle, and a deep lithospheric mantle. The bulk composition of all lithologies used in our models are listed in Tables 3.1 and 3.2. Rheological parameters are listed in Table 3.4 and reference strength envelopes for the initial conditions are shown in Fig. 3.2.

The degree of hydration of the incoming crustal units is as follows: pelagic sediments contain 7.36 wt% water (Rapp et al. 2008), oceanic upper (metabasalt) and lower (metagabbros) crusts contain 2.96 and 1.97 wt% water, respectively, to represent the effects of hydrothermal alteration (Carlson 2003). The sediments making up the miogeoclinal prism in the passive margin contain an initial water content of 7.55 wt%. For the serpentinized shallow upper mantle underneath the oceanic crust we assume a generous serpentinization degree of 20%, equivalent to an original water content of ~2.6 wt% (Schmidt and Poli 1998). The entire continental crust is assumed to be dry, while the lower crust of the arc contains 2 wt% of water (Takahashi et al. 2008). Note that in this work we use "water" for pure H_2O, although the actual aqueous fluid in a subduction environment may be different (i.e., silica-rich).

3.2.3 General and Boundary Conditions

The mechanical boundary conditions in our numerical domain are periodic on the lateral sides and free-slip at the top and bottom (Fig. 3.1a). Importantly, we do not impose velocity boundary conditions and therefore the dynamics of our simulations is controlled entirely by the balance between internal forces (e.g., buoyancy, shear resistance, etc.). The resolution varies between models, but typical nodal spacings are between 5.0 and 2.2 km, with around 4.6 and 15 million markers, respectively.

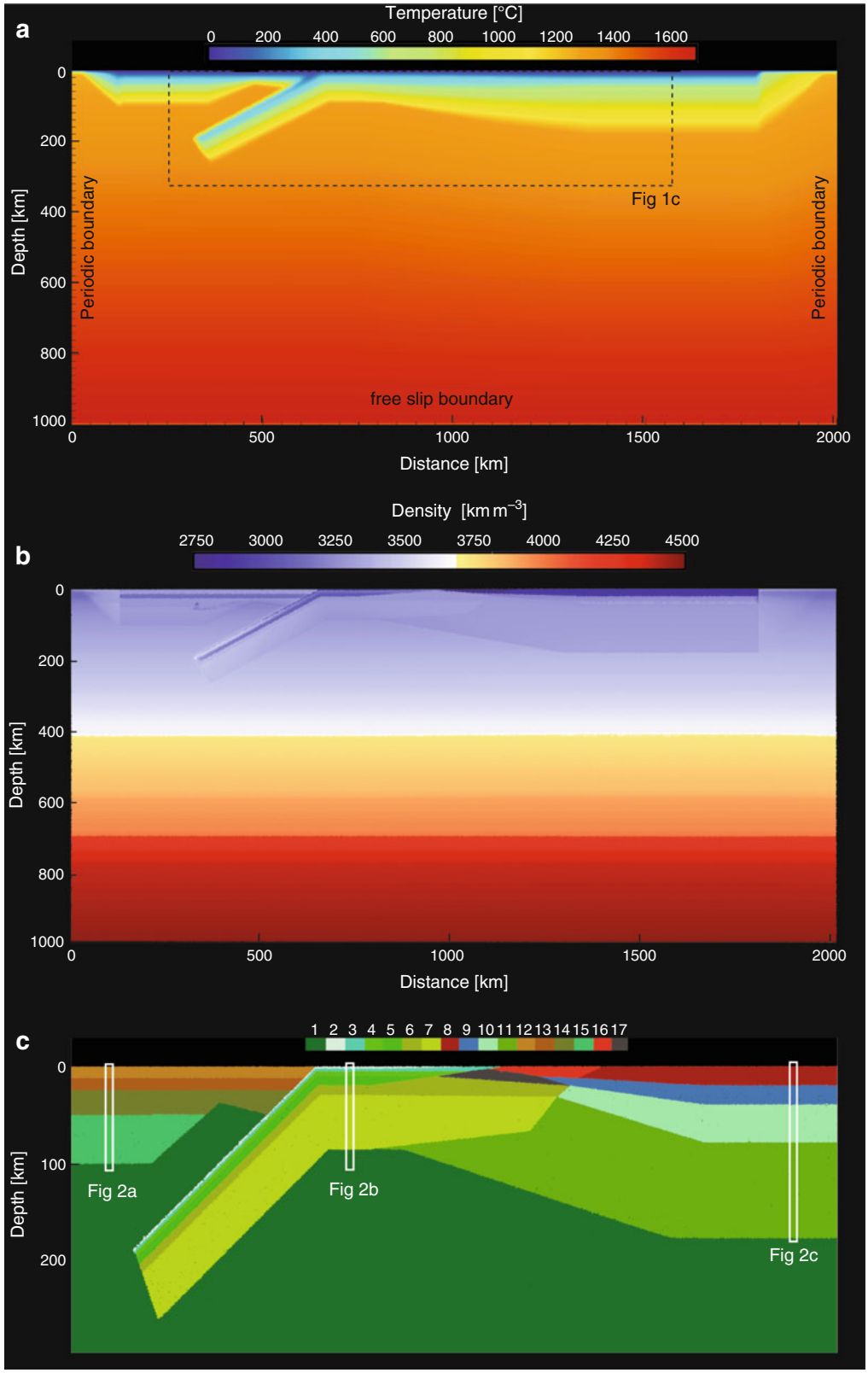
a
Temperature [°C]
0 200 400 600 800 1000 1200 1400 1600
Depth [km]
0 200 400 600 800 1000
Periodic boundary
Periodic boundary
Fig 1c
free slip boundary
0 500 1000 1500 2000
Distance [km]
b
Density [km m−3]
2750 3000 3250 3500 3750 4000 4250 4500
Depth [km]
0 200 400 600 800 1000
0 500 1000 1500 2000
Distance [km]
c
1 2 3 4 5 6 7 8 9 10 11 12 13 14 15 16 17
Depth [km]
0 100 200
Fig 2a
Fig 2b
Fig 2c

Table 3.1 Model bulk rock compositions for crustal layers [wt%]

Composition	Cont. UC[a]	Cont LC[b]	Arc MC[c]	Oce. UC[d]	Oce. LC[e]	Pelag. sed.[f]	Prism sed.[g]	Underplating[h]	Cont LC felsic[i]
SiO_2	65.81	53.52	65.80	48.99	52.58	54.32	60.69	53.63	63.67
TiO_2	0.66	0.82	0.48	1.27	0.59	0.84	0.64	0.60	0.69
Al_2O_3	15.31	16.94	15.70	14.89	13.83	17.42	12.34	14.11	15.04
FeO	5.34	8.59	4.49	9.86	6.74	7.79	5.40	6.88	6.04
MgO	2.82	7.26	1.82	7.56	12.48	3.08	2.57	12.73	3.60
CaO	4.10	9.61	5.03	11.26	10.52	1.54	6.17	10.73	5.26
Na_2O	3.31	2.66	3.91	2.70	1.20	3.93	2.52	1.22	3.40
K_2O	2.65	0.61	0.79	0.49	0.09	3.73	2.11	0.09	2.31
H_2O	0*	0*	1.99	2.96	1.97	7.36	7.55	0*	0*

*Initial water content, these values change as the materials are hydrated/dehydrated
[a]Estimated using 70% of upper crust composition and 30% of middle crust composition from Rudnick and Gao (2003)
[b]From Rudnick and Gao (2003)
[c]Recast from the middle (tonalitic) crust composition of Takahashi et al. (2008)
[d]Recast from the normal MORB composition in Schilling et al. (1983)
[e]Recast from Behn and Kelemen (2003)
[f]Recast from the MAG-1 composition of Rapp et al. (2008)
[g]Recast from the GLOSS composition of Plank and Langmuir (1998)
[h]Same as Oce. LC but dry
[i]Middle crust composition of Rudnick and Gao (2003)

Table 3.2 Model bulk rock compositions for mantle domains [wt%]

Composition	Sublith. Mantle[a]	Harzburg. Mantle[b]	Tecton mantle[c]	Cont. upp. Mantle[d]
SiO_2	45.34	43.28	44.84	45.60
TiO_2	0.00	0.00	0.00	0.00
Al_2O_3	4.53	1.11	2.63	1.79
FeO	8.16	7.26	8.28	7.31
MgO	38.08	47.62	41.51	43.51
CaO	3.53	0.61	2.52	1.74
Na_2O	0.36	0.12	0.18	0.05
K_2O	0.03	0.00	0.03	0.00
H_2O	0.00	0.00	0.00	0.00

[a]Recast from McDonough and Sun (1995)
[b]Recast from the average Slave xenoliths composition in Afonso et al. (2008a)
[c]Recast from the average Tecton peridotite composition in Afonso et al. (2008a)
[d]Representative average of the first 100 km of continental lithospheric mantle from Fernàndez et al. (2010)

We assume incomplete hydration of mantle lithologies in the mantle wedge due to the channelization of fluids (Hyndman and Peacock 2003), which is not explicitly included in our simulations. We therefore assign a maximum water content of 4%, in agreement with inferences from seismic studies (Hyndman and Peacock 2003; Carlson and Miller 2003).

As subducted lithologies reach saturation conditions, water is released through dehydration reactions (cf. Tatsumi and Eggins 1995) and starts its migration towards the surface (see details in Appendix A.5). Eventually, it may reach lithologies at undersaturated conditions (typically in the mantle wedge) that will incorporate all or some of this water by hydration

Fig. 3.1 (**a**) Initial thermal structure and mechanical boundary conditions of our reference model. The dashed rectangle refers to the zoom in Fig. 1c. (**b**) Initial density structure of the reference model. (**c**) The different colours indicate rock types (different bulk compositions): 1 = Sublithospheric mantle, 2 = pelagic sediments, 3 = oceanic upper crust, 4 = oceanic lower crust, 5 = serpentinized mantle, 6 = harzburgitic (depleted) mantle, 7 = deep oceanic lithospheric mantle (Tecton composition), 8 = upper continental crust, 9 = lower continental crust, 10 = harzburgitic (depleted) shallow continental mantle, 11 = deep continental lithospheric mantle (Tecton composition, 12 = arc upper crust, 13 = arc lower crust, 14 = arc shallow mantle (harzburgitic), 15 = deep arc mantle (Tecton composition), 16 = sediments of the miogeoclinal prism, 17 = underplating. Refer to Tables 1 and 2 for compositions.

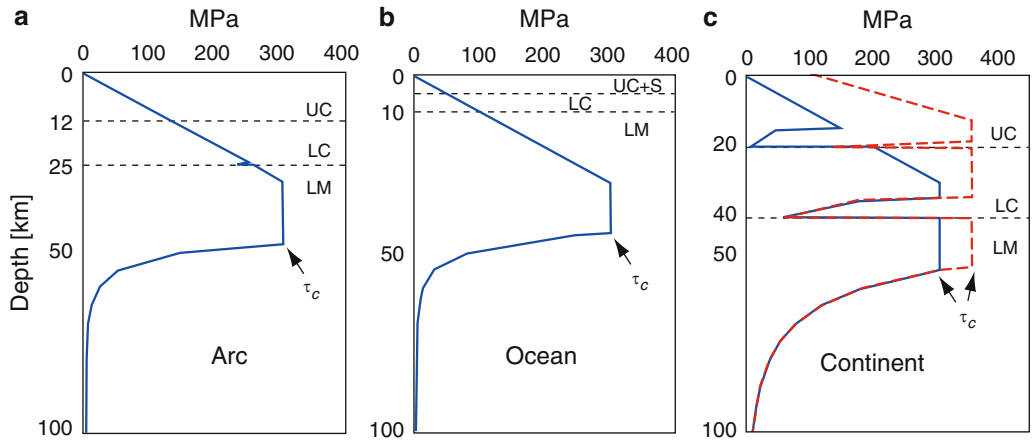

Fig. 3.2 Representative strength envelopes for the arc, ocean and continental domains (strain rate $=10^{-16}$ s^{-1}). The solid blue and dashed red lines in the continental domain indicate two end-member cases used in our simulations (strong vs soft crust). τ_c is the critical yield stress used to simulate high-pressure failure. See text for details.

reactions. If not all of the incoming water is consumed by unsaturated lithologies, the remaining water keeps being advected until it is totally consumed in hydrating other parts of the model or until it reaches the surface. Figure 3.3 shows the water content (i.e., bound water in hydrous assemblages) in four important lithologies as a function of temperature, pressure, and initial bulk water content.

Melting of the mantle is modelled as batch melting (Appendix A.4), including the extraction of water from partially molten rocks through an appropriate bulk partition coefficient. The amount of melt extracted from mantle parcels is tracked through the simulation and used to compute depletion effects on the bulk density and solidus temperature of the residue (Appendix A.4). In the present work we do not model the chemical interaction between melts and the solid mantle (e.g., metasomatic silica enrichment).

3.3 Results

In this section we summarize the main results of a series of 80 numerical simulations of continental subduction. First we describe the evolution and general aspects of a reference model that satisfy a number of geophysical and geological evidence, in which the only kinematic boundary condition is a zero horizontal velocity in the far-end of the continental plate (i.e., fixed far-end). This is done in order to simulate trench retreat in our reference model, but we relax this condition in subsequent simulations. Secondly, we analyze a number of factors with the potential to exert an influence on the dynamics of the system, and discuss their implications for interpreting arc–continent collisional settings.

3.3.1 The Reference Model

The evolution of the reference model is characterized by four main stages (Fig. 3.4). The first stage is the verticalization of the slab under the force of gravity. Since the initial angle of subduction is considerably shallow, this stage is characterized by fast velocities in the sublithospheric mantle (Figs. 3.4a–c and 3.5). Dip-slip motion along the interface between the two plates (i.e., subduction channel) initiates during this stage, in which the convergence velocity between the plates steadily increases until a quasi-stable oceanic subduction configuration is reached (Fig. 3.5). During this-quasi-stable subduction stage the magnitude of both plate and convecting mantle velocities remains almost constant (Stage 2 in Fig. 3.5), reflecting a steady balance between internal forces (e.g., negative buoyancy vs viscous resistance). The arrival of the passive margin perturbs the convergence velocity only slightly, given that the increase in the negative buoyancy provided by the subduction of the dense underplating material is somewhat counterbalanced

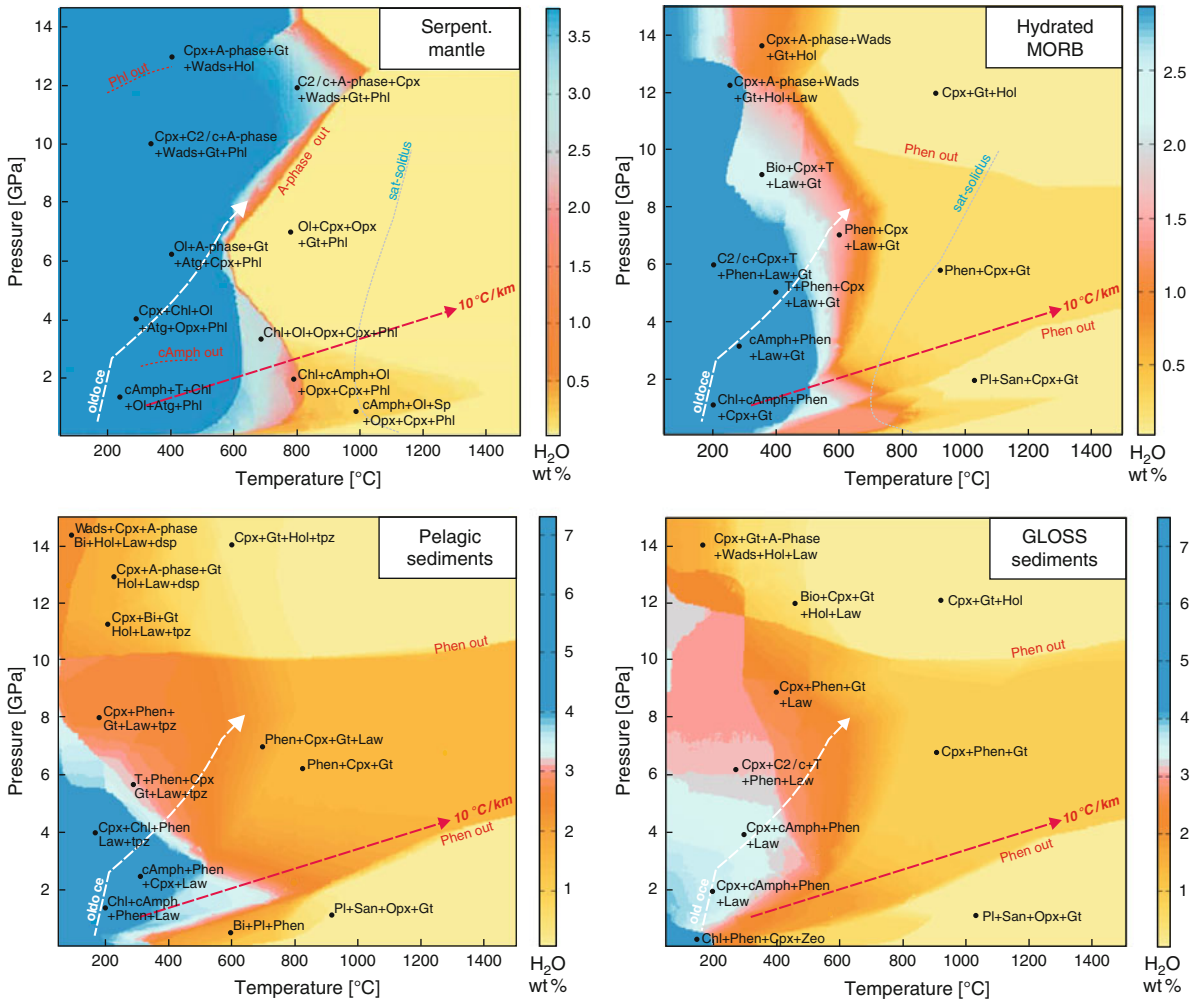

Fig. 3.3 Stable mineral assemblages and bound water content for four relevant rock types as a function of pressure and temperature. These plots were calculated using an augmented/modified version of the Holland and Powell (1998) thermodynamic database (see Appendix A.6). Two illustrative geotherms for a "hot" and "cold" slab are shown. Note that the scales saturate at water contents of 4 %.

by the low density sediments of the miogeoclinal prism (Fig. 3.1c). We stress here that model velocities are not imposed as boundary conditions, but emerge self-consistently in the simulations as response to internal forces. For the range of values adopted for the rheological parameters (Table 3.4), the velocities in our simulations are comparable to those measured by geodetic surveys (Sella et al. 2002).

The third stage begins with the arrival of the continental crust to the trench (Fig. 3.4 g–i). At this point the convergence velocity increases during a short period of time due to a concomitant increase in the total negative buoyancy of the slab. This latter increase is consequence of two main effects: (1) densification of the subducted crust due to changes in the mineral assemblages (i.e., low-pressure to high-pressure facies), and (2) increase in the thermal thickness of the lithospheric mantle (i.e., more cold material being subducted). We note that the first effect is likely overestimated in the present model given the assumptions of complete thermodynamic equilibrium and dry lithologies for the continental crust (see Table 3.1). We return to (1) and (2) in Sects. 3.3 and 3.6.2.

The fourth and final stage in the evolution of the system is a rapid decrease in convergence velocities

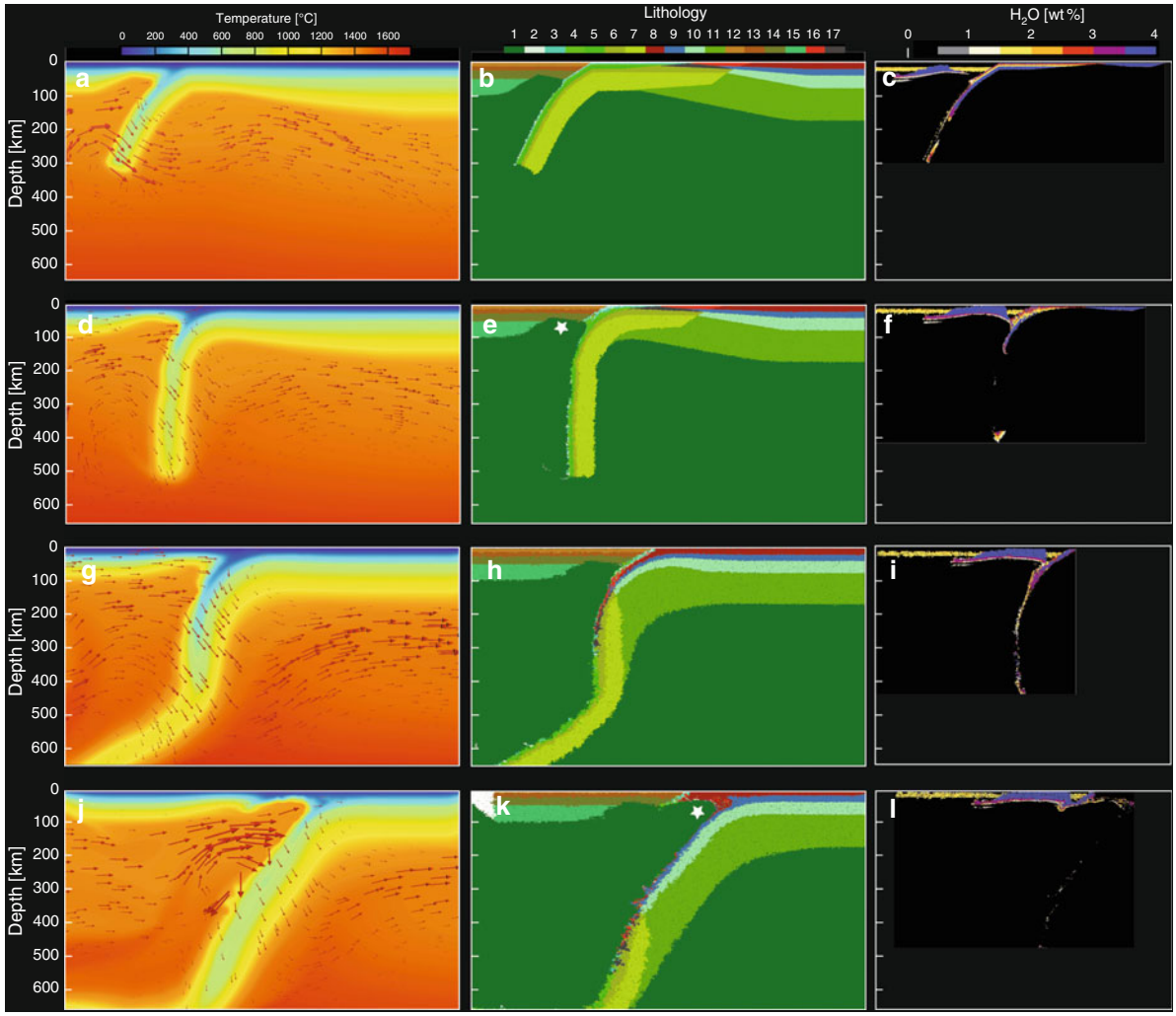

Fig. 3.4 Evolution of the reference model discussed in the text. Left column depicts thermal and velocity structures. Middle column shows the rock types (numbers as in Fig 1c). Right column depicts bound water content. The white stars in e anf k denote the location of partial melting. See text for details.

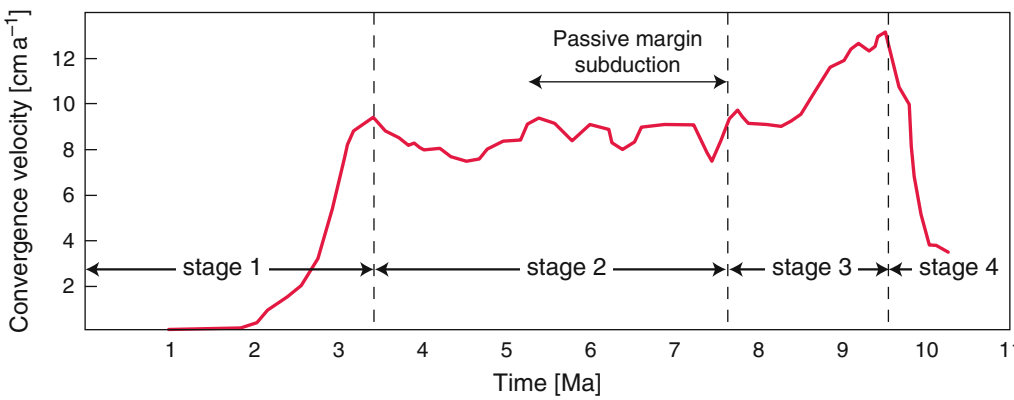

Fig. 3.5 Evolution of convergence velocity predicted by our reference model (Fig. 4). The different stages discussed in the text are shown.

due to the delamination at lower crustal levels of the continental lithospheric mantle (Figs. 3.4j–l and 3.5). This stage is similar to the "decoupled collision regime" of Faccenda et al. (2009). As discussed later, the occurrence of such a delamination and its final configuration are largely controlled by the brittle (plastic) rheological model assumed for the crustal components and by the rheological structure of the lithospheric mantle.

A few interesting observations can be made from this simulation. For instance, by looking at the convergence velocity only (Fig. 3.5, from stage 2), one could assign the dramatic slow down from ~9 to < 4 cm a^{-1} to an increase in positive buoyancy of the subducting continental plate (note that the increase during stage 3 is relatively small and short-lived and therefore difficult to identify in reconstructions based on geological/geophysical data). Indeed, a similar evolution of surface velocities (abrupt decrease) has been identified for the Asia-India collision (Guillot et al. 2003) and recently interpreted in terms of the total buoyancy of the Indian plate (Capitanio et al. 2010). Although this scenario is a generally accepted rule of thumb for continental collision, and likely applicable to the Asia-India, our reference model shows another potential scenario. In the simulation, the slow down in the convergence between the colliding plates is not a consequence of a decrease in the total negative buoyancy of the subducting plate, but the result of a mechanical decoupling between the mantle and crust. This decoupling effectively isolates two portions of the originally coherent continental plate, each with different rheological behavior and buoyancy. While the lithospheric mantle (and part of the lower crust) sinks into the convecting mantle due to its large negative buoyancy, the "lighter" crust remains unsubducted with its shallowest parts relatively rigid. Notably, although the continental lithospheric mantle is highly depleted in fusible components (intrinsically buoyant), the thermal structure of the sinking portion makes it more dense than the "fertile" sublithospheric mantle. This will be true as long as the entire sinking volume remains mechanically coherent. Additionally, for similar reasons (i.e., mechanical coherence), the deeper and denser portion of the (oceanic) slab exerts an extra "pull" on the upper continental portion, thus favoring its sinking.

The delamination process described above also causes a lateral shift of the locus of partial melting as well as a change in the amount of melting. Prior to delamination, the locus of partial melting is located below the arc (star in Fig. 3.4e), where the upper plate is thinner. The amount of partial melting in this zone generated in each time step during the retreat of the slab varies between 1 and 5%. At first, these values seem too low when compared with predictions from kinematic models of subduction, which usually depict values of ca. 10–20% at 2.5–3 GPa (e.g., Tatsumi and Eggins 1995; Katz et al. 2003). This apparent discrepancy between these two kind of models can be understood as follows. In kinematic models, the slab is forced to subduct with a constant angle and velocity, neglecting the actual balance of internal forces. Such configuration results in a typical corner flow in the mantle wedge, where hot and fertile (i.e., unmelted) material is continuously brought up to shallow depths as consequence of the circulation generated by the imposed velocity on the slab (e.g., Hebert et al. 2009). When this hot material reaches depths of ca. 50 km, it experiences decompression melting and then it is dragged back into deeper levels according to the corner flow circulation. Moreover, most "petrological" models of partial melting in the mantle wedge assume an initial thermal distribution given by a kinematic model (usually a corner flow) and then estimate "instantaneous" melt fractions adopting a batch (equilibrium) model (e.g., Katz et al. 2003). In reality, however, the amount of melting that a mantle parcel can experience is a function of previous events of melt extraction. This is a consequence of the fact that the solidus of a residual peridotite after melt extraction is higher than that of a fertile peridotite (Jordan 1978). In our simulations, the amount of melt generated by a mantle parcel during a time step considers this depletion effect (Appendix A.4) and therefore the material in the mantle wedge is less susceptible to melting, unless it is either hydrated or replaced by fertile mantle. The former occurs at shallow levels below the arc, where temperatures are low enough to allow stabilization of water in the assemblage, and therefore reduce the solidus. The latter is more unlikely in the reference model because of the sub-horizontal flow generated below the arc by the retreating slab (Fig. 3.4). In other words, the typical circulation pattern predicted by a corner flow model does not occur when the slab is in rollback. However, as shown in Sect. 3.5, simulations in which either the arc is fixed or both plates are allow to move freely, exhibit much less trench retreat and a flow pattern in the mantle wedge similar to a corner flow.

The space created by the delamination of the lithospheric mantle is rapidly filled by rising sublithospheric mantle (Fig. 3.4j–l). This has two major effects in the system: (1) the arc magmatism ceases to exist due to lack of water input from subducted material and the modification of the flow, and (2) the migration of the locus of partial melting, which is displaced towards the forearc following the tip of the delamination (star in Fig. 3.4k). The maximum amount of (dry) melting generated in the mantle in each time step is now ~2–2.5%. Whether the delamination process stops or continues until all the continental mantle has been recycled into the mantle depends on several factors such as the thermal/mechanical heterogeneities in the lithosphere, total length of the continent, and the rheological properties of the crust. Parallel simulations in which rheological heterogeneities (i.e., small lateral variations) are included in the lithosphere indicate that the delamination process stops shortly after its initiation (within a few Ma) due to the development of a necking instability and the final breakoff of the slab. Finally, we note that the development of such a delamination seems to be controlled by the fixed continental plate condition (i.e., forced rollback). Models in which the subducting continental plate is allowed to move horizontally (see below) do not promote delamination.

Several features predicted by the reference model resemble geological observations in collisional settings. For instance, the evolution of the surface velocities are compatible with estimations of convergence velocity across the Himalayas, Uralides, and Appalachians (e.g., Dahlen and Suppe 1988; Guillot et al. 2003). The decline of arc volcanism shortly after the arrival of continental crust has also been identified in a number of arc–continent collisional settings (e.g., Uralides, Caledonides). On the other hand, the uplift and possible volcanism predicted in the forearc following the initiation of the delamination is more ambiguous. There are no modern equivalents of this stage in an arc–continent setting (although a remarkably similar evolution has been proposed for Eastern Anatolia; see Keskin 2007), and it is not clear whether available geological evidence in past arc–continent collisions is consistent with this evolutionary model. However, this final stage in our reference model is indeed consistent with geological and geophysical evidence in decoupled orogens in continent–continent collisional settings (e.g., Northern Apennines, Carpathians).

3.3.2 Compositional Effects

It is now generally accepted that the composition of the continental lithospheric mantle is far from homogenous and that different compositional domains are characterized by different physical responses (e.g., Griffin et al. 2009; Afonso et al. 2010). It is therefore genuine to ask whether such compositional stratifications and lateral variations can influence the dynamics of an arc–continent collision. In order to test this we conducted experiments in which the composition of the uppermost lithospheric mantle varies between a highly depleted composition (harzburgitic mantle in Table 3.2) to a slightly depleted one (Tecton mantle in Table 3.2). We stress that these two end-members are based on estimations from a large number of xenoliths recovered in many different continental environments (Griffin et al. 2009) and on integrated petrological-geophysical modelling of passive margins (Fernàndez et al. 2010; Fullea et al. 2010).

As shown in Fig. 3.6a, the only noticeable difference between these two models is that the one with a relatively fertile composition tends to generate faster convergence when the continental lithospheric mantle begins to subduct. Although the first order behavior of the system is not affected, the maximum difference in convergence velocities exceeds ~10 cm yr^{-1}, which suggest that compositional heterogeneities in the lithospheric mantle also have the potential to affect the evolution of an arc–continent collision. Even more depleted compositions than the one used in our models for the uppermost subcontinental lithospheric mantle have been suggested (Griffin et al. 2009). However, changing the composition from harzburgitic to dunitic in the shallow lithospheric mantle result in a slight decrease of the overall density of the plate, and thus we do not expect to see large differences in the general evolution of our models.

3.3.3 Lithospheric Structure of the Passive Margin and Continental Plate

It is expected that the thermal structure of the passive margin and continental lithosphere will influence the dynamics of continental subduction. However, predicting

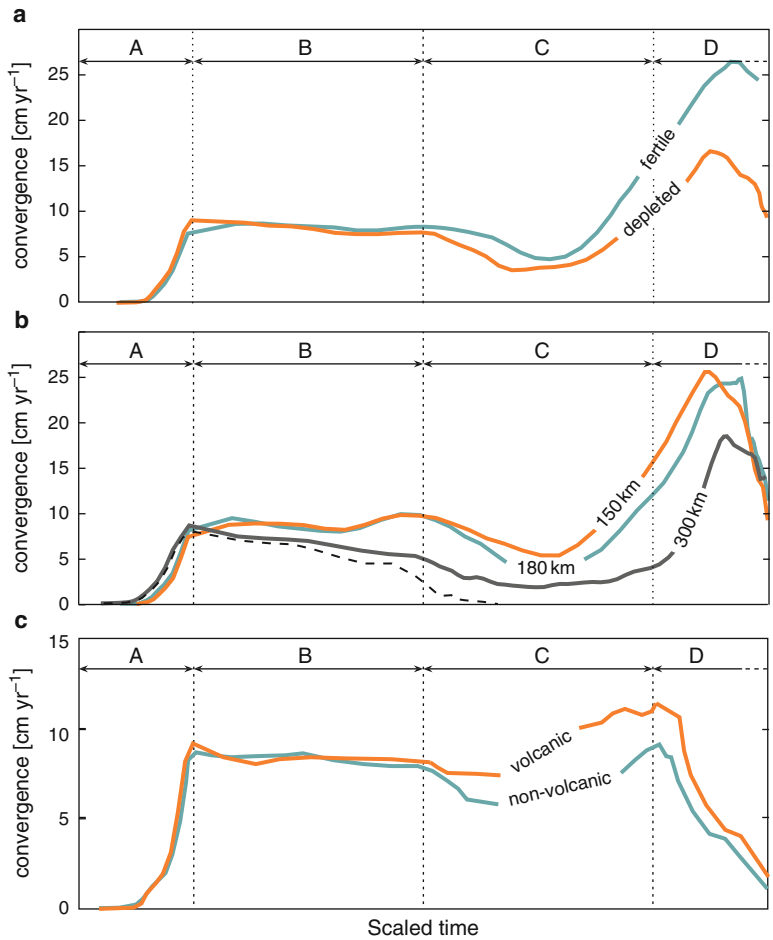

Fig. 3.6 (**a**) Evolution of convergence velocity for models with depleted vs fertile continental lithospheric mantle. (**b**) Evolution of convergence velocity for models with different thermal thicknesses in the continental plate. Numbers indicate thermal thickness in km. The dashed line represents a model with a thickness of 300 km in which the pre-exponetial factor of the lithospheric mantle has been changed from 1.1×10^5 to 1.0×10^4. (**c**) As in (a) and (b) but for different types of passive margin (see Fig. 7). The curves have been smoothed in comparison with that in Fig. 5. For the three panels A = verticalization of the slab, B = subduction of oceanic lithosphere, C = subduction of passive margin, D = subduction of continental crust. Note that the absolute time has been scaled in all models to force the curves to fit a unique temporal division of A,B,C, and D stages and that all models include "soft" rheologies for the passive margin and continental crust and a fixed far-end condition (i.e. zero horizontal velocity in the far-end of the continental plate).

the response of the system to an increase or decrease in the thermal thickness is not straightforward due to the trade-off between buoyancy and viscosity. For instance, a thicker lithosphere will be denser in average (more negatively buoyant) than a thin lithosphere, and thus it should promote faster subduction. On the other hand, a colder plate means a higher viscosity, making the plate more resistant to deformation and thus favoring subduction stall. We tested possible influences of the thermal structure by running three simulations in which the thermal thickness of the continental plate varies from 150 to 300 km. Since the lateral extent of the passive margin remains the same in all three models, the thermal structure of the mantle part of the passive margin also changes accordingly (i.e., the thicker the plate the thicker the passive margin). Figure 3.6b shows the convergence velocities predicted by the three models. These results indicate that the long-term effect of increasing the thermal thickness of the subducting plate is to slow down

subduction. In other words, the "stiffening" effect is more important than the increase in negative buoyancy. Indeed, a parallel simulation with a thermal thickness of 300 km (dashed black line in Fig. 3.6b) in which the viscosity of the lithospheric mantle was slightly increased within uncertainty limits resulted in total subduction stall and slab breakoff (Sect. 3.7).

3.3.4 Volcanic Versus Non-volcanic Passive Margins

The nature of the volcanic margin (i.e., volcanic vs non-volcanic) is likely to affect collision dynamics due to their different geometries and compositions. Briefly, a typical volcanic margin is narrower than a non-volcanic one, and includes a relatively thick "magma crust" composed of heavily intruded continental crust plus underplated mafic to ultra-mafic material (the so-called high-velocity bodies, Geoffroy 2005). The reference model described above is based on the structure of the Namibian volcanic margin, and thus we assume this model to represent a typical volcanic margin. For the non-volcanic case, we modified the passive margin structure of the reference model to accommodate a thinner crust of less mafic composition (Fig. 3.7). Note that the rheology of this new body changes accordingly to be consistent with the new composition (see Tables 3.4 and 3.5).

The resulting convergence velocities from two simulations that differ only in the geometry and composition of the passive margin are shown in Fig. 3.6c. To the first-order, the evolution of both models are similar, and they only differ in the absolute value of their convergence velocity. The volcanic passive margin becomes slightly faster once the passive margin begins to subduct, and remains faster for as long as the slab remains mechanically coherent. The maximum absolute difference in velocity occurs during the subduction of the passive margin and reaches a peak value of ~ 2.5 cm yr^{-1}, although for most of the simulation is 2 cm yr^{-1}.

3.3.5 Models with Free Plates

We carried out experiments in which both plates were allowed to move freely in response to the large-scale circulation. In this case, the continental plate is 1,000 km long (i.e., 500 km longer than in the reference model) and the numerical box was extended to a total of 3,000 km. This models could be representative of a scenario in which the continental plate is bounded in the far end by a mid-ocean ridge. Two snapshots of the thermal and velocity fields for the same model are shown in Fig. 3.8, from which it is evident that the dynamics of the system is considerably different from those in which the continental plate is fixed at the far end (Fig. 3.4). The convergence velocity in this case is dominated by the motion of the subducting plate rather than the arc. This indicates that when both plates are free to move (i.e., both having a mid-ocean ridge as the

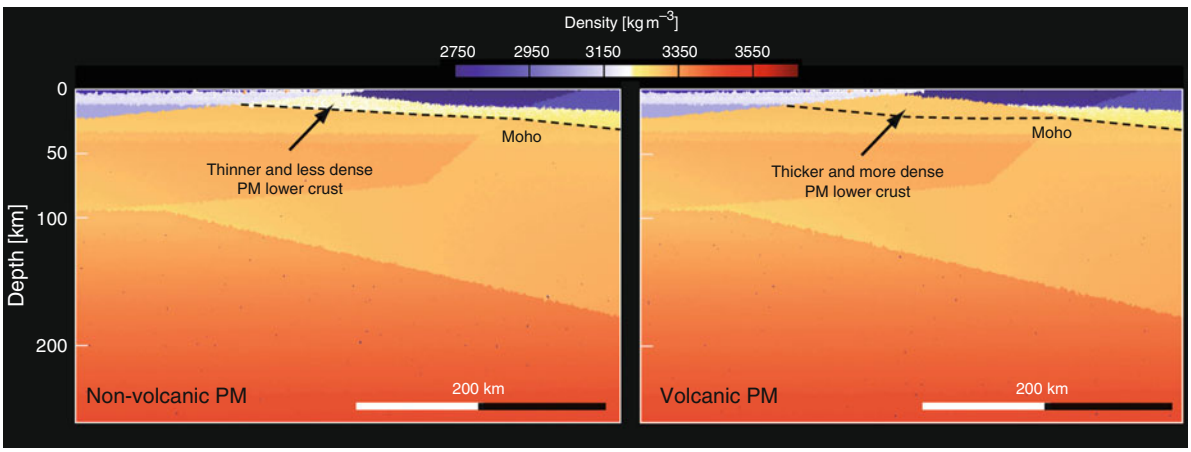

Fig. 3.7 Initial density structures for two different models of passive margins tested in this study. See text for details.

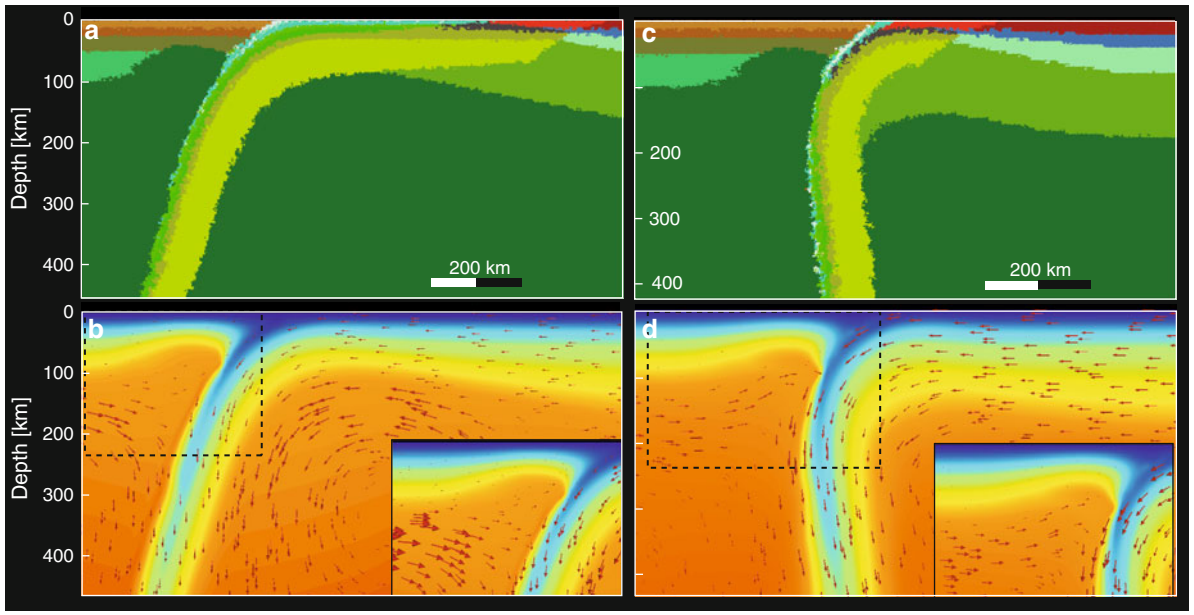

Fig. 3.8 Two snapshots at different times from a simulation with both plates free. The dashed boxes in b and d refer to the zoom in the lower corner. Scales are as in Fig. 1a and c.

far end boundary), it is easier for the system to "slide" the long continental plate over the low viscosity asthenosphere than produce a slab rollback. The latter involves the widespread deformation (motion) of large volumes of deep and viscous sublithospheric material, which is inefficient in terms of dissipation of available potential energy. Contrarily, when the horizontal component of the velocity in the continental plate is towards the trench, deformation is localized only along narrow areas adjacent to the slab and in the low viscosity asthenosphere (Fig. 3.8b, d). This scenario is favored by the strong non-linear dependence of viscosity on strain rate (Appendix A.3) and represents a more efficient mechanism of energy dissipation. Note that although the continental plate moves towards the trench, the global flow results in a slow trench retreat.

A consequence of this type of motion is that the mantle wedge beneath the arc experiences a circulation pattern more similar to a typical corner flow (zooms in Fig. 3.8b, c). As previously mentioned, this type of circulation favors a continuous replenishment of hot fertile mantle into the mantle wedge, which in turn favors larger degrees of melting. However, although the actual large scale flow is substantially different from the one produced by slab rollback, we see no significant difference in the general pattern and absolute values of convergence velocities between the two cases. Also, the delamination at lower crustal levels described above do not occur in models with free plates, which end in either a slab breakoff or in the subduction of large section of continental lithosphere, depending on the rheological parameters assumed in the simulations (see next section).

3.3.6 Rheological Effects: The Ghost in the Machine

Capturing in a numerical model the whole range of possible rheological behaviors observed in both laboratory experiments and natural rock samples is a difficult task, partly because of the physical nature of the deformation mechanisms, but also due to the large experimental uncertainties in rheological parameters. The outcomes of any thermomechanical simulation are strongly dependent on the rheological parameters assumed for the materials, particularly when non-linear (i.e., non-Newtonian) constitutive relations are employed. In this section we briefly explore the influence that these assumed rheological properties

have on our simulations, as well as the implications for interpreting processes associated to collisional settings. A thorough and systematic analysis of these effects will be presented elsewhere (Zlotnik and Afonso, in preparation).

3.3.6.1 Detachment of the Oceanic Crust

It has long been suggested that the contrast in density and rheological behavior between the subducted oceanic crust and the underlying serpentinized mantle could result in a separation (decoupling) of the eclogitized oceanic crust from the rest of the slab (e.g., Ringwood 1982; van Keken et al. 1996, and references therein). Whether this process occurs in reality has important implications for the interpretation of geochemical and seismological data (van Keken et al. 1996; Lee and Chen 2007, and references therein). In our simulations, different modes of spontaneous separation of either the entire oceanic crust or part of it occur depending on the rheological stratification assumed for the oceanic domain. We observe large portions of oceanic crust detaching from the rest of the slab only for extremely low critical yield stresses ($\tau_c \lesssim 100$ MPa) in the lower oceanic crust and serpentinized mantle (Fig. 3.9a). When yield stresses in better agreement with experimental results are used (e.g., Shimada 1993; Renshaw and Schulson 2004), the volume of detached oceanic crust decrease, but do not cease to occur in our models (Fig. 3.9d). These detachments occur in response to the difference in buoyancy and rheology between the eclogitized crust and the surrounding mantle bodies (Fig. 3.9b, e).

An interesting consequence of separating the oceanic crust from the slab is related to the significant change in negative buoyancy that the slab experiences, even when the volume of detached crust is not large. As seen in Fig. 3.9b, e, the oceanic crust is the denser part of the slab at all depths down to the top of the lower mantle and it contributes approximately between 12 and 16% to the total negative buoyancy of the slab (depending on the slab´s total length). Indeed, our simulations (Fig. 3.9c, f) show a sudden decrease in convergence velocity whenever a portion of the oceanic crust is separated from the rest of the slab. Although whether these detachments get trapped at the bottom of the transition zone or sink into the lower mantle is beyond the scope of this chapter, we note that it mainly depends on the large scale flow, the viscosity contrast assumed between the upper and lower mantle, and the temperature difference between the detachments and the surrounding mantle.

3.3.6.2 The Rheology of the Continental Crust

There is no doubt that the rheology of continental crustal units plays a major role in the dynamics of the collision (e.g., Toussaint et al. 2005; Burov and Yamato 2008; Warren et al. 2008). However, the choice of representative creep laws for the different units making up the continental crust is not always straightforward. The viscous behavior of the continental upper crust has been traditionally modelled using the creep law of a "wet quartzite" (e.g., Ranalli 1995; Afonso and Ranalli 2004; Nikolaeva et al. 2008; Faccenda et al. 2009), although arbitrarily stronger creep laws have been also used (e.g., Li and Gerya 2009). On the other hand, there is much less agreement as to what creep law should be adopted for the continental lower crust. In lack of more reliable data, several choices are usually tested in the literature, ranging from relatively soft "felsic granulite" laws to much stronger "dry mafic diabase" laws (cf. Afonso and Ranalli 2004). Arguably, the modelling of the brittle behavior of rocks is even more problematic. Although most authors adopt a plastic criterion to model brittle failure, the assumed criterion varies considerably amongst different authors. In this paper we use a modified version of the von Mises criterion that accounts for material strengthening with pressure (see Appendix A.3). In contrast to most previous studies, we use a constant maximum yield stress to account for the experimentally observed phenomenon of "high-pressure failure" (e.g., Shimada 1993; Renshaw and Schulson 2004; Zang et al. 2007). We vary this yield stress between 300 and 350 MPa in agreement with experimental and theoretical estimations.

We carried out a number of simulations in which we set "soft" and "strong" rheologies to the entire crust, as well as mixed cases (e.g., strong UC and soft LC, see Tables 3.3–3.5). We find that models with a soft upper crust are characterized by two main mechanical features. Firstly, the upper crust remains mechanically decoupled from the lower crust at most conditions, even at very low strain rates ($\lesssim 1 \times 10^{-17}$ s^{-1}). Secondly, the upper crust yields viscously and/or

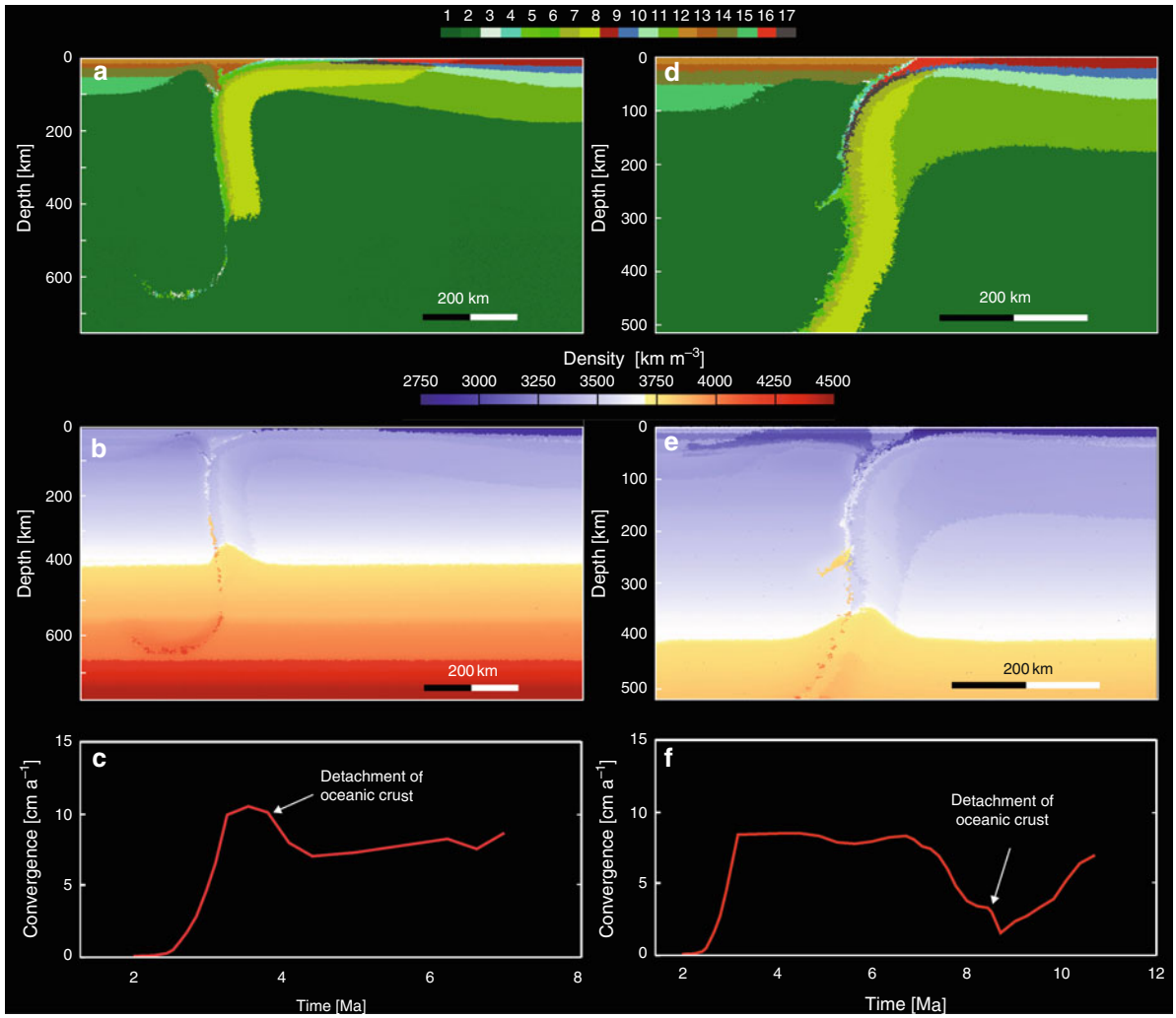

Fig. 3.9 Two different detachments of oceanic crust from the slab. In the left column the yield stress of the oceanic lower crust and serpentinized mantle (4 and 5) is 60 MPa. In the right column the yield stress of the oceanic lower crust and serpentinized mantle is 300 MPa (Table 4). Bottom panels (c and f) show the evolution of the convergence velocity for these two models.

plastically under relatively low stress levels, facilitating widespread deformation instead of localized concentration of strains. These two factors, and the fact that the upper crust is intrinsically less dense than the other lithologies involved in the collision, favor crustal thickening rather than subduction of the upper crust. When this is the case, subduction of significant volumes of upper continental down to depths >100–140 km crust is difficult to achieve in our simulations (Fig. 3.10). We observe that after an episode of accumulation of upper crust material and forced subduction to depths of ~100 km, a second episode of rapid (pulse-like) exhumation occurs in response to the build up of a critical volume of positively buoyant material (sediments + upper crust). This reinforces observations from recent works (Sobolev and Babeyko 2005; Gerya et al. 2006; Warren et al. 2008; Yamato et al. 2008; Beaumont et al. 2009; Li and Gerya 2009) in which pulse-like exhumation episodes from depths of about 100–160 km have been found to be not only possible but an integral part of orogenic cycles. However, exhumation from depths >200 km, as suggested by mineralogical evidence (e.g., Haggerty and Sautter 1990; Ye et al. 2000; Green et al. 2000; Song et al.

Table 3.3 Creep parameters

Lithology	A	n	E	V	Model bodies
Quartzite (wet)[a]	3.2×10^{-4}	2.3	154	0	*contUC, arcUC, oceSed, pmSed*
Quartzite (hard)[a]	3.2×10^{-7}	2.3	154	0	*contUC*
"Undried" diabase (wet)[b]	2.0×10^{-4}	3.4	260	0	*oceLC, arcLC*
Mafic granulite[c]	1.4×10^{4}	4.2	445	0	*contLC*
Diabase[c]	1.0×10^{2}	3.4	260	0	*oceUC*
Maryland diabase (dry)[d]	8.0	4.7	485	0	*under*
Diff. creep peridotite (wet)[e]	1.0×10^{6}	1.0	350	4	*mantle*
Disl. creep peridotite (wet)[e]	9.0×10^{1}	3.5	520	11	*mantle*
Diff. creep peridotite (dry)[e]	1.5×10^{9}	1.0	375	4	*mantle*
Disl. creep peridotite (dry)[e]	1.1×10^{5}	3.5	530	14	*mantle*

Units: pre-exponential parameter, A, in $\mathrm{Mpa}^{-n}\ s^{-1}$; Activation energy, E, in kJ mol^{-1}; Activation volume, V, in J mol^{-1} Mpa^{-1}. Activation volume is taken $= 0$ if no conclusive experimental results are available
Model bodies abbreviations: *cont* continent, *arc* arc, *oce* ocean, *UC* upper crust, *LC* lower crust, *under* underplating
References: [a]Kirby and Kronenberg 1987, [b]Shelton and Tullis 1981, [c]Kirby 1983, [d]Mackwell et al. 1998, [e]Hirth and Kohlstedt 2003

Table 3.4 Setup of the reference model

			Creep parameters	Plastic params (μ/c_0/max)	Composition	RHP (μW m^{-3})
Continent	Crust	Upper	Wet quartzite	0.6/100/300	cont. UC	1.2
		Lower	Mafic granulite	0.6/100/300	cont. LC	0.4
	Mantle	Upper	Dry peridotite		cont. UM	0.0
		Upper	Wet peridotite		Tecton	0.0
Ocean	Crust	Sedim.	Wet quartzite	0.4/0/300	Pelag. Sedim.	0.9
		Upper	Diabase	0.4/0/300	oce. UC	0.4
		Lower	Maryland diabase	0.4/0/300	oce. LC	0.4
	Mantle	Upper	Dry peridotite		Harzburg.	0.0
		Upper	Wet peridotite		Tecton	0.0
Arc	Crust	Upper	Wet quartzite	0.4/0/300	oce. UC	0.2
		Lower	Maryland diabase	0.4/0/300	oce. LC	0.0
	Mantle	Upper	Dry peridotite		Harzburg.	0.0
		Upper	Wet peridotite		Tecton	0.0
Passive margin	Volcanic	Sedim.	Wet quartzite	0.4/0/300	Prism sed.	0.8
		Under	Maryland diabase	0.4/0/300	Under.	0.0
	Non volcanic	Sedim.	Dry peridotite	0.4/0/300	Prism sed.	0.8
		Under	Wet peridotite	0.4/0/300	cont. LC	0.0
Sub lith	Mantle		Wet peridotite		Sublith. mantle	

2004; Liu et al. 2007; Scambelluri et al. 2008), has not been observed in these studies.

Models with a stronger upper continental crust are more strongly coupled to the lower crust and show less accumulation and larger subducted volumes of upper crust material before the systems stalls (Fig. 3.10). Although the density of the upper continental crust remains lower than the surrounding mantle down to depths of ~250–300 km, its higher intrinsic viscosity and low temperatures keep it mechanically coupled to the rest of the slab, allowing a more continuous subduction of this unit. However, should separation from the lower crust occur by any means at depths $<$ 250–300 km, small pieces of upper crust could potentially return to shallower depths by their own buoyancy and get entrained within the units comprising the orogen. We have not observed this in our simulations, but its importance to reconcile mineralogical observations with numerical simulations warrants more work towards this end. Below these depths, however, our simulations predict a sudden increase in the density of subducted continental material due to the appearance of stishovite, CAS, and K-hollandite in the assemblage (see Fig. 3.11), and the increase of modal

Table 3.5 Selected representative experiments discussed in the text

Model	Continent		P. margin structure	Cont. rheology		P.M. rheology		Oce. rheology		Boundary conditions
	Thickness	Mantle comp.		Creep	Plastic	Creep	Plastic	Creep	Plastic	
0024	180	Depleted	Volcanic						Soft[a]	Fixed cont.
0093	180	Fertile	Non-volcanic							Fixed cont.
0096	150	Depleted	Volcanic							Fixed cont.
0098	300	Depleted	Volcanic							Fixed cont.
0100	180	Depleted	Volcanic				Strong[b]			Fixed cont.
0102	180	Depleted	Non-volcanic				Strong[b]			Fixed cont.
0109	180	Depleted	Volcanic	Strong[c,d]						Fixed cont.
0110	180	Depleted	Volcanic	Strong[c]			Strong[b]			Fixed cont.
0111	180	Depleted	Volcanic	Strong[c]						Fixed cont.
0122	180	Depleted	Non-volcanic							Fixed cont.
0123	180	Depleted	Volcanic							Fixed cont.
0124	180	Depleted	Volcanic		Strong[e]		Strong[f]			Fixed cont.
0126	180	Depleted	Volcanic							Free plates
0202	180	Depleted	Volcanic	Strong[d]						Fixed cont.

[a]0/0/50 MPa
[b]0/0/250 MPa
[c]Upper crust: Quartzite (hard)
[d]Lower crust: Maryland Diabase
[e]0.6/100 MPa/350 MPa
[f]0.6/100 MPa/250 MPa

garnet. This new assemblage remains denser than the surrounding mantle down to the bottom of the transition zone (~660 km depth), where the ambient mantle rich in Mg-perovskite becomes denser. These predictions are in good agreement with estimations from high-T-P experiments on natural and synthetic samples with compositions representative of continental material (see Appendix A.6). It is therefore difficult to imagine a mechanism that could exhume significant volumes of subducted continental material once it has reached 250–300 km depth, although geochemical signatures could be "picked up" by ascending plumes (Hart et al. 1992; Workman et al. 2004). We thus conclude that this depth range effectively mark the "point of no return" for subducted continental material, in agreement with previous estimations from laboratory experiments (e.g., Irifune et al. 1994; Dobrzhinetskaya and Green 2007).

Note that regardless of the average rheology assumed for the continental crust or the final configuration (delamination vs slab breakoff), its lower section is prone to deep subduction and recycling for all tested conditions (Figs. 3.1, 3.4, 3.10, 3.12). The main reason for this is its high intrinsic density (e.g., Fig. 3.10), which in turn results from the dry mafic composition assumed. Although this mafic composition is based on best available estimates from outcrops, geophysical evidence, and xenoliths (Rudnick and Gao 2003), it is likely that more felsic components exist in the lower crust in some continental areas. This could somewhat restrict the amount of continental crust that can be subducted during the collision. Perhaps more important is the dry assumption. There is abundant evidence that the continental lower crust contains bound water, although the actual amount is difficult to constrain and could vary significantly across different tectonic settings (cf. Ague 2003; Rudnick and Gao 2003). Allowing for initial water contents of $\gtrsim 1\%$ in the lower crust decreases its average density (at crustal conditions) by ~ 3% due to the presence of hydrous phases (e.g., amphiboles, micas, etc.) and increases the pressure (~ 0.5 GPa) at which a low-T eclogitic assemblage (breakdown of plagioclase) first appears. It follows from the above arguments that the amount of subducted continental lower crust estimated from our simulations should represent an upper limit.

3.3.7 The Aftermath: Slab Breakoff

Although the original model of slab breakoff (Davis and Blanckenburg 1995) was proposed to explain a number of common observations in continent–

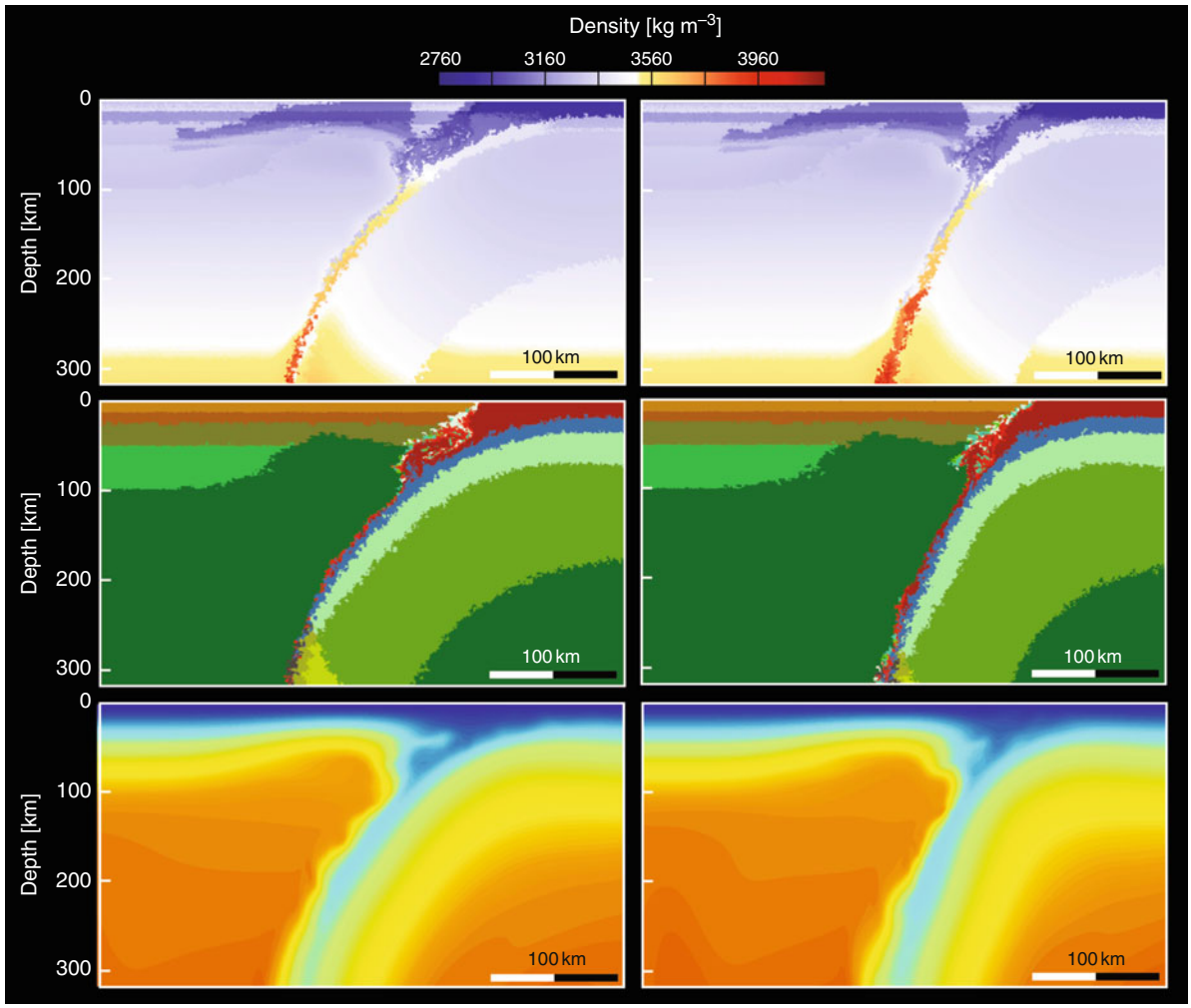

Fig. 3.10 Two snapshots of two different simulations in which the rheological parameters for the continental crust are different. Left column represents the case of a "soft" continental crust, whereas the right column includes a "strong" continental crust. Upper panels show density structure; middle panels show rock type; lower panels depict temperature field (scales as in Fig. 1a and c). See Tables 1–5 for the actual rheological parameters.

continent collision environments such as anomalous rates of uplift, metamorphic facies, post-orogenic bimodal magmatism, and P-T paths of exhumed rocks (cf. Davis and Blanckenburg 1995, 1998), it has been also suggested to be an integral part of arc–continent collisions (e.g., Dewey 2005). In our models, the necessary condition for the development of slab breakoff is that displacement along the main fault (i.e., subduction fault) decrease to values < 0.8 cm yr^{-1}. With such low values, the main fault can be considered effectively locked. As a result, the large negative buoyancy of the slab generates a significant state of tension along its entire length, which eventually get localized in regions where the slab is weakest. In our simulations this region is consistently located on the continental side of the slab (Fig. 3.12), where the high strain rates created in response to the bending of the lithosphere generate a pronounced low in the effective viscosity. No simulation in which the passive margin is subducted predicted either symmetrical necking or strain localization in the arc side. The latter does not take place due to two main factors: (1) at the time of fault locking, the arc side of the fault has been significantly cooled by thermal diffusion due to the adjacent subduction of cool material and therefore its viscosity is

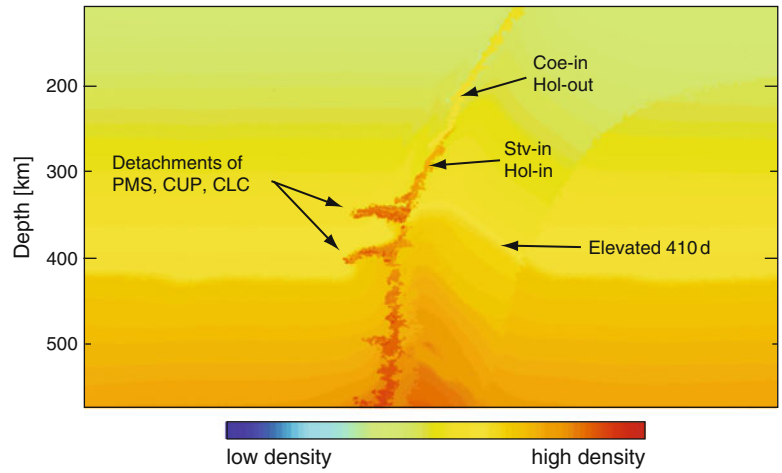

Fig. 3.11 Density structure of subducted continental material in a model with strong continental crust. Note the large jump in density due to the appearance of high-density phases stishovite and K-hollandite in the assemblages. PMS = passive margin sediments, CUP = continental upper crust, CLC = continental lower crust. The detachments tend to nucleate near the transition between "low-density" and "high-density" assemblages in response to the difference in buoyancy between the latter and the surrounding mantle.

relatively high; (2) there is no significant bending in the arc to produce high strain rates and thus low viscosity.

In contrast, models with unrealistically strong rheologies in the passive margin tend to stop subduction before significant portions of the passive margin can subduct. In this case, slab breakoff results from symmetrical necking at deeper levels, entirely within oceanic lithosphere (Fig. 3.13). This general pattern of symmetrical necking at deeper levels compares with the results obtained by Gerya et al. (2004) for intraoceanic subduction zones. However, geological evidence for partial if not total subduction of the passive margin (e.g., Urals, Caledonides) suggest that this model of slab breakoff is not entirely representative of arc–continent collisional settings.

The evolution of the slab breakoff (and all the processes associated with it) depicted in Fig. 3.12 is rapid, taking < 2 Ma to completely detach the slab after fault locking. This timescale agrees well with estimations in real arc-collisional settings (e.g., Dewey 2005). A short episode of hydrous melting ($\lesssim 1\%$) in the lithospheric mantle associated with mantle upwelling below the forearc is also observed. Although we do not model melting of crustal units, we expect a concomitant melting episode in adjacent parts of the crust. A similar short-lasted and volumetrically small episode of partial melting occurs below the arc once the slab is completely detached and sublithospheric mantle flow becomes continuous between the remaining lithosphere and the sinking slab (Fig. 3.12f). Mantle melting in the forearc thus precedes melting below the arc by ~ 0.8–1.0 Ma.

Another consequence on the breakoff evident in our simulations is the isostatic rebound of the orogen (Davis and Blanckenburg 1995) and the beginning of rapid exhumation of buoyant parcels in the orogenic wedge (Fig. 3.14b). Although the actual mechanism and timing of exhumation is beyond the scope of this paper, we highlight the following points: (1) exhumation of rocks in the orogenic wedge is an integral and self-consistent output in our experiments, (2) the orogenic wedge is highly heterogeneous in terms of its rock types (Fig. 3.14a), but with an average composition close to that of the upper crust, (3) the average degree of hydration in the orogenic wedge is high (Fig. 3.14c). Since a large variety of quartzofeldespatic rocks produce granitic melts by dehydration melting at temperatures between 800 and 1,100°C (e.g., Patiño Douce and McCarthy 1998), it is likely that at least some of the rocks being exhumed after the breakoff will experience dehydration melting and/or release of water-rich fluids (Vry et al. 2009). Together with the aforementioned observation of partial melting in the mantle, this offers a sound explanation to the common observation of post-collisional bimodal (granitic and basaltic) magmatism (Davis and

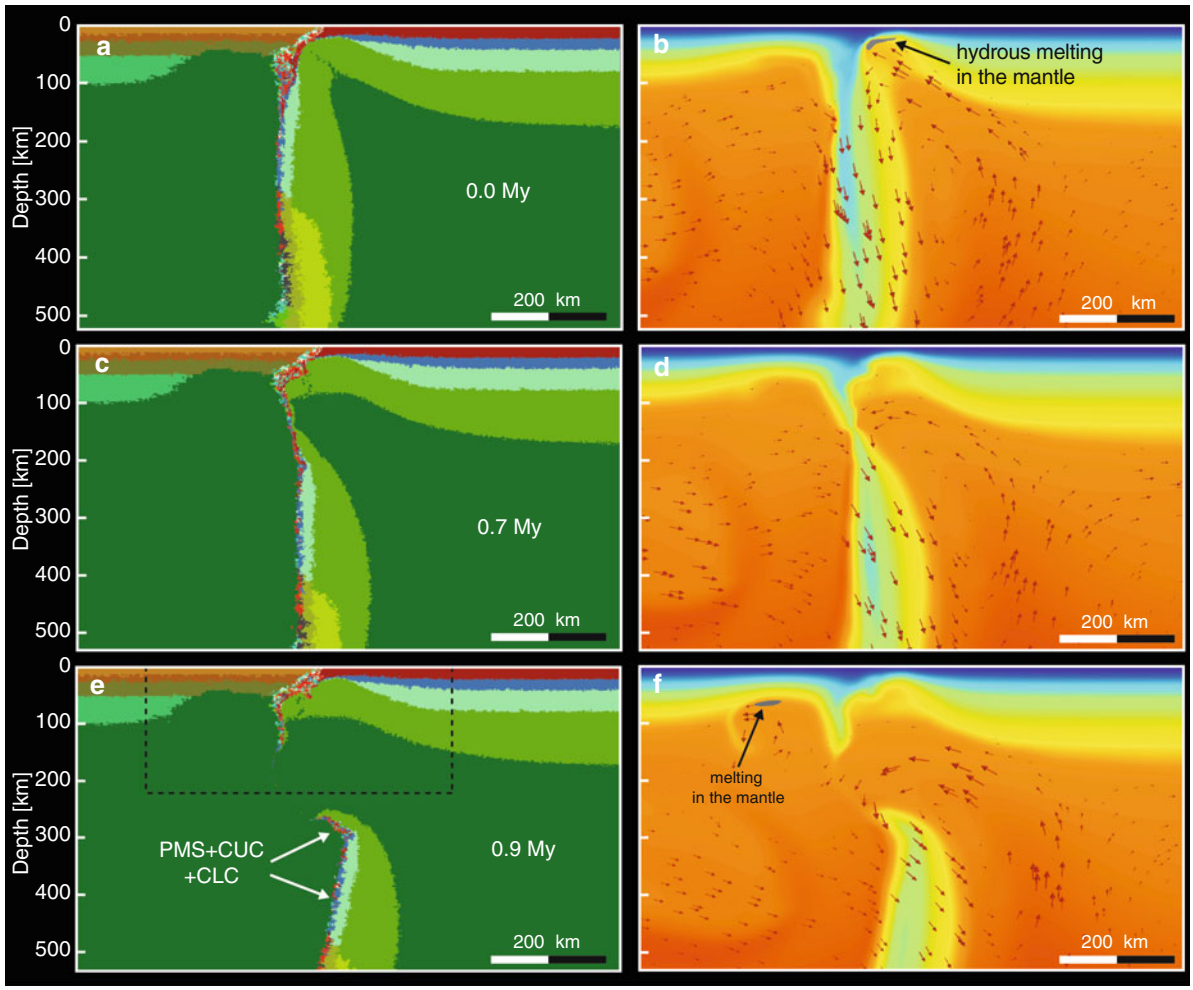

Fig. 3.12 Evolution of a typical slab breakoff in our simulations. Left column shows rock types (scale as in Fig. 1c). Right column depicts the thermal and velocity structures (scale as in Fig. 1a). Dashed box in e refers to the zoom in Fig. 15.

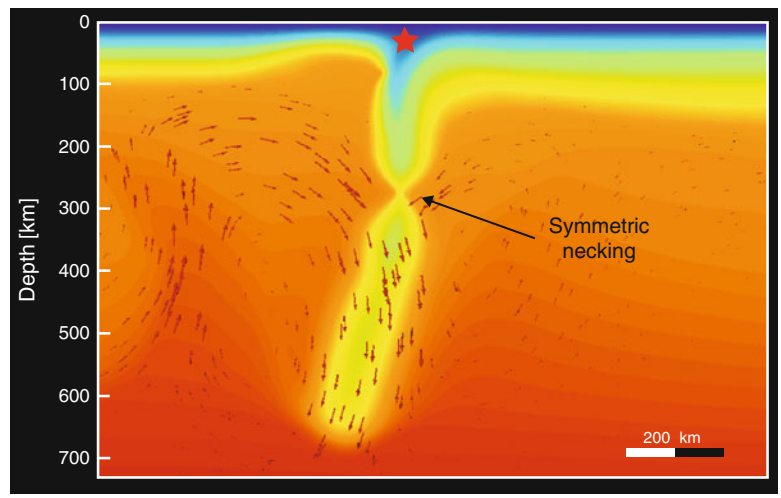

Fig. 3.13 Symmetric necking and slab breakoff arising in a model with extremely strong passive margin (yield stress = 1000 MPa and coefficient of friction = 0.8). The star indicates the location of the tip of the miogeoclinal prism.

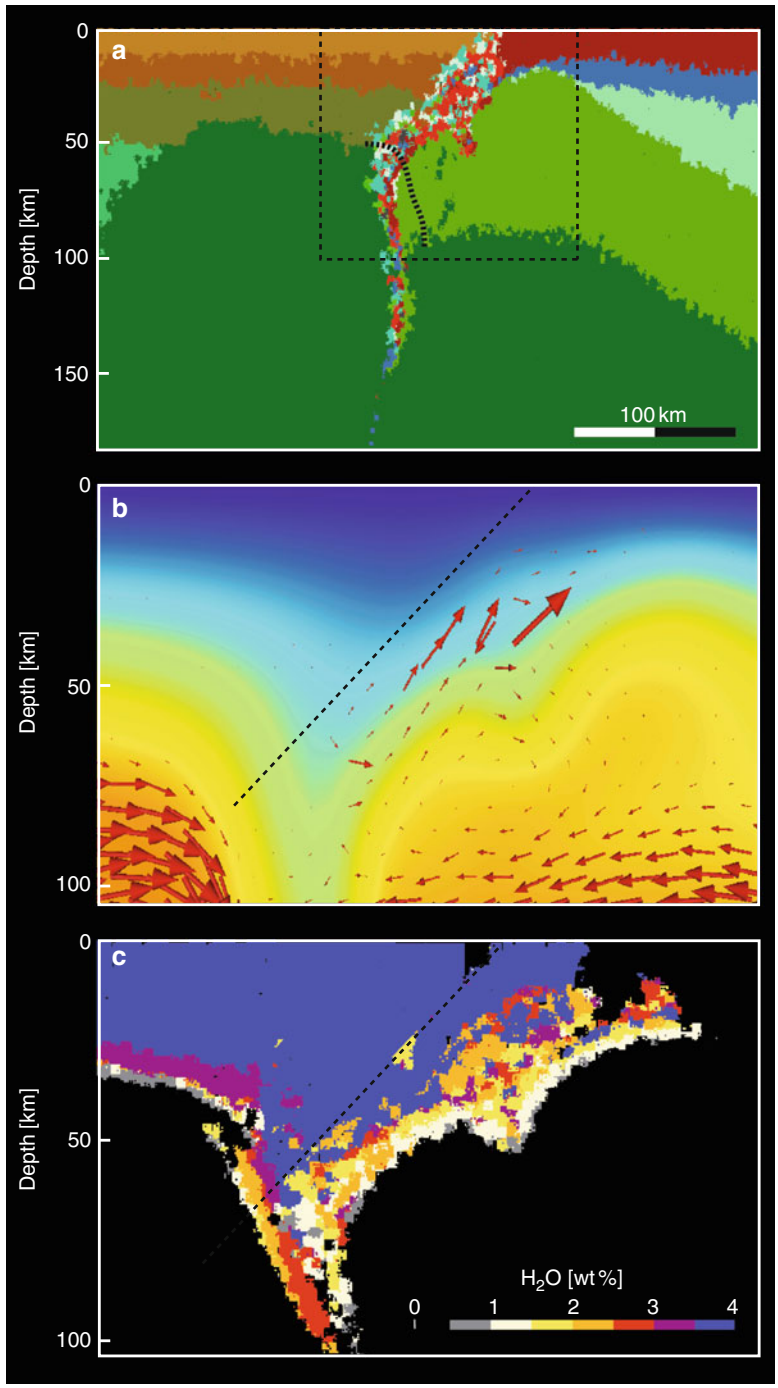

Fig. 3.14 (**a**) Rock types in the zoom box of Fig. 12e. Note the highly heterogeneous nature of the suture zone. The thick dotted line indicates the portion of the suture that is convectively removed in later times (after ~ 2.0 My). The based box refers to the zoom in (b) and (c). (**b**) Temperature and velocity fields in the suture zone. The dashed line indicates where the boundary between the arc and the suture is. (**c**) Bound water content in the assemblages. Note that large parts of the suture have water contents $> 2\%$.

Blanckenburg 1995) and existence of paired seismic and electrical conductivity anomalies in active orogens (Vry et al. 2009).

3.4 Summary and Conclusions

In this paper we have used 2D numerical simulations to study the large-scale dynamics of an arc/microcontinent–continent collision. We have not imposed velocity boundary conditions to either force or stop continental subduction, and therefore the velocities obtained in our simulations emerge self-consistently from the balance between internal forces in our numerical domain. We have also coupled our thermomechanical solvers to a petrologcial/thermodynamic model, which allowed us to obtain realistic estimates of all relevant physical properties and track metamorphic reactions within a wide range of pressures, temperatures, and bulk compositions.

Although our models are complex enough to capture most of the first-order physical processes relevant to subduction environments, they still are a simplification of reality. Importantly, we have not addressed systematically the role of compositional variations within the continental crust and its original degree of hydration. These two factors could play a significant role in the evolution of the collision and the recycling of continental derived material into the deep mantle. Also, partial melting of crustal lithologies has not been explicitly included in our simulations. Arguably, the latter effect may not be a first order factor in the large-scale evolution of the collision, but it is likely relevant in discussions of smaller-scale features across the orogen. Another important factor that has not been included in our study is the effect of the third dimension. Compared to full 3D models, 2D models generally require more energy for the onset and development of certain processes such as slab breakoff or the internal deformation of plates. For instance, the occurrence of a slab breakoff in 3D models typically evolve from a slab tearing instead of a full necking along the slab (e.g., Yoshioka and Wortel 1995). In this sense, the energy involved in our models should be considered an upper bound of that required in real cases.

Despite these limitations, there are a number of significant generalizations that can be made from the results of this investigation. These are:

1. The buoyancy increase due to subduction of continental material may not be the only explanation for the typical decrease in convergence velocity estimated in collisional settings after the arrival of continental crust to the trench. Delamination of the lithospheric mantle at lower crust levels after a period of continental subduction can result in a similar pattern of convergence velocities. This scenario is favoured in settings dominated by slab rollback.
2. The thermal structures of the continental plate and passive margin play important roles in the evolution and final configuration of the collision. The strengthening effect due to the colder temperatures in a thick continental plate overcomes the effects of its extra negative buoyancy. Thus, the overall effect of increasing the thermal thickness of the continental plate is to reduce convergence velocities, stalling subduction, and thus impede deep recycling of continental material.
3. When both the arc and the continental plate are free to move (e.g., bounded by mid-ocean ridges), the system evolves as forward subduction rather than as slab rollback. Although the circulation pattern in the sublithospheric mantle and in the mantle wedge are significantly different between these two cases, the general pattern and absolute values of the resulting convergence velocities are similar. Replenishment of fertile mantle in the mantle wedge and enhanced partial melting is favored in forward subduction scenarios.
4. The composition of the continental lithospheric mantle exerts a moderate influence on the overall evolution of the collision system. Since the highly depleted part of continental mantle seems to be restricted to shallow depths only ($<$60–80 km), the thermal effect is usually more important and the overall buoyancy of the lithospheric mantle at the beginning of the collision is negative.
5. The rheology of the continental crust is a major factor controlling both the duration of continental subduction and the volume of continental material that can be subducted. Strong crusts favor deep subduction of continental materials while soft crusts tend to accumulate at shallow depths. In the latter case, the decoupling between the upper crust and the rest of the lithosphere effectively restrict the increase of positive buoyancy of the slab, which remains negatively buoyant at all conditions.

6. Subducted continental crust remains buoyant with respect to the surrounding mantle down to depths of ~ 250–300 km. Potential detachments from the slab will therefore result in upwelling of these continental portions. However, the characteristic cold temperatures in the uppermost part of the slab result in a strong mechanical coupling between the crustal and mantle components, hindering the possibility of detachments.
7. Subducted continental crust that reaches depths >250–300 km becomes significantly denser than the surrounding mantle due to the appearance of high-density phases. This proves extra negative buoyancy to the slab and inhibit the return of subducted crust to the surface (point of no return).

Acknowledgments We would like to thank the editors D. Brown and P. Ryan for inviting us to contribute to this special volume. We are also indebted to all the participants of the field trip IGCP 524 (Ireland) for stimulating discussions and explanations in the field. We thank S. Saxena and W. Yong for unselfishly sharing their databases and helping in the implementation of new end-members, and G. Ranalli, G. Houseman, and B. Kaus for their detailed reviews and suggestions. Discussions with F. Capitanio, M. Faccenda, S. Turner, T. Rushmere, K. Grant and B. Schaefer were particularly useful. We also thank the team at VPAC and the geodynamics research group at Monash for their support. Most figures were produced with the open-source visualization package Paraview. This work has been supported by Macquarie University (JCA) and Monash University (SZ) grants and by the Monash e-Research Centre and ITS-Research Support Services through the use of the Monash Sun Grid cluster. This is contribution 659 from the Australian Research Council National Key Centre for the Geochemical Evolution and Metallogeny of Continents (http://www.gemoc.mq.edu.au).

Appendix A

A.1 Governing Equations

The dynamics of the problem analyzed in this paper is governed by the usual conservation equations of fluid dynamics (under the continuum hypothesis), namely the conservation of mass, momentum, and energy (cf. Batchelor 1967; Kundu 1990). The conservation of mass is the most obvious condition and requires

$$\frac{\partial \rho}{\partial t} + \frac{\partial (\rho u_i)}{\partial x_i} = 0 \tag{3.1}$$

where t is time, ρ bulk density, u_i velocity, and x_i refers to a Cartesian coordinate system. Equation (3.1) is also known as the *continuity equation*.

The conservation of momentum is the result of applying Newton´s law of motion to an infinitesimal fluid element. In its differential form it reads

$$\rho\left(\frac{\partial u_i}{\partial t} + u_j \frac{\partial u_i}{\partial x_j}\right) = \rho g - \frac{\partial P}{\partial x_i} + \frac{\partial \tau'_{ij}}{\partial x_j} \tag{3.2}$$

where

$$\begin{aligned}\tau'_{ij} &= 2\mu\left[\frac{1}{2}\left(\frac{\partial u_i}{\partial x_j} + \frac{\partial u_j}{\partial x_i}\right) - \frac{1}{3}\left(\frac{\partial u_i}{\partial x_i}\right)\delta_{ij}\right] \\ &= 2\mu\left(\epsilon_{ij} - \frac{1}{3}\epsilon_{ii}\delta_{ij}\right)\end{aligned} \tag{3.3}$$

is the deviatoric part of the total stress tensor $\sigma_{ij} = -P\delta_{ij} + \tau'_{ij}$ for a Newtonian fluid, P is pressure (i.e., $-1/3\ \sigma_{ii}$), g the acceleration of gravity, μ the dynamic shear viscosity, δ_{ij} the Kronecker delta, and ε_{ij} the strain rate tensor (cf. Batchelor 1967). Equation (3.2) is the 3D general form of the Navier-Stokes equation of motion. Note that the so-called *Stokes assumption*, in which the bulk viscosity is neglected, has been adopted in (3.3) (Kundu 1990).

The equation of conservation of energy relevant to our study includes five terms:

$$\rho\frac{DE}{Dt} = \sigma_{ij}\frac{\partial u_i}{\partial x_j} + H + \rho Ls\frac{D\chi}{Dt} + \rho Lm\frac{DF}{Dt} - \frac{\partial q}{\partial x_i} \tag{3.4}$$

where E the is internal energy per unit mass, H the internal heat generation (volumetric) due to radioactive decay, Ls the latent heat of transformation arising from solid-solid phase changes, Lm the latent heat of melting, q the conductive heat flow, χ the mass fraction of the new phase across a divariant solid-state reaction, F the mass fraction of melt, and D/Dt refers to the material derivative. The first term in the right-hand side of (3.4) is a *mechanical contribution* due to compressions and deformations of a fluid element without change of its velocity (Batchelor 1967). Using the above definition of total stress tensor σ_{ij}, (3.4) can be rewritten as

$$\rho\frac{DE}{Dt} = -P\frac{\partial u_i}{\partial x_i} + \Phi + H + \rho Ls\frac{D\chi}{Dt} + \rho Lm\frac{DF}{Dt} - \frac{\partial q}{\partial x_i} \tag{3.5}$$

where

$$\Phi = 2\mu\left[\epsilon_{ij} - 1/3\frac{\partial u_i}{\partial x_i}\delta_{ij}\right]^2 = \tau'_{ij}\epsilon_{ij} \tag{3.6}$$

is the *viscous dissipation* through shear deformation [i.e., there are no volume changes associated with the tensor Equation (3.6)], sometimes referred to as "shear heating" in the literature. Using the following thermodynamic identities

$$TdS = dE + PdV \tag{3.7}$$

$$dV = -\frac{d\rho}{\rho^2} \tag{3.8}$$

which imply

$$\frac{TDS}{Dt} = \frac{DE}{Dt} - \frac{P}{\rho^2}\frac{D\rho}{Dt} \tag{3.9}$$

we can rewrite (3.5) as

$$\rho T\frac{DS}{Dt} = \Phi + H + \rho Ls\frac{D\chi}{Dt} + \rho Lm\frac{DF}{Dt} - \frac{\partial q}{\partial x_i} \tag{3.10}$$

where we made use of (3.1) to eliminate the terms affected by P. Equation (3.7) implicitly includes all the "non-conventional" entropy production terms (e.g., due to phase changes) in the E term. Recalling that for a homogeneous fluid the rate of change of entropy is

$$\frac{DS}{Dt} = \frac{Cp}{T}\frac{DT}{Dt} - \frac{\alpha}{\rho}\frac{DP}{Dt} \tag{3.11}$$

we obtain the more familiar form

$$\begin{aligned}\rho Cp\left(\frac{DT}{Dt} - \frac{T\alpha}{\rho Cp}\frac{DP}{Dt}\right)\\ = \Phi + H + \rho Ls\frac{D\chi}{Dt} + \rho Lm\frac{DF}{Dt} - \frac{\partial q}{\partial x_i}\end{aligned} \tag{3.12}$$

where α is the coefficient of thermal expansion and Cp the isobaric specific heat capacity. Since we introduce latent heat effects directly into the energy equation, α and Cp do not need to be replaced by their "effective" or "apparent" counterparts in the phase change temperature range (e.g., Reddy and Gartling 2000; Li and Gerya 2009). Note that the second term on the left-hand side of (3.12) can be written as

$$\frac{T\alpha}{\rho Cp}\frac{DP}{Dt} = \left(\frac{\partial T}{\partial P}\right)_S\frac{DP}{Dt} = \frac{T\alpha}{\rho Cp}\left(\frac{\partial P}{\partial t} + u_i\frac{\partial P}{\partial x_i}\right) \tag{3.13}$$

For the Earth's mantle it is appropriate to neglect the term $\partial P/\partial t$ and assume that the vertical gradient in P is dominant and equal to ρg (i.e., hydrostatic profile; Schubert et al. 2001). Accordingly, (3.13) becomes

$$\begin{aligned}\rho Cp\left(\frac{DT}{Dt} - \frac{H_{ad}}{\rho Cp}\right) = \Phi + H + \rho Ls\frac{D\chi}{Dt}\\ + \rho Lm\frac{DF}{Dt} - \frac{\partial q}{\partial x_i}\end{aligned} \tag{3.14}$$

where $H_{ad} \equiv T\alpha\rho u_z g$ is the energy gained/lost by adiabatic compression/decompression and u_z is the vertical component of velocity. An alternative useful form of this latter relation is

$$\begin{aligned}\rho Cp\left(\frac{\partial T}{\partial t} + u_i\frac{\partial T}{\partial x_i}\right)\\ = \frac{\partial}{\partial x_i}\left(-k_{ij}\frac{\partial T}{\partial x_i}\right) + \Phi + H + H_{ad} + \rho Ls\frac{D\chi}{Dt} + \rho Lm\frac{DF}{Dt}\end{aligned} \tag{3.15}$$

where k_{ij} is the thermal conductivity tensor. Equations (3.1), (3.2), and (3.15) represent the fundamental set of equations governing the heat transfer and flow of a compressible Newtonian fluid. The insertion of an equation of state describing density as a function of other intensive variables (e.g., P, T, F, χ) completes the definition of the mathematical problem (except for the non-Newtonian case). In what follows, we describe a number of approximations and modifications to the fundamental set of equations.

A.2 Approximations

We adopt a modified version of the *extended Boussinesq approximation* (e.g., Christensen and Yuen 1985) in solving the system (3.1), (3.2), and (3.15). The Prandlt Pr and Match M numbers of a fluid determine the effects of inertia and compressibility on the flow

(cf. Jarvis and McKenzie 1980; Schubert et al. 2001). For the Earth's mantle, the product $Pr\ M^2$ is $\ll 1$ (Jarvis and McKenzie 1980), and therefore the material can be considered incompressible except in regions affected by phase transitions (see below). Equation (3.1) thus becomes

$$\frac{\partial u_i}{\partial x_i} = 0 \tag{3.16}$$

Likewise, given the effectively infinite Prandlt number of the mantle, inertia terms in the momentum (3.2) are neglected. Using (3.16), we rewrite (3.2) as

$$0 = \rho g - \frac{\partial P}{\partial x_i} + \frac{\partial}{\partial x_j}\left[\mu\left(\frac{\partial u_i}{\partial x_j} + \frac{\partial u_j}{\partial u_i}\right)\right] \tag{3.17}$$

Besides the inertia terms, the only difference between the (3.2) (compressible fluid) and (3.17) (incompressible fluid) is a term that includes the divergence $\nabla = \partial/\partial x_i$ of the velocity field

$$-\frac{\partial}{\partial x_j}\left[\frac{2}{3}\mu\left(\frac{\partial u_i}{\partial x_i}\right)\delta_{ij}\right]$$

The energy equation is made compatible with (3.16) by removing the term affected by the divergence of velocity in the viscous dissipation term (3.6), which becomes

$$\Phi = 2\mu\epsilon_{ij}{}^2 \tag{3.18}$$

The latent heats L in the energy equation can be written as $\Delta S\ T$, where ΔS is the entropy change of the phase transformation (solid-solid or solid-melt). Since entropy is an extensive quantity, the magnitude of ΔS in a rock experiencing a phase transition will depend on the actual amount of matter being transformed. For instance, although the ΔS associated with the spinel-garnet transformation is ~25 J Kg^{-1} K^{-1} in the system $MgAl_2O_4$ (spinel) + 4 $MgSiO_3$ (orthopyroxene) $\rightleftarrows$ $Mg_3Al_2Si_3O_{12}$ (pyrope) + Mg_2SiO_4 (forsterite), it becomes only ~4 J Kg^{-1} K^{-1} in a natural lherzolite with 4.5 wt% Al_2O_3 (see also Iwamori et al. 1995). Similarly, our thermodynamic calculations (see below) indicate that most metamorphic reactions typically involve $\Delta S < 8$ J Kg^{-1} K^{-1}. Such ΔS values result in local variations of the order of 5–10°C in the thermal structure and thus they can be ignored without losing any generality in large-scale models. On the other hand, reactions involving large mass fractions, such as the olivine-wadsleyite phase transitions in lherzolites (~60 vol% of the rock), can result in ΔS of the order of 30–45 J Kg^{-1} K^{-1}. In this case, the local thermal perturbation close to the phase transition can be as high as 60–70°C for fast vertical flow, and therefore the contribution from latent heat release should not be neglected in the energy equation. We introduce latent heat effects by approximating the material derivative of χ by (no time effects)

$$\frac{D\chi}{Dt} \equiv u_i \frac{\partial \chi}{\partial x_i} \tag{3.19}$$

where $\partial\chi/\partial x_i$ is assumed to be a step function (i.e., sharp transition) which is zero everywhere except at the transition, where it takes a value of $1/u_i\ \Delta t$. Appropriate values of ΔS are calculated as a function of bulk rock composition using a Gibbs free energy minimization formalism (see below).

The latent heat of melting is addressed in a similar manner, except that in this case the material derivative DF/Dt is a continuous function based on a parameterization of partial melting as a function of P, T, water content, and depletion (see below).

As stated above, the incompressibility assumption (3.16) is appropriate for modelling flow within the Earth as long as the Boussineq assumptions are fulfilled. This is not longer the case when density changes produced by mineral phase transitions are included in the model. Neglecting volume changes associated with phase transitions in the conservation equations has the net effect of "creating/destroying" mass when the material experiences a phase change (i.e., mass conservation is not ensured). This carries the obvious consequence of over/underestimating the buoyancy forces of the model, which in the case of a subducting plate has a major long-term effect on its buoyancy and thus on the dynamics of the model. We tackle this problem by modifying (3.16) and (3.17) to account for compressibility (i.e., non-zero divergence of the velocity field) in the regions affected by phase transitions. Equation (3.16) thus becomes

$$\frac{\partial u_i}{\partial x_i} = -\frac{1}{\rho}\frac{\partial \rho}{\partial x_i}u_i \approx -\frac{1}{\rho}\frac{\Delta \rho}{\Delta t} \tag{3.20}$$

where the material change in density $\frac{\Delta\rho}{\Delta t}$ is computed in each Lagrangian particle as the difference between the density in the current and previous time step (we only account for density changes due to mineral phase transitions, density variations related to melting are not included). The application of this non-zero divergence generates a localized velocity field that effectively compresses/expands the material at the time of the transition, therefore enforcing local mass conservation. In practice, since our numerical box is closed, we apply the mass correction only to lithospheric materials. This plays the role of simulating an "open" domain (i.e., sublithospheric convecting mantle can flow through the boundaries of the box to compensate for lithospheric volume changes). We note that this correction is not equivalent to modelling a fully compressible material, but rather numerically impose the changes in volume needed to conserve the mass in specific regions of the simulation domain, i.e., lithospheric materials. Similar strategies have been used by (e.g., Warren et al. 2008; Burov and Yamato 2008).

Equations (3.16) through (3.20) are solved using the finite-element platform *Underworld* (Moresi et al. 2003), which has been modified accordingly to account for all the processes described in this paper. The numerical accuracy of the mass correction term included in (3.20) is evaluated in each simulation by keeping track of the mass of the subducting plate trough time. However, this calculation is not trivial due to the difficulty in estimating the volumes of all bodies (i.e., the geometry of a body is defined by a set of moving particles that tend to mix with the particles of surrounding materials during the evolution of the model). We circumvent this problem by constructing Voronoi diagrams based on the particles and computing the mass of each particle as the product of its density times the area of the corresponding Voronoi cell. Therefore, the mass of a body is simply the sum of the mass of its constituents particles. We find that typical accumulated errors associated with mass conservation are $<1\%$.

A.3 Rheological Relationship

Our numerical models have both plastic (brittle) and viscous (Newtonian and non-Newtonian) rheologies. The brittle behaviour of rocks is assumed to follow a modified version of the von Mises criterion, in which the material yields (plastically) when the following condition is met

$$\sqrt{\tau'_{II}} \geq c_0 + \mu(\rho g z) \tag{3.21}$$

where τ'_{II} is the second invariant of the deviatoric stress tensor, c_0 is the "cohesive strength" and μ the coefficient of internal friction. Parameters c_0, and μ are specific for each material and vary among simulations. High-pressure failure of rocks (e.g., Shimada 1993; Renshaw and Schulson 2004) is modelled assuming a critical (constant) yield stress τ_c between 250 and 350 MPa (See Fig. 3.2).

The assumed general flow law for both diffusion and dislocation mechanisms has the following form (e.g. Hirth and Kohlstedt 2003)

$$\dot{\epsilon} = A(\sigma)^n d^{-m} \Psi_{H_2O} \exp\left(-\frac{E^* + PV^*}{R\,T}\right) \tag{3.22}$$

where d is the average grain-size, σ the differential stress, A the pre-exponential factor, n the stress exponent, m the grain-size exponent, E^* the activation energy, V^* the activation volume, R the gas constant, and Ψ_{H_2O} a parameter dependent on the water content (see below). Note that the activation energy E^* and volume V^* already include the T and P dependence of OH^- dissolution in olivine (cf. Hirth and Kohlstedt 2003; Karato 2008). Applying the Levy-von Mises formalism to purely viscous fluids (Ranalli 1995; Karato 2008) allows defining the effective viscosity as

$$\eta = \frac{1}{2}(\tau'_E)^{1-n} A^{-1} = \frac{1}{2}(\dot{\epsilon}_E)^{\frac{1-n}{n}} A^{-\frac{1}{n}} \tag{3.23}$$

where τ'_E and $\dot{\epsilon}_E$ are the "effective" second invariants of the deviatoric stress tensor $[= (\frac{1}{2}\tau'_{ij}\tau'_{ij})^{1/2}]$ and of the strain rate tensor $[= (\frac{1}{2}\dot{\epsilon}_{ij}\dot{\epsilon}_{ij})^{1/2}]$, respectively. Parameter A is a factor derived from the empirical Equation (3.22) and the type of experiment [for details see Chap. 4 of Ranalli (1995) and Chap. 3 of Karato (2008)]. All relevant parameters used to solve (3.21)–(3.23) are listed in Table 3.3.

Since diffusion and dislocation creep are thought to act simultaneously in the mantle, two different viscosities η_{diff} and η_{disl} are computed separately and then

combined into an effective viscosity η_{eff}. The latter is computed as the harmonic mean of η_{diff} and η_{disl}:

$$\frac{1}{\eta_{\text{eff}}} = \left(\frac{1}{\eta_{\text{diff}}} + \frac{1}{\eta_{\text{disl}}}\right) \tag{3.24}$$

This expression is truncated if the resulting viscosity is either greater or lower than two imposed cutoff values (10^{18} to 10^{24} Pa s). Although grain-size may change due to grain growth and dynamic recrystallization processes, its dependence on mantle flow conditions is poorly known and therefore we consider only constant grain sizes. For average grain sizes $d \gtrsim 3.5$ mm, dislocation creep represents an important component of the effective viscosity at depths < 200 km. For smaller values of d, diffusion creep becomes dominant. In this context, we note that synthetic seismological models of oceanic mantle suggest $d \gtrsim 3.5$ mm (Afonso et al. 2008a, b). All simulations shown in this work are carried out with a constant $d = 5$ mm.

A.4 Melting Model

We adopt a simple melting model based on the parameterizations of Katz et al. (2003). Melting of crustal components are not considered in the present work. The melt fraction of mantle rocks as a function of P, T, water content, and depletion ξ is expressed as

$$F_{(T,P,H_2O,\xi)} = \left(\frac{T - T_s}{T_l - T_s}\right)^{\beta 1} \tag{3.25}$$

where

$$T_s = A_1 + A_2 P + A_3 P^2 - \Delta T_w + \Delta T_\xi \tag{3.26}$$

$$T_l = B_1 + B_2 P + B_3 P^2 - \Delta T_w + \Delta T_\xi \tag{3.27}$$

Parameters A_n and B_n are fitting parameters obtained from regressions through a large number of experimental data (Katz et al. 2003). ΔT_w is a parameter that takes into account the temperature decrease in the solidus caused by the presence of water and has the simple form (Katz et al. 2003)

$$\Delta T_w = K X_{H_2O}^{\gamma} \tag{3.28}$$

where $K = 43$°C wt%$^{-\gamma}$, $\gamma = 0.75$, and X_{H_2O} is the weight percent of water in the melt. The latter is obtained assuming batch melting and a representative bulk partition coefficient D_w (Katz et al. 2003). Although it is expected that in natural systems D_w will vary with P,T, and bulk composition, here we adopt a constant $D_w = 0.008$ as a representative average for our simulations; this value is in agreement with various experimental estimations (cf. Hirschmann 2006). The concomitant extraction of bound water during melting of hydrous assemblages is tracked using the same bulk partition coefficient D_w as above.

In our simulations we assume "instantaneous" batch melting during each time step. Thus, all melt generated during a time step is extracted in the next time step, except for a small amount that remains in the solid assemblage as residual porosity (see below). The ΔT_ξ parameter is introduced here to include the effect of incremental depletion on the solidus temperature. This effect, not considered in the original parameterization of Katz et al. (2003), arises due to the progressive extraction of fusible elements from the solid rock by partial melting, which in turn increases the solidus temperature of the solid residue. We adopt the following linear form

$$\Delta T_\xi = 250F \tag{3.29}$$

where the result is in °C and F is in weight fraction (e.g., $0 < F < 1$). The numerical value 250 is identical to that estimated by Phipps Morgan (2001) and used by Afonso et al. (2008a). The effect of melt depletion on bulk density is accounted for by tracking the total amount of melt extraction F_T experienced by mantle particles and applying the following correction: $\rho_r = \rho_s - \zeta F_T$, where ρ_r is the bulk density of the residual peridotite, ρ_s is the bulk density of the unmelted (fertile) mantle, and ζ is a correction factor $= 2$ kg m^{-3} $\%F^{-1}$. For instance, if a mantle parcel has experienced a total of 10% melt extraction at a certain time of the simulation, the density of the residual solid assemblage will be 20 kg m^{-3} less than its fertile counterpart at identical P-T conditions.

The density of the partially melted rock is computed as

$$\rho_{eff} = \rho_s(1 - F) + \rho_m F \tag{3.30}$$

where ρ_s is the density of the solid aggregate and ρ_m is the density of the melt. The former is retrieved from the energy minimization scheme; the latter is estimated as a linear function of P and T according to the relation

$$\rho_m = \rho_0 + \left(\frac{\partial \rho_0}{\partial T}\right)_P (T - T_0) + \left(\frac{\partial \rho_0}{\partial P}\right)_T (P - P_0) \quad (3.31)$$

where ρ_0 is a reference value at $P_0 = 1$ atm and $T_0 = 800$ K. The derivatives are estimated using the-method of Lange and Charmichael (1987) for a melt with an average MgO content of 10 wt%. The results are $(\partial \rho_0/\partial T)_P \sim -10^{-4}$ kg m^{-3} K^{-1} and $(\partial \rho_0/\partial P)_T$ ~0.065 kg m^{-3} Gpa^{-1}. We assume the existence of a critical residual porosity F_c below which melts are immobile (Wark et al. 2003). Here we use a conservative value of 1% for F_c. When the calculated F at a certain P-T-H_2O condition becomes greater than F_c, the "excess" melt (i.e., $F - F_c$) is extracted from the solid and transported instantaneously to the surface. This assumption is entirely justified by the high velocities of melts in the mantle wedge (e.g., Turner et al. 2001) in comparison to the duration of a typical time step in our simulations (50,000–200,000 years).

A.5 Darcy Flow of Water

Aqueous fluids released by dehydration reactions are assumed to migrate through the solid matrix as porus flow along the solid grain boundaries (Darcy's flow). The effect of adding water into nominally-anhydrous minerals by diffusion is neglected here due to its minute contribution to the water balance compared to hydration/dehydration reactions.

Neglecting compaction effects and assuming that pressure variations from the lithostatic state are small (Burov and Yamato 2008), the fluid (melt or aqueous) velocity relative to the matrix velocity obeys the relation

$$V_f - V_s = \frac{\Delta \rho g k_\phi}{\mu_f \phi} \quad (3.32)$$

V_f and V_s are the velocities of the fluid and solid matrix, respectively, ϕ the fluid fraction, μ_f the dynamic viscosity of the fluid, and $\Delta\rho$ the density difference between the solid aggregate and the fluid. The permeability k_ϕ is given by (Wark et al. 2003)

$$k_\phi = \frac{d^2 \phi^3}{270} \quad (3.33)$$

where d is the mean grain diameter (5 mm). As stated in (3.32), the densities and viscosities of the aqueous fluids are required to compute their velocities. Here we estimate the density with the Pitzer-Sterner equation of state for pure water (Pitzer and Sterner 1994). This assumption will underestimate the real density of fluids as the solubility of silica-rich components in water increases significantly at high pressures (Audetat and Keppler 2004), thus increasing the density of the fluid. The viscosities are somewhat more problematic due to their order-of magnitude variations over conditions pertaining to the mantle wedge (Audetat and Keppler 2004). In order to avoid overcomplicating the model with poorly constrained parameters, here we assume the viscosities of fluids to be constants and equal to 1 Pa s.

A.6 Thermodynamic Databases and Free Energy Minimization Strategy

We compute stable assemblages and all their relevant bulk properties (ρ, C_p, α, bulk modulus, etc.) by free energy minimization using the software Perple_X (Connolly 2009). All calculations were performed in the system K_2O–Na_2O–TiO_2–FeO–CaO–MgO–Al_2O_3–SiO_2 + H_2O (KNTFCMAS + H_2O), which accounts for ≳99 wt% of the Earth´s crust and mantle. All stable assemblages and relevant physical properties were computed *a priori* as function of P, T, bulk composition, and water content and saved in "look-up" tables with a spacing of 75 MPa for P, 5.6 K for T, and 1 wt% for water content. Given the size of our numerical domain and the large range of compositions, we used two different thermodynamic databases and formalisms. For ultramafic *upper mantle* lithologies and for *all* crustal materials, we used an augmented-modified version of the Holland and Powell (1998) database (revised in 2002). The original data set has been augmented with the following phases:

CAS* ($CaAl_4Si_2O_{11}$), K-hollandite* ($KAlSi_3O_8$), Si-wadeite* ($K_2Si_4O_9$), K-Cymrite* ($KAlSi_3O_8{\cdot}H_2O$), Mg-majorite ($Mg_4Si_4O_{12}$), Na-majorite ($Na_2Al_2Si_4O_{12}$), Ca-perovskite* ($CaSiO_3$), Mg-wadsleyite (Mg_2SiO_4), Fe-wadsleyite (Fe_2SiO_4), high-pressure (C2/c) clinoferrosilite ($Fe_4Si_4O_{12}$), and high-pressure (C2/c) clinoenstatite ($Mg_4Si_4O_{12}$); * denotes stoichiometric phases (i.e., not part of a solid-solutions). The so-called NAL and Egg phases as well as Ca-ferrite are stable at very high-pressures along subduction P-T paths (e.g., Ono 1999; Miyajima et al. 2001). However, they are not included in the present version of the database due to their small volume fraction in comparison with other dominant phases.

In order to obtain a reliable internally consistent data set within the system KNTFCMAS + H_2O for the wide range $0 < P < 30$ GPa and $273 < T < 2{,}000$ K, the following phases in the original Holland and Powell (1998) database had to be slightly modified (always within experimental uncertainty): forsterite, fayalite, ferrosilite, enstatite, stishovite, tschermakite, Ca-tschermakite, Mg-tschermakite, grossular, pyrope, diopside, and A-phase. The modification involved mainly a refitting of the polynomials describing C_p and α to make them compatible with high-pressure experiments, and in some cases a slight modification of the enthalpies of formation and molar volumes. However, we stress that the predictions of the original database at low and moderate (crustal and shallow upper mantle) T-P conditions were not affected to any significant extent by these modifications, since they mostly apply at high-pressure conditions. A full description of all solid-solution models and end-members will be published elsewhere (Afonso and Zlotnik, in preparation).

Our database has been calibrated based on experimental results in simplified systems. The thermodynamic parameters of the mentioned phases were refined in successive steps in a hierarchical manner. First, a consistent database was obtained for the MS, FS, MAS, and FAS systems. Succeeding refining stages considered the ternary systems KAS, CAS, FMS, CMS, and quaternary systems KAS + H_2O, CMAS, FMAS. A subsequent comparison against experimental results in complex system such as NKCMFAS, KNTFCMAS + H_2O, and KCMAS + H_2O showed good agreement, and permitted a final refining of some phases and/or solutions (e.g., garnets and clinopyroxenes). Figure 3.15 shows a comparison of calculated phase diagrams for a peridotite using three different databases. It can be seen that at low P-T conditions our database (Fig. 3.15b) predicts similar equilibrium assemblages than the original database of Holland and Powell (1998) (Fig. 3.15a). At higher pressures, however, the original database fails to predict representative assemblages due to the lack of solid solution models for the solubility of pyroxenes into garnet, the transformation of olivine into wadsleyite, and the high-pressure monoclinic polymorph of orthopyroxene with C2/c symmetry. At high P-T conditions our phase diagram is therefore more similar to that predicted from the high-pressure database of Xu et al. (2008) (Fig. 3.15c).

Figure 3.16 shows the high T-P experimental results of Irifune and Isshiki (1998) together with predictions from our database for the same P-T and compositional conditions. Although the agreement with the experimental data is good, there are some differences at high pressures. Firstly, the experiments of Irifune and Isshiki (1998) did not constrain the amount of the monoclinic (clinopyroxene-structured) polymorph of orthopyroxene (e.g., Woodland and Angel 1997; Akashi et al. 2009), and therefore we cannot constrain well the effect that the presence (and disappearance) of the C2/c phase will have on the transfer of atomic species between garnet and clinopyroxene (see also Fig. 3.15). Although the behaviour of the C2/c phase in our calculations is in perfect agreement with experiments in the simple system FMS, it is still uncertain how this phase behaves in more complex systems such as the one in Fig. 3.16. Secondly, our database predicts high pressure garnets ($P > 10$ GPa) with relatively low contents in Na and high in Fe with respect to experiments on continental crust compositions (Irifune et al. 1994; Wu et al. 2009). Clinopyroxene, on the other hand, tend to be deficient in Fe and Mg. Although we have modified some end-member properties to make the database more reliable at high pressures, the above observations suggest that the solution models adopted in this study from experiments at low-moderate pressures require further refinements. Unfortunately, there are only a few high-P-T experiments in complex systems that could be used for this purpose, and not all of them are consistent (e.g., Irifune et al. 1994; Wu et al. 2009). Despite this limitation, Figs. 3.16 and 3.17 shows that our database reproduce high-P-T experimental observations satisfactorily for a wide range of compositions.

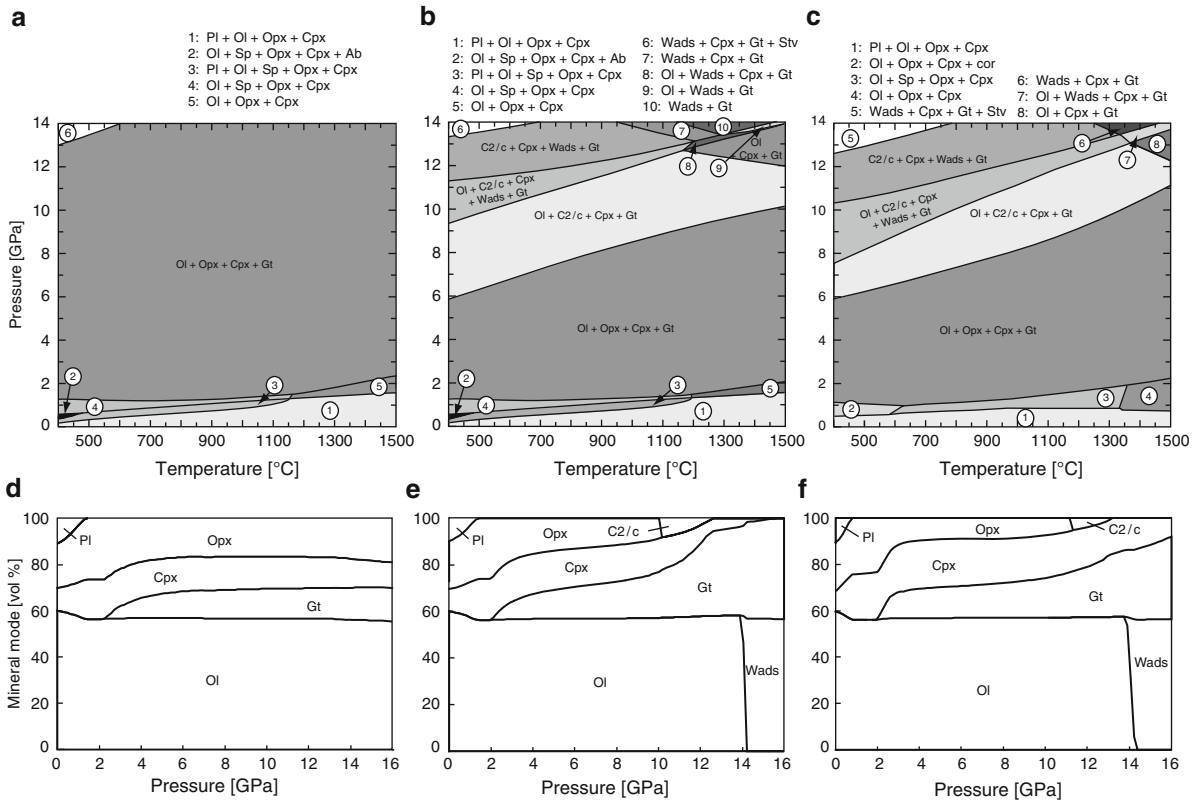

Fig. 3.15 Predicted phase diagrams of dry peridotite using the database of Holland and Powell (1998) (**a**), our augmented/modified version (**b**), and the database of Xu et al. (2008) (**c**). (d), (e) and (f) are the respective modal proportions along a 1330 °C adiabat.

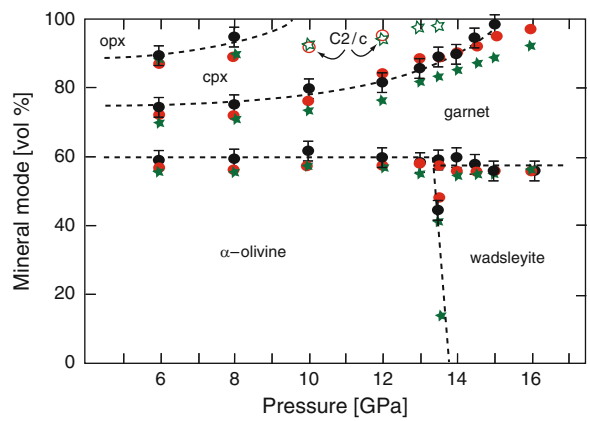

Fig. 3.16 Comparison between experimental and theoretical phase proportions in dry pyrolite. Black circles with error bars are from Irifune and Ito (1998) based on high-T-P experiments. Red (grey) circles are predictions from our dataset. Stars are predictions from the dataset of Xu et al. (2008).

The above discussion indicates that our database will predict reliable phase diagrams up to $\lesssim$30 GPa only for felsic, intermediate, and mafic compositions. For ultramafic compositions, however, predictions are only reliable up to ~15 GPa (i.e., above the wadsleyite-ringwoodite transition). Therefore, for mantle materials below this transition we use the thermodynamic database and formalism of Xu et al. (2008). This database

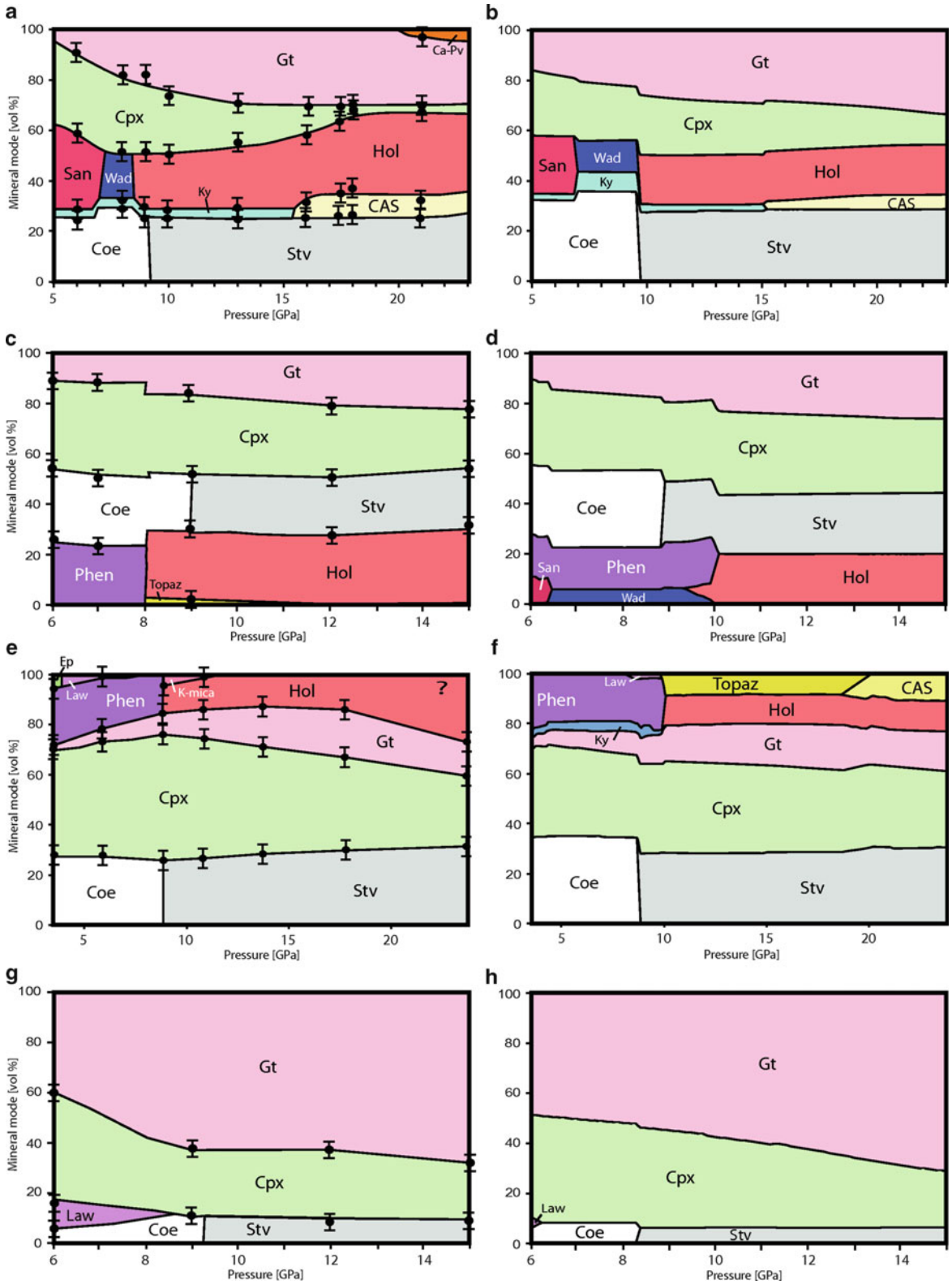

Fig. 3.17 Comparison between experimental results (left column) and predictions from our dataset (right column). Experimental studies are (a) Irifune et al. (1994), (c) Ono (1998), (e) Wu et al. (2009), (g) Ono (1998).

is suitable for ultramafic compositions (but not for felsic, intermediate, or hydrated compositions) at transition zone and lower mantle conditions in the simplified system NCFMAS. For similar NCFMAS compositions, the differences in bulk ρ, α, and seismic velocities between the two databases are $< 1\%$, $\lesssim 1.5$, $< 0.8\%$, respectively. Therefore, the discontinuity of such properties when passing from our database to that of Xu et al. (2008) is unlikely to have any significant effect on the dynamics of the system. In practice, we combine both databases at the Ol-Wads transition, where the properties of the system have a natural and significant discontinuity (i.e., the so-called 410d). We apply an interpolation function to smooth out the sharp contrasts in the physical properties.

References

Afonso JC, Ranalli G (2004) Crustal and mantle strengths in continental lithosphere: is the jelly sandwich model obsolete? Tectonophysics 394:221–232

Afonso JC, Fernàndez M, Ranalli G, Griffin W, Connolly J, (2008a) Integrated geophysical-petrological modelling of the lithospheric-sublithospheric upper mantle: methodology and applications. Geochem Geophys Geosyst 9. doi:10.1029/2007GC001834

Afonso JC, Zlotnik S, Fernàndez M (2008b) The effects of compositional and rheological stratifications on small-scale convection under the oceans: implications for the thickness of oceanic lithosphere and seafloor flattening. Geophys Res Lett 35:L20308. doi:10.1029/2008GL035419

Afonso JC, Ranalli G, Fernndez M, Griffin W, O'Reilly S, Ulrich F (2010) On the vp/vs – mg correlation in mantle peridotites: implications for the identification of thermal and compositional anomalies in the upper mantle. Earth Planet Sci Lett 289:606–618

Ague J (2003) Fuid flow in the deep crust. In: Rudnick RL, Holland HD, Turekian KK (eds) The crust, vol 3, Treatise on geochemistry. Elsevier, Oxford, pp 195–228

Akashi A, Nishihara Y, Takahashi E, Nakajima Y, Tange Y, Funakoshi K (2009) Orthoenstatite/clinoenstatite phase transformation in MgSiO3 at high-pressure and high-temperature determined by in situ X-ray diffraction: implications for nature of the X discontinuity. J Geophys Res 114: B04206. doi:10.1029/2008JB005894

Audetat A, Keppler H (2004) Viscosity of fluids in subduction zones. Science 303:513–516

Batchelor GK (1967) An introduction to fluid dynamics. Cambridge University Press, UK

Beaumont C, Jamieson RA, Butler JP, Warren CJ (2009) Crustal structure: a key constraint on the mechanism of ultra-high-pressure rock exhumation. Earth Planet Sci Lett 287: 116–129

Behn M, Kelemen P (2003) The relationship between seismic P-wave velocity and the composition of anhydrous igneous and meta-igneous rocks. Geochem Geophys Geosys 4:1041. doi:10.1029/2002GC000393

Burov E, Yamato P (2008) Continental plate collision, p-t-t-z conditions and unstable vs stable plate dynamics: insights from thermomechanical modelling. Lithos 103:178–204

Capitanio F, Morra G, Goes S, Weinberg R, Moresi L (2010) India-sia convergence driven by the subduction of the greater indian continent. Nature Geosci 3. doi: 10.1038/NGEO725

Carlson RW and Miller (2003) Bound water content of the lower oceanic crust estimated from modal analyses and seismic velocities of oceanic diabase and gabbro. Geophys Res Lett RG1001.

Carlson RL, Miller D (2003) Mantle wedge water contents estimated from seismic velocities in partially serpentinized peridotites. Geophys Res Lett 30. doi:10.1029/2002GL016600

Chopin C (2003) Ultrahigh-pressure metamorphism: tracing continental crust into the mantle. Earth Planet Sci Lett 212:1–14

Christensen U, Yuen D (1985) Layered convection induced by phase transitions. J Geophys Res 90:10291–10300

Clift P, Vannucchi P (2004) Controls on tectonic accretion versus erosion in subduction zones: implications for the origin and recycling of the continental crust. Rev Geophys 42, RG2001. doi:10.1029/2003RG000127

Connolly JAD (2009) Geodynamic equation of state: what and how. Geochem Geophys Geosyst 10, Q10014. doi:10.1029/2009GC002540

Dahlen F.A, Suppe J (1988) Mechanics, growth, and erosion of mountain belts. In: Clark S.P, Jr., Burchfield B.C, and Suppe J (eds) Processes in continental lithospheric deformation. Geol. Soc. Am. Spec. Pap., 218:161–178

Davis J, Blanckenburg F (1995) Slab breakoff: q model of lithosphere detachment and its test in the magmatism and deformation of collisional orogens. Earth Planet Sci Lett 129:85–102

Davis J, Blanckenburg F (1998) Thermal controls on slab breakoff and the rise of high-pressure rock during continental collisions. In: Hacker B, Liou J (eds) When continents collide. Dordrecht, Kluwer, pp 97–115

Dewey JF (2005) Orogeny can be very short. Proc Natl Acad Sci USA 102:15286–15293

Dobrzhinetskaya LF, Green HW (2007) Experimental studies of mineralogical assemblages of metasedimentary rocks at earths mantle transition zone conditions. J Metam Geol 25:83–96

Ernst W, Liou J (2008) High and ultrahigh pressure metamorphism: past results and future prospects. Am Mineral 93:1771–1786

Faccenda M, Minelli G, Gerya T (2009) Coupled and decoupled regimes of continental collision: numerical modeling. Earth Planet Sci Let 278:337–349

Fernàndez M, Afonso J, Ranalli G (2010) The deep lithospheric structure of the Namibian volcanic margin. Tectonophysics 481:68–81

Fullea J, Fernàndez M, Afonso JC, Vergés J, Zeyen H (2010) The structure and evolution of the lithosphere-asthenosphere boundary beneath the Atlantic-Mediterranean transition region. Lithos 120(1–2):74–95

Geoffroy L (2005) Volcanic passive margins. C R Geosci 337:1395–1408

Gerya T, Yuen D, Maresch W (2004) Thermomechanical modelling of slab detachment. Earth Planet Sci Lett 226:101–106
Gerya T, Connolly J, Yuen D, Gorczyk W, Capel A (2006) Seismic implications of mantle wedge plumes. Phys Earth Planet Int 156:59–74
Griffin WL, O'Reilly S, Afonso J, Begg G (2009) The composition and evolution of lithospheric mantle: a re-evaluation and its tectonic implications. J Petrol 50:1185–1204
Green H, Dobrzhinetskaya L, Bozhilov K.N. (2000). Mineralogical and experimental evidence for very deep exhumation from subduction zones. J. Geodyn., 30:61–76
Guillot S, Garzanti E, Baratoux D, Marquer D, Maheo G, Sigoyer J (2003) Reconstructing the total shortening history of the nw himalaya. Geochem Geophys Geosys 4:1064. doi:10.1029/2002GC000484
Haggerty S.E, Sautter V (1990) Ultradeep (greater than 300 kilometers), ultramafic upper mantle xenoliths. Science, 248:993–996
Hart SR, Hauri EH, Oschman LA, Whitehead JA (1992) Mantle plumes and entrainment: isotopic evidence. Science 256: 517–520
Hebert L, Antoshechkina P, Asimow P, Gurnis M (2009) Emergence of a low-viscosity channel in subduction zones through the coupling of mantle flow and thermodynamics. Earth Planet Sci Lett 278:243–256
Hirschmann MM (2006) Water, melting, and the deep Earth's H2O cycle. Ann Rev Earth Planet Sci 34:629–653
Hirth G, Kohlstedt DL (2003) Rheology of the upper mantle and the mantle wedge: a view from the experimentalists. In: Eiler J (ed) Inside the subduction factory, vol 138, Geophysical monograph., pp 83–105
Holland T, Powell R (1998) An internally consistent thermodynamic data set for phases of petrological interest. J Metam Geol 16:309–343
Hyndman R, Peacock S (2003) Serpentinization of the forearc mantle. Earth Planet Sci Lett 212:417–432
Irifune T, Isshiki M (1998) Iron partitioning in a pyrolite mantle and the nature of the 410-km seismic discontinuity. Nature 392:702–705
Irifune T, Ringwood A, Hibberson W (1994) Subduction of continental crust and terrigenous and pelagic sediments: an experimental study. Earth Planet Sci Lett 126:351–368
Iwamori H, McKenzie D, Takahashi E (1995) Melt generation by isentropic mantle upwelling. Earth Planet Sci Lett 134:253–266
Jarvis G, McKenzie D (1980) Convection in a compressible fluid with infinite prandtl number. J Fluid Mech 96:515–583
Jordan TH (1978) Composition and development of the continental tectosphere. Nature 274:544–548
Karato S-I (2008) Deformation of Earth materials: an introduction to the rheology of the solid Earth. Cambridge University Press, Cambridge, UK, 463 p
Katz RF, Spiegelman M, Langmuir C (2003) A new parameterization of hydrous mantle melting. Geochem Geophys Geosyst 4(9):1073. doi:10.1029/2002GC000433
Keskin M (2007) Eastern Anatolia: a hotspot in a collision zone without a mantle plume. In: Foulger G, Jurdy D (eds) Plates, plumes and planetary processes. Geological Society of America Special Paper, vol 430. The Geological Society of America, pp 693–722, doi:10.1130/2007.2430
Kirby S.H., Kronenbrg A.K., (1987) Rheology of the lithosphere:selected topics. Rev. Geophys. 25:1219–1244
Kirby S.H. (1983) Rheology of the lithosphere. Rev. Geophys., 21:1458–1487
Kundu PK (1990) Fluid mechanics. Academic, California, USA
Lange R, Charmichael I (1987) Densities of Na2O, K2O, CaO, MgO, FeO, Fe2O3, Al2O3, TiO2, SiO2 liquids: new measurements and derived partial molar properties. Geochim Cosmochim Acta 51(11):2931–2946
Lee C-TA, Chen W-P (2007) Possible density segregation of subducted oceanic lithosphere along a weak serpentinite layer and implications for compositional stratification of the earth's mantle. Earth Planet Sci Lett 255:357–366
Li Z, Gerya T (2009) Polyphase formation and exhumation of high- to ultrahigh-pressure rocks in continental subduction zone: numerical modeling and application to the Sulu ultrahigh-pressure terrane in eastern china. J Geophys Res 114: B09406. doi:10.1029/2008JB005935
Liu L, Zhang J, Green H, Jin Z, Bozhilov K.N. (2007) Evidence of former stishovite in metamorphosed sediments, implying subduction to > 350 km. Earth Planet. Sci. Lett., 263: 180–191
Mackwell S.J., Zimmerman M.E., Kohlstedt D.L., (1998) High-temperature deformation of dry diabase with application to tectonics on Venus. J. Geophys. Res. 103:975–984
McDonough WF, Sun S (1995) The composition of the Earth. Chem Geol 120:223–253
Miyajima N, Yagi T, Hirose K et al (2001) Potential host phase of aluminum and potassium in the earths lower mantle. Am Mineral 86:740–746
Moresi L, Dufur F, Mühlhaus H (2003) A lagrangian integration point finite element method for large deformation modeling of viscoelastic geomaterials. J Comp Phys 184:476–497
Nakagawa T, Tackley P, Deschamps F, Connolly J (2009) Incorporating self-consistently calculated mineral physics into thermochemical mantle convection simulations in a 3-D spherical shell and its influence on seismic anomalies in Earths mantle. Geochem Geophys Geosys 10:Q03004. doi:10.1029/2008GC002280
Nikolaeva K, Gerya T, Connolly J (2008) Numerical modelling of crustal growth in interoceanic volcanic arcs. Phys Earth Planet Int 171:336–356
Ono S (1998) Stability limits of hydrous minerals in sediment and mid-ocean ridge basalt compositions: implications for water transport in subduction zones. J Geophys Res 103:18253–18267
Ono S (1999) High temperature stability limit of phase egg, AlSiO3(OH). Contrib Mineral Petrol 137:83–89
Patiño Douce A, McCarthy T (1998) Melting of crustal rocks during continental collision and subduction. In: Hacker B, Liou J (eds) When continents collide. Dordrecht, Kluwer, pp 27–55
Phipps Morgan J (2001) Thermodynamics of pressure release melting of a veined pudding mantle. Geochem Geophys Geosys 2, 2000GC000049
Pitzer K, Sterner S (1994) Equations of state valid continuously from zero to extreme pressures for h2o and co2. J Chem Phys 101(4):3111–3116
Plank T, Langmuir C (1998) The chemical composition of subducting sediment and its consequences for the crust and mantle. Chem Geol 145:325–394

Ranalli G (1995) Rheology of the Earth, 2nd edn. Chapman & Hall, London
Ranalli G, Pellegrini R, D'Offizi S (2000) Time dependence of negative buoyancy and the subduction of continental lithosphere. J Geodyn 30:539–555
Rapp R, Irifune T, Shimizu N, Nishiyama N, Norman MD, Inoue T (2008) Subduction recycling of continental sediments and the origin of geochemically enriched reservoirs in the deep mantle. Earth Planet Sci Lett 271:14–23
Reddy J, Gartling D (2000) The finite element method in heat transfer and fluid dynamics, 2nd edn. CRC Press, USA
Renshaw C, Schulson E (2004) Plastic faulting: brittle-like failure under high confinement. J Geophys Res 109: B09207. doi:10.1029/2003JB002945
Ringwood AE (1982) Phase transformations and differentiation in subducted lithosphere: implications for mantle dynamics, basalt petrogenesis, and crustal evolution. J Geol 90:611–643
Rudnick RL, Gao S (2003) Composition of the continental crust. In: Rudnick RL, Holland HD, Turekian KK (eds) The crust, vol 3, Treatise on geochemistry. Elsevier, Oxford, pp 1–64
Scambelluri M, Pettke T, van Roermund H.L.M. (2008) Majoritic garnets monitor deep subduction fluid flow and mantle dynamics. Geology, 36:59–62
Schilling J, Zajac M, Evans R, Johnston T, White W, Devine J, Kingsley R (1983) Petrologic and geochemical variations along the Mid-Atlantic Ridge from 29 degrees N to 73 degrees N. Am J Sci 283:510–586
Schmidt M.W, Poli S (1998) Experimentally based water budgets for dehydrating slabs and consequences for arc magma generation. Earth Planet. Sci. Lett., 163:361–379
Schubert G, Turcotte DL, Olson P (2001) Mantle convection in the Earth and planets. Cambridge University Press, Cambridge, UK
Sella GF, Dixon T, Mao A (2002) Revel: a model for recent plate velocities from space geodesy. J Geophys Res 107(B4), 2081, doi:10.1029/2000JB000033
Shimada M (1993) Lithosphere strength inferred from fracture strength of rocks at high confining pressures and temperatures. Tectonophysics 217:55–64
Sobolev S, Babeyko A (2005) What drives orogeny in the Andes? Geology 33:617–620
Song S, Zhang L, Niu Y. (2004) Ultra-deep origin of garnet peridotite from the North Qaidam ultrahigh-pressure belt, Northern Tibetan Plateau, NW China. Am. Min., 89: 1330–1336
Takahashi N, Kodaira S, Tatsumi Y, Kaneda Y, Suyehiro K (2008) Structure and growth of the Izu-Bonin-Mariana arc crust: 1 seismic constraint on crust and mantle structure of the Mariana arcback-arc system. J Geophys Res 113: B01104. doi:10.1029/2007JB005120
Tatsumi Y, Eggins S (1995) Subduction zone magmatism. Blackwell, Oxford, UK
Tirone M, Ganguly J, Morgan J (2009) Modeling petrological geodynamics in the Earths mantle. Geochem Geophys Geosys 10:Q04012. doi:10.1029/2008GC002168
Toussaint G, Burov E, Avouac J-P (2005) Tectonic evolution of a continental collision zone: a thermomechanical numerical model. Tectonics, TC6003, doi:10.1029/2003TC001604
Turner S, Evans P, Hawkesworth C (2001) Ultrafast source-to-surface movement of melt at island arcs from 226ra-230th systematics. Science 292:1363–1366, doi: 10.1126/science.1059904
van Keken P, Karato S-I, Yuen D (1996) Rheological control of oceanic crust separation in the transition zone. Geophys Res Lett 23:1821–1824
Vry J, Powell R, Golden K, Petersen K (2009) The role of exhumation in metamorphic dehydration and fluid production. Nat Geosci 3:31–35
Wark D, Williams C, Watson E, Price J (2003) Reassesment of pore shapes in microstructurally equilibrated rocks, with implications for permeability of the upper mantle. J Geophys Res 108:2050. doi:10.1029/2001JB001575
Warren C, Beaumont C, Jamieson RA (2008) Formation and exhumation of ultra-high-pressure rocks during continental collision: role of detachment in the subduction channel. Geochem Geophys Geosys 9(4). doi:10.1029/2007GC001839
Woodland A, Angel R (1997) Reversal of the orthoferrosilite – high-P clinoferrosilite transition, a phase diagram for FeSiO3 and implications for the mineralogy of the Earth's upper mantle. Eur J Mineral 9:245–254
Workman R, Hart S, Jackson M, Regelous M, Farley KA, Blusztajn J, Kurz M, Staudigel H (2004) Recycled metasomatized lithosphere as the origin of the Enriched Mantle II (EM2) end-member: evidence from the Samoan volcanic chain. Geochem Geophys Geosyst 5, Q04008, doi:10.1029/2003GC000623
Wu Y, Fei Y, Jin Z, Liu X (2009) The fate of subducted upper continental crust: an experimental study. Earth Planet Sci Lett 282:275–284
Xu W, Lithgow-Bertelloni C, Stixrude L, Ritsema J (2008) The effect of bulk composition and temperature on mantle seismic structure. Earth Planet Sci Lett 275:70–79
Yamato P, Agard P, Burov E, Le Pourhiet L, Jolivet L, TiberiBurov C (2007) Burial and exhumation in a subduction wedge: mutual constraints from thermomechanical modeling and natural P-T-t data (schistes lustrs, western alps). J Geophys Res 112:B07410. doi:10.1029/2006JB004441
Yamato P, Burov E, Agard P, Le Pourhiet L, Jolivet L (2008) HP-UHP exhumation during slow continental subduction: self-consistent thermodynamically and thermomechanically coupled model with application to the western alps. Earth Planet Sci Lett 271:63–74
Ye K, Cong B, Ye D (2000) The possible subduction of continental material to depths greater than 200 km. Nature, 407:734–736
Yoshioka S, Wortel M (1995) 3D numerical modeling of detachment of subducted lithosphere. J Geophys Res 100 (20):223–244
Zang SX, Weia R, Ninga J (2007) Effect of brittle fracture on the rheological structure of the lithosphere and its application in the ordos. Tectonophysics 429:267–285
Zhai S, Ito E (2008) Phase relations of CaAl4Si2O11 at high-pressure and high-temperature with implications for subducted continental crust into the deep mantle. Phys Earth Planet Int 167(3–4):161–167

Chapter 4
The Seismic Structure of Island Arc Crust

A.J. Calvert

4.1 Introduction

Intraoceanic island arcs are considered to have been important building blocks in the formation of Earth's continental crust, with some of the oldest preserved crust created through amalgamation of island arcs and oceanic plateaux in the Middle to Late Archean, for example the Archean Superior Province of Canada (Hoffman 1989; Card 1990). Since the collision of island arcs with continental crust is presently occurring in locations such as Timor, Taiwan and northeastern South America, the addition of island arcs to existing continents is likely to have been a major contributor to continental growth throughout much of Earth's history. Studies of inferred arc terranes within continental regions can reveal much about the tectonic processes that incorporated arc crust into the continents, as well as some aspects of the original island arc crust, such as its age of formation; however, the lack of preservation of ancient, pre-collisional island arcs implies that we must look to modern islands arcs to understand many fundamental aspects of the island arc crust that became involved in past arc–continent collisions.

Modern ocean island arcs (Leat and Larter 2003) (Fig. 4.1 in Chap. 2) occur where one oceanic plate subducts beneath another whose stress state ranges from clearly extensional, such as the Tonga arc where back-arc spreading occurs, to neutral or mildly compressional such as the Aleutian arc (Jarrard 1986). Upper plates that are subject to a higher degree of compression are predominantly continental, though the Solomon arc, which is in collision with the Ontong Java plateau is an exception to this rule (Miura et al. 2004). In addition, some island arcs such as Japan have been built on, or contain some component of, remnant continental crust, and as such they cannot be considered pure island arc systems. In this paper, I will contrast the crustal structure of non-extended and extended island arc systems, including in the latter the inactive remnant arcs that are generated by arc rifting and separated from the active arc by back-arc spreading. Given the same magmatic input, an arc that is subject to one or more episodes of back-arc rifting will contain thinner crust than an arc that has not been so affected. This variation in the thickness of present-day island arc crust is one observation that will be emphasised due to its influence on the process of arc–continent collision and the resultant preservation of arc crust.

4.2 Island Arc Regimes

Metamorphic dehydration reactions within the subducted oceanic lithosphere release water into the overlying mantle wedge, generating melts that rise to form arc volcanoes, which define the location of the magmatic axis of the active arc (Stern 2002). The magmatic arc massif, whose abrupt seaward limit defines the magmatic front, averages approximately 100 km in width over all subduction zones (d'Ars et al. 1995), and is largely below sea-level in island arc settings. Volcanism can extend into the back-arc region, resulting in a less well-defined transition from arc to back-arc. The forearc lies between the magmatic front and the trench, and in the case of accretionary convergent margins will grow through

A.J. Calvert
Department of Earth Sciences, Simon Fraser University, 8888 University Drive, Burnaby, BC V5A 1S6, Canada
e-mail: acalvert@sfu.ca

D. Brown and P.D. Ryan (eds.), *Arc-Continent Collision*, Frontiers in Earth Sciences,
DOI 10.1007/978-3-540-88558-0_4,

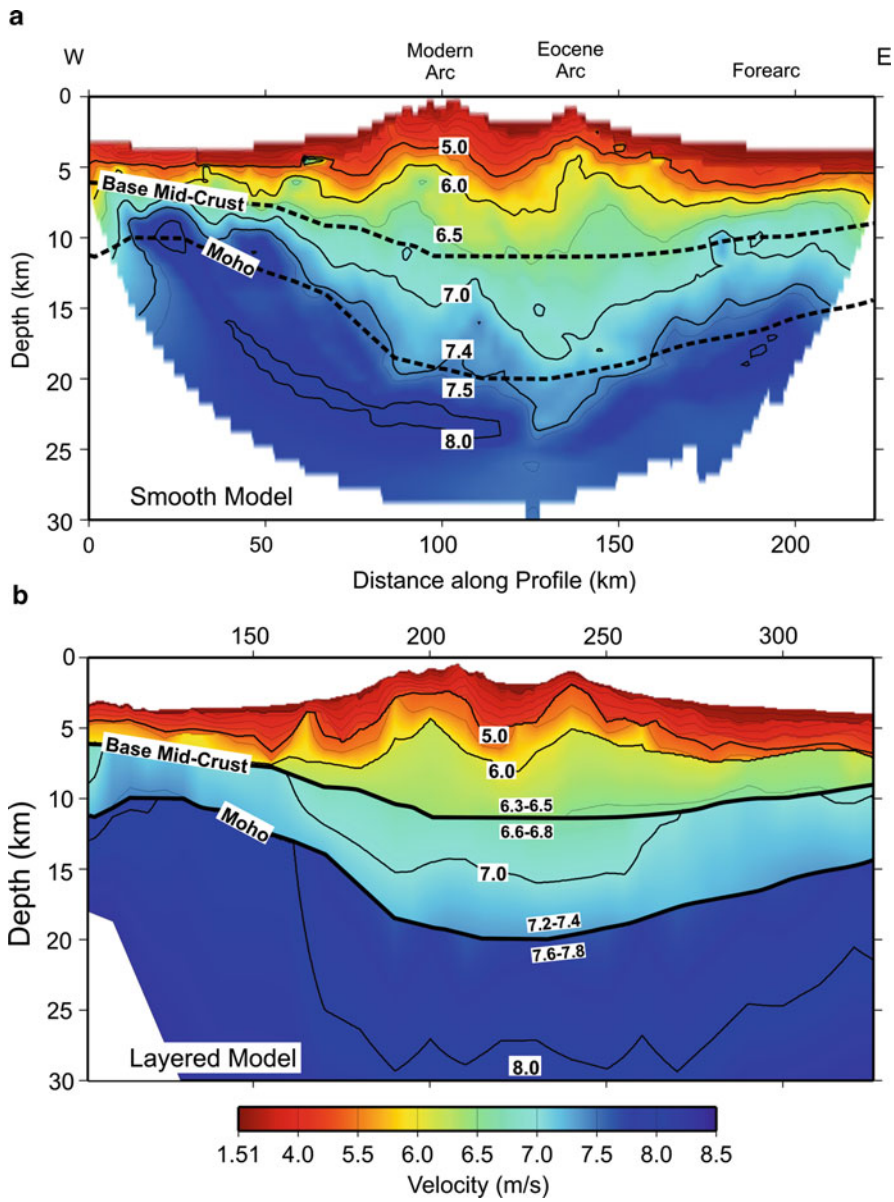

Fig. 4.1 Comparison of velocity models across the Mariana island arc. (**a**) Vertical section extracted from a 3D model derived using first arrival tomography. The 3D velocity model indicates that crustal velocities extend to greater depth beneath the frontal arc than the modern arc. (**b**) 2D velocity model obtained using first arrivals and wide-angle reflections from laterally continuous interfaces. The Moho and the base of the middle crust identified using wide-angle reflections (Takahashi et al. 2007) are shown by the *continuous heavy black lines*, and also indicated in (**a**) by *dashed lines*; the velocity contrasts across these interfaces are also shown. Vertical exaggeration is 4:1.

the addition of sediment, and perhaps igneous crust, scraped from the subducting plate to form an accretionary prism. In non-accretionary, and perhaps even accretionary settings, subduction erosion may remove material from the seaward edge of the forearc by slumping into the trench or from the base of the forearc crust (Von Huene and Scholl 1991). The width of the forearc averages 160 km (Gill 1981).

When the upper plate of an island arc system is under tension, back-arc basins form through the rifting

of the arc massif (Karig 1970), with the initial rift usually occurring within 50 km of the volcanic arc (Taylor and Karner 1983), which weakens the lithosphere due to its high heat flow and the presence of melt in a locally thickened crustal section (Molnar and Atwater 1978; Kuzsnir and Park 1987). Although arc rifting primarily occurs on the back-arc side of the arc, it can also be centered on the arc, or even in the forearc, resulting in the latter case in the two magma sources, associated with subducting slab and upwelling asthenosphere, migrating past one another as back-arc spreading develops (Martinez and Taylor 2006). When rifting occurs on the back-arc side of the arc massif, the remnant arc separates from the still unified magmatic arc and forearc through back-arc spreading. In this situation, the remnant arc will be quite narrow, and may not include any of the original volcanic edifices, e.g. the Kyushu-Palau Ridge (Kobayashi et al. 1995; Nishizawa et al. 2007). When rifting is centered on the arc volcanoes, as occurred in the Mariana arc, arc volcanism is greatly attenuated by the interaction between the different magmatic sources, but the arc will reestablish itself at the appropriate location above the slab as the back-arc spreading centres migrate away (Hussong and Uyeda 1981). If rifting occurs in the forearc, then the remnant arc will be uncommonly wide as seems to be the case with the Lau Ridge west of the Tonga-Kermadec subduction zone, and the active magmatic arc must shut down and reestablish itself closer to the trench as the back-arc basin opens (Martinez and Taylor 2006). Thus remnant arcs, which are typically identified by their associated seafloor ridges, can vary significantly in width and crustal thickness depending on the rifting process that created them.

Over the last 50 years, island arcs have been subject to a broad range of geoscientific studies, with recent emphasis on geochemical cycling through the subduction system and the magmatic evolution of the arc. One specific focus of interest has been the estimation of the volume of andesitic crust within the arc, because such crust has a similar composition to continental crust, and the widespread existence of such crust within island arcs would imply that arcs can indeed be the building blocks of continental crust. Although tonalitic rocks have been exhumed, for example, in the Tanzawa collision zone in Japan (Nitsuma 1989; Kawate and Arima 1998), seismic refraction surveys are required to constrain the subsurface distribution of such rocks in modern arcs from the inferred seismic velocities. In addition, seismic surveys can constrain the thickness of arc crust, and the vertical extent of the crust–mantle transition. In terms of arc–continent collision, crustal thickness and composition, which is closely related to density, are two key characteristics of arc crust that help determine the evolution of the process.

4.3 Seismic Studies of Arc Crust

Seismic refraction surveys of island arcs date back at least 40 years, and the early results, which include the Aleutian (Grow 1973), Kurile (Gorshkov 1970), Izu-Bonin-Mariana (Murauchi et al. 1968), New Britain (Wiebenga 1973) and Tonga-Kermadec (Shor et al. 1971) arcs are summarized by Gill (1981). These surveys indicated a 6–9 km thick upper crustal layer with P wave velocities of 5.0–5.7 km s^{-1} overlying a 10–15 km thick lower crust with velocities of 6.5–7.0 km s^{-1}. The P wave velocities of the deepest, underlying layer varied from 7.5–8.2 km s^{-1}, raising some uncertainty about whether values less than 7.8 km s^{-1} in fact represented lowermost arc crust or uppermost mantle. As an alternative to a sharp crust–-mantle transition, Jacob and Hamada (1972) used surface wave data from earthquakes to postulate the existence of a crust–mantle transition zone between 20 and 40 km depth beneath the Aleutian arc, and this issue remains relevant today. These early seismic refraction results demonstrated the first order characteristics of much arc crust, namely a 15–25 km thick crust and the absence of a thick, laterally continuous layer with velocities of approximately 6.1 km s^{-1}, as commonly found in continental interiors (Christensen and Mooney 1995).

Seismic surveying and data analysis techniques have evolved significantly over the last two decades, and densely sampled 2D profiles and 3D areal surveys can now constrain well 20 km wide lateral velocity variations in middle and lower arc crust, e.g. Takahashi et al. (2007) and Calvert et al. (2008). With this degree of resolution, modern seismic surveys have reached the point where lateral velocity variation (a proxy for compositional variation) in the middle crust can be correlated with geochemical variations in surface volcanoes (Kodaira et al. 2007a). This paper reviews the seismic structure of two island arcs that represent end members of the present-day spectrum of island arc

systems, because they have been recently studied using modern seismic techniques:

1. Aleutian arc: initiated in the Eocene and not significantly affected by extension and arc rifting
2. Izu-Bonin-Mariana arc-back-arc system: initiated in the Eocene and variably affected by localised extension plus two episodes of arc rifting and back-arc spreading, which have produced two remnant arcs now separated from the modern magmatic arc

These seismic surveys reveal the degree of along-strike variability of both active and remnant arcs, both of which can eventually become involved in arc–continent collision. The seismic structure of the southern part of the Lesser Antilles arc is also presented to demonstrate the effect of late sedimentary input as an arc approaches and collides with a continent.

In addition, the average variation of seismic P wave velocity with depth is derived for several recently surveyed island arcs. These individual velocity functions and a global average for all island arcs are contrasted with the average velocity variation of continental crust.

4.3.1 Seismic Methodologies and Model Comparisons

The seismic velocity models included in this paper come from different seismic refraction surveys, and more importantly, have been analysed using different techniques. Therefore, a general understanding of these methods will help to explain the different characteristics of the velocity models presented, and facilitate comparisons between them. Seismic surveys of island arcs are predominantly marine with land recording on the islands. Recent field surveys have comprised closely spaced (50–250 m) airgun shots recorded by sparsely distributed receivers usually spaced at larger intervals of 5–30 km along an approximately linear profile. All velocity models shown here have essentially been derived from the arrival times of two types of seismic wave: diving (refracted) arrivals that turn in the subsurface as they propagate directly from source to receiver and arrivals reflected upward at wide-angle from relatively sharp, flat to shallowly dipping boundaries in the crust.

Diving waves are relatively easy to identify in field data, at least at shorter source–receiver offsets (<50–100 km), because they are mostly first arrivals. P wave velocity models can be derived by tomographic inversion of first arrival travel times alone, and although there are a variety of approaches, those methods frequently used in crustal seismology produce velocity models that vary smoothly both in depth and laterally; the sharp changes in velocity that occur at the top of the igneous crust or at the Moho tend to be smoothed out.

The additional inclusion of wide-angle reflections can improve the resolution of velocity models, because the existence of a reflection requires a relatively sharp change in seismic velocity. This information can be incorporated into the velocity model by including laterally continuous interfaces across which the seismic properties suddenly change. In many crustal velocity models, these interfaces are continuous for 100 km or more, producing characteristically layered models. Figure 4.1 contrasts the greater lateral variability of a velocity model derived by first arrival tomography (Zelt and Barton 1998) with a layered model, in which wide-angle reflections have been included (Zelt and Smith 1992). Since wide-angle reflections are secondary arrivals, their identification can be influenced by various types of noise and the sparse distribution of the recording instruments. Thus the reflection points of the identified wide-angle reflections do not usually extend over the full length of the interfaces included in most velocity models. Essentially, improved vertical resolution in the model is obtained at the cost of including parts of an interface from which no reflections have been identified, raising the possibility that this section of the interface may not exist; the constraint of an interface can, however, be assessed from the distribution of reflecting points along the boundary. An alternate approach to determining where interfaces should be introduced into the velocity model is to locate, or "migrate", reflection arrival time picks in the distance-depth domain of the model using velocities derived only from a tomographic inversion of first arrivals (Ito et al. 2005; Fujie et al. 2006). The envelope of these migrated picks indicates the position and degree of lateral continuity of subsurface reflectors.

In the following examples of seismic velocity models, only the first order characteristics of the models that would likely be well-constrained by any travel

time inversion approach are discussed. A general description of the constraint of the velocity models is presented, but the reader is referred to the original publications for full details of ray coverage, model assessment procedures and checkerboard tests.

4.4 Aleutian Arc

4.4.1 Tectonic History

The present-day Aleutian arc, which developed in the Eocene, extends 3,000 km from the Kamchatka peninsula in the west to the Gulf of Alaska in the east (Fig. 4.2). Unimak Pass at the southwestern end of the Alaska Peninsula marks the eastward transition from subduction of the Pacific Plate beneath oceanic lithosphere attached to the North America plate to subduction beneath accreted terranes and continental crust. Along the oceanic part of the subduction zone, convergence varies from 6.3 cm yr^{-1} to the NNW in the east to 7.4 cm yr^{-1} towards the NW in the west (DeMets and Dixon 1999). Due to the arcuate geometry of the trench, the relative velocity vector changes from almost trench-normal in the Gulf of Alaska to almost trench-parallel in the west.

At approximately 60 Ma, the Kula plate was subducting beneath the Beringian and southwestern Alaskan margins, which both included the Peninsula and Chugach terranes, corresponding respectively to the arc and forearc of the accreted Jurassic Talkeetna arc complex (Plafker et al. 1994). Between 56 and 42 Ma, a series of southward and westward jumps in the location

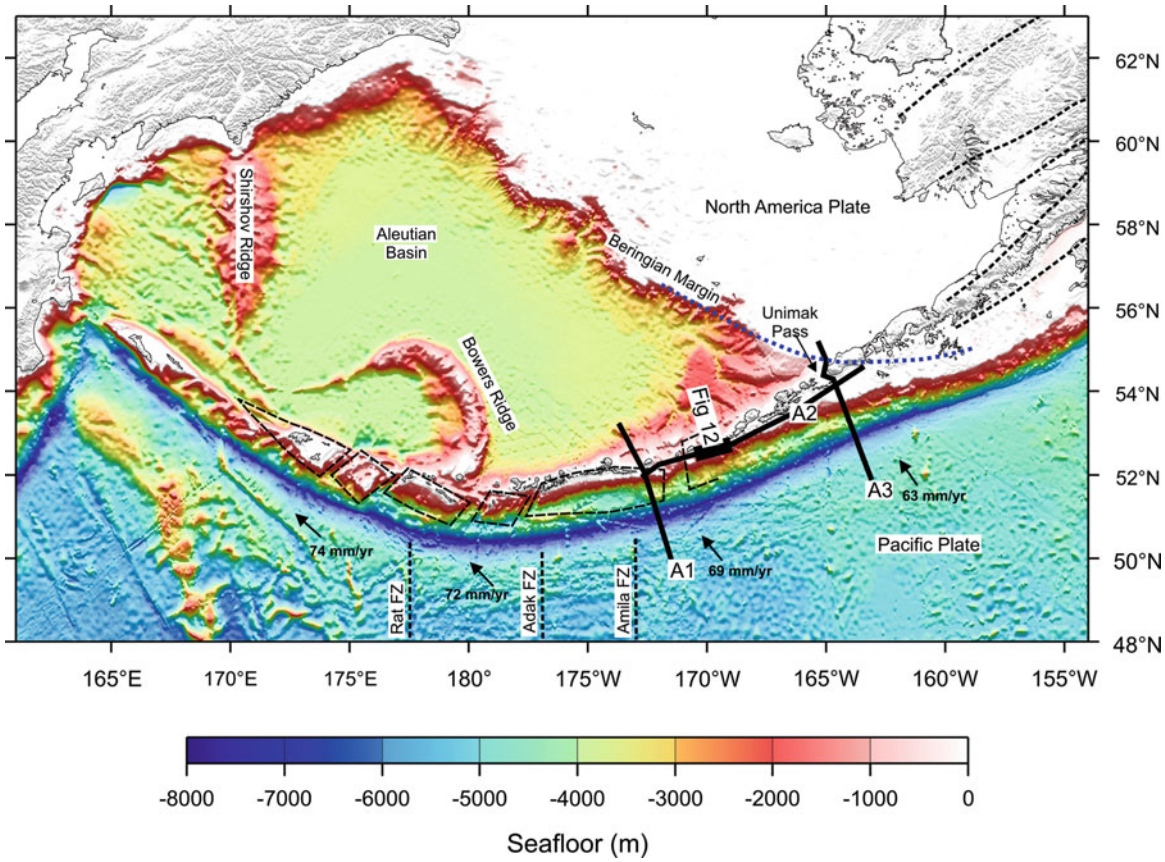

Fig. 4.2 Bathymetry of the Aleutian arc showing the location of the three lines acquired as part of the 1994 survey. *Long dashed black lines* indicate the segmentation and block rotation along the arc (Geist et al. 1988). The transition from an oceanic to a continental style of subduction occurs near Unimak Pass, and the *blue dashed line* shows the inferred location of the Beringian margin (Lizarralde et al. 2002). *Short black dashed lines* on the Pacific plate show the location of fracture zones. The convergence rate and direction at the trench is indicated by the *arrows*. Seafloor depth scale is the same as in Fig. 4.1 of Gerya in Chap. 2.

of subduction trapped a large remnant of the Kula plate against the North American plate, transforming the Beringian margin into a passive margin, and creating to the south an intraoceanic subduction zone where the Pacific plate now subducts beneath oceanic lithosphere of the former Kula plate (Scholl et al. 1992; Plafker and Berg 1994). Lizarralde et al. (2002) used seismic and potential field data to infer that the southward limit of the former Beringian margin lies just north of the Alaskan peninsula near Unimak Pass (blue dashed line in Fig. 4.2). In the oceanic section of the subduction zone, the full width of the arc massif is segmented along strike into blocks that have been subject to clockwise rotation (Geist et al. 1988).

4.4.2 Seismic Survey

Three wide-angle seismic profiles were shot over the Aleutian island arc (Fig. 4.2) by the *R/V Ewing* in 1994 using an airgun array with a total volume of 8,400 in^3:

- Line A1 was located across the oceanic part of the arc and employed 14 ocean-bottom seismometers (OBS) spaced every 20 km over the arc massif (Holbrook et al. 1999)
- Line A2 was more sparsely recorded along the inner forearc by effectively ten land stations and two OBS that were spaced 20–120 km apart and offset 20–60 km from the airgun line (Fliedner and Klemperer 1999)
- Line A3 was acquired across the arc at Unimak Pass using 16 OBS spaced 15–30 km apart (Lizarralde et al. 2002)

Although line A3 is approximately located at the along-strike transition from the oceanic to the continental arc, the interpretation of the former Beringian margin close to the northern end of this line implies that most of line A3 is located over arc crust with an oceanic affinity (Lizarralde et al. 2002).

4.4.3 Seismic Velocity Models

4.4.3.1 Cross-Arc Lines

On lines A1 and A3, diving rays, intracrustal reflections, and PmP reflections from the arc Moho plus a few reflections from the top and occasionally bottom of the subducting oceanic crust were identified in the wide-angle seismic data. P wave velocity models for lines A1 (Holbrook et al. 1999) and A3 (Lizarralde et al. 2002) were both derived by 2D travel time inversion of the wide-angle data with some additional travel times from normal incidence data using the methodology of Zelt and Smith (1992). In both models, the arc crust is divided into five layers, with three layers corresponding to the upper crust, separated by laterally continuous interfaces across which velocity discontinuities are present (Fig. 4.3). The crust is 25–32 km thick below the arc massif, but thins across the forearc to 12–15 km where the mantle wedge terminates towards the trench. On line A3, the upper and middle crust are generally well-constrained by both diving rays and wide-angle reflection raypaths. The arc Moho is located by PmP reflections under the arc massif, but the depth of the Moho is only inferred below the forearc. The position of the subducting oceanic crust is constrained by both normal incidence and wide-angle reflections south of the trench. Under the arc massif the subducting oceanic crust has been inserted into the model to be consistent with a small number of reflections and the Wadati-Benioff seismicity; below 20 km depth, the subducting crust is probably not well-located by the wide-angle survey alone.

The crustal architecture of the arc massif inferred for lines A1 and A3 is generally similar. Beneath a layer of volcaniclastic sediments of variable thickness, the upper igneous arc crust exhibits P wave velocities of 4.0–5.9 km s^{-1}, and the middle crustal layers have velocities of 6.5–6.9 km s^{-1}. The thickening of the mid-crustal layer on line A3 just seaward of the volcanic line may be linked to imbrication in the more complex tectonic environment at the tip of the Alaskan peninsula. The 12–20 km thick lower crust has velocities of 6.9–7.5 km s^{-1}; this lower layer thins under the forearc where it exhibits the highest velocities: 7.2 km s^{-1} on line A1 and 7.5 km s^{-1} on line A3. Neither line across the arc provides evidence for a significant volume of arc crust with velocities of 6.0–6.5 km s^{-1}.

4.4.3.2 Along-Strike Variation

Velocity models derived from seismic profiles acquired across an island arc may not always be representative of the arc along its full length due to the locations selected, and lines along the strike of the arc, such as

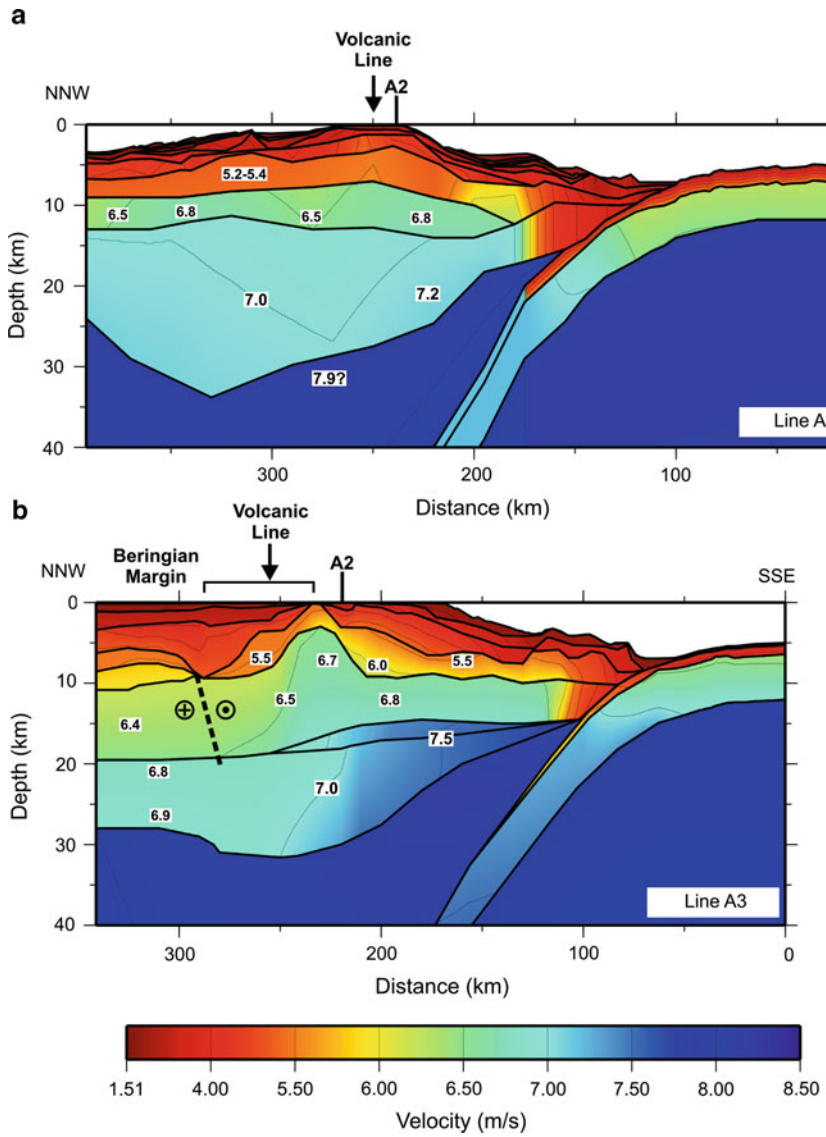

Fig. 4.3 Seismic velocity models across the Aleutian arc. (**a**) Western line A1 across the oceanic part of the arc (Holbrook et al. 1999); (**b**) Eastern line A3 in the region where the Aleutian arc changes from oceanic to continental (Lizarralde et al. 2002). The two velocity models are aligned at the location of the trench. The former Beringian margin, which may have been largely strike-slip late in its history, is shown by the *dashed black line* towards the NNW end of line A3. The upper plate crust to the south probably comprises relict Kula oceanic crust and overlying accretionary complex. The bar above line A3 marks the section of the line that was deviated around Unimak island. Vertical exaggeration is 4:1.

line A2, can identify anomalous regions that would not otherwise be detected. Due to the offset by 20–60 km of land receivers from the line of airgun shots, the travel times of diving rays and wide-angle reflections picked along line A2 were initially inverted by Fliedner and Klemperer (1999) using a 3D methodology (Hole 1992; Hole and Zelt 1995). However, the sparse distribution of the sources and receivers is more amenable to a 2.5-D inversion approach, in which ray-tracing is carried out in three dimensions, but the velocity structure is not allowed to vary perpendicular to the arc (van Avendonk et al. 2004). Using a tomographic velocity model from first arrivals recorded by a 4.2 km towed hydrophone streamer in the simultaneous normal incidence survey to fix the shallow structure, a velocity model was derived for 800 km

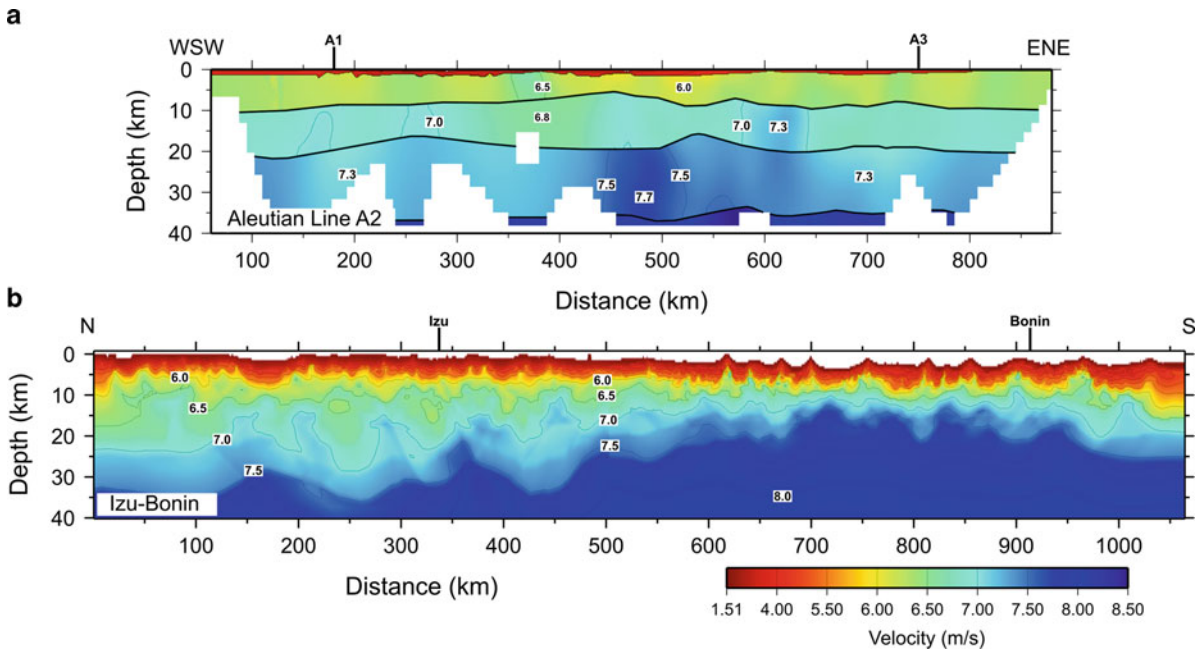

Fig. 4.4 Seismic velocity models along the Aleutian and Izu-Bonin arcs. (**a**) Line A2 is located over the inner forearc (Shillington et al. 2004); (**b**) Combined velocity models along the modern volcanic line of the Izu and Bonin arcs (Kodaira et al. 2007b). Velocities are displayed with the same scale as Fig. 4.3. Vertical exaggeration is 4:1.

along the strike of the arc (Fig. 4.4a) including the intersections with lines A1 and A3 (Shillington et al. 2004). In this model, the interfaces required to reproduce the arrival times of wide-angle reflections define three layers corresponding to the igneous arc crust, which is approximately 35 km thick. The upper crust is characterized by relatively high P wave velocities of 6.0–6.5 km s^{-1}; velocities are 6.5–7.3 km s^{-1} in the mid-crustal layer, and 7.3–7.7 km s^{-1} in the lower crustal layer.

Some differences in the crustal thickness and model velocities at the intersections of line A2 with the orthogonal profiles, A1 and A3, can be observed; for example, the crust is approximately 27 and 30 km thick on lines A1 and A3 respectively versus 35 km on the strike line A2 at the corresponding locations. Line A2 exhibits higher velocities throughout the crust than either line A1 or A3 at the same depth. This is most evident in the upper crust at a depth of ~5 km where there is a discrepancy of ~0.9 km s^{-1}, which diminishes to <0.2 km s^{-1} near the base of the crust. The discrepancy in the shallow velocities is attributable to the additional incorporation into line A2 of well-constrained velocities inferred from refractions recorded by the towed hydrophone streamer. Differences in deeper velocities may be attributable to an easier identification of wide-angle reflections on line A2 where the seafloor varies little; however, the sparse receiver distribution along line A2 introduces some uncertainty in the continuity of interfaces along strike. The intersections with lines A1 and A3 also occur near the ends of line A2 where only unreversed phases are present and the ray density is low (Shillington et al. 2004). In addition, the 3D structure of the arc, which cannot be resolved in this sparse survey, represents an additional source of uncertainty.

4.5 Izu-Bonin-Mariana Arc-Back-Arc System

4.5.1 Tectonic History

The Izu-Bonin(Ogasawara)-Mariana (IBM) subduction zone, along which Late Cretaceous to Early Jurassic ocean crust of the Pacific plate descends beneath the Philippine Sea plate, extends 2,800 km from Guam in the south to Japan in the north (Fig. 4.5), where the northern end of the volcanic arc is colliding with

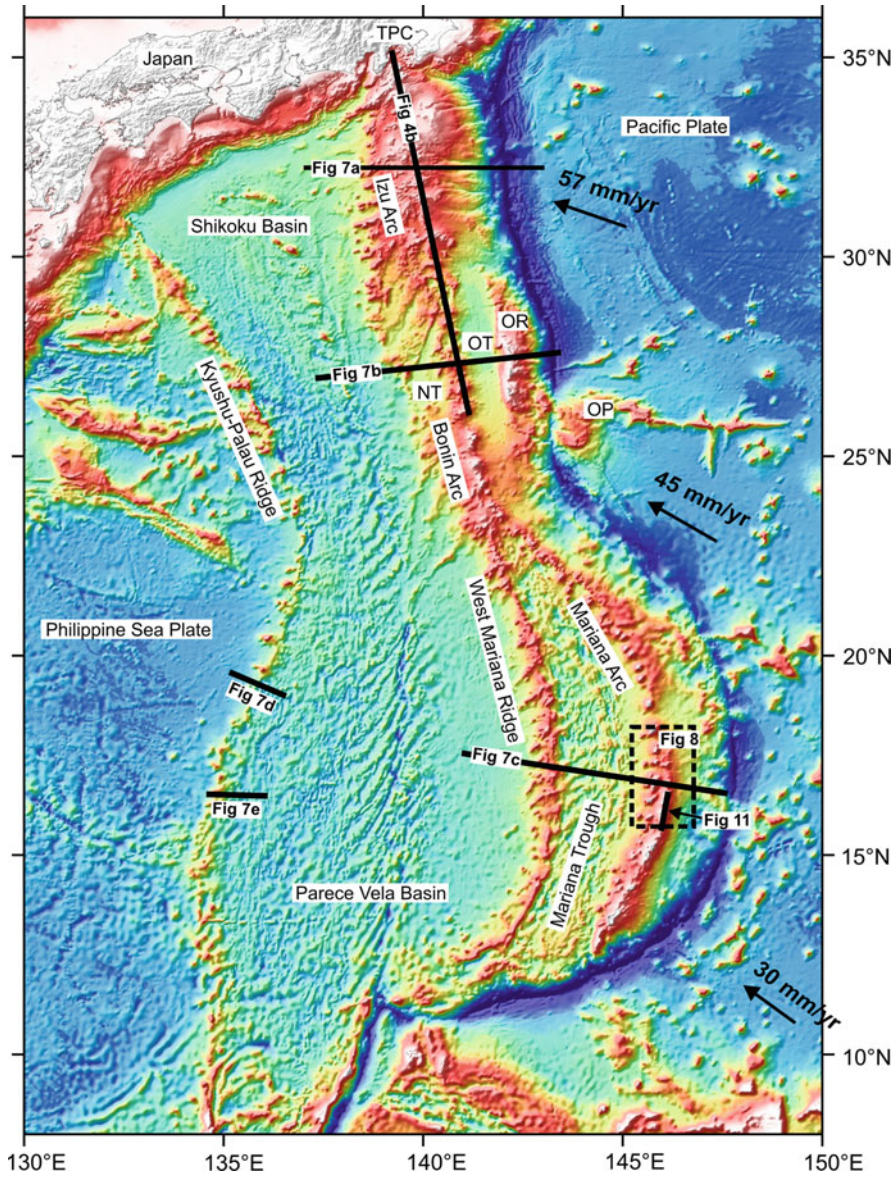

Fig. 4.5 Bathymetry of Izu-Bonin-Mariana arc-back-arc system with the location of seismic lines. The seismic lines are identified by their figure numbers within the chapter. The *dashed black rectangle* indicates the location of the 3D survey of Calvert et al. (2008). The convergence of the Pacific plate at the trench is indicated by the *arrows*. *OR* Ogasawara Ridge; *OT* Ogasawara Trough; *OP* Ogasawara Plateau; *NT* Nishinoshima Trough; *TPC* Tanzawa plutonic complex. Seafloor depth scale is the same as in Fig. 4.2.

the main Japanese island of Honshu (Stern et al. 2003). The convergence between these two plates varies between 2.4 cm yr^{-1} to the NW at 12°N to 6.1 cm yr^{-1} to the WNW at 34°N (Seno et al. 1993). A well-developed back-arc spreading centre exists west of the Mariana segment of the subduction zone, and estimates of the full spreading rate vary between 3.0 and 4.3 cm yr^{-1} (Bibee et al. 1980; Hussong and Uyeda 1981), implying that the convergence rate across the Mariana Trench is approximately 6–7 cm yr^{-1}. The strongly arcuate geometry of the Mariana segment of the subduction zone, which has arisen as a result of

back-arc spreading, implies oblique convergence along most of the trench with orthogonal convergence occurring only in the southern part of the Mariana arc system.

The IBM subduction zone was initiated in the Early Eocene (~50 Ma) (Fig. 4.6) (Taylor 1992; Stern and Bloomer 1992; Ishizuka et al. 2006), perhaps by the transformation to a trench of a fracture zone or weak line in the Pacific plate as a result of a change in the plate tectonic regime (Uyeda and Kanamori 1979). Early arc magmatism was characterized by boninitic magmas and very rapid crustal production rates until the modern-style island arc became established by the Late Eocene (~35 Ma) (Stern and Bloomer 1992). Early localised extension and partial rifting of the Bonin arc during the Eocene separated the Ogasawara ridge, which now forms part of the forearc (Ishizuka et al. 2006). In the Oligocene, rifting of the early arc began in the south at ~29 Ma and in north at ~25 Ma, and had developed along the entire IBM arc by 22 Ma (Taylor 1992, Kobayashi et al. 1995). Back-arc spreading along most of the IBM system up to 15 Ma created the Shikoku basin in the north and the Parece Vela basin in the south, which separated the remnant Kyushu-Palau ridge in the west from the still active IBM arc in the east (Hussong and Uyeda 1981; Kobayashi et al. 1995, Okino et al. 1999). The Mariana segment of the arc was subject to another rifting episode at ~8 Ma, with seafloor spreading commencing at 3–4 Ma (Bibee et al. 1980; Crawford et al. 1981). Back-arc spreading in the Mariana Trough continues, separating the West Mariana Ridge from the presently active Mariana arc that formed 3–4 Ma ago ~40 km west of the remnant Eocene arc (Fryer 1995; Stern et al. 2003). After 5 Ma, the rear side of the Izu-Bonin arc was also affected a by second episode of

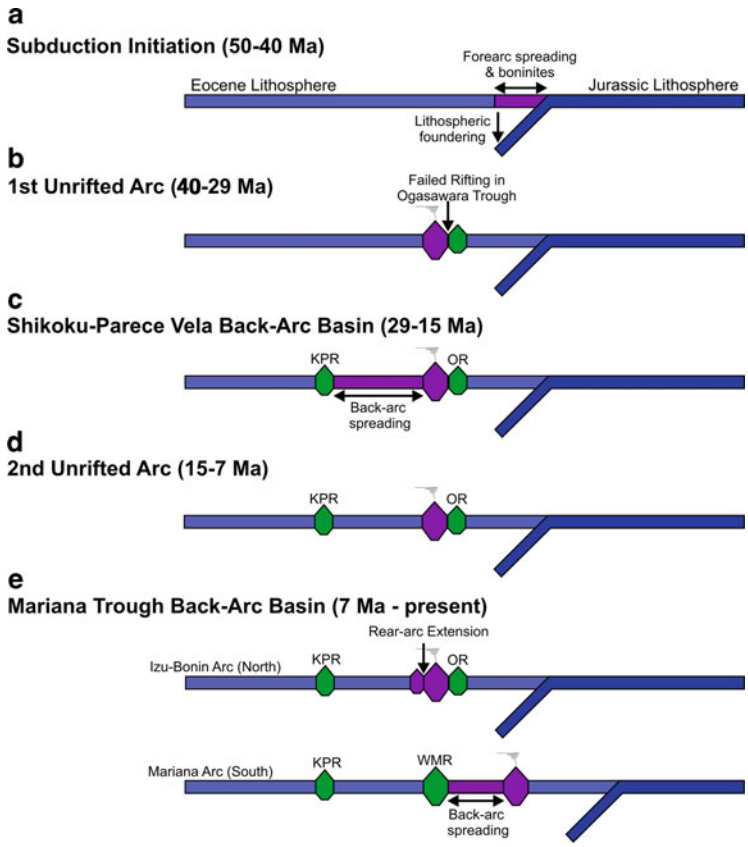

Fig. 4.6 Cartoon showing a simplified history of the Izu-Bonin-Mariana arc-back-arc system (after Stern et al. 2003). *Red* regions are currently or recently magmatically active; *green* areas represent inactive rifted arc crust. *OR* Ogasawara ridge, *KPR* Kyushu-Palau ride, *WMR* West Mariana ridge.

rifting, which created rift basins that have not yet developed into spreading centres (Taylor 1992).

The distance of the Mariana arc from continental areas has restricted the sedimentary input to the subduction zone to pelagic and volcaniclastic sediments. No significant accretionary wedge has developed because most of the incoming sediment is subducted and the forearc is also subject to erosion (Clift and Vannucchi 2004).

4.5.2 Seismic Surveys

More seismic surveys have been acquired over the IBM arc-back-arc system than any other island arc on Earth. Consequently it is possible to contrast seismic velocity models across the arc representing different evolutionary histories, and to constrain them with strike lines where available.

The Izu arc lies at the northern end of the IBM arc-back-arc system, and although affected by Oligocene arc rifting early in its history, the seafloor is shallower than 2,000 m over a width of more than 150 km, in contrast to the more southerly elements of the IBM arc. A seismic survey of the Izu arc was acquired in 1992, and this survey is historically important, because of the first inference of a laterally extensive mid-crustal layer with a P wave velocity of 6.1–6.3 km s^{-1}, which was interpreted to be granitic (Suyehiro et al. 1996). The wide-angle line across the Izu arc (Fig. 4.5) was recorded using 26 OBS spaced every 15–30 km, and shot using a 3-airgun 2,258 in^3 source, supplemented by 71 dynamite shots spaced every 2.5 km (Takahashi et al. 1998).

Further south, the Bonin arc has been subject to a more complex history of rifting than the Izu arc, and the seismic line across the arc, which was acquired in 2005, crosses the Eocene Ogasawara forearc ridge and two failed rifts, the Nishinoshima trough and the Ogasawara trough, located respectively west and east of the present-day volcanic line. The wide-angle seismic survey employed 110 OBS spaced every 5 km to record shots from an airgun array with total volume 12,000 in^3 (Takahashi et al. 2009). A 1,060 km-long profile was also acquired along the axis of the Izu-Bonin arc to show the along-strike variation in arc structure; shot in two phases this survey employed 103 OBS each time and the same 12,000 in^3 airgun array (Kodaira et al. 2007a, b).

Unlike the Izu-Bonin arc, the Mariana arc has undergone two episodes of rifting that developed to full back-arc spreading: initially in the Oligocene and later in the late Miocene. A seismic profile was acquired from the forearc, across the arc, the present-day back-arc spreading centre and the West Mariana ridge, which is the Miocene remnant arc. This line used 106 OBS spaced at 5–10 km intervals and an airgun array with total volume 12,000 in^3 (Takahashi et al. 2007, 2008). The Kyushu-Palau ridge, which is the older remnant arc, has a narrower expression in the seafloor bathymetry than the West Mariana ridge. The variation in crustal structure along the Kyushu-Palau ridge has been revealed by four profiles that were acquired across this remnant arc in 2004 using up to 200 OBS spaced at 5 km intervals, and a 8,040 in^3 airgun array (Nishizawa et al. 2007); two representative velocity models derived from this survey (Fig. 4.5) are included here. A 3D refraction survey, which involves an areal distribution of sources and receivers, has also been acquired over the central section of the Mariana arc (Calvert et al. 2008); 53 OBS were laid along three north–south lines and four north–south and seven east–west airgun lines were shot with a 10,810 in^3 airgun array.

4.5.3 Seismic Velocity Models

4.5.3.1 Cross-Arc Lines

The seismic velocity models across the arc are aligned at the trench and presented in Fig. 4.7 north to south with the Izu arc at the top. The two included seismic profiles from the Kyushu-Palau ridge lie at approximately the same latitude as the line across the Mariana arc and are shown on the left in Fig. 4.7, but these parts of the remnant arc actually originated further to the north, because the Parece Vela basin opened obliquely.

The crust of the Izu arc is inferred to be 18–21 km thick over at least 130 km of the east–west oriented

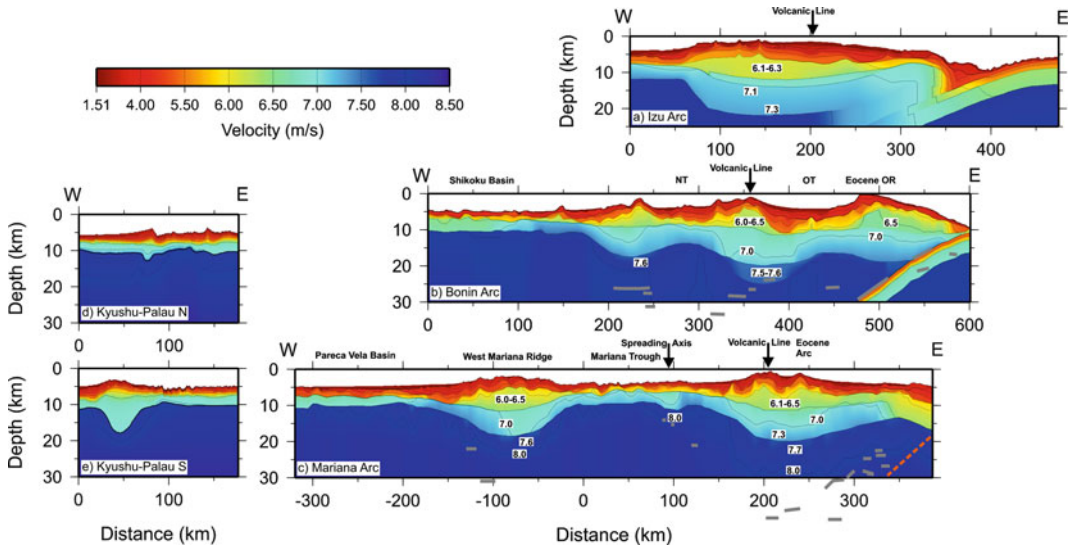

Fig. 4.7 Seismic velocity models across the Izu-Bonin-Mariana arc-back-arc system. (**a**) Line across the Izu arc (Suyehiro et al. 1996); (**b**) Line across the Bonin arc (Takahashi et al. 2009); (**c**) Line across the Mariana arc and remnant West Mariana ridge (Takahashi et al. 2007); (**d**) Northern line across the Kyushu-Palau ridge (Nishizawa et al. 2007); (**e**) Southern line across the Kyushu-Palau ridge (Nishizawa et al. 2007). The velocity models across the modern arc are aligned at the location of the trench. The lines across the Kyushu-Palau ridge are separated from the western end of the Mariana line by over 300 km of the Parece Vela basin, which is not shown here. The location of the top and bottom of the subducting oceanic crust beneath the Bonin forearc are constrained by wide-angle reflections. Beneath the Mariana forearc, the more steeply dipping oceanic crust is not resolved in this survey, but its approximate position is indicated by the *dashed orange line*. Grey line segments, some of which are at >30 km depth, indicate sub-Moho reflectors. Vertical exaggeration is 4:1.

profile (Fig. 4.7a), but the limited number of PmP reflections suggest that this thickness is not well constrained and the Moho is not identified at all under the forearc (Suyehiro et al. 1996; Takahashi et al. 1998). The midcrustal layer with velocities of 6.1–6.3 km s^{-1}, which reaches a maximum thickness of 7 km, also extends laterally over more than 100 km. This layer was introduced into the velocity model to reproduce the observed intracrustal reflections, and is also included, albeit in a less continuous form, in the velocity models across the Bonin and Mariana arcs. Although similar velocities are observed in the profile along-strike, the different tomographic approach used for inversion of the travel times of the strike line produces a velocity model with greater lateral heterogeneity (Fig. 4.4b), suggesting that greater compositional variation may be present in the middle crust of the Izu arc than implied by the first survey.

The velocity model across the Bonin arc shows the variation in crustal thickness caused by the two episodes of failed rifting here; the crust under the forearc Ogasawara ridge and the modern arc is as thick as 20 km, and the rear part of the arc reaches 15 km, but in the rift zones the crust thins to 9–12 km (Fig. 4.7b) with 2–3 km of this thickness comprising sedimentary rocks (Takahashi et al. 2009). The greater thicknesses of arc crust include mid-crustal regions with velocities of 6.0–6.5 km s^{-1} that are absent from the rift zones. In addition, Pn arrivals and some reflections from the upper mantle constrain velocities immediately below the inferred, laterally continuous (top)-Moho interface to be 7.5–7.6 km s^{-1}, leading to the interpretation of a crust-mantle transition zone up to 5 km thick beneath the thickest sections of arc crust. Under the rift zones, the Moho is inferred to be a sharp boundary.

In the Mariana arc, the initial Eocene arc lies 40 km east of the modern arc, but the crust, which is approximately 20–22 km thick (Takahashi et al. 2007; Calvert et al. 2008), does not appear to thin significantly between the two arcs (Figs. 4.1b and 4.7c) unlike the Bonin arc where the lateral separation due to rifting is greater at 150 km. However, the thickness of the mid-crustal

region with velocities of 6.1–6.5 km s^{-1}, is reduced by half between the Mariana modern and Eocene arcs. The crust of the 120 km-wide West Mariana ridge is up to 17 km thick, including a mid-crustal layer with velocities of 5.6–6.5 km s^{-1}. The smaller, 50 km-wide Kyushu-Palau ridge is 7–14 km thick (Fig. 4.7d, e), and lacks a significant region with velocities of 6.0–6.5 km s^{-1}, presumably due to its removal from the rear part of the arc massif. Velocities of 7.6–7.7 km s^{-1} inferred immediately below the top-Moho interface beneath the West Mariana ridge and the Mariana arc suggest crust–mantle transition zones are present beneath both the active arc and the remnant arc.

4.5.3.2 Along-Strike Variation

The velocity models obtained from the along-strike surveys reveal the variation in crustal structure of the Izu-Bonin arc from the collision zone with Japan in the north to the extended Bonin arc in the south (Kodaira et al. 2007b) (Fig. 4.4b). The seismic surveys were acquired along the modern volcanic line, and did not extend onto the failed rifts of the Bonin arc: the Nishi-noshima trough and the Ogasawara trough. Velocity models were derived independently using a multi-step procedure for each of the two ~500 km-long surveys, and then combined. In the first stage, a velocity model was derived using tomographic inversion of first arrivals, and this model was then locally updated to reproduce the arrival times of the wide-angle intracrustal reflections with these locations determined through migration of these second arrival picks (Kodaira et al. 2007a). This latter approach results in a model that lacks intracrustal interfaces that are continuous over large distances, e.g. more than 100 km, and variations in crustal velocity and thickness that occur over less than 50 km are quite apparent (Fig. 4.4b). The most striking feature of the velocity model, however, is the change in crustal thickness from 35 to 10 km, which is inferred from the 7.6 km s^{-1} velocity contour, and occurs over a distance of ~300 km. The thickness of the northern Izu arc is 26–35 km, but the Bonin arc is only 9–22 km thick. Lower average crustal velocities, more representative of an intermediate crustal composition, are inferred beneath the basaltic volcanoes of both the Izu and Bonin arcs, but higher velocities implying a more mafic crustal composition are found beneath rhyolitic arc volcanoes (Kodaira et al. 2007a).

4.5.3.3 3D Velocity Variation of the Mariana Arc

In contrast to 2D profiles, a 3D seismic survey can reveal the variation in seismic velocity throughout a subsurface volume, and the 3D velocity model obtained for the Mariana arc extends 240 km along strike (Calvert et al. 2008). Various crustal layer isopachs can thus be calculated from the thicknesses between iso-velocity contours. For example, an estimate of the igneous crustal thickness can be obtained from the depth interval between the 2.9 and 7.4 km s^{-1} contours (Fig. 4.8a). The igneous crust of the Eocene Mariana arc is thickest in the southern half of the main survey grid, reaching 22–24 km, and thins to 18–20 km further north. Along the modern arc, the crustal thickness reaches 20 km beneath most of the volcanoes, but decreases to approximately 16 km between them; this variation in crustal thickness is partly due to the inclusion of the volcanic edifices in the igneous crustal estimate. To the east of the Eocene arc, the forearc crust has a thickness of 13–16 km in the northern part of the survey grid, but the crust thins to 9–10 km in the south.

Isopachs of intermediate and mafic composition crust can be defined by the velocity ranges 6.0–6.5 km s^{-1} and 6.5–7.4 km s^{-1} respectively (Fig. 4.8b, c). Disregarding structures extending less than 20 km along strike, which are probably beyond the limit of resolution of the 3D tomographic inversion, the thickness of intermediate crust varies between 2 and 5 km along the modern arc, and only reaches a significant thickness near Sarigan, where three volcanoes have merged into a larger structure. Along the Eocene arc, intermediate composition crust is better developed, but it is not of uniform thickness along strike, varying between 3 and 6 km. Along the modern arc, the thickness of the mafic lower crust exceeds 12 km near the volcanic centers, but thins to 5–9 km between them, consistent with the inference that the modern arc is built on arc crust thinned by rifting (Oakley et al. 2009). Although thicker along the Eocene arc, the mafic lower crust thins from 15–18 km in the southern part of the survey grid to 12–15 km in the north. Along the modern arc, many of the thickness contours define approximately

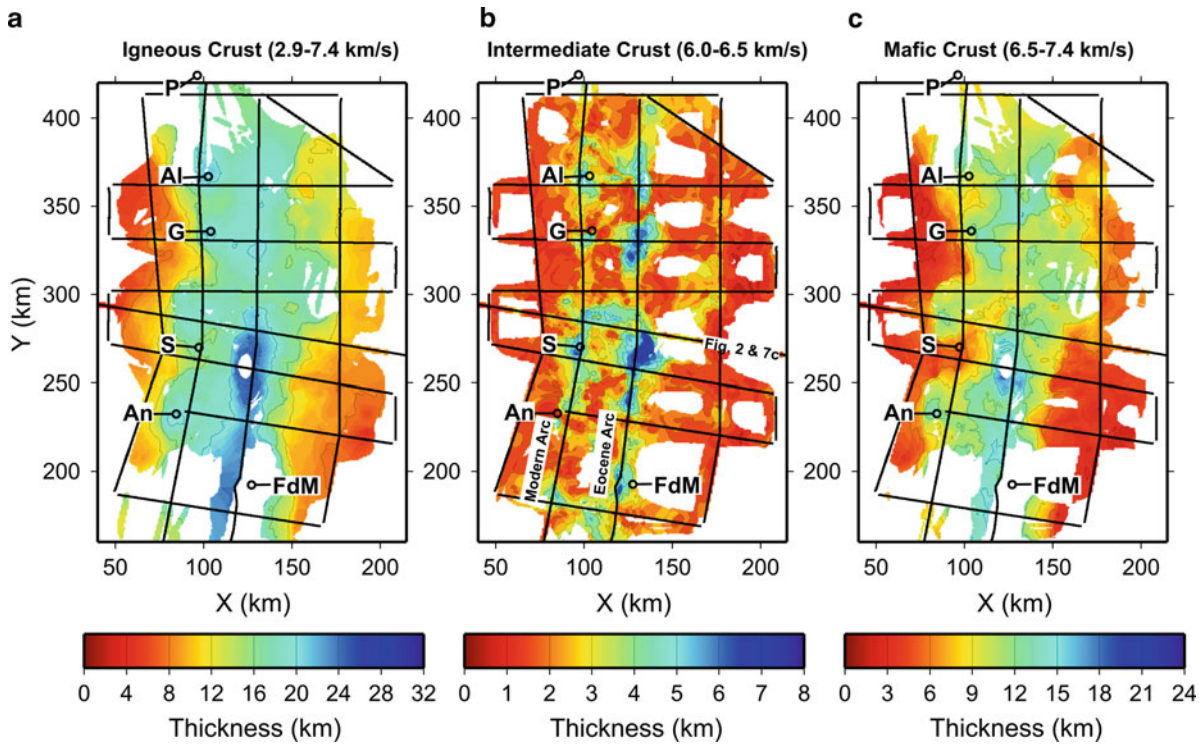

Fig. 4.8 Isopachs calculated from 3D tomographic velocity model: (**a**) Igneous crust (2.9–7.4 km s^{-1}); (**b**) Middle crust (6.0–6.5 km s^{-1}); (**c**) Lower crust (6.5–7.4 km s^{-1}). Note that the color-scale for the isopach thicknesses varies between different parts of this figure. P, Al, G, S, and An are the active volcanic islands of Pagan, Alamagan, Guguan, Sarigan and Anatahan. FdM is Ferdinand de Medinilla on the Eocene arc.

circular features, for example near Alamagan, Sarigan, and Anatahan, indicating focused crustal accretion over the last 4 Ma. In contrast, the contours beneath the Eocene arc are subparallel to strike, implying that these variations tend to even out over a longer period.

4.6 Lesser Antilles Arc

4.6.1 Tectonic History

The present arcs in the Caribbean region comprise a Great Caribbean island arc system that was originally formed in the Pacific Ocean, but migrated into the Atlantic Ocean as the Caribbean plate moved eastward (Burke 1988). At ~55 Ma, the Caribbean plate began to collide with South America in northwest Venezuela, resulting in the termination of subduction and volcanism in the Leeward Antilles arc (Fig. 4.9) as the collision migrated eastward. The Lesser Antilles arc initiated 12–15 Ma ago, and is separated from the Aves Ridge by the Grenada basin, which is believed to be underlain by oceanic crust (Boynton et al. 1979). The Aves Ridge is an extinct or remnant island arc that was originally active between ~90–55 Ma ago, and thus cannot be a remnant arc associated with the modern Lesser Antilles arc. The Grenada basin may have formed through back-arc spreading, e.g. Bouysse (1988), or, alternatively, the basin may have been created when an eastward jump in subduction trapped a piece of oceanic or forearc crust (Malfait and Dinkelman 1972). The Tobago and Grenada basins might originally have been continuous and only become separated with the more recent growth of the Lesser Antilles arc (Speed and Walker 1991);

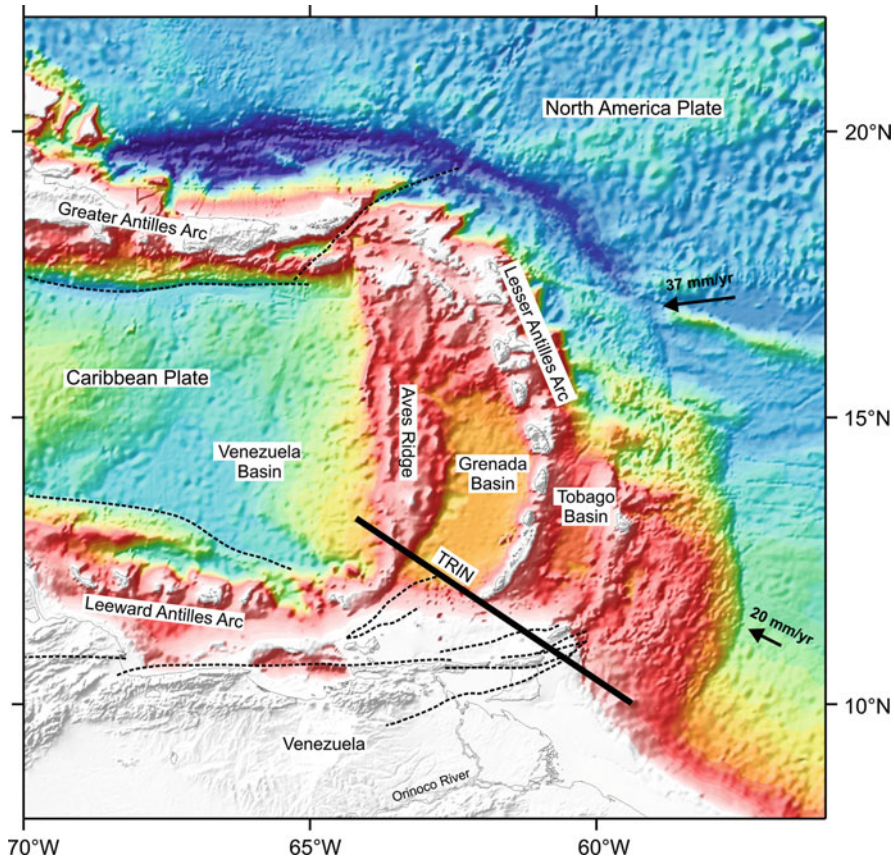

Fig. 4.9 Bathymetry of Lesser Antilles arc with the location of the TRIN seismic line. *Dashed black lines* indicate faults [after Christeson et al. (2008)]. The trench is well defined along the northern section of the arc, but further south the trench is obscured by the accretionary wedge that has evolved due to the high sediment input from the South American continent. The Aves ridge is interpreted to be a remnant arc that may have been active until ~55 Ma (Bouysse 1988). Seafloor depth scale is the same as in Fig. 4.2.

however, the complex nature of the Caribbean arc system means that many aspects of its evolution are still not well understood.

4.6.2 Seismic Survey and Velocity Model

A seismic survey, which employed 39 OBS spaced at 11–16 km intervals and an airgun source with volume 6,947 in^3, was acquired across the southern section of the Lesser Antilles arc (Fig. 4.9) in 2004 (Christeson et al. 2008). The crust of the active arc is approximately 24 km thick, and the crust of the remnant arc, the Aves ridge, is 26 km thick (Fig. 4.10). PmP reflections were recorded beneath the Aves ridge, Grenada basin and Tobago basin, but a Moho reflector appears to be absent beneath the active arc. In the back-arc basin and forearc of the Lesser Antilles arc, the top of the igneous crust probably lies close to the 4.5–5.0 km s^{-1} isovelocity contours due to its age and burial. Thus the back-arc and forearc basins are filled with a sedimentary section that is up to 12 km thick and overlies 4–10 km of igneous crust (Christeson et al. 2008). In general, the forearc region and back-arc basin of an island arc system represent a significant accommodation space that will rapidly fill if there is a high sediment input as is the case where the Lesser Antilles arc is close to the Orinoco river of South America.

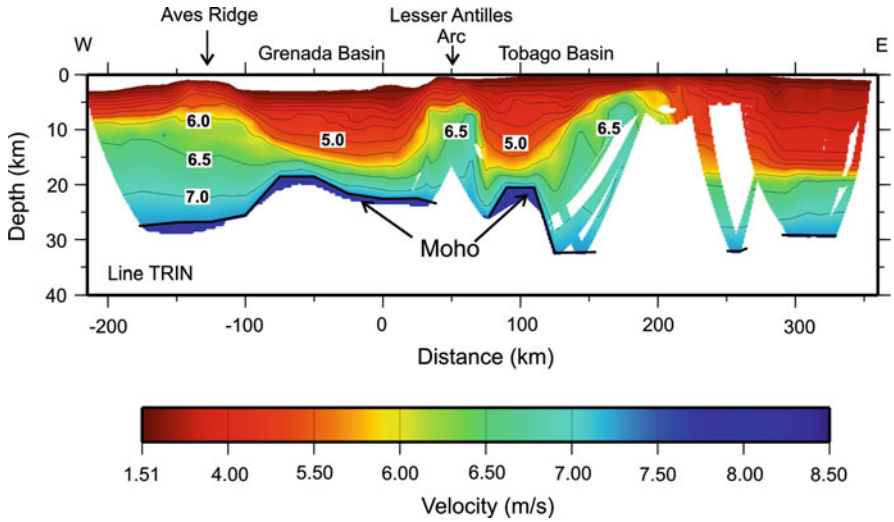

Fig. 4.10 Seismic velocity model across the southern section of the Lesser Antilles arc–continent collision zone (Christeson 2008). The base of the crust is primarily defined by PmP reflections from the Moho, which is shown by a *heavier black line* where constrained. The velocity model is not well-defined east of the Tobago basin due to the low ray coverage.

4.7 Deep Seismic Reflectivity Beneath Island Arcs

4.7.1 Wide-Angle Reflections

Wide-angle surveys of island arcs record reflections from within arc crust, the crust–mantle-transition and the uppermost mantle. These reflections are routinely incorporated into the derivation of the velocity models (see Sect. 3.1), but reflectors within the mantle wedge are somewhat surprising since they are not commonly observed in other tectonic environments. Deep reflectors beneath the Mariana and Bonin arcs, which have been located using migration of travel time picks, are shown in Fig. 4.7b, c. Since the migration of relatively sparse data can generate artifacts, the steeply dipping limbs have been excluded, and the reflectors are mostly shown as subhorizontal. Within the Mariana arc-back-arc system, reflectors occur in the uppermost mantle beneath the forearc, active arc, rear arc and remnant arc, with depths varying between 20 and 42 km (Takahashi et al. 2008). In the case of the Bonin arc, intra-mantle reflectors occur similarly across the arc system at depths of 22–32 km, and reflections are also recorded from the top of the subducting slab (Takahashi et al. 2009).

Although some mantle reflectors in the vicinity of the active arc could be attributable to melt, the existence of such reflectors beneath the remnant West Mariana ridge suggests that they are produced during the generation of island arc crust, frozen into the uppermost mantle and preserved by arc-rifting. Inferred velocity contrasts across the mantle reflectors are 7.6–7.9 km s^{-1} beneath the active Bonin arc (Takahashi et al. 2009) and perhaps as large as ~7.6–8.3 km s^{-1} beneath the Mariana arc (Takahashi et al. 2008).

4.7.2 Normal-Incidence Reflections

In principle, normal-incidence multichannel seismic reflection surveys can map laterally varying structures in the sub-surface with much greater resolution than more sparsely sampled wide-angle surveys. However, the interpretation of normal-incidence reflection data across island arcs is very challenging, because complex long-period water-layer multiples are generated by the deep variable seafloor, and high-amplitude coherent noise is produced by scattering from the rugose bathymetry around the seismic line. To illustrate the potential of this methodology, two unmigrated seismic sections are presented from areas

where the seafloor is relatively shallow; in such areas, water-layer multiples will decay more rapidly with recording time, and reflections from the lower crust and Moho can be more easily identified.

As with most island arcs, the seafloor depth of the IBM arc system is almost everywhere greater than ~200 m; however, shallow seafloor exists around the island of Farallon de Medinilla on the Eocene part of the Mariana arc. The hard seafloor produces a sequence of high amplitude multiple reflections in the data, but these have largely dissipated by a recording time of ~8 s (Fig. 4.11). Coherent dipping linear arrivals due to scattering around the seismic line (Larner et al. 1983) are also present. Nevertheless beneath the shallow seafloor, sub-horizontal low frequency reflections can be identified between 8 and 11.5 s in a 15-fold stack processed from the airgun shooting line from the 3D survey shown in Sect. 5.3.3. The 7.4 km s^{-1} isovelocity contour, which was interpreted to be the top of the crust–mantle transition zone in a coincident wide-angle seismic survey (Calvert et al. 2008), occurs at a depth of ~24 km here, corresponding to 9.0–9.5 s. The existence of reflections up to 2 s below this contour suggests that the crust–mantle transition extends down to ~32 km, if the downward termination of seismic reflections marks the top of the upper mantle.

The Aleutian arc differs from other intraoceanic arcs in that the seafloor is <200 m along most of the arc massif. Thus imaging of reflections from the deeper crust and upper mantle is not strongly affected by interfering water layer multiples. In fact high amplitude reflections from the top of the subducting Pacific plate visible in a 40-fold stack from line A2 (Fig. 4.2) demonstrate good signal penetration through the arc crust and mantle wedge (Fig. 4.12). These reflections from the top of the plate originate up-dip, i.e., out of the plane of this section. At the west end of the section, the downward termination of lower crustal reflections correlates closely with the position of the Moho inferred by Shillington et al. (2004), but further east the deepest identifiable lower crustal reflections, which are somewhat lower in amplitude, are ~2 s shallower than the Moho.

Despite seismic imaging difficulties, the lack of reported reflections from the igneous crust of island arcs suggests that arc crust is not strongly reflective. Yet the reflection data presented here show that lower crustal reflectors with an apparent lateral continuity of <10 km in unmigrated data can exist beneath island

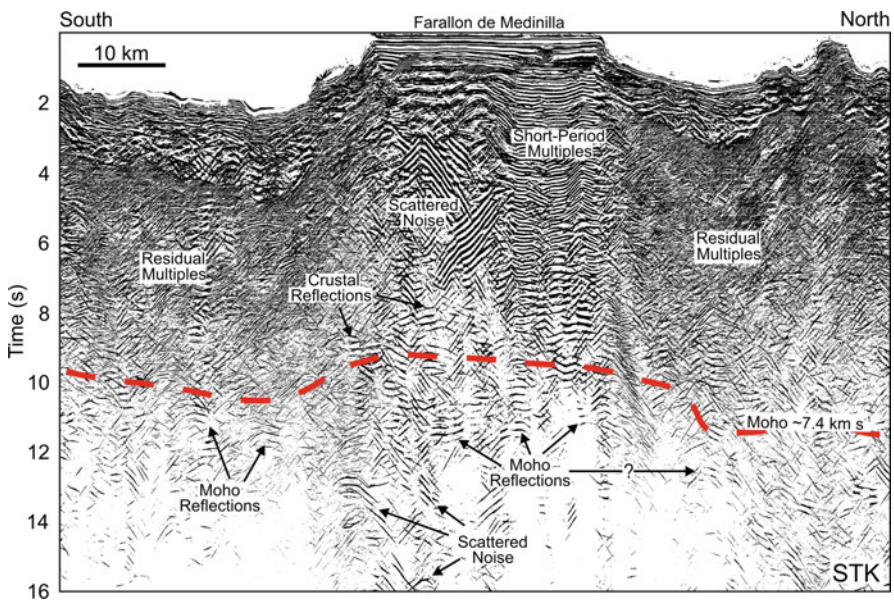

Fig. 4.11 Seismic reflection section along the inactive Eocene section of the Mariana arc. Low frequency reflections, which are laterally continuous over 4–8 km, can be identified between 8 and 11.5 s beneath the shallow seafloor around the island of Farallon de Medinilla. At earlier times, the section is dominated by interfering coherent noise. Reflections up to 2 s below the 7.4 km s^{-1} isovelocity contour, which was interpreted to represent the top of the crust–mantle transition in a coincident wide-angle seismic survey (Calvert et al. 2008), indicate that this transition zone may be ~8 km thick here.

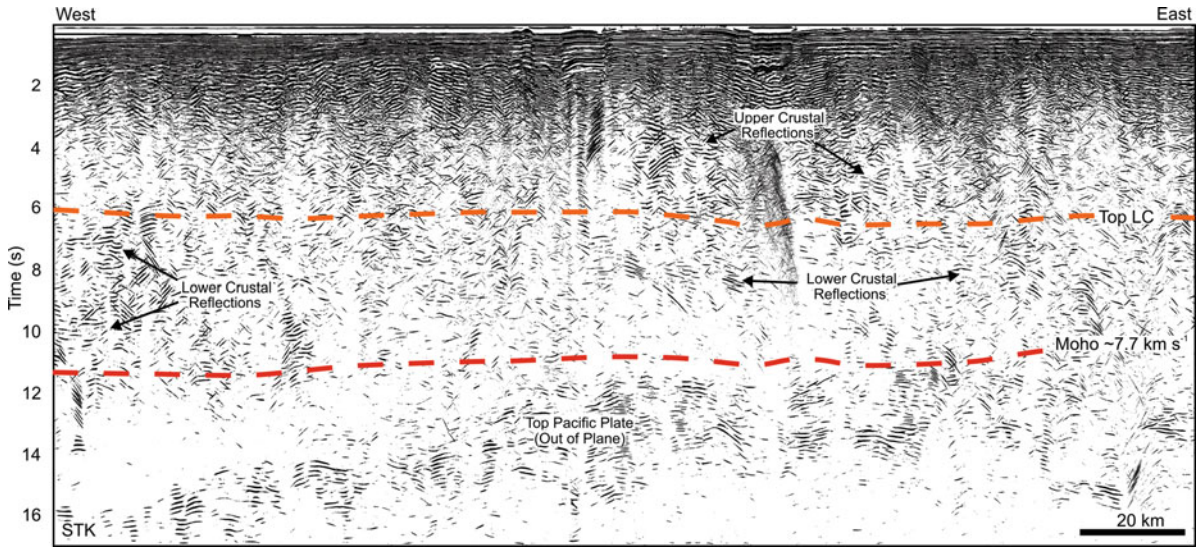

Fig. 4.12 Seismic reflection section along the Aleutian arc. Lower crustal reflections can be identified between 6 and 11 s at the western part of the section and between 6 and 8.5 s further east. Clear reflections from the top of the subducting Pacific plate indicate good signal penetration through the arc crust, but the top of the plate is deeper than it appears in this section, because these reflections originate up dip and out of the plane of this image. The times of the Moho and the top of the lower crust are derived from the velocity model of Shillington et al. (2004).

arcs. In extended arcs, some reflections in the igneous crust might indicate faults or shear zones, but in many cases the characteristics of these deep reflections, or their absence, are likely attributable to magmatic processes, and reflection surveys have the potential to constrain their lateral variability.

4.8 Interpretation of Seismic Velocity Models

The seismic velocities of rocks are affected by a number of factors, including mineralogy, porosity, pore fluid, temperature and confining pressure. In the interpretations of seismic velocity models from island arcs, porosity is considered to be a significant effect mainly in the upper crust, where volcaniclastic sediments and talus from the volcanic edifices can serve to reduce seismic velocities in the upper few kilometres; in the middle and lower crust, porosities are very low although seismic velocities can be affected if certain crack geometries are widespread (Hyndman and Shearer 1989). No localized velocity anomalies that could be interpreted as magma bodies have been inferred in any of the velocity models shown here, implying that the dimensions of any melt zone must be less than the limit of resolution of seismic refraction surveys. Given the magmatism associated with island arcs, it is likely, however, that there are significant lateral variations in temperature within the crust, which could extend over several tens of kilometers. The P wave velocities of igneous crustal rocks decrease with increasing temperature (Birch 1943; Kern 1978; Christensen 1979), and, in the absence of melting, a reduction in lower crustal velocity of 0.12 km s^{-1} has been suggested for the Aleutian arc relative to the same depth in the forearc region (Fliedner and Klemperer 1999). The thermal structure of most island arcs is not well known, but a similar difference in velocities is predicted at a depth of 20 km if the geothermal gradient varies from a high value of 40°C km^{-1} in the active arc to 25°C km^{-1} in the forearc. Given the relatively small effect of temperature on the magnitude of seismic velocity variation at a given depth, most authors interpret velocity variations inferred in the middle and lower crust in terms of mineral composition related to the volcanic arc's magmatic evolution. Such interpretations can be better constrained by a comparison of seismic velocity

models with laboratory measurements of velocity on samples from exhumed island arc crust or continental areas with similar lithologies.

4.8.1 Constraints from Laboratory Measurements

1D velocity-depth profiles were obtained for eight island arcs by laterally averaging the best constrained parts of their respective 2D seismic velocity models (Table 1), and then converted from depth to lithostatic pressure using an empirical relation between velocity and density (Brocher 2005). All profiles were also corrected to a common temperature of 25°C using a conservative geothermal gradient of 25°C km^{-1} and a thermal coefficient of -0.4 m s^{-1}°C^{-1}, which is consistent with a broad range of crustal rocks (Rudnick and Fountain 1995) and produces an increase in the observed velocities of 0.2 km s^{-1} at a depth of 20 km. These corrected 1D seismic velocity profiles are compared to the velocity variation with confining pressure of a number of representative lithologies from two regions where island arc crust has been exhumed: the Tanzawa plutonic complex (Nitsuma 1989) on the Japanese island of Honshu (TPC in Fig. 4.5) and the Kohistan-Ladkh terrane (Bard et al. 1980) of northern Pakistan and northwestern India (Fig. 4.13). Some average velocity functions, e.g. from the Tonga and South Sandwich arcs, only extend as far as the middle crust while others extend into to the uppermost mantle, e.g. the Mariana arc. The envelope of all velocity functions, which is shaded grey is relatively broad at pressures above 0.5 GPa, because the thickness of the crust varies from arc to arc.

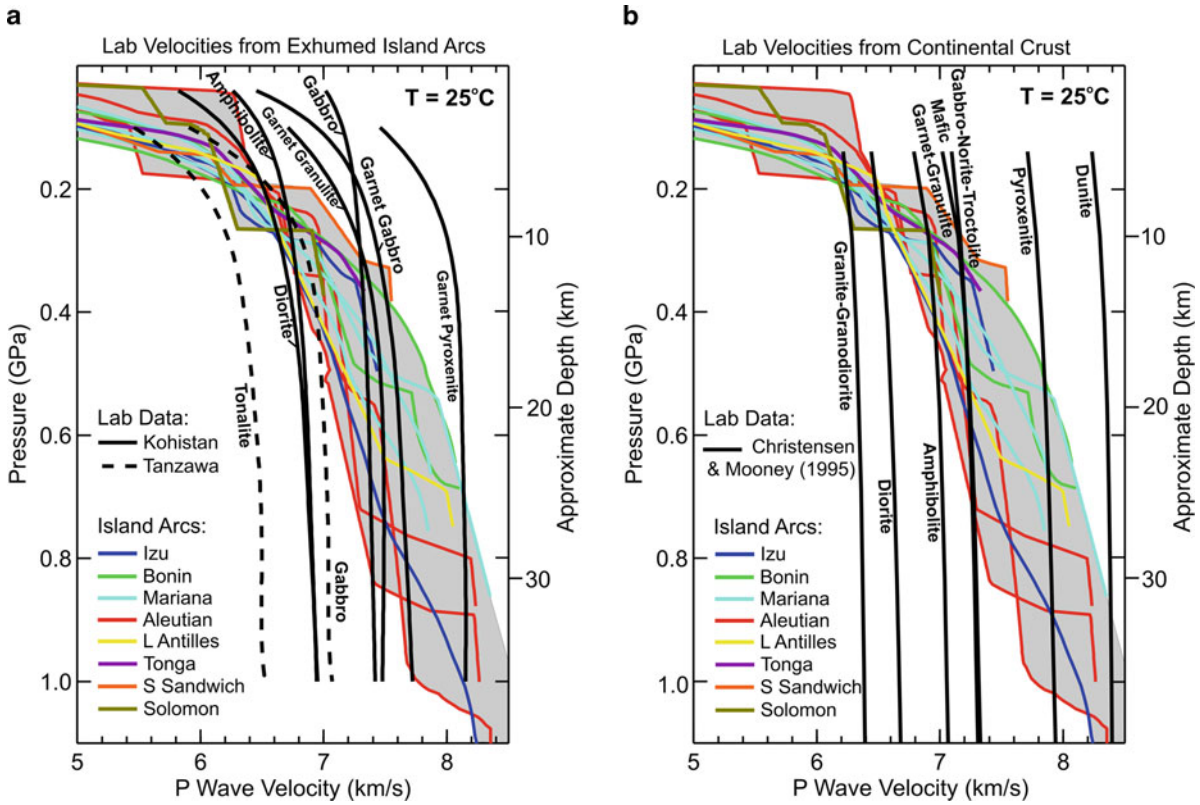

Fig. 4.13 Comparison of island arc velocity functions with laboratory measurements of P wave velocity in cores from: (**a**) Exhumed sections of island arcs; (**b**) Continental crust. The arc velocity profiles were obtained by averaging laterally the best constrained parts of the 2D velocity models, followed by conversion to confining pressure and correction to a constant temperature of 25°C using a thermal coefficient of -0.4 m s^{-1}°C consistent with most igneous rocks (Rudnick and Fountain 1995). The *shaded grey area* represents the range of velocities inferred in island arcs from wide-angle seismic surveys. The sources for the arc velocity profiles are listed in Fig. 4.14.

As pointed out by Behn and Keleman (2003), it is impractical to invert P wave velocity data for whole rock geochemistry, or to even determine in detail the SiO_2 content of igneous rocks; however, the comparison of seismic refraction models with measurements on core samples data and velocities calculated for given compositions can guide a first order interpretation.

The suite of tonalitic and gabbroic plutons of the Tanzawa plutonic complex was exhumed in the collision between the northernmost Izu arc and the Honshu arc that began ~7 Ma ago (Kawate and Arima 1998; Yamamoto and Kawakami 2005). These plutons intruded volcanic rocks, hemipelagic sediments, and volcaniclastic sediments of the Miocene Tanzawa Group whose metamorphism indicates a maximum depth of approximately 6 km (Arai 1987). Once thought to be the middle crust of the Izu arc, recent U-Pb geochronology has shown that while one tonalite has an age of 9 Ma, the others are approximately 4–5 Ma old and thus syncollisional (Tani et al. 2010). Measurements of P wave velocity versus confining pressure for three tonalites (56–71% SiO_2) and three gabbros (43–54% SiO_2) (Kitamura et al. 2003) were each averaged and fit with a fifth-order polynomial to create a lithology-specific velocity variation (dashed lines in Fig. 4.13a).

The exposed Cretaceous Kohistan arc was obducted during the collision of India with Eurasia, and comprises a near-complete crustal section extending from upper crustal volcanics to the uppermost mantle. The arc initially developed in an intra-oceanic setting, but formed an Andean-style margin after its accretion to Euriasia (Burg in Chap. 10; DeBari et al., in Chap. 5). Using velocity measurements published by Miller and Christensen (1994), representative velocity variations with pressure have been calculated for diorite (44–76% SiO_2), amphibolite (47–57% SiO_2), gabbro (43–50% SiO_2) and garnet gabbro (41–52% SiO_2 with 30–50% garnet) and these data are shown with solid lines in Fig. 4.13a. Lab measurements from Kono et al. (2009) have been used to derive velocity variations for garnet granulite (49–52% SiO_2 with 24–37% garnet) and garnet pyroxenite (41–48% SiO_2 with 15–60% garnet); the garnet granulites of Kono et al. (2009) are similar rocks to the garnet gabbros of Miller and Christensen (1994).

At low confining pressures, the laboratory P wave velocities increase notably with increasing pressure due to the closure of microcracks in the sample (Kitamura et al. 2003), but at pressures greater than ~0.5 GPa, the velocity variation with pressure is considerably less, and the difference in velocity of the various lithologies is related to their different (to first order mafic) mineral content. A similar relationship is seen with velocity measurements on lithologies from a broad range of continental crust (Fig. 4.13b). The velocity variation within specific lithologies at a given confining pressure is indicated by standard deviations from Christensen and Mooney (1995), which typically range from ~0.1–0.25 km s^{-1}, with gabbro-norite-troctolite being at the upper end of this range. Gabbros from the Kohistan arc have higher velocities than those from the Tanzawa plutonic complex, consistent with this finding.

At pressures greater than 0.2 GPa, the tonalites from the Tanzawa plutonic complex exhibit lower velocities than those found in any island arc, even allowing for a reasonable velocity variation between different samples. This observation indicates that voluminous tonalite is only likely to occur in island arcs at depths less than ~8 km. The relatively high velocities in the upper crust of the Aleutian arc suggest the presence of significantly more mafic rocks. Although the geothermal gradient and thermal coefficient introduce some uncertainty, island arc velocity profiles derived from seismic refraction surveys are consistent with a composition somewhere between diorite and gabbro at pressures of 0.2–0.3 GPa. At greater pressures, seismic velocities correspond to gabbroic rocks with a lower quartz content. Temperature-corrected P wave velocities greater than approximately 7.4 km s^{-1} may indicate the presence of garnet in gabbros with a low plagioclase content or pyroxenites characteristic of restites (Kitamura et al. 2003).

4.8.2 Upper Arc Crust

In general, the upper crust of island arcs can be viewed as a layer of sedimentary rocks derived through a range of processes overlying igneous crust, but in detail the uppermost crust is commonly heterogenous due to volcanism and intrusion into the upper crustal section, as demonstrated in the Tanzawa plutonic complex. In many arc velocity models, an uppermost, relatively low velocity sedimentary layer has been defined using coincident multichannel seismic reflection data, stacking velocities and/or velocities from first arrival tomography of the towed streamer data. These sediments

accumulated in small basins within the arc massif, on the flanks of the arc itself or in the deep ocean basin. The base of this layer is typically defined by a sharp increase in velocity in the models, and may directly overlie the igneous crust, for example as interpreted along the strike of the Aleutian arc where the velocities beneath the sedimentary layer are 6.0–6.5 km s^{-1}. In other arcs, the increase in velocity at the base of the upper sedimentary layer is smaller, but a high velocity gradient exists in the underlying layer, with velocities increasing downward from ~3.5 km s^{-1} to >5.0 km s^{-1} over a few kilometers. Such a region may correspond to interbedded, and variably metamorphosed volcanics, hemipelagic and volcaniclastic sediments intruded by plutons of different ages and composition.

At shallow depths, basaltic rocks can have relatively low velocities, making them difficult to identify on the basis of P wave velocity alone. For example, velocities as low as 2.5–3.0 km s^{-1} have been inferred in the extrusive basaltic layer of 0–3 Ma old oceanic crust using OBS surveys, and a gradual increase in velocity to 3.5–4.5 km s^{-1} by 4–5 Ma, and to 4.0–5.5 km s^{-1} at ages greater than 50 Ma due to porosity reduction has been documented (White 1984). In island arcs, the increase in velocity with depth may be partly associated with a comparable reduction in porosity through compaction and the filling of pores by hydrothermal circulation, and an increasing prevalence of intrusive rocks. The base of the upper crust has been interpreted in most arc velocity models to be located where the high velocity gradient, which is characteristic of the upper crust, decreases sharply and the P wave velocity reaches approximately 6.0 km s^{-1}, but this value is 6.5 km s^{-1} in the case of the line along the Aleutian arc. This strike line suggests that the upper crust of the Aleutian arc is largely basaltic, because the velocities are 6.0–6.5 km s^{-1} at depths as shallow as 2 km where fracture porosity reduces P wave velocity values. At such shallow depths, felsic rocks would likely have velocities below 6.0 km s^{-1}, but the unknown porosity is a source of significant uncertainty.

4.8.3 Middle Arc Crust

The middle crust has been defined in different studies both in terms of seismic velocity and as the region between intracrustal reflectors with some degree of lateral continuity along a seismic profile. In surveys across the IBM arc system, for example, the mid-crust is interpreted to be the region with velocities between 6.0 and 6.5 km s^{-1} between two intracrustal reflectors, e.g. Takahashi et al. (2007). Kodaira et al. (2007a) refer to the region with these velocities as the upper middle crust and a deeper region with velocities of 6.5–6.8 km s^{-1} as the lower middle crust; however, Takahashi et al. (2007) and Calvert et al. (2008) associated velocities of 6.5–6.8 km s^{-1} with the upper part of the lower crust. In the Aleutian arc, which is generally characterized by higher seismic velocities, the mid-crustal layer has velocities of 6.5–7.3 km s^{-1} with the upper and lower boundaries constrained by intracrustal reflections. With the greater thickness of Aleutian arc crust, the base of the middle crust occurs here at a depth of 15–20 km, and it is worth noting that these depths correspond to the lower crust along much of the IBM arc, and even the upper mantle in those parts of the Bonin arc where the crust has been thinned by rifting. Thus the term middle crust is not used in a way that is consistent between surveys, in part due to the different approaches to analysis of the various seismic surveys, but also due to the term's implicit relation to overall crustal thickness. Here I shall assume that arc crust can be loosely divided into upper, middle and lower regions with approximate relative proportions of 3, 4, and 5 respectively, and the term middle crust will be used loosely to refer to that third of the crust between the upper and lower regions. Where a region predominantly within the middle crust is bounded by two intracrustal reflectors, the term mid-crustal layer, which allows a broad range of seismic velocities within it, will be used. Inferred crustal composition is better associated with regions characterized by a specific range of seismic velocities (but with the implicit assumption of a depth range, i.e., confining pressure) than a generalised "middle crust".

Based on seismic velocity measurements on samples from the Tanzawa plutonic complex, velocities of 6.0–6.5 km s^{-1}, which are too low to be most gabbroic rocks at depths of 5–15 km, indicate the presence of tonalitic rocks, but the higher end of this velocity range is too high to be consistent with pure tonalite. Mapping of the Tanzawa plutonic complex suggests that the middle to upper crust of the Izu arc includes plutonic rocks that range from pyroxene-hornblende gabbronorite to relatively quartz rich tonalite (Kawate and Arima 1998). It is an oversimplification to

associate a single lithology with velocities of 6.0–6.5 km s^{-1}, which probably represent a region of average "intermediate" composition similar to quartz gabbro that comprises tonalite, diorite and gabbro. Within the IBM arc, the thickness of the region in the upper and middle crust with velocities of 6.0–6.5 km s^{-1} varies between 2 and 8 km. Such seismic velocities are only found in the uppermost crust of the Aleutian arc.

P wave velocities of 6.5–6.8 km s^{-1} indicate a crust more dominated by gabbroic lithologies. Velocities lower than 6.9 km s^{-1} are difficult to simulate in pristine gabbros using models of mantle melting (Korenaga et al. 2002), but the velocities of gabbroic rocks recovered from ocean crust by drilling are 6.5–7.4 km s^{-1} (Iturrino et al. 1991; Iturrino et al. 1996). These lowest velocities in oceanic crust may arise from ridge-crest faulting and thermal contraction (Korenaga et al. 2002). Faulting associated, for example, with arc rifting in the IBM arc-back-arc system or block rotation in the Aleutian arc could locally reduce gabbroic velocities in island arcs. It is also possible that velocities of 6.5–6.8 km s^{-1} indicate a region comprising plutons of both gabbroic and intermediate composition with a reduction in the volume of intermediate composition rocks with increasing depth and seismic velocity. The rugose velocity contours shown in some of the velocity models, e.g. along the Izu-Bonin arc could be an indication of this heterogeneity. There is also a large range of velocities, 6.5–7.3 km s^{-1}, within the mid-crustal layer of the Aleutian arc, but the average velocity of 6.92 km s^{-1} indicates a primarily gabbroic composition with lower velocities perhaps associated with the local presence of more felsic rocks (Shillington et al. 2004).

4.8.4 Lower Arc Crust

In many surveys of arc crust, the Moho is usually located using PmP reflections, because few Pn diving waves are observed at offsets >120 km. The lower crust is commonly bounded below by this reflector. Seismic velocities in the lower crustal layers beneath the Izu, Bonin and Mariana arcs are 6.8–7.3 km s^{-1}, 6.7–7.4 km s^{-1}, and 6.8–7.4 km s^{-1} respectively. In the lines across the Aleutian arc, velocities of 6.9–7.2 km s^{-1} were inferred in this layer along line A1 in the west and 6.9–7.5 km s^{-1} along line A3 in the east; velocities of 6.8–6.9 km s^{-1} at the northernmost end of line A3 could indicate the presence of continental crust associated with the former Beringian margin. As discussed above, these velocities are essentially consistent with the presence of quartz-poor gabbroic plutons; however, velocities as high as 7.4–7.5 km s^{-1} may indicate either ultramafic cumulates or perhaps partially intruded, partially serpentinized peridotite as suggested beneath the forearc of line A3 (Lizarralde et al. 2002). Lower crustal velocities of 7.3–7.7 km s^{-1} derived along the strike of the Aleutian arc are higher than found on the intersecting profiles, but the interpretation of a mixture of mafic and ultramafic rocks, including garnet-bearing assemblages, is generally similar (Shillington et al. 2004). Along line A2, higher velocities occur at the centre of a structural block, leading Shillington et al. (2004) to suggest that lower temperatures here result in relatively high pressure fractionation and a greater volume of mafic restite.

4.8.5 Crust–Mantle (Moho) Transition Zone

The thickness of arc crust is often constrained by PmP reflections, but where large offset Pn arrivals are well recorded velocities immediately beneath the Moho reflector have been found to be significantly lower than typical upper mantle velocities; velocities of 7.7 and 7.6 km s^{-1} were found below the Mariana arc and remnant West Mariana ridge respectively (Takahashi et al. 2007). An upper mantle velocity of 7.8 km s^{-1} is only attained 4 and 3 km below the Moho reflector respectively, suggesting the presence of a vertically distributed crust–mantle transition. Although the presence of melts or serpentinized mantle peridotites might explain low velocities under the modern arc, neither explanation is likely to apply beneath the remnant arc where there is no water rising from the subducting slab. It seems more plausible that a gradual crust–mantle transition zone is a primary feature of island arc formation.

Kodaira et al. (2007a) similarly interpret a 5–10 km thick layer with velocities of 7.2–7.6 km s^{-1} at the base of the Izu-Bonin arc crust. Sato et al. (2009) modelled the elastic response of wide-angle reflections from the top and bottom of the Izu crust–mantle transition, and

estimated that the P wave velocity contrasts varied from approximately 0.2–0.4 km s^{-1} along the arc; where the contrast at the top of the layer was high, the contrast at the base was relatively low, and vice versa. If the uppermost mantle comprises olivine cumulates, i.e., dunite, formed during initiation of the arc, then the crust–mantle transition zone is probably a mixture of olivine cumulates and mafic restite (Tatsumi et al. 2008). The laterally varying velocity perturbations at the top and bottom of the crust–mantle transition could thus indicate the relative proportion of these two components; for example, a small upper velocity contrast over a larger lower contrast would indicate a lower proportion of olivine cumulate (Sato et al. 2009). In thicker arcs, pyroxenites may be more likely to occur at the crust–mantle transition than dunite (DeBari et al., in Chap. 5). This form of heterogeneity in the Mariana crust–mantle transition could generate the normal incidence seismic reflections tentatively identified over a depth range of ~24–32 km beneath Farallon de Medinilla in the Mariana arc (Fig. 4.11).

Most PmP reflections appear to originate from the top of the crust–mantle transition layer, and fewer wide-angle reflections are recorded from the base, e.g. Takahashi et al. (2009), perhaps because the contrast at the base of the crust–mantle transition is commonly smaller than at the top (Sato et al. 2009). Thus under an island arc, the interface that generates PmP reflections is best considered a top-Moho reflector, and the crustal thickness estimates quoted in this paper relate either to this reflector or a proxy for it, such as an isovelocity contour.

During repeated episodes of basaltic underplating, reaction of plagioclase with clinopyroxene can produce garnet in mafic restite if the depth is greater than approximately 25 km (Behn and Keleman 2006; Tatsumi et al. 2008), increasing the seismic velocity to 7.3–7.7 km s^{-1} (see also Fig. 4.13); however, the depth at which garnet occurs is quite sensitive to the geotherm. At depths greater than 30 km, garnet-producing reactions can also increase the seismic velocity of pyroxenites (Kono et al. 2009). Thus an alternative suggestion is that reflectors at the crust–mantle transition or within the uppermost mantle wedge might arise from a sudden downward increase in the proportion of garnet (Shillington et al. 2004; Takahashi et al. 2008). In the Kohistam paleo-arc, the crust–mantle transition is exposed as a continuous mafic-ultramafic layered intrusion progressing downward in paleodepth from garnet gabbro/garnet granulite, to garnet pyroxenite, to pyroxenite/dunite; the presence of garnet is due to the 36–45 km depth of the lowermost crust in a mature arc (Garrido et al. 2006). At the transition from garnet gabbro to garnet pyroxenite, the P wave velocity increases from 7.3–7.7 to 7.9–8.3 km s^{-1} due to disappearance of plagioclase which determines the base of the Moho transition zone in this setting (Kono et al. 2009). The presence of garnet will increase the average seismic velocity of the deep crust, but it is uncertain whether its distribution will cause seismic reflections. A crust–mantle transition zone is also observed in relatively thin arcs such as the Bonin arc; the 7.5 km s^{-1} contour lies at a depth of 15–20 km (Fig. 4.7b). In this shallower setting, the crust–mantle transition is likely to be a gradual change from mafic to ultramafic lithologies with minimal garnet present.

4.9 In Situ 1D Velocity-Depth Functions

Average in situ 1D velocity-depth functions have been obtained for several island arcs by laterally averaging sections of 2D velocity models derived by various authors (Table 4.1 in Appendix). The envelope of these velocity functions is shaded grey area in Fig. 4.14a. Line A3 across the Aleutian arc extends onto the continental crust of the Beringian margin, which is characterized by a mid-crustal layer of 6.4 km s^{-1} and a lower crust with velocities of 6.8–6.9 km s^{-1} (Fig. 4.2), and the proximity of this crust to the volcanic line is sufficient to perturb the average 1D velocity-depth function here into the range of continental profiles (dashed red line in Fig. 4.14a).

A seismic profile oriented along an island arc samples a greater volume of arc crust, and is thus likely to be more representative. The difference in the shape of the four 1D velocity functions along the IBM arc is primarily due to the variation in crustal thickness between the arcs (Fig. 4.14b). The Izu arc, which is well characterized by the recent survey of Kodaira et al. (2007a), is up to 35 km thick, and its average velocity profile in the middle and lower crust differs from that of the Aleutian arc by <0.3 km s^{-1}. In fact, the most striking difference between the Izu and Aleutian arcs is the presence of velocities of 6.0–6.5 km s^{-1} in the upper 5 km of the Aleutian arc, which is well

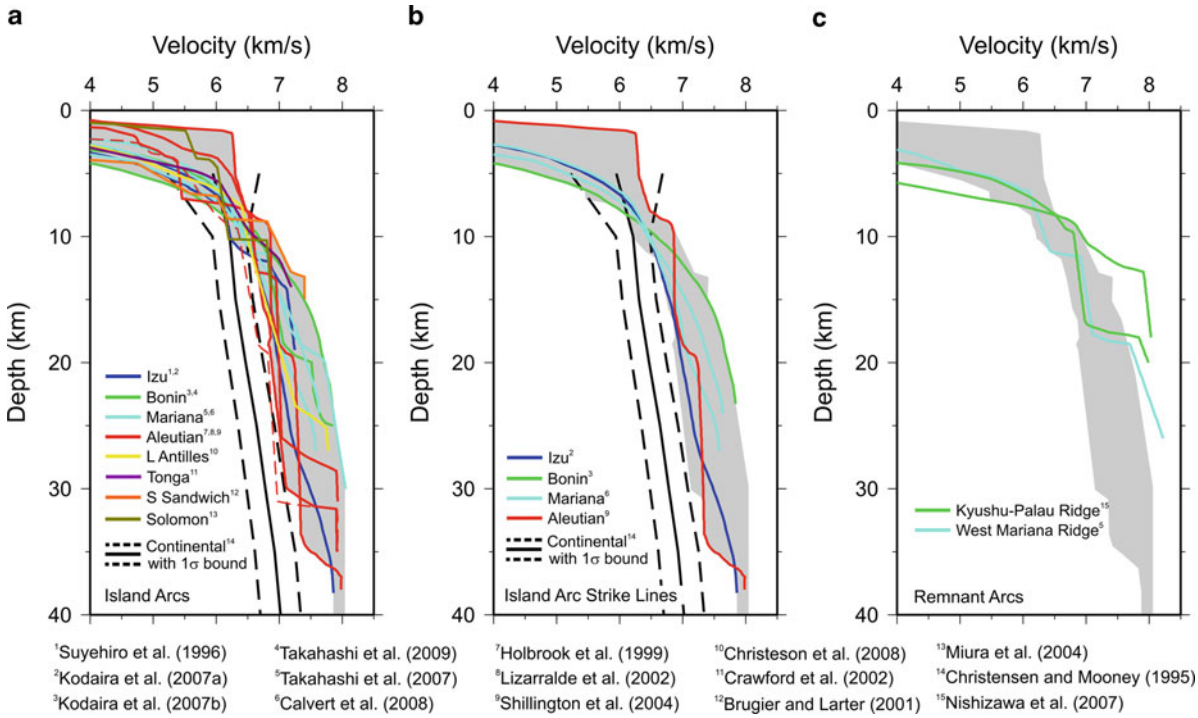

Fig. 4.14 Comparison of in situ island arc velocity profiles with the range of velocity values estimated for continental crust from wide-angle seismic surveys: (**a**) All island arc surveys; (**b**) Lines along island arcs, which represent a relatively large volume of arc crust; (**c**) Remnant arcs. The *grey shaded area* encompasses 1D velocity profiles from a broad range of island arcs. The *dashed red line* is derived from around the volcanic line on line A3 across the Aleutian arc, but the velocities in this profile are lowered by continental crust of the former Beringian margin.

constrained by streamer tomography (Shillington et al. 2004). These higher velocities may be attributable to the erosion of an original carapace of relatively high porosity flows and volcaniclastic rocks, resulting in an extensive, high velocity arc massif with a seafloor less than 200 m deep (Fig. 4.2), in contrast to the deep water settings of most other island arcs.

Remnant arcs tend to fall outside the envelope of functions for active island arcs due to their variable seafloor depth and crustal thickness, which are controlled by the original locus of arc rifting. For example, some crustal sections of the Kyushu-Palau ridge are only slightly thicker than oceanic crust (Fig. 4.7d), because rifting occurred in the rear arc.

The velocity depth functions used to represent continental crust in Fig. 4.14 were obtained after removal of the sedimentary basins (Christensen and Mooney 1995), and any comparison with island arc crust should, strictly speaking, use arc velocity functions referenced to the top of the igneous crust. Identification of the top of the igneous crust in island arcs is not straightforward due to the presence of high porosity volcanic rocks and intrusions within the shallow sedimentary section. Taking the 3.5 km s^{-1} isovelocity contour to be an approximation to this boundary, as is so at mid-ocean ridges (White 1984), a representative 1D velocity function for island arcs has been calculated using this datum (Fig. 4.15). (See Table 4.2 in Appendix for tabulation of reference velocity functions for this datum, as well as seafloor and mean sea level datums). Above a depth of ~8 km, island arc velocities are similar to those of continental crust and consistent with the presence of felsic rocks; however, seismic velocities in the uppermost crust can also be lowered by the increased porosity found there, and, as mentioned previously, the velocities in the uppermost crust are also consistent with porous mafic rocks. At depths greater than ~8 km, island arc crust is on average characterized by higher in situ seismic velocities, and is hence more mafic, than continental crust. Generation of continental crust directly from island arcs would require the removal of the large volume of crust that presently exists at depths greater than 10 km.

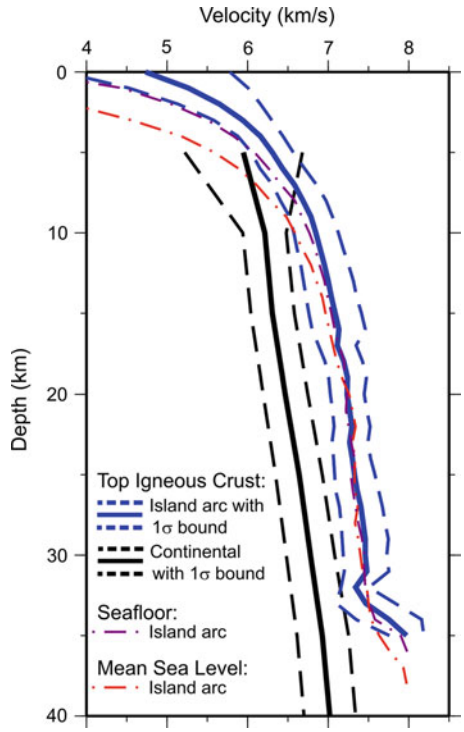

Fig. 4.15 Comparison of the average seismic velocity functions for island arcs with that of continental crust from Christensen and Mooney (1995). The different depth datum levels are indicated. Note that the range of data included in the island arc average decreases below 30 km depth, because there are few velocity models that extend this deep.

4.10 Evolution of Island Arc Crust

Although 1D velocity functions reveal the typical average velocity variation with depth in island arc crust, significant lateral variations can be present along strike; for example, the thickness of crust with velocities of 6.0–6.8 km s^{-1} increases beneath, or close to, basaltic volcanoes along the Izu arc, and decreases beneath rhyolitic volcanoes (Kodaira et al. 2007a). A variation in the thickness of crust with velocities of 6.0–7.0 km s^{-1} is also observed along the Eocene Mariana arc (Calvert et al. 2008), but as with the Izu arc, most of the lateral variation is associated with velocities greater than 6.5 km s^{-1}. Thicker regions of crust with velocities of 6.0–6.8 km s^{-1} have been interpreted to indicate locally elevated generation of tonalitic crust; however, at depths greater than 8 km the crust is intermediate to mafic in terms of its average bulk composition. Over the >40 Ma life of the IBM arc, repeated episodes of magmatic intrusion into the lower crust have resulted in anatexis and intracrustal differentiation; see, for example, Tatsumi et al. (2008) and DeBari et al., in Chap. 5. While intermediate composition magmas generated by this process rose into the upper crust, some of these magmas may have solidified at depths as great as 20 km, reducing the seismic velocities from those characteristic of quartz-poor gabbro.

Generation of intermediate composition magma by melting of basaltic crust will produce a residuum of pyroxenite restite (Nakajima and Arima 1998), implying an increase in the volume of high-velocity mafic rocks in the lower crust. However, thickening of the lower crust beneath thicker regions of inferred intermediate composition is not typically observed; in tomographic velocity models the mafic lower crust commonly becomes thinner (Calvert et al. 2008), as can be observed at 180 km, 250 km, 320 km in Fig. 4.4b in the case of the Izu arc. Two alternative explanations for the observed decrease in the thickness of the high velocity lower crust beneath regions of growth in intermediate crust are:

1. With an in situ P wave velocity of 7.3–7.6 km s^{-1} (Behn and Keleman 2006), pyroxenite restite can lie below the Moho in several velocity models, suggesting that the generation of intermediate composition melts can raise the level of the interpreted Moho, a seismologically defined boundary, within a petrologic lower crust and produce an apparent thinning of high velocity lower crust (Tatsumi et al. 2008).
2. With a density of 3.2–3.9 g cm^{-3} (Nakajima and Arima 1998), which is similar to or greater than peridotite in the uppermost mantle, restite may have detached from the arc crust and foundered. If this speculation is correct, then arc crust with a relatively thin high velocity lower crust could be an indication that this delamination process has occurred. In a detailed analysis of the stability of arc lower crust, Behn and Keleman (2006) show that pyroxenite and gabbronorite characteristic of arc lower crust can become denser than underlying harzburgite at pressures greater than ~0.85 GPa, i.e., ~30 km depth, due to the decrease in the amount of plagioclase and the formation of garnet in some rocks. Gravitational instability has thus been suggested if arc crust grows to more than 30 km thick; however, some island arcs, e.g. the Bonin arc, may not reach such thicknesses due to multiple episodes of extension that limit their vertical growth.

4.11 Comparison of Aleutian and IBM Arcs

In terms of seismic structure, the northern Izu arc, whose rear arc was subject to one episode of rifting in the Oligocene that created the relatively thin Kyushu-Palau ridge (Okino et al. 1994), appears most similar to the Aleutian arc with a somewhat less mafic composition, and a crustal thickness of 26–35 km versus the 35 km of the Aleutian arc. In contrast, the Bonin arc was subject to extension in the Eocene, which placed the Ogasawara Ridge in the forearc (Ishizuka et al. 2006), rifting of the rear arc in the Oligocene to remove the Kyushu-Palau ridge, and probably another episode of extension to create the Nishinoshima Trough, whose origin is poorly understood. As a result, the Bonin arc and forearc extend over 400 km from the trench, and comprise three distinct crustal blocks, none of which exceeds a thickness of 20 km, separated by thinned arc crust 10–12 km thick (Fig. 4.7b). The broad region of thin, 10–17 km thick, arc crust identified on the strike line (Fig. 4.4b) is likely a consequence of separation of the Ogasawara ridge, consistent with the suggestion that much of the arc crust was generated early in its history (Stern and Bloomer 1992). As indicated by the along-strike velocity profiles in Fig. 4.14b, the Mariana arc has a seismic structure intermediate between the northern Izu and Bonin arcs, which is presumably due to the Mariana arc massif being subject to less extension than the Bonin arc.

Arc rifting may result in the addition of high velocity magmatic material to the base of both the active and remnant arcs by decompression melting similar to that which has created magmatic underplates at some passive continental margins (Takahashi et al. 2008). In the case of the Mariana arc and West Mariana ridge, this characteristic mafic underplate appears to be a relatively small proportion (<5–8%) of the total crustal volume, but modification of arc crust by rifting is an issue that merits more detailed study.

Since the Eocene the average magmatic production rates of the Aleutian and Mariana arcs are estimated to be 82 km^3/km/Ma (Holbrook et al. 1999) and 80 km^3/km/Ma (Calvert et al. 2008) respectively, which fall within the range of 30–85 km^3/km/Ma derived for several arcs in the western Pacific (Dimalanta et al. 2002). Although these estimates of average productivities of the Aleutian and IBM arcs appear to be generally similar, differences in the distribution and volume of crust within these two arcs could be attributable to spatial and temporal variations in the magmatic flux from the mantle in addition to the effects of extension and arc rifting.

4.12 Implications for Arc–Continent Collision

Most island arcs, including both the Aleutian and IBM arcs, lie distant from continental areas and are subject to a restricted terrigenous sediment supply. As an island arc approaches a continental margin the sediment input to the arc will increase, very significantly in some cases due to uplift and erosion in the collision zone, and a thick sedimentary section can develop on the flanks of the island arc, across the forearc, and fill

the back-arc basin, if present. The Lesser Antilles arc is an example of this situation where sediment derived primarily from the northern margin of South America has formed a large accretionary wedge east of the Tobago basin, obscuring the trench in the southern part of the subduction zone (Fig. 4.9). Therefore prior to collision, the crust surrounding an island arc is likely to develop a much thicker sedimentary section due to this relatively late sedimentary input than implied by the tomographic velocity models from the Aleutian and IBM arcs, which now lie far from continental sediment sources.

Along-strike variations in the thickness of island arc crust, which ranges from 10–35 km in the case of the Izu-Bonin arc, will strongly influence the structural style of any arc–continent collision in which it is involved. Thin crust may be either obducted or underplated depending on its composition, and hence buoyancy, relative to a passive continental margin. Thick arc crust may be accreted to the edge of the incoming margin; for example, the 35 km-thick Stikinia arc terrane is interpreted to have partly overridden and accreted to the paleo-margin of western North America (Cook et al. 2004). The transition between these two processes might occur over distances along the strike of the arc as small as 300 km, the distance over which the Izu-Bonin arc thins from 35 to 10 km. Since the incoming arc will often be oblique to the margin this distance may be smaller along the strike of the collision zone. The seismic velocity variations inferred within the mid-crust of the Izu arc suggest that compositional variations at a scale of 50 km may also be apparent in accreted arc rocks.

Where a rifted island arc and its associated remnant arc are involved in arc–continent collision, the final post-collision geometry after closure of the ocean basin may contain a repetition of arc rocks with similar ages separated by younger arc rocks from the successor arc created after the initial collision, assuming that there has been not flip in subduction polarity.

4.13 Conclusions

A compilation of 1D seismic (P wave) velocity functions from eight island arcs, which are derived from well-constrained velocity models extending over 2,000 km of island arc crust, shows that overall island arc crust is predominantly mafic. At depths greater than 8–10 km, i.e., confining pressures >0.2 GPa, arc crust is characterized by in situ seismic velocities greater than 6.5 km s^{-1}, clearly distinguishing it from typical continental crust (Fig. 4.15). Although felsic-intermediate rocks such as tonalite may be present over a broad depth range, such rocks can only predominate at depths less than 8 km; however, it is not possible to determine their proportion accurately at these relatively shallow depths, because the seismic velocities of mafic rocks can be significantly reduced by fluid-filled porosity.

In detail, island arc crust is characterized by its lateral variability, both across the arc as might be expected, but also along the arc. The crustal thickness of an island arc can be qualitatively related to the amount of extension it has undergone with the thickest 35 km island arc crust found in the Aleutian arc where extension has been minimal. The crust of the Izu arc, which has only been subject to removal of the Kyushu-Palau ridge from the rear arc thus limiting the volume of crust lost, is 26–35 km thick. In contrast the Bonin arc has been thinned by at least three episodes of extension, two of which did not lead to back-arc spreading, resulting in a 400 km wide arc and forearc with laterally variable 10–22 km thick crust. The average velocity profiles of other island arcs appear to lie between these end members, but the lower arc crust is not always well constrained in these other locations. Forearc crust commonly thins to 10–12 km close to the trench, but igneous crust as thick as 16 km has been observed in the Mariana and Bonin forearcs, suggesting that significant lateral variability can be present. Forearc crust can also thicken prior to collision through the accumulation of a thick sedimentary section derived from the approaching continent.

Arc crust can vary in thickness from 10–35 km over 300 km along strike, while the forearc can vary from 9–16 km over 50 km. Such changes in crustal thickness, and perhaps composition, due to an island arc's tectonic and magmatic evolution are likely to have a strong influence on the fashion in which arc–continent collision unfolds, resulting in significant along-strike variations in the character of preserved arc crust; for example, island arcs that have not been subject to extension are likely to have a relatively thick mafic middle and lower crust that may be less susceptible to obduction onto an incoming passive margin.

The seismic surveys reviewed here have been acquired using different parameters, especially numbers of recording seismometers, and analysed using different methodologies. The characteristics of the derived velocity models are a consequence of the methods used to produce them, with the assumption of lateral continuity often necessitated by a large receiver spacing. Comparisons of different island arc systems would be greatly facilitated by the use of similar, densely sampled acquisition geometries, which provide greater confidence in secondary phase identifications and permit the use of similar tomographic inversion techniques. 2D profiles across an arc are required to determine the broader tectonic setting and to allow estimation of magmatic flux from arc growth rates, but intriguing recent results have come from seismic profiles along arcs; strike profiles are an effective way of identifying both large-scale variations in arc structure and localised tectonic features that merit further detailed study. 3D surveys, which provide seismic velocity throughout a large crustal volume, can provide more robust estimates of arc growth, but at the cost of additional field effort.

The large-scale P wave velocity structure of many island arcs has been well determined over the last two decades. Looking forward, complementary S wave velocity models could help discriminate mafic and ultramafic lithologies in the lowermost arc crust (Behn and Keleman 2006). Seismic waveform inversion methods, which require an OBS spacing of ~1 km, can provide higher resolution velocity models, and have the potential to reveal the way tonalitic intrusions are distributed in the upper crust. Great progress has been made in understanding the seismic velocity structure of the lowermost arc crust and upper mantle wedge. However, combining a 3D active source survey with coincident passive recording where high levels of intraplate seismicity are present in a relatively shallowly subducting slab could generate the dense ray coverage necessary to refine velocity models at depths of 25–40 km, and better constrain deep magmatic processes. Coherent scattered noise and water-layer multiples usually obscure deep reflections, where present, in multichannel seismic profiles; progress on these two issues, which likely requires some form of 3D acquisition, might allow seismic reflection surveys to provide a complementary, higher resolution perspective on island arcs.

Acknowledgements I am very grateful to those who generously contributed seismic velocity models for this paper: G. Christeson, W. Crawford, S. Holbrook, S. Kodaira, E. Kurashimo, R. Larter, D. Lizarralde, S. Miura, A. Nishizawa, D. Shillington, N. Takahashi, and H. van Avendonk. Constructive reviews by Steve Holbrook and an anonymous reviewer plus comments from Sue DeBari improved the final manuscript. The bathymetry data for all the maps were obtained from the National Oceanic and Atmospheric Administration ETOPO1 global relief model (Amante and Eakins 2009). This project was supported by the Natural Sciences and Engineering Research Council of Canada.

Appendix

Table 4.1 lists the sections of the various wide-angle velocity models that were laterally averaged to create the 1D velocity-depth functions shown in Figs. 4.13 and 4.14. The x-coordinates correspond to those used originally in the publications cited. A maximum depth, below which the velocities are not considered well constrained, was chosen for each velocity function, and velocity functions are only displayed above these depths.

Representative 1D velocity depth functions for island arc crust were calculated by averaging the sections of the 2D arc velocity models listed in Table 4.1 (but excluding the continental part of Aleutian line A3) using three difference reference datums: mean sea level, the seafloor (taken to be the 1.52 km s^{-1} isovelocity contour), and the top of the igneous crust (Fig. 4.15). In many island arc settings, the top of the igneous crust is not well defined due to low velocity, high porosity volcanic rocks and intrusions into the overlying sedimentary section; so the 3.5 km s^{-1} contour was used to approximate this boundary. To obtain a 1D velocity model for a particular reference datum, e.g. the seafloor, each velocity model was depth-shifted so that the velocity value immediately below the datum was aligned at zero across the 2D model. This results in higher velocities at zero depth than the selected datum value due to discretization of the velocity models. All the 2D models were then averaged. The contribution of a particular velocity model to the average velocity functions depends on the length of the model in Table 4.1. Thus the long-strike lines along the Aleutian and Izu, Bonin and Mariana contribute more to the average than relatively short dip lines, such as that across South Sandwich arc.

Table 4.1 Locations of derived 1D velocity-depth functions

Arc	Profile	Xmin	Xmax	Xmax-Xmin	Zmax	References
Aleutian	A1 – Dip	234	269	35	31	Holbrook et al. (1999)
Aleutian	A2 – Strike	180	750	570	38	Shillington et al. (2004)
Aleutian	A3 – Dip-Cont	235	275	40	35	Lizarralde et al. (2002)
Aleutian	A3 – Dip-Ocean	219	255	36	35	Lizarralde et al. (2002)
Bonin	Dip	340	380	40	25	Takahashi et al. (2009)
Bonin	Strike	700	950	250	23	Kodaira et al. (2007b)
Izu	Dip	150	250	100	19	Suyehiro et al. (1996)
Izu	Strike	150	450	300	38	Kodaira et al. (2007a)
L. Antilles	Dip	40	65	25	27	Christeson et al. (2008)
Mariana	Dip	185	215	30	35	Takahashi et al. (2007)
Mariana	Strike – Modern	80	250	170	24	Calvert et al. (2008)
Mariana	Strike – Eocene	100	360	260	27	Calvert et al. (2008)
Solomon	Dip	260	280	20	14	Miura et al. (2004)
S. Sandwich	Dip	300	320	20	15	Brugier and Larter (2001)
Tonga	Dip	50	140	90	14	Crawford et al. (2002)
Remnant Arc						
Kyushu Palau	Dip – KPr20	69	81	22	18	Nishizawa et al. (2007)
Kyushu Palau	Dip – SPr5	38	52	14	20	Nishizawa et al. (2007)
West Mariana	Dip	−105	−70	35	26	Takahashi et al. (2007)

Table 4.2 Reference 1D velocity-depth functions for island arcs (km s^{-1})

Depth (km)	Velocity below mean sea level	Standard deviation	Velocity below seafloor	Standard deviation	Velocity below top igneous crust	Standard deviation
0	1.503	0.024	3.249	1.648	4.730	1.047
1	2.649	1.496	4.438	1.322	5.265	0.740
2	3.795	1.781	5.054	0.960	5.652	0.511
3	4.561	1.398	5.505	0.654	5.940	0.360
4	5.180	0.952	5.828	0.452	6.160	0.281
5	5.587	0.667	6.085	0.332	6.306	0.261
6	5.888	0.487	6.259	0.278	6.433	0.277
7	6.106	0.365	6.410	0.295	6.581	0.274
8	6.279	0.269	6.584	0.299	6.689	0.286
9	6.481	0.284	6.672	0.286	6.788	0.268
10	6.586	0.254	6.770	0.263	6.848	0.277
11	6.681	0.233	6.838	0.268	6.901	0.286
12	6.786	0.196	6.896	0.281	6.954	0.296
13	6.855	0.210	6.953	0.290	7.002	0.308
14	6.926	0.235	6.990	0.308	7.040	0.316
15	6.968	0.251	7.037	0.322	7.085	0.329
16	7.011	0.268	7.082	0.329	7.131	0.332
17	7.060	0.287	7.130	0.330	7.115	0.235
18	7.104	0.299	7.202	0.318	7.193	0.232
19	7.170	0.286	7.198	0.235	7.239	0.234
20	7.259	0.291	7.232	0.238	7.235	0.211
21	7.303	0.289	7.222	0.215	7.266	0.216
22	7.342	0.291	7.255	0.218	7.296	0.223
23	7.298	0.241	7.285	0.226	7.270	0.226
24	7.332	0.249	7.326	0.237	7.297	0.232
25	7.329	0.256	7.282	0.228	7.329	0.248
26	7.336	0.246	7.310	0.237	7.361	0.265
27	7.364	0.251	7.343	0.256	7.408	0.267

(*continued*)

Table 4.2 (continued)

Depth (km)	Velocity below mean sea level	Standard deviation	Velocity below seafloor	Standard deviation	Velocity below top igneous crust	Standard deviation
28	7.336	0.256	7.373	0.270	7.435	0.275
29	7.373	0.269	7.420	0.270	7.460	0.285
30	7.403	0.281	7.446	0.279	7.457	0.269
31	7.429	0.291	7.446	0.264	7.477	0.276
32	7.477	0.289	7.463	0.270	7.337	0.173
33	7.497	0.295	7.511	0.327	7.468	0.368
34	7.536	0.330	7.582	0.428	7.754	0.405
35	7.633	0.378	7.903	0.312	7.974	0.215
36	7.769	0.363	7.978	0.211		
37	7.933	0.205				
38	7.976	0.213				

References

Amante C, Eakins BW (2009) Arc-minute global relief model: procedures, data sources and analysis. Technical memorandum NESDIS NGDC-24, NOAA, Boulder

Arai T (1987) Tectonics of Tanzawa mountains: constraints from metamorphic petrology. J Geol Soc Jpn 93:185–200

Bard JP, Maluski P, Matte P et al (1980) The Kohistan sequence, crust and mantle of an obducted island arc. Geol Bull Univ Peshawar 13:87–94

Behn MD, Keleman PB (2003) Relationship between P-wave velocity and the composition of anhydrous igneous and meta-igneous rocks. Geochem Geophys Geosyst. doi:10.1029/2002GC000393

Behn MD, Keleman PB (2006) Stability of arc lower crust: Insights from the Talkeetna arc section, south central Alaska, and the seismic structure of modern arcs. J Geophys Res. doi:10.1029/2006JB004327

Bibee LD, Shor GG Jr, Lu RS (1980) Inter-arc spreading in the Mariana Trough. Mar Geol 35:183–197

Birch F (1943) Elasticity of igneous rocks at high temperatures and pressures. Geol Soc Am Bull 54:263–286

Bouysse P (1988) Opening of the Grenada back-arc basin and evolution of the Caribbean Plate during the Mesozoic and early Paleogene. Tectonophysics 149:121–143

Boynton CH, Westbrook GK, Bott, MHP et al (1979) A seismic refraction investigation of crustal structure beneath the Lesser Antilles island arc. Geophys JR astr Soc 58: 371–393

Brocher TM (2005) Empirical relations between elastic wavespeeds and density in the Earth's crust. Bull Seismol Soc Am 95:2081–2092

Brugier N, Larter R (2001) Crustal structure and rate of growth of the South Sandwich arc from wide-angle seismic data. Eur Union Geosc Prog Abs 392–393

Burke K (1988) Tectonic evolution of the Caribbean. Annu Rev Earth Planet Sci 16:201–230

Calvert AJ, Klemperer SL, Takahashi N et al (2008) Three-dimensional crustal structure of the Mariana island arc from seismic tomography. J Geophys Res. doi:10.1029/2007JB004939

Card KD (1990) A review of the Superior Province of the Canadian Shield, a product of Archean accretion. Precambrian Res 48:99–156

Christensen NI (1979) Compressional wave velocities in rocks at high temperatures and pressures, critical thermal gradients, and crustal low velocity zones. J Geophys Res 84: 6849–6857

Christensen NI, Mooney WD (1995) Seismic velocity structure and composition of the continental crust. J Geophs Res 100: 9761–9788

Christeson G, Mann P, Escalona A et al (2008) Crustal structure of the Caribbean – northeastern South America arc-continent collision zone. J Geophys Res. doi:10.1029/2007JB005373

Clift P, Vannucchi P (2004) Controls on tectonic accretion versus erosion in subduction zones: implications for the origin and recycling of the continental crust. Rev Geophys. doi:10.1029/2003RG000127

Cook FA, Clowes RM, Snyder DB et al (2004) Precambrian crust beneath the Mesozoic northern Canadian Cordillera discovered by Lithoprobe seismic reflection profiling. Tectonics. doi:10.1029:2002TC001412

Crawford AJ, Beccaluva L, Serri G (1981) Tectono-magmatic evolution of the West Philippine-Mariana region and the origin of boninites. Earth Planet Sci Lett 54:346–356

Crawford WC, Hidebrand JA, Dorman LM, Webb SC, Wiens DA (2002) Tonga Ridge and Lau Basin crustal structure from seismic refraction data. J Geophys Res. doi:10.1029/2001JB001435

d'Ars JB, Jaupart C, Sparks RSJ (1995) Distribution of volcanoes in active margins. J Geophys Res 100:20421–20432

DeMets C, Dixon TH (1999) New kinematic models for Pacific-North America plate motion from 3 Ma to present: I. Evidence for steady motion and biases in the NUVEL-1A model. Geophys Res Lett 26:1921–1924

Dimalanta C, Taira A, Yumul GP Jr et al (2002) New rates of western Pacific island arc magmatism from seismic and gravity data. Earth Planet Sci Lett 202:105–115

Fliedner MM, Klemperer SK (1999) Structure of an island-arc: wide-angle studies in the eastern Aleutian Islands, Alaska. J Geophys Res 104:10667–10694

Fryer P (1995) Geology of the Mariana Trough. In: Taylor B (ed) Back-arc basins: tectonics and magmatism. Plenum, New York

Fujie G, Ito A, Kodaira S et al (2006) Confirming sharp bending of the Pacific plate in the northern Japan trench subduction zone by applying a travel time mapping method. Phys Earth Planet Int 157:72–85

Garrido CJ, Bodinier J-L, Burg J-P et al (2006) Petrogenesis of mafic garnet granulite in the lower crust of the Kohistan paleo-arc complex (Northern Pakistan): implications for intra-crustal differentiation of island arcs and generation of continental crust. J Petrol 47:1873–1914

Geist EL, Childs JR, Scholl DW (1988) The origin of summit basins of the Aleutian Ridge: implications for block rotation of an arc massif. Tectonics 7:327–342

Gill JB (1981) Orogenic andesites and plate tectonics. Springer, Berlin

Gorshkov GS (1970) Volcanism and the upper mantle. Plenum, New York

Grow JA (1973) Crustal and upper mantle structure of the central Aleutian arc. Geol Soc Am 84:2169–2192

Hoffman PF (1989) Precambrian geology and tectonic history of North America. In: Bally AW, Palmer PR (eds) The Geology of North America: an Overview, vol A. Geol Soc Am, Boulder

Holbrook WS, Lizarralde D, McGeary S et al (1999) Structure and composition of the Aleutian island arc and implications for continental growth. Geology 27:31–34

Hole JA (1992) Nonlinear high-resolution three-dimensional seismic travel time tomography. J Geophys Res 97: 6553–6562

Hole JA, Zelt BC (1995) 3-D finite-difference reflection travel times. Geophys J Int 121:427–434

Hussong DM, Uyeda S (1981) Tectonic processes and the history of the Mariana arc, a synthesis of the results of Deep Sea Drilling Project Leg 60. In: Hussong DM (ed) Initial Reports of the Deep Sea Drilling Project, Vol 60. Ocean Drilling Program, College Station

Hyndman RD, Shearer PM (1989) Water in the lower continental crust – modelling magnetotelluric and seismic reflection results. Geophys J Int 98:343–365

Ishizuka O, Kimura J, Li YB et al (2006) Early stages in the evolution of Izu-Bonin arc volcanism: new age, chemical, and isotopic constraints. Earth Planet Sci Lett 250:385–401

Ito A, Fujie G, Kodaira S et al (2005) Bending of the subducting oceanic plate and its implication for rupture propagation of large interplate earthquakes off Miyagi, Japan, in the Japan trench subduction zone. Geophys Res Lett. doi:10.1029/2004GL022307

Iturrino GJ, Christensen NI, Kirby S, Salisbury MH (1991) Seismic velocities and elastic properties of oceanic gabbroic rocks from Hole 735B. Proc Ocean Drill Program Sci Results 118:227–244

Iturrino GJ, Miller DJ, Christensen NI (1996) Velocity behavior of lower crustal and upper mantle rocks from a fast-spreading ridge at Hess Deep. Proc Ocean Drill Program Sci Results 147:417–440

Jacob KH, Hamada K (1972) The upper mantle beneath the Aleutian island arc from pure-path Rayleigh-wave dispersion data. Bull Seismol Soc Am 62:1439–1454

Jarrard RD (1986) Relations among subduction parameters. Rev Geophys 24:217–284

Karig DE (1970) Ridges and basins of the Tonga-Kermadec island arc system. J Geophys Res 75:239–254

Kawate S, Arima M (1998) Petrogenesis of the Tanzawa plutonic complex, central Japan: exposed felsic crust of the Izu-Bonin-Mariana arc. Island Arc 7:342–358

Kern H (1978) The effect of high temperature and high confining pressure on compressional wave velocities in quartz-bearing and quartz-free igneous and metamorphic rocks. Tectonophysics 44:185–203

Kitamura K, Ishikawa M, Arima M (2003) Petrological model of the northern Izu-Bonin-Mariana arc crust: constraints from high pressure measurements of elastic wave velocities of the Tanzawa plutonic rocks, central Japan. Tectonophysics 371:213–221

Kobayashi KS, Kasuga S, Kl O (1995) Shikoku Basin and its margins. In: Taylor B (ed) Back-arc basins: tectonics and magmatism. Plenum, New York

Kodaira S, Sato T, Takahashi N et al (2007a) Seismological evidence for variable growth of crust along the Izu intraoceanic arc. J Geophys Res. doi:10.1029/2006JB004593

Kodaira A, Sato T, Takahashi N et al (2007b) New seismological constraints on growth of continental crust in the Izu-Bonin intra-oceanic arc. Geology 35:1031–1034

Kono Y, Ishikawa M, Harigane Y et al (2009) P- and S-wave velocities of the lowermost crustal rocks from the Kohistan arc: implications for seismic Moho discontinuity attributed to abundant garnet. Tectonophysics 467:44–54

Korenaga J, Kelemen PB, Holbrook WS (2002) Methods for resolving the origin of large igneous provinces from crustal seismology. J Geophys Res. doi:10.1029/2001JB001030

Kusznir, NJ, Park RG (1987) The extensional strength of the continental lithosphere: its dependence on geothermal gradient, and crustal composition and thickness. In: Coward MP, Dewey JF, Hancock, PL (eds) Continental extensional tectonics. Geol Soc, London.

Larner K, Chambers YM et al (1983) Coherent noise in marine seismic data. Geophysics 48:854–886

Leat PT, Larter RD (2003) Intra-oceanic subduction systems: introduction. In: Larter RD, Leat PT (eds) Intra-oceanic subduction systems: tectonic and magmatic processes, vol 219, Geol Soc Lon Spec Pub., pp 1–17

Lizarralde D, Holbrook WS, McGeary S et al (2002) Crustal structure of a volcanic arc, wide-angle results from the western Alaska Peninsula. J Geophys Res. doi:10.1029/2001JB000230

Malfait BT, Dinkelman MG (1972) Circum-Caribbean tectonic and igneous activity and the evolution of the Caribbean plate. Geol Soc Am Bull 83:251–271

Martinez F, Taylor B (2006) Modes of crustal accretion in back-arc basins: Inferences from the Lau Basin. In: Christie DM et al (eds) Back-arc spreading systems: Geological, biological, chemical and physical interactions. Am Geophys Union, Washington

Miller DJ, Christensen NI (1994) Seismic signature and geochemistry of an island arc: a multidisciplinary study of the Kohistan accreted terrane, northern Pakistan. J Geophys Res 99:11623–11642

Miura S, Suyehiro K, Takahashi N et al (2004) Seismological structure and implications of collision between the Ontong Java plateau and Solomon island arc from ocean bottom seismometer-airgun data. Tectonophysics 389: 191–220

Molnar P, Atwater T (1978) Interarc spreading and Cordilleran tectonics as alternatives related to the age of subducted oceanic lithosphere. Earth Planet Sci Lett 41:330–340

Murauchi S, Den N, Asano S et al (1968) Crustal structure of the Philippine Sea. J Geophys Res 73:3143–3171.

Nakajima K, Arima M (1998) Melting experiments on hydrous low-K tholeiite: implications for the genesis of tonalitic crust in the Izu-Bonin-Mariana arc. Island Arc 7:359–373

Nishizawa A, Kaneda K, Katagiri Y et al (2007) Variation in crustal structure along the Kyushu-Palau Ridge at 15–21°N on the Philippine Sea plate based on seismic refraction profiles. Earth Planets Space 59:e17–e20

Nitsuma N (1989) Collision tectonics in the South Fossa Magna, Central Japan. Mod Geol 14:3–18

Oakley AJ, Taylor B, Moore GF, Gooliffe A (2009) Sedimentary, volcanic, and tectonic processes of the central Mariana Arc: Mariana Trough back-arc basin formation and the West Mariana Ridge. Geochem Geophys Geosyst. doi:10.1029/2008GC002312

Okino K, Shimakawa Y, Nagaoka S (1994) Evolution of the Shikoku Basin. J Geomagn Geoelectr 46:463–479

Okino K, Ohara Y, Kasuga S et al (1999) The Philippine Sea: new survey results reveal the structure and the history of the marginal basins. Geophys Res Lett 26:2287–2290

Plafker G, Berg HC (1994) Overview of the geology and tectonic evolution of Alaska. In: Plafker G, Berg HC (eds) The Geology of North America, vol G-1, The Geology of Alaska. Geol Soc Am, Boulder

Plafker G, Moore JC, Winkler GR (1994) Geology of the southern Alaska margin. In: Plafker G, Berg HC (eds) The Geology of North America, vol G-1, The Geology of Alaska. Geol Soc Am, Boulder

Rudnick LR, Fountain MD (1995) Nature and composition of the continental crust: a lower crustal perspective. Rev Geophys 33:267–309

Sato T, Kodaira S, Takahashi N et al (2009) Amplitude modeling of the seismic reflectors in the crust-mantle transition layer beneath the volcanic front along the northern Izu-Bonin island arc. Geochem Geophys Geosyst. doi:10.1029/2008GC001990

Scholl DW, Stevenson AJ, Mueller S et al (1992) Exploring the notion that southeast-Asian-type escape tectonics and trench clogging are involved in regional-scale deformation of Alaska and the formation of the Aleutian-Bering sea region. In: Flower M, McCabe R, Hilde T (eds) Southeast Asia structure, tectonics and magmatism, Proc Geod Res Inst Symp. Texas A&M Univ, College Station

Seno T, Stein S, Gripp AE (1993) A model for the motion of the Philippine Sea plate consistent with NUVEL and geological data. J Geophys Res 98:17941–17948

Shillington DJ, van Avendonk HJA, Holbrook WS et al (2004) Composition and structure of the central Aleutian island arc from arc-parallel wide-angle seismic data. Geochem Geophys Geosyst. doi:10.1029/2004GC000715

Shor GG Jr, Kirk HK, Menard HW (1971) Crustal structure of the Melanesian area. J Geophys Res 76:2562–2586

Speed RC, Walker JA (1991) Oceanic crust of the Grenada basin in the southern Lesser Antilles arc platform. J Geophys Res 96:3835–3851

Stern RJ (2002) Subduction zones. Rev Geophys. doi:10.1029/2001RG000108

Stern RJ, Bloomer SH (1992) Subduction zone infancy: examples from the Eocene Izu-Bonin-Mariana and Jurassic California arcs. Geol Soc Am Bull 104:1621–1636

Stern RJ, Fouch MJ, Klemperer SL (2003) An overview of the Izu-Bonin-Mariana subduction factory. In: Eiler JM (ed) Inside the subduction factory. Am Geophys Union, Washington

Suyehiro K, Takahashi N, Ariie Y et al (1996) Continental crust, crustal underplating, and low-Q upper mantle beneath an island arc. Science 272:390–392

Takahashi N, Suyehiro K, Shinohara M (1998) Implications from the seismic crustal structure of the northern Izu-Bonin arc. Island Arc 7:383–394

Takahashi N, Kodaira S, Klemperer S et al (2007) Crustal structure and evolution of the Mariana intra-oceanic island arc. Geology 35:203–206

Takahashi N, Kodaira S, Tatsumi Y et al (2008) Structure and growth of the Izu-Bonin-Mariana arc crust: 1. Seismic constraint on crust and mantle structure of the Mariana arc–back-arc system. J Geophys Res. doi:10.1029/2007JB005120

Takahashi N, Kodaira S, Tatsumi Y et al (2009) Structural variations of arc crusts and rifted margins in the southern Izu-Ogasawara arc-back arc system. Geochem Geophys Geosyst. doi:10.1029/2008GC002146

Tani K, Dunkley DJ, Kimura J-I et al (2010) Syncollisional rapid granitic magma formation in an arc-arc collision zone: evidence from the Tanzawa plutonic complex, Japan. Geology 38:215–218

Tatsumi Y, Tani K, Kogiso T et al (2008) Structure and growth of the Izu-Bonin-Mariana arc crust: 2. Arc evolution, continental crust formation, and crust-mantle transformation. J Geophys Res. doi:10.1029/2007JB005121

Taylor B (1992) Rifting and volcano-tectonic evolution of the Izu-Bonin-Mariana arc. In: Maddox E (ed) Proceedings of the ocean drilling program, scientific results, Vol 126. Ocean Drilling Program, College Station

Taylor B, Karner GD (1983) On the evolution of marginal basins. Rev Geophys Space Phys 21:1727–1741

Uyeda S, Kanamori H (1979) Back-arc opening and the mode of subduction. J Geophys Res 84:47–56

Van Avendonk HJA, Shillington DJ, Holbrook WS, Hornbach MJ (2004) Inferring crustal structure in the Aleutian island arc from a sparse wide-angle seismic data set. Geochem Geophys Geosyst. doi:10.1029/2003GC000664

Von Huene R, Scholl DW (1991) Observations at convergent margins concerning sediment subduction, subduction erosion, and the growth of continental crust. Rev Geophys 29: 279–316

White RS (1984) Atlantic oceanic crust: Seismic structure of a slow-spreading ridge. In: Gass IG (ed) Ophiolites and oceanic lithosphere, vol 13. Geol Soc Lon, London

Wiebenga WA (1973) Crustal structure of the New Britain-New Zealand region. In: Coleman PJ (ed) The Western Pacific. Western Australia University Press, Perth

Yamamoto Y, Kawakami S (2005) Rapid tectonics of the late Miocene Boso accretionary prism related to the Izu-Bonin arc collision. Island Arc 14:178–198

Zelt CA, Barton PJ (1998) 3-D seismic refraction tomography: a comparison of two methods applied to data from the Faroes Basin. Geophys J Int 103:7187–7210

Zelt CA, Smith RB (1992) Seismic traveltime inversion for 2-D crustal velocity structure. Geophys J Int 108:16–34

Chapter 5
Vertical Stratification of Composition, Density, and Inferred Magmatic Processes in Exposed Arc Crustal Sections

S.M. DeBari and A.R. Greene

5.1 Introduction

Earth's crust is primarily generated in oceanic settings via divergent and convergent margin processes. In divergent margins, the crust is ultimately recycled back into the mantle, whereas at convergent margins, the resulting island arc crust becomes the buoyant nucleus of new continental crust. The collision of island arcs with continental margins is well accepted as a dominant process of post-Archean continental growth (e.g., Rudnick and Gao 2003). The goal of this paper is to describe what we know about island arc crust from exposed crustal sections, and summarize the inferred processes that produce this crust and its characteristics. From this, we can also better understand modern arcs, and the nature of continental crust.

The net magmatic input into island arc crust at convergent margins is dominated by fluid-fluxed melting of the mantle wedge to produce basalt (e.g., Tatsumi 2005). However, net magmatic output at arc volcanoes is commonly more silicic than basalt (andesite, e.g., Gill 1981). Thus, the arc crust acts as a distiller to modify mantle-derived magmas. The geochemistry and diversity of the crystal cargo of extrusive products of arc magmatism lead us to inferences about those distillation processes, but complementary evidence from plutonic exposures is usually lacking. In this paper, the exposed crustal sections of paleo-arcs provide both the intrusive and extrusive record of these processes.

S.M. DeBari
Geology Department, Western Washington University, Bellingham, WA 98225, USA
e-mail: debari@geol.wwu.edu

A.R. Greene
Department of Geology and Geophysics, SOEST, University of Hawai'i, Honolulu, HI 96822, USA

In linking the formation of island arcs to the formation of continental crust, a few central points about continental crust are important to consider. Continental crust is high-standing and thick, with an average "andesitic" bulk composition (Rudnick and Gao 2003; Taylor and McLennan 1985, and references therein). The best estimates show that upper continental crust is granodioritic in composition (66.6 wt.% SiO_2, 2.5 wt.% MgO), rich in incompatible elements, and depleted in compatible elements (Rudnick and Gao 2003). Their mid-crust estimate is intermediate in composition (63.5 wt% SiO_2, 3.6 wt% MgO), and their lower crust is mafic (53.4 wt% SiO_2, 7.2 wt% MgO). The weighted average produces an andesitic bulk composition of 60.6 wt% SiO_2 and 4.7 wt% MgO. The bulk continental crust estimate is depleted in Nb, with a subchondritic Nb/Ta ratio (12.4; Rudnick and Gao 2003). Calculations using this Nb depletion suggest that at least 80% of the continental crust was generated in convergent margins (Barth et al. 2000; Plank and Langmuir 1998).

If we accept the compositional estimate of Rudnick and Gao (2003), as well as the convergent margin origin for continental crust, then study of exposed crustal sections of island arcs becomes even more relevant. First, the compositional stratification in continental crust is also present in exposed island arcs, and may be related to similar processes. Second, an andesitic bulk composition complicates the simple premise of one-stage melting of the mantle to produce continental crust. Melts of the mantle are basaltic, thus some return flow of mafic components to the mantle are required to balance the geochemical budget of continental crust formation. Several hypotheses have been proposed for this (see summary in Rudnick and Gao 2003). Exposed island arc crustal sections can be used to test these hypotheses, especially with respect to evidence for crustal foundering (delamination).

D. Brown and P.D. Ryan (eds.), *Arc-Continent Collision*, Frontiers in Earth Sciences,
DOI 10.1007/978-3-540-88558-0_5,

However, there are some important distinctions between modern island arcs and continental crust as shown by modern arc seismic signatures. Calvert (2011) shows that at depths >8–10 km, island arcs have higher seismic velocities (i.e., have more mafic compositions) than continental crust, whereas at depths <8–10 km, seismic velocities are similar.

From the arc crustal sections described in this paper, we discuss differentiation processes that may account for compositional stratification within arcs. We also discuss evidence from these sections that strongly support lower crustal foundering of mafic and ultramafic compositions to produce a more felsic arc crustal composition. Finally, we relate this information to interpretation of geophysical signatures in arcs.

5.2 Exposed Crust and Upper Mantle Sections of Mesozoic Arcs

We summarize four exposed cross sections of accreted arcs (Fig. 5.1), three of which are island arcs and one which was built on a newly accreted continental margin. Some sections are more complete than others, and each are different thicknesses. However, all arc sections share common mid-crustal lithologies, and two of the four share common upper mantle and lower crustal lithologies. All share common lithological stratification with depth. Taken together, the petrologic story that each of these sections tells corroborates the others, and provides us with an unprecedented view into the workings of magmatic arcs.

In this paper, we define the crust-mantle boundary as the boundary between plagioclase-bearing and plagioclase-free lithologies. Thus the "Moho" described in the following sections marks the contact between gabbroic rocks above and ultramafic rocks below. Gabbroic rocks in the lower crust include lithologies such as gabbronorite (variably called two-pyroxene gabbro or two-pyroxene granulite by different authors) and garnet gabbro (also called garnet granulite). These lower crustal gabbroic rocks are understood to be cumulate in nature. Ultramafic rocks below the Moho are comprised of varying proportions of olivine and pyroxene. They may be residual mantle that has interacted with percolating melts, or purely cumulate.

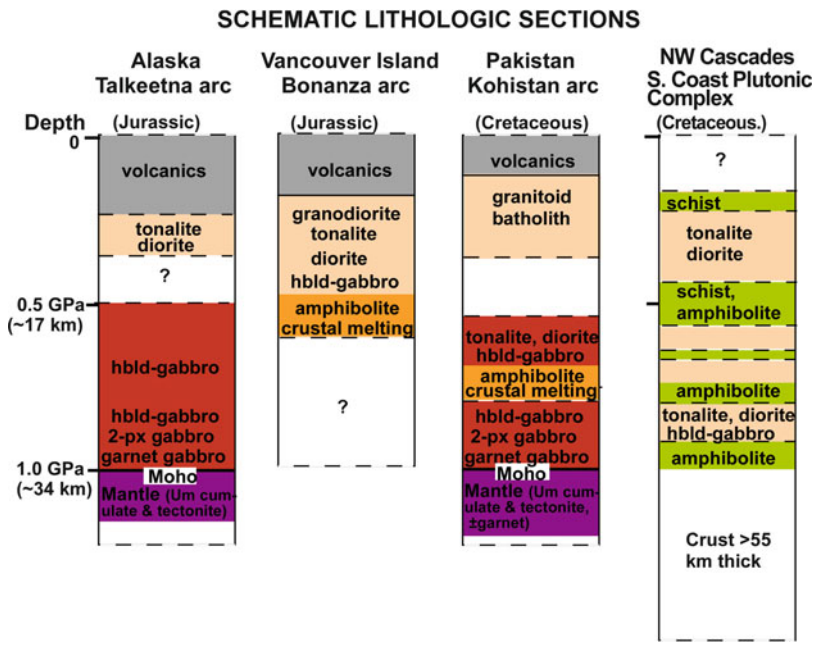

Fig. 5.1 Schematic lithologic sections of the four accreted arcs discussed in the text. Colors are meant to be broad generalizations of lithologic types. *Grey* is volcanic rocks (all compositions), *tan* is intermediate to felsic plutonic rocks (53–72 wt% SiO_2), *red* is gabbroic rock (typically cumulate) (45–52 wt% SiO_2), *purple* is ultramafic rock (pyroxenite, wehrlite, dunite and harzburgite) (<52 wt% SiO_2). *Orange regions* show crustal levels where partial melting has taken place. *Green areas* represent abundant metamorphic country rock that has not melted. The paleo-Moho is defined in this study as the transition between ultramafic rock (plagioclase absent) and gabbroic rock (plagioclase present).

In this paper we also use the term *felsic* to describe rocks with >63 wt% SiO_2 (extrusive dacite or intrusive tonalite), *intermediate* to describe rocks with ~52–63 wt% SiO_2 (extrusive andesite or intrusive diorite), and *mafic* to describe rocks with ~48–52 wt% SiO_2 (extrusive basalt to intrusive gabbro).

5.2.1 Talkeetna Arc, Alaska

The Jurassic Talkeetna island arc in south-central Alaska is an exhumed and tilted arc section where subarc mantle, lower crust, and middle and upper crust are now exposed at the surface (Burns 1985; DeBari and Coleman 1989). The arc is estimated to be exposed along at least 1,000 km of strike length (Plafker et al. 1989; Reed and Lanphere 1973) from the Chugach and Talkeetna Mountains in the east to the Lower Cook Inlet Region and Alaska Peninsula in the west (Fig. 5.2a).

The arc is interpreted to have formed in an oceanic subduction zone setting as a result of the northward dipping subduction (present-day coordinates) of the Farallon plate beneath the Peninsular terrane (Clift et al. 2005b; Plafker et al. 1989). Talkeetna arc magmatism is believed to have been active from ~200 Ma to at least 160 Ma (Plafker et al. 1989; Rioux et al. 2007, 2010). A trondhjemite pluton, dated at ~153 Ma, intrudes the central Talkeeetna Mountains, possibly marking the end of arc plutonism (Rioux et al. 2007). Cessation of magmatism, along with evidence for deformation, exhumation, and sedimentation at 160–150 Ma, is thought to reflect the collision of the Talkeetna arc with a tectonic block to the north (Clift et al. 2005b; Trop et al. 2005). It is unclear if the collision was between the Talkeetna arc and another terrane

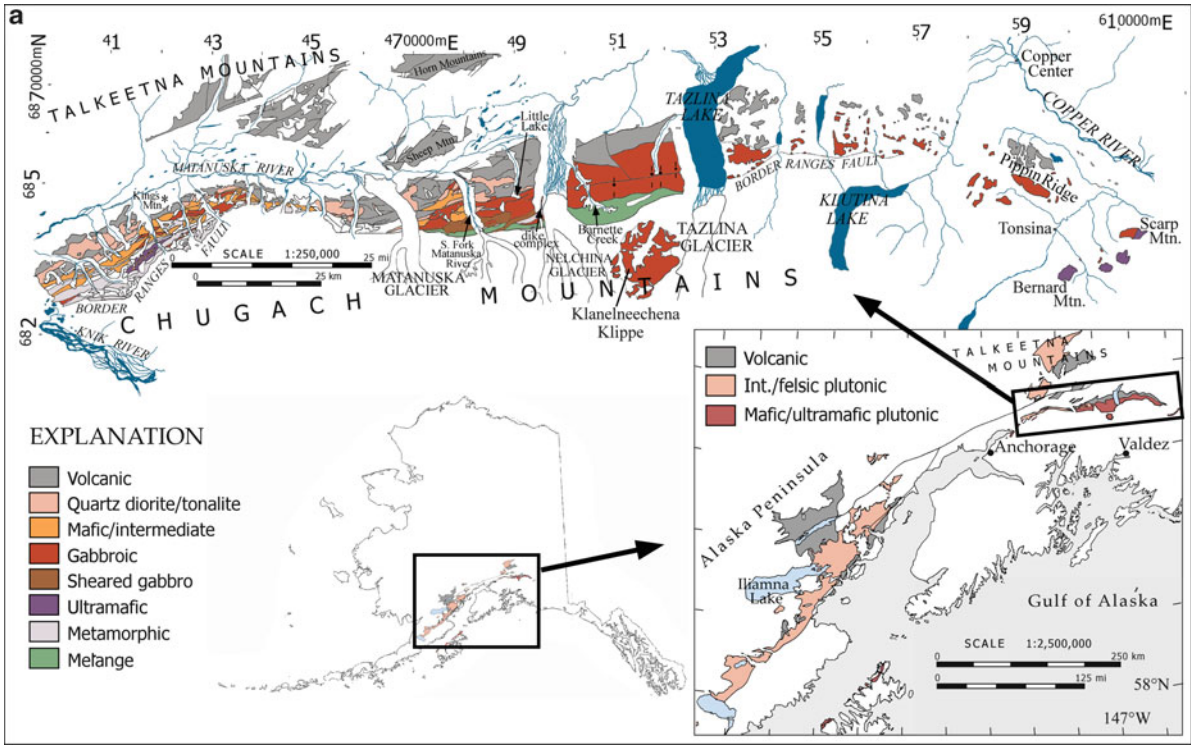

Fig. 5.2 (**a**) Map of the location of the Talkeetna arc in Alaska from Greene et al. (2006). The arc extends for over 1,000 km in an east west direction. The easternmost segment of the arc exposes the deepest crustal levels, and that region is shown in the most detail. The paleo-Moho is exposed in the far eastern region on Bernard and Scarp Mountains. Thick sections of cumulate gabbroic rock are exposed in the eastern part of the arc. The western part of the arc on the Alaska Peninsula exposes a much thicker section of intermediate and felsic plutonic rocks (Johnsen 2007; Reed and Lanphere 1973). (**b**) Detailed crustal section for the Talkeetna arc based on stratigraphic thickness of the volcanic section (Clift et al. 2005a) and geobarometry of Hacker et al. (2008). The paleo-Moho is defined as in Fig. 5.1 and the Bernard Mountain Moho section is shown in detail. A simplified cross section from Greene et al. (2006) is also included.

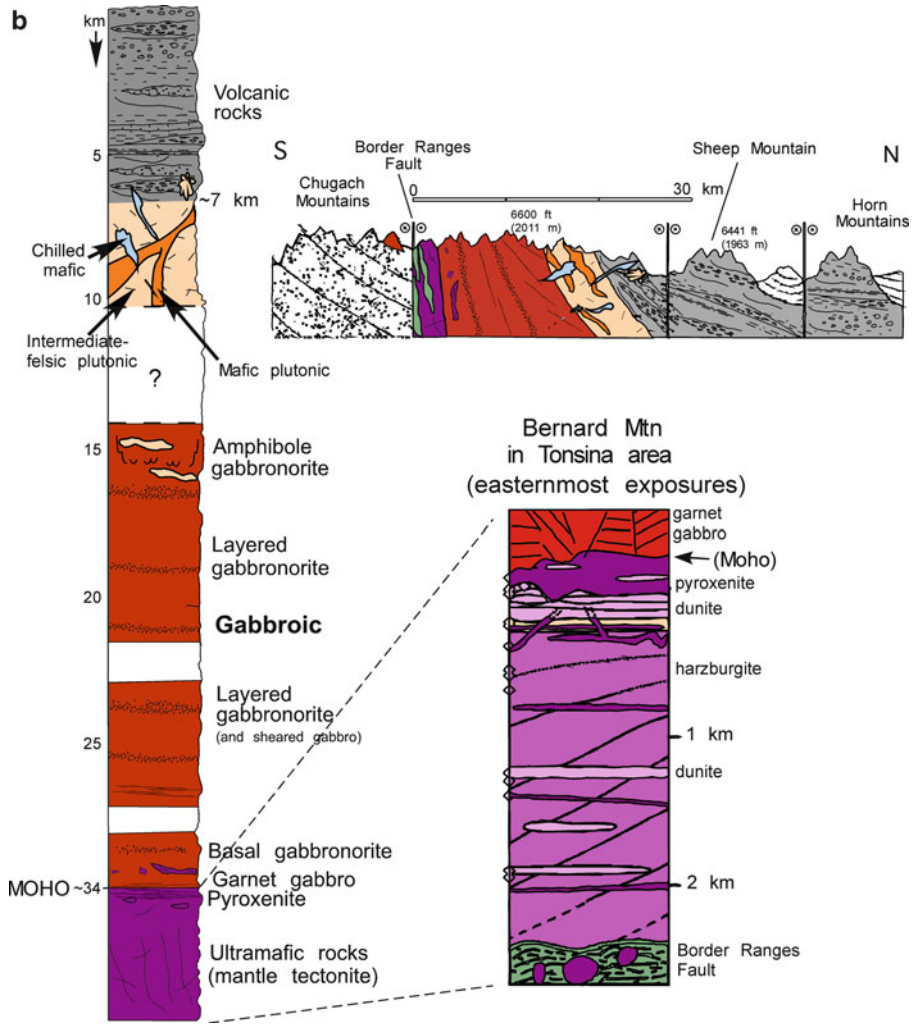

Fig. 5.2 (Continued)

(Wrangellia) or the accretion of the entire amalgamated terrane onto the margin of North America.

Clift et al. (2005b) interpret northward migration of magmatism in the arc to be due to tectonic erosion of the forearc while the arc was active. They interpret the juxtaposition of younger accreted trench sedimentary rocks (Chugach terrane) against the base of the Talkeetna arc sequence as a change from a state of tectonic erosion to accretion after collision-induced increase of sedimentary flux at ~160 Ma.

The arc crustal section, with an inferred original thickness of ~35 km (DeBari and Sleep 1991; Hacker et al. 2008) sits above a residual mantle section that includes ultramafic cumulate rocks. Pyroxenites and garnet-bearing gabbros are characteristic of the lowermost crust, layered gabbronorite in the lower and middle crust, gabbroic rocks and intermediate-felsic plutonic rocks in the middle-upper crust, and volcanic rocks in the uppermost crust. The arc is not physically exposed as a contiguous section, but most stratigraphic levels are present in plutonic and volcanic exposures in the Chugach and Talkeetna Mountains. There are no exposures of remnant oceanic crust upon which the arc was built. This led Clift et al. (2005a, b) to assume that the arc was extensional.

The upper crust of the arc includes a 7-km-thick volcanic section (Clift et al. 2005a) intruded by felsic to intermediate tonalites and quartz diorites. Hacker et al. (2008) infer that these upper crustal plutonic rocks crystallized at 0.13–0.27 GPa (5–9 km), which

agrees with the observed stratigraphic thickness of the volcanic rocks (Fig. 5.2b). These volcanic and shallow plutonic rocks are exposed over an enormous area of the Talkeetna Mountains and the Alaska Peninsula.

The middle crust of the arc is dominantly hornblende gabbronorite in its lower part, but upper middle crust lithology (9–15 km) is not well constrained due to a gap in geobarometric data (Hacker et al. 2008). In contrast, rocks of the lower middle crust and lower crust are layered gabbronorites (2-pyroxene gabbro) that are exposed semi-continuously for approximately 150 km in an E–W direction and 5–18 km in a N–S direction (Fig. 5.2a). These rocks were described by Greene et al. (2006), who evaluated their role as cumulates in arc differentiation. Hacker et al. (2008) infer that these plutonic rocks crystallized and equilibrated at 0.43–0.72 GPa (15–24 km) and 700–900°C (Fig. 5.2b). A klippe to the south of the main body of the arc consists of diorites with igneous garnet that crystallized at 0.7–1.0 GPa (24–34 km depth).

The lowermost crust and Moho of the arc is exposed in the far eastern part of the arc near Tonsina at Bernard and Scarp Mountains (Fig. 5.2a). The lithologies consist of gabbronorites ± hornblende ± garnet. Anhydrous assemblages give way to more abundant hornblende gabbronorites upward in the section. These lowermost crustal rocks yield equilibration pressures of 0.9–1.2 GPa (Hacker et al. 2008).

The Moho of the arc is best exposed on Bernard Mountain as a transitional boundary between garnet gabbros above (up to 10 volume % garnet) and cumulate pyroxenites below. These garnet gabbros crystallized at ~1.0 GPa and 875–1,000°C (30–35 km, Fig. 5.2b) (DeBari and Coleman 1989; Hacker et al. 2008). Beneath the paleo-Moho, 50–200 m of websterite and olivine clinopyroxenite overlie an ~100 m transition zone of coarse chromite-bearing dunite. Beneath that is ~2,500 m of residual spinel harzburgite with interlayered dunite. Residual mantle rocks have Moho-parallel foliation and display stretching lineations indicative of flow paralled to the arc axis (Mehl et al. 2003).

Studies focusing on the geochemistry of the Talkeetna arc have shown that lower crustal gabbronorites and upper crustal volcanic rocks can be related to a single type of parent magma, each group of rocks forming as a result of simple fractional crystallization (DeBari and Sleep 1991; Greene et al. 2006; Kelemen et al. 2003). Gabbronorites represent the crystallized cumulate pile and erupted volcanic rocks represent the remaining liquid following differentiation. Fractional crystallization was also used to explain the formation of middle-upper crustal intermediate and felsic plutonic rocks (Rioux et al. 2007, 2010; Johnsen 2007). Isotopic signatures from these intermediate-felsic plutonic rocks are mostly intra-oceanic with little or no involvement of continental crustal material (Amato et al. 2007; Rioux et al. 2007, 2010). However, in the westernmost end of the Talkeetna arc on the Alaska Peninsula, Johnsen (2007) showed that the youngest felsic plutonic rocks were probably produced by variable mixing of an andesitic parent magma with a partial melt of arc lower crust.

The bulk composition of the Talkeetna arc was originally calculated to be basaltic by DeBari and Sleep (1991) (51 wt% SiO_2 and 11 wt% MgO). However, their mass balance calculations may have over-estimated the ultramafic cumulate component. Greene et al. (2006) calculate a "primary magma" composition for the arc that would be in equilibrium with the mantle, based on the most primitive compositions erupted. This primary magma composition is also basaltic, and is similar to the bulk composition of DeBari and Sleep (1991). Hacker et al. (2008) also calculated a bulk composition based on their geobarometric reconstruction of the arc. They calculated a potential range of compositions from basalt to andesite (51–58 wt% SiO_2) and 4–11 wt% MgO. The wide range is due to extrapolations on a "missing" mid crustal component.

5.2.2 Kohistan Arc, Pakistan

The Kohistan arc of NE Pakistan represents an island arc that was obducted between the collision of the Indian and Eurasian plates. The arc extends for at least 300 km in an east–west direction, from the Nanga Parbat massif to northeastern Afghanistan. The arc is juxtaposed against the Asian plate to the north along the Karakorum-Kohistan Suture, and against the Indian plate to the south along the Indus Suture.

The arc developed in response to northward-directed subduction of the Tethyan lithosphere at the leading edge of the Indian plate during latest Jurassic to Cretaceous times (the oldest pluton is 154 ± 0.6 Ma, Schaltegger et al. 2003). The arc underwent a rifting episode at ~85 Ma to produce the voluminous

Chilas mafic intrusion (Khan et al. 1989; Schaltegger et al. 2002; Burg et al. 2006). Continued subduction resulted in complete consumption of the leading oceanic edge of the Indian plate, resulting in obduction of the arc onto the Indian continent at the site of the Indus suture (~60–45 Ma) (Burg (2011) and references therein). The timing of collision of the Kohistan arc on its northern end with the Karakorum (Eurasian) plate is controversial. It has long been thought that this collision pre-dated Kohistan arc rifting (e.g., Petterson and Windley 1985) such that after 100 Ma the Kohistan arc was an Andean-type continental arc. However, more recent work suggests that this northern collision post-dates collision of Kohistan with India (e.g., Khan et al. 2009, Burg 2011). It is unclear whether the Kohistan arc was ever Andean in nature.

The arc was tilted to the north during final docking of terranes. Subsequent uplift and erosion have exposed a cross section that consists of rocks from the upper mantle through the lower, middle and upper crust (Fig. 5.3). As with the Talkeetna arc, forearc sequences in the Kohistan arc are rare, suggesting tectonic erosion of the forearc may have occurred during arc magmatism or subsequent collision.

A detailed description of the exposed crustal levels can be found in Burg (2011). These are briefly reviewed below.

The shallowest part of the arc section consists of volcanic, sedimentary, and shallow-level granitic rocks in the northern part of the exposure. The volcanic rocks record all phases of arc evolution from intraoceanic arc, continental arc, and arc rifting (Petterson and Treloar 2004). The volcanic and sedimentary rocks are intruded by granitoids of the Kohistan batholith, the oldest of which predate suturing of Kohistan to Eurasia (154 $\pm$ 0.6 Ma, Schaltegger et al. 2003). Arc-related plutons of the batholith span ages from 112 to 38 Ma (Jagoutz et al. 2009; Petterson and Windley 1985, 1991; Schaltegger et al. 2003).

The middle crust of the arc is separated into a northern section (middle crust represented by calcalkaline plutons of the Kohistan batholith) and a southern section (middle crust represented by metadiorites, metagabbros, metasediments, and metavolcanics of the Southern Amphibolite Belt) (Fig. 5.3a). The intervening Chilas Complex is a massive body of layered gabbroic rocks up to 50 km wide (N–S) and 300 km long (E–W). This Complex is interpreted to be an intrusive body related to rifting of the Kohistan arc at ~85 Ma (Burg et al. 2006; Jagoutz et al. 2006, 2007; Khan et al. 1989) and thus is not strictly part of the arc crustal section. The Southern Amphibolite belt includes the Kamila amphibolite, and is 15–35 km thick. Some metabasalts within this belt are interpreted to be the oceanic remnant oceanic crust upon which the arc was built (Jan 1988; Khan et al. 1993), whereas others are related to arc magmatism (Burg 2011). Partial melting within this belt is interpreted to have occurred at ~97 Ma based on the presence of a granitic migmatite (Schaltegger et al. 2002).

The lowermost crust of the arc is exposed to the south of the Southern Amphibolite belt and consists of garnet-gabbros (granulites) that overlie and intrude the residual/cumulate rocks of the subarc mantle (Burg et al. 1998). These garnet-gabbros are ~5–6 km thick in the Jijal Complex (Fig. 5.3b). They consist of ~20–30 vol% garnet, plus plagioclase, clinopyroxene, amphibole, and oxides. Rare two-pyroxene gabbros from this section were dated at 118 $\pm$ 12 Ma by a Sm–Nd mineral isochron (Yamamoto and Nakamura 2000). They are overlain by metagabbro (98.9 $\pm$ 4 Ma, Schaltegger et al. 2002) that forms the southernmost part of the Southern Amphibolite belt.

The 2–3-km thick ultramafic section of the Kohistan arc is found in the Jijal and Sapat Complexes along the southernmost margin of the arc (Fig. 5.3b). Dunite, wehrlite, olivine-clinopyroxenite, and websterite lithologies are the most abundant lithologies in this basal section. Pyroxenite increases in abundance up section, as does the presence of amphibole. Pyroxene-rich ultramafic rocks grade into hornblende-, clinopyroxene-, and garnet-rich rocks. Modal abundances vary dramatically in short distances, with complex relationships between hornblendite, garnetite, and pyroxenite. Above these rocks, plagioclase appears in gabbronorites with Mg# <0.60 (Garrido et al. 2006). Clinopyroxene from the ultramafic rocks yields a Sm–Nd isochron of 117 $\pm$ 7 Ma, interpreted as a crystallization age (Dhuime et al. 2007). This section has some residual harzburgite (Bouilhol et al. 2009; Dhuime et al. 2007; Jan and Howie 1981; Miller et al. 1991; Burg 2011) and is interpreted as a melt-mantle reaction zone beneath the base of the arc (e.g., Burg et al. 1998; Dhuime et al. 2007).

The Kohistan arc preserves a geochemical record that spans arc inception, arc thickening, and subsequent uplift (Dhuime et al. 2007; Yoshino and Okudaira

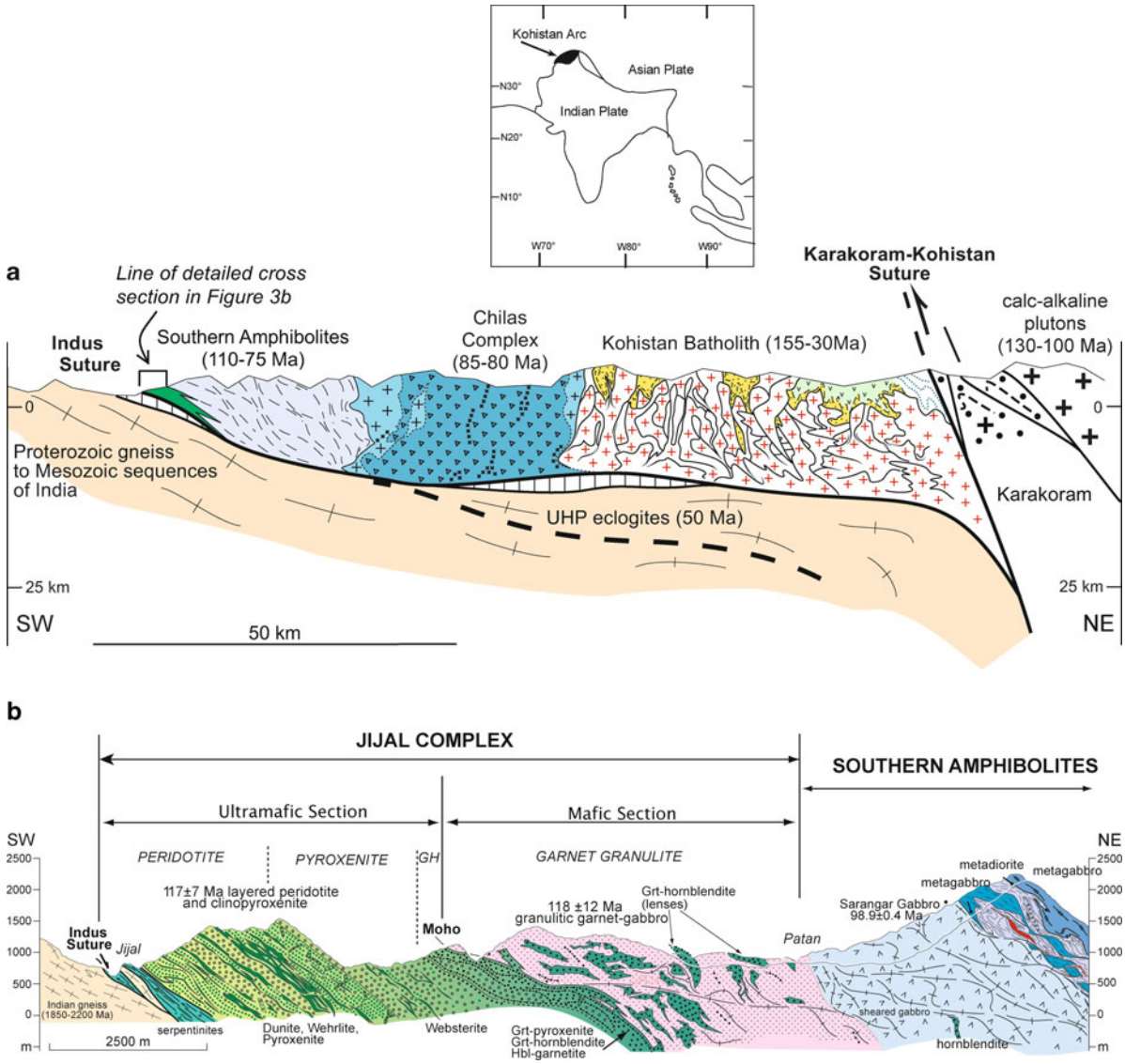

Fig. 5.3 (**a**) Simplified cross section through the Kohistan arc from Burg et al. (2006) and Burg (2011). The main units, the Southern Amphibolites, the Chilas Complex, and the Kohistan Batholith are described in the text. (**b**) Detail of the Moho section (south of the Southern Amphibolites) from Burg (2011) and Dhuime et al. (2007). GH is garnet-hornblendite/ pyroxenite and hornblende-garnetite rocks. The inset map shows the location of the Kohistan arc along the suture between the Indian and Asian plates.

2004). Metamorphic P-T-t paths of lower crustal rocks clearly indicate arc thickening due to magmatic input (Yoshino and Okudaira 2004; Yoshino et al. 1998). However, there is no consensus as to whether the arc underwent extensive intracrustal differentiation through melting of the lower crust (e.g., Garrido et al. 2006) or whether voluminous intermediate to felsic magmas of the upper crust (Kohistan batholith) are dominantly a result of fractional crystallization processes (Jagoutz 2010). In either case, more mafic rocks of the Kohistan batholith preserve geochemical evidence for evolution throughout the history of the collisional origin (increasing crustal component, Petterson et al. 1993; Petterson and Windley 1991).

5.2.3 Bonanza Arc, Vancouver Island

The Bonanza arc (500 km strike length) is a Jurassic arc crustal section (middle to upper crust) exposed on Vancouver Island and the Queen Charlotte Islands, Canada (DeBari et al. 1999) (Fig. 5.4). The arc is part of the much larger Wrangellia terrane that was accreted to western North America during the latest Jurassic to early Cretaceous. The arc is thought to be the southern extension of the Talkeetna arc described in Sect. 5.2.1 above (Plafker et al. 1989; Clift et al. 2005b).

The Bonanza arc was built on a thick oceanic basement comprising distinctive mid-Paleozoic arc volcanic rocks (Sicker Group), Pennsylvanian-Permian clastic rocks and limestones, and a remarkably uniform 6,000-m-thick sequence of Late Triassic tholeiitic flood basalts of the Karmutsen Formation (e.g., Greene et al. 2009 and references therein). These basalts are in turn overlain by Late Triassic-Early Jurassic shallow to deep-water carbonates and shales. The arc developed into and on this basement in response to eastward-directed subduction of Pacific ocean lithosphere during Early to Middle Jurassic times (Armstrong 1988).

Unroofing of the arc began with deposition of detritus derived from Bonanza Group volcanic rocks to form Middle Jurassic (Callovian) and Lower Cretaceous (Valanginian) conglomerates. This unroofing continued with Late Cretaceous granitoid-volcanic conglomerate deposited directly on unroofed Middle Jurassic Island Intrusions (Muller et al. 1974). Accretion to the North American margin may have occurred at this time (Monger et al. 1994). Afterwards,

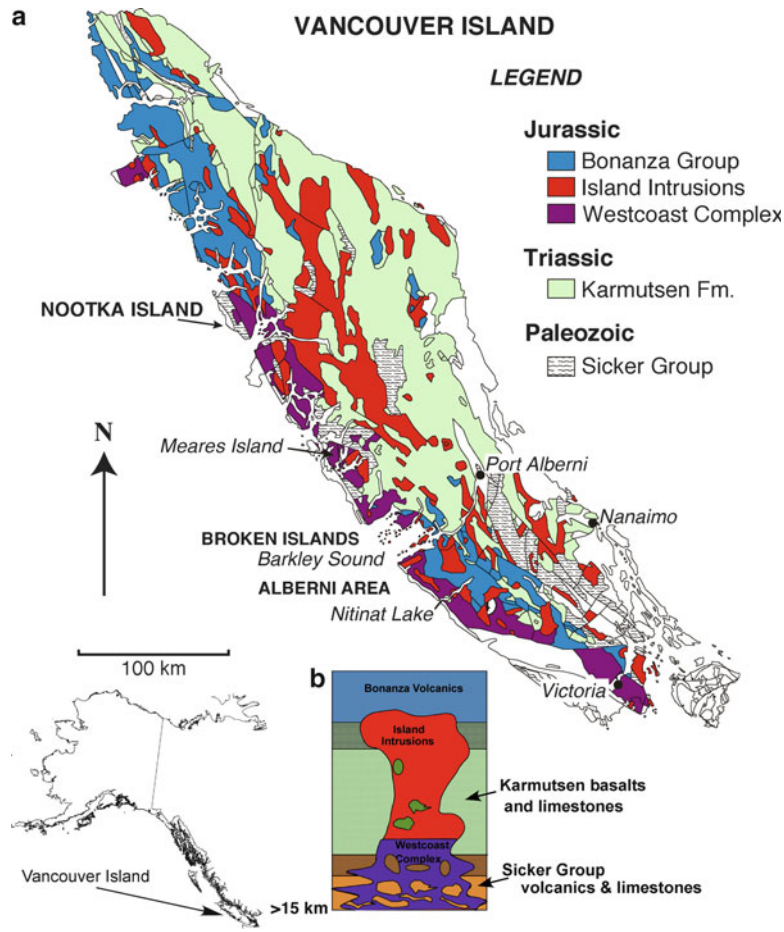

Fig. 5.4 (**a**) Map of Vancouver Island showing the main units of the Jurassic Bonanza arc (from DeBari et al. 1999). The deepest intrusive level of the arc is represented by the Westcoast Complex, the intermediate level is represented by the Island Intrusions, and the shallowest level is represented by the Bonanza Volcanics. (**b**) Schematic crustal section of the arc showing intrusive relationships between plutons and pre-existing country rock.

subduction continued under an Andean-type continental margin, and the locus of magmatism swept eastward to form the Late Jurassic to Cretaceous Coast Plutonic Complex. Late Cretaceous and younger contraction and possible sinistral transcurrent faulting along the continental margin further dismembered the arc (Monger et al. 1994; Plafker et al. 1989).

The exposed arc can be divided into discrete stratigraphic levels (DeBari et al. 1999). The Westcoast Complex represents the deepest exposed levels of the arc and displays a wide variety of lithologic types, including metamorphosed and migmatized segments of pre-existing crust (Sicker Group rocks) and mafic to intermediate plutonic rocks (190.3–186.6 Ma) representative of mantle-derived magmas (diorites to gabbros) (DeBari et al. 1999). The unit is composed of a heterogenous mixture of multiple magma types, partial melts, and restites. Stratigraphy of the pre-existing crust suggests that the deepest levels of the exposed arc represent depths of ~15–20 km (DeBari et al. 1999). This unit may have acted as a deep crustal "filter" where mantle-derived magmas stalled, fractionated, and interacted with older crust.

The higher levels of the arc are represented by the plutons of the Island Intrusions, whose ages overlap those of the Westcoast Complex (DeBari et al. 1999). These plutonic rocks are more texturally homogeneous than the deeper Westcoast Complex. They include diorite, quartz diorite, and granodiorite that intrude the Triassic Karmutsen Formation and overlying sediments. The lack of migmatized country rock and the general homogeneity of the plutons indicate that the mixing and homogenization processes were more or less complete before migration of magmas to these shallower crustal levels.

The Bonanza Group volcanic rocks record effusive magmatism and mark the highest crustal level of the arc. They are a thick sequence (up to 2,500 m) of lava flows, pyroclastic deposits, and thin interbedded sedimentary rocks. They conformably overlie Late Triassic-Early Cretaceous sediments and are intruded at their deepest levels by plutons of the Island Intrusions (Fig. 5.4).

Migmatitic partial melts of amphibolite country rock in the deep crust of the arc are tonalitic to trondhjemitic in composition. They have a very distinctive chemical signature, with depletions of Nb, Y, Zr, and the intermediate- and heavy-REE relative to the typical plutonic rocks of the Island Intrusions or WCC. These tonalites and trondhjemites were able to coalesce and migrate from their site of generation in the deep crust to shallower levels in the crust.

5.2.4 Southern Coast Plutonic Complex: WA Cascades

The >1,500-km-long Coast Plutonic Complex of British Columbia, and its southern extension in the crystalline core of the North Cascades, represents a voluminous Cretaceous to Paleogene magmatic arc (Armstrong 1988; Tabor et al. 1989) (Fig. 5.5). In Washington State, exposed plutons (96–45 Ma) represent various crustal levels of the arc from deep (~20–35 km) to shallow (~7 km) (Miller and Paterson 2001) (Fig. 5.5d). The base of the exposed section represents paleodepths of ~40 km; but the Cretaceous Moho was thought to be at depths >55 km as a result of arc contraction (Miller and Paterson 2001). Regional shortening resulted in crustal thickening and burial of supracrustal rocks to great depths of 25 to >40 km (Matzel et al. 2004; Valley et al. 2003; Whitney et al. 1999).

Arc plutons that range in age from 96 to 45 Ma intrude oceanic terranes of varying affinity that had only recently been accreted to each other (by 96 Ma) and to the margin of North America (Umhoefer and Miller 1996). From upper to lower paleodepths these include the Ingalls Ophiolite, the Chiwaukum schist (accretionary complex), and the Napeequa Complex (ocean floor assemblage) (Fig. 5.5d). Based on equilibration pressures, the Swakane gneiss is at the bottom of the stack (0.9–1.2 GPa; Matzel et al. 2004), but it has not been intruded by arc plutons. Matzel et al. (2004) conclude that Swakane protolith was arc-derived clastic sediments that were buried and metamorphosed after the most voluminous pulse of plutonism.

The base of the arc section at ~35 km comprises intermediate (tonalitic) plutons that intrude amphibolite facies (<700°C) country rock [e.g., (Miller et al. 2009)] (Fig. 5.5d). Miller and Paterson (2001) interpret low temperatures at such deep levels (in contrast to thinner arcs) to be a result of rapid crustal thickening. These low temperatures are responsible for the lack of

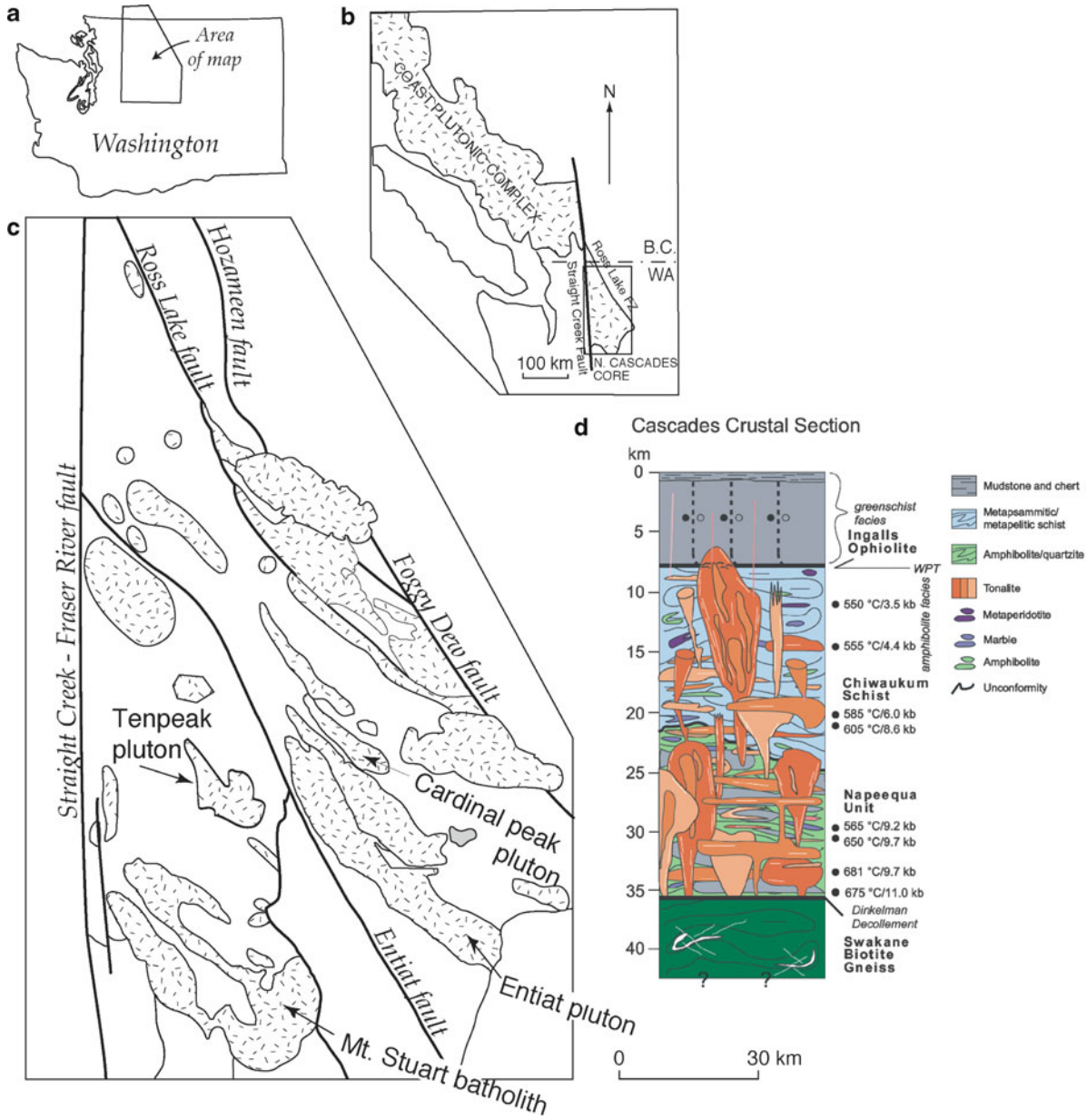

Fig. 5.5 Maps (**a**–**c**) showing region and detail of the southern Coast Plutonic Complex in Washington State after Miller et al. (2009). Schematic crustal section in (**d**) is from Miller et al. (2009) and is based on structural thicknesses and geobarometric constraints.

migmatization observed in host rocks at the 30–35 km level. However, cryptic evidence for host rock melting at deeper, currently unexposed levels of the arc is preserved in geochemical signatures in the tonalitic rocks (Dawes 1993; Parent 1999; Miller et al. in preparation).

Tonalite is the most abundant plutonic lithology at all levels of the crustal section (10–30 km). However, deeper plutons (>0.6 GPa, ~20 km) commonly display evidence for broadly synchronous mafic magmatism (Miller and Paterson 2001). These mafic compositions are most abundant as sheeted zones at

the margins of the plutons and suggest that mafic magmas, with minor crustal component, predominated at the early stages of pluton emplacement. As the plutons evolved, magma volume generated by partial melting at deep levels in the crust increased (Miller et al. in preparation). These crustal melts mixed with the mantle-derived magmas, producing hybrid compositions. Sheet-like emplacement may have continued, but the volume of magma increased and partially erased its record. Throughout the history of these plutons, mafic magmas and tonalitic hybrid magmas were injected simultaneously, as shown by intermingled mafic enclaves and mafic sheets (see later discussion).

Plutons that crystallized at shallower levels (< 0.6 GPa) are more homogeneous, presumably because hybridization was completed at greater crustal depth (Miller and Paterson 2001). These shallower plutons, and their erupted counterparts, may not record the cryptic history and variety of sources necessary for their genesis.

5.3 Depth-Specific Processes: Pre-collision

The sections described above expose multiple levels of island arc crust. Some expose only parts of the section, some expose more complete traverses. But taken together, these four sections show very clear commonalities and provide a fairly complete picture of arc crust from top to bottom (Fig. 5.1).

5.3.1 Crystal Fractionation and Production of Pyroxenite and Px-Gabbro Assemblages Near the Moho

In both the Kohistan arc and the Talkeetna arc, the crustal section includes paleo-Moho exposures. In the field, the Moho is clearly observed as a relatively sharp (10–100s of meters) boundary between plagioclase-bearing and plagioclase free lithologies [e.g., see photo in Fig. 10.10 of Burg (2011)]. It is a high temperature contact, where fabric on both sides of the Moho displays evidence for high-temperature flow (e.g., Burg et al. 2005; Mehl et al. 2003)

In exposures beneath the paleo-Moho, minor dunites and abundant pyroxenites (Fig. 5.6), indicate early crystal fractionation of olivine and pyroxene. At both Kohistan and Talkeetna, pyroxenite veins, dikes, and layers increase in abundance up section, such that cumulate pyroxenite is the dominant lithology near the Moho. Cumulate pyroxenite is ~500 m thick near the paleo-Moho exposures in Talkeetna (Fig. 5.2b), and several km thick in Kohistan (Fig. 5.3b).

Above the Moho, in the lower and mid crust of the Kohistan and Talkeetna arc sections, the plagioclase-bearing crystal assemblage is a cumulate consisting of plagioclase, clinopyroxene, orthopyroxene, oxide (Mg–Al spinel or Fe–Ti oxide), ± amphibole, ± garnet. Note that this assemblage is olivine free, indicative of the relatively high pressures at which this crystal fractionation occurred (~0.5–1.0 GPa, Hacker et al. 2008, Yoshino et al. 1998). However, some

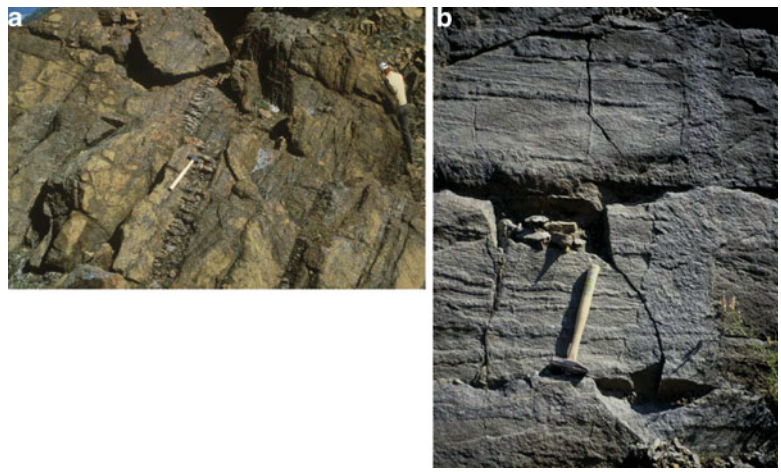

Fig. 5.6 Photographs of pyroxenite layers in the mantle sections of the Talkeetna and Kohistan arcs. (**a**) Shows sub-parallel layers of pyroxenite (dipping ~70°) in dunite at Talkeetna, with one layer adjacent to the hammer. (**b**) Shows sub-parallel pyroxenite layers and one cross-cutting pyroxenite layer within dunite at Kohistan. In the latter example, the pyroxenite stands out from the dunite background.

pyroxene + spinel-rich assemblages in the lower crust of the Talkeetna arc are thought to have formed from olivine + plagioclase assemblages crystallized at 0.1–0.6 GPa that later underwent pressure increase to ~1 GPa (Hacker et al. 2008).

In both arc sections, fractionation of the observed cumulate rocks was dominantly responsible for producing the more differentiated compositions in the upper sections of the respective arcs (Greene et al. 2006; Jagoutz 2010). Qualitatively, this can be seen in Fig. 5.7a, where positive Eu and Ti abundances in the cumulate rocks (from accumulation of plagioclase and oxides) are mirrored by low abundances of these elements in the more differentiated volcanic rocks.

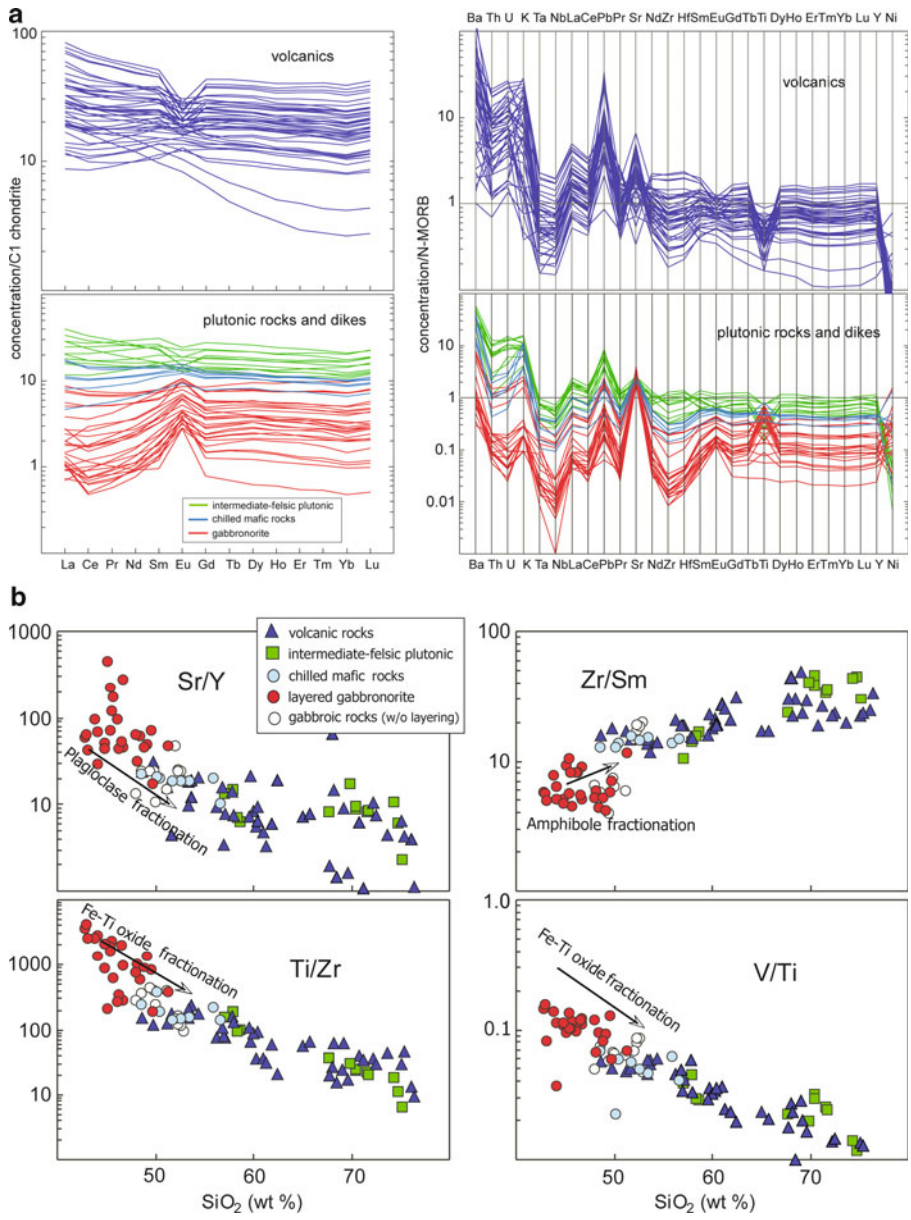

Fig. 5.7 (**a**) Normalization diagrams for volcanic rocks (*purple*), intermediate-felsic plutonic rocks (*green*), chilled mafic rocks (*blue*), and cumulate gabbronorite (*red*) from Talkeetna. Note that where some positive spikes (enrichment) occurs in cumulate gabbronorite (e.g., Eu, Ti), corresponding negative spikes (depletion) occurs in more differentiated rocks in the upper crust. Corresponding enrichment and depletion is shown more quantitatively for trace element ratios in (**b**). Figures are from Greene et al. (2006).

Ratios of Zr/Sm, V/Ti, Sr/Y, and Ti/Zr in the cumulate rocks are matched by reciprocal ratios of these elements in the volcanic rocks with increasing SiO_2 (Fig. 5.7b)

In the Talkeetna arc, Greene et al. (2006) quantitatively modeled the fractionation process using observed cumulate assemblages. The rare earth element (REE) abundances in clinopyroxene in the cumulate rocks were used to calculate REE abundances of liquids in equilibrium with those cumulates. The calculated equilibrium liquids closely match observed compositions in the volcanic rocks in the upper crust of the arc. Greene et al. (2006) also modeled the differentiation trend of the upper crustal volcanic rocks from basalt to andesite to predict calculated modes and compositions of fractionated minerals. Those predicted modes and compositions were a striking match to the observed cumulates in the lower crust. The basalt to andesite trend in the volcanic rocks was reproduced by ~73% fractionation of the observed lower crustal cumulate rocks.

Jagoutz (2010) modeled the fractionation process in the Kohistan arc by mass balance using observed volumes of cumulate rocks (dunite, wehrlite, pyroxenite, gabbro). He was able to produce the bulk of the upper crustal granitoids after 80% fractionation of the cumulate rocks, with some assimilation of leucocratic rock produced by deep crustal melting.

One critical outcome of the Greene et al. (2006) modeling in the Talkeetna arc is that a substantial section of cumulate pyroxenites must be missing from the base of the arc (Kelemen et al. 2003). These results are supported by the thermodynamic modeling of Behn and Kelemen (2006). In order to bring the most mafic Talkeetna liquid composition in Fe/Mg equilibrium with the mantle, a much larger, and more Mg-rich section of cumulate pyroxenites would be necessary. Even the most Mg-rich cumulates currently exposed in the arc were fractioned from liquids that had already themselves been fractionated. Thus, some fractionated cumulate material *should* be present beneath the exposed crustal section. Fractionation of the parental basaltic magma could have occurred at deeper levels in the mantle than exposed. However, modeling by Greene et al. (2006) shows that any mantle-derived parental basaltic magma must have fractionated ~25% pyroxene before it reached the paleo-Moho. Given that cumulate pyroxenites increase upward (toward the Moho) in the observed mantle section, most pyroxenites were more likely fractionated near the Moho, and should be exposed there. As discussed below, it is likely (and physically reasonable) that missing pyroxenite cumulates were removed by lower crustal foundering (delamination).

5.3.2 Densification of Crust and Lower Crustal Foundering at the Moho

In both the Talkeetna arc and the Kohistan arc, assemblages near the paleo-Moho are garnet bearing. These include garnet-pyroxenites as well as garnet gabbros (referred to as granulites by some authors) (Fig. 5.8). The garnet gabbros in both arcs form irregular veins and lenses within gabbronorite, and garnet percentages range from 1 to 40 volume %. Kohistan has a much thicker preserved garnet-bearing section than Talkeetna (~5 km vs. $\ll$1 km), but as discussed below, the Talkeetna arc may once have had a garnet-bearing section of comparable thickness.

The Jijal Complex at the base of the Kohistan arc includes a 5-km thick section of garnet gabbros equilibrated at 700–950°C and >1 GPa (Yamamoto 1993). There is no consensus on whether these garnet gabbros formed during igneous cooling (Ringuette et al. 1999), postmagmatic heating and crustal thickening (Yamamoto and Yoshino 1998; Yoshino and Okudaira 2004; Yoshino et al. 1998) or dehydration melting of hornblende (Garrido et al. 2006). In the Talkeetna arc, the garnet-bearing gabbros at the base of the section (at Bernard Mountain) formed through subsolidus cooling (DeBari and Coleman 1989). They record conditions at the base of the arc section of 900°C–1,000°C and ~1 GPa (Hacker et al. 2008).

The presence of garnet bearing lithologies at the Moho in both crustal sections has important implications. At pressures of 1–1.2 GPa, the slope of the garnet-in reaction for gabbronorites such as those in Kohistan and Talkeetna is nearly parallel to likely arc geotherms, making the stability of garnet highly sensitive to small changes in temperature (Fig. 5.9) (Behn and Kelemen 2006; Jull and Kelemen 2001). A shift from 1,000 to 800°C at 1 GPa will result in a density increase of more than 250 kg/m^3 due to the formation of garnet at lower temperature (Behn and Kelemen 2006). Thus as

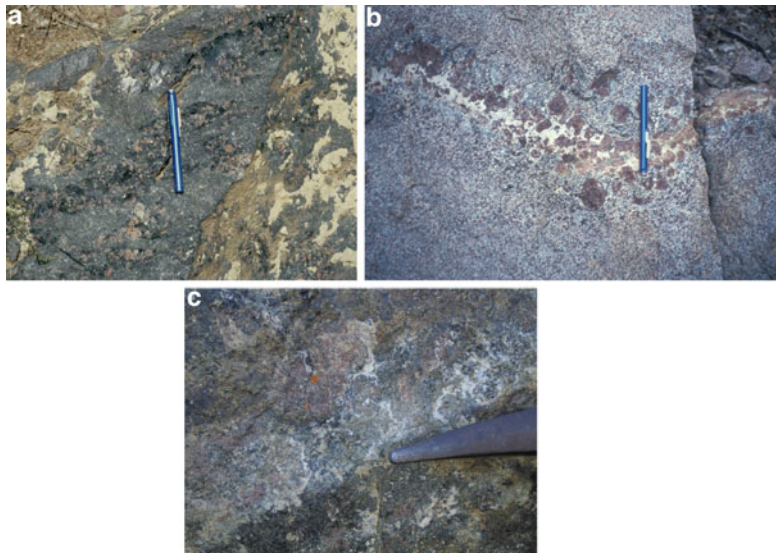

Fig. 5.8 Garnet-bearing lithologies from the Kohistan arc (**a** and **b**) and Talkeetna arc (**c**). The photo in (**a**) shows Kohistan garnet-hornblende pyroxenite in mantle rocks, whereas (**b**) and (**c**) show lower crustal garnet gabbros from Kohistan and Talkeetna, respectively. *Reddish* mineral grains are garnet, plagioclase is *white*, hornblende and pyroxene are *black*.

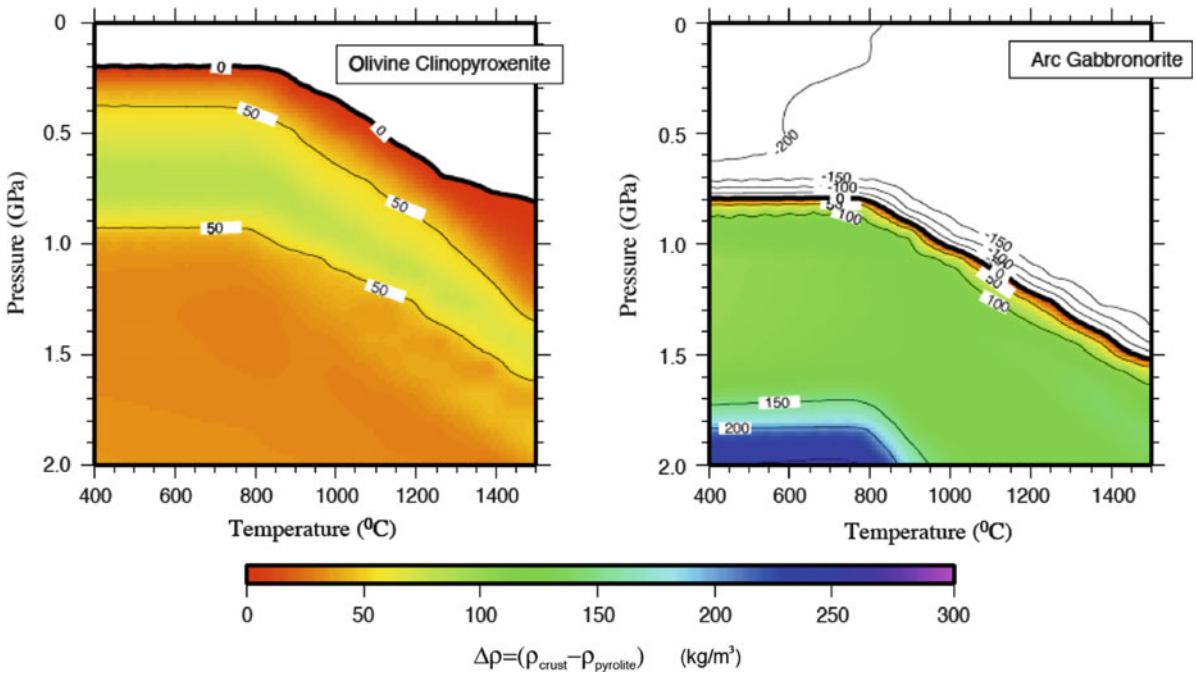

Fig. 5.9 Calculated density contrast (Δρ, kg/m^3) from Jull and Kelemen (2001) between crustal rock and pyrolite mantle. The colored regions are those in which the density contrast is positive, and hence the rock would be denser than the underlying mantle. In (**a**) the crustal rock is olivine clinopyroxenite and in (**b**) the crustal rock is arc gabbronorite. Both lithologies are typical of Talkeetna arc rocks near the Moho (1 GPa, 800–1,000°C). At those P-T conditions, these arc cumulates would have been denser than their underying mantle.

2-pyroxene gabbroic rocks cool at 1 GPa, or if the arc thickens, formation of garnet should be a common process. Jull and Kelemen (2001) show that Talkeetna garnet gabbros will be ~100 kg/m^3 denser than the underlying mantle at 800°C. The density contrast will be even greater for gabbronorites with Mg# >80 (Behn and Kelemen 2006). In Kohistan, no primitive gabbronorites with Mg# >80 are observed in the arc section,

providing evidence that those rocks may have been lost to the mantle (Behn and Kelemen 2006).

The presence of pyroxenite near the Moho also has important implications for lower crustal stability. Pyroxenite, even without garnet, is predicted to be denser than residual peridotite when the proportion of plagioclase is less than 6–8% (Behn and Kelemen 2006; Jull and Kelemen 2001). Thus the density contrast between pyroxenite and residual peridotite is less sensitive to temperature. Consequently, while pyroxenite is denser than residual mantle at 1,000°C and 1 GPa, gabbronorite will be less dense than mantle at these higher temperatures. Jull and Kelemen (2001) show that a 10 km thick ultramafic cumulate layer at the base of the crust at ~1,000°C would need 10 Ma to delaminate. But if temperatures or strain rates are higher, then ultramafic cumulate layers a few hundred meters thick may become unstable as quickly as they form. Arc gabbronorites on the other hand, need lower temperatures (~800°C).

Thus, the discrepancy between the observed proportions of pyroxenites near the Moho in the Talkeetna arc (<5% of the arc section) and the proportion required by crystal fractionation modeling described above (>25%) can be explained by gravitational instability. Dense ultramafic cumulates, probably together with dense garnet gabbros, may have foundered into the underlying mantle during the time that the Talkeetna arc was magmatically active, or in the initial phases of slow cooling (and sub-solidus garnet growth). Given the "missing" pyroxenites, the Talkeetna arc lower crust was interpreted by Behn and Kelemen (2006) to be an equilibrium configuration that was convectively stable relative to the underlying mantle. The denser, more primitive cumulates may have been removed via foundering into the asthenospheric mantle.

In the Kohistan arc, the Moho is also interpreted to be a site of active underplating, granulite facies metamorphism, and efficient recycling of ultramafic and garnet-bearing lower crust into the asthenospheric mantle (Dhuime et al. 2009; Garrido et al. 2007). This occurred during the main stage of oceanic arc development (105–91 Ma), prior to accretion to the continent. These authors use similar reasoning to Greene et al. (2006) – the evolved character of underplated magmas (Mg# <59) implies a thick cumulate sequence that is no longer preserved in the crustal section.

5.3.3 Crustal Melting

Three of the four crustal sections described above show clear evidence for crustal melting to produce intermediate compositions (shown in orange in Fig. 5.1). One section shows cryptic geochemical evidence for crustal melting at levels deeper than those exposed (southern Coast Plutonic Complex), whereas two sections (Kohistan and Bonanza) display clear field and geochemical evidence for partial melting of country rock at the level of exposure. These partial melts exist in situ in migmatite complexes and as extracted magmas in pods or stocks at shallower crustal levels (e.g., DeBari et al. 1999; Dhuime et al. 2009) (Fig. 5.10). In the Talkeetna arc, cryptic geochemical evidence for crustal melting occurs only in the far western part of the arc in the latest stages of magmatism (Johnsen 2007).

Interestingly, these migmatite complexes do not exist right at the Moho. Moho sections are generally anhydrous assemblages, with evidence for only late stage, crosscutting amphibole-bearing lithologies. In Kohistan, migmatites occur within the Southern Amphibolite unit at pressures 0.8–1.0 GPa (Fig. 5.3). In the Bonanza arc, migmatites are within the Westcoast Complex at >0.6 GPa (Fig. 5.4) (DeBari et al. 1999).

Where observed in the field, the partial melts are tonalitic, produced by partial melting of metabasalts and metagabbros. In the Kohistan and Bonanza arcs, the partial melts have REE patterns distinctive of hornblende-bearing sources (Dy/Yb < 3). In contrast, in the Coast Plutonic Complex, inferred partial melts from pressures >1.5 GPa (below the level of exposure) have steep REE patterns distinctive of garnet-bearing sources (Dy/Yb > 3).

5.3.4 Mingling, Mixing, and Homogenization: "MASH" Zone

One commonality between all crustal sections is the heterogeneous nature of the middle crust. All crustal sections at this level display complex relationships between multiple lithologies, at all scales, and over many kilometers of section (Fig. 5.11). In the Westcoast Complex of the Bonanza arc and the Southern Amphibolite belt of the Kohistan arc, outcrops over many square kilometers show complex relationships

Fig. 5.10 Field examples of migmatitic rocks where crustal melting has taken place. (**a**) Is in the Southern Amphibolites of the Kohistan arc and (**b**) is in the Westcoast Complex of the Bonanza arc. *Black* rocks are restite, *white* rocks are tonalitic partial melts.

between amphibolite facies host rock and multiple magma types (including partial melts). In the southern Coast Plutonic complex, where host rock abundance is higher, these complex relationships are evident in km-wide sheeted zones at pluton margins. In the mid crust of the Talkeetna arc, multiple magma types are complexly intermingled (Fig. 5.11), but without the presence of intermixed host rock.

These observed heterogeneous zones in all the crustal sections are a good match for the proposed "MASH" zone of Hildreth and Moorbath (1988). These authors proposed a zone in the deep arc crust where crustal melting, assimilation of host rock, stagnation, and homogenization takes place. However, the major difference between their model and the representations in crustal sections is that this MASH zone does not occur right at the Moho. The Moho is instead dominated by the cumulate products of crystal fractionation, corroborating the deep crustal "hot zone" model of Annen et al. (2006). The MASH zone occurs above that cumulate-dominated zone, presumably where magmas that had been variably differentiated by removal of crystal cumulates coalesce and mingle with host rocks and any partial melts.

5.4 Post-collision Geochemical Changes

In two of the arc crustal sections, Talkeetna and the southern Coast Plutonic Complex, arc magmatism continued after accretion to a continental margin (Clift et al. 2005b; Rioux et al. 2007; Tabor et al.

Fig. 5.11 Examples of magma mixing/mingling relationships between mafic and felsic magmas in the Coast Plutonic Complex, Bonanza arc, and Talkeetna arc. Flow textures in the mafic (*dark*) rocks suggest that all compositions were molten at the same time. (**a**) Shows physical mixing between basaltic compositions and plagioclase rich tonalites from the Tenpeak pluton in the Coast Plutonic Complex. Photos in (**b**) through (**d**) show basaltic dikes that were intruded into a more felsic magma chamber with various amounts of mixing and homogenization (**b** and **c** are from the Bonanaza arc and **d** is from the Talkeetna arc.

1989), or in the case of Talkeetna perhaps to another large terrane (Rioux et al. 2007). In both cases, this produced a thickened arc whose geochemical signature begins to reflect some incorporation of new basement rock, intracrustal melting and the segregation of garnet (either through partial melting or deep seated crystallization). In the eastern Talkeetna arc, Rioux et al. (2007) interpret plutonic rocks with more evolved initial isotopic ratios and the presence of xenocrystic zircons as reflecting docking to either the Wrangellia terrane or to North America. In the western Talkeetna arc, Johnsen (2007) correlates changing isotopic and trace element ratios to this same process.

Thickening of the arc due to the contractional processes is what is responsible for the generation of a more strongly calcalkaline, "continent-like" geochemical signature. For example, Johnsen (2007) shows that late-stage plutons in the western Talkeetna arc have much steeper rare earth element patterns ($[La/Yb]_N > 5$) than the older plutons (Fig. 5.12). He interprets this as change from a pure fractionation origin (fractionation of pyroxene, plagioclase, hornblende, and oxides from an andesitic parental magma) to a more complex origin involving fractionation combined with partial melting of overthickened crust. Similar interpretations are proposed for plutonic rocks of the southern Coast Plutonic Complex (crust >55 km thick) where trace element patterns are very steep ($[La/Yb]_N > 10$) and a role for garnet in magma genesis is required (DeBari et al. 1998, Miller et al. in preparation).

5.5 Relationship Between Inferred Magmatic Processes, Lithological "Stratification", and Geophysical Signature

In general, seismic velocity profiles in modern arcs show an increase of P-wave velocities (V_p) with depth (Fig. 5.13) with a clear segmentation into upper, middle, and lower crustal regions. Calvert (2011) reports a typical ratio of three parts upper crust to four parts middle crust to five parts lower crust. The depth of these segments depends on total thickness of the arc.

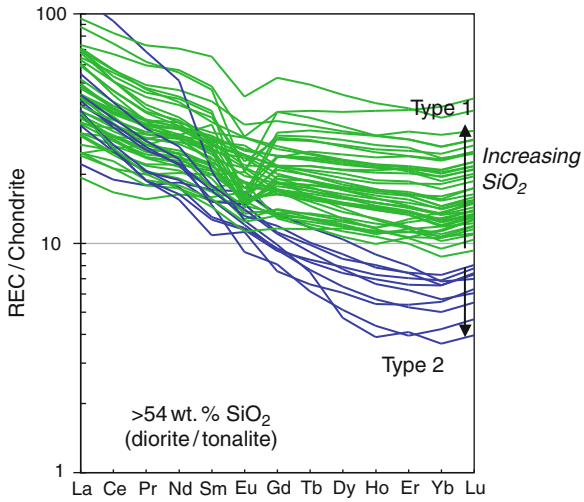

Fig. 5.12 REE patterns of Type 1 plutonic rocks from the western Talkeetna arc (*green*) compared to Type 2 plutonic rocks (*blue*). Type 1 patterns are from older plutons produced by crystal fractionation of pyroxene, plagioclase, hornblende, and magnetite. Type 2 patterns are found in younger plutons, and require some crustal melting and assimilation, and possibly a garnet component. Data from Johnsen (2007).138.

Figure 5.13 shows a comparison of V_p profiles for several modern arcs, compared to a V_p profile calculated in this study for the lithologies present in the Talkeetna crustal section.

Intriguingly, some modern arcs (e.g., Kurile, Izu Bonin, Mariana) have a thick layer of low-velocity upper middle crust (V_p = 6.0–6.5 km/s) that has been interpreted to be intermediate or felsic intrusive rock (e.g., Kodaira et al. 2007; Nakanishi et al. 2009; Takahashi et al. 2007). There has been much discussion about the presence of this layer in arcs as the unsubductable nucleus of continental crust (e.g., Tatsumi et al. 2008). Field analogues to this layer are observed in all crustal sections described above. Tonalite and diorite (the light blue fields in Fig. 5.1) are common upper middle crust lithologies in these arc sections. In contrast, the Aleutian arc middle crust has a V_p =6.5–6.9 km/s (Shillington et al. 2004), which is higher than the western Pacific arcs. Shillington et al. (2004) interpret this mid crustal layer to be dominantly gabbroic, with some proportion of more felsic rocks. Clearly more felsic rocks are produced in the Aleutians, given the composition of felsic plutons and volcanic rocks exposed at the surface (e.g., Romick et al. 1992).

The Honshu and Cascade arcs are continental, but both are built on juvenile continental crust. They both also have a middle crust with Vp = 6.0–6.5 km/s. In the Cascades, Parsons et al. (1998) interpret the 10 km-thick layer with Vp = 6.0–6.5 km/s to contain felsic intrusive rocks similar to plutonic inclusions in Mt. St. Helens' volcanic rocks. Laboratory experiments on P-wave velocities support this interpretation (Parsons et al. 1998).

Lower crustal P-wave velocities in modern arcs are high (>6.9 km/s, Fig. 5.13), indicative of rocks in dry "granulite facies" conditions (e.g., Rudnick and Fountain 1995). These granulite facies conditions are preserved in rocks from the lower crust of both Talkeetna and Kohistan. However, seismic velocities will be slower if the lithologies are hydrous (i.e., amphibole bearing). For example, P-wave velocities are lower in the lower crust of northeast Japan than in other arcs (V_p = 6.5–7.0 km/s) (Iwasaki et al. 2001). Nishimoto et al. (2005) interpret this lower velocity to be due to an extensively hydrated lower crust where hornblende, plagioclase, and magnetite are dominant, as represented by lower crustal xenoliths. This hydration may be due to infiltration of H_2O-rich magmas, a process locally documented in the deep crust of the Kohistan arc during decompression (Yamamoto and Yoshino 1998) and in the Talkeetna arc (DeBari and Coleman 1989).

Behn and Kelemen (2006) conclude that P wave velocities >7.4 km/s are indicative of lower crust that is denser than underlying mantle peridotite (e.g., the garnet-bearing gabbros or pyroxenites from Talkeetna), and can become convectively unstable. Interestingly, seismic refraction studies in modern arcs typically find lower crustal V_p < 7.4 km/s. This implies that, like the Talkeetna arc, either (1) gravitationally unstable material founders rapidly on geologic timescales, or (2) the missing high V_p cumulates crystallize beneath the Moho. Preservation of such a thick section of these dense rocks in Kohistan is surprising. However, their low Mg # (<0.60; Garrido et al. 2006; Jagoutz 2010) may suggest a greater density stability for these rocks (cf. Behn and Kelemen 2006).

The paleo-Moho in Kohistan and the Talkeetna arc sections is a sharp boundary between ultramafic rocks and plagioclase-abundant gabbroic rocks (generally <100 m transition zone). Both density and P-wave velocity would change rapidly over this type of

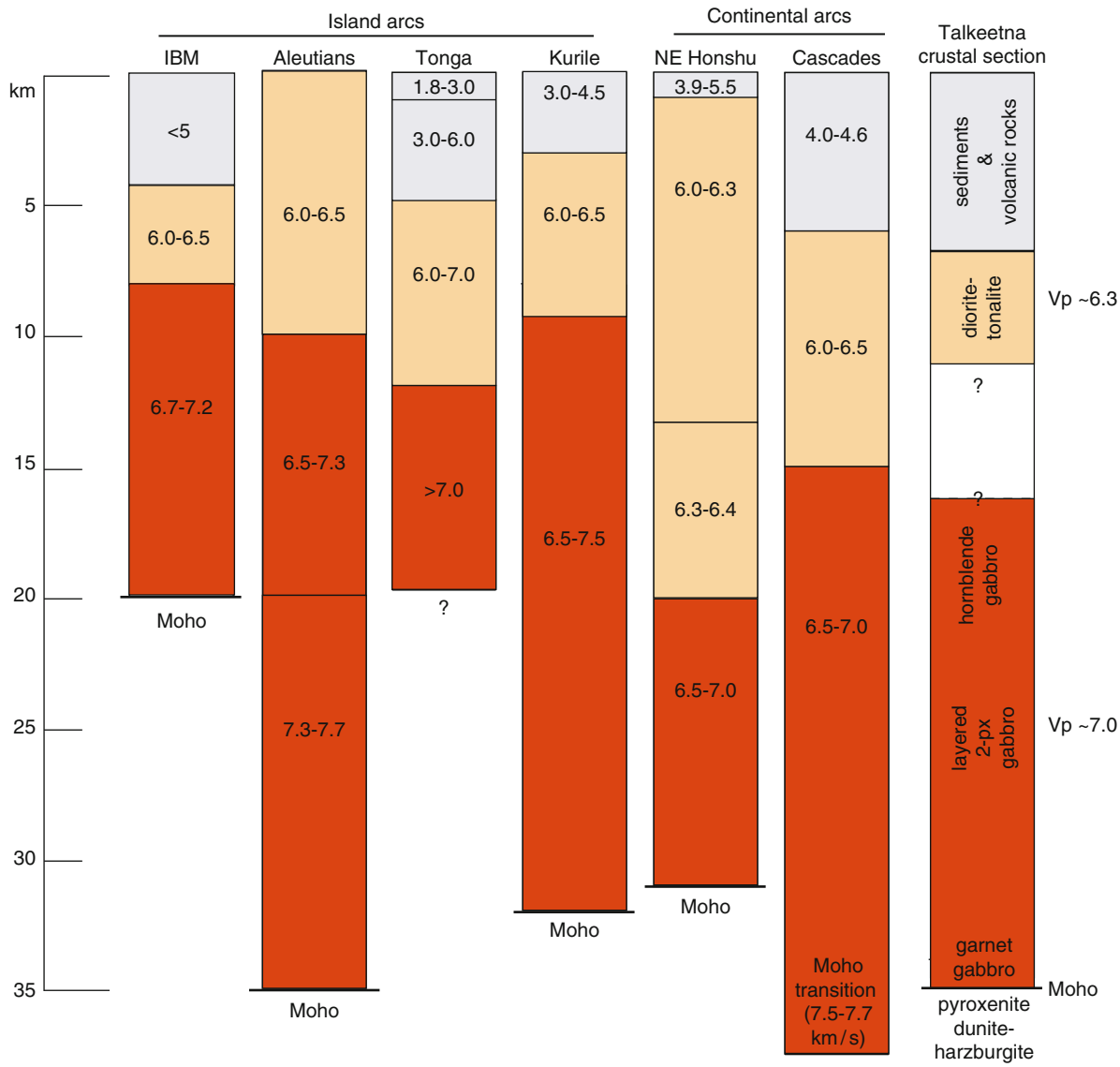

Fig. 5.13 Seismic velocity profiles of various modern island arcs and continental arcs compared to the Talkeetna crustal section. The Izu-Bonin arc is from Suyehiro et al. (1996), the Aleutian arc is from Shillington et al. (2004), the Tonga arc is from Crawford et al. (2003), the Kurile arc is from Nakanishi et al. (2009), NE Honshu is from Iwasaki et al. (2001), and the Cascade arc is from Parsons et al. (1998).

transition. Thus if these exposed sections are representative of modern arcs, seismic profiles should produce a sharp Moho. An interesting implication of the Moho as being a plagioclase-saturation boundary is that much of the "igneous" part of the arc (ultramafic cumulates) is not part of the crust. Experiments by Müntener et al. (2001) show that up to 50% of primary mantle-derive liquid could crystallize as ultramafic plutonic rocks before plagioclase saturation. Thus the arc crust is necessarily more felsic than the parental magma extracted from the mantle.

Many geophysical studies seek to link geophysical profiles from modern arcs with magmatic processes (e.g., Calvert et al. 2008; Nakanishi et al. 2009; Nishimoto et al. 2005; Shillington et al. 2004; Suyehiro et al. 1996). One particularly elegant model (Tatsumi et al. 2008) integrates petrologic modeling with seismic features of the Izu-Bonin-Mariana (IBM)

arc. They conclude that the IBM arc has gone through two stages of arc development. Stage 1 is the initial growth of the arc, where crystal fractionation is dominant, and a mafic-intermediate crust is created. The bulk composition is basaltic, with differentiated magmas in the upper crust and cumulates in the lower crust/upper mantle. In Stage 2, successive basaltic underplating causes partial melting of Stage 1 crust to produce more differentiated (andesitic) magmas. This can take place either by moderate degrees of melting of basaltic arc crust (which produces andesite and complementary mafic restite), or by smaller percent melting that produces felsic magma that mixes with differentiated basaltic magma to produce andesite. This latter process also leaves a restite.

These two stages (crystal fractionation dominated and crustal melting dominated) are clearly represented in the crustal sections described above (Fig. 5.14). Much of the exposed crustal section in the eastern Talkeetna arc (where the deepest exposures are) is a final product

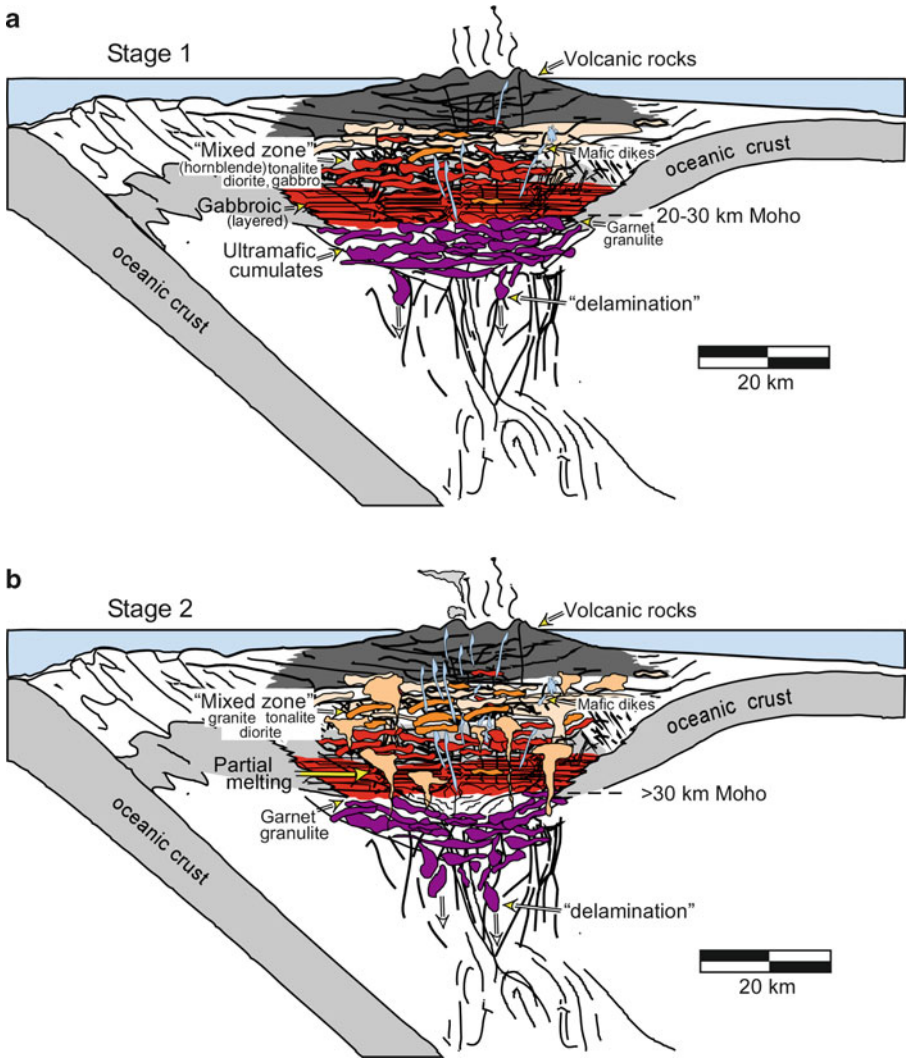

Fig. 5.14 Evolution of an arc through (**a**) Stage 1 and (**b**) Stage 2 phases, modified after Garrido et al. (2006). A Stage 1 arc is dominated by crystal fractionation and mingling/mixing processes, with arc crust generally <30 km thick. This stage occurs during early stages of arc development, but as indicated by the Talkeetna arc, this stage may persist for tens of millions of years. A Stage 2 arc has been thickened extensively, typically by arc contraction, and may be indicative of collision with another terrane. During this stage, crustal melting can be extensive. Delamination of dense cumulates as discussed in the text occrs during both of these stages.

of a Stage 1 arc, even with a 30 km crustal thickness. Intermediate and felsic plutons are exposed, but they are all clearly related by fractional crystallization. The seismic profile of the Mariana modern arc (Calvert et al. 2008) suggests that this arc is also in Stage 1. A Stage 2 arc, where crustal melting is important, is represented by the crustal sections from Kohistan, the Bonanza arc, and the Coast Plutonic Complex. Crustal melting must also have occurred locally in the later stages of the Talkeetna arc (Rioux et al. 2007; Johnsen 2007).

From the petrologic modeling, Tatsumi et al. (2008) calculate that much of the cumulate and restitic rock produced in the fractionation and partial melting processes must be below the Moho. This is required because the lower crustal thickness is too thin to accommodate the required rock material. This hypothesis of mass transfer across the Moho is strongly corroborated in the arc crustal sections (Fig. 5.14).

5.6 Conclusion

The arc-crustal sections described in this paper show that mantle-derived magmas pond and fractionate at the base of the crust, producing thick swaths of cumulate rocks. The seismic Moho is within these cumulate rocks, with plagioclase-bearing rocks (gabbros) above and plagioclase-absent rocks (pyroxenites and dunites) below. It is a relatively sharp boundary. As shown in both Kohistan and the Talkeetna arc, as the arc thickens through magma input (or by contraction) to >30 km, gabbroic rocks may become garnet-bearing either through crystallization of igneous garnet, by subsolidus garnet growth, or by growth of garnet during partial melting. Pyroxenites and garnet gabbros are denser than underlying mantle and are very likely removed via crustal foundering. Missing pyroxenites from the base of Talkeetna arc crust, coupled with high temperature flow fabrics in the underlying mantle, and a thin layer of garnet gabbros, provide strong evidence that the Moho can be a delamination feature. Missing ultramafic cumulates in the Kohistan arc also corroborate this hypothesis.

The lower middle crust of these arc sections is a zone of extreme inhomogeneity. This is the part of the crust where there is the best evidence for crustal melting, and where mantle-derived magmas at variable stage of differentiation mix with each other and with these crustal melts. The middle and upper crust is more homogeneous, more felsic, and much less dense than the rocks of the lower crust. This then becomes the unsubductable nucleus of continental crust, with compositions that range from diorite to quartz diorite to tonalite. Finally, the uppermost crust contains the volcanic pile that is variably intruded by upper crustal plutonic rocks.

As arcs thicken over time, especially after accretion, the development of garnet in the lower crust and the greater role for deep crustal melting has profound impacts on arc chemistry. These magmas become more felsic, and develop steeper rare-earth element patterns that more closely resemble continental crust.

References

Amato JM, Rioux ME, Kelemen PB, Gehrels GE, Clift PD, Pavlis TL, Draut AE (2007) U-Pb geochronology of volcanic rocks from the Jurassic Talkeetna Formation and detrital zircons from prearc and postarc sequences: implications for the age of magmatism and inheritance in the Talkeetna arc. In: Ridgway KD, Trop JM, Glen JMG, O'Neill JM (eds) Tectonic growth of a collisional continental margin: crustal evolution of southern Alaska. Geological Society of Americal Special Paper 431:253–271

Annen C, Blundy JD, Sparks RSJ (2006) The genesis of intermediate and silicic magmas in deep crustal hot zones. J Petrol 47(3):505–539

Armstrong RLA (1988) Mesozoic and early Cenozoic magmatic evolution of the Canadian Cordillera. Geol Soc Am Spec Pap 218:55–91

Barth MG, McDonough WF, Rudnick RL (2000) Tracking the budget of Nb and Ta in the continental crust. Chem Geol 165 (3–4):197–213

Behn MD, Kelemen PB (2006) Stability of arc lower crust: insights from the Talkeetna arc section, south central Alaska, and the seismic structure of modern arcs. J Geophys Res Solid Earth, 111, B11207, doi:10.1029/2006JB004327

Bouilhol P, Burg J-P, Bodinier JL, Schmidt MW, Dawood H, Hussain S (2009) Magma and fluid percolation in arc to forearc mantle: evidence from Sapat (Kohistan, Northern Pakistan). Lithos 107:17–37

Burg J-P (2011) The Asia-Kohistan-India collision. Review and discussion. In: Brown D, Ryan P (eds) Arc-continent collision: the making of an orogen, Frontiers in earth sciences. Springer, Heidelberg

Burg J-P, Bodinier J-L, Chaudhry S, Hussain S, Dawood H (1998) Infra-arc mantle-crust transition and intra-arc mantle diapirs in the Kohistan complex (Pakistani Himalaya): petro-structural evidence. Terra Nova 10(2):74–80

Burg J-P, Arbaret L, Chaudhry NM, Dawood H, Hussain S, Zeilinger G (2005) Shear strain localization from the upper mantle to the middle crust of the Kohistan arc (Pakistan).

In: Bruhn D, Burlini L (eds) High-strain zones: structure and physical properties, vol 245. Geological Society of London, Special Publications, London, pp 35–38

Burg J-P, Jagoutz O, Dawood H, Hussain SS (2006) Precollision tilt of crustal blocks in rifted island arcs: structural evidence from the Kohistan Arc. Tectonics 25, TC5005, doi:10.1029/2005TC001835

Burns LE (1985) The Border Ranges ultramafic and mafic complex, south-central Alaska: cumulate fractionates of island-arc volcanics. Can J Earth Sci 22:1020–1038

Calvert AJ (2011) The seismic structure of island arc crust. In: Brown D, Ryan P (eds) Arc-continent collision: the making of an orogen, Frontiers in earth sciences. Springer, Heidelberg

Calvert AJ, Klemperer SL, Takahashi N, Kerr BC (2008) Three-dimensional crustal structure of the Mariana island arc from seismic tomography. J Geophys Res Solid Earth 113, B01406, doi:10.1029/2007JB004939

Clift PD, Draut AE, Kelemen PB, Blusztajn J, Greene A (2005a) Stratigraphic and geochemical evolution of an oceanic arc upper crustal section: the Jurassic Talkeetna Volcanic Formation, south-central Alaska (vol 117, pg 902, 2005). Geol Soc Am Bull 117(9–10):1368–1373

Clift PD, Pavlis T, DeBari SM, Draut AE, Rioux M, Kelemen PB (2005b) Subduction erosion of the Jurassic Talkeetna-Bonanza arc and the Mesozoic accretionary tectonics of western North America. Geology 33(11):881–884

Crawford WC, Wiens DA, Dorman LM, Webb SC (2003) Tonga Ridge and Lau Basin crustal structure from seismic refraction data. J Geophys Res-Solid Earth 108(B4):2195, doi:10.1029/2001JB001435

Dawes RL (1993) Mid-crustal, Late Cretaceous plutons of the North Cascades: petrogenesis and implications for the growth of continental crust. Ph.D. Thesis, University of Washington, Seattle, 273 pages

DeBari SM, Coleman RG (1989) Examination of the deep levels of an island arc: evidence from the Tonsina ultramafic-mafic assemblage, Tonsina, Alaska. J Geophys Res 94(B4):4373–4391

DeBari SM, Sleep NH (1991) High-Mg, low-Al bulk composition of the Talkeetna island arc, Alaska: implications for primary magmas and the nature of arc crust. Geol Soc Am Bull 103:37–47

DeBari SM, Miller RB, Paterson SR (1998) Genesis of tonalitic plutons in the Cretaceous magmatic arc of the North Cascades: mixing of mantle-derived mafic magmas and melts of a garnet-bearing lower crust. Geol Soc Am Abstr Programs 30(7):257–258

DeBari SM, Anderson RG, Mortensen JK (1999) Correlation among lower to upper crustal components in an island arc: the Jurassic Bonanza arc, Vancouver Island, Canada. Can J Earth Sci 36(8):1371–1413

Dhuime B, Bosch D, Bodinier JL, Garrido CJ, Bruguier O, Hussain SS, Dawood H (2007) Multistage evolution of the Jijal ultramafic-mafic complex (Kohistan, N Pakistan): implications for building the roots of island arcs. Earth Planet Sci Lett 261(1–2):179–200

Dhuime B, Bosch D, Garrido CJ, Bodinier JL, Bruguier O, Hussain SS, Dawood H (2009) Geochemical architecture of the lower- to middle-crustal section of a paleo-island arc (Kohistan complex, Jijal-Kamila area, Northern Pakistan): implications for the evolution of an oceanic subduction zone. J Petrol 50(3):531–569

Garrido CJ, Bodinier JL, Burg J-P, Zeilinger G, Hussain SS, Dawood H, Chaudhry MN, Gervilla F (2006) Petrogenesis of mafic garnet granulite in the lower crust of the Kohistan paleo-arc complex (Northern Pakistan): implications for intra-crustal differentiation of island arcs and generation of continental crust. J Petrol 47(10):1873–1914

Garrido CJ, Bodinier JL, Dhuime B, Bosch D, Chanefo I, Bruguier O, Hussain SS, Dawood H, Burg J-P (2007) Origin of the island arc Moho transition zone via melt-rock reaction and its implications for intracrustal differentiation of island arcs: evidence from the Jijal complex (Kohistan complex, northern Pakistan). Geology 35(8):683–686

Gill JB (1981) Orogenic andesites and plate tectonics, vol 16. Springer, Berlin, p 390

Greene AR, DeBari SM, Kelemen PB, Blusztajn J, Clift PD (2006) A detailed geochemical study of island arc crust: the Talkeetna arc section, south-central Alaska. J Petrol 47(6):1051–1093

Greene AR, Scoates JS, Weiss D, Nixon GT, Kieffer B (2009) Melting history and magmatic evolution of basalts and picrites from the accreted Wrangellia oceanic plateau, Vancouver Island, Canada. J Petrol 50(3):467–505

Hacker BR, Mehl L, Kelemen PB, Rioux M, Behn MD, Luffi P (2008) Reconstruction of the Talkeetna intraoceanic arc of Alaska through thermobarometry. J Geophys Res-Solid Earth 113, B03204, doi:10.1029/2007JB005208

Hildreth W, Moorbath S (1988) Crustal contributions to arc magmatism in the Andes of central Chile. Contrib Mineral Petrol 98:455–489

Iwasaki T, Kato W, Moriya T, Hasemi A, Umimo N, Okada T, Miyashita K, Mizogami T, Takeda T, Sekine S, Matsushima T, Tashiro K, Miyamachi H (2001) Extensional structure in northern Honshu arc as inferred from seismic refraction/wide-angle reflection profiling. Geophys Res Lett 12:2329–2332

Jagoutz O (2010) Construction of the granitoid crust of an island arc. Part II: a quantitative petrogenetic model. Contrib Mineral Petrol 160:359–381

Jagoutz O, Muntener O, Burg J-P, Ulmer P, Jagoutz E (2006) Lower continental crust formation through focused flow in km-scale melt conduits: the zoned ultramafic bodies of the Chilas complex in the Kohistan island arc (NW Pakistan). Earth Planet Sci Lett 242(3–4):320–342

Jagoutz O, Muntener O, Burg J-P, Ulmer P, Pettke T, Burg J-P, Dawood H, Hussain S (2007) Petrology and Mineral Chemistry of Lower Crustal Intrusions: the Chilas Complex, Kohistan (NW Pakistan). J Petrol 48(10):1895–1953

Jagoutz O, Burg J-P, Hussain S, Dawood H, Pettke T, Iizuka T, Maruyama S (2009) Construction of the granitoid crust of an island arc part I: geochronological and geochemical constraints from the plutonic Kohistan (NW Pakistan). Contrib Mineral Petrol 158:739–755

Jan MQ (1988) Geochemistry of amphibolites from the southern part of the Kohistan arc, N-Pakistan. Mineralog Mag 52(365):147–159

Jan MQ, Howie RA (1981) The mineralogy and geochemistry of the metamorphosed basic and ultrabasic rocks of the Jijal complex, Kohistan, NW Pakistan. J Petrol 22(1):85–126

Johnsen M (2007) Geochemical composition of the western Talkeetna island arc crustal section, lower Cook Inlet region, Alaska: implications for crustal growth along continental margins. M.S. Thesis, Western Washington University, Bellingham, WA

Jull M, Kelemen PB (2001) On the conditions for lower crustal convective instability. J Geophys Res Solid Earth 106 (B4):6423–6446

Kelemen PB, Hanghoj K, Greene AR (2003) One view of the geochemistry of subduction-related magmatic arcs, with emphasis on primitive andesite and lower crust. In: Rudnick RL (ed) The crust, treatise on geochemistry, vol 3. Elsevier, Oxford, pp 593–659

Khan MA, Jan MQ, Windley BF, Tarney J, Thirwall MF (1989) The Chilas mafic-ultramafic igneous complex: the root of the Kohistan island arc in the Himalaya of northern Pakistan. Geol Soc Am Spec Pap 232:75–93

Khan MA, Jan MQ, Weaver BL (1993) Evolution of the lower arc crust in Kohistan, N. Pakistan: temporal arc magmatism through early, mature and intra-arc rift stages. In: Treloar PJ, Searle MP (eds) Himalayan tectonics, vol 74. Geological Society of London, Special Publications, London, pp 123–138

Khan SD, Walker DJ, Hall SA, Burke KC, Shah MT, Stockli L (2009) Did the Kohistan-Ladakh island arc collide first with India?, GSA Bulletin, v. 121, no. 3/4, doi:10.1130/B26348.1

Kodaira S, Sato T, Takahashi N, Miura S, Tamura Y, Tatsumi Y, Kaneda Y (2007) New seismological constraints on growth of continental crust in the Izu-Bonin intra-oceanic arc. Geology 35(11):1031–1034

Matzel JEP, Bowring SA, Miller RB (2004) Protolith age of the Swakane Gneiss, North Cascades, Washington: evidence of rapid underthrusting of sediments beneath an arc. Tectonics 23(6):TC6009, doi:10.1029/2003TC001577

Mehl L, Hacker BR, Hirth G, Kelemen PB (2003) Arc-parallel flow within the mantle wedge: evidence from the accreted Talkeetna arc, south central Alaska. J Geophys Res-Solid Earth 108(B8):2375, doi:10.1029/2002JB002233

Miller RB, Paterson SR (2001) Construction of mid-crustal sheeted plutons: examples from the north Cascades, Washington. Geol Soc Am Bull 113(11):1423–1442

Miller DJ, Loucks RR, Ashraf M (1991) Platinum-group element mineralization in the Jijal layered ultramafic-mafic complex, Pakistani Himalayas. Econ Geol 86:1093–1102

Miller RB, Paterson SR, Matzel JEP (2009) Plutonism at different crustal levels: insights from the ~5–40 km (paleodepth) North Cascades crustal section. In: Miller RB, Snoke AW (eds) Crustal cross sections from the western North America Cordillera and elsewhere: implications for tectonic and geologic processes. Geological Society of America Special Paper 456, pp 125–149

Monger JWH, van der Heyden P, Journeay JM, Evenchick CE, Mahoney JB (1994) Jurassic-Cretaceous basins along the Canadian Coast Belt: their bearing on pre-mid-Cretaceous sinistral displacements. Geology 22(2):175–178

Muller JE, Northcote KE, Carlisle D (1974) Geology and mineral deposits of Alert Bay – Cape Scott map area. Vancouver Island, British Columbia. Geological Survey of Canada, Paper 74–8, p 77

Muntener O, Kelemen PB, Grove TL (2001) The role of H2O during crystallization of primitive arc magmas under uppermost mantle conditions and genesis of igneous pyroxenites: an experimental study. Contrib Mineral Petrol 141(6): 643–658

Nakanishi A, Kurashimo E, Tatsumi Y, Yamaguchi H, Miura S, Kodaira S, Obana K, Takahashi N, Tsuru T, Kaneda Y, Iwasaki T, Hirata N (2009) Crustal evolution of the southwestern Kuril arc, Hokkaido Japan, deduced from seismic velocity and geochemical structure. Tectonophysics 472 (1–4):105–123

Nishimoto S, Ishikawa M, Arima M, Yoshida T (2005) Laboratory measurement of P-wave velocity in crustal and upper mantle xenoliths from Ichino-megata, NE Japan: ultrabasic hydrous lower crust beneath the NE Honshu arc. Tectonophysics 396(3–4):245–259

Parent L (1999) Petrology and petrogenesis of the Cardinal Peak Pluton, North Cascades, Washington. Geology Department, San Jose State University, San Jose, CA, 130 pages

Parsons T, Trehu AM, Luetgert JH, Miller K, Kilbride F, Wells RE, Fisher MA, Flueh E, St Brink U, Christensen NI (1998) A new view into the Cascadia subduction zone and volcanic arc: implications for earthquake hazards along the Washington margin. Geology 26(3):199–202

Petterson MG, Treloar PJ (2004) Volcanostratigraphy of arc volcanic sequences in the Kohistan arc, North Pakistan: volcanism within island arc, back-arc-basin, and intra-continental tectonic settings. J Volcanol Geoth Res 130(1–2): 147–178

Petterson MG, Windley BF (1985) Rb-Sr dating of the Kohistan arc-batholith in the trans-Himalaya of North-Pakistan, and tectonic implications. Earth Planet Sci Lett 74(1):45–57

Petterson MG, Windley BF (1991) Changing source regions of magmas and crustal growth in the Trans-Himalayas: evidence from the Chalt volcanics and Kohistan batholith, Kohistan, northern Pakistan. Earth Planet Sci Lett 102:326–341

Petterson MG, Crawford MB, Windley BF (1993) Petrogenetic implications of neodymium isotope data from the Kohistan batholith, North Pakistan. J Geol Soc Lond 150: 125–129

Plafker G, Nokleberg WJ, Lull JS (1989) Bedrock geology and tectonic evolution of the Wrangellia, Peninsular, and Chugach terranes along the trans-Alaska crustal transect in the Chugach Mountains and southern Copper River basin, Alaska. J Geophys Res 94(B4):4255–4295

Plank T, Langmuir CH (1998) The chemical composition of subducting sediment and its consequences for the crust and mantle. Chem Geol 145:325–394

Reed BL, Lanphere MA (1973) Alaska-Aleutian Range batholith: geochronology, chemistry, and relation to circum-Pacific plutonism. Geol Soc Am Bull 84:2583–2610

Ringuette L, Martignole J, Windley BF (1999) Magmatic crystallization, isobaric cooling, and decompression of the garnet-bearing assemblages of the Jijal sequence (Kohistan terrane, western Himalayas). Geology 27(2):139–142

Rioux M, Hacker B, Mattinson J (2007) Magmatic development of an intra-oceanic arc: high-precision U-Pb zircon and whole-rock isotopic analyses from the accreted Talkeetna arc, south-central Alaska. Geol Soc Am Bull 119(9–10): 1168–1184

Rioux M, Mattinson J, Hacker B, Kelemen P, Blusztajn J, Hanghoj K, Gehrels G (2010) Intermediate to felsic middle crust in the accreted Talkeetna arc, the Alaska Peninsula and Kodiak island, Alaska: an analogue for low-velocity middle

crust in modern arcs. Tectonics 29:TC3001, doi:10.1029/2009TC002541

Romick JD, Kay SM, Kay RW (1992) The influence of amphibole fractionation on the evolution of calc-alkaline andesite and dacite tephra from the central Aleutians, Alaska. Contrib Mineral Petrol 112:101–118

Rudnick RL, Fountain DM (1995) Nature and composition of the continental crust: a lower crustal perspective. Rev Geophys 33(3):267–309

Rudnick RL, Gao S (2003) Composition of the continental crust. In: Rudnick RL (ed) The crust, treatise on geochemistry, vol 3. Elsevier, Oxford, pp 1–70

Schaltegger U, Zeilinger G, Frank M, Burg J-P (2002) Multiple mantle sources during island arc magmatism: U-Pb and Hf isotopic evidence from the Kohistan arc complex, Pakistan. Terra Nova 14(6):461–468

Schaltegger U, Frank M, Burg J-P (2003) A 120 million years record of magmatism and crustal melting in the Kohistan batholith. Geophysical Research Abstracts, EGS-AGU-EUG Joint Assembly 5, Abstract 06816

Shillington DJ, Van Avendonk HJA, Holbrook WS, Kelemen PB, Hornbach MJ (2004) Composition and structure of the central Aleutian island arc from arc-parallel wide-angle seismic data. Geochem Geophys Geosyst 5:Q10006

Suyehiro K, Takahashi N, Ariie Y, Yokoi Y, Hino R, Shinohara M, Kanazawa T, Hirata N, Tokuyama H, Taira A (1996) Continental crust, crustal underplating, and low-Q upper mantle beneath an oceanic island arc. Science 272:390–392

Tabor RW, Haugerud RA, Miller RB (1989) Overview of the geology of the North Cascades. In: International Geologic Congress Trip T307. American Geophysical Union, p 62

Takahashi N, Kodaira S, Klemperer SL, Tatsumi Y, Kaneda Y, Suyehiro K (2007) Crustal structure and evolution of the Mariana intra-oceanic island arc. Geology 35(3):203–206

Tatsumi Y (2005) The subduction factory: how it operates in the evolving Earth. GSA Today 15(7):4–10

Tatsumi Y, Shukuno H, Tani K, Takahashi N, Kodaira S, Kogiso T (2008) Structure and growth of the Izu-Bonin-Mariana arc crust: 2. Role of crust-mantle transformation and the transparent Moho in arc crust evolution. J Geophys Res-Solid Earth 113, B02203, doi:10.1029/2007JB005121

Taylor SR, McLennan SM (1985) The continental crust: its composition and evolution. Blackwell, Oxford

Trop JM, Szuch DA, Rioux M, Blodgett RB (2005) Sedimentology and provenance of the Upper Jurassic Naknek Formation, Talkeetna Mountains, Alaska: bearings on the accretionary tectonic history of the Wrangellia composite terrane. Geol Soc Am Bull 117(5/6):570–588

Umhoefer PJ, Miller RB (1996) Mid-Cretaceous thrusting in the southern Coast Belt, British Columbia and Washington, after strike-slip fault reconstruction. Tectonics 15(3):545–565

Valley PM, Whitney DL, Paterson SR, Miller RB, Alsleben H (2003) Metamorphism of the deepest exposed arc rocks in the Cretaceous to Paleogene Cascades belt, Washington: evidence for large-scale vertical motion in a continental arc. J Metamorph Geol 21(2):203–220

Whitney DL, Miller RB, Paterson SR (1999) P-T-t evidence for mechanisms of vertical tectonic motion in a contractional orogen: north-western US and Canadian Cordillera. J Metamorph Geol 17(1):75–90

Yamamoto H (1993) Contrasting metamorphic P-T-time paths of the Kohistan granulites and tectonics of the western Himalayas, Journal of the Geological Society, London, v. 150, p. 843–856

Yamamoto H, Nakamura E (2000) Timing of magmatic and metamorphic events in the Jijal complex of the Kohistan arc deduced from Sm-Nd dating of mafic granulites. In: Khan MA, Treloar PJ, Searle MP, Jan MQ (eds) Tectonics of the Nanga Parbat Syntaxis and the Western Himalaya, vol 170. Geological Society of London, Special Publications, London, pp 313–319

Yamamoto H, Yoshino T (1998) Superposition of replacements in the mafic granulites of the Jijal complex of the Kohistan arc, northern Pakistan: dehydration and rehydration within deep arc crust. Lithos 43(4):219–234

Yoshino T, Okudaira T (2004) Crustal growth by magmatic accretion constrained by metamorphic P-T paths and thermal models of the Kohistan arc, NW Himalayas. J Petrol 45(11):2287–2302

Yoshino T, Yamamoto H, Okudaira T, Toriumi M (1998) Crustal thickening of the lower crust of the Kohistan arc (N. Pakistan) deduced from Al zoning in clinopyroxene and plagioclase. J Metamorph Geol 16(6):729–748

Chapter 6
The Generation and Preservation of Mineral Deposits in Arc–Continent Collision Environments

R.J. Herrington and D. Brown

6.1 Introduction

Studies of the relationship between arc–continent collision and the generation of mineral deposits are rare (e.g., Mitchell 1985), yet it has been recognised that some key processes associated with arc–continent collision could play a significant role in the formation of orebodies (e.g., Solomon 1990). The lack of literature focused on the relationship between mineral deposit formation and arc–continent collision needs to be addressed with modern study. However, the mining industry has already identified that in fossil orogens, zones of arc–continent collision are primary targets for mineral exploration since they are often rich in various types of mineral deposits that formed during the intra-oceanic subduction phase and following collision and accretionary events.

Dewey (2005) observed that arc–continent collision can generate very short orogenies largely as a result of the buoyancy-driven impedance to the continued subduction of continental crust. Dewey (op cit) also noted that arc or supra-subduction ophiolite obduction can occur, and may be followed rapidly by subduction zone jump and/or reversal. Subduction reversal (Casey and Dewey 1984; Dewey 2005), is also recognised as one of the most effective ways to change an accretionary continental margin into an active continental arc above a sub continental subduction zone (Clift et al. 2003). This change in subduction character will have a profound effect on the magmatic systems that are active in the arc and, de facto, the mineral deposits forming in the crust now above the subduction zone. Tectonically, subduction reversal may also result in major changes in the state of stress in the growing orogen as the compressive forces of mountain building are reorganised (Clift et al. 2003), implying a profound change that can have major implications for metallogenesis.

Arc–continent collisions have been recognised as fundamental mechanisms for continental growth (Taylor and McLennan 1995; Rudnick and Fountain 1995; Hoffman 1988). In its simplest terms, arc–continent collision can then preserve any mineral deposits that had formed in the oceanic arc rocks or microcontinent blocks that became accreted or obducted. Obduction is a particularly important process in the case of ophiolite preservation (Dewey 2005), since it is now recognised that the majority (if not all) ophiolites, with their mineral deposit endowment, are preserved by obduction on to continental passive margins (e.g., Cawood and Suhr 1992; Carlile and Mitchell 1994). It is apparent that in similar fashion, volcanic arc sequences can be accreted on to the continental margin (e.g., Brown et al. 2006), again preserving the mineral deposits formed in the arc. Each collision scenario is different, however, and the degree of scrape off and preservation from the slab is variable.

The largest diversity of mineral deposits is associated with convergent margin settings (e.g., Sawkins 1984; Groves and Bierlein 2007). Arc magmatism is one of the major mechanisms for mineral deposit formation (Mitchell and Garson 1981) and the arc magmas generated can be directly linked to the tectonics (Vigneresse 1995). In arc settings, magmatism is generated by partial melts of the overlying mantle wedge driven by the dehydration in the down going

R.J. Herrington
The Natural History Museum, London, UK
e-mail: r.herrington@nhm.ac.uk

D. Brown
Instituto de Ciencias de la Terra “Jaume Almera” CSIC, Barcelona, Spain
e-mail: d.brown@ija.csic.es

D. Brown and P.D. Ryan (eds.), *Arc-Continent Collision*, Frontiers in Earth Sciences,
DOI 10.1007/978-3-540-88558-0_6,

slab, which happens at a depth of around 100 km (e.g. Peacock 1993). In intra-oceanic arc settings, the oceanic mantle is likely to be already depleted as a result of partial melting at the mid-ocean ridges where the crust formed, but this depleted mantle will become enriched in volatiles, sulfur, silica and LILE above the subduction zone as the down going slab dehydrates (Tatsumi et al. 1986; Davidson 1996; de Hoog et al. 2001). The elements Ti, Nb, Ta are retained by the down going slab or in the slab melt in the form of rutile (Ryerson and Watson 1987; Foley and Wheller 1990; Prouteau et al. 1999). The mantle wedge becomes hydrated and progressively enriched in large-ion lithophile elements (LILE). As a result of the hydration, new phases such as amphibole and mica form (e.g., Tatsumi et al. 1986). This partially melts to form characteristic basalts with high water and LILE but anomalously low Ti, Nb and Ta (Ringwood 1977; Perfit et al. 1980; Pearce 1983; Plank and Langmuir 1988; Arculus 1994; Stolper and Newman 1994; Pearce and Peate 1995). In oceanic arc settings these melts erupt directly, usually as arc tholeiites, but as the arc crust thickens, differentiated andesites of calc-alkaline affinity will form (e.g., Carmichael 2002). In much thicker arc crust, dense mafic magma rising from the wedge can pond in the thicker crust adding heat and leading to crustal melting and assimilation by the primary basalt, which again leads to the chemistry of the melt being contaminated (Gill 1981; Hildreth 1981; Fyfe 1992).

Compression is expected to be the commonest tectonic scenario in a convergent continental margin setting, yet Hamilton (1995) recognised that extension is a common regime above subduction zones. For example, in cases where progressively older and colder oceanic slabs are being subducted, the down going slab tends to roll back leading to the process of trench suction, or trench pull, which actually becomes the main force driving subduction (Shemenda 1993). This process can lead to significant extension in the arc and back-arc but more significantly in the fore-arc. Extension encourages melting by decompression of the upwelling asthenosphere in both the fore-arc and back-arcs leading to magmatism derived from mantle melting. In the back-arc there may be no evidence of a geochemical contribution from the down going slab. McNulty et al. (1998) show how crustal shortening can be accommodated by extension and strike-slip faulting leading to extensional settings even within notionally compressional arcs. It is also clear from modern studies that convergence rate, relative convergence vector, slab dip and slab buoyancy are all important factors in subduction systems. Slab dip can change over a few million years which can lead to ephemeral or long-term changes in stress regimes in the arc.

In active magmatic arcs of both intra-oceanic and continental character, significant mineralization can be directly linked to the magmatism at the constructional stages of arc formation with different deposit types linked to specific tectonic settings and lithological associations within the arc (e.g., Sawkins 1984).

In this paper, we review the various types of mineral deposits found in intra-oceanic arcs, as well as those which can form during the processes involved in arc–continent collision. Various examples are used throughout the paper to illustrate these points.

6.2 Mineralization in Magmatic Arcs: The Links to Magmas

The mineral deposits that typify the early constructional phases of immature oceanic arcs are dominated by those related initially to mafic and ultramafic types of magmatic rocks (Fig. 6.1a). Most ophiolite suites in the ancient record are likely to have formed in such a setting with magmas largely derived from the supra-subduction mantle wedge with little or no contribution of components from the subducting slab. Orthomagmatic deposits can include distinctive ophiolitic podiform chromite deposits (Duke 1996), whilst in zones of extension, magmatic-hydrothermal volcanogenic or volcanic-associated (VMS) deposits form (Hannington et al. 2005). As arcs mature, more felsic magmas are generated and the deposits change to reflect this (Fig. 6.1b), with extension behind the arc, which may be increased due to slab roll-back, often resulting in back arc rifting or spreading. In such rift settings, submarine volcanic sequences are often associated with VMS deposits (Hannington et al. 2005). In these magmatic-hydrothermal systems, metals are mobilised from the underlying igneous rocks and associated sediments by heated seawater, which is convectively circulated by heat from the magmatic activity, precipitating sulfide masses at or near the seafloor. VMS systems are extremely common in submerged parts

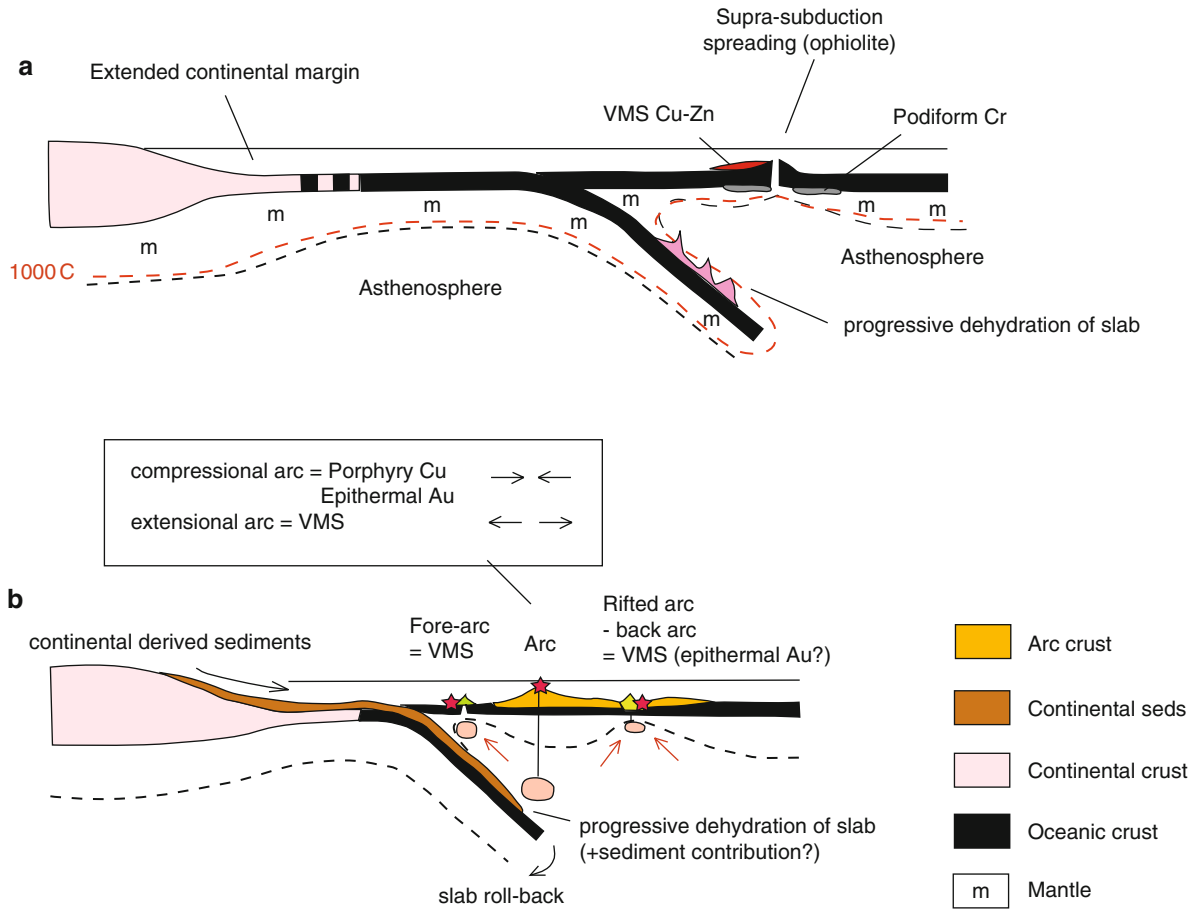

Fig. 6.1 (**a**) Simplified section of an early supra-subduction (infant arc) setting showing ophiolite formation and key related mineral deposits. (**b**) Section of maturing arc setting showing fore-arc and back-arc rifting and possible magma source regions. Subduction of continent derived sediment enters subduction channel and yields components to metasomatise the sub-arc mantle wedge. (compiled from various published sources including Winter 2001; Garson and Mitchell 1977; Robb 2005).

of modern volcanic arcs and ancient analogues are preserved in many fossil arc sequences (Hannington et al. 2005; Franklin et al. 2005). In more mature arcs, calc-alkaline magmas are generated, largely sourced from the mantle wedge but in a mature arc this may be metasomatised and additionally components sourced from the subducting slab may be added. Such calc-alkaline magmas can generate porphyry Cu–Mo–Au deposits and diverse styles of epithermal Au–Ag deposits. In the case of the porphyry copper and some of the epithermal deposits, mineralization can be directly related to fluids evolving from the cooling calc-alkaline magmas and thus the chemistry of these reflects the source region of the melt and its components (Seedorff et al. 2005). Although more common in continental arc settings (Sillitoe 2010), large porphyry copper deposits are common features of the oceanic arcs in the southwest Pacific (Garwin et al. 2005) along with associated epithermal Au–Ag deposits (Simmons et al. 2005). In a broad sense it is noted that the tectonic regime within an arc dictates the type of deposit formed (see Fig. 6.1b) and notable generalisations include the recognition that VMS deposits are related to periods of extension in active arcs (Allen et al. 2002) while porphyry Cu–Mo–Au deposits are restricted to largely contractual settings within the arc (Sillitoe 2010). From the above analysis, it is clear that the metal budgets in the mineralizing systems developed in arc rocks are directly related to the nature of the magmatism. It therefore follows that

any changes affecting where arc magmas are generated and therefore which components are incorporated into the magma will likely affect the nature of any mineral deposits formed from it.

6.3 Intra-oceanic Arcs, Magmas and Mineral Deposits

Figure 6.1a shows the hypothetical scenario of an intra-oceanic arc setting developed close to an approaching continental passive margin. In the cases where metasomatised and hydrated mantle wedge is partially melted, the magmas generated will contain a contribution of components which have migrated from the down-going slab. In more complex arcs there is also the opportunity for involvement of arc– crust interaction with the generated magmas, which can further complicate the scenario. Back arc settings may have melts generated which show little effect from the descending slab and may be derived directly from the mantle by decompression due to crustal extension and asthenospheric upwelling. Figure 6.1b indicates the hypothetical location of key mineral deposits that may be linked to each setting within the evolving arc.

The most important magmatic-hydrothermal deposits formed in arcs are VMS, Porphyry Cu–Mo–Au and epithermal Au–Ag deposits (Fig. 6.1b). VMS deposits can form in a range of tectonic settings in submerged parts of the active volcanic arc where heated seawater circulation is generated by interaction with heated crust. In more compressional parts of the arc, deeper sourced calc-alkaline magmas generated by the partial melting of metasomatised mantle can be host to porphyry Cu–Mo–Au and related epithermal Au–Ag deposits. These deposit types are commonly found preserved in arc–continent collision but in many cases the deposit may have formed well before the arc–continent collision event. Accretion or obduction during arc–continent collision is thus the event which preserves the deposits.

In a few cases, the arc–continent collision is an important modifier to ongoing arc magmatism. As continental material enters the subduction zone, a geochemical effect is recorded in the arc magmas. Arc magmas in an intra-oceanic arc setting in southern Sulawesi, for example, show that where the subducting slab carries a sediment load, the variations in the isotopic and geochemical signatures of the resulting magmas are explained by variable additions of fluid derived from dewatering of the subducting slab and an addition of subducted sediment to the mantle wedge (Elburg et al. 2002). Identifying such a process in more mature arcs, or those built on continental crust, is more difficult as purely mantle-derived melts may interact with the upper plate by assimilation, leading to contaminated melts that are impossible to distinguish from those contaminated by subducted sediment (e.g., Thirlwall et al. 1996; Gasparon and Varne 1998). Evidence from south Sulawesi suggests that the contamination effect of subducted continental material is seen some 3–5 Ma after its first subduction (Elburg et al. 2002), consistent with the observed 2–4 Ma lag between subduction of a geochemical tracer into the arc and its expression in the arc volcanic rocks (Turner et al. 1997).

During the collision process between the continental margin and the arc, the sedimentary signature in melts is likely to be most pronounced in post-collisional volcanic rocks as subduction slows. Slowing of the subducting slab can allow for higher temperatures to build in the down going slab, enabling a more effective transport of components from the sediment on the slab to the overlying mantle wedge (McInnes et al. 2001). As subduction continues, the continental slab is relatively buoyant and thus the subduction angle might be expected to shallow significantly. Shallowing of the subduction angle has been used to explain the migration of arc volcanism away from the active volcanic front toward the backarc region (e.g., Gutscher et al. 2000). With the arrival of the continental crust at the subduction zone, this might be one of the consequences of arc–continent collision that leads to a shift in the location of volcanism and possibly the formation of new mineral deposits (see data from the Urals below).

It is generally thought that the more buoyant continental crust can be exhumed during arc–continent collision due to density contrasts between it and the surrounding mantle (e.g., Chemenda et al. 1996; Afonso and Zlotnik 2011). This may not be the case in all scenarios, however (see Brueckner 2009), and the down going slab might continue to subduct where it will heat up and partially melt. There is increased recognition in the literature of the melting of subducted continental crust (e.g., Zhao et al. 2007; Auzanneau et al. 2006) and this may be the case where continental crust was subducted to great depth and was not subsequently exhumed (Afonso and Zlotnik 2011). The

intrusive rocks generated in such a setting are likely to be both silica and potassium enriched (Brueckner 2009) and "normal" arc magmatism would cease as the volatile flux causing partial melt of the mantle wedge stops.

6.4 Tracking Subduction of the Continental Slab: The Magmatic and Mineralization Response

The mineral deposits developed in the Magnitogorsk arc of the southern Urals have been described in detail elsewhere (Gusev et al. 2000; Herrington et al. 2002, 2005a, b). The magmatic-hydrothermal deposits formed during the intra-oceanic stage of arc formation can all be accommodated within the general models shown in Fig. 6.1, and largely relate to events unconnected with the arc–continent collision. However there are a number of deposits in the intra-oceanic arc that formed after the continental margin of Laurussia had entered the subduction zone (Brown et al. 2006).

The onset of arc–continent collision in the Urals can be fairly well constrained by the high-pressure metamorphism of the leading edge of the continental margin, as well as the magmatic and sedimentary record. The timing and evidence for it are given in detail by Brown et al. (2006, 2011). In the western part of the Magnitogorsk arc (closest to where the subduction zone was) arc magmas generated from a depleted MORB-like mantle source show some evidence for a slab component (Spadea and D'Antonio 2006). The most evolved sequences of these western lavas do show some evidence for the addition of a lead component from the down going slab seen expressed in both the volcanic rocks and the VMS deposits formed from them (Herrington et al. 2002). Volcanism in the western part of the arc ceased more or less at the time of the onset of arc–continent collision and this was accompanied by a distinctive shift of volcanism toward the back arc region in the east, to where intra-arc rifts were forming (Herrington et al. 2002, 2005a; Brown et al. 2006). Here large VMS deposits formed in conjunction with more primitive uncontaminated mantle-derived melts (Herrington et al. 2002). However, the culmination of volcanism in the Magnitogorsk arc is of alkaline to shoshonitic in composition and is developed in this eastern zone above the sequences hosting the VMS deposits. These alkaline rocks are interbedded with sediments that were deposited across the arc and onto the continental margin. These sediments contain clasts of exhumed high pressure rocks derived from the subducted continental margin, indicating that arc–continent collision was well underway when these rocks were deposited (Brown et al. 2006; Gusev et al. 2000). Small porphyry copper deposits are related to this late arc magmatism (Gusev et al. 2000), and there are similar late porphyries associated with Cu–Au porphyry mineralization in the latest arc rocks of the southern extension to the Magnitogorsk arc in Kazakhstan (Shatov et al. 2003). The composition of these late porphyries is consistent with an increased contribution of subducted slab to the melts. Muller and Groves (1993) have noted the association between potassic magmas and Cu–Au deposits in similar settings.

The Banda arcs, which are a continuation of the active intra-oceanic Sunda arc in Indonesia have been undergoing collision with the margin of the Australian continent since 3.5–2 Ma Audley-Charles (2004). There is seismic evidence that the Australian lithosphere has reached a depth of at least 300 km (McCaffrey 1989), and regional studies show that there is clear evidence for the contamination of magmas by subducted sediment (e.g., Whitford et al. 1977, 1981; Margaritz et al. 1978; Whitford and Jezek 1979; Hilton et al. 1992; Vroon et al. 2001). For example, the island of Wetar lies in the collisional part of the arc and distinctive gold-rich VMS deposits occur there (Scotney et al. 2005). Detailed studies show that the onset of contamination by continental sediments coincides with formation of magmas associated with these distinctive VMS deposits and a genetic link between them has been proposed (Herrington et al. 2011), suggesting that melt and other fluids released from the subducted continental margin might be implicated in the development of such gold-rich deposits.

6.5 Tectonic Response to Arc–Continent Collision

The response of the subduction system to the entrance of the continental crust into the subduction zone appears to be quite variable but important scenarios can be identified in the geological record, shown

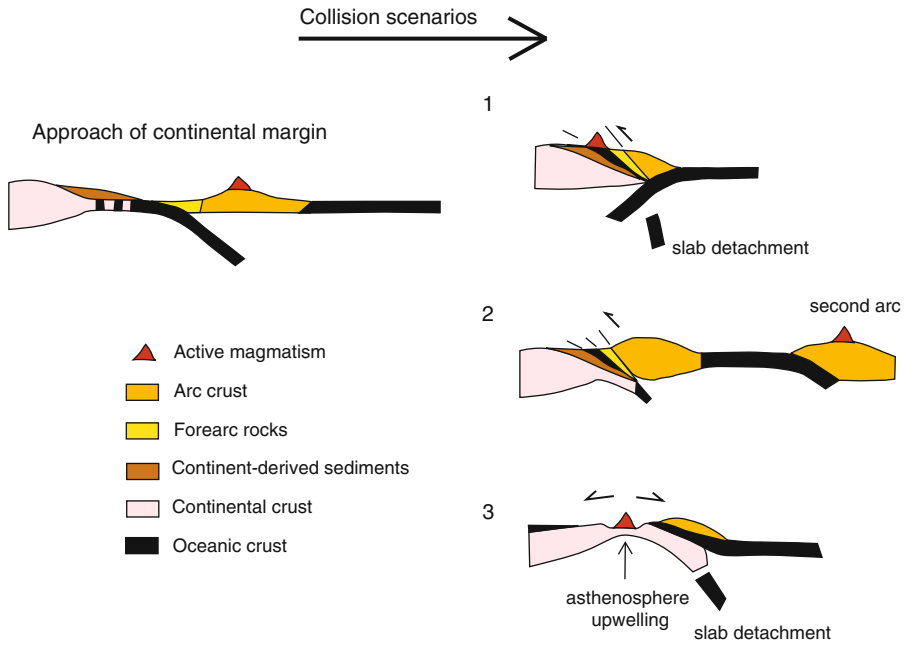

Fig. 6.2 Simplified sections showing key responses to arc–continent collision which have implications for mineral deposit formation (1) Accretion (and obduction) and arc reversal; (2) Accretion (and obduction) and subduction jump and (3) Accretion (and obduction) and post-collision extension (adapted from various published sources).

graphically in Fig. 6.2, which appear to have major implications for the formation of mineral deposits:

1. Accretion and subduction polarity reversal (arc reversal)
2. Accretion and subduction jump
3. Accretion and post collision extension

It is also further noted that in many cases, particularly those involving oblique convergence, much continued shortening can be accommodated along favourable oriented strike-slip faults which may result in a more complex response.

In all these scenarios, accretion of parts of the upper oceanic slab (including its arc rocks) to the continental margin occurs. In some cases this might include a full range of oceanic crust and arc sequences (e.g., Urals – see Brown et al. 2011), yet in some collisions, the detachment of upper crustal rocks from lower crustal material can occur in both the upper and lower plates (e.g., Draut et al. 2002; Brown et al. 2006). In the case of the lower plate, this could allow the depleted ultramafic part of the oceanic plate to possibly continue subducting whilst physically transferring upper crustal rocks to the approaching continental margin where they will be preserved as ophiolites or ultramafic allochthons. Therefore obducted and accreted rocks may host some of the deposits shown formed in the settings shown in Fig. 6.1. There are many well-documented cases of ophiolite obduction in the literature which likely relate to arc–continent collision in some form (e.g., Oman: Lippard et al. 1986; Bay of Islands, Canada: Casey and Dewey 1984; Cawood and Suhr 1992) and these have resulted in preservation of mineral deposits formed in the oceanic terranes. There is no recorded case of a mineral deposit in the subducted continental crust that has been returned to the surface hosted in medium to ultra-high-pressure rocks, although these are important markers for the timing of arc–continent collision events, as well as records of physical and chemical conditions in the subduction channel.

6.5.1 Scenario 1: Accretion and Subduction Polarity Reversal (Arc Reversal)

Dewey (2005) implies that a change in the location and polarity of the subduction zone is a common scenario in an arc–continent collision, although this does not always seem to be the case (e.g., Brown et al.

2006, 2011). A change in subduction location and polarity can lead to the development of a new active continental margin in which magmas derived from the newly subducting oceanic crust intrude the now defunct arc–continent collision zone to form a complex continental arc (Fig. 2.1). Magmatic-hydrothermal deposits that typify continental arcs and some mature intra-oceanic arc environments are porphyry Cu–Au–Mo deposits (e.g., Seedorff et al. 2005) and epithermal precious metal deposits (Simmons et al. 2005). The largest porphyry deposits form in generally compressional settings within arc settings and such settings are more common in continental arcs (Sillitoe 2010). Epithermal high-sulfidation deposits are often associated with the upper parts of porphyry Cu systems (Hedenquist et al. 1998) whilst low-sulfidation epithermal gold deposits may be associated with higher-level lower temperature parts of these systems (Simmons et al. 2005). Other deposit types linked to arc construction include granite-hosted Sn–W and reduced intrusion related Au mineralization (Robb 2005). VMS deposits can be found in more restricted or distal settings in continental arcs, usually in back arc rifts or fore-arc basins (Allen et al. 2002).

It has been demonstrated that arc magmatism in continental settings generated by subduction zone reversal following arc collision produce some of the largest and richest copper and gold deposits (Sillitoe 2010). Solomon (1990) recognised that peak mineralization in a magmatic arc often relates to the reversal in subduction zone polarity due to the generation of magmas from an already modified mantle. Further work has shown that the melting of metasomatised (subduction modified) mantle may generate highly oxidised magmas that are fluid rich, serving to destabilise mantle sulfides, releasing gold (McInnes and Cameron 1994). For example, peridotite xenoliths from mantle under the Tabar-Feni arc, which is the host to the giant Ladolam gold deposit, are enriched in the metals Cu, Au, PGE relative to depleted mantle and share isotopic characteristics with the ore deposit indicating that subduction modified mantle is implicated in the formation of large gold deposits in this kind of setting (McInnes et al. 2001). The magma responsible for generating this giant deposit was metasomatically enriched by a dehydrating subduction slab although not strictly in an arc–continent collision reversal (Kennedy et al. 1990; McInnes and Cameron 1994; McInnes et al. 2001; Muller et al. 2001).

It is also noted that elsewhere in the SE Asian and SW Pacific magmatic arcs, major tectonic reorganisation caused by (a) collision of the Australian Craton with the Philippines arc and, (b) the initial "soft" collision of the Ontong Java Plateau with the arc of Melanesia (Hall 2002; Hill and Hall 2003) has led to arc modification and subduction zone reversals in Papua New Guinea and the Philippines. Subduction reversal under the Philippines at around 17 Ma is linked with the formation of major gold deposits in the Camarines Norte and Bagio districts (Barley et al. 2002). Other important gold deposits formed following subduction zone reversal in the Late Oligocene, Middle Miocene and Pliocene rocks of Luzon and in Pliocene rocks of Mindanao, north Sulawesi and Bougainville (Barley et al. 2002).

The collision of the Ontong Java Plateau with the subduction zone at the Kilinailau Trench effectively blocked southwards subduction along the entire Manus-Kilinailau-Solomon Trench. To accommodate continued shortening, the arc reversed and the New Britain Trench developed south and inboard of the previous subduction zone, with northwards dipping subduction initiating by ca. 5 Ma under the Solomon Islands and Bougainville. Arc magmatism recommenced and the giant Panguna porphyry Cu–Au deposit formed at this time from melts generated from previously metasomatised arc mantle and crust (Williamson and Hancock 2005; Hill and Hall 2003).

Another recent example of arc–continent collision where mineralization may have been initiated by subduction zone reversal is in the case of the modern Kamchatka arc (Konstantinovskaya 2011). Here, the current subduction zone dips westward under the margin of the fused Okhotsk microplate and the margin of Eurasia. This plate configuration is the result of the collision of an intra-oceanic arc that had developed above an east-dipping subduction zone in the Paleogene. A further "soft" arc–continent collision occurred ca. 5 Ma with continued subduction outboard of the first arc–continent collision (Konstantinovskaya 2001, 2011). Major gold mineralization is linked to both of these latter events in which a period of Miocene magmatic activity and mineralization in the centre of Kamchatka (e.g., Sidorov 2008) was followed by Pliocene to Holocene magmatism accompanied by mineralization in the east (Lapukhov et al. 2007; Takahashi et al. 2006).

Arc–continent collision-related gold deposits are also found in the Grampian Orogen of Ireland, in both Tyrone and South Mayo (Dewey and Mange 1999; Chew et al. 2008), where a suite of 470 Ma calc-alkaline intrusions suggest that subduction zone reversal took place. No economic mineralization has yet been discovered that is directly associated with the magmatic products of this subduction zone reversal. However, significant orogenic vein-gold mineralization can be linked to a thrusting event at Curraghinalt and Cavinacaw in Tyrone (Wilkinson et al. 1999) which is interpreted to be related to the subduction zone reversal. Veins investigated at Curraghinalt show evidence that the first stage of mineralization was related to the 464 Ma thrusting event and migration of CO_2-rich hydrothermal fluid, which was later overprinted by a saline, basinal fluid during the Variscan orogeny (Earls et al. 1996). Along strike in the South Mayo region, a mineralized deformation zone occurs in the footwall of the Clew Bay Fault Zone and hosts significant orogenic gold deposits (Halls and Zhao 1995). The Clew Bay Fault Zone is a crustal-scale structure which correlates with the Highland Boundary Fault in Scotland, and relates to the subduction zone reversal in this region (Ryan and Dewey 1991). The host rocks to the gold deposit are interpreted either as having formed in a north-facing fore-arc basin developed over the Ordovician ophiolitic basement rocks over a southward dipping subduction zone (Dewey and Ryan 1990) which may have been in part syn- to post-collisional (McConnell et al. 2009). In a somewhat similar setting to Curraghinalt described above, the Cregganbaum gold deposit formed between 420–390 Ma, which is hosted in a well-defined stratigraphic and structural horizon of Arenig-age turbidites which contains ultramafic rocks and altered examples referred to as listvenites (Halls and Zhao 1995). The similar, larger gold deposit of Croag Patrick deposit is hosted in the same fore-arc assemblage to the northwest (Wilkinson and Johnston 1996).

6.5.2 Scenario 2: Accretion Without Subduction Zone Reversal

In some cases, arc–continent collision is not accompanied by subduction zone reversal (Clift et al. 2003) and in this case subduction may jump to a second arc (Fig. 6.2). In the Uralides, the collision between the Magnitogorsk Arc and the Laurussia margin in the Middle through Late Devonian is an excellent example of this. The geology, geochemistry and geophysics of this arc–continent collision is described in detail by Brown et al. (2006, 2011) and the reader is referred there. Mineral deposits related to the intra-oceanic arc stage have beed described earlier but here we discuss the response to the arc–continent collision itself.

The first feature of the collision is the development of the Sakmara allochthon which contains the Kempirsay "ophiolite", an ultramafic complex comprising mantle tectonites of mostly harzburgite composition, overlain by cumulates, massive gabbro, a well-developed sheeted dike complex, and basaltic pillow lavas capped with black shales (Savelieva and Nesbitt 1996; Savelieva et al. 1997, 2002; Melcher et al. 1999). A supra-subduction setting is proposed for this ophiolite complex (Melcher et al. 1999) and the Kempirsay massif contains the largest harzburgite-hosted chrome deposits in the world (Melcher et al. 1999; Thalhammer 1996). Associated volcanic complexes in the Sakmara zone also host VMS deposits and again a supra-subduction setting is suspected for these magmatic rocks (Herrington et al. 2002, 2005b). These sequences are quite distinct from the Devonian arc sequences of the Magnitogorsk arc (Herrington et al. 2002) described earlier and the Sakamara rocks were clearly emplaced as allochthons onto the continental margin together during the arc–continent collision resulting in their preservation.

The Main Uralian Fault, which marks the arc–continent collision suture, contains volcanic complexes that are host to small VMS deposits (Nimis et al. 2004; Herrington et al. 2005b). The presence of mass flows containing ultramafic clasts and detrital chromite in the host sequences point to the exposure of ultramafic crust on the seafloor at the time of deposit formation which together with the association of boninitic lavas suggests a supra-subduction setting (Nimis et al. 2003) developed as the fore-arc to the Magnitogorsk arc immediately to the east. Again, the arc–continent collision has preserved these unusual fore-arc rocks.

There are also a number of epigenetic, orogenic gold deposits along the Main Uralian Fault that are hosted in altered serpentinites, diabases sandstones

and shales (Dimkin et al. 1990; Koroteev et al. 1997; Kisters et al. 1999). Although the deposits are mostly small, two districts of Mindyak and Murtekti have produced more than 50 tonnes of gold (Kisters et al. 1999). All the deposits are epigenetic, ranging from disseminations in altered rock to discrete mineralized veins related to structures linked the Main Uralian Fault. Large-scale deformation had ceased on the Main Uralian Fault with the intrusion of the Syrostan batholith at around 327 ± 2 Ma (Montero et al. 2000) which suggests that the deposits may relate to deformation prior to this, during the period of arc–continent collision. There may then have been remobilisation of fluids during the continent-continent collision that followed which formed the Uralides (Brown et al. 2008).

6.5.3 Scenario 3: Accretion and Post Subduction Extension

One of the possible responses to arc–continent collision may be the detachment of the subducting slab from the lower plate resulting in the upwelling of the asthenosphere which is then expressed in both the deformation and magmatism in the collisional orogen (Davies and von Blanckenburg 1995). This scenario is illustrated in Fig. 6.3d.

One possible example of mineralization developed in such a setting is the Paleozoic Mount Read volcanic belt in Tasmania. Here medium to high-K calc-alkaline volcanic rocks, dominated by felsic facies with co-magmatic granitoids and late stage rhyolites, host very significant VMS deposits (Solomon and Groves 1994). These lavas were erupted in response to extension in an assembled Middle Cambrian crustal collage which resulting from the obduction of probable forearc crust onto the continental margin, which is likely to have occurred during arc–continent collision. This extension led to the upwelling of the asthenosphere which resulted in the formation of half-grabens accompanied by the eruption of the Mt Read volcanic rocks (Crawford and Berry 1992). This type of environment may be comparable to that which hosts the continental rift hosted VMS deposits found in the Iberian Pyrite Belt and Bathurst Districts (Allen et al. 2002).

A further example may be the proposed tectonic setting of the Grasberg porphyry Cu–Au deposit on Papua New Guinea. Cloos et al. (2005) propose that during continental collision, at around 7.5–4 Ma, the leading edge of the Australian Plate underthrust and became subducted under Papua New Guinea. They suggest asthenosphere upwelling resulted in adiabatic decompression and melting beneath the Australian Plate margin which produced the magmas that intruded into the overlying sediment package, leading to the formation of the giant porphyry deposit.

6.6 Summary

Major mineral deposit formation in arcs can be directly related to the magmatism and therefore ultimately to the tectonics (Vigneresse 1995). In all cases, the ingress of continental derived sediments and finally the continental crust itself can have both geochemical and physical effects on both the subduction and the nature and chemistry of the melts formed. This general scenario is illustrated in Fig. 6.3a where melts are generated largely in the mantle wedge but may be contaminated by components from the descending subducting slab, either as volatile inputs or more rarely as possible direct slab melts. An example of the former scenario is found in the Banda arc where magma contamination by subducted continental-derived sediment is linked to the formation of gold-rich VMS deposits (Scotney et al. 2005; Herrington et al. 2011). Also, the last stages of continental subduction in the Uralides are marked by the generation of K-rich magmas, potentially partly slab-derived melts, linked to porphyry Cu–Au deposits (Gusev et al. 2000; Shatov et al. 2003).

As the arc and continent collide, subduction of the continental slab will finally fail and we can envisage three main tectonic scenarios which will have an effect on mineral deposit formation (1) Accretion and arc reversal; (2) Accretion and arc stepping and (3) Accretion and post-orogenic collapse (see Fig. 6.2).

In all these cases there is likely to be obduction of some of the oceanic rocks and this is a key mechanism for the preservation of ophiolites and their mineral deposits. Some or all of the arc rocks also become accreted to the continental margin and this is also a major mechanism for the growth of continental crust (Clift et al. 2003).

In the first scenario of accretion and arc reversal, which may be the norm (Dewey 2005), subduction direction reverses and the once passive continental margin becomes an active destructive margin. A new

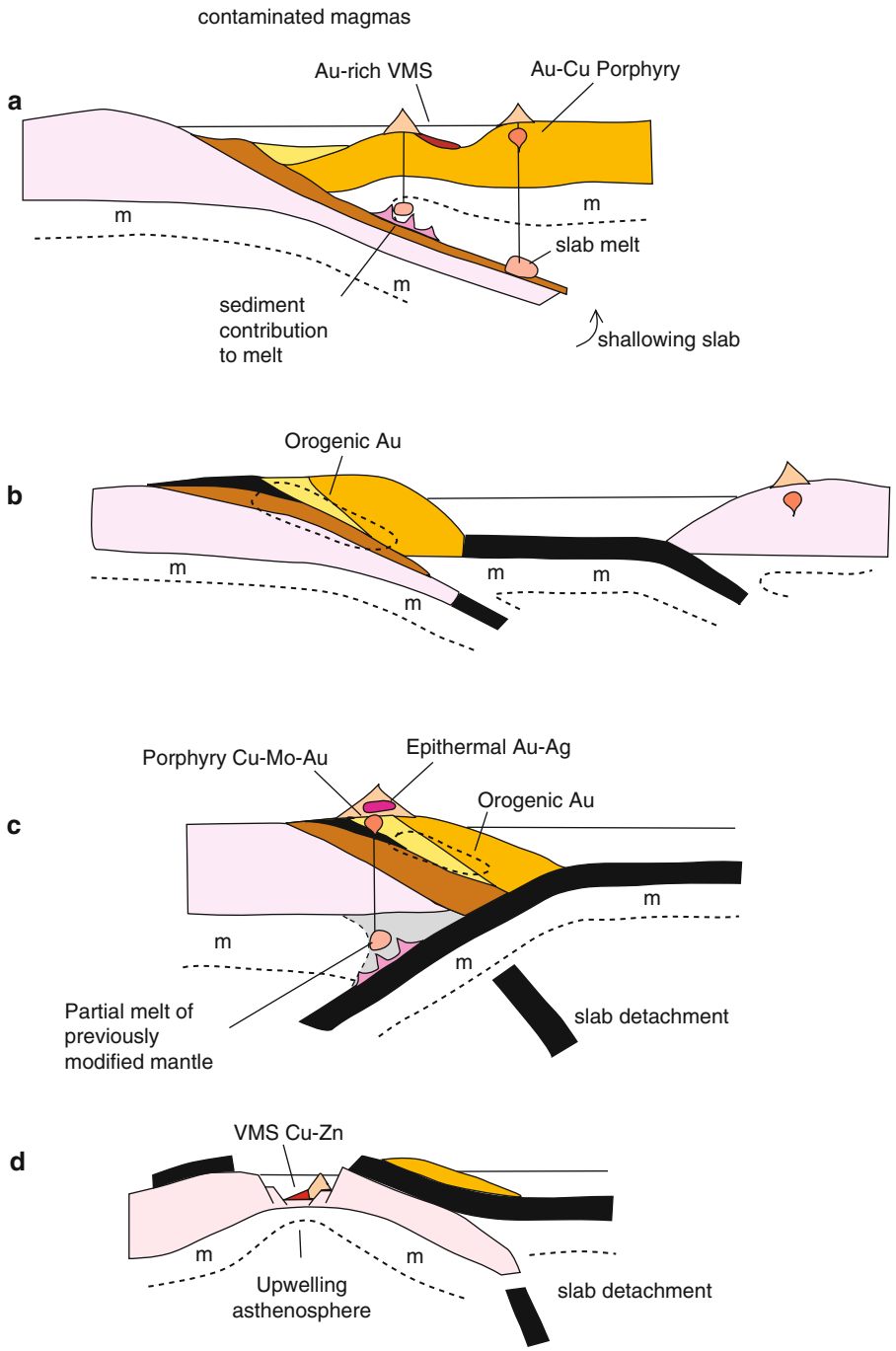

Fig. 6.3 Specific arc–continent collision scenarios with effects on mineral deposit systems: (**a**) Contamination of generated melts by subducted sediment (Au-rich VMS?) and possible slab melting (Au–Cu porphyries?); (**b**) Accretion and obduction linked to orogenic gold deposits, arc step leads to new locus for magmatism and mineral deposits; (**c**) Arc reversal and metasomatism of previously modified or new sub-continental mantle (Porphyry Cu–Au, epithermal Au–Ag); (**d**) Post collision extension (rift basins with VMS or porphyry Cu–Au deposits).

continental arc will develop and there is evidence that in arcs formed in this way (e.g., Kamchatka, Philippines) this flip is the trigger for major Cu and Au deposits to form (Fig. 6.3c). It appears that the flip, if inboard of the previous intra-oceanic arc could permit the melting of a mantle which has already been

modified and this results in magmas fertile for the formation of large magmatic-hydrothermal Cu and Au deposits (e.g., Solomon 1990; McInnes et al. 2001). A reversal like this is modelled in the case of the New Britain Trench which is related to the complex collisions of plates in southwest Pacific.

In the second scenario, obduction and accretion will occur but perhaps due to the mechanical competence of the oceanic slab attached to the continent, arc reversal is resisted and any shortening is accommodated on other subduction zones outboard of the former subduction zone (Fig. 2.2). This is the case for the Urals (see Brown et al. 2011; Herrington et al. 2005b) and in this case the old arc dies.

The last scenario may be rare but in the case of Tasman Fold System, arc–continent collision was marked by obduction of primitive supra-subduction rocks including boninites. Instead of arc reversal, slab detachment resulted in extension on the passive continental block (Fig. 6.3d) with formation of grabens in which VMS deposits formed (Crawford et al. 2003). It is possible that a similar scenario for the formation of the magmatism responsible for the Grasberg porphyry copper deposit might also be envisaged (Cloos et al. 2005).

Thus arc–continent collision is most critical as a mechanism for the preservation of supra-subduction zone ophiolite-hosted mineral deposits and those formed in intra-oceanic arcs. Nevertheless, the effects of the onset of collision can also subtly change magma chemistry in the intra-oceanic arc during its waning stages, affecting the associated mineral deposits. During the tectonic processes of the actual collision small to medium sized orogenic gold deposits may be formed.

The common effect of arc reversal is potentially one of the most important processes for the formation of continental arcs and their associated mineral deposit. Such continental arcs host major porphyry Cu–Au–Mo and epithermal Au–Ag deposits. Lastly, in rare cases, post collisional settings may be suitable sites for the formation of some VMS and porphyry Cu–Au deposits.

References

Afonso JC, Zlotnik S (2011) The subductability of continental lithosphere: the before and after story. In: Brown D, Ryan P (eds) Arc-continent collision: the making of an orogen, Frontiers in earth sciences. Springer, Heidelberg

Allen RL, Weihed P, Blundell DJ, Crawford T, Davidson G, Galley A, Gibson H, Hannington M, Herrington R, Herzig P, Large R, Lentz D, Maslennikov V, McCutcheon S, Peter J, Tornos F (2002) Global comparisons of volcanic-associated massive sulphide districts. In: Blundell D et al (eds) The timing and location of major ore deposits in an evolving orogen, vol 204. Geological Society of London, Special Publication, London, pp 13–37

Arculus RJ (1994) Aspects of magma genesis in arcs. Lithos 33:189–208

Audley-Charles MG (2004) Ocean trench blocked and obliterated by Banda fore-arc collision with Australian proximal continental slope. Tectonophysics 389:65–79

Auzanneau E, Vielzeuf D, Schmidt MW (2006) Experimental evidence of decompression melting during exhumation of subducted continental crust. Contrib Mineralog Petrol 152: 125–148

Barley ME, Rak P, Wyman D (2002) Tectonic controls on magmatic-hydrothermal gold mineralization in the magmatic arcs of SE Asia. Geol Soc Spec Publ 204:39–47

Brown D, Spadea P, Puchkov V, Alvarez-Marron J, Herrington R, Willner A, Heztel R, Gorozhanina Y (2006) Arc continent collision in the Southern Urals. Earth Sci Rev 79:261–287

Brown D, Juhlin C, Ayala C, Tryggvason A, Bea F, Alvarez-Marron J, Carbonell R, Seward D, Glasmacher U, Puchkov V, Perez-Estaun A (2008) Mountain building processes during continent-continent collision in the Uralides. Earth Sci Rev 89:177–195

Brown D, Herrington R, Alvarev-Marron J (2011) Processes of arc-continent collision in the Uralides. In: Brown D, Ryan P (eds) Arc-continent collision: the making of an orogen, Frontiers in earth sciences. Springer, Heidelberg

Brueckner HK (2009) Subduction of continental crust, the origin of post-orogenic granitoids (and anorthosites?) and the evolution of Fennoscandia. J Geol Soc 166:753–762

Carlile JC, Mitchell AHG (1994) Magmatic arcs and associated gold and copper mineralization in Indonesia. J Geochem Explor 50:91–142

Carmichael ISE (2002) The andesite aqueduct: perspectives on the evolution of intermediate magmatism in west-central (105–99°W) Mexico. Contrib Mineralog Petrol 143:641–663

Casey JF, Dewey JF (1984) Initiation of subduction zones along transform and accreting plate boundaries, triple-junctions evolution and fore-arc spreading centres – implications for ophiolite geology and obduction. Geol Soc Lond Spec Publ 13:269–290

Cawood PA, Suhr G (1992) Generation and obduction of ophiolites; constraints for the Bay of Islands Complex, western Newfoundland. Tectonics 11:884–897

Chemenda AI, Mattauer M, Bokun AN (1996) Continental subduction and a mechanism for exhumation of high-pressure metamorphic rocks: new modelling and field data from Oman. Earth Planet Sci Lett 143:173–182

Chew DM, Flowerdew MJ, Page LM, Crowley QC, Daly JS, Cooper M, Whitehouse MJ (2008) The tectonothermal evolution and provenance of the Tyrone Central Inlier Ireland Grampian imbrication of an outboard Laurentian microcontinent? J Geol Soc Lond 165:675–685

Clift PD, Schouten H, Draut AE (2003) A general model of arc-continent collision and subduction polarity reversal from Taiwan and the Irish Caledonides. Geol Soc Lond Spec Publ 219:81–98

Cloos M, Sapiie B, van Ufford AQ, Weiland RJ, Warren PQ, McMahon TP (2005) Collisional delamination in New Guinea: the geotectonics of subducting slab breakoff. GSA Spec Pap 400:1–51

Crawford AJ, Berry RF (1992) Tectonic implications of Late Proterozoic-early Paleozoic igneous rock associations in western Tasmania. Tectonophysics 214:37–56

Crawford AJ, Meffre S, Symonds PA (2003) 120 to 0 Ma tectonic evolution of the southwest Pacific and analogous geological evolution of the 600 to 220 Ma Tasman Fold Belt System. In: Hillis R.R., Muller R.D. (eds) Evolution and dynamics of the Australian plate. Geological Society of Australia Special Publication, Australia, pp 377–397

Davidson JP (1996) Deciphering the mantle and crustal signatures in subduction zone magmatism. Geophys Monogr 96: 251–262

Davies JH, von Blanckenburg F (1995) Slab breakoff; a model of lithosphere detachment and its test in the magmatism and deformation of collisional orogens. Earth Planet Sci Lett 129:85–102

de Hoog JCM, Mason PRD, van Bergen MJ (2001) Sulfur and chalcophile elements in subduction zones: constraints from a laser ablation ICP-MS study of melt inclusions from Galunggung Volcano, Indonesia. Geochim Cosmochim Acta 65:3147–3164

Dewey JF (2005) Orogeny can be very short. Proc Natl Acad Sci USA 102:15286–15293

Dewey JF, Mange M (1999) Petrography of Ordovician and Silurian sediments in the western Irish Caledonides: tracers of a short-lived Ordovician continent-arc collision orogeny and the evolution of the Laurentian Appalachian-Caledonian margin. Geol Soc Lond Spec Publ 164:55–107

Dewey JF, Ryan PD (1990) The Ordovician evolution of the South Mayo Trough, western Ireland. Tectonics 9:887–901

Dimkin AM, Necheukin VM, Sazonov VN (1990) Geology and geochemistry of the principal ore systems of the Urals. Nauka, Moscow, p 270 (in Russian)

Draut AE, Clift PD, Hannigan RE, Layne G, Shimizu N (2002) A model for continental crust genesis by arc accretion: rare earth element evidence from the Irish Caledonides. Earth Planet Sci Lett 203:861–877

Duke JM (1996) Podiform (ophiolitic) chromite. In: Eckstrand OR et al (eds) Geology of Canadian mineral deposit types, No 8. Geological Survey of Canada, Canada, pp 621–624

Earls G, Hutton D, Wilkinson JJ, Moles N, Parnell J, Fallick AE, Boyce AJ (1996) The gold metallogeny of northwest Northern Ireland: Northern Ireland geological Survey Report 049.96

Elburg MA, Van Leeuwen T, Foden J, Muhardjo (2002) Origin of geochemical variability by arc-continent collision in the Biru area, southern Sulawesi (Indonesia). J Petrol 43:581–606

Foley SF, Wheller GE (1990) Parallels in the origin of the geochemical signatures of island arc volcanics and continental potassic igneous rocks: the role of residual titanites. Chem Geol 85:1–18

Franklin JM, Gibson HL, Jonasson IR, Galley AG (2005) Volcanogenic massive sulfide deposits. In: Hedenquist JW et al (eds) Economic geology 100th anniversary volume. Society of Economic Geologists, Littleton, CO, pp 523–560

Fyfe WS (1992) Magma underplating of continental crust. J Volcanol Geoth Res 50:33–40

Garson MS, Mitchell AHG (1977) Mineralization at destructive plate boundaries: a brief review, vol 7. Geological Society, Special Publications, London, pp 81–97

Garwin S, Hall R, Watanabe Y (2005) Tectonic settings, geology and gold and copper mineralization in Cenozoic magmatic arcs of southeast Asia and the west Pacific. In: Hedenquist JW et al (eds) Economic geology 100th anniversary volume. Society of Economic Geologists, Littleton, CO, pp 891–930

Gasparon M, Varne R (1998) Crustal assimilation versus subducted sediment input in west Sunda arc volcanics: an evaluation. Mineral Petrol 64:89–117

Gill JB (1981) Orogenic andesites and plate tectonics. Springer, New York, NY, p 390

Groves DI, Bierlein FP (2007) Geodynamic settings of mineral deposit systems. J Geol Soc Lond 164:19–30

Gusev GS, Gushchin AV, Zaykov VV, Maslennikov VV, Mezhelovsky NV, Perevozchikov BV, Surin TN, Filatov EI, Shirai EP (2000) Geology and metallogeny of island arcs. In: Mezhelovsky NV et al (eds) Geodynamics and metallogeny: theory and implications for applied geology. Ministry of Natural Resources of the RF and GEOKART, Moscow, pp 213–295

Gutscher M-A, Maury R, Eissen J-P, Bourdon E (2000) Can slab melting be caused by flat subduction? Geology 28:535–538

Hall R (2002) Cenozoic geological and plate tectonic evolution of SE Asia and the SW Pacific: computer based reconstructions, model and animations. J Asian Earth Sci 20:353–431

Halls C, Zhao R (1995) Listvenite and related rocks: perspectives on terminology and mineralogy with reference to an occurrence at Cregganbaun, Co. Mayo, republic of Ireland. Miner Deposita 30:303–313

Hamilton WB (1995) Subduction systems and magmatism. Geol Soc Lond Spec Publ 81:3–28

Hannington MD, de Ronde CEJ, Petersen S (2005) Sea-floor tectonics and submarine hydrothermal systems. In: Hedenquist JW et al (eds) Economic geology, one hundredth anniversary volume, 1905–2005. Society of Economic Geologists, Littleton, CO, pp 111–141. ISBN 978-1-887483-01-8

Hedenquist JW, Arribas A Jr, Reynolds TJ (1998) Evolution of an intrusion-centred hydrothermal system: far Southeast-Lepanto porphyry and epithermal Cu-Au deposits. Econ Geol 93:373–404

Herrington RJ, Scotney PM, Roberts S, Boyce AJ, Harrison D (2011) Temporal association of arc-continent collision, progressive magma contamination in arc volcanism and formation of gold-rich massive sulphide deposits on Wetar Island (Banda Arc), Gondwana Research 19:583–593

Herrington RJ, Armstrong RN, Zaykov VV, Maslennikov VV, Tessalina SG, Orgeval J-J, Taylor RN (2002) Massive sulfide deposits in the South Urals: geological setting within the framework of the Uralide orogen. In: Brown D, Juhlin C, Puchkov V (eds) Mountain building in the Uralides: Pangea to present, vol 132. American Geophysical Union, Geophysical Monograph, pp 155–182

Herrington R, Maslennikov V, Zaykov V, Seravkin I, Kosarev I, Buschmann B, Orgeval J-J, Holland N, Tesalina S, Nimis P, Armstrong R (2005a) Classification of VMS deposits: lessons from the South Uralides. Ore Geol Rev 27: 203–237

Herrington RJ, Zaykov VV, Maslennikov VV, Brown D, Puchkov VN (2005b) Mineral deposits of the Urals and links to geodynamic evolution. In: Hedenquist JW et al (eds) Economic geology, one hundredth anniversary volume, 1905–2005. Society of Economic Geologists, Littleton, CO, pp 1069–1095. ISBN 978-1-887483-01-8

Herrington RJ, Puchkov VN, Yakubchuk AS (2005c) A reassessment of the tectonic zonation of the Uralides: implications for metallogeny. In: McDonald I, Boyce AJ, Butler IB, Herrington RJ, Polya DA (eds) Mineral deposits and earth evolution. Geological Society, Special Publications, London, pp 153–166

Hildreth W (1981) Gradients in silicic magma chambers: implications for lithospheric magmatism. J Geophys Res 86: 10153–10192

Hill KC, Hall R (2003) Mesozoic-Cenozoic evolution of Australia's New Guinea margin in a west Pacific context. Geol Soc Am Spec Pap 372:265–290

Hilton DR, Hoogewerff JA, van Bergen MJ, Hammerschmidt K (1992) Mapping magma sources in the east Sunda-Banda Arcs, Indonesia: constraints from helium isotopes. Geochim Cosmochim Acta 56:851–859

Hoffman PF (1988) United plates of America, the birth of a craton Early Proterozoic assembly and growth of Laurentia. Annu Rev Earth Planet Sci 16:543–603

Kennedy AK, Hart SR, Frey FA (1990) Composition and isotopic constraints on the Petrogenesis of alkaline arc lavas: Lihir Island, Papua New Guinea. J Geophys Res 95:6929–6942

Kisters AFM, Meyer FM, Seravkin IB, Znamensky SE, Kosarev AM, Ertl RGW (1999) The geological setting of lode-gold deposits in the central southern Urals: a review. Geol Rundsch 87:603–616

Konstantinovskaya EA (2001) Arc continent collision and subduction reversal in the Cenozoic evolution of the Northwest Pacific: an example from Kamchatka (NE Russia). Tectonophysics 333:75–94

Konstantinovskaya E (2011) Early Eocene arc-continent collision in Kamchatka, Russia: structural evolution and geodynamic model. In: Brown D, Ryan P (eds) Arc-continent collision: the making of an orogen, Frontiers in earth sciences. Springer, Heidelberg

Koroteev VA, de Boorder H, Necheukhin VM, Sazonov VN (2007) Geodynamic setting of the mineral deposits of the Urals. Tectonophysics 276:291–300

Lapukhov AS, Guzman B, Gorev VA, Solotchin EP, Travin AV (2007) The $^{40}Ar/^{39}Ar$ age of the epithermal gold-silver mineralization of the Asachinskoe Deposit, southern Kamchatka. J Volcanol Seismolog 1:405–409

Lippard SJ, Shelton AW, Gass IG (1986) The ophiolite of northern Oman. Geological Society of London, London, Memoir 11

Margaritz M, Whitford DJ, James DE (1978) Oxygen isotopes and the origin of high- 87Sr/86Sr andesites. Earth Planet Sci Lett 40:220–230

McCaffrey R (1989) Active tectonics of the eastern Sunda and Banda arcs. J Geophys Res 93:15163–15182

McConnell B, Riggs N, Crowley QG (2009) Detrital zircon provenance and Ordovician terrane amalgamation, western Ireland. J Geol Soc 166:473–484

McInnes BIA, Cameron EM (1994) Carbonated, alkaline hybridizing melts from a sub-arc environment: mantle wedge samples from the Tabar-Lihir-Tanga-Feni arc, Papua New Guinea. Earth Planet Sci Lett 122:125–144

McInnes BIA, Gregoire M, Binns RA, Herzig PM, Hannington MD (2001) Hydrous metasomatism of oceanic sub-arc mantle, Lihir, Papua New Guinea: petrologt and geochemistry of fluid-metasomatised mantle wedge xenoliths. Earth Planet Sci Lett 188:169–183

McNulty BA, Farber DL, Wallace GS, Lopez R, Palacios O (1998) Role of plate kinematics and plate-slip-vector partitioning in continental magmatic arcs: evidence from the Cordillera Blanca, Peru. Geology 26:827–830

Melcher F, Grum W, Thalhammer TV, Thalhammer OAR (1999) The giant chromite deposits at Kempirsai, Urals: constraints from trace element (PGE, REE) and isotope data. Miner Deposita 34:250–272

Mitchell AHG (1985) Mineral deposits related to tectonic events accompanying arc-continent collision. Trans IMM 94: B115–B125

Mitchell AHG, Garson MS (1981) Mineral deposits and global tectonic settings. Academic, London, p 404

Montero P, Bea F, Gerdes A, Fershtater G, Zin'kova E, Borodina N, Osipova T, Smirnov V (2000) Single-zircon evaporation ages and Rb-Sr dating of four major Variscan batholiths of the Urals: a perspective on the timing of deformation and granite generation. Tectonophysics 317:93–108

Muller D, Groves DI (1993) Direct and indirect associations between potassic igneous rocks, shoshonites and copper-gold mineralization at a convergent plate margin. Ore Geol Rev 8:383–406

Muller D, Franz L, Herzig PM, Hunt S (2001) Potassic igneous rocks from the vicinity of epithermal gold mineralization, Lihir Island, Papua New Guinea. Lithos 57:163–186

Nimis P, Omenetto P, Tesalina SG, Zaykov VV, Tartarotti P, Orgeval J-J (2003) Peculiarities of some mafic–ultramafic-hosted massive sulfide deposits from southern Urals. A likely forearc occurrence. In: Eliopoulos et al (eds) Proceedings of the seventh biennial SGA meeting mineral exploration and sustainable development, vol 1. Millpress, Rotterdam, The Netherlands, pp 627–630

Nimis P, Zaykov VV, Omenetoo P, Melekestseva IYu, Tesalina S, Orgeval J-J (2004) Peculiarities of some mafic-ultramafic and ultramafic hosted massive sulfide deposits from the Main Uralian Fault Zone, southern Urals. Ore Geol Rev 33:49–69

Peacock SM (1993) Large-scale hydration of the lithosphere above subducting slabs. Chem Geol 108:49–59

Pearce JA (1983) Role of the subcontinental lithosphere in magma genesis at active continental margins. In: Hawkesworth CJ, Norry MJ (eds) Continental basalts and mantle xenoliths. Shiva, Cheshire, UK, pp 230–249

Pearce JA, Peate DW (1995) Tectonic implications of the composition of volcanic arc magmas. Annu Rev Earth Planet Sci 23:251–285

Perfit MR, Gust DA, Bence AE, Arculus RJ, Taylor SR (1980) Chemical characteristics of island-arc basalts: implications for mantle sources. Chem Geol 30:227–256

Plank T, Langmuir CH (1988) An evaluation of the global variations in the major element chemistry of arc basalts. Earth Planet Sci Lett 90:349–370

Prouteau G, Scaillet B, Pichavant M, Maury RC (1999) Fluid-present melting of oceanic crust in subduction zones. Geology 27:1111–1114

Ringwood AE (1977) Petrogenesis in island arc systems. In: Talwani M, Pitman WC (eds) Island arcs, deep sea trenches, and back arc basins. American Geophysical Union [Maurice Ewing Series I], Washington DC, pp 311–324

Robb L (2005) Introduction to ore-forming processes. Blackwell, Malden, MA

Rudnick RL, Fountain DM (1995) Nature and composition of the continental crust: a lower crustal perspective. Rev Geophys 33:267–309

Ryan PD, Dewey JF (1991) A geological and tectonic cross-section of the Caledonides of western Ireland. J Geol Soc Lond 148:173–180

Ryerson FJ, Watson EB (1987) Rutile saturation in magmas: implications for Ti-Nb-Ta depletion in island-arc basalts. Earth Planet Sci Lett 86:225–239

Savelieva GN, Nesbitt RW (1996) A synthesis of the stratigraphic and tectonic setting of the Uralian ophiolites. J Geol Soc Lond 153:525–537

Savelieva GN, Sharaskin AY, Saveliev AA, Spadea P, Gaggero L (1997) Ophiolites of the southern Uralides adjacent to the East European continental margin. Tectonophysics 276:117–138

Savelieva GN, Sharaskin AYa, Saveliev AA, Spadea P, Pertsev A.N, Barbarina II (2002) Ophiolites and zoned mafic-ultramafic massifs of the Urals: a comparative analysis and some tectonic implications. In: Brown D et al (eds) Mountain building in the Uralides: Pangea to the present. Geophysical monograph 132, pp 135–153. ISBN 0-87590-991-4

Sawkins FJ (1984) Metal deposits in relation to plate tectonics. Springer, Berlin, p 261

Scotney PM, Roberts S, Herrington RJ, Boyce AJ, Burgess R (2005) The development of volcanic hosted massive sulfide and barite-gold orebodies on Wetar Island, Indonesia. Miner Deposita 40:76–99

Seedorf E, Dilles JD, Profett JM Jr, Einaudi MT, Zurcher L, Stavast WJA, Johnson DA, Barton MD (2005) Porphyry deposits: characteristics and origin of hypogene features. In: Hedenquist JW et al (eds) Economic geology 100th anniversary volume. Society of Economic Geologists, Littleton, CO, pp 251–298

Shatov VV, Seltmann R, Moon CJ (2003) The Yubileinoe porphyry Au(Cu) deposit, the south Urals: geology and alteration controls of mineralization. In: Eliopoulos DG et al (eds) Mineral exploration and sustainable development. Millpress, Rotterdam, The Netherlands, pp 379–382. ISBN 90 77017 77 1

Shemenda AI (1993) Subduction of thee lithosphere and back arc dynamics: insights from physical modelling. J Geophys Res 98:16167–16185

Sidorov AA (2008) "Postmineral" basaltoids and ore-bearing hydrothermal meineralizations. J Volcanol Seismolog 2: 143–148

Sillitoe RH (2010) Porphyry copper systems. Econ Geol 105: 3–41

Simmons SF, White NC, John DA (2005) Geological characteristics of epithermal precious and base metal deposits. In: Hedenquist JW et al (eds) Economic geology 100th anniversary volume. Society of Economic Geologists, Littleton, CO, pp 485–522

Solomon M (1990) Subduction, arc reversal and the origin of porphyry copper-gold deposits in island arcs. Geology 18: 630–633

Solomon M, Groves DI (1994) The geology and origin of Australia's mineral deposits: oxford monographs in geology and geophysics, 24. Oxford University Press, Oxford, p 1002

Spadea P, D'Antonio M (2006) Initiation and evolution of intra-oceanic subduction in the Uralides: geochemical and isotopic constraints from Devonian oceanic rocks of the Southern Urals, Russia. Island Arc 15:7–25

Stolper E, Newman S (1994) The role of water in the petrogenesis of Mariana trough magmas. Earth Planet Sci Lett 121: 293–325

Takahashi R, Matsueda H, Okrugin VM, Ono S (2006) Polymetallic and Au-Ag mineralizations at the Mutnovskoe Deposit in south Kamchatka, Russia. Resour Geol 56:141–156

Tatsumi Y, Hamilton DL, Nesbitt RW (1986) Chemical characteristics of fluid phase released from a subducted lithosphere and the origin of arc magmas: evidence from high-pressure experiments and natural rocks. J Volcanol Geoth Res 29:293–309

Taylor SR, McLennan SM (1995) The geochemical evolution of the continental crust. Rev Geophys 33:241–265

Thalhammer TV (1996) The Kempirsai ophiolite complex, south Ural: petrology, geochemistry, platinum-group minerals, chromitite deposits. Unpubl. Ph.D thesis, Mining University, Leoben, p 197

Thirlwall MF, Graham AM, Arculus RJ, Harmon RS, Macpherson CG (1996) Resolution of the effects of crustal assimilation, sediment subduction, and fluid transport in island arc magmas: Pb-Sr-Nd-O isotope geochemistry of Grenada, Lesser Antilles. Geochim Cosmochim Acta 60: 4785–4810

Turner S, Hawksworth C, Rogers N, Bartlett J, Worthington T, Hergt J, Pearce J, Smith I (1997) 238U-230Th disequilibria magma petrogenesis, and flux rates beneath the depleted Tonga-Kermedec island arc. Geochim Cosmochim Acta 61:4855–4884

Vigneresse JL (1995) Crustal regime of deformation and ascent of granitic magma. Tectonophysics 249:187–202

Vroon PZ, Lowry D, van Bergen MJ, Boyce AJ, Mattey DP (2001) Oxygen isotope systematics of the Banda Arc: low δ18O despite involvement of subducted continental material in magma genesis. Geochim Cosmochim Acta 65:589–609

Whitford DJ, Jezek PA (1979) Origin of late-Cenozoic lavas from the Banda arc, Indonesia; trace element and Sr Isotope evidence. Contrib Mineralog Petrol 68:141–150

Whitford DJ, Compston W, Nicholls IA, Abbott MJ (1977) Geochemistry of late Cenezoic lavas from eastern Indonesia: role of subducted sediments in petrogenesis. Geology 5:571–575

Whitford DJ, White WM, Jezek PA (1981) Neodymium isotopic composition of Quaternary island arc lavas from Indonesia. Geochim Cosmochim Acta 45:989–995

Wilkinson JJ, Johnston JD (1996) Pressure fluctuations, phase separation, and gold precipitation during seismic fracture propagation. Geology 24:395–398

Wilkinson JJ, Boyce AJ, Earls G, Fallick AE (1999) Gold remobilization by low-temperatue brines: evidence from the Curraghinalt gold deposit, Northern Ireland. Econ Geol 94:289–296

Williamson A, Hancock G (eds) (2005) The geology and mineral potential of Papua New Guinea. Papua New Guinea Department of Mining, Port Moresby, p 151

Winter JD (2001) An introduction to igneous and metamorphic petrology. Prentice-Hall, Upper Saddle River, NJ, p 697

Zhao Z-F, Zheng Y-F, Wei C-S, Wu Y-B (2007) Post-collisional granitoids from the Dabie orogen in China: Zircon U–Pb age, element and O isotope evidence for recycling of subducted continental crust. Lithos 93: 248–272

Part II
Specific Examples of Arc–Continent Collision

Chapter 7
The Nature of the Banda Arc–Continent Collision in the Timor Region

R. Harris

7.1 Introduction

Arc–continent collision is one of the most fundamental tectonic processes for the formation of new land, and the preservation on land of fragments of oceanic lithosphere (ophiolites). However, the tectonic evolution of arc–continent collision is commonly over-simplified in everything from introductory textbooks to complex tectonic models. Major unresolved issues include the response of the forearc during collision, controlling factors of deep continental subduction, possible slab delamination and the role of structural inheritance. Many of these issues have been addressed by detailed studies of arc–continent collisions in a variety of tectonic settings and stages of development. These studies reveal many common features, such as (1) arcuate orogens surrounding young, supra-subduction zone ocean basins, (2) high pressure metamorphism, (3) thrust sheets of forearc basement structurally overlying mélange in the hinterland of a continental fold and thrust belt, (4) reversal of sedimentation into a flexural trough, (5) contamination and modification of arc volcanism (6) arc accretion and suture zone development, and (7) uplift and exhumation of the orogenic wedge.

These common features attest to similar syn-collisional processes associated with plate kinematics that controls the personality of arc–continent collisions. I refer to these features as the tectonic *nurture* of the collision versus its tectonic *nature*, which is associated with pre-collisional or inherited features. For example, the arc–continent collision of Taiwan displays only some of the features listed above. Upper plate nappes and high-pressure metamorphic terranes are notably lacking in Taiwan. This contrast is mostly attributable to the young *nature* of the Asian continental margin versus the old and cold *nature* of most continental margins colliding with arcs, such as the Tethyan continental margins and those involving the northern Australian margin. Does the increased positive buoyancy and reduced strength of warm continental margins resist subduction more than cold continental margins? Is a continental margin with high heat flow, as in Taiwan, more likely to thrust over the forearc versus under it to some extent as in most arc–continent collisions? Deciphering the relative contribution of these inherited features versus plate kinematics in arc–continent collisions is one of the most important aspects to reconstructing how continental crust is formed and shaped – its *nurture* versus its *nature*.

Active collisions are key to addressing these issues. They provide both the tectonic nature and nurture of the collision at a variety of temporal and spatial scales. If the continental margin is oblique to the plate boundary then it can be analyzed in the fourth dimension of time where various phases of collision are manifest along orogenic strike. Taiwan is the most intensely studied example, but the Banda arc–continent collision of the Timor region also provides a classic example of an active, oblique arc–continent collision that differs in some very important aspects from Taiwan. The plate kinematics or *nurture* of each is very similar, but they are very different in *nature*.

The Timor region in many respects is more typical of arc–continent collisions in general (Searle and Stevens 1984), yet it is not nearly as well constrained by geological research as Taiwan and because of this is used as a "one collision fits all" analog for almost any tectonic scenario. Only recently has improved

R. Harris
Brigham Young University, Provo, UT, USA
e-mail: ramelau@gmail.com

D. Brown and P.D. Ryan (eds.), *Arc-Continent Collision*, Frontiers in Earth Sciences,
DOI 10.1007/978-3-540-88558-0_7,

political stability in the Timor region permitted sustained geological research for the first time in over 30 years. The purpose of this paper is to present some of the new discoveries resulting from these studies and how they help us better understand the role of structural heritage versus plate kinematics in shaping active arc–continent collisions and interpreting ancient ones.

7.2 The Banda Orogen

The Banda arc–continent collision or Banda Orogen forms a tectonic buffer zone at the triple junction between the huge Indo-Australian, Pacific and Asian plates. It consists of a complex array of island arcs, marginal basins, continental fragments and ophiolites amalgamated by repeated plate boundary reorganizations over the past 200 million years (Hamilton 1979; Pubellier et al. 2004; Harris 2003). Many of the oceanic terranes in the mix were emplaced onto the edges of partially subducted continental margins that began arriving at the triple junction during the mid-Tertiary. The last remains of a series of ocean basins that once separated the Sunda Shelf of Asia from the Sahul Shelf of Australia are closing and setting the stage for a collision between these two continents (Fig. 7.1).

The young deformation in the Banda Orogen is used as a modern analog for the Jurassic amalgamation of Alaska at the mega-triple junction between North America, Kula and Asian Plates (i.e., Silver and Smith 1983; Harris et al. 1987; Audley-Charles and Harris 1990). It has also been used in several papers to support various models for the Jurassic and Cretaceous amalgamation in the Mediterranean mega-triple junction between Africa, Europe and the Tethys (i.e., Searle and Stevens 1984). The 180° bend of the Banda Orogen around the young Banda Sea ocean basin is also similar to several Mediterranean orogenic loops and others such as the Yukon-Koyukuk (Alaska). However, in these orogens ophiolites are nearly all that remains of what once was likely a complex plate boundary system.

The initial closure stage presented by the Banda Orogen offers a unique perspective into how the *nature* of the colliding plates influences the transformation of arcs and passive margins into continents. This transformation includes the poorly understood transitions from subduction to collision, from an accretionary wedge to a fold and thrust belt, from arc volcanism to arc accretion and forearc destruction.

7.2.1 NNE-Directed Subduction Beneath the SE Asian Continent–Ocean Transition

The Banda Arc traces back to the "Great Indonesian Arc" of Early Cretaceous to Oligocene time, which stretched at least from India to the Sunda Shelf (Lytwyn et al. 2001) and most likely eastward beyond the Shelf into oceanic lithosphere all of the way to the Philippines and Halmahera (Hall 2002). This arc collapsed during a Tertiary regional extensional event that opened up several new marginal basins throughout SE Asia (Hall 2002).

The most recent expression of northward subduction of Indo-Australian oceanic lithosphere along the SE Asian Plate is the Late Neogene Sunda arc. The Sunda Arc replaced the Great Indonesian Arc and in many places is mounted on top of its forearc subduction complex. As one of the premier active volcanic arcs, the Sunda Arc stretches for nearly 6,000 km from Myanmar, where it is terminated by continental collision with India, to the Banda Arc where it is transitional with the Banda arc–continent collision. The active accretionary wedge of the Sunda arc consists mostly of Late Paleogene to Recent cover sediments and seamounts accreted from the subducting Indian Ocean sea floor (Hamilton 1979). Where these are thick the accretionary wedge rises above sea level to form a series of arc-parallel islands, such as those off of the coast of Sumatra in the NW and in the Lesser Sunda Islands of the Timor region in the SE.

The uplift of the Lesser Sunda Islands is an expression of how the *nature* of both the lower plate of the Sunda subduction system changes from oceanic to continental. The upper plate also changes from the continental Sunda Shelf to a series of composite oceanic basins due to backarc extension. Where the Australian continent enters the Sunda Trench the subduction system is transformed into a collision between the Banda intra-oceanic arc upper plate and

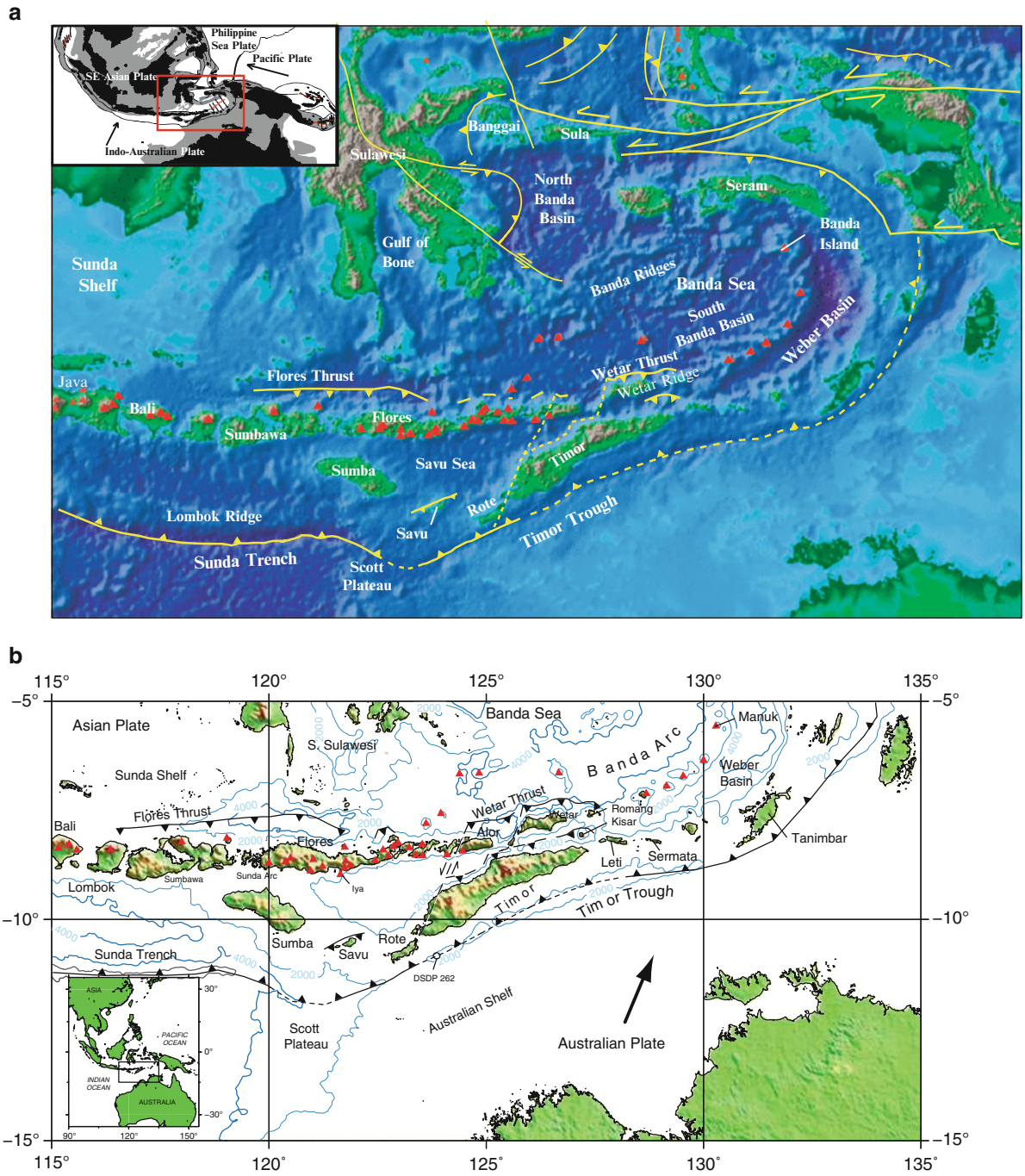

Fig. 7.1 (**a**) DEM of the Banda Arc region showing active faults (*yellow*, *dashed* is poorly defined) and active volcanoes (*red triangles*). *Inset* is plate tectonic map of the SE Asian region with plate vectors. Continental crust is grey and oceanic crust white. *Red box* is area of larger maps. (**b**) Topographic location map of places referred to in text.

long-lived passive continental margin lower plate. The collision actually involves the entire NW part of the Australian continent including the western part of New Guinea. However, the focus of this paper is on the western part of the Banda Orogen, which is the Timor region.

7.2.2 Seismic Tomography

Tomographic images to depths of 1,400 km across the Banda arc–continent collision show that the entire region is underlain by subducted lithosphere (Widiyantoro and van der Hilst 1997; Hafkenscheid et al. 2001). Up to 5,400 km of convergence is estimated along the Sunda Arc system from a high P-wave velocity anomaly that stretches beneath the Banda Arc region from Java to the southern Philippines. The subducting Indian Ocean plate begins to lose its seismic and tomographic expression below 600 km depth where it merges with a more diffuse zone of high-velocity mantle that underlies the entire region at depths of 600–1,400 km. Tomographic images of the Pacific side of the Banda Arc also connect westward subducting slabs to a high P-wave velocity zone at depth that is interpreted as a slab graveyard.

These results indicate that an entire ocean has been consumed along the Sunda arc-trench system, and that the Australian continent on the other side of this large ocean basin has finally arrived at the subduction zone. What happens when an ocean basins pulls a continent embedded in it into a subduction zone remains a topic of great debate, especially in the Timor region (Audley-Charles 1981; Price and Audley-Charles 1987; McCaffrey et al. 1985; Charlton 1991; Harris and Wu 1991; Sandiford 2008; Fichtner et al. 2010). The debate is about whether the subducting slab stays intact and allows deep continental subduction or the oceanic part breaks off preventing deep subduction and causing isostatic rebound of the continent. Much of the debate is driven by the assumption that deep subduction of continental lithosphere is not possible. However, since the discovery of micro-diamonds and other ultra-high pressure minerals in several collision zones (i.e., Sobolev and Shatsky 1990; Ernst and Liou 2000), there is now direct evidence for deep subduction of continental crust (>350 km).

In the Banda Arc not only are high-pressure assemblages found (Kaneko et al. 2007), but also the youngest arc volcanics are contaminated by deep subduction of cratonic material (van Bergen et al. 1993; Elburg et al. 2004). These features attest to subduction of the passive continental margin to at least 120 km depth. Evidence for deeper subduction without slab break off is provided by tomographic studies that show a 200 km thick zone of high seismic velocities (thickness of Australian continental lithosphere) extending to at least 400 km (Fichtner et al. 2010; Spakman and Hall 2010). The arc above this zone is contaminated by continental crust indicating that the high velocity zone is part of the Australian continent (Fichtner et al. 2010). These results differ significantly from tomograms of the Taiwan arc–continent collision (Wu et al. 2007), which show no evidence of deep subduction. These differences are consistent with the low heat flow (40 mWm^{-2}) reported for NW Australia (Cull 1982) versus high heat flow (95 mWm^{-2}) reported for the southern China continental margin subducting beneath Taiwan (Lee and Cheng 1986).

7.3 Collisional Setting

One of the most significant advantages of studying the Banda arc–continent collision is that the pre-collisional characteristics of the arc and continent are both preserved. Both can be progressively tracked into the collision zone along orogenic strike and inspected at various stages of collisional development. Throughout this process it becomes increasingly apparent just how much the *nature* of the lower plate matters in the tectonic evolution of an arc–continent collision. The better we understand the structural and stratigraphic heritage of the lower plate, the better we can constrain how much structural inheritance influences mountain building processes.

7.3.1 Lower Plate: NW Australian Passive Margin and Scott Plateau

The Australian continental margin has a complex structural heritage that causes many lateral discontinuities that are exploited by arc–continent collision. The passive margin formed after Permian to Jurassic intra-cratonic rifting of Gondwana. Middle-Late Jurassic breakup evolved into Early Cretaceous (Berriasian) sea-floor spreading in the adjacent Wharton Basin (Falvey 1972; Larson 1975). The Wharton Basin is one of the oldest remaining ocean basins on the

planet, which is a significant inherited feature that adds to the negative buoyancy and strength of the lower plate entering the Banda arc–continent collision zone.

7.3.1.1 Structural Evolution

The early stages of Gondwana rifting produced intracratonic basins of similar style and tectonic setting to those found in the North Sea (Spencer et al. 2005). These NW-SE striking basins filled with Permian to Jurassic siliciclastics, carbonates and some volcanic rocks known as the Gondwana Sequence (Fig. 7.2). This early phase of intracratonic rifting is later overprinted by breakup-related extension that produced a nearly perpendicular set of ENE-WSW rift basins that form the Australian continental margin (Fig. 7.3). These rift basins are underlain by a Jurassic breakup unconformity that separates the pre-breakup Gondwana Sequence from the post-breakup Australian Continental Margin Sequence (Fig. 7.2).

During Gondwana breakup some of the earlier NW-SE intra-cratonic rifts were exploited to form a rifted margin with rectangular continental plateaus, such as the NW protruding Scott Plateau (Longley et al. 2002). The Scott Plateau is made up of thinned continental crust 17–18 km thick (Symonds et al. 1998) and rises 2–3 km above the oceanic crust that surrounds it on three sides (Fig. 7.4). Like the Exmouth Plateau to the south it protrudes perhaps as much as 500 km out beyond the ENE-WSW Australian continental shelf (Longely et al. 2002). Magnetic lineations in oceanic crust surrounding the Scott Plateau, and rift basins within the continental plateau, are oriented ENE-WSW. These basins are truncated by transform faults on the NE and SW sides of the plateau.

The transform boundary on the NE side of the Scott Plateau, not the NW facing rifted margin, is colliding with the Sunda-Banda forearc (Fig. 7.4). This collisional geometry brings the ENE-WSW oriented rift basins of the Scott Plateau into the collision zone sub-parallel to their axes. The islands of Sumba, Savu and Rote emerge in the orogenic wedge adjacent to where some of these basins have entered into trench end-on.

The protrusion of the Scott Plateau also causes different parts of the continental margin to collide at different times with the Java Trench. Generally, the continental margin is oriented ENE-WSW from Timor to Rote (Fig. 7.4). The continental margin moves NNE at a rate of 68 km/Ma relative to the Asian Plate (Nugroho et al. 2009). As it collides with the E-W Sunda Trench the arc–continent collision propagates WSW at 110 km/Ma (Harris 1991). This plate kinematic solution predicts that the collision initiated in central Timor by at least 6 Ma and has propagated WSW to its current point of initiation south of Sumba Island (Fig. 7.3). However, irregularities in the shape of the continental margin to form the Scott Plateau protrusion (Keep et al. 2002) cause it to collide with the Sunda Trench at around 3.5 Ma (Fortuin et al. 1997), which is much earlier than the immediately surrounding areas.

Structural inheritance in this instance exerts a major control on where collision initiates and how it propagates. For example, collision propagates along the ENE-WSW part of the continental margin from central Timor to Rote as predicted (Roosmawati and Harris 2009). But the protrusion of the Scott Plateau allowed it to arrive at the Sunda Trench much earlier than adjacent parts of the Australian continental margin. The collision of the Scott Plateau propagates southeastward along its NE edge from Sumba to Savu to Rote. Evidence of these irregularities would be difficult to detect in ancient arc–continent collisions where mostly orthogonal convergence, straight continental margins, and rifted versus transform boundaries are assumed.

7.3.1.2 Gondwana Sequence

The Permian to Jurassic Gondwana Sequence of the Timor region represents the pre-breakup sedimentary cover of the Australian continental margin. It consists of two groups of rocks: the Kekneno Group (Simons 1940; Audley-Charles 1968), which has a proximal source, and the more distal facies Aileu and Maubisse Formations (Fig. 7.2). Part of this group is also inferred as the protolith of the Aileu metamorphic Complex along the north coast of East Timor (Audley-Charles 1968).

The Kekneno Group is exposed mostly in fensters through structurally overlying nappes of the Banda forearc (Banda Terrane). It consists of Permian to Jurassic siliciclastics with minor interbedded limestone

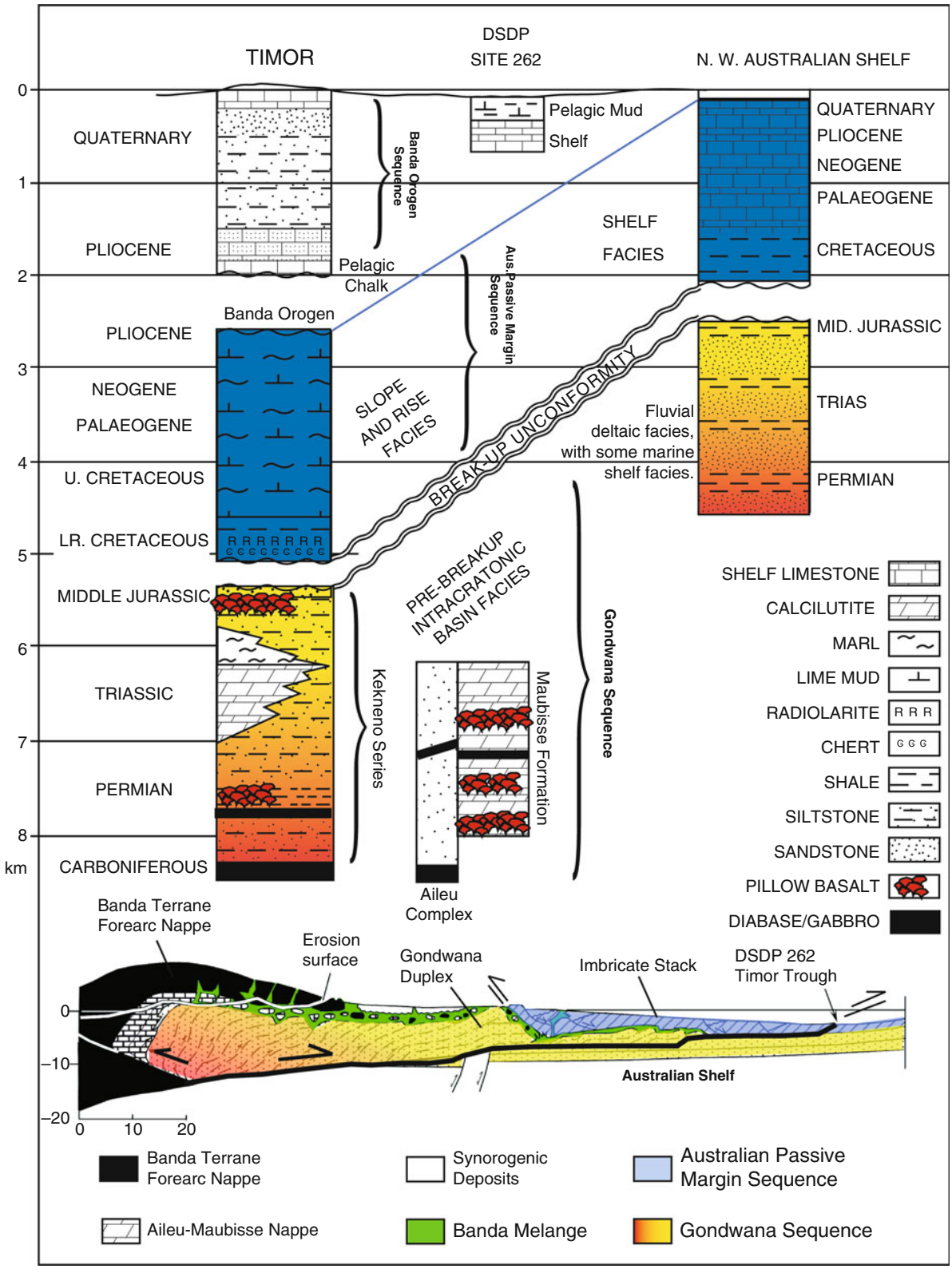

Fig. 7.2 Stratigraphic correlation between in situ and accreted (Timor) lithologies of the Australian continental margin. Cross section is modified from Harris (1991).

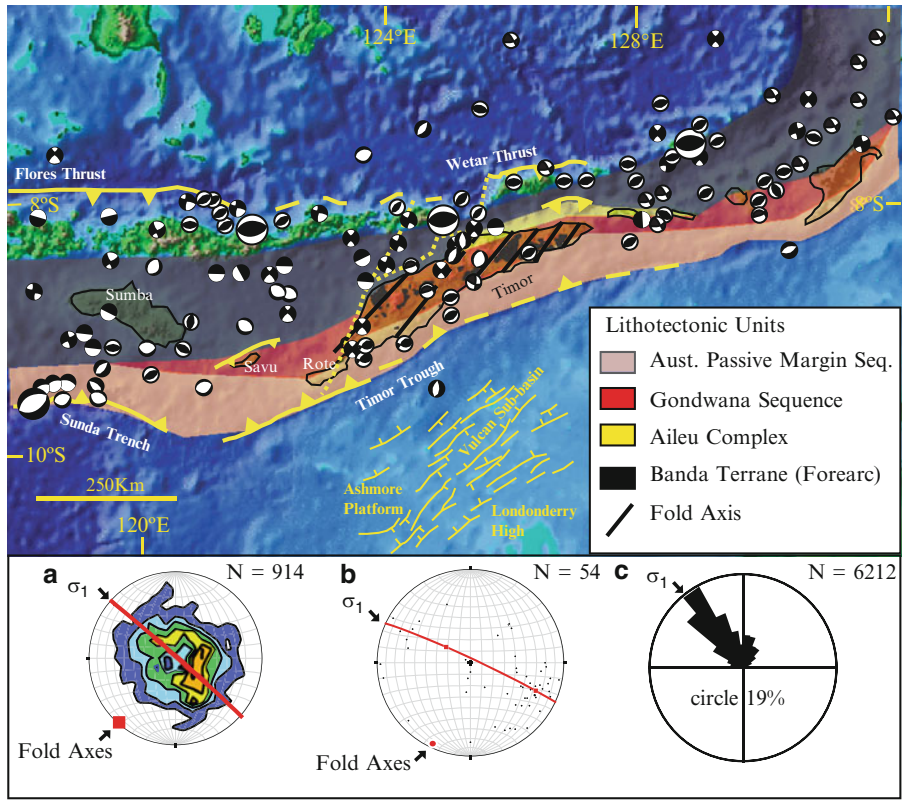

Fig. 7.3 Map showing extent of major lithotectonic units in the Banda Orogen, fault plane solutions, active faults (*thick yellow*) and inherited structure (*thin yellow*). The Banda Terrane (*dark grey*) is forearc crust that forms klippen overlying the Gondwana Sequence in Timor. *Black lines* are hinge lines of antiforms in Timor, which parallel the inherited structure of the northwest Australian continental margin (from Petkovik et al. 2000). Stereographs show (**a**) contour of poles to bedding planes and (**b**) poles to axial planes in folded Gondwana Sequence lithologies. Pi-circle (*red*) approximates maximum compressive stress (σ1), Pi-pole is approximation of fold hinge lines. (**c**) Mode one fracture measurements from synorogenic deposits throughout Timor and Alor (Mikolas and Harris 1986). The large pedal is parallel to σ1, which is perpendicular to fold axes and axial surfaces in pre-orogenic rocks (above) and to P-Axes from shallow earthquakes (Das 2004). The secondary direction is parallel to the plate motion vector measured by GPS (Nugroho et al. 2009).

and volcanics (see review papers by Charlton et al. 2002, 2009). The volcanics are mafic in composition with affinities to rift basin basalt (Berry and Jenner 1982). Similar rocks to the Kekneno Group are well documented in drill cores of the Australian continental margin (Charlton 1989).

Petrologic studies of Kekneno Group sandstone in Timor (Audley-Charles 1968; Bird and Cook 1991; Zobell 2007; Haig et al. 2008), Savu (Harris et al. 2009) and Rote (Roosmawati and Harris 2009) indicate it is texturally immature, consists of quartz to lithic wackes with large subangular framework grains of fresh twinned feldspar, mica, and lithic fragments. These relations indicate a proximal source, which according to discriminate diagrams was a recycled orogen.

U/Pb age determinations of detrital zircon grains collected from Timor, Savu and Kisar yield major peaks at 301 Ma and 1882 Ma (Zobell 2007; Harris 2006). The youngest grain analyzed in Triassic sandstone is 234.6 ± 4 Ma and the oldest grains are Archean, with a maximum age of 2725.3 ± 37.6 Ma. The youngest grains in the Aileu Complex are 198 ± 8 Ma (Major et al. 2009). The most likely source region with matching age distributions is Argoland (Zobell 2007), which rifted from the Australian continent during Jurassic breakup of Gondwana and has since accreted to Asia (Stampfli and Borel 2002).

a

PRESENT

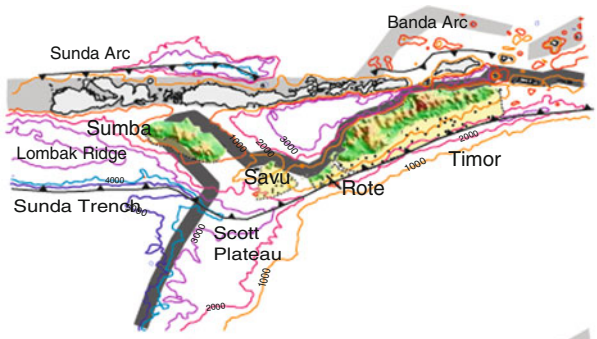

Timor - collision with Australian Shelf and rapid uplift (1-10 mm/a)
- Closure of forearc

Sumba - rapid uplift in north (0.5 mm/a), extensional collapse in south

Savu - uplift on north coast (>0.3 mm/a) from north-directed Savu Thrust, subsidence in south

Rote - uplift with highest rates (1.5 mm/a) along south coast near Timor Trough

Banda volcanic arc - accretion to lower plate, uplift and northward shift of volcanism

b

2 Ma

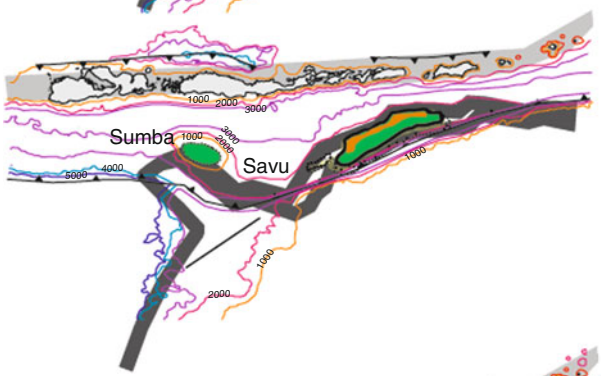

Timor - shortening, uplift and lateral expansion of island emergence.

Sumba - rapid uplift of coral terraces from collision with Scott Plateau prong (?)

Savu - rapid uplift from 2-3 km depth to surface

Rote - initiation of uplift

Banda volcanic arc
- backarc thrust development
- contamination front spreads east and west

c

4 Ma

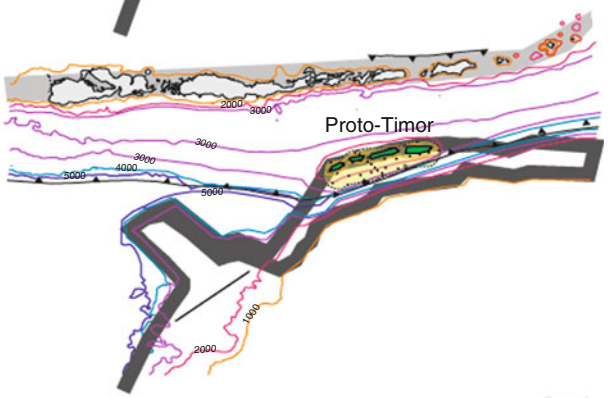

Timor - emergence to sea level from shortening of accreted Australian continental margin cover units
- uplift and erosion of Banda Terrane
- shallow exhumation of Aileu Complex

Sumba -3-4 km deep forearc basin

Savu and Rote - 3 km deep forearc ridge (Lombak Ridge Phase)

Banda volcanic arc - contamination by continental crust

d

6.0 Ma

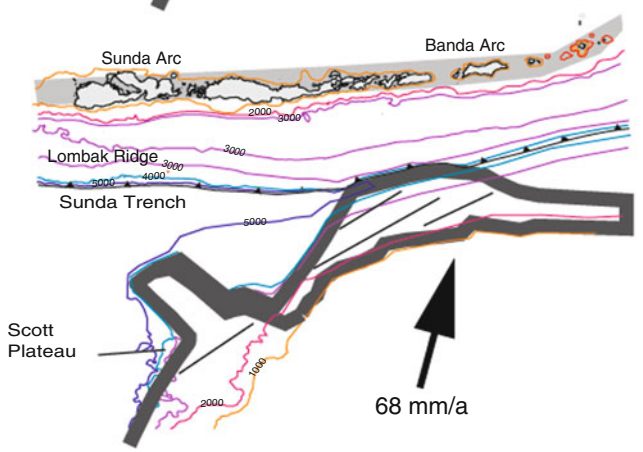

Timor - deep accretionary ridge underthrust by most distal parts of Australian basement. (Savu Phase).
- metamorphism of Aileu Complex

Banda volcanic arc - subduction zone volcanism

Aileu Complex

The Aileu Complex consists of late Carboniferous-Jurassic psammite intruded by mafic plutons that grades southward into limestone and basalt associated with the Maubisse Formation (Audley-Charles 1968; Berry and Grady 1981; Prasetyadi and Harris 1996). On the north coast of central East Timor these units are metamorphosed into pelitic schist, marble, phyllite and amphibolite, and are intruded by gabbroic and lherzolitic bodies of unknown age. In some places there are so many intrusions that only screens of metapsammite are found, which is interpreted as a rift event, which may explain the sillimanite grade rocks reported by Berry and Grady (1981). The earliest phase of metamorphism is overprinted by metamorphism associated with latest Miocene onset of collision in central Timor (Berry and McDougall 1986; Harris et al. 2000). Minimum P-T estimates for these rocks along retrograde paths are as high as 9 ± 1.2 kbars and 826 ± 37°C in Timor (Major et al. 2009) and 10 kbars and 600°C on Leti Island to the east of Timor (Kadarusman et al. in press).

Maubisse Formation

The Maubisse Formation consists of volcanic rocks interbedded with a distinctive red, sparitic crinoidal limestone and micritic units interbedded with red shale that were deposited during the Early Permian through Triassic (de Roever 1940; Audley-Charles 1968; Charlton et al. 2002). The volcanic rocks represent a bimodal suite with mostly basalt including common pillow lavas and volcaniclastics, with minor occurrences of rhyolite and some syenitic intrusives (Major et al. 2009). Geochemical studies indicate within-plate and ocean-ridge basalt, which is interpreted as representing the onset of rifting (Berry and Jenner 1982). Clastic sedimentary units found in the Maubisse Formation fine toward the south (Carter et al. 1976). Rocks similar to the Maubisse Formation are documented on the Sahul Shoals of the undeformed Australian continental margin (Archbold 1988).

7.3.1.3 Australian Passive Margin Sequence

The formation of the present NW Australian passive margin is marked in the stratigraphic record by a Middle Jurassic breakup unconformity at the top of the Gondwana Sequence (Fig. 7.2). Overlying the unconformity is a condensed succession of Early Cretaceous pelagic iron- and manganese-rich shale and mudstone interlayered with radiolarian chert and semi-consolidated foraminiferal and nannochalk (von Rad and Exon 1983). Exposures of these deposits are found throughout the Banda Orogen and are known as the Nakfunu Formation (Rosidi et al. 1979). They indicate rapid subsidence and development of slope and rise passive margin sedimentary environments. Overlying the Nakfunu Formation is a dense Cretaceous to Tertiary calcilutite interbedded with mudstone and some turbidites in both the present passive margin of Australia and in the Banda Orogen (Charlton 1989). These deposits are known as the Ofu Formation. Most of the accreted slope and rise facies Australian passive margin deposits outcrop in the southern parts of Timor and Rote as part of an imbricate thrust stack (Figs. 7.2 and 7.3). On the present passive margin these slope deposits grade into shelf facies successions of sandstone and shale conformably overlain by thick successions of Cenozoic carbonate up to 3,000–4,000 m thick (Smith and Ross 1986; Balke and Burt 1976). No shelf facies post-breakup successions are recognized in the orogenic wedge. However, upper Pliocene shelf facies limestone was encountered at the bottom of DSDP 262, which drilled into a 2,298 m deep section of the Timor trough

Fig. 7.4 Palinspastic map of the Banda arc-continent collision using a plate velocity (68 mm/a) and direction (015°) of convergence relative to the Asian Plate (Nugroho et al. 2009). Shortening of the Australian continental margin is shown by progressive narrowing. Green represents land near sea level, *brown* – mountains, *yellow* – turbidite deposition and *light grey* – zone of active volcanism. Bathymetry in "B" to "D" is speculative except where constrained by analysis of foraminifera (Roosmawati and Harris 2009). ENE–WSW lines in "D" are approximate axes of rift basins on Australian continental margin (see Fig. 7.3). Collision of Australian passive margin initiates in the Timor region and propagates westward toward Rote. Collision of the Scott Plateau initiates south of Sumba and propagates SE to Savu and Rote. Modified from Roosmawati and Harris (2009).

near the deformation front (Fig. 7.2). The shelf facies material documents rapid subsidence of the continental margin from sea level to >2,000 m depth in <2.5 Ma (Hamilton 1979).

7.3.1.4 Mechanical Stratigraphy

The major mechanical boundary layers of the Australian continental margin cover are the ~1,000 m thick succession of Late Triassic to Jurassic mudstone known as the Wai Luli Formation and the pelagic mud of the immediately overlying Nakfunu Formation (Harris et al. 1998). Both of these units straddle the breakup unconformity (Fig. 7.2). Most of the clay minerals in the mudstone are smectite-rich, which retain large amounts of water and produce high fluid over-pressures. Wells that penetrate this stratigraphic interval both in the Timor fold and thrust belt (Sani et al. 1995) and on the NW Australian margin (Kingborough et al. 1991) commonly experience borehole blowouts due to very high pore fluid pressures. Triaxial tests of mudstone from the breakout zones show extreme ductility at surface temperatures and differential stress of only 40–70 MPa (Kingborough et al. 1991). The mechanical weakness of this inherited structure and others found near the base of the Permian exert a major control on how the Australian continental margin cover sequences are accreted to the Banda Arc.

7.3.1.5 Shortening of the Australian Continental Margin

As the Australian continental margin arrives at the Sunda Trench its pre- and post-rift sequences are incorporated into the Banda orogenic wedge by both underplating-duplexing and frontal accretion processes, respectively (Fig. 7.5). There are also components of subduction channel flow and diapirism associated with the development and remobilization of thick mélange occurrences. Seismic reflection profiles across the deformation front in the Timor Trough show active décollement propagation into Jurassic and Early Cretaceous mudstone near the breakup unconformity (Breen et al. 1986; Karig et al. 1987; Masson et al. 1991). Large mud diapirs are seen rising from the décollement zone and forming mud ridges (blow-outs) on the seafloor. Some of the diapirs rise seaward of the thrust front and may influence the eventual position of the next forward-stepping thrust fault (Breen et al. 1986). Above the breakup unconformity-level décollement, post-breakup Australian Passive Margin Sequences are frontally accreted to the orogenic wedge as a stack of imbricate thrust sheets (Fig. 7.6) with no lithologies older than Jurassic found in the thrust stack.

The imbricate thrust stack that forms at the front of the orogenic wedge is best exposed in the Kolbano Mountains region of southern west Timor (Fig. 7.5b). The Oetuke River canyon cut through the Kolbano Mountains and exposes at least 25 imbricate thrust sheets in only 13 km of section (Fig. 7.6). The faults repeat a <500 m thick succession of Cretaceous to Pliocene Australian Passive Margin Sequence. The thrust sheets take the shape of truncated fault-propagation folds with mostly overturned forelimbs. The deformed section restores into an originally 27 km long section that is shortened by a minimum of 58%. Axial planar pressure solution cleavage is well developed throughout most of the section and represents a significant amount of volume loss during deformation.

The pre-breakup Gondwana Sequence underthrusts the imbricate stack to deeper levels of the subduction channel where it then stacks up into a thrust duplex zone (Fig. 7.5). The roof of the duplex is near the breakup unconformity-level décollement and the floor is near the base of the Permian. These boundary conditions produce fault-propagation folded thrust sheets 1–3 km thick that repeat various parts of the Permian to Jurassic Gondwana Sequence (Fig. 7.5). The duplex zone first emerges on the Island of Savu at the rear of the orogenic wedge (Harris et al. 2009).

Savu exposes at least four separate thrust sheets of the Triassic to Jurassic Babulu and Wai Luli Formation, which is the upper part of the Gondwana Sequence (Fig. 7.7). Another duplex consisting of lower Gondwana Sequence lithologies is inferred below the one exposed on the surface. The Savu Thrust carries the duplex stack and mélange over the Banda Terrane nappe along the north coast of the island (Fig. 7.7). Seismic reflection profiles across the Savu Thrust show that it consists of a series of northward younging thrust faults that deform the

youngest beds on the seafloor. A well drilled on the north coast of Savu penetrated through synorogenic chalk deposits before hitting mélange overlying the top of the Banda Terrane nappe (Harris et al. 2009).

The lower Gondwana Sequence thrust duplex is exposed in several structural windows through the Banda Terrane nappe of Timor (Harris 1991). A structural transect by Zobell (2007) through one of these structural windows in the Cribas region of East Timor reveals several repetitions of mostly Permian to Triassic thrust sheets (Fig. 7.8). The Banda Terrane nappe rests in a synformal region between two

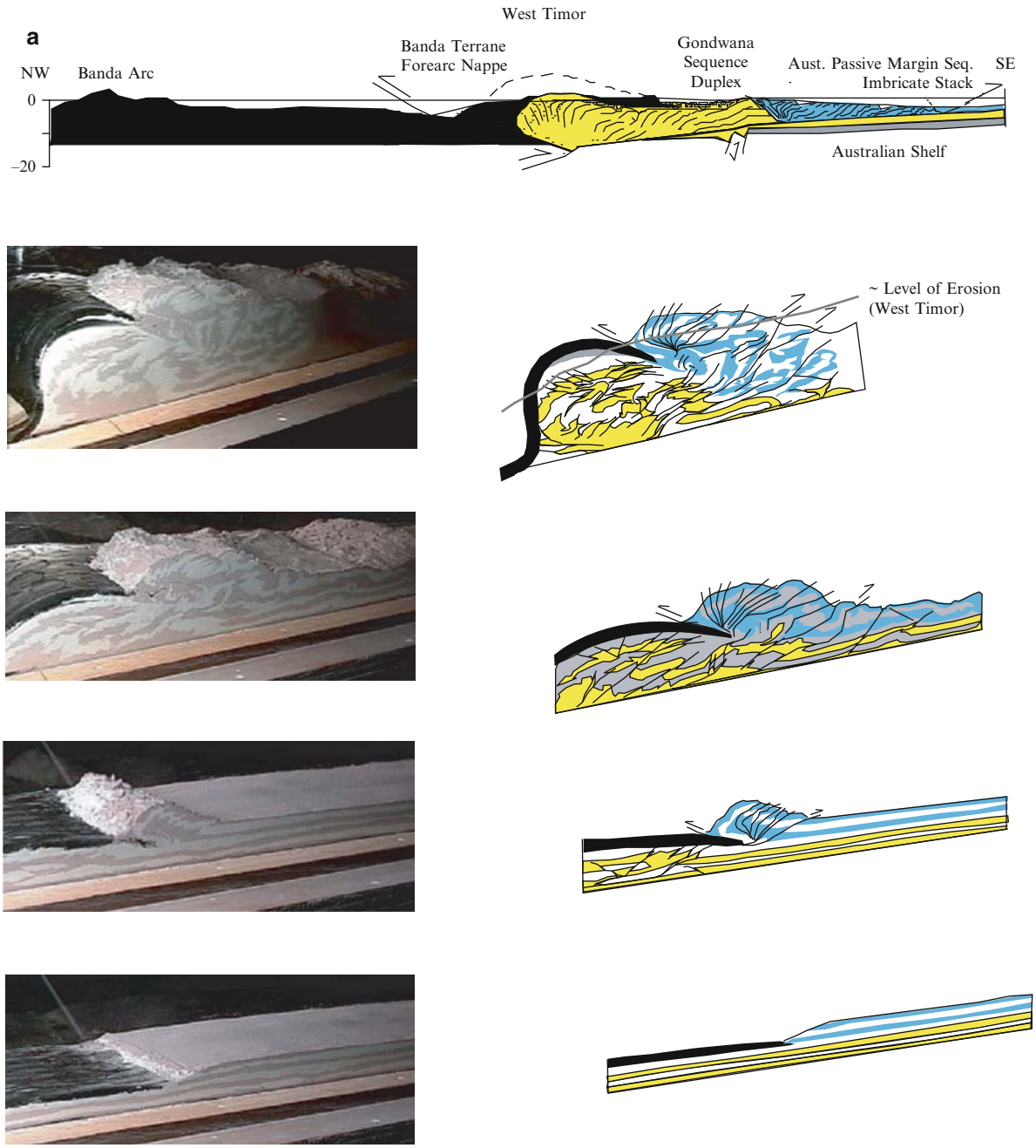

Fig. 7.5 (continued)

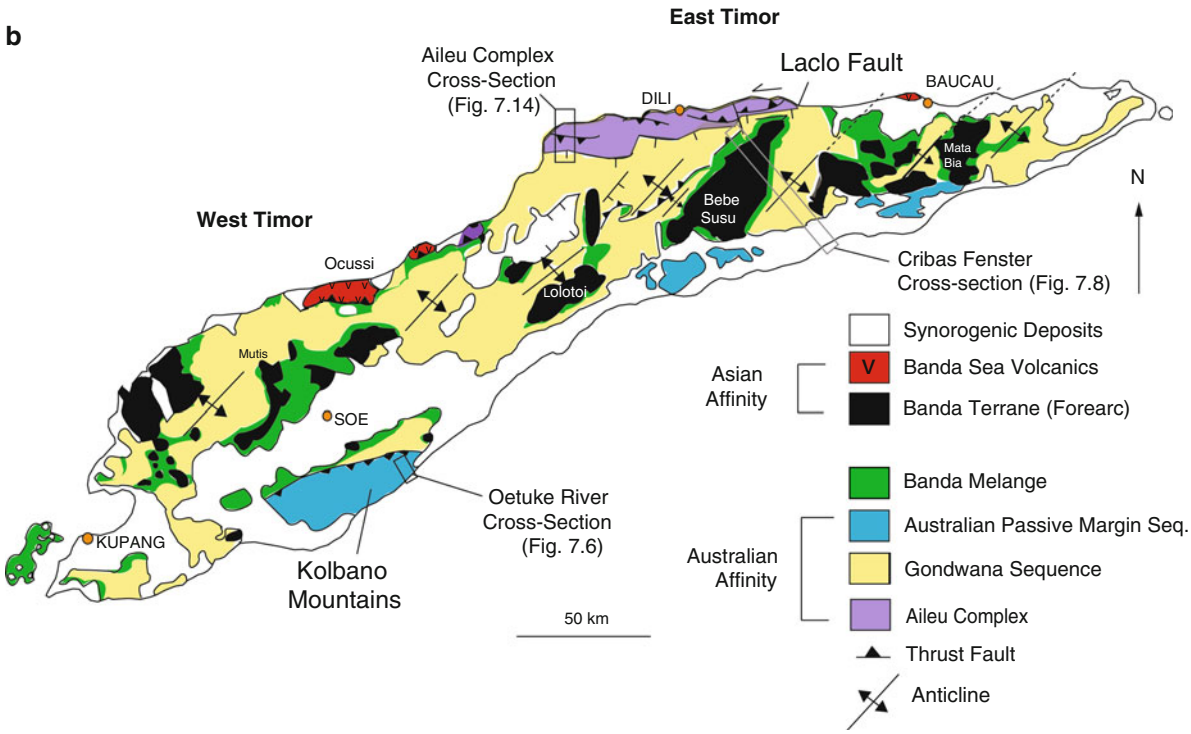

Fig. 7.5 (**a**) Analog sandbox model testing how a strong upper plate structural lid influences orogenic wedge geometry (modified from Vorkink 2004). Materials are scaled to the rheology and thickness of the Australian continental margin (*red* and *white*) and Banda Terrane (*black*). In coming continental margin cover successions are detached at two levels. The Australian Passive Margin Sequence is frontally accreted to form an imbricate thrust stack (*blue*). Gondwana Sequence lithologies (*yellow*) are subduct further before detaching and deform into a fold-dominant duplex system. The Banda Terrane is represented by black plasticene that is driven back into an asymmetric retro-antiform by under stacking of Gondwana Sequence units. Compare to cross-section through West Timor (modified from Harris 1991). The line of section is shown on map. (**b**) Generalized geologic map of Timor taken mostly from Audley-Charles (1968), Rosidi et al. (1979) and Harris et al. (2000). Asian affinity Banda Terrane massifs are interpreted as structurally overlying Australian affinity Gondwana Sequence lithologies. Banda Mélange (*green*) is found surrounding and beneath the Banda Terrane klippe. The NW-SE rectangles are the locations of two detailed structural transects and cross sections (see Figs. 7.6 and 7.8).

structural culminations of the duplex. Between the lower Gondwana Sequence duplex and the structurally overlying Banda Terrane nappe is a zone of mélange. Line balanced reconstructions of the duplex estimate at least 48% shortening of an initial 100 km long undeformed section (Zobell 2007).

Gross area balanced cross sections across the orogenic wedge indicate that after only 3–4 m.y. the space available in the wedge would fill with Australian continental margin lithologies (Vorkink 2004; Zobell 2007). This calculation assumes that the wedge extends to at least 30 km depth, which is the depth of metamorphism of the highest-pressure parts of the Aileu Complex. It also assumes 100% accretion of a constant thickness Permian to Pliocene continental margin cover. What the estimate does not take into account are deeper duplexes of Pre-Permian units that may have stacked beneath the lower Gondwana Sequence duplex or even stacks of metamorphic basement or metamorphosed Gondwana Sequence as found in the Aileu Complex. These estimates hint that the hinterland region of the Banda orogen, which is all that is exposed throughout the Banda Arc, formed in less than 3–4 m.y. and is currently being exhumed. Most of the shortening associated with ~70 km/Ma of plate convergence is taken up in other locations such as the back arc region (Wetar and Flores Thrust systems), the rear of the accretionary wedge and at the deformation front in the Timor Trough (Fig. 7.2).

7.3.1.6 Banda Mélange

The Banda Mélange occurs extensively throughout the Banda Orogen and is exposed at the front of, and in erosional windows through the Banda Terrane nappe, and as diapirs (Fig. 7.5). It consists mostly of a pervasively deformed scaly clay-rich matrix with little to no internal continuity that incases a highly mixed assemblage of neighboring blocks of a variety of sizes, rock types, ages and metamorphic grade.

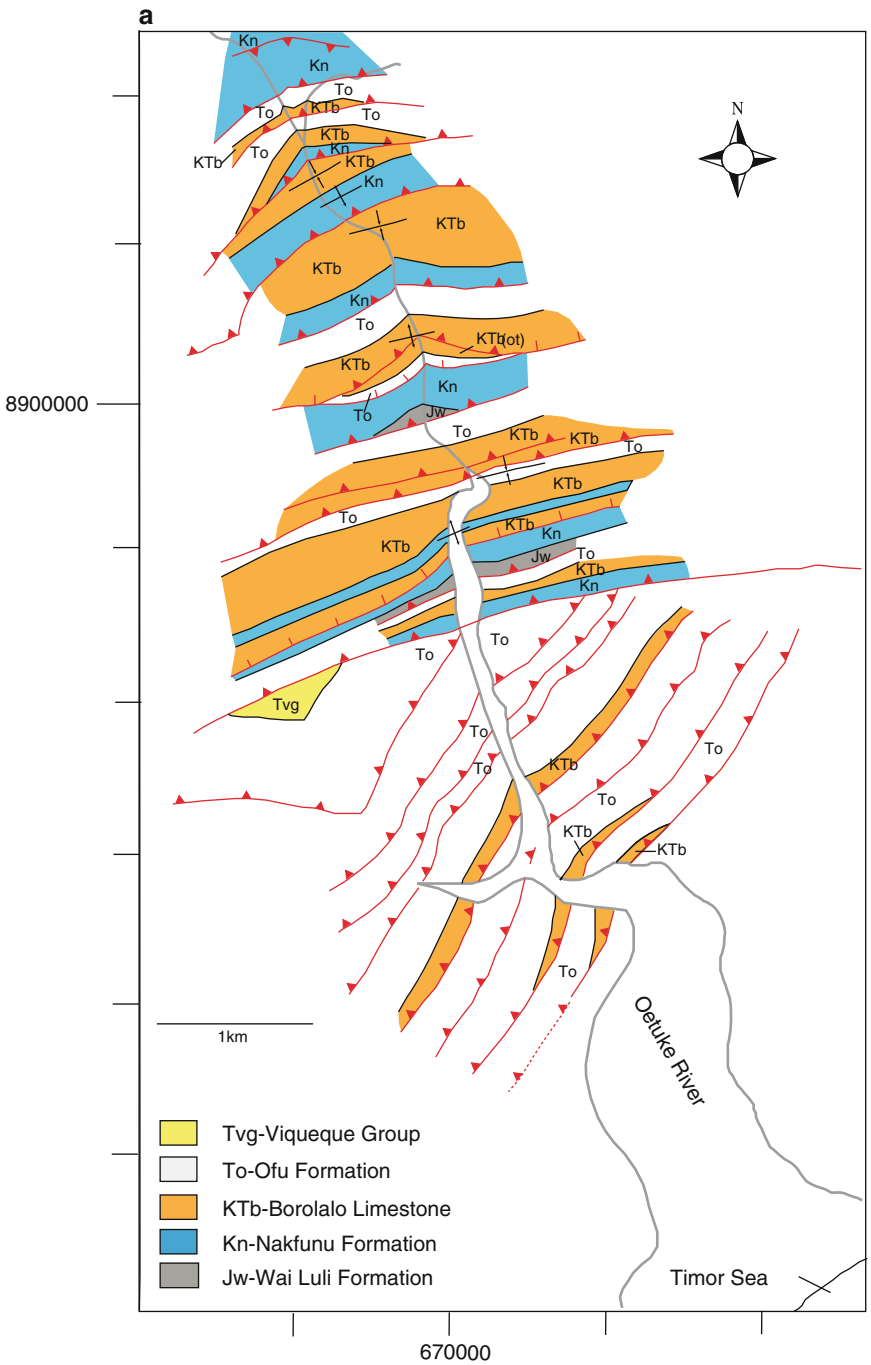

Fig. 7.6 (continued)

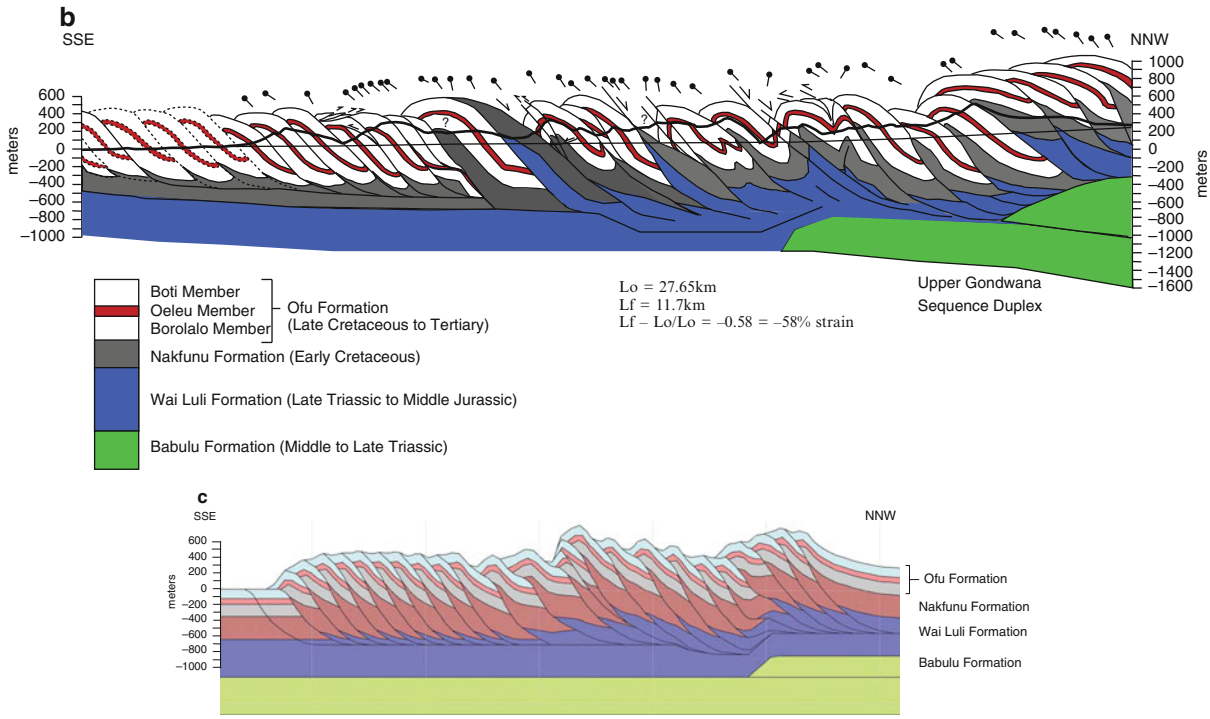

Fig. 7.6 Oetuke River structural transect (see Fig. 7.5 for location). (**a**) Structural map of the lower Oetuke River, which cuts through an imbricate thrust stack of Australian Passive Margin Sequence units. Thrust faults with triangle and normal faults with line on hanging-wall. (**b**) Cross section along the Oetuke river with dip symbols and topographic profile (*heavy black line*). (**c**) Pre-extensional forward model of cross section using Lithotect software. Imbricate thrust sheets continue offshore where they are imaged by reflection seismic profiles.

Biostratigraphic analysis of the scaly clay matrix yields a less mixed assemblage of palynoflora, nannoflora, and microfauna mostly derived from Jurassic and Cretaceous clay-rich units near the breakup unconformity. However, the large range of taxa (Lower Triassic to Pliocene) indicates a high level of mixing that is not consistent with sedimentary processes.

The mélange was mapped in Timor as the Bobonaro scaly clay (Audley-Charles 1968), and like many mélanges was initially interpreted as an olistostrome, but later recognized as primarily a tectonic feature (Barber et al. 1986; Harris et al. 1998). It is referred to here as the Banda Mélange due to its ubiquitous occurrence throughout the Banda Orogen and most common structural position at the base, and immediately in front of Banda Terrane nappes (Fig. 7.2). Other occurrences are also documented that may relate to secondary sedimentary and diapiric processes (Audley-Charles 1968; Barber et al. 1986; Masson et al. 1991).

Stratal disruption within the Banda mélange involves mostly viscous flow at low temperatures due to the *nature* of the expandable clay that feeds into the mélange from the Wai Luli Formation. There are at least two phases of deformation: a pervasive mostly coaxial layer-parallel extension and more localized non-coaxial shear. Layer-parallel extension is characterized by boudinage with viscous flow of clay-rich layers out from between competent layers. Calcite fibers in bed normal fractures throughout mélange blocks indicate coaxial strain about an axis normal to bedding during hydro-fracturing, which attests to fluid pressures at least 95% of lithostatic. Non-coaxial shear is localized throughout the mélange, particularly in broken formation of the Gondwana Sequence near the base of the mélange and along the base of the Banda Terrane roof thrust near the top of the mélange, which is consistent with flow in a subduction channel (Shreve and Cloos 1986).

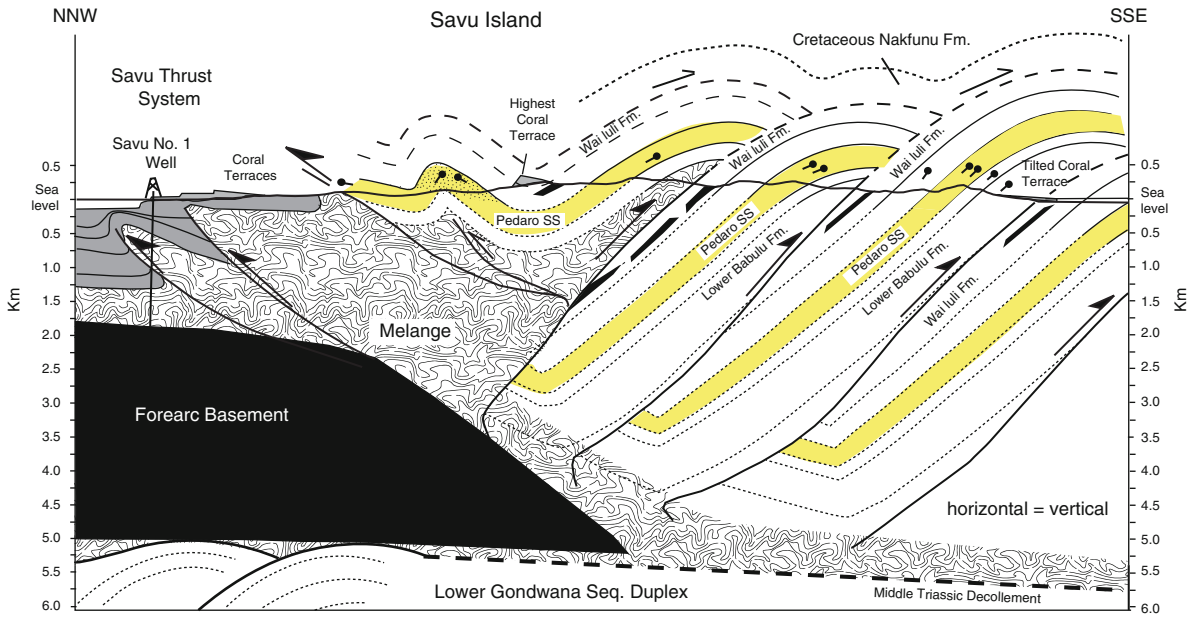

Fig. 7.7 Composite cross section across Savu (modified from Harris et al. 2009). *Upper* Gondwana Sequence duplex of Triassic Babulu Formation and Jurassic Wai Luli Formation as seen at base of Oetuke River section (Fig. 7.6). *Black lines* within the Wai Luli Formation are pillow basalt layers. Grey is latest Miocene to Pleistocene pelagic chalk (Batu Putih Formation) synorogenic cover. Savu No. 1 well drilled through synorogenic cover into top of Banda Terrane forearc basement. Active Savu Thrust carries rear of orogenic wedge and mélange over forarc basin deposits. The structure of northern section is according to seismic profiles off the north coast and from drilling data. Folds and thrust faults are determined from field mapping (Harris et al. 2009). Dip measurements are given by *black dots* with line pointing in direction of dip. Black bodies in Wai Luli Formation are basalt. Detachment depth is estimated from the projected depth of the Sumba Ridge and stratigraphic thickness of units incorporated into thrust sheets. Cretaceous units are interpreted as a roof thrust for the Upper Triassic–Jurassic duplex. Assuming no subduction erosion, the southern edge of the forearc was the initial position of the pre-collisional Sunda Trench. Southward-tilted coral terraces are shown at both coast lines and above the syncline.

Block types are highly mixed but vary in abundance from top to bottom and north to south throughout the mélange. Serpentinized mantle and deep crustal lithologies from the Banda Terrane (Fig. 7.9) are more abundant near the top and to the north while upper crustal oceanic material and Gondwana Sequence lithologies are most abundant in the lower and southern sections. The middle of the mélange is a chaotic mixture of both types, with ubiquitous Gondwana Sequence lithologies such as the sandstone and siltstone from the Kekneno Group, and pink crinoidal limestone and associated pillow basalt of the Maubisse Formation.

Mantle material incorporated into the mélange is mixed with early-accreted lithologies sourced from the upper most oceanic crust (pillow basalt, chert, manganese nodules). Sandstone blocks and matrix is also sourced from the upper part of the Gondwana Sequence and the distal most Australian Passive Margin Sequence. These lithologies dominate in mélange exposed near the south coast along with predominately crustal versus mantle material from the forearc upper plate. Dense blocks supplied from the forearc upper plate sink through the low-density mud and mix with lower plate lithologies. Mud extrusion around the edges of many of these blocks is still active and observed in several places throughout Timor forming fresh mud lumps on the surface.

7.3.1.7 Mud Diapirism

Diapirs of matrix-rich mélange locally rise from overpressured horizons up through the Banda Orogenic wedge. The most common sites are at the deformation front in the Timor Trough, at the front of the Banda

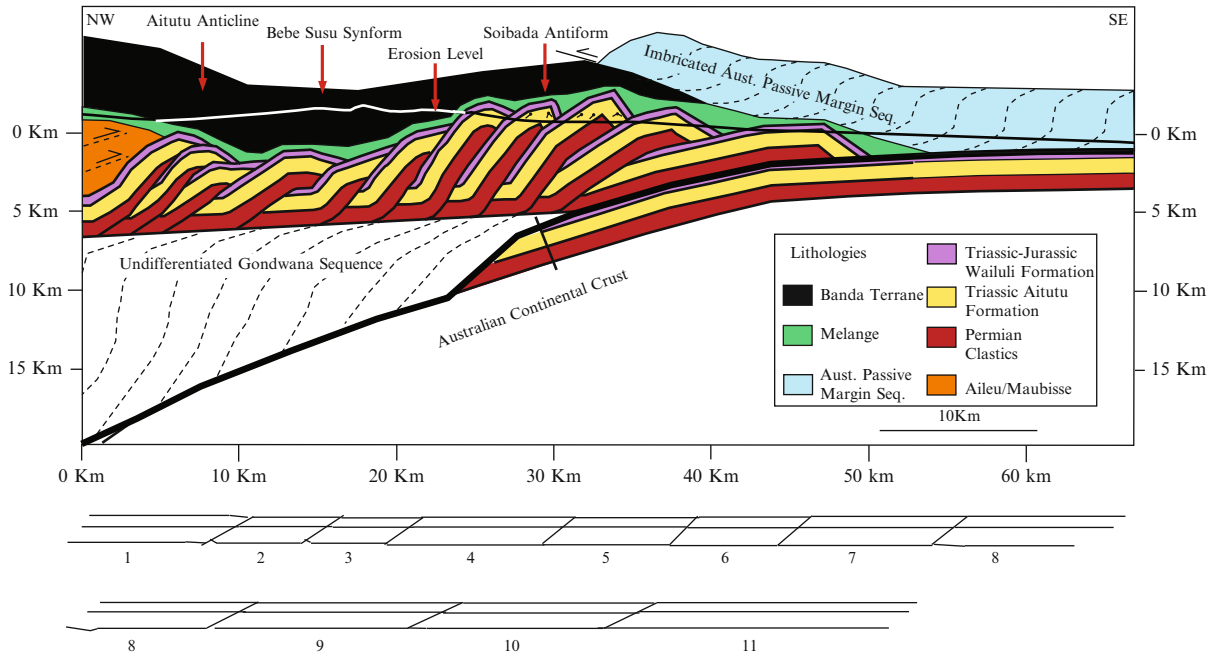

Fig. 7.8 Cribas fenster cross-section (modified from Zobell 2007). See Fig. 7.5b for line of section. Duplex of mostly Permian to Triassic *lower* Gondwana Sequence lithologies beneath the Banda Terrane as seen at base of Savu cross section (Fig. 7.7). Balanced reconstruction (below). Thrust sheets on restored section are numbered in order of deformation (1 is accreted first). Green zone is mixed block and clay mélange that represents the original subduction channel. Current erosional level is shown.

Terrane nappe, along the retrowedge thrust front (Savu Thrust) and faults cross-cutting the orogen (Barber et al. 1986; Harris et al. 1998). Many active diapir fields are imaged offshore (Breen et al. 1986; Masson et al. 1991). Onshore diapirs are found intruding into basal synorogenic chalk and turbidites and along fault zones (Harris et al. 1998).

Seismic profiles and side-scan sonar images across the deformation front show disturbed areas in the subsurface that connect with mud diapirs on the surface. The disrupted horizons rise from near the breakup unconformity where drilling on the NW Australian continental margin has documented over-pressured mudstone. The diapirs form a series of mud ridges 20 km long and up to 300 m high that parallel the thrust front within the Timor Trough (Breen et al. 1986). The mud ridges define the deformation front, which deforms the bedded continental margin units by diapirism before they are accreted to the thrust front.

Large diapirs are also imaged along the Savu Thrust at the rear of the accretionary prism (Reed et al. 1986). Some of these diapirs are exposed on the island of Savu and consist of block in clay mélange with blocks derived from both the Gondwana Sequence and Banda Terrane.

Another large occurrence of mélange diapirs is found at the 123° East discontinuity (Barber et al. 1986), which forms the western edge of Timor and intersects the islands of Semau and Rote (Fig. 7.1). A line of several diapir islands rise along this NNE-SSW zone that is sub-parallel to the direction of plate convergence. Each island consists of active mud volcano fields extruding block in clay mélange through eroded lag deposits of a variety of block types. Systematic block counts on these islands and in exposures of mélange throughout the Timor region document a high degree of mixing under conditions of hydrofracturing (Harris et al. 1998).

The characteristics associated with the Banda mélange are most consistent with subduction channel versus sedimentary processes (Harris et al. 1998). These characteristics include the extensive occurrence of the mélange, its structural position at the base of forearc nappes and at active thrust fronts,

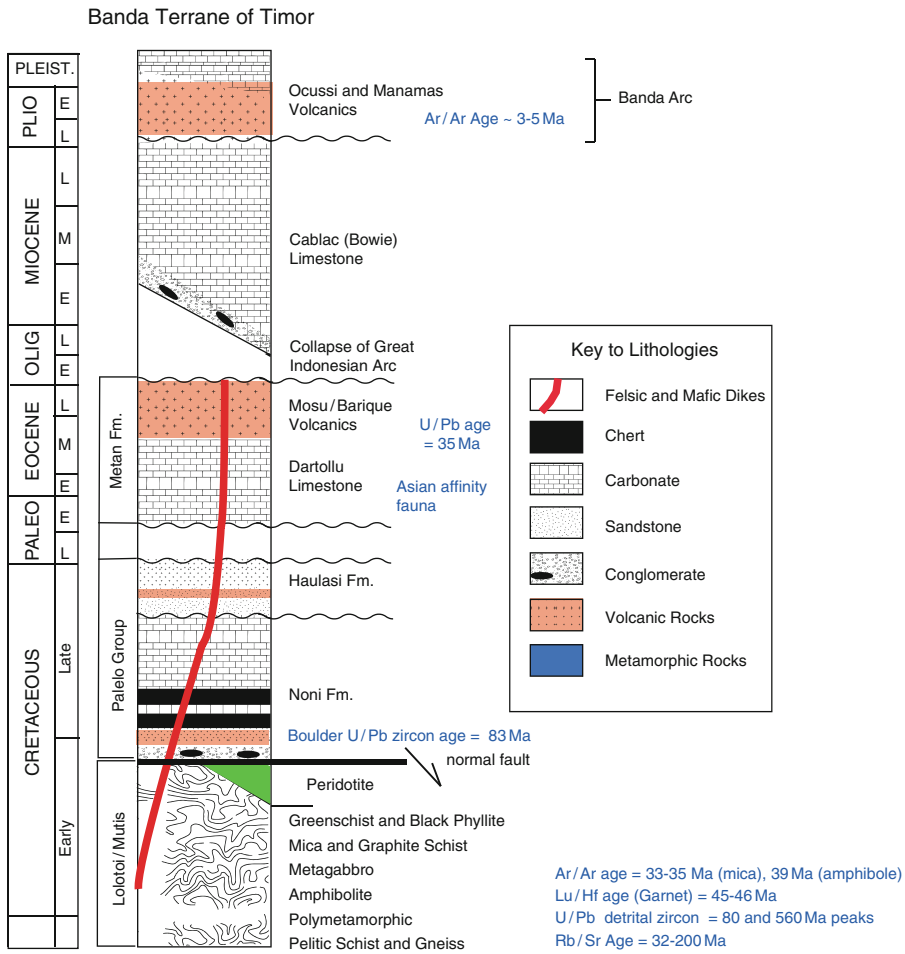

Fig. 7.9 Lithologies and ages of the Banda Terrane (Banda forearc). Modified from Harris (2006).

the high degree of block dispersal and mixing, intense viscous strain, hydro-fracturing, mix of fossil assemblages and perhaps most significant, its lack of any synorogenic sedimentary features. A thick layer of deep marine chalk (see Batu Putih Formation below) overlies the Banda Mélange in many places. The chalk uniformly yields planktic foraminifera of stage N18 (5.6–5.2 Ma) and indicates water depths near the lysocline (>3 km) (Roosmawati and Harris 2009). These data indicate that the mélange was being covered with chalk near the trench and during the earliest stages of arc–continent collision. The common occurrence of mélange beneath the Banda Terrane also extends it from near the surface at the trench into the subduction channel where it can mix with mantle material and blocks of much higher temperature and pressure conditions moving up the channel (e.g. Shreve and Cloos 1986). Even in the northern most exposures of the mélange, where it would have been in deeper parts of the channel, the clay matrix is not metamorphosed indicating a very flat trajectory into the subduction zone.

The part of the Banda Mélange that is overlain by the Batu Putih Formation can be traced from exposures onshore to the accretionary ridge offshore that forms in front of the Banda Terrane upper plate (Harris et al. 1998). Offshore seismic reflection profiles across the ridge show chaotic reflectors immediately beneath well-bedded sediments (Harris et al. 2009). Wells drilled through this contact confirm that it consists of pelagic chalk deposits overlying mélange with a variety of block types encountered in the wells (Audley-Charles

1968; Harris et al. 1998, 2009). The accretionary ridge collapses to the south where it is underthrust by the Australian continental margin south of Savu. Where this occurs the surface slope of the ridge decreases dramatically from 6° to 2° causing the deformation front to bulge southward by more than 100 km (Harris 1991). The collapse opened several slope basins (Fig. 7.7) in this part of the accretionary wedge, which are well documented by marine geophysical studies by van der Werff (1995).

Extensional collapse of the orogenic wedge early in its collisional history explains the ubiquitous layer-parallel extension in the mélange, its close association with diapirism and the overlying pelagic chalk (Harris et al. 1998). The contact between the mélange and overlying chalk is ubiquitously irregular due to diapirism and remobilization of the scaly clay. It is difficult to interpret this contact as sedimentary in origin. Also, massive submarine landslides, such as olistostomes, are notably lacking in seismic reflection profiles or sonar images of the seafloor throughout the Banda Arc (Breen et al. 1986; Masson et al. 1991). In some ways the collapse of the orogenic wedge mimics a mega-landslide, but the fundamental processes are associated with weakening of the décollement at the base of the accretionary wedge by overpressured mudstones of the underthrust Australian continental margin. The relationships are much more consistent with highly overpressured mud "blowing out" of the subduction channel as seen in seismic reflection profiles across the deformation front (Breen et al. 1986).

7.3.2 Upper Plate: Banda Arc–Forearc Complex

The Banda Arc formed due to subduction of Cretaceous to Jurassic age oceanic lithosphere attached to an irregular-shaped continental margin. The combination of these factors resulted in a strongly arcuate pattern of trench retreat that opened supra-subduction zone ocean basins. In the case of the Banda Arc, and many other subduction zones like it, if the upper plate cannot move or keep pace with a retreating trench, it must stretch by internal extension and magmatism (Elsasser 1971; Schellart et al. 2002). The young north and south Banda Sea ocean basins in the upper plate separate highly attenuated ridges of continental and arc material pulled away from the pre-existing continental arc (Harris 2006). The ocean basins opened from NW to SE (Honthaas et al. 1998; Hinschberger et al. 2001) as the Banda Trench retreated into the large continental embayment west of New Guinea (Fig. 7.10). The direction of trench retreat is recorded by the SE migration of active volcanism in individual volcanoes of the Banda Arc producing linear hot-spot tracks with the active volcanoes at the eastern edges of the tracks (Fig. 7.1). Additional bending of the northern part of the Banda Arc may have involved oroclinal bending associated with left lateral shear with the Pacific Plate (Silver et al. 1985). These variable directions of trench retreat produced a spoon-shaped subducting slab (Hamilton 1979).

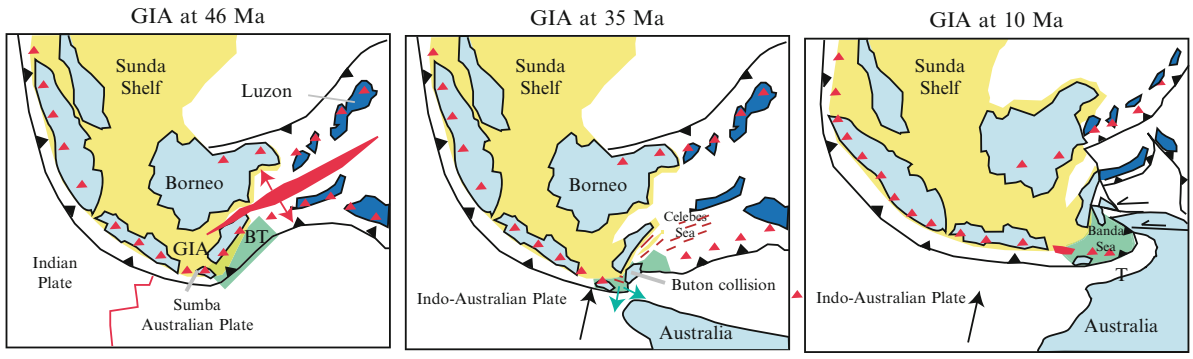

Fig. 7.10 Reconstruction of the collapse of the Great Indonesian Arc (GIA), opening of the Banda Sea, dispersal of the Banda Terrane (BT - green) and development of the Banda Arc (from Harris 2006). Red lines - active rifting, Red triangles - active volcanism, T - Timor.

The orogenic loop of the Banda Arc and other orogens is interpreted in various ways that emphasize buoyancy forces (Dewey 1988), asthenospheric escape (Flower et al. 2001) and plate kinematics (Dilek and Harris 2004), such as the combination of northward convergence of Australia and westward convergence of the Pacific plate to produce the bend in the eastern Banda Arc (e.g. Silver et al. 1985). However, Schellart and Lister (2004) show that although each of these geodynamic processes may contribute, the dominant mechanism for the progressive out-bowing of most arcs is slab rollback, which is also most consistent with data from the Banda Arc.

Examples of other orogenic systems comparable to the Banda Arc are the Yukon–Koyukuk Arc of northern Alaska (Harris et al. 1987), the Carpathian, Betic–Rif, Tyrrhenian, and Aegean arcs of the Mediterranean region (Harris 1992; Royden 1993; Milsom et al. 2001), and the Scotia and Caribbean arcs of the western Atlantic (Schellart and Lister 2004). Each of these orogens has collapsed toward an unconstrained margin associated with subduction zone rollback (Malinverno and Ryan 1986; Doglioni et al. 1999a and b). Space created in the wake of the collision zone is filled with highly attenuated continental and arc crustal fragments embedded in new oceanic lithosphere, which produces a composite marginal basin.

Several continental and arc fragments are scattered throughout the Banda Sea, such as the NEC-Lucipara Ridges, which form the northern boundary of the South Banda Basin, and the Wetar Ridge, which forms its southern boundary. Geochemical and geochronological analysis of samples dredged from both of these ridges on either side of the South Banda Basin show strong affinities suggesting that they once formed a single magmatic arc that was split by the opening of the South Banda Basin (Honthaas et al. 1998). The southern part of the South Banda Basin is now being overthrust by the Wetar Ridge along the Wetar Thrust, which takes up some of the convergence between the Australia and Asia plates (Silver et al. 1983; Genrich et al. 1996; Nugroho et al. 2009). Loading associated with the Wetar Thrust may explain the anomalous depth versus young age of the South Banda Basin.

Fragments of the Wetar Ridge and southern Banda Sea ocean floor that are incorporated into the Banda Orogen are known as the Banda Terrane (Harris 1992). The Banda Terrane is exposed in situ in Sumba and on Timor as nappes thrust over partially subducted Australian continental margin lithologies (Harris 1991). The nappes are part of the Banda forearc that was uplifted by duplexing of the Gondwana Sequence beneath it. The uplift and exposure of sections of a forearc due to continental underthrusting provides a rare opportunity to observe the composition of forearc basement still attached to an active arc, and reveal how forearc nappes are emplaced onto continents or destroyed in suture zones.

7.3.2.1 Banda Terrane

Oceanic lithosphere is commonly inferred to occupy the forearc of intra-oceanic arc systems. However, the Banda forearc includes large fragments of arc-derived meta-sediment that were intruded by arc-related plutons and metamorphosed during another life as part of the Great Indonesian Arc. The lack of oceanic lithosphere in the forearc and occurrence of arc rocks at its southern edge attests to a significant amount of subduction erosion (e.g. Scholl et al. 2008). The forearc fragments are known as the Banda Terrane (Audley-Charles and Harris 1992). The Banda Terrane consists mostly of a mix of pelitic and mafic metamorphic rocks consisting of gneiss, schist and greenstone (Lolotoi Complex of East Timor and Mutis Complex of West Timor) that is structurally overlain by Cretaceous to Miocene sedimentary and volcanic cover units (Fig. 7.9). The cover units are remnants of a Cretaceous-Early Tertiary forearc succession (Palelo Group and Metan Formation), which is depositionally overlain by Oligocene-Miocene massive limestone (Bowie Limestone).

Petrologic analysis of the Lolotoi/Mutis metamorphic complex indicates a mostly Cretaceous sedimentary origin with deposition of inter-layered volcanogenic and pelitic sedimentary successions (shale-greywacke) and arc-related volcanic deposits (basalt to basaltic andesite compositions). Provenance interpretations obtained from various geochemical discriminant diagrams from these rocks indicate mixed MORB and volcanic arc affinities for the igneous units and intermediate to mafic continental and oceanic arc sources for the sedimentary successions (Harris 2006; Standley and Harris 2009). The protolith studies point to a proximal forearc basin setting on the southern edge of the eastern Great Indonesian Arc

before it collapsed to form the Banda Sea floor and current Banda Arc.

Protolith age estimates are obtained from Rb/Sr and U/Pb age analyses. The Rb/Sr ages from 12 whole rock samples of pelitic schist and gneiss found throughout the Mutis Complex of West Timor (Earle 1981) yield a poorly defined isochron with maximum and minimum ages of 200 to 32 Ma (Harris 2006). Detrital zircons from para-amphibolite of the Lolotoi Complex in East Timor yield U/Pb ages as young as 82 Ma, which provides a maximum deposition age for the metamorphic protolith (Harris 2006). The age distribution has spikes at 663, 120 and 87 Ma, which is typical for the Great Indonesian Arc of Asia, but very different from Australian affinity lithologies (see above).

Metamorphism of the Mutis and Lolotoi Complexes is attributed to subduction zone processes occurring beneath the arcward part of the forearc basin. Various mineral assemblages yield pressure-temperature estimates of 5–10 kbar and 530–680°C, which resulted in upper greenschist and amphibolite facies metamorphism (Brown and Earle 1983; Sopaheluwakan et al. 1989; Standley and Harris 2009). The age of peak metamorphism is well constrained at 45–46 Ma by Lu–Hf age analysis of garnet (Standley and Harris 2009), which was followed by rapid uplift based on $^{40}Ar/^{39}Ar$ cooling ages for hornblende of 39 Ma and biotite of 34 Ma (Harris 2006).

The sedimentary and volcanic units faulted down against the Mutis and Lolotoi Complexes consist of a distinctive basal unit of Aptian–Turonian radiolarian chert with interbedded tuffaceous clastics, volcanic units and carbonate (Haile et al. 1979; Earle 1983). This succession is unconformably overlain by a conglomerate with metamorphic and felsic igneous clasts, quartzite and chert. One of the andesitic cobbles in the conglomerate overlying the Lolotoi metamorphic rocks yields an U/Pb age of 83 Ma with Jurassic xenocrysts.

Late Cretaceous turbiditic successions and Paleogene tuffs and lavas overlie the conglomerate. The volcanic rocks consist of agglomerates with a tuffaceous matrix, pyroxene basalt and andesite lavas, and andesitic and dacitic tuffs (some associated with ignimbritic eruptions). Geochemical analysis of these volcanic rocks and those with volcanic protoliths in the metamorphic complexes uniformly indicate subduction-related affinities with overlap of the two different groups on most discriminate diagrams (Standley and Harris 2009). Samples of the same age from Sumba (Lytwyn et al. 2001) along with dredge samples collected from the Wetar Strait north of Timor (Harris 1992) and the South Banda Basin (Honthaas et al. 1998) also show overlap (Standley and Harris 2009). An age determination from a dacitic volcanic unit yields a mean U/Pb age of 35 Ma, with one zircon core of 67.8 Ma (Harris 2006).

Closely related to the volcanic rocks is a distinctive Eocene carbonate that includes calcirudites with volcanic clasts and a pure microfaunal assemblage with characteristic large foraminifera. These fauna are only found in low latitude, shallow marine environments of Sundaland and some Pacific islands (Lunt 2003).

A major hiatus in deposition occurs throughout the Oligocene (Carter et al. 1976), which is also found in wells drilled throughout the Sunda Shelf region (Curray 1989). The hiatus is also coincident with exhumation of the Lolotoi and Mutis metamorphic complexes. By Oligocene time the metamorphic rocks had reached the surface and were unconformably overlain by basal conglomerates and limestone of the Oligocene to mid-Miocene Bowie Limestone.

The Bowie Limestone (formerly the Cablac Limestone) of West Timor consists of hard, commonly massive units of calcilutite, oolitic limestone, calcarenite, and intra-formational breccia, agglomerate and tuffaceous units that are well exposed on or around Banda Terrane klippen in West Timor. Identical units are also found associated with the Mata Bia and Cablac massifs of East Timor, (Fig. 7.5) which is why the limestone was initially named the Cablac Limestone by Audley-Charles (1968). However, rocks of Triassic age also make up some of the Cablac Massif (Haig and McCartain 2007), so the name of the unit has been changed to the Bowie Limestone (Haig et al. 2007). At the base of the Bowie Limestone is a distinctive conglomerate, first reported by T'Hoen and Van Es (1926) in West Timor and is also reported from the Mata Bia massif in East Timor (Harris 2006), which consists of clasts from older Banda Terrane units, such as polymetamorphic pelitic schist and a range of volcanic and some plutonic clasts, Eocene *nummulites* fragments and large Oligocene foraminifera embedded in a carbonate matrix. Near the top of the Bowie Limestone in West Timor are an increasing abundance of ash layers interbedded with Middle Miocene marl (Carter et al. 1976). These deposits

may document the birth of the subaerial Banda Arc (see below), which yields Late Miocene ages from nearby arc volcanics in Wetar and Alor (Abbott and Chamalaun 1981; Elburg et al. 2005).

Exhumation of the metamorphic basement of the Banda Terrane was assisted by normal faults that juxtapose various Cretaceous to Eocene cover units with the Eocene metamorphic rocks. This tectonic scenario is consistent with apatite fission track model ages that indicate cooling below 120°C during the Oligocene, then renewed burial into the partial annealing zone until rapid Pliocene–Pleistocene uplift (Standley and Harris 2009).

Late Miocene to Pliocene opening of the Banda Sea further fragmented the Great Indonesian Arc and transported the Banda Terrane southward and eastward until it became captured in the forearc of the Banda Arc. Collision from Early Pliocene to the present has uplifted much of the Banda Terrane, which is one of the few places on the planet where large sections of the forearc of an active arc are exposed. The uplift of the metamorphic rocks from the partial annealing zone of apatite was so recent that no new fission-tracks are found.

Structural analyses and observations of contact relationships (Standley and Harris 2009) show that during tectonic emplacement, the Banda Terrane was thrust over Gondwana Sequence units of the Australian continental margin as indicated by extensive outcrops of mélange and broken formation at the structural base of the Banda Terrane (see mélange above). This phase of deformation is recorded in the Banda Terrane by parallelism between the orientations and transport directions of structurally underlying Gondwana Sequence and the latest phases of deformation of the Banda Terrane (Standley and Harris 2009). Duplex stacking of Gondwana Sequence units beneath the Banda Terrane uplifted it from a forearc basement position to higher than 2,500 m elevation in places. Erosion has removed much of the likely continuous metamorphic terrane leaving only isolated klippen with similar orientations of structural features (Harris 2006).

Due to the obliquity between the Australian continental margin and the Banda Trench, allochthonous thrust sheets of the Banda Terrane in Timor can be traced laterally along orogenic strike to autochthonous units in the present forearc of the westernmost Banda Arc island of Sumba (Harris 1991). Forearc basement exposed in Sumba is traceable eastward along the submarine Sumba Ridge (Reed et al. 1986) to the mostly flat-lying thrust sheets of Banda Terrane in Timor (Fig. 7.5). Various structural expressions of the Banda Terrane are found along orogenic strike and provide a rare glimpse of progressive modes of forearc nappe emplacement during an active arc–continent collision.

7.3.2.2 Ophiolite?

Mafic and ultramafic bodies associated with the Banda Terrane are commonly reported as a dismembered ophiolite, but no characteristic ophiolite sequence is found, neither is an age or compositional relationship demonstrated for the assortment of fragments that are documented (Harris and Long 2000). It is not clear which of the mafic and ultramafic bodies are part of the upper plate Banda Terrane or the most distal edge of the lower plate Australian continental margin. Lherzolitic and gabbroic bodies identical in composition to those found intruding the Aileu Complex (see above) are dredged from the distal Australian continental margin (Nicholls et al. 1981). These bodies were emplaced and exhumed during continental breakup and in Timor are now thrust back over the continental margin during Latest Miocene to Pliocene arc–continent collision.

The best candidate for a supra-subduction zone ophiolite is the 3–5 Ma Ocussi volcanic pile on the north coast of West Timor, which structurally overlies the Gondwana Sequence (Harris 1992). However, nothing more than pillow basalt and sheet flows overlain by Pliocene forearc sedimentary successions are found. These steeply dipping volcanic units have $^{40}Ar/^{39}Ar$ ages (3–5 Ma) and supra-subduction zone (SSZ) geochemical characteristics similar to dredge samples from other parts of the southern Banda Sea Basin (Harris 1992). A similar body of pillow basalt with SSZ characteristics also occurs near Baucau in East Timor (Standley and Harris 2009). Ultramafic blocks in mélange at the base of both of these nappes are geochemically depleted with an estimated 20–25% partial melting (Harris and Long 2000). Based on these relations, the Ocussi and Baucau volcanics are interpreted as the emergent tip of part of the SSZ ocean basin that formed within the eastern Sunda Arc in a similar way to the southern Banda Basin.

Another possible subduction-related ultramafic body is the fault-bounded Hili Manu lherzolite of central East Timor. Nd and Sr isotopes, REE and associated harzburgite of this ultramafic body show similar patterns to other ultramafic bodies with known supra-subduction zone crustal affinities (Falloon et al. 2006). Based on these new data it is possible that the gabbro and lherzolitic bodies along the north coast of Timor and even those found within the Banda Terrane may be associated with rifting of south Banda Basin immediately before or during collision initiation.

Several lines of evidence indicate that the most recent phase of extension of the Banda Basins was synchronous with the arrival of the Australian continental margin at the Java Trench and the onset of arc–continent collision. For example, the first part of the Australian continental margin to accrete to the edge of the southern Banda Basin, the Aileu Complex, yields reliable $^{40}Ar/^{39}Ar$ metamorphic cooling ages of around 5 Ma (Berry and McDougall 1986), which overlap those of the South Banda Basin. These concordant ages indicate that the distal part of the Australian continental margin had already accreted to the edge of the Asian plate, and cooled from 600 to 350°C, around the same time as the Banda Basins were opening and forming new oceanic lithosphere. The synorogenic sedimentary record of Timor (see below) also dates the initial emergence and erosion of the Banda arc–continent collision at around this time (Audley-Charles 1986; Fortuin and de Smet 1991). These relations are consistent with those documented for other arc–continent collisions like in Oman where supra-subduction zone ophiolites have ages that overlap those of its tectonic emplacement over continental margins (Harris 1992).

Although the Banda Terrane was probably emplaced over the continental margin of Australia in a similar way to Oman-type ophiolite nappes its composition is more akin to a composite forearc terrane. It inherits its metamorphism and early deformational history from its previous life as part of a proximal forearc basin of a continental arc. The composition and age relations of the Banda Terrane do not fit the conventional model for oceanic lithosphere constituting the basement of intra-oceanic forearcs. Age and compositional relations are mixed. Most of the forearc formed and was metamorphosed during an event distant in time and space from the Banda Orogen, while the Ocussi Volcanics show a direct relationship with the arc–continent collision it is incorporated into. Other places where similar relations to the Ocussi body may occur is in the Weber Basin, which is a forearc region along orogenic strike to the east that consists of oceanic lithopshere >7,000 m deep (Bowin et al. 1980). Parts of the Weber Basin are uplifted in the hinterland of the Banda Orogen near Tanimbar and represents a large ophiolite in the initial stages of emplacement onto the Australian continental margin, an ophiolite as large as any known (Harris 1992).

7.3.2.3 Banda Volcanic Arc

The Banda volcanic arc is an extension of the eastern Sunda Arc, both of which are considered intra-oceanic volcanic arcs mounted on mostly oceanic crust (Fig. 7.1a). Both arcs formed by subduction of Indian Ocean floor. However, the Banda volcanic arc is younger (0–8 Ma, Honthaas et al. 1998; Elburg et al. 2005), due to its association with opening of the Banda Sea, and is contaminated by subduction of continental material. The contamination causes some of the most extreme compositional variation known from island arcs, including everything from tholeiitic through calcalkaline and shoshonitic to leucititic compositions. It also manifests the widest range of K_2O values and lowest He^3/He^4 ratios known (Wheller et al. 1987). These variations result from mixing of peridotitic and contaminated mantle with continental material in the source region. Both spatial and temporal geochemical variations are observed that relate directly to lateral variations in composition and structure or the "nature" of the lower plate subducting beneath the arc (Whitford et al. 1977, 1981; Whitford and Jezek 1979; Hilton and Craig 1989; Hilton et al. 1992; Vroon et al. 1993; van Bergen et al. 1993).

The spatial transition from parts of the arc that are not contaminated by continental crust and those that are, happens around Iya Volcano in central Flores (Fig. 7.1b). Although there are exceptions to this, such as non-contaminated volcanoes to the east and some that are contaminated to the west, central Flores marks the current position of the main westward propagating continental contamination front.

A notable exception to this pattern is found in Sumbawa (Fig. 7.1b) where recent shoshonitic to high-K volcanoes yield higher Pb and He isotopic values than the low-K volcanoes surrounding them or

lavas from earlier eruptions (Elburg et al. 2004). The Sumbawa segment of the volcanic arc is adjacent to the Sumba segment of the collision, which has evolved in a different manner than the Timor region (see Sumba below). Contamination of the Sumbawa volcanoes is predicted by models for the evolution of the Sumba segment of the Banda Orogen resulting from subduction of the Scott Plateau continental prong ahead of the arrival of continental crust into immediately adjacent parts of the arc (Harris 1991; Keep et al. 2003; Fleury et al. 2009).

Tracking continental contamination of the arc through time is possible in the parts of the volcanic arc that are deeply eroded due to shifts in the position of active magmatism, such as in Wetar Island (Fig. 7.1) north of central Timor and Ambon Island near Seram. The earliest signs of contamination are found in cordierite- and garnet-bearing rhyolite and dacite lavas in Ambom (ambonites) and Wetar. These volcanics yield reliable $^{40}Ar/^{39}Ar$ ages of around 5 Ma (Elburg et al. 2005). This age is consistent with a 4.9 Ma $^{40}Ar/^{39}$ age for volcanic rocks with clear evidence of continental contamination reported by Scotney et al. (2005). The most contaminated volcanics on Wetar yield a $^{40}Ar/^{39}$ age of 2.4 Ma (Herrington et al. 2011) indicating increased contamination through time.

These age and geochemical data indicate that continental contamination started at least by around 5 Ma near Wetar and has swept westward to its present position in central Flores. The contamination front also spread eastward from Wetar (e.g. Whitford et al. 1977; Elburg et al. 2005) where volcanoes become progressively less contaminated toward Banda Island (Fig. 7.1b). In a similar pattern to that of continental contamination, cessation of volcanism along the axis of the Banda Arc started at Wetar (<2.4 Ma) then progressed to Romang (<1.7 Ma) and Alor (<1.3 Ma) to the east and west, respectively (Fig. 7.1b).

Since the cessation of volcanism in the Wetar segment of the arc new volcanic centers have risen out of the Banda Sea north of Wetar, Alor and eastern Flores (Fig. 7.1). Active volcanism in this region is enigmatic because it happens above a deep part of the Benioff zone. However, compositionally the samples collected from these 0–0.4 Ma volcanoes are very similar to slightly contaminated volcanic rocks of Wetar, with the exception of high Mg values (Schwartz et al. 1984). The fact that continental contamination is detected in these new volcanoes is difficult to explain unless the continent is taking a very shallow trajectory into the subduction zone and has shifted or re-established the asthenospheric wedge 90 km to the north of the Benioff zone (Harris 2003). The Wetar volcanic ridge is shifted 45 km to the north of the main axis of volcanism along strike slip faults imaged on the sea floor off the west coast of Wetar (Breen et al. 1989a, b).

The location of the abandoned segment of the arc and its high levels of continental contamination is consistent with many other lines of evidence that demonstrate collision initiated in the Central Timor/Wetar region and therefore more continental crust is subducted there than any other part of the Banda Orogen (Harris 1991). The youngest volcanic rocks in Wetar present an end-member of extreme continental contamination among studied volcanic arcs worldwide with $^{87}Sr/^{86}Sr$ ratios as high as 0.7223, $^{206}Pb/^{204}Pb$ ratios as high as 19.6, $^{143}Nd/^{144}Nd$ ratios as low as 0.5195 and He^3/He^4 ratios much lower than normal (2.0 average). These anomalous compositions require the incorporation of large amounts of subducted continental sediment into the magma source regions of these volcanoes (Vroon et al. 1993; Elburg et al. 2005; Scotney et al. 2005).

Much of the compositional variation in the volcanic rocks can be traced directly to the composition of sediment entering the subduction zone. Lead isotope variations, and trace element abundances in the volcanic rocks parallel variations found in the sediment dredged from the seafloor entering the trench (Vroon et al. 2001). Incompatible trace-element ratios in these volcanics, such as K/Rb and La/Th, are unique among island arcs (Vroon et al. 2001). Common trace elements used to detect a subduction component, such as the Nb and Ta anomalies, can be traced directly to similar anomalies found in the sediment entering the subduction zone (Vroon et al. 1993).

Bulk mixing calculations by Vroon et al. (1993) indicate that the amount of the subducted continental material increases along the Banda Arc from 0.1% near the northward bend in the arc (Island of Manuk, Fig. 7.1b) to as much as 5.0% toward the central Timor/Wetar region. The composition, age and thickness of sediment entering the subduction zone also vary depending on the structure of the continental margin. For example, greater amounts of contamination by Proterozoic and Paleozoic sedimentary rocks is

detected where the Bonaparte Gulf Basin is subducting (Vroon et al. 1993), which is one of the only basins containing thick sections of these sediments on the NW continental margin of Australia (Harrowfield and Keep 2005). The large of amount of subducted sediment in the Banda Orogen provides a modern analog for how subducted sediment can produce mantle heterogeneities, such as the EMII anomaly found in ocean-island basalts (e.g. Ben Othman et al. 1989).

Continental contamination of arcs may also play a previously unrecognized role in mineralization. The economic Au–Ag–Hg-bearing barite units mined on the island of Wetar are related to Pliocene (4.7–2.4 Ma) pumping of marine hydrothermal fluids through fracture networks that vented onto the seafloor as smoker systems (Scotney et al. 2005). The timing of this event is coincident with the first evidence of contamination of the subduction system by continental crust.

7.3.3 Banda Orogen Sequence

The subduction of the Australian continental margin beneath the Banda Arc produced a submarine orogenic wedge that is overlain by synorogenic sedimentary successions known as the Banda Orogen Sequence (Fig. 7.11). The sediments most likely unconformably overlie the Banda Mélange, but the contact is irregular due to remobilization of the scaly clay. Unconformities are found with most other units from both the

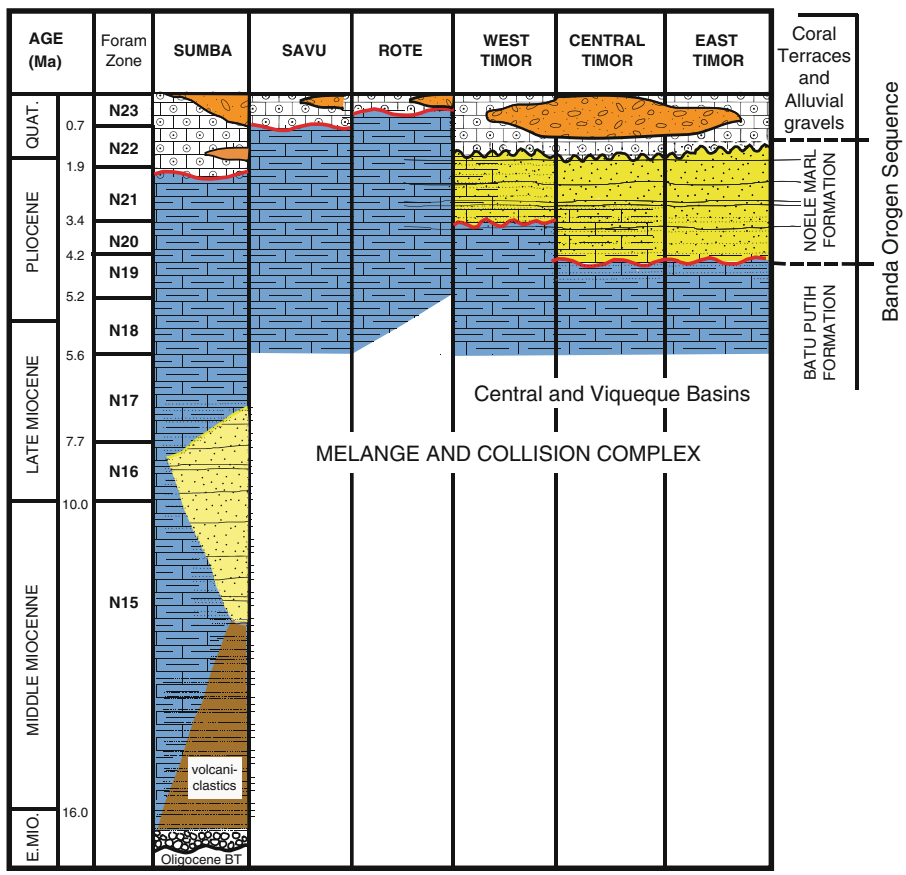

Fig. 7.11 Spatial and temporal distribution of Banda Orogen Sequence synorogenic sedimentary rocks from East Timor to Sumba. Changes in lithofacies and depth of deposition through time indicate the arc-continent collision propagated westward along the Australian passive margin from East and Central Timor to Rote, and along the eastern edge of the Scott Plateau from Sumba to Rote. The Noele Marl Formation is most likely currently being deposited in offshore basins of Rote and Savu. Modified from Roosmawati and Harris (2009).

Australian continental margin and the Banda Arc, which form the Banda orogenic wedge. The basal unit of the Banda Orogen Sequence is a distinctive pelagic chalk succession, which documents the birth of the accretionary prism and much of its uplift history. These are overlain in places by turbidites shed from the first land created by the rise of the orogenic wedge above sea level. As the orogen emerged close to sea level it was encrusted in coral reefs and locally buried by fluvial gravels that form the uppermost units of the sequence.

The basal unit of the Banda Orogen Sequence is known as the Batu Putih Formation (Audley-Charles 1968), which consists of a few hundreds of meter thick massive, foraminifera-rich calcareous pelagite and chalk deposits with some calcilutite and vitric tuff horizons. The depositional environment is consistent with deep, low energy, open sea conditions of the Banda forearc with no terrigenous input in the basal section and some mica and metamorphic rocks fragments in the upper section (Haig and McCartain 2007). The basal contact between the Batu Putih Formation and underlying accretionary wedge is poorly defined. In the type location it is interpreted by Haig and McCartain (2007) as unconfomable. However, it is very irregular in places. In many places the contact is highly disturbed by remobilization of mélange.

Detailed biostratigraphic age analyses by Haig and McCartain (2007) of the type location of the Viqueque Group in East Timor yield ages of Neogene foraminifera zone N18 for the basal Batu Putih Formation. This age corroborates those obtained by Kenyon (1974) from the type locality of the Batu Putih Formation in the Central Basin of West Timor. The earliest sign of turbidite deposition within the Batu Putih Formation is during N20 (4.2–3.35 Ma). The youngest age of the Batu Putih Formation varies westward from N19 (5.2–4.2 Ma) in East Timor (Haig and McCartain 2007) to N20 (4.2–3.4 Ma) in western-most Timor (Kenyon 1974) to N22-N23 (1.9–0.7 Ma) in Rote and Savu (Roosmawati and Harris 2009), and is latest Pliocene in Sumba (Fig. 7.11).

Overlying the Batu Putih Formation in Timor is the Noele Marl Formation, which consists of calcilutite and marl interbedded with turbiditic sandstone, and tuffaceous material (Fig. 7.11). These deposits become more clastic-rich up section, and the clasts also coarsen upwards. The clasts are dominated by metamorphic rock fragments. The oldest turbidites of the Noele Marl Formation ranges in age from N21 (3.35 Ma) in East Timor (Haig and McCartain 2007), to N22 (4.2–0.7 Ma) in West Timor. The absence of the Noele Marl in Rote, Savu and Sumba (Fig. 7.11) indicates that these islands are at different stages of collisional evolution than Timor. During the time of Noele Marl Formation deposition in Timor, Batu Putih Formation pelagic deposits were deposited on the accretionary ridge (Savu and Rote) and in the forearc basin (Sumba) to the west. The lack of turbidite deposition in the synorogenic rocks exposed on these islands indicates that they are the first parts of the orogenic wedge in these regions to emerge above sea level and experience erosional exhumation, which happened much earlier in Timor (Roosmawati and Harris 2009).

The upper part of the Banda Orogen Sequence consists of the Quaternary Baucau (coral limestone) Formation and the Ainaro (gravel) Formation (Audley-Charles 1968). These two units are commonly interbedded along the coast and represent the emergence to sea level of the Banda orogenic wedge (coral) and uplift and erosion (gravels) of the islands mostly during the Quaternary (Fig. 7.11). Both of these units are uplifted and form marine and fluvial terraces throughout Timor and other islands that are locally warped by ongoing deformation (see Uplift History below).

7.3.3.1 Synorogenic Basins and Foredeep

The Banda Orogen Sequence accumulates to thicknesses of >3,000 m in slope basins that formed during the collapse of the accretionary wedge shortly after initial underthrusting of the Australian Continental Margin (Figs. 7.12 and 7.13). Sonar mapping of the seafloor and seismic reflection profiles show that most of these basins are half-grabens with top-down-to-the-south basin bounding faults (van der Werff 1995). Some strike-slip faults are also found that may link many of these basins to pull-apart structures (Mark Quigley, Brendan Duffy and Myra Keep, personal communication). Some of the basins also manifest structures that suggest some tectonic inversion during collision, but generally most basins show few contractional structures (Fig. 7.13). Much of the deformation within the basins originally interpreted as shortening (Kenyon 1974) is disturbed mostly by local diapiric movement of the underlying Banda Mélange.

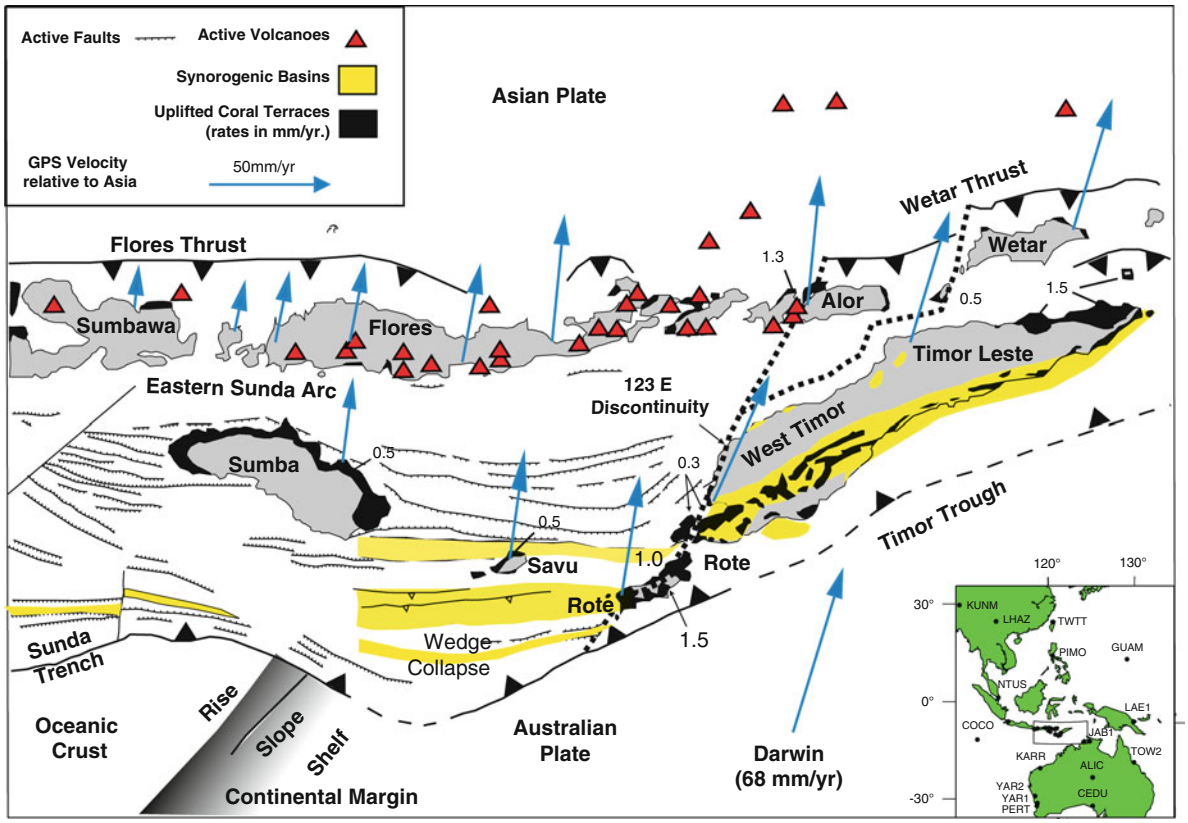

Fig. 7.12 Neotectonic map of the Timor Region showing active faults, active volcanism, surface uplift rates and GPS velocities. Velocities are plotted relative to Asian reference frame (see stations on *inset* map). Synorogenic basins open during collapse of the accretionary wedge east of Sumba and are uplifted due to subduction of the Australian continental margin. Uplift rates vary throughout the region and correlate best with proximity to active faults. Sea floor structure from van der Werff (1995). Uplift rates from Cox et al. (2006). GPS velocities from Nugroho et al. (2009).

The Banda Orogen Sequence progrades into the 3 km deep Timor Trough, which is a classic example of an under-filled collisional foredeep. Drilling data from DSDP 262, which was drilled 400 m into sediments in the Timor Trough, indicates a yield of mostly pelagic ooze, containing nannofossils, foraminifers, and radiolaria overlying Pleistocene age shallow water shelf strata (Veevers et al. 1974). The pelagic sediment documents the rapid subsidence of the Australian Shelf as it flexes downward from near sea level to enter into the Timor Trough. Modeling of the flexure indicates an effective elastic thickness of 25 km (Lorenzo et al. 1998) and only 200 m of forebulge uplift. This contrasts with an effective elastic thickness of 11 km for the China continental margin as it bends beneath the Taiwan arc–continent collision (Ma and Song 2004). However, unlike Taiwan, a foreland basin has not yet developed in the Banda Orogen. The difference may be related to the greater rigidity of the Australian continental margin, which is more than 100 Ma older than the China margin, and the lack of source sediment coming from the Australian continent.

7.4 Initiation of Collision

When collision initiated in the Banda Orogen depends upon how "collision" is defined. Most commonly the time of collision initiation is interpreted as the age of: (1) the youngest material accreted from the subducted continental margin, (2) the oldest synorogenic deposits, (3) metamorphism of continental margin lithologies, and (4) continental contamination and extinction of the volcanic arc.

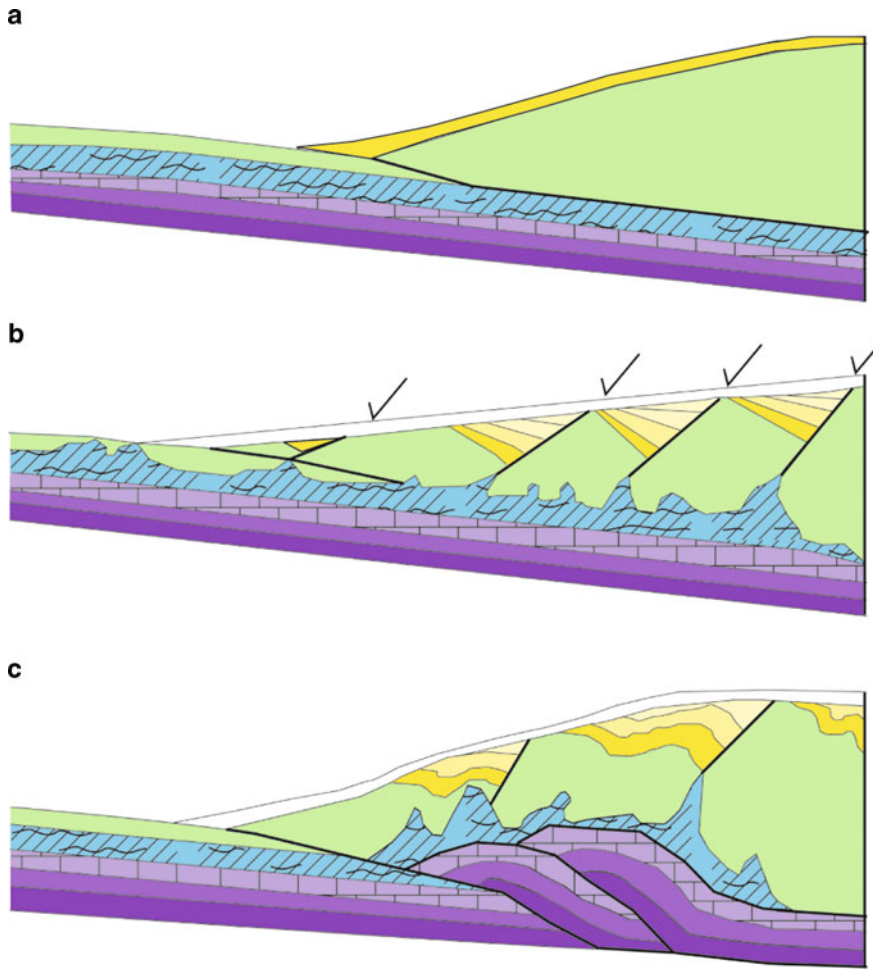

Fig. 7.13 Idealized structural evolution of accretionary wedge collapse south of Savu. (**a**) pre-collisional geometry with slope angle of 5–6°. Green is accretionary wedge and mélange overlain by Batu Putih formation pelagic chalk (*yellow*). (**b**) Underthrusting of continental margin with highly over-pressured Cretaceous and Jurassic mudstone (*blue*) weakens décollement causing collapse of the accretionary wedge to the south, opening of synorogenic slope basins, diapirism and collisional mélange development. Surface slope decreases to 2–3°. (**c**) Development of Gondwana Sequence duplex (*purple*) uplifts the orogenic wedge and may cause mild inversion of slope basins.

7.4.1 Youngest Passive Margin Lithologies

If collision is distinguished from subduction by underthrusting of continental versus oceanic lithosphere, then where collision is initiating in the Banda Arc is easy to pin point by where the distal most edge of the Scott Plateau is entering the Java Trench south of Sumba (Fig. 7.1). However, due to the obliquity between the Australian continental margin and the trench the age of collision, and the irregular shape of the continental margin, collision initiation varies along orogenic strike. In older parts of the Banda Orogen evidence for collision initiation, according to this definition, may be constrained by identifying the youngest continental margin lithologies that were accreted to the deformation front. However, identifying these lithologies can be difficult because as the continental margin approaches the accretionary wedge both are overlain by the same sedimentary units. Ideally the age of collision initiation could be bracketed across

an angular unconformity where the youngest known continental margin rocks of the accretionary wedge are unconformably overlain by undeformed synorogenic deposits close to the same age. However, these types of relations are difficult to constrain.

The youngest distinguishable continental margin units incorporated into the Banda Arc accretionary wedge form an imbricate stack that is partially exposed along the south coast of Timor (Audley-Charles 1968; Rosidi et al. 1979) and in Savu and Rote (Harris et al. 2009; Roosmawati and Harris 2009). The best exposures are in the Kolbano Mountains along the cross-strike Oetuke River in West Timor (Fig. 7.6). This drainage exposes a southward-verging imbricate stack of at least 21 separate thrust sheets consisting mostly of slope and rise facies pelagic lithologies that range from Upper Jurassic Tithonian to Lower Pliocene Zanclian stage (Sawyer et al. 1993). Unconformably overlying the imbricate stack are successions of Pliocene chalk and calcilutite of foraminifera stage N18-19 (5.6–4.2 Ma). The youngest units of the Australian Passive Margin Sequence found to date in East Timor yield ages of 8 Ma (Keep and Haig 2010).

7.4.2 Oldest Synorogenic Deposits

The oldest synorogenic deposit is calcareous pelagite at the base of the Batu Putih Formation (Kenyon 1974; Audley-Charles 1986; Haig and McCartain 2007), which yields ages of (N18, 5.6–5.2 Ma). Locally, Late Miocene calcilutite and tuffaceous lithologies are found at the base of the chalk (Kenyon 1974; Haig and McCartain 2007) that may represent the earliest pre-collisional synorogenic deposits. The first turbidite in the Batu Putih Formation (N20, 4.2–3.35 Ma) and those that define the Noele Marl Formation (N21, 3.35–1.9 Ma) document the emergence of the Timor Island above sea level and the initiation of erosional exhumation. As mentioned earlier, the age of this transition decreases to the west where in Rote and Savu there is no record of it at all, but is likely happening offshore of these islands (Roosmawati and Harris 2009). These ages document the rise of the orogenic wedge from pelagic depths of >3,000 m to the surface between 5.6 and 4.2 Ma in East Timor and later to the west.

7.4.3 Metamorphic Cooling Ages

There are two distinct metamorphic complexes exposed throughout the Banda Orogen: the Asian affinity complexes of the Banda Terrane, which were metamorphosed ~40 m.y. prior to the Banda Orogen (see 7.3.2.1 above), and the Australian affinity Aileu Complex. The age of metamorphic cooling of the Aileu Complex was investigated initially by Berry and Grady (1981) who report K/Ar ages for biotite and white mica of 5.4–5.7 ± 0.2 Ma and amphibole ages of 7.7–16.5 Ma. Nearly identical ages were produced by Berry and McDougall (1986) using $^{40}Ar/^{39}Ar$ methods. However, only one white mica age yields an acceptable plateau age (5.36 ± 0.05 Ma). Reanalysis of these data using ISOPLOT yields unacceptable MSWD values (>60) for inverse isochron plots for every age determination except the one white mica age (Major et al. 2009). Therefore, there is only one reliable age of metamorphism for the Aileu Complex, which indicates that it experienced metamorphic cooling to around 420°C (closure temperature of white mica, Kirshner et al. 1996) at 5.4 Ma.

The age of exhumation of the Aileu Complex is further constrained by fission-track analyses of apatite grains (Harris et al. 2000). Nearly all of the fission-tracks are highly to completely annealed, which indicates a low-temperature exhumation age of <4 Ma. These ages are also consistent with plate reconstructions (Hall 2002; Roosmawati and Harris 2009) of when the NW Australian continental margin arrived at the collision zone (Fig. 7.4).

7.4.4 Arc Contamination and Extinction

The age of arc extinction is commonly used as an indicator of collision initiation, but in the Banda Arc it is obvious that volcanism continued after collision initiation and still may not have ceased completely. The deeply eroded Wetar to Alor section of the arc is not active currently and the youngest volcanic rocks are 2.5 and 1.3 Ma, respectively (see Banda Arc above). However, there are lavas on these islands that show ^{238}U-^{230}Th disequilibrium that limits their age to <350,000 years (Vroon et al. 1993). There is

also a line of active volcanoes north of the Wetar-Alor segment that are similar in composition to the Banda Arc (Schwartz et al. 1984). Dredge samples from a submerged seamount in this region yield ages of 0.4 Ma (Morris et al. 1984). There is abundant evidence from multiple sources that arc–continent collision initiated in the Wetar to Alor segment of the arc significantly earlier than volcanism ceased (see above). It is also important to note that there are well-documented inactive segments of the Sunda Arc to the west that are not related to collision. For example, there is a 200 km long extinct segment of Sunda Arc in central Java. For these reasons it is advisable to reconsider how arc volcanism is modified by collision (Vroon et al. 1993).

The age of continental contamination of the Banda Arc provides a minimum age of collision initiation that would be at least 2 m.y. too young due to the time it takes for the edge of the continent to reach the depths of arc magma generation. Evidence for contamination shows up in volcanic rocks of Wetar as early as 5 Ma (Scotney et al. 2005), which is consistent with other minimum ages of collision initiation mentioned earlier. The Wetar segment of the Banda volcanic arc is also offset northward from the rest of the arc by 40 km. Instead of ramming into the accretionary wedge as in Taiwan, the Banda volcanic arc is accreting to the lower plate and moving mostly with it along the Wetar Thrust to the north of the arc (see Fig. 7.12). These geochemical and structural modifications to the volcanic arc are adjacent to the oldest part of the collision based on other indicators, such as the position of the Aileu Complex, highest topographic relief and oldest synorogenic sedimentary rocks.

Unlike Taiwan, volcanism is still active in most parts of the collision zone in the Banda Orogen. The West Timor to Sumba section of the collision, which is at least 3 m.y. old, is adjacent to the active, but contaminated volcanoes of Flores Island and those between Flores and Alor. A similar situation is found in the Wetar to Alor arc segment where continental contamination of arc volcanics is found as early as 5 Ma, but arc volcanism persisted on Wetar until at least 2.5 Ma (Scotney et al. 2005) and may be still active. East of Romang the active volcanism is part of the collision zone that stretches nearly all of the way to Seram (Fig. 7.1).

7.4.5 Summary

The above indicators of collision initiation in Timor converge at a Latest Miocene age (< 8 Ma). Taking into account the lag times between collision initiation and (1) emergence and erosion of the orogen at 4.2 Ma, (2) metamorphism and later metamorphic cooling to 420°C at 5.3 Ma, and (3) continental margin underthrusting (< 8 Ma) and eventual contamination of the volcanic arc at Wetar by at least 5 Ma, the collision initiated south of Wetar at around 8 Ma. The age of collision initiation young's to the west towards Rote Island, but initiated earlier in Sumba due to the Scott Plateau protrusion.

7.5 Tectonic Features of the Banda Orogen

Due to the Scott Plateau protrusion the Banda Orogen is shaped by two arc–continent collisions. The first is the arrival of the NW Australian continental margin to Banda Trench at around 8 Ma in the central Timor/Wetar region. This collision propagated to the west in a time-space equivalent manner to just beyond Rote Island. Its propagation to the east is only constrained by the eastern propagation of the contamination front. The second collision is the arrival of the Scott Plateau at the Sunda Trench at around 3 Ma to form the Sumba Ridge. This collision propagated from Sumba to the SE through Savu to Rote Island (Harris et al. 2009; Roosmawati and Harris 2009). Both of the collisions merge in the Rote region to form the western Banda Orogen.

Serial sections through the collision reveal various orogenic phases of collision propagation (Fig. 7.15). These include, (1) the birth of Savu Island above the Savu Thrust and collapse of the accretionary wedge south of the Island, (2) deformation along a lateral ramp in Rote, (3) development of the Gondwana Sequence duplex beneath the Banda Terrane in West Timor, (4) folding, uplift and detachment (?) of the Banda Terrane tectonic lid, (5) forearc closure and cessation of volcanism in central Timor, (6) forearc sinking, arc accretion and northward translation adjacent to

Wetar, (7) strong coupling of the lower plate creating an oblique-slip extensional system (East Timor), and exhumation of metamorphic rocks (East Timor).

7.5.1 Sumba Ridge: Collision with a Continental Plateau

The most vivid expression of the initiation of collision in the Banda Orogen is the abrupt uplift of the Sunda forearc basin from 5 km below sea level to the surface to form the island of Sumba. Sumba Island is the emergent part of the Sumba Ridge (Fig. 7.4), which stretches in a NW-SE direction from the distal continental margin of Australia under the Sunda trench and forearc all of the way to the volcanic arc. The Sumba Ridge uplifts the Sunda Trench and forearc by at least the same amount as the 2–3 km difference in bathymetry between the Scott Plateau and the Jurassic oceanic crust that surrounds it. The Sunda Trench becomes the Timor Trough at this point. However, an additional 20–30 km of shortening in the region or a thicker crust is needed to lift Sumba up from its forearc basin origins to the surface and expose its basement rocks. Gravity data from Sumba (Chamalaun et al. 1981) indicate that whatever the uplift mechanism is, it must involve continental-type crust, which underlies the forearc basement exposed at the surface.

The Sumba Ridge also indents the Sunda Arc and shifts it around 30 km northward near the island of Sumbawa (Fig. 7.1). The indentation is accommodated by slip along the Flores Thrust, which has propagated over 300 km to the west near Lombak Island and nearly the same distance to the east. The volcanoes in the region of the indentation are contaminated with continental crust and include the explosive giant of Tambora.

The Sumba Ridge is likely the expression of the subducted NE edge of the Scott Plateau (Harris 1991; Keep et al. 2003), which arrived at the Sunda Trench at around 3 Ma (Fig. 7.4). Subduction of the Scott Plateau presents an end member of arc–continent collision of semi-buoyant thinned continental lithosphere with only a thin veneer of cover sediment. The initial stages of collision in the Sumba region are even characterized as that of a seamount asperity forcing wedge taper adjustments of shortening followed by extension (Fleury et al. 2009).

The collision of the Scott Plateau is also manifest in the volcanic arc and backarc region. Volcanoes above where the Scott Plateau is subducted show evidence of recent continental contamination (see Volcanic Arc above) to the west of the main contamination front, which is in central Flores. Adjacent to this region in western Flores arc volcanism has ceased.

7.5.2 Transition from Subduction to Collision: Uplift and Shortening of the Forearc

Where the Scott Plateau intersects the deformation front the Sunda Trench becomes the Timor Trough and manifests many structural features not seen in the accretionary prism to the west. Differences in the way incoming material is accreted is described by Breen et al. (1986). In the Sunda Trench the thin sedimentary cover blanketing the Indian Ocean seafloor is picked up by horizontal propagation of short décollements into small, accreted slices that shorten along closely spaced thrusts and conjugate strike-slip faults. Seismic images of the accretion zone show chaotic reflections interpreted as mélange. Where the Scott Plateau enters the Timor Trough (between 120°40′ E and 121°, Fig. 7.1b) Breen et al. (1986) report décollements propagating up to 15 km south of the thrust front into significantly thicker sections of incoming layered successions allowing for the accretion of long slabs of lower plate material (Fig. 7.6). The length/thickness ratio of these thrust sheets is more like what is found in fold-thrust zones. The thrust front is well defined by a vertical separation along faults and folds 2–4 km long that occur throughout the lower slope. Mud diapirism is also seen for the first time and produces ridges of mud volcanoes south of the thrust front in the lower plate that are sourced from the décollement. The décollement is traced as a strong to moderate reflector into what is interpreted as Cretaceous shale (Reed 1985; Karig et al. 1987). Exposures of this unit in Timor show that it is actually a mudstone composed of expandable clays (see Banda Mélange above) that overlie pre-rift Gondwana Sequence cover sediment of the Australian continental margin.

Another difference in the deformation pattern between subduction in the Sunda Trench and collision in the Timor Trough is the partitioning of strain away from the deformation front in the later. In the Sunda Trench a sharp boundary is found between the lower and upper slope of the accretionary wedge (Karig et al. 1987; Breen et al. 1986). Seismic reflection and sonar data show that this boundary marks the northern limit of the deformation front where recently accreted sediments are disturbed. In most places along the Sunda Trench this boundary is 20–30 km from the deformation front, with no evidence of any deformation in parts of the arc-trench system beyond this narrow zone. This observation implies that in the Sunda Trench most of the convergence between Indo-Australia and SE Asian Plates occurs at very high strain rates within only the lower slope region of the accretionary wedge, which is consistent with the abundance of mélange generated in this zone. The only other site of convergence in the zone of subduction is the Flores Thrust to the north of the Sunda volcanic arc. However, it is most likely a product of subduction of the Scott Plateau and its impingement on the Sunda volcanic arc.

Distribution of strain away from the deformation front due to underthrusting of the Scott Plateau south of Sumba involves: (1) initiation of northward-verging thrust systems (Flores and Savu thrusts), (2) shift of shallow seismicity away from the trench into the forearc and backarc, (3) uplift of the forearc basin (Sumba) and ridge (Savu), (4) abrupt widening of the accretionary wedge by >100 km, (5) formation of top-down-to-the-south half graben slope basins, and (6) extensive mud diapirism. Features 1–3 may relate to increased coupling due to positive buoyancy of the underthrust continental plate. Features 4–7 are most likely caused by adjustments of the accretionary wedge to basal décollement weakening as over-pressured Australian continental slope units enter the trench (Harris et al. 1998).

7.5.3 Savu: Initiation of the Retro-Wedge Thrust System and Fore-Wedge Collapse

Savu Island emerged from the sea at around 0.8 Ma where it was encrusted with coral terraces (Harris et al. 2009). The coral terraces are tilted to the south away from active thrust fault near the north shore (Fig. 7.7). Erosional windows through the coral terraces reveal that Savu is composed mostly of Triassic to Jurassic Gondwana Sequence with some Cretaceous Australian Passive Margin Sequence that are stacked by thrust faults (Harris et al. 2009). The thrust sheets are up to 2 km thick and verge to the south in the southern part of the island and to the north near the north shore (Fig. 7.7). Along the north coast and immediately offshore are splays of the active Savu Thrust, which offset uplifted coral terraces on shore and rupture all of the way to the surface in several places offshore (Harris et al. 2009). The island is part of the ENE-WSW Savu-Rai Jua Ridge that corresponds to a rift basin of the same orientation within the Scott Plateau lower plate and the position of the Lombak forearc accretionary ridge on the upper plate. Analysis of foraminifera within synorogenic deposits reveal that the accretionary ridge at Savu was uplifted from depths of 2.5 km below sea level to the surface between ~1.5 and 0.7 Ma, which is also when the NE edge of the subducted Scott Plateau arrived beneath Savu (Fig. 7.4).

The SSE dipping Savu Thrust forms where the rear of the accretionary wedge ramps up over the uplifted edge of the Banda forearc basement. Its orientation and that of most other thrusts and fold axes on the island parallels the ENE-WSW structural grain of NW Australian continental margin rift basins (Fig. 7.3). Even before the Australian continental margin arrives at the Timor Trough some of its rift basins are inverted to form anticlines with fold axes oriented parallel to east-northeast–west-southwest rift basins (Dore and Stewart 2002). In many ways, the Savu–Rai Jua ridge can also be considered an inverted rift basin of the Scott Plateau. Bedding attitude measurements throughout Savu show a dominantly ENE-WSW strike, which is also the orientation of fold hinge lines and thrust faults (Fig. 7.3). These observations show that the pattern of deformation in Savu during the earliest phases of arc–continent is more strongly influenced by structural inheritance than NNE plate convergence, which would produce fold axes and thrust faults that strike WNW. This same pattern persists into more advanced stages of collision. South of Timor, the thrust front also rotates to parallelism with the structural grain of the northwest Australian continental margin (Fig. 7.1).

One of the most unique features of the transition from subduction to collision is the abrupt change in surface slope angle of the accretionary wedge from 6° to the west at the Lombak Ridge to around 2° south of Savu. The collapse of the accretionary wedge to the south is like a massive submarine slump that opens rift basins in the upper slope and causes mud-cored folds and thrusts at its toe (Figs. 7.12 and 7.13). The mega-slump is most likely caused by décollement weakening associated with underthrusting of highly over-pressured Jurassic to Cretaceous mudstone (see Banda Mélange above). In many ways the structure of the accretionary wedge south of Savu is similar to the structure of the slumping sedimentary wedge of the northern Gulf of Mexico.

7.5.4 West Timor: Anatomy of the Collision Revealed

Traveling from west to east on the only paved road through the island of Timor is like climbing up through an enormous plunging antiform. On the west coast all that is exposed are coral terraces encrusting the most recently uplifted part of the WSW propagating Banda Orogen. Below the coral veneer is a thick section of synorogenic deposits of the Central Basin (Fig. 7.5) that document rapid uplift of the accretionary wedge from depths of >3 km to the surface during the past 3 Ma (Kenyon 1974; De Smet et al. 1990). Further to the east and deeper into the antiform is a landscape that is a chaotic mix of two very different worlds (Fig. 7.5). To the north are the steep spires of deeply eroded Asian affinity rocks of the Banda Terrane. To the south are piles of dismembered thrust sheets of Gondwana Sequence. Between the two is a block and scaly clay mélange, which is a chaotic mixture of the rocks on either side.

Erosional windows through the Banda Terrane reveal that it structurally overlies the mélange and Gondwana Sequence. The mélange formed as part of the original subduction channel at the base of the Banda Terrane that was eventually clogged by and included parts of the Gondwana Sequence. The Gondwana Sequence is folded and thrust, but not enough structural relief is available to make out the pattern of deformation. However, the repetition of Permian to Jurassic successions indicate that it is detaching near the base of the Permian and is overlain by a roof thrust above which the rest of the Cretaceous to Tertiary section (Australian Passive Margin Sequence) is found.

To find the Australian Passive Margin Sequence requires braving the tortuous dirt roads to the Kolbano Mountains along the south coast of West Timor. The lower part of the Oetuke River exposes an astonishing section of at least 24 imbricate thrust repetitions each around 200–300 m thick of Early Cretaceous to Late Tertiary slope and rise deposits (Figs. 7.6 and 7.7). The thrust sheets are deformed mostly by fault-propagation folding with the thrust faults truncating the overturned forelimb. The structural relief increases upstream until at its headwaters the river breaches the basal décollement in the Wai Luli Formation. North of this point mostly only Gondwana Sequence lithologies are exposed in what is interpreted as a thrust duplex (Harris 1991).

In the northern part of West Timor uplift and erosion exposes several large massifs of the Banda Terrane along strike of the submerged Sumba ridge to the west that is exposed in Sumba. These nappes cover much of the Gondwana Sequence duplex that varies in structural relief beneath them making it difficult to establish any lateral continuity of the underlying structure. The erosional level is such that the subduction channel beneath the Banda Terrane nappes is well exposed in several key places. It shows evidence of high fluid pressures associated with hydrofracturing of both lower and upper plate blocks along a basal and roof décollement that may have been active simultaneously. Traction along the basal shear zone of the channel pulls continental material deeper into the channel while at the same time material is plucked from the structurally overlying Banda Terrane roof thrust, which may explain the strongly attenuated nature of these nappes.

South of the Gondwana Sequence duplex zone the Banda Terrane is tilted southward and even extends to the south coast of the island in East Timor where it was penetrated by wells (Audley-Charles 1968). North of the duplex the Banda Terrane nappe is tilted steeply northward and is likely detached from its roots and carried by backthrusts over itself (Fig. 7.5). The best example of northward back tilting is the steepening to vertical dips of alternating pillow basalt and sheet flow

layers of the Occusi nappe on the north coast of West Timor (Fig. 7.5).

7.5.5 East Timor: Fall of the Forearc and Rise of the Hinterland

The one paved road through Timor enters East Timor (Timor Leste) along the north coast of the central part of the island where two new features appear on the eastern horizon. The closest is a large mountain range (Aileu Range) of metamorphic rocks of the Australian affinity Aileu Complex. The other feature is the deeply eroded Banda volcanic arc island of Alor. Only 30 km separates the coast of Alor from the western-most north coast of East Timor. Between the two is the nearly 3 km deep Wetar Strait. The Wetar Strait is the site of the Wetar Suture proposed by Price and Audley-Charles (1983) to explain the narrow gap between the Banda volcanic arc and Australian continental margin material. They inferred a large fault that ruptured through the entire Australian Plate and moved it over the forearc. The location of the thrust at the base of the north-facing slope of the accretionary wedge (Fig. 7.14) is confirmed by seismic reflection profiles across the Wetar Strait (Breen et al. 1989a, b; Snyder et al. 1996). However, it is not known whether the fault ruptures through the entire lithosphere or connects with the basal décollement like a more advanced stage of the Savu Thrust (Fig. 7.7).

Additional confirmation of the northward motion of the orogenic wedge is provided by structural field mapping of the Aileu Complex (Prasetyadi and Harris 1996). These studies locate several top-to-the north thrust faults near the north coast of East Timor and a switch to top-to-the-south motion near the crest of the Aileu Range (Fig. 7.14).

The metamorphic fabric of the Aileu is characterized by an initial flattening (S0 = S1), which is overprinted by an axial planar foliation (S2) associated with isoclinal and nearly recumbent folds with generally top-to-the-south vergence. Berry and McDougall (1986) suggest that mica in the Aileu Complex records the age of S2 (~6 Ma). Rf-ϕ analysis of quartz grains yield a nearly horizontal prolate ellipsoid with the long (x) axis oriented N-S (Fig. 7.14). These features are overprinted by low-angle generally top-to-the-north thrust faults in the northern part of the range and top-to-the-south thrust faults in the central and southern parts of the range (Fig. 7.14). The last phase of deformation is the development of high-angle normal faults with an array of orientations, but predominately top-down-to-the-north sense of shear along the north coast.

The structure of the Aileu metamorphic complex documents an initial layer-parallel extensional phase most likely associated with compaction and perhaps even a rift-related thermal event associated with passive margin development. A close association with rifting is indicated by a series of enigmatic intrusions of lherzolite and gabbro bodies (Fig. 7.14) into mica schist mostly in the western part of the Aileu Complex (Prasetyadi and Harris 1996). The later layer-parallel shortening phase is most likely associated with arc–continent collision. Subsequent brittle deformational phases document uplift by retro-wedge motion to the north and extensional exhumation.

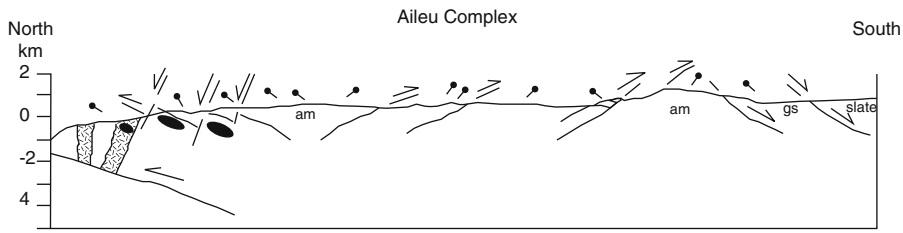

Fig. 7.14 Cross section across the Aileu Complex near the border of West and East Timor (modified from Prasetyadi and Harris 1996). See Fig. 7.5 for location. Stippled areas are mafic and ultramafic intrusions. Abbreviations for metamorphic grade: am – amphibolite facies, gs – green schist facies. Ellipses are in the x–z plane and show relative amounts of strain and direction of stretching from Rf-ϕ analysis of quartz grains. Normal faults are the youngest features and cross cut northward verging faults near the intrusions and accommodate exhumation on the southern part of the complex. The Laclo Fault is similar to these top-down-to-the-south normal faults, but with some left-lateral strike-slip motion.

7.5.5.1 Where is the Banda Forearc?

Retro-wedge motion along the Wetar Suture is used to explain the progressive closure of the Banda forearc north of Timor (Price and Audley-Charles 1983; Harris 1991). What happens to the forearc, and in many cases the arc complex as well, during arc–continent collision is poorly understood. If the thrust in the Wetar Strait completely over-rides the northern Banda forearc basin then the forearc basement should be beneath Timor. If this is the case then it would produce a gradually decreasing gravity high from the north coast toward the center of the island (Zobell 2007). However, what is observed is perhaps the steepest gravity gradient known that increases sharply from the north coast but does not extend south beneath Timor (Zobell 2007). Modeling this pattern from a combination of detailed gravity measurements across central Timor (Chamalaun et al. 1981) and regional data (Kaye 1990) predicts a geometry very different from those proposed by Price and Audley-Charles (1983) and Harris (1991, 2003). The most viable way to reasonably reconcile the predicted and observed gravity values is to subduct the majority of the forearc with the Australian lower plate. A similar solution to is also presented by Richardson and Blundell (1996) for gravity data collected east of Timor.

7.5.5.2 Structure of the Gondwana Duplex

At the same time as the forearc is sinking into the subduction zone the adjacent hinterland of the orogenic wedge is rising. Enough uplift and erosion has occurred in Central Timor to expose the lower Gondwana Sequence duplex that structurally underlies the Banda Terrane roof thrust. Although structural studies of this package of rocks are hampered by lack of good biostratigraphic data, there are a few key marker units for identifying various stratigraphic intervals, such as the distinctive Triassic limestone of the Aitutu Formation. The Aitutu Formation is repeated several times in N-S transects along drainages through the Ramelau Range (Fig. 7.8). Most of the repetition is associated with abrupt breaks in stratigraphy that both dip and face upward to the NNW indicating thrust versus fold repetition. Fault-propagation folds are observed at wavelengths of up to 1–2 km (Fig. 7.8). The overall pattern of deformation is one of ENE-WSW striking folds and thrusts.

Space considerations require that there are likely multiple levels of detachment within the Gondwana Sequence that produce multiple duplex zones. For example, in Savu a duplex of upper Gondwana Sequence forms in front of the Banda Terrane nappe while the lower section of the Gondwana Sequence that is exposed in northern Timor is inferred to stack up beneath it (Fig. 7.8).

7.5.5.3 Late-Stage Oblique-Slip Normal Faulting

The general pattern of ENE-WSW folds and thrusts is disturbed by normal faults with significant amounts of oblique slip that crosscut the Gondwana Sequence duplex . These faults are only now being recognized on shore in places where they down-drop thick sections of the Banda Orogen Sequence (synorogenic deposits) and juxtapose them against much deeper structural levels. Perhaps the largest of these structures is the Laclo Fault, which was first recognized by Berry and Grady (1981). This fault dips at a moderate angle to the south and juxtaposes the upper parts of the Gondwana Sequence duplex against amphibolite to granulite facies sections of the Aileu Complex. More recent studies of the fault recognize kinematic indicators that vary from top-down-to-the-south to left-lateral strike-slip motion along the fault. The Laclo River separates the Laclo Fault zone and its thin hangingwall of Gondwana Sequence to the north from the largest Banda Terrane massif on the island (Fig. 7.5), which is most likely preserved due to top-down-to-the-south faulting on the Laclo Fault. The oblique-slip nature of these faults may reflect the increased coupling between the Banda Orogenic wedge and the Australian continental margin. A series of NE-SW left-lateral wrench faults formed at around 3 Ma in parts of the Australian continental margin near the Timor Trough (Clough et al. 2000).

7.5.5.4 Eastern East Timor Plateau

East of the Aileu Complex the north coast of Timor displays two very important features that help interpret the evolution of arc–continent collision. The first is large section of ultramafic rocks associated with mélange that structurally overlies the Gondwana Sequence duplex and exposes the subduction channel that these rocks entered (Harris and Huang 2010). The

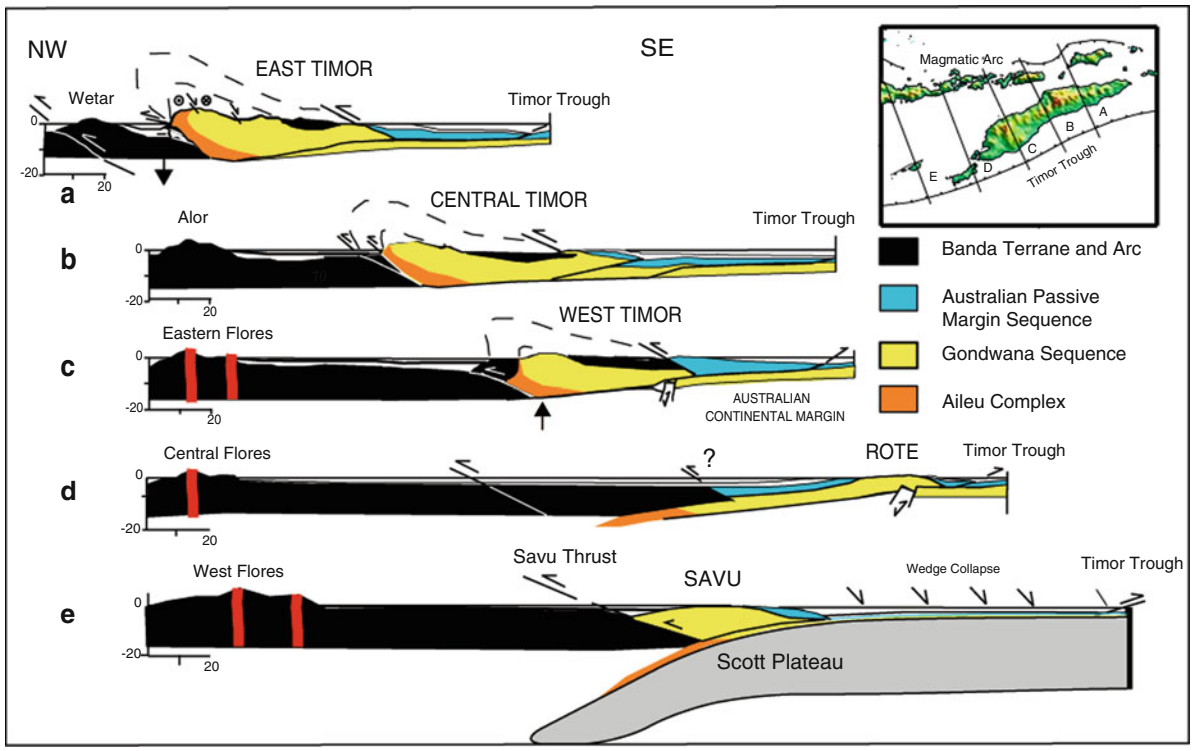

Fig. 7.15 Serial sections through the Banda arc-continent collision from East Timor (**a**) to Savu (**e**). Initiation of retrowedge thrust (Savu Thrust) and collapse of overcritical wedge south of Savu. Shortening of subcritical wedge in Rote begins progressive northward translation of the Timor Trough as coupling increases with the Australian lower plate. In Wetar the arc is also translated northward as it couples with the lower plate. Active volcanism (*red lines*) ceases in Alor and Wetar, but is still active during collision in C–E. In the Timor region the southern edge of the forearc is folded and uplifted as a passive roof thrust by accretion of Australian continental margin cover units beneath it. North of Timor progressive closure of the forearc requires it to sink into the subduction zone (downward arrow). Maximum coupling with the lower plate in East Timor results in mostly left-lateral oblique extension.

second feature is an unprecedented series of uplifted coral terraces that rise to a high plateau over 600 m above sea level. At least 25 individual terraces are found in some places, and most of them are warped into what may be ENE-WSW trending anticlines and synclines that intersect the north coast of Timor at oblique angles (Cox et al. 2006). The warping of the terraces demonstrates active deformation in the region over the past 0.1 Ma.

7.5.6 Uplift History

Investigating the pattern of uplift throughout the Banda Orogen provides a way to test a fundamental unresolved question about the geodynamics of collisions generally. The question is about how much uplift is due to crustal shortening versus lithospheric scale processes, such as buoyancy of subducted continental lithosphere, and delamination or tearing off of the oceanic slab. Crustal shortening is documented throughout the Banda Orogen, and enough material has been brought into the orogenic wedge over the past 8 Ma to fill all of the space needed to account for its size and topography. However, much of the incoming sediment may have subducted and not accreted. One test of crustal shortening versus slab-tear is the longevity of uplift. If most of the uplift is from shortening during collision propagation then there should also be a pattern of *sustained* uplift that young's in the direction of collision propagation to the west and east, which is what is observed. In contrast, a pulse of rapid, simultaneous uplift throughout variously shortened parts of the orogen followed by no uplift would be more consistent with a whole

lithosphere process. The rate of uplift through time is also a key to distinguishing between these two mechanisms or the relative contributions of each.

The emergence of several islands throughout the Banda Orogen over the past few million years provides a rare glimpse of the temporal distribution of vertical strain in an active arc–continent collision over time scales of 10^3 to 10^6 years. Multiple proxies for measuring both *surface* and *rock* uplift rates are available including the rates of sediment discharge, thermochronology of metamorphic rocks, depth versus age relations from benthic and planktic foraminifers in synorogenic deposits, rates of patterns of uplift from flights of coral terraces and other geomorphic features such as stream asymmetry.

7.5.6.1 Erosion Exhumation and Sediment Discharge

The Banda Arc provides the rare opportunity to measure both *rock* and *surface* uplift rates throughout the same orogen. This comparison provides a way to test the significance of erosional or tectonic exhumation in young mountain systems. It is commonly assumed that erosional exhumation positively correlates with total annual precipitation or rates of uplift, which is manifest by high amounts of sediment discharge in streams. However, measurements of sediment discharge in Seram and Timor are markedly different even though these islands of similar size and shape have nearly identical uplift patterns, topography, geomorphology, rock types, and basin catchment size (Cecil et al. 2003). The only other major factor controlling sediment discharge that may account for differences in sediment discharge on these islands is climate.

The Banda Arc straddles two different climate zones and provides a natural laboratory for testing the extent that climate may control rates of erosional exhumation (Harris et al. 2008). The southern part of the Banda Arc (Timor) is seasonal and has a lengthy, 8-month dry season with around 1,300 mm/a of rainfall during its short rainy season. The northern Banda Arc (Seram) is perhumid with little to no dry season. During some months Seram receives up to 600 mm of precipitation, with a total of 3,250 mm/a. However, even though the total amount of rainfall in Seram is nearly three times that of Timor, sediment discharge in Timor during its short rainy season is more than 27 times that of the annual sediment discharge in Seram. Timor annualized sediment concentration is 0.7×10^6 metric tons/km^3 of water discharged. This value is 60% of that of the Ganges/Bramaputra River system (Cecil et al. 2003).

These data are consistent with other indicators of sediment discharge rates found in Seram and Timor. The rivers of Seram are characterized by meandering, acidic blackwater with exceedingly low solute and suspended-sediment concentrations, but with significant amounts of terrestrial organic matter. They also have limited fluvial bed loads, primarily as point bars, which diminish downstream into estuaries without sediment fill derived from fluvial systems. The coastal regions where the rivers discharge are mud-dominated, sediment-starved, host large stands of mangrove and have few, if any coral reefs. In contrast, the rivers of Timor are braided from the mountains to the coast where sedimentation keeps pace with rising sea level to produce deltas. Riverbed sediment is dominated by cobbles and pebbles with lesser amounts of sand-size material, which also characterizes the beaches. The coastlines are mostly estuary and mangrove free and have thick encrustations and large build-ups of coral.

With most other factors nearly equal, it is evident that seasonality of climate, not total amounts of precipitation is the major controlling factor of erosional exhumation in the Banda Arc (Cecil et al. 2003). The protracted dry season in the Timor region results in less vegetative cover and higher rates of sediment run off into streams. Higher rates of erosional exhumation in Timor may explain why deeper structural levels are exposed there compared to Seram.

7.5.6.2 Thermochronology

Rock uplift rates for the metamorphic core of the Banda Orogen are inferred from a combination of pressure and temperature estimates, $^{40}Ar/^{39}Ar$ cooling ages, and apatite fission track analyses. Using the only reliable $^{40}Ar/^{39}Ar$ age determination from white mica in the Aileu Complex discussed above (5.3 Ma) along with the pressure and temperature estimates for these rocks (600–700°C and 8–10 kbars, Major et al. 2009) yields a geothermal gradient of around 20–25°C/km and long-term rock uplift rates of around 3 mm/yr over the past 5 m.y. Fission track analyses of apatite grains

in the same rocks show uplift from the partial annealing zone (80–120°C) to the surface in <4 m.y. (Harris et al. 2000). This requires a rock uplift rate of 1-2 mm/yr over the past 4 m.y. The exposure of these metamorphic rocks in the part of the orogen with the most shortening is consistent with uplift caused by crustal shortening associated with extensional and erosional exhumation versus regional lithospheric processes.

7.5.6.3 Foraminifers in Synorogenic Deposits

Synorogenic foraminifera-rich chalk and turbidites provide depth and age constraints for tracking when various parts of the Banda Orogen emerged from an accretionary wedge at pelagic depths to where they are exposed at the surface. Although there is some erosion of these deposits after they reached the surface, the majority of their ascent was in a submarine environment, with little to no erosion. Therefore, the record of vertical movements is interpreted as mostly *surface* versus *rock* uplift.

The Batu Putih Formation chalk at the base of the Banda Orogen Sequence has scarce benthonic foraminifera, but those that are found are characteristic of very deep water (>3 km). Abundant planktonic foraminifer's of biozone Neogene (N) 18 (5.6–5.2 Ma) are partially dissolved indicating water depths near the lysocline (~ 3 km). In early emerging parts of the Banda Orogen the Batu Putih Formation is overlain by turbidites of the Noele Marl Formation, which varies in age along strike from N20 (4.2–3.4 Ma) in East Timor and N21 (3.4–1.9 Ma) in West Timor (Audley-Charles 1986) and Sumba (Fortuin et al. 1997). However, in between the large islands of Timor and Sumba the deep water conditions of the Batu Putih Formation continued until N21 as in Savu (1.9–07 Ma) and N23 (<0.7 Ma) as in Rote (Fig. 7.11).

These data indicate that collision of the Australian continental margin with the Banda Arc initiated much earlier in Timor and Sumba than in Savu and Rote where it has just begun. A rough pattern of westward propagation of uplift exists between East Timor and Rote, and eastward propagation of uplift from Sumba to Savu. The pattern of westward propagation is consistent with underthrusting and shortening of the NE-SW trending part of the Australian continental margin beneath the E-W Sunda Trench. Underthrusting of the Scott Plateau beneath the western-most part of the Banda Orogen explains SE propagation of uplift from Sumba (2–3 Ma) to Savu (1.0–0.5 Ma) and then to Rote (0.2 Ma). Average rates of *surface* uplift of the Batu Putih Formation pelagic deposits during the past 2 m.y. in Rote and Savu are ~1.5 and 2.3 mm/a, respectively (Roosmawati and Harris 2009).

7.5.6.4 Uplifted Coral Terraces

Uplifted coral terraces throughout the Banda orogen reveal how strain is distributed over the past of 10^3 to 10^5 years. U-series age analysis of the lowest coral terraces yields surface uplift rates that vary by almost an order of magnitude from 0.2 to 1.5 mm/a (Fig. 7.12). The pattern of uplift correlates best with proximity to active faults. Merritts et al. (1998) calculated coral uplift rates on the south coast of Rote, which is near the deformation front, of 1–1.5 mm/a. Coral terraces on the north coast of Savu, which are associated with the north-directed Savu thrust system, yield uplift rates at least 0.3 mm/a (Harris et al. 2009). A series of islands along the western edge of West Timor yield uplift rates of 0.2–0.3 mm/a on Semau Island and the adjacent coast of West Timor (Merritts et al. 1998; Jouannic et al. 1988). Both of these sites are part of a linear zone of uplift along the 123° East structural discontinuity. Eastern Sumba has uplifted coral terraces just on its north and east coast at rates as high as 0.5 mm/a (Pirazzoli et al. 1991). A south dipping thrust fault has been mapped offshore of this region (van der Werff 1995). The previously mentioned uplifted coral terraces along the north coast of East Timor may correlate with the retrowedge thrust system imaged by seismic offshore to the north and rates of uplift vary from 0.3 to 1.5 mm/a (Cox et al. 2006). Uplifted terraces on the north coasts of Alor and Wetar (Fig. 7.12) may be associated with uplift along the Wetar Thrust. On Atuaro Island, which is much further from the Wetar Thrust, Chappell and Veeh (1978) measured uplift rates of 0.5 mm/yr. These uplifted terraces are used as evidence for slab tear by Sandiford (2008).

However, most of these flights of coral terraces are warped at short wavelengths. For example, coral terraces are tilted north in Sumba, SSE in Savu, NNW in Rote and generally south along the north coast of Timor. In all of these cases the tilt is away from

zones of active thrusting and folding. In Sumba the forearc is ramping up and over the northern edge of the Scott Plateau along what is most likely a north dipping thrust (Fleury et al. 2009). In Savu the coral terraces form on the back of the accretionary wedge, which is ramping up over the forearc basin on the south dipping Savu Thrust (Harris et al. 2009). In Rote coral terraces form on the front of the accretionary wedge where it is ramping up over the Australian continental margin (Merritts et al. 1996; Roosmawati and Harris 2009). The north coast of East Timor may be uplifted by ramping of the rear of the accretionary wedge over the base of the volcanic arc (Cox et al. 2006). Localized uplift of circular islands surrounded by others with no uplift is also common and may be associated with diapirism (Major 2010). Generally, the pattern of uplift is consistent with short wavelength deformational processes with highly variable rates that correlate with loading rates measured along active faults by GPS.

7.5.7 Active Faults

Active faults in the Banda Orogen are found near where islands emerge and flights of coral terraces are uplifted (Fig. 7.12). The Wetar and Flores Thrusts along the backside of the volcanic arc are well defined on the seafloor and by sonar, seismic reflection studies and shallow seismicity. The amount of slip along the Wetar Thrust is estimated at around 50 km from the size of the fold and thrust belt it has produced (Silver et al. 1986). The fold and thrust belt associate with the Flores Thrust (Silver et al. 1983) decreases in size in both directions away from Western Flores, which implies that it has propagated away from where the arc-trench system was first impacted by the Scott Plateau.

The Savu Thrust within the forearc is recognized as a site of active shortening from several lines of evidence (Harris et al. 2009). Reflection seismic profiles show several active splays of the thrust system breaking the surface of the sea floor. Some of the thrust strands offset uplifted Pleistocene coral terraces along the north coast of Savu. Also, GPS measurements show up to 7 mm/a of strain accumulation across the fault (Fig. 7.12).

Similar relations are found along the Timor Trough where thrust splays cut the seafloor and GPS measurements across the structure document a strain accumulation rate of 21 mm/a. The lack of seismicity at the deformation front has led some to interpret it as inactive. However, thrust mechanism earthquakes throughout the island of Timor document that the basal décollement linked to the Timor Trough is still active and the deformation front has seismic potential (Harris et al. 1997).

The characteristics of the Timor Trough are similar in many ways to the northern part of the Sunda arc-trench system in the Sumatra region where subduction is oblique and the trench is overstuffed with sediment, which is typical of arc-trench systems that produce mega-thrust earthquakes (Scholl et al. 2008). Historical accounts from Dutch outposts in the Banda Islands document earthquakes of this magnitude with tsunami run-ups of 20 m that trace back to the Timor Trough (Major et al. 2008). The bad news is that it has been nearly 200 years since the last recorded event.

Active thrust faults are also imaged breaking through to the sea floor from reflection seismic profiles across the southern edge of the Wetar Strait north of East Timor (Breen et al. 1986; Snyder et al. 1996). These faults extend east at least as far as Kisar Island. Kisar rises up in the middle of the Wetar Strait and exposes the Aileu Complex overlain by several flights of coral terraces with uplift rates of 1.5 mm/a (Major et al. 2010).

The 123° East discontinuity, which stretches from the island of Rote along the western edge of West Timor and into a linear volcanic field west of Alor, has several shallow earthquakes with left-lateral strike-slip fault plane solutions. The fault zone is also imaged in seismic lines off the NW coast of West Timor (Karig et al. 1987). This linear structure most likely represents a transcurrent fault or lateral ramp that separates two segments of the Banda Orogen with differing amounts of shortening and coupling to the Australian plate. Across the discontinuity the forearc rises from around 1,000 m below sea level to >2,000 m above sea level in the mountains of West Timor. Differences in GPS velocities are also observed across the structure (Nugroho et al. 2009).

7.5.8 GPS Measurements

Another way to define where collision initiates and how strain is partitioned in the Banda arc–continent collision is with geodetic measurements. Although

these measurements only record movement over a very short temporal range (decade or less), they correspond very closely with predictions over geological time scales using plate kinematic models, such as NUVEL-1.

The obliquity of collision allows documentation of different strain regimes at various stages of collision development. A series of campaign-style GPS measurements throughout the Banda Orogen over the past two decades (Fig. 7.12) reveal that large sections of the SE Asian Plate are progressively accreting to the edge of the Australian continent by distribution of strain away from the deformation front to newly forming forearc and backarc plate boundary segments (Genrich et al. 1996; Nugroho et al. 2009). These segments or crustal blocks have a nearly uniform GPS velocity field, indicating little if any internal deformation. Each crustal segment of the arc–continent collision is 400–500 km in strike length and moves parallel to the subducting Australian Plate, but at different rates.

West of the collision in the Sunda continental arc nearly all of the 68 mm/a of convergence between the Australian oceanic plate and the Asian continental margin (Tregoning et al. 1994) is taken up within a narrow 30 km wide zone near the Sunda Trench (Stockmal 1983; Sieh et al. 1999). No component of the NNE subducting lower plate is detected on the islands of Java or Bali, which indicates a decoupled subduction system in this region (Nugroho et al. 2009).

East of Bali the consistent pattern of decoupled subduction changes to one of increasing amounts of coupling with the lower plate eastward (Fig. 7.12). This is expressed as movement of arc and forearc islands relative to the rest of the Asian Plate and in the same direction as the lower plate. The first hint of coupling with the lower plate is found on the island of Lombok, which is across the famous "Wallace Line" from Bali. The deep water between these islands that limited faunal migration into the eastern Sunda Arc marks the edge of the Sunda Shelf. At this boundary the *nature* of the crust the Sunda Arc is mounted on changes from continental to transitional or oceanic.

GPS measurements on Lombak and Sumbawa Islands show slight amounts of movement relative to Asia in nearly the same direction as the lower plate and at around 20% of its velocity. Most, if not all, of this movement is taken up along the Flores Thrust, which is shoving the Sunda Arc over transitional backarc crust. The Flores thrust has propagated into this area from the collision with the Scott Plateau 500 km to the east. At face value, these GPS measurements document that collision is initiating in the Lombak region due to its partial movement with the lower plate and the propagation of the Flores Thrust into its backarc. Yet, the Sunda Arc is still a subduction zone in every other way.

The uniform velocity and direction of movement of the Lombak-Sumbawa segment changes at the Komodo Islands, between the Islands of Sumbawa and Flores (Fig. 7.12). Across this 125 km distance the direction and velocity of the upper plate changes so that Komodo Island moves in the same direction as the lower plate, like the rest of the crust to the east, but at a velocity slightly higher than the 400 km long arc segment to the west, but much less than the 400 km long arc segment to the east. In the 30 km of distance between the stations we measured on Komodo and Flores Islands the percentage of movement with the lower plate jumps from 25% to 40% (Nugroho et al. 2009). The fact that the upper plate is moving more with the lower plate is not surprising since there is other compelling evidence of collision in this region, such as the uplift of the forearc basin and ridge to form the island of Sumba. What is surprising, however, is that the velocity is nearly constant over 400 km of arc crust to the west and another 400 km of arc crust to the east, but changes abruptly in this narrow straight. There is no evidence of a major fault zone in the region, although the data available is sparse.

The GPS measurements reveal two important processes associated with the mechanical behavior of arc accretion that is not very well understood. First, the arc is not adhering to the lower plate in a progressive manner, but rather in large jumps where a 400 km long segment of the arc becomes partially attached with uniform velocities throughout the segment, then more attached uniformly. The second process is diffusive versus localized shear as no fault zone is observed across the boundary between the two crustal blocks although there is seismicity.

The next accreting crustal segment of the arc to the east of the Komodo Islands is the Flores-Savu-Sumba block. It also shows nearly uniform directions and velocities of movement among its stations, with some notable exceptions. One of these is the 7 ± 1 mm/a difference in velocity between the Island of Savu and western Flores, which crosses the Savu Thrust. This

result is consistent with other evidence that the Savu Thrust is active (see Active Faults below).

The northern boundary of this arc segment is the Flores Thrust, which is well imaged by sonar and seismic reflection data (Silver et al. 1983) and according to GPS measurements accumulates around 22 mm/a of strain. Earthquakes along this thrust of magnitudes >7.5 are consistent with fault segments and rupture lengths of similar size to the strike length of crustal blocks based on our GPS measurements.

The eastern boundary of the Flores-Savu-Sumba block lies near the 123°E structural discontinuity (Fig. 7.1). The Timor–Alor-Wetar crustal block to the east of the discontinuity moves at 63% of the motion of the Australian Plate, which is close to the 70% predicted from total shortening based on structural studies throughout Timor (Harris 1991).

Although the Timor–Alor-Wetar segment is interpreted as accreted to the Australian continent (Genrich et al. 1996), there remains around 21 mm/a of Australian Plate motion unaccounted for between Timor and Darwin, Australia (Nugroho et al. 2010). This motion is most likely taken up along the basal décollement of the Banda Orogen that surfaces at the Timor Trough.

7.5.9 Seismic Gaps

The pattern of seismicity in the Banda Orogen mimics in many ways the distribution of strain documented by GPS measurements and along active faults. Shallow earthquakes around Timor Island have mostly thrust fault plane solutions and depths consistent with slip along a basal décollement attached to the deformation front in the Timor Trough (Fig. 7.3). Although many researchers invoke major amounts of strike-slip motion along lineaments cross-cutting the Banda Orogen, there is little evidence of strike-slip geomorphic features in the region and few strike-slip fault plane solutions.

In terms of deeper earthquakes associated with the Benioff zone beneath the Sunda and Banda Arcs there is a nearly continuous zone of seismicity from the shallow depths all of the way to around 600 km. However, a notable lack of seismicity is observed at intermediate depths (71–300 km) in places where arc volcanism has mostly ceased. Although lack of seismicity at these depths is common in many subduction zones it is distinct throughout the 500 km strike-length of the Alor-Wetar segment of the Banda Arc (Cardwell and Isacks 1978). Similar low levels of seismic activity at this depth also occur along two other abandoned volcanic arc segments in central Java and western Flores.

A combination of factors in the Alor-Wetar arc segment, such as the intermediate level seismic gap, lack of volcanism, the high relief of the inactive arc segment and the regionally extensive uplift of coastlines has led to a slab rupture hypothesis (McCaffrey et al. 1985; McCaffrey 1989; Sandiford 2008). Several characteristics of the earthquakes in the region are used to support this hypothesis. However, tomographic images of the area do not support slab tear (Spakman and Hall 2010; Fichtner et al. 2010). After relocating more than 800 earthquakes in the Banda Arc region, Das (2004) warned that existing models often explain some observations but ignore others, such as the fact that the only parts of the Indonesian arc-trench systems with continuous seismicity from the surface to below 600 km are those under the highest stress in regions of greatest arc curvature. In other words, adjacent slabs may be separated by a structural discontinuity that allows for different amounts of slab stress and produce a "seismic gap" that does not relate to tearing at all.

Another consideration is the effect of distributed heterogeneities within the slab, such as preexisting faults (Silver et al. 1995; Kirby et al. 1996). The intermediate depth seismic gap in the Alor-Wetar region may be a function of the multi-deformed and extremely heterogeneous *nature* of the subducting plate in this region, which involves the irregular northern rifted continental margin of Australia.

A gap in shallow seismicity also exits throughout the eastern part of East Timor. However, in this same region there are also many other indicators of active deformation, such as the warped coral terraces and seismic reflection images of thrust faults rupturing the seafloor. Due to the small temporal range of the earthquake record it is possible that the shallow seismic gap may be a locked fault segment, and that uplift is co-seismic. Numerical models (Yang et al. 2006) show that uplift of inactive segments of the volcanic arc can be explained by increased coupling with the lower plate and does not require a slab tear.

7.5.10 Numerical Modeling

Quantifying horizontal and vertical strain through GPS and surface uplift rate measurements, and shear stress data from fault plane solutions, provides a way to numerically model deformation patterns in the Banda Arc. One of the key questions these models address is whether the observed pattern of vertical and horizontal movements (Fig. 7.12) can be replicated by simply a progressive eastward increase in plate coupling or does

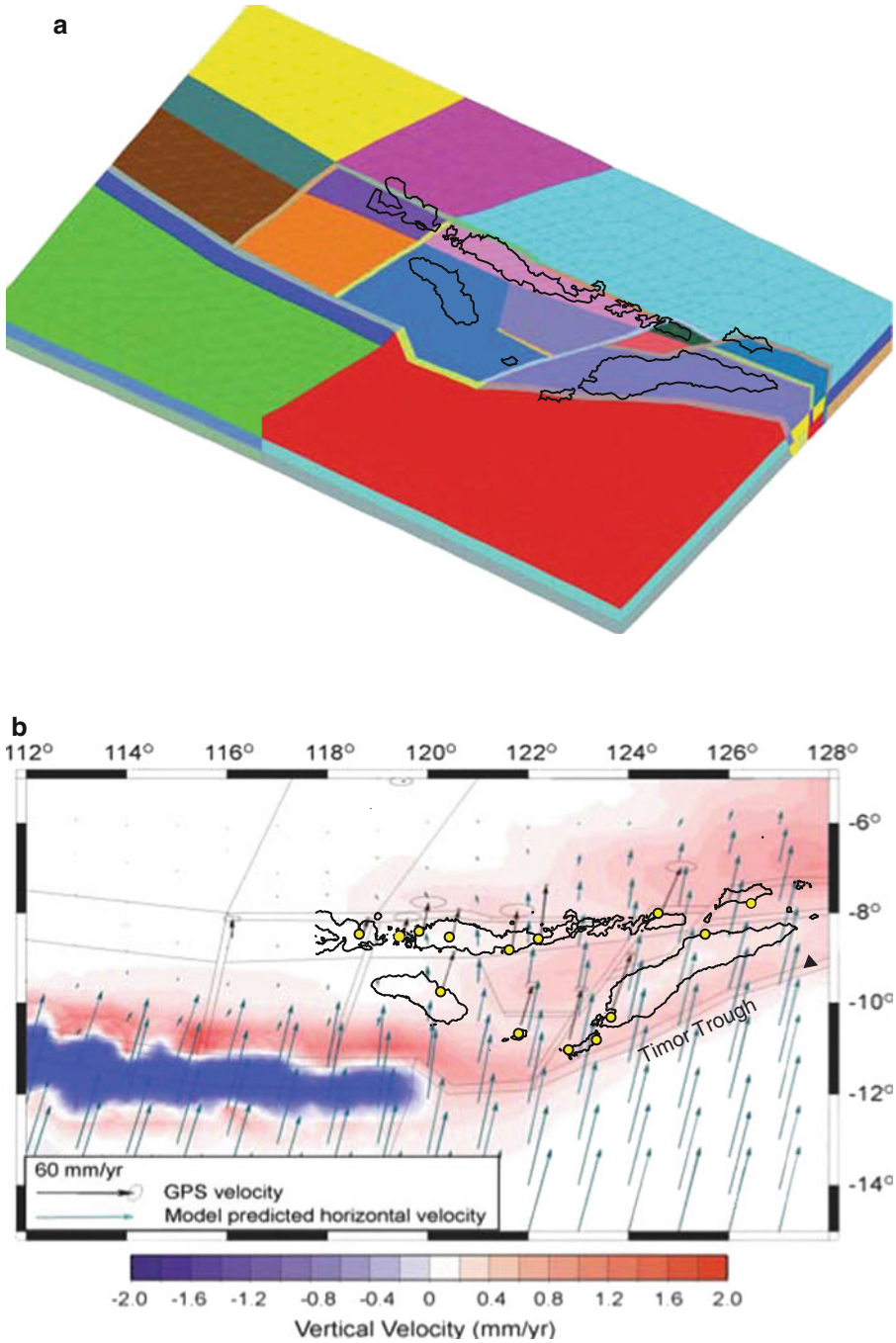

Fig. 7.16 (continued)

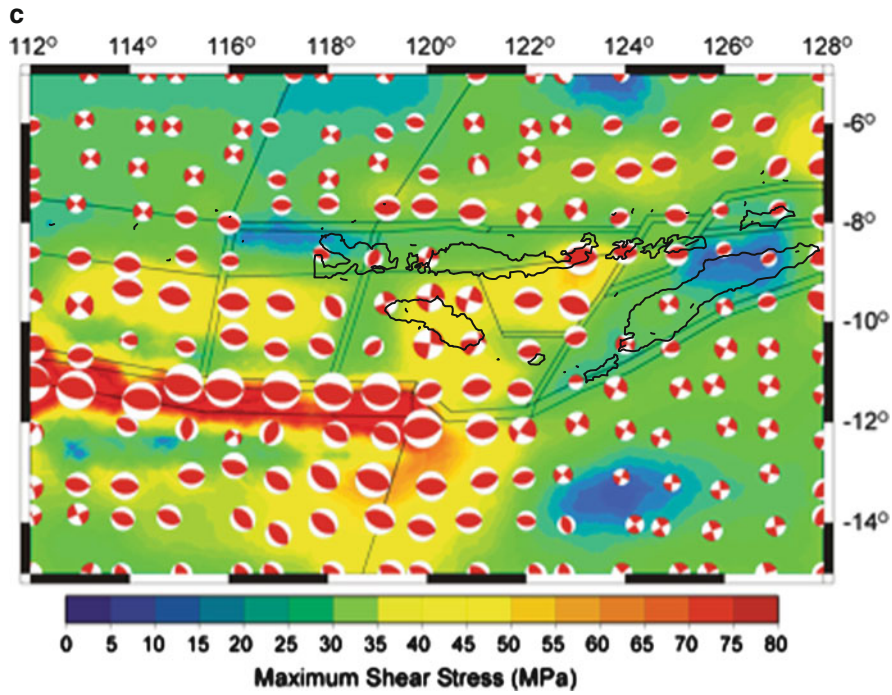

Fig. 7.16 Three-dimensional finite element model of the Banda Arc (modified from Yang et al. 2006). (**a**) vertically exaggerated reference model with vertical variation in rheology and segmented crustal domains. For assumptions and model conditions see Yang et al. (2003). (**b**) Best fit model to GPS velocities (*blue arrows*). Viscosity along faults increases eastward simulating increased plate coupling. Predicted uplift rates are shown in color gradient. The model predicts uplift rates of 0.5 mm/a and greater for the inactive Alor to Wetar arc segment without slab tear or any other lithospheric process. (**c**) Shear stress prediction using model B. Shear stress in MPa is shown as color gradient. Fault plane solutions predict types and size of earthquakes associated with stress field.

it require other processes, such as slab tear or large amounts of strike-slip movement?

This question was investigated by Yang et al. (2006) using a 3-D power-law viscous flow model (Fig. 7.16a). The model includes vertical variations of rheology with major active fault zones simulated as weak zones using a special fault element (Goodman et al. 1968). The model includes only the crust (30 km thick). The velocity boundary conditions are constrained by GPS velocities that are applied to the edges of the model domain. Topographic loading is calculated from Etopo 5 data. Spring elements are applied on the surface and bottom of the model to simulate isostatic restoring forces. The evolution of the finite strain is calculated using the finite element method (Yang et al. 2003).

A series of forward models were used to explore the effects of major factors on vertical and horizontal strain partitioning, such as variation in coupling and plate boundary reorganization. The model that fits the GPS velocity field (Fig. 7.16b) also predicts a similar surface uplift rate pattern to what is observed (Fig. 7.12). What is especially telling are surface uplift rates of >0.5 mm/a predicted by the model for the Alor to Wetar segment of the Banda Arc, which is close to rates measured from uplifted coral terraces in the region. The model demonstrates that increased coupling alone according to the pattern provided by the GPS velocity field can account for uplift of the abandoned arc segment without having to invoke an additional slab tear component. The result is also consistent with several other indicators that the collision is mostly progressive versus episodic.

Model C shows the shear stress field predicted by model B, which is very similar to observed shallow earthquake fault plane solutions for the region (compare with Fig. 7.3). The model also shows the importance of strain partitioning with most of the

convergence distributed away from the deformation front, but not all. This result is consistent with only partial accretion of the volcanic arc and at least 21 mm/a of strain accumulation across the deformation front in the Timor Trough. Fitting the strain partitioning also puts constraints on the crustal rheology (effective viscosity) in the range of 10^{22} to 10^{23} Pa s.

7.6 Conclusion

The Australian Plate pulls into the Sunda and Banda Trenches a passive margin with many inherited features that strongly influence the way arc–continent collision is expressed in the Timor region. Some of its characteristics provide modern analogs for other arc–continent collisions. However, in older orogens where the collision process is complete it may be difficult to detect these features. For example, in most collisions lower plate heterogeneities that influenced the collision are completely buried by a thick fold and thrust belt or overprinted by metamorphism. Perhaps even more critical is the loss to subduction of the forearc and arc, which contain a crucial record of pre- and syn-collisional events.

One of the most profound inherited controlling factors of the Banda arc–continent collision is the thermo-mechanical influence of an old and cold lower plate. This single attribute may account for most of the tectonic differences the arc–continent collisions of Taiwan and Timor. Some of these features unique to the Banda arc–continent collision:

- Pre-collisional trench retreat, extensional collapse and subduction erosion of the upper plate to form a forearc consisting of highly attenuated arc crust separated by young supra-subduction zone ocean basins. The last phase of opening of the southern Banda Basin happened during collision initiation.
- Collision of an irregularly shaped continental margin.
- Initial collapse of the accretionary wedge as overpressured mudstones of the continental margin are subducted and weaken the basal décollement.
- Massive mud diapirism by remobilization of overpressured mudstone.
- Mélange development due to diapirism coupled with subduction channel processes where material from the upper part of the lower plate mixes with blocks plucked from the lower part of the upper plate.
- Extrusion of mélange along the subduction channel and out onto the sea floor at the deformation front.
- Opening followed by inversion of accretionary wedge slope basins.
- Partitioning of strain away from the deformation front into the forearc and backarc, and the development of new plate boundary segments as plate coupling increases.
- Emplacement of nappes of the upper plate onto the shortened continental margin.
- Increased coupling of the arc to the continent one ~400 km long arc segment at a time.
- Uplift primarily from crustal shortening through the development of multiple detachments and duplex systems.
- Closure and eventual burial or sinking of the forearc.
- Deep subduction of the continental lower plate to depths where it experiences a high-pressure metamorphism and contaminates the volcanic arc. The contamination front initiates at Wetar Island at ~5 Ma and spreads laterally in space and time.
- Continued subduction of the continent to depths of at least 400 km with no slab break off.
- Active arc volcanism several millions of years after collision initiation and even after initiation of arc accretion.
- Movement of the arc partially with the lower plate and development of a backarc fold and thrust belt without subduction polarity reversal.

Acknowledgements I would like to thank the National Science Foundation for support of much of my research in the Banda Arc region. Major grants were also provided by Chevron/Texaco and Union Texas Petroleum. Logistical support in Indonesia is provided primarily by the GRDC and Universitas Pengbangunan Nasional (UPN) Yogyakarta. Field research relied heavily on the invaluable assistance of several faculty and students from UPN, especially the assistance of Carolus Prasetyadi. In East Timor I appreciate the assistance of SERN directors and staff, and several East Timorese field assistants who have accompanied me over the past 20 years. I have also enjoyed rich collaborations with colleagues in the field including Mike Audley-Charles, Carolus Prasetyadi, Sahat Tobing, Rob Sawyer, Dorothy Merritts, Nova Roosmawati, Hendro Nugroho and many others including several graduate students whose names appear as authors and co-authors in this manuscript. The manuscript benefited from reviews by Mike Sandiford, Sebastien Meffre, Carl Hoiland and Tim Charlton.

References

Abbott MJ, Chamalaun FH (1981) Geochronology of some Banda Arc volcanics. In: Barber AJ, Wiryosujono S (eds) The geology and tectonics of Eastern Indonesia, vol 2. Geological Research and Development Centre, Special Publications, Bandung, Indonesia, pp 253–268

Archbold NW (1988) Permian brachiopoda and bivalvia from Sahul Shoals No. 1, Ashmore Block, northwestern Australia. Proc R Soc Victoria 100:33–38

Audley-Charles MG (1968) The geology of Portuguese Timor. Geological Society of London Memoir, vol 4. 76 pp

Audley-Charles MG (1986) Rates of Neogene and Quaternary tectonic movements in the southern Banda Arc based on micropaleontology. Geol Soc London 143:161–175

Audley-Charles MG (1983) Reconstruction of western Gondwanaland. Nature 306(5938):48–50

Audley-Charles MG (1981) Geometrical problems and implications of large scale over-thrusting in the Banda Arc-Australian margin collision zone, vol 9. Geological Society of London, Special Publication, London, pp 407–416

Audley-Charles MG, Harris RA (1990) Allochthonous terranes of the Southwest Pacific and Indonesia. Phil Trans R Soc London 331:571–587

Balke B, Burt D (1976) Arafura Sea area, Economic geology of Australia and Papua New Guinea 3. Australas Inst Min Metall Monogr 7:209–214

Barber AJ, Audley-Charles MG (1976) The significance of the metamorphic rocks of Timor in the development of the Banda Arc, eastern Indonesia. Tectonophysics 30: 119–128

Barber AJ, Tjokrosapoetro S, Charlton TR (1986) Mud volcanoes, shale diapirs, wrench faults and mélanges in accretionary complexes, Eastern Indonesia. AAPG Bulletin 70:1729–1741

Ben Othman D, White WM, Patchett J (1989) The geochemistry of marine sediments, island arc magma genesis, and crust-mantle recycling. Earth Planet Sci Lett 94:1–21

Berry RF, Grady AE (1981) Deformation and metamorphism of the Aileu Formation, north coast, East Timor and its tectonic significance. J Struct Geol 3(2):143–167

Berry RF, Jenner GA (1982) Basalt geochemistry as a test of the tectonic models of Timor. J Geol Soc London 139:593–604

Berry RF, McDougall I (1986) Interpretation of (super 40) Ar/(super 39) Ar and K/Ar dating evidence from the Aileu Formation, East Timor, Indonesia. Chem Geol Isot Geosci 59(1):43–58

Bird PR, Cook SE (1991) Permo-Triassic successions of the Kekneno area. West Timor: Implications for paleogeography and basin evolution. J Southeast Asian Earth Sci 6:359–371. doi:10.1016/0743-9547(91)90081-8

Bowin C, Purdy GM, Johnston C, Shor G, Lawver L, Hartono HMS, Jezek P (1980) Arc-continent collision in Banda Sea region. Bull AAPG 64:868–915

Breen NA, Silver EA, Roof S (1989a) The Wetar backthrust belt, eastern Indonesia: the effects of accretion against an irregularly shaped arc. Tectonics 8:85–98

Breen NA, Silver EA, Hussong DM (1986) Structural styles of an accretionary wedge south of the island of Sumba. Indonesia, revealed by Sea Marc II side scan sonar. Geol Soc Am Bull 97:1250–1261. doi:10.1130/0016-7606

Breen NA, Silver EA, Roof S (1989b) The Wetar backthrust belt, eastern Indonesia: the effects of accretion against an irregularly shaped arc. Tectonics 8:85–98

Brown M, Earle MM (1983) Cordierite-bearing schists and gneisses from Timor, eastern Indonesia. P–T implications of metamorphism and tectonic implications. J Metamorph Geol 1:183–203

Cardwell RK, Isacks BL (1978) Geometry of subducted lithosphere beneath the Banda Sea in eastern Indonesia from seismicity and fault plane solutions. J Geophys Res 83:2825–2838

Carter DJ, Audley-Charles MG, Barber AJ (1976) Stratigraphical analysis of island arc-continental margin collision in eastern Indonesia. Geol Soc London 132:179–198

Cecil CB, Dulong FT, Harris RA, Cobb JC, Gluskoter HG, Nuroho H, (2003) Observations on climate and sediment discharge in selected tropical rivers, Indonesia. In: Cecil CB, Edgar T (eds) Climate Controls on Stratigraphy, vol 77. Soc. Sedimentary Geology Special Publication, pp 29–50

Chamalaun FH, Grady AE, von der Borch CC, Hartono HMS (1981) The tectonic significance of Sumba. Bull Geol Res Develop Centre Bandung 5:1–20

Chappell J, Veeh HH (1978) Late Quaternary tectonic movements and sea-level changes at Timor and Atauro Island. Geol Soc Am Bull 89:356–368

Charlton TR (1989) Stratigraphic correlation across an arc-continent collision zone: Timor and the Australian Northwest Shelf. Aust J Earth Sci 36:263–274

Charlton TR (1991) Post-collisional extension in arc–continent collision zones, eastern Indonesia. Geology 19:28–31

Charlton TR, Barber AJ, Harris RA, Barkham ST, Bird PR, Archbold NW, Morris NJ, Nicoll RS, Owen HG, Owen RM, Sorauf JE, Taylor PD, Webster GD, Whittaker JE (2002) the Permian of Timor; stratigraphy, palaeontology and palaeogeography. J Asian Earth Sci 20(6):719–774

Charlton TR, Barber AJ, McGowan AJ, Nicoll RS, Roniewicz E, Cook SE, Barkham ST, Bird PR (2009) The Triassic of Timor; lithostratigraphy, chronostratigraphy and palaeogeography. J Asian Earth Sci 36(4–5):341–363

Clough M, Keep M, Longley I (2000) Neogene structural modifications of petroleum systems of the Timor Sea. AAPG Bull 84(9):1412–1413

Cox NL, Harris RA, Merritts D (2006) Quaternary uplift of coral terraces from active folding and thrusting along the northern coast of Timor–Leste. Eos Trans AGU 87(52): T51D-1564

Cull JP (1982) An appraisal of Australian heat-flow data. BMR J Aust Geol Geophys 7(1):11–21

Curray JR (1989) The Sunda Arc: a model for oblique plate convergence. Neth J Sea Res 24:131–140

Das S (2004) Seismicity gaps and the shape of the seismic zone in the Banda Sea Region from relocated hypocenters. J geophys Res 109. doi:10.1029/2004JB003192

de Roever WP (1940) Geological investigation in the Southwestern Moetis region (Netherlands Timor), Ph.D. Thesis, University of Amsterdam, 244 pp.

De Smet MEM, Fortuin AR, Troelstra SR, Van Marle LJ, Karmini M, Tjokrosapoetro S, Hadiwasastra S (1990)

Detection of collision-related vertical movements in the Outer Banda Arc (Timor, Indonesia), using micropaleontology data. J Southeast Asian Earth Sci 4(4):337–356

Dewey JF (1988) Extensional collapse of orogens. Tectonics 7:1123–1139

Dilek Y, Harris RA (2004) Continental margins of the Pacific Rim: Tectonophysics Special Issue, V. 392, 348 p

Doglioni C, Guegen E, Harabaglia P, Mongelli F (1999a) On the origin of west directed subduction zones and applications to the western Mediterranean, vol 156. Geological Society of London, Special Publication. pp 541–561

Doglioni C, Harabaglia P, Merlini S, Mongelli F, Peccerillo A, Piromallo C (1999b) Orogens and slabs vs. their direction of subduction. Earth Sci Resour 45:167–208

Dore AG, Stewart IC (2002) Similarities and differences in the tectonics of two passive margins; the Northeast Atlantic margin and the Australian North West Shelf. In: Keep M, Moss SJ (eds) Sedimentary basins of Western Australia. Petroleum Exploration Society of Australia Symposium Proceedings, vol 3. pp 89–117

Ernst WG, Liou JG (2000) Ultra-high pressure metamorphism and geodynamics in collision type orogenic belts. In: Ultra-high pressure metamorphism and geodynamics in collision type orogenic belts, vol 4, International Book Series. Bellwether, Geological Society of America, Columbia, MD, 293 p

Earle MM (1981) The metamorphic rocks of Boi, Timor, eastern Indonesia. In: Barber AJ, Wiryosujono S (eds) The geology and tectonics of Eastern Indonesia, vol 2. Geological Research and Development Centre, Special Publications, Bandung, Indonesia, pp 239–251

Earle MM (1983) Continental margin origin for cretaceous radiolarian chert in western Timor. Nature 305:129–130

Elburg MA, Foden JD, van Bergen MJ, Zulkarnain I (2005) Australia and Indonesia in collision: geochemical sources of magmatism. J Volcanol Geotherm Res 140: 25–47

Elburg MA, van Bergen MJ, Foden JD (2004) Subducted upper and lower continental crust contributes to magmatism in the collision sector of the Sunda-Banda arc, Indonesia. Geology 32:41–44

Elsasser WM (1971) Sea-floor spreading as thermal convection. J Geophys Res 76:1101–1112

Falloon TJ, Berry RF, Robinson P, Stolz AJ (2006) Whole-rock geochemistry of the Hili Manu peridotite, East Timor; implications for the origin of Timor ophiolites. Aust J Earth Sci 53(4):637–649

Falvey DA (1972) Sea-floor spreading in the Wharton Basin (north-east Indian Ocean) and the break-up of eastern Gondwanaland. Aust Petrol Explor Assoc J 12:86–88

Fichtner A, De Wit M, van Bergen M (2010) Subduction of continental lithosphere in the Banda Sea region: combining evidence from full waveform tomography and isotope ratios. Earth Planet Sci Lett 297(3–4):405–412

Fleury JM, Pubellier M, de Urreiztieta M (2009) Structural expression of fore-arc crust uplift due to subducting asperity. Lithos 113(1–2):318–330

Flower MFJ, Russo RM, Tamaki K, Hoang N (2001) Mantle contamination and the Izu–Bonin–Mariana (IBM) 'high-tide mark': evidence for mantle extrusion caused by Tethyan closure. Tectonophysics 333:9–34

Fortuin AR, De Smet MEM (1991) Rates and magnitudes of late Cenozoic vertical movements in the Indonesian Banda Arc and the distinction of eustatic effects, vol 12. International Association of Sedimentologist, Special Publication, pp 79–89

Fortuin AR, van der Werff W, Wensink H (1997) Neogene basin history and paleomagnetism of a rifted and inverted forearc region, on- and offshore Sumba, eastern Indonesia. J Asian Earth Sci 15:61–88

Genrich JF, Bock Y, McCaffrey R, Calais E, Stevens CW, Subarya C (1996) Accretion of the southern Banda arc to the Australian plate margin determined by Global Positioning System measurements. Tectonics 15:288–295. doi:10.1029/95TC03850

Goodman RE, Taylor RL, Brekke TL (1968) A model for the mechanics of jointed rock. American Society of Civil Engineers, New York, pp 637–659

Grady AE, Berry RF (1977) Some Paleozoic–Mesozoic stratigraphic-structural relationships in Timor Leste and their significance to the tectonics of Timor. J Geol Soc Aust 24:203–214

Guilou H, Arnaud N, Honthaas C, Rehault J, Maury RC, Bellon H, Hemond C, Malod J, Cornee J, Villeneuve M, Cotten J, Burhanuddin S, Guillou H, Arnaud N (1998) Neogene back-arc origin for the Banda Sea basins: geochemical and geochronological constraints from the Banda ridges (East Indonesia). Tectonophysics 298:297–317

Hafkenscheid SH, Buiter MR, Wortel W, Spakman HB (2001) Modeling the seismic velocity structure beneath Indonesia: a comparison with tomography. Tectonophysics 333:35–46

Haig DW, McCartain E (2007) Carbonate pelagites in the post-Gondwana succession (Cretaceous-Neogene) of East Timor. Aust J Earth Sci 54(6):875–889

Haig DW, McCartain E, Barber L, Backhouse J (2007) Triassic–Lower Jurassic foraminiferal indices for Bahaman-type carbonate-bank limestones, Cablac Mountain, East Timor. J Foraminiferal Res 37:248–264

Haig DW, McCartain EW, Keep M, Barber L (2008) Re-evaluation of the Cablac Limestone at its type area, East Timor; revision of the Miocene stratigraphy of Timor. J Asian Earth Sci 33(5–6):366–378

Haile NS, Barber AJ, Carter DJ (1979) Mesozoic cherts on crystalline schists in Sulawesi and Timor. Geol Soc London 136:65–70

Hall R (2002) Cenozoic geological and plate tectonic evolution of SE Asia and the SW Pacific: computer-based reconstructions, model and animations. J Asian Earth Sci 20: 353–431

Hamilton W (1979) Tectonics of the Indonesian region. U.S. Geology Survey Professional Paper 1078, pp 1–345

Harris RA (1991) Temporal distribution of strain in the active Banda Orogen. A reconciliation of rival hypotheses. J Southeast Asian Earth Sci 6:373–386

Harris RA (1992) Peri-collisional extension and the formation of Oman-type ophiolites in the Banda Arc and Brooks Range. In: Parson LM, Murton BJ, Browning P (eds) Ophiolites and their modern oceanic analogues, vol 60. Geological Society of London, Special Publication, London, pp 301–325

Harris RA (2003) Geodynamic patterns of ophiolites and marginal basins of the Indonesian and New Guinea regions.

In: Dilek Y, Robinson PT (eds) Ophiolite in Earth history, vol 218. Geological Society of London, Special Publication, London, pp 481–505

Harris R (2006) Rise and fall of the eastern Great Indonesian Arc recorded by the assembly, dispersion and accretion of the Banda Terrane, Timor. Gondwana Res 10:207–231

Harris RA, Audley-Charles MG (1987) Taiwan and Timor Neotectonics: a comparative review. Memoir Geological Society of China, vol 9. pp 45–61

Harris RA, Wu S (1991) Postcollisional extension in arc-continent collision zones, eastern Indonesia. Geology 20(1):92–93

Harris RA, Long T (2000) The Timor ophiolite, Indonesia. Model or myth? In: Dilek Y, Moores EM, Elthon D, Nicolas A (eds) Ophiolites and oceanic crust. New insights from field studies and the Ocean Drilling Program. Geologic Society of America Special Paper vol 349, pp 321–330

Harris RA, Huang CY (2010) Linking mélange types and occurrences with active mélange forming processes in Timor and Taiwan. Geological Society of America, Tectonic Crossroads Mtg., abstract 49-1, pp 84–85

Harris RA, Stone DB, Turner DL (1987) Tectonic implications of paleomagnetic and geochronologic data from the Yukon-Koyukuk basin, Alaska. Geol Soc Am Bull 99:362–375

Harris RA, Donaldson K, Prasetyadi C (1997) Geophysical disaster mitigation in Indonesia using GIS, vol 5. Buletin Teknologi Mineral pp 2–10

Harris RA, Sawyer RK, Audley-Charles MG (1998) Collisional mélange development: geologic associations of active mélange-forming processes with exhumed mélange facies in the western Banda orogen: Indonesia. Tectonics 17:458–480

Harris RA, Kaiser J, Hurford A, Carter A (2000) Thermal history of Australian passive margin cover sequences accreted to Timor during Late Neogene arc-continent collision, Indonesia. J Asian Earth Sci 18:47–69

Harris RA, Cecil CB, Dulong FT, Nugroho H (2008) Is sediment discharge controlled more by climate or tectonics? Studies of suspended and dissolved loads from rivers in active orogens of Indonesia. Himalayan Geol 29(3):32–33

Harris RA, Vorkink MW, Prasetyadi C, Zobell E, Roosmawati N (2009) Transition from subduction to arc-continent collision: geological and neotectonic evolution of Savu, Indonesia. Geosphere 5:1–20. doi:10.1130/GES00209.1

Harrowfield M, Keep M (2005) Tectonic modification of the Australian North-West Shelf: episodic rejuvenation of long-lived basin divisions. Basin Res 17(2):225–239

Herrington RJ, Philip A, Scotneybe M, Roberts S, Adrian B, Boyce C, Harrison D (2011) Temporal association of arrested subduction, progressive magma contamination in arc volcanism and formation of gold-rich massive sulphide deposits on Wetar Island (Banda arc). Gondwana Res

Hilton DR, Craig H (1989) A helium isotope transect along the Indonesian archipelago. Nature 342(6252):906–908

Hilton DR, Hoogewerff JA, van Bergen MJ, Hammerschmidt K (1992) Mapping magma sources in the East Sunda-Banda arcs, Indonesia; constraints from helium isotopes. Geochimica et Cosmochimica Acta 56(2):851–859

Hinschberger F, Malod J-A, Dyment J, Honthaas C, Rehault J, Burhanuddin S (2001) Magnetic lineations constraints for the back-arc opening of the Late Neogene south Banda Basin (eastern Indonesia). Tectonophysics 333:47–59

Hinschberger F, Malod JA, Rehault JP, Villeneuve M, Royer JY, Burhanuddin S (2005) Late Cenozoic geodynamic evolution of eastern Indonesia. Tectonophysics 404(1–2):91–118

Honthaas C, Rehault J, Maury R, Bellon H, Hemond C, Malod JA, Cornee JJ, Villeneuve M, Cotten J, Burhanuddin S, Guillou H, Arnaud N (1998) A Neogene back-arc origin for the Banda Sea basins: geochemical and geochronological constraints from the Banda ridges (East Indonesia). Tectonophysics 298:297–317

Jouannic C, Hoang CT, Hantoro WS, Delinom RM (1988) Uplift rate of coral reef terraces in the areas of Kupang, West Timor: preliminary results. Palaeogeogr Palaeoclimatol Palaeoecol 68:259–272

Kadarusman A, Maruyama S, Kaneko Y, Ohta T, Ishikawa A, Sopaheluwakan J, Omori S in press. World's youngest blueschist belt from Leti Island in the non-volcanic Banda outer arc of eastern Indonesia. Gondwana Res 18(1):189–204

Kaneko Y, Maruyama S, Kadarusman A, Ota T, Ishikawa M, Tsujimori T, Ishikawa A, Okamoto K (2007) On-going orogeny in the outer-arc of the Timor–Tanimbar region, eastern Indonesia. Gondwana Research 11:218–233

Karig DE, Barber AJ, Charlton TR, Klemperer S, Hussong DM (1987) Nature and distribution of deformation across the Banda Arc-Australian collision zone at Timor. Geol Soc Am Bull 98:18–32

Kaye SJ (1990) The structure of Eastern Indonesia: an approach via gravity and other geophysical methods. Unpublished Ph. D. thesis, University of London, 290 pp

Keep M, Haig DW (2010) Deformation and exhumation in Timor: Distinct stages of a young orogeny. Tectonophysics [Tectonophysics]. Vol. 483, no. 1-2, pp. 93-111

Keep M, Longley I, Jones R (2003) Sumba and its effect on Australia's northwestern margin. In: Hills RR, Mueller RD (eds) Special Paper Geological Society of America, vol 372. pp 309–318

Keep M, Clough M, Langhi L, Moss SJ (2002) Neogene tectonic and structural evolution of the Timor Sea region, NW Australia. In: Keep M, Moss SJ (eds) Sedimentary Basins of Western Australia. Proceedings of the Petroleum Exploration Society of Australia Symposium, vol 3, pp 341–353

Kenyon CS (1974) Stratigraphy and sedimentology of the Late Miocene to Quaternary deposits in Timor. Ph.D. Dissertation, University of London

Kirby SH, Engdahl ER, Denlinger R, Roger P (1996) Intermediate-depth intra-slab earthquakes and arc volcanism as physical expressions of crustal and uppermost mantle metamorphism in subducting slabs. Geophys Monogr 96: 195–214

Kirschner DL, Cosca MA, Masson H, Hunziker JC (1996) Staircase 40Ar/39Ar spectra of fine-grained white mica: timing and duration of deformation and empirical constraints on argon diffusion. Geology 24:747–750

Kingborough RH, Williams AF, Hillis RR (1991) Borehole stability on the Northwest Shelf of Australia. SPE 23015, Soc. Petrol. Engin., Perth, Australia, pp 653–662

Larson RL (1975) Late Jurassic sea-11oar spreading in the eastern Indian Ocean. Geology 3:69–71

Lee C-R, Cheng W-T (1986) Preliminary heat flow measurements in Taiwan. In: Proceedings of the Fourth Circum-Pacific Energy and Mineral Resources Conference, Singapore

Longley IM, Buessenschuett C, Clydsdale L (2002) The North West Shelf of Australia – A Woodside perspective. In: Keep M, Moss S (eds) Sedimentary basins of Western Australia. Petroleum Exploration Society of Australia Symposium proceedings, vol 3. pp 27–88

Lorenzo JM, O'Brien GW, Stewart J, Tandon K (1998) Inelastic yielding and forebulge shape across a modern foreland basin; northwest shelf of Australia, Timor Sea. Geophys Res Lett 25(9):1455–1458

Lunt P (2003) Biogeography of some Eocene larger foraminifera, and their application in distinguishing geological plates. Palaeontologia Electronica 6:1–22

Lytwyn J, Rutherford E, Burke K, Xia C (2001) The geochemistry of volcanic, plutonic, and turbiditic rocks from Sumba, Indonesia. J Asian Earth Sci 19:481–500

Ma K-F, Song Teh-Ru Alex (2004) Thermo-mechanical structure beneath the young orogenic belt of Taiwan. Tectonophysics 388(1–4):21–31

Major J (2010) The tectonic significance and origin of Kisar, Indonesia, AAPG Bulletin, vol. 94, no. 1, pp.132

Major JR (2010) Metamorphism, thermochronology and uplift of the Aileu Complex on Kisar Island, Banda arc-continent collision, unpublished MSc. Thesis, Brigham Young University, 150 p

Major JR, Harris RA, Robinson JS (2008) Earthquake and tsunami history and hazards of eastern Indonesia. Eos Trans AGU 89(53), Fall Meet. Suppl., Abstract T53E-2009

Major JR, Harris RA, Chiang H, Prasetyadi C, Shen C (2009) Variation in deformational mechanisms in the Banda Arc: uplift and tectonic implications of Kisar, Indonesia. Eos Trans AGU 90(52), Fall Meet. Suppl., Abstract T33B-T1915

Malinverno A, Ryan WBF (1986) Extension in the Tyrrhenian Sea and shortening in the Apennines as result of arc migration driven by sinking of the lithosphere. Tectonics 5:227–245

Masson DG, Milsan J, Barber AJ, Simumbang N, Dwiyanto B (1991) Recent tectonics around the island of Timor, eastern Indonesia. Mar Pet Geol 8:35–49

McCaffrey R, Molnar P, Roecker SW, Joyodirwiryo YS (1985) Microearthquake seismicity and fault plane solutions related to arc continent collision in the eastern Sunda Arc, Indonesia. J geophys Res 90:4511–4545

McCaffrey R (1989) Seismological constraints and speculations on Banda Arc tectonics. Neth J Sea Res 24:141–152

Merritts, Dorothy, Eby, Rebecca, Harris, Ron, Edwards, R. Lawrence, and Cheng, Hai (1998) Variable Rates of Late Quaternary Surface Uplift Along the Banda Arc-Australian Plate Collision Zone, Eastern Indonesia, In: Stewart IS, Vita-Finzi C (eds) Coastal Tectonics, Geological Society of London Special Publications No. 146, p. 213–224

Mikolas M, Harris RA (1986) Variations of stress in time and space of an oblique arc-continent collision; analysis of fractures in synorogenic deposits of Timor, Abstracts with Programs. Geol Soc Am 28(5) p 91

Milsom J, Sardjono R, Susilo A (2001) Short-wavelength, high-amplitude gravity anomalies around the Banda Sea, and the collapse of the Sulawesi orogen. Tectonophysics 333:61–74

Morris JD, Gill JB, Schwartz D, Silver EA (1984) Late Miocene to recent Banda Sea volcanism, III, Isotopic compositions. EOS Trans AGU 65:1135, V22A-04

Myra K, David HW (2010) Deformation and exhumation in Timor: distinct stages of a young orogeny. Tectonophysics 483(1–2):93–111

Nicholls LA, Ferguson J, Jones H, Marks GP, Mutter JC (1981) Ultramafic blocks from the ocean floor southwest of Australia. Earth Planet Sci Lett 56:362–374

Nugroho H, Harris RA, Amin WL, Bilal M (2009) Active plate boundary reorganization in the Banda arc-continent collision: insights from new GPS measurements. Tectonophysics 479:52–65. doi:10.1016/j.tecto.2009.01.026

Peter Petkovic, Clive DN Collins, Doug M Finlayson (2000) Crustal structure across the Vulcan Sub-basin from seismic refraction and gravity data, Exploration Geophysics 31:287–294

Pirazzoli PA, Radtke U, Hantoro WS, Jouannic C, Hoang DT, Causse C, Borel Best M (1991) Quaternary raised coral-reef terraces on Sumba Island, Indonesia. Science 252: 1834–1836

Prasetyadi C, Harris RA (1996) Hinterland structure of the active Banda arc-continent collision, Indonesia: constraints from the Aileu Complex of East Timor. In: Proceedings of the 25th Convention of the Indonesian Association of Geology pp 144–173

Price NJ, Audley-Charles MG (1983) Plate rupture by hydraulic fracture resulting in overthrusting. Nature (London) 306 (5943):572–575

Price NJ, Audley-Charles MG (1987) Tectonic collision processes after plate rupture. Tectonophysics 140 (2–4):121–129

Pubellier M, Monnier C, Maury RC, Tamayo R (2004) Plate kinematics, origin and tectonic emplacement of supra-subduction ophiolites in SE Asia. Tectonophysics 392(1–4): 9–36

Reed DL, Silver EA, Prasetyo H, Meyer AW (1986) Deformation and sedimentation along a developing terrane suture: Sunda forearc, Indonesia. Geology 14:1000–1003. doi: 10.1130/0091-7613

Reed DL (1985) Structure and stratigraphy of eastern Sunda forearc, Indonesia: geologic consequences of arc-continent collision. Unpublished Ph.D. thesis, Scripps Institute of Oceanography, La Jolla, California

Richardson AN, Blundell DJ (1996) Continental collision in the Banda Arc. In: Hall R, Blundell D (eds) Tectonic evolution of Southeast Asia, vol 106. Geological Society of London, Special Publication, London, pp 47–60

Roosmawati N, Harris RA (2009) Surface uplift history of the incipient Banda arc-continent collision: geology and synorogenic foraminifera of Rote and Savu Islands, Indonesia. Tectonophysics 479:95–110. doi:10.1016/j.tecto.2009.04.009

Rosidi HMO, Suwitopiroyo K, Tjokrosapoetro S (1979) Geological map Kupang–Atambua Quadrangle, Timor 1:250, 000. Geological Research Centre, Bandung, Indonesia

Royden LH (1993) The tectonic expression of slab-pull at continental convergent boundaries. Tectonics 12:303–325

Sani K, Jacobson ML, Sigit R (1995) The thin-skinned thrust structures of Timor. In: Indonesian Petroleum Association 24th Annual Convention, Jakarta, pp 277–293

Sandiford M (2008) Seismic moment release during slab rupture beneath the Banda Sea. Geophys J Int 174(2):659–671

Sawyer, RK, Sani K, Brown S (1993) The stratigraphy and sedimentology of west Timor, Indonesia. Paper presented

at 22nd Convention of the Indonesian Petroleum Association, Jakarta, pp 1–20
Schellart WP, Lister GS (2004) Tectonic models for the formation of arc-shaped convergent zones and back arc basins. Geol Soc Am Spec Pap 283:237–258
Schellart WP, Lister GS, Jessell MW (2002) Analogue modeling of back-arc extension. J Virtual Explor 7:25–42 (on line)
Scholl DW, Keranen K, Kirby SH, Blakely RJ, Wells RE, Ryan HF, von Huene R, Fisher MA (2008) Abstracts with Programs. Geol Soc Am 40(6) pp 160
Schwartz O, Gill JB, Duncan RA (1984) Late Miocene to recent Banda Sea Volcanism: II petrology. EOS Trans AGU 65(45) p 1135, abstract V22A-03
Scotney PM, Roberts S, Herrington RJ, Boyce AJ, Burgess R (2005) The development of volcanic hosted massive sulfide and Barite-Gold ore bodies on Wetar Island, Indonesia. Mineralium Deposita 40:76–99
Searle MP, Stevens RK (1984) Obduction processes in ancient, modern and future ophiolites. In: Gass LG, Lippard SL, Shelton AW (eds) Ophiolites and oceanic lithosphere, vol 13. Geological Society of London, Special Publication, London, pp 303–320
Shreve RL, Cloos M (1986) Dynamics of sediment subduction, mélange formation, and prism accretion. J Geophys Res 91 (B10):10229–10245
Sieh K, Ward SN, Natawidjaja D, Suwargadi BW (1999) Crustal deformation at the Sumatran subduction zone revealed by coral rings. Geophys Res Lett 26:3141–3144
Silver PG, Beck SL, Wallace TC, Meade C, Myers SC, James DE, Kuehnel R (1995) Rupture characteristics of the deep Bolivian earthquake of 9 June 1994 and the mechanism of deep-focus earthquakes. Science 268:69–73
Silver EA, Smith RB (1983) Comparison of terrane accretion in modern Southeast Asia and the Mesozoic North American Cordillera. Geology 11(4):198–202
Silver EA, Reed R, McCaffrey R, Joyodiwiryo Y (1983) Back arc thrusting in the eastern Sunda arc, Indonesia: a consequence of arc-continent collision. J Geophys Res 88:7429–7448. doi:10.1029/JB088iB09p07429
Silver EA, Gill JB, Schwartz D, Prasetyo H, Duncan RA (1985) Evidence of submerged and displaced borderland, north Banda Sea, Indonesia. Geology 13:687–691
Silver EA, Breen NA, Prasetyo H, Hussong DM (1986) Multibeam study of the Flores backarc thrust belt, Indonesia. J Geophys Res 91:3489–3500. doi:10.1029/ JB091iB03p03489
Simons AL (1940) Geological investigations in northeast Netherlands Timor. Geol Exped Lesser Sunda Islands 1:107–213
Smith MR, Ross JG (1986) Petroleum potential of northern Australian continental shelf. Am Assoc Petrol Geol Bull 20:1700–1712
Snyder DB, Prasetyo H, Blundell DJ, Pigram CJ, Barber AJ, Richardson A, Tjokrosapoetro S (1996) A dual doubly vergent orogen in the Banda arc-continent collision zone as observed on deep seismic reflection profiles. Tectonics 15:34–53
Sobolev NV, Shatsky VS (1990) Diamond inclusions in garnets from metamorphic rocks; a new environment for diamond formation. Nature 343(6260):742–746
Sopaheluwakan I, Helmers H, Tjokrosapetro S, Surya Nila E (1989) Medium pressure metamorphism with inverted gradient. Associated with ophiolite nappe emplacement in Timor, Netherlands. J Sea Res 24:333–343
Spakman W, Hall R (2010) Surface deformation and slab–mantle interaction during Banda arc subduction rollback. Nat Geosci 3:562–566. doi:10.1038/ngeo917
Spencer A, Chew K, Leckie G (2005) The discovery patterns of the resources of the rift and gas provinces of the North Sea compared with some analogous provinces worldwide. In: Dore AG, Vining BA (eds) Petroleum geology; north-west Europe and global perspectives. proceedings of the 6th petroleum geology conference, vol 6. Pp 25–33
Stampfli GM, Borel GD (2002) A plate tectonic model for the Paleozoic and Mesozoic constrained by dynamic plate boundaries and restored synthetic oceanic isochrones. Earth Planet Sci Lett 196(1–2):17–33
Standley C, Harris RA (2009) Banda forearc basement accreted to the NW Australian continental margin: a geochemical, age and structural analysis of the Lolotoi metamorphic complex of East Timor. Tectonophysics 479:66–94. doi:10.1016/ j.tecto.2009.01.034
Stockmal GS (1983) Modeling of large-scale accretionary wedge deformation. J Geophys Res 88:8271–8287
Symonds PA, Planke S, Frey O, Skogseid J (1998) Volcanic evolution of the western Australian continental margin and its implications for basin development. Petroleum Exploration Society of Australia Proceedings, vol 2. pp 33–54
T'Hoen CWAP, Van Es LJC (1926) The exploration for minerals in the island of Timor. Jaarb Mijn Ned Indie 2:1–80
Tregoning P, Brunner FK, Bock Y, Puntodewo SSO, McCaffrey R, Genrich JF, Calais E, Rais J, Subarya C (1994) First geodetic measurement of convergence across the Java Trench. Geophys Res Lett 21:2135–2138
Van Bergen MJ, Vroon PZ, Hoogewerff JA (1993) Geochemical and tectonic relationships in the East Indonesian arc-continent collision region: Implications for the subduction of the Australian passive margin. Tectonophysics 223:97–116
van der Werff W (1995) Cenozoic evolution of the Savu Basin, Indonesia: forearc basin response to arc-continent collision. Mar Petrol Geol 12:247–262
Veevers JJ, Falvey DA, Hawkins LV, Ludwig WJ (1974) Seismic Reflection Measurements of Northwest Australian Margin and Adjacent Deeps. AAPG Bull 58(9):1731–1750
von Rad U, Exon NF (1983) Mesozoic-Cenozoic sedimentary and volcanic evolution of the starved passive continental margin off NW Australia. In: Watkins JS, Drake CL (eds) Studies in continental margin geology. American Association of Petroleum Geologists Memoir, vol 34. pp 253–281
Vorkink (2004) Incipient tectonic development of the active Banda arc-continent collision : geologic and kinematic evolution of Savu Island, Indonesia. MSc. Thesis, Brigham Young University, 87 p
Vroon PZ, Van Bergen MJ, White WM, Varekamp JC (1993) Sr–Nd–Pb Isotope systematics of the Banda Arc, Indonesia: Combined subduction and assimilation of continental material. J Geophys Res 98:22349–22366
Vroon PZ, Lowry D, van Bergen MJ, Boyce AJ, Mattey DP (2001) Oxygen isotope systematics of the Banda Arc: Low δ18O despite involvement of subducted continental material in magma genesis. Geochimica et Cosmochimica Acta 65:589–609

Wang Z, Zhao D, Wang J, Kao H (2006) Tomographic evidence for the Eurasian lithosphere subducting beneath south Taiwan. Geophys Res Lett 33(18):L1830

Wheller GE, Varne R, Foden JD, Abbott MJ (1987) Geochemistry of Quaternary volcanism in the Sunda-Banda are, Indonesia, and three-component genesis of island-arc basaltic magmas. J Geotherm Volcanol Res 32:137–160

Whitford DJ, Jezek PA (1979) Origin of late-Cenozoic lavas from the Banda arc, Indonesia; Trace element and Sr Isotope evidence: Contributions to Mineralogy and Petrology. Pages 68:141–150

Whitford DJ, Compston W, Nicholls IA, Abbott MJ (1977) Geochemistry of late Cenezoic lavas from eastern Indonesia: Role of subducted sediments in petrogenesis. Geology 5:571–575

Whitford DJ, White WM, Jezek PA (1981) Neodymium isotopic composition of Quaternary island arc lavas from Indonesia. Geochimica et Cosmochimica Acta 45:989–995

Widiyantoro S, van der Hilst R (1997) Mantle structure beneath Indonesia inferred from high-resolution tomographic imaging. Geophys J Int 130:167–182

Wortel MJR, Spakman W (2000) Subduction and slab detachment in the Mediterranean-Carpathian region. Science 290:1910–1917

Yang Y, Liu M, Stein S (2003) A 3-D geodynamic model of lateral crustal flow during Andean mountain building. Geophys Res Lett 30(21):2093. doi:10.1029/2003GL018308

Yang Y, Liu M, Harris RA (2006) From subduction to arc-continent collision: geodynamic modeling of strain partitioning and mountain building in the Indonesia Archipelago. Eos Trans AGU 87(52) T41C-1589

Yih-Min Wu, Chien-Hsin Chang, Li Zhao, J Bruce H Shyu, Yue-Gau Chen, Kerry Sieh, and Jean-Philippe Avouac (2007) Seismic tomography of Taiwan: Improved constraints from a dense network of strong motion stations, Journal of Geophysical research, vol. 112, B08312, doi:10.1029/2007JB004983

Zobell E (2007) Origin and tectonic evolution of Gondwana sequence units accreted to the Banda Arc: a structural transect through central East Timor. M.S. thesis, Provo, Utah, Brigham Young University, 75 p

Chapter 8
The Arc–Continent Collision in Taiwan

T. Byrne, Y.-C. Chan, R.-J. Rau, C.-Y. Lu, Y.-H. Lee, and Y.-J. Wang

8.1 Introduction

Geologists have long been fascinated with the map view curvature of mountain belts (Chamberlain and Shepard 1923; Dana 1866) and one of the many challenges has been to relate orogenic curvature to orogenic processes. Marshak (2004) presents a modern summary and overview of map-view curves and proposes fundamental differences between fold-and-thrust belts that form in pre-deformational basins and belts that form adjacent to obstacles or promontories. The former often form salients whereas the later form recesses or syntaxes in the orogenic belt. Macedo and Marshak (1999) examined the structural consequence of irregularities in the footwall in more detail and pointed out the in the majority of cases, fold and thrust belts tend to advance over pre-deformational sedimentary basins. Thomas (2006) also recently reviewed the importance of structural inheritance in the formation of the Appalachian orogenic belt and reached a similar conclusion – map view curvature often mimics irregularities in the initial continental margin.

In this chapter, we examine the tectonic setting and geologic history of the arc–continent collision in Taiwan, looking in particular at the role of continental margin geometry in the subducting passive margin of the South China Sea. A previously recognized magnetic anomaly along the northern margin of the South China Sea serves as a proxy for the edge of continental crust of normal thickness (~30 km) in this area and can be traced into the central part of Taiwan. The magmatic arc south of Taiwan also appears to record the progressive subduction of oceanic, transitional and continental crust from south to north, defining pre-, early and late collision zones, respectively. One of our objectives is to examine the arc–continental collision, exposed primarily on the island of Taiwan, in the context of this progressive evolution from pre- to late-stage collision. We propose that the continental crust involved in the late stage of the collision is of normal thickness but highly irregular in map view. Based on a combination of magnetic, seismic, geodetic, and topographic data we propose that a continental margin promontory and associated transform fault played, and continues to play, a critical role in the development of the active arc–continent collision in Taiwan.

8.2 Tectonic Setting and Regional-Scale Orogenic Processes

The Taiwan orogenic system is the result of collision of the Luzon arc with the Asian continental margin as

T. Byrne
Center for Integrative Geosciences, University of Connecticut, Storrs, CT, USA
e-mail: timothybyrne@earthlink.net

Y.-C. Chan
Institute of Earth Sciences, Academia Sinica, Taipei, Taiwan, ROC

R.-J. Rau
Department of Earth Sciences, National Cheng Kung University, Tainan, Taiwan, ROC

C.-Y. Lu
Department of Geological Sciences, National Taiwan University, Taipei, Taiwan, ROC

Y.-H. Lee
Earth and Environmental Sciences, National Chung Cheng University, Chiayi, Taiwan, ROC

Y.-J. Wang
Institute of Geophysics, National Central University, Jhungli, Taiwan, ROC

D. Brown and P.D. Ryan (eds.), *Arc-Continent Collision*, Frontiers in Earth Sciences,
DOI 10.1007/978-3-540-88558-0_8,

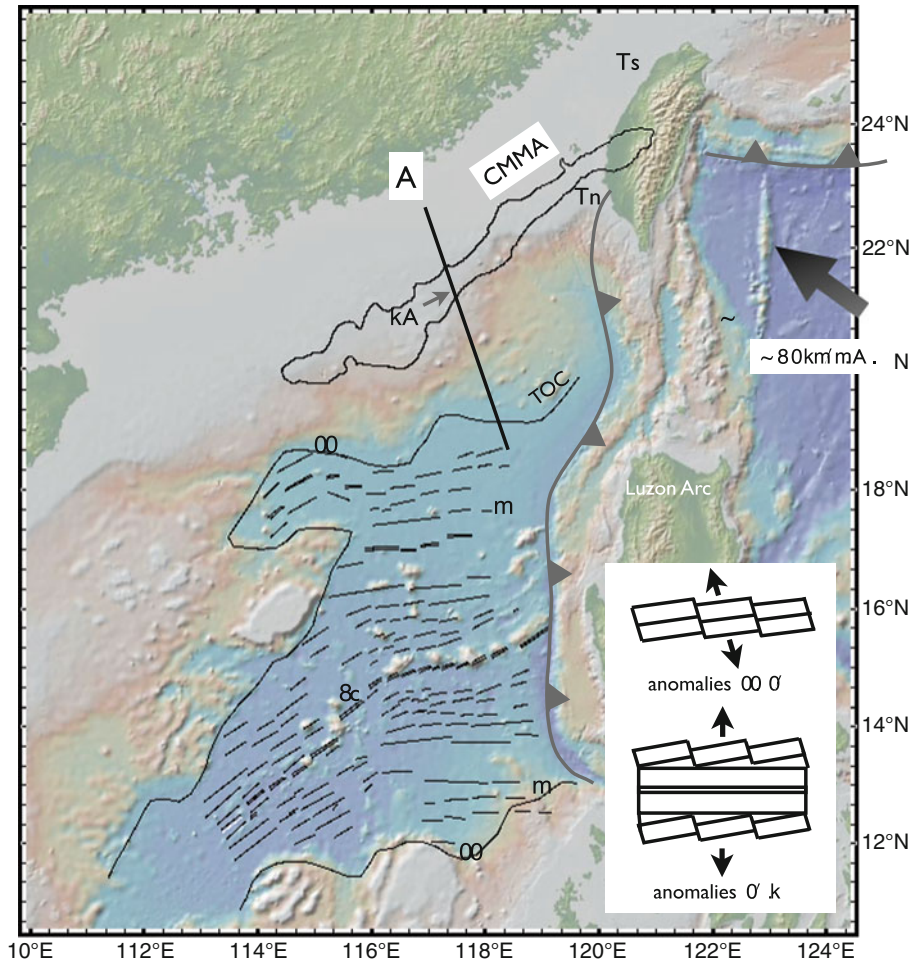

Fig. 8.1 Regional map of South China Sea showing ocean floor magnetic anomalies (from Briais et al. 1989) and continental margin magnetic anomaly (CMMA) from (Hsu et al. 1998). Ts = Taishi Basin; Tn = Tainan Basin; TOC = transitional-ocean crust boundary; black numbers = magnetic anomaly numbers; A = cross-section line in Fig. 8.3; "B" locates Batan Island and *arrow* locates shot-point station 7A in Fig. 8.3. Note westward retreat of Luzon arc over oceanic crust. In this and subsequent figures large *black arrow* shows relative motion vector od Philippine Sea plate with respect to Eurasia. Base map is from GeoMapApp (http://www.geomapap.org) using topography from Ryan et al. (2009).

the South China Sea closes by east-dipping subduction (Fig. 8.1). In the vicinity of Taiwan, the NUVEL-1 global plate motion model predicts that the Philippine Sea plate moves to the NW (~305°–310°) at a rate of 70 km/Ma relative to the Eurasian plate (Seno et al. 1993). Recent GPS data support a similar orientation (~305°–310°) with a slightly larger magnitude (82 km/Ma) (Yu et al. 1997). This relative plate motion vector is 15°–20° clockwise with respect to the orthogonal to the mountain belt; that is, convergence is slightly oblique in the collision zone.

In addition, the obliquity between the north-trending Luzon volcanic arc and the northeast-trending Asian passive continental margin suggests a time-for-space equivalence, thereby providing an opportunity to study the progression from subduction to collision (Fig. 8.2). That is, different positions along the mountain belt may be viewed as different time slices across the collision. Based on the current geometries of the arc and continental margin and current plate kinematics, the collision appears to be propagating southward at a rate of approximately 60 km/Ma (Byrne and Liu 2002b). However, this rate may have varied through time as the geometry of the colliding boundaries and relative plate motions may have changed over time. Suppe (1981) was the first to take advantage of the

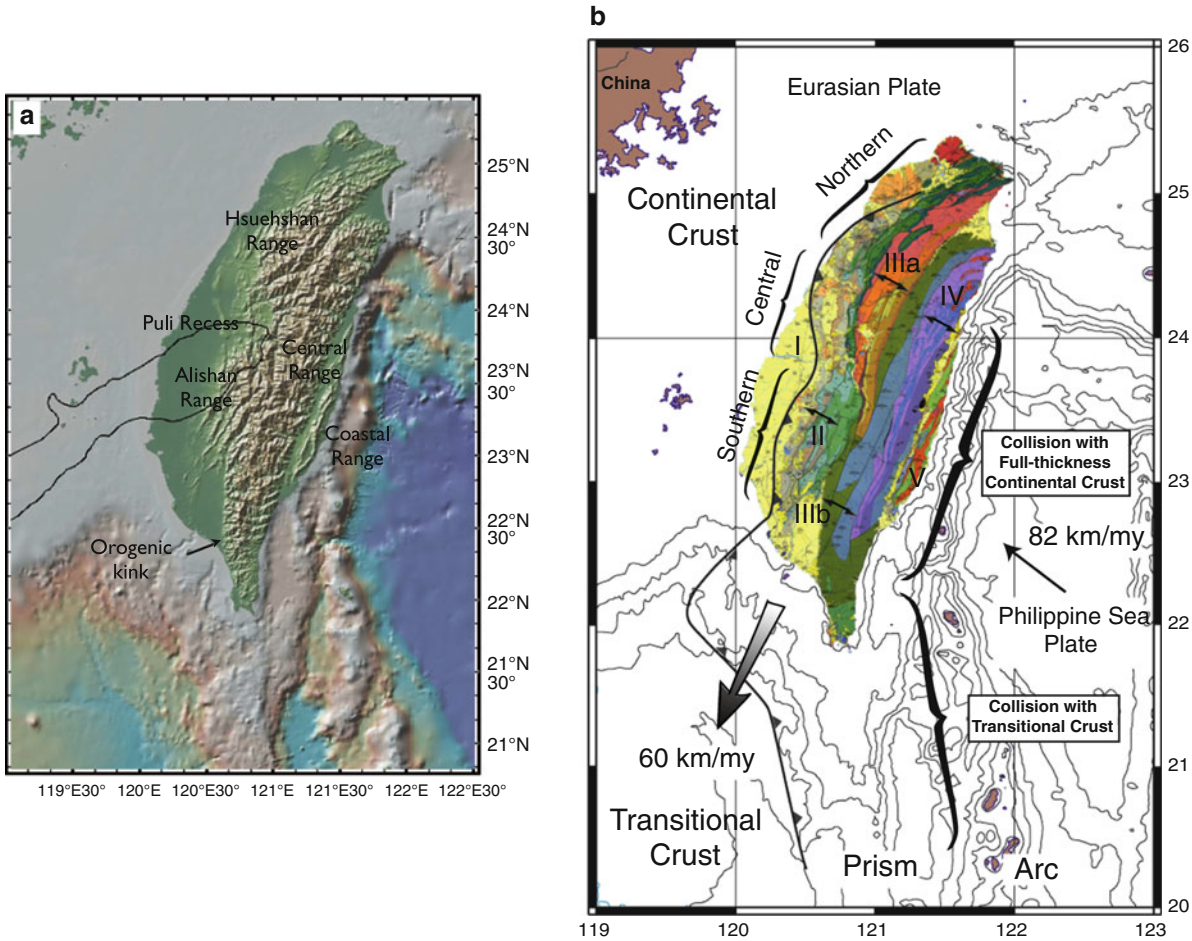

Fig. 8.2 (**a**) Topographic and (**b**) geologic (Chen 2000) maps of Taiwan. I – Coastal Plain; II – fold-and-thrust belt; IIIa and IIIb – slate belts; IV – pre-Tertiary metamorphic belt; V – Coastal Range. *Small arrow*: plate convergence vector, *large arrow*: propagation direction based on plate kinematics (Byrne and Liu 2002b). Note "kink" in southern Taiwan boundary between early and late collision. *Thin black line* in (A) shows outline of CMMA in Fig. 8.1. Base map is from GeoMapApp in (**a**) (http://www.geomapap.org) using topography from Ryan et al. (2009).

space-time equivalence in Taiwan and proposed an evolutionary scenario for the orogen. Assuming a steadily propagating collision and observations of a relatively uniform wedge width, cross-sectional area, and topographic slope, Suppe (1981), building on earlier work by Chapple (1978), inferred that both the size and shape of Taiwan were steady over million-year time scales. Dahlen et al. (1984) and Davis et al. (1983) incorporated this concept of a steady size and shape and proposed the critical wedge theory for steady-state orogens. The key assumption behind the steady-state model is that stresses within the wedge and along the basal décollement are at the Coulomb yield stress. As a result, a critical wedge maintains a constant taper angle (topographic slope + basal slope), which is a function of the décollement dip and the mechanical strengths of the wedge interior and base. Davis et al. (1983) interpreted the relative uniformity of the topographic slope of western Taiwan as evidence of a steady taper angle and, hence, steady crustal strength over the duration of the collision.

Though steady propagation continues to be a fundamental assumption underpinning many recent studies of Taiwan (e.g., Fuller et al. 2006; Stolar et al. 2007b; Willett et al. 2003), there is ongoing debate about whether collision propagation is instead punctuated (e.g., Lee et al. 2006; Mouthereau et al. 2002; Mouthereau and Lacombe 2006) or much slower than previously expected (e.g., Simoes et al. 2007). Indeed, one of the first detailed studies of geomorphic

parameters in the eastern Central Range (Willemin and Knuepfer 1994) indicated higher uplift rates in the central part of the range rather than in the south as predicted by the propagation interpretation. Recent research along the western Central Range also suggests higher uplift rates in the middle of the range (Byrne et al. 2009). These results are consistent with completely reset fission track ages of detrital zircons from southern Taiwan that show exhumation ages substantially older than predicted by southward propagation (e.g., 6 Ma vs. <1 Ma., Lee et al. 2006). In contrast to these results, Ramsay et al. (2007) have recently shown that the geomorphic patterns and indices in the southern most part of the Central Range are consistent with southward propagation, although the age and rates are not well constrained.

Several alternative models of the orogen have been proposed since the original critical wedge interpretations (Davis et al. 1983; Dahlen et al. 1984; Dahlen and Barr 1989). These early models, rather than treating the Central Range as a rigid backstop, have attempted to explain both the regional-scale topography and vergence of deformation of the Taiwan orogen. One of the first alternative models proposed that the orogen is a doubly vergent critical wedge (Koons 1990; Willett et al. 1993) consisting of a shallow-tapered western wedge, which extends from the toe of the fold-and-thrust belt to the main topographic divide, and a more steeply-tapered eastern wedge, which extends from the divide to the eastern edge of the Central Range (e.g., Willett et al. 2003; Whipple and Meade 2004, 2006).

A second model, presented by Carena et al. (2002), proposes that the Taiwan orogen, from the fold-and-thrust belt to the eastern Central Range, is a single west-vergent critical wedge. The rollover in topography at the main divide is explained by roll-over of the basal decollément (i.e., maintenance of a constant taper requires an eastward-dipping topographic slope). The backstop in this model, though not explicitly specified by Carena et al. (2002), is presumably the Luzon Arc and Coastal Range onshore.

Simoes et al. (2007) proposed a third model, which departs from critical wedge theory, that holds that the main components of the Taiwan orogen (e.g., the Hsüehshan, Backbone, and Central Ranges) act as rigid blocks and slide past each other along high-angle reverse faults (Simoes et al. 2007). In this model, the wedge is bounded to the east by a steeply dipping normal fault that raises the eastern Central Range over the Longitudinal Valley; the geometry and sense of slip along this fault are required to explain high maximum temperatures achieved by material inferred to be underplated beneath the Central Range. Because the physical basis for underplating is not known with certainty, the spatial patterns of mass influx and efflux are not necessarily related in the model of Simoes et al. (2007), and therefore, there is a wider range of allowable responses to surface erosion than in the critical wedge model.

Finally, Yamato et al. (2009) present a fully coupled thermomechanical numerical model that is consistent with much of the geological and geophysical data from Taiwan. Similar to a limited number of earlier studies (Wu et al. 1997; Lin 2000; Lin et al. 1998), Yamato et al. (2009) conclude that the orogen is "thick-skinned". In this context, they propose that deep-seated materials from the Chinese crust drive exhumation and erosion of the Central Range. In contrast to previous studies (e.g., Simoes et al. 2007), however, Yamato et al. (2009) propose that exhumation is related to frontal accretion of the whole (bi-layered, in their model) Asian continental crust. Their results also imply that the eastward increase in metamorphic grade across the orogen is related to the initial depth of the rocks, rather than significant subduction.

Investigations of the age of collision initiation have also been inconclusive. A relatively rapid increase in rates of deposition (Chen et al. 2001) and the age of the oldest sediments derived from the orogen (Lundberg and Dorsey 1990; Huang et al. 2006) suggest the collision initiated 3–4 Ma (Suppe 1984). Paleomagnetic data also show that collision-related clockwise rotation of the arc in the Coastal Range started about 2–3 Ma. These ages, however, may be minimum estimates because the northern part of the arc appears to be partially subducted beneath northern Taiwan and the Ryukyu arc. Older ages for collision initiation (~ 6 Ma) come from age of basin subsidence in the foreland, interpreted to be related to orogenic loading (Lin et al. 2003; Lin and Watts 2002; Simoes and Avouac 2006), and from fission track ages of completely reset detrital zircons from the Central Range (Liu et al. 2000, 2001; Lee et al. 2006). Lee et al. (2006) have recently proposed that both suites of ages may be correct and that the collision progressed in stages.

In northern Taiwan, the polarity of subduction is reversed and the volcanic rocks of the Luzon arc and the oceanic crust of the Philippine Sea plate are subducting to the northeast along the Ryuku trench (Suppe 1984; Yu et al. 1997; Wu et al. 2009). Subduction of the

Philippine Sea plate is evidenced by patterns of deep seismicity coinciding with high P-wave velocities (Wu et al. 2009; Rau and Wu 1995; Chou et al. 2009). Subduction in this area has also resulted in westward propagation of the Okinawa Trough into northeastern Taiwan, generating extension and orogenic collapse (Teng 1996). These data support the interpretation that the Taiwan orogenic system exhibits the full range of tectonic behavior from pre-collision in the southern offshore region, to active collision in southern and central Taiwan, to post-collision in northern Taiwan.

8.3 Geologic Background

Within the collision zone, continental shelf, slope, and rise sediments of the passive margin and part of the underlying basement have been deformed, metamorphosed and accreted (Byrne and Liu 2002a; Ho 1975, 1982; Suppe 1984), forming three tectonostratigraphic units that parallel the topographic grain of the island (Fig. 8.2). The units increase in metamorphic grade and deformational complexity from west to east, forming an active fold-and-thrust belt of Miocene to Quaternary sediments, a slate belt of Eocene to Miocene sediments, and a belt of pre-Tertiary metamorphic rocks. The boundaries between the units appear to be major fault zones, although none of the boundaries appears to be seismically active. All three belts are recognized along the length of the orogen; however, there are significant differences along strike, particularly north and south of the recess, or embayment, of the topographic centered on the city of Puli (Fig. 8.2).

The fold-and-thrust belt appears to display the most variation along strike, particularly around the Puli recess (Fig. 8.2a). North of this recess, a relatively thick, Miocene and younger sedimentary section (up to 8 km) is deformed into a series of tight, north to northeast-trending regional-scale folds with up to 7–8 km of structural relief (e.g., the Chuhuangkeng anticline, Ho 1976; Hung and Wiltschko 1993; Lacombe et al. 2001; Mouthereau et al. 2002; Namson 1981). In the area of the Puli recess in central Taiwan, imbricate sheets of Miocene to Quaternary sedimentary rocks characterize the fold-and-thrust belt, consistent with classic fold-and-thrust belts (e.g., Yue et al. 2005). The north-trending Chelungpu thrust, which generated vertical coseismic displacements of up to 10 m in the 1999 M 7.6 Chi-Chi earthquake, crops out in the middle of this section of the fold-and-thrust belt. The southern section of the fold-and-thrust belt (i.e., south of the recess) is wider than the belt to the north and balanced cross-sections and limited seismic reflection data suggest that it is characterized by duplex structures and/or basement (pre-Miocene)-involved imbricate thrusting (Ho 1976, 1988; Hung and Wiltschko 1993; Mouthereau et al. 2002). Thus, the thrust belt shows large variations in structural style from north to south, with regions in northern Taiwan where a thick sedimentary section is deformed, a central region where the stratigraphic section is thinner and a more classic thrust belt is present, and a southern region where the décollement appears to cut deeper in to the pre-Miocene (i.e., "basement").

The slate belt comprises two sub-belts generally west and east of the Lishan fault (Units IIIa and IIIb in Fig. 8.2b). The western sub-belt is exposed primarily in the Hsüehshan Range although it also continues southward across the Puli recess, where the bedrock is often laterized (Hsieh, M.-L. 2008, personal communication) and continues into the western edge of the Central Range where the sub-belt pinches out. In the Hsüehshan Range an east-dipping cleavage on the west side of the range and a west-dipping cleavage on the east side form a regional-scale popup structure (Clark et al. 1993). In contrast, the eastern sub-belt of the slate belt crops out in the Central Range where it displays a well developed, southeast-dipping structural fabric (Fisher et al. 2002, 2007). Incremental strain markers show a top-to-the-northwest sense of shear (Fisher et al. 2002) throughout the slate belt in this range. Southeast of the Puli recess, the eastern sub-belt supports the highest peak in the orogen (Yushan 3,952 m) and exposes the oldest sediments of the pre-collisional passive margin (the Eocene Shihpachungchi Formation). In the southern Central Range, the slaty cleavage is less penetrative and pencil cleavages are locally present. Further south, in the Hengchun Peninsula, penetrative cleavages are rare to non-existent. These observations show strong along- and across-strike structural variability internal to the slate belt.

The Tananao schist, a complex of multiply deformed metasediment, marble, and granite in the eastern Central Range, is interpreted as exhumed Eurasian continental basement (Ho 1986). Regionally, the Tananao schist has been subdivided into two belts: (1) the High T/Low P Tailuko belt (of Taroko gorge) and (2) the High P/Low T greenstones and schists of the Yuli belt.

Together, these belts are interpreted to represent the remnants of a late Mesozoic subduction complex that was thinned during Tertiary rifting prior to being incorporated into the Taiwan orogenic wedge (Yui et al. 1990). The interpretation of fabrics and paleotemperatures in the Tananao schist, however, is hampered by the difficulty in differentiating Mesozoic deformation and metamorphism from features related to the ongoing collision.

The Longitudinal Valley, a relatively straight basin that separates the Asian basement and cover of the Central Range from the accreted arc complex of the Coastal Range represents one of the most enigmatic morphotectonic features in Taiwan. The mountain fronts that define the western and eastern margins of the valley are in places demonstrably active (e.g., Lee et al. 2001, 2002) or recently active (e.g., Shyu et al. 2006) fault zones with shortening rates on individual faults locally as high as 15 mm per year (Angelier et al. 1997; Lee et al. 2002). Moreover, leveling surveys across the southern part of the valley indicate uplift of both the Central and Coastal Ranges relative to the valley floor at a rate of ~3 cm per year (Liu and Yu 1990). Thus, the flanks of the Longitudinal Valley are everywhere a site of rapid horizontal and vertical deformation, yet this feature persists along the length of the active collision zone.

The Coastal Range of easternmost Taiwan represents the northern extension of the Luzon volcanic arc and forearc basin that has collided with and accreted to Taiwan. The arc complex consists of a lower Miocene sequence of intermediate to mafic volcanic and shallow intrusive rocks, a middle to upper Miocene sequence of marine pyroclastics, andesitic tuff, lapilli tuff and tuff breccia, and finally, an arc-fringing carbonate reef complex (Ho 1986). The arc complex is unconformably overlain by a 4–6.5-km-thick collisional Plio-Pleistocene basin sequence derived from the Central Range to the west (Dorsey 1992). This syncollisional sequence records rapid subsidence of the arc complex and unroofing of the mountain belt to the west, with increasing metamorphic grade of lithic fragments up section (Dorsey 1992). A series of Holocene elevated shorelines along the east coast of the Coastal Range indicates active uplift, with rapid uplift rates of ~2.5 to >8 mm per year (Liew et al. 1993). However, recent compilations of continuous GPS in the northern Coastal Range (Lin et al. 2010) show significant subsidence relative to the Longitudinal Valley and the Central Range. These results are consistent with interpretations of seismicity and Vp tomography indicating subduction of the arc beneath the Ryukyu subduction zone.

8.4 The Chinese Passive Margin: The Collisional Footwall

The South China Sea is a relatively large marginal basin of mid-Tertiary age surrounded on three sides by blocks of continental crust (Fig. 8.1). The middle of the basin is composed of oceanic crust and preserves several sets of magnetic anomalies (Hayes and Taylor 1978). The northern and southern margins are passive margins that formed as the basin opened whereas the western boundary appears to be a left-lateral transfer zone that may connect to the Red River fault in China. In fact, Briais et al. (1993) have argued that the basin formed in conjuncture with large (500–600 km) left-lateral displacements along the Red River fault as India collided with Eurasia. Briais et al. (1993) also completed a detailed study of the anomalies in the middle of the basin and proposed a complicated spreading history that included asymmetric spreading, propagating ridges and ridge jumps. In general, however, the history is marked by three directions of spreading (Fig. 8.1 inset): an initial phase of NW–SE spreading (32–30 Ma; anomalies 11 and 10), a middle phase of N–S spreading (30–24 Ma; anomalies 10–6b) and a late phase of NW–SE spreading (24–18 Ma; anomalies 6b to 5a). The earliest phase of NW–SE spreading appears to have defined the generally geometry of the continental margins, including the area of the arc–continent collision in Taiwan.

Nissen et al. (1995) investigated the structure and general composition of the margin of the South China Sea south of the collision and documented a relatively wide zone of transitional crust (~250 km across strike, Fig. 8.3) composed of thinned continental crust, volcanic and other igneous rocks, and a high velocity lower crust. Nissen et al. (1995) interpreted the high velocity lower crust as underplated gabbroic rocks and proposed that the steep boundary between these rocks and more continental-like rocks in the lower crust to the north was responsible for a magnetic anomaly observed at the surface. Wang et al. (2006) recently confirmed this transition in the lower crust

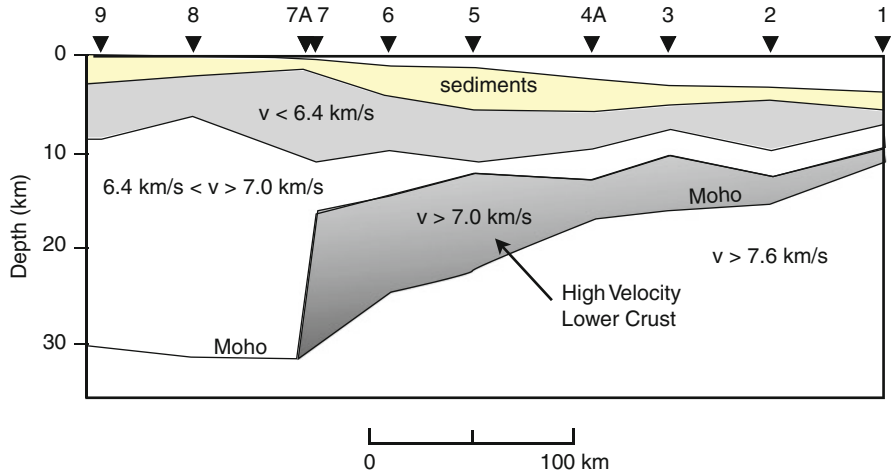

Fig. 8.3 Geophysical cross-section from Nissen et al. (1995). Numbers show range of velocities (km/s) in crustal layers. Note dramatic thinning of continental crust from a normal thickness of ~30 to ~5 km from at shot-point 7A. Dark shaded layer below thinned crust (labeled) is interpreted by Nissen et al. (1995) to be gabbroic in composition.

using higher resolution data from ocean bottom seismometers. The magnetic map of this region shows a northeast trending linear high that lies just landward of the continental shelf (Fig. 8.1) (Wang et al. 2002; Hsu et al. 1998), consistent with Nissen's (1995) interpretation that it can be used as a proxy for the boundary between continental and transitional crust.

The magnetic high also continues into central Taiwan where it is parallel to the seaward edge of a previously recognized basement high (Fig. 8.4) (i.e., Peikang High; see also Cheng 2004 for a similar interpretation). The magnetic high (Fig. 8.4a), however, extends further northeast into central Taiwan and appears to be truncated or offset long a northwest-trending fault or fracture zone (Fig. 8.4a). The apparent fracture zone is parallel to the early spreading direction in the South China Sea (i.e., NW–SE, Fig. 8.1) and orthogonal to the trend of pre-breakup (~58–30 Ma) sedimentary basin (e.g., the Nanjihtao Basin, Lin et al. 2003) along the margin. We therefore propose that the northwest trending truncation of the magnetic anomaly represents a partially subducted continental margin fracture zone in the passive margin of Eurasia.

Seismic reflection data and subsidence records of deep wells provide additional constraints on the evolution of the margin in the area of Taiwan and show two en echelon, post-rift sedimentary basins, centered on the magnetic anomaly (Fig. 8.4b). The northern, or Taishi, basin, records deposition throughout the Eocene, Oligocene and Miocene and is preserved both offshore northwestern Taiwan (Lin et al. 2003; Teng 1987) and in the sedimentary record of the Hsüehshan Range (Teng 1987). The southern, or Tainan, basin records deposition of Miocene sediments and is preserved offshore southwest of Taiwan; an earlier record of Eocene to Oligocene deposition may have been removed by late Oligocene uplift and erosion in this area (Lin et al. 2003). The eastern slate belt in the southern Central Range, which is also missing an Oligocene section, may be the exhumed equivalent of the Tainan Basin. The slate belt, however, also exposes Eocene sediments, suggesting that both sedimentary basins may have contained Eocene sediments.

The magnetic anomaly between the two en echelon basins widens slightly and the anomaly's seaward edge curves from 60° to 75°, consistent with the recognized reorientation of the spreading direction in the South China Sea at the time of anomaly 10 (~30 Ma) (Fig. 8.1 inset). Normal faults that bound the Tainan Basin south of the anomaly are also slightly curved. North of the anomaly, the western edge the Taishi Basin (30–6.5 Ma) (Fig. 8.4b) occupies the triangular zone between the anomaly and the fracture zone (Fig. 8.4), suggesting that the basin propagated across the fracture zone as the spreading direction changed and the magnetic anomaly rotated seaward. This slight reorientation and extension north of the anomaly may have also isolated a fragment of continental crust, forming the Peikang High.

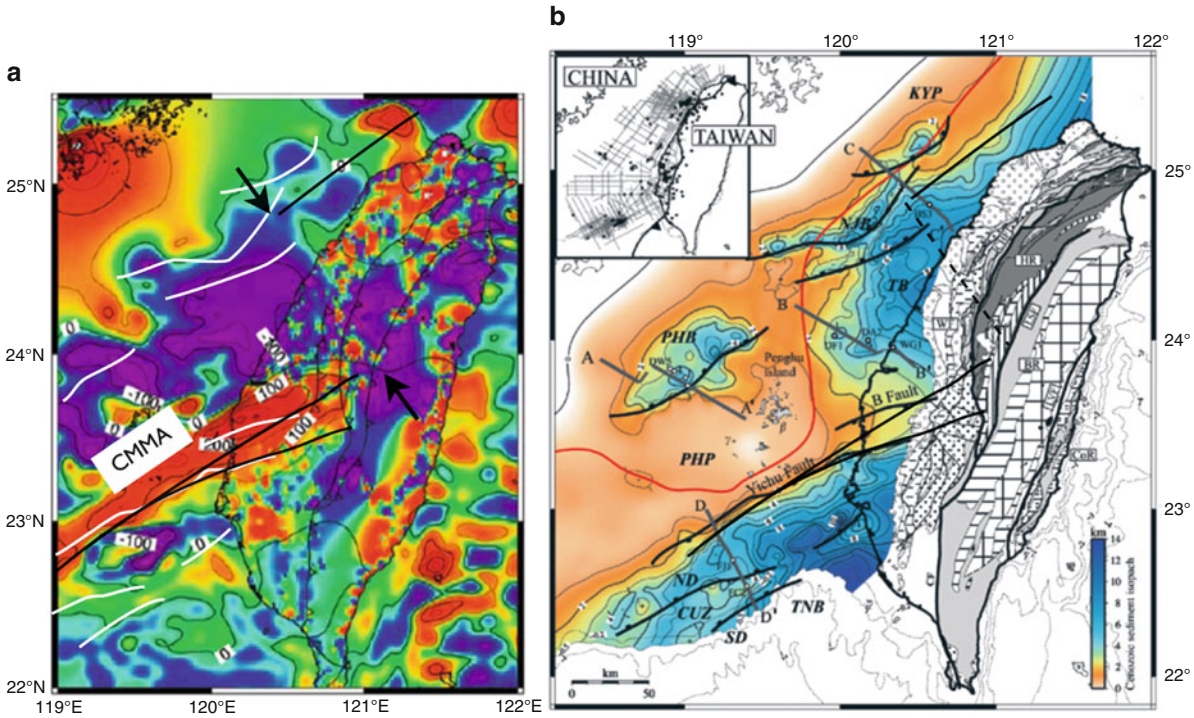

Fig. 8.4 (**a**) Magnetic anomaly (Cheng 2004) and (**b**) depth to Mesozoic basement (Lin et al. 2003) maps. *Arrows* in (**a**) show trend and extent of interpreted fracture zone that truncates magnetic anomaly. *Dashed black line* in (**b**) shows Interpreted fracture zone. *Straight black lines* show interpreted edge of continental crust based on magnetic anomaly and Mesozoic basement morphology; these lines are shown in subsequent figures for reference. *White lines* in (**a**) are normal faults shown as *black lines* in (**b**). Contours in (**a**) are nanoteslas. CUZ = Central Uplift Zone; KYP = Kuanyin Platform; ND = Northern Depression; NJB = Nanjihtao Basin; PHB = Penghu Basin; PHP = Penghu Platform (or high); SD = Southern-Depression,TNB = Tainan Basin,TB5 = Taihsi Basin; BR = Backbone Range; CoR = Coastal Range; HR = Hsüehshan Range; WF = Western Foothills. Major faults: CF = Chaochou; CHF = Chuchih, LSF = Lishan; LVF = Longitudinal Valley.

The western edge of the Taishi Basin, which crosses the proposed fracture zone and laps onto the Peikang High, preserves a progressively thicker Miocene section from southwest to northeast (Fig. 8.4b). For example, near the Peikang High the Miocene is only a few hundred meters thick whereas northeast of the fracture zone it is 2–3 km thick. The rates of deposition during the Miocene also increase to the northeast from 35 m/Ma near the Peikang High to 120–190 m/Ma north of the fracture zone (Lin et al. 2003; Mouthereau et al. 2002). Although this change in deposition may be gradational, previous authors have proposed that it may also occur in two northwest-trending steps, one near the Peikang High (recognized as the Pakushan transfer zone) (Deffontaines et al. 1994; Mouthereau et al. 2002) and the second parallel to the proposed fracture zone (recognized as the Sanyi-Puli transfer zone) (Lee et al. 1997; Rau and Wu 1995; Deffontaines et al. 1994, 1997).

In summary, rifting in the South China Sea appears to have formed a relatively wide area of transitional crust, including a continental margin magnetic anomaly (CMMA). Based on geophysical data along the margin in the South China Sea, the CMMA serves as a proxy for the edge of a continental crust of normal thickness (~30 km). In Taiwan, the anomaly appears to be truncated by a northwest-trending fracture zone, defining a continental margin prong or promontory. Two post-rift sedimentary basins formed "en echelon" north and south of the truncated anomaly and the northern basin appears to have propagated across the fracture zone during a change in spreading direction. In the following sections we evaluate the role that the wide zone of transitional crust and the continental promontory, including its sedimentary cover, played in the collision. For easy reference, the black lines (continuous and dashed) in Fig. 8.4 are used in subsequent figures to represent the seaward edge of the continental margin.

8.5 Luzon Magmatic Arc: The Collisional Hanging Wall

The Luzon arc records subduction-related volcanism since at least the early Miocene (16–15 Ma) (Yang et al. 1995, 1996) and provides important clues to the evolution of the collision as the subducting plate changes from oceanic to continental crust. Although the arc is generally typical of subduction zone magmatic arcs and broadly andesitic in composition, several regional-scale segments have been recognized along strike. For example, the segments north and south of Luzon Island appear to have been pinned, or slowed, by thicker crust in the subducting plate (Fig. 8.1). In the north, the "S-shaped" inflection in the deformation front (Fig. 8.1) correlates with the boundary between oceanic crust in the south to transitional crust in the north whereas in the south, collision of the Palawan Ridge appears to be limiting westward migration of the arc. As a result, the central segment (Luzon) has retreated westward over the oceanic crust of the South China Sea. Similar arc geometries above oceanic lithosphere with changing physical properties along strike have been documented at a number of margins around the world (Wallace et al. 2005; Vogt et al. 1976; McCabe 1984), consistent with the observations from Luzon.

The northern segment (e.g., north of Luzon) also appears to be segmented. Well-developed, stratavolcanoes of Quaternary age occur in northern Luzon Island and as far north as Batan Island (20.5°N, Fig. 8.1), about 100 km south of Taiwan. Relatively young K–Ar ages (30 ka) have also been reported from the islands just south of Taiwan, but volcanic activity this far north appears to be more limited. The volcanic rocks in the area of Batan Island are also distinctive in containing mantle xenoliths and geochemical signatures that suggest the involvement of enriched mantle considered to reside in the continental lithosphere (Yang et al. 1995, 1996). Yang et al. (1996) has also recognized a double arc, with older arc rocks to the west, south of Batan but not north of it. Yang et al. (1996) has also pointed out that this unusual along-strike change in arc character and composition correlates with a relatively abrupt change in the dip of the slab from shallow in the south to nearly vertical in the north, possibly resulting in a tear in the slab in this area and allowing lateral flow of Eurasian mantle. Yang et al. (1996) suggested that the partial subduction of the inactive South China Sea spreading center beneath Luzon resulted in shallowing of the subduction zone, leading lateral flow of the mantle and arc contamination.

Alternatively, the area of the proposed broken slab (approximately Batan Island) also correlates with the transition from oceanic to transitional crust in the subducting plate. We, therefore, propose that westward retreat of the central segment of the Luzon arc over oceanic crust caused shallowing of the slab in this area, leading to the tear proposed by Yang et al. (1996). In this interpretation, the pinning of the arc north of Luzon by the subduction of transitional crust marks the initial stages of the arc–continent collision in Taiwan. This initial collision, however, is between the arc and transitional crust rather than between the arc and continental crust of normal thickness.

Collision of transitional crust with the arc also appears to be recorded in the geology and morphology of the arc and forearc north of Batan Island. At about 21°N lat. (about 50 km north of Batan, Fig. 8.1) the accretionary prism associated with the Manilla Trench widens from about 30 km to nearly 60 km, consistent with subduction thicker crust and/or the influx of offscraped or underplated materials into the wedge. Slightly further north (~ 21.25°N) a well-defined back thrust (i.e., a west-dipping thrust) in the Luzon forearc signals the collapse of the forearc (Malavieille and Trullenque 2009), indicating that the colliding materials are of sufficient strength to transmit horizontal stresses within the forearc. Detailed structural studies of the forearc in this area also show that the back thrust overlies a more significant, east-dipping thrust that separates the underthrusted forearc from relatively undeformed arc. Cheng (2008), based on P-wave tomography has also proposed that the relatively thin crust of the forearc is progressively thrust beneath the arc from about 21°N to 23°N where it appears to lie completely beneath the arc.

Paleomagnetic studies of the arc rocks in the Coastal Range of Taiwan provide additional information about the kinematics and timing of the collision. Lee et al. (1991) collected sedimentary samples from 132 sites that overlie the arc volcanic rocks and range in age from early Pliocene to Pleistocene. Based on the age and paleomagnetic characteristics of each site, Lee et al. (1991) divided the range into northern, central and southern sections. He also recognized an older and a younger suite of sites in each section. The results

show that all three geographic sections record 20° to 25° of clockwise rotation, and that the rotations are diachronous from north to south. In the north, rotation of the arc occurred 2–3 Ma, whereas in the central section it occurred 2.1–1.7 Ma and in the south it occurred after about 1.4 Ma. The data also suggest that the rotations occurred relatively quickly at each site (~0.5 m.y.), and that the rotation migrated southward at about 70 km/Ma. This migration rate is only slightly higher than the most recent calculations for the rate of collision propagation of 60 km/Ma (Byrne and Liu 2002b). A sharp clockwise bend in the topographic grain of the orogen about 70 km south of the Coastal Range (at about 22.3°N lat) is also consistent with this propagation rate and suggests that the bend in the topographic grain marks the area of active, collision-related oroclinal bending.

Finally, isotopic and geochronologic data from accreted volcanic centers in the Coastal Range show a systematic trend in geochemical signatures and in the age of youngest volcanism. In the north, the top of the volcanic rocks yield dates of NN11 (< 8–5 Ma, Chi et al. 1981) and 6–5 Ma (40Ar/39Ar; Lo and Onstott 1995) whereas the top of the same stratigraphic horizon in the south yields ages of 5.6 Ma (40Ar/39Ar; Lo and Onstott 1995). Volcanism in the offshore Lutao and Lanhsu Islands ended at 1.5 Ma and 0.5–0.04 Ma (Yang et al. 1995), respectively. Thus, both the microfossil and radiometric ages indicate that the initial arc–continent collision began at ca. 6–5 Ma in the north and propagated southward. A progressive increase in continental contamination of magmas also correlates with progressively younger ages the volcanic rocks and is interpreted to reflect the systematic increase in continentally derived sediments through time (Dorsey 1992).

In summary, the arc south of Taiwan records significant changes in its structure, age and chemical signature hundreds of kilometers before it collides with the continental margin of China in the area of Taiwan. These along-strike changes appear to reflect the subduction of a relatively wide zone of transitional crust rather than well-developed oceanic crust. We propose therefore that the "early collision zone" extends from Batan Island (i.e., approximate boundary of oceanic to transitional crust in the subduction plate) to the zone of active oroclinal bending (i.e., the kink in topography) in southern Taiwan. This is an along-strike distance of about 200 km, which, assuming a collision propagation rate of 60 km/m.y., suggests that the initial collision (of transitional crust) may have started nearly 3 Ma before the arc collided with continental crust of normal thickness. In addition, because the trend of the boundary between transitional and oceanic crust strikes more easterly than the strike of the continental margin, the propagation rate of the collision with transitional crust would have been slower by about a third. The collision (initially with transitional crust), therefore, may have started 6–7 Ma.

8.6 The Collision Zone: Implications of Transitional Crust and a Continental Margin Promontory in Collision Kinematics, Dynamics and Exhumation

Here we examine the arc–continent collision in Taiwan in more detail and evaluate the role that subducting crust of variable composition and thickness may have played, and may continue to play, in the development of the orogenic system. In the previous sections we proposed that the boundary between oceanic and transitional crust marks the transition from normal subduction, south of the boundary, to collision north of the boundary. That is, the subduction-collision transition occurs about 200 km of Taiwan, near Batan Island. This location of the transition is significantly farther south than most previous interpretation that place the transition closer to Taiwan (Huang et al. 2006; Suppe 1984; Malavieille and Trullenque 2009). Teng (1990) is a notable exception as he also recognized the wide zone of transitional crust and proposed that the collision may have started 6–8 Ma. Based on the clear correlation between changes in the subducting plate and the growth of the prism and the collapse of the forearc to the north, we propose a two-staged collision: An early stage of the collision from Batan (i.e., ~ lat 21°N) northward to the "kink" or orocline in the orogenic topography in southern Taiwan (Figs. 8.1 and 8.2) and a late, or current stage of the collision from the kink to northern Taiwan where the Central Range is subsiding on the southern flank of the Okinawa Trough and the arc is subducting beneath the Ryukyu trench.

8.6.1 Early Stage of the Collision

This stage of the collision is primarily preserved in the off shore region south of Taiwan, which is only accessible remotely, and on the Hengchun Peninsula. Available data indicate that as progressively thicker transitional crust is subducted from south to north the depth of the sea floor at the Manila Trench shallows and the composition of the sediments on the subducting plate changes from dominantly hemipelagic clays and silts in the south to silts and sands in the north (Yu and Huang 2009). Seismic reflection data also show that at shallow structural levels near the deformation front the décollement is relatively deep as nearly all of the sediments on the subducting plate are being accreted (Yu and Huang 2009; McIntosh et al. 2005). Thus, at deeper structural levels in the prism, where the décollement probably steps to deeper levels, blocks of transitional crust also may be incorporated into the prism.

Detailed geophysical studies across the early collision in southern Taiwan also show sediment accretion and suggest the possible involvement of crustal rocks. For example, McIntosh et al. (2005) recognized a relatively high P-wave velocity core beneath the Hengchun Peninsula in southern Taiwan with velocities that are consist with either metamorphosed accretionary prism materials or accreted basement from the subducting transitional crust. In addition, Cheng (2008) (Fig. 8.5) has recognized blocks of anomalously high velocity and density further north in the southern Central Range. The blocks were mapped using high-resolution seismic tomography of both Vp and Vs waves integrated with a gravity model. The Vp and Vs waves also provide Poisson's ratio (σ). Cheng (2008) was able to recognize at least 3 km-sized

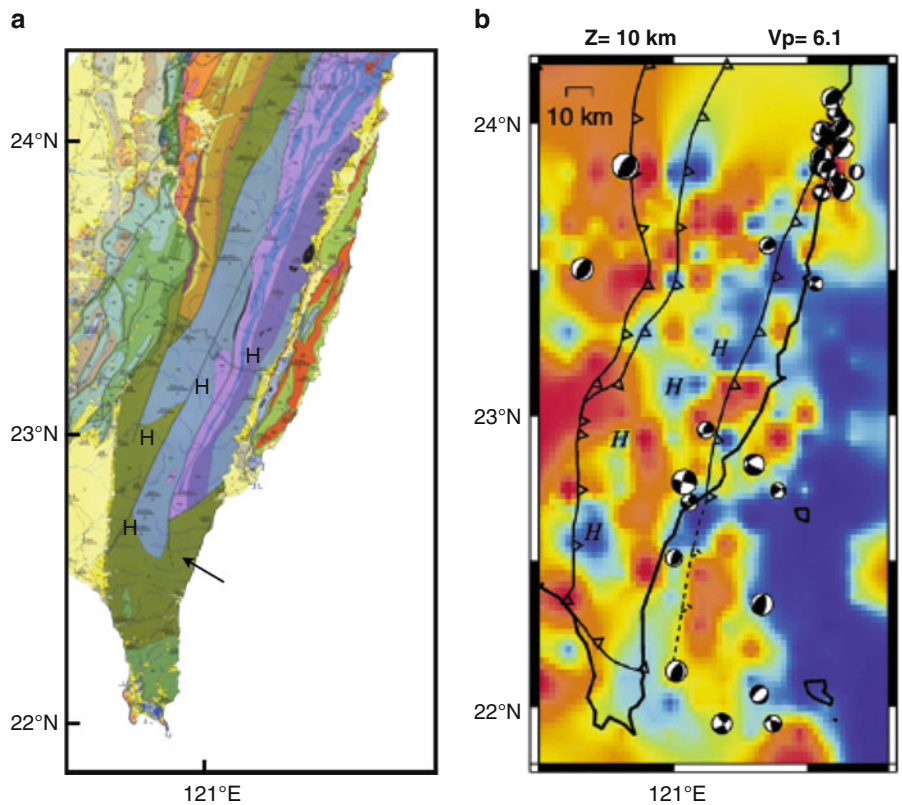

Fig. 8.5 (**a**) Geologic map of the southern Central Range (Chen 2000) and (**b**) map view of Vp velocity structure at 10 km depth (Cheng 2008). "H" shows locations of high velocity anomalies interpreted as accreted blocks of mafic (transitional?) crust. Note strip of mafic rocks in Central Range and locations of anomalously old reset fission track ages [*arrow* in (**a**)](Liu et al. 2001; Lee et al. 2006).

blocks in the upper and middle crust of the Central Range with anomalously high Vp and high σ, which he interpreted as representing slivers of mafic crust. Because the blocks are interpreted to be slivers in the continental materials of the Central Range (i.e., the pre-Tertiary metamorphic rocks and/or slate belt), Cheng (2008) also proposed that the subducted transitional crust was unusually wide.

Additionally, the only exposed tectonic slivers of mafic rocks that are part of the late Tertiary collision crop out in the area of mafic blocks described by Cheng (2008) (Fig. 8.5). The exposed mafic unit occurs along the faulted contact between the slate belt and the pre-Tertiary metamorphic rocks (Chen 2000). The rocks have not been studied in detail or dated, but may represent pieces of accreted oceanic crust or mantle, or part of an underplated gabbroic sequence. In any case, their occurrence is consistent with geophysical data that indicate similar bodies at depth and suggest the involvement of transitional crust in the early stages of the collision. Eroded equivalents of these mafic blocks may also be preserved in the Kenting mélange (Huang et al. 1985), which is exposed on the southwestern tip of the Central Range.

Evidence for an early stage to the collision in Taiwan also comes from unexpectedly old exhumation ages of accreted sediments exposed in the Central Range. For example, Liu et al. (2001) obtained completely reset zircon fission track ages from sandstones in both northern and southern Taiwan. Liu et al. (2001) interpreted the northern ages as evidence that collision started 6 Ma or earlier. This interpretation is also consistent with cooling ages (4–3.6 Ma) Liu (2000) obtained from sandstone boulders eroded from the Central Range and deposited in the northern Coastal Range, and with the age of the earliest foreland basins (~6.5 Ma; Lin et al. 2003; Simoes and Avouac 2006; Teng 1987).

More recently, Lee et al. (2006) have confirmed the older zircon ages in southern Taiwan documented an additional subset of "old" grains and identified a suite of younger ages for completely reset detrital zircon and apatite grains. Based on these new data, Lee et al. (2006) proposed a multiple stage collision that started ~6 Ma in both northern and southern Taiwan (Fig. 8.6). The younger ages and their distribution in southern Taiwan also suggest to Lee et al. (2006) that the area records an increase in exhumation rates starting about 1–3 Ma and that this stage of relatively rapid uplift may be propagating southward into the area of Hengchun Peninsula. This proposed increase in exhumation cooling supports the hypothesis that the collision is composed of early and late stages.

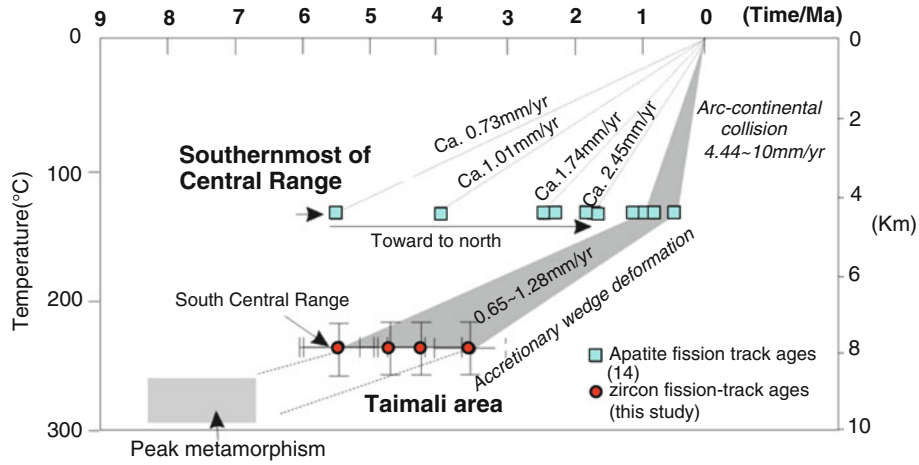

Fig. 8.6 Compilation of completely reset detrital apatite and zircon fission track ages from sandstones in the southern Central Range (from Lee et al. 2006). Data from Taimali area (*shaded*) show a change in exhumation cooling rates from ~1 mm/yr to up to 10 mm/yr at ~1 Ma whereas apatite data from southernmost Central Range show a progressive decrease in ages from south to north. Proposed increase in cooling at ~2 Ma is consistent with the transition from early to late collision stages proposed here.

8.6.2 Late Stage of the Collision

Our discussion of the late stage of the collision progresses from a review of the current state of stress (seismicity) and surface displacements (GPS) to signatures in the topography and structural fabrics and finally to crustal-scale observations and possible evolutionary scenarios of the orogen. Our overall goal is to understand the possible link between the subducting continental margin and the kinematics and dynamics in the early and late stages of the collision. The results strongly suggest: 1) that the continental margin promontory has had significant impact on the evolution of the orogen; 2) that the youngest stage of the collision is fundamentally three-dimensional, and 3) that the southward propagation inferred from the tectonic setting may only apply to the relatively recent history of the Coastal Range and the southern tip of the Central Range.

8.6.2.1 Seismicity

Three well-defined patterns of seismicity in west-central Taiwan appear to reveal the partially subducted continental margin and associated fracture zone. One of the patterns is defined by a steeply dipping, planar cluster of seismicity, generally recognized as the Sanyi-Puli seismic zone (Wu et al. 2004), which parallels the proposed fracture zone (Fig. 8.7a). This zone of activity was particularly well-defined prior to the 1999 Chi-Chi earthquake (Wu et al. 2004) and is composed of an upper cluster of seismicity that extends from 5 to 15 km and a lower cluster that extends from 20 to 35 km. Preliminary analyses of focal mechanisms (Wu and Rau 1998; Wu et al. 2004) indicate a complex zone of deformation but with many events recording left-lateral motions on NW-striking planes. The second pattern of seismicity developed in the few months after the Chi-Chi earthquake and occurs

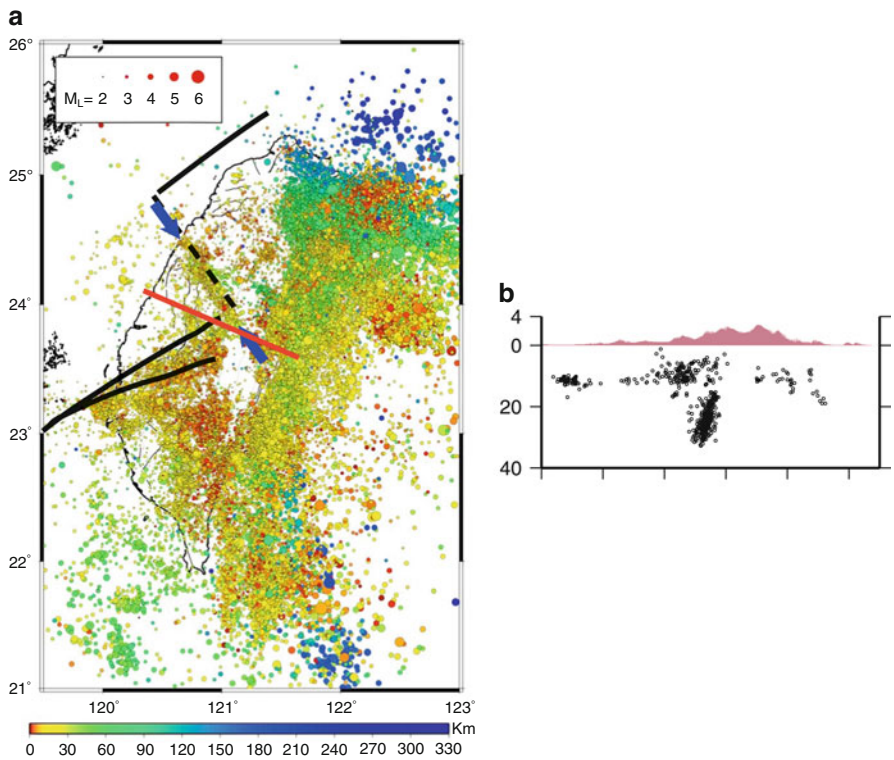

Fig. 8.7 (**a**) Pre- Chi-Chi seismicity (1990–1995; Lin et al. 2010) that shows Sanyi-Puli seismic zone (delimited with blue arrows) and seismicity along the southern edge of continental promontory. Note Sanyi-Puli zone parallels proposed continental margin facture zone (*dashed line*). (**b**) Post-Chi-Chi seismicity (20 Sept. 1999 to 31 Dec. 1999) along a vertical profile in central Taiwan (location shown in (**a**)) (from Wu et al. 2004). Note steeply west-dipping zone of seismicity in the middle of the section that correlates with the eastern edge of the promontory.

at the southeast end of the Sanyi-Puli zone (Fig. 8.7b). This zone also extends to nearly 40 km. The pattern of seismicity defines a planar, steeply west-dipping zone and focal mechanism solutions yield mostly top-to-the-east, or thrust, sense of slip (Wu et al. 2004). This cluster correlates spatially with the proposed eastern corner of the continental margin (Fig. 8.7b). The third seismic pattern occurs along the southeast edge of the magnetic anomaly and could equally be described as a seismic–aseismic transition in map view. This zone trends slightly oblique to the structural grain of the fold-and-thrust belt but parallel to the trend of the rifted margin (Fig. 8.7a) (Lin et al. 2003). This seismic–aseismic transition is present in both pre- and post-Chi-Chi data. Earthquakes south of the magnetic anomaly are relatively shallow (<20 km) and have a variety of focal mechanism solution, although Hsu et al. (2008) has recently proposed that the dominant focal mechanism solutions in this area changed from mostly strike-slip to most normal before and after the Chi-Chi earthquake. Taken together these zones of seismicity define a triangular zone in central Taiwan with relatively low seismicity, which approximates the boundary of the proposed continental margin promontory (Fig. 8.7a).

In addition to the clusters of seismicity that define the perimeter of the promontory, the distribution and magnitude of co-seismic slip associated with the 1999 Mw 7.6 Chi-Chi earthquake also correlate with the promontory (Fig. 8.8). The surface rupture of the Chelungpu fault, which slipped during the earthquake, generally trends north–south, slightly oblique to the structural grain of the orogen. Figure 8.8a shows the distribution of slip greater than 1 m based on GPS data

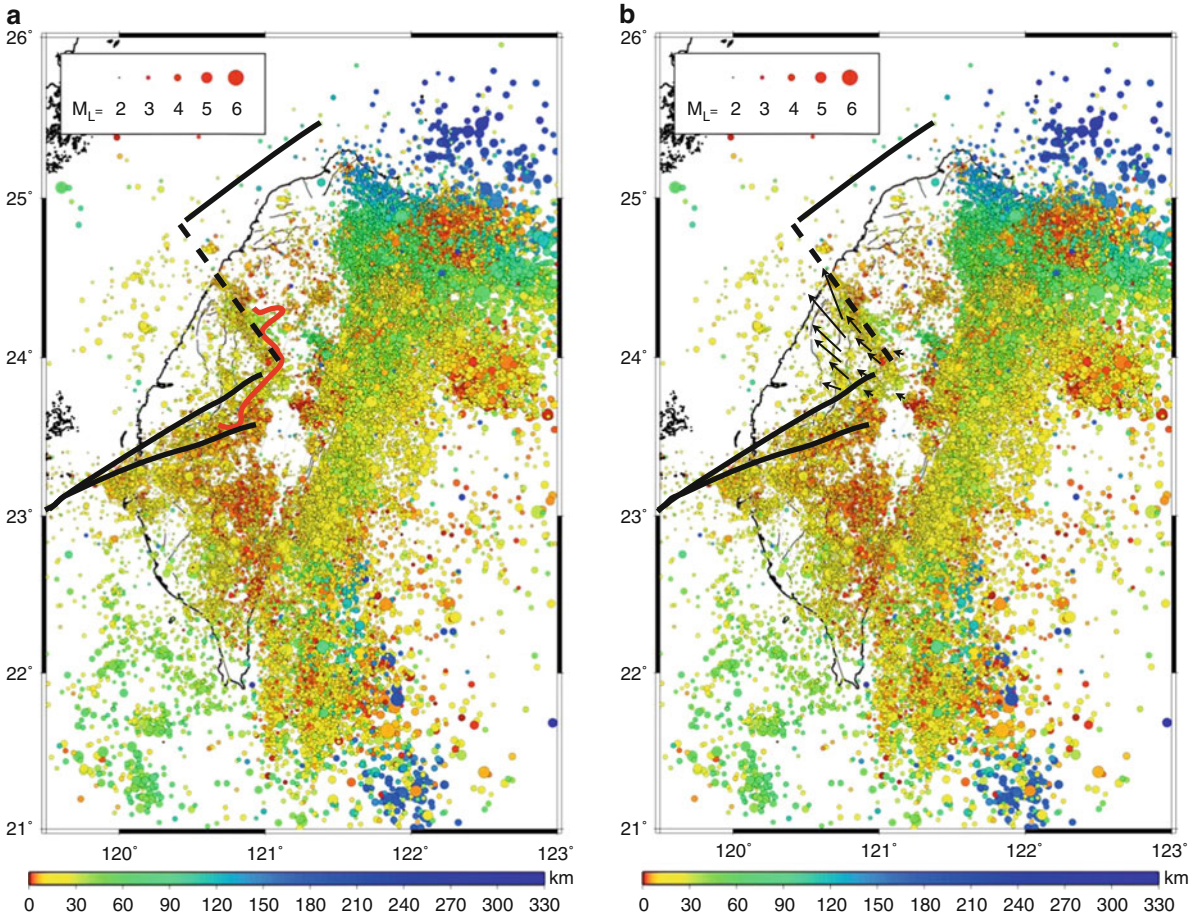

Fig. 8.8 Co-seismic slip associated with the 1999 Mw 7.6 Chi-Chi earthquake based on GPS data (Yu et al. 2003; Hsu et al. 2003). (**a**) *Curved line* shows distribution of area that slipped greater that 1 m (Hsu et al. 2003) and (**b**) *arrows* show representative slip vectors (Yu et al. 2003).

(Yu et al. 2003; Hsu et al. 2003) overlain on the proposed interpretation of the continental margin. Although irregular, the 1 m contour generally follows both the southeastern and northeastern boundaries of the promontory. The magnitude of co-seismic slip also varies systematically across the promontory. In the southern end of the Chelungpu fault, near field displacements are about 1.5 m. whereas at the north end of the fault, displacements are greater than 10 m (Yang et al. 2000). This along-strike increase in displacements correlates with the increase in width of the promontory (Fig. 8.8b), measured parallel to the plate convergence vector. One possibility, therefore, is that the geometry of the promontory limited the area of pre-elastic strain accumulation as well as subsequence seismic displacements.

The earthquake also illuminated a steeply dipping, planar zone of seismicity southeast of the Chelungpu fault a few hours after the main shock (Wu et al. 2004). Seismicity started near the southern end of the Chelungpu rupture, in the area of the previously recognized Luliao fault zone (Lee et al. 1999; Wu et al. 2004), and propagated southeast for about 50 km, crossing geologic boundaries at an acute angle (Fig. 8.9). The seismicity extends to 12–13 km and is dominated by left-lateral focal mechanisms (Wu and Rau 1998). The Luliao seismic zone therefore has the geometric and kinematic characteristics of a tear fault

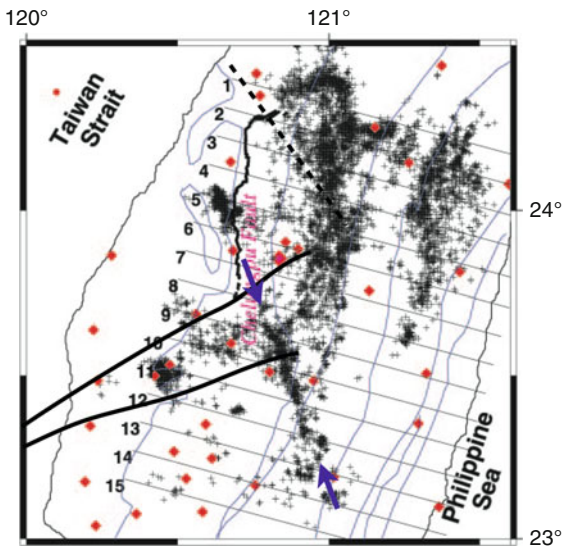

Fig. 8.9 Post-Chi-Chi seismicity in central Taiwan showing the Luliao seismic zone (*blue arrows*) (from Wu et al. 2004). *Black lines* = geologic boundaries.

in the fold and thrust belt, although the southeastern end of the zone extents into the slate belt, which overlies the edge of the Peikang High in this area. The zone also generally correlates with the edge of the Taishi Basin and is broadly equivalent to the previously recognized Pakuashan transfer zone (Mouthereau et al. 2002; Deffontaines et al. 1997).

Island-wide kinematics interpreted from focal mechanisms also appear to reflect collision with the promontory. Yeh et al. (1991), using earthquakes prior to 1987, recognized a regional fanning of the trend of $\sigma 1$ from NW in northern Taiwan to SW in southern Taiwan and proposed that reflected collision with the Peikang high. Rau and Wu (1998), using a larger data set, documented a relatively heterogeneous stress field throughout Taiwan with thrust faulting common in the fold and thrust belt and strike-slip and normal faulting in more common in the Central Range. They also suggested that strike-slip faulting was unusually common around the Peikang high. Wu et al. (2004) and Hsu et al. (2008) confirmed many of these patterns and emphasized the importance of both deep and shallow normal faulting in the Central Range.

Finally, a generally aseismic area, both pre- and post-Chi-Chi, occurs in the higher elevations (>1,500 m) of the Central Range between the continental margin promontory and the arc (Fig. 8.10) (Wu et al. 2004, 2007; Hsu et al. 2008). Hsu et al. (2008) also noted that focal mechanisms of earthquakes just to the northeast and southwest of this aseismic zone are dominantly extensional. They (Hsu et al. 2008) proposed that this along-strike change in seismicity reflected an along-strike change in the magnitude of horizontal stresses with a constant vertical stress. That is, they proposed that at elevations >1,500 m $\sigma 1$ is vertical and that the area of aseismicity is an area of high horizontal stress, relative to the areas of extension to the north and south. This interpretation is consistent with our proposal that the continental margin promontory is colliding with the arc in the area of high horizontal stresses (Fig. 8.10), which appears to limit extensional failure in this area.

8.6.2.2 Global Positioning System (GPS) Displacements and Strain

Yu et al. (1997) conducted an island-wide survey from 1990 to 1995 that produced the first comprehensive

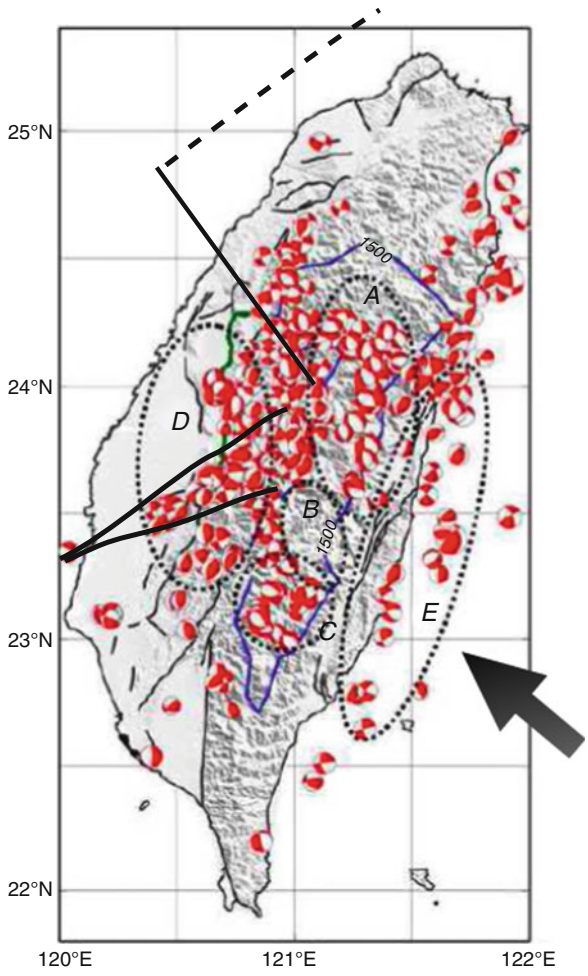

Fig. 8.10 Seismicity and focal mechanisms between July 1999 and July 2001 (i.e., mostly after the Chi-Chi earthquake) (from Hsu et al. 2008) showing aseismic zone at elevations >1,500 m (*blue line*). with extensional focal mechanisms to northeast and southwest. Areas: A = mostly normal faulting; B = aseismic; C = normal faulting and strike-slip; D and E = mostly thrusting with σ_1 northwest-trending.

view of surface deformation across Taiwan. Their data confirmed the wide distribution of deformation associated with the collision and illuminated a fanning of velocity vectors around a basement high in west-central Taiwan (Fig. 8.11a). Geological and geophysical data as well as physical and numerical models seemed to confirm the importance of this high in the deformation of the Taiwan orogen (Lacombe et al. 2001, 2003; Lu and Malavieille 1994), although it remained poorly defined.

Several authors have used the 1990–1995 GPS data (Yu et al. 1997) to examine different aspects of the collision (e.g., Chang et al. 2003; Bos and Spakman 2003), including Chang et al. (2003) who re-calculated the velocity field (using a linear interpolation algorithm) to map strain rate tensors over an approximately 11 km grid. Chang et al. (2003) also mapped the ratio of the two horizontal strain rate components at each grid node (Fig. 8.11b). For example, 100% extension means both strain rates are extensional whereas 100% compression means both strain rates are compressional. A strike-slip regime would have strain rates of opposite sign.

The resulting deformation mode map (Fig. 8.11b) shows two dominant belts – a western belt of compression in the fold-and-thrust and an eastern belt of extension in the Central Range. A less prominent belt of compression also occurs in the Coastal Range, which, in the central part of the range, expands westward nearly crossing the Central Range and linking up with compression belt in the west. The western and eastern belts are also composed of sub-domains; two sub-domains of compression in the west and three sub-domains of extension in the east, separated by a narrow zones of strike-slip deformation. The northern zone of compression overlies the western deformation front of the Hsüehshan Range whereas the southern zone, which is nearly twice as wide, overlies the southern fold and thrust belt and fills the triangle zone of the proposed continental margin promontory. The northern sub-domain of extension probably reflects westward propagation of the Okinawa Trough into the Central Range whereas the two southern sub-domains of extension correlate with the extensional zones at high elevations in the Central Range recognized by Hsu et al. (2008), although the southern sub-domain extends slightly further south. In any case, the correlation between the large zone of compression in southwestern Taiwan with the proposed continental margin promontory shows that it strongly influences deformation within the orogen.

The west to southwest fanning of the GPS vectors in southern Taiwan is perhaps one of the most striking features of the GPS data. Yu et al. (1997) proposed that the fanning reflected deflection and possibly extrusion of the orogen to the southwest as it collided with the Peikang High. Subsequent analysis and additional data confirmed the importance of the high in deflecting the orogen (e.g., Gourley 2006; Hickman et al. 2002; Angelier et al. 2009; Ching et al. 2007), although the geometry of the extruding block was not

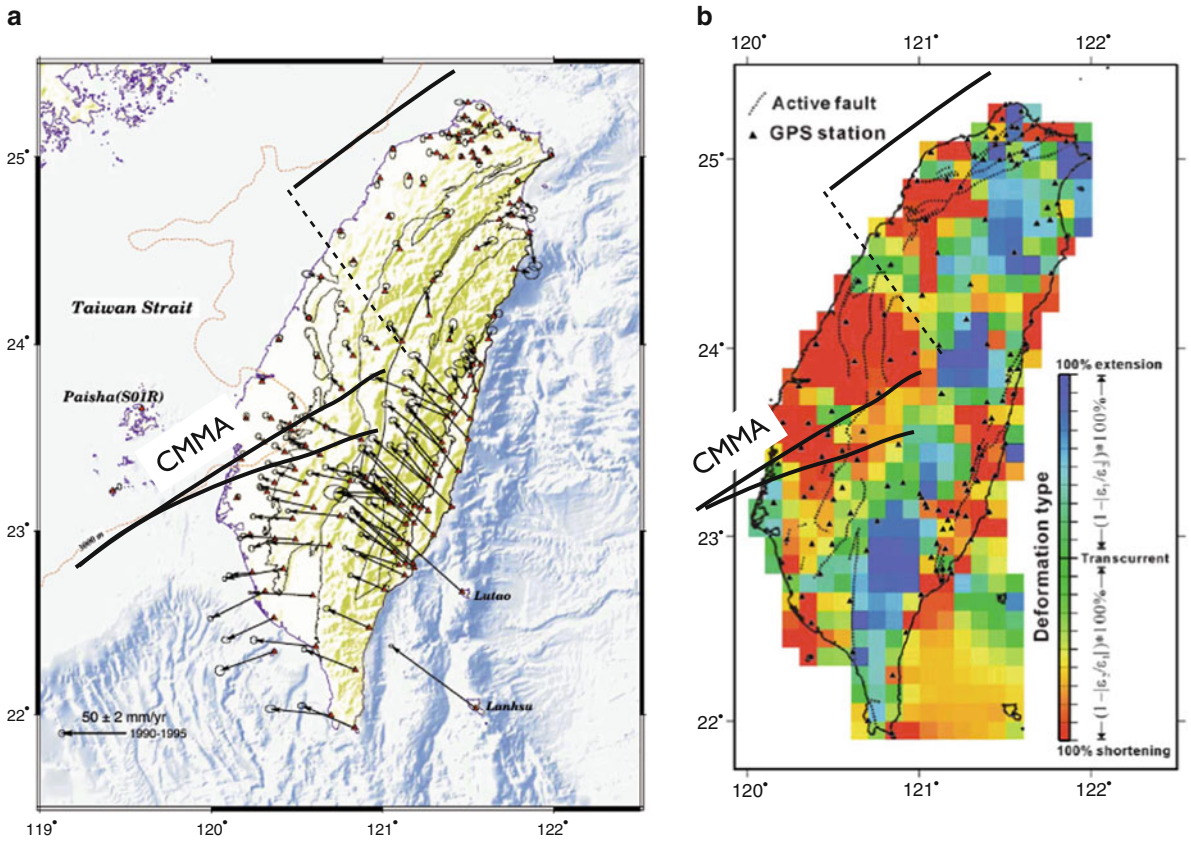

Fig. 8.11 (**a**) GPS displacements from 1990 to 1995 (from Yu et al. 1997) and (**b**) deformation modes (from Chang et al. 2003) based on data shown in (**a**). Displacements in (**a**) are relative to Penghu Island (station S01R), located in the Chinese continental margin.

well defined. To elucidate the extruding block, particularly the block boundaries, we re-plotted the vectors referenced to the central part of the Central Range (Fig. 8.12); that is, relative to a reference frame close to arc and opposite the continental margin prong. In this frame of reference, the GPS displacements in southern Taiwan show general flow of the upper crust to the southwest at about 3–5 cm per year. This regional-scale southwest flow is associated with right-lateral displacements on the west in the area of the Chishan fault and left-lateral displacements on east in the area of the western Central Range (Fig. 8.12). Left-lateral shear in the western Central Range is also associated with significant extension; thus, this zone may be a zone of left-lateral transtension.

Since the Chi-Chi earthquake, over 300 permanent GPS stations have been installed throughout Taiwan, providing continuous, island-wide coverage for the first time (Lin et al. 2010) as well as more detailed insights into the collision kinematics. Lin et al. (2010) used continuous GPS data collected from 110 stations from 1 January 2003 to 31 December 2005 characterized the surface deformation after the 1999 Chi-Chi earthquake. At the broadest scale, these data confirm the importance of the continental margin promontory as defined by the truncated magnetic anomaly and the Sanyi-Puli seismic zone. The strain rate data also show the three areas of extension identified by Chang et al. (2003) and Yu et al. (1997) and more clearly define the band of compression between the promontory and the Coastal Range (Fig. 8.13a). The eastern and western boundaries of the extruding block in southern Taiwan also display clockwise and counterclockwise rotational strains, respectively, consistent with regional-scale lateral flow of at least the upper crust (Fig. 8.13b). The post-Chi-Chi GPS displacement data, when

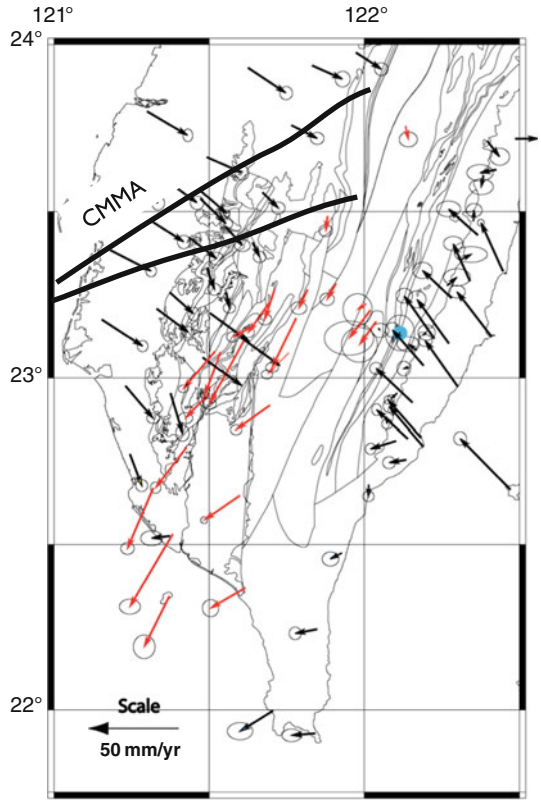

Fig. 8.12 GPS displacements from Yu et al. (1997) and Hickman et al. (2002) plotted with respect to a reference frame in the eastern Central Range (*blue dot*).

compared to the pre-Chi-Chi data, also show significant displacements in Central Range southeast of the area that moved during the 1999 Chi-Chi earthquake (Fig. 8.14) (Lin et al. 2010), suggesting that post-seismic processes are still active (Hsu et al. 2007). Lin et al. (2010) propose that these relatively large post-Chi-Chi displacements may reflect a viscoelastic response or afterslip of the Chi-Chi earthquake (e.g., Perfettini and Avouac 2004; Hsu et al. 2007). In any case, these displacements occur between the promontory and arc, the area of higher horizontal compression, which is consistent with our proposal that the promontory plays a critical role in the dynamics of the orogen.

8.6.2.3 Topography

Detailed studies of the topography along the length of the orogen show significant anomalies in the context of a propagating steady-state orogen. In one of the earliest quantitative studies of the topography of the Central Range, Willemin and Knuepfer (1994) showed that the middle part of the range is narrower, shorter and steeper than the range to the north and south (Fig. 8.15). Suppe (1981) also recognized the narrowing of the range in this area, but proposed that overall the orogen maintained an average width of 90 km throughout its length. More recently, however, Stolar et al. (2007a) quantified the topographic variability in the portion of the Central Range conventionally thought to be in steady state and found that variations in mean elevation and cross-sectional area are significant – up to 30% of the mean value. The anomalies correspond to the Hsüehshan Range in the north and to the continental promontory in central Taiwan. At smaller scales, Wobus et al. (2006) and Stolar et al. (2007a) have documented ubiquitous hanging tributary valleys and knickpoints along major rivers in the eastern Central Range, indicating a combination of non-uniformity and transience in the tectonic and erosional forcing of the Central Range landscape. Shyu et al. (2006) have also been mapped several thrust faults by along the eastern range front in the central part of the range. Despite uncertainty about the age of faulting, these observations imply that tectonic activity is, or has been recently, higher in the middle part of the range than in the south, which is opposite from predictions of the southward propagation model.

8.6.2.4 Penetrative Fabrics

One of the most prominent features of the Central Range is a penetrative, slaty cleavage that forms a fan across the range (Fig. 8.16) (e.g., Stanley et al. 1981; Crespi et al. 1996; Fisher et al. 2002; Ho 1988). On the western flank of the range the cleavage dips east and is associated with top-to-the-west asymmetric structures (e.g., folds, thrusts and shear zones). On the eastern flank, the cleavage dips west, asymmetric structures appear to be overturned, and the cleavage is often overprinted by a second or third crenulation (Fisher et al. 2002). Although the origin of cleavage fan is undoubtedly complex (Yeh et al. 2001; Fisher et al. 2002, 2007; Pulver et al. 2002), a recent compilation of cleavage data from the range (Fig. 8.16) (Lu et al. 2010) shows that the apex of the fan (i.e., where the cleavage has vertical dip), consistently lies just east of the ridge crest nearly the entire length of the

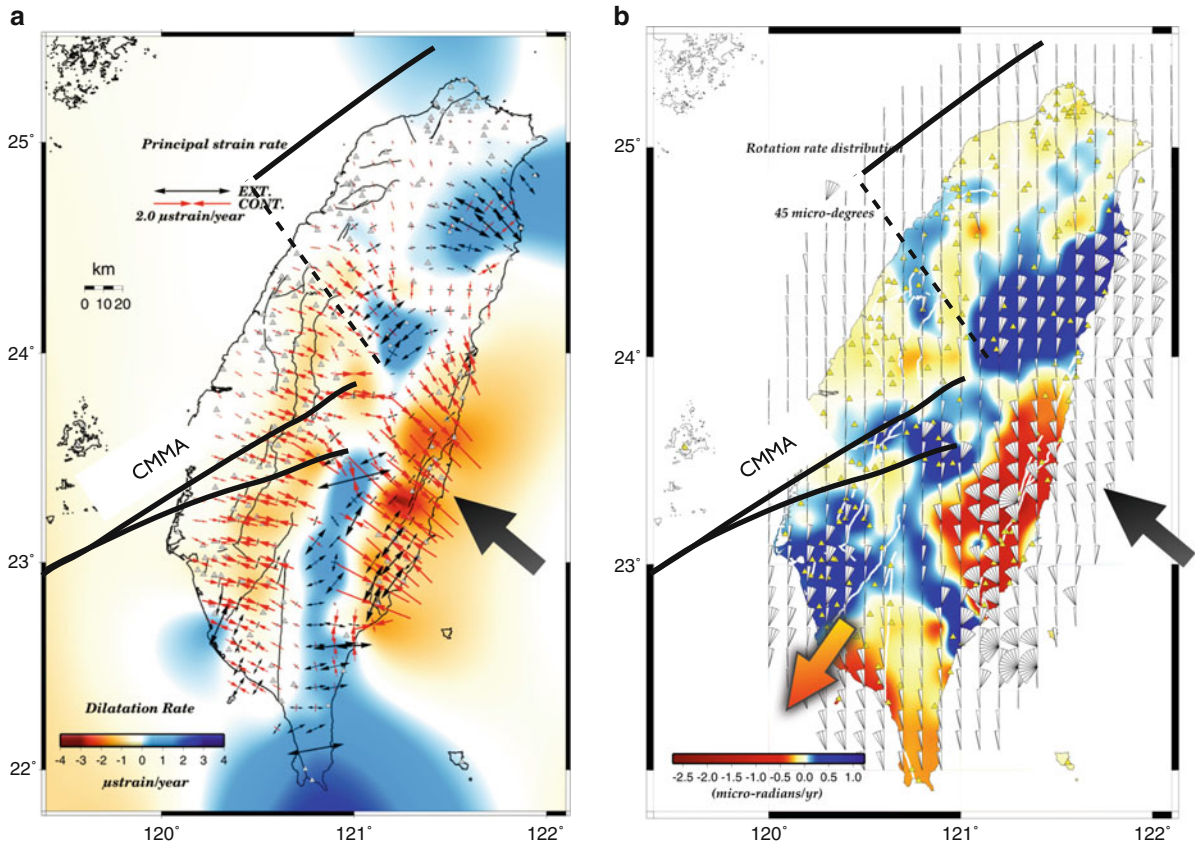

Fig. 8.13 (**a**) Dilatational and (**b**) rotational strain rate data from continuous GPS data collected after the 1999 Chi-Chi earthquake (2003–2005) (Lin et al. 2010).

orogen. This consistency is maintained even in the central section of the range where the range is anomalously steep and narrow (described above).

Topographic development is normally considered to be relatively young, especially in Taiwan where uplift and exhumation rates are relatively high, and slaty cleavage is normally considered to form substantially deeper in the crust (e.g. at depths equivalent to 200° to 300°); thus, the correlation of the cleavage geometry with the topographic crest is unexpected. With the available data, several interpretations are possible: (1) The slaty cleavage formed at earlier stage of the orogen whereas the fan of cleavage formed contemporaneously with the topography; (2) Both the cleavage and cleavage fan formed during an earlier stage of the collision and were subsequently deformed as the topography developed; (3) The cleavage and the cleavage fan formed at relatively shallow structural levels (e.g., due to anomalously high heat flow) and at about the same time as the topography. Although we are not able to eliminate any of these possibilities, the consistency between the cleavage fan and the topography argues that the topographic anomaly reflects a crustal-scale processes, suggesting the continental margin promontory is driving both the tectonic and topographic evolution.

8.6.2.5 Crustal-Scale Structure, Thickening and Exhumation

The crustal-scale structure in the central part of Taiwan provides additional constraints on the evolution of the orogen and the role of the promontory. A variety of geophysical tools have been used to understand the three-dimensional structure (e.g., Wu et al. 2004, 2007; Cheng 2004; Kim et al. 2005) and the structure of orogen appears to be relatively complex (compare e.g., Wu et al. 1997; Willett et al. 2003; Simoes et al. 2007; Suppe et al. 2010). We start

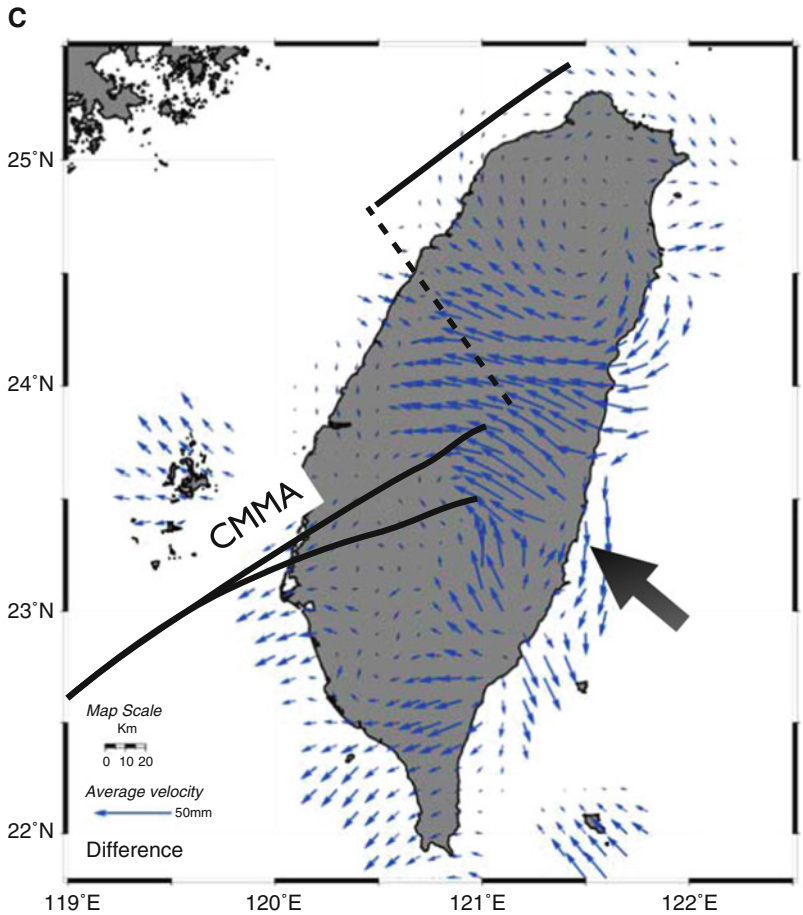

Fig. 8.14 Difference between GPS velocities collected before (from 1990 to 1995) and after (2003 to 2005) the Chi-Chi earthquake in terms of average annual velocity (from Lin et al. 2010).

with a recent interpretation of the crustal thickness (Wang et al. 2010a) and then examine horizontal sections of the P-wave velocity in the middle and lower crust which will then be complemented with higher resolution vertical cross-sections of seismic wave velocity and attenuation models. This compilation suggests that an area of thickened crust with relatively high P- and S-wave attenuation lies between the colliding continental margin promontory and the volcanic arc.

Wang et al. (2010a) recently analyzed receiver functions from the "Broadband Array in Taiwan for Seismology" catalog to estimate variations in crustal thickness (H) and Vp/Vs ratio (k) in the collision. Waveforms and travel times of 220 carefully selected teleseismic events and a two-stage weighted stacking process were used to reduce errors and increase the signal-to-noise ratio. In fact, high quality receiver functions can provide higher resolution H values than seismic tomography, which often yields higher resolution images of the crustal interior. The receiver function results suggest two viable models. One model, preferred by Wang et al. (2010a), shows the Moho as a 52 km deep elongate depression with gradients that cuts across the orogen at nearly right angles, including the Puli embayment and the Hsüehshan Range. The second model shows a shallower maximum depth for the Moho (~40 km in central Taiwan) and more uniform crustal thicknesses beneath the Central and Hsüehshan Ranges. We prefer this second model (Fig. 8.17a) because the uniform crustal thickness beneath the main ranges is more consistent with P-wave and gravity inversions. Both models, however, show the thickest crust in central Taiwan, primarily between the promontory and the arc, with thinner crust to the north and moderately thick crust to the south.

The relatively thick crust in central Taiwan is consistent with P- and S-wave velocity inversions and gravity data. For example, Cheng (2004) preformed a sequential inversion of travel-times and gravity data to image the three-dimensional velocity structure in

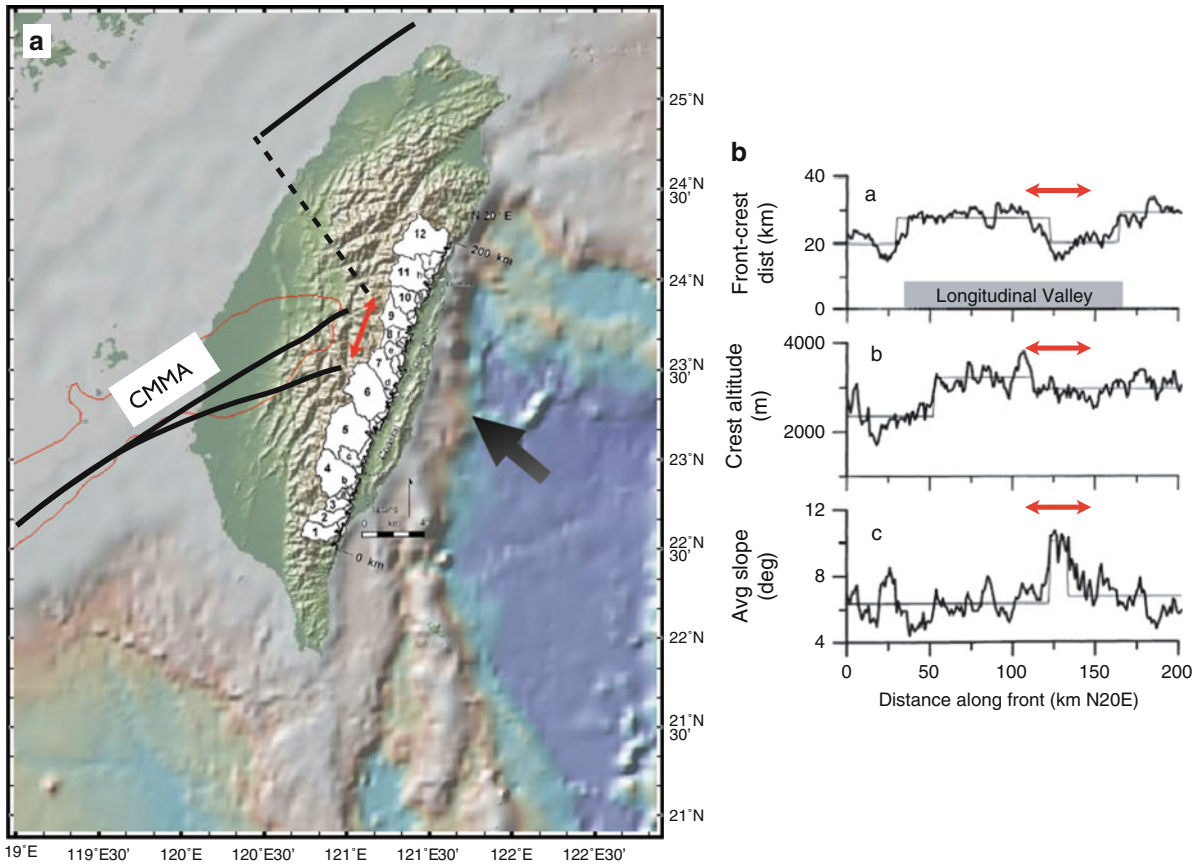

Fig. 8.15 (**a**) Watersheds and (**b**) along-strike variations in critical geomorphic parameters along the eastern flank of the Central Range (from Willemin and Knuepfer 1994). *Red double arrow* shows same along-strike section in (**a**) and (**b**).

central Taiwan. His results show an elongated "S" shaped low velocity zone at a depth of 25 km (Fig. 8.17b). The northern segment of the "S" lies beneath the Hsüehshan Range whereas the southern segment is much wider and extends beneath parts of both the Alishan and Central Ranges in central Taiwan. Kim et al. (2005) and Wu et al. (2007) obtained broadly similar results using P-wave tomography.

Wu et al. (2009) recently completed a high resolution study of the velocity structure in northern Taiwan and their results show confirm the presence of a low-velocity zone beneath the Hsüehshan Range (i.e., the northern segment of the "S" in Fig. 8.18a). In addition, their data show that the low velocity zone dips east about 45° to a depth of about 60 km (Fig. 8.18a). This east-dipping crustal layer was also identified by Lin and Roecker (1993) using the Vp tomography of Roecker et al. (1987) and carefully selected arrival times of P and S waves. Finally, recent attenuation models of the crust in northern Taiwan using both P- and S-waves (i.e., Qp and Qs) also confirm the moderate east dip (Fig. 8.18b) and show that the east-dipping zone of low Vp correlates with a zone of high Qp (i.e., low attenuation), which is overlain by a zone of low Qp and high Vp (Fig. 8.18).

At a more regional scale, P-wave attenuation data (Wang et al. 2010b) show a well-developed high Q zone at 19 km in the area of the proposed promontory and low Q zones beneath the Hsüehshan Range and in the central part of the Central Range (Fig. 8.19). The low Q zones wrap around the northern and eastern sides of the promontory and mimic the low velocity mid-crust identified by Cheng (2004). Wang et al. (2010b) interpret the low Q values in the Hsüehshan and Central Ranges to be related to recent and relatively rapid exhumation. Lee et al. (2010) (see also Lee et al. 2009) also completed a more detailed study of the attenuation in the central part of the Central

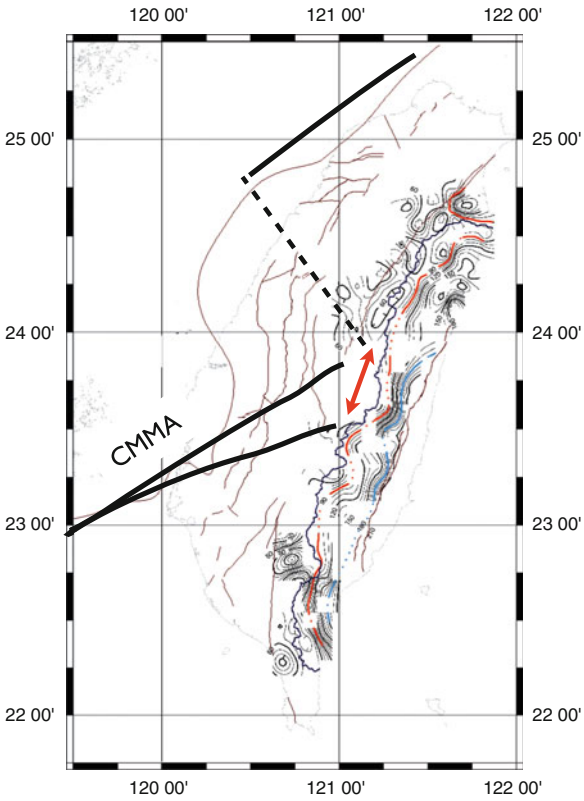

Fig. 8.16 Contour map of cleavage dip in the Central Range; *red line* = vertical dip; *blue* = overturned and horizontal cleavage (from Lu et al. 2010). *Black continuous line* just west of vertically dipping cleavage represents the topographic divide. *Red double arrow* is the same as in Fig. 8.15.

Range (box in Fig. 8.19) and show a low Q (high attenuation) zone that extends to 20–30 km. Using the observed attenuation values and published laboratory experiments, Lee et al. (2010) also estimated the temperatures in the area of the lowest Q values (~20 km depth) to be in the range of 680° to 750°C. These values are consistent with high heat-flow values (200–300 mW m^{-2}) measured by Lee and Cheng (1986) and suggest the possible presence of molten rocks at depth (Lee et al. 2010).

The area of high Q further southwest in the Central Range (Fig. 8.19) correlates with the outcrops of mafic rocks along the western boundary of the Tananao schists and may reflect the presence of more mafic blocks at depth. Cheng (2008) also recognized blocks of anomalously high velocity and density in this area (Fig. 8.5). That is, the along-strike change in attenuation in the Central Range (Fig. 8.19) may reflect changes in rock composition, rather than changes in the rate of exhumation.

In the southern most extent of the Central Range, velocity models and joint gravity-velocity inversions also suggest east-dipping crustal layers although relatively large blocks with anomalous density and attenuation values are also present. Cheng (2008) identified relatively thick crust (~30 to 40 km) in the southern Central Range, consistent with the receiver function analysis, and km-scale, east-dipping, high velocity layers. At least one of the layers projects to the surface near the Chaochou fault along the western Central Range. McIntosh et al. (2005) also recognized east-dipping high velocity layers in the southern Central Range using a geophysical survey that combined land and marine data.

8.6.2.6 Thermochronology and Exhumation

A number of studies have documented the complex thermal history recorded in the orogen since the early work of Lo and Onstott (1995) and Tsao (1996), including possible complications related to a continental margin promontory (e.g., Liu et al. 2001). For example, Liu et al. (2001; 1999), using completely reset detrital zircon grains, documented regional-scale patterns both across and along the structural grain of the orogen. These early data show younger exhumation cooling ages in the eastern Central Range and relatively older ages in the western Central and Hsüehshan Ranges. Liu et al. (2001) proposed that this orogen-scale pattern reflected different exhumation rates with relatively slow rates in the west (~1 mm per year) and much faster rates (~5 mm per year) in the east. More recent fission track data, much of which are compiled in Fuller et al. (2006), are consistent with this pattern; completely reset detrital zircon ages range from 6.4 to 2.9 Ma in the western Central Range range and from 3.0 to 0.8 Ma in the eastern part of the range. Reset detrital apatite ages and (U–Th)/He ages of zircons across are also consistent with a general decrease in the age of exhumation cooling east to west across the range.

Liu et al. (2001) also documented a single relatively old completely reset detrital zircon (~6 Ma, based on fission track) in southern Central Range that appeared to be anomalous in the context of southward propagation model. Liu suggested that this anomalous age might be related to collision of the Peikang high, although specific details on the geometry and timing were not provided. Relatively old completely reset apatite fission track ages have also

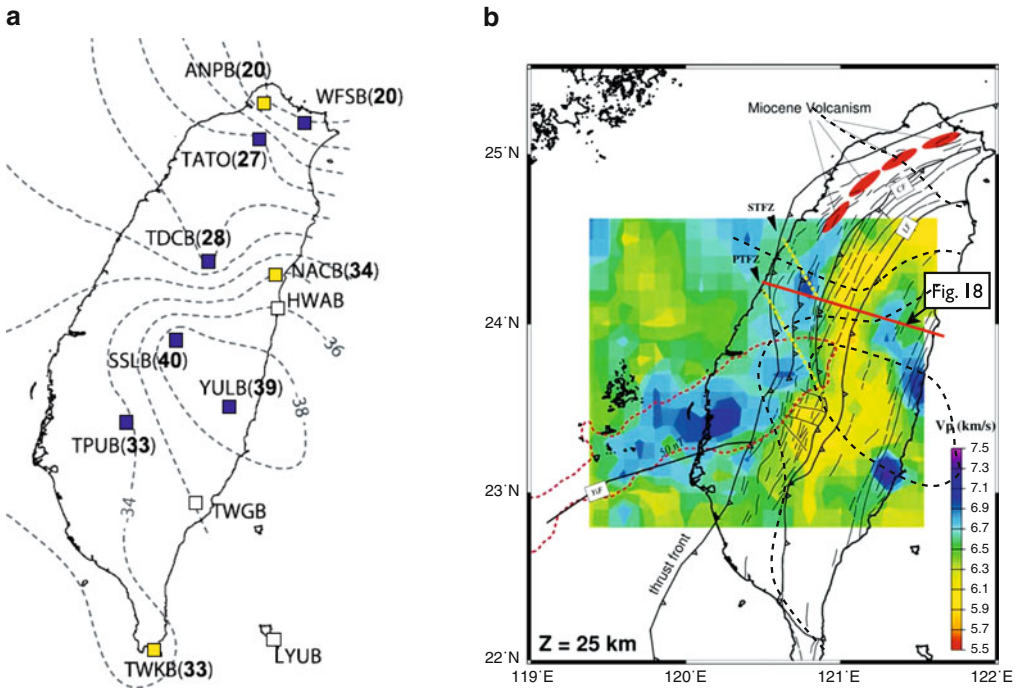

Fig. 8.17 (**a**) Depth to Moho beneath Taiwan (Wang et al. 2010a) and (**b**) P-wave velocity structure (at depth 25 km) in central Taiwan based a sequential inversion of travel-times and gravity data (Cheng 2004). Note the elongate "S" formed by the low-velocity crust centered on the promontory (*red dashed line* shows magnetic high) *dashed black lines* are the same as in (**a**).

been documented in southern Taiwan (Willett et al. 2003), supporting the early work of Liu et al. (2001). Willett et al. (2003) proposed a pre-collision thermal event, possibly related to burial on a relatively warm ocean floor or in an accretionary prism prior to the collision. More recently, Lee et al. (2006) used these older ages, as well as additional zircon fission track ages, to argue for a two-stage evolution of the orogen – an early accretion stage with relatively slow exhumation (evidenced by the older ages) followed by collision associated with faster exhumation (Fig. 8.6). Byrne et al. (2008) interpreted this temporal evolution in exhumation rates to a progressive collision rather than accretion followed by collision. In either case, the change in rates reflects fundamental changes in the processes supporting the orogen-scale topography.

8.6.2.7 Stratigraphic Record

Stratigraphic records preserved in the Western Foothills can also be used to interpret the history of the collision and are consistent with a multi-stage collision (Teng 1990; Chang and Chi 1983). In the Western Foothills, a basal unconformity separates an onlapping foreland basin sequence above from passive margin sequences below and marks the base of the Taiwan foreland sedimentation (Lin and Watts 2002; Yu and Chou 2001). In the Taishi Basin, Lin et al. (2003) estimated the age of the unconformity to be 6.5 Ma based on age-diagnostic fossil assemblages and a dated basalt layer 25 m beneath the unconformity. The foreland sediments generally record an upward increase in grain size and sediment accumulation rate reflecting, in part, the westward migration of the developing orogenic system and the progradation of orogenic sediments. In more detail, however, Chen et al. (2001) have documented an anomalously high sedimentation accumulation rates in both northern and southern Taiwan during the last 1.25 Ma (Fig. 8.20). From about 2.5 Ma to 1.25 Ma both areas record rates of ~900 m/m.y. At 1.25 Ma accumulation rates in northern Taiwan jumped nearly one order of magnitude to 900 m/100k years whereas in southern Taiwan the increase was less (~1,900 m/m.y.) but still substantially higher than typically measured in

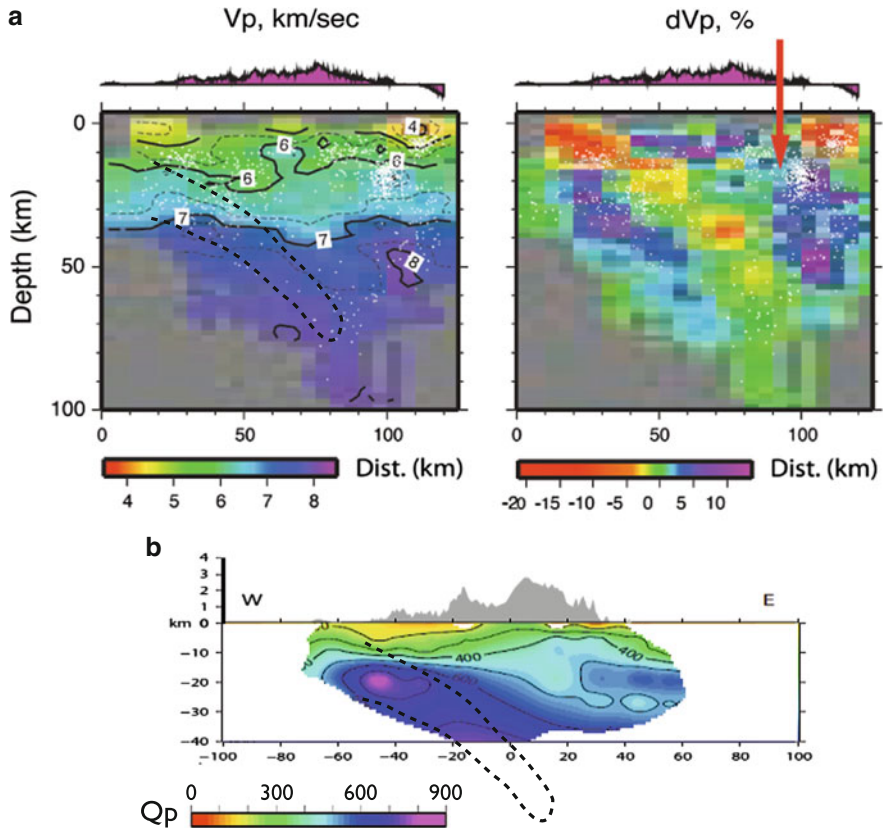

Fig. 8.18 Cross-sections showing contours of (**a**) Vp and dVp from (from Wu et al. 2009) and (**b**) P-wave attenuation (from Wang et al. 2010b); all at the same vertical and horizontal scales. Cross-section locations are shown in Figs. 8.17b and 8.19. *Dashed black line* in (**a**) and (**b**) is approximate distribution of low dVp.

foreland basins (e.g., 100–1,000 m/m.y., Jordon 1995). Although various interpretations are possible, the increase in accumulation rates correlate with the increase in exhumation cooling proposed by Liu et al. (2001) and substantiated with more extensive dating by Lee et al. (2006).

Simoes and Avouac (2006) also examined the spatial distribution of foreland sediments through time and proposed a southward propagation of the depositional center of the basin. Although Simoes and Avouac (2006) emphasized the southward propagation of the basins from 3.3 Ma to ~0 Ma, their data show that the basin was essentially stationary in northern Taiwan from 6.5 to 3.3 Ma. One possibility, therefore, is that this early foreland basin was constrained at its southern end, perhaps by a topographic or bathymetric barrier, and propagated southward only after this barrier was breached. In fact, a comparison of the reconstructed continental margin promontory suggests that this early foreland basin was constrained by the continental margin fracture zone. (Fig. 8.21).

Finally, the only two mélanges recognized in Taiwan appear to be sedimentary olistostromes that formed as the Central Range initially emerged above sea level. The Kenting and Lichi melanges crop out in the southern tips of the Central and Coastal Ranges, respectively, and contain distributed blocks of sandstone, shale, limestone (marble) and various compositions of igneous rocks, ranging from andesite to basalt, in a shale or mudstone matrix (Page and Suppe 1981; Page and Lan 1983; Chang et al. 2000; Huang et al. 1985; Tsan, 1974). The mafic igneous rocks in both units have also been interpreted to be remnants of ophiolites (e.g., blocks in the Lichi constitute the "east Taiwan ophiolite") (Page and Suppe 1981). Available fossil data indicate a limited range of age for the Lichi ranges (from 3.7 to 3.5 Ma) and a wider range for the Kenting (~10 Ma to <1 Ma) (Fig. 8.20)

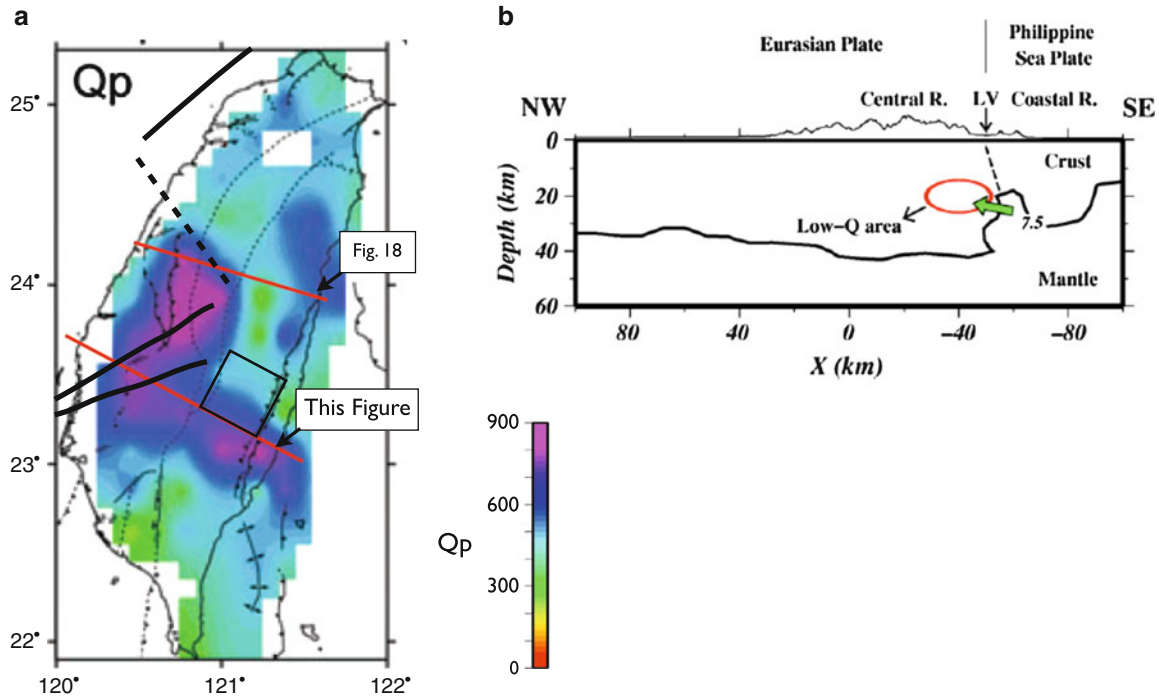

Fig. 8.19 (**a**) Map view of P-wave attenuation (at 19 km) from Wang et al. (2010b) and cross-section show (from Lee et al. 2010) showing the location of the low-Q zone (red ellipse) in a simplified crustal section (from Kim et al. 2005). Approximate Moho is shown by 7.5 km/sec contour.

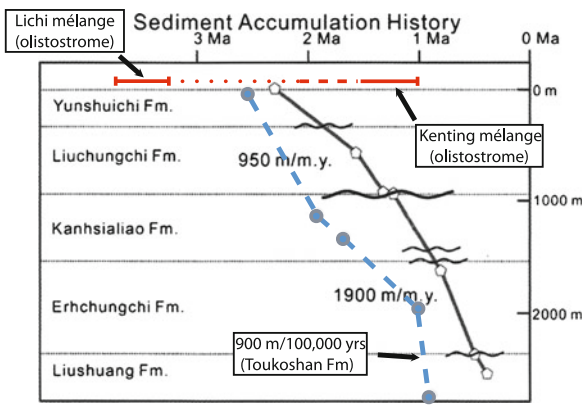

Fig. 8.20 Plot of sediment accumulation rates versus time in northern (*dashed blue line*) and southern stratigraphic sections (*gray line*) of the foreland basin (Tsaohuchi and Chengwenchi sections, respectively of Chen et al. 2001). *Wavy lines* show unconformities. Depositional ages of Lichi and Kenting olistostromes are shown for reference (see text for discussion).

(Huang et al. 2008; Chang et al. 2009). Page and Suppe (1981) carefully documented the age and stratigraphic relations of the Lichi mélange and showed that it stratigraphically interfingers with more coherent sedimentary units, confirming to these authors that the units are stratigraphic rather than tectonic. Page and Lan (1983) made the same argument for the Kenting mélange although the outcrop and stratigraphic relations were less clear. Huang et al. (1985), Huang et al. (2008) and Harris and Huang (2010) have proposed that both mélanges formed through tectonic processes or a combination of tectonic and diapiric processes (Harris and Huang 2010). Chang et al. (2000, 2009) showed, however, that although tectonic deformation substantially altered the original stratigraphy, the initial mixing of the various lithologies was the result of an olistostrome, as proposed by Page and Suppe (1981) and Page and Lan (1983). The low grade of thermal alternation ($< 100°C$) in both mélanges also indicates limited burial, consistent with their initial formation as olistostromes (see e.g., Byrne 1994). Both units are therefore interpreted to represent relatively large submarine slide deposits that formed as the Central Range and the magmatic arc emerged above sea level. The interpreted ages of deposition correlate with the proposed change in rates of exhumation cooling in the Central Range and with the increase in

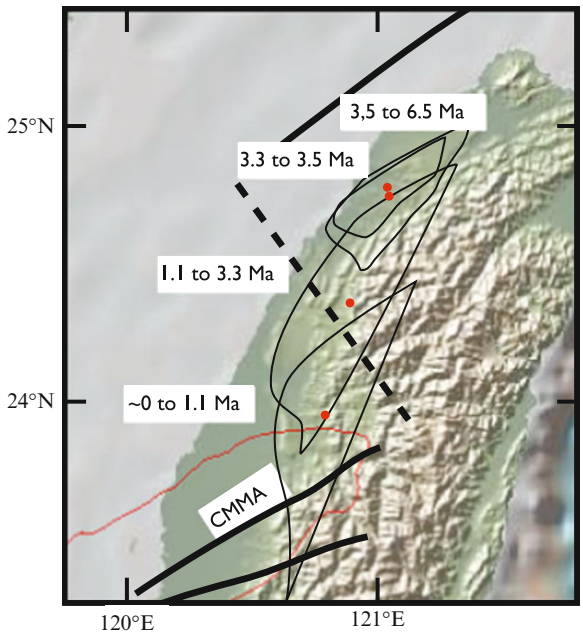

Fig. 8.21 *Black closed lines* show foreland basin depositional centers (from Simoes and Avouac 2006). Distribution of depositional centers suggests that the basin formed initially north of the proposed fracture zone (*dashed line*) and propagated southward as the arc collided with continental margin promontory.

rate of sediment accumulation in the foreland, suggesting the increase in rates of exhumation may have lead to at least local catastrophic failure and land sliding.

8.7 Discussion

Previous interpretations of the arc-collision in Taiwan have treated the Chinese continental margin as a relatively homogeneous passive margin that progressively collides with the arc (e.g., Byrne and Liu 2002a; Suppe 1984; Willett et al. 2003). Our compilation of a wide range of geological and geophysical data suggest, however, that the colliding passive margin was more heterogeneous than previously thought and that these heterogeneities have played, and continue to play, a significant role in the kinematics and dynamics of the orogen. The wide area of transitional crust southwest of Taiwan (~250 to 300 km across the margin) is consistent with geological data from Taiwan that indicate a relatively early history of accretion and exhumation (e.g., ~ 6 Ma to ~2 Ma). For example, if we assume that plate convergence (80 km/Ma) is partitioned approximately equally between shortening in the arc and deformation in the accretionary prism, as it is today, then during the last 3 m.y. (when the arc appears to have first rotated due to the collision) approximately 120 km of transitional crust could have been consumed through underthrusting in the prism. This results in between 130 and 180 km of transitional crust to be consumed prior to 3 Ma. Depending on the degree of partitioning between arc deformation and underthrusting in the prism, transitional crust may have first collided with the arc between 7.5 and 4.5 Ma (3 Ma plus 1.5 to 4.5). The rocks accreted during this early stage of the collision (7.5–4.5 Ma) are most likely exposed in the Hsüehshan and Central Ranges, or have been removed by erosion (e.g., the Taiwan ophiolite).

We propose that the late stage of the collision (~3–2 Ma to present) involved continental crust of more normal thickness (~30 km) and that this crust formed a regionally significant, and relatively rigid, continental promontory. Considering that the interpreted apex of the promontory still lies beneath central Taiwan, the volume of continental crust, of normal thickness, that has been underthrusted or subducted is fairly limited. Limited underthrusting of continental crust is also consistent with recent thermomechanical numerical models of the collision (Yamato et al. 2009). Although underthrusting of continental crust is interpreted to be relatively limited, the continental margin promontory and en echelon sedimentary basins north and south of it, appear to have dominated the growth of the orogen during the late-stage of the collision.

Perhaps the most conspicuous consequence of the colliding promontory is the map view curvature of the fold and thrust belt (Figs. 8.2 and 8.22) with a central zone of anomalously north-trending folds and thrusts. Our interpretation of this map-view curvature is that in southern Taiwan, thick continental crust of the promontory limited westward propagation of the fold and thrust belt; that is, the promontory acted as a buttress. In the north, the thick sedimentary sequences of the Taishi Basin allowed the thrust belt to propagate substantially west of the promontory, resulting in a left-lateral accommodation zone between the northern and southern thrust belts (Fig. 8.22). Left-lateral shear appears to be accommodated at deep structural levels by slip along the Sanyi-Puli seismic zone, which is reactivating a continental margin fracture. At shallow structural levels south of this zone, left-lateral shear is

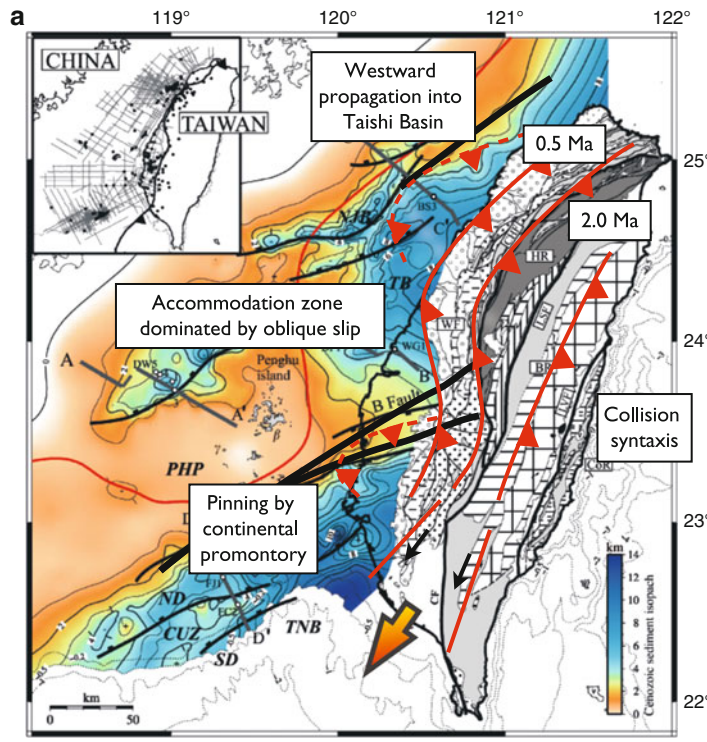

Fig. 8.22 Map showing depth to Mesozoic basement (Lin et al. 2003) and geology of Taiwan. *Red lines* with barbs show proposed development of Taiwan orogen from 2–3 Ma to present. *Dashed red lines* with barbs show are of reactivated normal faults (from Mouthereau et al. 2002). Ages are based on syn-tectonic stratigraphy in the central section of the fold-and-thrust belt. Note that the southern fold-and-thrust belt is in pinned by the continental margin promontory (*black line*) as the northern belt propagates northwest, resulting in an accommodation zone dominated by faults and folds with oblique slip. See Fig. 8.4 for abbreviations.

accommodated by the development of a thin-skinned fold and thrust belt in which slip is both oblique and partitioned along strike (e.g., see co-seismic slip during the Chi-Chi earthquake, Fig. 8.8). Geochronologic data from sedimentary basins between thrust sheets (i.e., "piggyback" basins) also document foreland propagation beginning about 2 Ma (Fig. 8.22) (Lee et al. 1996). If the slip pattern recorded during the Chi-Chi earthquake is representative of the long-term displacement, it would explain the progressive westward rotation of increasingly younger thrust sheets. In essence, the central Taiwan fold and thrust belt is interpreted to be a wide accommodation zone between thrust systems advancing at different rates. The southern boundary of this accommodation zone also appears to have been illuminated, at least in part, as the Luliao seismic zone just after the Chi-Chi earthquake (Wu et al. 2004).

The recognition of a continental margin promontory beneath central Taiwan and its correlation with a change in geometry of the fold and thrust belt in map view suggests that it may represent a recess or syntaxis in the fold and thrust belt. The correlation between the apex of the promontory and the thickest crust with the highest P-wave attenuation (e.g., compare Figs. 8.18 and 8.20) suggests that this should be an area of maximum rock uplift and exhumation, consistent with other orogenic syntaxes recognized around the world (Khan et al. 2000). This interpretation is also consistent with geomorphic indices from the central part of the Central Range that indicate high rates of uplift (Stolar et al. 2007b), with the absence of seismicity in this area (e.g., Hsu et al. 2008) and the presence of high heat flow (Lee and Cheng 1986). Although detailed thermochronologic and kinematic data are limited in central Taiwan, the available data suggest a recent increase in rates of exhumation consistent with the interpretation that the prong collided relatively recently (< 2 Ma).

The presence of a crustal-scale buttress in southern Taiwan and the collision of the continental margin prong may have also initiated lateral extrusion in the southern part of the orogen (Ching et al. 2007; Lacombe et al. 2001; Angelier et al. 2009). Again, detailed kinematic and geochronologic data are limited in this area of Taiwan, but two aspects of the available data suggest significant crustal involvement. First, GPS and geologic data suggest that extrusion is asymmetric with the western part of the extruding block being characterized by right-lateral transpression whereas the eastern part of the block is

characterized by left-lateral transtension (see e.g., Figs. 8.13 and 8.22). This asymmetry may reflect the regional-scale boundary conditions of east-dipping subduction and southwest-directed extrusion of the Central Range, suggesting that the extruding block involves the entire orogen from the décollement to the surface. In this context, transpression in the west reflects the combined effects of underthrusting and extrusion whereas transtension in the east reflects southwest-directed extrusion. Second, the area of transtension in the southern Central Range includes nearly the entire southern half of the Central Range (Fig. 8.13) with numerous peaks over 3,000 m. If the extensional regime indicated by the GPS (Yu et al. 1997) and brittle fault data (Crespi et al. 1996) is representative of relatively long-term rates (e.g., 3–2 Ma) then the surface topography must be supported by flow in the middle to lower crust. One possibility, therefore, is that crustal material flows from the syntaxis to the southwest. Again, suggesting involvement of at least the middle and upper crust.

Finally, the observations and interpretations presented above for the late-stage development of the orogen involve only limited southward propagation. Although paleomagnetically determined rotations in the arc show southward propagation, how this progressive collision-related propagation is transmitted into the orogen is less clear. In fact, available fission track ages indicate exhumation cooling began in both northern and southern Taiwan about 6 Ma (Liu et al. 2000, 2001; Lee et al. 2006). The southward migration of the foreland basin identified by Simoes and Avouac (2006) (Fig. 8.21) may also reflect the change in the depth of basement in the down-going plate from north to south, rather than propagation of the collision. For example, the foreland basin may have been restricted to the area of the Taishi Basin north of the continental margin fracture early in the collision and then propagated southward across the fracture zone and onto thicker crust as the continental margin promontory collided 2–3 Ma. Evidence for southward propagation also appears to be present in the southern Central Range (e.g., Willett et al. 2003; Wiltschko et al. 2010), but this may be a local response to crustal flow. For example, Ramsay et al. (2007), used geomorphic parameters and kinematic models from the southeastern flank of the range to argue for a rapid increase in rock uplift rates from the area of the orocline (Fig. 8.2) to about 23°N. One possibility, however, is that the increase in the rate of uplift, which increases towards the proposed orogenic syntaxis, is driven by lateral crustal flow away from the syntaxis. Fission track ages of completely reset detrital apatites from this area of the Central Range are consistent with this interpretation and suggest that the increase in the rate of uplift occurred about 2 Ma (Fig. 8.6) (Lee et al. 2006).

8.8 Summary

The compilation of a variety geological and geophysical data sets suggests that the Taiwan orogenic belt, which is often presented as a relatively simple, propagating orogen, has evolved in a least two stages and involved both lateral and vertical extrusion. The initial collision occurred between the Luzon arc and transitional crust of the South China Sea about 6 Ma. Based on observations from the South China Sea south of Taiwan the transitional crust was composed of thinned continental crust and newly formed mafic rocks. Rocks of similar composition are currently exposed in the Central Range of Taiwan and are inferred to be present at depth from seismic velocity data. The initial collision and accretion of transitional crust was followed by a more significant collision with a continental margin promontory of more normal (~30 km) thickness. This later stage of the collision is still active.

The continental margin promontory, as revealed primarily by magnetic data and the distribution of seismicity before and after the Chi-Chi earthquake, is only partially subducted beneath Taiwan. In western Taiwan, the promontory divides the fold-and-thrust belt into three parts – a northern salient, a central fold-and-thrust belt that fans from northeast- to north-striking and a southern salient offset left laterally from the northern fold and thrust belt. The central fold-and-thrust belts, therefore, represents an accommodation zone between two fold-and-thrust belts. In the Central Range, the apex of the partially subducted promontory correlates with an area in the orogenic belt that is relatively, narrow, steep and low in elevation. This area also has anomalously high P- and S-wave attenuation, suggesting relatively high rates of exhumation. In southwest Taiwan, the promontory, previously recognized as the Peikang High, limited the westward propagation of the fold-and-thrust belt. As a result, shortening in southern Taiwan

has been accommodated by vertical and lateral flow of at least the middle and upper crust.

The classic model of Taiwan as a southward propagating orogen with space-time equivalence may therefore be too simple. Instead, the kinematics and dynamics of the orogenic belt appear to be dominated by the presence of a partially subducted continental margin promontory and associated fracture zone. This relatively rigid promontory forms the apex of an orogenic syntaxis in central Taiwan that divides the orogen both along and across strike, resulting in structural domains with distinct deformational patterns and histories. Future studies therefore might focus on defining these various domains and on understanding how they interact temporally and spatially.

Acknowledgements We are grateful to the many colleagues in Taiwan who have kindly shared their data and ideas, and helped with the numerous logistical challenges over the years. We also acknowledge and appreciate support from the Department of Geological Sciences at the National Taiwan University and the Institute of Earth Sciences, Academia Sinica. Support from the Fulbright Foundation (to Byrne) and the National Science Foundation (EAR0711353 and EAR0738979) is also gratefully acknowledged. The ideas and conclusions were improved through numerous discussions with Jon Gourley, Jon Lewis, Chung Huang, Dave Mirakian and Hao-Tsu Chu. The support and patience of the editors, Dennis Brown and Paul Ryan is greatly appreciated.

References

Angelier J, Hsu HT, Lee JC (1997) Shear concentration in a collision zone: kinematics of the active Chihshang fault in the Longitudinal Valley, eastern Taiwan. Tectonophysics 274:117–144

Angelier J, Chang T-Y, Hu J-C, Chang C-P, Siame L, Lee J-C, Deffontaines B, Chu H-T, Lu C-Y (2009) Does extrusion occur at both tips of the Taiwan collision belt? Insights from active deformation studies in the Ilan Plain and Pingtung Plain regions: Tectonophysics 466:356–376.

Bos AG, Spakman W (2003) Surface deformation and tectonic setting of Taiwan inferred from GPS velocity field. J Geophys Res 108(B10):2458–2476

Briais A, Tapponnier P, Pautot G (1989) Constraints of Sea Beam data on crustal fabrics and seafloor spreading in the South China Sea. Earth Planet Sci Lett 95:307–320

Briais A, Patriat P, Tapponnier P (1993) Updated interpretation of magnetic anomalies and seafloor spreading stages in the South China Sea – implications for the Tertiary Tectonics of Southeast Asia. J Geophys Res 98(B4):6299–6328

Byrne T (1994) Sediment melanges – an example of the interplay of deformation and diagenesis. In: Maltman A (ed) Geological deformation of sediments. Chapman and Hall, London, pp 239–260

Byrne T, Liu C-S (2002a) Geology and geophysics of an arc-continent collision, Taiwan, vol 358, Geological Society of America Special Paper. Geological Society of America, Boulder, CO

Byrne T, Liu C-S (2002b) Preface: introduction to the geology and geophysics of Taiwan. In: Byrne T, Liu C-S (eds) Geology and geophysics of an arc-continent collision, Taiwan, vol 358, Geological Society of America Special Paper. Geological Society of America, Boulder, CO, pp v–vii

Byrne T, Chan Y-C, Lee Y-H, Lee J-C, Rau R-J (2008) Reconstructing Taiwan: a new view of a classic Orogen. In: Geological Society of America, National Meeting, Houston, TX. Geological Society of America Abstracts with Programs. pp T82 321–324

Byrne T, Daniels M, Miller J (2009) Footwall geometry and topography in the Taiwan arc-continent collision. In: Geological Society of America Northeastern Section-44th Annual Meeting, Portland, Maine. Geological Society of America Abstracts with Programs, p 3

Carena S, Suppe J, Kao H (2002) Active detachment of Taiwan illuminated by small earthquakes and its control of first-order topography. Geology 30(10):935–983

Chamberlain RT, Shepard FB (1923) Some experiments in folding. Journal of Geology 31:490–512

Chang SL, Chi WR (1983) Neogene nannoplankton biostratigraphy in Taiwan and the tectonic implications. Petrol Geol Taiwan 19:93–147

Chang C-P, Angelier J, Huang C-Y (2000) Origin and evolution of a mélange: the active plate boundary and suture zone of the Longitudinal Valley, Taiwan. Tectonophysics 325:43–62

Chang CP, Chang T-Y, Angelier J, Honn K, Lee J-C, Yu S-B (2003) Strain and stress field in Taiwan oblique convergent system: constraints from GPS observation and tectonic data. Earth Planet Sci Lett 214:115–127

Chang CP, Angelier J, Huang CY (2009) Evolution of subduction indicated by melanges in Taiwan. In: Lallemand S, Funiciello F, Lallemand S, Funiciello F (eds) Subduction zone geodynamics. Springer, Berlin, pp 207–225. doi:10.1007/978-3-540-87974-9

Chapple WM (1978) Mechanics of thin-skinned fold-and-thrust belts. Geol Soc Am Bull 89:1189–1198

Chen C-H (2000) Geologic map of Taiwan. Central Geological Survey, Ministry of Economic Affairs, Taipei

Chen W-S, Ridgeway KD, Horng C-S, Chen Y-G, Kai-Shuan S, Yeh M-G (2001) Stratigraphic architecture, magnetostratigraphy, and incised-valley systems of the Pliocene-Pleistocene collisional marine foreland basin of Taiwan. Geol Soc Am Bull 113:1249–1271

Cheng W-B (2004) Crustal structure of the High Magnetic Anomaly Belt, western Taiwan and its implications for continental margin deformation. Marine Geophys Res 25 (1–2):79–83. doi:10.1007/s11001-005-0735-3

Cheng W-B (2008) Tomographic imaging of the convergent zone in Eastern Taiwan – a subducting forearc sliver revealed? Tectonophysics. doi:10.1016/j.tecto.2007.11.010

Chi WR, Namson J, Suppe J (1981) Stratigraphic record of plate interactions in the Coastal Range of eastern Taiwan. Memoirs Geol Soc China 4:491–530

Ching K-E, Rau RJ, Lee J-C, Hu J-C (2007) Contemporary deformation of tectonic escape in SW Taiwan from GPS observations, 1995–2005. Earth Planet Sci Lett 262:601–619

Chou H-C, Kuo B-Y, Chiao L-Y, Zhao D, Hung S-H (2009) Tomography of the westernmost Ryukyu subduction zone and the serpentinization of the fore-arc mantle. J Geophys Res 114. doi:10.1029/2008JB006192

Clark MB, Fisher DM, Lu C-Y, Chen C-S (1993) The Hsüehshan Range of Taiwan: a crustal-scale pop-up structure. Tectonics 12(1):205–217

Crespi J, Chan Y-C, Swaim M (1996) Synorogenic extension and exhumation of the Taiwan hinterland. Geology 24(3): 247–250

Dahlen FA, Barr TD (1989) Brittle frictional mountain building 1. Deformation and mechanical energy budget. J Geophys Res 94(B4):3906–3922

Dahlen FA, Suppe J, Davis D (1984) Mechanics of fold-and-thrust belts and accretionary wedges: cohesive Coulomb theory. J Geophys Res 89:10,087–10,101

Dana JD (1866) A textbook of geology. Theodore Bliss, Philadelphia

Davis D, Suppe J, Dahlen FA (1983) Mechanics of fold-and-thrust belts and accretionary wedges. J Geophys Res 88: 1153–1172

Deffontaines B, Lee J-C, Angelier J, Carvalho J, Rudant J-P (1994) New geomorphic data on the active Taiwan orogen: a multisource approach. J Geophys Res 99(B10):20,243–20,266

Deffontaines B, Lacombe O, Angelier J, Chu H-T, Mouthereau F, Lee CT, Deramond J, Lee J-F, Yu M-S, Liew P-M (1997) Quaternary transfer faulting in the Taiwan foothills: evidence from a multisource approach. Tectonophysics 274:61–82

Dorsey RJ (1992) Collapse of the Luzon volcanic arc during onset of arc-continent collision: evidence from a Miocene-Pliocene unconformity, eastern Taiwan. Tectonics 11: 177–191

Fisher DM, Lu C-Y, Chu H-T (2002) Taiwan Slate Belt: insights into the ductile interior of an arc-continent collision. In: Byrne TB, Liu C-S (eds) Geology and geophysics of and an arc-continent collision, Taiwan, vol 358, Geological Society of America Special Paper. Geological Society of America, Boulder, CO, pp 93–106

Fisher DM, Willett S, Yeh E-C, Clark MB (2007) Cleavage fronts and fans as reflections of orogen stress and kinematics in Taiwan. Geology 35(1):65–68

Fuller C, Willett SD, Fisher DM, Lu C-Y (2006) A thermomechanical wedge model of Taiwan constrained by fission-track thermochronometry. Tectonophysics 425:1–24

Gourley JR (2006) Syn-tectonic extension and lateral extrusion in Taiwan: the tectonic response to a basement high promontory. University of Connecticut, Storrs

Harris R, Huang C.Y, Linking melange types and occurrences with active melange-forming process in Timor and Taiwan, in Proceedings Annual Meeting, Geological Society of America, Denver, CO, 2010, Geological Society of America, p. Paper 49–41

Hayes DE, Taylor BR (1978) Magnetic anomalies. In: Hayes DE (ed) Geophysical Atlas of East and Southeast Asian Seas, vol MC 25, Map and Charts Ser. Geological Society of America, Boulder, CO

Hickman JB, Wiltschko DV, Hung J-H, Fang P, Bock Y (2002) Structure and evolution of the active fold-and-thrust belt of southwestern Taiwan from Global Positioning System analysis. In: Byrne T, Liu C-S (eds) Geology and geophysics of an arc-continent collision, Taiwan, vol 358, Geological Society of America Special Paper. Geological Society of America, Boulder, CO, pp 75–92

Ho CS (1975) An introduction to the geology of Taiwan – Explanatory text of the geologic map of Taiwan. Ministry of Economic Affairs, Taipei

Ho CS (1976) Foothills tectonics of Taiwan. Bull Geol Surv Taiwan 25:9–28

Ho CS (1982) Tectonic evolution of Taiwan: explanatory text of the geologic map of Taiwan. Ministry of Economic Affairs, Taipei, Taiwan, Republic of China

Ho CS (1986) A synthesis of the geologic evolution of Taiwan. Tectonophysics 125:1–16

Ho CS (1988) An introduction to the geology of Taiwan – explanatory text of the geologic map of Taiwan, 2nd edn. Ministry of Economic Affairs, Taipei, Taiwan, Republic of China

Hsu S-K, Liu C-S, Shyu C-T, Liu S-Y, Sibuet J-C, Lallemand S, Wang C, Reed DL (1998) New Gravity and Magnetic Anomaly Maps in the Taiwan-Luzon Region and their Preliminary Interpretation. Terr Atmos Ocean Sci 9(3):509–532

Hsu Y-J, Simons M, Yu S-B, Kuo L-C, Chen H-Y (2003) A two-dimensional dislocation model for interseismic deformation of the Taiwan mountaion belt. Earth Planet Sci Lett 211:287–294

Hsu Y-J, Segall P, Yu S-B, Kuo L-C, Williams C (2007) Temporal and spatial variations of postseismic deformation following the 1999 Chi-Chi, Taiwan earthquake. Geophys J Int 169:367–379. doi:10.1111/j.1365-246X.2006.03310.x

Hsu Y-J, Yu S-B, Simons M, Kuo L-C, Chen H-Y (2008) Interseismic crustal deformation in the Taiwan plate boundary zone revealed by GPS observations, seismicity, and earthquake focal mechanisms. Tectonophysics. doi:10.1016/j.tecto.2008.11.016

Huang CY, Cheng YM, Yeh CC (1985) Genesis of the Kenting Formation in the Hengchun Peninsula, southern Taiwan. Ti-Chih (Geology) 6:21–38

Huang C-Y, Yuan P, Tsao S-J (2006) Temporal and spatial records of active arc-continent collision in Taiwan: a synthesis. Geol Soc Am Bull 118(3/4):274–288. doi:10.1130/B25527.1

Huang CY, Chien C-W, Yao B, Chang CP (2008) The Lichi Melange: a collision melange formation along early arcward backthrusts during forearc basin closure, Taiwan arc-continent collision. In: Draunt AE, Clift PD, Scholl D (eds) Formation and applications of the sedimentary record in arc collision zones, vol 436. Geological Society of America, Boulder, pp 127–154

Hung JH, Wiltschko DV (1993) Structure and kinematics of arcute thrust faults in teh Miaoli-Cholan area of western Taiwan. Petrol Geol Taiwan 8:59–96

Jordon TE (1995) Retroarc Foreland and related basins. In: Busby C, Ingersoll R (eds) Tectonics of sedimentary basins. Blackwell, Oxford, pp 331–362

Khan M, Treloar P, Searle M, Jan M (eds) (2000) In: Tectonics of the Nanga Parbat Syntaxis and the Western Himalaya, vol 170. Geological Society of London, Special Publications, London. doi:10.1144/GSL.SP.2000.170.01.01

Kim K-H, Huang B, Yeh Y-H, Shen P, Chiu J-M, Pujol J, Chen K-C (2005) Three-dimensional Vp and Vs structural models associated with the active subduction and collision tectonics in the Taiwan region. Geophys J Int 162(1):204–220

Koons PO (1990) The two-sided orogen: collision and erosion from the sandbox to the Southern Alps, New Zealand. Geology 18:679–682

Lacombe O, Mouthereau F, Angelier J, Deffontaines B (2001) Structural, geodetic and seismological evidence for tectonic escape in sw Taiwan. Tectonophysics 333:323–345

Lacombe O, Mouthereau F, Angelier J, Chu H-T, Lee J-C (2003) Frontal belt curvature and oblique ramp development at an obliquely collided irregular margin: geometry and kinematics of the NW Taiwan fold-thrust belt. Tectonics 22 (3). doi:10.1029/2002TC001436

Lee Y-H, Byrne T, Lo W (2010) Exhumation History and Segmentation of the Hsuehshan Range, Central Taiwan Revealing by Low Temperature Thermochronology Data, American Geophysical Union: Taipei, AGU, p. T54A-01

Lee C-R, Cheng W-T (1986) Preliminary heat flow measurements in Taiwan. In: Proceedings of the fourth circum-pacific energy and mineral resources conference, Singapore

Lee T-Q, Kissel C, Barrier E, Laj C, Chi W-R (1991) Paleomagnetic evidence for a diachronic clockwise rotation of the Coastal Range, eastern Taiwan. Earth Planet Sci Lett 104: 245–257

Lee J-C, Lu C-Y, Chu H-T, Delcaillau B, Angelier J, Deffontaines B (1996) Active Deformation and Paleostress Analysis in the Pakua Anticline Area of Western Taiwan. Terr Atmos Ocean Sci 7(4):431–446

Lee J-C, Deffontaines B, Angelier J, Chu H-T, Hu J-C, Lacombe O, Mouthereau F, Yeh Y-H, Bureau D, Carvalho J, Lu C-Y, Liew P-M, Rudant J-P, Li F-C, Jeng J-C, Lee C-T (1997) Morphoneotectonic map of Taiwan. Central Geologic Survey, Ministry of Economic Affairs, R.O.C

Lee Y-H, Hsieh M-L, Lu S-D, Shih T-S, Wu W-Y, Sugiyama Y, Azuma T, Kariya Y (1999) Slip vectors of the surface rupture of the 1999 Chi-Chi earthquake, western Taiwan. J Struct Geol 25:1917–1931

Lee J-C, Angelier J, Chu H-T, Hu J-C, Jeng F-S (2001) Continuous monitoring of an active fault in a plate suture zone: a creepmeter study of the Chihshang Fault, eastern Taiwan. Tectonophysics 333:219–240

Lee J-C, Hu J-C, Rau RJ (2002) Near-surface seasonal creeping and subsurface repeated seismicity on the plate-suture thrust fault in Chihshang, Eastern Taiwan. Eos Trans AGU 83(47) FallMeet Suppl, Abstract T61B-1276

Lee Y-H, Chen C-C, Liu T-K, Ho H-C, Lu H-Y, Lo W (2006) Mountain building mechanisms in the Southern Central Range of the Taiwan Orogenic Belt – from accretionary wedge deformation to arc–continental collision. Earth Planet Sci Lett 252:413–422. doi:10.1016/j.epsl.2006.09.047

Lee C-P, Hirata N, Huang B, Huang W-G, Tsai Y-B (2009) Anomalous seismic attenuation along the plate collision boundary in southeastern Taiwan: observations from a linear seismic array. Bull Seismol Soc Am 99:2662–2680. doi:10.1785/0120080302

Lee C-P, Hirata N, Huang B-S, Huang W-G, Tsai Y-B (2010) Evidence of a highly attenuative aseismic zone in the active collision orogen of Taiwan. Tectonophysics 489:128–138. doi:10.1016/j.tecto.2010.04.009

Liew P-M, Pirazzoli PA, Hsieh M-L, Arnold M, Barusseau JP, Fountugne M, Giresse P (1993) Holocene tectonic uplift deduced from elevated shorelines, eastern Coastal Range of Taiwan. Tectonophysics 222:55–68

Lin C-H (2000) Thermal modeling of continental subduction and exhumation constrained by heat flow and seismicity in Taiwan. Tectonophysics 324:189–201

Lin CH, Roecker SW (1993) Deep earthquakes beneath central Taiwan: mantle shearing in an arc-continent collision. Tectonics 12(3):745–755

Lin AT-S, Watts A (2002) Origin of the west Taiwan basin by orogenic loading and flexure of a rifted continental margin. J Geophys Res 107(B9):2185. doi:10.1029/2001JB000669

Lin C-H, Yeh Y-H, Yen H-Y, Chen K-C, Huan B-S, Roecker SW, Chiu J-M (1998) Three-dimensional elastic wave structure of the Hualien region of Taiwan: evidence of active crustal exhumation. Tectonics 17:89–103

Lin A, Watts A, Hesselbo P (2003) Cenozoic stratigraphy and subsidence history of the South China Sea margin in the Taiwan region. Basin Res 15:453–478. doi:10.1046/j.1365-2117.2003.00215.x

Lin K-C, Hu J-C, Ching K-E, Angelier J, Rau R-J, Yu S-B, Tsai C-S, Shin T-C, Huang M-H (2010) GPS crustal deformation, strain rate and seismic activity after the 1999 Chi-Chi earthquake in Taiwan. J Geophys Res 115 (B07404) 22 pp

Liu CC, Yu SB (1990) Vertical crustal movements in eastern Taiwan and their tectonic implications. Tectonophysics 183:111–119

Liu T-K, Chen Y-G, Chen W-S, Jiang S-H (2000) Rates of cooling and denudation of the Early Penglai Orogeny, Taiwan, as assessed by fission-track constraints. Tectonophysics 320:69–82

Liu T-K, Hsieh S, Chen Y-G, Chen W-S (2001) Thermo-kinematic evolution of the Taiwan oblique-collision mountain belt as revealed by zircon fission track dating. Earth Planet Sci Lett 186:45–56

Lo C-H, Onstott TC (1995) Rejuvenation of K-Ar systems for minerals in the Taiwan Mountain Belt. Earth Planet Sci Lett 131:71–98

Lu C-Y, Malavieille J (1994) Oblique convergence, indentation and rotation tectonics in the Taiwan mountain belt. Earth Planet Sci Lett 121:93–108

Lu C-Y, Chan Y-C, Kuo L-C, Chang K, Lee J-C (2010) Geohazards in related to neotectonic patterns of taiwan based on recent multi-source data. Paper presented at the EOS Trans. AGU, Taipei, Taiwan

Lundberg N, Dorsey RJ (1990) Rapid Quaternary emergence, uplift, and denudation of the Coastal Range, eastern Taiwan. Geology 18:638–641

Macedo JM, Marshak S (1999) Controls on the geometry of fold-thrust belt salients. Geol Soc Am Bull 111:1808–1822

Malavieille J, Trullenque G (2009) Consequences of continental subduction on forearc basin and accretionary wedge deformation in SE Taiwan: insights from analogue modeling. Tectonophysics. doi:10.1016/j.tecto.2007.11.016

Marshak S (2004) Salients, recesses, arcs, orocline, and syntaxes – a review of ideas concerning the formation of map-view curves in fold-thrust belts. In: McClay KR (ed) Thrust tectonics and hydrocarbon systems, vol 82, AAPG Memoir. American Association of Petroleum Geologists, Tulsa, pp 131–156

McCabe R (1984) Implications of paleomagnetic data on the collision-related bending of island arcs. Tectonics 4: 409–428

McIntosh K, Nakamura Y, Wang T-K, Shih R-C, Chen A, Liu C-S (2005) Crustal-scale seismic profiles across Taiwan and the western Philippine Sea Plate. Tectonophysics 401: 23–54

Mouthereau F, Lacombe O (2006) Inversion of the Paleogene Chinese continental margin and thick-skinned deformation in the Western Foreland of Taiwan. J Struct Geol 28: 1977–1993.

Mouthereau F, Deffontaines B, Lacombe O, Angelier J (2002) Variations along the strike of the Taiwan thrust belt: basement control on the structural style, wedge geometry and kinematics. In: Byrne T, Liu C-S (eds) Geology and geophysics of an arc-continent collision, Taiwan, vol 358, Geologic Society of America Special Paper. Geologic Society of America, Boulder, CO

Namson J (1981) Detailed structural analysis of the western foothills belt in the Miaoli-Hsinchu area, Taiwan: I Southern Part. Petrol Geol Taiwan 18:31–51

Nissen S, Hayes DE, Bochu Y, Weijun Z, Yongqin C, Xiaupin N (1995) Gravity, heat flow, and seismic constraints on the processes of crustal extension: Northern margin of the South China Sea: Journal of Geophysical Research, v. 100, no. B11, p. 22,447–422,483

Nissen S, Hayes DE, Buhl P, Diebold J, Bochu Y, Weijun Z, Yongqin C (1995) Deep penetration seismic soundings across the northern margin of the South China Sea. J Geophys Res 100(B11):22407–22433

Page B, Lan CY (1983) The Kenting melange and it's tectonic events. Mem Geol Soc China 5:227–248

Page BM, Suppe J (1981) The Pliocene Lichi melange in Taiwan: its plate tectonic and olistostromal origin. Am J Sci 281:193–227

Perfettini H, Avouac J-P (2004) Postseismic relaxation driven by brittle creep: a possible mechanism to reconcile geodetic measurements and the decay rate of aftershocks, application to the Chi-Chi earthquake, Taiwan. J Geophys Res 109 (B02304). doi:10.1029/2003JB002488

Pulver MH, Crespi JM, Byrne TB (2002) Lateral extrusion in a transpressional collisional zone: an example from the pre-Tertiary metamorphic basement of Taiwan. In: Byrne TB, Liu C-S (eds) Geology and geophysics of an arc-continent collision, Taiwan, vol 358, Geological Society of America Special Paper., pp 107–120

Ramsay LA, Walker RT, Jackson J (2007) Geomorphic constraints on the active tectonics of southern Taiwan. Geophys J Int. doi:10.1111/j.1365-246X.2007.03444.x

Rau R-J, Wu F (1995) Tomographic imaging of lithospheric structures under Taiwan. Earth Planet Sci Lett 133:517–532

Rau R-J, Wu FT (1998) Active tectonics of Taiwan orogeny from focal mechanisms of small-to-moderate-sized earthquakes. Terr Atmos Ocean Sci 9:755–778

Roecker SW, Yeh YH, Tsai Y-B (1987) Three-dimensional P and S wave velocity structures beneath Taiwan deep structure beneath an arc continent collision. J Geophys Res 92: 10547–10570

Ryan WBF, et al. (2009) Global Multi-Resolution Topography synthesis, Geochem. Geophys. Geosyst., 10, Q03014, doi:10.1029/2008GC002332

Seno T, Stein S, Gripp AE (1993) A model for the motion of the Philippine Sea plate consistent with NUVEL-1 and geologic data. J Geophys Res 98:17941–17948

Shyu JH, Sieh K, Chen Y-G, Chung L-H (2006) Geomorphic analysis of the Central Range fault, the second major active structure of the Longitudinal Valley suture, eastern Taiwan. Geol Soc Am Bull 118(11/12):1447–1462. doi:10.1130/B25905.1

Simoes M, Avouac J-P (2006) Investigating the kinematics of mountain building in Taiwan from the spatiotemporal evolution of the foreland basin and western foothills. J Geophys Res 111. doi:10.1029/2005JB004209

Simoes M, Avouac J-P, Beyssac O, Goffe B, Farley K, Chen Y-G (2007) Mountain building in Taiwan: a thermokinematic model. Journal of Geophysical Research 112. doi:10,1029/2006JB004824

Stanley RS, Hill AB, Chang HC, Hu HN (1981) A transect through the metamorphic core of the Central Mountains, southern Taiwan. Memoirs Geol Soc China 4:443–473

Stolar D, Roe GH, Willett S (2007a) Controls on the patterns of topography and erosion rate in a critical orogen. J Geophys Res 112 (F04002)

Stolar D, Willett S, Montgomery DR (2007b) Characterizing topographic steady state in Taiwan. Earth Planet Sci Lett 261: 421–431

Suppe J (1981) Mechanics of mountain building and metamorphism in Taiwan. Memoir Geol Soc China 4:67–89

Suppe J (1984) Kinematics of arc-continent collision, flipping of subduction and back-arc spreading near Taiwan. Memoirs Geol Soc China 6:21–33

Suppe J, Wu YM, Carena S, Ustaszewski K (2010) Deep and shallow structure of the Taiwan arc-continent collision. In: West. Pac. Geophys. Meet. Suppl., Taipei, Taiwan. Eos Trans AGU. pp Abstract T22A-01

Teng LS (1987) Stratigraphic records of the late Cenozoic Penglai orogeny of Taiwan. Acta Geologica Taiwanica 25: 205–224

Teng LS (1990) Geotectonic evolution of late Cenozoic arc-continent collision in Taiwan. Tectonophysics 183:57–76

Teng LS (1996) Extensional collapse of the northern Taiwan mountain belt. Geology 24(10):949–952

Thomas W (2006) Tectonic inheritance at a continental margin. GSA Today 16(2):4–11

Tsan SF (1974) The Kenting formation: a note on Hengchun Peninsula stratigraphy. Proc Geol Soc China 17:131–133

Tsao S (1996) The geological significance of illite crystallinity, zircon fission-track ages and K-Ar ages of metasedimentary rocks of the Central Range. M.S., National Taiwan University, Taipei

Vogt PR, Lowrie A, Bracey D, Hey R (1976) Subduction of aseismic oceanic ridges: effects on shape, seismicity, and other characteristics of consuming plate boundaries. Geol Soc Am Spec Publ 172:59

Wallace L, McCaffery R, Beaven J, Ellis S (2005) Rapid microplate rotations and backarc rifting at the transition between collision and subduction. Geology 33(11):857–860

Wang C, Huang C-P, Ke L-Y, Chien W-J, Hsu S-K, Shyu C-T, Cheng W-B, Lee C-S, Teng LS (2002) Formation of the Taiwan Island as a solitary wave along the Eurasian continental plate margin: magnetic and seismological evidence. Terr Atmos Ocean Sci 13(3):339–354

Wang TK, Chen M-K, Lee C-S, Xia K (2006) Seismic imaging of the transitional crust across the northeastern margin of the South China Sea. Tectonophysics 412:237–254

Wang H-L, Chen H-W, Zhu L (2010a) Constraints on average Taiwan Reference Moho Discontinuity Model – receiver function analysis using BATS data. Geophys J Int 183: 1–19. doi:10.1111/j.1365-246X.2010.04692.x

Wang Y-J, Ma K-F, Mouthereau F, Eberhart-Phillips D (2010b) Three-dimensional Qp- and Qs-tomography beneath Taiwan orogenic belt: implications for tectonic and thermal structure. Geophys J Int 180(2):891–910. doi:10.1111/j.1365-246X.2009.04459

Whipple KX, Meade B (2004) Controls on the strength of coupling among climate, erosion, and deformation in two-sided, frictional orogenic wedges at steady state. J Geophys Res 109. doi:10.1029/2003JF000065

Whipple KX, Meade B (2006) Orogen response to changes in climatic and tectonic forcing. Earth Planet Sci Lett 243: 218–228. doi:10.1016/j.epsl.2005.12.022

Willemin J, Knuepfer P (1994) Kinematics of arc-continental collision in the eastern Central Range of Taiwan inferred from geomorphic analysis. J Geophys Res 99(B10):20, 267–20, 280

Willett S, Beaumont C, Fullsack P (1993) Mechanical model for the tectonics of doubly vergent compressional orogens. Geology 21(4):371–374

Willett S, Fisher DM, Fuller C, Yeh E-C, Lu C-Y (2003) Erosion rates and orgenic-wedge kinematics in Taiwan inferred from fission-track thermochronometry. Geology 31(11):945–948

Wiltschko D, Hassler L, Hung J-H, Liao H-S (2010) From Accretion to Collision: Motion and evolution of the Chaochou Fault, Southern Taiwan. Tectonics 29 (TC2015)

Wobus CW, Crosby BT, Whipple KX (2006) Hanging valleys in fluvial systems: controls on occurrence and implications for landscape evolution. J Geophys Res 111. doi:10.1029/2005JF000406

Wu FT, Rau RJ (1998) Seismotectonics and identification of potential seismic source zones in Taiwan. Terr Atmos Ocean Sci 9:739–754

Wu F, Rau R-J, Salzberg D (1997) Taiwan orogeny: thin-skinned or lithospheric collision? Tectonophysics 274:191–220

Wu FT, Chang LS, Wu YM (2004) Precisely relocated hypocenters, focal mechanism and active orogeny in central Taiwan. In: Malpas J, Fletcher CJ, Ali JR, Aitchison JC (eds) Aspects of the tectonic evolution of China, vol 226. Geological Society of London Special Publications, London, pp 333–354

Wu YM, Chang C-H, Zhao L, Shyu B, Chen Y-G, Sieh K, Avouac J-P (2007) Seismic tomography of Taiwan: improved constraints from a dense network of strong motion stations. J Geophys Res 112 (B08312). doi:10.1029/2007JB004983

Wu FT, Liang W, Lee J-C, Benz H, Villasenor A (2009) A model for the termination of the Ryukyu subduction zone against Taiwan: a junction of collision, subduction/separation, and subduction boundaries. Journal Geophysical Research 114 (B07404). doi:10.1029/2008JB005950

Yamato P, Mouthereau F, Burov E (2009) Taiwan mountain building: insights from 2-D thermomechanical modeling of a rheologically stratified lithosphere. Geophys J Int 176: 307–326. doi:10.1111/j.1365-246X.2008.03977

Yang TF, Tien JL, Chen C-H, Lee T, Punongbayan R (1995) Fission-track dating of the Taiwan-Luzon Arc: eruption ages and evidence for crustal contamination. J Asian Earth Sci 11:81–93

Yang T, Lee T, Chen C-H, Cheng S-N, Knittel U, Punongbayan R, Rasdas A (1996) A double island arc between Taiwan and Luzon: consequence of ridge subduction. Tectonophysics 258:85–101

Yang M, Rau R-J, Yu JC, Yu TT (2000) Geodetically observed surface displacements of the 1999 Chi-Chi, Taiwan, earthquake. Earth Planet Sci Lett 52:403–413

Yeh YH, Barrier E, Lin CH, Angelier J (1991) Stress tensor analysis in the Taiwan area from focal mechanisms of earthquakes. Tectonophysics 200:267–280

Yeh E-C, Fisher DM, Lu C-Y (2001) The structural evolution in the eastern central range of Taiwan. In: Program proceedings of the international symposium on East Asian Tectonics, Taipei, Taiwan, p 178

Yu H-S, Chou Y-W (2001) Characteristics and development of the flexural forebulge and basal unconformity of Western Taiwan Foreland Basin. Tectonophysics 333:277–291

Yu H-S, Huang Z-Y (2009) Morphotectonics and sedimentation in convergent margin basins: an example from juxtaposed marginal sea basin and foreland basin, Northern South China Sea. Tectonophysics 466:241–254. doi:10.1016/j.tecto.2007.11.007

Yu S-B, Cheng H-Y, Kuo L-C (1997) Velocity field of GPS stations in the Taiwan area. Tectonophysics 274:41–59

Yu S-B, Hsu Y-J, Kuo L-C, Chen H-Y, Liu C-C (2003) GPS measurement of postseismic deformation following the 1999 Chi-Chi, Taiwan, earthquake. J Geophys Res 108 (B11). doi:10.1029/2003JB002396

Yue L-F, Suppe J, Hung J-H (2005) Structural geology of a classic thrust belt earthquake: the 1999 Chi-Chi earthquake Taiwan (Mw = 7.6). J Struct Geol 27(11):2058–2083

Yui T-F, Wu TW, Jahn BM (1990) Geochemistry and plate-tectonic significance of the metabasites from the Tananao Schist Complex of Taiwan. J Southeast Asian Earth Sci 4:357–368

Chapter 9
Early Eocene Arc–Continent Collision in Kamchatka, Russia: Structural Evolution and Geodynamic Model

E. Konstantinovskaya

9.1 Introduction

Kamchatka Peninsula is located at the triple junction of the Pacific, North American and Eurasian major plates. Minor plates of the Sea of Okhotsk and of the Bering Sea accommodate the major plate interaction (Fig. 9.1).

Three arc terranes are recognised in the accretionary basement of the Kamchatka orogen (Fig. 9.1). The Jurassic – Early Cretaceous Kvakhona arc (Figs. 9.2 and 9.3) was incorporated in the basement of Western Kamchatka in the Early Cretaceous (Bondarenko 1992). The crystalline basement of Western Kamchatka is exposed in the Sredinny metamorphic massif and composed of amphibolites, granulites and granites (Khanchuk 1985; Shul'diner et al. 1987).

The Avhaivayam-Valagina arc extends for more than 1,000 km from South Kamchatka to the Olyutorsky region of Koryak highland (Fig. 9.1). The arc terrane is most likely composite and formed from individual arc segments of slightly different age. The Kamchatka segment (Ozernoy-Valagina arc) is Campanian-Danian in age (Fig. 9.2), whilst the Olutorsky arc segment is Maastrichtian-Paleocene in age (Bogdanov et al. 1990; Zinkevich et al. 1993; Astrakhantsev et al. 1987). The time of collision also varies along the strike of the Achaivayam-Valagina arc from Early Eocene in the southwest to the early Mid Eocene in the northeast (Konstantinovskaya 2001; Soloviev 2005). The Early Eocene collision of the Ozernoy-Valagina arc with the Asian margin (Western Kamchatka) in South Kamchatka (Fig. 9.2) is the subject of this paper.

The Late Cretaceous – Early Paleogene Kronotsky arc that is exposed on the eastern peninsulas of Kamchatka (Figs. 9.1 and 9.3) was probably emplaced at the Kamchatka margin along the Grechishkin suture zone either in the Late Miocene (Fig. 9.2) (Bakhteev et al. 1997; Konstantinovskaya 2001) or between the Late Eocene and the Early Miocene with a minor shortening in the Miocene (Alexeiev et al. 2006).

In this paper, the alternative models of the Early Eocene arc–continent collision in South Kamchatka are discussed based on a review of the geological and geochronological data and the author's physical modelling results. Several problematic issues of the arc–continent collision are focused.

The volcanic units of the Ozernoy-Valagina arc were thrust to the northwest along the Iruney-Vatyna Nappe (Fig. 9.3) over the Sredinny metamorphic massif in South Kamchatka (Zinkevich et al. 1994; Konstantinovskaya 2001), and over a Cretaceous-Early Eocene, continental-derived turbidite series in North Kamchatka (Soloviev 2005). The SE-vergent Vetlovsky thrust bounds the arc along its southeastern margin (Fig. 9.3). In South Kamchatka, Iruney Nappe and Vetlovsky thrust were formed subsequently in the Early Eocene during the arc–continent collision (Fig. 9.2). Based on physical modeling data, it was suggested that the syncollisional thrusting to the northwest and to the southeast occurred subsequently at the both arc sides may have been related to subduction reversal (Konstantinovskaya 2000, 2001). Otherwise, a slab detachment was proposed to be characteristic of the latest stages of the arc–continent collision (Shapiro et al. 2008; Luchitskaya et al. 2008).

E. Konstantinovskaya
Institut national de la recherche scientifique, Centre Eau, Terre et Environnement (INRS-ETE), 490 de la Couronne, Quebec, QC, Canada G1K 9A9
e-mail: Elena.Konstantinovskaya@ete.inrs.ca

D. Brown and P.D. Ryan (eds.), *Arc-Continent Collision*, Frontiers in Earth Sciences,
DOI 10.1007/978-3-540-88558-0_9,

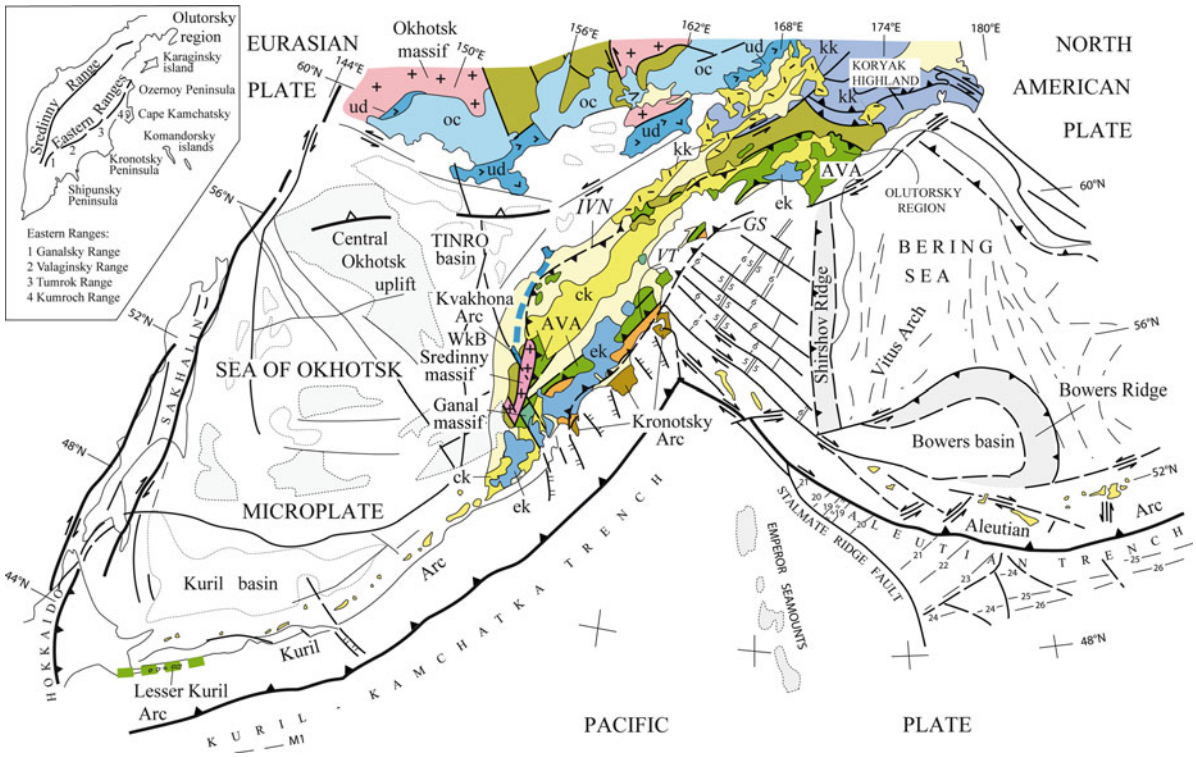

Fig. 9.1 Geodynamic setting of Kamchatka, modified after Konstantinovskaya (2001) and based on data from Kharakhinov (1996) and Nokleberg et al. (1994). The *inset* map shows the location of the Kamchatka ranges and peninsulas. Abbreviations are as follows: (ek) Eastern Kamchatka; (ck) Central Kamchatka; (kk) Koryak-Kamchatka; (oc) Okhotsk-Chukotka, (ud) Uda-Murgal volcanic belts; (WkB) West Kamchatka offshore basin; (AVA) Achaivayam-Valagina Arc, (*IVN*) Iruney-Vatyna Nappe, (*VT*) Vetlovsky thrust, (*GS*) Grechishkin suture.

The lithological variations in sedimentary and volcanic successions of the Ozernoy-Valagina arc are discussed in order to reconstruct the arc behaviour and changes of detrital sources during the arc–continent collision. The physical modeling results help to associate the geological data with the crustal and lithospheric deformations occurred in the arc and forearc area during the arc–continent collision.

Another major problem of the Early Eocene arc–continent collision in South Kamchatka is related to deformation and metamorphism occurred within the continental margin of Western Kamchatka during the collision. This issue is directly connected to the nature of the Sredinny metamorphic massif. The massif was previously considered as an uplift of Precambrian or Cretaceous basement of Western Kamchatka (Khanchuk 1985; Vinogradov et al. 1988, 1991). Recently, new U–Pb (SHRIMP) age data on the metamorphic rocks and granites of the Sredinny massif have been reported suggesting the peak of metamorphism and anatexis in gneisses of the massif occurred during the Early Eocene arc–continent collision (Bindeman et al. 2002; Soloviev 2005; Luchitskaya et al. 2008; Hourigan et al. 2009). Structural observations have also revealed the presence of post-collision, normal ductile faulting along the eastern side of the Sredinny metamorphic massif (Kirmasov et al. 2004).

Whether the peak metamorphism in the continental margin was related to delamination of crustal slices and tectonic thickening of the crust or to burial due to the arc obduction is still debatable. The syncollisional exhumation of metamorphic crust was produced either by a compressional and buoyancy-driven squeezing up of subducted slices of continental crust and erosional unloading or by density inversion, diapiric uplift and crustal thinning. The evidence of syncollisional exhumation is discussed based on lithological analysis of sedimentary units of the forearc and foreland basins.

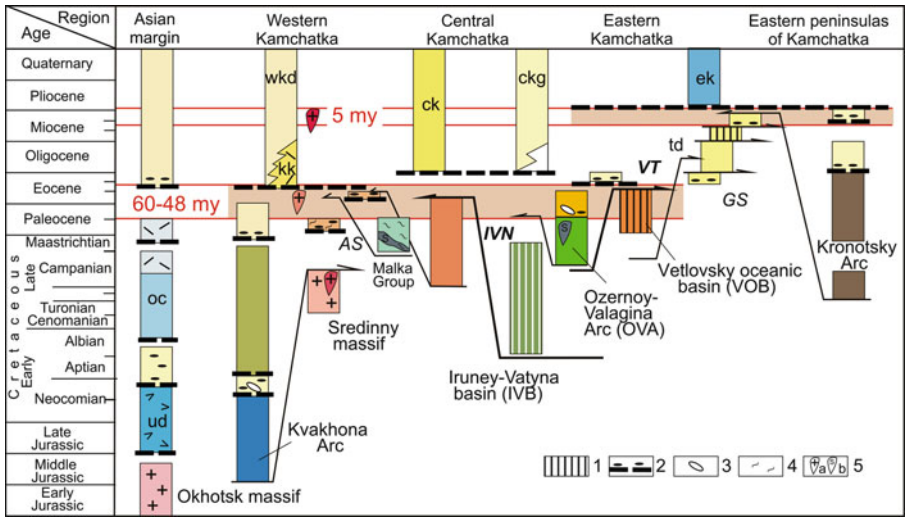

Fig. 9.2 Chronodiagram representing time vs. simplified lithotectonic units and major tectonic events for Kamchatka, modified after Konstantinovskaya (2001). (1) oceanic crust rocks (basalts, diabases and/or pelagic sediments); (2) major unconformity and basal conglomerates; (3) olistostromal deposits; (4) penetratively deformed and/or regionally metamorphosed rocks; (5) granite (a) and pyroxenite and gabbro-syenite (b) intrusions. The onshore Cenozoic depressions are as follows: (wkd) Western Kamchatka, (ckg) Central Kamchatka graben, (td) Tushevsky; (*AS*) Andrianovka suture. Other symbols as in Fig. 9.1.

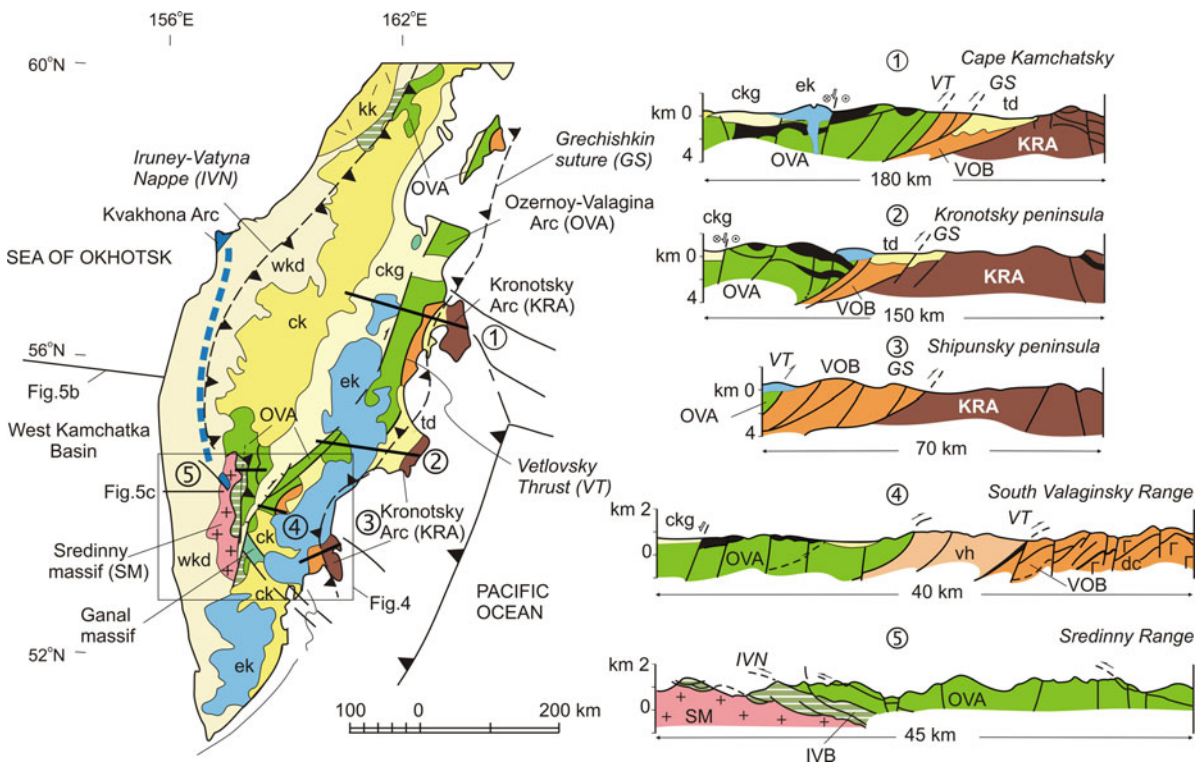

Fig. 9.3 Tectonic map and cross-sections of Kamchatka, modified after Konstantinovskaya (2001). Based on data from Zinkevich and Tsukanov (1992) and Zinkevich et al. (1994). Locations of Figs. 9.4 and 9.5b, c are shown. wkd – Western Kamchatka depression, vh – Vakhvina Group, dc – Diabase Complex Other symbols as in Figs. 9.1 and 9.2.

9.2 Geological Framework

9.2.1 Geodynamic Settings of Kamchatka

The Sea of Okhotsk microplate (Fig. 9.1) is considered either as a microcontinent (Jolivet et al. 1988; Zonenshain et al. 1990; Sengor and Natalin 1996; Nokleberg et al. 1998; Konstantinovskaya 2001; Bindeman et al. 2002) or as an oceanic plateau (Watson and Fujita 1985; Bogdanov and Chekhovich 2002; Bogdanov and Dobretsov 2002) that collided with the eastern margin of Asia in the Late Cretaceous. Results from seismic tomography (Van der Voo et al. 1999) demonstrate the presence of slab remnants of Jurassic age that were subducted beneath the Okhotsk-Chukotka volcanic belt prior this collision.

The Okhotsk-Chukotka volcanic belt (late Early to Late Cretaceous) is an Andean-type magmatic arc that extends over 3,000 km along the eastern margin of the Asian continent (Fig. 9.1). The volcanic assemblages of the belt were emplaced before the end of the Albian to Early Cenomanian (Fig. 9.2), based on floral stratigraphic data (Filatova 1988). In the Okhotsk segment of the belt, the youngest volcanic section of calc-alkaline (subduction related) type was recently dated by the $^{40}Ar/^{39}Ar$ method to between 85.5 ± 1.3 Ma and 80.7 ± 0.8 Ma (Hourigan and Akinin 2004). This may constrain the docking time of the Sea of Okhotsk microplate to the Asian margin at about 81 Ma. The capping basalts of the section, dated to between 77.5 ± 1.1 Ma and 74.0 ± 1.2 Ma, have within-plate type geochemical features and are possibly related to a phase of extension (Hourigan and Akinin 2004).

Western Kamchatka is considered to be a part of the Sea of Okhotsk microplate (Gladenkov et al. 1997; Sedimentary basins 1987), or to form a separate Western Kamchatka microplate that collided with the Sea of Okhotsk microplate in the Early Maastrichtian (Bogdanov and Chekhovich 2002). In the present geodynamic framework (Fig. 9.1), the regions of the West Kamchatka Basin and the Central-Okhotsk uplift in the Sea of Okhotsk differ from Western Kamchatka in their thicknesses and seismic velocities. The West Kamchatka Basin and the Central-Okhotsk uplift are characterised by a subcontinental type of crust with thicknesses of 25 and 30 km, respectively, reduced as a result of the Mid Eocene and Miocene extension (Kharakhinov et al. 1996). The crustal thickness in the southern part of Western Kamchatka varies from 30 km on the western coast of the peninsula to 44–46 km in the region of the Sredinny metamorphic massif, its seismic velocities being typical of those of the continental crust (Kharakhinov et al. 1996; Tectonic Map 2000). The Moho depth ranges between 30 and 40 km across Kamchatka (Levin et al. 2002). In the present study, Western Kamchatka is considered as the frontal (facing SE) part of the Sea of Okhotsk microplate whose crystalline basement was deformed and metamorphosed during the Early Eocene collision between the Achaivayam-Valagina arc and the continental margin of Asia.

9.2.2 Post-collisional Volcanic Belts and Sedimentary Depressions of Kamchatka

Three longitudinal volcanic belts were developed on the accretionary basement of the Kamchatka orogen (Figs. 9.2 and 9.3): the Koryak-Kamchatka (Middle Eocene–Oligocene), the Central Kamchatka (Oligocene-Quaternary) and the Eastern Kamchatka (Pliocene-present) belts. A calc-alkaline supra-subduction series of volcanites is characteristic for the eastern side of the Central Kamchatka belt, whereas a high-alkaline series is localised along its western side (Avdeiko and Volynets 2000). The active volcanoes of the Eastern Kamchatka belt and the Kuril arc occur above the northwest-dipping subduction zone of the Pacific plate (Figs. 9.1 and 9.3). Seismic tomography data suggest that subducting lithosphere of the Pacific plate terminates at the Aleutian–Kamchatka junction and becomes progressively shallower towards its northern edge (Gorbatov et al. 1997; Bijwaard et al. 1998).

Three longitudinal depressions of Cenozoic age bound the volcanic belts: Western Kamchatka, Central Kamchatka and Tushevsky (Fig. 9.2).

The Western Kamchatka depression of the Kamchatka orogen is located to the west of the Central Kamchatka volcanic belt (Fig. 9.3). The 1–4 km-thick sedimentary fill is Upper Paleocene-Quaternary in the deepest parts of the basin and Middle Miocene–Quaternary above the basement highs (Buryak et al. 1988). The basinal depression was mostly formed as a result of a regional extension and subsidence that

affected the Sea of Okhotsk microplate from the Mid Eocene and reached its peak during the Miocene. The early stages of the depression evolution were contemporary to the Early Eocene arc–continent collision and discussed with more details below.

The Central Kamchatka graben separates the Central and Eastern Kamchatka volcanic belts (Fig. 9.3). The sedimentary fill of the graben is Oligocene-Quaternary in the north and Miocene-Quaternary in the south, with a total thickness 5.5–6.5 km (Nurmukhamedov 2001). The Central Kamchatka graben is asymmetrical in cross section, with a faulted eastern margin and in the west ascending gradually towards the Sredinny Range (Fig. 9.3). The NE-SW-trending active faults along the eastern flank of the graben dip steeply west and reveal mostly normal offsets with up to about 2 km of displacement; there is also a minor dextral strike-slip component (Kozhurin 2004; Kozhurin et al. 2006). The dominant dextral strike-slip offsets are typical for the northeastern splay fault in the Kamchatsky Cape (Kozhurin 2004). The Central Kamchatka graben (Fig. 9.2) started to open progressively from the NE to the SW from Oligocene to Miocene time (Zinkevich et al. 1993). The late Pleistocene–Holocene lavas at the northern end of the Central Kamchatka depression north of the edge Pacific slab (Aleutian-Kamchatka junction) originated as a consequence of low-grade decompression melting of the Pacific asthenospheric mantle, related to the Quaternary detachment of a fragment of the subducting Pacific slab (Portnyagin et al. 2005).

The Tushevsky depression is located between the Eastern Kamchatka volcanic belt and the eastern peninsulas of Kamchatka (Fig. 9.3) and consists of Middle Eocene–Upper Miocene turbidite deposits (Fig. 9.2). Flute casts, cross-lamination structures, and drag folds in soft-sediment slumps document a principal sediment transport from the west and northwest in the Upper Eocene and Lower and Middle Miocene deposits of the depression (Alexeiev et al. 1999; Marsaglia et al. 1999). The Grechishkin collisional suture that affects the structure of the Tushevsky depression (Fig. 9.3) is recognised as a long-lived, syn-sedimentary thrust zone, which developed during Late Eocene to Late Miocene east-directed transverse compression (Bakhteev et al. 1997). Miocene pelagic siliceous rocks (Fig. 9.2) that occur in tectonic slices within this zone on the Kronotsky Peninsula (Fig. 9.1, inset map) contain radiolaria groups similar to those of Japan and the Kuril Islands (Bakhteev et al. 1997) and testify to a prolonged Late Eocene-Late Miocene accretion along the Grechishkin suture zone.

9.2.3 Lithotectonic Complexes and Structures of the Continental Margin

9.2.3.1 The Southern Part of Western Kamchatka Depression

The southern part of Western Kamchatka depression consists of the Kolsky and Kolpakova depressions separated by the Sobolev salient (Fig. 9.4). The inland sedimentary cover extends to the offshore West Kamchatka Basin in the Sea of Okhotsk (Fig. 9.5b, c), where five seismo-stratigraphic sequences are recognised (Kharakhinov 1996). The Paleocene–Eocene deposits (0.2–1.2 km thick) rest with an angular unconformity upon the Upper Cretaceous basement and fill individual grabens close to the Kamchatka coast. The syn-sedimentary west-vergent thrust affects the Cretaceous basement along its western margin (Fig. 9.5b).

The Kolpakova depression is bounded by the Sredinny metamorphic massif to the east and the Sobolev basement salient to the south (Fig. 9.4). The Cretaceous (pre-Santonian) basement rocks of the depression consist of folded and faulted greenschist-facies sandstones and mudstones of the *Kikhchik Group* (Sedimentary basins 1987) (Fig. 9.5c). The sedimentary cover of the Kolpakova depression is up to 4 km thick and consists of a Paleogene-Neogene, upward-deepening succession (Table 9.1) that overlaps basement rocks with an angular unconformity (Buryak et al. 1988; Sedimentary basins 1987). The proluvial lobes conglomerates and breccias of the Upper Paleocene *Khulgun Formation* at the base of the cover are not continuous and occur along the margins of the basement highs. The Upper Paleocene-Lower Eocene, coarse clastic sequences of the *Napan Formation* fill a paleotopography around the Sobolev salient and west of the Sredinny uplift (Bakun et al. 1994). The Paleogene sequences of the Kolpakova depression pinch out to the south towards the Sobolev salient, where Middle Miocene deposits overlie Cretaceous basement. The basement highs controlled the transgressive marine

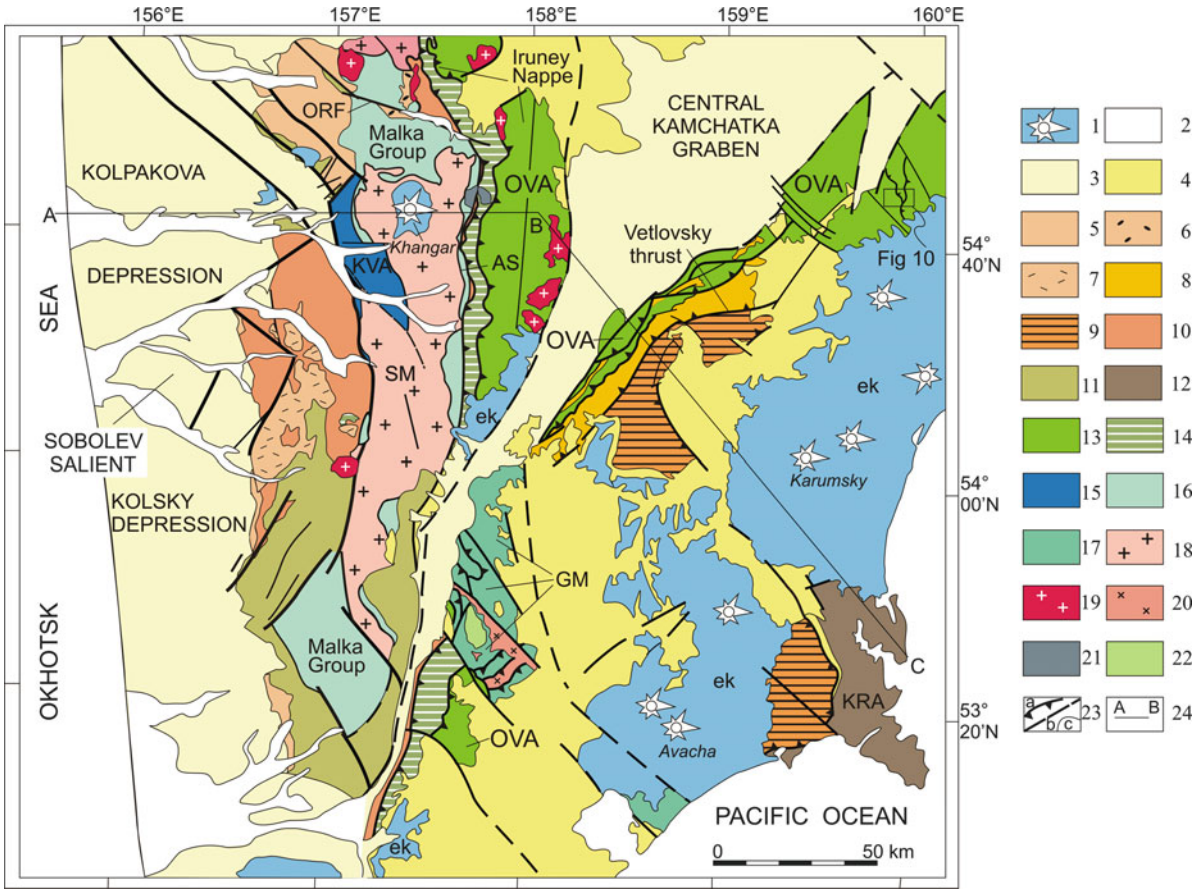

Fig. 9.4 Tectonic map of South Kamchatka, after Konstantinovskaya (2002). Based on data from the Geological map of Kamchatka (1981) and Rikhter (1991). (1) Pliocene–Holocene volcanic rocks; (2) Holocene alluvial deposits; (3) Neogene–Quaternary sedimentary rocks; (4) Middle Eocene–Miocene sedimentary and volcanic rocks; (5) Paleogene sedimentary rocks, Western Kamchatka depressions; (6) Lower Eocene conglomerates, Baraba Formation; (7) Paleocene (?)–Eocene volcanites, Cherepanova Formation; (8) Upper Paleocene–Lower Eocene turbidites, Tal'niki Formation and Vakhvina Group; (9) Paleocene–Lower Eocene rocks, Vetlovsky Complex; (10) Upper Cretaceous-Lower Paleocene turbidites, Khozgon and Pumshum formations; (11) Lower-Upper Cretaceous (pre-Santonian) turbidites, Kikhchik Group; (12) Cretaceous-Paleogene rocks, Kronotsky arc (KRA); (13) Campanian–Danian rocks, Ozernoy–Valagina arc (OVA); (14) Campanian–Maastrichtian marginal sea rocks, Iruney Formation; (15) Middle–Upper Jurassic–Neocomian rocks, Kvakhon arc (KVA); (16–18) non-differentiated metamorphic rocks of the Malka Group (16), of the Ganal massif (GM), (17) and non-differentiated gneisses and granites of the Sredinny massif (SM) (18); (19) Miocene granites; (20) synkinematic plagiogranite, GM; (21) subalkaline ultrabasite (a) and gabbro (b) intrusions (63.0 ± 0.6 and 70.4 ± 0.7 Ma) (22) Yurchik gabbro pluton (71 ± 4.3 Ma); (23) thrust faults (a), other faults (b), and conformable stratigraphic contacts (c); (24) profile line. ORF is the Oblukovina river fault. Other symbols as in Fig. 9.1. Line A-B-C shows the location of Fig. 9.5a, box – Fig. 9.10.

sedimentation in the Kolpakova depression in the Mid Eocene – Oligocene, as shown by the well log data (Bobylev and Bakun 1992)

Horst-anticlines and graben-synclines (Fig. 9.5c) are recognised in the structure of the sedimentary cover of the Kolpakova depression (Krylov et al. 1988). The horst-anticline zones, which are promising targets for hydrocarbon occurrences, are morphologically related to the uplifted blocks of Cretaceous basement (Kozyanin 1990; Burlin and Kozyanin 1995). The basement blocks are thrown up along the west-vergent thrusts (Fig. 9.5c) with relative displacements from a few hundred to several thousand metres (Kozyanin 1990). The basement rocks of the Sredinny Range are thrust above (Fig. 9.5c) the sedimentary cover of the Kolpakova depression along the high-amplitude west-vergent thrust, along which sedimentary rocks displaced under the basement to a depth of

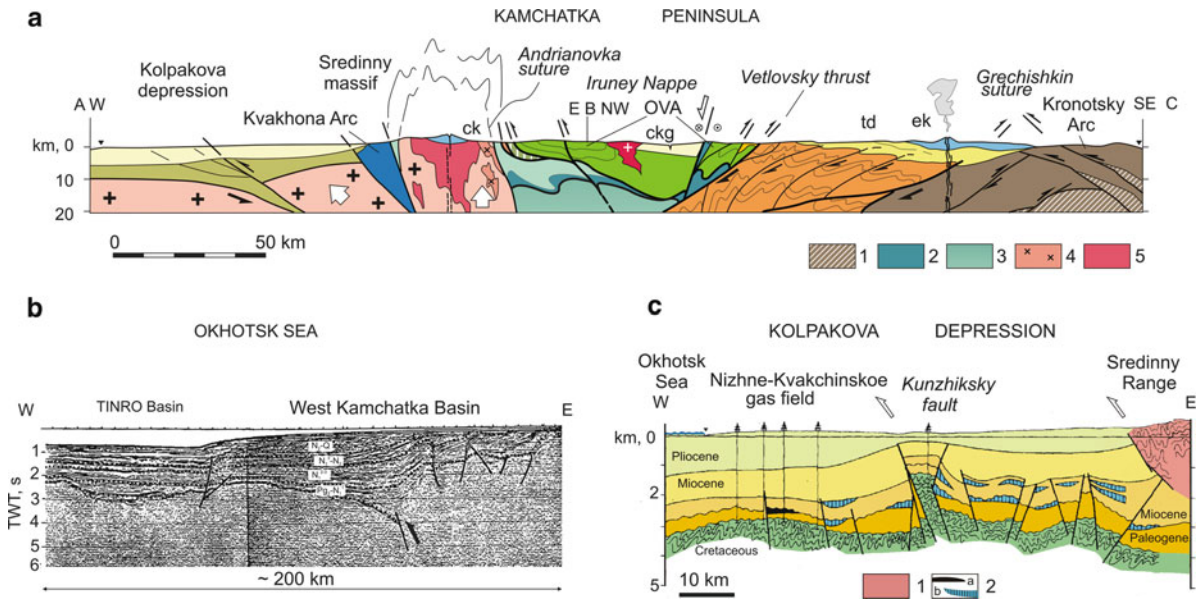

Fig. 9.5 (**a**) Interpretative profile along line A–B–C, modified after Konstantinovskaya (2002). Legend: (1) Paleogene and (2) Cretaceous oceanic crust; (3) mantle lithosphere of subducted fore-arc block; (4) syncollisional equigranular granites (52 ± 2 Ma); (5) Krutogorov gneissic granites (80–78 Ma). Other symbols as in Fig. 9.4. (**b**) Seismic time section across the southwestern part of the offshore West Kamchatka basin, after Kharakhinov (1996); *Arrow* shows the west-vergent thrust that affects Cretaceous basement (**c**) Interpretation of seismic profile across the onshore Kolpakova depression, after Kozyanin (1990). Petroliferous sandstones and conglomerates are confined to the unconformity surface between Paleogene and Neogene rocks. (1) basement rocks of the Sredinny Range; (2) gas-condensate pools (a) and predicted pools (b). See Figs. 9.3 and 9.4 for locations of profiles.

Table 9.1 Sedimentary units of the Kolpakova depression, Western Kamchatka, after Bobylev and Bakun (1992) and Bakun et al. (1994)

Age	Unit	Lithology	Thickness (m)
Upper Paleocene	*Khulgun Formation*	Proluvial, unsorted, coarse conglomerates and breccias composed of sandstone, argillaceous chert and shale fragments cemented by a gravel–sand matrix	15–350
Upper Paleocene–Lower Eocene	*Napan Formation*	Alluvial–lagoonal sequence of rhythmically interbedded sandstones (<15 m) and mudstones (8–17 m) with lenses and interlayers of large-pebble conglomerate (0.4 m); contains fossil plant detritus and silicified fauna remnants	50–149
Middle–Upper Eocene	*Snatol' Formation*	Transgressive marine sequence of a deepening-upward series of siltstones and sandstones with local conglomerates at the base	50–150
Upper Eocene–Lower Oligocene	*Kovach Formation*	Marine sequence of irregular interbeds of clayey sandstones with small pebbles, porous sandstones and mudstones; contains interlayers of clayey limestone (<0.3 m), nest-like calcite accumulations and fossil fauna remnants	10–60
Lower Miocene	*Voyampol' Group*	Deep-water marine sequence of predominantly mudstones	up to 3,000
Middle–Upper Miocene and Pliocene	*Kavran Group*	Deltaic and coastal-marine volcaniclastic molasse	

more than 3 km (Kozyanin 1990; Burlin and Kozyanin 1995). The westward thrusts that affect the sedimentary cover of the inland Kolpakova depression and the offshore West Kamchatka Basin occurred mostly at the end of the Miocene (Fig. 9.5b, c). This faulting, however, seems to be inherited from the westward

thrusting and uplift of blocks of crystalline basement that occurred in Western Kamchatka in the Late Paleocene-Early Eocene and controlled accumulation of the coarse proluvial deposits and later basin paleotopography and sedimentation in the Kolpakova depression until the Oligocene.

9.2.3.2 Sredinny Metamorphic Massif

The Sredinny metamorphic massif is 30–40 km wide and extends N–S over 200 km (Fig. 9.4), and displays a heterogeneous (Fig. 9.6) fold-and-thrust structure (Rikhter 1995). The lower structural level (parautochthon) crops out in the central part of the massif and it is composed of amphibolite- and granulite-facies metamorphic rocks of the *Kolpakova Group* (Khanchuk 1985; Rikhter 1995; Tararin 2008). The amphibolite-facies gneisses with a kyanite-biotite-garnet assemblage are the result of the regional metamorphism of a terrigenous protolith that occurred at conditions of 560–660°C and 0.59–0.69 GPa (Tararin 2008). Superimposed granitisation and migmatisation processes occurred at amphibolites facies at 620–660°C and 0.19–0.30 GPa (Tararin 2008) and are thought to be associated with decompression melting and exhumation. The granulite-facies rocks are characterised by an orthopyroxene-garnet-cordierite-orthoclase assemblage and formed at temperatures of 830–840°C around gabbro-granitoid intrusions of the Oligocene-Miocene, Lavkinskii Intrusive Complex (Tararin 2008), indicating that the granulites are associated with contact metamorphism and are younger and unrelated to the regional-scale, amphibolite-facies event.

The Kolpakova Group rocks have been dated by the Rb–Sr whole-rock method to 127–140 and 60–70 Ma (Vinogradov and Grigor'ev 1994; Vinogradov et al. 1988, 1991). The U–Pb (SHRIMP) dating of zircons from the Kolpakova Group gneisses (Bindeman et al. 2002) revealed a broad age range: Precambrian and Palaeozoic detrital nuclei with ages of 2.9–2.5, 1.7–2.1 and ~1 Ga, and other ages of 460–175, 150–120, and 96–75 Ma with a maximum of 77 ± 2 Ma. Most of the older detrital zircon nuclei are surrounded by rims of 77 Ma (Fig. 9.6), which suggests that there was a regional metamorphic event in the Campanian (Bindeman et al. 2002). Small, irregularly shaped, metamorphic zircons without zonal structure were separated from the same gneiss samples and gave ages of 47–53 Ma (Early Eocene) (Bindeman et al. 2002).

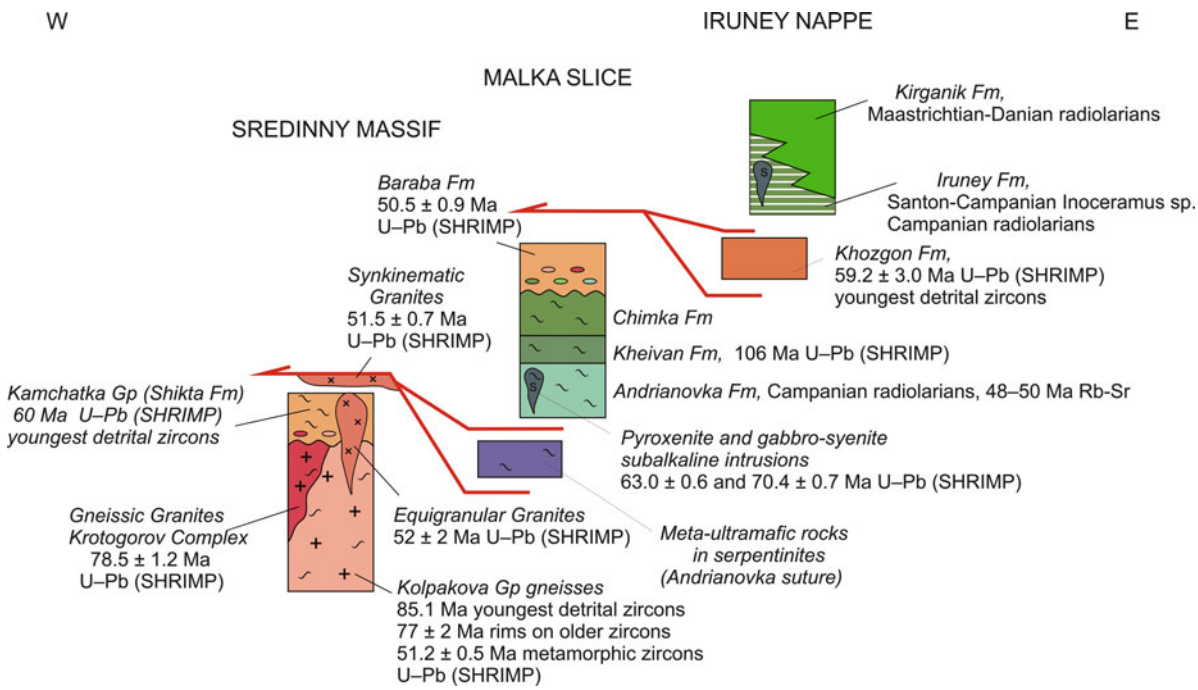

Fig. 9.6 Correlation of lithotectonic units and age data for the Sredinny massif, after data from Rikhter (1995), Luchitskaya et al. (2008) and Hourigan et al. (2009). The units are not drawn to scale.

The U–Pb (SHRIMP) dating of zircons from the gneisses of the Kolpakova Group obtained more recently (Soloviev 2005; Hourigan et al. 2009) has confirmed the wide variation of detrital zircon ages from 85.1 to 1,859 Ma (Fig. 9.6). The outer rims growing over zircon grains from the leucosome and the melanosome of the Kolpakova migmatite were dated to 51.2 ± 0.5 Ma and the metamorphic monazites from the migmatised garnet–biotite gneiss of the Kolpakova Group were dated to 52.4 ± 0.7 Ma and 51.7 ± 0.7 Ma (Soloviev 2005; Hourigan et al. 2009). This implies that the peak of metamorphism and anatexis in gneisses of the Kolpakova Group occurred at 52 ± 0.2 Ma during the Early Eocene (Fig. 9.7).

The gneissic granites of the *Krutogorov Complex* (Fig. 9.6) cut through the gneisses and migmatites of the Kolpakova Group (Rikhter 1995). Structural observations in the gneissic granites and in the Kolpakova gneisses testify to the emplacement of the granites close to the time of metamorphism of the gneisses (Khanchuk 1985). The U–Pb (SHRIMP) age of the Krutogorova Complex gneissic granites is 78.5 ± 1.5 Ma

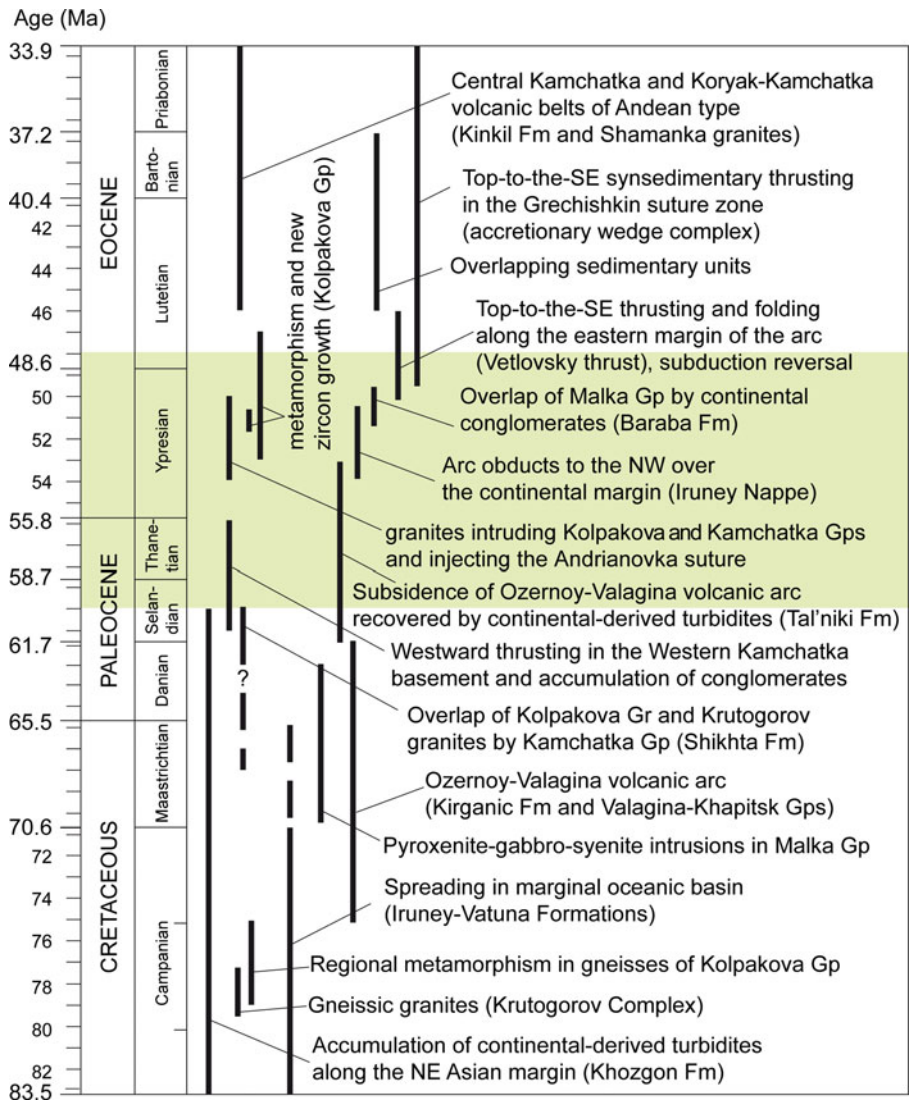

Fig. 9.7 Correlation of tectonic, metamorphic, magmatic and sedimentary events that occurred in the continental margin, fore-arc and arc areas before, during and after the Early Eocene, Kamchatka arc-continent collision. The *green* shading indicates the time of collision. See text for the age references for different events.

(Luchitskaya et al. 2008; Hourigan et al. 2009) and is coeval (Fig. 9.7) with the outer rims of zircon in the Kolpakova gneisses (77 ± 2 Ma) (Bindeman et al. 2002). The source rocks for the Krutogorov granites were both mafic metavolcanic and metasedimentary in nature, and were involved in heating at the base of accretionary wedge (Luchitskaya et al. 2008).

The biotite schist and plagiogneiss with garnet, staurolite, kyanite and sillimanite of the *Kamchatka Group* (Shikhta Formation) lie unconformably upon and overlap (Fig. 9.6) the rocks of the Kolpakova Group and Krutogorova Complex (Khanchuk 1985; Tararin 1988; Rikhter 1995). The protolith of the Kamchatka Group schists corresponds to shales with rare interlayers of polymict and arkosic sandstones (Rikhter 1993). A conglomerate containing pebbles and boulders of the underlying gneisses of the Kolpakova Group and granites of the Krutogorov Complex marks the angular unconformity at the base of the Kamchatka Group (Shul'diner et al. 1987; Rikhter 1995). PT estimates indicate temperatures of 550–650°C for the formation of the schists of Kamchatka Group (Hourigan et al. 2009). The U–Pb (SHRIMP) age of zircons from schists of the Kamchatka Group ranges from 2,048 Ma to 55.2 ± 3.3 Ma (Hourigan et al. 2009). The youngest of these grain ages is considered to be metamorphic in origin, whilst the next youngest population of zircons of inferred detrital origin is about 60 Ma (Fig. 9.7), implying a Paleocene stratigraphic age for the sedimentary protolith of the Kamchatka schists (Hourigan et al. 2009).

Metavolcanic and metasedimentary rocks of the Middle Jurassic–Neocomian *Kvakhona Complex* (Fig. 9.4) are thrust above the gneisses of the Sredinny massif along its western margin (Kuznetsov 1994). Tectonic slices of picrites, basalts (Alestar Formation) and serpentinite mélange occur at the base of the Kvakhona Nappe. The Kvakhona Complex rocks are unconformably overlain by Lower to Upper Cretaceous, quartz–feldspar turbidites (*Kikhchik Group* and *Khozgon Formation*) (Sidorchuk and Khanchuk 1981; Khanchuk 1985; Shul'diner et al. 1987). The Kvakhona Complex rocks are likely to represent the oceanic arc terrane that was incorporated in the metamorphic basement of Western Kamchatka at the end of the Early Cretaceous (Bondarenko 1992; Kuznetsov 1994).

The amphibolite- and greenschist-facies rocks of the *Malka Group* were thrust westwards over the metamorphic rocks of the Sredinny massif along its eastern margin (Figs. 9.4 and 9.5a). The tectonic contact between the metapelitic rocks of the Kamchatka Group and metavolcanites of the Andrianovka Formation (Fig. 9.6) is marked by lenses of ultramafic rocks in a meta-serpentinite matrix (Rikhter 1995) and has been described as the Andrianovka suture (Kirmasov et al. 2004).

Garnet amphibolites (*Andrianovka Formation*) form the lower part of the Malka Group (Fig. 9.6), and derive from island-arc volcanic rocks (Rikhter 1993). The PT estimates indicate 525–560°C and 0.64–0.68 GPa (Hourigan et al. 2009). Low-grade quartzites occurring in the Andrianovka Formation contain remnants of Santonian-Early Campanian radiolaria (Soloviev 2005). The Malka Group amphibolites were dated by the Rb–Sr whole-rock method to 48–50 Ma (Bondarenko 1992), which may represent the age of exhumation.

Chlorite phyllites and biotite–garnet schists of the *Kheivan Formation* structurally overlie the amphibolites of the Andrianovka Formation (Rikhter 1995; Kirmasov et al. 2004). U–Pb (SHRIMP) ages of zircons from the schists of the Kheivan Formation scatter from 106 to 2,650 Ma (Soloviev 2005; Hourigan et al. 2009). The peaks in the age distribution fall in the terminal Early Cretaceous and the Palaeoproterozoic. As the youngest dates mark the time of sedimentation, the age of the protolith was estimated as Early Cretaceous (Soloviev 2005; Hourigan et al. 2009). Albite–actinolite schists and quartzites formed from greenschist tuffs and cherts constitute the *Chimka Formation*, and conformably overlie the phyllites of the Kheivan Formation (Khanchuk 1985; Rikhter 1995).

The metamorphic rocks of the Malka Group have been suggested to represent amphibolites- and greenschist-facies rocks of the Ozernoy-Valagina arc units, based on the fact that Cretaceous radiolaria fossils were found in the metavolcanites of the Andrianovka Formation (Kirmasov et al. 2004; Soloviev 2005). If this interpretation is accepted, the boundary between the metamorphic rocks of the Sredinny massif and the units of the Ozernoy-Valagina arc could be placed at the base of the Malka Group between metapelitic schists of the Kamchatka Group and metavolcanites of the Andrianovka Formation, along the Andrianovka suture with its thin tectonic slices of serpentinite

(Fig. 9.6). Top-to-the-east, normal shear displacement has been recognised at deeper structural levels in the schists of the Kamchatka Group (Kirmasov et al. 2004). This deformation stage is considered to relate to post-collisional extension and exhumation of the high-grade core of the Sredinny massif (Kirmasov et al. 2004).

9.2.3.3 Early Eocene Granites in the Sredinny Metamorphic Massif

The Th–Pb (SHRIMP) ages of monazites (51.9 ± 0.7 Ma and 52.1 ± 0.6 Ma) and U–Pb (SHRIMP) ages of zircons (50.1 ± 1.7 to 54.9 ± 0.5 Ma) were obtained from equigranular granites in both the central and the northern part of the Sredinny metamorphic massif (Luchitskaya et al. 2008; Hourigan et al. 2009). These Early Eocene granites form plutons (2 km × 2 km up to 8 km × 12 km) which cut through schists of the Kamchatka Group and gneisses of the Kolpakova Group and contain xenoliths of the gneisses (Fig. 9.6). Synkinematic granite injected along the Andrianovka suture (Fig. 9.6) was dated by the U–Pb method (SHRIMP) to 51.5 ± 0.7 Ma (Soloviev 2005; Hourigan et al. 2009). The Early Eocene episode of granite formation (52 ± 2 Ma) in the Sredinny massif was coeval (Fig. 9.7) with a peak of metamorphism and anatexis in the Kolpakova gneisses which occurred either at 51.2 ± 0.5 Ma (Soloviev 2005; Hourigan et al. 2009) or at 47–53 Ma (Bindeman et al. 2002).

9.2.3.4 Sedimentary and Volcanic Cover of the Sredinny Metamorphic Massif

Continental conglomerates and sandstones of the *Baraba Formation* occur in the northern part of the Sredinny massif (Fig. 9.4). A thick sequence of conglomerates at the base of the Baraba Formation overlaps, above an angular unconformity, metamorphic rocks of the Malka Group (Fig. 9.6) (Shapiro et al. 1986; Soloviev et al. 2004). Clasts of chert similar to the rocks of the Iruney Formation and fragments of phyllite from the underlying Malka Croup occur at the base of the conglomerate succession. Granitic and higher-grade metamorphic clasts are found higher in the section (Shapiro et al. 1986; Soloviev et al. 2007; Shantser and Chelebaeva 2005). Fossil floral remnants found in the rocks the Baraba Formation have been described as Late Campanian (Shantser and Chelebaeva 2005). Zircons from a dacitic tuff at the bottom of the Baraba Formation have provided a U–Pb (SHRIMP) age of 50.5 ± 1.2 Ma (Soloviev et al. 2007; Hourigan et al. 2009), which corresponds to the Early Eocene (Fig. 9.7).

The conglomerates containing the Paleocene fossil flora overlie the Malka Group rocks not far from the Baraba Formation (Fig. 9.4), on the leftbank of the Oblukovina river and in the upper reaches of the Krutogorova River (Slyadnev et al. 1997).

Felsic and intermediate, continental, volcanic and subvolcanic rocks of the *Cherepanova Formation* occur locally along the western margin of the Sredinny massif (Fig. 9.4) (Slyadnev et al. 1997). A K–Ar radiological age for these volcanites was determined at 59–65 Ma (Paleocene), and for the subvolcanic bodies at 55 Ma (Slyadnev et al. 1997). The basalts and dacites of the continental-type bimodal series occur in the vicinity of Chernaya Mt. at the western margin of the Sredinny massif (Shantser and Fedorov 1997). Fragments of fossil flora from the tuffs of the upper part of the Chernaya Mt. series are of the Mid Eocene age (Chelebaeva and Brattseva 1986).

9.2.4 Ozernoy-Valagina Arc

9.2.4.1 Lithotectonic Units

Lithotectonic units of the arc are exposed in the Eastern Ranges (e.g. *Valagina* and *Khapitsk groups*) and on the eastern slopes of the Sredinny Range of Kamchatka (*Iruney* and *Kirganik formations*) (Figs. 9.3 and 9.4). The arc units consist mostly of basalts and andesites, whereas picrites and dacites are less abundant. Massif lavas and pillow lavas are associated with agglomeratic breccia and conglomerates, coarse-grained and psammitic tuffs, volcaniclastic sandstones, siltstones, siliceous shales, hyaloclastites, cherts and jaspers. The volcanic rock sequences are preserved in tectonic slices of 1–2 km thickness or less. The cherts and mudstones from the volcanic and volcaniclastic units are dated by radiolarian remnants as Campanian-Danian (Fig. 9.7) in the Eastern Ranges and as Maastrichtian-Danian (Kirganik Formation) in

the Sredinny Range (Konstantinovskaya et al. 1993; Zinkevich et al. 1994).

A differentiated tholeiite, boninite, calc-alkaline and alkaline, mafic and ultramafic volcanic series of intra-oceanic arc type has been recognised in the volcanic rocks of the Ozernoy-Valagina arc (Konstantinovskaya 1992; Magakyan et al. 1993; Kamenetsky et al. 1993, 1995). The rocks are characterised by a rare earth element (REE) distribution typical for island arcs (Fig. 9.8), by a strong high field strength element (HFSE) depletion in comparison with REE, and by a high enrichment in large-ion lithophile

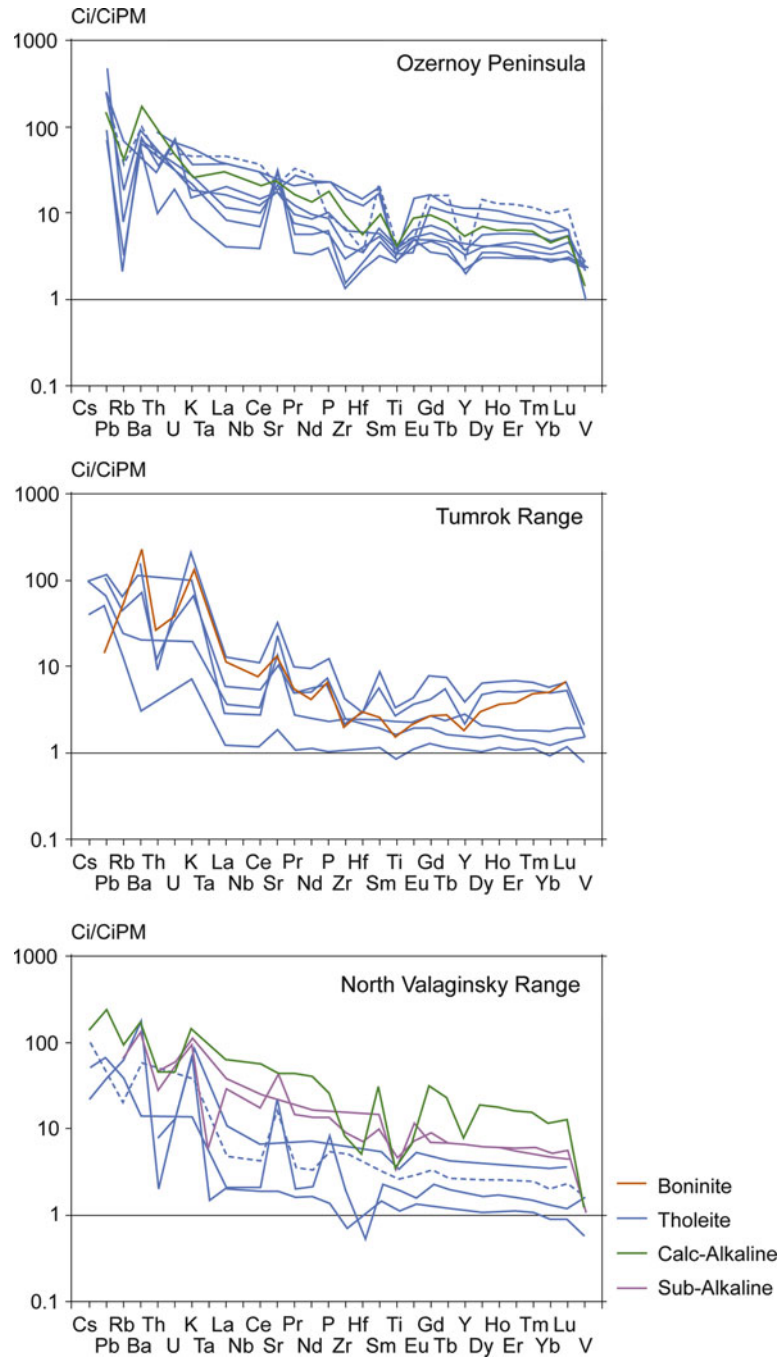

Fig. 9.8 Geochemical composition of volcanic (*solid lines*) and plutonic (*dashed lines*) rocks from the Ozernoy-Valagina arc, Eastern Ranges of Kamchatka, modified after Magakyan et al. (1993). The element contents are normalised to primitive mantle compositions, after Sun and McDonough (1989).

elements (LILE), P, K and H_2O (Magakyan et al. 1993; Kamenetsky et al. 1995). Depleted concentrations of REE, P, Ta, Th, Zr, Hf, Ti and Y, and high Mg and Cr contents in picrites and basalts (Magakyan et al. 1993), as well as on exceptionally primitive composition of the phenocrysts and their magmatic inclusions (Kamenetsky et al. 1995), provide direct evidence of a mantle origin for the primary melts, which were highly magnesian. Enrichment of LILE (Ca, Ba, Pb, K, Sr) in the volcanic rocks could be a result of a subduction-related fluid influx. The primary melts were produced under high-pressure (30–50 kbar) and high-temperature (1,500–1,700°C) conditions by partial melting of a refractory peridotitic mantle (Kamenetsky et al. 1995).

The contrasting depletion in HFSE and enrichment in LILE in the volcanic rocks varies along the strike of the Ozernoy-Valagina arc, being most marked in the arc series of the southern Kamchatka in comparison with northern Kamchatka (Fig. 9.8). These variations could be a result of a heterogeneous mantle source and subducting plate component along the strike of the arc.

9.2.4.2 Plutonic Facies

The multiphase dunite–clinopyroxenite, clinopyroxene–gabbro and syenite subalkaline intrusions are localised along the eastern slopes of the Sredinny Range (Fig. 9.4) both in volcanic rocks of the Iruney and Kirganik formations and in the amphibolites of the Andrianovka Formation (Malka Group) (Flerov and Koloskov 1976; Flerov et al. 2001). The rocks of the intrusions are characterised by low HFSE contents, low Sr and Nd isotope ratios and high LILE contents relative to MORB that most likely indicate a depleted magma source combined with ingress of mantle fluids (Flerov et al. 2001). The multiphase massifs are interpreted as fragments of conduits of Upper Cretaceous island-arc complexes (Flerov et al. 2001). The Left Andrianovka zoned massif, which is restricted to the Andrianovka Formation (Malka Group) on the eastern slope of the Sredinny Range, is composed of a dunite-clinopyroxenite core with gabbro along the margins and is cut by subordinate syenite intrusions (Hourigan et al. 2009). Zones of mylonitisation within the syenite indicate that the Left Andrianovka massif was emplaced (Fig. 9.6) prior to deformation and metamorphism of amphibolites of the Andrianovka Formation at the base of the Iruney Nappe (Kirmasov et al. 2004; Hourigan et al. 2009).

K–Ar dating of biotite from the multiphase massifs of the Sredinny Range gave ages of 52 ± 3, 55 ± 3, and 53 ± 1 Ma, and a K–Ar whole-rock age of 56 ± 4 Ma (Shantser and Gladenkov 1997). Flerov and Koloskov (1976) reported a 48 ± 2 Ma biotite K–Ar age from a biotite pyroxenite of the Left Andrianovka Massif. U–Pb (SHRIMP) zircon dating of a syenite from this massif (Hourigan et al. 2004) yielded crystallisation ages of 63.0 ± 0.6 and 70.4 ± 0.7 Ma, Maasrichtian–Danian (Fig. 9.7), which is consistent with an origin for the multiphase intrusions as magma conduits at the base of the Ozernoy-Valagina arc.

The amphibolites of the Ganal metamorphic massif and the Yurchik gabbro pluton are exposed in the Ganalsky Range, immediately to the south-southeast of the Sredinny massif (Fig. 9.4). The amphibolites of the Ganal massif represent metamorphosed tholeiitic basalts and greywackes (German 1978; Rikhter 1991). U–Pb SHRIMP zircon ages obtained from amphibolites (zircon cores, 66 ± 2 Ma) and from the Yurchik gabbro pluton (71 ± 4.3 Ma) in the Ganal metamorphic massif (Bindeman et al. 2002) are similar to ages from the Left Andrianovka massif (Hourigan et al. 2009). The absence of zircons older than Late Cretaceous, and the absence of any inherited cores in the Ganal amphibolites, may indicate either that the mafic protolith did not contain older zircons or that no older zircon cores have survived the 66 Ma metamorphism (Bindeman et al. 2002). The rather primitive whole-rock values of $^{87}Sr/^{86}Sr = 0.703$ and ε_{Nd} from −3 to +9.5 (Vinogradov et al. 1991) are consistent with metamorphism of young oceanic crust with marine sediments. The Ganal massif is interpreted as the lower crust of an intra-oceanic (Ozernoy-Valagina) island arc that experienced a 66 Ma, high-grade metamorphism and emplacement of the Yurchik gabbro (Bindeman et al. 2002), the 71 ± 4 Ma crystallisation age of which is consistent with its synmetamorphic origin (German 1978).

Alaskan-type, platinum-bearing plutons and potassium-enriched, mafic to ultramafic volcanic rocks are temporally and spatially associated with the volcanic units in the northern (Olutorsky) segment of the Achaivayam-Valagina arc (Astrakhantsev et al. 1987, 1991; Batanova and Astrakhantsev 1992). The compositions of the principal mineral phases in the Galmoenan intrusive rocks are typical of primitive

island-arc magmas in intra-oceanic settings (Batanova et al. 2005), and closely resemble the mineral compositions of the Ozernoy-Valagina ultramafic volcanic rocks (Kamenetsky et al. 1995). The temporal and spatial association of intrusive and extrusive arc units, and the similarity of their mineral compositions, suggest that both suites were formed from similar parental magmas. Fluxing of a highly refractory mantle wedge (similar to the accepted source of boninites) by chlorine-rich aqueous fluids was likely responsible for the both high degree of partial melting and the geochemical characteristics of the magmas, including their enrichment in platinum-group elements (Batanova et al. 2005).

9.2.4.3 Lateral Facies

The Ozernoy-Valagina arc units are replaced laterally by the Iruney marginal sea facies represented by the Iruney and the Khozgon formations (Fig. 9.6) that are squeezed up between the arc and the Sredinny metamorphic massif (Fig. 9.5a) (Konstantinovskaya 1997, 2000, 2001).

The *Iruney Formation* consists of a proximal, volcaniclastic-cherty facies and a distal, deep-water, cherty-mudstone facies (Konstantinovskaya 1992, 1997). Massive tuff and pillow lava flows of tholeiitic and calc-alkaline basalt occur locally in the proximal facies. The proximal-facies, fine-grained turbidites of the Iruney Formation have similar REE signatures to the basalts and andesites of the Kirganik Formation, whilst the distal-facies mudstones are similar in their REE contents to recent, deep-water, pelagic sediments (Konstantinovskaya 1997).The distal cherts are characterised by a well-pronounced negative Ce anomaly in the PAAS-normalised REE patterns that is characteristic for sedimentary environments of deep-water (>2 km depth) oceans (Konstantinovskaya 1997). The Iruney Formation is dated (Fig. 9.7) as Santonian-Campanian by remnants of an Inoceramus fauna, and as Campanian-Maastrichtian by radiolaria (Konstantinovskaya 1992, 1997; Zinkevich et al. 1994).

The Campanian-Paleocene *Khozgon Formation* is composed of quartz-feldspar turbidites, rarely with layers of cherts, and MORB-type basalts (Fedorov 1986; Zinkevich et al. 1994). The U–Pb (SHRIMP) age of the youngest detrital zircons from the Khozgon Formation is 59.2 ± 3.0 Ma (Hourigan et al. 2009), which corresponds to the Paleocene (Fig. 9.6).

9.2.4.4 Sedimentary Cover

Quartz–feldspar turbidites containing Late Paleocene–Early Eocene planktonic foraminifera (*Tal'niki Formation*) conformably overlie the volcanic units of the Ozernoy-Valagina arc in the South Valaginsky Range (Konstantinovskaya et al. 1993; Bakhteev et al. 1994). The stratigraphic transition from coarse-grained volcaniclastic rocks to thin-bedded, fine-grained, quartz–feldspar turbidites is sharp; several olistostrome conglomerates with felsic volcanic clasts are observed within the first few tens of metres in the turbidites (Fig. 9.9).

The sandstones from the Upper Paleocene–Lower Eocene turbidites of southern Kamchatka contain up to 20–35% quartz, 20–35% feldspar fragments and 35–50% rock fragments (Shapiro et al. 1992) that correspond to quartz–feldspathic and feldspar–quartzose graywackes. The rock fragments include both volcanic and sedimentary rocks. Less common are fragments of metamorphic rocks, such as quartz–mica schist and micaceous quartzite. The high concentration of metamorphic-group minerals, notably garnet, and the low content of the pyroxene-group minerals are characteristic for the heavy fraction of the turbidite sandstones (Shapiro et al. 1992).

The Upper Paleocene–Lower Eocene, quartz-feldspar turbidites of southern Kamchatka are characterised by a higher content of metamorphic clastics in the heavy fraction in comparison with the Upper Cretaceous–Middle Eocene, quartz-feldspar turbidites in northern Kamchatka (Shapiro et al. 1992). This may reflect the presence of a metamorphic clastic source, most likely the Sredinny massif that contributed detritus to the quartz-feldspar turbidites in the arc area of southern Kamchatka during the Late Paleocene–Early Eocene.

The transition from the volcaniclastic units of the Ozernoy-Valagina arc to the quartz–feldspar turbidites Tal'niki Formation may be associated with abrupt termination of volcanic activity in the arc and its rapid subsidence with change in the detrital source from volcanic one to metamorphic one.

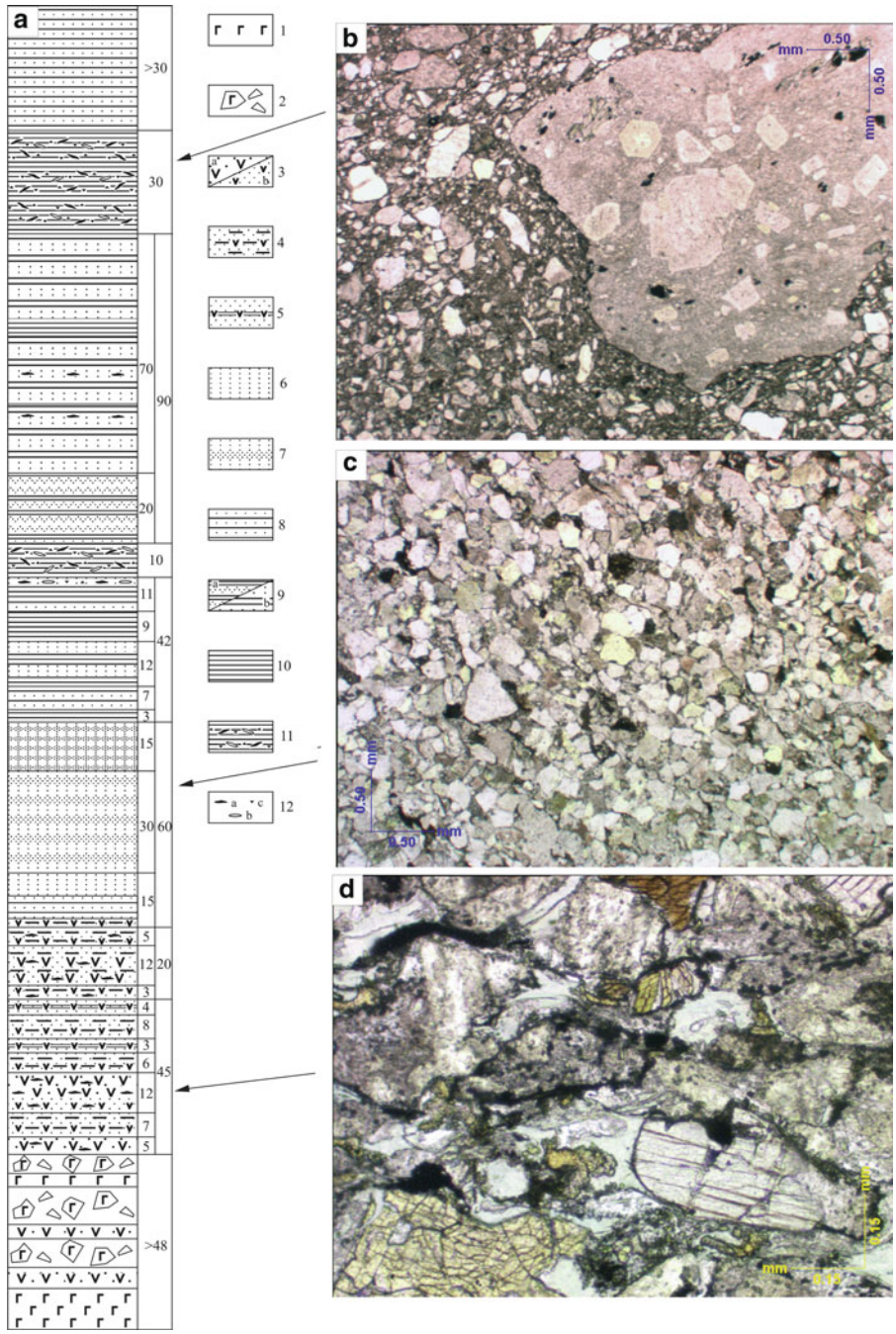

Fig. 9.9 (**a**) Stratigraphic succession of the transition zone from the Ozernoy-Valagina arc rocks (Valagina Group) to its quartz-feldspar (Q-Fsp) sedimentary cover (Tal'niki Formation), South Valaginsky Range, modified after Konstantinovskaya (2003). (1) basalt, (2) basalt agglomerate, (3) basalt tuff, (4–5) volcaniclastic sandstone and cherty siltstone, massive (6) and layered (7) Q-Fsp sandstone, (8–10) Q-Fsp fine- and medium-grained sandstone and siltstone, (11) olistostromal layer with fragments of shale (12a), tuff (12b) and carbonate nodules (12c); (**b–d**) photomicrographs of thin-sections of volcaniclastic coarse sandstone (b), Q-Fsp fine-grained sandstone (c), olistostromal layer with felsic volcanic fragments (d). Arrows show the stratigraphic locations of the thin-sections.

9.2.4.5 Tectonic Structure

The axial part of the Ozernoy-Valagina arc is exposed in the North Valaginsky Range and the Ozernoy Peninsula (Fig. 9.1). In the North Valaginsky Range, the arc units occur in gently dipping, NW-vergent tectonic nappes folded in a large open antiform (Fig. 9.10). Steep, SE-vergent reverse faults also deform the nappes (Fig. 9.10) and represent a second phase of deformation in the Ozernoy-Valagina arc (Zinkevich et al. 1990).

Tectonic slices of serpentinite mélange (Fig. 9.3) emplaced between the nappes of volcanic rocks in Eastern Kamchatka (North Valaginsky and North Kumroch Ranges, Ozernoy Peninsula, and Karaginsky Island). Blocks of ophiolitic peridotite, gabbro, amphibolite, diabase, basalt and jasper varying in size from a few metres to over a kilometre in diameter are present in serpentinite mélange. Clasts of pyroxenite, gabbro, plagiogranite, and the Jurassic-Lower Cretaceous cherts were recognised in the Middle-Upper Maastrichtian cherty breccias dated by radiolaria remnants (Konstantinovskaya 1989). Clasts of pyroxenites and plagiogranites were found also in the agglomeratic breccias (Konstantinovskaya 1989). The ophiolitic rocks associated with the Ozernoy-Valagina

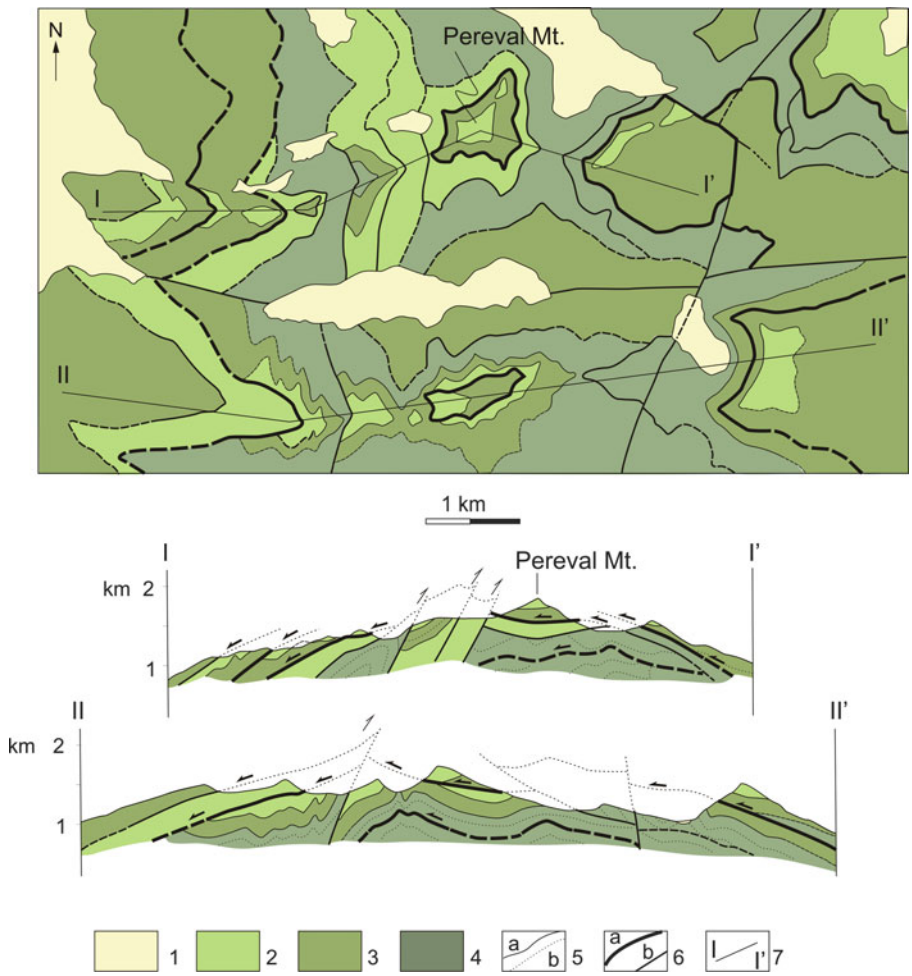

Fig. 9.10 Detailed geological map and cross-sections of the Mt Pereval area, North Valaginsky Range, after Konstantinovskaya (2003). (1) Quaternary deposits; (2–4) Campanian-Danian rocks of the Ozernoy-Valagina arc: (2) upper unit of coarse volcaniclastic rocks, (3) middle unit of cherty-volcaniclastic rocks, (4) low unit of cherty-mudstone rocks; (5) stratigraphic contact (a) and marker layer (b), (6) low-angle NW vergent thrusts (a) and later high-angle faults with SE vergence, (7) location of cross-sections. See Fig. 9.4 for the map location.

arc are considered to represent the oceanic basement of an arc that was remobilised along fairly flat-lying detachments and squeezed in the form of a serpentinite tectonic mélange along the nappe contacts during the arc emplacement.

The western border of the Ozernoy-Valagina arc is exposed on the eastern slopes of the Sredinny Range in southern Kamchatka (Fig. 9.4). The Maastrichtian-Danian volcanic arc units of the Kirganik Formation are thrust above the Santonian-Maasrtichtian volcaniclastic sandstones, siltstones and cherts of the Iruney Formation (Fig. 9.3, profile 5). The volcanic and cherty-volcaniclastic units are folded in NW-vergent moderately inclined folds and affected by NW-vergent thrusts. The structurally lower nappes are composed mostly of pelagic cherts, jaspers, shales and, less commonly, basalt flows (Konstantinovskaya 1997). The rocks are characterised by vertical or steeply overturned dips and affected by a penetrative cleavage. Thin tectonic slices of Campanian-Paleocene, quartz-feldspar turbidites of the Khozgon Formation are recognised beneath the frontal thrusts of the Iruney pelagic cherts (Fedorov 1986; Zinkevich et al. 1994).

The rocks of the Ozernoy-Valagina arc and Iruney marginal sea (Kirganik, Iruney and Khozgon formations) are folded and thrust to the NW over the metamorphic rocks of the Malka Group of the Sredinny massif and the conglomerates of the Baraba Formation (Figs. 9.4 and 9.5a). The base of the Iruney Nappe in the northeastern part of the Sredinny massif is a NW-vergent, low-angle fault. To the south of the Oblukovina transfer fault (Fig. 9.4), a steep fault zone (Fig. 9.5a) separates non-metamorphic rocks of the Iruney and Khozgon formations from metavolcanic rocks of the Andrianovka Formation (Rikhter 1995; Zinkevich et al. 1994; Konstantinovskaya 2002). To the west of the fault, the Andrianovka Formation consists of greenschists that pass westwards into amphibolites with a steep, east-dipping foliation (Rikhter 1995).

The terrigenous rocks containing Mid Eocene fossil remnants overlap deformed volcanic and volcaniclastic rocks of the Maastrichtian-Danian, Kirkanik Formation (Shantser and Gladenkov 1997), indicating that the westward thrusting of the Ozernoy-Valagina arc units most likely occurred between the Late Paleocene and the end of the Early Eocene.

The eastern border of the Ozernoy-Valagina arc in southern Kamchatka crops out in the South Valaginsky Range (Fig. 9.4). A tectonic slice of serpentinite mélange with blocks of ultramafic rocks and gabbros emplaced onto the volcanic arc rocks constitutes of the uppermost structural allochthon (Fig. 9.3, profile 4). Campanian-Danian arc units (*Valagina Group*) and conformably overlying, Upper Paleocene-Lower Eocene, quartz-feldspar turbidites (*Tal'niki Formation*) are folded in inclined and overturned SE-vergent folds and thrust to the southeast above the strongly folded and faulted, quartz-feldspar turbidites (*Vakhvina Group*) which are similar in age to the Tal'niki Formation (Bakhteev et al. 1994). Isoclinal folds and SE-vergent, imbricated thrusts characterise the rocks of the Vakhvina Group.

Quartz-feldspar turbidites of the Vakhvina Group are emplaced to the southeast above Paleocene–Lower Eocene rocks of the Vetlovsky Complex along the Vetlovsky thrust (Figs. 9.3, profile 4 and 9.5a). Tectonic mélange occurs along the Vetlovsky thrust fault (Zinkevich et al. 1993). Ultramafic rocks, gabbro and sedimentary rocks from the overlying units constitute the blocks floating in the serpentinite matrix of the mélange.

The *Vetlovsky Complex* rocks are strongly disrupted by SE-vergent, imbricate thrusts. Volcaniclastic sandstones, siltstones and cherty siltstones with fine-grained tuff interlayers constitute the major part of the Complex with less common tectonic lenses of basalt, chert, jasper, micritic limestone, and Fe-bearing shale (Zinkevich et al. 1993; Konstantinovskaya et al. 1993; Bakhteev et al. 1994). Early and Late Paleocene and Early Eocene, planktonic foraminifera fossils (Fig. 9.2) have been determined from the rocks of the Vetlovsky Complex (Bakhteev et al. 1994). Late Paleocene foraminifera fossils from the micritic limestones were found to be typical for the tropical areas of an open, pelagic, oceanic depositional setting (Bakhteev et al. 1994). Pillow lavas of basalt, diabase, mafic tuffs and agglomerates (*Diabase Complex*) compose the structurally lower tectonic sheet in front of the Vetlovsky Complex (Fig. 9.3, profile 4). The mafic volcanic rocks of the Diabase Complex are characterised by a typical tholeiitic MORB geochemical composition (Zinkevich et al. 1993). The ophiolitic fragments from the Vetlovsky and Diabase Complexes most likely represent the Early Paleocene-Early Eocene oceanic crust that accreted to the eastern margin of the Ozernoy-Valagina arc.

The Middle Eocene mudstone–sandstone succession (Fig. 9.2) overlaps with an angular unconformity the SE-vergent, fold-and-thrust structure and the tectonic mélange along the Vetlovsky thrust in the South Valaginsky Range (Bakhteev et al. 1994). The basal conglomerates of the succession contain Mid Eocene mollusc fossils. Southeastward displacement along the Vetlovsky thrust at the eastern border of the Ozernoy-Valagina arc in southern Kamchatka is limited to the late Early Eocene (Fig. 9.2), because of the fact that Upper Paleocene-Lower Eocene rocks are involved in the thrusting and the neoautochthon is Middle Eocene in age (Konstantinovskaya 2002, 2003).

The contact between the Paleocene–Lower Eocene, Vetlovsky oceanic units and the Middle Eocene–Upper Miocene units of the Tushevsky depression extends northeastwards for about 300 km (Fig. 9.3) and represents a system of steep, NW-dipping, synsedimentary thrusts known as the Grechishkin collisional suture (Bakhteev et al. 1997). Exotic Miocene pelagic cherts form tectonic slices (Fig. 9.2) within the turbidite deposits of the Tushevsky depression, limiting the accretion of the Kronotsky arc to the end of the Miocene (Bakhteev et al. 1997). The structure bounded by the Vetlovsky thrust and the Grechishkin suture most likely represents an accretionary wedge developed between the Mid Eocene and the Late Miocene at the eastern side of the accreted Ozernoy-Valagina arc, in front of the coeval Central Kamchatka volcanic belt (Figs. 9.2 and 9.3).

The discussed above geological data reveal several deformation and/or metamorphic events (Fig. 9.7) occurred within the continental margin, fore-arc and arc area during the Early Eocene arc–continent collision in South Kamchatka that need to find an explanation from tectonic processes operating at crustal and lithospheric scales. For example, what could be the tectonic process responsible for the peak of metamorphism and anatexis occurred in the continental margin (Sredinny massif) during the arc–continent collision? How could we explain the termination of volcanic activity and rapid subsidence of the Ozernoy-Valagina arc at the early stages of the collision before any deformation occurred in the arc area? What could produce the complete destruction of the forearc basin existed between the arc and the margin (Sredinny massif) in South Kamchatka? What could be the reason of the subsequent of thrusting to the northwest (Iruney Nappe) and to the southeast (Vetlovsky thrust) occurred respectively at the both sides of the arc during the Early Eocene? The physical modeling results presented below help to address these questions.

9.3 Modelling Results

The 2D analogue modelling performed for the Taiwan arc–continent collision (Chemenda et al. 2001) is also relevant for the Early Eocene, arc–continent collision on Kamchatka (Konstantinovskaya 2002, 2003). The model (Fig. 9.11) consists two converging parts, the continental part (the Asian margin) and the oceanic part (the Vetlovsky plate). The oceanic lithosphere is composed of one layer thinned (weakened) in the

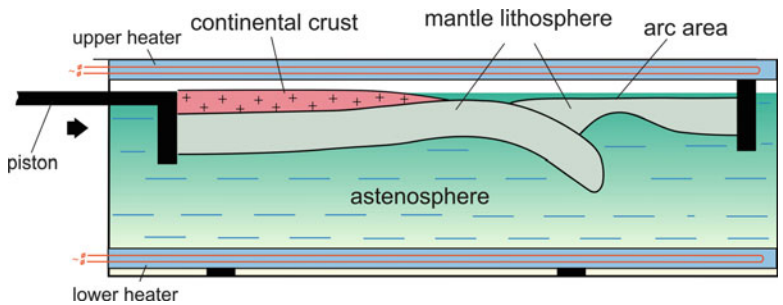

Fig. 9.11 Scheme of 2D modelling, modified after Chemenda et al. (2001). The model consists two converging parts, the continental part (the Asian margin) and the oceanic part (the Vetlovsky plate). The oceanic lithosphere is composed of one layer. The continental lithosphere has two layers: the mantle (made of the same material as the oceanic lithosphere) and the crust. The lithosphere is underlain by a low-viscosity astenosphere, which in the experiments is distilled water. Convergence is driven by a piston moving at a constant rate.

arc (Ozernoy-Valagina) area. The continental lithosphere has two layers: the mantle (made of the same material as the oceanic lithosphere) and the crust. The lithosphere is underlain by a low-viscosity asthenosphere, which in the experiments is distilled water. Convergence is driven by a piston moving at a constant rate. More details on model settings and material properties for the 3 experiments described below may be consulted in Chemenda et al. (2001).

In *experiment 1* (Fig. 9.12), the material that was used for the continental crust corresponded to a low-strength thinned continental margin. As the margin began to subduct (Fig. 9.12a–c), tectonic delamination of continental crust occurred along the low-angle

Fig. 9.12 Photos of stages of deformation of the model in cross-sections in Experiment 1, modified after Chemenda et al. (2001).

thrust fault directed toward the continent. The crustal slice was detached from its mantle base and accreted to the frontal part of the overriding plate. The structure of the margin was thickened due to the crustal slice delamination.

Advance of the thickened continental margin into the subduction zone slowed down or temporarily ceased, whilst shortening stress strongly increased in the overriding plate. Deformation was localised in the weakest part of the overriding plate, i.e., in the arc area (Fig. 9.12d), where the plate subsequently failed (Fig. 9.12e). In this experiment, the fore-arc lithosphere block underthrust the arc area that had experienced fast uncompensated subsidence. The frontal part of the fore-arc block with its accreted crustal slice underwent rapid uplift (Fig. 9.12d–e).

When the fore-arc block had completely subducted beneath the arc area (Fig. 9.12f–g), the advance of the continental margin accelerated to accommodate the plate convergence. The arc was thus obducted over the continental margin. Further crustal delamination and thrusting occurred in the structure of the continental margin. Slices of continental crust were detached from its base and accreted in front of the obducted arc (Fig. 9.12g) to form the crustal-scale accretionary prism at the end of the experiment (Fig. 9.13a).

In *experiment 2*, the initial settings were similar to those in experiment 1, but erosion was applied to the area of uplift in the frontal part of the fore-arc block, to which a slice of continental crust was accreted (Fig. 9.13b). The erosional unload caused the previously subducted crustal slice to squeeze up on account of the high horizontal compression and the buoyancy force. A normal fault displacement occurred between the rising crustal slice and the subducting fore-arc block (Fig. 9.13b). The eroded material from the exhumed slice of continental crust filled both the fore-arc and the foreland basins.

In *experiment 3* (Fig. 9.14), the strength of the subducting crust was set at about two times greater than in the previous experiments. This experiment was prepared to study deformation in the lithosphere after the stage of subduction reversal. The overriding plate was pre-cut as shown in Fig. 9.14a. The underthrusting of the oceanic plate beneath the arc started simultaneously with the subduction of the continental margin (Fig. 9.14b–c). The advance of the continental margin plate in the subduction zone continued until it met the

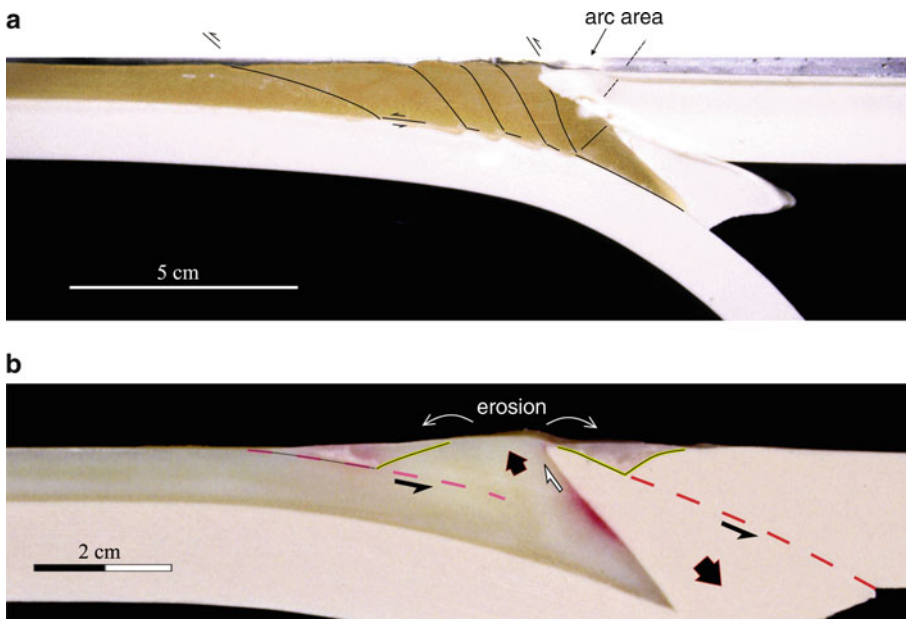

Fig. 9.13 Photos of the last stage of model deformation in Experiment 1 without erosion (**a**) and in Experiment 2 with erosion (**b**), modified after Chemenda et al. (2001). The conditions are the same in both experiments, but in experiment 2 the upper part of the crustal slice has been eroded after failure and crustal thickening in the margin. The eroded material is deposited on both sides of the growing relief.

Fig. 9.14 Photos of stages of the model deformation in cross-sections in Experiment 3, modified after Chemenda et al. (2001). The material used for the crust is two times stronger than in Experiments 1 and 2. Before the experiment started, the overriding plate was cut as shown in (**a**).

oceanic plate at depth (Fig. 9.14d). The oceanic plate then caused the subducted lithosphere of the continental margin plate to rupture (Fig. 9.14e), and the new oceanic subduction became stable whilst the advance of the continental margin stopped (Fig. 9.14f).

The presented above experimental data contribute to our understanding of the tectonic processes that could have occurred at the crustal and lithospheric scale during the Early Eocene arc–continent collision in Kamchatka. Crustal thickening by thrust faulting along the margin and erosion-induced syncollisional exhumation a crustal slice detached from the mantle base, subsidence of the arc and subduction of the fore-arc lithosphere block and subduction reversal are proved to be the possible features of arc–continent collision discussed in the physical models. The correlation between geological and modeling data is summarised in the geodynamic model of the collision in Kamchatka in the next section.

9.4 Evolutionary Geodynamic Model of the Collision in Kamchatka

2D and 3D reconstructions of the paleogeodynamic settings that existed in the NW Pacific region during Paleocene – Early Eocene time have been proposed on the basis of geological and paleomagnetic data (Konstantinovskaya 2001; Shapiro et al. 2008; Hourigan et al. 2009).

According to the paleomagnetic data, the Ozernoy–Valagina arc formed in the Pacific Ocean at about 48°N, to the southeast of its present position, and

approached the Asian margin in the late Early Paleocene (Pechersky et al. 1997; Shapiro et al. 1997; Kovalenko 2000; Levashova et al. 2000). At this time, the SE-facing frontal part of the Asian continental margin was located along Western Kamchatka and incorporated in the Sea of Okhotsk microplate (Konstantinovskaya 2000, 2001). The continental margin in the Sea of Okhotsk microplate was uplifted above the sea level and there was no sedimentation in the Early Paleocene in this area. The basement of Western Kamchatka (Sredinny massif) included Cretaceous continental blocks (Kolpakova Group and Krutogorov Complex, see Discussion) and accreted fragments of the Middle Jurassic–Neocomian, Kvakhona arc terrane (Fig. 9.15a). The heterogeneous structure of the margin could be responsible for the relatively weak strength of the crust within it. The quartz-feldspar turbidite series accumulated at the base of slopes and along of the continental margin (Kamchatka Group and Khozgon Formation), and the deep-water cherts, jaspers and shales (Iruney Formation) were deposited in the Iruney marginal sea that separated the Ozernoy-Valagina arc and the Asian margin (Konstantinovskaya 1997, 2001).

As the weak continental margin entered the subduction zone (Fig. 9.15b), long-lasting, syn-sedimentary, west-vergent thrusts started to develop in the basement of Western Kamchatka in the Late Paleocene at the beginning of the collision. Crustal blocks were uplifted and eroded, and coarse clastic conglomerates accumulated in the lower slopes of the basement highs. The uplifted blocks of the Sredinny

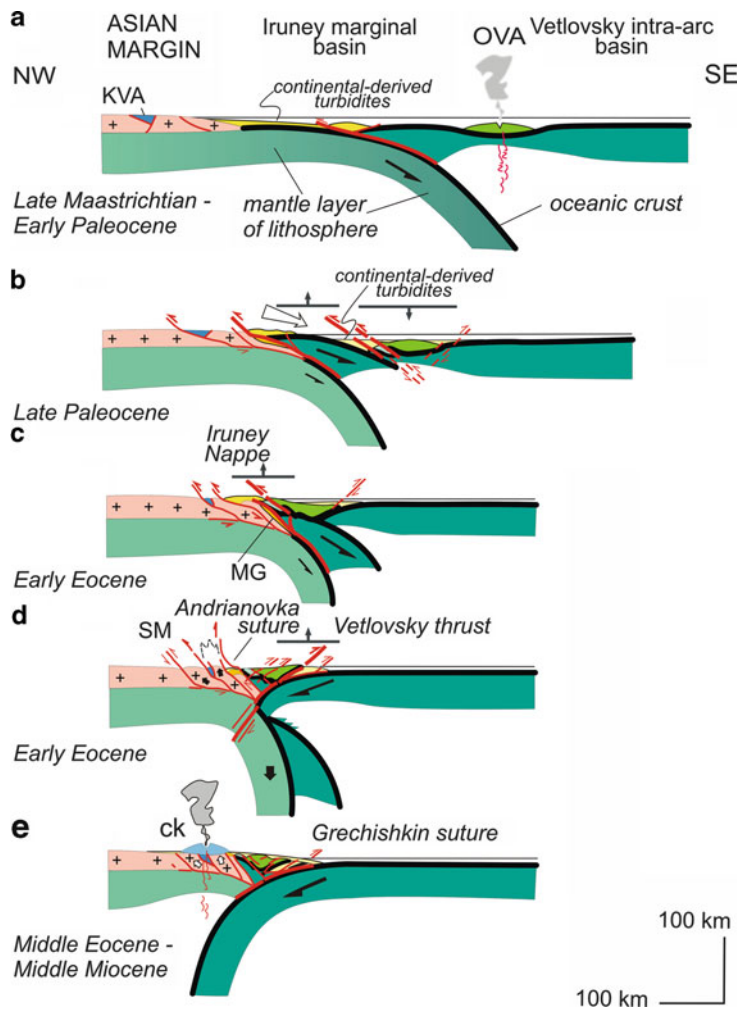

Fig. 9.15 Geodynamic model of the collision between the Ozernoy-Valagina arc and the Asian continental margin (Western Kamchatka), modified after Konstantinovskaya (2002). The subsequent collisional stages include: (**b**) continental margin faulting and thickening; (**c**) a metamorphic event in the margin, fore-arc block subduction and arc obduction; (**d**) erosion and exhumation in the margin and subduction reversal. Abbreviations: (SM) Sredinny massif, (MG) Malka Group, (OVA) Ozernoy-Valagina arc, (KVA) Kvakhona Arc, (ck) Central Kamchatka volcanic belt.

massif and Sobolev salient controlled the sedimentation in the Kolpakova depression from the Late Paleocene until the Oligocene (Bobylev and Bakun 1992; Bakun et al. 1994). The westward thrusting and thickening that occurred in the margin could have been initiated by the delamination of crustal slices from their mantle base and accretion in front of the overriding plate (Fig. 9.15b–c). Thickening in the margin most likely led to heating, and to the migmatisation and granite injection that occurred in the margin in the Early Eocene (52 ± 2 Ma) during the arc–continent collision (Fig. 9.15c), as is supported by the U–Pb SHRIMP dating of zircons from gneisses of the Kolpakova Group and from granites in the Sredinny massif (Luchitskaya et al. 2008; Hourigan et al. 2009).

Erosion of the squeezed up blocks of continental crust resulted in exhumation of Cretaceous metamorphic rocks in the Sredinny massif (Fig. 9.15d). The eroded material was deposited both in the Kolpakova depression and in the arc area. The 48 Ma Rb-Sr age from the schist of the Andrianovka Formation indicates that cooling from peak (amphibolite-facies) metamorphic conditions to below about 300°C was rapid (Hourigan et al. 2009). The normal faults recognised in the Andrianovka suture along the eastern margin of the Sredinny massif (Kirmasov et al. 2004) are considered to have controlled the exhumation of the metamorphic units.

Volcanism in the Ozernoy–Valagina arc ceased in the Mid Paleocene (about 60 Ma), the arc structures rapidly subsided, and the continental-derived, quartz-feldspar turbidites (Tal'niki Formation) started to accumulate in the arc area (Fig. 9.15b). This may have been resulted from the subduction of a cold, fore-arc, lithosphere block beneath the arc. The accretionary prism experienced uplift as a part of the fore-arc block during the underthrusting of the continental margin and the arc underwent subsidence (Fig. 9.15b). Deposition of the chaotic units at the lower stratigraphic level of the turbidite succession occurred under the unstable conditions of the arc subsidence. The accumulation of Upper Paleocene-Lower Eocene deposits of the Tal'niki Formation could have resulted from the erosion of the Upper Cretaceous-Lower Paleocene, quartz-feldspar turbidites of the Khozgon Formation that formed the NW-facing accretionary prism in front of the Ozernoy-Valagina arc. The supply of metamorphic-group minerals present in the heavy fraction of sandstones of the Tal'niki Formation may have resulted from the erosion of the Sredinny massif.

After the closure of the forearc basin, the Ozernoy–Valagina arc was thrust above the continental margin in the Early Eocene to form the Iruney Nappe (Fig. 9.15c). The metamorphic rocks of the Malka Group may have represented a tectonic slice of the arc (or of an older fore-arc) basement involved in the underthrusting during the northwestward emplacement of the Iruney Nappe.

In the late Early Eocene, the units of the Ozernoy–Valagina arc and the overlapping quartz-feldspar turbidites of the Tal'niki Formation were simultaneously folded and thrust to the southeast along the Vetlovsky thrust fault on the eastern side of the arc (Fig. 9.15d). The south-eastward thrusting was most likely a result of the subduction reversal and northwestward underthrusting of the Vetlovsky oceanic plate under the Ozernoy–Valagina arc along its eastern side (Fig. 9.15d). The SE-facing accretionary prism (Vetlovsky Complex) with its enclosed tectonic lenses of Paleocene–Early Eocene rocks of oceanic crust then developed due to further subduction of the Vetlovsky plate at the back of the arc (Fig. 9.15d). The complete accretion of the Ozernoy-Valagina arc to the margin and the end of the Early Eocene arc-continent collision in South Kamchatka may be dated by the Middle Eocene mudstone–sandstone succession that overlaps with a structural disconformity the SE-vergent Vetlovsky thrust in the South Valaginsky Range (Bakhteev et al. 1994).

The continuing NW-dipping subduction of the Vetlovsky oceanic plate under the accreted Ozernoy–Valagina arc could have resulted in its collision with the SE-dipping continental margin plate that had earlier been subducted beneath the arc (Fig. 9.15d). The Vetlovsky plate most likely cut off the former subducted plate and continued to subduct (Fig. 9.15e), as has been shown in the experiments (Fig. 9.14). Subsequently, the northwestward subduction of the Vetlovsky oceanic plate beneath the accretionary margin resulted in the emplacement of the superimposed Central-Kamchatka volcanic belt in the Oligocene (Fig. 9.15e).

The total duration of the arc–continent collision in Kamchatka was about 12 Ma (Fig. 9.7) from the Late Paleocene (just after 60 Ma), when the continental crust entered the subduction zone and the fore-arc

block start to subduct and the arc volcanism stopped, to the late Early Eocene (48 Ma), when the buried crustal slice was exhumed to 300°C, and subduction reversal led to the southeastward thrusting at the back side of the deformed arc. The shift from tholeiitic insular arc volcanism (Fig. 9.8) in the Ozernoy-Valagina arc before the arc–continent collision (Fig. 9.15a) to the Andian-type, calc-alkaline, volcanic activity in the Central-Kamchatka volcanic belt on the continental margin after the collision (Fig. 9.15e) records the reversal of subduction polarity.

9.5 Discussion of the Problematic Issues

The above proposed model of Early Eocene arc–continent collision in Kamchatka is one of several possible scenarios. Many of the aspects of the collision model presented here would probably be accepted by most researchers whereas some of the features would conceivably be regarded as debatable.

One of the crucial questions for the geodynamic model of the arc–continent collision in Kamchatka is the nature of the Sredinny metamorphic massif – does it represent a pre-existing (Cretaceous) continental crust (Bindeman et al. 2002) or was it formed as a result of syncollisional metamorphism of Paleocene terrigenous turbidites (Hourigan et al. 2009). Another controversial questions concern the nature of heating and the mode of burial and exhumation occurred along the continental margin during the collision in Kamchatka. Finally, either subduction reversal or slab detachment occurred at the final stage of the collision in the late Early Eocene. The next sections address these problems.

9.5.1 Source of Detrital Sediments Served the Protolith of the Sredinny Massif

The gneisses of the Kolpakovka Group in the Sredinny massif were formed from sediments with depositional ages no older than Late Cretaceous (Campanian), with the youngest ages of detrital zircon at 96 Ma (Bindeman et al. 2002) or 85 Ma (Hourigan et al. 2009). These gneisses are characterised by a large spectrum of zircon ages (Archaean, Proterozoic and Phanerozoic) with 31% of the zircons with Precambrian cores in the zircon population (Bindeman et al. 2002). The sedimentary series of the Sredinny massif are predominantly of a felsic terrigenous nature, and the gneisses of the massif show relatively primitive whole-rock $^{87}Sr/^{86}Sr$ values (0.703–0.706) that likely indicate a high degree of weathering of feldspars in the source area. This evidence supports the continental nature of the zircon source that could have been an extensive polychronous area with a complex age pattern that experienced high erosion rates, i.e., the Precambrian craton of Siberia with its deeply eroded platform cover (Bindeman et al. 2002). The presence of Palaeozoic-Triassic detrital zircons and detrital and/or volcanic, Late Jurassic to Early Cretaceous zircons implies the proximity of a long-lived Phanerozoic magmatic arc or arcs on or near a Precambrian continental margin as a source area, such as the Tuva-Mongol, Uda-Murgal, Okhotsk-Chukotka arcs (Bindeman et al. 2002).

The terrigenous schists from the Kamchatka Group, which represents the metamorphosed cover of the Kolpakova gneisses and Krotogorov granites in the Sredinny massif, contain the youngest detrital zircons of Paleocene age, 60 Ma (Hourigan et al. 2009). The non-metamorphosed quartz-feldspar sandstones from the Khozgon Formation also contain detrital zircons of Paleocene age (Hourigan et al. 2009). The sedimentary successions of the Kamchatka Group and the Khozgon Formation in South Kamchatka, and of the Ukelayat Group in the Olutorsky region, accumulated as a thick marine series of turbidites along the northeast Asian margin and demonstrate a similarity of U–Pb zircon grain-age distributions with Early Proterozoic, Mesozoic and Early Cenozoic peaks suggesting a common sedimentary source region (Hourigan et al. 2009). The Early Proterozoic peak in the zircon populations indicates that the source region most likely included the Siberian Craton, which is characterised by a distinctive peak in magmatic activity at 1.9 Ga (Rosen 2002). The Okhotsk-Chukotka Volcanic Belt, which was active from about 105 to 80 Ma (Filatova 1988; Hourigan and Akinin 2004), could have supplied the Mesozoic zircons. The Paleocene (62.5–63.0 Ma) hypabyssal rocks of the Omgon Range, Western Kamchatka (Ledneva et al. 2006), could have been the source for the Paleocene detrital zircons in the Khozgon Formation and the Kamchatka Group.

9.5.2 Campanian Metamorphic Event Along the Margin

Bindeman et al. (2002) suggested that the episode of 77 Ma zircon growth, as overgrowth rims around detrital zircon cores of different ages, was most likely the main episode of high-grade regional metamorphism and migmatisation that generated the paragneisses of the Kolpakova Group and the granites of the Krutogorov Complex in the Campanian.

In contrast, Hourigan et al. (2009) rejected the idea of a Campanian metamorphic event in the Sredinny massif and proposed that the Kolpakova and Kamchatka groups represent sediments of the northeast Asian continental margin which were metamorphosed once in the Early Eocene during the arc–continent collision. Hourigan et al. (2009) argued that the composite samples of the Kolpakova Group gneisses used in the study of Bindeman et al. (2002) may have been contaminated by samples of the Krutogorova granites. However, this is debatable because the 77 Ma zircon overgrowth rim data were obtained from samples taken from both north and south of the Sredinny massif over a distance of 150 km apart.

There is another argument in support of a Campanian metamorphic event in the rocks of the Kolpakova Group of the Sredinny massif. The Krutogorova granites that cut through gneisses of the Kolpakova Group (Rikhter 1995) are dated to 78–80 Ma (Luchitskaya et al. 2008; Hourigan et al. 2009), i.e., the granites were intruded into the Kolpakova gneisses in the Campanian. Furthermore, the observations of lineations in the gneissic granites of the Krutogorov Complex and the schistosity in the Kolpakova gneisses testify to the emplacement of the granites close to the time of metamorphism of the gneisses (Khanchuk 1985). This conclusion is consistent with the recent U–Pb SHRIMP ages of zircons from the Krutogorov granites (78.5 $\pm$ 1.5 Ma) (Hourigan et al. 2009) and overgrowth rims around zircon cores in the Kolpakova gneisses (77 Ma) (Bindeman et al. 2002).

If the above-mentioned arguments are accepted, the amphibolite-facies metamorphism of continental-derived sediments (Kolpakova Group gneisses) and the emplacement of the Krutogorov granites occurred in the Western Kamchatka basement (Sredinny massif) in the Campanian (80–77 Ma). The major, coeval tectonic event in the Sea of Okhotsk region was the collision of a non-subducting microcontinent or oceanic plateau of the Sea of Okhotsk microplate with the Asian margin, which occurred in the Campanian and resulted in the magmatic hiatus within the Okhotsk-Chukotka volcanic belt (Watson and Fujita 1985; Sengor and Natalin 1996; Bogdanov and Dobretsov 2002). The arc-related magmatism in the Okhotsk sector of the belt ceased at about 81 Ma, whilst the within-plate or extension-related magmatism occurred locally from 78 to 73 Ma (Hourigan and Akinin 2004). If the basement of Western Kamchatka represents the southeastern (facing the Pacific), Cretaceous, accretionary boundary of the Sea of Okhotsk microplate, the peak metamorphism and granite formation within the accretionary wedge could have been related to a regional tectonic reorganisation (and probable rotation) of the microplate provoked by its docking against the Asian continent in the Campanian.

9.5.3 Early Eocene Metamorphism and Granite Formation Along the Margin During the Arc–Continent Collision

SHRIMP U-Pb ages of zircon overgrowths and metamorphic monazite extracted from migmatite and gneiss of the Kolpakova Group indicate that peak metamorphism and anatexis occurred at 51.6 $\pm$ 1.4 Ma (Hourigan et al. 2009). This conclusion is in accordance with the results of Bindeman et al. (2002), who extracted small, irregularly shaped, unzoned metamorphic zircons of 53–47 Ma (SHRIMP U–Pb ages) from the Kolpakova gneisses. The youngest zircons with a SHRIMP U–Pb age of 55.2 $\pm$ 3.3 Ma from the Kamchatka Group are considered as metamorphic in origin (Hourigan et al. 2009). The equigranular granites that cut through metamorphic rocks of the Kolpakova and Kamchatka groups, and synkinematic granites that intruded along the Andrianovka suture, have been dated by the Th–Pb and U–Pb SHRIMP method to 52 $\pm$ 2 Ma (Soloviev 2005; Luchitskaya et al. 2008; Hourigan et al. 2009).

The Early Eocene episode of granite formation (52 $\pm$ 2 Ma) and the peak of metamorphism and anatexis in the Kolpakova gneisses and Kamchatka schists in the Sredinny massif were coeval with the emplacement of the Ozernoy-Valagina arc over the

margin (Konstantinovskaia and Bindeman 2001; Konstantinovskaya 2002; Soloviev 2005; Luchitskaya et al. 2008; Hourigan et al. 2009). Heating is estimated to have been rapid, at rates approaching 80°C/m.y. (Hourigan et al. 2009). The geochemistry of the equigranular granites testifies to their similarity to syn-collisional, subduction-related granites (Luchitskaya et al. 2008).

9.5.4 Burial by Delamination of Crustal Slices and Tectonic Thickening of the Margin or Due to the Arc Obduction

The Early Eocene episode of granite formation and peak of metamorphism and anatexis that occurred in the continental margin (Sredinny massif) during the arc–continent collision (Figs. 9.6 and 9.7) may have been associated with the tectonic thickening of the crust produced by the delamination of crustal slices from their mantle base and their accretion in front of the overriding plate, as appears to be supported by the physical modelling results (Fig. 9.12). In the experiment (Fig. 9.12c–d), the deformation of the continental margin predates the arc obduction, as is likely the case for the Kamchatka arc–continent collision (Fig. 9.15b–c), where the westward thrusting in the margin started in the Late Paleocene and the arc obduction occurred in the Early Eocene (Fig. 9.7) (Konstantinovskaya 2001, 2002).

Alternatively, Hourigan et al. (2009) proposed that the continental margin sediments could have been deeply buried beneath a mafic structural lid of the Olutorsky (Ozernoy-Valagina) arc during the arc obduction. In this model, the structural burial of the margin is provoked by the arc obduction, and consequently started during or after this event. Thermal modelling demonstrates that about 10–20 m.y. is necessary to produce anatectic melts and mobilise the lower portions of a crustal section thickened by thrusting under typical thermal conductivity values and boundary conditions (England and Thompson 1984). Structural burial and attendant heating rates in the continental margin during the Kamchatka arc–continent collision are estimated to have been exceedingly rapid, up to 80°C/my, probably caused either by mantle-derived mafic melts (Hourigan et al. 2009) or by the ascent of asthenospheric magma initiated by syn-collisional slab breakoff (Luchitskaya et al. 2008). As follows from this model, the arc obduction over the margin should have occurred at least just after 60 Ma in order to have provoked burial and metamorphism of the Kamchatka Group sediments (detrital age 60 Ma) and granite injection in the margin at 52 Ma. In this scenario, there is no time left for the deformation of the forearc basin and subduction of the fore-arc lithosphere block that were initially located between the arc and the continental margin.

9.5.5 Exhumation by Compression- and Buoyancy-Driven Squeezing up and Erosional Unload or by Density Inversion, Diapiric Uplift and Crustal Thinning

The syn-collisional exhumation model proposed in the present study is driven mostly by erosion of the squeezed up slice of continental crust represented by Cretaceous metamorphic rocks in the Sredinny massif (Fig. 9.15d), which is also supported by the experimental results (Fig. 9.13b). The normal fault displacement that occurred between the rising crustal slice and the subducting fore-arc block in the experiment (Fig. 9.13b) may correspond to the normal faults recognised along the Andrianovka suture along the eastern margin of the Sredinny massif (Kirmasov et al. 2004). The eroded material was deposited both in the Kolpakova foreland depression and in the arc area (Tal'niki Formation).

In the post-collisional exhumation model of Hourigan et al. (2009), the Sredinny massif is considered as a gneiss dome that was exhumed due to a combination of ductile and brittle thinning of the crust caused by diapiric ascent of a low-density, low-viscosity, continental material beneath a dense structural lid of the obducted island arc. The gravitational collapse model cannot be applied as a mechanism for the dome exhumation because there is no evidence for any significant topography at Kamchatka at the end of the collision. In contrast, Kamchatka is considered to have been a low-standing orogen in the Early Eocene, invaded by a marine transgression in the Mid Eocene (Bobylev and Bakun 1992; Gladenkov et al. 1997). In the absence of significant topography, the model of

density inversion with the addition of mantle-derived or in situ generated decompression melts is suggested to have contributed to the dome initiation and uplift in the form of a diapir (Hourigan et al. 2009). These authors recognised, however, that there is no evidence for any major break in metamorphic grade within the Sredinny Range that would indicate excision of metamorphic section accompanying exhumation by low-angle normal faulting. Further studies need to prove that crustal thinning occurred in the Sredinny massif at 52–48 Ma, as proposed by Hourigan et al. (2009), because this area, even after the Miocene regional extension that affected the entire Sea of Okhotsk microplate, is still characterised by the thickest crust of the Kamchatka Peninsula, i.e., 44–46 km (Kharakhinov et al. 1996) or 40 km (Levin et al. 2002).

9.5.6 Subduction Reversal or Slab Detachment

The subduction reversal and subsequent truncation of the former, subducted, continental margin plate by the oceanic plate probably occurred at the final stage of the Kamchatka arc–continent collision in the late Early Eocene (Fig. 9.15d). This model helps to explain the syn-collisional, SE-vergent thrusting at the rear side of the collided arc (Figs. 9.2 and 9.5a) and the onset of volcanic activity in the Central Kamchatka volcanic belt that was ultimately formed upon on the deformed basement of South Kamchatka in Oligocene time.

Another scenario suggests that the involvement of pre-collision sialic crust (Kolpakova Group) in the Eocene subduction zone at about 54 Ma ago led to the slab break-off that, in turn, initiated the ascent of asthenospheric magma and caused anomalously rapid heating, metamorphism and emplacement of granitic magma at 52 $\pm$ 2 Ma within the margin (Shapiro et al. 2008; Luchitskaya et al. 2008). Further studies may help to prove whether the Early Eocene granite (or other magma) emplacement was widespread in Western Kamchatka as one may expect in the case of a slab break-off, or whether it was limited and related to the regional crustal thickening in the Sredinny massif. A complete slab break-off would have resulted in a rapid isostatic rise of the crust above the break-off zone and deep erosion of the crust (Atherton and Ghani 2002). However, it is known that a marine transgression invaded the whole of the Kamchatka Peninsula in the Mid Eocene just after the arc–continent collision (Bobylev and Bakun 1992; Gladenkov et al. 1997).

9.6 Conclusions

The proposed model of the Early Eocene collision of the Ozernoy-Valagina (Olutorsky) arc with the continental margin of Asia in South Kamchatka takes into account all the recently published geological data and the author's previous geological and physical modelling results.

Western Kamchatka, whose crystalline basement is exposed in the Sredinny massif, is considered as the frontal (SE-facing) part of the Sea of Okhotsk microplate. The terrigenous felsic series with the youngest detrital ages of zircons of 85 Ma represent the protolith of the Kolpakova Group of the massif. The Campanian (80–77 Ma) episode of high-grade regional metamorphism and migmatisation resulted in the formation of paragneisses of the Kolpakova Group and granites of the Krutogorov Complex that marks a stage of the generation of continental crust in Western Kamchatka. This episode could be related to a regional tectonic reorganisation (and probably rotation) of the Sea of Okhotsk microplate provoked by its docking against the Asian continent in the Campanian, as recorded by the termination of the arc-related magmatism in the Okhotsk sector of the Okhotsk-Chukotka volcanic belt at about 81 Ma.

The Early Eocene (52 $\pm$ 2 Ma) episode of granite formation and peak of metamorphism and anatexis that occurred along the continental margin (Sredinny massif) during the arc–continent collision may have been related to the tectonic thickening of the crust produced by the delamination of crustal slices from just above the top of the mantle and their accretion in front of the overriding plate, as is supported by the physical modelling data.

Erosion of a squeezed up slice of continental crust resulted in the syn-collisional exhumation of Cretaceous metamorphic rocks in the Sredinny massif. The normal fault displacement that is observed between the rising crustal slice and the subducting fore-arc block in the experiment may correspond to the normal faults recognised in the Andrianovka suture along the

eastern margin of the Sredinny massif. The eroded material was deposited both in the Kolpakova foreland depression and in the arc area (Tal'niki Formation).

The subduction reversal and subsequent truncation of the former subducted continental margin plate by the oceanic plate occurred at the final stage of the Kamchatka arc–continent collision in the late Early Eocene. This model helps to explain the occurrence of the SE-facing accretionary prism at the rear side of the collided arc and the onset of volcanic activity in the Central Kamchatka volcanic belt that was formed upon on the deformed basement of South Kamchatka in the Oligocene.

Further studies could be carried out in Kamchatka to obtain the SHRIMP age dating of the Tal'niki Formation as a stratigraphic record the Sredinny massif exhumation. The age of the amphibolites from ophiolitic blocks of serpentine melanges associated with nappes of the Ozernoy-Valagina arc could help to date the beginning of the arc detachment during the collision in Kamchatka.

Acknowledgements I am grateful to Dennis Brown who invited me to participate in the IGCP524 Project "Arc–Continent Collision" and to contribute to this Special Volume. My special thanks to two anonymous reviewers for detailed corrections and constructive suggestions that helped to improve the manuscript.

References

Alexeiev DV, Tsukanov NV, Lewerenz S, Freitag R, Gaedicke C, Holl HG (1999) Middle Eocene collision of the Kronotskiy terrane with Kamchatka: new evidence from provenance analysis of the Upper Eocene to Middle Miocene Tyushevka sandstones. In: AGU Fall Meeting EOS Trans, San Francisco, pp F953–F954

Alexeiev DV, Gaedicke C, Tsukanov NV, Freitag R (2006) Collision of the Kronotskiy arc at the NE Eurasia margin and structural evolution of the Kamchatka–Aleutian junction. Int J Earth Sci (Geol Rundsch) 95:977–993

Astrakhantsev OV, Kazimirov AD, Krylov KA, Fedorov PI (1987) Tectonics and structure of the Vatyna nappe frontal part (Koryak Highland). Doklady Akademii Nauk SSSR 295:157–160

Astrakhantsev OV, Batanova VG, Perfiliev AS (1991) Structure of the Galmoenan dunite-clinopyroxenite-gabbro massif (South Koryak Region). Geotectonics 25:132–144

Atherton MP, Ghani AA (2002) Slab breakoff: a model for Caledonian, Late Granite syn-collisional magmatism in the orthotectonic (metamorphic) zone of Scotland and Donegal, Ireland. Lithos 62:65–85

Avdeiko GP, Volynets ON (2000) The Kuril-Kamchatka island arc system. In: Bogdanov NA, Khain VE (eds) Explanatory notes to tectonic map of the sea of Okhotsk Region (scale 1:250 000). Institute of the Lithosphere of Marginal and Inner Seas, Russian Academy of Sciences, Moscow, Russia, pp 123–124

Bakhteev MK, Ben'yamovskii VN, Bragin NYu, Vitukhin DI, Morozov OA, Sinel'nikova VN, Tikhomirova SR, Shatser AE (1994) New data on Mesozoic-Cenozoic stratigraphy of the Eastern Kamchatka (Valaginsky Range). Stratigr Geol Correlation 2(6):555–562

Bakhteev MK, Morozov OA, Tikhomirova SR (1997) Structure of the Eastern Kamchatka ophiolite free collisional suture – Grechishkin thrust. Geotectonics 31(3):236–246

Bakun NN, Bobylev VV, Bushkova OP, Ivanov SV (1994) Formation Conditions of the Gas-Bearing Upper Paleocene-Lower Oligocene Deposits of the Kolpakova Trough (Western Kamchatka). Geol Petrol Gas 2:30–34 (in Russian)

Batanova VG, Astrakhantsev OV (1992) Tectonic position and origin of zoned mafic-ultramafic plutons of the North Olyutor zone (Koryak upland). Geotectonics 26:153–165

Batanova VG, Pertsev AN, Kamenetsky VS, Ariskin AA, Mochalov AG, Sobolev AV (2005) Crustal evolution of island-arc ultramafic magma: Galmoenan pyroxenite-dunite plutonic complex, Koryak Highland (Far East Russia). J Petrol 46(7):1345–1366

Bijwaard H, Spakman W, Engdahl ER (1998) Closing the gap between regional and global travel time tomography. J Geophys Res B: Solid Earth 103(B12):30055–30078

Bindeman IN, Vinogradov VI, Valley JW, Wooden JL, Natal'in BA (2002) Archean protolith and accretion of crust in Kamchatka: SHRIMP dating of zircons from sredinny and ganal massifs. J Geol 110:271–289

Bobylev VV, Bakun NN (1992) A hiatus in the Oligocene of the Kolpakova trough (Western Kamchatka). Tikhookean Geol 4:140–144

Bogdanov NA, Chekhovich VD (2002) On collision between West Kamchatkan and Sea of Okhotsk Plates. Geotectonics 36(1):63–76

Bogdanov NA, Dobretsov NL (2002) The Okhotsk volcanic plateau: Russian Geology and Geophysics 43:87–99

Bogdanov NA, Tilman SM, Chechovich VD (1990) Late Cretaceous–Cenozoic history of the Koryak–Kamchatka region and the Commander Basin of the Bering Sea. Int Geol Rev 32:1185–1201

Bondarenko GE (1992) The Jurassic-Valanginian evolution of Kamchatka, Abstract of Cand. Sc. (Geol.–Min.) Dissertation, Geol. Inst. Ross. Akad. Nauk., Moscow

Burlin YuK, Kozyanin KV (1995) In: Sokolov BA (ed) Bedding-parallel deformations in the sequence of the West Kamchatka Trough as an oil and gas exploration target. VNIIZarubezhgeologiya, Moscow, pp 188–194

Buryak VA, Bakulin YuI, Bespalov VYa, Vrublevskii AA, Gagaev VN, Galichanin EN, Kirillova GL, Loshak NP, Nigai EV, Plyaskin VA, Troyan VB (1988) Petroleum potential of the Southern Far East and adjacent regions (A Comparative Analysis). IKARP DVO RAN, DVIMS i Dal'geolkom MPR RF, Mezhreg. Assots. Dal'nii Vostok i Zabaikal'e, Khabarovsk, 282 p

Chelebaeva AI, Brattseva GM (1986) On the climate stratigraphy of the Paleogene on the basis of Paleoflora: the Northern

Pacific and adjacent regions, (Correlation of the Cenozoic Strata of the Far East). Geol Inst Akad Nauk SSSR, Moscow, pp 157–209

Chemenda AI, Yang R-K, Stephan J-F, Konstantinovskaia EA, Ivanov GM (2001) New results from physical modelling of arc-continent collision in Taiwan. Tectonophysics 333: 159–178

England PC, Thompson AB (1984) Pressure-temperature-time paths of regional metamorphism I. Heat transfer during the evolution of regions of thickened continental crust. J Petrol 25:894–928

Fedorov PI (1986) The comparison of petrochemical compositions of Upper Cretaceous volcanic rocks of the Northern Kamchatka. In: Essays of the geology of the Far East of USSR. Moscow, Nauka, pp 124–136 (in Russian)

Filatova NI (1988) Perioceanic volcanogenic belts. Nedra, Moscow, 264 p, (in Russian)

Flerov GB, Koloskov AV (1976) Alkaline basaltic magmatism in Central Kamchatka. Nauka, Moscow (in Russian)

Flerov GB, Fedorov PI, Churikova TG (2001) Geochemistry of the Late Cretaceous-Paleogene potassic rocks of the early evolution phase of the Kamchatka Island Arc. Petrology 9(2): 161–179

Geological map of Kamchatka (scale 1: 1 000 000) (1981) VSEGEI, USSR

German LL (1978) Ancient crystalline complexes of Kamchatka. Moscow, Nedra, 128 p (in Russian)

Gladenkov YuB, Shantser AE, Chelebaeva AI, Sinel'nikova VN, Antipov MP, Ben'yamovskii VN, Brattseva GM, Polyanskii BV, Stupin SI, Fedorov PI (1997) The Lower Paleogene of Western Kamchatka. GEOS, (Trudy Geol. Inst. Russ. Acad. Sci, issue 488), Moscow, 367 p (in Russian)

Gorbatov A, Kostoglodov V, Suarez G, Gordeev E (1997) Seismicity and structure of the Kamchatka subduction zone. J Geophys Res 102:17883–17898

Hourigan JK, Akinin VV (2004) Tectonic and chronostratigraphic implications of new 40Ar/39Ar geochronology and geochemistry of the Arman and Maltan-Ola volcanic fields, Okhotsk-Chukotka volcanic belt, northeastern Russia. GSA Bull 116(5–6):637–654

Hourigan JK, Soloviev AV, Ledneva GV, Garver JI, Brandon MT, Reiners PW (2004) Timing of syenite intrusions on the eastern slope of the Sredinnyi Range, Kamchatka: rate of accretionary structure exhumation. Geochem Int 42(2):97–105

Hourigan JK, Brandon MT, Soloviev AV, Kirmasov AB, Garver JI, Stevenson J, Reiners PW (2009) Eocene arc-continent collision and crustal consolidation in Kamchatka, Russian Far East. Am J Sci 309:333–396

Jolivet L, Cadet JP, Lalevee F (1988) Mesozoic evolution of Northeast Asia and the collision of the Okhotsk microcontinent. Tectonophysics 149:89–109

Kamenetsky VS, Portnyagin MV, Sobolev AV, Danushevskiy LV (1993) Magma composition and crystallisation conditions on the picrite-basalt suite in the Tumrok Ridge, East Kamchatka. Geochem Int 30:58–73

Kamenetsky VS, Sobolev AV, Joron JL, Semet MP (1995) Petrology and geochemistry of Cretaceous ultramafic volcanics from Eastern Kamchatka. J Petrol 36:637–662

Khanchuk AI (1985) Evolution of Ancient sialic crust in East Asian Island Arc systems. Dal'nevost. Geol. Inst, Dalnevost. Nauchn. Tsentr Akad. Nauk SSSR, Vladivostok, 150 p

Kharakhinov VV (1996) Tectonics and history of sedimentary basins development. In: Rodnikov AG, Tuezov IK, Kharakhinov VV (eds) Structure and dynamics of the lithosphere and asthenosphere of the Okhotsk Sea region. Nat. Geophys. Com., Russ. Acad. Sci, Moscow, Russia, pp 256–305, in Russian

Kharakhinov VV, Baboshina VA, Tereshchenkov AA (1996) Structure of the Earth's Crust. In: Rodnikov AG, Tuezov IK, Kharakhinov VV (eds) Structure and dynamics of the lithosphere and asthenosphere of the Okhotsk Sea region. Nat Geophys Com, Russ Acad Sci, Moscow, Russia, pp 91–111, in Russian

Kirmasov AB, Solov'ev AV, Hourigan JK (2004) Collision and postcollision structural evolution of the Andrianovka suture, Sredinny range, Kamchatka. Geotectonics 38(4): 294–316

Konstantinovskaia EA, Bindeman IN (2001) Continental margin of Kamchatka Peninsula, Russia: the mode and nature of crustal growth in the accretionary Orogen. Eos Trans, vol 82, no. 47 (Fall Meet. Suppl. Abstracts)

Konstantinovskaya EA (1989) Exotic sedimentary breccias in the Ozernoy Peninsula (Eastern Kamchatka) and its tectonic significance. Geotectonics 5:93–98

Konstantinovskaya EA (1992) The Eastern Kamchatka in the Cretaceous. Ph.D. Thesis. Geological Institute USSR Academy of Sciences, Moscow, USSR (in Russian)

Konstantinovskaya EA (1997) The Late Cretaceous marginal sea of Kamchatka Peninsula. Lith Min Res 32:50–64

Konstantinovskaya EA (2000) Geodynamics of an Early Eocene arc–continent collision reconstructed from the Kamchatka Orogenic Belt, NE Russia. Tectonophysics 325:87–105

Konstantinovskaya EA (2001) Arc-continent collision and subduction reversal in the Cenozoic evolution of the Northwest Pacific; an example from Kamchatka (NE Russia). Tectonophysics 333:75–94

Konstantinovskaya EA (2002) The mechanism of continental crust accretion: an example of Western Kamchatka. Geotectonics 36:67–87

Konstantinovskaya EA (2003) Tectonics of the East Asian Margins: structural evolution and geodynamic modelling. Scientific World, Moscow, 223 p (in Russian)

Konstantinovskaya EA, Zinkevich VP, Tsukanov NV, Garanina SA (1993) In: Pushcharovskii YuM (ed) Composition, structure, and geodynamic setting of the Upper Cretaceous-Lower Paleogene structural-lithologic associations of the East Kamchatkan Ranges. Nauka, Moscow, pp 59–113

Kovalenko DV (2000) Paleomagnetism of the geologic complexes of Kamchatka and Southern Koryakia, Abstract of Doctoral (Geol.–Min.) Dissertation, IL RAN, Moscow

Kozhurin AI (2004) Active faulting at the Eurasian, North American and Pacific plates junction. Tectonophysics 380:273–285

Kozhurin A, Acocella V, Kyle PR, Lagmay FM, Melekestsev IV, Ponomareva V, Rust D, Tibaldi A, Tunesi A, Corazzato C, Rovida A, Sakharov A, Tengonciang A, Uy H (2006) Trenching studies of active faults in Kamchatka, eastern Russia: Palaeoseismic, tectonic and hazard implications. Tectonophysics 417:285–304

Kozyanin VK (1990) Classification and prediction of hydrocarbon accumulations in the Kolpakova Trough in Western Kamchatka. Tikhookean Geol 5:71–75

Krylov NA, Burlin YuK, Lebedev LI (1988) Petroleum basins of continental margins. Nauka, Moscow

Kuznetsov NB (1994) Pre-Late Cenozoic tectonics of the basement of the Kuril-Kamchatka Island Arc, Abstract of PhD (Geol.–Min.) Thesis, Moscow State University, Moscow, 27 p

Ledneva GV, Nosova AA, Soloviev AV (2006) "Calc-Alkaline" Magmatism of the Omgon Range: evidence for Early Paleogene Extension in the Western Kamchatka Segment of the Eurasian Continental Margin. Petrology 14:154–186

Levashova NM, Shapiro MN, Beniamovsky VN, Bazhenov ML (2000) Paleomagnetism and geochronology of the Late Cretaceous–Paleogene Island Arc complex of the Kronotsky Peninsula, Kamchatka, Russia: kinematic implications. Tectonics 19(5):834–851

Levin V, Park J, Brandon M, Lees J, Peyton V, Gordeev E, Ozerov A (2002) Crust and upper mantle of Kamchatka from teleseismic receiver functions. Tectonophysics 358:233–265

Luchitskaya MV, Soloviev AV, Hourigan JK (2008) Two stages of granite formation in the Sredinny Range, Kamchatka: tectonic and geodynamic setting of granitic rocks. Geotectonics 42(4):286–303

Magakyan RG, Kolesov GM, Romashova TV, Konstantinovskaia EA (1993) Geochemical features of the Cretaceous island-arc magmatism from the Eastern Kamchatka. In: Puchsharovskiy YuM (ed) Accretional tectonics of the Eastern Kamchatka. Nauka, Moscow, Russia, pp 114–155 (in Russian)

Marsaglia KM, Mann P, Hyatt RJ, Olson HC (1999) Evaluating the influence of aseismic ridge subduction and accretion on detrital modes of forearc sandstone: an example from the Kronotskiy peninsula in the Kamchatka forearc. Lithos 46:17–42

Nokleberg WJ, Parfenov LM, Monger JWN, Baranov BV, Byalobzhesky SG, Bundtzen TK, Feeney TD, Gordey KP, Grantz A, Khanchuk AI, Natal'in BA, Natapov LM, Norton IO, Patton WW, Plafker G Jr., Scholl DW, Sokolov SD, Sosunov GM, Stone DB, Tabor RW, Tsukanov NV, Vallier TL, Wakita K (1994) Circum-North Pacific Tectono-stratigraphic Terrane Kamchatka. Map. USGS Open-File Report 94–714, 108 p

Nokleberg WJ, Parfenov LM, Monger JWH, Norton IO, Khanchuk AI, Stone DB, Scholl DW, Fujita K (1998) Phanerozoic tectonic evolution of the Circum-North Pacific: Reston, Virginia. U. S. Geological Survey, Open-File Report, OF 98–0754, 125 p

Nurmukhamedov AG (2001) Resistivity structure of the upper crust along the Nizhnyaya Oblukovina-Adrianovka Line (Kamchatka). Tikhookean Geol 20(2):13–23

Pechersky DM, Levashova NM, Shapiro MN, Bazhenov ML, Sharapova ZV (1997) Paleomagnetism of Paleogene volcanic series of the Kamchatsky Mys Peninsula, East Kamchatka: the motion of an Active Island Arc. Tectonophysics 273:219–237

Portnyagin M, Hoernle K, Avdeiko G, Hauff F, Werner R, Bindeman I, Uspensky V, Garbe-Schonberg D (2005) Transition from arc to oceanic magmatism at the Kamchatka-Aleutian junction. Geology 33:25–28

Rikhter AV (1991) Structure of metamorphic complexes in the Ganal Range, Kamchatka Massif. Geotectonics 1:98–108

Rikhter AV (1993) Structure of metamorphic rocks in Eastern Kamchatka. In: Pushcharovskii YuM (ed) Accretionary tectonics of Eastern Kamchatka. Nauka, Moscow, pp 28–58

Rikhter AV (1995) Structure of metamorphic complex of the Central Kamchatka massif. Geotectonics 29(1):65–72

Rosen OM (2002) Siberian craton – a fragment of a Paleoproterozoic supercontinent. Russian J Earth Sci 4:103–119

Sedimentary Basins of the USSR Far East and Their Petroleum Potential (1987) In: Voronkov YuS (ed) Nedra, Leningrad, 263 p

Sengor AMC, Natalin BA (1996) Paleotectonics of Asia: fragments of a synthesis. In: Yin A, Harrison M (eds) The tectonic evolution of Asia. Cambridge University Press, London, pp 486–641

Shantser AE, Chelebaeva AI (2005) Late Cretaceous in the Central Kamchatka. GEOS, Moscow, 116 p, (in Russian)

Shantser AE, Fedorov PI (1997) In: Yu.B.Gladenkov (ed) The Lower Paleogene of Western Kamchatka. GEOS, Moscow, pp 117–128 (Tr. Geol. Inst. Russ. Acad. Sci, issue 488)

Shantser AE, Gladenkov YuB (1997) Geologic evolution and paleogeographic changes in the Early Paleogene of Western Kamchatka. In: Gladenkov YuB (ed) The Lower Paleogene of Western Kamchatka. GEOS, Moscow, pp 129–137 (Tr. Geol. Inst. Russ. Acad. Sci, issue 488)

Shapiro MN, Raznitsin YuN, Shantser AE, Lander AV (1986) Structure of northeastern framework of the metamorphic rocks in the Sredinny Range of Kamchatka. In: Pushcharovsky YuM (ed) Essays on geology of the East USSR. Nauka, Moscow, pp 5–21 (in Russian)

Shapiro MN, Markevich PV, Grechin VI, Konstantinovskaya EA (1992) Upper Cretaceous and Lower Paleocene sandstones of Kamchatka: composition and sources. Lithol Mineral Resour 6:94–106

Shapiro MN, Pecherskii DM, Lander AV (1997) Absolute movement velocities and directions of subduction zones in the geologic past. Geotectonics 31(2):89–99

Shapiro MN, Soloviev AV, Hourigan JK (2008) Lateral structural variability in zone of Eocene Island-Arc–Continent collision, Kamchatka. Geotectonics 42(6):469–487

Shul'diner VI, Khanchuk AI, Vysotskii SV (1987) In: Belousov VV (ed) Pre-Late Mesozoic basement of the Kamchatka fold zone and the tectonic setting of its formation. Nauka, Moscow, pp 6–53

Sidorchuk IA, Khanchuk AI (1981) Mesozoic Glaucophane Schist complex on the Western slope of the Sredinnyi Range in Kamchatka. Geol Geofiz 3:150–155

Slyadnev BI, Sokolkov VA, Markovskii BA (1997) Barab conglomerates: structure, composition, and origin (Kamchatka). Tikhookean Geol 16(1):83–88

Soloviev AV (2005) Study of tectonic processes in regions of lithospheric plate convergence by fission-track dating and structural analysis. Abstract of Doctoral (Geol.–Min.) Dissertation, GIN RAS, Moscow, 49 p, (in Russian)

Soloviev AV, Hourigan JK, Brandon MT, Garver JI, Grigorenko ES (2004) Age of the Baraba formation from the U/Rb (SHRIMR) Dating (Sredinny Range, Kamchatka): geological implications. Stratigr Geol Correlation 12:418–424

Soloviev AV, Palechek TN, Shapiro MN, Johnston SA, Garver JI, Ol'shanetskii DM (2007) New data on the Baraba formation age (the Sredinny Range of Kamchatka). Stratigr Geol Correlation 15:112–119

Sun SS, McDonough WF (1989) Chemical and isotopic systematic of oceanic basalts: implications for mantle composition and processes. Geol Soc Amer (Spec Publ) 42: 313–345

Tararin IA (1988) Metamorphism evolution in the Middle Kamchatka metamorphic zone. Tikhookean Geol 7(1):63–70

Tararin IA (2008) Granulites of the Kolpakovskaya series in the Sredinny range, Kamchatka: a myth or reality? Petrology 16: 193–209

Tectonic Map of the Sea of Okhotsk Region (scale 1:250 000) and Explanatory Notes (2000) In: Bogdanov NA, Khain VE (eds) Institute of the Lithosphere of Marginal and Inner Seas, Russian Academy of Sciences, Moscow, Russia

Van der Voo R, Spakman W, Bijwaard H (1999) Mesozoic subducted slabs under Siberia. Nature 397:246–249

Vinogradov VI, Grigor'ev VS (1994) Rb–Sr Age of rocks from the Sredinny Range of Kamchatka. Dokl Akad Nauk 339(5): 645–649

Vinogradov VI, Grigoriev VS, Leites AM (1988) Age of metamorphism of the rocks from the Sredynniy Range of Kamchatka. Izvestia Acad Nauk SSSR Ser Geol 9:30–38 (in Russian)

Vinogradov VI, Grigor'ev VS, Kastrykina VM (1991) Age of metamorphic rocks from basement of Kamchatka. Sov Geol 7: 58–65 (in Russian)

Watson BF, Fujita K (1985) Tectonic evolution of Kamchatka and the Sea of Okhotsk implications for the Pacific Basin. In: Howell DG (ed) Tectonostratigraphic terranes of the Circum-Pacific region: Houtson. Circum-Pacific Council for Energy and Mineral Resources, Texas, pp 333–348

Zinkevich VP, Tsukanov NV (1992) The Vetlovsky collisional suture of eastern Kamchatka. Trans (Dokl) USSR Acad Sci Earth Sci Sect 324:638–642

Zinkevich VP, Konstantinovskaya EA, Magakyan R, Tsukanov NV (1990) Accretionary structure of the eastern Kamchatka. Trans (Dokl) USSR Acad Sci Earth Sci Sect 312:1186–1190 (in Russian)

Zinkevich VP, Konstantinovskaya YeA, Tsukanov NV, Rikhter AV, Kamenetsky VS, Magakyan R, Sobolev AV, Karpenko SF, Garanina SA, Danyushevsky LV, Kononkova NN, Portnyagin MV, Kolesov GM, Romashova TV (1993) In: Pushcharovsky YuM (ed) Accretionary tectonics of Eastern Kamchatka. Nauka, Moscow, 272 p, (in Russian)

Zinkevich VP, Kolodyazhny SY, Bragina LG, Konstantinovskaya YA, Fedorov PI (1994) Tectonics of the eastern edge of Kamchatka's Sredinny metamorphic massif. Geotectonics 28:75–90

Zonenshain LP, Kuzmin MI, Natapov LM, Page BM (1990) Geology of the USSR; a plate-tectonic synthesis, vol 21. American Geophysical Series, Washington DC, 242 p

Chapter 10
The Asia–Kohistan–India Collision: Review and Discussion

J.-P. Burg

10.1 Introduction

The Himalaya mountain range reaches the Hindu Kush and Karakoram in northern Pakistan where the Himalayan Orogen consists of three tectonic units (Fig. 10.1a and b): To the north, the late Cretaceous–Miocene Karakoram Batholith borders the Eurasian plate. To the south, deformed and metamorphosed shelf and platform Mesozoic sediments cover the Precambrian–Paleozoic Indian plate. Between the Indian and Karakoram (Eurasian) plates, the Kohistan Complex is bound by two suture zones: the Karakoram–Kohistan Suture (KKS), to the north, and the Indus Suture (IS), to the south. In this paper, the term Shyok Suture is avoided to describe the KKS because the Shyok is a river several hundred kilometres away, to the east of the described area, in India, where the Shyok Suture separates the Ladakh Arc from the Karakoram/Eurasian margin (Gansser 1980; Thakur 1981; Thakur and Misra 1984). Although there are notable similarities between Kohistan and Ladakh, there are also differences raising the possibility that tectonic processes were not all identical for these two lateral equivalents. For instance, large volcanic areas like the Deosai Plateau, on the Ladakh side (e.g., Honegger et al. 1982; Reuber 1989; Robertson and Degnan 1994), point to different exhumation/erosion (Van der Beek et al. 2009), hence tectonic/isostatic processes. With this respect, a documented eastward increase of both the continental signature in the chemistry of basalts and the proportion of sediments to volcanic material suggests that the Ladakh island arc, although intra-oceanic for much of its length, was pinned to the Eurasian continental margin at its eastern end (Rolland et al. 2000). Accordingly, tectonic processes have likely varied eastward (Burg 2007), just as modern systems show lengthwise variations (e.g., Stern et al. 2003). To avoid confusion, we deal here with the Kohistan section only, i.e. that part of the island arc with adjacent continents that lays to the west of the Nanga Parbat Syntaxis (Fig. 10.1a). "Northern Suture Zone" (Frank et al. 1977) is another denomination avoided here because there are other Mesozoic suture zones further north (e.g., Zanchi et al. 2000; Hildebrand et al. 2001). Indus Suture is preferred to Main Mantle Thrust for the Kohistan–India boundary because the mantle peridotites squeezed in the contact zone are rather rare and the "thrust" displays many normal faulting features (Burg et al. 1996; Vince and Treloar 1996; Anczkiewicz et al. 2001). Therefore "Main Mantle Thrust" does not reflect the geological reality. Its hint of similarity with the Main Central Thrust and Main Boundary Thrust in the Himalayas brings further confusion since these two latter thrusts are proven, intra-continental shear zones whereas the southern border of Kohistan actually is a suture zone between two different plates.

The geological Kohistan has been identified as an obducted island arc by (Tahirkheli et al. 1979), an interpretation that has been accepted and consolidated by much work that followed, and partly referenced hereafter. Most authors agree that the intra-oceanic arc developed during the Mesozoic in the equatorial area of the Tethys Ocean above a north-dipping subduction (Yoshida et al. 1996; Van der Voo et al. 1999). In that case, there was a wide oceanic basin between Kohistan and Eurasia (Fig. 10.2), whose southern margin was ca. 20° in the northern hemisphere (Schettino and

J.-P. Burg
Department of Earth sciences, ETH- and University Zurich, Sonneggstrasse 5, CH 8092 Zurich, Switzerland
e-mail: jean-pierre.burg@erdw.ethz.ch

D. Brown and P.D. Ryan (eds.), *Arc-Continent Collision*, Frontiers in Earth Sciences,
DOI 10.1007/978-3-540-88558-0_10,

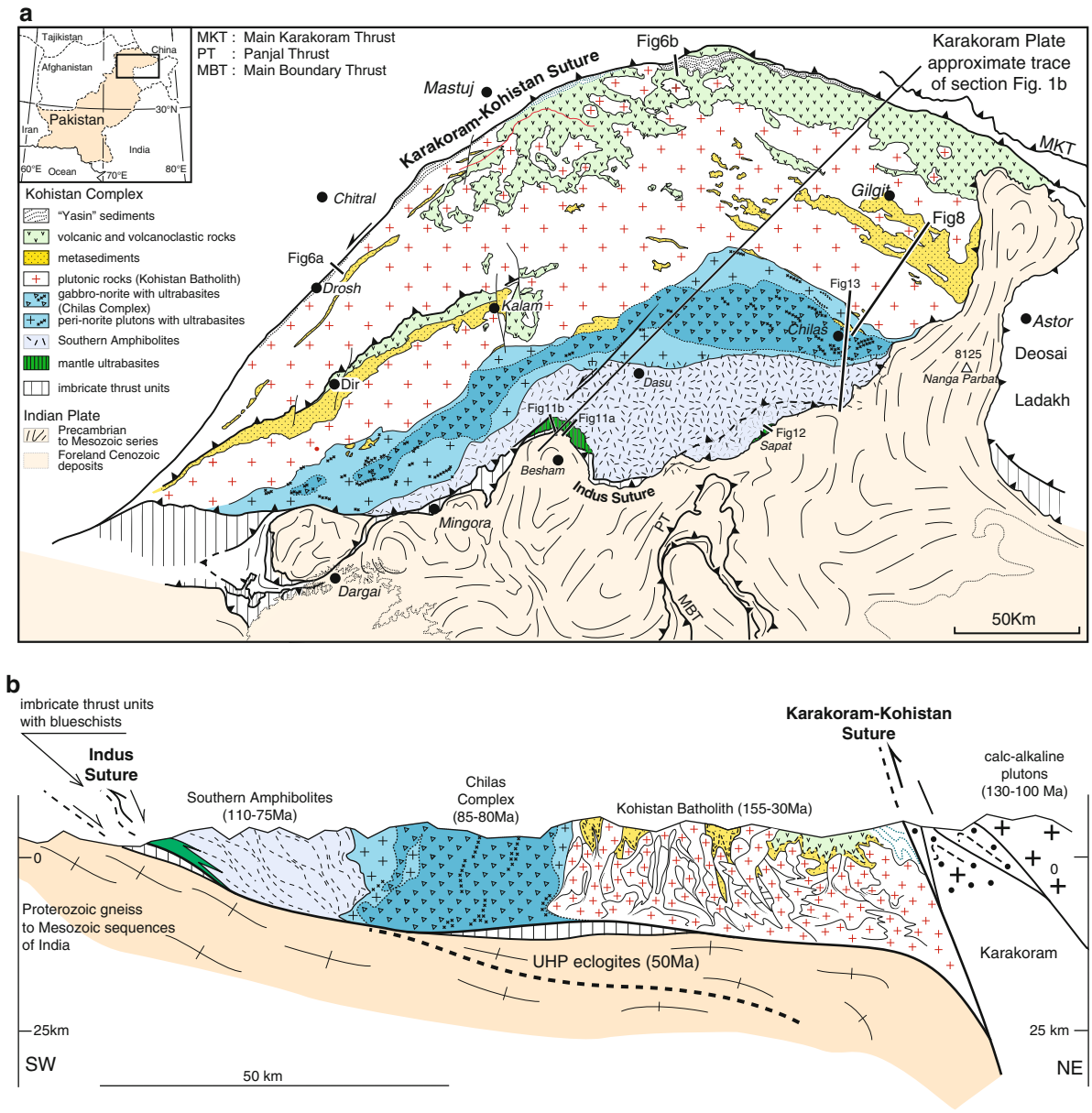

Fig. 10.1 (**a**) Structural/lithological sketch map of Kohistan. (**b**) Synthetic cross section located in **a**.

Scotese 2005). Alternatively, some authors suggest that Kohistan developed near the Eurasian continental margin, on the southern side of a rather narrow, rifted oceanic back-arc basin (Coward et al. 1987; Khan et al. 1993; Bignold and Treloar 2003).

This paper reviews previous work and shows that improved geological, geochemical and geochronological information placed in the light of numerical and analogue modelling orientates tectonic scenarios towards new considerations. A minimum age for initiation of subduction is given by the 154 ± 0.6 Ma calc-alkaline Matum Das intrusion (Schaltegger et al. 2003), which is older than previously foreseen. Early Cretaceous convergence is likely absorbed in two parallel and simultaneous subduction zones, on both sides of Kohistan but, at ~85 Ma, arc rifting with associated decompression melting resulted in the intrusion of the Chilas Complex (Khan et al. 1989; Schaltegger et al. 2002; Burg et al. 2006; Jagoutz et al. 2006; Jagoutz et al. 2007), which marked a change in convergence

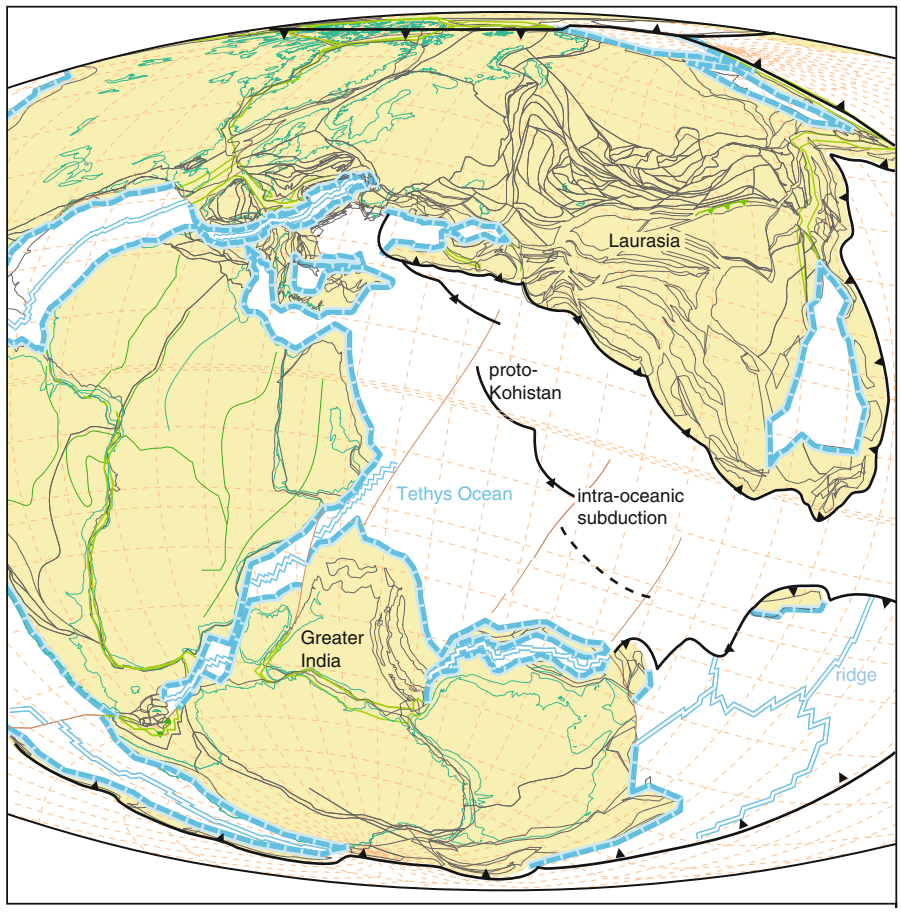

Fig. 10.2 Location of Kohistan at ca. 130 Ma, just after major plate reorganisation. Mollweide projection centred at 58 E, generated from Stampfli and Borel (2002) to place the major continental masses. *Black line* subduction with *filled triangles* in hanging plate. *Blue lines* extensional sites with *barbed lines* in hanging wall; *double blue line* ridges. In this figure, the inferred subduction within Tethys derives from the Early Cretaceous ridge, which has been inverted during major plate reorganization at 135 Ma.

processes. The widespread extensional event affects both the arc and the Karakoram margin of Eurasia; it is likely due to slab rollback on the southern side of Kohistan. Syn-convergence extension has divided a northern, active and southern, inactive arc separated by a trough. Finally, closure of forearc, intra-arc and back-arc basins took place during Eocene–Oligocene times as part of the collisional locking of both sutures and full collision between India and Asia.

10.2 Plate Tectonic Context

Geophysical studies, principally of marine magnetic anomaly data, provide good constraints on the position of India with respect to Asia with a strong emphasis on the last 80 Ma (Patriat and Achache 1984; Klootwijk et al. 1992). However, the tectonic framework is available for the last 190 Ma.

10.2.1 Wrenching-Spreading Tethys

More or less equatorial spreading, combined with sinistral wrenching between Gondwana and Laurasia, dominated Tethys until the Mid to late Jurassic (155–140 Ma, Savostin et al. 1986; Ricou 1994; Stampfli and Borel 2002; Schettino and Scotese 2005). Southwestward propagating spreading ridges that carved-up Gondwana (rifting of the Argo-Burma Terrane from NW Australia and separation of Madagascar/India from Africa) formed at that time (Besse

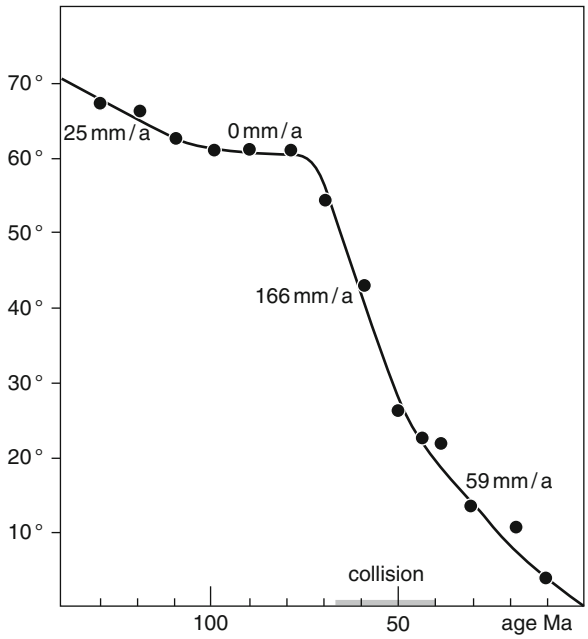

Fig. 10.3 Latitudinal separation and convergence rate between India and Eurasia for a point now at 29°N, 87°E after Besse and Courtillot (1988).

and Courtillot 1988) and preceded major plate reorganization at 135 Ma. Latitudinal convergence between India and Eurasia, at the end of this period, is slow (Fig. 10.3).

10.2.2 Closing Tethys

At about 140 Ma, India stopped rotating slowly clockwise and started the anticlockwise rotation that would last to the present (Schettino and Scotese 2005). Coeval, northward motion of India started at that time and seems to have been through a no-latitudinal-convergence stage between 100 and 80 Ma (Fig. 10.3). India travelled about 5,200 km until a visible change in its apparent polar wander path at 40 Ma. Rapid closure of Tethys (15–25 cm/a, Molnar and Tapponnier 1975) began around 80 Ma (Fig. 10.3), perhaps with the second major plate reorganization at 70 Ma, and remained fast until the onset of tectonic interaction between the continental parts of the Indian and Asian plates around 55 Ma ago (Patriat and Achache 1984; Klootwijk et al. 1992). However, Pelobatid amphibian fossils on both plates suggest that India and Asia were already linked at 67 Ma (Jaeger et al. 1989) by continental bridges along intervening continental blocks such as the Kabul Block (Treloar and Coward 1991) or intra-oceanic island arcs located at near-equatorial latitudes (Burg 2007). Closure of Tethys near the Cretaceous / Tertiary boundary is further constrained by lithostratigraphic and structural information on both sides of the Kohistan arc. To the east, obduction and subsequent interaction between India and Asia is dated at >50 Ma in the Ladakh Himalaya (Green et al. 2008) and at about 65 Ma in the Central Himalayas (Burg and Chen 1984; Ding et al. 2005). To the south-southwest, in the Waziristan–Kurram regions, obduction started also at ca. 65 Ma (Beck et al. 1996).

Very rapid convergence is usually attributed to a long slab of the Tethys Ocean pulling India, thus enhancing fast movement; buoyancy resistance to subduction of continental India triggered slow convergence (ca. 5 cm/a) after 42 Ma (Molnar and Tapponnier 1975; Schettino and Scotese 2005).

10.2.3 Continental Collision: Continental Impingement

Paleomagnetic results from Southern Tibet compared with apparent polar wander paths for the Indian plate show that collision processes involving India began at equatorial latitudes (Klootwijk et al. 1992). Since initial collision, India has moved ca. 2,000 km further north while rotating slightly anticlockwise (Schettino and Scotese 2005). Steady, slow convergence (Fig. 10.3) is assigned to deformability of the welded Indian and Asian continental lithospheres but it cannot be determined to what extent crustal shortening, lateral escape of continental blocks and closure of small basins accommodated this indentation. Crustal growth of the Tibetan Plateau for about 20 Ma may have forced further deceleration of the India/Asia convergence rate (Molnar and Stock 2009).

10.2.4 Place of Kohistan

The paleogeographic position of the Kohistan island arc is uncertain because of remagnetization and weak

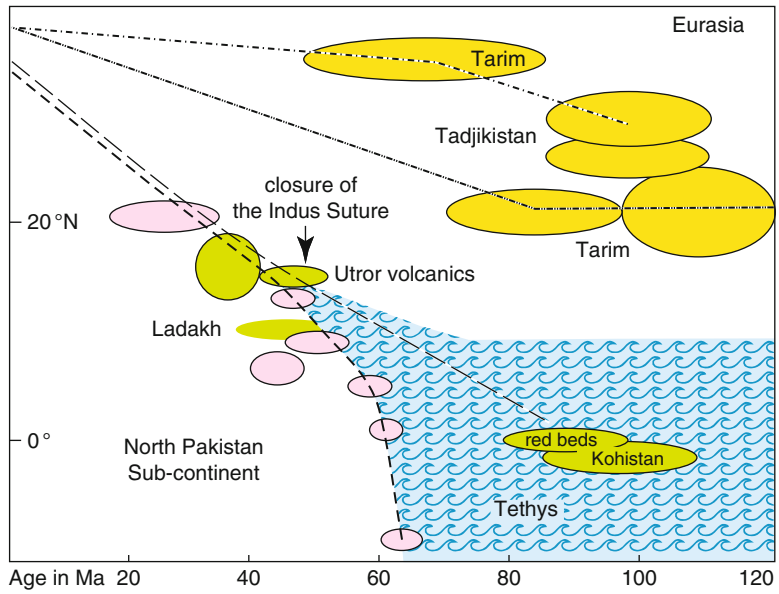

Fig. 10.4 Paleolatitudes of Kohistan (*green*) and neighbouring terranes (Eurasia, *yellow*; India, *pink*) after Yoshida et al. (1996). Northern boundary of Tethys = southern shore of Asia after Chen et al. (1993).

age determination. Kohistan is placed in the equatorial zone and close to the Karakoram margin in the late Cretaceous (100–80 Ma, Fig. 10.4). The Tadjikistan and Tarim basins of Eurasia were at that time more than 2,000 km to the north of Kohistan while India was still in the southern hemisphere. As emphasized by Zaman and Torii (1999), the wide separation during the Cretaceous between Kohistan and Asia (Figs. 10.2 and 10.4) is at odds with interpretations that place Kohistan against the southern margin of Asia in the Late Cretaceous.

In middle Eocene times (ca 45 Ma) there is no measurable difference in latitude between India and Kohistan (Yoshida et al. 1996), which points to complete suturing along the Indus Suture (Figs. 10.3 and 10.4).

10.3 Kohistan: Structure and Lithology of an Arc System

The lithological organisation of Kohistan has led previous authors to define a lithostratigraphic pile from the structurally deepest ultramafic rocks, the Jijal and Sapat Complexes along the Indus Suture, to sediments and volcanic rocks apparently occupying the structurally highest position in the footwall of, and within the KKS. This sequence has been listed by Bard (1983a) and refined by Treloar et al. (1996) and Searle et al. (1999). Kohistan was interpreted as a stack of calc-alkaline plutons intrusive into the Tethys oceanic crust and overlain by the co-genetic calc-alkaline lavas and derivative sediments. However, this "lithostratigraphic" succession hides the facts that nearly all rock types occur throughout the geological Kohistan and that, if north-dipping attitudes are dominant in the south, south-dipping structures are common in the northern parts. The "complete section of the island arc edifice" is more complex than the general view of an arc simply tilted to the north and eroded after collision. Referring to protolith composition, this review distinguishes rocks with upper-crustal (lavas and sediments), mid- to deep crustal (plutonic) and mantle origins to emphasize the complexity and multiplicity of "complete sections" exposed in Kohistan. The description omits the meta-ophiolites that represent the "basement" lithosphere on which the island arc was established.

10.3.1 Upper Crust

Upper crustal sequences pertain to two geographically distinct domains: (1) in the north, along and in the Karakoram–Kohistan Suture zone, and (2) further

south, as scattered outcrops over the rest of the Kohistan Arc (Fig. 10.1).

10.3.1.1 Along the Karakoram–Kohistan Suture Zone

The suture zone is essentially a fault zone that varies in width from few metres to several kilometres. Rocks from both Karakoram and Kohistan sides usually display little strain up to the fault zone so that detailed sedimentary (Robertson and Collins 2002), volcanic (Petterson and Treloar 2004) and plutonic (Heuberger et al. 2007) features and macrofossils (Pudsey et al. 1985b) can be well identified (Fig. 10.5). There is no regional strain gradient towards this faulted suture zone.

Sedimentary and volcanic rocks along the western to northern margin of the arc crop out episodically in two types of settings (Pudsey et al. 1985a; Pudsey 1986; Heuberger 2004): dismembered rock formations in the tectonic imbrication of the Karakoram–Kohistan Suture are allochthonous with respect to contiguous sequences "attached" to the Kohistan Batholith.

Allochthonous Sequences

The Karakoram–Kohistan Suture was described as a chaotic arrangement of large lenses of limestone, sandstone, conglomerate and mafic to ultramafic rocks in a matrix of slates (Coward et al. 1982). Referring to the weak strain of rocks on both sides of the suture and in the suture itself, it was concluded that the KKS represents a small, oceanic and marginal basin (Pudsey et al. 1985a; Coward et al. 1986). In support of this interpretation is the absence of large accretionary wedge, complete ophiolite, blueschists and, conversely, the presence of terrigenous quartzose sediments, presumably derived from Eurasia (Robertson and Collins 2002).

Despite intense tectonic imbrication, there is some order in the tectonic slices (Fig. 10.6). Within the fault zone, from Karakoram to Kohistan, the imbricate lithologies can be assigned to three tectonic units: (1) the former Karakoram active margin, (2) the North-Tethys oceanic basin and (3) the Kohistan Paleo-Island Arc (Robertson and Collins 2002; Heuberger 2004; Heuberger et al. 2007). Most oceanic slices are

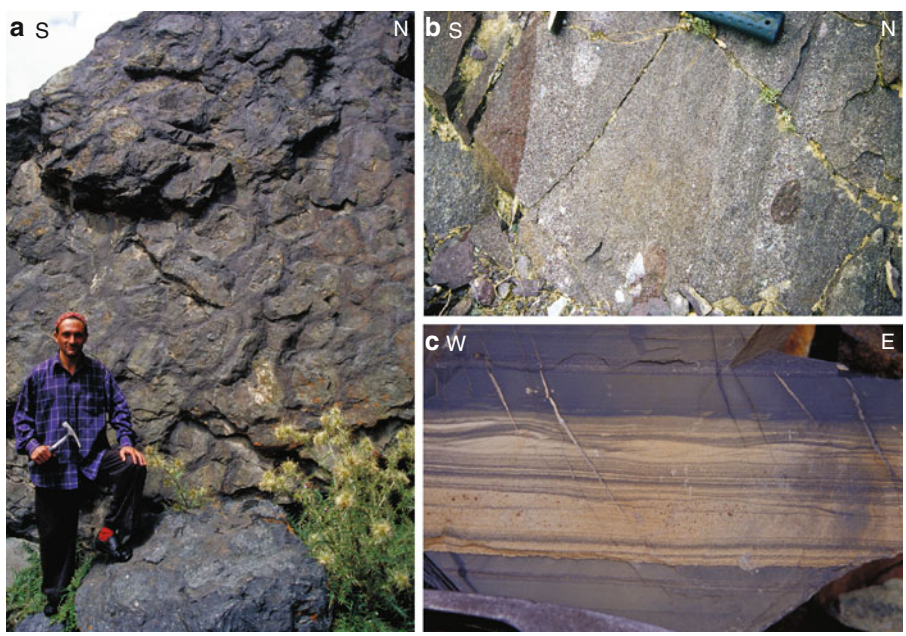

Fig. 10.5 Examples of weakly strained rocks in the footwall of the Karakoram Kohistan Suture. (**a**) undeformed pillows of the Kohistan (Chalt) volcanics ca. 2,000 m from the suture (S of Yasin GPS: N36°20′38.62″; E073°20′12.09″); (**b**) weakly foliated red shales and graded volcanoclastic (Yasin) sediments ca. 100 m from the suture (Yasin GPS: N36°22′31.98″; E073°19′20.95″). (**c**) nearly unschistosed, non-metamorphic turbidites of rippled sandstone (light colour) and black shales, ca. 350 m from the suture (Qurkulti Bar, GPS: N36°24′31.3″; E073°27′47.8″).

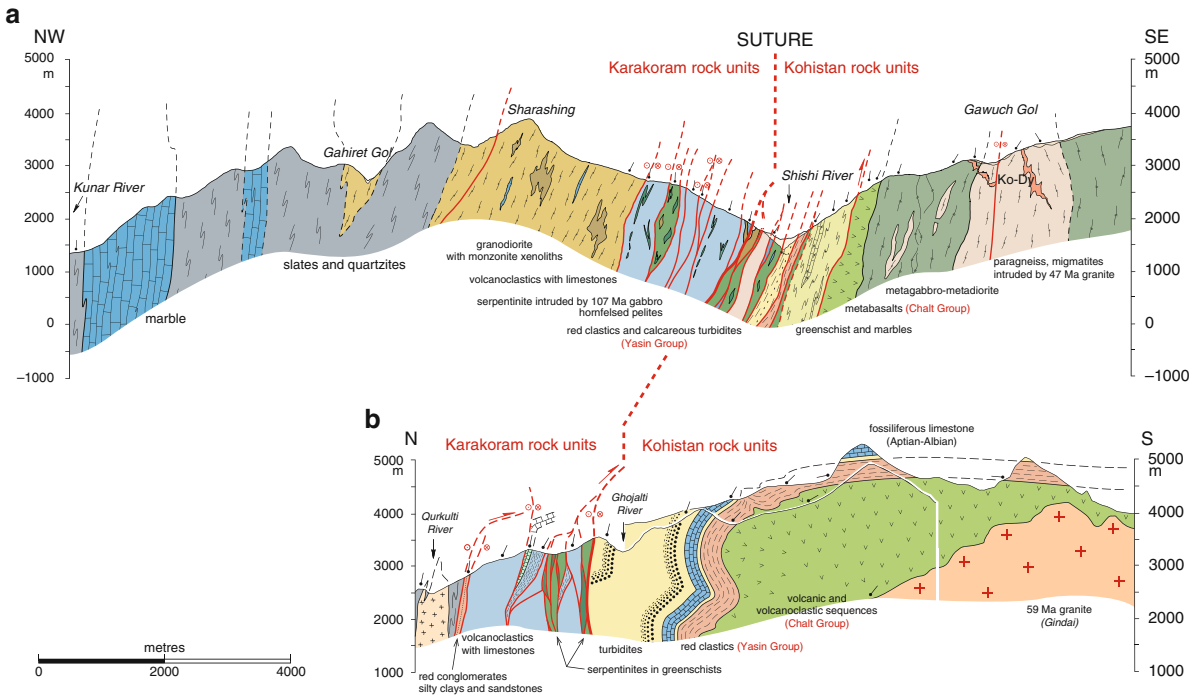

Fig. 10.6 Section across the Karakoram Kohistan Suture (**a**) after Heuberger (2004) and (**b**) unpublished. Colours and symbols correspond to lithologies written next to them, described in the text.

linked to Karakoram (unpublished analysis of heavy minerals pointing to a continental source in the Yasin region), with direct evidence that ultramafic rocks essentially belonged to the Karakoram forearc and were already serpentinised before being intruded by a 90–130 Ma quartz-monzodiorite (Heuberger et al. 2007). Serpentinites occur all along the KKS as massive lenticular bodies and thin schistose shreds along major faults, in continuity with reacted ultramafic rocks identified as talc-magnesite carbonates and schists. The rarely preserved original paragenesis of ultramafic rocks suggests a harzburgitic protolith. The scattered occurrence of ophicarbonates further suggests that the meta-harzburgites were brecciated near or at the sea floor (Heuberger 2004).

Imbricate, Karakoram and oceanic components include shallow water, volcano-detritic sediments including debris flows and conglomerates (e.g., Robertson and Collins 2002), pelagic to hemipelagic sediments, andesitic and low-grade volcanic rocks (including pillow lavas) and calc-alkaline plutonic rocks. Rudist reef-limestone within green basaltic to andesitic volcanites have an unclear origin since they may have deposited on either the Karakoram or Kohistan terranes, or both. In the Drosh region (Fig. 10.1a), limestones with benthic fauna, abundant quartz pebbles in clastic and volcanoclastic sediments with very variable sedimentary facies suggest a dynamic depositional environment, perhaps a delta near sites of active volcanism in Cretaceous times (Heuberger 2004).

Imbricate rocks ascribed to the Kohistan side include locally hornfelsed metapelites and sandstones, calcareous turbidites, red conglomerates, shales and sandstones, greenschists and metavolcanic rocks (Fig. 10.6a). One of these sandstones contains a 120 ± 31 Ma detrital fission track age on zircon (Zeitler 1985). The red, clastic rocks represent alluvial fan or delta deposits in an oceanic basin close to volcanic centers. On the edges of Kohistan, foraminiferae-bearing micritic limestones are interlayered with lavas, tufs and volcanoclastic sandstones. These limestones, along with rudist-bearing massive limestones (Fig. 10.6b), are interpreted as fragments of the volcanic arc shelf redeposited in deeper and more distal parts of a marine basin.

Silty clays, sandstones and conglomerates with pebble to cobble sized clasts occur along the northern limits of the suture zone (Fig. 10.6b). The pebble size

and red color of these clastic rocks indicates a position close to the shore line. Fission track ages of detrital zircon are ca 69 Ma for one conglomerate and 58.1 ± 9.8 and 55.0 ± 3.1 Ma for Karakoram rocks unconformably covered by this conglomerate (Zeitler 1985). Although only maximum ages are recorded, this red clastic series could be equivalent to the Tertiary "molasse" reported far to the east, in the Skardu area (Robertson and Collins 2002).

In summary, the KKS exposes rocks from both the Karakoram forearc and Kohistan backarc basins, which both received volcano-detritic sediments. Fossiliferous limestones represent the foundered Cretaceous shelf of both sides. The lack of complete ophiolite implies that either there was no oceanic lithosphere between the two arcs or that it entirely subducted below Karakoram. In the latter case, the obducted Karakoram forearc was floored by serpentinites now found as tectonic wedges and slices in the fault zone that delineates the Karakoram Kohistan Suture.

Contiguous Sequences

Contiguous sequences, a belt in the footwall of the allochthonous sequences (Fig. 10.1), consist of dominantly volcanic rocks below dominantly sedimentary units (Fig. 10.6). The volcanic sequence (Chalt Volcanic Group) is comprised of pillowed (Fig. 10.5a) and non-pillowed lavas intruded, to the south, by various plutons of the Kohistan Batholith. The lavas are calc-alkaline basalts, andesites, minor rhyolites and rare boninites interlayered with tuffs, agglomerates and thin ignimbrites (Petterson et al. 1990; Khan et al. 1997). A Strombolian volcanic centre was identified (Petterson and Treloar 2004). Some pillow lavas are primitive island-arc-type, tholeiites. High-Mg basalts have been attributed to the formation of a back-arc spreading center (Bignold et al. 2006). These volcanic rocks, interlayered with minor volcanoclastic sediments, conformably grade upward into the dominantly sedimentary sequence, the Yasin Group (e.g., Ivanac et al. 1956; Pudsey et al. 1985a; Pudsey 1986). This group consists of interlayered, calcite-rich shales, tuffs, sands and conglomerates (Figs. 10.5b, 10.6a and b). Orbitoid foraminiferae are abundant in shales; limestones contain a rich and well preserved, Aptian–Albian fauna of rudists, gastropods, chondrodonts, corals and other shelly fragments (*Orbitolina* and *Hippuritid Rudists* fossils, ca. 100–120 Ma; Douvillé 1926; Ivanac et al. 1956; Pudsey et al. 1985b). Rudist forms are typical of the northern realm of the Tethys Ocean (Pudsey et al. 1985b). In places (and in the locus typicus, Yasin city, Fig. 10.1a) clastic organization of fossils indicates proximal deposits of reef debris (talus breccia) interlayered with sandstones and gravels. In other places, the carbonate platform of massive limestone is up to 400 m thick (Fig. 10.6b). This remarkable, stratigraphic level passes upwards into immature turbidites, which start with coarse conglomerates. The turbiditic sequence (Fig. 10.5c, shales, wackes, siltstones, sandstones, micritic limestones and limestone conglomerates, graywackes) displays upward thinning with a gradual change to siltstones and shales. Black shales smelling of organic matter in several places confirm that sediments on the Kohistan side, and thus likely the North Kohistan shore, were not buried to depth equivalent to low-grade metamorphic conditions. Increasingly distal environment indicates that, at some stage, the subsidence rate exceeded growth rate and the platform was drown so that younger strata were deposited in a deep-water, marine environment. Andesitic sills and dikes with chilled margins and alteration rims are common.

10.3.1.2 Within Arc Occurrences

Greenschist to lower amphibolite facies volcano-sedimentary units occur in the northern and northwestern parts of Kohistan between and intruded by the plutons of the Kohistan Batholith. Their geographic separation led to a list of local names whose multiplicity reflects the difficulty of making solid correlation from one name "group" to the next and with the Yasin and Chalt groups of the Karakoram–Kohistan Suture (Khan et al. 1994; Treloar et al. 1996). Intrusions and tectonic dismemberment have obliterated much of the primary relationships, which further hampers correlation. A confusing consequence is that the same formation names (e.g., Gashu, Shamran, Teru and Dir) were used to lump volcanic formations unconformable upon eroded Kohistan Batholith plutons (Matsushita and Huzita 1965; Danishwar et al. 2001) and older, intruded volcanic rocks. What follows is a tentative ordering (Table 10.1), knowing that discontinuity

Table 10.1 Tentative stratigraphy and equivalence (see text for details)

N-Kohistan (Yasin–Drosh)	N-Batholith (Jaglot–Gilgit)	S-Batholith (Dir–Kalam)	Age constraints
Teru volcanics			
Unconformity			
Shamran volcanics		Utror volcanics	61–58 55 ± 2 Ma
		Baraul Banda slates	Contain ca 60 Ma fossils
		Unconformity	
Turbidites	Thelichi slates-marbles	Peshmal Schists	Intruded by 75 Ma plutons
Yasin sediments			Contain ca. 110 Ma fossils
Chalt volcanics	Gashu volcanics	Mankial volcanics	Intruded by 75 Ma plutons
	Gilgit turbidites		Intruded by 85 Ma pluton

of outcrops, similar petrology and geochemistry of volcanic rocks as well as heterogeneous facies inherent to volcanoclastic sequences render correlations extremely uncertain.

Unconformable Sequences

Unconformable volcanic rocks (depending on authors, Teru, Shamran or Utror Groups) cover northwestern Kohistan and likely cap its "upper crust" stratigraphy. This stratigraphic assignment is consistent with $^{40}Ar/^{39}Ar$ ages of 43.8 ± 0.5 and 32.5 ± 0.4 Ma measured on lavas whose geochemistry indicates that subduction-related volcanism lasted until at least 33 Ma (Khan et al. 2004). They also reveal that parts of Kohistan had been deeply eroded by that time. In fact, the unconformity (chilled lavas against underlying granitoids, Hamidullah and Onstott 1992; Danishwar et al. 2001) might be "old" if the 58 ± 1 $^{40}Ar/^{39}Ar$ hornblende age (Treloar et al. 1989b) dates one of these lavas and if the 50–55 Ma fission track ages of zircons in some plutonic rocks (Zeitler 1985) denote cooling during erosional denudation. In that case, it is possible that these unconformable volcanics correlate with the youngest Paleocene–Eocene lavas found further south (Sullivan et al. 1993), but additional work is required to ascertain this equivalence.

Intruded Sequences

The intruded (underlying?), hence low grade to amphibolite facies volcanic and sedimentary sequences (Dir, Kalam, Chalt, Pashmal, Jaglot, Thelichi, Gilgit, Majne Groups) seem to start with bottom conglomerates, quartzites and clastic limestones with a mid-Jurassic to Cretaceous fauna (Kraig 1981 in Bender and Raza 1995). These rocks apparently seal a paleotopography (alluvial fans) and are overlain by, or in lateral equivalence with a turbiditic sequence (Gilgit Formation, lobe facies inferred from the few cm thick alternation of pelitic and fine, locally graded sandy material Fig. 10.7). The turbidites pass upward and transitionally to sandstones and pelites interbedded with volcanic breccias, locally pillowed calc-alkaline basalts, andesites, tuffs, minor ignimbrites and rhyolites (Utror, Peshmal = Gashu = Chalt Volcanics? Khan et al. 1994). Lava geochemistry confirms an arc environment (Bignold et al. 2006). Marbles and cherts occur with volcanoclastic sediments and slates (Thelichi Formation) in the upper part of the sequence (Fig. 10.8). These upper, thinly laminated slate units perhaps correlate with the Baraul Banda slates,

Fig. 10.7 Alternating sandy and pelitic beds in biotite-garnet paragneiss providing evidence for the turbidite protolith of the Gilgit formation (SW Gilgit).

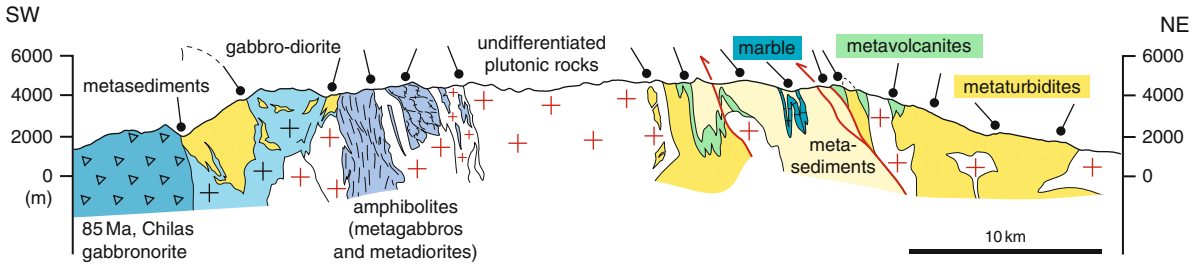

Fig. 10.8 Unpublished section across the so-called Jaglot Syncline (Coward et al. 1986) in the Kohistan Batholith.

in SW Kohistan, which contain late Paleocene (60–55 Ma) fossiliferous limestones (Kakar et al. 1971; Sullivan et al. 1993). Depositional models for the largest outcrop (Dir–Kalam, Fig. 10.1) infer rapid subsidence in extensional, restricted fore- or intra-arc basins that widened enough to evolve into quiet, deep water basins (Treloar et al. 1996; Shah and Shervais 1999). These sediments and volcanic rocks may just as well represent an oceanic back-arc basin of conjectured size (Khan et al. 1996). In any case, there is no evidence that ophiolitic rocks floored any of these basins.

If given ages and correlations are confirmed, the metamorphic volcano-sedimentary sequences encounteredwithin the Kohistan Batholith include sequences older than the Aptian–Albian limestone in the footwall of the KKS and younger sequences demonstrated by Paleocene fossiliferous limestone and, if they do not belong to the unconformable sequence, by 58 ± 1, and 55 ± 2 Ma basaltic andesites (hornblende, ^{40}Ar–^{39}Ar age, Treloar et al. 1989b).

Metamorphic conditions are quite disparate, which in itself is untypical for regional metamorphism expected for a subduction/collision event. For example, nearby samples may show heating for one but cooling for the other during decompression to ca. 0.8 GPa; corresponding temperatures are high, ca. 715°C. The first case is attributed to "syntectonic" plutons (Chamberlain et al. 1989). Indeed, most metamorphic rocks are due to contact effects, which explains the wide range of cooling ages over Kohistan, away from the Nanga Parbat Syntaxis (Treloar et al. 1989b; Krol et al. 1996).

The southernmost, scattered exposures of "upper-crustal" rocks are shortly described with the Southern Amphibolites of the Plutonic crust.

10.3.2 Plutonic Crust (Mid- to Lower Crust)

The plutonic crust, the largest portion of Kohistan, is comprised of three units. One of them, the Chilas Gabbronorite, separates the Kohistan Batholith to the north from the Southern Amphibolites (essentially meta- gabbros, diorites and tonalites; Fig. 10.1, e.g., Bard 1983b; Treloar et al. 1996; Searle et al. 1999).

10.3.2.1 Kohistan Batholith

Kohistan Batholith is a denomination that gathers calc-alkaline granitoids with a wide range of shape, size, age and mineralogical compositions intrusive into older plutonic, sedimentary and volcanic formations. Gabbros, diorites, tonalites, granodiorites and granites that built the Batholith derive from mantle melts evolved through amphibole-dominated fractionation and assimilation of the arc crust (Jagoutz et al. 2009).

Multiple intrusions are locally shaped like dyke swarms that suggest opening of the back-arc basin possibly as early as c. 135 Ma (K–Ar whole-rock age, Khan et al. 2007). Pioneering geochemical studies (Petterson and Windley 1985, 1991) suggested that the Kohistan Batholith evolved through three main stages. The first plutonic stage (102–85 Ma) would be composed of a bi-modal sequence of foliated gabbro-diorites and quartz-monzodiorites. Stage 2 consists of undeformed gabbros, diorites and granites that intruded between 85 and 40 Ma with a general mafic to acid trend. Stage 3 refers to swarms of ca. 30 Ma old leucogranite sheets and dykes (Rb–Sr ages at 34 ± 14

and 29 ± 8 Ma, Petterson and Windley 1985; U–Pb zircon at 30.4 ± 0.6 Ma, Schaltegger et al. 2003). These dykes were ascribed to crustal melting of the underlying, partially molten Indian crust, well after collision with the subcontinent. However, some of the concordant zircons have εHf up to +10, which shows that these granites also contain a juvenile component (Schaltegger, personal communication). Stage 1 and early stage 2 plutons have isotopic signatures characteristic of a mantle derivation and their Sr and Nd contents indicate an increasing crustal component, with the latest magmas being entirely crustally derived (Petterson and Windley 1991; Petterson et al. 1993). This evolution was interpreted as the result of arc thickening and lower arc melting following suturing to Asia. Geochronological and geochemical work carried out since then has shown that calc-alkaline magmatism began earlier, in Jurassic times (154 ± 0.6 Ma, Schaltegger et al. 2003) and that arc magmatism covers the 112–38 Ma time span (Table 10.2, Jagoutz et al. 2009). Gaps in age data used to infer periodic magmatic activity (Treloar et al. 1996) may reflect incompleteness of sampling or the spatial variability of magmatic episodes. Besides, many K–Ar and Ar–Ar ages between ca. 80 and 40 Ma (Treloar et al. 1989b) likely reflect cooling of neighbouring plutons.

10.3.2.2 Gabbronorite (Chilas Complex)

A large body of gabbronorites (Fig. 10.1) was first interpreted as a layered magma chamber (Bard 1983b; Jan et al. 1984; Khan et al. 1989, 1993) intruded into the arc in Cretaceous times (ca. 85 Ma, Zeitler et al. 1980; 85.73 ± 0.15 Ma, Schaltegger et al. 2002). In details, this so-called Chilas Complex is a multiple intrusion of norites, noritic gabbros and two-pyroxene-quartz-diorite enclosing a string of diverse ultramafic-mafic-anorthosite (UMA) lenses (Jan and Howie 1981). Magmatic structures such as mineral layers, slumps, graded beds and faults are abundant in the vicinity of the UMA. The gabbronorite was re-equilibrated under granulite-facies conditions (750–850°C, 0.6–0.8 GPa, Jan and Howie 1980; Yamamoto 1993; Yoshino and Okudaira 2004). The Sm–Nd age of 69.5 ± 9.3 Ma from the northwestern border of the main body refers to cooling below ca. 700°C (Yamamoto and Nakamura 1996). Cooling through 500°C (K–Ar and ^{40}Ar–^{39}Ar hornblende ages) was around 80 Ma (Treloar et al. 1989b). This apparent contradiction (700°C younger than 500°C) emphasises the heterogeneity of the thermal and structural history, likely controlled by local and short thermal pulses.

The Chilas Complex was pictured as a gigantic, isoclinal anticline, implying that the thickness of this presumed huge stratiform intrusion was about half or less the <40 km map width of gabbronorites (Coward et al. 1982, 1986). The subalkaline geochemistry (Khan et al. 1989) and structural arguments emphasize that, instead, the Chilas Complex intruded the early arc during extension (Burg et al. 1998, 2006) up into metasediments and metavolcanics of the Kohistan Batholith, to the north and, to the south, into the Southern (Kamila) Amphibolites (Figs. 10.1 and 10.8, Treloar et al. 1996).

10.3.2.3 Meta-gabbros to Trondhjemites (Southern Amphibolites, Kamila Amphibolites)

The so-called Kamila or Southern Amphibolites often indistinctly refer in the literature to a 15–35 km thick pile of interwoven, sheet-like intrusions (predominantly calc-alkaline gabbros and diorites with subordinate tonalites, granites and trondhjemites) and to mafic rocks of possible pre-arc, ophiolitic origin that screen the intrusions (Khan and Thirlwall 1988; Jan 1988; Khan et al. 1993; Treloar et al. 1996; Bignold et al. 2006). Other "enclaves" expose meta-volcanic rocks with arc signature (mainly basalts and locally pillowed basaltic andesites, tuffs and agglomerates, Fig. 10.9a), metasediments (including calc-silicate rocks, Fig. 10.9b) and meta-plutonic rocks. This rock unit generally makes the hanging wall of the Indus Suture where mantle lenses are absent.

The present description refers to the gabbroic to granitic plutonic rocks, which were variably sheared in amphibolite (550–680°C, 0.9–1.0 GPa) to greenschist facies conditions (Bard 1983b; Jan 1988; Treloar et al. 1990; Chamberlain et al. 1991; Arbaret et al. 2000; Burg et al. 2005). U–Pb ages on zircons spread from ca. 110 to ca. 75 Ma (Table 10.3). Ar–Ar cooling ages on hornblendes cluster around 83 Ma (Treloar et al. 1989b) and recalculated cooling through ca 500°C occurred by 76 ± 4 Ma (Wartho et al. 1996). These ages are consistent with the 82 Ma age of

Table 10.2 High-temperature (near intrusion) geochronological data on plutonic rocks of the Kohistan Batholith

Rock type (*location*)	Age (Ma)	References
Method: U–Pb zircon		
Tonalite (*Matum Das*)	154.0 ± 0.6	Schaltegger et al. (2003)
Meta-diorite *(Mirkhani)*	111.52 ± 0.4	Heuberger et al. (2007)
Tonalite (*Tak Gah*)	79.34 ± 0.34	Jagoutz et al. (2009)
Quartz-diorite *(Bibior)*	75.1 ± 4.5	Jagoutz et al. (2009)
Granite *(N-Matiltan)*	72.3 ± 5.1	Jagoutz et al. (2009)
Granite *(Makarkhar)*	70.3 ± 5.0	Jagoutz et al. (2009)
Tonalite *(Khiner Gah)*	67.6 ± 5.8	Jagoutz et al. (2009)
Diorite *(Shunji)*	64.5 ± 0.5	Khan et al. (1996)
Diorite *(Biusho)*	62.1 ± 4.9	Jagoutz et al. (2009)
Granite *(Roshai Dab)*	57.3 ± 5.3	Jagoutz et al. (2009)
Meta-gabbro *(N-Ziarat)*	49.8 ± 0.15	Heuberger et al. (2007)
Granite dyke *(Beorai Gol)*	47.4 ± 0.5	Heuberger et al. (2007)
Diorite *(N-Dir)*	42.1 ± 3.7	Jagoutz et al. (2009)
Granitoid *(Pingal)*	41.0 ± 0.5	Khan et al. (1996)
Granite dyke *(Beorai Gol)*	38.73 ± 0.2	Heuberger et al. (2007)
Granite (*Parri*)	30.4 ± 0.6	Schaltegger et al. (2003)
Aplite *(Confluence)*	30.2 ± 0.3	Krol et al. (1996)
Method: Rb–Sr whole rock		
Tonalite (*Matum Das*)	102 ± 12	Petterson and Windley (1985)
Granite *(Shunji)*	65.4	Khan et al. (2004)
Granitoid (*Gilgit*)	54 ± 4	Petterson and Windley (1985)
Granite (*Gindai*)	59 ± 2	Debon et al. (1987)
Leucogranite *(Jaglot)*	49.1 ± 11	George et al. (1993)
Granodiorite (*Shirot*)	40 ± 6	Petterson and Windley (1985)
Aplite-pegmatite (*Confluence*)	34 ± 14	Petterson and Windley (1985)
Granite (*Parri*)	29 ± 8	Petterson and Windley (1985)
Granite (*Parri*)	26.2 ± 1.2	George et al. (1993)
Method: Ar/Ar Hornblende		
Diorite (*near Kalam*)	94 ± 4	Treloar et al. (1989b)
Diorite (*near Kalam*)	81 ± 3	Treloar et al. (1989b)
Mafic sheet (*N-Gilgit*)	82 ± 3	Treloar et al. (1989b)
Diorite (*Kalam*)	78 ± 1	Treloar et al. (1989b)
Diorite (*Kalam*)	76 ± 2	Treloar et al. (1989b)
Diorite (South-Kalam)	75.9 ± 0.4	Krol et al. (1996)
Mafic (*Jutal*) dyke	75 ± 2	D. Rex in Petterson and Windley (1985)
Mafic sheet (*N-Gilgit*)	74 ± 3	Treloar et al. (1989b)
Mafic sheet (*N-Gilgit*)	71 ± 3	Treloar et al. (1989b)
Diorite (*Gabral*)	64.0 ± 0.8	Hamidullah and Onstott (1992)
Pluton (*Gupis*)	63 ± 1	Treloar et al. (1989b)
Granitoid (*Gupis*)	61 ± 3	Treloar et al. (1989b)
Diorite (*Dainyar*)	54 ± 1	Treloar et al. (1989b)
Diorite (*Kalam*)	48 ± 1	Treloar et al. (1989b)
Diorite (*Dir*)	45.2 ± 0.4	Zeitler (1985)
Method: Ar/Ar Biotite		
Tonalite (*Matiltan*)	73.6 ± 0.2	Hamidullah and Onstott (1992)
Granite (*Naz Bar*)	58 ± 1	Treloar et al. (1989b)
Method: K–Ar whole rock		
Dolerite dyke *(S-Gilgit)*	134 ± 3	Khan et al. (2007)
Granite (*Gindai*)	50.3 ± 1.7	Casnedi et al. (1978)
Granite (*Gindai*)	37.4 ± 1.6	Casnedi et al. (1978)
Method: K–Ar Biotite		
Granite (W Yasin)	62 ± 3	Pudsey (1986)
Granitoid *(Pingal)*	57 ± 2	Treloar et al. (1989b)
Granitoid *(SE-Gakuch)*	43 ± 2	Treloar et al. (1989b)

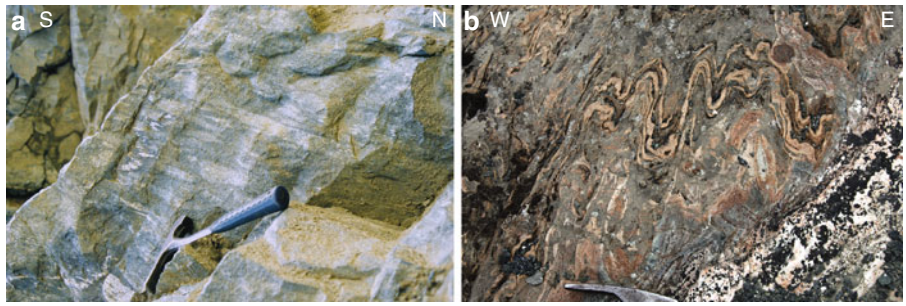

Fig. 10.9 Greenschist to amphibolite facies rocks enclaved in the Southern Amphibolites (**a**) volcanic agglomerate (GPS: N35°17′48.6″; E073°57′44.5″). (**b**) Folded cherts in calcsilicate-bearing rocks (GPS: N35°17′40.9″; E073°48.7″).

Table 10.3 High-temperature (near intrusion) geochronological data on plutonic rocks of the Southern Amphibolites

Rock type	Age (Ma)	References
Method: U–Pb zircon		
Amphibolite xenolith *(Dur Banda Khwar)*	110.7 ± 4.9	Yamamoto et al. (2005)
Tonalite vein *(Kiru)*	107.7 ± 1.8	Yamamoto et al. (2005)
Tonalite *(Sapat)*	106.83 ± 0.24	Bouilhol (2008)
Hornblende-trondjhemite *(Sapat)*	104.83 ± 0.30	Bouilhol (2008)
Hornblende-trondjhemite *(Sapat)*	104.38 ± 0.78	Bouilhol (2008)
Garnet-tonalite *(Sapat)*	103.0 ± 1.1	Bouilhol (2008)
Hornblende-tonalite *(Sapat)*	99.48 ± 0.69	Bouilhol (2008)
Gabbro *(Sarangar)*	98.9 ± 0.4	Schaltegger et al. (2002)
Granite *(Dur Banda Khwar)*	97.1 ± 0.2	Schaltegger et al. (2002)
Tonalite *(Buto Gah)*	95.03 ± 0.09	Bouilhol et al. (2011)
Tonalite vein *(Dur Banda Khwar)*	94.0 ± 1.9	Yamamoto et al. (2005)
Tonalite *(Buto Gah)*	93.57 ± 0.1	Bouilhol et al. (2011)
Diorite *(S-Kiru)*	91.8 ± 1.4	Schaltegger et al. (2002)
Foliated tonalite *(Dur Banda Khwar)*	89.5 ± 3.3	Yamamoto et al. (2005)
Ky- pegmatite (S-Khwaza Khela)	82.8 ± 1.1	Schaltegger et al. (2002)
Tonalite dike *(ENE-Patan)*	82.0 ± 2.0	Yamamoto et al. (2005)
Anorthositic vein *(Chachung)*	81.0 ± 1.6	Yamamoto et al. (2005)
Tonalite vein *(Sehgal)*	80.6 ± 4.5	Yamamoto et al. (2005)
Trondhjemitic vein *(Sehgal)*	75.8 ± 1.7	Yamamoto et al. (2005)
Trondhjemite *(Dur Banda Khwar)*	75.7 ± 1.4	Yamamoto et al. (2005)
Method: Sm–Nd isochron		
Two-pyroxene gabbro *(Patan)*	118.0 ± 12	Yamamoto and Nakamura (2000)
Garnet-granulite *(Patan)*	91.0 ± 6.3	Yamamoto and Nakamura (2000)
Garnet-granulite *(Patan)*	94.0 ± 4.7	Yamamoto and Nakamura (2000)
Garnet hornblendite *(Ganbir)*	83.0 ± 10	Yamamoto and Nakamura (2000)
Garnet-granulite *(S-Patan)*	95.7 ± 2.7	Anczkiewicz and Vance (2000)
Garnet-granulite *(Khwaza Khela)*	94.6 ± 5.3	Anczkiewicz and Vance (2000)
Method: Ar–Ar Hn		
Diorite *(N-Patan)*	85.8 ± 0.6	Zeitler (1985)
Sheared amphibolite *(S-Kamila)*	83 ± 1	Treloar et al. (1989b)
Sheared amphibolite *(S-Kamila)*	83 ± 3	Treloar et al. (1989b)

kyanite-pegmatites (Schaltegger et al. 2002) whose high-pressure assemblages (1.0–1.2 GPa) suggest cooling (510–600°C) during crustal thickening (Jan and Karim 1995).

To the southeast, a mylonitic to ultramylonitic zone pervaded by Southern Amphibolite tonalites delineates the top, northern boundary of a distinctly metamorphic unit that includes massive pyroxenites and which is

associated with the Sapat ultramafic rocks (Jan et al. 1993; Bouilhol 2008) (Fig. 10.1a). The 93.57 ± 0.1 Ma tonalite (Table 10.3) intrudes the mylonites, thus corroborating the relative antiquity of the Sapat metagabbroic unit within the frame of the arc history. Although the sample location is not precise enough to ascertain it, the Ar–Ar biotite age of 73.8 ± 0.7 seems to concern this unit, which would then have been cooling through 300–320°C at that time, like the Southern Amphibolites (Chamberlain et al. 1991).

The garnet-granulite (Jan and Howie 1980, 1981), often lumped with mantle rocks under the Jijal–Patan Complex designation, actually is a calc-alkaline gabbro intrusive, at the arc root level, into the uppermost lithologies of the sub-arc, reacted mantle (Burg et al. 1998). The intrusive contact (Fig. 10.10) is the lower boundary of the arc crust. Granulite facies overprint essentially marks isobaric cooling at 1.5 ± 0. 4 GPa from crystallization temperatures (≥950°C Yamamoto 1993; Ringuette et al. 1999) to metamorphic temperatures of T ~750°C. The granulite facies event was followed by cooling down to ca 550°C and decompression down to 0.33 GPa. The Sm–Nd mineral age of 118 ± 12 Ma from the top of the garnet-granulite was interpreted as dating the emplacement of the granulitic gabbro (Yamamoto and Nakamura 2000). Sm–Nd and Rb–Sr isochrons at c. 95 Ma date the cooling through ca 700°C (Yamamoto and Nakamura 2000; Anczkiewicz and Vance 2000).

10.3.3 Mantle

Separate occurrences of ultramafic-mafic rock associations, with differing ages, represent different types of mantle, all related to volcanic arc processes. Jijal and Sapat are direct hanging walls of the Indus Suture. The Chilas UMA occur as a string within the gabbro-norite. In these three locations, the relationships with neighbouring mafic rocks document mantle–crust transitions. Sporadic outcrops of ultramafic rocks in the northern area, close to the Karakoram–Kohistan Suture (Heuberger 2004, and unpublished mapping), require analytical work to be specified.

10.3.3.1 Jijal

The Jijal mantle section (Bard et al. 1980; Bard 1983b; Miller et al. 1991; Williams et al. 2004; Garrido et al. 2007; Dhuime et al. 2009) includes more than 3 km thick ultramafic rocks grading from garnet- and plagioclase-free replaced peridotites and a few pyroxenites dominate in the lowest part through an up-section increasing amount of websterite and pyroxenite within dunite and rare harzburgite to hornblendite and garnetite atop the sequence (Figs. 10.10 and 10.11). This rock succession represents the sub-arc mantle increasingly metasomatized upward by REE-depleted melts at ca 117 Ma (Dhuime et al. 2007). Pressure conditions are similar to those calculated from the overlying granulitic gabbro (Jan and Howie 1981).

10.3.3.2 Sapat

The up to c. 2 km thick Sapat mantle section exposes meta-harzburgites, dunites and pyroxenites (Jan et al. 1993; Arif and Jan 2006; Bouilhol et al. 2009) which are strongly serpentinised at their eastern tip, near Babusar Pass. They represent the refractory mantle below the lower-crustal metagabbros and trondhjemites that include pegmatitic pyroxenite bodies

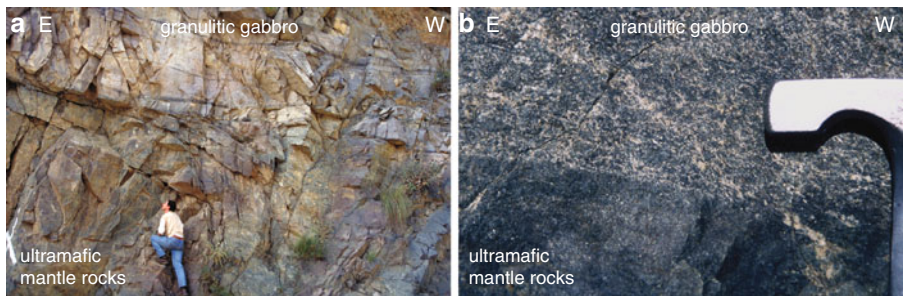

Fig. 10.10 Intrusive contact of the granulitic gabbro into mantle ultramafic rocks (**a**) outcrop scale (note enclaves and schlieren in the gabbro, and (**b**) detail showing the sharp contact between the ultramafic rocks and the overlying granulites cut by a feldspar vein (GPS: N35°04′19.9″; E072°57′55.5″). This outcrop was regrettably quarried in March 2005.

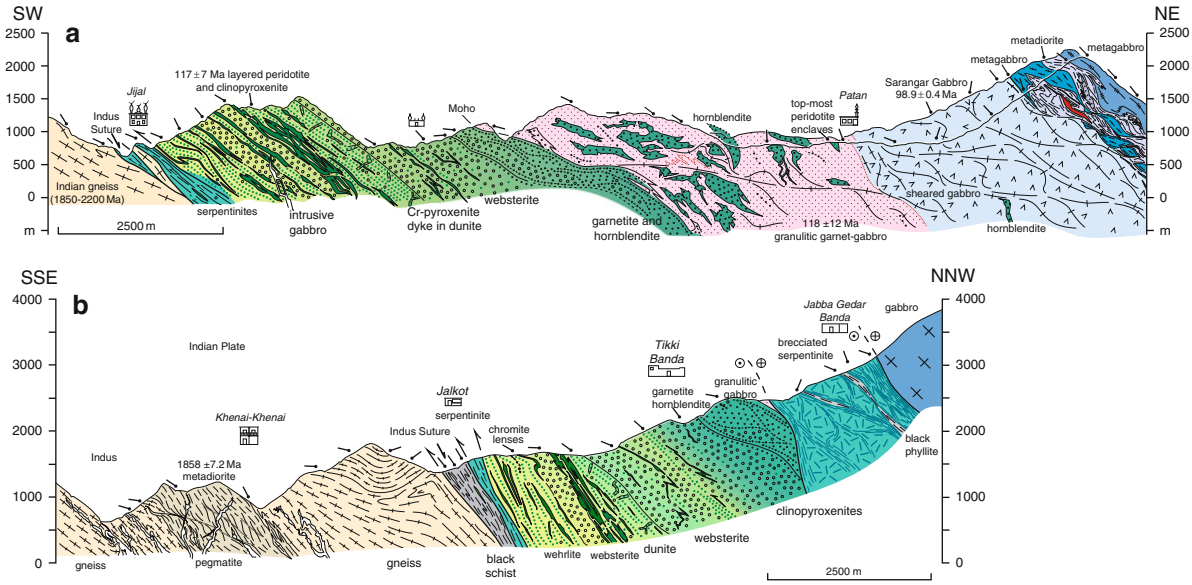

Fig. 10.11 Sections across the mantle–crust transition zone in the Jijal-Patan Complex of southern Kohistan (**a**) section line parallel to, and slightly west of the KKH-Indus Valley, upgraded from Burg et al. (2005); (**b**) section line parallel to, and slightly west of the Ranolia Khwar (Valley), upgraded from Zeilinger (2002).

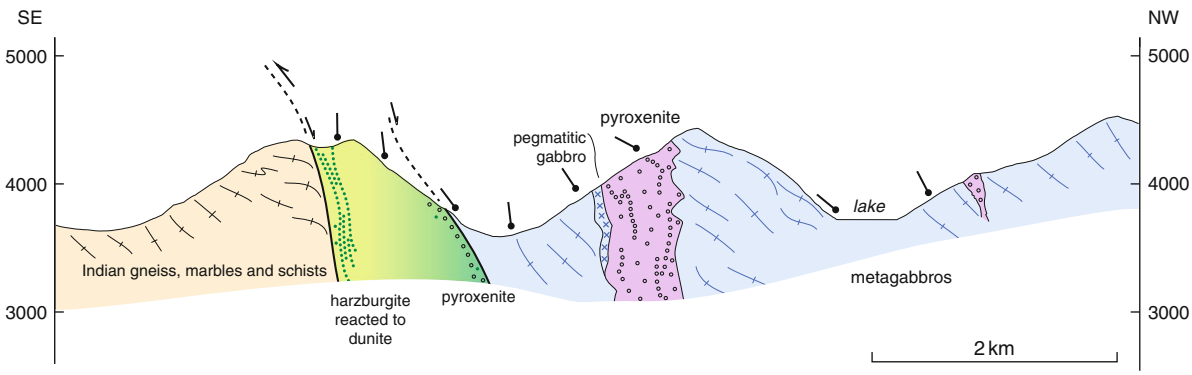

Fig. 10.12 Section across the mantle–crust transition zone in the Sapat Complex of southern Kohistan.

(Fig. 10.12). The contact between the ultramafic and metagabbro units is a ductile to brittle fault zone following, and locally deviating from the crust mantle transition. Field relations, micro-textures, bulk and mineral chemistry authenticate dunites to be the product of reactions between highly depleted (εHf ~ +16) primitive arc-melts and percolated meta-harzburgites (Bouilhol et al. 2009). Taking into account the highly refractory composition of the Sapat mantle, its structural position along the southern border of Kohistan, the evidence for interaction with highly depleted arc melts and the sub-solidus interaction with volatile-rich arc fluids, the Sapat ultramafic rocks are a distinct Kohistan unit ascribed to the frontal side of the arc. This ultramafic sequence differs from the sub-arc Jijal ultramafic section in terms of petrological significance and age (Sapat formed continuously between 106 and 99 Ma, Bouilhol 2008; Bouilhol et al. 2011).

A refractory mantle like the Sapat ultramafics occurs also in back-arc regions, but the structural position of the Sapat rocks in the south of the Kohistan arc excludes such an origin. Since this mantle portion has suffered extensive hydration upon cooling, due to fluids of supra-subduction origin, the Sapat ultramafic sequence and crust–mantle transition have likely formed during a magmatic episode affecting the most frontal part of the Kohistan arc.

10.3.3.3 Chilas

The ultramafic-mafic-anorthosite lenses in the Chilas gabbronorite were interpreted as the core of the already mentioned enormous antiform. This structural interpretation implied that the Jijal ultramafic rocks are deep level, metamorphic equivalents of the Chilas Complex (Coward et al. 1986). In fact, the scattered UMA outcrops represent intra-arc, lower-crustal mantle melt conduits emplaced during rifting of the Kohistan island-arc (Burg et al. 1998, 2006). Gravity-driven mesostructures and the orientation of hornblende-pegmatite swarms suggest that the steep attitude of the UMA (Fig. 10.13) is nearly original (Burg et al. 2006). Petrological and geochemical analyses indicate that the UMA and the surrounding gabbronorite originate from the same parental magma, but evolved along different mineral fractionation trends (Jagoutz et al. 2006, 2007). A Sm–Nd age of 100 ± 11 Ma was obtained from whole rocks and mineral separates of mafic and ultramafic rocks (Jagoutz et al. 2006). It is older than the ~85 Ma intrusion age of the gabbronorite and notably older than an internal gabbronorite Sm–Nd "errorchrone" (~70 Ma Yamamoto and Nakamura 1996). The age difference suggests enduring magmatic activity. These ages are further arguments to preclude any correlation with the 117 Ma Jijal and the 105 Ma Sapat ultramafic rocks.

10.4 Evolution of the Kohistan Island Arc

The wealth of information summarized in the previous paragraphs allows reassessment of the traditional interpretations.

10.4.1 Ages of Kohistan

A minimum age for initiation of subduction and subsequent installation of the proto-Kohistan arc is given by the 154 ± 0.6 Ma calc-alkaline Matum Das intrusion (Table 10.2), in temporal coincidence with the Mid Jurassic change in plate motions (Schettino and Scotese 2005).

The increasing contribution of slab melt components in magmas of the Jijal mantle rocks and overlying deep and mid crustal plutonic rocks between 117 and 90 Ma attests for active subduction at that time (Schaltegger et al. 2002; Dhuime et al. 2009; Bouilhol et al. 2011). This period was the major igneous event on the southern side of Kohistan, with pervasive metasomatism of the mantle, magma underplating and

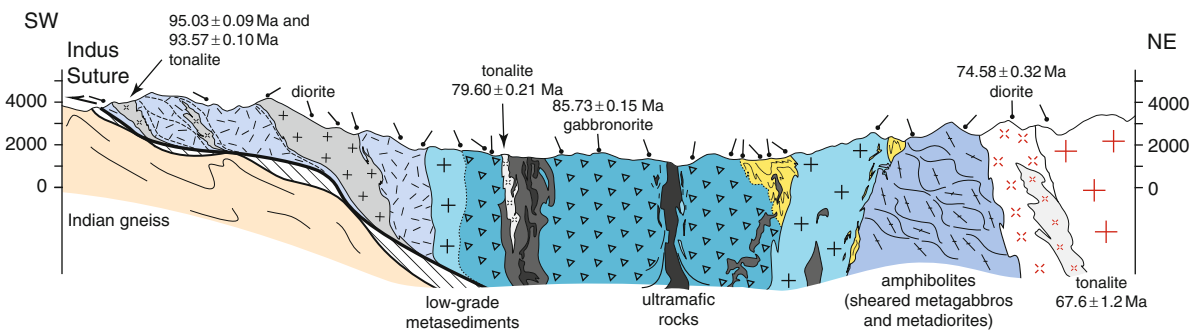

Fig. 10.13 Section across the Chilas Complex and adjoining lithologies (upgraded from Jagoutz et al. 2009).

granulite-facies metamorphism of deepest crustal rocks. Meanwhile, granites were generated by dehydration-melting of hornblende-rich, early plutonic rocks in the root of the arc. Granulite facies pressures indicate that the arc reached a nearly 50 km thickness resulting from underplating and within-crust intrusions and accumulation of lavas.

At about 100 Ma, on the northern shores of the Kohistan arc, subsidence rates exceeded growth rates and the carbonate platform was drowned. The deposition base initially close to sea level started to evolve in shallow water, feeding the adjacent depressions with calcareous debris and organic matter, which were rapidly buried by volcanoclastic turbidity currents in black shales.

At ~85 Ma, intra arc extension with associated decompression melting resulted in the voluminous intrusion of the Chilas Complex and related plutonic rocks (Khan et al. 1989; Schaltegger et al. 2002; Burg et al. 2006; Jagoutz et al. 2006, 2007). Extension was associated with intra-arc basins (e.g., the intruded sequences) which remained marine until at least Eocene times (fossil-bearing limestone). The forearc interpretation for the within-Kohistan, basins was only supported by similarity of detrital sediments with sediments off the coasts of present-day magmatic arcs (Sullivan et al. 1993). This comparison is not discriminatory since similar turbidites are also common in back-arc basins (Bahk and Chough 1983; Taylor 1995). Therefore, following Treloar et al. (1996) and, owing to their geographic distribution in Kohistan, the intruded sequences should represent remnants of an (or several) intra-arc basin(s).

Still, geochemistry shows that Chilas magmas derived from mantle wedge with a slab-derived component increasingly present in plutonic rocks dated up to 42 Ma (Petterson and Windley 1991; Jagoutz et al. 2007, 2009). These plutonic rocks have permanently intruded earlier plutonic, volcanic and sedimentary sequences present in and on the arc, and this protracted plutonism is responsible for deformation and metamorphism found with different intensity and grades throughout the Kohistan Batholith. The significance of the <42 Ma, unconformable lavas remains unclear, owing to the lack of detailed work. The confluence aplites and granites at 30 Ma (U–Pb age, Parri granite, Table 10.2) may sample molten, Indian continental crust.

The duality of Kohistan is a clear result of the systematic dating program. The Southern Amphibolites are all between ca 120 and 75 Ma (Table 10.3). Ar–Ar cooling ages on hornblendes cluster around 83 Ma (Treloar et al. 1989b).

Ages in the Kohistan Batholith span the whole range 150–30 Ma, 150–40 Ma if one excludes the non-subduction related 30 Ma granites and aplites (Table 10.2).

This bears an important consequence: magmatism ceased to the south of the Chilas Complex during the Late Cretaceous while it covers a wider time span to the north of the Chilas Complex, where all young lavas are also preserved.

10.4.2 Subduction Polarity

The geometry of paleo-subduction zones is generally inferred from structural, kinematic and geochemical data. Structural and kinematic data take into consideration the framework of the main tectonic units along with their relative movements. Geochemistry typifies and dates magmatism and its chemical evolution on either side of the considered suture, whether it exposes ophiolites or not. These criteria are now discussed for the two suture zones that border Kohistan.

10.4.2.1 Karakoram–Kohistan Suture

The significance of the KKS in terms of subduction polarity is disputed. Taken at face value, the position of the Karakoram Batholith alone requires that the slab was dipping underneath this continental margin of Asia. However, structural evidence is more complex, with north-vergent structures and strike-slip faulting obscuring earlier events and showing that Kohistan was transported over Karakoram, at least in places (Coward et al. 1986, 1987; Heuberger 2004).

Timing constraints placed by the intrusion of the calc-alcaline, composite batholith on the Karakoram margin point to initiation of subduction at about 130 Ma (Heuberger et al. 2007); this magmatism seems to have stopped at ca. 95 Ma (Le Fort et al. 1983), which would be the age of cessation of subduction but not the end of tectonic activity along the Karakoram–Kohistan suture. It does not mark the end of magmatic activity in the Kohistan arc either, which lasted until 40–30 Ma ago (Table 10.2). Apatite

fission track ages indicate that, away from the Nanga Parbat Syntaxis, no or little vertical differential movement has taken place along this fault zone since 11–13 Ma (Heuberger et al. 2007).

The volcanic record further clarifies the subduction geometry. On the Karakoram side, across the suture, no calc-alkaline magmatism is younger than 95 Ma. Conversely, the unconformable volcanic rocks and ca. 50 Ma metagabbros on the Kohistan side (Table 10.2) should indicate subduction beneath northern Kohistan until 45–35 Ma, later than the accepted closure of the "main" subduction along the Indus Suture. Admittedly, this age and space distribution does not specify the subduction polarity but raises the question whether there was a flip between 95 and 50, which would explain structural observation of north-vergent thrust zones and folds and be consistent with the existence of intra-arc or inter-arc oceanic basins hosting Eocene–Paleocene fossiliferous limestones and other sediments in the (Kohistan) hanging wall plate. A long-lasting and complex closure history of the Karakoram–Kohistan suture would give reasons for the recurrent dispute on the collision time and geometry of this zone, also along its eastern, Shyok continuation.

This working hypothesis implies that cessation of Cretaceous subduction beneath the Karakoram was no collision but perhaps a renewed sedimentation history of the basin. This proposition is consistent with the post- 100 Ma Yasin sediments grading into a deep marine basin between the late-Cretaceous Kohistan and Karakoram margins. It further fits the alkaline magmatism at 88 ± 4 Ma that dates extension within the Karakoram margin as ultimate magma products of "subduction-related" plutonism (Debon and Khan 1996). This latter point has several consequences:

1. It casts doubts on the relationship between deformation in Kohistan and collision along the KKS: It is difficult to imagine intense compressional stresses and strain between two coeval extensional sites as Karakoram and Chilas at 90–85 Ma.
2. It raises the question as to what may have stopped subduction below Karakoram around 95 Ma. A possibility is that there was no more oceanic lithosphere to subduct and that the arrival of the Kohistan arc in the trench halted subduction, for buoyancy reasons. This event would fit the "gentle docking" envisioned in models that placed closure of the KKS between 102 and 75 Ma. Alternatively, this situation leaves the forearc basin of Karakoram open, even if it is somewhat deformed.
3. Then when did the northern oceanic domain close and how? If it were relatively small, it may have closed later without lithospheric subduction. If the basin was large (which would be the case if the high-Mg basalts do represent the installation of a spreading center, as evoked by (Bignold and Treloar 2003), there has been subduction. In the absence of evidence on the Karakoram side, a second subduction may well have been dipping below Kohistan. South-dipping subduction along this suture has been a proposal in various models (Jan and Asif 1981; Andrews-Speed and Brookfield 1982; Khan et al. 1997). This scenario is discussed in the next section. For the moment we retain that structural, kinematic and geochronological evidence are ambiguous from ca. 85 to ca 12 Ma. The 11–13 Ma age is a bound from similar fission track apatite ages on both sides of the KKS (work in progress); these ages show that the rocks on either side passed the apatite partial annealing zone together; accordingly, no or little vertical differential movement has taken place along this fault zone since the late Miocene.

10.4.2.2 Indus Suture

Trace element and isotopic compositions of Kohistan igneous rocks express an increasing slab component with time and demonstrate that the juvenile arc formed away from any old, continental influence, hence likely above an intra-oceanic subduction zone (e.g., Petterson and Windley 1985, 1991; Treloar et al. 1996; Khan et al. 1997; Bignold et al. 2006). The general morphology of the Indus suture, with Kohistan over India and tectonic slivers of ophiolites, accretionary wedge sediments, blueschists, and southward senses of shear in deformed rocks (Kazmi et al. 1984; Treloar et al. 1989a; Anczkiewicz et al. 1998) documents the north-dipping subduction that most investigators agreed upon. These ophiolites, imbricate "mélange" and blueschists signal a major suture zone. Accordingly, there is little doubt that the Indus Suture absorbed most of the Tethys oceanic lithosphere over Mesozoic times and that the corresponding subduction was plunging beneath Kohistan. This conclusion is consistent with tectonic interpretations of the eastern

continuations of this suture in Ladakh (e.g., Rolland et al. 2000) and farther east in South Tibet (e.g., Allègre and 34 co-authors 1984; Yin and Harrison 2000).

10.5 Tectonic Model for Kohistan Arc Collisions with Asia and India

Several workers suggested that the Karakoram–Kohistan–Shyok Suture originated earlier than the Indus Suture (Frank et al. 1977; Coward et al. 1982; Petterson and Windley 1985; Treloar et al. 1996; Searle et al. 1999). Others favoured a younger age (Tahirkheli 1979; Klootwijk et al. 1979; Brookfield and Reynolds 1981; Thakur 1981; Bard 1983b).

The tectonic model that the author tends to consider is illustrated in Figs. 10.14–10.19. Besides considering geological and geochemical constraints, it satisfies magnetic and paleomagnetic constraints: (1) northward movement of India with respect to Eurasia reflects the existence of subduction zones in the Tethys Ocean during the magnetic quiet zone at about 120 Ma (Schettino and Scotese 2005); (2) India continued to move rapidly north until about 50 Ma ago (Patriat and Achache 1984; Klootwijk et al. 1992); (3) India then continued to move north at a much slower rate, which implies several hundred kilometres of tertiary convergence for completion of suturing and intracontinental shortening (Besse et al. 1984; Schettino and Scotese 2005).

10.5.1 Double, North-Dipping Subduction

The first constraint is that any model requires double subduction during Early Cretaceous times (130–95 Ma) because arc-related magmatism of that age is established within both the Karakoram Eurasian margin and Kohistan. The simplest solution would plead that both were attached and represent the same arc. This is not sustainable because paleomagnetic data indicate that Karakoram and Kohistan were thousands of kilometres apart and geochemical data demonstrate a Karakoram continental basement while Kohistan was installed on an oceanic lithosphere.

Khan et al. (1997) suggested that the juvenile arc was generated above a south-dipping subduction zone. Their model implies that the major oceanic basin, between Karakoram and Kohistan, closed between two subduction zones, one dipping north beneath Karakorum and the other dipping south beneath Kohistan. This tectonic system is intrinsically plausible as exemplified by coeval and opposite subduction systems presently closing the Molucca (Silver and Moore 1978; Hall and Wilson 2000) and Adriatic (e.g., Doglioni et al. 2007) Seas. This system tolerates ending subduction below Karakoram at about 95 Ma but does not explain what happens with the south-dipping subduction below the Kohistan island arc. The model requires that the Kohistan island arc was attached to the leading front of northward-moving Indian plate. All data point to the existence of a large oceanic basin

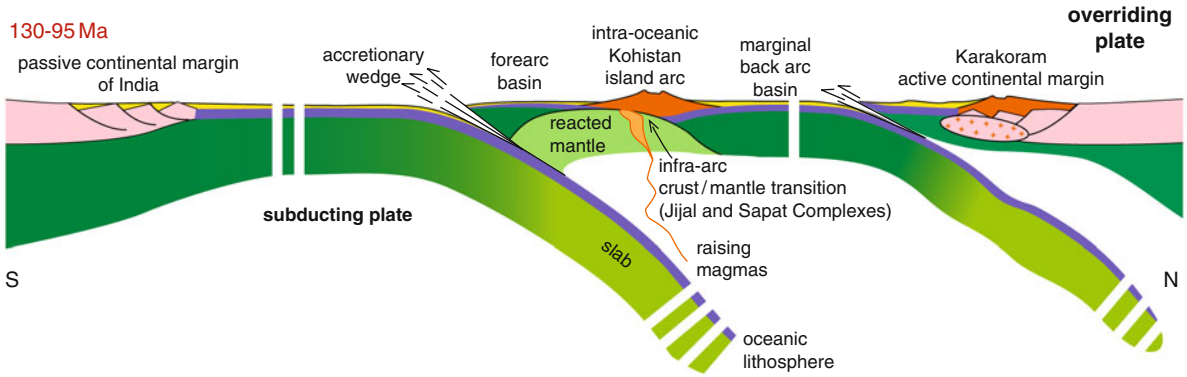

Fig. 10.14 Tectonic setting of Kohistan between two, north-dipping subduction zones in Cretaceous times.

Fig. 10.15 Structural relationship between plutons of the Kohistan Batholith (GPS: N35°59′20.4″; E074°19′35.4″); note that the foliated rock (*bottom* part of image, below the hammer) is younger than the non-foliated rock (*top-left* part of picture).

between India and Kohistan, and the ensuing Indus Suture has to be closed at some stage. Geochemical arguments for this solution were disputed by Bignold and Treloar (2003). It is therefore difficult to admit south-dipping subduction (actually double, divergent subduction) in the Cretaceous KKS. Consequently, perhaps conservatively, it is more consistent to accept the classical model of two parallel, north-dipping subduction zones in Early Cretaceous times, one along the KKS and one along the Indus Suture (Fig. 10.14).

10.5.2 Continental Arc–Island Arc Docking: Karakoram–Kohistan

Geological evidence from Karakoram suggests that the KKS subduction zone choked by ca 95 Ma. To accommodate the lack of evidence for subduction of a large oceanic tract, Pudsey (1986) argued that the KKS represented a collapsed back-arc basin. However, this argument can be answered with a non-accretionary margin (Stern 2002) along Karakoram and cessation of subduction does not mean that the two arcs fully collided.

The timing of collision of the Kohistan arc with the Eurasian active margin remains contentious because constraints, mostly imported from the eastern Shyok segment, are partly controversial. Using structural-metamorphic arguments, Tahirkheli (1979) and Bard (1983b) considered closure of the Karakoram–Kohistan Suture to postdate collision with India at 60–50 Ma; paleomagnetic data support this interpretation (Khan et al. 2009). Conversely, closure of the KKS before that of the Indus Suture was inferred from structural observations and few Rb–Sr whole rock ages (Petterson and Windley 1985, and many followers). The argument was essentially based on the assumption that only collision between Karakoram and Kohistan could produce foliation and metamorphism older than India–Asia collision at 60–50 Ma, even older than the 85 Ma Chilas gabbronorite. However, this interpretation minimizes the role of widespread and long-lasting plutonism as a thermal and strain source. The assumption that foliated rocks must be older than non-foliated rocks is wrong when it concerns plutonic rocks, as field observation can prove (Fig. 10.15). Consequently, the contention that the suture must have formed between 102 and 75 Ma is poorly constrained.

This discussion leaves open the question between cessation of convergence / subduction and full closure of the basin with collision of the Karakoram forearc with the Kohistan back arc. Structural and geochronological data show that tectonic and magmatic activity along the KKS existed until ca 30 Ma, and the time gap leaves time to close the 95 Ma remnant oceanic basin, which comprised at least the Karakoram forearc. By comparison with modern continental forearcs, the width of this basin could have been anything from a 50 km wide straight to a more than 500 km wide sea.

Several hypotheses are allowed for the fate of the KKS slab. Breakoff would trigger important magmatism and strong isostatic rebound of both plates (e.g., Gerya et al. 2004). There is no evidence for either sign. Numerical simulation of double subduction shows that both thermal absorption and/or eduction (reversed subduction) are possible (Fig. 10.16). In the latter case, one would expect exhumation of high-pressure rocks and prominent evidence for top-to the-north sense of shear. Since both are lacking in the KKS, the slab has likely faded through thermal dissipation.

10.5.3 Arc Rifting: Slab Rollback

The magmatic structures of the Chilas gabbronorite and associated plutonic rocks document a bulk south-dipping extensional system (Burg et al. 2006).

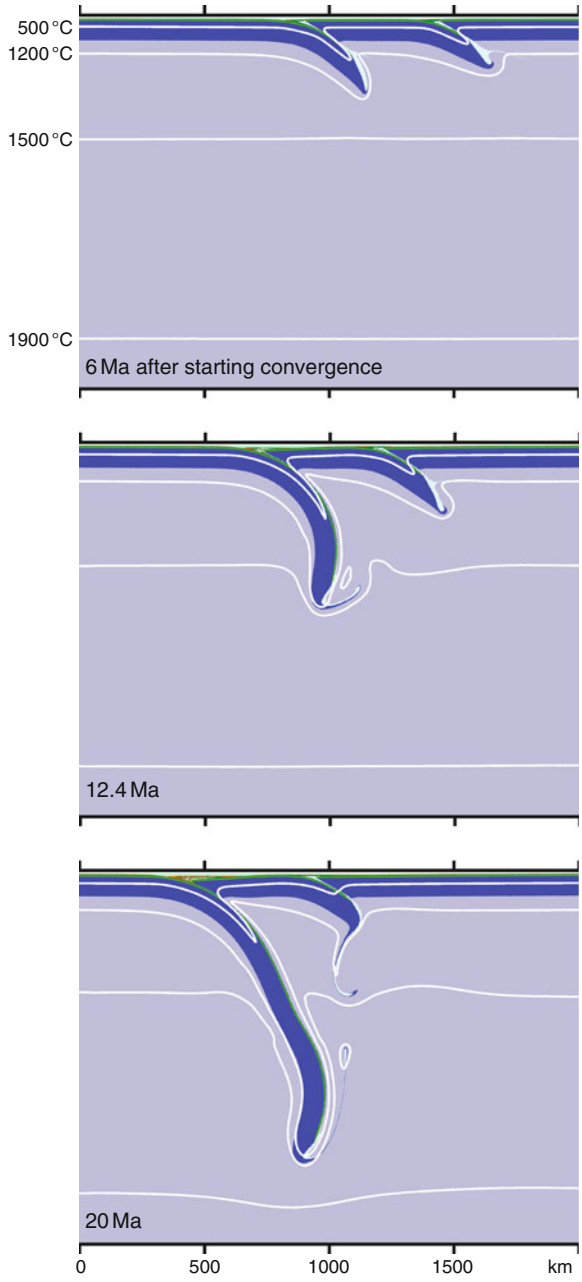

Fig. 10.16 Numerical models of double subduction: Unpublished stages of experiment 14 of Mishin et al. (2008). Lithosphere age = 50 Ma. Note eduction (un-subduction) of the right-side slab between 12.4 and 20 Ma, once roll back of the main slab absorbs total convergence.

Structural observations support geochemical and petrological arguments for arc rifting at the time of emplacement, ca 85 Ma ago (Khan et al. 1989; Jagoutz et al. 2006). Contemporaneous alkaline plutonism in Karakoram (Debon and Khan 1996) suggests that the whole system was then extensional. Structural, petrological, geochemical and geochronological signatures are sufficient to accept that Kohistan was split along its length into two parts; within arc, restricted marine basins (those that host the "intruded") existed in between (Fig. 10.17). The general north-dipping attitude of the Southern Amphibolites (Fig. 10.1b) and their partial exhumation (regionally distributed $^{39}Ar/^{40}Ar$ cooling/unroofing ages at 83–80 Ma, Treloar et al. 1989a) are attributed to extensional tilting. This (gravitational collapse?) event marks the end of magmatic activity in this part of the arc.

Structural, petrological, geochemical and geochronological data are also sufficient to exclude a wide separation and a ridge between an active and a remnant arc component. One could argue that extension was focused in the bigger back-arc now disappeared within the Karakoram–Kohistan Suture. This rifted basin could be compared to the Woodlark Basin, with its lateral transition from continental to oceanic rifting (e.g., Taylor et al. 1995, if the high-Mg basalts in the Karakoram Kohistan Suture do represent a spreading center and if the Kohistan–Ladakh system was anchored to a continent to the east (Rolland et al. 2000). In addition to lack of evidence, this eventuality would complicate final closure of the KKS in which, in any case, no ophiolite has been found, so far.

The crustal thickness of Kohistan was ca 50 km sometime around 100 Ma (granulites) and was reduced, at least locally, to 20–25 km during extension (depth of Chilas). The narrow, thick arc of earlier times is comparable to the 50–55 Ma old Aleutian arc (e.g., Holbrook et al. 1999). The extended, hence wider and thinner Kohistan Arc can be compared to the mature, 48 Ma old Izu-Bonin arc (e.g., Takahashi et al. 1998).

In view of modern references such as the Lau Basin behind the Tonga Trench (e.g., Martínez and Taylor 2002) and the Mariana Trough and Trench (e.g., Taylor 1995; Takahashi et al. 2007), rifting apart Kohistan was tentatively linked to rollback (Treloar et al. 1996; Burg et al. 2006). Rollback of the Tethys oceanic slab may have started as early as 105 Ma ago (Kapp et al. 2005), which coincidentally is the age of the Sapat Complex. Slab rollback and subsequent widespread extension in the hanging wall plate can also have

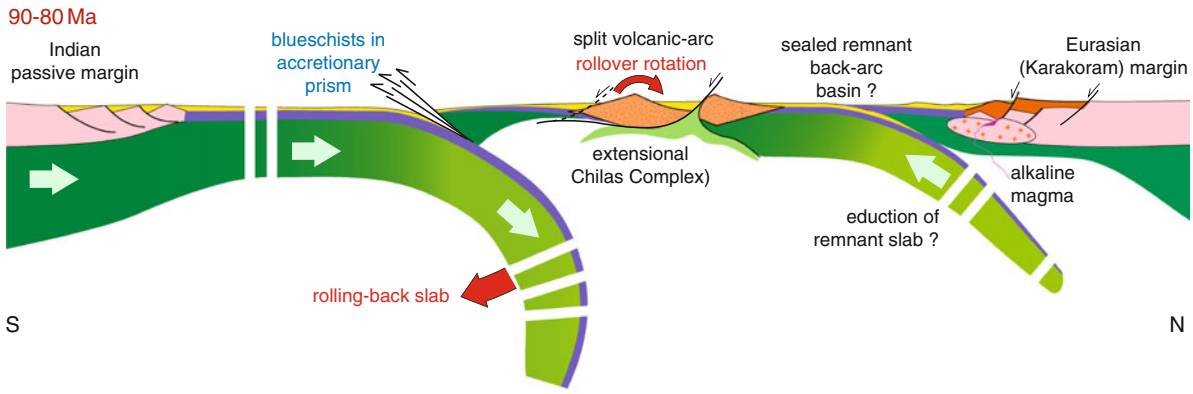

Fig. 10.17 Tectonic interpretation across the Kohistan island arc in Late Cretaceous times. Eduction along the Karakoram–Kohistan Suture inferred from models, Fig. 10.16.

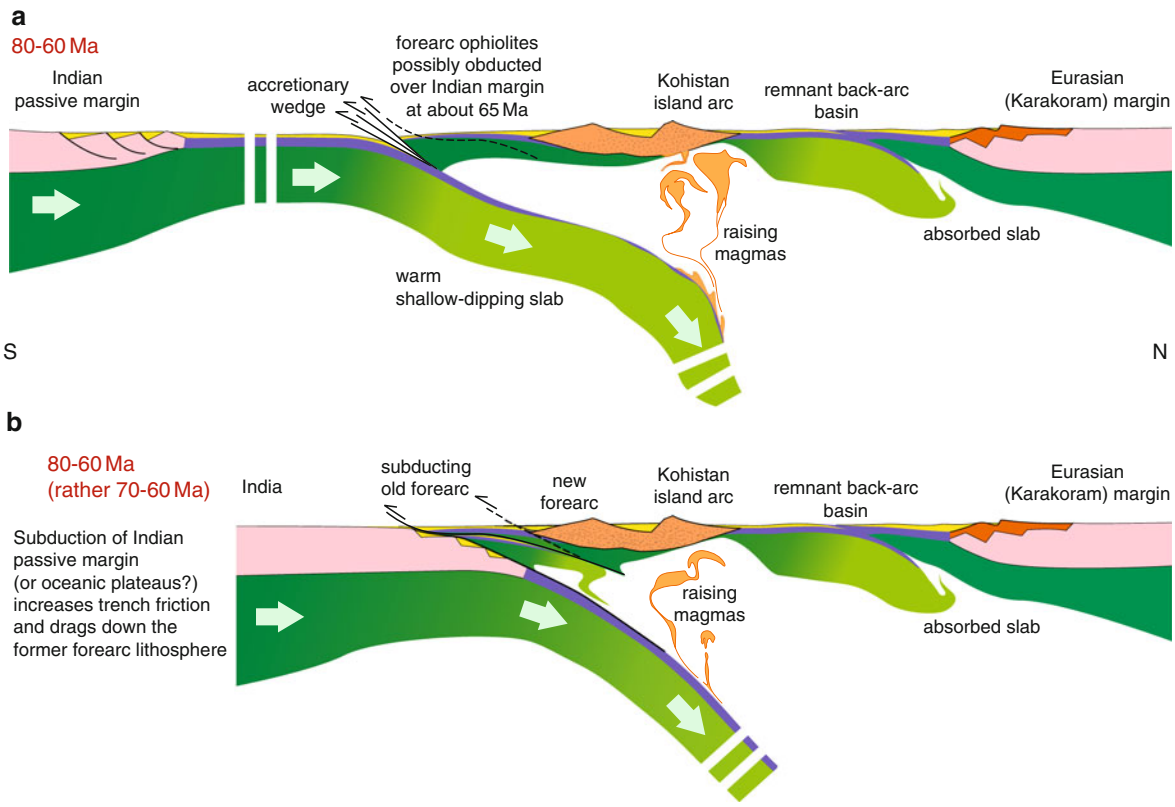

Fig. 10.18 Tectonic interpretations across the Kohistan island arc in Late Cretaceous – Paleocene times. The two scenari (**a** and **b**) are discussed in the text. Note that arrival of oceanic plateaus into the trench could also drag down the forearc lithosphere as in (**b**), although the leading edge of India would be far from the trench, as in (**a**).

(1) favoured exhumation of the blueschists in the accretionary wedge of the Indus Suture, between 90 and 80 Ma (Anczkiewicz et al. 2000) and (2) triggered cessation of the KKS subduction, which became kinematically unnecessary.

10.5.4 Single Subduction

The large amount of convergence and the fast rate at which India drifted over late-Cretaceous–Paleocene

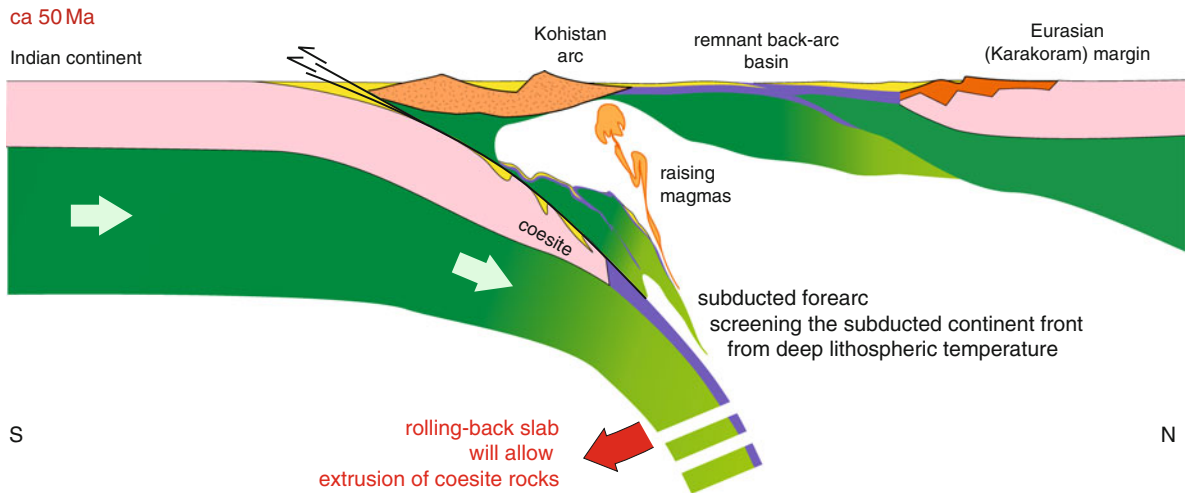

Fig. 10.19 Tectonic interpretation across the collisional system Karakoram/Kohistan island arc/India in early Eocene times.

times (Fig. 10.3) are obvious sources for the post-80 Ma, abundant magmatism in the previous rear-arc now represented by the Kohistan Batholith.

If the arc-trench gap depends on the dip angle of subduction (e.g., Condie 1997; Kearey et al. 2009), then northward shift of the magmatic front in Kohistan can be due to flattening of the slab. One mechanism for flat-slab subduction is buoyancy (e.g., Uyeda 1984). Either young Tethys lithosphere became subducted, marking the approach and entry of the oceanic ridge into the trench, or a submarine plateau made the flat portion of the subducted Tethys plate. Another mechanism for a shallow angle of descent is trench rollback due to fast convergence rate (Christensen 1996; van Hunen et al. 2000).

Assessing the contribution of each of these two mechanisms is difficult. For simplicity, and because it is sufficient and data-supported, fast convergence alone is involved in the interpretation drawn in Fig. 10.18a. A corollary is contemporaneous roll back, which may actually have been active until 55–50 Ma to allow space for extrusion of ultra-high pressure crustal slivers of the Indian leading edge within the trench region (O'Brien et al. 2001; Kaneko et al. 2003, Fig. 10.19).

Analogue modelling of intra-oceanic subduction systems (Boutelier et al. 2003) offers an additional explanation for the temporal and spatial variation of magmatic activity: The magmatic front might move with the trench while the forearc is subducted (Fig. 10.18b). Forearc subduction would explain the scarce evidence for it and the accretionary wedge, the absence of large ophiolite nappes (they would derive from the hanging plate of the subduction system, Fig. 10.18a) along with the relatively cold temperatures recorded by deeply subducted parts of the Indian continent (Fig. 10.19). A complex balance of subduction rates in front of and at the back of the forearc would allow coeval slab rollback while the old frontal arc (the Southern Amphibolites, including Jijal and Sapat complexes) became the new forearc.

10.5.5 Arc–Continent Collision: Kohistan–India

At ca 55 Ma, tectonic interaction between the continental parts of India and Asian began and frontal parts of the Indian continent were subducted down to the coesite stability field before 45 Ma (Kaneko et al. 2003; Parrish et al. 2006). Arc magmatism was still active, generated from the main Tethys slab or/and from the oceanic forearc (Fig. 10.19). Buoyancy resistance of the subducting Indian continent built up stresses to enter into a high compressional regime (Chemenda et al. 1996; Beaumont et al. 1996). This corresponds to the marked slowdown (ca 20 to ca 5 cm/a) in the northward migration of India toward Asia at this time (Klootwijk et al. 1992). In the light of

events reported on both sides of the Asia–Kohistan–India system, in Waziristan (Beck et al. 1996) and Ladakh (Green et al. 2008; Searle and Treloar 2010), obduction was a precursor phase that started at about 65 Ma (Anczkiewicz et al. 1998).

10.5.6 Collision: Closure of All Basins

Increases horizontal stresses in the system lead to its total closure until locking of the sutures in Eocene–Miocene times, as suggested by earlier authors (Brookfield and Reynolds 1981; Reynolds et al. 1983).

Along the KKS, metamorphic rocks are low grade and no ophiolite is known: ultramafic rocks are serpentinites from the Karakoram forearc. The most efficient solution to close the remnant basin while avoiding burial of exposed rocks consists in underthrusting most of the Karakoram forearc below Karakoram and most of the Kohistan backarc below Kohistan (Fig. 10.20). Flip with new subduction below the arc is a process supportively obtained in analogue models (Chemenda et al. 2001). Since the KKS basin was not very wide, the amount of convergence partitioned between the two opposite systems was too small to produce lithospheric subduction, at least below Karakoram. Divergent underthrusting deserves consideration on several levels: (1) it provides ultimate southward "subduction" that may have produced the unconformable, Eocene lavas and the 30 Ma plutons; (2) it is consistent with both south- and north-vergent structures described in the KKS; (3) late locking of this basin would explain Eocene– Miocene

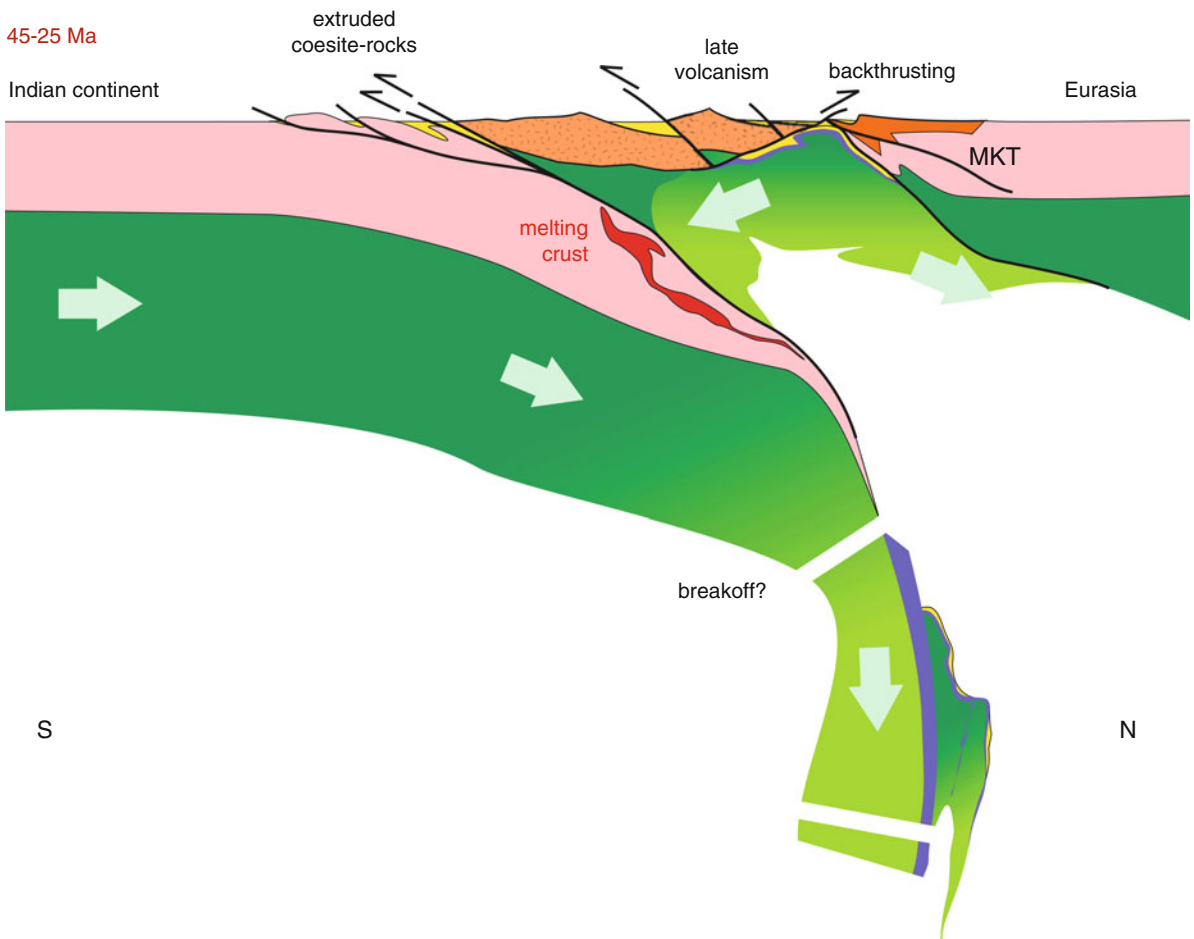

Fig. 10.20 Tectonic interpretation across the collisional system Karakoram/Kohistan island arc/India in Eocene – Oligocene times. Breakoff is inferred from an event suspected in Ladakh (Mahéo et al. 2009) and the Himalayas (Chemenda et al. 2000), but for which direct evidence is not known on the Kohistan section.

thrusting (the Main Karakoram Thrust = MKT on Fig. 10.20) and wrenching during metamorphism in the Karakoram block, next to the KKS and in the eastern parts of Karakoram (Fraser et al. 2001; Searle et al. 2010); and (4) it is consistent with terrestrial fauna trespassing the Shyok Suture in Eocene–Oligocene times (ca. 38 Ma) only (Sharma 1987). Acceptably, some of the 40–30 Ma granitic stocks and dykes were formed by partial melting processes of the Indian plate and/or back arc sediments, and of the arc crust and underlying mantle.

Within-arc basins with till Eocene sedimentation were likely inverted at that time (Fig. 10.20).

Drag folds and shear sense criteria particularly abundant in low-grade, graphitic schists of the suture zone indicate top-to-the-north normal movement (Burg et al. 1996; Vince and Treloar 1996; Anczkiewicz 1998). These structures are attributed to upward extrusion of the deeply subducted and buoyant continental rocks thrust over the incoming tail of the Indian continent (Anczkiewicz et al. 1998; O'Brien et al. 1999; Treloar et al. 2003). This is an important part of the Himalayan deformations that will further develop with syn- and post-metamorphic thrust imbrication at the expenses of the Indian continent (Treloar et al. 1989a), with cooling through 500°C between 40 and 35 Ma (Treloar et al. 1989b).

Apatite fission track ages indicate that suturing and basin closure were achieved by ca 15 Ma along both the KKS (Heuberger et al. 2007) and the Indus Suture (Zeitler 1985; Zeilinger et al. 2007).

10.6 Conclusion

Kohistan geology establishes the existence of a fossil, obducted island arc. It also establishes the unstable life of such an arc, punctuated by important variations in tectonic settings and magmatic production and location. From the Jijal and Sapat mantles upward to the metasediments and metavolcanic rocks exposed to the south of the Chilas Complex, there already is a "complete" crustal section through an island arc. There is another "complete" section from the Chilas UMA to the metasediments and metavolcanic rocks included in the Batholith. Complete means that these sections contain lower, middle and upper crustal elements expected to be seen in the island arc; however, metamorphism and tectonism are pervasive to the point that it can nowhere be said that the crustal sections are intact. One could counter that, conversely, the intense, syn-metamorphic fabrics is integral part of an arc. Flat seismic reflectors recorded in present-day systems (e.g., Holbrook et al. 1999; Iwasaki et al. 2002; Takahashi et al. 2007) might delineate this bulk shear fabric.

An important part of the Kohistan history involves arc-normal extension as arc-building process at a mature stage. The older crustal components are, in general, preserved in the southern, frontal part; the corresponding Southern Amphibolites preserve only crustal formation processes for the period before rifting occurred. On the other hand, a more complete history of crustal formation is preserved in the northern, rear part (the Kohistan Batholith). An old arc system might be represented by rare, very old plutonic rocks such as Matun Das, which crystallized about 70 Ma earlier before most of the other plutonic rocks of the Batholith. The corresponding proto-arc might document instabilities during the wrenching, sinistral drift of Gondwana with respect to Eurasia.

This presentation is limited to Kohistan because along-island-arc variations towards Ladakh can be expected. However, some tectonic processes should be shared. In particular, the model discussed here does not stop activity of the north-arc suture with Cretaceous "soft collision". Two temporally unrelated events explain and reconcile a long-lasting controversy. The northbound of "Greater India" reached the intraoceanic island arc during the Paleocene. Early continental subduction refers to obduction and progressively increased horizontal stresses until compression was strong enough to trigger full collision and close all oceanic basins during Eocene–Miocene times. Cessation of calc-alkaline magmatism in Kohistan signs the waning stages of this full collision while high-stress continental collision begins.

Aknowledgements The author has carried out and supervised geological investigations on Kohistan over more than 15 years. This contribution summarizes his personal view stemming out of this effort shared with Master and PhD students and collaborators in Pakistan, in particular Prof. N.M Chaudhry from Lahore, and S.S. Hussain and H. Dawood from the Museum of Natural History at Islamabad. All were co-authors of publications referred to in this synthesis and all participated in developing the ideas presented here. G. Stampfli generously helped in generating Fig. 10.2. Pointed reviews from Mike Searle and Paul Ryan have been essential to improve this presentation of the Kohistan Arc.

References

Allègre CJ, 34 co-authors (1984) Structure and evolution of the Himalayan-Tibet orogenic belt. Nature 307:17–22

Anczkiewicz R (1998) Structural and geochronological study of the India-Kohistan arc collision, Lower Swat region of Pakistan, NW Himalaya. PhD, # 12771, ETH, Zürich

Anczkiewicz R, Vance D (2000) Isotopic constraints on the evolution of metamorphic conditions in the Jijal-Patan complex and the Kamila Belt of the Kohistan arc, Pakistan Himalaya. In: Khan MA, Treloar PJ, Searle MP, Jan MQ (eds) Tectonics of the Nanga Parbat syntaxis and the western Himalaya, vol 170. Geological Society Special Publication, London, pp 321–331

Anczkiewicz R, Burg J-P, Hussain SS, Dawood H, Ghazanfar M, Chaudhry MN (1998) Stratigraphy and structure of the Indus Suture in the Lower Swat, Pakistan, NW Himalaya. J Asian Earth Sci 16 (2-3):225–238. doi:10.1016/S0743-9547(98)00003-8

Anczkiewicz R, Burg J-P, Villa IM, Meier M (2000) Late Cretaceous blueschist metamorphism in the Indus Suture Zone, Shangla region, Pakistan Himalaya. Tectonophysics 324 (1–2):111–134

Anczkiewicz R, Oberli F, Burg J-P, Villa IM, Günther D, Meier M (2001) Timing of normal faulting along the Indus Suture in Pakistan Himalaya and a case of major $^{231}Pa/^{235}U$ initial disequilibrium in zircon. Earth Planet Sci Lett 191 (1-2): 101–114. doi:10.1016/S0012-821X(01)00406-X

Andrews-Speed CP, Brookfield ME (1982) Middle Paleozoic to Cenozoic geology and tectonic evolution of the northwestern Himalaya. Tectonophysics 82 (3-4):253–275

Arbaret L, Burg J-P, Zeilinger G, Chaudhry N, Hussain S, Dawood H (2000) Pre-collisional anastomosing shear zones in the Kohistan arc, NW Pakistan. In: Khan MA, Treloar PJ, Searle MP, Jan MQ (eds) Tectonics of the Nanga Parbat Syntaxis and the Western Himalaya, vol 170. Geological Society Special Publications, London, pp 295–311

Arif M, Jan MQ (2006) Petrotectonic significance of the chemistry of chromite in the ultramafic–mafic complexes of Pakistan. J Asian Earth Sci 27 (5):628–646. doi:10.1016/j.jseaes.2005.06.004

Bahk KS, Chough SK (1983) Provenance of turbidites in the Ulleung (Tsushima) back-arc basin, East Sea (Sea of Japan). Journal of Sedimentary Research 53 (4):1331–1336

Bard J-P (1983a) Metamorphic evolution of an obducted island arc: Example of the Kohistan sequence (Pakistan) in the Himalayan collided range. Geol Bull Univ Peshawar 16:105–184

Bard J-P (1983b) Metamorphism of an obducted island arc: Example of the Kohistan sequence (Pakistan) in the Himalayan collided range. Earth Planet Sci Lett 65:133–144

Bard J-P, Maluski H, Matte P, Proust F (1980) The Kohistan sequence: Crust and mantle of an obducted island arc. Geological Bulletin of the University of Peshawar 11:87–94

Beaumont C, Ellis S, Hamilton J, Fullsack P (1996) Mechanical model for subduction-collision tectonics of Alpine-type compressional orogens. Geology 24 (8):675–678. doi:10.1130/0091-7613(1996)024<0675:MMFSCT>2.3.CO;2

Beck RA, Burbank DW, Sercombe WJ, Khan AM, Lawrence RD (1996) Late Cretaceous ophiolite obduction and PalEocene India-Asia collision in the Westernmost Himalaya. Geodinamica Acta 9 (2-3):114–144

Bender FK, Raza HA (1995) Geology of Pakistan, vol 25. Beträge zur regionalen Geologie der Erde. Gebrüder Borntraeger, Berlin

Besse J, Courtillot V (1988) Paleogeographic maps of the continents bordering the Indian Ocean since the early Jurassic. J Geophys Res 93 (B10):11971–11808

Besse J, Courtillot V, Pozzi J-P, Westphal M, Zhou YX (1984) Paleomagnetic estimates of crustal shortening in the Himalayan thrusts and Zangbo suture. Nature 311 (5987):621–626

Bignold SM, Treloar PJ (2003) Northward subduction of the Indian Plate beneath the Kohistan island arc, Pakistan Himalaya: New evidence from isotopic data. J Geol Soc London 160 (3):377–384

Bignold SM, Treloar PJ, Petford N (2006) Changing sources of magma generation beneath intra-oceanic island arcs: An insight from the juvenile Kohistan island arc, Pakistan Himalaya. Chem Geol 233:46–74

Bouilhol P (2008) Structural, petrological and geochemical constraints on the transfer and evolution of arc magmas in the mafic-ultramafic Sapat Complex (Kohistan, Pakistan). PhD, # 18181. ETH, Zürich

Bouilhol P, Burg J-P, Bodinier J-L, Schmidt MW, Dawood H, Hussain S (2009) Magma and fluid percolation in arc to forearc mantle: Evidence from Sapat (Kohistan, Northern Pakistan). Lithos 107 (1-2):17–37. doi:10.1016/j.lithos.2008.07.004

Bouilhol P, Schaltegger U, Chiarada M, Ovtcharova M, Stracke A, Burg J-P, Dawood H (submitted) Timing of juvenile arc crust formation and evolution in the Sapat complex (Kohistan-Pakistan). Chem Geol 280 (3–4). doi: 10.1016/j.chemgeo.2010.11.013

Boutelier D, Chemenda A, Burg J-P (2003) Subduction versus accretion of intra-oceanic volcanic arcs: Insight from thermo-mechanical analogue experiments. Earth Planet Sci Lett 212 (1-2):31–45

Brookfield ME, Reynolds PH (1981) Late Cretaceous emplacement of the Indus suture zone ophiolitic mélange and an Eocene-Oligocene magmatic arc on the northern edge of the Indian plate. Earth Planet Sci Lett (55):157–162

Burg J-P (2007) Two orogenic systems and a transform-transfer fault in the Himalayas: Evidence and consequences. Earth Science Frontiers 13 (4):27–46

Burg J-P, Chen GM (1984) Tectonics and structural zonation of Southern Tibet, China. Nature 311 (5983):219–223

Burg J-P, Chaudhry MN, Ghazanfar M, Anczkiewicz R, Spencer D (1996) Structural evidence for back sliding of the Kohistan arc in the collisional system of northwest Pakistan. Geology 24 (8):739–742

Burg J-P, Bodinier J-L, Chaudhry MN, Hussain S, Dawood H (1998) Infra-arc mantle-crust transition and intra-arc mantle diapirs in the Kohistan Complex (Pakistani Himalaya): Petro-structural evidence. Terra Nova 10 (2):74–80

Burg J-P, Arbaret L, Chaudhry MN, Dawood H, Hussain S, Zeilinger G (2005) Shear strain localization from the upper mantle to the middle crust of the Kohistan Arc (Pakistan). In: Brunhn D, Burlini L (eds) High-strain zones: Structure and physical properties, vol 245. Geological Society, Special Publication, London,

Burg J-P, Jagoutz O, Dawood H, Hussain SS (2006) Precollision tilt of crustal blocks in rifted island arcs: Structural evidence

from the Kohistan Arc. Tectonics 25 (TC5005). doi:10.1029/2005TC001835

Casnedi R, Desio A, Forcella F, Nicoletti M, Petrucciani C (1978) Absolute age of some granitoid rocks between Hindu Raj and Gilgit river (W. Karakorum). Rendiconti della Accademia Nazionale dei Lincei 64:204–210

Chamberlain CP, Zeitler PK, Jan MQ (1989) The dynamics of the suture between the Kohistan island arc and the Indian plate in the Himalaya of Pakistan. J metamorphic Geol 7(1):135–149

Chamberlain CP, Zeitler PK, Erickson E (1991) Constraints on the tectonic evolution of the Northwestern Himalaya from geochronologic and petrologic studies of Babusar Pass, Pakistan. J Geol 99 (6):829–849. doi:10.1086/629555

Chemenda AI, Mattauer M, Bokun AN (1996) Continental subduction and a mechanism for exhumation of high-pressure metamorphic rocks: New modelling and field data from Oman. Earth Planet Sci Lett 143 (1-4):173–182. doi:10.1016/0012-821X(96)00123-9

Chemenda AI, Burg J-P, Mattauer M (2000) Evolutionary model of the Himalaya-Tibet system: Geopoem based on new modelling, geological and geophysical data. Earth Planet Sci Lett 174 (3-4):397–409. doi: 10.1016/S0012-821X(99)00277-0

Chemenda AI, Yang R-K, Stephan J-F, Konstantinovskaya EA, Ivanov GM (2001) New results from physical modelling of arc–continent collision in Taiwan: Evolutionary model. Tectonophysics 333 (1-2):159–178. doi:10.1016/S0040-1951(00)00273-0

Chen Y, Courtillot V, Cogné J-P, Besse J, Yang ZY, Enkin R (1993) The configuration of Asia prior to the collision of India: Cretaceous paleomagnetic constraints. J Geophys Res 98 (B12):21927–21941

Christensen UR (1996) The influence of trench migration on slab penetration into the lower mantle. Earth Planet Sci Lett 140 (1-4):27–39. doi:10.1016/0012-821X(96)00023-4

Condie KC (1997) Plate tectonics and crustal evolution. fourth edition edn. Butterworth-Heinemann, Oxford

Coward MP, Jan MQ, Rex DC, Tarney J, Thirlwall M, Windley BF (1982) Geotectonic framework of the Himalaya of N Pakistan. J Geol Soc London 139:299–308

Coward MP, Windley BF, Broughton RD, Luff IW, Petterson MG, Pudsey CJ, Rex DC, Khan MA (1986) Collision tectonics in the NW Himalayas. In: Coward MP, Ries AC (eds) Collision tectonics, vol 19. Geological Society Special Publication, London, pp 203–219

Coward MP, Butler RWH, Khan MA, Knipe RJ (1987) The tectonic history of Kohistan and its implications for Himalayan structure. J Geol Soc London 144:377–391

Danishwar S, Stern RJ, Khan MA (2001) Field relations and structural constraints for the Teru volcanic formation, northern Kohistan terrane, Pakistani Himalayas. J Asian Earth Sci 19 (5):683–695

Debon F, Khan NA (1996) Alkaline orogenic plutonism in the Karakorum batholith: The Upper Cretaceous Koz Sar complex (Karambar valley, N. Pakistan). Geodinamica Acta 9 (4):145–160

Debon F, Le Fort P, Dautel D, Sonet J, Zimmermann JL (1987) Plutonism in western Karakorum and northern Kohistan (Pakistan): A composite Mid-Cretaceous to upper Cenozoic magmatism. Lithos 20 (1):19–40. doi:10.1016/0024-4937(87)90022-3

Dhuime B, Bosch D, Bodinier J-L, Garrido CJ, Bruguier O, Hussain SS, Dawood H (2007) Multistage evolution of the Jijal ultramafic-mafic complex (Kohistan, N Pakistan): Implications for building the roots of island arcs. Earth Planet Sci Lett 261 (1-2):179–200. doi:10.1016/j.epsl.2007.06.026

Dhuime B, Bosch D, Garrido CJ, Bodinier J-L, Bruguier O, Hussain SS, Dawood H (2009) Geochemical architecture of the lower- to middle-crustal section of a paleo-island arc (Kohistan Complex, Jijal-Kamila Area, Northern Pakistan): Implications for the evolution of an oceanic subduction zone. J Petrol 50 (3):531–569. doi:10.1093/petrology/egp010

Ding L, Kapp P, Wan XQ (2005) Paleocene–Eocene record of ophiolite obduction and initial India-Asia collision, south central Tibet. Tectonics 24 (TC3001). doi:10.1029/2004TC001729

Doglioni C, Carminati E, Cuffaro M, Scrocca D (2007) Subduction kinematics and dynamic constraints. Earth Sci Rev 83 (3-4):125–175. doi:10.1016/j.earscirev.2007.04.001

Douvillé H (1926) Fossiles recueillis par Hayden dans le Kashmir en 1906 et les Pamirs en 1914: Leur description. Rec Geol Surv India 58 (4):349–357

Frank W, Gansser A, Trommsdorff V (1977) Geological observations in the Ladakh area (Himalayas). A preliminary report. Schweiz Mineral Petrogr Mitt 57:89–113

Fraser JE, Searle MP, Parrish RR, Noble SR (2001) Chronology of deformation, metamorphism, and magmatism in the southern Karakoram Mountains. Geol Soc Amer Bull 113 (11):1443–1455. doi:10.1130/0016-7606(2001)113<1443:CODMAM>2.0.CO;2

Gansser A (1980) The significance of the Himalayan suture zone. Tectonophysics 62 (1-2):37–52. doi:10.1016/0040-1951(80)90134-1

Garrido C, Bodinier J-L, Dhuime B, Bosch D, Chanefo I, Bruguier O, Hussain S, Dawood H, Burg J-P (2007) Origin of the island arc Moho transition zone via melt-rock reaction and its implications for intracrustal differentiation of island arcs: Evidence from the Jijal complex (Kohistan complex, northern Pakistan). Geology 35 (8):683–686. doi:10.1130/G23675A

George MT, Harris NBW, Butler RWH (1993) The tectonic implications of contrasting granite magmatism between the Kohistan island arc and the Nanga Parbat-Haramosh Massif, Pakistan Himalaya. In: Treloar PJ, Searle MP (eds) Himalayan tectonics, vol 74. Geological Society Special Publication, London, pp 173–191

Gerya TV, Yuen DA, Maresch WV (2004) Thermomechanical modelling of slab detachment. Earth Planet Sci Lett 226 (1-2):101–116. doi:10.1016/j.epsl.2004.07.022

Green OR, Searle MP, Corfield RI, Corfield RM (2008) Cretaceous-Tertiary carbonate platform evolution and the age of the India-Asia Collision along the Ladakh Himalaya (Northwest India). J Geol 116 (4):331–353

Hall R, Wilson MEJ (2000) Neogene sutures in eastern Indonesia. J Asian Earth Sci 18 (6):781–808

Hamidullah S, Onstott T (1992) $^{40}Ar/^{39}Ar$ evidence for Late Cretaceous formation of the Kohistan island arc, NW, Pakistan. Kashmir Journal of Geology 10:105–122

Heuberger S (ed) (2004) The Karakoram-Kohistan Suture zone in NW Pakistan - Hindu Kush Mountain Range. vdf Hochschulverlag AG, Zürich

Heuberger S, Schaltegger U, Burg J-P, Villa IM, Frank M, Dawood H, Hussain S, Zanchi A (2007) Age and isotopic constraints on magmatism along the Karakoram-Kohistan Suture Zone, NW Pakistan: Evidence for subduction and continued convergence after India-Asia collision. Swiss JGeosci 100 (1):85–107. doi:10.1007/s00015-007-1203-7

Hildebrand PR, Noble SR, Searle MP, Waters DJ, Parrish RR (2001) Old origin for an active mountain range: Geology and geochronology of the eastern Hindu Kush, Pakistan. Geol Soc Amer Bull 113 (5):625–639

Holbrook WS, Lizarralde D, McGeary S, Bangs N, Diebold J (1999) Structure and composition of the Aleutian island arc and implications for continental crustal growth. Geology 27 (1):31–34

Honegger K, Dietrich V, Frank W, Gansser A, Thoni M, Trommsdorff V (1982) Magmatism and metamorphism in the Ladakh Himalayas (the Indus-Tsangpo Suture zone). Earth Planet Sci Lett 60 (2):253–292

Ivanac JF, Través DM, King D (1956) The geology of the northwest portion of the Gilgit Agency. Records of the Geological Survey of Pakistan, Quetta 8 (2):1–27 and 23 tables

Iwasaki T, Yoshii T, Ito T, Sato H, Hirata N (2002) Seismological features of island arc crust as inferred from recent seismic expeditions in Japan. Tectonophysics 366 (1-4):53–66

Jaeger J-J, Courtillot V, Tapponnier P (1989) Paleontological view of the ages of the Deccan Traps, the Cretaceous/Tertiary boundary, and the India-Asia collision. Geology 17 (4):316–319

Jagoutz O, Müntener O, Burg J-P, Ulmer P, Jagoutz E (2006) Lower continental crust formation through focused flow in km-scale melt conduits: The zoned ultramafic bodies of the Chilas Complex in the Kohistan island arc (NW Pakistan). Earth Planet Sci Lett 242 (3-4):320–342

Jagoutz O, Müntener O, Ulmer P, Pettke T, Burg J-P, Dawood H, Hussain SS (2007) Petrology and mineral chemistry of lower crustal intrusions: The Chilas Complex, Kohistan (NW Pakistan). J Petrol 48 (10):1895–1953. doi:10.1093/petrology/egm044

Jagoutz O, Burg J-P, Hussain S, Dawood H, Pettke T, Iizuka T, Maruyama S (2009) Construction of the granitoid crust of an island arc part I: Geochronological and geochemical constraints from the plutonic Kohistan (NW Pakistan). Contrib Mineral Petrol 158 (6):739–755. doi:10.1007/s00410-009-0408-3

Jan MQ (1988) Geochemistry of amphibolites from the southern part of the Kohistan arc, N. Pakistan. Mineral Mag 52: 147–159

Jan MQ, Asif M (1981) A speculative tectonic model for the evolution of NW Himalaya and Karakoram. Geological Bulletin of the University of Peshawar 14:199–201

Jan MQ, Howie RA (1980) Ortho- and clinopyroxenes from the pyroxene granulites of Swat Kohistan, northern Pakistan. Mineral Mag 43:715–726

Jan MQ, Howie RA (1981) The mineralogy and geochemistry of the metamorphosed basic and ultrabasic rocks of the Jijal complex, Kohistan, NW Pakistan. J Petrol 22 (1):85–126

Jan MQ, Karim A (1995) Coronas and high-P veins in metagabbros of the Kohistan island arc, northern Pakistan: Evidence for crustal thickening during cooling. J metamorphic Geol 13 (3):357-366. doi:10.1111/j.1525-1314.1995.tb00225.x

Jan QM, Khattak MUK, M.K. P, Windley BF (1984) The Chilas Stratiform Complex: field and mineralogical aspects. Geol Bull Univ Peshawar 17:153–169

Jan MQ, Khan MA, Qazi MS (1993) The Sapat mafic-ultramafic complex, Kohistan arc, North Pakistan. In: Treloar PJ, Searle MP (eds) Himalayan tectonics, vol 74. Geological Society Special Publication, London, pp 113–121

Kakar SK, Mian SB, Khan J (1971) The geology of the Jandul valley, western Dir. Geol Bull Univ Peshawar 6:54–73

Kaneko Y, Katayama I, Yamamoto H, Misawa K, Ishikawa M, Rehman HU, Kausar AB, Shiraishi K (2003) Timing of Himalayan ultrahigh-pressure metamorphism: Sinking rate and subduction angle of the Indian continental crust beneath Asia. J metamorphic Geol 21 (6):589–599

Kapp P, Yin A, Harrison TM, Ding L (2005) Cretaceous-Tertiary shortening, basin development, and volcanism in central Tibet. Geol Soc Amer Bull 117 (7/8):865–878. doi:10.1130/B25595.1

Kazmi AH, Lawrence RD, Dawood H, Snee LW, Hussain SS (1984) Geology of the Indus Suture Zone in the Mingora - Shangla area of Swat, North Pakistan. Geol Bull Univ Peshawar 17:127–144

Kearey P, Klepeis KA, Vine FJ (2009) Global tectonics. third edn. Wiley-Blackwell, Oxford

Khan MA, Thirlwall MF (1988) Babusar amphibolites: arc tholeiites from the southern Kohistan arc, N. Pakistan. Geol Bull Univ Peshawar 21:147–158

Khan MA, Jan MQ, Windley BF, Tarney J, Thirlwall MF (1989) The Chilas mafic-ultramafic igneous complex: The root of the Kohistan Island Arc in the Himalaya of northern Pakistan. Spec Pap Geol Soc Am 232:75–93

Khan MA, Jan MQ, Weaver BL (1993) Evolution of the lower arc crust in Kohistan, N. Pakistan: Temporal arc magmatism through early, mature and intra-arc rift stages. In: Treloar PJ, Searle MP (eds) Himalayan tectonics, vol 74. Geological Society Special Publication, London, pp 123–138

Khan T, Khan MA, Qasim Jan M (1994) Geology of a part of the Kohistan terrane between Gilgit and Chilas, northern areas, Pakistan. Geol Bull Univ Peshawar 27:99–112

Khan T, Khan MA, Jan MQ, Naseem M (1996) Back-arc basin assemblages in Kohistan, Northern Pakistan. Geodinamica Acta 9 (1):30–40

Khan MA, Stern RJ, Gribble RF, Windley BF (1997) Geochemical and isotopic constraints on subduction polarity, magma sources, and paleogeography of the Kohistan intra-oceanic arc, northern Pakistan Himalaya. J Geol Soc London 154 (6):935–946

Khan SD, Stern RJ, Manton MI, Copeland P, Kimura JI, Khan MA (2004) Age, geochemical and Sr–Nd–Pb isotopic constraints for mantle source characteristics and petrogenesis of Teru Volcanics, Northern Kohistan Terrane, Pakistan. Tectonophysics 393:263–280. doi:10.1016/j.tecto.2004.07.038

Khan T, Murata M, Karim T, Zafar M, Ozawa H, Rehman HU (2007) A Cretaceous dike swarm provides evidence of a spreading axis in the back-arc basin of the Kohistan paleo-island arc, northwestern Himalaya, Pakistan. J Asian Earth Sci 29 (2-3):350–360

Khan SD, Walker DJ, Hall SA, Burke KC, Shah MT, Stockli L (2009) Did the Kohistan-Ladakh island arc collide first with India? Geol Soc Amer Bull 121 (3/4):366–384. doi:10.1130/B26348.1

Klootwijk CT, Shah SK, Sharma ML, Gergan J, Tirkey B (1979) The extent of Greater India, II. Palaeomagnetic data from the Ladakh intrusives at Kargil, northwestern Himalayas. Earth Planet Sci Lett 44 (1):47–64. doi:10.1016/0012-821X(79)90007-4

Klootwijk CT, Gee JS, Peirce JW, Smith GM, McFadden PL (1992) An early India-Asia contact: Paleomagnetic constraints from Ninetyeast Ridge, ODP Leg 121. Geology 20 (5):395–398. doi:10.1130/0091-7613(1992)020<0395:AEIACP>2.3.CO;2

Krol MA, Zeitler PK, Copeland P (1996) Episodic unroofing of the Kohistan Batholith, Pakistan: Implications from K-feldspar thermochronology. J Geophys Res 101 (B12):28149-28164

Le Fort P, Michard A, Sonet J, Zimmermann J-L (1983) Petrography, geochemistry and geochronology of some samples from the Karakorum axial batholith (Northern Pakistan). In: Shams FA (ed) Granites of Himalayas, Karakoram and Hindu Kush. Punjab University, Lahore, pp 377–387

Mahéo G, Blichert-Toft J, Pin C, Guillot S, Pêcher A (2009) Partial melting of mantle and crustal sources beneath South Karakorum, Pakistan: Implications for the Miocene geodynamic evolution of the India-Asia convergence zone. J Petrol 50 (3):427–449. doi:10.1093/petrology/egp006

Martínez F, Taylor B (2002) Mantle wedge control on back-arc crustal accretion. Nature 416:417–420. doi:10.1038/416417a

Matsushita S, Huzita K (1965) Geology of the Karakoram and Hindu Kush. Results of the Kyoto University scientific expedition to the Karakoram and Hindu Kush. Kyoto University Press, Kyoto

Miller DJ, Loucks RR, Ashraf M (1991) Platinum-group element mineralization in the Jijal layered ultramafic-mafic complex, Pakistani Himalayas. Econ Geol 86 (5):1093–1102

Mishin YA, Gerya TV, Burg J-P, Connolly JAD (2008) Dynamics of double subduction: Numerical modeling. Phys Earth Planet Inter 171 (1-4):280–295. doi:10.1016/j.pepi.2008.06.012

Molnar P, Stock JM (2009) Slowing of India's convergence with Eurasia since 20 Ma and its implications for Tibetan mantle dynamics. Tectonics 28:TC3001. doi:10.1029/2008TC002271

Molnar P, Tapponnier P (1975) Cenozoic tectonics of Asia: Effects of a continental collision. Science 189:419–426

O'Brien PJ, Zotov N, Law R, Khan MA, Jan MQ (1999) Coesite in eclogite from the Upper Kaghan Valley, Pakistan: A first record and implications. Terra Nostra 99/2:109–111

O'Brien PJ, Zotov N, Law R, Khan MA, Jan MQ (2001) Coesite in Himalayan eclogite and implications for models of India-Asia collision. Geology 29 (5):435–438

Parrish RR, Gough SJ, Searle MP, Waters DJ (2006) Plate velocity exhumation of ultrahigh-pressure eclogites in the Pakistan Himalaya. Geology 34 (11):989–992. doi:10.1130/G22796A.1

Patriat P, Achache J (1984) India-Eurasia collision chronology has implications for crustal shortening and driving mechanism of plates. Nature 311:615–621

Petterson MG, Treloar PJ (2004) Volcanostratigraphy of arc volcanic sequences in the Kohistan arc, North Pakistan: volcanism within island arc, back-arc-basin, and intra-continental tectonic settings. J Volcanol Geotherm Res 130 (1-2):147–178

Petterson MG, Windley BF (1985) Rb-Sr dating of the Kohistan arc-batholith in the Trans-Himalaya of north Pakistan, and tectonic implications. Earth Planet Sci Lett 74 (1):45–57

Petterson MG, Windley BF (1991) Changing source regions of magmas and crustal growth in the Trans-Himalayas: evidence from the Chalt volcanics and Kohistan batholith, Kohistan, northern Pakistan. Earth Planet Sci Lett 102 (3/4):326–341

Petterson MG, Windley BF, Luff IW (1990) The Chalt volcanics, Kohistan, N. Pakistan: High-Mg tholeiitic and low-Mg calc-alkaline volcanism in a Cretaceous island arc. In: Sharma KK (ed) Geology and geodynamic evolution of the Himalayan collision zone: A synthesis, vol 17. *Physics and Chemistry of the Earth*, pp 19–30

Petterson MG, Crawford MB, Windley BF (1993) Petrogenetic implications of neodymium isotope data from the Kohistan Batholith, North Pakistan. J Geol Soc London 150 (1):125–129

Pudsey CJ (1986) The Northern Suture, Pakistan: margin of a Cretaceous island arc. Geol Mag 123 (4):405–423

Pudsey CJ, Coward MP, Luff IW, Shackleton RM, Windley BF, Jan MQ (1985a) Collision zone between the Kohistan arc and the Asian plate in NW Pakistan. Trans R Soc Edinburgh 76:463–479

Pudsey CJ, Schroeder R, Skelton PW (1985b) Cretaceous (Aptian/Albian) age for island-arc volcanics, Kohistan, N Pakistan. Him Geol 3:150–168

Reuber I (1989) The Dras arc: Two successive volcanic events on eroded oceanic crust. Tectonophysics 161 (1-2):93–106. doi:10.1016/0040-1951(89)90305-3

Reynolds PH, Brookfield ME, McNutt RH (1983) The age and nature of Mesozoic-Tertiary magmatism across the Indus Suture Zone in Kashmir and Ladakh (N.W. India and Pakistan). Geol Rundsch 72 (3):981–1004

Ricou L-E (1994) Tethys reconstructed: plates, continental fragments and their boundaries since 260 Ma from Central America to South-eastern Asia. Geodinamica Acta 7 (4):169–218

Ringuette L, Martignole J, Windley BF (1999) Magmatic crystallization, isobaric cooling, and decompression of the garnet-bearing assemblages of the Jijal sequence (Kohistan terrane, western Himalayas). Geology 27 (2):139–142

Robertson AHF, Collins AS (2002) Shyok Suture Zone, N Pakistan: Late Mesozoic-Tertiary evolution of a critical suture separating the oceanic Ladakh Arc from the Asian continental margin. J Asian Earth Sci 20 (3):309–351

Robertson A, Degnan P (1994) The Dras arc Complex: lithofacies and reconstruction of a Late Cretaceous oceanic volcanic arc in the Indus Suture Zone, Ladakh Himalaya. Sediment Geol 92 (1-2):117–145

Rolland Y, Pêcher A, Picard C (2000) Middle Cretaceous back-arc formation and arc evolution along the Asian margin: The Shyok Suture Zone in northern Ladakh (NW Himalaya). Tectonophysics 325:145–173

Savostin LA, Sibuet J-C, Zonenshain LP, Le Pichon X, Roulet M-J (1986) Kinematic evolution of the Tethys Belt from the Atlantic Ocean to the Pamirs since the Triassic. Tectonophysics 123 (1-4):1–35. doi:10.1016/0040-1951(86)90192-7

Schaltegger U, Zeilinger G, Frank M, Burg J-P (2002) Multiple mantle sources during island arc magmatism: U-Pb and Hf

isotopic evidence from the Kohistan arc complex, Pakistan. Terra Nova 14 (6):461–468

Schaltegger U, Frank M, Burg J-P (2003) A 120 million years record of magmatism and crustal melting in the Kohistan Batholith. Geophysical Research Abstracts; EGS-AGU-EUG Joint Assembly 5:EAE03-A-08307

Schettino A, Scotese CR (2005) Apparent polar wander paths for the major continents (200 Ma to the present day): a palaeomagnetic reference frame for global plate tectonic reconstructions. Geophys J Int 163 (2):727–759

Searle MP, Treloar PJ (2010) Was late Cretaceous – Palaeocene obduction of ophiolite complexes the primary cause of crustal thickening and regional metamorphism in the Pakistan Himalaya? In: Kusky TM, Zhai M-G, Xiao W (eds), The evolving continents: Understanding processes of continental growth. vol 338. Geological Society Special Publication, London, pp. 345–359

Searle MP, Khan AM, Fraser JE, Gough SJ, Jan QM (1999) The tectonic evolution of the Kohistan-Karakoram collision belt along the Karakoram Highway transect, north Pakistan. Tectonics 18 (6):929–949

Searle MP, Parrish RR, Thow AV, Noble SR, Phillips RJ, Waters DJ (2010) Anatomy, age and evolution of a collisional mountain belt: The Baltoro granite batholith and Karakoram Metamorphic Complex, Pakistani Karakoram. J Geol Soc London 167 (1):183–202. doi:10.1144/0016-76492009-043

Shah MT, Shervais JW (1999) The Dir-Utror metavolcanic sequence, Kohistan arc terrane, northern Pakistan. J Asian Earth Sci 17 (4):459–475

Sharma KS (1987) Crustal growth and two-stage India-Eurasia collision in Ladakh. Tectonophysics 134:17–28

Silver EA, Moore JC (1978) The Molucca Sea collision zone, Indonesia. J Geophys Res 83 (B4):1681–1691

Stampfli G, Borel GD (2002) A plate tectonic model for the Paleozoic and Mesozoic constrained by dynamic plate boundaries and restored synthetic oceanic isochrons. Earth Planet Sci Lett 196 (1-2):17–33. doi:10.1016/S0012-821X(01)00588-X

Stern RJ (2002) Subduction zones. Rev Geophys 40 (4). doi:10.1029/2001RG000108

Stern RJ, Fouch MJ, Klemperer SL (2003) An overview of the Izu-Bonin-Mariana subduction factory. In: Eiler J (ed) Inside the subduction factory, vol 138. Geophysical monograph, vol American Geophysical Union, pp 175–222

Sullivan MA, Windley BF, Saunders AD, Haynes JR, Rex DC (1993) A palaeogeographic reconstruction of the Dir Group: evidence for magmatic arc migration within Kohistan, N. Pakistan. In: Treloar PJ, Searle MP (eds) Himalayan tectonics, vol 74. Geological Society Special Publication, London, pp 139–160

Tahirkheli RA (1979) Geology of Kohistan and adjoining Eurasian and Indo-Pakistan continents, Pakistan. Geol Bull Univ Peshawar 11:1–30

Tahirkheli RAK, Mattauer M, Proust F, Tapponnier P (1979) The India Eurasia Suture Zone in Northern Pakistan: Synthesis and interpretation of recent data at plate scale. In: Farah A, De Jong KA (eds) Geodynamics of Pakistan. Geological Survey of Pakistan, Quetta, pp 125–130

Takahashi N, Suyehiro K, Shinohara M (1998) Implications from the seismic crustal structure of the northern Izu–Bonin arc. Island Arc 7 (3):383–394. doi:10.1111/j.1440-1738.1998.00197.x

Takahashi N, Kodaira S, Klemperer SL, Tatsumi Y, Kaneda Y, Suyehiro K (2007) Crustal structure and evolution of the Mariana intra-oceanic island arc. Geology 35 (3):203–206. doi:10.1130/G23212A.1

Taylor B (1995) Backarc basins: Tectonics and magmatism. Plenum Press, New York

Taylor B, Goodliffe A, Martínez F, Hey R (1995) Continental rifting and initial sea-floor spreading in the Woodlark basin. Nature 374:534-537. doi:10.1038/374534a0

Thakur VC (1981) Regional framework and geodynamic evolution of the Indus-Tsangpo suture zone in the Ladakh Himalaya. Trans R Soc Edinburgh 72:89–97

Thakur VC, Misra DK (1984) Tectonic framework of the Indus and Shyok suture zones in eastern Ladakh, northwest Himalaya. Tectonophysics 101:207–220

Treloar PJ, Coward MP (1991) Indian plate motion and shape: constraints on the geometry of the Himalayan orogen. Tectonophysics 191 (3-4):189–198

Treloar PJ, Broughton RD, Williams MP, Coward MP, Windley BF (1989a) Deformation, metamorphism and imbrication of the Indian plate, south of the Main Mantle Thrust, north Pakistan. J metamorphic Geol 7 (1):111–125. doi:10.1111/j.1525-1314.1989.tb00578.x

Treloar PJ, Rex DC, Guise PG, Coward MP, M.P. S, Windley BF, Petterson MG, Jan MQ, Luff IW (1989b) K/Ar and Ar/Ar geochronology of the Himalayan collision in NW Pakistan: constraints on the timing of suturing, deformation, metamorphism and uplift. Tectonics 8 (4):881–909

Treloar PJ, Brodie KH, Coward MP, Jan MQ, Khan MA, Knipe RJ, Rex DC, Williams MP (1990) The evolution of the Kamila Shear Zone, Kohistan, Pakistan. In: Sallisbury MH, Fountain DM (eds) Exposed cross-sections of the continental crust. Kluwer Academic Press, Amsterdam, pp 175–214

Treloar PJ, Petterson MG, Qasim Jan M, Sullivan MA (1996) A re-evaluation of the stratigraphy and evolution of the Kohistan arc sequence, Pakistan Himalaya: implications for magmatic and tectonic arc-building processes. J Geol Soc London 153 (5):681–693. doi:10.1144/gsjgs.153.5.0681

Treloar PJ, O'Brien PJ, Parrish RR, Khan MA (2003) Exhumation of early Tertiary, coesite-bearing eclogites from the Pakistan Himalaya. J Geol Soc London 160:367–376

Uyeda S (1984) Subduction zones: Their diversity, mechanism and human impacts. GeoJournal 8:381–406

Van der Beek P, Van Melle J, Guillot S, Pêcher A, Reiners PW, Nicolescu S, Latif M (2009) Eocene Tibetan plateau remnants preserved in the northwest Himalaya. Nature Geoscience 2 (5):364–368. doi:10.1038/NGEO503

Van der Voo R, Spakman W, Bijwaard H (1999) Tethyan subducted slabs under India. Earth Planet Sci Lett 171 (1):7–20

van Hunen J, van den Berg AP, Vlaar NJ (2000) A thermo-mechanical model of horizontal subduction below an overriding plate. Earth Planet Sci Lett 182 (2):157–169. doi:10.1016/S0012-821X(00)00240-5

Vince KJ, Treloar PJ (1996) Miocene north-vergent extensional displacements along the Main Mantle Thrust, NW Himalaya, Pakistan. J Geol Soc London 153:677–680

Wartho J-A, Rex DC, Guise PG (1996) Excess argon in amphiboles linked to greenschist facies alteration in the Kamila

Amphibolite Belt, Kohistan island arc system, northern Pakistan: Insights from $^{40}Ar/^{39}Ar$ step-heating and acid leaching experiments. Geol Mag 133 (5):595–609

Williams HM, McCammon CA, Peslier AH, Halliday AN, Teutsch N, Levasseur S, Burg J-P (2004) Iron isotope fractionation and the oxygen fugacity of the mantle. Science 304:1656–1659

Yamamoto H (1993) Contrasting metamorphic P-T-time paths of the Kohistan granulites and tectonics of the western Himalayas. J Geol Soc London 150:843–856

Yamamoto H, Nakamura E (1996) Sm-Nd dating of garnet granulites from the Kohistan complex, northern Pakistan. J Geol Soc London 153 (6):965–969

Yamamoto H, Nakamura E (2000) Timing of magmatic and metamorphic events in the Jijal complex of the Kohistan arc deduced from Sm-Nd dating of mafic granulites. In: Khan MA, Treloar PJ, Searle MP, Jan MQ (eds) Tectonics of the Nanga Parbat Syntaxis and the Western Himalaya, vol 170. Geological Society Special Publication, London, pp 313–319

Yamamoto H, Kobayashi K, Nakamura E, Kaneko Y, Kausar AB (2005) U-Pb zircon dating of regional deformation in the lower crust of the Kohistan arc. Int Geol Rev 47 (10):1035–1047

Yin A, Harrison TM (2000) Geologic evolution of the Himalayan-Tibetan orogen. Ann Rev Earth Planet Sci 28:211–280

Yoshida M, Zaman H, Ahmad MN (1996) Paleopositions of Kohistan Arc and surrounding terranes since Cretaceous time: The paleomagnetic constraints. Proceedings of Geoscience Colloquium, Geoscience Laboratory Project, Islamabad, Pakistan 15:83–101

Yoshino T, Okudaira T (2004) Crustal growth by magmatic accretion constrained by metamorphic P-t paths and thermal models of the Kohistan Arc, NW Himalayas. J Petrol 45 (11):2287-2302. doi:10.1093/petrology/egh056

Zaman H, Torii M (1999) Palaeomagnetic study of Cretaceous red beds from the eastern Hindukush ranges, northern Pakistan: palaeoreconstruction of the Kohistan-Karakoram composite unit before the India-Asia collision. Geophys J Int 136 (3):719–738

Zanchi A, Poli S, Fumagalli P, Gaetani M (2000) Mantle exhumation along the Tirich Mir Fault (NW Pakistan): Pre-mid-Cretaceous accretion of the Karakorum Terrane to the Eurasian margin. In: Khan AM, Treloar PJ, Searle MP, Jan MQ (eds) Tectonics of the Nanga Parbat Syntaxis and the Western Himalaya, vol 170. Geological Society, Special Publication, London, pp 237–252

Zeilinger G (2002) Structural and geochronological study of the Lowest Kohistan Complex, Indus Kohistan region in Pakistan, NW Himalaya. PhD, # 14421, ETH, Zürich

Zeilinger G, Seward D, Burg J-P (2007) Exhumation across the Indus Suture Zone: a record of back sliding of the hanging wall. Terra Nova 19 (6):425–437, doi: 410.1111/j.1365-3121.2007.00767.x

Zeitler PK (1985) Cooling history of the NW Himalaya, Pakistan. Tectonics 4 (1):127–151

Zeitler P, Tahirkheli RAK, Naeser C, Johnson N, Lyons J (1980) Preliminary fission track ages from the Swat valley, Northern Pakistan. Geol Bull Univ Peshawar 13:63–65

Chapter 11
Processes of Arc–Continent Collision in the Uralides

D. Brown, R.J. Herrington, and J. Alvarez-Marron

11.1 Introduction

Extending for nearly 2,500 km from near the Aral Sea in the south to the islands of Novaya Zemlya in the Arctic Ocean (Fig. 11.1a), the Uralide Orogen of Russia records the Paleozoic collision of two intra-oceanic arcs with the margin of what was then Laurussia. The Tagil and Magnitogorsk volcanic arcs (Fig. 11.1) developed during the Late Ordovician to Devonian (Tagil) and the Early Devonian to Early Carboniferous (Magnitogorsk) in an intra-oceanic setting (Yazeva and Bochkarev 1996; Seravkin et al. 1992; Brown and Spadea 1999; Spadea et al. 1998, 2002; Herrington et al. 2002; Brown et al. 2006a) and began to collide with the continental margin of Laurussia in the late Middle Devonian (Magnitogorsk) and the Early Carboniferous (Tagil) (Puchkov 1997; Brown and Spadea 1999; Brown et al. 2006a). There appears to have been tectonic quiesence along this margin of Laurussia until the latest Carboniferous, when continent–continent collison began as the Kazakstanian collage and finally Siberia collided with the margin to form the Uralide orogen (Brown et al. 2008). The Uralides have remained largely intact since the Paleozoic, allowing its well-preserved arc–continent collisions to be compared with great detail to those that are active today (Puchkov 1997: Brown et al. 1998, 2001, 2006a; Brown and Spadea 1999; Alvarez-Marron et al. 2000). In this paper we present a review of the arc–continent collisions in the Uralides, placing emphasis on the tectonic processes that took place in the South Urals (Fig. 11.1b) where there is a larger amount of data available and where the area was less affected by the subsequent continent–continent collision that formed the Uralide Orogen.

11.2 Tectonostratigraphic Framework of the Uralides

From west to east the Uralides are divided into a number of tectonic zones; the undeformed foreland basin, the foreland thrust and fold belt, the Magnitogorsk-Tagil Zone, the East Uralian Zone, and the Trans-Uralian Zone (Fig. 11.1a). For descriptive purposes, the Uralides are divided geographically into the South, Middle, North, Cis-Polar and Polar Urals (Fig. 11.1a).

The foreland basin comprises undeformed Late Carboniferous to Early Triassic syn-tectonic sediments that were derived from the growing Uralide orogen to the east (Mizens 1997; Chuvashov 1998). The foreland thrust and fold belt comprises deformed Late Carboniferous to Early Triassic sediments of the foreland basin, Paleozoic platform margin and continental slope rocks, Archean, Mesoproterozoic and Neoproterozoic rocks of the East European Craton (part of Laurussia). In the South Urals it also includes the Middle to Late Devonian arc–continent collision accretionary complex (hereafter referred to as accretionary complex) related to the collision of the Magnitogorsk Arc with the Laurussia continental margin (Kamaletdinov 1974; Brown et al. 1997, 2004, 2006b). The Magnitogorsk-Tagil Zone consists of Late

D. Brown and J. Alvarez-Marron
Instituto de Ciencias de la Tierra "Jaume Almera", CSIC, c/Lluís Solé i Sabarís s/n, 08028 Barcelona, Spain

R.J. Herrington
Department of Mineralogy, Natural History Museum, Cromwell Road, London SW7 5BD, England, UK

D. Brown and P.D. Ryan (eds.), *Arc-Continent Collision*, Frontiers in Earth Sciences,
DOI 10.1007/978-3-540-88558-0_11,

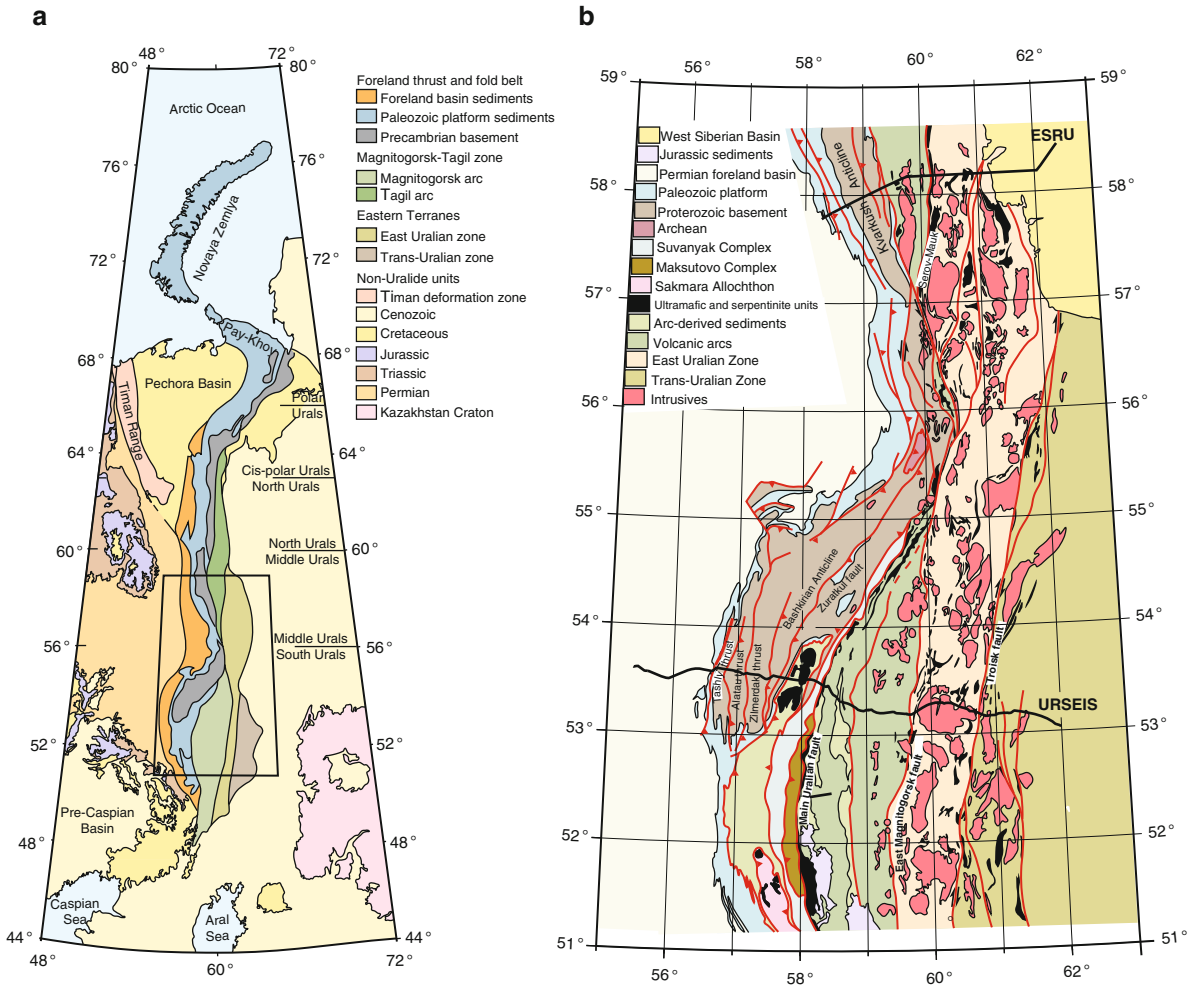

Fig. 11.1 (**a**) Map showing the different zones of the Urals and its geographic divisions from north to south. The box indicates the area discussed in this paper. (**b**) Geological map of the South and part of the Middle Urals showing the location of the ESRU and URSEIS seismic profiles. The legend shows the disposition of the various tectonic units discussed in this paper.

Ordovician to Devonian intra-oceanic island arc volcanic rocks and overlying volcaniclastic sediments of the Magnitogorsk and Tagil island arcs (Seravkin et al. 1992; Maslov et al. 1993; Brown and Spadea 1998; Brown et al. 2001; Spadea et al. 2002; Herrington et al. 2002). The Magnitogorsk-Tagil Zone is sutured to the former continental margin rocks of Laurussia along the Main Uralian Fault. The East Uralian Zone is composed predominantly of deformed and metamorphosed volcanic arc fragments with minor amounts of Precambrian and Paleozoic rocks thought to represent continental crust (Puchkov 1997, 2000; Friberg et al. 2000). The East Uralian Zone was extensively intruded by Carboniferous and Permian granitoids (Fershtater et al. 1997; Bea et al. 1997, 2002), forming the "main granite axis" of the Uralides. The East Uralian Zone is juxtaposed against the Magnitogorsk-Tagil Zone along the East Magnitogorsk – Serov-Mauk strike-slip fault system. The Trans-Uralian Zone is composed of Carboniferous volcano-plutonic complexes (Puchkov 1997, 2000). Ophiolitic material and high-pressure rocks have also been reported (Puchkov 2000). The contact between the East Uralian and Trans-Uralian zones is only exposed in the South Urals, where it is a mélange made up predominantly of serpentinite. Rocks that unequivocally belong to either the Kazakhstan or Siberia plates do not outcrop in the Uralides, although

geophysical and borehole data indicate that they are present in the subsurface. The remainder of this paper will deal with the arc–continent collision units.

11.3 The Continental Margin of Laurussia in the Devonian

Rifting during the Late Cambrian to Early Ordovician led to the formation of what appears to have been a roughly curvi-linear continental margin of the part of Laurussia that was to become involved in the Uralide arc–continent collisions. While the South and Middle Urals part of the Laurussia margin appears not to have had any major re-entrants or salients, there is a significant bend in the trend of the Main Uralian Fault (continent margin-oceanic terrane suture in the Uralides, see Sect. 11.7 below) between approximately 54° and 56° North that coincides with the Perm-Bashkir Arch, a crystalline basement high that may represent the remanents of a promotory marked by outcropping Archean and Proterozoic rocks (Fig. 11.2). The margin of Laurussia that entered the subduction zone in the Late Devonian was highly structured, with deep crustal discontinuities oriented at both low and high

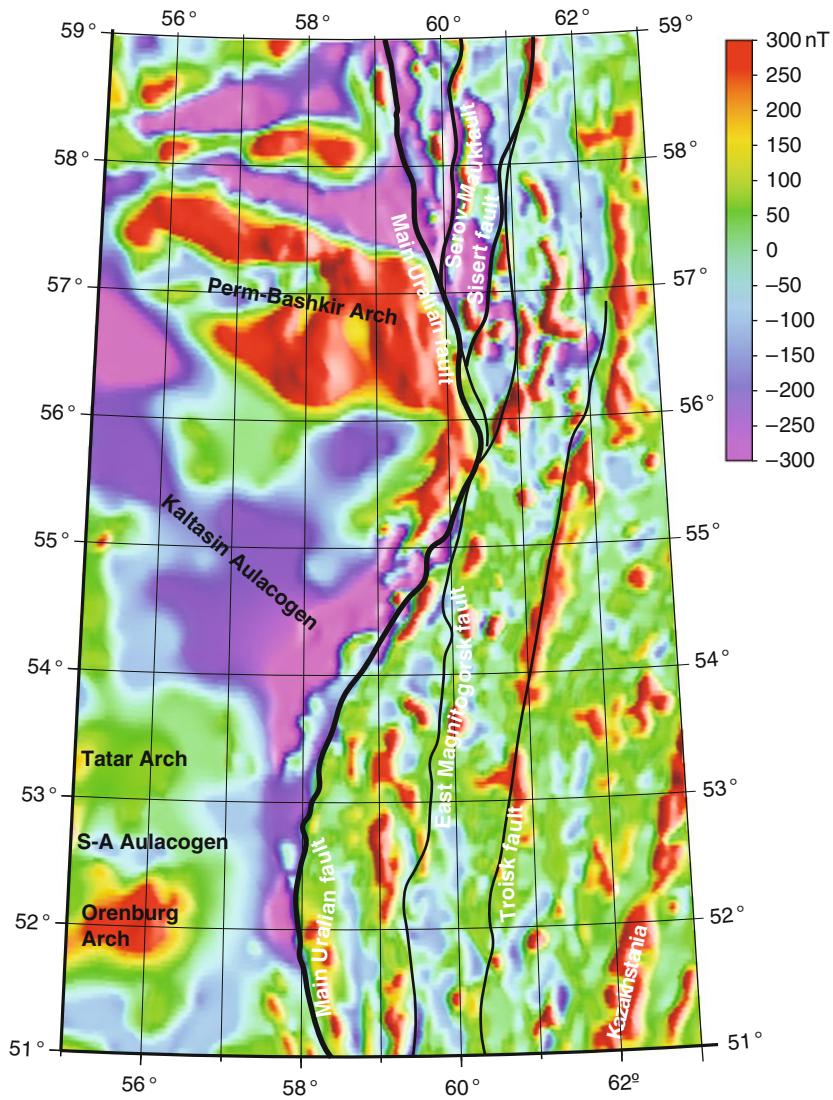

Fig. 11.2 Aeromagnetic map of the South and Middle Urals showing the main structures that were present in the margin of Laurussia prior to the arc–continent collision. The Main Uralian Fault marks the boundary between what was continental crust and what was island arc. The *blues* and *purples* indicate rift area that have thick sedimentary fill, whereas *green* and *red* are areas with little sedimentary cover above the magnetic crystalline rocks.

angles to the inferred orientation of the subduction zone (Brown et al. 1999). Structures in the basement included several deep aulacogens developed in the Archean crystalline rocks (Fig. 11.2) and filled with up to 15 km of Riphean-aged sediments (Maslov et al. 1997; Brown et al. 1999), giving a structural grain at a high angle to the Devonian subduction zone. Along the eastern part of the margin, the Riphean sediments and the underlying Archean rocks were affected by an orogenic event in the Late Precambrian (Puchkov 2000) that juxtaposed them along faults roughly parallel to that of the Devonian subduction zone (Brown et al. 1999) (see Sect. 11.9).

The Archean and Proterozoic basement gneisses, as well as the Proterozoic sedimentary rocks that were deposited in the aulocogens (Kozlov et al. 1989; Maslov et al. 1997), outcrop extensively along the South and Middle Urals, in the Bashkirian and Kvarkush anticlines, respectively (Fig. 11.1b). Along the eastern flanks of both these anticlines Precambrian rocks were affected by a Neoproterozoic III to Early Cambrian tectonothermal event that locally reached granulite and eclogite facies metamorphism (Puchkov 1997; Giese et al. 1999; Glasmacher et al. 1999, 2001, 2004; Beckholmen and Glodny 2004). Unmetamorphosed Neoproterozoic III sediments along the western flanks of both the Bashkirian and Kvarkush antiforms are thought to have been deposited in a foreland basin setting to this tectonothermal event (Brown et al. 1996; Puchkov 1997). In the south, both Ordovician and Silurian clastic rocks can unconformably overlie basement locally, whereas westward the Lower Devonian is unconformable on basement. In the South and Middle Urals, the shelf sediments of the Paleozoic continental margin are made up of about 4,000 m of limestones with thin intercalations of clastics. The pelagic sediments of the margin are preserved in allochthons overlying the shelf complex and are represented by deep-water terrigenous and cherty rocks with, locally, subordinate limestones (Puchkov 2002). Ordovician, Silurian and Lower Devonian barrier reefs were also developed.

It is not possible to determine the width of the thinned, extended Paleozoic Laurussia continental margin. However, an idea of its width and architecture can be obtained by analogy to today's non-volcanic rifted continental margins. These typically range between 150 and 400 km in width and consist of highly structured, thinned continental and transitional crust overlain by a several kilometer thick carapace of sediments (Keen and Dehler 1997; Sayers et al. 2001; Bauer et al. 2000; Funck et al. 2004; Reston 2009). If we assume that the margin of Laurussia was similar to today's passive margins, then we can predict that the thinned part of it was somewhere between 150 and 400 km wide (Fig. 11.3).

Reflection and refraction seismic data (see Sect. 11.9) indicate that the current thickness of the crust beneath what would have been the Devonian platform is on the order of 40–45 km (Echtler et al. 1996; Knapp et al. 1996; Steer et al. 1998; Tryggvason et al. 2001; Juhlin et al. 1998; Friberg et al. 2002; Brown et al. 2002; Kashubin et al. 2006), providing a reasonable estimate for its thickness during the Paleozoic.

11.4 The Tagil Arc

The Tagil Arc formed in the paleo-Uralian ocean as a result of east-direct (today's coordinates) subduction. The Tagil Arc stratigraphy begins with Late Ordovician to Early Silurian bimodal basalt and rhyolite, with intercalated cherts and carbonates, and is transitional upward into a sequence of Silurian-age tuffs, basalt, andesitic-basalt, and calc-alkaline andesite (Herrington et al. 2005). Zoned mafic-ultramafic complexes intrude the lower sequence of basalts and sheeted dike complexes. The intrusions have been dated at 428 ± 7 Ma (Bosch et al. 1997) and are thought to be comagmatic with the calc-alkaline lavas higher in the sequence (Friberg 2000). Stratigraphically upward, there is more volcaniclastic sediments, trachytic extrusions and turbidites. These are overlain by up to 2 km of limestone and calc-alkaline volcanic rocks. Calc-alkaline activity continued in the eastern part of the Tagil Arc through the Middle Devonian and into the Late Devonian (Frasnian), synchronous with the Magnitogorsk Arc rocks described below. The poorly exposed and structurally deformed and dismembered Tagil Arc has received considerably less attention in aspects such as its geochemical and isotopic characteristics than the Magnitogorsk Arc. Therefore, in what follows we place the majority of the emphasis on the Magnitogorsk Arc and its collision with the margin of Laurussia.

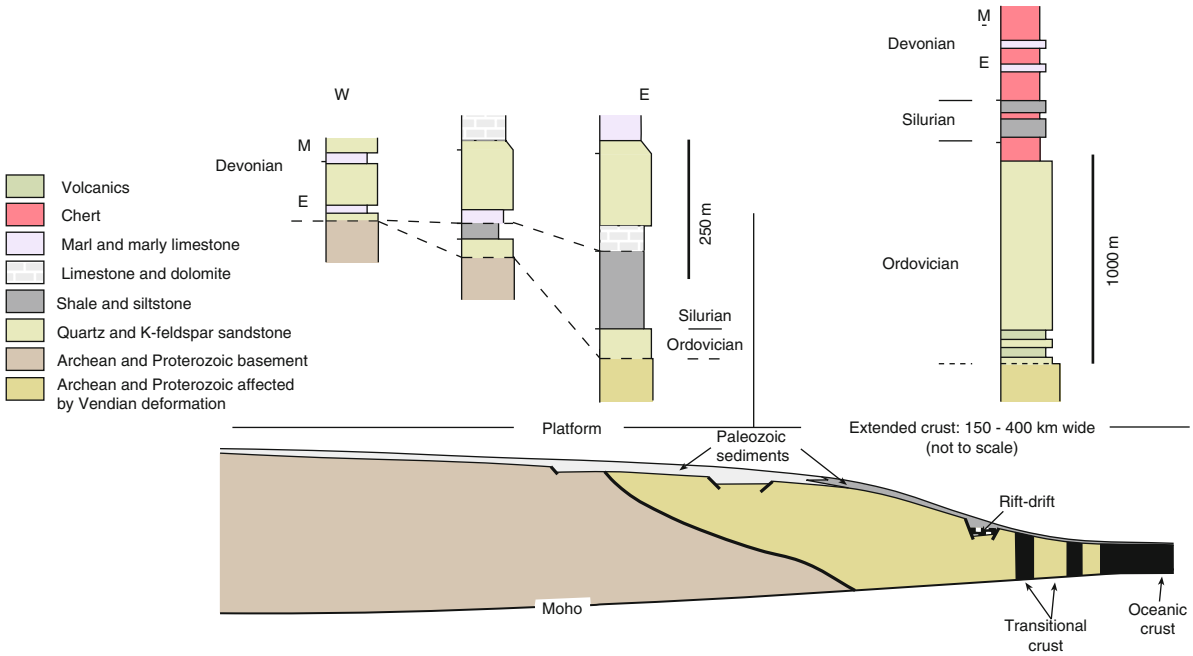

Fig. 11.3 A schematic section of the Laurussia margin in the Middle Devonian in the South Urals, just prior to collision with the Magnitogorsk Arc. The Paleozoic platform stratigraphy that was present at this time is represented by three schematic stratigraphic columns outcropping along the Belaya River, at the southern end of the Bashkirian Anticlinorium (see Brown et al. 1997a, b). A schematic, composite rift-drift, slope, and rise facies stratigraphic column is interpreted from weakly deformed rocks found in the Sakmara Allochthon (after Puchkov 2002). Note that the extended part of the margin is not drawn to the same horizontal scale as the platform.

11.5 The Magnitogorsk Arc

Unlike the Tagil Arc, the Magnitogorsk Arc is only weakly deformed and is unmetamophosed, providing an excellent opportunity to study a Devonian arc. Nevertheless, with the exception of the Karamalytash anticline it is not possible to put age constraints on the timing of the little deformation that there is (Brown et al. 2001, 2006a) and it could be related to either the Devonian arc–continent collision or to the Late Carboniferous to Early Triassic continent–continent collision (Brown et al. 2008).

11.5.1 The Volcanic Rocks

The oldest part of the Magnitogorsk Arc exposed in the South Urals is represented by the Emsian-age Baimak-Buribai Formation which is composed of picrite, high-Mg basalt, basaltic andesite, and andesite lava flows intercalated with pyroclastics, hyaloclastites, agglomerates, volcaniclastics, thin beds of tuffaceous chert, and, locally, boninitic lavas and dikes (Kuz'min and Kabanova 1991; Spadea et al. 1998). The boninites are chemically primitive (Mg# 81–68) and very low in TiO_2 (Fig. 11.4), are strongly depleted in high field-strength elements (HFSE) with respect to normal mid-ocean ridge basalt (N-MORB), and have a flat rare earth element (REE) pattern (Fig. 11.5). The picrites have a Mg# of 81.4, very low TiO_2, and are the most HFSE-depleted rocks among the high-Mg lavas. The high-Mg basaltic andesite and andesite are lower in MgO (Mg# 73–62) and slightly higher in TiO_2 than the boninites (Fig. 11.4), are depleted in HFSE, and have a flat REE to slightly light rare earth element (LREE)-depleted pattern (Fig. 11.5). The island arc tholeiites (IAT), basaltic andesites and andesites have Mg# in the 68–42 range, low TiO_2 (0.4–0.8 wt%), have low and variable HFSE MORB-normalized values, and a flat or slightly LREE-enriched pattern. The calc-alkaline (CA) basalts, basaltic andesites and andesites Mg# in the 71–36 range, have higher TiO_2 contents than the other petrologic groups (0.5–1 wt%), have depleted to slightly enriched N-MORB normalized patterns, and

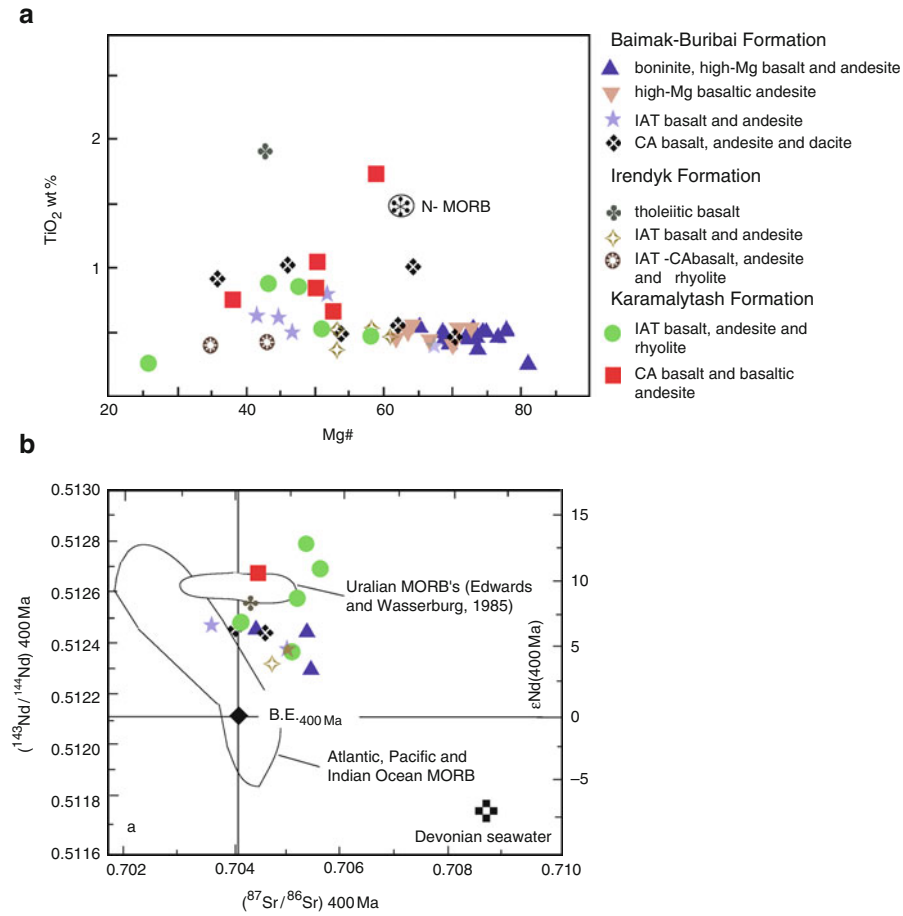

Fig. 11.4 (**a**) TiO_2 versus Mg# for Magnitogorsk Arc Devonian extrusive rocks (after Spadea et al. 2002; Brown et al. 2006a). (**b**) Initial $^{143}Nd/^{144}Nd$ versus $^{87}S/^{86}Sr$ (back calculated to 400 Ma) for representative Magnitogorsk Zone Devonian extrusive rocks (after Spadea et al. 2002; Brown et al. 2006a). The fields of Atlantic, Pacific and Indian MORB back calculated to 400 Ma, and Uralian MORB. The isotopic composition of Devonian seawater is from Burke et al. (1982) for Sr, and from Shaw and Wasserburg (1985) for Nd.

have a relatively high REE content with a LREE-enriched pattern. Spadea et al. (1998, 2002) and Brown and Spadea (1999) interpret the Baimak-Buribai Formation to have been erupted in a suprasubduction-zone setting at an early stage of intra-oceanic convergence.

From the latter part of the Emsian through the lowermost Eifelian, volcanism in the Magnitogorsk Arc evolved from the high-Mg basalts of the Baimak-Buribai Formation to island-arc calc-alkaline suites of the uppermost Baimak-Buribai and Irendyk formations. The Irendyk Formation consists of lava flows intercalated with pyroclastics, hyaloclastites, agglomerates, volcaniclastics, and, locally, thin beds of tuffaceous chert. Irendyk tholeiitic basalt has MORB-type characteristics with a high Fe_2O_3, with Mg# 43, a N-MORB type HFSE pattern that is about 20 times chondritic, is LREE depleted, and REE enriched (Figs. 11.4 and 11.5). IAT basalts and basaltic andesite are moderately fractionated (Mg# 61–54), typically low in TiO_2, are HFSE depleted (except P) with respect to MORB, and have a flat REE pattern that is ten times less than chondritic. IAT andesites and dacites are low Mg# (44–35), low TiO_2 (around 0.4 wt%), with MORB-type incompatible HFSE patterns and marked Ti depletion, and have REE contents that are more than ten times chondritic and a marked negative Eu anomaly (Spadea et al. 2002).

The uppermost Eifelian Karamalytash Formation outcrops in the central and eastern part of the Magnitogorsk Arc. It is composed of aphyric and plagioclase or

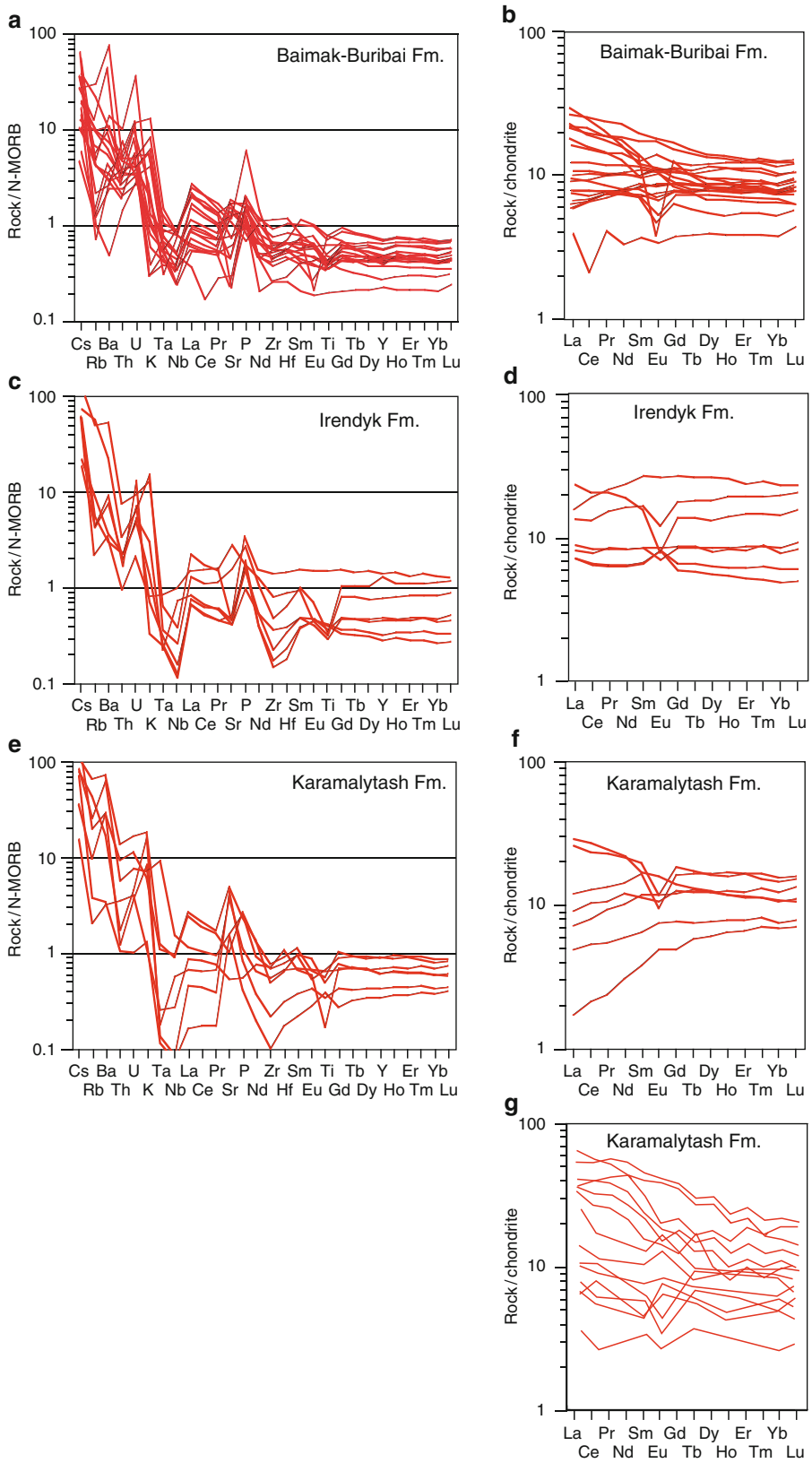
a
Baimak-Buribai Fm.
Rock/N-MORB
100
10
1
0.1
Cs Ba U Ta La Pr P Zr Sm Ti Tb Y Er Yb
Rb Th K Nb Ce Sr Nd Hf Eu Gd Dy Ho Tm Lu
b
Baimak-Buribai Fm.
Rock/chondrite
100
10
1
La Pr Sm Gd Dy Er Yb
Ce Nd Eu Tb Ho Tm Lu
c
Irendyk Fm.
Rock/N-MORB
100
10
1
0.1
Cs Ba U Ta La Pr P Zr Sm Ti Tb Y Er Yb
Rb Th K Nb Ce Sr Nd Hf Eu Gd Dy Ho Tm Lu
d
Irendyk Fm.
Rock/chondrite
100
10
1
La Pr Sm Gd Dy Er Yb
Ce Nd Eu Tb Ho Tm Lu
e
Karamalytash Fm.
Rock/N-MORB
100
10
1
0.1
Cs Ba U Ta La Pr P Zr Sm Ti Tb Y Er Yb
Rb Th K Nb Ce Sr Nd Hf Eu Gd Dy Ho Tm Lu
f
Karamalytash Fm.
Rock/chondrite
100
10
1
La Pr Sm Gd Dy Er Yb
Ce Nd Eu Tb Ho Tm Lu
g
Karamalytash Fm.
Rock/chondrite
100
10
1
La Pr Sm Gd Dy Er Yb
Ce Nd Eu Tb Ho Tm Lu

clinopyroxene phyric basalt, and rhyolite with minor basaltic andesite and quartz andesite. In the central part of the zone, the IAT basaltic andesite of the Karamalytash Formation has a Mg # between 58 and 44, TiO_2 in the 0.4–0.8 wt% range, and other HFSE are slightly to strongly depleted with respect to MORB (Figs. 11.4 and 11.5). The REE patterns are flat to variably LREE depleted. Calc-alkaline basalt and basaltic andesite have a Mg# between 52 and 38, is low in TiO_2 (0.63–0.72 wt%), is characterized by low N-MORB-normalized HSFE patterns, and are LREE enriched. In the eastern part of the Magnitogorsk Arc, the lower part of the Karamalytash Formation is characterized by high-Mg basalts with primitive REE patterns (Bochkarev and Surin 1996). These basalts have an arc tholeiite signature, although they are poor in Ti (Frolova and Burikova 1997). Rhyolites display two different affinities, one with a fractionated tholeiite signature and a second with a calc-alkaline signature (Gusev et al. 2000). Tholeiites have low Zr/Y ratios (5–7), indicative of an arc setting. The calc-alkaline rocks have LREE enrichment patterns with strong positive Eu anomalies.

From the Eifelian onwards volcanism shifted entirely to the eastern part of the Magnitogorsk Arc (Puchkov 1997; Gusev et al. 2000; Herrington et al. 2002), to the East Magnitogorsk volcanic front. In the northeast part of the Magnitogorsk Arc, the Givetian Kurosan Formation is composed of a continuous series of predominantly basalt to rhyodacite that is enriched in K and LREE (Figs. 11.4 and 11.5). Elevated Sr isotope values are suggestive of a contaminated magma source (Spadea et al. 2002). The Givetian to lowermost Frasnian Ulutau Formation consists mainly of andesite and dacite lava flows, near-vent breccias and sills intruded into tuffaceous and volcaniclastic sandstone and agglomerate (Yazeva et al. 1989). It comprises a series of largely calc-alkaline basaltic andesite through to rhyolite, with basaltic andesite and andesite forming around 40% of the sequence (Gusev et al. 2000). The Ulutau Formation is low-K calc-alkaline. Volcanism continued sporadically across the Magnitogorsk Arc until the earliest Bashkirian epoch of the Late Carboniferous, although they do not have a subduction zone geochemical signature. The East Magnitogorsk volcanic front was the primary source for the Late Devonian suture forearc sediment that is discussed below.

11.5.2 Forearc Basin Sediments

The Middle to Late Devonian Aktau Formation outcrops along the western margin of the central and southern part of the Magnitogorsk Arc (Fig. 11.6a). It consists of up to 150 m of uppermost Eifelian to lowermost Frasnian interbedded tuffaceous sandstone, chert and jasper, and minor conglomerate overlain by the Frasnian Mukas chert and Frasnian to Tournaisian volcaniclastics of the Zilair Formation (Maslov and Artyushkova 1991). The Aktau Formation is thought to be a remnant of the forearc basin to the Irendyk volcanic front that remained isolated from sediment input from elsewhere in the Magnitogorsk Arc until the latest Frasnian (Brown et al. 2001, 2006a).

The Magnitogorsk forearc basin consists of up to 5,000 m of westward thickening Givetian to Famennian chert and volcaniclastic sediments that overlie the volcanic edifice (Fig. 11.6b). The lowest unit is the Givetian Jarlykapovo Formation (Fig. 11.6), which consists of several tens of meters to approximately 200 m of jasper and chert that overlie the Irendyk Formation and is coeval with the Karamalytash Formation. The Bugulygyr jasper, which directly overlies the Karamalytash Formation, is correlated with the uppermost part of the Jarlykapovo Formation. The Jarlykapovo Formation (including the Bugulygyr jasper) often displays intense syn-sedimentary deformation locally (Brown et al. 2001, 2006a).

The Givetian to lowermost Frasnian Ulutau Formation stratigraphically overlies the Jarlykapovo Formation. The Ulutau Formation sediments were sourced from the volcanic sequences of the same name in the east (see Sect. 5.1). It ranges in thickness from several hundred to approximately 2,000 m, and consists of volcanomictic sandstone, with thin interbeds of tuffaceous chert, and, locally, thin beds of siliceous shale. Olistostromes, on the order of several hundreds of square meters, are widespread. These contain reworked Ulutau material, volcanics and, locally, blocks of limestone (Kopteva 1981; Brown et al. 2001, 2006a).

Fig. 11.5 Mid Ocean Ridge Basalt (N-MORB)-normalized incompatible element diagrams and chondrite-normalized rare earth elements diagrams for the Baimak-Buribai Fm. (**a** and **b**), the Irendyk Fm. (**c** and **d**) and the Karamalytash Fm. (**e** and **f**) (redrafted from Spadea et al. 2002). (**g**) Chondrite-normalized rare earth elements diagram for the Karamalytash Fm. in the eastern area of the Magnitogorsk Arc (redrafted from Herrington et al. 2002).

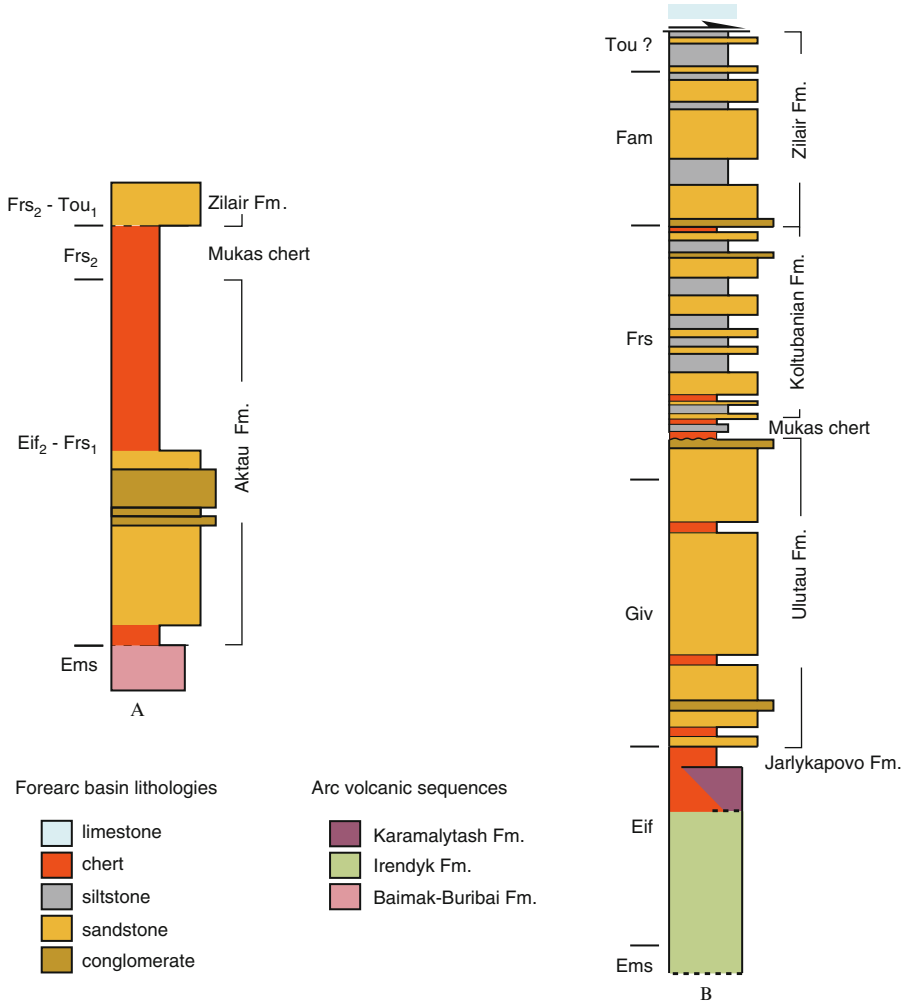

Fig. 11.6 (**a**) Schematic stratigraphic column of the Aktau synform (after Maslov and Artyushkova 1991). (**b**) A simplified stratigraphic column of the suture forearc basin sediments (after Brown et al. 2001; Maslov et al. 1993).

The tuffaceous Mukas chert outcrops throughout the Magnitogorsk Arc. It forms a 10–100 m thick unit and everywhere overlies the Ulutau Formation. The Mukas chert often displays chaotic folding, brecciation, and slumping on a variety of scales. The Frasnian-age Koltubanian Formation is composed of up to 1,500 m of westward-thickening volcanomictic siliceous sandstone, with interbeds of tuffaceous chert, grading into siliceous siltstones in the upper part of the formation. Locally, within the Koltubanian Formation, coherent slumps can be mapped for hundreds of meters in structural thickness, and up to a kilometer in length (Kopteva 1981; Brown et al. 2001, 2006a).

Conformably overlying the Koltubanian Formation, the latest Frasnian and Famennian Zilair Formation and the eastern time equivalent of the Zilair Formation in the South Urals accretionary complex (see below). It consists of up to 2,000 m of westward-thickening volcanomictic sandstone and siltstone. Olistostromes on the scale of 10–100 m wide and larger are common in the Lower Zilair formations. A spectacular example is the Biyagodinskay olistostrome, which has an outcrop area of c. 250 to c. 300 km^2, and a thickness of several hundred meters (Kopteva 1981; Brown et al. 2001, 2006a; Veymarn et al. 2004). Syn-sedimentary deformation is less common in the upper units of the Zilair Formation.

The sediments of the forearc basin are overlain by Early Carboniferous conglomerate and limestone. Locally, the contact is a steeply east-dipping

extensional fault (Brown et al. 2001). The forearc region is locally intruded by Middle to Late Carboniferous gabbroic dikes (Seravkin et al. 1992). Undeformed Jurassic clastic sediments unconformably overlie the forearc sediments, the Early Carboniferous sediments, and the Main Uralian Fault.

11.6 Arc–Continent Collision Accretionary Complexes

11.6.1 The Magnitogorsk Accretionary Complex

The Magnitogorsk accretionary complex is related to the collision of the Magnotogorsk Arc with the Laurussia margin (Brown et al. 1998, 2006a; Brown and Spadea 1999; Alvarez-Marron et al. 2000) and is one of the key units for deciphering the arc–continent collision history. Therefore, it is described in some detail below. It is made up of the Timirovo thrust system, the Zilair Nappe, the Suvanyak Complex, the Uzyan Allochthon, the Sakmara Allochthon, and the Maksutovo Complex (Figs. 11.7 and 11.8).

The Timirovo thrust system outcrops continuously for nearly 100 km along the northwestern margin of the accretionary complex. It is composed of highly sheared Middle Devonian reef limestone with local intercalations of arkosic sandstone (Brown et al. 1997a, b; Alvarez-Marron et al. 2000; Fernandez et al. 2004). Metamorphic grade is low, and the regional conodont color alteration index ranges from 4.5 to 5 (Vladimir Baryshev, pers. comm.). Kinematic indicators (σ and δ clasts, S-C fabrics, and extensional crenulation cleavages) together with the stretching lineation, indicate a top-to-the-WSW sense of movement (Brown et al. 1997a, b; Alvarez-Marron et al. 2000; Fernandez et al. 2004).

The Zilair Nappe consists of latest Frasnian and Famennian polymictic and greywacke turbidites of the Zilair Formation interpreted to have been deposited in a foreland-basin setting to the arc–continent collision (Mizens 1997, 2004; Brown et al. 1998, 2006a; Brown and Spadea 1999; Alvarez-Marron et al. 2000). The Zilair Formation has a structural thickness of 5–6 km and it youngs westward, with fine-grained, thin-bedded turbidites being more common in the west, whereas thicker beds of sandstones and conglomerates appear in the east (Keller 1949; Pazukhin et al. 1996; Puchkov et al. 1998). The metamorphic grade in the Zilair Nappe increases eastward from anchizone to greenschist facies (chlorite zone) (Bastida et al. 1997). The structure of the Zilair Nappe is that of a large-scale synform with a west-verging ramp anticline at the front with a well-developed, moderately east-dipping, penetrative axial planar pressure solution cleavage (Alvarez-Marron et al. 2000; Brown et al. 1998, 2004, 2006a). Along the eastern margin of the nappe, folds verge to the east and the cleavage fans until it dips westward.

The Suvanyak Complex consists predominantly of moderately to strongly deformed chlorite and white mica-bearing metaquartzite, quartz and albite schist, and chlorite and white mica phyllite thought to represent the Paleozoic slope sediments of the Laurussia continental margin (Zakharov and Puchkov 1994; Puchkov 1997). Its regional-scale structure is that of an upright antiform (the Uraltau Antiform) that folds an earlier, locally penetrative foliation (Hetzel et al. 1998; Alvarez-Marron et al. 2000). Zones of intense shearing, with rare top-to-the-west shear sense indicators are found locally. The metamorphic grade appears to increase eastward from lower to middle greenschist facies.

The Uzyan Allochthon (Brown et al. 2006a) is made up of Ordovician to Middle Devonian quartz sandstone, siltstone, and shale, with layers of chert predominating in the top of the succession (Puchkov 2002). These sediments are thought to have been deposited in a deep-water environment on the continental slope and rise. Metamorphism in the Uzyan Allochthon sediments reaches lower greenschist facies. The Kraka massif structurally overlies the sediments of the Uzyan Allochthon. Kraka is composed predominantly of weakly metamorphosed lherzolite, but also contains dunite, harzburgite, pyroxenite, wehrlite, and gabbro, all folded into an open synform and with a well developed foliation (Savelieva 1987; Savelieva et al. 2002). The basal contact between Kraka and the underlying sediments is a several hundred meter-thick tectonic mélange. On the basis of its normal mid-ocean ridge basalt REE signature, Savelieva et al. (1997) interpret Kraka as a fragment of oceanic mantle, although enrichment of large ion lithophile elements has led Fershtater and Bea (1996) to suggest that it may be a fragment of the continental

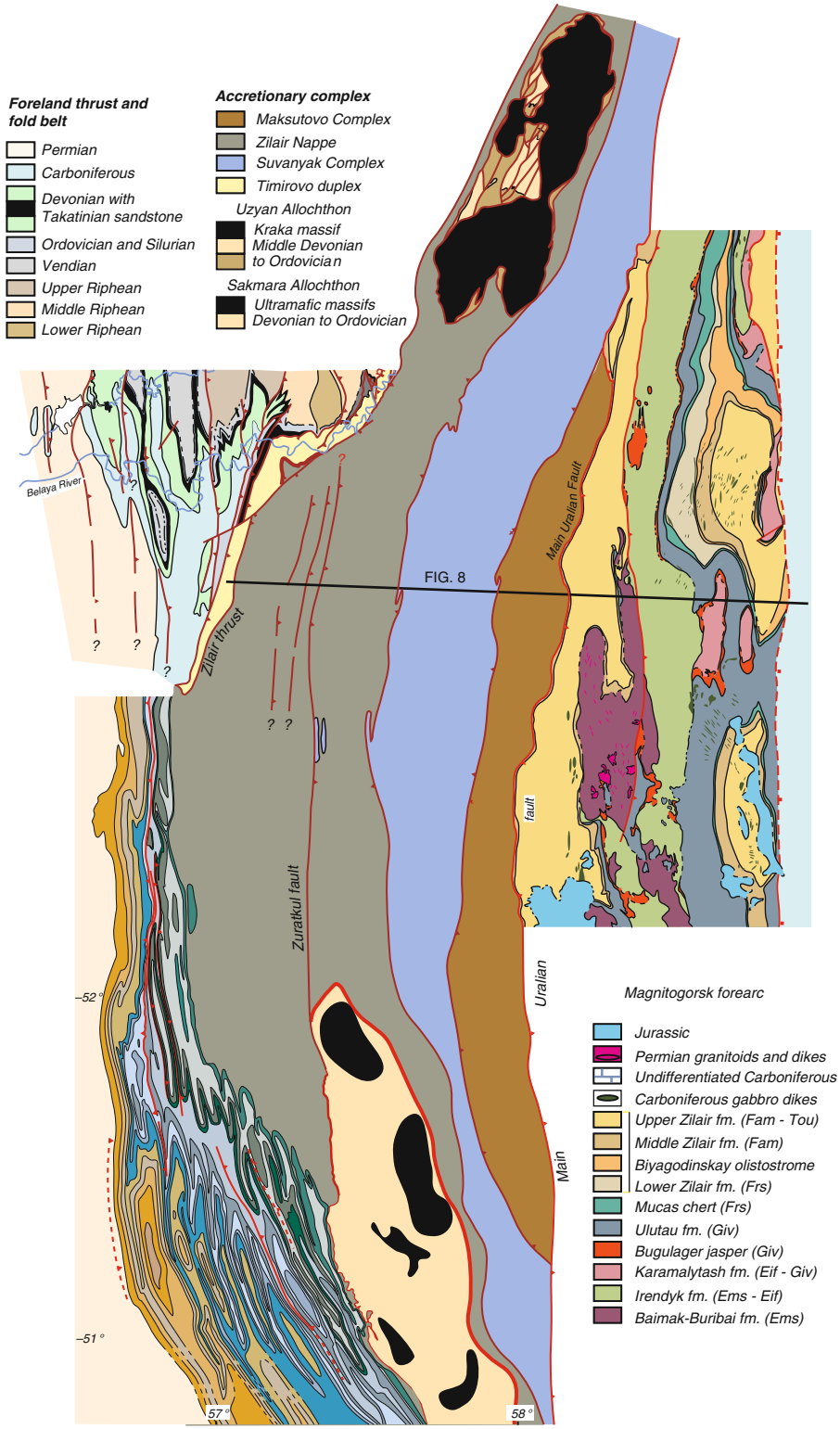

Fig. 11.7 Geological map of part of the South Urals foreland thrust and fold belt, the Magnitogorsk accretionary complex, and the western part of the Magnitogorsk Arc. The *black line* shows the location of the cross section in Fig. 11.8.

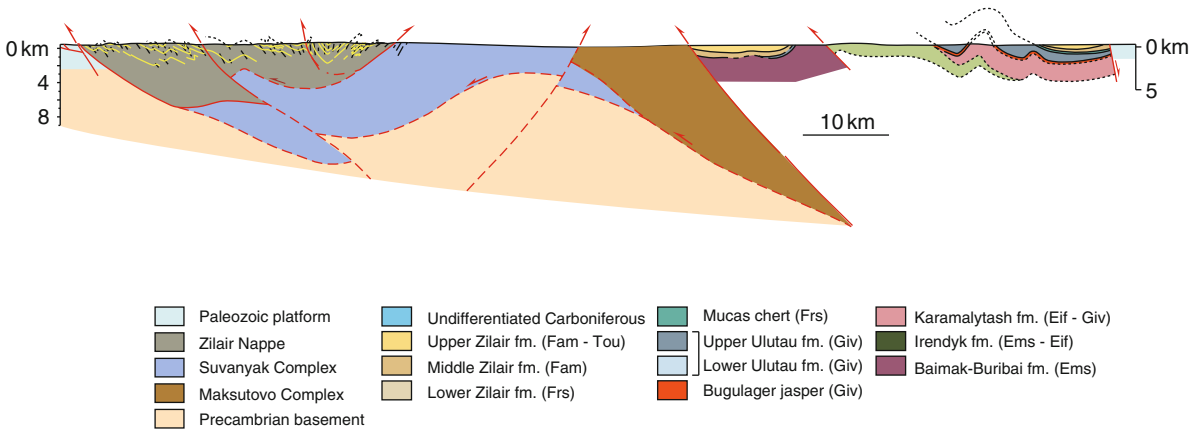

Fig. 11.8 Geological cross section showing the structural relationships between the different units within the accretionary complex and the Magnitogorsk Arc. The cross section is based on reflection seismic profile R114 (Brown et al. 1998, 2006a) and on our geological field mapping (Alvarez-Marron et al. 2000).

mantle. Paleontological and radiometric age data are not available for Kraka. The structure of the Uzyan Allochthon is not well known because of poor exposure in the sedimentary rocks, but it appears to consist of several thin, west-verging thrust sheets, overlain by the Kraka massif.

The Sakmara Allochthon is made up of several imbricate thrust sheets consisting of Ordovician to Devonian shale, sandstone, chert and limestone interpreted to have been deposited on the continental slope and rise (Puchkov 2002). Thrust sheets and a mélange consisting of pillow lava and chert, tuffaceous turbidites, polymictic olistostromes, belonging to oceanic and island arc crust, all in a serpentinite matrix, structurally overlie these. The Kempirsay and Khabarny ultramafic massifs form the uppermost thrust sheets. The best studied of these, Kempirsay, is composed of mantle tectonite of mostly harzburgite composition, accompanied by cumulates, gabbro, a sheeted dike complex, and basaltic pillow lavas capped with Middle Ordovician shale (Ivanov and Puchkov 1990; Saveliev and Savelieva 1991; Savelieva and Nesbitt 1996; Savelieva et al. 1997, 2002; Melcher et al. 1999). Two Sm–Nd isochron ages (397 ± 20 and 396 ± 33 Ma) were determined from Kempirsay gabbros (Edwards and Wassenburg 1985), but more recently Sm–Nd isochrons from two lherzolite samples yielded ages of 487 ± 54 Ma, and a U–Pb zircon age of 420 ± 10 Ma was obtained from dikes of pyroxene gabbro composition crosscutting ultramafic rocks (see Savelieva et al. 2002).

The Maksutovo Complex is composed of two tectono-metamorphic units that are structurally juxtaposed (Lennykh 1977; Zakharov and Puchkov 1994; Dobretsov et al. 1996). The structurally lowest unit consists predominantly of glaucophane-bearing metasediment and minor amounts of mafic eclogite and blueschist. Eclogite mineral phases record prograde growth zoning and a clockwise P-T path, with pressure conditions having been estimated at about 2.0 + 0.3 GPa and 550 ± 50°C, followed by retrograde blueschist and greenschist facies conditions that indicate cooling during exhumation (Beane et al. 1995; Hetzel et al. 1998; Schulte and Blümel 1999). Recently, microdiamond aggregates have been described from the Maksutovo Complex (Bostick et al. 2003), suggesting that a minimum pressure of 3.2 Gpa and a temperature of 650°C may have been reached. However, Sr-isotope equilibrium among eclogite facies phases and among eclogite facies fluid veins and host rock, together with the prograde fabrics recorded in them, indicate that these rocks do not record any evidence of retrograde metamorphism from this apparent ultrahigh-pressure event (Hetzel et al. 1998; Glodny et al. 2002). The age of eclogite facies metamorphism in the lower unit has been constrained by various isotopic systems at a mean of 378 ± 6 Ma (Matte et al. 1993; Lennykh et al. 1995; Beane and Connelly 2000; Hetzel and Romer 2000; Glodny et al. 2002), or Frasnian. U–Pb dating of zircons have yielded slightly older ages of 388 ± 4 (Leech and Willingshofer 2004). The upper unit of the

Maksutovo Complex is composed of Paleozoic metasedimentary and metavolcanic rocks. A serpentinite mélange at the base of the upper unit (and in contact with the lower unit) contains metarodingites that pseudomorph lawsonite. These rocks experienced peak metamorphic conditions of 0.8 GPa and <450°C (Dobretsov et al. 1996; Hetzel et al. 1998), although recent estimates by Schulte and Sindern (2002) suggest that pressures = 1.8–2.1 GPa and a temperatures of 520–540°C may have been reached. The lower and upper units were structurally juxtaposed after eclogite facies metamorphism in the lower unit along a top-to-the ENE retrograde shear zone (Hetzel 1999) that yielded Rb–Sr and Ar–Ar ages of 360 ± 8 Ma (Beane and Connelly 2000; Hetzel and Romer 2000). Retrograde conditions in the upper unit have been determined to be >0.45 GPa at T < 440°C at 339 Ma (Schulte and Sindern 2002). Ar–Ar white mica ages from retrograde shear zones in the Maksutovo Complex range from 370 to 332 Ma (Beane and Connelly 2000; Hetzel and Romer 2000) and Rb-Sr ages cluster around 360 Ma (Hetzel and Romer 2000). The lower unit of the Maksutovo Complex is thought to have been derived from the Laurussia continental margin, whereas the upper unit has been interpreted as containing remnants of the Uralian ocean crust (Hetzel 1999) and fragments of island arc material (e.g., Dobretsov et al. 1996). The structure of the Maksutovo Complex is not well known, although Hetzel et al. (1998) and Leech and Ernst (2000) show it to be complexly deformed with, locally, two foliations developed during prograde metamorphism and two foliations developed during retrograde metamorphism (Hetzel et al. 1998). Final emplacement appears to have taken place between about 340 Ma (the youngest Ar–Ar ages) and the cooling through 110°C at about 300 Ma according to apatite fission track modeling (Leech and Stockli 2000). The Maksutovo Complex is unconformably overlain by Lower Jurassic sediments.

11.6.2 The Tagil Accretionary Complex

A well-developed accretionary complex such as that found in the South Urals is not present in the Middle Urals. The Bardym thrust stack (e.g., Zhivkovich and Chekhovich 1985; Puchkov 2002) may, however, represent a fragment of an accretionary complex. In the Bardym thrust stack, the Paleozoic continental slope deposits comprise about 200 m of Middle to Late Ordovician clastic sediments, with interbeds of limestone, diabase, and tuffs (Puchkov and Ivanov 1982). The Silurian is made up of about 350 m of predominantly chert. The Devonian consists of about 1,000 m of chert, clastics, and basalt. The volcanic arc deposits in the Bardym thrust stack consist of about 1,000 m of Silurian to Lower Devonian andesite, andesitic basalt, tuffs, and rare chert, overlain by about 300 m of Lower Devonian(?) trachybasalt, trachyandesite and tuff.

11.7 The Main Uralian Fault

The paleo-margin of Laurussia is juxtaposed against the Magnitogorsk and Tagil arcs along the Main Uralian Fault. However, on the basis of geological, potential field, topographic, and reflection seismic data, Ayarza et al. (2000) have suggested that the current Main Uralian Fault is not everywhere the remnant of the same, coeval paleosubduction zone along which arc–continent collision occurred. In the South Urals it appears to be the original arc-continent suture, whereas in the Middle Urals it represents the westernmost strand of an extensive Late Carboniferous to Permian age strike-slip fault system that reactivated the original suture and displaced part of the Tagil Arc to the north. For this reason the remainer of this section will concentrate on the Main Uralian Fault in the South Urals.

In the South Urals, the Main Uralian Fault is an up to 10 km wide mélange consisting predominantly of serpentinite in which fragments of Devonian suprasubduction zone volcanics and sediments are found. Kinematic criteria that reliably indicate a consistent movement direction are lacking. Reflection seismic profiling suggests that the Main Uralian Fault dips eastward and extends at least into the middle crust (Echtler et al. 1996; Knapp et al. 1996; Brown et al. 1998, 2008). In the northernmost part of the South Urals (c. 55° N), it has been intruded by rocks of the Syrostan batholith that has a deformed phase dated at 333 ± 3 Ma, and an undeformed phase dated at 327 ± 2 (Montero et al. 2000) thereby dating the end of tectonic activity along the Main Uralian Fault in the South Urals (Ayarza et al. 2000).

The Main Uralian Fault contains olistostromes and several lenticular or wedge-shaped slabs of mantle ultramafic rocks that measure up to 1 km^2 in size (e.g., Nurali, Mindyak, Baiguskarovo and others). These bodies are mostly lherzolitic in composition, with an upper unit consisting of a crust-mantle transition zone made of mantle restites and ultramafic cumulates that are intruded by gabbro and diorite (Savelieva 1987; Savelieva et al. 1997, 2002; Garuti et al. 1997). The Mindyak lherzolite, is of special interest since its geochemical signature suggests an intra-oceanic suprasubduction zone setting (Scarrow et al. 1999). Garnet-tschermakite/pargasite-diopside-bearing blocks within a tectonic breccia in the upper mantle sequences of the Mindyak massif represent metamorphosed gabbros that originally crystallised at low pressures followed by low temperature rodingite alteration and then metamorphism under upper mantle conditions (T ~ 800°C and P ~ 1 GPa) (Cortesogno et al. 1998) at approximately 415–410 Ma (Savelieva et al. 1999; Scarrow et al. 1999), suggesting that it was subducted and metamorphosed during the early stages of intra-oceanic subduction.

11.8 Provenance of Syn-Collisional Sediments

The provenance of syn-collisional sediments has only been studied in the South Urals where the Zilair Formation represents sediments that were deposited during the late stage of arc–continent collision in a forearc and foreland-basin setting. Sedimentary clasts dominate in the Zilair Formation, although metamorphic lithoclasts make up a large percentage of the clasts (Brown et al. 1996, 2006a; Gorozhaninia and Puchkov 2001; Willner et al. 2002) (Fig. 11.9). Among the transparent heavy minerals, metamorphic minerals dominate, including epidote, garnet, tourmaline, amphibole, titanite and chloritoid, and possibly most or all of the rutile and apatite (Arzhavitina 1978; Arzhavitina and Arzhavitin 1991; Willner et al. 2002). Volcanic lithoclasts of basic to acid composition are also abundant in the Zilair Formation, as are clasts derived from a mafic to ultramafic source (Willner et al. 2002). When plotted on the discrimination diagrams of Dickinson (1985) the Zilair Formation falls across the fields assigned to magmatic arcs and into the mixed orogen source field (Fig. 11.9). Similarly, a plot of the three major types of lithoclasts (sedimentary, metamorphic and volcanic) shows that the Zilair Formation does not conform with any one of the discrimination fields established by Ingersoll and Suzcek (1979). In all three types of plot there is a broad scatter indicating a mixture of materials from different sources. The same clast signature is found in the Zilair Formation in both the accretionary complex and Magnitogorsk Zone (i.e. in the foreland and forearc basins, respectively). Also, there is no variation in clast spectrum with the age of deposition.

The strong angularity of the majority of the clasts, together with the presence of low stability minerals such as K-feldspar, amphibole, pyroxene, biotite, garnet or carbonate, and the frequent local enrichment of specific heavy minerals, point to a very low degree of transport abrasion and therefore a nearby source area (Willner et al. 2002). The source of volcanic lithoclasts in the Zilair Formation was the Magnitogorsk Arc and/or volcanic rocks that are found as blocks within the Main Uralian Fault zone. Metamorphic clasts appear to have been derived from the Suvanyak and Maksutovo complexes, whereas the source of mafic to ultramafic clasts was most likely the ophiolite and peridotite units derived from the Main Uralian Fault.

11.9 Current Crustal Structure of the Middle and South Urals

The ESRU, URSEIS (Fig. 11.10), and reprocessed Russian reflection/refraction seismic surveys provide significant data for interpreting the current crustal structure of the Uralides (Echtler et al. 1996; Knapp et al. 1996; Carbonell et al. 1996, 1998, 2000; Steer et al. 1995, 1998; Tryggvason et al. 2001; Friberg et al. 2000, 2002; Kashubin et al. 2006; Brown et al. 2002, 2008) and provides insights into the nature of the Laurussia margin prior to arc–continent collision. In the Middle Urals (ESRU) (Fig. 11.10a) and Southern Urals (URSEIS) (Fig. 11.10b) the crust of the former Laurussia margin thickens eastward from ~40 km to ~48 km, and is imaged by sub-horizontal to east-dipping reflectivity. Many of these east-dipping reflections can be related to the Precambrian evolution of the rocks that made up the Laurussia margin

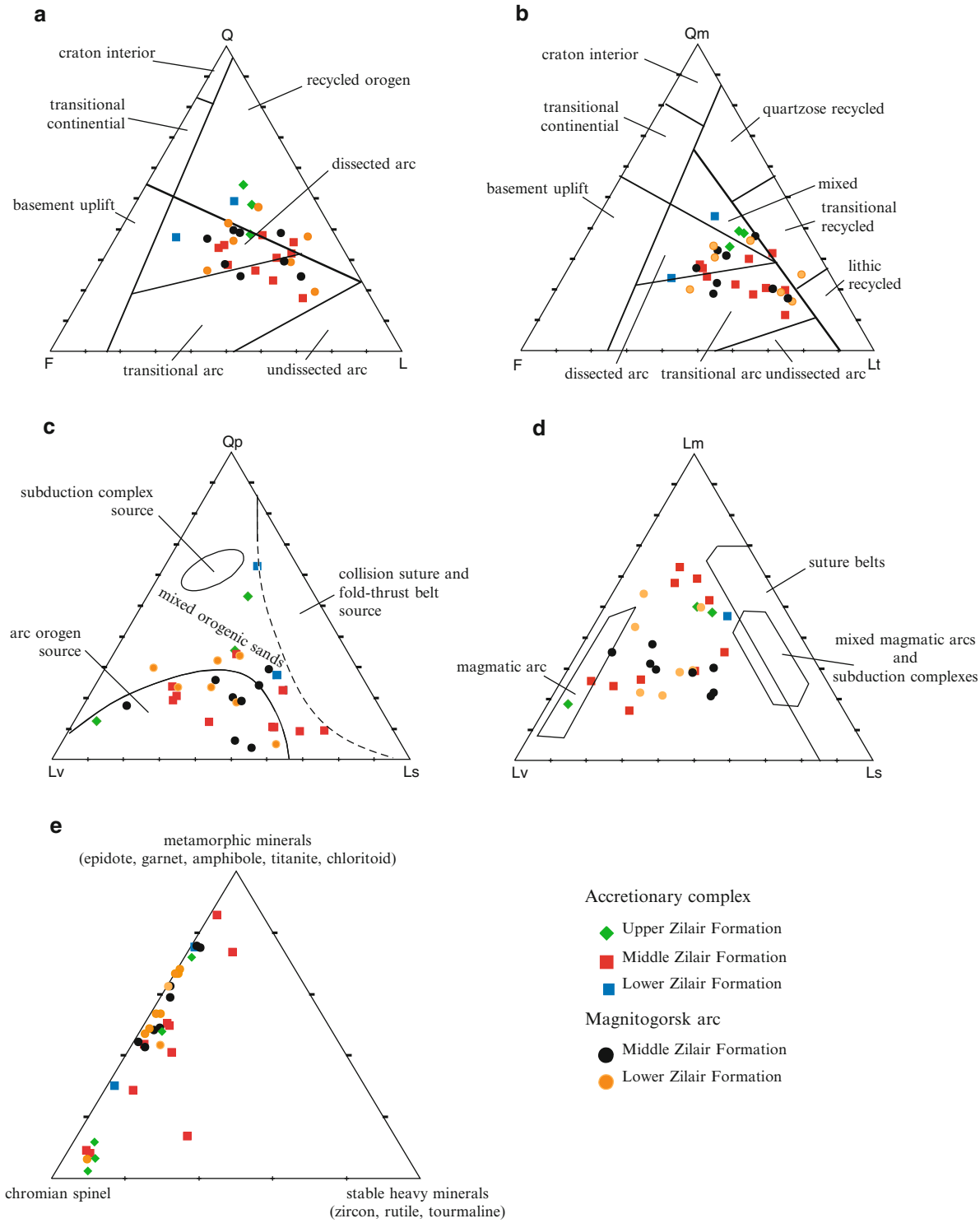

Fig. 11.9 The light mineral spectrum of the Zilair Formation in the accretionary complex and the Magnitogorsk Arc (redrafted from Willner et al. 2002; Brown et al. 2006a). (**a**–**c**) discrimination diagrams after Dickinson (1985). Qm = monocrystalline quartz, Qp = polycrystalline quartz, Lt = L + Qp, Ls = sedimentary lithoclasts, Lv = volcanic lithoclasts. (**d**) Variation of sedimentary (L_S), metamorphic (L_m) and volcanic lithoclasts (L_V). Discrimination fields after Ingersoll and Suzcek (1979). (**e**) Variation of metamorphic heavy minerals, stable heavy minerals, and chrome spinel.

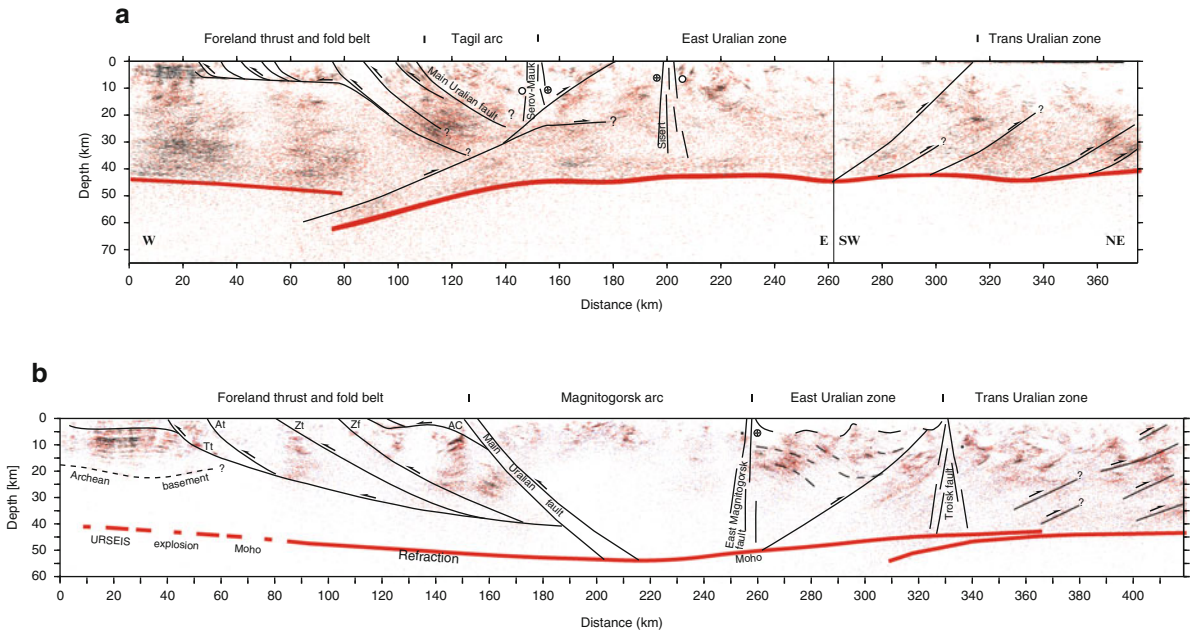

Fig. 11.10 Interpreted line drawings of the depth migrated ESRU (**a**), and URSEIS (**b**) reflection seismic profiles (after Brown et al. 2008). These profiles show, in part, the structure of the Laurussia margin prior to arc–continent collision and the current juxtaposition of the Tagil and Magnitogorsk arcs relative to the paleomargin rocks.

(Tryggvason et al. 2001; Brown et al. 2002, 2008), clearly indicating that it was highly structured at the time of arc–continent collision. The suture zone between the Laurussia margin and the accreted terranes, the Main Uralian Fault, is poorly imaged in the URSEIS section, but in the ESRU section it is imaged as a zone of east-dipping reflectivity that extends from the surface into the middle crust; it marks an abrupt change to weakly subhorizontal reflectivity in the Tagil arc (e.g., Ayarza et al. 2000). East of the Main Uralian Fault, the Magnitogorsk (South Urals) and the Tagil (Middle Urals) arcs display moderate to weak upper crustal reflectivity, and diffuse middle to lower crustal reflectivity. The Moho beneath the Magnitogorsk Arc is poorly imaged in the reflection data, but based on refraction data is interpreted to be at 50–55 km depth (Thouvenot et al. 1995; Juhlin et al. 1996; Carbonell et al. 1998; Brown et al. 2008), whereas in the ESRU data the Moho beneath the Tagil Arc is clearly imaged, but may be related to more recent tectonothermal processes (Kashubin et al. 2006; Juhlin et al. 2007). East of the arc complexes, the wide zone of anastomosing strike-slip faulting and granitoids of the East Uralian zone is imaged in the seismic sections as clouds of diffuse reflectivity interspersed with, or cut by sharp, predominantly west-dipping reflections. In the Southern and Middle Urals, west-dipping reflectivity of the Trans-Uralian zone extends from the middle crust into the lower crust where it appears to merge with the Moho (Echtler et al. 1996; Knapp et al. 1996; Steer et al. 1998; Friberg et al. 2000, 2002; Kashubin et al. 2006; Brown et al. 2002, 2008). This reflectivity has been interpreted to be related to the Late Carboniferous to Triassic continent–continent collision that formed the Uralide Orogen (e.g., Brown et al. 2008).

11.9.1 Velocity Structure

In the GRANIT profile of the Middle Urals (Juhlin et al. 1996) (Fig. 11.11a), Vp in the upper crust ranges from about 5.5 kms^{-1} near the surface to around 6.4 kms^{-1} at roughly 15 km depth across the former continental margin, and about 10 km depth in the Tagil and East Uralian zones. In the middle crust, Vp ranges from 6.4 up to 6.8 kms^{-1} at about 30 km depth across-all tectonic units. Lower crustal velocities reach as high as 7.6 kms^{-1} in the lowermost crust before

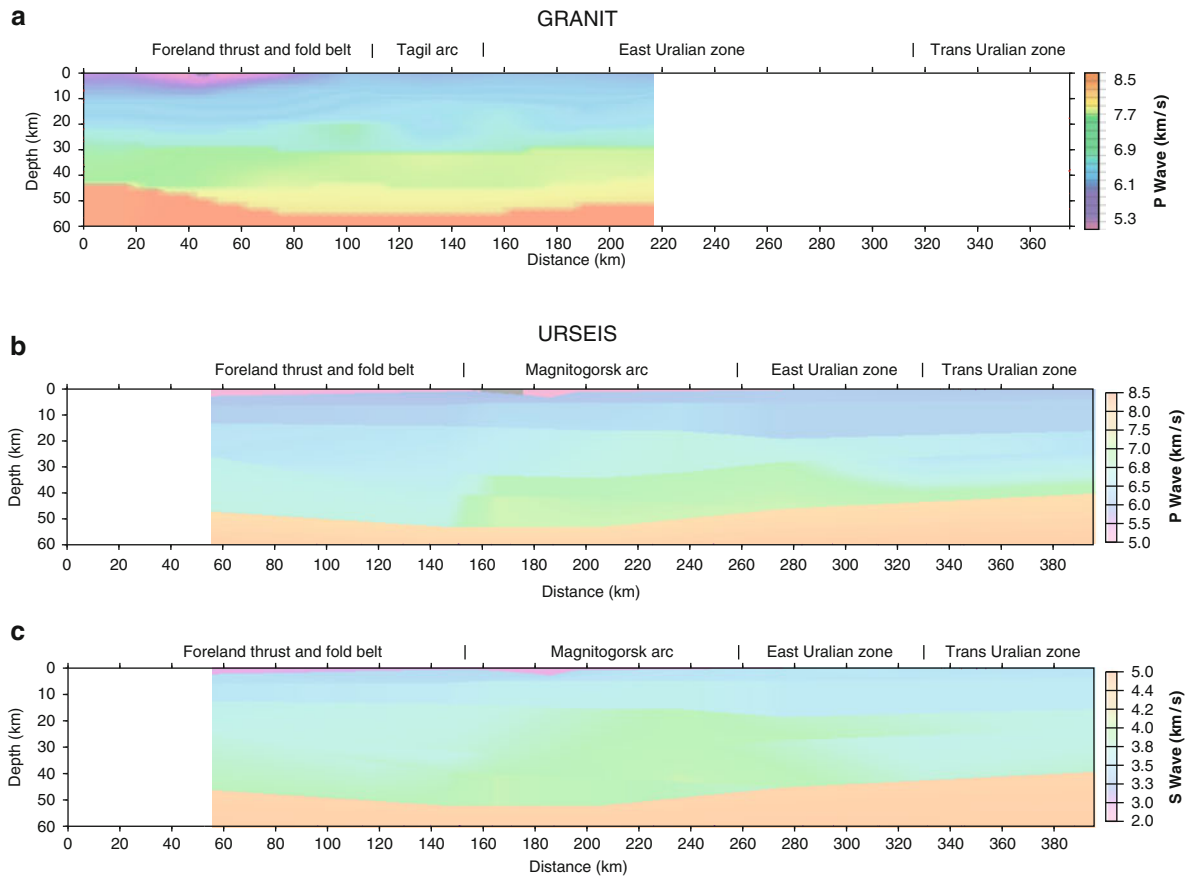

Fig. 11.11 (**a**) P-wave velocity model of the GRANIT data plotted in the reference frame of the ESRU profile. (**b**) P-wave velocity model of the URSEIS wide-angle data plotted in the reference frame of the reflection profile. (**c**) S-wave velocity model of the URSEIS wide-angle data plotted in the reference frame of the reflection profile. Note that, especially in the case of the South Urals, that there is still a significant velocity contrast from rocks of the Laurussia margin to those of the arcs.

reaching an upper mantle velocity greater than 8.0 kms^{-1}. Beneath the easternmost part of the former continental margin, and extending eastward beneath the Tagil and East Uralian zones, the crust thickens by approximately 10 km, reaching c. 60 km. Velocities in this thickened zone increase from 7.6 to 7.8 kms^{-1} before attaining mantle velocities of greater than 8.0 kms^{-1}. The lower crustal P-wave velocities along the GRANIT profile are high compared to those in the South Urals (Carbonell et al. 2000) and to the global average (Christensen and Mooney 1995), but similar to those interpreted from thickened crust in central Finland (Moisio and Kaikkonen 2004).

In the South Urals, upper crustal Vp (Fig. 11.11b) reaches up to 6.2 kms^{-1} to a depth of approximately 13 km in the former continental margin and Magnitogorsk Arc. Eastward, in the East and Trans-Uralian zones, the upper crustal Vp reaches 6.2–6.3 kms^{-1} at a depth of between 15 and 18 km. Below these depths there is a gradual increase in Vp to values of up to 6.7 kms^{-1}. In the westernmost part of the former margin, there is a jump in Vp from 6.5 to 6.7 kms^{-1} at about 25–30 km depth that disappears eastward. From the Main Uralian Fault eastward there is a velocity increase from 6.4 kms^{-1} at the base of the upper crust to between 6.6 and 6.8 kms^{-1} at the top of the middle crust and then a gradual increase up to 7.0 kms^{-1} above the Moho. Vp in this area also increases eastward to a maximum in the eastern part of the Magnitogorsk Arc and the western part of the East Uralian Zone, after which it decreases again. The lowermost crust to the east of the Main Uralian Fault is characterized by an eastward-thinning band of Vp of 7.0–7.1 kms^{-1}. The Moho is marked by an increase

in Vp to >8.0 kms^{-1}. Crustal thickness increases from c. 42 km in the west and to c. 53 km eastward beneath the Magnitogorsk Arc.

In the South Urals, upper crustal Vs (Fig. 11.11c) in the former continental margin reaches 3.5–3.6 kms^{-1} at a depth of about 13 km, increasing in the Magnitogorsk arc to 3.9 kms^{-1}, and decreasing again to a maximum of 3.6 kms^{-1} at about 15–17 km depth in the East and Trans-Uralian zones. Below this depth there is an increase in Vs to between 3.7 and 3.9 kms^{-1} and then a gradual increase from 3.9 to 4.0 kms^{-1} at the Moho. Vs in the middle and lower crust increases eastward to a maximum in the eastern part of the Magnitogorsk Arc and the western part of the East Uralian Zone, after which it decreases again. The lowermost crust in the eastern part of the Magnitogorsk arc and the western part of the East Uralian Zone is marked by a high Vs in which velocities reach 3.9–4.0 kms^{-1}. The Moho is characterized by an increase from crustal velocities of ≤4.0 kms^{-1} to mantle velocities of >4.6 kms^{-1}.

11.9.2 Crustal Composition of the South Urals Derived from Geophysical Data

Petrophysical modeling (Brown et al. 2003; Brown 2007) (Fig. 11.12) of the URSEIS data in the South Urals suggests that the average composition of the upper crust of the deformed former Laurussia margin is best characterized by phyllite and perhaps slate and mica quartz schist. Granite and biotite gneiss both fall within the acceptable values, but since neither fit the known geology they are discarded. The velocity and density data for the middle crust fall outside the values for most of the measured rock types, although the composition may be best characterized by mica quartz schist, felsic granulite and paragranulite. The lower crust of the former Laurussia margin is likely composed of amphibolite and mafic granulite, which is in keeping with the lithology of the Archean crystalline basement in outcrop.

The composition of the upper part of the middle crust of the Magnitogorsk Arc is not well constrained by the velocity and density data, but on the basis of surface geology is interpreted to consist of zeolite to prehnite-pumpellyite facies basalt and its intrusive equivalents (diabase, diorite, and tonalite). The lower part of the middle crust fits the parameters for greenschist facies basalt, amphibolite, and mafic granulite quite well. The Magnitogorsk Arc lower crust appears to be composed of gabbro-norite, mafic garnet granulite or hornblendite.

The upper and middle crust of the East Uralian and Trans-Uralian zones is best characterized by low metamorphic grade sediments, basalt, granite, and/or felsic gneiss. The middle crust in the East Uralian Zone, and extending into the lower crust in the Trans-Uralian Zone, is best characterized by greenschist facies basalt, amphibolite, and mafic granulite (and

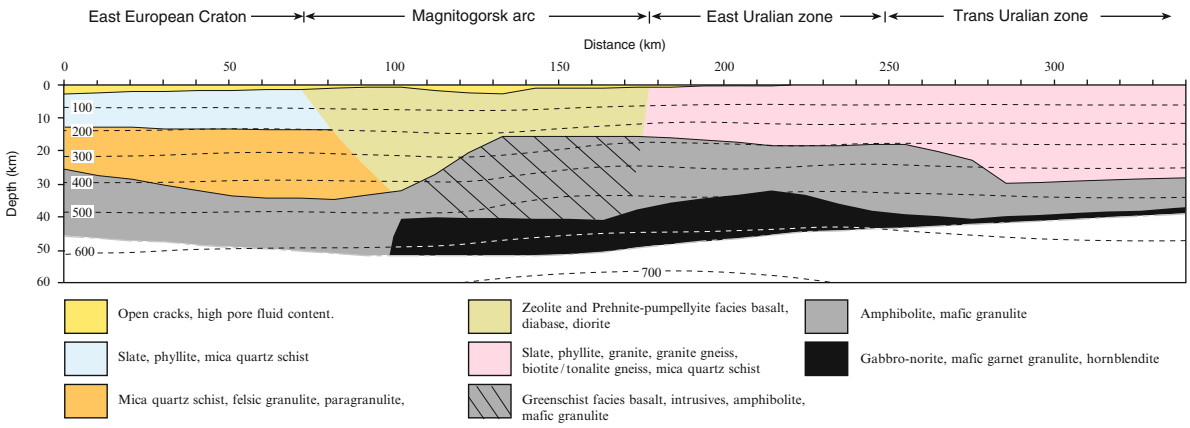

Fig. 11.12 Crustal composition model along the URSEIS transect determined from physical properties data (after Brown et al. 2003). The model clearly demonstrates that there is a strong contrast in physical properties (in particular seismic velocities and density) from the former continental margin to the Magnitogorsk Arc, suggesting that inherited continental crustal inhomogeneties still exist after some 360 My.

to a lesser extent anorthosite and anorthositic granulite). The lower crust in the East Uralian Zone, and the lowermost crust in the Trans-Uralian Zone is best characterized by gabbro-norite, mafic garnet granulite and/or hornblendite.

11.10 Discussion

The convergent tectonic evolution of the Uralides began in the Middle Devonian in the South Urals as the Magnitogorsk island arc began to collide with the margin of Laurussia (Zonenshain et al. 1984, 1990; Puchkov 1997, 2000; Brown and Spadea 1999; Alvarez-Marron 2002; Brown et al. 2006a). It is less clear when the Tagil Arc began to collide, but active collision appears to have been taking place by the Early Carboniferous (Zonenshain et al. 1984, 1990; Puchkov 1997, 2000). Below, we develop a detailed model for the arc–continent collisions that took place in the Uralides (Fig. 11.13). Much of the emphasis is placed on the South Urals, since the Magnitogorsk Arc is much better preserved and exposed than the Tagil Arc, and it has therefore been more extensively studied.

11.10.1 Intra-Ocean Subduction and Arc Formation

The Baimak-Buribai Formation boninites of the Magnitogorsk Arc have been interpreted to have erupted in a forearc position, similar to other boninites worldwide (Crawford et al. 1989; Tatsumi and Maruyama

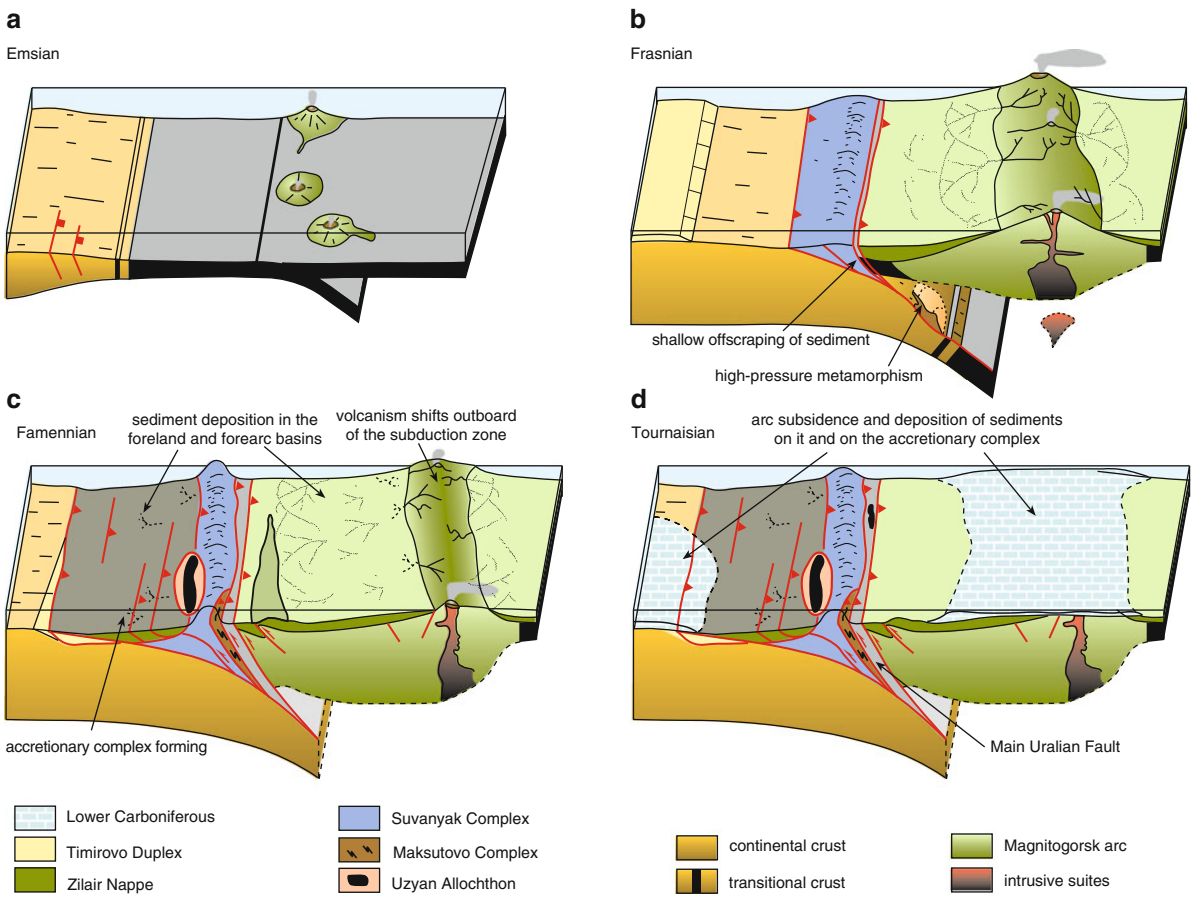

Fig. 11.13 Model outlining the tectonic processes through time that took place during arc–continent collision in the South Urals in the (**a**) Eifelian, (**b**) Frasnian, (**c**) Famennian, (**d**) Tournaisian.

1989; Arndt 2003), and therefore to mark the early stage of subduction-related melting and the initiation of development of the arc (Spadea et al. 1998; Brown and Spadea 1999; Brown et al. 2006a) (Fig. 11.13a). By the end of the Emsian, volcanism had changed from arc-tholeiite to the calc-alkaline suites of the uppermost Baimak-Buribai and Irendyk formations, and continued as a mature intra-oceanic arc well into the Eifelian. On the basis of geochemical and isotopic data, Spadea and D'Antonio (2006) suggest a depleted MORB-type mantle component in the Baimak-Buribai Formation and an enriched, subduction-related component (fluids and melts) with increased pelagic sediment input for the younger Irendyk and Karamalytash formations.

11.10.2 Arc–Continent Collision

The first indication of arc–continent collision in the geological record of the Uralides is the Maksutovo Complex eclogites in the South Urals where part of the continental crust that had entered the subduction zone had reached ca. 70 km depth, and perhaps as much as 120 km, by the middle part of the Frasnian (378 Ma) (Fig. 11.13b). However, the earlier history is difficult to constrain since there are no time markers in the geological record that can be used. For example, the geochemistry of the Magnitogorsk Arc volcanic rocks do not reflect any input from the subducting continent margin, nor are there zircons in the volcanic and plutonic sequences that were recycled from the subducting continental crust (Fershtater et al. 2007). The increasing Nd isotope ratios in the Karamalytash Formation relative to those of the intra-oceanic Baimak-Burbai and Irendyk formations is contradictory to the patterns observed in the Australia – Banda Arc collision or the Grampian arc–continent collision of Ireland where a variable or decreasing Nd isotope ratio in the arc–continent collision-related volcanic rocks relative to the intra-oceanic sequences is thought to be indicative of a continental crustal source in the former (Draut et al. 2002; Elburg et al. 2005; Herrington et al. 2011). Similarly, the LREE patterns of the Magnitogorsk rocks do not indicate any continental crust contribution to the Karamalytash melts as they do in the Grampian of Ireland, for example (Draut et al. 2002, 2009). Therefore, in order to make an estimate of when the leading edge of the Laurussia margin could have entered the subduction zone, we look at published examples of the subduction of continental crust at various velocities and subduction angles (e.g., Ranalli et al. 2000; Li and Liao 2002). These models show that, at subduction velocities ranging from 2.5 to 10 cm per year and subduction angles of between 30° and 70°, approximately 0.5 and 3 My would have been needed for the leading edge of the Laurussia continental margin to reach the 70 km depth recorded by the Maksutovo high-pressure rocks. Adding this to the age of the high pressure metamorphism recorded in the Maksutovo Complex (378 Ma) we get a rough estimate of between 378.5 and 381 Ma (early Frasnian) for the entrance of the continental crust into the subduction zone in the South Urals. It is not possible to make such an estimate for the Middle Urals.

With the entrance of the continental crust into the subduction zone, the Paleozoic rise and slope sediments of the continental margin were shallowly underthrust beneath the crust and upper mantle of the forearc. The uppermost continental crust was subsequently detached within the sedimentary carapace and thrust westward along with the overlying forearc mantle. These rocks are currently represented by the Uzyan and Sakmara allochthons in the South Urals and possibly the Bardym thrust sheet in the Middle Urals. With continued subduction of the continental crust, parts of the slope and rise sediments were more deeply subducted, deformed and metamorphosed to lower and middle greenschist facies before being completely offscraped and exhumed to form the Suvanyak Complex. Similar processes to those suggested above have been interpreted in areas of active arc–continent collision such as Timor, Papua New Guinea, and Taiwan, where sedimentary offscraping and forearc crust and mantle obduction is currently taking place or has taken place in the recent past (Jahn et al. 1986; De Smet et al. 1990; Charlton et al. 1991; Abbott et al. 1997; Huang et al. 2000, 2006). These processes can also be inferred from analogue and thermo-mechanical modeling results, which suggest that shallow offscraping and exhumation of sediments is an integral part of arc–continent collision (van den Beukel 1992; Chemenda et al. 2001; Boutelier et al. 2003, 2004). With continued subduction, the continental crust reached depths of at least 50–70 km (and perhaps as much as 120 km) by the late Frasnian, where it was metamorphosed to eclogite facies before

starting its journey back up the subduction/exhumation channel.

The next indicator of arc–continent collision in the South Urals is the onset of deposition of the Zilair Formation sediments in the latest Frasnian (c. 376 Ma) (Fig. 11.13c). The Zilair sediments point to the presence of a sub-aerial accretionary complex (which included the first high-pressure rocks to reach the surface), that was being eroded and distributing sediments both to the foreland basin in the west and the forearc basin in the east (Brown et al. 1998, 2006a; Brown and Spadea 1999; Willner et al. 2002). The variety of clast types in the Zilair Formation, especially in the forearc basin, indicate that the East Magnitogorsk volcanic front also formed subaerial mountain ranges that provided sediments to the submarine foreland and suture forearc basins. The fact that both basins shared the same two source areas throughout their history suggests that they were linked and remained so until the end of arc–continent collision (Willner et al. 2002). Both the foreland and the forearc basins display evidence that widespread slumping and deformation was taking place during the latest Frasnian to the early Fammenian. As arc–continent collision was progressing, volcanism continued in the East Magnitogorsk volcanic front, and thrusting, folding, and sediment deposition were taking place in the forearc region throughout the Frasnian and Famennian. This is indicated by the onlapping geometry of the forearc basin sediments over the Karamalytash anticline, which is suggestive of a growth fold geometry and indicates that deformation and sedimentation were active simultaneously (Brown et al. 2001). The uplift of the South Urals accretionary complex, the widespread syn-sedimentary deformation in the Koltubanian Formation, and the initiation of growth of the Karamalytash anticline indicate basin instability and deformation that was caused by the arrival of the full thickness of the Laurussia continental crust at the subduction zone in the Frasnian (Brown et al. 1998, 2001, 2006a; Brown and Spadea 1999).

11.10.3 The Subduction Channel

The Mindyak lherzolite and the Maksutovo Complex provide important information about the physical conditions and the processes that were active in the subduction zone during intra-oceanic subduction and arc–continent collision, respectively (Brown et al. 2000, 2006a). These complexes indicate that the temperature conditions within the subduction zone were quite different during the early intra-oceanic stage, where it reached ca. 800°C at 30 km depth (data from the Mindyak lherzolite), compared to the arc–continent collision stage where it was <440°C at around 15 km, 550°C at 60 km and, possibly, about 650°C at 110 km depth (Maksutovo Complex data). Numerical modeling of intra-oceanic subduction zones shows a pronounced cooling with time as geotherms are depressed (e.g., Peacock 1996). Modeling shows that with the entrance of the continental crust into a subduction zone, relative heating may take place in the upper 50 km or so of the subduction zone (van den Beukel 1992). Second, the variation of the ages and P-T conditions obtained from the Mindyak and Maksutovo Complex high-pressure rocks indicates that an important flux of material was taking place from deep within the subduction zone from the early stages of intra-oceanic subduction to the final stages of arc–continent collision. This suggests that there was a mass flow of material along a subduction channel in which concomitant subduction, high-pressure metamorphism, exhumation and subduction-erosion of material was continuously taking place. Third, there is widespread textural and isotopic evidence from both the prograde and retrograde Maksutovo Complex eclogite and blueschist that indicate that there was a free fluid phase in the subduction channel (Glodny et al. 2002) during subduction of the continental crust. This fluid phase may have been the result of influx either from underplated and/or metamorphosed sediments of the continental margin, and it likely acted to trigger and catalyze reactions and growth of eclogite facies minerals (Glodny et al. 2002).

11.10.4 Arc–Continent Collision Stops

Arc–continent collision stopped in the South Urals at the end of the Devonian (Fig. 11.13d) and in the Middle Urals perhaps by the late Early Carboniferous. In the South Urals, the Magnitogorsk Arc subsided, and Early Carboniferous sediments were

deposited on top of it and along the western margin of the accretionary complex. From beginning to end, arc–continent collision in the South Urals lasted about 20–30 My. It is not possible to constrain the duration of arc–continent collision in the Middle Urals. In arc–continent collision zones such as Papua New Guinea, Timor, and Taiwan (Sibuet and Hsu 2004; Abers and McCaffrey 1994; Charlton 1991), active seismicity indicates that continental crust continues to underthrust the arc 3–9 My after its entry into the subduction zone. In somewhat older examples, such as along the northern Caribbean Plate margin, collision of the Greater Caribbean arc with the margin of North America began during the Late Paleocene in Cuba and continues to be active today in Hispaniola (Mann et al. 1991), more than 55–60 My later. In other Paleozoic orogens, such as the Grampian Orogeny in the Caledonides of Britain and Ireland, or the Taconic Orogeny of the Appalachians, arc–continent collision appears to have lasted about 8–10 My (e.g., Cousineau and St-Julien 1992; van Staal 1994; Dewey 2005). These examples, together with that of the Urals, suggest that arc–continent collision appears to be a short-lived event, generally lasting from 10 to 20 My, although longer-lived events do take place. However, the duration of an arc–continent collision orogeny depends on factors such as subduction velocity and shape and thickness of the continental margin involved (e.g., Ranalli et al. 2000; Li and Liao 2002). Furthermore, determining when the continental crust entered the subduction zone in a fossil orogen may be difficult. The Uralides case clearly shows that the sediments derived from the growing accretionary complex began to arrive in the foreland and suture forearc basins later than the peak high-pressure metamorphic event that affected the continental margin. The pressure and temperature conditions recorded in the high-pressure rocks, together with the age of the peak metamorphic event, indicates that the continental crust entered the subduction zone much earlier still. Finally, the geochemistry of the volcanic rocks do not record any clear evidence of the continental crust being in the subduction zone or contributing to the geochemical signature of arc-related volcanism. Importantly, there is no evidence in the South Urals that points to a change in subduction zone polarity during the late stages of arc–continent collision, or immediately following it.

11.10.5 Growth and Destruction of the Continental Crust

There is general agreement that the accretion of intra-oceanic volcanic arcs to a continental margin is one of the major processes in which new material has been added to the continental crust throughout geological time (Rudnick 1995; Rudnick and Fountain 1995). The means by which, or even if, continental crust is recycled back into the mantle is less well understood. In the case of the South Urals, where there is clear evidence for the subduction of the continental margin, if it is assumed that an average thickness of 10 km of the Laurussia margin was subducted to around 120 km depth along the entire c. 400 km length of the presently exposed collision zone (with only minor return of material to the surface as high-pressure rocks) and a current Moho depth of c. 50 km, then about 280,000 km^3 of continental crust has been lost to the present day mantle (Fig. 11.14). If a crustal thickness of 20 km is assumed for the Magnitogorsk arc, and a width of c. 100 km, then approximately 800,000 km^3 of new material accreted to the margin. This rough calculation suggests that a net volume of around 520,000 km^3 of material was added to the Laurussia margin during its collision with the Magnitogrsk arc. If this is applied to the Middle Urals as well, then we see that the volumes of material involved are considerable, even when compared to that for sediment subduction (Clift and Vannucchi 2004; Clift et al. 2009). Caution is urged, however, in the interpretation of this volume since the uncertainties (assumptions of thickness, length etc.) in the calculation are large.

In the Middle Urals, Bea et al. (2001), Krasnobaev et al. (2005), and Fershtater et al. (2007) have reported that zircons from subduction-related ultramafic massifs and granitoids record inherited ages that suggest that there was at least some recycling of the Laurussia margin into the Tagil Arc plutonic rocks. With the current data set, however, we are unable to say more about the growth and destruction of the continental crust during the collision of the Tagil Arc.

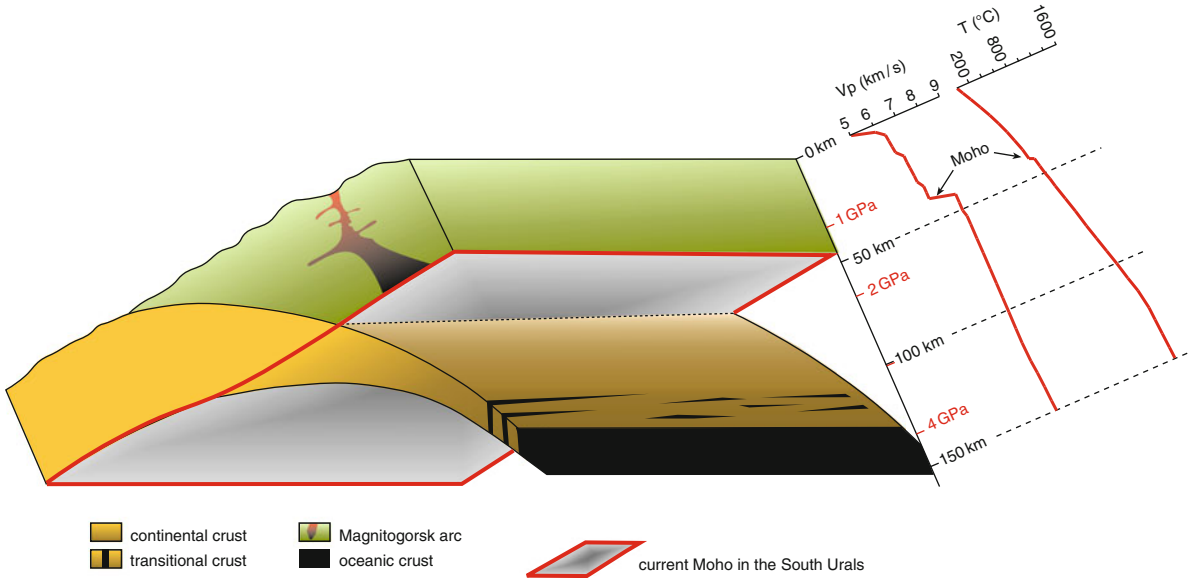

Fig. 11.14 Schematic diagram representing a view from below of the subducted continental margin of Laurussia beneath the Magnitogorsk Arc at an intermediate stage in the arc–continent collision. The position of the present day Moho derived from geophysical data is shown, as are the P-wave velocities and the thermal structure with depth. On the basis of various types of geophysical data Brown (2008) suggested that part of the continental and transitional crust shown below the present day Moho has either been assimilated into the mantle or its physical properties have changed to those of the mantle so that it can no longer be imaged by geophysical methodologies.

11.11 Conclusions

The geochemistry of the Magnitogorsk Arc volcanic rocks, the structure of the arc–continent collision accretionary complex and the forearc, the high-pressure rocks beneath and along the suture zone, the mafic and ultra-mafic ophiolitic material, and the syn-tectonic sediments show the Paleozoic tectonic processes recorded in the South Urals (Fig. 11.15). These can be favorably compared with those in currently active settings such as the west Pacific. For example, boninitic lavas found in the oldest arc volcanics provide a geodynamic marker that records the onset of intra-oceanic subduction and the development of a proto-arc. While the geochemical and isotopic signatures of the Magnitogorsk Arc volcanic rocks are indicative of intra-oceanic subduction, they do not record clear evidence of the subduction of the continental crust. There was apparently no recycling of Precambrian zircons into the Magnitogorsk Arc rocks, further suggesting that the subducted margin rocks may not have played a significant role in the arc volcanism and plutonism. High-pressure/low temperature rocks along the backstop of the accretionary complex were in part derived from continental margin material, and the Frasnian age of their high-pressure metamorphism provides a constraint for determining the timing of the entry of the continental crust into the subduction zone. The pressure, temperature, and thermochronology data of the Maksutovo Complex and high-pressure mafic rocks along the arc-continent suture, provide evidence for changing physical conditions over time in the subduction zone. The flux of material along it suggests the presence of a subduction channel along which material moved. The sediments overlying the volcanic arc record near surface processes such as growth folding. The widespread occurrence of debris flows within these sediments is thought to represent seismic events, and may be related to the arrival of the full thickness of the continental crust at the subduction zone. During the late stage of collision turbidites of the Zilair Formation were deposited in a forearc basin and a foreland basin separated by a subaerial part of the accretionary complex. These sediments represent eroded material from the magmatic arc and the

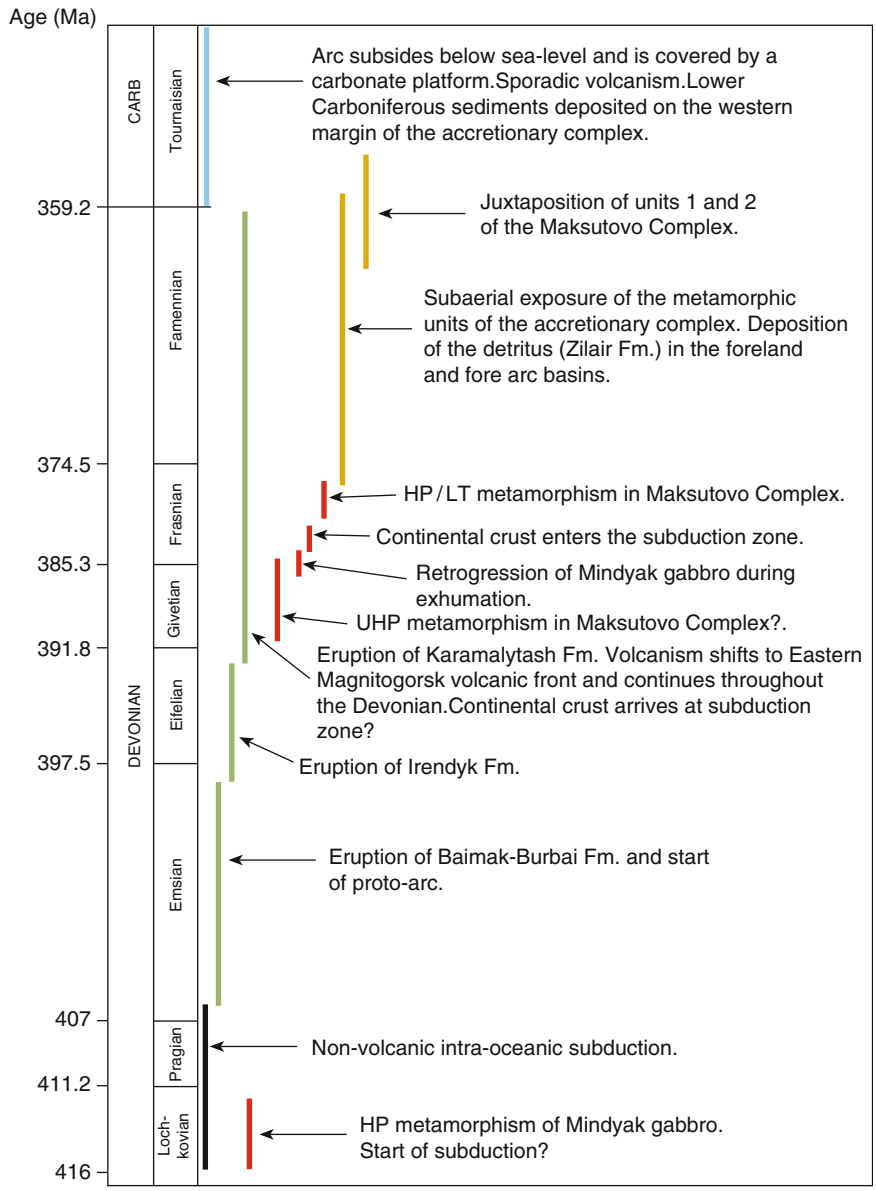

Fig. 11.15 Time/process evolutionary diagram for intra-oceanic subduction and arc–continent collision in the South Urals (after Brown et al. 2006a).

growing accretionary complex. From beginning to end, the arc–continent collision in the South Urals lasted about 20 My and possibly as much as 30 My.

High-pressure rocks derived from the mafic ganulite that currently makes up the middle and lower crust of the South Urals do not occur in outcrop, suggesting that much of the subducted margin remained in the upper mantle. However, extensive geological, geochemical, and geophysical data do not unequivocally clarify this. Crustal delamination and foundering into the mantle can be ruled out, and recycling through the volcanic arc system appears to have been minor. While the metamorphic products of subducted continental crust can remain in the mantle for long periods of time, in the Southern Urals it has not been imaged by the available geophyscial data sets. A possible explanation for this is that the progressive metamorphism of mafic granulite to eclogite assemblages would have altered its physical properties to those of typical mantle lithologies, making them difficult to detect by geophysical methods. It is estimated that the volume of continental crust that was subducted

and lost to the mantle was approximately one-third of the volume that was added to the Laurussia margin by the accretion of the Magnitogorsk arc. Finally, Petrophysical modeling of geophysical data in the South Urals indicate that there still remains a significant juxtaposition of material in the lower crust across the arc-continent suture, suggesting that crustal differentiation processes and homogenization of the lower crust has not been active.

Less can be said about the processes that took place in the Middle Urals, with the collision of the Tagil Arc. However, the recycling of Precambrian zircons into the volcanic and plutonic rocks of the Tagil Arc suggest that, unlike in the South Urals crustal melting processes took place in the Middle Urals and that a certain volume of the continental margin crustal material was recycled back into the arc.

Acknowledgements Much of this work was carried out as part of ESF's Europrobe and GEODE programmes. We would like to thank all of our coleagues who took part in these research efforts and whose results are presented here. However, we take full responsibility for the interpretations. Reviewers Torgeir Andersen and Vicky Pease are thanked.

References

Abbott LD, Silver EA, Anderson RS, Smith R, Ingle JC, Kling SA, Haig D, Small E, Galewsky J, Sliter W (1997) Measurement of tectonic surface uplift rate in a young collisional mountain belt. Nature 385:501–507

Abers GA, McCaffrey R (1994) Active arc-continent collision: earthquakes, gravity anomalies, and fault kinematics in the Huon-Finisterre collision zone, Papua New Guinea. Tectonics 13:227–245

Alvarez-Marron J (2002) Tectonic processes during collisional orogenesis from comparison of the South Urals with the Central Variscides. In: Brown D, Juhlin C, Puchkov V (eds) Mountain building in the Uralides: pangea to present, vol 132, American Geophysical Union, Geophysical Monograph., pp 83–100

Alvarez-Marron J, Brown D, Perez-Estaun A, Puchkov V, Gorozhanina Y (2000) Accretionary complex structure and kinematics during Paleozoic arc-continent collision in the South Urals. Tectonophysics 325:175–191

Arndt N (2003) Komatiites, kimberlites, and boninites. J Geophys Res 108. doi: 10.1029/2002JB002157

Arzhavitina MY (1978) Mineral composition of the terrigenous rocks of the Zilair-Formation in the Magnitogorsk syncline (in Russian). Mineral chemistry of volcanogenic and sedimentary deposits of the South Urals. Geological Institute of the Russian Academy of Sciences, Ufa, Russia, pp 48–55

Arzhavitina MY, Arzhavitin PV (1991) Mineral components of the terrigenous flysch in the Magnitogorsk Syncline (in Russian). Nappe tectonics and its importance for ore deposits. Geological Institute of the Russian Academy of Sciences, Ufa, Russia, pp 82–83

Ayarza P, Brown D, Alvarez-Marron J, Juhlin C (2000) Contrasting tectonic history of the arc-continent suture in the Southern and Middle Urals: implications for the evolution of the orogen. J Geol Soc 157:1065–1076

Bastida F, Aller J, Puchkov VN, Juhlin C, Oslianski A (1997) A cross section through the Zilair Unit (South Urals). Tectonophysics 276:253–264

Bauer K, Neben S, Schreckenberger B, Emmermann R, Hinz K, Fecher N, Gohl K, Schulze A, Rumbull RB, Weber K (2000) Deep structure of the Namibia continental margin as derived from integrated geophysial studies. J Geophys Res 105:25829–25853

Bea F, Fershtater G, Montero P, Smirnov V, Zin'kova E (1997) Generation and evolution of subduction-related batholiths from the central Urals: constraints on the P-T history of the Uralian orogen. Tectonophysics 276:103–116

Bea F, Fershtater GB, Montero P, Whitehouse M, Levin VY, Scarrow JH, Austrheim H, Pushkariev EV (2001) Recycling of continental crust into the mantle as revealed by Kytlym dunite zircons, Ural Mts, Russia. Terra Nova 13:407–412

Bea F, Fershtater G, Montero P (2002) Granitoids of the Urals: implications for the evolution of the orogen. In: Brown D, Juhlin C, Puchkov V (eds) Mountain building in the Uralides: pangea to present, vol 132, American Geophysical Union, Geophysical Monograph., pp 211–232

Beane RJ, Connelly JH (2000) $^{40}Ar/^{39}Ar$, U-Pb and Sm-Nd constraints on the timing of metamorphic events in the Maksyutov Complex, southern Ural Mountains. J Geol Soc 157:811–822

Beane RJ, Liou JG, Coleman RG, Leech ML (1995) Petrology and retrograde P-T path for eclogites of the Maksyutov Complex, South Urals Mountains, Russia. The Island Arc 4:254–266

Beckholmen M, Glodny J (2004) Timanian blueschist-facies metamorphism in the Kvarkush metamorphic basement, Northern Urals, Russia, in *The Neoproterozoic Timanide Orogen of Eastern Baltica,* edited by D.G. Gee and V. Pease, *Geol. Soc*. London Mem 30:125–134

Bochkarev VV, Surin TN (1996) REE in Middle Devonian boninite-like basalts of the Urals (in Russian). Yearbook-1995. Institute of Geology and Geochemistry, Yekaterinburg Russia, pp 85–93

Bosch D, Krasnobayev AA, Efimov A, Savelieva G, Boudier F (1997) Early Silurian ages for the gabbroic section of the mafic-ultramafic zone from the Urals. In: Oxburgh ER (ed) EUG 9, Terra Nova. Cambridge Publications, Strasbourg, p 121

Bostick BC, Jones RE, Ernst WG, Chen C, Leech ML, Beane RJ (2003) Low-temperature microdiamond aggregates in the Maksyutov Metamorphic Complex, South Ural Mountains, Russia. American Mineralogist 88:1709–1717

Boutelier D, Chemenda A, Burg J-P (2003) Subduction versus accretion of intra-oceanic volcanic arcs: insight from thermo-mechanical analogue experiments. Earth Planet Sci Lett 212:31–45

Boutelier D, Chemenda A, Jorand C (2004) Continental subduction and exhumation of high-pressure rocks: insights from thermo-mechanical laboratory modeling. Earth Planet Sci Lett 222:209–216

Brown D (2007) Modal mineralogy and chemical composition of the Uralide lower crust determined from physical properties data. Tectonophysics 433:39–51

Brown D, Spadea P (1999) Processes of forearc and accretionary complex formation during arc-continent collision in the Southern Ural Mountains. Geology 27:649–652

Brown D, Puchkov V, Alvarez-Marron J, Perez-Estaun A (1996) The structural architecture of the footwall to the Main Uralian Fault, South Urals. Earth-Sci Rev 40:125–147

Brown D, Alvarez-Marron J, Perez-Estaun A, Gorozhanina Y, Baryshev V, Puchkov V (1997) Geometric and kinematic evolution of the foreland thrust and fold belt in the southern Urals. Tectonics 16:551–562

Brown D, Juhlin C, Alvarez-Marron J, Perez-Estaun A, Oslianski A (1998) Crustal-scale structure and evolution of an arc-continent collision zone in the South Urals, Russia. Tectonics 17:158–171

Brown D, Alvarez-Marron J, Perez-Estaun A, Puchkov V, Ayala C (1999) Basement influence on foeland thrust and fold belt development: an example from the southern Urals. Tectonophysics 308:459–472

Brown D, Hetzel R, Scarrow JH (2000) Tracking arc-continent collision subduction zone processes from high-pressure rocks in the South Urals. J Geol Soc 157:901–904

Brown D, Alvarez-Marron J, Perez-Estaun A, Puchkov V, Ayarza P, Gorozhanina Y (2001) Structure and evolution of the Magnitogorsk forearc basin: identifying upper crustal processes during arc-continent collision in the South Urals. Tectonics 20:364–375

Brown D, Juhlin C, Tryggvason A, Steer D, Ayarza P, Beckholmen M, Rybalka A, Bliznetsov M (2002) The crustal architecture of the Southern and Middle Urals from the URSEIS, ESRU, and Alapaev reflection seismic surveys. In: Brown D, Juhlin C, Puchkov V (eds) Mountian building in the Uralides: pangea to present, vol 132, American Geophysical Union, Geophysical Monograph., pp 33–48

Brown D, Carbonell R, Kukkonen I, Ayala C, Golovonova I (2003) Composition of the Uralide crust from seismic velocity (Vp, Vs), heat flow, gravity, and magnetic data. Earth Planet Sci Lett 210:333–349

Brown D, Alvarez-Marron J, Perez-Estaun A, Gorozhanina Y, Puchkov V (2004) The structure of the south Urals foreland fold and thrust belt at the transition to the Precaspian Basin. J Geol Soc 161:813–822

Brown D, Spadea P, Puchkov V, Alvarez-Marron J, Herrington R, Willner AP, Hetzel R, Gorozhanina Y (2006a) Arc-continent collision in the Southern Urals. Earth-Sci Rev 79:261–287

Brown D, Juhlin C, Tryggvason A, Friberg M, Rybalka A, Puchkov V, Petrov G (2006b) Structural architecture of the Southern and Middle Urals foreland from reflection seismic profiles. Tectonics 25. doi: 10.1029/2005TC001834

Brown D, Juhlin C, Ayala C, Tryggvason A, Bea F, Alvarez-Marron J, Carbonell R, Seward D, Glasmacher U, Puchkov V, Perez-Estaun A (2008) Mountain building processes during continent-continent collision in the Uralides. Earth-Sci Rev 89:177–195

Burke WH, Denison RE, Hetherington EA, Koepnick RB, Nelson HF, Otto JB (1982) Variation of seawater $^{87}Sr/^{86}Sr$ through Phanerozoic time. Geology 10:516–519

Carbonell R, Perez-Estaún A, Gallart J, Diaz J, Kashubin S, Mechie J, Stadtlander R, Schulze A, Knapp JH, Morozov A (1996) A crustal root beneath the Urals: wide-angle seismic evidence. Science 274:222–224

Carbonell R, Lecerf D, Itzin M, Gallart J, Brown D (1998) Mapping the Moho beneath the Southern Urals. Geophys Res Lett 25:4229–4233

Carbonell R, Gallart J, Perez-Estaun A, Diaz J, Kashubin S, Mechie J, Wenzel F, Knapp J (2000) Seismic wide-angle constraints on the crust of the southern Urals. J Geophys Res 105:13755–13777

Charlton TR (1991) The structural evolution of the Timor collision complex, eastern Indonesia. J Struct Geol 13: 489–500

Chemenda A, Hurpin D, Tang J-C, Stefan J-F, Buffet G (2001) Impact of arc-continent collision on the conditions of burial and exhumation of UHP/LT rocks: experimental and numerical modeling. Tectonophysics 342:137–161

Christensen NI, Mooney WD (1995) Seismic velocity structure and composition of the continental crust: a global view. J Geophys Res 100:9761–9788

Chuvashov VI (1998) Dynamics of the evolution of the Uralian foredeep. Geotectonics 32:186–200

Clift P, Vannucchi P (2004) Controls on tectonic accretion versus erosion in subduction zones; implications for the origin and recycling of the continental crust. Rev Geophys 42. doi: 8755-1209/04/2003RG000127

Clift P, Schouten H, Vannucchi P (2009) Arc-continent collisions, sediment recycling and the maintenance of the continental crust. In: Cawood P, Kroener A (eds) Accretionary Orogens in space and time, vol 318. Geological Society of London (Special Publication), London, pp 75–103

Cortesogno L, Gaggero L, Savelieva G, Scarrow JH, Spadea P, (1998) Garnet pyroxenites from the Mindyak Massif, South Urals: records of early accretion of crust and lithospheric mantle. EUROPROBE Uralides Workshop, Moscow, Progamme with Abstracts, p 191

Cousineau PA, St-Julien P (1992) The Saint-Daniel mélange: evolution of an accretionary complex in the Dunnage Terrane of the Quebec Appalachians. Tectonics 11:898–909

Crawford AJ, Falloon TJ, Green DH (1989) Classification, petrogenesis and tectonic setting of boninites. In: Crawford AJ (ed) Boninites and related rocks. Unwin Hyman, London, pp 1–49

De Smet MEM, Fortuin AR, Troelstra SR, Van Mrale LJ, Karmini M, Tjokosaproetro S, Hadiwasastra S (1990) Detection of collision-related vertical movements in the Outer Banda Arc (Timor, Indonesia), using micropaleontological data. J Southeast Asian Earth Sci 4:337–356

Dewey JF (2005) Orogeny can be very short. Proc Am Acad Sci 102:15286–15293

Dickinson WR (1985) Interpreting provenance relations from detrital modes of sandstones. In: Zuffa GG (ed) Provenance of Arenites, vol 148, Nato ASI Series C. Reidel, Dordrecht, pp 333–361

Dobretsov NL, Skatshy VS, Coleman RG, Lennykh VI, Valizer PM, Liou J, Zhang R, Beane RJ (1996) Tectonic setting and petrology of ultrahigh-pressure metamorphic rocks in the

Maksyutov Complex, Ural Mountains, Russia. Int Geol Rev 38:136–160

Draut A, Clift PD, Hannigan RE, Layne G, Shimizu N (2002) A model for continental crust genesis by arc accretion: rare earth element evidence from the Irish Caledonides. Earth Planet Sci Lett 203:861–877

Draut A, Clift PD, Amato JM, Blustajn J, Schouten H (2009) Arc-continent collision and the formation of continental crust: a new geochemical and isotopic record from the Ordovician Tyrone Igneous Complex, Ireland. J Geol Soc 166:485–500

Echtler HP, Stiller M, Steinhoff F, Krawczyk CM, Suleimanov A, Spiridonov V, Knapp JH, Menshikov Y, Alvarez-Marron J, Yunusov N (1996) Preserved collisional crustal architecture of the South Urals – Vibroseis CMP-profiling. Science 274:224–226

Edwards RL, Wassenburg GJ (1985) The age and emplacement of obducted oceanic crust in the Urals from Sm-Nd and Rb-Sr systematics. Earth Planet Sci Lett 72:389–404

Elburg MA, Foden JD, van Bergen MJ, Zulkarnain I (2005) Australia and Indonesia in collision: geochemical sources of magmatism. J Volcanol Geoth Res 140:25–47

Fernandez FJ, Brown D, Alvarez-Marron J, Prior DJ, Perez-Estaun A (2004) Microstructure and crystallographic fabric of calcite mylonites at the base of the South Urals accretionary prism. J Geol Soc 161:67–79

Fershtater GB, Bea F (1996) Geochemical typification of the Ural ophiolites (in Russian). Geokhimiya 3:195–218

Fershtater GB, Montero P, Borodina NS, Pushkarev EV, Smirnov V, Zin'kova E, Bea F (1997) Uralian magmatism: an overview. Tectonophysics 276:87–102

Fershtater GB, Krasnobaev AA, Bea F, Montero P, Borodina NS (2007) Geodynamic setting and history of the Paleozoic intrusive magmatism of the Central and Southern Urals: results of zircon dating. Geotectonics 41:465–486

Friberg M, Larionov A, Petrov GA, Gee DG (2000) Paleozoic amphibolite-granulite facies magmatic complexes in the hinterland of the Uralide Orogen. Int J Earth Sci 89:21–39

Friberg M, Juhlin C, Beckholmen M, Petrov GA, Green AG (2002) Paleozoic tectonic evolution of the Middle Urals in light of the ESRU seismic experiments. J Geol Soc 159:295–306

Frolova TI, Burikova IA (1997) Geosyncline volcanism (by the example of the eastern slope of the South Urals) (in Russian). Moscow State University, Moscow, 163 pp

Funck T, Jackson HR, Louden KE, Dehler SA, Wu Y (2004) Crustal structure of the northern Nova Scotia rifted continental margin (eastern Canada). J Geophys Res 109. doi: 10.1029/2004JB003008

Garuti G, Fershtater G, Bea F, Montero P, Pushkarev EV, Zaccarini F (1997) Platinum-group elements as petrological indicators in mafic-ultramafic complexes of the central and South Urals: preliminary results. Tectonophysics 276:181–194

Giese U, Glasmacher U, Kozlov VI, Matenaar I, Puchkov VN, Stroink L, Bauer W, Ladage S, Walter R (1999) Structural framework of the Bashkirian anticlinorium, SW Urals. Geologische Rundschau 87:526–544

Glasmacher UA, Reynolds P, Alekseev A, Puchkov VN, Taylor K, Gorozhanin V, Walter R (1999) $^{40}Ar/^{39}Ar$ thermochronology west of the main Uralian fault, Southern Urals, Russia. Geologische Rundschau 87:515–525

Glasmacher UA, Bauer W, Giese U, Reynolds P, Kober B, Puchkov VN, Stroink L, Alekseev A, Willner A (2001) The metamorphic complex of Beloretzk, SW Urals, Russia – a terrane with a polyphase Meso- to Neoproterozoic thermo-dynamic evolution. Precambrian Res 110:185–213

Glasmacher UA, Bauer W, Clauer N, Puchkov VN (2004) Neoproterozoic metamorpishm and deformation at the southeastern margin of the East European Craton Uralides, Russia. Int J Earth Sci 93:921–944

Glodny J, Bingen B, Austrheim H, Molina JF, Rusin A (2002) Precise eclogitization ages deduced from Rb/Sr mineral systematics: the Maksyutov Complex, South Urals, Russia. Geochimica et Cosmochimica Acta 66:1221–1235

Gorozhaninia EN, Puchkov VN (2001) The model of sedimentation in the forearc trough of the Magnitogorsk volcanic arc in the Late Devonian (in Russian). In: Puchkov VN, Salikhov DN (eds) Geology and perspectives of the resource base widening of Baskortostan and Neighboring territories. Ufimian Geoscience Centre, RAS, Ufa, pp 5–13

Gusev GS, Gushchin AV, Zaykov VV, Maslennikov VV, Mezhelovsky NV, Perevozchikov BV, Surin TN, Filatov EI, Shirai EP (2000) Geology and metallogeny of island arcs (in Russian). In: Mezhelovsky NV (ed) Geodynamics and metallogeny: theory and implications for applied geology. Ministry of Natural Resources of the RF and GEOKART, Moscow, pp 213–295

Herrington RJ, Armstrong RN, Zaykov VV, Maslennikov VV, Tessalina SG, Orgeval J-J, Taylor RNA (2002) Massive sulfide deposits in the South Urals: geological setting within the framework of the Uralide Orogen. In: Brown D, Juhlin C, Puchkov V (eds) Mountain building in the Uralides: pangea to present, vol 132, American Geophysical Union, Geophysical Monograph., pp 155–182

Herrington RJ, Zaykov VV, Maslennikov VV, Brown D, Puchkov VN (2005) Mineral deposits of the Urals and links to geodynamic evolution. In: Hedenquist JW, Thompson JFH, Goldfarb RJ, Richards JP (eds) Economic geology, vol 100., pp 1069–1095

Herrington RJ, Scotney PM, Roberts S, Boyce AJ, Harrison D (2011) Temporal association of arrested subduction, progressive magma contamination in arc volcanism and formation of gold-rich massive sulphide deposits on Wetar Island (Banda arc). Gondwana Research

Hetzel R (1999) Geology and geodynamic evolution of the high-P/low-T Maksyutov Complex, South Urals, Russia. Geologische Rundschau 87:577–588

Hetzel R, Romer RL (2000) A moderate exhumation rate for the high-pressure Maksyutov Complex, South Urals, Russia. Geol J 35:327–344

Hetzel R, Echtler HP, Seifert W, Schulte BA, Ivanov KS (1998) Subduction- and exhumation-related fabrics in the Paleozoic high-pressure–low-temperature Maksyutov Complex, Antingan area, South Urals, Russia. Geol Soc Am Bull 110:916–930

Huang C-Y, Yuan PB, Lin C-W, Wang TK, Chang C-P (2000) Geodynamic processes of Taiwan arc-continent collision and comparison with analogs in Timor, Papua New Guinea, Urals and Corsica. Tectonophysics 325:1–22

Huang C-Y, Yuan PB, Tsao S-J (2006) Temporal and spatial records of active arc-continent collision in Taiwan: a synthesis. Geol Soc Am Bull 118:274–288

Ingersoll RV, Suzcek CA (1979) Petrology and provenance of Neogene sand from Nicobar and Bengal fans, DSDP Sites 211 and 218. J Sediment Petrol 49:1217–1228

Ivanov KS, Puchkov VN (1990) Geology of the Sakmara zone of the Urals (new data) (in Russian). RAS, Sverdlovsk

Jahn BM, Martineau F, Peucat JJ, Cornichet J (1986) Geochronology of the Tananao schist complex, Taiwan, and its regional tectonic significance. Tectonophysics 125:103–124

Juhlin C, Knapp JH, Kashubin S, Bliznetzov M (1996) Crustal evolution of the Middle Urals based on seismic reflection and refraction data. Tectonophysics 26:21–34

Juhlin C, Friberg M, Echtler H, Green AG, Ansorge J, Hismatulin T, Rybalka A (1998) Crustal structure of the Middle Urals: results from the (ESRU) Europrobe Seismic Reflection Profiling in the Urals Experiments. Tectonics 17: 710–725

Juhlin C, Brown D, Rybalka A, Petrov G (2007) Moho imbrication in the Middle Urals. Terra Nova 19:189–184

Kamaletdinov MA (1974) The nappe structures of the Urals (in Russian). Nauka, Moscow, 229 pp

Kashubin S, Juhlin C, Friberg M, Rybalka A, Petrov G, Kashubin A, Bliznetsov M, Steer D (2006) Crustal structure of the Middle Urals based on reflection seismic data. In: Gee D, Stephenson R (eds) European lithosphere dynamics, vol 32. Geological Society, London, pp 427–442, Memoirs

Keen CE, Dehler SA (1997) Extensional styles and gravity anomalies at rifted continental margins: some North Atlantic examples. Tectonics 16:744–754

Keller BM (1949) The Paleozoic flysch formation in the Zilair synclinorium of the South Urals and comparable complexes (in Russian). Trudy Institute of Geology Nauka, Moscow, 165 pp

Knapp JH, Steer DN, Brown LD, Berzin R, Suleimanov A, Stiller M, Lüschen E, Brown D, Bulgakov R, Rybalka AV (1996) A lithosphere-scale image of the South Urals from explosion-source seismic reflection profiling in URSEIS '95. Science 274:226–228

Kopteva VV (1981) Sedimentary-tectonic breccias of the Gadilevo unit (South Urals) (in Russian). Lithology and raw materials 1:55–68

Kozlov VI, Krasnobaev AA, Larionov NN, Maslov AV, Sergeeva ND, Bibikova EV, Genina LA, Ronkin YuL (1989) The lower riphean of the Southern Urals. Nauka, Moscow, 208 p

Krasnobaev AA, Fershtater GB, Bea F, Montero P (2005) Polygenic zircons in the Adui Batholith, the Central Urals. Doklady Earth Sci 410:1096–1100

Kuz'min MI, Kabanova L Ya (1991) Boninite series of the South Urals: geologic and petrographic description, compositional peculiarities and problems of origin (in Russian). Nauka, Miass, pp 156–173

Leech ML, Ernst WG (2000) Petrotectonic evolution of the high to ultrahigh-pressure Maksyutov Complex, Karayanova area, south Ural Mountains: structural and oxygen isotope constraints. Lithos 52:235–253

Leech ML, Stockli DF (2000) The late exhumation history of the ultrahigh-pressure Maksyutov Complex, south Ural Mountains, from new apatite fission-track data. Tectonics 19: 153–167

Leech ML, Willingshofer E (2004) Thermal modeling of the UHP Maksyutov Complex in the south Urals. Earth Planet Sci Lett 226:85–99

Lennykh VI (1977) Eclogite and glaucophane schist belts in the south Urals (in Russian). Nedra, Moscow, pp 1–158

Lennykh VI, Valiser PM, Beane R, Leech M, Ernst WG (1995) Petrotectonic evolution of the Makysutov complex, southern Ural Mountains, Russia: implications for ultrahigh-pressure metamorphism. Int Geol Rev 37:584–600

Li L, Liao X, (2002) Slab breakoff depth: a slowdown subduction model. Geophys Res Lett 29. doi: 10.1029/2001GL013420

Mann P, Draper G, Lewis JF (1991) Geologic and tectonic development of the North America-Caribbean Plate Boundary in Hispañola. Geological Society of America Special Paper 262, 401 pp

Maslov VA, Artyushkova OV (1991) Paleontology and stratigraphy of the Devonian and Carboniferous of the Urals (Aktau suite, Magnitogorsk megasynclinorium). Ufimsky Nauchno Tsentr pp 46–53

Maslov VA, Cherkasov VL, Tischchenko VT, Smirnova IA, Artyushkova OV, Pavlov VV (1993) On the stratigraphy and correlation of the Middle Paleozoic complexes of the main copper-pyritic areas of the South Urals (in Russian). Ufimsky Nauchno Tsentr, Ufa, 129 pp

Maslov AV, Erdtmann B-D, Ivanov KS, Ivanov SN, Krupenin MT (1997) The main tectonic events, depositional history, and the paleogeography of the South Urals during the Riphean – Early Paleozoic. Tectonophysics 276: 313–335

Matte P, Maluski H, Caby R, Nicolas A, Kepezhinskas P, Sobolev S (1993) Geodynamic model and $^{39}Ar/^{40}Ar$ dating for the generation and emplacement of the high-pressure (HP) metamorphic rocks in SW Urals, vol 317, Academie de Sciences Comptes Rendus, ser. II., pp 1667–1674

Melcher F, Grum W, Thalhammer TV, Thalhammer OAR (1999) The giant chromite deposits at Kempirsai, Urals: constraints from trace element (PGE, REE) and isotope data. Mineralium Deposita 34:250–272

Mizens GA (1997) On the stages of formation of the Uralian foredeep. Geotectonics 31:374–385

Mizens GA (2004) Devonian paleogeography of the South Urals. Geol Q 48:205–216

Moisio K, Kaikkonen P (2004) The present day rheology, stress field and deformation along the DSS profile FENNIA in the central Fennoscandian Shield. J Geodyn 38:161–184

Montero P, Bea F, Gerdes A, Fershtater G, Zinkova E, Borodina N, Osipova T, Smirnov V (2000) Single-zircon evaporation ages and Rb-Sr dating of four major Variscan batholiths of the Urals – a perspective of the timing of deformation and granite generation. Tectonophysics 317:93–108

Pazukhin VN, Puchkov VN, Baryshev VN (1996) New data on the stratigraphy of the Zilair series (S. Ural) (in Russian). Yearbook – 95. Institute of Geology, Ufimian Science Centre, Ufa, pp 34–41

Peacock SM (1996) Thermal and petrologic structure of subduction zones (overview). In: Bebout GE, Scholl DW, Kirby SK, Platt JP (eds) Subduction top to bottom, vol 96, American Geophysical Union, Geophysical Monograph., pp 119–134

Puchkov VN (1997) Structure and geodynamics of the Uralian orogen. In: Burg J-P, Ford M (eds) Orogeny through time, vol 121. Geological Society (Special Publication), London, pp 201–236

Puchkov VN (2000) Paleogeodynamics of the central and South Urals (in Russian). Pauria, Ufa, 145 pp

Puchkov V (2002) Paleozoic evolution of the East European continental margin involved in the Uralide orogeny. In: Brown D, Juhlin C, Puchkov V (eds) Mountain building in the Uralides: pangea to present, vol 132, American Geophysical Union, Geophysical Monograph., pp 9–32

Puchkov V, Ivanov K (1982) Geology of allochthonous bathyal complexes of the Ufimian amphitheater. Sverdlovsk Scientific Center, RAS, 61 p

Puchkov VN, Perez-Estaun A, Brown D, Alvarez-Marron J, (1998) The marginal fold and thrust belt of an orogen: structure and origin (at the example of the Bashkirian Urals) (in Russian). Herald of Geology, Geochemistry, Geophysics and Mining Branch of the Russian Academy of Science, vol 1. pp 70–99

Ranalli G, Pellegrini R, D'Offizi S (2000) Time dependence of negative buoyancy and the subduction of continental lithosphere. J Geodyn 30:539–555

Reston TJ (2009) The structure, evolution and symmetry of the magma-poor rifted margins of the North and Central Atlantics: a synthesis. Tectonophysics 468:6–27

Rudnick RL (1995) Making continental crust. Nature 378: 571–578

Rudnick RL, Fountain DM (1995) Nature and composition of the continental crust: a lower crustal perspective. Rev Geophys 33:267–309

Saveliev AA, Savelieva GN (1991) The Kempersay ophiolite massif: main features of the structure and composition (in Russian). Geotectonics 6:57–65

Savelieva GI (1987) Gabbro-ultramafic assemblages of Uralian ophiolites and their analogues in the recent oceanic crust. Nauka, Moscow, 242 pp

Savelieva GN, Nesbitt RW (1996) A synthesis of the stratigraphic and tectonic setting of the Uralian ophiolites. J Geol Soc 153:525–537

Savelieva GN, Sharaskin AY, Saveliev AA, Spadea P, Gaggero L (1997) Ophiolites of the southern Uralides adjacent to the East European continental margin. Tectonophysics 276: 117–138

Savelieva GN, Pertsev AN, Astrakhantsev O, Denisova EA, Boudier F, Bosch D, Puchkova AV (1999) The Kytlym Pluton, North Urals: structure and emplacement history. Geotectonics 33:119–141

Savelieva GN, Sharaskin AY, Saveliev AA, Spadea P, Pertsev AN, Babarina II (2002) Ophiolites and zoned mafic-ultramafic massifs of the Urals: a comparative analysis and some tectonic implications. In: Brown D, Juhlin C, Puchkov V (eds) Mountain building in the Uralides: pangea to present, vol 132, American Geophysical Union, Geophysical Monograph., pp 135–154

Sayers J, Symonds PA, Direen NG, Bernardel G (2001) Nature of the continent-ocean transition on the non-volcanic rifted margin of the central Great Australian Bight. In: Wilson RCL, Whitmarsh RB, Taylor B, Froitzheim N (eds) Non-volcanic rifting of continental margins: a comparision of evidence from land and sea, vol 187. Geological Society (Special Publication), 76, p 51

Scarrow JH, Savelieva GN, Glodny J, Montero P, Pertsev A, Cortesogno L, Gaggero L (1999) The Mindyak Paleozoic lherzolite ophiolite, South Urals: geochemistry and geochronology. Ofioliti 24:239–246

Schulte BA, Blümel P (1999) Prograde metamorphic reactions in the high-pressure Maksyutov Complex, Urals. Geologische Rundschau 87:561–576

Schulte BA, Sindern S (2002) K-rich fluid metasomatism at high-pressure metamorphic conditions: Lawsonite decomposition in rodingitized ultramafite of the Maksyutov Complex, South Urals (Russia). J Metamorph Geol 20: 529–541

Seravkin I, Kosarev AM, Salikhov DN (1992) Volcanism of the South Urals (in Russian). Nauka, Moscow, 197 pp

Shaw HF, Wasserburg GJ (1985) Sm-Nd in marine carbonates and phosphates: implications for Nd isotopes in seawater and crustal ages. Geochimica et Cosmochimica Acta 49:503–518

Sibuet J-C, Hsu S-K (2004) How was Taiwan created? Tectonophysics 379:159–181

Spadea P, D'Antonio M (2006) Initiation and evolution of intra-oceanic subduction in the Uralides: geochemical and isotopic constraints from Devonian oceanic rocks of the South Urals, Russia. Island Arc 15:7–25

Spadea P, Kabanova LY, Scarrow JH (1998) Petrology, geochemistry and geodynamic significance of Mid-Devonian boninitic rocks from the Baimak-Buribai area (Magnitogorsk Zone, South Urals). Ofioliti 23:17–36

Spadea P, D'Antonio M, Kosarev A, Gorozhanina Y, Brown D (2002) Arc-continent collision in the South Urals: petrogenetic aspects of the forearc complex. In: Brown D, Juhlin C, Puchkov V (eds) Mountain building in the Uralides: pangea to present, vol 132, American Geophysical Union, Geophysical Monograph., pp 101–134

Steer DN, Knapp JH, Brown LD, Rybalka AV, Sokolov VB (1995) Crustal structure of the Middle Urals based on reprocessing of Russian seismic reflection data. Geophys J Int 123:673–682

Steer DN, Knapp JH, Brown LD, Echtler HP, Brown DL, Berzin R (1998) Deep structure of the continental lithosphere in an unextended orogen: an explosive-source seismic reflection profile in the Urals (Urals Seismic Experiment and Integrated Studies (URSEIS 1995)). Tectonics 17:143–157

Tatsumi Y, Maruyama S (1989) Boninites and high-Mg andesites: tectonics and petrogenesis. In: Crawford AJ (ed) Boninites and related rocks. Unwin Hyman, London, pp 112–132

Thouvenot F, Kashubin SN, Poupinet G, Makovskiy VV, Kashubina TV, Matte Ph, Jenatton L (1995) The root of the Urals: evidence from wide-angle reflection seimics. Tectonophysics 250:1–13

Tryggvason A, Brown D, Perez-Estaun A (2001) Crustal architecture of the southern Uralides from true amplitude processing of the URSEIS vibroseis profile. Tectonics 20: 1040–1052

van den Beukel J (1992) Some thermomechanical aspects of the subduction of continental lithosphere. Tectonics 11: 316–329

van Staal CR (1994) Brunswick subduction complex in the Canadian Appalachians: record of the Late Ordovician to Late Silurian collision between Laurentia and the Gander margin of Avalon. Tectonics 13:946–962

Veymarn AB, Puchkov VN, Abramova AN, Artyushkova OV, Baryshev VN, Degtyaryov KE, Kononova LI, Maslov VA, Mosejchuk VM, Pazukhin VN, Pravikova NV, Tevelev AV, Yarkova AV (2004) Stratigraphy and geological events at the boundary of the Famennian/ Frasnian ages in the South Urals. Geology Q 48:233–244

Willner AP, Ermolaeva T, Gorozhanina YN, Puchkov VN, Arzhavitina M, Pazukhin VN, Kramm U, Walter R (2002) Surface signals of an arc-continent collision: the detritus of the Upper Devonian Zilair formation in the South Urals, Russia. In: Brown D, Juhlin C, Puchkov V (eds) Mountain building in the Uralides: pangea to present, vol 132, American Geophysical Union, Geophysical Monograph., pp 183–210

Yazeva RG, Bochkarev VV (1996) Silurian island arc of the Urals: structure, evolution and geodynamics. Geotectonics 29:478–489

Yazeva RG, Puchkov VN, Bochkarev VV (1989) Relics of the active continental margin in the Urals. Geotectonics 3:76–85

Zakharov OA, Puchkov VN (1994) On the tectonic nature of the Maksutovo complex of the Ural-Tau zone (in Russian). Ufimian Science Centre, Ufa, 28 pp

Zhivkovich AY, Chekhovich PA (1985) Paleozoic formation and tectonics of the Ufimian amphitheater. Nauka, Moscow, 183 p

Zonenshain LP, Korinevsky VG, Kazmin VG, Pechersky DM, Khain VV, Mateveenkov VV (1984) Plate tectonic model of the south Urals development. Tectonophysics 109:95–135

Zonenshain LP, Kuzmin MI, Natapov LM (1990) Uralian foldbelt. In: Page BM (ed) Geology of the USSR: a plate-tectonic synthesis, vol 21, Geodynamic series. American Geophysical Union, Washington, DC, pp 27–54

Chapter 12
The Record of Ordovician Arc–Arc and Arc–Continent Collisions in the Canadian Appalachians During the Closure of Iapetus

A. Zagorevski and C.R. van Staal

12.1 Introduction

Arc–continent collision is the major process that adds juvenile magmatic rocks to continental margins effectively offsetting the crustal losses incurred during subduction of both continental crust and continentally-derived sediments (e.g., von Huene and Scholl 1991). Application of the term "arc–continent collision" requires collisional orogenesis that can be defined as "a plate interaction of the sort that causes a re-arrangement of plate motions, generally with the initiation of a new subduction zone and the creation of mountains" and "should leave a clear evidence in the rock record . . . such as accreted exotic terranes" (Cloos 1993). A variety of collision types have been defined in literature (see Cawood et al. 2009 for a review) reflecting either the tectonic configuration of the type localities (e.g., *Cordilleran-*, *Alpine-*, *Pacific-*, *Turkic-* or *Altaid-* types, etc.) and the style of accretion (i.e., *accretionary* vs. *collisional* orogens). Further subdivisions specifically address the pre- to syn accretionary history of the involved terranes (i.e., *retreating* vs. *advancing* orogens) or intensity of deformation and metamorphism (i.e., *hard* vs. *soft* collision).

The Northern Appalachian orogen records Late Cambrian to Devonian accretion of multiple outboard exotic terranes to the Laurentian margin (Figs. 12.1 and 12.2; see van Staal et al. 1998, 2009b; van Staal 2005 for a review). The clear evidence of accreted terranes is present at all scales, ranging from broad subdivision of the Northern Appalachians into zones and subzones (Fig. 12.2; Williams and Hatcher 1983; Williams et al. 1988; Williams 1995a) to the more intricate subdivision of accreted terranes to a kilometric-scale fault-bound tectonic slabs (e.g., van Staal et al. 2003; Zagorevski et al. 2006). Overall, prior to the Alleghenian collision of Laurentia with Gondwana, the Appalachians can be classified as an *accretionary* orogen, that grew to the southeast (present coordinates) through sequential accretion of arc, backarc, microcontinent-derived terranes and seamounts accompanied by southeast-ward migration of magmatism and deformation (e.g., van Staal 2005). However, this classification neglects the details of the tectonic processes involved in the various accretionary events. For example, during parts of its history, the Northern Appalachian orogen varied from *Pacific* (e.g., van Staal et al. 1998) to *Alpine* (Dewey 1969), *accretionary* (Lissenberg et al. 2005b) to *collisional* orogen (van Staal et al. 2007). During the various tectonic stages, the orogen was also periodically changed from *retreating* (e.g., Zagorevski et al. 2006) to *advancing* (e.g., Lissenberg et al. 2005b). Hence, the Appalachians highlight the temporal changes in the overall dynamic setting an orogen may undergo during its evolution. These changes in dynamic history and the available high resolution geological constraints allow inferences to be made on how different plate configurations affect arc–continent collision zones.

In this contribution, we focus the discussion on the interactions between the Laurentian margin and outboard arc terranes during the Ordovician. Three arc–continent collision styles are reviewed and distinguished on the basis of different tectonic configurations that have the colliding arc in a unique upper or lower plate setting (i.e., obduction vs. underplating). The first

A. Zagorevski
Geological Survey of Canada, 601 Booth St, Ottawa, ON, Canada K1A 0E8
e-mail: Alex.Zagorevski@NRCan-RNCan.gc.ca
C.R. van Staal
Geological Survey of Canada, 625 Robson St, Vancouver, BC, Canada V6B5J3

D. Brown and P.D. Ryan (eds.), *Arc-Continent Collision*, Frontiers in Earth Sciences,
DOI 10.1007/978-3-540-88558-0_12,

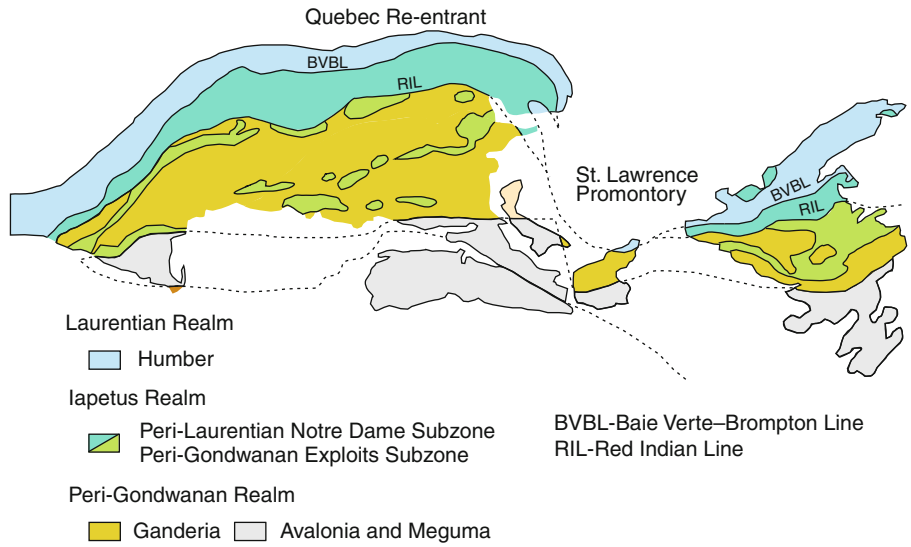

Fig. 12.1 Tectono-stratigraphic subdivisions of Northern Appalachians (modified from Hibbard et al. 2006).

setting is an arc–continent collision with the subduction of a passive margin beneath an active arc (van Staal et al. 2007) analogous to Taiwan and Banda arc–continent collision zones. The second setting is subduction of a young, still evolving oceanic arc-back-arc basin system beneath an active continental margin (e.g., Lissenberg et al. 2005b; Zagorevski et al. 2006, 2009), which has a modern analogue in the subduction and accretion of the Izu-Bonin Arc along the Ruykyu trench (Soh et al. 1998). The third style is the collision between an active continental margin with an outboard island arc, with doubly dipping subducting oceanic slabs intervening between the two arc systems (e.g., van Staal et al. 1998; Zagorevski et al. 2008). A modern analogue is represented by the southward propagating arc–arc collision in the Molucca Sea south of the Philippines (e.g., Pubellier et al. 1999). The orogenesis that occurs in the above examples produces distinctly different products and tectonic styles and influences the degree of preservation of arc complexes, and ophiolites, as well the nature and types of syn-orogenic sedimentary basins.

12.2 Northern Appalachians

The Northern Appalachians were divided into the Humber, Dunnage, Gander, Avalon and Meguma zones or terranes (Fig. 12.2; Williams 1988), which is a first order line of evidence for the presence of several major discrete terranes in this orogen and the need for different Ordovician to Devonian collisional events to accrete them to a progressively expanding (paleo-South) Laurentian margin (e.g., Williams 1995a; van Staal et al. 1998). The Humber Zone represents the remnants of a passive margin built upon the leading edge of Laurentia during the Cambrian and Early-Middle Ordovician, whereas the Gander, Avalon and Meguma zones represent micro-continental ribbons (including their juvenile additions acquired prior to their accretion to Laurentia) that were derived from Gondwana (Williams 1995b). The Dunnage zone preserves the vestiges of predominantly supra-subduction zone terranes that developed in the Cambro-Ordovician Iapetus Ocean. They include slices of forearc, arc, back-arc, and rare seamount crust and mantle. The implied oceanic nature of these terranes is somewhat misleading, because many of these island arc terranes were underlain by extended continental rather than true oceanic crust (van Staal et al. 1998; Rogers et al. 2006; Zagorevski et al. 2006, 2007a; Zagorevski et al. in press). Based on an extensive set of different lines of evidence, the majority of the various Dunnage Zone terranes formed either close to the Laurentian or Gondwanan margins of Iapetus in supra-subduction zone settings. This paleogeography is reflected by the partitioning of the Dunnage Zone terranes into the peri-Laurentian Notre Dame and peri-Gondwanan Exploits subzones (Fig. 12.2;

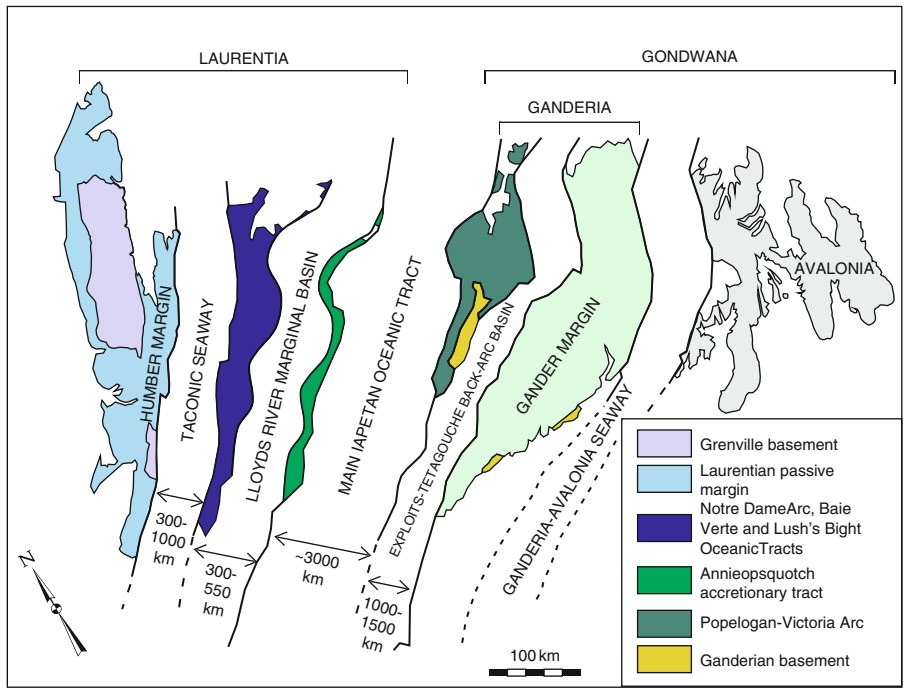

Fig. 12.2 Tectono-stratigraphic subdivisions of Newfoundland expanded to show seaways that occurred outboard of Laurentian margin (modified from Williams 1995b and van Staal et al. submitted).

Williams 1995b). Most, if not all, of oceanic lithosphere that formed in the Iapetus Ocean was subducted and is not preserved.

The Notre Dame Subzone is bounded by the Baie Verte – Brompton Line to the west and the Red Indian Line to the east. It comprises the Lushs Bight and Baie Verte Oceanic Tracts (e.g., Hibbard 1983; van Staal et al. 1998; Skulski et al. 2009), the Notre Dame Arc (Whalen et al. 1997; van Staal et al. 1998, 2007) and the Annieopsquotch accretionary tract (van Staal et al. 1998; Lissenberg et al. 2005b; Zagorevski et al. 2009). Zircon inheritance and isotope characteristics (e.g., Swinden et al. 1997; Whalen et al. 1997; Lissenberg et al. 2005b; Zagorevski et al. 2006; van Staal et al. 2007) indicate that many of the arc terranes of the Notre Dame Subzone appear to be, at least in part, built on thin Laurentian crust. They were sequentially accreted to the Laurentian margin as separate or composite blocks. These accretionary events produced the poly-phase Late Cambrian to Late Ordovician (495–450 Ma) Taconic orogeny (Szybinski 1995; Lissenberg et al. 2005b; van Staal et al. 2007; Zagorevski et al. 2007b), which was principally caused by the closure of the Taconic seaway (Waldron and van Staal 2001), the Lloyds River marginal basin (Lissenberg et al. 2005b; Zagorevski et al. 2009) and the main tract of Iapetus itself (van Staal et al. 2007; Zagorevski et al. 2008) (Fig. 12.2). The grouping of multiple accretionary events into the Taconic orogeny was done because they either overlap- or follow each other closely in time and space, and hence, generally cannot be separated individually on an orogen-wide scale. These Taconic events exemplify three unique tectonic configurations that are reviewed and discussed in the following sections.

To the east of the Annieopsquotch accretionary tract and the Red Indian Line (Fig. 12.2), the Exploits Subzone is represented by the Ordovician Popelogan-Victoria Arc – Tetagouche-Exploits back-arc system that was built on a Cambrian to Early Ordovician Penobscot arc founded on peri-Gondwanan Neoproterozoic basement (e.g., Colman-Sadd et al. 1992a; van Staal et al. 1996; O'Brien et al. 1997; MacLachlan et al. 2001; Rogers et al. 2006; Zagorevski et al. 2007a). The Popelogan-Victoria Arc is the first peri-Gondwanan terrane to arrive at the Laurentian margin following the closure of the main tract of the Iapetus Ocean. Its accretion marks the end of the strictly peri-Laurentian Taconic Orogeny and the start of the Late Ordovician-Silurian Salinic Orogeny – related

accretionary events that involved both Laurentian and peri-Gondwanan rocks (e.g., van Staal et al. 2009b).

12.3 Soft Versus Hard Collision

In this paper, arc–continent collisions are termed either *hard* or *soft*. This usage follows earlier papers (e.g., van Staal et al. 1998), although the detailed difference between these two processes has not been formally defined. We acknowledge that an objective difference is difficult to define other than in a qualitative way; h*ard* collision is herein used where the overriding plate, either arc or supra-subduction zone forearc ophiolite, has been significantly tectonically thickened in proximity to the suture zone due to internal deformation and was associated with high-grade metamorphism and progressive widening of the subduction channel into its hangingwall (van Staal et al. 2009b). This is broadly equivalent to collisional orogens of Cawood et al. (2009) and collisional orogenesis of Cloos (1993). The only arc-collision described herein that represents a *hard* collision is the Taconic Notre Dame Arc – Humber margin collision. All other collisions discussed herein are considered *soft*, as they are not associated with significant thickening and metamorphism. These types are broadly equivalent to accretionary orogens of Cawood et al. (2009). It should be noted that the principal manifestations of the differences between soft and hard collisions are highly dependent on the erosion level.

12.4 The Taconic Seaway

The Early to Middle Ordovician closure of the Taconic seaway and the resultant collision between the Humber margin and Dashwoods played a crucial role in development of the Taconic orogen in the Northern Appalachians (Fig. 12.3; van Staal et al. 2007), but it cannot be understood without the knowledge of the initial configuration of the Laurentian margin . A protracted series of rift-related magmatic events and paleomagnetic constraints suggest that Iapetus opened in several phases (Cawood et al. 2001). The rift-drift transition preserved on the Humber margin (Williams and Hiscott 1987; Cawood et al. 2001; Cawood and Nemchin 2001), the last gasp of rift-related magmatism, and formation of c. 555–540 Ma transitional crust (Waldron and van Staal 2001; van Staal et al. 2008) represent opening of the relatively narrow Taconic seaway following an inboard ridge jump from the main Iapetus tract, which had opened earlier (Waldron and van Staal 2001; Hibbard et al. 2007; van Staal et al. 2007). The Humber margin sediments probably transcended the continental-oceanic boundary during the Cambrian (Waldron and van Staal 2001). This inference is supported by tectonic interleaving of Fleur de Lys Group sediments (part of Humber margin) with c. 560–550 Ma (van Staal et al. 2008) transitional crust (Birchy Complex and correlatives: Hibbard 1983; Winchester et al. 1992) along the Baie Verte – Brompton Line in Newfoundland. In general, it is likely that at least part of the Taconic seaway's oceanic crust was overlain by a considerable thickness of Laurentian-derived clastic sediments. The latter were probably assembled into an accretionary wedge during the Taconic subduction and became the source for the late syntectonic S-type granitic sheets (459–455 Ma) that are restricted to the high strain zone marking the Baie Verte – Brompton Line in Newfoundland (Fig. 12.4; Brem et al. 2008; van Staal et al. 2009b).

Opening of the Taconic seaway led to separation of a single or several micro-continent ribbons derived from the Laurentian margin collectively called Dashwoods in the Northern Appalachians (Waldron and van Staal 2001). Dashwoods subsequently became the basement to the Ordovician Notre Dame Arc (Fig. 12.2). The extent of Dashwoods basement along the length of the Appalachian orogen is contentious and poorly known at present. The presence of Dashwoods-like basement has been detected in the subsurface beneath the Notre Dame Arc both in Newfoundland (van Staal et al. 2007) and southern Quebec (Gerbi et al. 2006a, b) and hence most of the arc is continental at the latitude of Canada; however, the Notre Dame Arc may transgress from a continental to an oceanic substrate along strike.

12.5 Closure of the Taconic Seaway

Early Ordovician, east-directed (present coordinates) subduction in the Taconic Seaway was either initiated following a subduction polarity flip or a step-back from an earlier, relatively soft accretion, between an

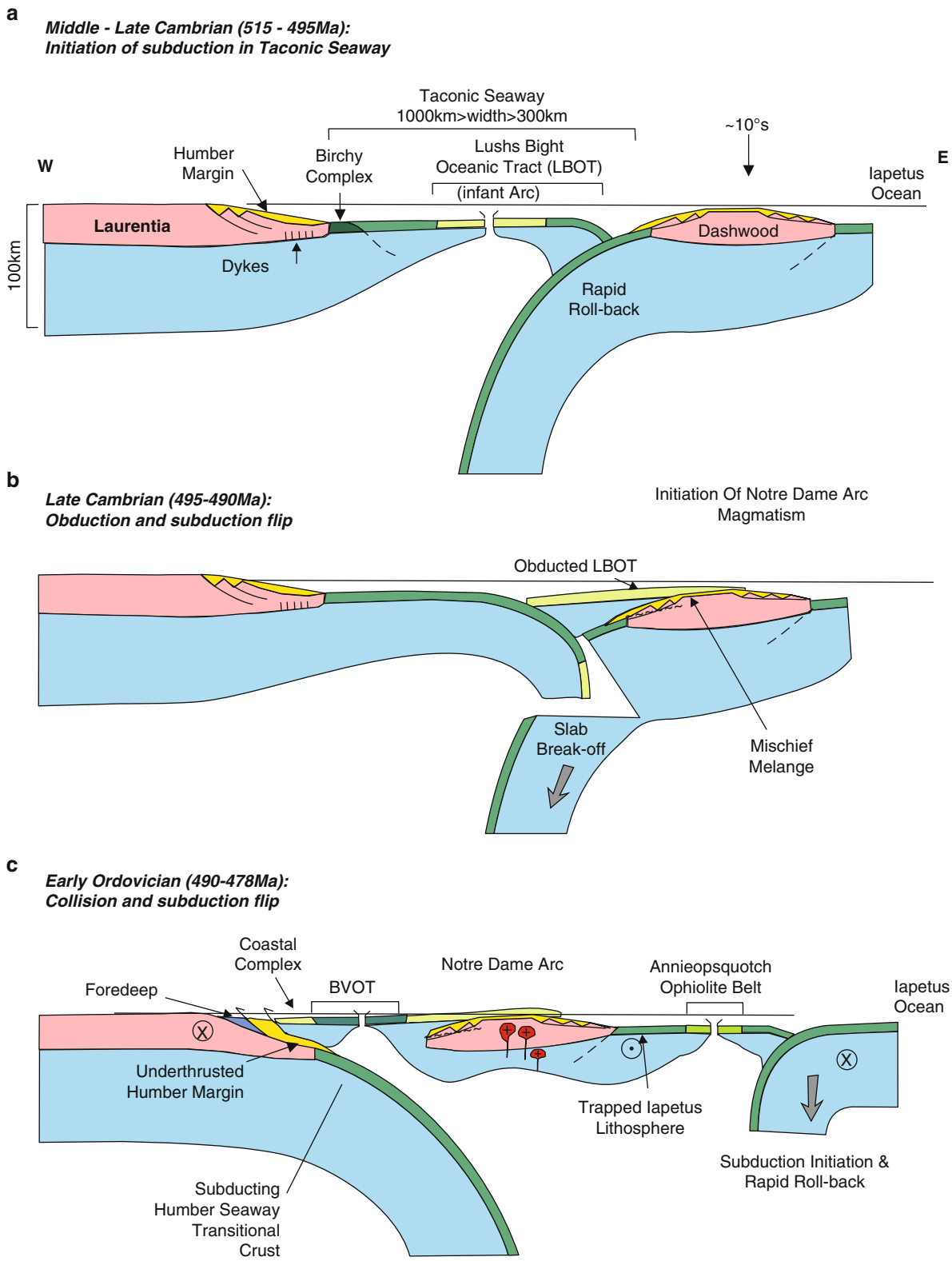
a
Middle - Late Cambrian (515 - 495Ma):
Initiation of subduction in Taconic Seaway
Taconic Seaway
1000km>width>300km
~10°s
W
E
Humber
Margin
Birchy
Complex
Lushs Bight
Oceanic Tract (LBOT)
(infant Arc)
Iapetus
Ocean
Laurentia
Dashwood
100km
Dykes
Rapid
Roll-back
b
Late Cambrian (495-490Ma):
Obduction and subduction flip
Initiation Of Notre Dame Arc
Magmatism
Obducted LBOT
Slab
Break-off
Mischief
Melange
c
Early Ordovician (490-478Ma):
Collision and subduction flip
Coastal
Complex
Notre Dame Arc
Annieopsquotch
Ophiolite Belt
Foredeep
BVOT
Iapetus
Ocean
Underthrusted
Humber Margin
Trapped Iapetus
Lithosphere
Subduction Initiation &
Rapid Roll-back
Subducting
Humber Seaway
Transitional
Crust

Fig. 12.4 S-type granitoid located in the Baie Verte – Brompton Line deformation zone in Newfoundland.

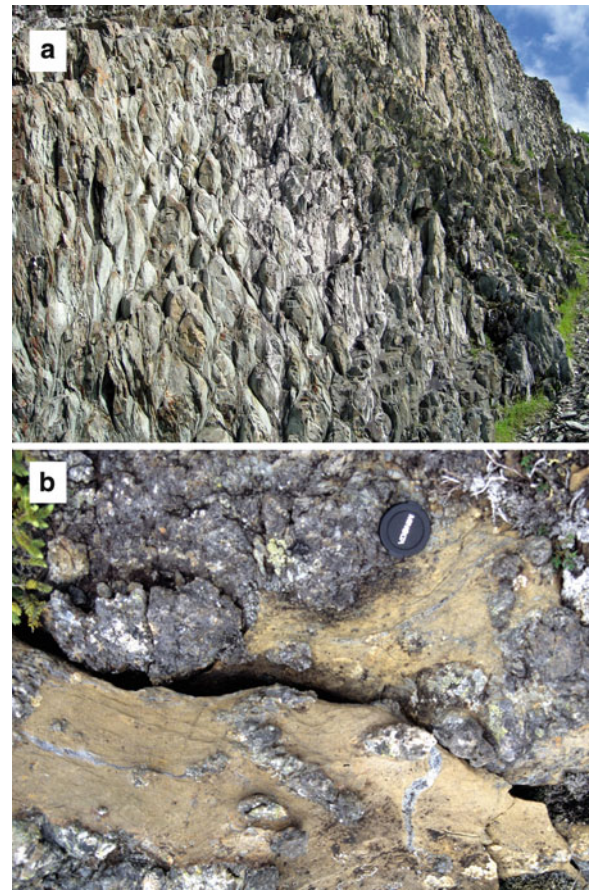

Fig. 12.5 Lushs Bight oceanic tract. (**a**) Deformed Lushs Bight pillow basalts. (**b**) Lushs Bight ultramafic rocks intruded by Notre Dame Arc dykes.

outboard supra-subduction zone Lush's Bight Oceanic Tract (LBOT; Fig. 12.5) and Dashwoods (Fig. 12.3; van Staal et al. 2007). Although the LBOT occupied the upper plate in this tectonic event, it is at present poorly known whether it originally formed outboard or inboard of Dashwoods (cf. van Staal et al. 2007) due to inadequate geochronological, metamorphic and structural studies (van Staal et al. 2009b). The presence of LBOT remnants in a forearc position (Jenner et al. 1991; Kurth et al. 1998) during the final closure of the Taconic seaway, supports formation of the LBOT in the Taconic seaway. The previously proposed outboard position of the LBOT (van Staal et al. 1998, 2007) requires that Dashwoods was completely subducted beneath the LBOT; this requirement is removed if one accepts the inboard kinematic model (Fig. 12.3). If the latter suggestion is correct, a subduction polarity flip is required in the Taconic seaway at ca. 490 Ma. Regardless of which tectonic process was responsible for accretion of the LBOT, subsequent initiation of eastward-directed subduction in the Taconic seaway led to formation of the 490–484 Ma supra-subduction zone Baie Verte Oceanic Tract (Dunning and Krogh 1985; Jenner et al. 1991), which was situated close to the leading edge of Dashwoods, i.e. in a forearc position to the first phase of the Notre Dame Arc (489–475 Ma: van Staal et al. 2007).

The Notre Dame Arc was created by B-subduction of the Taconic seaway's oceanic lithosphere and culminated in prolonged A-subduction of the Humber margin beneath Dashwoods (Fig. 12.3; 475–459 Ma: van Staal et al. 2007). West-directed subduction had

Fig. 12.3 Cambrian–Early Ordovician tectonic evolution of the Humber margin and outboard peri-Laurentian terranes (modified from van Staal et al. 2007, 2009b). (**a**) Subduction initiation and rapid hinge retreat of the west-dipping (present coordinates) Dashwoods plate is responsible for formation of the Lushs Bight oceanic tract infant arc terrane in the Taconic Seaway. (**b**) Subduction flip in the Taconic Seaway follows obduction of Lushs Bight oceanic tract onto Dashwoods. (**c**) Subduction in the Taconic Seaway produces the Baie Verte oceanic tract and Notre Dame Arc and led to the Taconic arc–continent collision. The collision results in subduction flip and initiation of west-directed subduction outboard of Dashwoods. The latter led to formation of the Annieopsquotch ophiolite belt (Lissenberg et al. 2005a).

already initiated outboard of Dashwoods by ca. 480 Ma (Lissenberg et al. 2005a; see following). Collision started along first and second order promontories in the Humber margin, and culminated in underplating and locally significant tectonic thickening of the Notre Dame Arc and its underlying Dashwoods infrastructure in south-western Newfoundland (van Staal et al. 2007).The locally intense deformation and metamorphism of the arc and its basement are hallmarks of a hard collision and the principal manifestation of the Taconic orogeny in Newfoundland (van Staal et al. 2009b). The recent and in part still ongoing Luzon arc-China collision exposed in Taiwan (e.g., Huang et al. 2000) can be considered to represent a modern analogue of the Taconic collision on basis of evidence for shortening and partial subduction of the Luzon arc-forearc system in parts of Taiwan (e.g. Tang and Chemenda 2000; Chemenda et al. 2001; Hirtzel et al. 2009). However, the mid-crustal and deeper roots of the Luzon arc are not yet exhumed, and hence the impact of the collision on the overriding arc is still poorly known.

12.6 Evolution of the Humber Margin and Diachroneity of the Taconic Collision

The first manifestation of convergence between the Humber margin and Notre Dame Arc during the closure of the Taconic seaway is tectonic loading of Laurentia's leading edge when it approached and entered the trench. Evidence of this early part of the Taconic convergence and collision is mainly preserved in the stratigraphic record of the Humber margin (Fig. 12.6), where the influence of Taconic tectonism (loading) is first recorded both in the Early Ordovician (~480 Ma) deep water clastic strata (i.e., Cow Head Group breccias) and a disconformity in the platform rocks in western Newfoundland (i.e., Boat Harbour Formation: Knight et al. 1991). Continuous underthrusting of the margin and the resultant west-directed propagation (present coordinates) of a foreland bulge and a trailing foreland basin onto the margin (Jacobi 1981) reflects progressive emplacement of the leading edge of the overriding plate (forearc and ophiolite; Figs. 12.3 and 12.7) further onto the Humber margin. The obducted ophiolites emerged above sea level

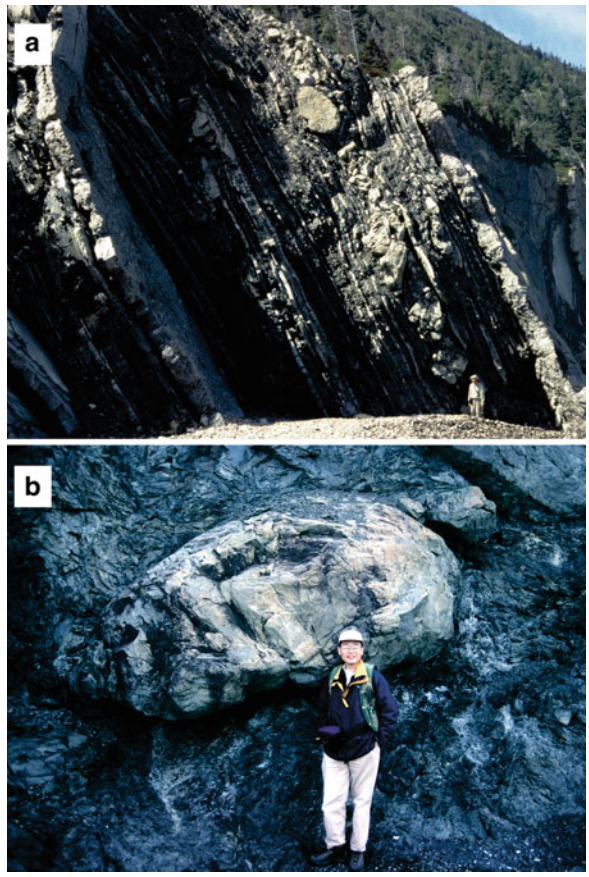

Fig. 12.6 Humber margin. (**a**) Cape Cormorant Formation polymictic conglomerates record progressive unroofing of the Cambrian to Ordovician Laurentian margin carbonate shelf during arc–continent collision. J. Waldron for scale. (**b**) Knocker in mélange at the base of Humber Arm allochton recording emplacement of Baie Verte oceanic tract onto the Laurentian margin. S. Lin for scale.

and started to supply detritus to the adjacent foreland basin later during the Early Ordovician (Stevens 1970).

Re-entrants and promontories (Fig. 12.8) appear to have had a major influence on the evolution and longevity of the collisional processes. The generation of the c. 465 Ma Mont Albert Complex ophiolite in Gaspe, Quebec (Malo et al. 2008) took place after obduction of the ca. 484 Ma Bay of Islands Ophiolite Complex and foreland basin development near promontories (Cawood and Suhr 1992; van Staal et al. 2007). Hence, subduction of relatively old, dense oceanic lithosphere must have continued in adjacent re-entrants. First order re-entrant – promontory pairs (Fig. 12.8; Thomas 1977) provide the simplest explanation why the collision appears to have started later

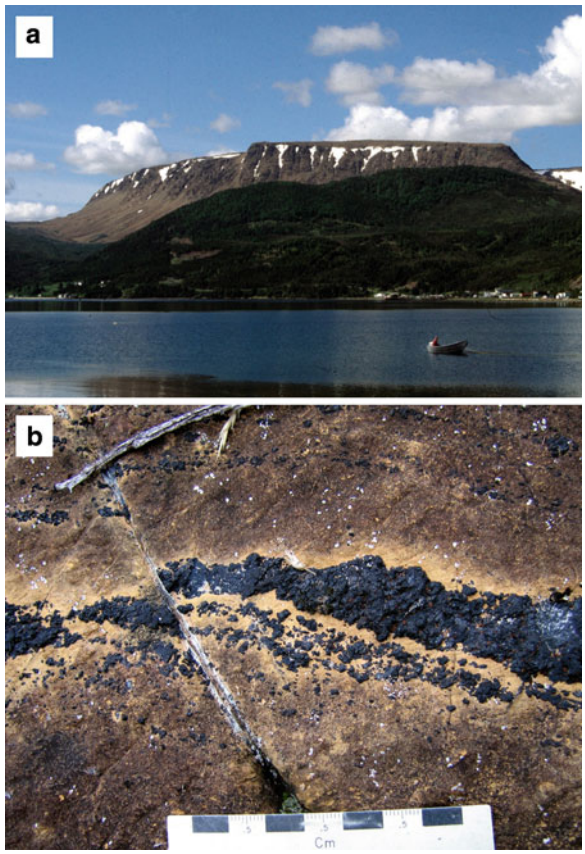

Fig. 12.7 Baie Verte oceanic tract. (**a**) Tablelands plateau in Gros Morne National Park represent the mantle of the Baie Verte oceanic tract that was obducted onto the Laurentian margin. (**b**) Metasomatized mantle with chromite-layers of the Advocate ophiolite (Bedard and Escayola, 2010) of the supra-subduction zone Baie Verte oceanic tract in Newfoundland.

and continued longer in the Quebec re-entrant compared to the adjacent St. Lawrence promontory (e.g., Knight et al. 1991; Hiscott 1995). It also provides a mechanism for the long-lasting A-subduction of parts of the Humber margin (c. 20 my). That is, B-subduction of trapped old oceanic lithosphere in first and second order re-entrants was the principal driving force of the A-subduction of the adjacent promontories culminating in Middle Ordovician (c. 464 Ma) eclogite formation in the Baie Verte peninsula (Jamieson 1990; van Staal et al. 2009a). Such a mechanism demands that the slab pull of the remaining oceanic lithosphere trapped in the re-entrants and still attached to the Humber margin at depth exceeded the buoyancy forces of the progressively underthrusted continental margin some of which may have had properties approaching that of transitional crust.

12.7 Evolution of the Taconic Terranes Accreted to the Humber Margin

The outboard terranes accreted to the Humber margin during closure of the Taconic seaway comprise the oceanic forearc material, which include parts of the LBOT (e.g. c. 505 Ma Coastal Complex: Jenner et al. 1991; Kurth et al. 1998), the Baie Verte oceanic tract and the trailing continental Notre Dame Arc built upon Dashwoods (van Staal et al. 2007). It is inferred from available data in Newfoundland that obduction onto the Humber margin here started at c. 480 Ma (Knight et al. 1991) and initiation of east-directed subduction took place at c. 490 Ma (van Staal et al. 2007). Hence, all tectonic events that predate this, such as the earliest oceanic detachment (e.g. St. Anthony complex) and emplacement of part of the LBOT and its assembly with Dashwoods (Fig. 12.5b) between 500 and 495 Ma are kinematically unrelated and not dealt with herein.

12.7.1 Baie Verte Oceanic Tract

The Baie Verte oceanic tract (BVOT) mainly comprises tectonised ophiolitic slivers spatially closely associated with the Baie Verte – Brompton Line that extends from northern Newfoundland through southern Quebec into New England (Williams and St-Julien 1982). All constituent layers of an ideal Penrose ophiolite (Anonymous 1972) are locally preserved; although undisturbed, intact sections are absent. The basalts, dikes and gabbros have compositions ranging between boninite and island arc tholeiite; the tholeiites being erupted last (Bedard et al. 2000; Skulski et al. 2009). Boninites also dominate the ophiolites of the BVOT in Quebec (e.g. Schroetter et al. 2003; De Souza et al. 2008; Page et al. 2008). The age of the oceanic rocks of the BVOT ranges between 490 and 484 Ma in Newfoundland (Dunning and Krogh 1985; Cawood et al. 1996; Skulski et al. 2009) and between 480 and 465 Ma in Quebec (Whitehead et al. 2000;

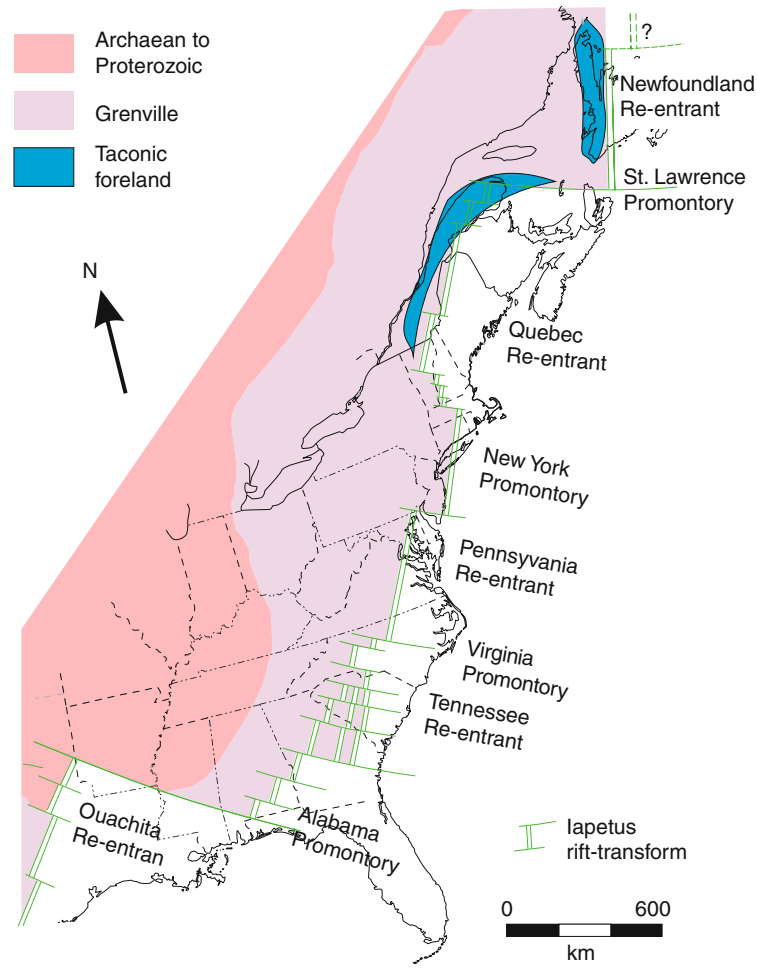

Fig. 12.8 The geometry of the Laurentian margin following breakup of Rodinia and opening of Iapetus Ocean (modified from Thomas 2005).

Pincivy et al. 2003). Deformed trondhjemite and tonalite intrusions of the Rowe-Hawley belt along strike in southern Vermont yielded ages between 496 and 486 Ma (Ratcliffe et al. 1998), indicating that the two dated ophiolites of the BVOT in Quebec significantly postdate an already established history of subduction and orogenesis near the Laurentian margin in this part of the Northern Appalachians. Nevertheless, the younger ages in Quebec are consistent with the diachroneity of events expected when moving from a first order promontory to an adjacent re-entrant.

The BVOT ophiolites in northern and west-central Newfoundland lies unconformably beneath c. 481 to 467 Ma extensional arc-like cover sequence previously referred to as the Snooks Arm arc (van Staal et al. 2007). The Snooks Arm arc comprises a mixture of E-MORB and calc-alkaline volcanic rocks (Bedard et al. 2000) whose chemical compositions and the presence of inherited zircons suggest interaction with continental crust during their ascent (Skulski et al. 2009). Combining the above data with evidence from the adjacent Humber margin (e.g. Knight et al. 1991), they suggest that obduction of the BVOT forearc was underway at c. 480 Ma in Newfoundland. Oceanic detachment and obduction had started slightly later in Quebec, between 477 and 470 Ma (Whitehead et al. 1996, 2000). Possible analogues of the Snooks Arm sequence are the Bolton Igneous Group in Quebec and correlatives in adjacent Vermont, which erupted in the arc-trench gap

between 477 and 458 Ma (Kim et al. 2003); however, a stratigraphic linkage with the older forearc ophiolites has not yet been documented there. Although the tectonic setting of the Snooks Arm cover sequence and correlatives elsewhere is still contentious, we tentatively interpret them as having formed after the onset of the obduction of the underlying forearc ophiolite as a result of localised, accelerated rollback driven by relatively old oceanic lithosphere trapped in nearby second order re-entrants (Fig. 12.6 in van Staal et al. 2007). This process locally steepened the downgoing slab, initiated upper plate extension and promoted a renewed injection of asthenosphere beneath the already partially obducted BVOT in such localities.

12.7.2 Notre Dame Arc

The Notre Dame Arc is anomalously well exposed in Newfoundland and has been studied in detail resulting in a very extensive, high-quality radiometric database (Whalen et al. 2006; van Staal et al. 2007). The Notre Dame Arc generally comprises low metamorphic grade volcanic rocks in the north, near the beginning of the Newfoundland re-entrant; whereas upper amphibolite or granulite facies and plutonic rocks predominate opposite the St. Lawrence promontory in the south (Fig. 12.9). The deepest exhumed rocks are thus exposed in the south and the arc system preserves a tilted section from supra- to infrastructure going from north to south. The first, B-subduction related phase of the continental Notre Dame Arc was active between 489 and 475 Ma in Newfoundland and was followed by a magmatic gap until c. 465 Ma, which combined with other structural and geochronological evidence suggest that a hard collision between the Notre Dame Arc and the Humber margin was established here by at least 470 Ma (van Staal et al. 2007).

The equivalent of the Notre Dame Arc in Quebec and adjacent New England is poorly preserved, but detailed studies in the Chain Lakes massif, an exposed Dashwoods correlative, reveal that the B-subduction related phase of the arc was active by at least 477 Ma, possibly already at 486 Ma, and continued until at least 472 Ma (Gerbi et al. 2006a, b). Hard collision between the arc and the Humber margin had also started by c. 470 Ma. Between 470 and

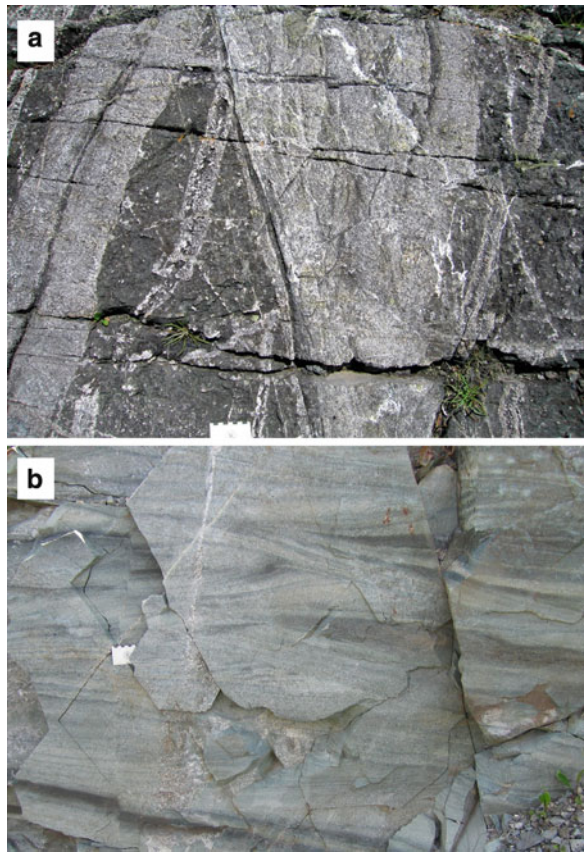

Fig. 12.9 Notre Dame arc. (**a**) Pyroxenite and hornblendite cut by Early Ordovician diorite and tonalite in the roots of the Notre Dame arc. (**b**) Cross-bedded, mafic-derived sandstone of the Middle Ordovician Cutwell Group form the suprastructure of the Notre Dame Arc.

460 Ma, the Notre Dame Arc in Newfoundland was significantly thickened as a result of continuous A-subduction of the downgoing Humber margin and progressive widening of the subduction channel into its hangingwall (van Staal et al. 2009b). Collision was terminated with slab breakoff that triggered a very voluminous pulse of syn-tectonic, upper plate granitoid magmatism between 464 and 459 Ma, known as the second phase of the Notre Dame Arc (van Staal et al. 2007). This phase is strictly speaking not an arc, because it significantly postdates obduction of the forearc and the onset of A-subduction-induced arc thickening. This event has only been studied in detail in Newfoundland, but the coeval continental Ascot "arc" in southern Quebec (Tremblay et al. 1994) is correlated with this event (van Staal et al. 2007).

12.8 Characteristics of the Taconic Collision

From the foregoing we conclude that the Taconic collision between the Laurentian Humber margin and the Notre Dame Arc involved a series of very complex, diachronous events. The generation of forearc supra-subduction zone ophiolites in the Taconic seaway between Newfoundland and Quebec spanned more than 30 my (490–456 Ma). Based on evidence preserved in the stratigraphic record of the Humber margin and the timing of the supply of ophiolite-derived detritus to the adjacent marine foreland basins, formation of several of the forearc ophiolites postdate or overlap in age with the time of obduction onto the margin of other ophiolites along strike. Formation and emplacement of some even appear to have overlapped with the onset and duration of the hard collision between the arc and the Humber margin. Evidently first and second order promontory – re-entrant pairs in the Humber margin seem to have played an enormously important role in this process (Fig. 12.8). Ophiolites such as the Bay of Island and Mont Albert complexes and perhaps even the Thetford Mines complex may have been generated as supra-subduction zone oceanic lithosphere in deep re-entrants where mainly Mediterranean-style subduction continued as a result of roll back of trapped oceanic lithosphere (van Staal et al. 2007), whereas convergence had slowed down significantly in the adjacent promontories. Such syn-collisional ophiolites were classified as peri-collisional by Harris (1992), and it is these that preferentially have preserved metamorphic soles. Because the closure of the Taconic seaway was oblique, obducted ophiolitic segments that were once opposite to a promontory may over time have been transported opposite still subducting re-entrants, such that now they were subjected to the local roll-back induced extension, creating a post-obduction, extensional arc-like sequence such as the Snooks Arm cover to the BVOT. The major irregularities in the margin are probably also the reason why ophiolites are so well preserved only in re-entrants or along the bordering margins of promontories. Where the forearc lithosphere became caught-up in the collision between the arc and the leading edge of promontories, such as in south-western Newfoundland (core of the St. Lawrence promontory), little or no BVOT is preserved and presumably was removed by extensive erosion following uplift (van Staal et al. 2007).

12.9 Annieopsquotch Accretionary Tract: Closure of the Lloyds River Marginal Basin

The remnants of the opening and closing of the Lloyds River marginal basin are preserved in the Annieopsquotch accretionary tract in Newfoundland (Fig. 12.10; Lissenberg et al. 2005a, b; Zagorevski et al. 2006). Correlatives of these rocks are poorly preserved or completely masked by younger cover sequences in the Northern Appalachians outside of Newfoundland (e.g., Dupuis et al. 2009). Hence, the following discussion is solely based on relationships observed in central Newfoundland. The Annieopsquotch accretionary tract forms a structural collage of multiple arc and ophiolite terranes that were accreted to the Iapetus-facing margin of Dashwoods with its Notre Dame Arc supra-structure. The oldest rocks in the Annieopsquotch accretionary tract are c. 480 Ma supra-subduction zone ophiolite rocks (Annieopsquotch ophiolite belt, Dunning 1987), which record formation of an east-facing infant arc (Figs. 12.11 and 12.12a; Lissenberg et al. 2005a). Inception of west-directed subduction outboard of Dashwoods thus closely coincides with the initiation of the collision between the Notre Dame Arc and the St. Lawrence promontory in the Taconic Seaway (see above). Hence, the initiation of west-directed subduction and magmatism in the Annieopsquotch accretionary tract is attributed to a subduction polarity flip from east dipping subduction in the Taconic seaway to west-dipping subduction outboard of Daswoods (Lissenberg et al. 2005a; van Staal et al. 2007). The evolution of the Annieopsquotch accretionary tract is complex and characterized by formation of multiple arc and ophiolite belts from c. 480 Ma to c. 460 Ma (e.g., Dunning 1987; Zagorevski et al. 2006), followed by their accretion to the Notre Dame Arc, commonly within ~5 my of their formation (Lissenberg et al. 2005b).

Formation of the Annieopsquotch ophiolite belt was followed by development of an overall extensional arc-backarc system at c. 473 Ma (Figs. 12.12b and 12.13), referred to as the Roberts Arm-Lloyds River arc system. Most of the early arc material preserved

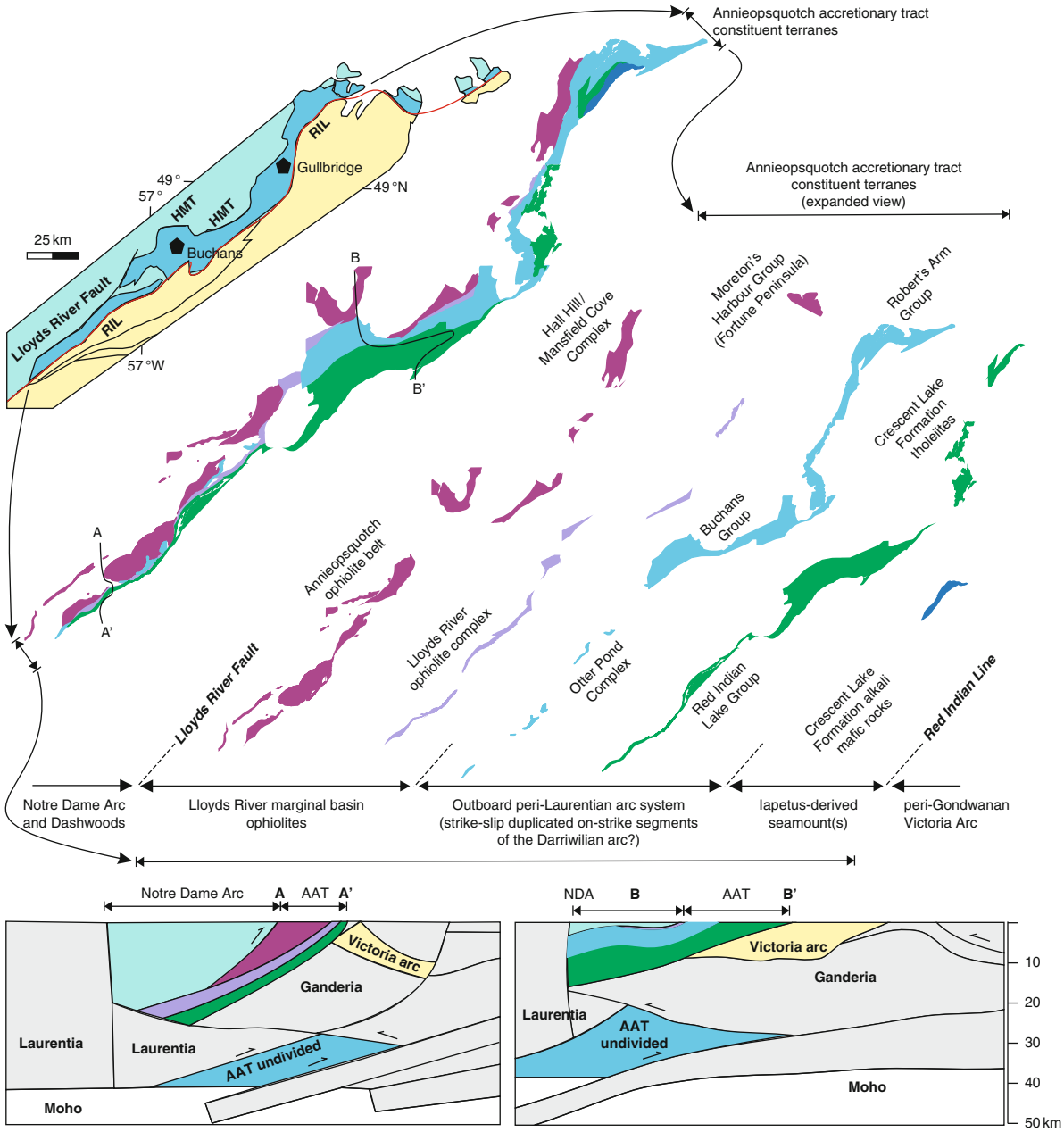

Fig. 12.10 Tectono-stratigraphic subdivisions of the Annieopsquotch accretionary tract expanded to show the aspect ratios of the constituent terranes (modified from Zagorevski et al. 2009).

in the Annieopsquotch accretionary tract in Newfoundland (e.g., c. 473 Ma Mink Lake formation: Zagorevski et al. 2006) appears, somewhat surprisingly, to have been built predominantly upon Laurentian-derived crust characterized by Proterozoic and Achaean inheritance rather than oceanic crust. We have interpreted this basement to represent a rifted-off promontory of Dashwoods (Zagorevski et al. 2006), which transcended onto oceanic (Annieopsquotch ophiolite belt) crust along strike. Remnants of the c. 473 Ma oceanic arc are only locally preserved (e.g. parts of Roberts Arm belt). This complex island arc system evolved over time until c. 462 Ma and underwent multiple episodes of rifting marked by the

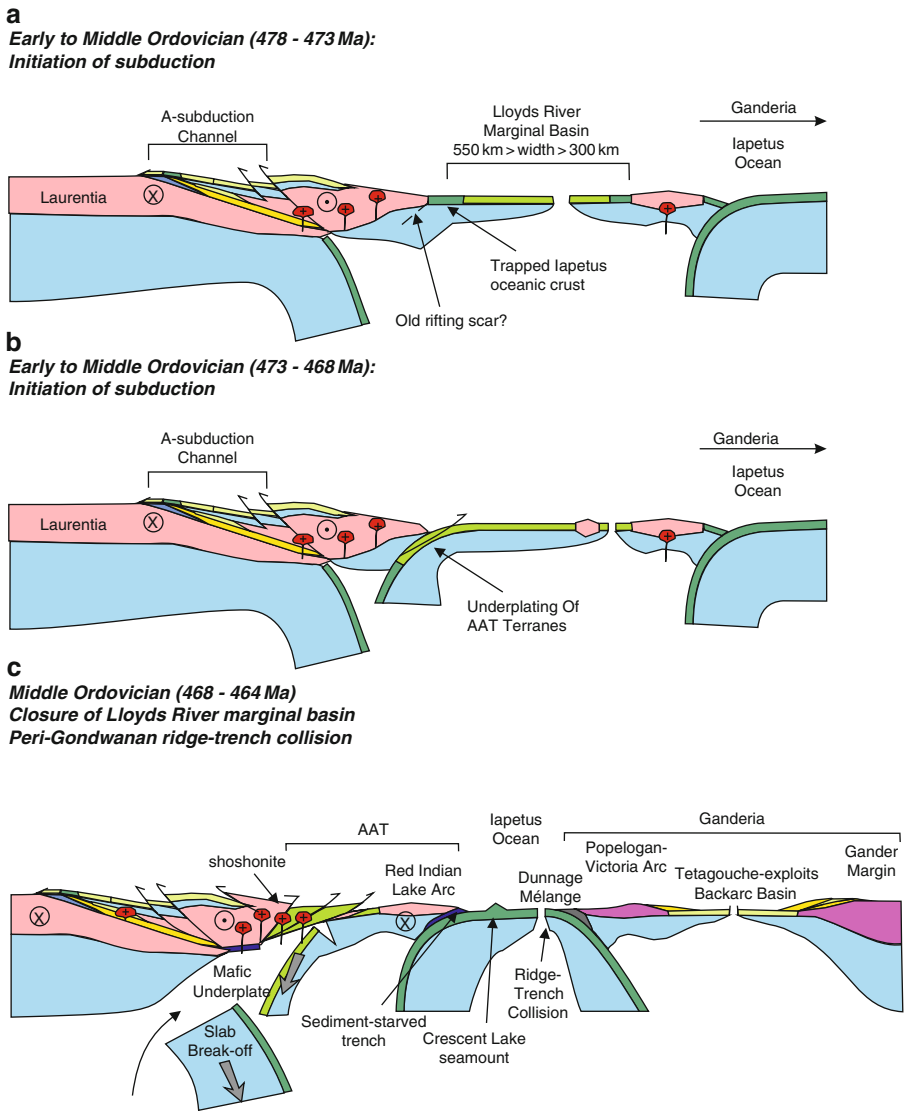

Fig. 12.11 Early to Middle Ordovician tectonic evolution of the Humber margin and outboard peri-Laurentian terranes (modified from van Staal et al. 2007, 2009b). (**a**) Formation of the Annieopsquotch ophiolite belt (AAT) is followed by development of extensional arc outboard of Dashwoods (Zagorevski et al. 2006) synchronous with on-going collision in the Taconic Seaway. (**b**) On-going convergence in the Taconic Seaway places Lloyds River marginal basin under compression initiating subduction at an old rifting scar at the Dashwoods – Iapetus oceanic crust interface. Lloyds River marginal basin terranes are underplated beneath Dashwoods forming an accretionary tract (Lissenberg et al. 2005b). (**c**) The outboard arc is accreted to Dashwoods accompanied by stitching magmatism in the AAT and slab-breakoff. The Red Indian Lake arc continues to be active following a short magmatic gap, unconformity and syntectonic sedimentation. The Popelogan – Victoria arc on the southern margin of Iapetus collides with a ridge resulting in arc-trench gap deformation and magmatism. The width of the AAT is exaggerated for clarity.

formation of back-arc basin ophiolites and rifted arc assemblages (Zagorevski et al. 2006; Zagorevski and Rogers 2009).

Accretion of parts of the Annieopsquotch accretionary tract to the now composite Laurentian margin (Humber margin + Dashwoods) had commenced by c. 470 Ma (Fig. 12.11; Lissenberg et al. 2005b). This event is marked by burial of the Annieopsquotch ophiolite belt, formation of c. 470 Ma amphibolite facies tectonites, and c. 468 Ma stitching plutonism

along the Annieopsquotch ophiolite belt and Lloyds River ophiolite complex boundary (Lissenberg et al. 2005b). This accretion and associated burial to moderate and deep depths is coeval with outboard arc magmatism. Hence, the early development of the Annieopsquotch accretionary tract necessitates subduction in a relatively narrow and young marginal basin (Lloyds River basin) that forms the backarc to the younger outboard arc terranes of the Annieopsquotch accretionary tract (Lissenberg et al. 2005b; Zagorevski et al. 2009). The cause of the initiation of subduction in such a relatively young (~10 my) basin remains unclear. However, it may be related to several factors (1) old oceanic lithosphere that probably formed shortly after opening of Iapetus may have been trapped between Dashwoods and AOB and hence was inherently subductable (Fig. 12.11), and (2) far-field compressive stresses induced by the southerly motion of Laurentia as suggested by its relatively robust paleomagnetic dataset (see van Staal et al. 1998, Fig. 12.8) may have placed the young Lloyds River marginal basin into compression (i.e., introversion of Murphy et al. 2009).

The Annieopsquotch accretionary tract thus forms a *retreating* and an *accretionary* orogen of Cawood et al. (2009) depending on whether composite Laurentian margin or outboard arc are used as a reference point. The setting of the Annieopsquotch accretionary tract terranes relative to the subduction zone is fundamentally different from the setting of the Notre Dame Arc relative to the passive margin of Laurentia. Instead of emplacement of the arc onto the continental margin (i.e. obduction), the Annieopsquotch accretionary tract terranes were thrust beneath the Notre Dame Arc as a result of B-subduction and the underplating of relatively young marginal basin and extended arc lithosphere.

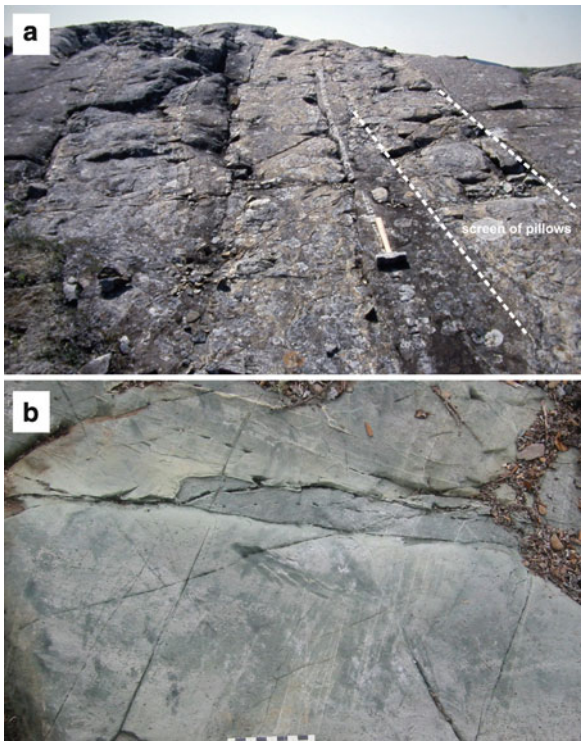

Fig. 12.12 Ophiolites of the Lloyds River marginal basin. (**a**) c. 480 Ma Annieopsquotch ophiolite belt sheeted dyke complex with screen of pillow basalt. (**b**) c. 473 Ma Lloyds River ophiolite complex vesicular sheeted dykes.

Fig. 12.13 Robert's Arm arc represented by the c. 473 Ma Mink Lake Formation basalt.

12.10 Structure of the Accreted Terranes in the Annieopsquotch Accretionary Tract

The most notable feature of the Annieopsquotch accretionary tract is the very long and narrow aspect ratio of the tract and its accreted terranes (Fig. 12.10; e.g., Zagorevski et al. 2009). The terranes form a thrust stack with a combined structural thickness of <15 km and individual terranes rarely exceed 5 km in stratigraphic thickness (e.g., van der Velden et al. 2004; Lissenberg et al. 2005b; Zagorevski et al. 2006). The ophiolite belts generally comprise cumulate gabbro, isotropic

gabbro, trondjhemite, sheeted dykes and pillow basalt (Fig. 12.12; Dunning and Chorlton 1985; Lissenberg et al. 2004; Zagorevski et al. 2006). Although ultramafic rocks do occur locally (Lissenberg et al. 2006), well developed ultramafic cumulate and mantle sections typical of the Baie-Verte Oceanic Tract ophiolites (e.g., Bedard et al. 1998; Bedard and Escayola 2010) are rare, and where present occur as small, isolated bodies (Lissenberg et al. 2006; Lissenberg and van Staal 2006). The arc terranes preserve predominantly supracrustal sections; minor granodiorite to diorite subvolcanic plutons occur only locally near the stratigraphic and structural base (e.g., Thurlow and Swanson 1987; Bostock 1988; Kerr and Dunning 2003; Zagorevski et al. 2006; Zagorevski and Rogers 2008). The large tracts of middle and lower crust plutonic and metamorphic rocks typical of the Notre Dame Arc are notably absent. Zagorevski et al. (2009) interpreted these relationships to be the direct result of the lower plate setting of the terranes during arc–arc collision. The transfer of the terranes from the lower plate to the upper plate was probably accomplished by step-down of the decollement to the brittle-ductile transition in the subducting crust, the location of which is probably controlled by thermal and/or fluid-induced weakening, similar to observations in other accretionary margins (e.g., Kimura and Ludden 1995; Calvert 1996). Most of the lower, dominantly mafic crust and lithospheric mantle of the accreted arc and backarc segments thus was delaminated and completely subducted, which is the expected norm for subduction of relatively young arc systems (Boutelier et al. 2003).

12.11 Patterns of Sedimentation

Sedimentary rocks in the Annieopsquotch accretionary tract are generally scarce, but are preserved between the Annieopsquotch ophiolite belt and Dashwoods along the Lloyd's River fault system (Fig. 12.10; Lissenberg et al. 2006; Lissenberg and van staal 2006). Here they are intensely migmatised and invaded by plutonic rocks and hence their original sedimentary protolith is difficult to discern. Elsewhere in the Annieopsquotch accretionary tract, they predominantly comprise tuffaceous to epiclastic rocks derived from proximal volcanic centres. Basinal shale, chert, jasperite and limestone are widespread, but volumetrically very minor relative to volcanic and epiclastic rocks. The interpreted peri-Laurentian position of the Annieopsquotch accretionary tract (Johnson et al. 1991; van Staal et al. 1998; Lissenberg et al. 2005a, b; Zagorevski et al. 2009; Cutts et al. 2010) may seem at odds with the lack of Laurentian-derived clastic rocks in such a tectonic setting. The scarcity of such rocks preserved during the accretion of backarc and remnant arc may be due to several processes. Foremost, the accreted terranes were underplated at depth (Zagorevski et al. 2009); hence, any sedimentary record of the accretion, including a forearc basin built upon the backarc basin's oceanic crust, may be lost through either subduction erosion along the Lloyds River trench (Fig. 12.11) or due to subsequent erosion to the present crustal level. In addition, sediments may have been largely assimilated by the slab break-off related voluminous granitoid magmatism of the second phase of the Notre Dame Arc that massively invaded the boundary between the arc and the Annieopsquotch accretionary tract between c. 464 and 460 Ma (Lissenberg et al. 2005b; van Staal et al. 2007). Alternatively, underplating of the Annieopsquotch accretionary tract terranes may not have had a lasting or noticeable impact on the Notre Dame Arc as these terranes are characterized by thinned crust (e.g., Zagorevski et al. 2006; Zagorevski and Rogers 2009) and did not have sufficient buoyancy to cause significant orogenesis (cf. Cloos 1993; Soh et al. 1998).

The arc terranes in the Annieopsquotch accretionary tract show a Middle Darriwilian (c. 467 Ma) regional unconformity (e.g., Zagorevski et al. 2006; Coombs 2009). It is marked by erosion of the underlying volcanic rocks and a polymictic breccia-conglomerate, locally spectacularly developed, derived from Late Cambrian to Early Darriwilian volcano-plutonic arc terranes (Fig. 12.14; Coombs 2009 and McNicoll et al. unpublished data), which generally correspond to those found in the Annieopsquotch accretionary tract and the composite Laurentian margin. The presence of this unconformity links all the arc terranes in the Annieopsquotch accretionary tract dynamically together and it is probably related to final closure of the Lloyds River marginal basin and accretion of the backarc and arc complexes to the Notre Dame Arc (Lissenberg et al. 2005b). Hence, the unconformity is a product of a collision between the outboard arc-and the Notre Dame Arc; the latter was magmatically inactive at

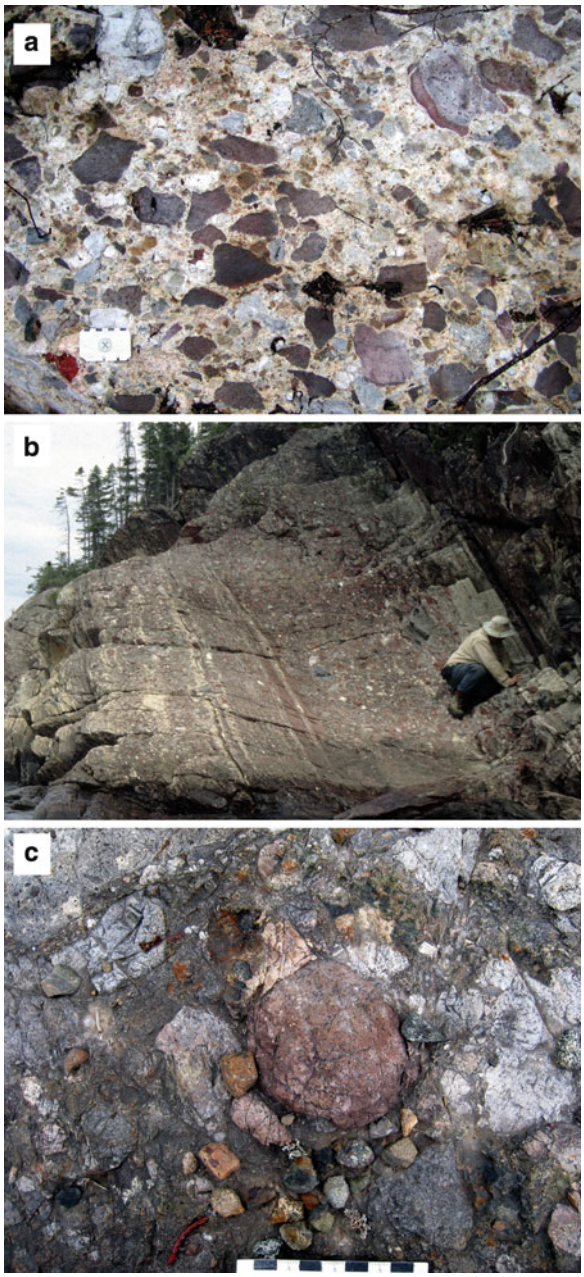

Fig. 12.14 Regional unconformity in the Annieopsquotch accretionary tract records the termination of subduction in the Lloyds River marginal basin and accretion of the outboard Robert's Arm arc to Dashwoods. (**a**) Breccia-conglomerate above Skidder formation contains andesitic clasts that have no known source in the AAT. (**b**) Breccia-conglomerate in the Red Indian Lake group contains mostly locally derived volcanic clasts above a shallow angular unconformity. (**c**) Breccia-conglomerate and sandstones in the Robert's Arm group record emergence of Early Ordovician arc in Early Darriwilian (McNicoll et al. unpublished data).

this time (magmatic gap of van Staal et al. 2007). Compared to the Notre Dame Arc-Humber margin collision, this collision was soft because neither the accreted arc nor the Notre Dame Arc rocks on Dashwoods show evidence of regionally penetrative deformation and structural thickening outside the relatively narrow subduction channel (Szybinski 1995; Lissenberg et al. 2005b; Lissenberg and van Staal 2006).

12.12 Iapetus Ocean

The development of the Annieopsquotch accretionary tract arc terranes outboard of the Notre Dame Arc while the latter is undergoing collision with the inboard Laurentian Humber margin, coincides with arc volcanism in the peri-Gondwanan realm of Iapetus Ocean (Figs. 12.11 and 12.15). Hence, the Iapetus ocea was subducting along its northern and southern margins at the same time (van Staal et al. 1998). This complex consumption of the Iapetus Ocean culminated in the collision of the peri-Gondwanan arc terrane with the active composite Laurentian margin in a configuration that is similar to the Molucca and Solomon Sea collision zones.

12.13 Peri-Laurentian Arc

The eastern most arc terranes of the Annieopsquotch accretionary tract represent fragments of the Middle Ordovician peri-Laurentian Red Indian Lake arc, which is the renewal of the east–facing arc following its accretion at c. 467 Ma due to the closure of the Lloyds River basin (e.g., Lissenberg et al. 2005b; Zagorevski et al. 2006). It is characterized by continentally influenced bimodal calc-alkaline and tholeiitic arc magmatism, suggesting an overall extensional setting marked by development of back-arc or intra-arc rift basins (Zagorevski et al. 2006; Zagorevski and Rogers 2009). Although volcanic rocks of the Red Indian Lake arc are generally well preserved (Fig. 12.16), the remnants of the associated forearc basin are poorly represented. Arc-derived turbidites and mass-flows interlayered with tuff beds, such as the Moores Cove Formation (e.g. Dec et al. 1997) situated along the Red Indian Line in the Notre

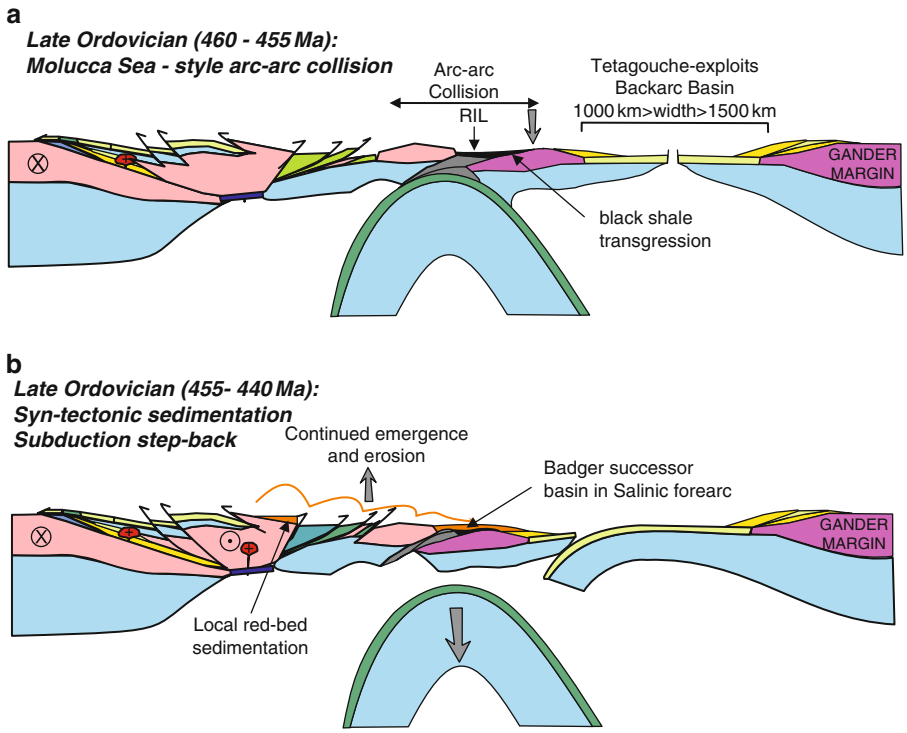

Fig. 12.15 Middle Ordovician tectonic evolution of the outboard peri-Laurentian and peri-Gondwanan terranes (modified from van Staal et al. 2007, 2009b). (**a**) Collision of the peri-Laurentian Red Indian Lake arc with peri-Gondwanan Popelogan-Victoria arc. During the collision the Red Indian Lake arc occupies an upper plate setting forming an emergent orogen that loads the Victoria arc (Zagorevski et al. 2008). Victoria arc is drowned resulting in black shale transgression and deep marine syn-tectonic sedimentation. (**b**) Subduction steps back into the Exploits-Tetagouche backarc basin placing the Badger successor basin into forearc position with respect to Salinic subduction.

Dame Bay area, are situated in the forearc position and may represent some of the potential remnants of the forearc basin (Fig. 12.17). However, overall, the forearc basin does not seem to have been extensive. In the Robert's Arm area in north-central Newfoundland, the Red Indian Lake arc volcanic and volcaniclastic rocks are in direct contact with an accreted seamount consisting of alkalic diabase, pillow basalt, mafic sandstone and conglomerate, and limestone (Fig. 12.18; Bostock 1988; Zagorevski 2008). The lack of forearc-like sedimentary rocks separating the arc from the accreted seamount suggests that the forearc basin was not extensive and that subduction was probably erosive.

12.14 Peri-Gondwanan Arc

The southern margin of the Iapetus Ocean is characterised by development of the Early-Middle Ordovician Popelogan-Victoria arc system that forms suprastructure to the Cambrian to Early Ordovician Penobscot Arc built on a ribbon rifted-off the peri-Gondwanan Ganderian microcontinent (Figs. 12.11 and 12.15; e.g., van Staal et al. 1996, 1998; Rogers et al. 2006). The Penobscot arc was terminated after it was reassembled with the Gander margin following a soft arc–continent collision history (i.e., c. 485 Ma Penobscot Orogeny: Colman-Sadd et al. 1992a; Zagorevski et al. 2007a; Zagorevski et al. 2010), which entirely took place in the peri-Gondwanan realm and is not discussed herein. Similar to the arc terranes in the Annieopsquotch accretionary tract, the Popelogan-Victoria arc was predominantly extensional throughout its history and was accompanied by a wide backarc basin floored by oceanic lithosphere. This is the Tetagouche-Exploits back-arc basin (van Staal et al. 1991, 2003; O'Brien et al. 1997; Valverde-Vaquero et al. 2006) whose closure during the Silurian

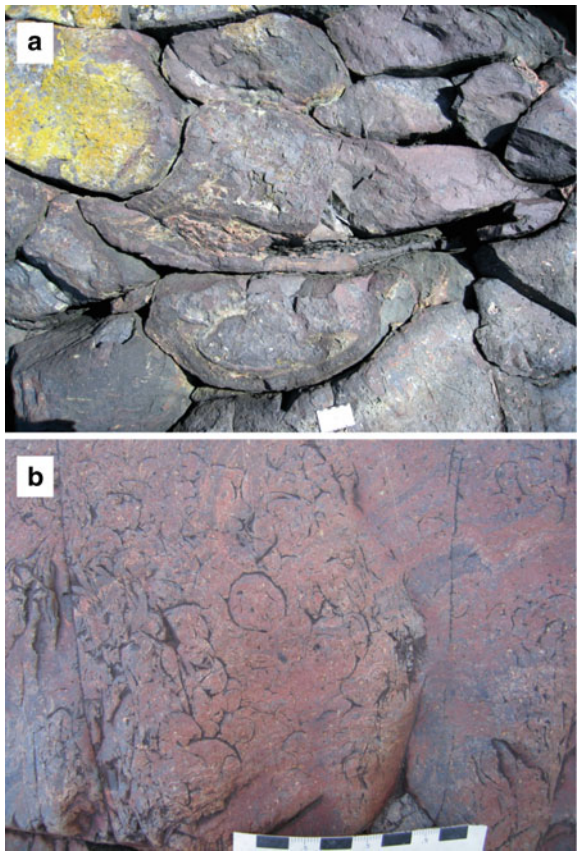

Fig. 12.16 Red Indian Lake arc. (**a**) Overturned calc-alkaline pillow basalt of the Middle Ordovician Robert's Arm Group. (**b**) Perlitic, flow-banded, tholeiitic rhyolite in the Middle Ordovician intra or back-arc rift, Mary March Brook formation (Zagorevski and Rogers 2009).

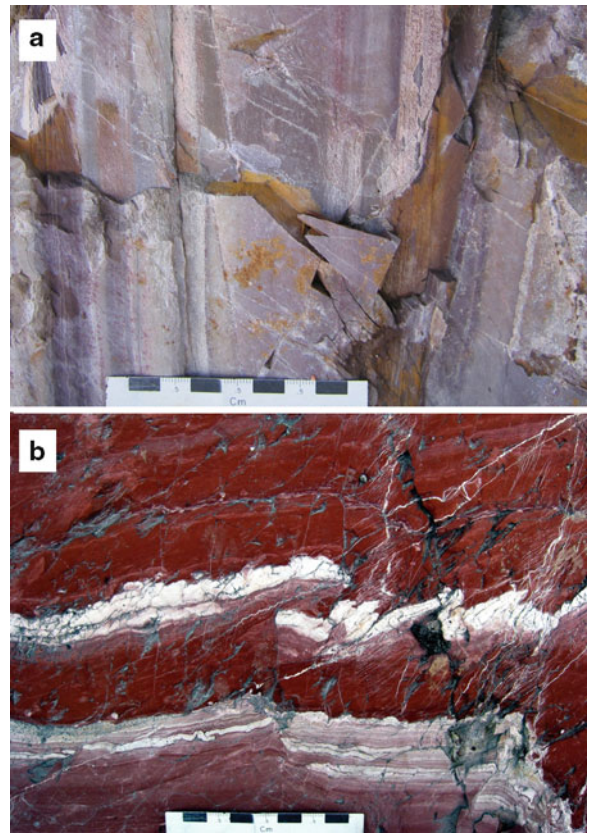

Fig. 12.17 Red Indian Lake fore-arc. (**a**) Epiclastic sediments of the Moores Cove Formation in the Notre Dame Bay may represent a peri-Laurentian fore-arc fragment. (**b**) Interbedded red shale, radiolarian jasperite and felsic tuff in the Crescent Lake formation along the Red Indian Line is in direct tectonic contact with an accreted seamount. Jasperite, red shale and haematized volcanic rocks are typical of Darriwilian succession in the Northern Appalachians.

was the main cause of the Salinic orogeny (van Staal et al. 2009b).

The main magmatic front of the Victoria Arc is not well preserved in Newfoundland, and the magmatism is dominated by a bimodal association of E-MORB/continental rift-like basalt and calc-alkaline rhyolite/dacite (Zagorevski et al. 2010). Unlike the terranes in the Annieopsquotch accretionary tract, the Popelogan-Victoria arc and Tetagouche-Exploits backarc system were characterized by an abundance of epiclastic sediments. The pre-collisional architecture of the Victoria Arc was dominated by asymmetric volcanoclastic turbidite basins above the Penobscot Arc basement (e.g., O'Brien et al. 1997). Forearc strata are probably locally preserved along the western margin of the Victoria Arc in Newfoundland (e.g., Upper Wild Bight Group: MacLachlan and Dunning 1998b; MacLachlan et al. 2001); however, they are difficult to differentiate from intra-arc and backarc-basin strata in the absence of a clearly defined magmatic front.

The western-most extent of the Victoria arc is marked by an extensive belt of mélange (Dunnage Mélange tract: Williams 1994) that in part defines the suture zone between the peri-Laurentian and peri-Gondwanan realms, namely the Red Indian Line (Williams 1995b). The mélange is locally intruded by c. 469 Ma syn-tectonic quartz-feldspar porphyry (Coaker Porphyry) indicating that mélange formation predates the collision with the peri-Laurentian Red Indian Lake Arc (see following). Presence of basaltic knockers of metric to kilometric scale in the mélange has led to proposals that it represents part of an accretionary prism with incorporated seamounts (i.e., Summerford

Fig. 12.18 Mafic-derived, cross-bedded sandstone on a flank of an accreted seamount. Remnants of the Iapetus oceanic crust are sparsely preserved along Red Indian Line and appear to be limited to small, clipped-off seamounts.

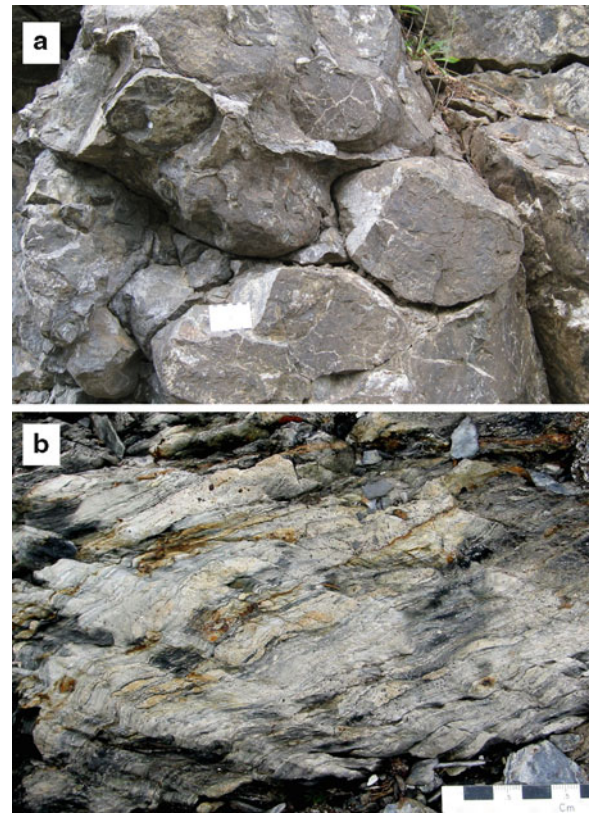

Fig. 12.19 Victoria arc. (**a**) Overturned pillow basalts of the Summerford Group. Summerford Group has been previously interpreted as an accreted seamount (Wasowski and Jacobi 1985), but may represent reworked Victoria arc during Ordovician trench-ridge collision. (**b**) Broken formation along the Red Indian Line displaying boudinaged Upper Ordovician tuff beds in epiclastic siltstone and shale.

Group: Wasowski and Jacobi 1985; Fig. 12.19a). Since the basalts are identical to the arc basalts in the Victoria arc (O'Brien et al. 1997; MacLachlan and Dunning 1998b; Zagorevski 2008) and that the Coaker porphyry samples Cambrian to Early Ordovician metamorphic and plutonic arc basement and lithospheric mantle (e.g., Lorenz 1985; van Staal et al. 2010), the mélange does not represent an accretionary prism. Rather, tectonism and magmatism in the forearc, combined with enriched or transitional tholeiitic-alkaline mafic magmatism and calc-alkaline felsic magmatism in the arc suggests that Victoria Arc had collided with a ridge before the terminal closure of the Iapetus (van Staal et al. 2010), consistent with independent evidence from New Brunswick (van Staal et al. 1998; Rogers and van Staal 2003; Wilson 2003, compare to Schoonmaker and Kidd 2006). The subsequent formation of a slab window led to magmatism in the arc-trench gap and the anomalous bimodal association of E-MORB and calc-alkaline rhyolite/dacite.

12.15 Constraints on the Timing of Collision

The collision of the Red Indian Lake Arc with the Popelogan- Victoria arc marks the closure of the main tract of Iapetus and juxtaposition of the peri-Laurentian and peri-Gondwanan realms. Timing of this collision is marked by a sequence of events starting with shut-off of arc volcanism, formation of a narrow zone of black shale mélange along the suture zone and syn-collisional black shale sedimentation due to tectonic loading of the downgoing Popelogan-Victoria arc (Zagorevski et al. 2008). The volcanism shut-off occurs within a few million years in both arcs. The youngest arc volcanism in the Red Indian Lake arc occurs at ca. 460 Ma (Zagorevski et al. 2006). The Victoria arc remains sporadically magmatically active until ca. 457–453 Ma (Fig. 12.19b; Zagorevski et al. 2008). Limited paleomagnetic data from volcanic rocks associated with these peri-Gondwanan, black shale-bearing rocks suggests that this magmatism was occurring near the Laurentian margin (Potts et al. 1995; Todaro et al. 1996), consistent with arrival of the leading peri-Gondwanan terranes at the Laurentian

margin. The formation of Sandbian-Katian black shale mélange belt along the Red Indian Line (e.g., Nelson 1981; McConnell et al. 2002; Zagorevski et al. 2007b), lack of involvement of tectono-stratigraphic units younger than 453 Ma, constrains the timing of this collision and related deformation. Since, the collision did not involve significant tectonic thickening and was not associated with high-grade metamorphism it is considered to be a soft collision.

12.16 Patterns of Sedimentation

The most striking difference between the peri-Laurentian and peri-Gondwanan collided arcs is the pattern of syn- to post-collisional sedimentation. The entire Notre Dame subzone is characterized by a Late Ordovician/Silurian unconformity, while the Exploits subzone generally displays continuous Late Ordovician to Silurian sedimentation (Williams 1995b). These stratigraphic contrasts arose as a result of the geometry of the collision. The Red Indian Lake arc occupied an upper plate setting relative to the partially subducted Victoria Arc (e.g., van der Velden et al. 2004). Hence, the Red Indian Lake arc, and the Annieopsquotch accretionary tract in general, were uplifted resulting in a newly emergent orogen that fringed the adjacent, strongly deformed Notre Dame Arc, which was uplifted slightly earlier during the Middle Ordovician. The latter was locally unconformably overlain at c. 453 Ma by a thick sequence of alluvial conglomerate and sparsely interlayered volcanic rocks (Dube et al. 1996), which grade upwards into the Silurian red beds that overlie all rocks of the Notre Dame Subzone with angular unconformity (e.g., Colman-Sadd et al. 1992b; Williams 1995b).

In contrast to the Notre Dame Subzone, the Popelogan-Victoria arc displays continuous marine sedimentation across the Ordovician – Silurian boundary (e.g., Wilson et al. 2004; Colman-Sadd et al. 1992b; Williams 1995b; Williams et al. 1995) both in Newfoundland and in mainland Canada. Although most elements of the down-going arc and associated collision process are preserved in New Brunswick and Maine, they are largely masked by younger Silurian to Devonian sedimentary and volcanic rocks. Hence, discussion below is mainly based on evidence gathered in Newfoundland. The earliest signs of the collision in Newfoundland include formation of olistostromal and tectonic mélange

Fig. 12.20 Badger Group successor basin above Victoria Arc – poorly sorted matrix supported boulder conglomerate with granitoid boulders derived from the Notre Dame Subzone.

(e.g., Nelson 1981; McConnell et al. 2002) followed by deposition of a transgressive Sandbian-Katian sequence of black shale and manganese-rich sediments above the Victoria Arc and trailing backarc elements (e.g., Colman-Sadd et al. 1992b; Williams 1992). The black shale transgression likely resulted from the partial subduction and loading of the Victoria arc by the overriding Red Indian Lake arc (Zagorevski et al. 2008). The influx of volcanic and plutonic arc, ophiolitic and metamorphic detritus (Fig. 12.20; e.g., Nelson and Casey 1979; Lash 1994) marks the emergence of the Notre Dame Arc and Annieopsquotch accretionary tract (McNicoll et al. 2001; Waldron et al. 2008) to the north. The lack of metamorphic detritus higher grade than greenschist facies (Lash 1994) suggests that the Taconic orogen in northern Newfoundland maintained a relatively low relief and was not characterized by exhumation of deep seated rocks at this time. In contrast, high grade amphibolite facies orthogneisses derived from Notre Dame Arc plutonic rocks were exhumed by Katian time in southern Newfoundland, confirming its position opposite to a large promontory (Dube et al. 1996; van Staal et al. 2007).

12.17 Structure of the Accreted Terranes

The structure of the peri-Gondwanan Victoria Arc contrasts the structure of the peri-Laurentian Red Indian Lake arc and other Annieopsquotch accretionary tract

terranes. Although plutonic complexes and cumulate rocks of the Victoria Arc are not exposed at the present erosion level, its Late Neoproterozoic to Early Ordovician basement is generally well preserved and exposed (e.g., O'Brien et al. 1997; MacLachlan and Dunning 1998a; Rogers et al. 2006; Zagorevski et al. in press). The Victoria also extends to a significant depth (i.e. van der Velden et al. 2004) suggesting that in contrast to the accreted upper crustal arc slices in the Annieopsquotch accretionary tract (Zagorevski et al. 2009), the arc was accreted as large coherent crustal blocks, without delamination of most of its basement, probably because subduction could step-back into the weak back-arc basin behind it rather than delaminate the downgoing arc (Boutelier et al. 2003).

12.18 Discussion

The closure of the Humber Seaway, Lloyds River marginal basin and main Iapetus tract resulted in sequential accretion of terranes to the Laurentian margin. The geometry of the Laurentian margin and its rifted-off micro-continents appear to have the most fundamental influence on the development of the outboard arcs and their accretion, especially during the Early to Middle-Ordovician Taconic orogeny. Specifically, the first and second order promontories and re-entrants necessitate diachronous tectonic history and structural styles along the strike of the orogen adding to, and further complicating, the oblique convergence histories of the outboard terranes. Whereas geometry of the margin plays the central role, the tectonic configuration of the arc–continent collision zone produces distinctly different products and tectonic styles and influences the degree of preservation of arc complexes, and ophiolites, as well the nature and types of syn-orogenic sedimentary basins. The study of ophiolitic rocks in collision zones provides a good starting point for discussion of arc–continent collision. Although this may seem counterintuitive, ophiolites have a relatively simple structure when compared to arcs; hence, they tend to provide a lot of information on the nature, geometry and tectonic evolution of collision zones. Since ophiolites are usually accreted within several million years of their formation (e.g. Thetford mines complex: Whitehead et al. 2000; Schroetter et al. 2003; Annieopsquotch ophiolite belt and Lloyds River ophiolite complex: Lissenberg et al. 2005b) they also provide information on the local tectonic setting and structure of the adjacent arc. For example, rifting and formation of a backarc basin reduces crustal thickness and half-width of arc blocks and hence effects the behaviour of the arc in collision zone (Cloos 1993). Finally, erosion of ophiolitic cumulates and mantle yields abundant chromite that is easily identified in the sedimentary record of an arc–continent collision zone (Stevens 1970).

12.19 Nature of Ophiolites in Newfoundland and Quebec

The oceanic crust that was accreted to the Laurentian margin during the arc–continent collisions in Newfoundland represents five distinct tectonic settings (1) the rifted continental margin – ocean transition represented by the Birchy complex (Hibbard 1983; Winchester et al. 1992; van Staal et al. 2008; i.e., Ligurian-type ophiolite of Dilek 2003); (2) the syn-collisional forearc spreading ophiolites of the Baie Verte Oceanic tract, which were generated in reentrants. Examples are the Bay of Islands, Thetford Mines and Mont Albert ophiolite complexes (Cawood and Suhr 1992; Schroetter et al. 2003; i.e., the peri-collisional ophiolites of Harris 1992 and Tethyan or Mediterranean-type ophiolites of Dilek 2003); (3) the subduction initiation/development of nascent arc ophiolite of the Baie Verte oceanic tract and AOB (Lissenberg et al. 2005a; van Staal et al. 2007); (4) the backarc basin ophiolites of the Lloyds River marginal basin (Zagorevski et al. 2006); and (5) seamount fragments derived from the subducting Iapetus crust (i.e., Caribbean-type ophiolite of Dilek 2003). The nature of the oceanic lithosphere is strongly influenced by the initial structure and tectonic setting, and the syn- and post-accretionary history. Many Newfoundland ophiolites are structurally disrupted and do not fulfil the Penrose definition of ophiolites (Anonymous 1972); hence, the following discussion is based on a fragmentary record and the possibility that some ophiolitic components have been structurally excised from the northern Appalachians has to be acknowledged. The Ligurian-type ophiolites of the rifted Humber margin (Winchester et al. 1992; van Staal

et al. 2008) are not discussed further as their preservation probably is related to decoupling from the downgoing Humber margin during the earliest stages of obduction of the Baie Verte oceanic tract rather than the subsequent collisional processes themselves (van Staal et al. 2009a, b).

Comparison of the ophiolitic rocks between Humber Seaway, Lloyds River marginal basin and main Iapetus tract reveal significant differences in the volume, structure, and preservation of ophiolites. The only ophiolites that conform to the typical Penrose stratigraphy (Anonymous 1972) are the peri-collisional ophiolites of the Baie Verte Oceanic Tract, such as the Bay of Island and Thetford Mines complexes. These ophiolites preserve a metamorphic sole, tectonized mantle, cumulate, gabbro, sheeted dyke, and basalt zones along the entire length of Northern Appalachians (e.g., Cawood and Suhr 1992; Schroetter et al. 2003). The remarkable preservation of all components of ophiolitic stratigraphy is the direct result of their tectonic setting. These ophiolites occupied an upper plate setting, were formed close to the Laurentian margin and were obducted shortly after their formation (Fig. 12.3; e.g., Cawood and Suhr 1992; van Staal et al. 2007).

The Annieopsquotch accretionary tract ophiolites that formed in the Lloyds River marginal basin, in general, contrast the BVOT ophiolites. These ophiolites do not conform to the Penrose stratigraphy as the mantle component is generally missing. The crustal section is well-preserved and locally consists of cumulate, gabbro, sheeted dyke and basalt zones associated with abundant trondhjemite and locally rhyolite (e.g., Dunning 1987; Lissenberg et al. 2004, 2005a; Zagorevski et al. 2006; Cutts et al. 2010). The general lack of mantle stems from the lower plate setting of the ophiolites at the time of accretion (Fig. 12.11; Zagorevski et al. 2009). These ophiolites were underplated at depth by step down of decollement to the brittle-ductile transition in the oceanic crust and transfer of the crustal section to the upper plate. The key element for the preservation of the Annieopsquotch accretionary tract ophiolites is their young age at the time of their accretion, which indicates that the brittle-ductile transition was located near the base of the crust. Hence, the mantle was decoupled from the crust and continued to subduct enabling accretion of aerially extensive, but thin slabs of ophiolite. This process has been imaged seismically in the New Britain accretionary wedge, east of Papua New Guinea's Huon peninsula (Bernstein-Taylor et al. 1992a, b).

The Iapetus oceanic crust that is preserved along the Red Indian Line is yet again distinct from the Taconic Seaway and Lloyds River marginal basin. The Red Indian Line suture zone is remarkably poor in remnants of oceanic crust. The preserved oceanic crust appears to be limited to upper crustal section of clipped-off seamount(s) and potentially some basaltic knockers in the mélange belts that delineate the suture zone. The paucity of ophiolitic rocks does not appear to be dependent on the age of the subducting Iapetus slab, as the oceanic crust that remained in the Middle Ordovician was proximal to the ridge that collided with the Popelogan-Victoria Arc by c. 469 Ma (e.g., van Staal et al. 2010). The tectonic setting of the collision zone was likely a key factor in the (lack of) preservation of ophiolites as the oceanic crust was tectonically buried under Popelogan-Victoria Arc and Red Indian Lake arc. Hence, if ophiolites were accreted during the collision, they are likely to have been deeply buried and they are not exposed at present crustal level (Fig. 12.15). Similar relationships are observed in the Molucca Sea collision zone where the only preserved ophiolitic rocks (i.e., Pujada-Miangas Ridge) form part of the Sangihe forearc basement and hence not part of the Molucca Sea slab (Bader et al. 1999).

12.20 Nature of Accreted Arcs in Newfoundland

The highly variable initial structure of modern arc complexes (e.g., Barker et al. 2003; Boutelier et al. 2003; McIntosh et al. 2005) renders inferences on their evolution during collision much more difficult than ophiolites; however, the evolution of the Ordovician arcs during accretion and collision appears to mimic the evolution of the associated ophiolites. The closure of the Taconic Seaway through east-directed subduction resulted in obduction of nascent arc and/or syn-collisional ophiolites of the Baie Verte Oceanic tract and long-lived underthrusting (A-subduction) of the Humber margin beneath the Notre Dame Arc. This collision is characterized by variable degrees of thickening of the Notre Dame Arc through widening of the

subduction channel, characteristic of a hard collision. Underplating of Humber margin sedimentary rocks culminated in volumetrically minor S-type magmatism channelled along the suture zone (Brem et al. 2008; van Staal et al. 2009b). The preservation and varying degrees of shortening and unroofing of the arc along strike were strongly influenced by its upper plate setting, and convergence with a highly irregular margin characterised by deep re-entrants. Initial collision during the Early Ordovician (480–475 Ma) led to little or no penetrative deformation of the arc. Its only manifestation is universal uplift and unroofing of the Tremadoc arc plutons along its whole length in Newfoundland (e.g., Skulski et al. 2009) mirroring the uplift and exhumation of the Baie Verte oceanic tract ophiolitic rocks (Stevens 1970) preserved in the adjacent forearc. The Taconic orogen was exhumed to deep metamorphic levels in the middle Ordovician in the south, probably due to its prolonged collision with the St. Lawrence promontory (e.g., van Staal et al. 2007), but appears to have maintained a relatively low relief until Late Ordovician – Early Silurian in the north. Here, accelerated uplift and exhumation may have been triggered by the sequential accretion of the Annieopsquotch accretionary tract terranes and Victoria Arc. Hence, the present exposure of the deep crustal metamorphic rocks in the Notre Dame Arc (e.g., Owen et al. 2000; Pehrsson et al. 2003) appears to be the result of superimposition of multiple collisions on a hard collision zone.

The arc terranes of the Annieopsquotch accretionary tract also mirror the relationships preserved in the associated ophiolitic rocks. The arc terranes preserved predominantly upper crustal sections characterized by volcano-sedimentary succession and only minor plutonic rocks. The accretionary mechanism of the arc terrenes is unlikely to have differed significantly from the ophiolitic rocks (Zagorevski et al. 2009) as the arcs never reached significant thickness due to protracted rifting and formation of intra arc or backarc ophiolites. Hence, they did not attain the necessary thickness or half-width to have the buoyancy required for collisional orogenesis as defined by Cloos (1993). Emergence of these terranes during accretion of the Red Indian Lake arc to the Notre Dame Arc was marked by predominantly volcanic detritus (e.g., Zagorevski et al. 2006; Coombs 2009) with minor plutonic and metamorphic rocks (e.g. Bostock 1988) in rare sedimentary successions that are most likely syn-collisional. Similar to the closure of the northern part of the Taconic Seaway, the orogen that formed during the closure of the Lloyds River Marginal basin maintained a low relief.

In contrast to the accreted peri-Laurentian terranes, the Popelogan-Victoria arc was neither exhumed to deep crustal level nor decoupled from its basement. Instead the arc was accreted as a more or less coherent (± minor internal imbrication) crustal block that comprises basement and its volcano-sedimentary suprastructure (Figs. 12.10 and 12.15; e.g., Rogers et al. 2006; Zagorevski et al. 2007a; Zagorevski et al. 2010). The accretion of the Popelogan-Victoria arc marks a change in the tectonic architecture of the composite Laurentian margin. The Late Ordovician-Early Silurian subduction of the Tetagouche-Exploits backarc basin caused universal uplift and emergence of the accreted peri-Laurentian terranes above sea level. This process persisted until the Late Silurian and culminated in the Salinic collision with the Gander margin (van Staal et al. 2009b), allowing erosion to continue to deep crustal levels followed by continental red bed sedimentation and volcanism (c. 430 Ma Springdale Group and equivalents: e.g., Chandler et al. 1987). The progressively emerging, polyphase orogen provided abundant plutonic and metamorphic detritus to the Late Ordovician to Early Silurian Badger Basin that formed immediately east of the Red Indian Line, mainly above the largely subsided Victoria Arc (e.g., Williams et al. 1995). During this time, the Victoria Arc occupied the arc-trench gap setting with respect to the downgoing Tetagouche-Exploits backarc slab (van Staal 1994; van Staal et al. 2009b) and the newly emerging continental Early Silurian Salinic arc (Whalen et al. 2006).

Taconic accretion of the Popelogan Victoria arc and the Red Indian Lake arc are both considered soft, because neither were highly thickened, metamorphosed or penetratively deformed during this process. Whereas the development of an emergent orogen in the peri-Laurentian realm following accretion may be mistakenly attributed to a hard collision along the Red Indian Line, the dominant ages of deformation and metamorphism in the Notre Dame Subzone are too old (Early-Middle Ordovician). Instead, the Late Ordovician buoyancy-driven uplift of the Annieopsquotch accretionary tract and adjacent Notre Dame Arc were simply superimposed on the effects of a pre-existing hard collision zone that, at least in

Newfoundland, was already characterized by Middle Ordovician Taconic deformation and metamorphism (e.g., Szybinski 1995; Pehrsson et al. 2004; Lissenberg et al. 2005b; van Staal et al. 2007). Although the accretion of the Popelogan Victoria arc may have had the potential for collisional orogenesis in the sense of Cloos (1993), either the arc did not have the sufficient size or, more likely, the Salinic step-back of subduction into the Exploits-Tetagouche backarc basin (Fig. 12.15) terminated convergence along the Red Indian Line and hence, any major shortening by internal deformation in the accreted terranes.

12.21 Preservation of Forearc Basins and Accretionary Wedges

Evidence for the forearc basins and accretionary wedges associated with the subduction and accretion of the Ordovician arc systems is generally poorly preserved or missing. The main exceptions are the forearc remnants preserved in the Dunnage Mélange tract, Newfoundland and the syn-collision forearc basin rocks in Quebec. The Dunnage Mélange and related forearc rocks (i.e. Upper Wild Bight Group: MacLachlan and Dunning 1998b) are associated with the Victoria arc (475–457 Ma) and preserve Middle to Late Ordovician collisions with a mid-Iapetus ridge (e.g., van Staal et al. 2010) and with peri-Laurentian terranes. Whereas the Dunnage Mélange tract is very well preserved in north-central Newfoundland, it is not laterally continuous. Hence, its preservation is probably related to the promontory – re-entrant configuration of the composite Laurentian margin. The syn-collision forearc basin rocks preserved in Quebec were deposited on the Thetford Mines ophiolite complex during its obduction (Schroetter et al. 2005); however, little or no evidence was preserved of the arc-trench gap rocks formed during the preceding period of B-subduction.

Similar to the preservation of the forearc basins, there is generally little evidence of the arc-trench gap rocks associated with the arc terranes that were originally positioned outboard of Laurentia (i.e., Notre Dame, Roberts Arm and Red Indian Lake arcs). Although their absence could be explained by deep erosion following deformation and uplift in areas of intense shortening along promontories in the margin, their absence in areas where the arc volcanics are relatively well preserved presents a conundrum. We think that the reason for their absence is due to a combination of factors: (1) B-subduction was short-lived (~10 my) as is the case for the Notre Dame Arc-Humber margin and hence there was little time to form an outerarc high to trap significant arc-derived sediment in a forearc basin; (2) little or no input of terrigeneous and arc-derived clastics in the trench and/or the forearc basin, which if it was a major responsible factor suggest that the island arc and opposite margin had relative low relief akin to intraoceanic subduction sytems; and (3) subduction erosion of the forearc terranes was important. We especially called upon the latter mechanism to explain the lack of geochronological evidence for metamorphism of the Taconic wedge during the Notre Dame Arc-Humber margin collision in Newfoundland (van Staal et al. 2009a, b). In addition to these factors, subduction or underthrusting of the forearc block beneath the arc, such as in the Taiwan collision zone (McIntosh et al. 2005) and along the Huon Peninsula (Abbott et al. 1994), may have been an important process for removing much of the remaining evidence of the forearcs and accretionary prisms.

12.22 Magmatic Characteristics of Accreted Terranes

Extensive petrological studies indicate that most Ordovician island arcs in the Canadian Appalachians contained significant proportion of island arc tholeiite, regardless whether they had an oceanic or extended continental basement (e.g., Swinden et al. 1997; MacLachlan et al. 2001; Lissenberg et al. 2005b; Rogers et al. 2006; Zagorevski et al. 2006, 2007a; McNicoll et al. 2008; Hinchey and McNicoll 2009). Calc-alkaline volcanic rocks are common but generally comprise bimodal transitional tholeiitic to calc-alkaline or low-K calc-alkaline series (e.g., Rogers 2004; Zagorevski 2008). These characteristics suggest that convergence rates associated with these arcs were generally high and the arc crust generally relatively thin (Coulon and Thorpe 1981; Leeman 1983; Plank and Langmuir 1988; Mantle and Collins 2008) resulting in the general absence of andesite (for exception see Coombs 2009) and high K calc-alkaline to shoshonitic volcanic series. Rifting of the arcs culminated in development of oceanic backarc basins characterized

by either backarc MORB – E-MORB (e.g., Jenner and Swinden 1993; Zagorevski et al. 2006) or bimodal calc-alkaline rhyolite/dacite – E-MORB associations (e.g., O'Brien et al. 1997; Rogers et al. 2003; Zagorevski et al. 2007a) analogous to East Scotia Ridge/Lau Basin (Hawkins and Allan 1994; Fretzdorff et al. 2002) and Sea of Japan (Pouclet et al. 1995) respectively.

Boninite is locally voluminous, and dominates some ophiolite belts such as the Baie Verte oceanic tract, both in Newfoundland (Bedard et al. 1998; Bedard et al. 2000) and Quebec/New England (e.g., Kim and Jacobi 2002). These were produced in a narrow time window during the Middle Cambrian to Early Ordovician (510–480 Ma) when Iapetus changed from a diverging to a rapidly contracting ocean through formation of new subduction zones along their opposite margins (van Staal and Hatcher 2010) and fringing seaways. They appear either related to subduction initiation and formation of nascent arcs (e.g., van Staal et al. 1998, 2007; Lissenberg et al. 2005b) or during spreading induced by Mediterranean-style subduction driven by slab rollback of old oceanic lithosphere trapped in deep re-entrants (e.g., Schroetter et al. 2003).

12.23 Conclusions

The Canadian Appalachians and the Newfoundland segment in particular, have preserved extensive evidence of very complex tectonic processes that occurred during Ordovician arc–continent collisions along the composite Laurentian margin. Evidence for these processes is commonly poorly preserved or cryptic in other along-strike segments of the Appalachian and British Caledonides, resulting in simpler tectonic models outside of Newfoundland. However, increasingly larger datasets allow identification and refinement of these processes outside of Newfoundland (e.g., Chew et al. 2003; Dupuis et al. 2009). The degree of complexity established in the Canadian Appalachians is largely driven by a progressively expanding database based on long-lived multidisciplinary thematic studies. Particularly the integration of structural studies with detailed geochronology, geochemistry and isotope tracer studies was a main driving force for development of the new models and constraining the presented tectonic evolutionary models.

Geological evidence necessitates that relatively young marginal basins (10–15 my) associated with the Ordovician arcs on both sides of Iapetus were closed regularly. Hence, the Appalachians repeatedly switched between a retreating and an advancing accretionary orogen of Cawood et al. (2009). Although the reasons why these marginal basins closed remain poorly constrained, the geometry of the resulting collisions is relatively well understood. The primary control on the collision is exerted by the promontory – re-entrant geometry of the margins. Secondary control is the configuration of the collisions themselves. In the Ordovician, three configurations of arc–continent collisions are preserved along the Laurentian margin. These three configurations resulted in different composition and preservation of ophiolites and arcs, as well as in different patterns of sedimentation. Ophiolites are most constructive in studying these configurations. Taiwan and Banda-style collision result in obduction of Penrose-type syn-collisional ophiolites onto the continental margin (i.e., closure of the Taconic seaway: Cawood and Suhr 1992). Izu-style collision results in underplating of nascent arc and back-arc ophiolites below the continental margin (i.e., closure of the Lloyds River marginal basin: Lissenberg et al. 2005b; Zagorevski et al. 2009). Molucca Sea-style collision does not appear to preserve ophiolites but does result in significant syn-post collisional sedimentation (i.e., closure of the main Iapetus tract and formation of Badger Basin: Zagorevski et al. 2008).

The relationships we have deduced largely echo the complexities observed in the SW-Pacific and adjacent parts of the Indonesian archipelago (e.g., van Staal et al. 1998). Similar to the SW-Pacific, the identified arc complexes in the Canadian Appalachians are typically extensional due to slab retreat, relatively primitive and short-lived (5–20 my). Their evolution was interrupted by very short periods of orogenesis (2–5 my), mainly evidenced by arc shut-off and/or uplift, such as documented in the Notre Dame Arc (e.g., Whalen et al. 2006; van Staal et al. 2007), in the peri-Laurentian Roberts Arm arc during the Middle Ordovician (Zagorevski et al. 2006; Coombs 2009), in the peri-Gondwanan Penobscot arc during the Early Ordovician (Colman-Sadd et al. 1992a; Zagorevski et al. 2007a; Zagorevski et al. 2010) and in the Victoria arc in the Late Ordovician (Zagorevski et al. 2008). The resultant hard and soft collisions have resulted in formation of small orogens,

re-arrangement of plate motions indicated by initiation of new subduction zone by step-back, and left clear evidence in the form of accreted terranes.

Acknowledgements This is a contribution to the Geological Survey of Canada Targeted Geoscience Initiative (2001–2010; GSC contribution #20100258) and IGCP 524: Arc–continent collision. GAC Newfoundland Section, and in particular A. Kerr (GSNL) are thanked for organizing and providing us with a venue for our fieldtrips that greatly contributed to discussion of the relationships in Newfoundland. P. Ryan, J. Dewey and D. Brown are thanked for organizing the Ireland fieldtrip which lead to many stimulating discussions of the Caledonide-Appalachian connections. This manuscript has benefited from numerous discussions with J. Bedard, S. Castonguay, V. McNicoll, N. Rogers and Tom Skulski and reviews by N. Rogers, J. Dewey and J.B. Murphy.

References

Abbott LD, Silver EA, Galewsky J (1994) Structural evolution of a modern arc-continent collision in Papua New Guinea. Tectonics 13(5):1007–1034

Anonymous (1972) Penrose field conference on ophiolites. Geotimes 17(12): 22–24

Bader AG, Pubellier M, Rangin C, Deplus C, Louat R (1999) Active slivering of oceanic crust along the Molucca Ridge (Indonesia-Philippine); implication for ophiolite incorporation in a subduction wedge? Tectonics 18(4):606–620

Barker DHN, Christeson GL, Austin JA, Dalziel IWD (2003) Backarc basin evolution and Cordilleran orogenesis; insights from new ocean-bottom seismograph refraction profiling in Bransfield Strait, Antarctica. Geology (Boulder) 31 (2):107–110

Bedard JS, Escayola M (2010) The Advocate Ophiolite mantle, Baie Verte, Newfoundland: regional correlations and evidence for metasomatism. Can J Earth Sci 47(3): 237–253

Bedard JH, Lauziere K, Tremblay A, Sangster A (1998) Evidence for forearc seafloor-spreading from the Betts Cove Ophiolite, Newfoundland; oceanic crust of boninitic affinity. Tectonophysics 284(3–4):233–245

Bedard JH, Lauziere K, Tremblay A, Sangster A, Douma SL, Dec T (2000) Betts Cove Ophiolite and its cover rocks, Newfoundland. Geol Surv Can 550:76

Bernstein-Taylor BL, Brown KM, Silver EA, Kirchoff-Stein KS (1992a) Basement slivers within the New Britain accretionary wedge; implications for the emplacement of some ophiolitic slivers. Tectonics 11(4):753–765

Bernstein-Taylor BL, Kirchoff-Stein KS, Silver EA, Reed DL, Mackay M (1992b) Large-scale duplexes within the New Britain accretionary wedge; a possible example of accreted ophiolitic slivers. Tectonics 11(4):732–752

Bostock HH (1988) Geology and petrochemistry of the Ordovician volcano-plutonic Robert's Arm Group, Notre Dame Bay, Newfoundland. Geological Survey of Canada Bulletin 369, Geological Survey of Canada, p 84

Boutelier D, Chemenda A, Burg JP (2003) Subduction versus accretion of intra-oceanic volcanic arcs; insight from thermo-mechanical analogue experiments. Earth Planet Sci Lett 212(1–2):31–45

Brem AG, Wintsch R, Lin S, van Staal CR, Davis DW, McNicoll VJ (2008) The Middle Ordovician to Early Silurian voyage of the Dashwoods Microcontinent, west Newfoundland; based on new U/Pb and (super 40) Ar/ (super 39) Ar geochronological, and kinematic constraints. Am J Sci 307(2): 311–338

Calvert AJ (1996) Seismic reflection constraints on imbrication and underplating of the northern Cascadia convergent margin. Can J Earth Sci 33(9):1294–1307

Cawood PA, Nemchin AA (2001) Paleogeographic development of the East Laurentian margin; constraints from U-Pb dating of detrital zircons in the Newfoundland Appalachians. Geol Soc Am Bull 113(9):1234–1246

Cawood PA, Suhr G (1992) Generation and obduction of ophiolites; constraints for the Bay of Islands Complex, western Newfoundland. Tectonics 11(4):884–897

Cawood PA, Sangster AL, van Gool JAM, Dunning GR (1996) Geological development of eastern Humber and western Dunnage zones; Corner Brook-Glover Island region, Newfoundland. Can J Earth Sci 33:182–198

Cawood PA, McCausland PJA, Dunning GR (2001) Opening Iapetus; constraints from the Laurentian margin in Newfoundland. Geol Soc Am Bull 113(4):443–453

Cawood PA, Kroner A, Collins WJ, Kusky TM, Mooney WD, Windley BF (2009) Accretionary orogens through Earth history. In: Cawood PA, Kroner A (eds) Earth accretionary systems in space and time. The Geological Society, Special Publications, London, pp 1–36

Chemenda A.I, Yang R.-K, Stephan J.-F, Konstantinovskaya E.A, Ivanov G.M. (2001) New results from physical modeling of arc-continent collision in Taiwan: evolutionary model, Tectonophysics, 333:159–178

Chandler FW, Sullivan RW, Currie KL (1987) The age of the Springdale Group, western Newfoundland, and correlative rocks; evidence for a Llandovery overlap assemblage in the Canadian Appalachians. Trans R Soc Edinb Earth Sci 78(1): 41–49

Chew D.M, Daly S.J, Magna T, Page L.M, Kirkland C.L, Whitehouse M.J, Lam R (2010) Timing of ophiolite obduction in the Grampian orogen, GSA Bulletin; November/ December 2010; 122(11/12):1787–1799; doi: 10.1130/ B30139.1

Cloos M (1993) Lithospheric buoyancy and collisional orogenesis; subduction of oceanic plateaus, continental margins, island arcs, spreading ridges, and seamounts. Geol Soc Am Bull 105(6):715–737

Colman-Sadd SP, Dunning GR, Dec T (1992a) Dunnage-Gander relationships and Ordovician orogeny in central Newfoundland; a sediment provenance and U/Pb age study. Am J Sci 292(5):317–355

Colman-Sadd SP, Stone P, Swinden HS, Barnes RP (1992b) Parallel geological development in the Dunnage Zone of Newfoundland and the Lower Palaeozoic terranes of southern Scotland: an assessment. Trans R Soc Edinb Earth Sci 83:571–594

Coombs A (2009) Geochemical and zircon provenance of peri-Laurentian ophiolite to arc transition, central Newfoundland. Memorial University of Newfoundland

Coulon C, Thorpe RS (1981) Role of continental crust in petrogenesis of orogenic volcanic associations. Tectonophysics 77:79–93

Cutts JA, Zagorevski A, McNicoll V, Carr S (2010) Tectonostratigraphic setting of the Moreton's Harbour Group and its implications for the evolution of the Laurentian Margin. GSA Abstr Programs 42(1), p 164

De Souza S, Tremblay A, Daoust C, Gauthier M (2008) Stratigraphy and geochemistry of the Lac-Brompton ophiolite, Canada: evidence for extensive forearc magmatism and mantle exhumation in the Southern Quebec Ophiolite Belt. Can J Earth Sci 45(9):999–1014

Dec T, Swinden HS, Dunning RG (1997) Lithostratigraphy and geochemistry of the Cottrells Cove Group, Buchans-Roberts Arm volcanic belt; new constraints for the paleotectonic setting of the Notre Dame Subzone, Newfoundland Appalachians. Can J Earth Sci 34(1):86–103

Dewey JF (1969) Evolution of the Appalachian/Caledonian orogen. Nature 222:124–129

Dilek Y (2003) Ophiolite concept and its evolution. In: Dilek Y, Newcomb S (eds) Ophiolite concept and the evolution of geological thought. Geological Society Special Paper 373, Geological Society of America (GSA), United States, pp 1–16

Dube B, Dunning GR, Lauziere K, Roddick JC (1996) New insights into the Appalachian Orogen from geology and geochronology along the Cape Ray fault zone, Southwest Newfoundland. Geol Soc Am Bull 108(1):101–116

Dunning GR (1987) Geology of the Annieopsquotch Complex, Southwest Newfoundland. Can J Earth Sci 24(6):1162–1174

Dunning GR, Chorlton LB (1985) The Annieopsquotch ophiolite belt of Southwest Newfoundland; geology and tectonic significance. Geol Soc Am Bull 96(11):1466–1476

Dunning GR, Krogh TE (1985) Geochronology of ophiolites of the Newfoundland Appalachians. Can J Earth Sci 22 (11):1659–1670

Dupuis C, Malo M, Bedard J, Davis B, Villeneuve M (2009) A lost arc-back-arc terrane of the Dunnage oceanic tract recorded in clasts from the Garin Formation and McCrea Melange in the Gaspe Appalachians of Quebec. Geol Soc Am Bull 121(1–2):17–38

Fretzdorff S, Livermore RA, Devey CW, Leat PT, Stoffers P (2002) Petrogenesis of the back-arc East Scotia Ridge, South Atlantic Ocean. J Petrol 43(8):1435–1467

Gerbi CC, Johnson SE, Aleinikoff JN (2006a) Origin and orogenic role of the Chain Lakes massif, Maine and Quebec. Can J Earth Sci 43:339–366

Gerbi CC, Johnson SE, Aleinikoff JN, Bedard JH, Dunning GR, Fanning CM (2006b) Early Paleozoic development of the Maine-Quebec Boundary Mountains region. Can J Earth Sci 43(3):367–389

Harris RA (1992) Peri-collisional extension and the formation of Oman-type ophiolites in the Banda Arc and Brooks Range. In: Parson LM, Murton BJ, Browning P (eds) Ophiolites and their modern oceanic analogues. Geological Society, Special Publication, London, pp 301–325

Hawkins JW, Allan JF (1994) Petrologic evolution of Lau Basin Sites 834 through 839. In: Hawkins J et al (eds) Proceedings of the Ocean Drilling Program, scientific results. Ocean Drilling Program, College Station, TX, pp 427–470

Hibbard J (1983) Geology of the Baie Verte Peninsula, Newfoundland. Memoir – Government of Newfoundland and Labrador, Department of Mines and Energy, Mineral Development Division

Hibbard J, van Staal C, Rankin D, Williams H (2006) Lithotectonic map of the Appalachian Orogen, Canada – United States of America. Geological Survey of Canada, Map 2096A. Scale 1: 500 000

Hibbard JP, Wintsch RP, van Staal CR, Rankin DW (2007) A comparative analysis of pre-Silurian crustal building blocks of the northern and the southern Appalachian Orogen. Am J Sci 307(1):23–45

Hinchey JG, McNicoll V (2009) Tectonostratigraphic architecture and VMS mineralization of the southern Tulks Volcanic Belt: new insights from U-Pb geochronology and lithogeochemistry. Current Research – Newfoundland Geological Survey Branch, Report 09–1

Hirtzel J, Chi W.-C, Reed D, Chen L, Liu C.-S, Lundberg N, (2009) Destruction of Luzon forearc basin from subduction to Taiwan arc–continent collision, Tectonophysics, 479: 43–51.

Hiscott R.N. (1995) Middle Ordovician clastic rocks (Humber zone and St. Lawrence platform), In: Williams H, (ed) Geology of the Appalachian-Caledonian orogen in Canada and Greenland: Ottawa, Geological Survey of Canada, Geology of Canada, p. 87–98.

Huang CY, Yuan PB, Lin CW, Wang TK, Chang CP (2000) Geodynamic processes of Taiwan arc-continent collision and comparison with analogs in Timor, Papua New Guinea, Urals and Corsica. Tectonophysics 325:1–21

Jacobi RD (1981) Peripheral bulge; a causal mechanism for the Lower/Middle Ordovician unconformity along the western margin of the Northern Appalachians. Earth Planet Sci Lett 56:245–251

Jamieson RA (1990) Metamorphism of an early Palaeozoic continental margin, western Baie Verte Peninsula, Newfoundland. J Metamorph Geol 8(3):269–288

Jenner GA, Swinden HS (1993) The Pipestone Pond Complex, central Newfoundland; complex magmatism in an eastern Dunnage Zone ophiolite. Can J Earth Sci 30(3):434–448

Jenner GA, Dunning GR, Malpas J, Brown M, Brace T (1991) Bay of Islands and Little Port complexes, revisited; age, geochemical and isotopic evidence confirm suprasubduction-zone origin. Can J Earth Sci 28(10):1635–1652

Johnson RJE, van der Pluijm BA, Van der Voo R (1991) Paleomagnetism of the Moreton's Harbour Group, northeastern Newfoundland Appalachians; evidence for an Early Ordovician island arc near the Laurentian margin of Iapetus. J Geophys Res 96:11689–11701

Kerr A, Dunning GR (2003) A note on the U-Pb zircon age of the Woodford's Arm granite, and its relationship to the Roberts Arm Group, Central newfoundland (NTS2E/12). Current Research Report, Report: 03–1, pp 47–50

Kim J, Jacobi RD (2002) Boninites; characteristics and tectonic constraints, northeastern Appalachians. Phys Chem Earth 27 (1–3):109–147

Kim J, Coish R, Evans M, Dick G (2003) Supra-subduction zone extensional magmatism in Vermont and adjacent Quebec; implications for early Paleozoic Appalachian tectonics. Geol Soc Am Bull 115(12):1552–1569

Kimura G, Ludden J (1995) Peeling oceanic crust in subduction zones. Geology (Boulder) 23(3):217–220

Knight I, James NP, Lane TE (1991) The Ordovician St. George unconformity, Northern Appalachians, Newfoundland; effects of lithospheric dynamics on the Sauk-Tippecanoe sequence boundary. Geol Soc Am Bull 103:1200–1225

Kurth M, Sassen A, Suhr G, Mezger K (1998) Precise ages and isotopic constraints for the Lewis Hills (Bay of Islands Ophiolite); preservation of an arc-spreading ridge intersection. Geology 26(12):1127–1130

Lash GG (1994) Detrital modes of the Riding Island Graywacke, north-central Newfoundland; evidence for deposition in a collisional successor basin in the Dunnage Zone. Can J Earth Sci 31(1):176–181

Leeman WP (1983) The influence of crustal structure on compositions of subduction-related magmas. J Volcanol Geoth Res 18:561–588

Lissenberg CJ, van Staal CR (2006) Feedback between deformation and magmatism in the Lloyds River Fault Zone, an example of episodic fault reactivation in an accretionary setting, Newfoundland Appalachians. Tectonics 25:TC4004

Lissenberg CJ, Bedard JH, van Staal CR (2004) The structure and geochemistry of the gabbro zone of the Annieopsquotch Ophiolite, Newfoundland; implications for lower crustal accretion at spreading ridges. Earth Planet Sci Lett 229 (1–2):105–123

Lissenberg CJ, van Staal CR, Bedard JH, Zagorevski A (2005a) Geochemical constraints on the origin of the Annieopsquotch ophiolite belt, Newfoundland Appalachians. Geol Soc Am Bull 117(11–12):1413–1426

Lissenberg CJ, Zagorevski A, McNicoll VJ, van Staal CR, Whalen JB (2005b) Assembly of the Annieopsquotch accretionary tract, Newfoundland Appalachians; age and geodynamic constraints from syn-kinematic intrusions. J Geol 113(5):553–570

Lissenberg CJ, McNicoll VJ, van Staal CR (2006) The origin of mafic-ultramafic bodies within the northern Dashwoods Subzone, Newfoundland Appalachians. Atlantic Geol 42 (1):1–12

Lorenz BE (1985) A study of the igneous intrusive rocks of the Dunnage Melange, Newfoundland. Canada

MacLachlan K, Dunning G (1998a) U-Pb ages and tectonomagmatic relationships of early Ordovician low-Ti tholeiites, boninites and related plutonic rocks in central Newfoundland, Canada. Contrib Mineralog Petrol 133(3):235–258

MacLachlan K, Dunning GR (1998b) U-Pb ages and tectonomagmatic relationships of Middle Ordovician volcanic rocks of the Wild Bight Group, Newfoundland Appalachians. Can J Earth Sci 35:998–1017

MacLachlan K, O'Brien BH, Dunning GR (2001) Redefinition of the Wild Bight Group, Newfoundland; implications for models of island-arc evolution in the Exploits Subzone. Can J Earth Sci 38(6):889–907

Malo M, Ruffet G, Pincivy A, Tremblay A (2008) A 40Ar/39Ar study of oceanic and continental deformation processes during an oblique collision: Taconian orogeny in the Quebec reentrant of the Canadian Appalachians. Tectonics 27: TC4001

Mantle GW, Collins WJ (2008) Quantifying crustal thickness variations in evolving orogens; correlation between arc basalt composition and Moho depth. Geology (Boulder) 36 (1):87–90

McConnell BJ, O'Brien BH, Nowlan GS (2002) Late Middle Ordovician olistostrome formation and magmatism along the Red Indian Line, the Laurentian Arc-Gondwanan Arc boundary, at Sops Head, Newfoundland. Can J Earth Sci 39(11):1625–1633

McIntosh K, Nakamura Y, Wang TK, Shih RC, Chen A, Liu CS (2005) Crustal-scale seismic profiles across Taiwan and the western Philippine Sea. Tectonophysics 401(1–2):23–54

McNicoll V, van Staal CR, Waldron JWF (2001) Accretionary history of the northern Appalachians: SHRIMP study of Ordovician-Silurian syntectonic sediments in the Canadian Appalachians, vol 26. Geological Association of Canada/ Mineralogical Association of Canada Annual Meeting Abstracts, St. John's, NL, p 100

McNicoll VJ, Squires GC, Kerr A, Moore PJ (2008) Geological and metallogenic implications of U-Pb zircon geochronological data from the Tally Pond area, central Newfoundland: Current Research (2008) Newfoundland Department of Mines and Energy Geological Survey, Report 08–01, pp 173–192

Murphy JB, Nance RD, Cawood PA (2009) Contrasting modes of supercontinent formation and the conundrum of Pangea. Gondwana Res 15:408–420

Nelson KD (1981) Melange development in the Boones Point Complex, North-central Newfoundland. Can J Earth Sci 18 (3):433–442

Nelson KD, Casey JF (1979) Ophiolitic detritus in the Upper Ordovician flysch of Notre Dame Bay and its bearing on the tectonic evolution of western Newfoundland. Geology (Boulder) 7:27–31

O'Brien B, Swinden HS, Dunning GR, Williams SH, O'Brien FHC (1997) A peri-Gondwanan arc-back arc complex in Iapetus; Early-Mid Ordovician evolution of the Exploits Group, Newfoundland. Am J Sci 297(2):220–272

Owen JV, Jones AP, Greenough JD (2000) Petrology of the Cormacks Lake Complex, Newfoundland; decompressional reaction relations in cordierite + orthoamphibole-bearing gneisses and associated rocks. Mineralog Mag 64(4 (425)):711–724

Page P, Bedard JH, Schroetter J-M, Tremblay A (2008) Mantle petrology and mineralogy of the Thetford Mines ophiolite complex. Lithos 100(1–4):255–292

Pehrsson SJ, Pereira CPG, van Staal CR, Herd R, McNicoll V (2003) The Cormacks Lake Complex, Dashwoods Subzone; a window into the deeper levels of the Notre Dame Arc: Current Research – Newfoundland. Geological Survey Branch, pp 115–125

Pehrsson S, van Staal CR, McNicoll V, Whalen JB (2004) Tectonic evolution of the Dashwood Microcontinent and its accretion to the Laurentian margin. Abstr Programs – Geol Soc Am 35(3):98

Pincivy A, Malo M, Ruffet G, Tremblay A, Sacks PE (2003) Regional metamorphism of the Appalachian Humber Zone of Gaspe Peninsula; (super 40) Ar/ (super 39) Ar evidence for crustal thickening during the Taconian Orogeny. Can J Earth Sci 40(2):301–315

Plank T, Langmuir CH (1988) An evaluation of the global variations in the major element chemistry of arc basalts. Earth Planet Sci Lett 90:349–370

Potts SS, van der Pluijm BA, Van der Voo R (1995) Paleomagnetism of the Pennington Mountain Terrane; a near-Laurentian back arc basin in the Maine Appalachians. J Geophys Res 100(B7):10003–10011

Pouclet A, Lee J-S, Vidal P, Cousens B, Bellon H (1995) Cretaceous to Cenozoic volcanism in South Korea and in the Sea of Japan: magmatic constraints on the opening of the back-arc basin. In: Smellie JL (ed) Volcanism associated with extension at convergent plate margins, pp 169–191

Pubellier M, Bader AG, Rangin C, Deffontaines B, Quebral R (1999) Upper plate deformation induced by subduction of a volcanic arc; the Snellius Plateau (Molucca Sea, Indonesia and Mindanao, Philippines). Tectonophysics 304(4): 345–368

Ratcliffe NM, Hames WE, Stanley RS (1998) Interpretation of ages of arc magmatism, metamorphism, and collisional tectonics in the Taconian Orogen of western New England. Am J Sci 298(9):791–797

Rogers N (2004) Red Indian Line geochemical database. Geological Survey of Canada Open File 4605

Rogers N, van Staal CR (2003) Volcanology and tectonic setting of the northern Bathurst mining camp; Part II, mafic volcanic constraints on back-arc opening. Econ Geol Monogr 11: 181–201

Rogers N, van Staal CR, Theriault R (2003) Volcanology and tectonic setting of the northern Bathurst mining camp; Part 1, extension and rifting of the Popelogan Arc. Econ Geol Monogr 11:157–179

Rogers N, van Staal CR, McNicoll V, Pollock J, Zagorevski AW, Whalen J (2006) Neoproterozoic and Cambrian arc magmatism along the eastern margin of the Victoria Lake Supergroup: a remnant of Ganderian basement in central Newfoundland? Precambrian Res 147(3–4):320–341

Schoonmaker A, Kidd WSF (2006) Evidence for a ridge subduction event in the Ordovician rocks of north-central Maine. Geol Soc Am Bull 118(7/8):897–912

Schroetter J-M, Page P, Bedard JH, Tremblay A, Becu V (2003) Forearc extension and sea-floor spreading in the Thetford Mines ophiolite complex. Geol Soc Spec Publ 218:231–251

Schroetter J.-M, Tremblay A, Bedard J.H, Villeneuve M.E, (2006) Syncollisional basin development in the Appalachian orogen—The Saint-Daniel Mélange, southern Québec, Canada, *GSA Bulletin*; January/February 2006; 118(1/2): 109–125; doi: 10.1130/B25779.1

Skulski T, Castonguay S, van Staal CR, Rogers N, McNicoll V, Kerr A, Escayola M (2009) Baie Verte Peninsula: an evolving geological story. In: Rogers N, Kerr A (eds) Geological Association of Canada, Newfoundland and Labrador Section Annual Field Trip Guide, Geological Association of Canada

Soh W, Nakayama K, Kimura T (1998) Arc–arc collision in the Izu collision zone, central Japan, deduced from the Ashigara Basin and adjacent Tanzawa Mountains. Island Arc 7(3): 330–341

Stevens RK (1970) Cambro-Ordovician flysch sedimentation and tectonics in west Newfoundland and their possible bearing on a proto-Atlantic Ocean. Spec Pap Geol Assoc Can 7:165–177

Swinden HS, Jenner GA, Szybinski ZA (1997) Magmatic and tectonic evolution of the Cambrian-Ordovician Laurentian margin of Iapetus; geochemical and isotopic constraints from the Notre Dame Subzone, Newfoundland, vol 191. Memoir – Geological Society of America, pp 337–365

Szybinski ZA (1995) Paleotectonic and structural setting of the western Notre Dame Bay area, Newfoundland Appalachians, Ph.D. thesis. Memorial University of Newfoundland

Tang J.-C., Chemenda (2000) Numerical Modelling of Arc-Continent Collision: Application to Taiwan, Tectonophysics 325:23–42

Thomas W.A. (1977) Evolution of Appalachian - Ouachita salients and recesses from reentrants and promontories in the continental margin: American Journal of Science 277: 1233–1278

Thomas WA (2005) Tectonic inheritance at a continental margin. GSA Today 6(2):4–11

Tremblay A, Lafleche M.R, McNutt R.H, Bergeron M, (1994) Petrogenesis of Cambro-Ordovician subduction-related granitic magmas of the Quebec Appalachians, Canada: Chemical Geology, 113(3–4):205–220.

Thurlow JG, Swanson EA (1987) Stratigraphy and structure of the Buchans Group. Paper – Geol Surv Can 86–24:35–46

Todaro SM, Stamatakos J, van der Pluijm BA, Van der Voo R (1996) Near-Laurentian paleogeography of the Lawrence Head Volcanics of central Newfoundland, Northern Appalachians. Tectonophysics 263:107–121

Valverde-Vaquero P, van Staal CR, McNicoll V, Dunning GR (2006) Mid-Late Ordovician magmatism and metamorphism along the Gander margin in central Newfoundland. J Geol Soc Lond 163(2):347–362

van der Velden AJ, van Staal CR, Cook FA (2004) Crustal structure, fossil subduction, and the tectonic evolution of the Newfoundland Appalachians; evidence from a reprocessed seismic reflection survey. Geol Soc Am Bull 116 (11–12):1485–1498

van Staal CR (1994) Brunswick subduction complex in the Canadian Appalachians; record of the Late Ordovician to Late Silurian collision between Laurentia and the Gander margin of Avalon. Tectonics 13(4):946–962

van Staal CR (2005) North America; northern Appalachians. In: Selley RC, Cocks LRM, Plimer IR (eds) Encyclopedia of geology. Elsevier, Oxford, pp 81–92

van Staal CR, Hatcher RD Jr (2010) Global setting of Ordovician orogenesis. In: Finney SC, Berry WBN (eds) The Ordovician Earth System. Geological Society of America Special Paper 466:1–11

van Staal CR, Winchester JA, Bedard JH (1991) Geochemical variations in Middle Ordovician volcanic rocks of the northern Miramichi Highlands and their tectonic significance. Can J Earth Sci 28(7):1031–1049

van Staal CR, Sullivan RW, Whalen JB (1996) Provenance of tectonic history of the Gander Zone in the Caledonian/ Appalachian Orogen; implications for the origin and assembly of Avalon. Spec Pap Geol Soc Am 304:347–367

van Staal CR, Dewey JF, Mac Niocaill C, McKerrow WS (1998) The Cambrian-Silurian tectonic evolution of the Northern Appalachians and British Caledonides; history of a complex, west and southwest Pacific-type segment of Iapetus. In: Blundell DJ, Scott AC (eds) Lyell: the past is the key to the present. Geological Society, Special Publication, London, pp 199–242

van Staal CR, Wilson RA, Rogers N, Fyfee LR, Langton JP, McCutcheon SR, McNicoll V, Ravenhurst CE (2003)

Geology and tectonic history of the Bathurst Supergroup, Bathurst mining camp, and its relationships to coeval rocks in southwestern New Brunswick and adjacent mine; a synthesis. Econ Geol Monogr 11:37–60

van Staal CR, Whalen JB, McNicoll VJ, Pehrsson S, Lissenberg CJ, Zagorevski A, van Breemen O, Jenner GA (2007) The Notre Dame Arc and the Taconic Orogeny in Newfoundland In: Hatcher RD Jr, Carlson MP, McBride JH, Martinez Catalan JR (eds) 4-D framework of continental crust, Geological society of America Memoir, v. 200 pp 511–552

van Staal CR, McNicoll V, Hibbard J, Skulski T (2008) New data on the opening of the Taconic Seaway in Newfoundland. Abstr Program – Geol Soc Am 40(2):75

van Staal CR, Castonguay S, McNicoll V, Brem A, Hibbard J, Skulski T, Joyce N, Anonymous (2009a) Taconic arc-continent collision confirmed in the Newfoundland Appalachians. Abstr Program – Geol Soc Am. Geological Society of America (GSA), Boulder, CO, p 4

van Staal CR, Whalen JB, Valverde-Vaquero P, Zagorevski A, Rogers N (2009b) Pre-Carboniferous, episodic accretion-related, orogenesis along the Laurentian margin of the northern Appalachians. In: Murphy JB, Keppie JD, Hynes AJ (eds) Ancient orogens and modern analogues. Geological Society London Special Publication, London, pp 271–316

van Staal CR, Zagorevski A, McNicoll V (2010) Origin of the Early-Middle Ordovician Dunnage Melange tract, Newfoundland Appalachians: Ridge-trench collision immediately prior to accretion of Ganderia's leading edge to Laurentia. GSA Abstr Programs 42(1):174

von Huene R, Scholl DW (1991) Observations at convergent margins concerning sediment subduction, subduction erosion, and the growth of continental crust. Rev Geophys 29 (3):279–316

Waldron JWF, van Staal CR (2001) Taconian Orogeny and the accretion of the Dashwoods Block; a peri-Laurentian microcontinent in the Iapetus Ocean. Geology (Boulder) 29(9): 811–814

Waldron JWF, Floyd JD, van Staal CR, McNicoll VJ, Simonetti A, Heaman LM (2008) Detrital zircons from syntectonic sandstones in Scotland and Newfoundland; similarities and contrasts in Appalachian/Caledonide convergence history. GSA Abstr Programs 40(2):75

Wasowski JJ, Jacobi RD (1985) Geochemistry and tectonic significance of the mafic volcanic blocks in the Dunnage Melange, north central Newfoundland. Can J Earth Sci 22 (9):1248–1256

Whalen JB, Jenner GA, Longstaffe FJ, Gariepy C, Fryer BJ (1997) Implications of granitoid geochemical and isotopic (Nd, O, Pb) data from the Cambrian-Ordovician Notre Dame Arc for the evolution of the central mobile belt, Newfoundland Appalachians, vol 191. Memoir – Geological Society of America, pp 367–395

Whalen JB, McNicoll VJ, van Staal CR, Lissenberg CJ, Longstaffe FJ, Jenner GA, van Breemen O (2006) Spatial, temporal and geochemical characteristics of Silurian collision-zone magmatism: an example of a rapidly evolving magmatic system related to slab break-off. Lithos 89(3–4): 377–404

Whitehead J, Reynolds PH, Spray JG (1996) 40Ar/39Ar age constraints on Taconian and Acadian events in the Quebec Appalachians. Geology 24(4):359–362

Whitehead J, Dunning GR, Spray JG (2000) U-Pb geochronology and origin of granitoid rocks in the Thetford Mines ophiolite, Canadian Appalachians. Geol Soc Am Bull 112 (6):915–928

Williams H (1992) Melanges and coticule occurrences in the Northeast Exploits Subzone, Newfoundland. Paper – Geological Survey of Canada, Report, vol 92-01D, pp 121–127

Williams H (1994) The Dunnage Melange, Newfoundland, revisited Current Research – Geological Survey of Canada, Report, vol 1994-D, pp 23–31

Williams H (1995a) Chapter 2: Temporal and spatial divisions. In: Williams H (ed) Geology of the Appalachian-Caledonian orogen in Canada and Greenland. Geological Survey of Canada, pp 23–42

Williams H (1995b) Chapter 3: Dunnage Zone – Newfoundland. In: Williams H (ed) Geology of the Appalachian-Caledonian orogen in Canada and Greenland. Geological Survey of Canada, pp 142–166

Williams H, Hatcher RD Jr (1983) Appalachian suspect terranes. Memoir – Geological Society of America, vol 158, pp 33–53

Williams H, Hiscott RN (1987) Definition of the Iapetus rift-drift transition in western Newfoundland. Geology (Boulder) 15:1044–1047

Williams H, St-Julien P (1982) The Baie Verte-Brompton Line; early Paleozoic continent-ocean interface in the Canadian Appalachians

Williams H, Colman-Sadd SP, Swinden HS (1988) Tectonic-stratigraphic subdivisions of central Newfoundland. Paper – Geological Survey of Canada, vol 88-1B, pp 91–98

Williams H, Lafrance B, Dean PL, Williams PF, Pickering KT, van der Pluijm BA (1995) Chapter 4: Badger belt. In: Williams H (ed) Geology of the Appalchian – Caledonian orogen in Canada and Greenland. Geology of Canada, pp 403–413

Wilson RA (2003) Geochemistry and petrogenesis of Ordovician arc-related mafic volcanic rocks in the Popelogan Inlier, northern New Brunswick. Can J Earth Sci 40(9):1171–1189

Wilson RA, Burden ET, Bertrand R, Asselin E, McCracken AD (2004) Stratigraphy and tectono-sedimentary evolution of the Late Ordovician to Middle Devonian Gaspé Belt in northern New Brunswick: evidence from the Restigouche area. Canadian Journal of Earth Sciences 41:527–551.

Winchester JA, Williams H, Max MD, van Staal CR (1992) Does the Birchy Complex of Newfoundland extend into Ireland? J Geol Soc Lond 149(Part 2):159–162

Zagorevski A (2008) Preliminary geochemical database of the Buchans-Robert's Arm Belt, central Newfoundland. Geological Survey of Canada Open File 5986, 1 CD-ROM

Zagorevski A, Rogers N (2008) Stratigraphy and structural geology of the Ordovician volcano-sedimentary rocks in the Mary March Brook area. Current Research (2008) Newfoundland Department of Mines and Energy Geological Survey, Report 08–01, pp 111–123

Zagorevski A, Rogers N (2009) Geochemical characteristics of the Ordovician volcano-sedimentary rocks in the Mary March Brook area. Current Research (2009) Newfoundland Department of Mines and Energy Geological Survey, Report 09–01, pp 271–288

Zagorevski A, Rogers N, McNicoll V, Lissenberg CJ, van Staal CR, Valverde-Vaquero P (2006) Lower to Middle Ordovician evolution of peri-Laurentian arc and back-arc

complexes in the Iapetus: constrains from the Annieopsquotch Accretionary Tract, central Newfoundland. Geol Soc Am Bull 118(3/4):324–342

Zagorevski A, McNicoll V, van Staal C, Rogers N (2007a) Upper Cambrian to Upper Ordovician peri-Gondwanan island arc activity in the Victoria Lake Supergroup, central Newfoundland: tectonic development of the northern Ganderian margin. Am J Sci 307(2):339–370

Zagorevski A, McNicoll V, van Staal CR (2007b) Distinct Taconic, Salinic and Acadian deformation along the Iapetus suture zone, Newfoundland Appalachians. Can J Earth Sci 44:1567–1585

Zagorevski A, van Staal CR, McNicoll V, Rogers N, Valverde-Vaquero P (2008) Tectonic architecture of an arc-arc collision zone, Newfoundland Appalachians. In: Draut A, Clift PD, Scholl DW (eds) Formation and applications of the sedimentary record in arc collision zones. pp 309–334

Zagorevski A, Lissenberg CJ, van Staal CR (2009) Dynamics of accretion of arc and backarc crust to continental margins: inferences from the Annieopsquotch Accretionary Tract, Newfoundland Appalachians. Tectonophysics 479(1–2):150–154

Zagorevski A, Rogers N, van Staal CR, McNicoll V, Pollock J (2010) Middle Cambrian to Ordovician arc-back–arc development on the leading edge of Ganderia, Newfoundland Appalachians. In: Tollo R, Bartholomew J, Karabinos P, Hibbard J (eds) From Rodinia to Pangea: the lithotectonic record of the Appalachian Region: Geological Society of America Memoir 206:367–396, doi: 10.1130/B25779.1

Chapter 13
Arc–Continent Collision in the Ordovician of Western Ireland: Stratigraphic, Structural and Metamorphic Evolution

P.D. Ryan and J.F. Dewey

Western Ireland comprises a short section of a complex Ordovician arc–continent collision event, the Grampian (in British Isles) – Taconic (in North America) Orogeny (Fig. 13.1), that is traced 6,000 km from Alabama to the Shetland Islands (Dewey and Shackleton 1984). This orogeny is accepted as being the result of collision between north or west-facing oceanic arcs within the Iapetus Ocean (present coordinates) and the margin of the Laurentian landmass. There is considerable along strike variation in the system (Fig. 13.2). The Neoproterozoic – early Palaeozoic geology of the Laurentian margin varied from carbonate bank development in the south to thick clastic rift basins in the north. The Grampian Orogeny was marked by arc accretion in western Ireland and New England and by ophiolite obduction in Newfoundland and the Shetland Islands. There was a variable response of the Laurentian margin to this event with flexural foreland basins only being recorded in the Taconic sector. There were also differing degrees of lower plate metamorphism. The subsequent Caledonian-Acadian and Alleghanian Orogenies have produced variable amounts of reworking of the Grampian – Taconic tract. Whilst the geology of the West of Ireland is not representative of this tract as a whole, it is one of the most well exposed, most accessible and certainly the most studied such region. Original field relationships are well-preserved because much of the upper plate has been affected by only low grade metamorphism and gentle folding during the later orogenic events. This region, therefore, provides an unique laboratory for studying the arc–continent collision process. This article reviews the geology of western Ireland, presents a summary of the evidence for this being an fossil arc collision zone and then concentrates on those features that help inform wider knowledge of this process.

P.D. Ryan
Earth and Ocean Sciences, National University of Ireland Galway, Galway, Ireland
e-mail: paul.ryan@nuigalway.ie

J.F. Dewey
Department of Geology, UC Davis, One Shields Avenue, Davis, CA 95616, USA

13.1 The Ordovician Geology of Western Ireland

The geology of western Ireland is divided into five zones from north to south, whose boundaries are marked by major faults: North Mayo; Clew Bay; South Mayo; Connemara; and South Connemara (Fig. 13.1a–c).

North Mayo contains a Grenvillian basement (Daly 1996, 2001; Daly and Flowerdew 2005) overlain by Neoproterozoic sediments of the Dalradian Supergroup deposited from pre-720 Ma to post 595 Ma (Condon and Prave 2000). Basement and cover were deformed and metamorphosed by the 475–462 Ma Grampian Orogeny (Daly and Flowerdew 2005; Flowerdew et al. 2009). Evidence for high pressure-low temperature metamorphism is found in the southern-most Dalradian Supergroup (Gray and Yardley 1979) and in the pre- or early Grampian eclogites of the Slishwood Division (Flowerdew et al. 2005). Fabrics indicate that early convergence was associated with NW-directed dextral transpression (Harris 1995). North Mayo is interpreted as comprising part of the Laurentian passive margin to the Iapetus Ocean which opened in latest Neoproterozoic times, the Dalradian sediments having been deposited during rifting and

D. Brown and P.D. Ryan (eds.), *Arc-Continent Collision*, Frontiers in Earth Sciences,
DOI 10.1007/978-3-540-88558-0_13,

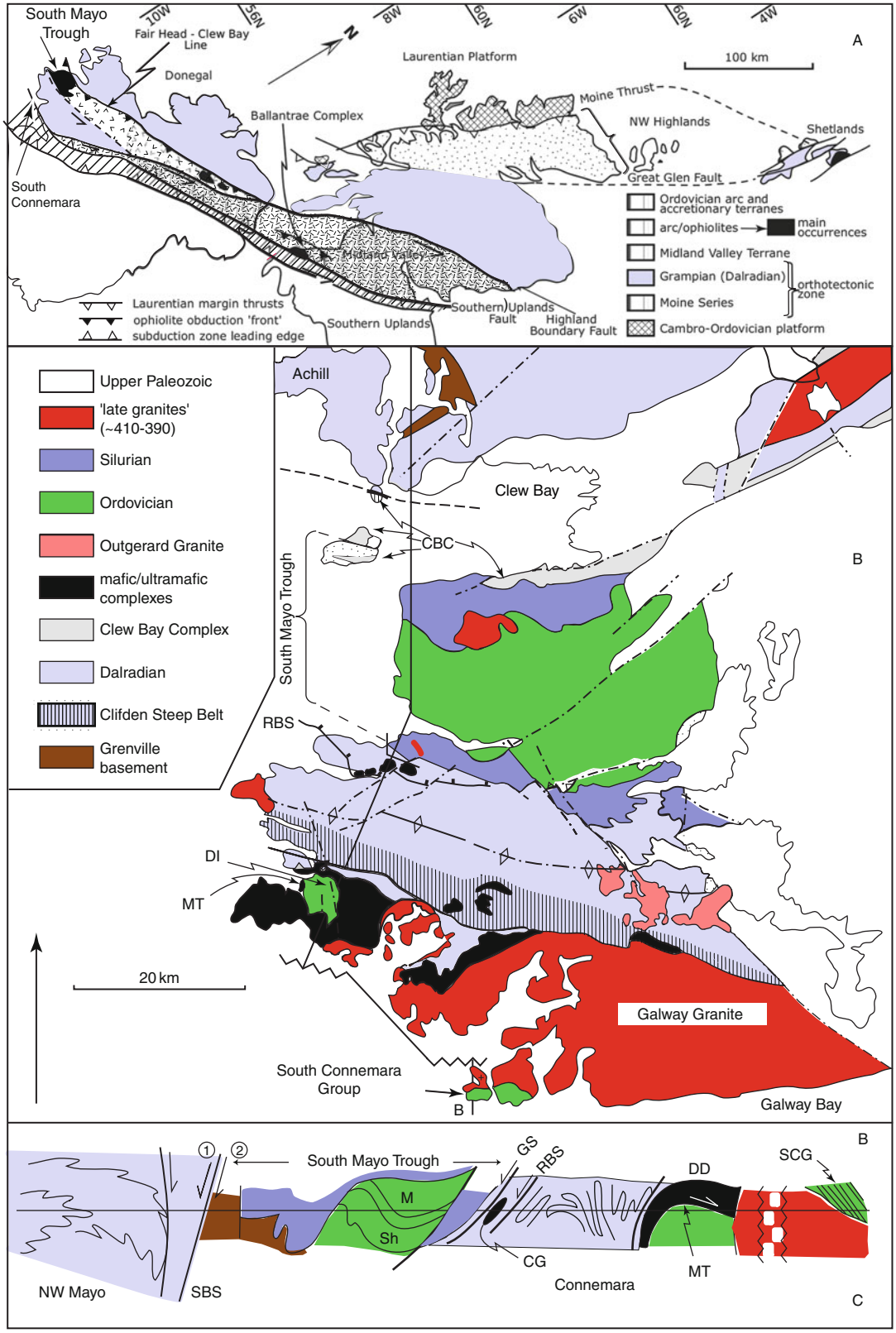
South Mayo Trough
Fair Head - Clew Bay Line
Donegal
Ballantrae Complex
South Connemara
Laurentian Platform
Moine Thrust
NW Highlands
Shetlands
Great Glen Fault
100 km
A
Ordovician arc and accretionary terranes
arc/ophiolites
main occurrences
Midland Valley Terrane
Grampian (Dalradian)
orthotectonic zone
Moine Series
Cambro-Ordovician platform
Laurentian margin thrusts
ophiolite obduction 'front'
subduction zone leading edge
Southern Uplands
Southern Uplands Fault
Highland Boundary Fault
Upper Paleozoic
'late granites' (~410-390)
Silurian
Ordovician
Outgerard Granite
mafic/ultramafic complexes
Clew Bay Complex
Dalradian
Clifden Steep Belt
Grenville basement
Achill
Clew Bay
CBC
B
South Mayo Trough
RBS
DI
MT
20 km
Galway Granite
South Connemara Group
B
Galway Bay
B
South Mayo Trough
GS
RBS
DD
SCG
M
Sh
CG
MT
NW Mayo
SBS
Connemara
C

break-up of Rodinia (Strachan and Holdsworth 2000). The southern margin of this zone, referred to as the Grampian Terrane (Murphy et al. 1991), is marked by a strong magnetic lineament (Max and Riddihough 1975; Max et al. 1983), the Fair Head – Clew Bay Line (FCL) regarded as the westward continuation of the Highland Boundary fault (HBF) in Scotland (Fig. 13.1a). In Britain and Ireland the FCL-HBF is taken to mark contact between the Laurentian margin and the arcs accreted during the Grampian Orogeny (van Staal et al. 1999).

The highly-sheared Clew Bay Complex lies south of the FCL (Fig. 13.1b). It comprises two main components: a sedimentary melange (Dewey and Ryan 1990) with a mature continental provenance (Dewey and Mange 1999; Chew 2003), and a dismembered ophiolite in the south (Ryan et al. 1983b). The age of the complex is uncertain (Williams et al. 1996), however, a Cambro-Ordovician age is likely on provenance grounds (Dewey and Mange 1999) and it shares the same 460 Ma S2 fabric as the Dalradian to the north of the FCL (Chew et al. 2003). Provenance studies also suggest a stratigraphic linkage between this complex and the South Mayo Trough by the early-mid Ordovician times and is interpreted as an accretionary complex above a north-verging subduction zone (Dewey and Ryan 1990).

The South Mayo Trough (Figs. 13.1b and 13.3) contains a thick sequence of Lower to Middle Ordovician sediments that are preserved in a large syncline, the Mweelrea-Partry Syncline. A Silurian continental to marine sequence unconformably overlies both limbs implying that the Ordovician rocks lay in a broad syncline prior to Silurian deposition. The northern limb contains a 9 km thick Floian – Darriwillian (approximately 480–463 Ma, Arenig-Llanvirn in the classic British Stages, Figs. 13.2 and 13.5) conformable sequence. The lower portion has a primitive arc, ophiolitic and poly-metamorphic sedimentary source, whilst juvenile metamorphic with subordinate evolved arc detritus occurs at higher levels (Dewey and Mange 1999; Clift et al. 2009). The southern limb is disrupted by faulting, but similar provenance trends are observed, particularly at higher stratigraphic levels. Volcanic complexes, which lie mainly in the southern limb, are of primitive arc affinities near the base (Ryan et al. 1980; Clift and Ryan 1994; Draut et al. 2004) and show an increasing proportion of Laurentian-derived melt up section (Draut et al. 2004). Volcanic activity continued throughout the history of the basin with ash band marker horizons occurring at all levels. The South Mayo Trough is interpreted as a fore-arc basin that preserves a record of initial arc development, incipient subduction of the Laurentian margin and of the subsequent exhumation and erosion of the Grampian orogenic belt (Dewey and Ryan 1990). South Mayo is correlated north-westwards along strike (Fig. 13.1a) with the Ordovician volcanics of Charlestown and the Furongian-Floian Tyrone Volcanic Group (Floian, 493–473 Ma, Cooper et al. 2008; Draut et al. 2009). These complexes, the Clew Bay Complex, and their eastern correlatives are grouped into the North-western Terrane of Murphy et al. (1991)

Connemara contains rocks of the Dalradian Supergroup and can be divided into four zones (Fig. 13.1b). The northern zone comprises low-grade Southern Highland Group strata, with syntectonic (D2/D3) mafic/ultramafic intrusions (474.5 ± 1.0, Friedrich et al. 1999b). A low-angle extensional slide, the Renvyle–Bofin slide, separates them from a zone of uppermost Appin Group, Argyll Group and lowermost Southern Highland Group c. 5 km thick, arranged in north-verging, polyphase, recumbent folds, refolded into the Connemara antiform, affected by medium to high-grade Barrovian metamorphism (Yardley 1976). These rocks were intruded by the late to post-tectonic Oughterard Granite suite (462.5 ± 1.2 Ma, Friedrich et al. 1999b). Fold axial surfaces steepen southwards into the Clifden Steep Belt, which contains syntectonic mafic intrusions (470.1 ± 1.4 Ma, Friedrich et al. 1999b). Further south, a zone of sillimanite-grade semipelites injected by huge volumes of syntectonic gabbros and ultramafics (Errisbeg Complex) and 467 ± 2 Ma (Friedrich et al. 1999a) quartz diorites

Fig. 13.1 (continued) Geology of the Grampian zone redrawn from Dewey (2005). (**a**) Schematic tectonic map of the Irish and British Caledonides. (**b**) Schematic tectonic map of the western Irish Caledonides. *DD* Delaney Dome, *MT* Mannin Thrust. (**c**) Schematic geologic section along line AB on B above. *CG* Currywongaun Gabbro, *GS* Gowlaun Slide, *M* Mweelrea, *SH* Sheeffry, *SBS* South Achill Beg Slide, *SCG* South Connemara Group, *1 and 2*, first and second movement sense on SBS, all other abbreviations, symbols, and ornament are as in (**b**).

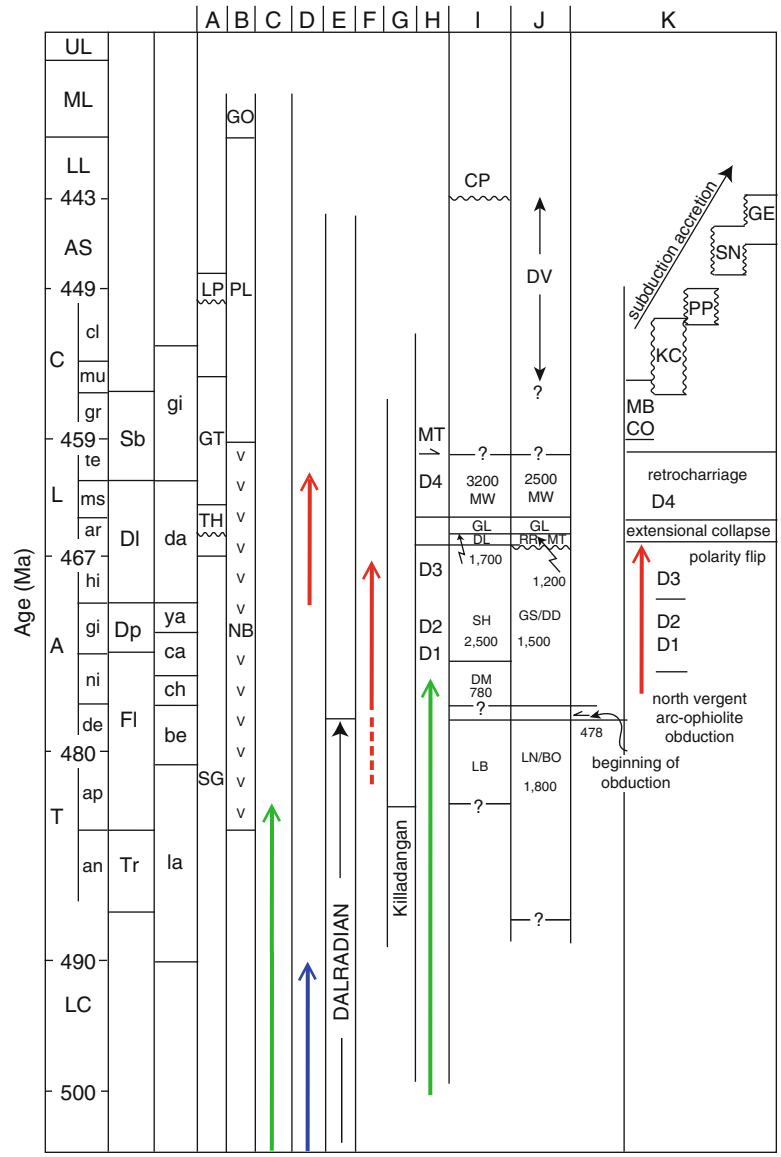

Fig. 13.2 Grampian and Taconic stratigraphic data, modified after Dewey (2005). Key to columns: A, Western Newfoundland Ordovician Shelf; B, Notre Dame Bay arc stratigraphy; C, West Newfoundland ophiolites; D, Quebec -New England; E, Scottish Highlands; F, Achill; G: Clew Bay Complex; H, Connemara and Scottish ophiolites; I, north limb of SMT; J, south limb of SMT(thicknesses in I and J in meters); K, Southern Uplands accretionary prism. The following abbreviations are used: *CO* Corsewall, *CP* Croagh Patrick, *DD* Delaney Dome, *Dp* Dapingian, *DL* Derrylea, *Dl* Darriwillian, *DM* Derrymore, *DV* Derryveeny, *Fl* Floian, *GE* Glenlee, *GL* Glenummera, *GO* Goldson, *GS* Glensaul, *GT* Goose Tickle, *KC*, Kirkcolm, *KD* Killadangan, *LB* Letterbrock, *LN* Lough Nafooey, *LP* Long Point, *MB* Marchburn, *MN* Maumtrasna, *MT* Mannin Thrust, *MW* Mweelrea, *NB* New Bay, *PL* Point Leamington, *PP* Portpatrick, *RR* Rosroe, *Sb* Sandbian, *SG* Saint George, *SH* Sheeffry, *SI* Shinnel, *TH* Table Head. Key to timescale: *A* Arenig, *AS* Ashgill, *C* Caradoc, *L* Llanvirn, *LC* Late Cambrian, *LL* Lower Llandovery, *ML* Middle Llandovery, *T* Tremadoc, *Tr* Tremadoc (IUGS usage), *UL* Upper Llandovery. Key to Ordovician graptolite zones: an, *Anisograptus*; ap, *Tetragraptus approximatus*; ar, *Didymograptus artus*; cl, *Dicranograptus clingani*; de, *Didymograptus deflexus*; gi, *Isograptus gibberulus*; gr, *Nemagraptus gracilis*; hi, *Didymograptus hirundo*; ms, *Didymograptus murchisoni*; mu, *Diplograptus multidens*; ni, *Didymograptus nitidus*; te, *Glyptograptus teretiusculus*. Key to the Australian Ordovician graptolite zones in ascending stratigraphic order: *la* Lancefieldian, *be* Bendigoian, *ch* Chewtonian, *ca* Castlemainian, *ya* Yapeenian, *da* Darriwillian, *gi* Gisbornian. Australian and British zones were correlated following the scheme of Paskevicius (2007). The various *coloured arrows* represent: supra-subduction zone ophiolites (*green*), prograde regional metamorphism (*red*) and blueschist facies metamorphism (*blue*).

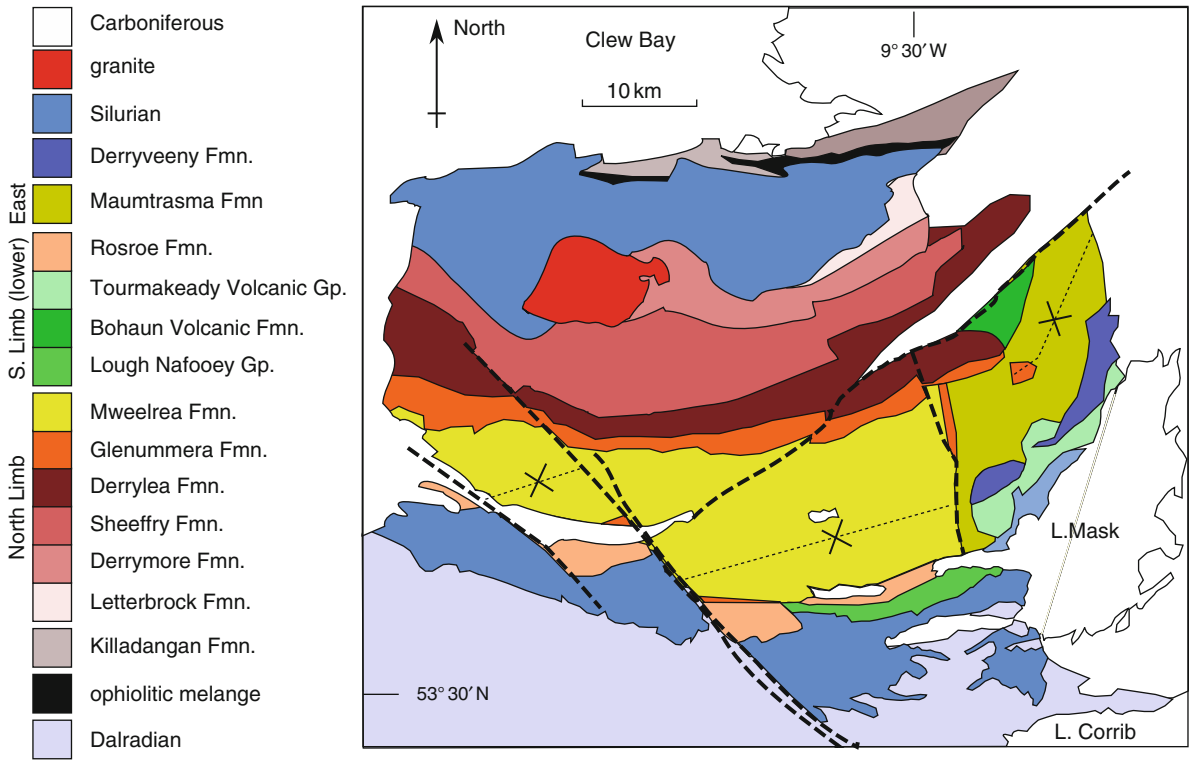

Fig. 13.3 Geological map of the Ordovician of the South Mayo Trough. Conformable geological contacts are shown as *thin lines*; unconformable or faulted contacts as *medium thickness lines*. Caledonian and later major faults as *heavy dashed lines*. The following abbreviations are used: *Fmn* Formation, *L* Lough, *S* south. The axial trace of the Mweelrea- Partry syncline is shown as a *heavy dotted line*.

(Leake 1986, 1989) record gentler northward dips and were thrust SE over low-grade evolved arc rocks dated at 474.6 ± 5.5 Ma (Friedrich 1998; Draut and Clift 2002) that show chemical similarities to volcanic rocks within the South Mayo Trough, suggesting that Connemara lay structurally beneath an evolved arc by Darriwillian (Llanvirn) times (Draut and Clift 2002). The radiometric studies bracket the metamorphic maximum to c. 475–467 Ma (Floian) with rapid uplift, formation of the Connemara antiform and retrogressive metamorphism by 462 Ma (Darriwillian). The contact between Connemara and South Mayo is obscured by a narrow Silurian sub-aerial to marine tract which contains abundant arc derived detritus (Menuge et al. 1995). However, structural and geophysical considerations suggest that it is a pre-Silurian major fault with c. 15 km of downthrow to the north (Dewey et al. 1970a; Ryan and Archer 1978). Connemara has clear stratigraphic affinities with the Laurentian margin (Grampian Terrane) and is interpreted as the lower plate of the Grampian Orogeny subsequently emplaced to its present position by post-Grampian, pre-Silurian lateral motion (Hutton 1987).

The arrival of Connemara to its present structural level is recorded in conglomerates of the Mweelrea and Derryveeney Formations (Fig. 13.3) which are covered unconformably by the Silurian of north Galway (Graham et al. 1991) suggesting that it was providing high level granitic detritus since 464 Ma and high grade metamorphic detritus by pre-Llandovery times (Graham et al. 1991; McConnell et al. 2009).

The South Connemara Complex (Ryan and Dewey 2004) comprises a tectonic melange incorporating abyssal cherts, mafic volcanics of mid-ocean ridge basalt (MORB) affinities (Ryan et al. 1983a) and trench sediments with abundant metamorphic, granitic and some rhyolitic detritus (Ffrench and Williams 1984). This complex is interpreted as forming in a late Ordovician south-verging trench (Ryan and Dewey 2004) and it marks the line of the Southern Upland Fault in western Ireland (Fig. 13.1b) which is the northern boundary of the south verging subduction-accretion complexes of the post-Grampian Central terrane.

13.2 Nature of the Crust and Lithosphere

Deep geophysical experiments, both onshore (Brown and Whelan 1995; Lowe and Jacob 1989) and offshore (Klemperer et al. 1991), constrain the current upper lithospheric structure of western Ireland. The current Moho rests at about 30 km (Lowe and Jacob 1989; Klemperer et al. 1991). The FCL is now a north-dipping structure (Ryan et al. 1983b; Klemperer et al. 1991) that can be traced to the Moho. North of the FCL a pervasive south-dipping reflectivity is linked to a Neoproterozoic volcanic margin to Laurentia (Ryan 2008). Magnetic sources to the south of the FCL, generally presumed to be the Ordovician arc complexes, occur in the upper 15 km (Brown and Whelan 1995). The lower crust south of the FCL has a shallow north-dipping seismic reflection fabric that can be traced from the latest Silurian Iapetus Suture in the south to a "keel" in the Moho offshore of Donegal. This coupled with structural evidence from Connemara, Clew Bay, North Mayo and Donegal (Clift et al. 2004; Alsop and Hutton 1993) for a late Ordovician reversal in sense of thrusting is consistent with rapid southwards directed collapse (Fig. 13.1c), perhaps associated with post-flip back-arc extension that preserved upper plate rocks before they could be eroded (Clift et al. 2004).

13.3 The Grampian Orogeny

The Grampian (Taconic) Orogeny was an early to mid-Ordovician (Floian to Darriwillian) short-lived arc collision event (Dewey 2005) that effected the Laurentian margin and was followed by a subduction polarity reversal (Dewey and Shackleton 1984; Ryan and Dewey 1991, 2004) in mid- to late Ordovician times. Evidence from South Mayo and Connemara suggest that initial island arc–continent "collision" during the Floian was "soft", meaning continental sediment entered the subduction channel, (Draut and Clift 2001) and that this was followed by Darriwillian "hard" collision associated with an increasing continental component in the arc melts when the continental margin entered the subduction channel (Draut and Clift 2001; Draut et al. 2004). This change in arc chemistry was coeval with both the change in sedimentary provenance within the South Mayo Trough and the emplacement of the syntectonic D2/3 gabbros in Connemara at 475–470 Ma (Floian-Dapingian) (Dewey and Mange 1999; Clift et al. 2004). Radiometric evidence from both North Mayo and Connemara suggests that the entire event took less than 15 my, with initial collision taking 4.5–6.5 my followed by subduction flip which took from 3.5 to1.5 my and then a period of rapid exhumation and cooling to greenschist-facies conditions with associated flip-related volcanism in Connemara, which lasted probably about 4 my (Dewey and Mange 1999; Soper et al. 1999; Draut and Clift 2001). Present data suggests exhumation and cooling may have lasted for 11 my in North Mayo (Flowerdew et al. 2005).

Evidence of post-Grampian subduction polarity reversal is found in the mid- to late Ordovician and Silurian strata of South Mayo and North Connemara, which contain abundant arc detritus (Williams et al. 1992; Menuge et al. 1995; Dewey and Mange 1999) and probably formed in a supra-subduction zone setting (Williams and Harper 1991; Menuge et al. 1995) geometrically requiring north-dipping subduction. The late Ordovician Mannin Thrust (Draut and Clift 2002) probably formed as deformation transferred into the back arc during, or prior to, subduction reversal (Fig. 13.1b, c). The Connemara antiform may reflect Andean style shortening (e.g. Kay et al. 2005) in the thermally weakened proto-back arc during or immediately after subduction flip . The South Connemara complex, south of Connemara, is interpreted as forming in a late Ordovician south-verging trench (Ryan and Dewey 2004).

Tectonic models for the Ordovician and Silurian of western Ireland have long recognised the link with modern arc systems. Mitchell and McKerrow (1975) pointed out the similarities with Burma, but their model for the Grampian Orogeny only required subduction beneath Laurentia. Dewey and Shackleton (1984) related the Grampian event to the northward obduction of a nappe of ophiolitic and accretionary prism rocks onto Laurentia. Dewey and Ryan (1990) developed a model in which the Ordovician strata of the north limb of the Mweelrea/Partry Syncline accumulated in a fore-arc basin with the arc whose composition evolved up-section (Ryan et al. 1980; Clift and Ryan 1994; Draut and Clift 2002) lying in the south limb of this fold. The Clew Bay Complex was

interpreted as an accretionary prism with an ophiolitic back stop (Dewey and Ryan 1990). Ryan and Dewey (1991) further developed the model to include post-Grampian subduction flip. Dewey and Mange (1999) presented a model, based on a comprehensive high resolution heavy mineral data set throughout the region, that established the dominance of juvenile Grampian metamorphic detritus in the upper part of the Ordovician succession. Thus the strata of the South Mayo Trough as now seen as recording the complete record of arc–continent collision.

13.4 Mineral Deposits

The Grampian and North-western terranes in Ireland represent a significant orogenic gold province with proven reserves of one million ounces. In the west of Ireland at Leckanvey, quartz veins within Silurian quartzites overlying ophiolitic melanges within the Clew Bay zone host 498,000 tonnes of ore at 9.94 gm/tonne. An east-west shear zone in Ordovician turbidites at Cregganbaun within the South Mayo Trough, which have abundant mafic and ultramafic detritus (see below), contains 530,000 tonnes of ore at 6 gm/tonne . Upper Dalradian rocks of the Grampian terrane immediately north of the Tyrone Volcanic Group have significant deposits (Cox 2005) at Cavanacaw with two million tonnes at 6.9 gm/tonne and Curraghinalt with 470,000 tonnes at 17 gm/tonne. The primary mineralisation is attributed to post-Grampian Caledonian magmatism affecting the structurally underlying Tyrone Volcanic Group (Parnell et al. 2000). In general, whilst the gold mineralisation might have been sourced from the Ordovician arc complexes of the North-western Terrane, available evidence suggests that it was emplaced post-tectonically with Grampian and Caledonian structures providing conduits along which later (?) Carboniferous brines ascended (Parnell et al. 2000).

The features that are currently best understood within the Ordovician of western Ireland that have relevance to the study of arc–continent collision elsewhere are: the sedimentary and volcanic record of the arc–continent collision process preserved within the South Mayo Trough; the timing, duration and nature of the events in the upper (South Mayo Trough) and lower plates (Connemara and North Mayo); and the inferred topographic record of the collision process with the preservation of sections of both the upper and lower plate. The remainder of this article will focus on these items.

13.5 The Sedimentary and Volcanic Record of Arc–Continent Collision in the South Mayo Trough

This account will first review the field relationships and geochemistry of the sedimentary record and then the volcanic complexes within the South Mayo Trough. The stratigraphic sequence within the South Mayo Trough for both limbs of the Mweelrea-Partry syncline is shown in Fig. 13.4a. Stratigraphic dates are quoted using the equivalent Australian Ordovician graptolite zones following Skevington and Archer (1971) allowing absolute ages to be attributed using the scale of Sadler et al. (2009). Correlations with the new IUGS Ordovician stages and the classic British stages are provided in Fig. 13.5. A total of 533 geochemical analyses have been compiled from various sources, 186 of volcanic rocks and 347 of sedimentary rocks. This compilation suffers from some drawbacks; not all samples have been analysed for the same suite of elements; different analytical techniques have been used; and there is a shortage, by modern standards, of isotopic data. However, they provide a useful insight into the chemical evolution of both the arc and its associated fore-arc basin during arc–continent process. In the following geochemical diagrams, red is used for formations that pre-date arc–continent collision, green for those formations believed to have been coeval with collision, and blue for those associated with post-collision subduction flip.

13.5.1 Stratigraphy of the South Mayo Trough

The stratigraphy of the South Mayo Trough (Figs. 13.1b, 13.3 and 13.4) has been studied for more than 100 years. Knowledge of the northern

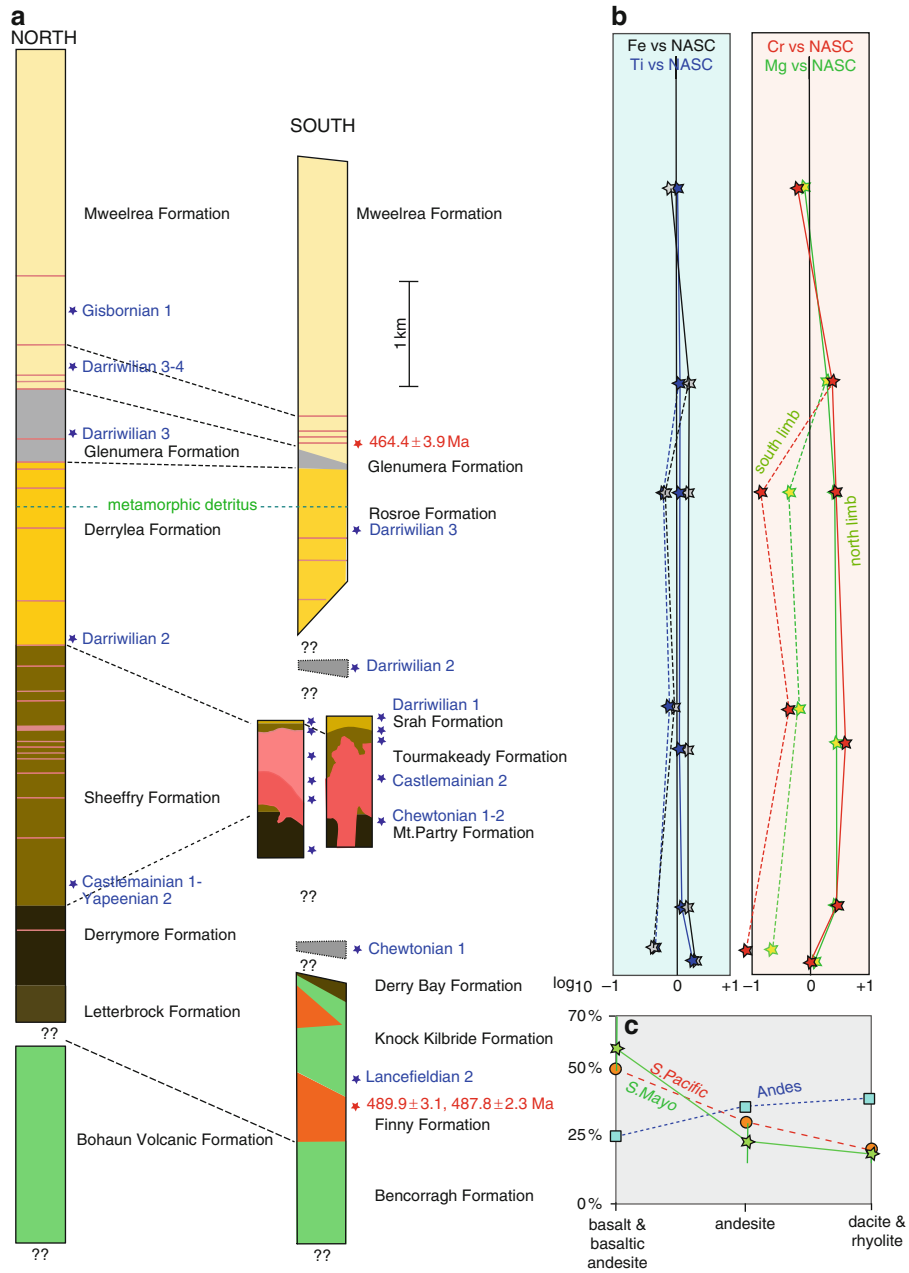

Fig. 13.4 The Ordovician stratigraphy of South Mayo. (**a**) Stratigraphic columns for the north and south limb successions. *Blue stars* represent palaeontological control. Australian graptolite zones are abbreviated *La* Lancefieldian, *Ch* Chewtonian, *Ca* Castlemainian, *Ya* Yapeenian, *Da* Darriwillian, *Gi* Gisbornian followed by the zone number. *Red stars* represent U-Pb dates plus errors (details in the text). (**b**) Plots of mean: Fe (*black*); Ti (*blue*); Mg (*green*); and Cr (*red*) for each formation normalised against the North American Shale Composite. (**c**) Plots of relative volumes of basalt and basaltic andesite; andesite; and dacite and rhyolite for the South Mayo Trough compared to that of the South Pacific arcs and the Andes.

succession is based primarily on the works of Stanton (1960), Dewey (1963), McManus (1972), and Pudsey (1984a). Archer (1977), Ryan et al. (1980), Graham et al. (1989) describe the fault-bounded southern limb succession. Dewey and Mange (1999: Appendix 1) provide the most recent synthesis. Palaeontological

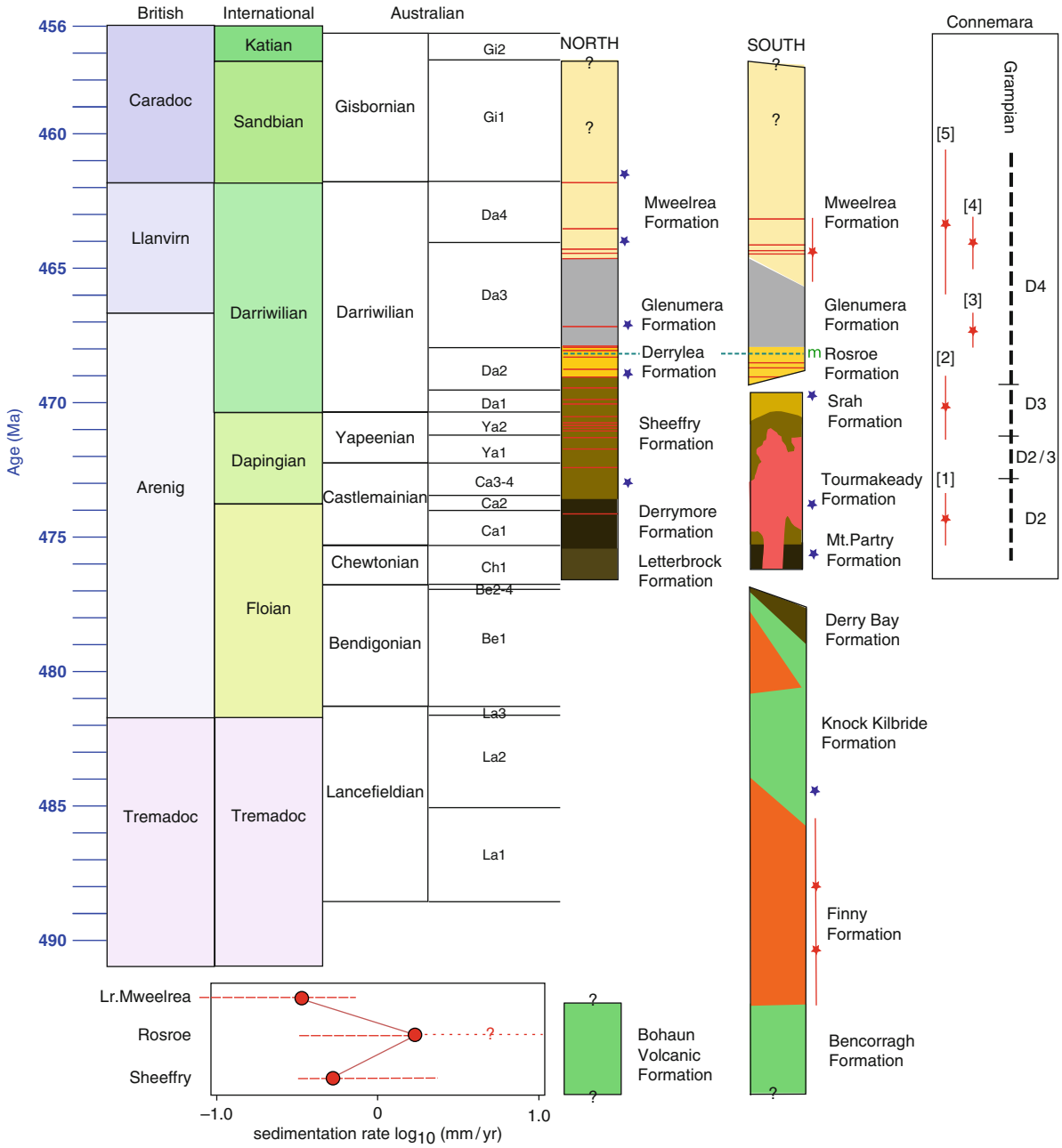

Fig. 13.5 Stratigraphic and absolute ages for the Ordovician succession of South Mayo. The standard British Ordovician stages, those of the IUGS and the Australian ordovician graptolite zones are assigned absolute ages following the scheme of Sadler et al. (2009). The absolute ages for events in Connemara are represented by *red stars* with *error bars* and the corresponding deformation events by D1-4. The numbers refer to: [1] Currywongaun gabbro; [2] Cashel - Lough Wheelaun gabbro; [3] Connemara anatexite; [4] Connemara quartz diorite; [5] Oughterard granite (Freidrich et al. 1999a, b). The plot in the *bottom left* shows the estimated sedimentation rates for the Sheeffry, Derrylea/Rosroe and Mweelrea Formations on a $\log_{10}$ scale.

controls are provided by graptolites and locally shelly faunas of Laurentian affinity, which are reviewed in Skevington and Archer (1971), Pudsey (1984a), Graham et al. (1989) and Harper and Parkes (2000). More recent works are cited in the text.

The northern limb succession (Figs. 13.3 and 13.4) comprises a ~9 km thick conformable succession containing, in ascending stratigraphic order, the Letterbrock, Derrymore, Sheeffry, Derrylea, Glenummera and Mweelrea Formations (Dewey and Mange 1999). The biostratigraphical age constraints used are those of Pudsey (1984a) unless stated otherwise. The Letterbrock Formation (>250 m), has a northerly provenance and comprises slates, greywackes and conglomerates containing ophiolitic and continental detritus. The Derrymore Formation (780 m) of felspathic sandstone turbidites with rare fuchsite/chromite/pyrite shear zones whose provenance is from the north, north-east and east. The Sheeffry Formation (2,500 m) has green to grey-green turbidites containing significant silicic and mafic volcanic detritus with white-weathering silicic tufts and submarine lahars, fuchsite-brunerite shear zones. It contains a graptolite fauna near the base of Arenig (*hirundo* or *extensus* zone) age (Castlemaine 1 – Yapeen 2, 475.44–470.54 Ma). The provenance is from the north, east and south. The Derrylea Formation (1,700 m) is made up of massive greywacke turbidites, with common ferroan dolomite/ siderite/ankerite nodules, green slates and cream-weathering porcellanous tufts. Dark green chromite and chlorite-rich turbidites are derived from the north and east whilst paler grey-green turbidites with abundant clear and smoky quartz and alkali felspar were derived from the south. Towards the top of the formation, metamorphic detritus (staurolite, garnet and metamorphic quartz) becomes important. A graptolite fauna near its base is of *hirundo* zone age or higher (Darriwillian 2, 469.57–467.94 Ma). The overlying Glenummera Formation (600 m) comprises grey-green slates, mudrocks, cherty argillites with minor thin sandstones and has a shelly fauna of Llanvirn age (? Darriwillian 3, 467.94–463.04 Ma). Litharenites with volcanic, granitic and metamorphic detritus of the Mweelrea Formation (>3,200 m) were deposited in humid alluvial fans, fan deltas and braided rivers that flowed westwards (Pudsey 1984b). This formation contains six ignimbrite horizons and three marine slate bands that thicken to the northwest. Graptolites from the first marine band are assigned a *murchisoni* zone age (Darriwillian 3–4; 467.94–460.86 Ma) and a shelly fauna from the third marine band (Harper et al. 2010) a Sandbian age (460.86–456.0 Ma)

The southern limb contains two fault-bounded volcanic complexes (described below), the Lough Nafooey Group and the Tourmakeady Volcanic Group, which are in fault contact with the Rosroe, Glenummera and Mweelrea Formations (Figs. 13.3 and 13.4). The Rosroe Formation (>1,200 m), which is generally taken as a correlative of the Derrylea Formation and of the conglomeratic Maumtrasma Formation to the east (Fig. 13.3), contains deep-water marine proximal fans of coarse, thick, channel sandstones with common volcanic, granitic and, towards the top, metamorphic detritus which were derived principally from the south, southeast and east. It is palaeontologically dated (Skevington and Archer 1971) to the *murchisoni* zone (Darriwillian 3, 467.94 Ma–463.04 Ma). The Glenummera Formation thins southwards (300 m) as does the Mweelrea Formation (>2,500 m) but both are lithologically similar to their northern counterparts.

13.5.1.1 Heavy Mineral Studies

Heavy mineral suites (Fig. 13.6), gross lithological assemblages, and quartz/feldspar/lithic ratios in the sedimentary rocks of the South Mayo Trough (Dewey and Mange 1999) record the sedimentary response of the South Mayo Trough to tectonic events in neighbouring terranes. The Letterbrock Formation was derived from a source of ophiolitic and mature continental detritus that lay to the north, consistent with derivation from the Killadangan Formation and the Deer Park Complex. The Sheeffry and lower Derrylea Formations record the continued progressive erosional denudation of an ophiolitic source to the north and an evolved arc source to the south, of a similar composition to the coeval volcanism of the southern succession (see below). The upper Derrylea and upper Rosroe Formations record the sudden appearance of garnet and staurolite indicating the abrupt unroofing of a Grampian Barrovian amphibolite facies source to the north (Dewey and Mange 1999; Clift et al. 2004). The finer grained Glenummera Formation represents either a period of low Grampian elevation during waning collapse or the relocation of the depocentre to a site

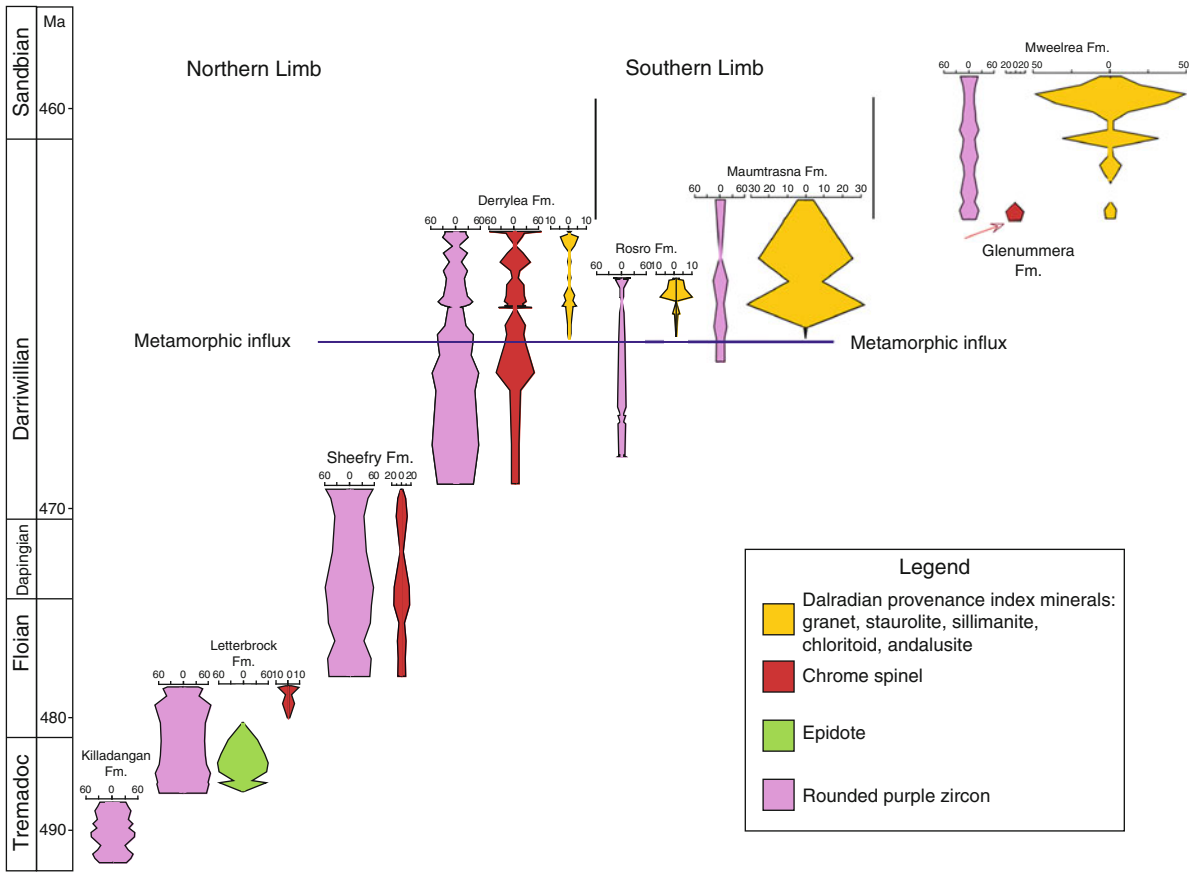

Fig. 13.6 Summary plot of heavy mineral distribution by formation within the Ordovician of South Mayo, redrawn after Dewey and Mange (1999). The numbers on the *scale bars* refer to percentages of a particular mineral suite.

no longer preserved. The fluviatile Mweelrea Formation and its ignimbrite bands records the establishment of the new silicic, interpreted as a post-flip, arc (Ryan and Dewey 1991) and the final stages of erosional unroofing of the Grampian Orogen, during a renewed, Andean-style, shortening phase (Clift et al. 2004).

13.5.1.2 Sedimentary Geochemistry

Several major studies have been carried out on the geochemistry of the sandstones and shales of South Mayo. Early studies (Wrafter and Graham 1989) and Ryan et al. (1995) concentrated on the anomalous nature of the sediments in the north limb succession of the South Mayo Trough. Later studies have used sedimentary discriminant diagrams to test the tectonic setting of the Ballytoohey and Killadangan Formations of the Clew Bay Complex (Harkin et al. 1996) and of the main South Mayo Trough succession and interbedded tuffs (Ryan and Williams 2007). Wrafter and Graham (1989) reported high Ti and Fe concentrations of mafic provenance in the Letterbrock and Derrymore Formations with the overlying Sheeffry and Derrylea Formations having high Cr, Ni, and Mg concentrations of ultramafic provenance, a sequence they interpreted as the result of the progressive unroofing of an ophiolite. Ryan et al. (1995) show that such anomalous values are unique to South Mayo and are not recorded within other Irish Ordovician volcaniclastic terranes. Harkin et al. (1996) report that the sandstones of the Clew Bay complex were derived from a transitional continental provenance, possibly a passive continental margin, and lack any significant ophiolite detritus. Ryan and Williams (2007) use sedimentary discriminant diagrams to propose an active margin setting for the Ordovician Mweelrea and Rosroe Formations and a passive margin setting for the Derrylea and Sheeffry Formations.

This latter result for the Derrylea and Sheeffry Formations is not consistent with the high resolution heavy mineral studies of Dewey and Mange (1999).

The mean compiled values for each formation (Fig. 13.4b) show that high mean Mg and Cr, normalised against the North American Shale Composite (NASC, Gromet et al. 1984), are recorded for the Derrymore, Sheeffry, Derrylea and Glenummera Formations but are not present in the sediments of the south limb older than the Glenummera Formation. The extreme contrast in Mg and Cr values for the two limbs, with the north limb succession having values between 6 and 9 times higher than that of the south limb illustrates the marked difference in their sources. A similar contrast is not present for Ti and Fe and it is not clear that the argument that the values for the Derrymore Formation represent the stripping of the upper portion of an ophiolite (Wrafter and Graham 1989) can be sustained. It is more likely that an ultramafic source supplied material to the north limb succession from Derrymore to Glenummera times. Plotting all available analyses (Fig. 13.7a) and their means (Fig. 13.7b) on the discriminant diagram of Roser and Korsch (1988), the diagram found by Ryan and Williams (2007) to give the best agreement with their tectonic interpretation, confirms their result with the Sheeffry and Derrylea Formations plotting in the P4 quartzose sedimentary provenance field (P1/P4 overlap) and places Glenummera and the Derrymore Formations in the same field implying a mature provenance. This result is almost certainly a product of the high negative weighting given to MgO in both Discriminant Functions 1 and 2 (Roser and Korsch 1988) and, although it confirms the presence of ultramafic detritus, it probably has no further tectonic significance. We, therefore, prefer the interpretation of Dewey and Mange (1999) that the main input to these formations was from an accretionary prism containing a significant ultramafic component in a fore-arc setting, an explanation also consistent with the nature of the associated volcanism (see below). The interpretation of Ryan and Williams (2007), that the Sheeffry and Derrylea Formations were sourced from a passive margin containing significant mafic to ultramafic igneous complexes, could produce the same compositional plot, but implies a totally different tectonic setting. This, perhaps, illustrates the potential dangers of using sedimentary discriminants in an arc–continent collisional setting. For example, individual sand compositions in the Luzon fore-arc vary dramatically following sequential deposition from the Taiwan Orogen, the Chinese margin and the Luzon arc (Yen and Lundberg 2006). Also, Liu et al. (2008) show that submarine canyons transport clay minerals from the same three sources into the northern part of the South China Sea, which is currently adjacent to a passive margin.

There are a few isotopic studies on the sediments of the South Mayo Trough. Rb, Sr, Sm and Nd data from the Derryveeny Formation, which unconformably overlies the Tourmakeady Volcanic Formation and lies beneath Silurian strata (Fig. 13.3) suggest derivation of both high grade migmatite and granitoid clasts from the Connemara Dalradian indicating a pre-Silurian age for the docking of Connemara (Graham et al. 1991). Harkin et al. (1996) suggest a possible Laurentian source for the sedimentary component of the Clew Bay Complex on the basis of Sm–Nd model ages. A U–Pb study on detrital zircons (McConnell et al. 2009) demonstrates that within the Mweelrea Formation, east-derived sandstones probably originated from along-strike equivalents of the Lough Nafooey Group and the Clew Bay Complex, whilst zircons from south-derived sandstones were probably sourced from the Connemara metagabbro and orthogneiss suite. This implies that Connemara had docked with respect to South Mayo by Sandbian times (460.86–456.35 Ma), a conclusion supported by single crystal $^{40}Ar/^{39}Ar$ muscovite ages (Idleman et al. 2004) which show a rapid influx of mid-Ordovician aged micas at high levels in the Derrylea Formation, coincident with the influx of juvenile metamorphic detritus recorded in the heavy mineral studies (Dewey and Mange 1999). Clift et al. (2009) dated detrital zircons from the Rosroe, Maumtrasma and Derryveeny Formations and reveal a provenance dominated by erosion from the upper levels of the Dalradian Supergroup affected by the Grampian Orogeny which lay to the north-east with a minor proportion (<20%) being contributed by the colliding arc. In summary, current isotopic evidence suggests: a Laurentian provenance for continentally derived sediments and Grampian dates for the juvenile metamorphic detritus within the upper stratigraphic levels of the South Mayo Trough; a mature Laurentian provenance for sediments within Clew Bay Complex, which contain no juvenile metamorphic material (Dewey and Mange 1999); and that Connemara was supplying sediment to the South Mayo Trough by 464 Ma (Darriwillian).

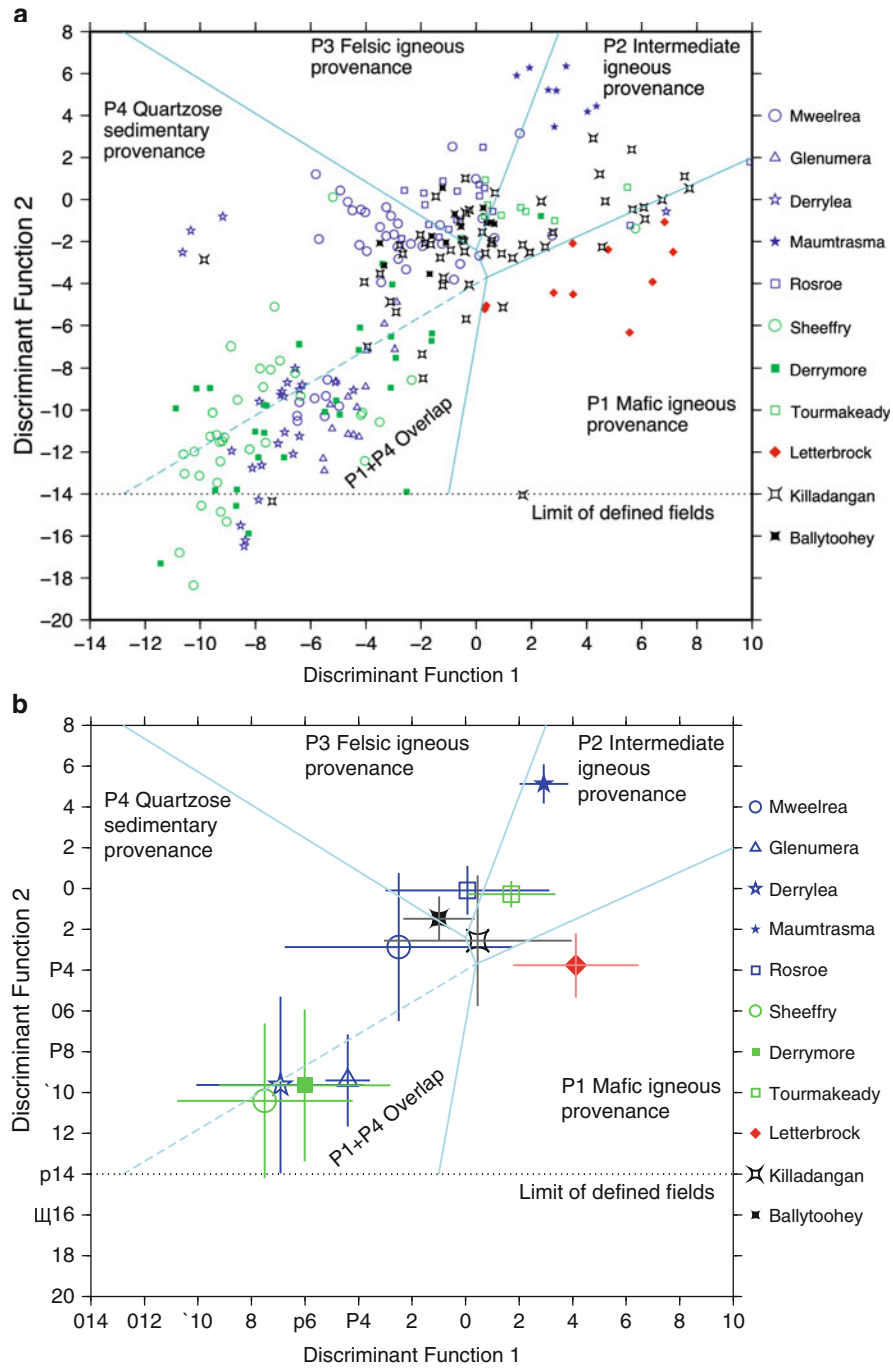

Fig. 13.7 Discriminant plot for sands and shales from the Ordovician of the South Mayo Trough, fields after Roser and Korsch (1988). Plot (**a**) shows all data and plot (**b**) the means for each formation estimated from the compiled data.

13.5.2 The Volcanic Evolution of the South Mayo Trough

13.5.2.1 Field Relationships

The Lough Nafooey Group (Figs. 13.3 and 13.4a) of the south limb succession of the Mweelrea-Partry syncline represents the oldest dated rocks within the South Mayo Trough and comprises, in ascending stratigraphic order: the Bencorragh Formation, the Finny Formation, the Knock Kilbride Formation and the Derry Bay Formation (Ryan et al. 1980). The Bencorragh Formation is a minimum of 850 m thick and comprises well-formed vesicular pillows with some

pillow breccia. There is little interstitial sediment and the vesicle size decreases up section. The overlying Finny Formation is about 500 m in thickness and dominated by andesitic coarse-grained epiclastic breccias interbedded, near the top, with pillow basalts and radiolarian cherts. The Knock Kilbride Formation (~ 800 m) comprises interbedded pillow basalts with chert interstitial fillings and epiclastic andesitic breccias. A shale horizon near the base of this formation yields a graptolite assemblage which indicates a late Tremadoc age, correlating with the *A. victoriae* Biozone in the Cow Head Group in western Newfoundland and Lancefieldian 2 (La2) of Australasia (Williams and Harper 1994) suggesting an age of between 485.15–483.7 Ma. The Derry Bay Formation marks the onset of marine volcaniclastic sandstone deposition, which continued in the south limb succession until the mid-Llanvirn (Darriwillian, 467.94–463.04 Ma). The upper limit for the age of the Lough Nafooey Group is provided by an isolated outcrop yielding a *D. protobifidus* (Chewtonian 1, 476.68–475.44 Ma) assemblage (Dewey et al. 1970b), and the lower limit by an U–Pb secondary ionization mass spectrometry (SIMS) zircon ages of 489.9 ± 3.1 Ma and 487.8 ± 2.3 Ma from a plagiogranite clast in overlying Silurian conglomerates unequivocally derived from the Finny Formation (Chew et al. 2007). The age of the base of the Bencorragh Formation is unknown, but the lack of interstitial sediment suggests a rapid rate of eruption. The Lough Nafooey Group is of anchimetamorphic, probably burial metamorphic grade (Ryan et al. 1980).

The Tourmakeady Volcanic Group (Graham et al. 1989) comprises, in ascending stratigraphic order, the Mount Partry, Tourmakeady and Srah Formations (Figs. 13.3 and 13.4a). It is of low pressure early-diagenetic metamorphic grade (Rice and Williams 2010). The Mount Partry Formation (~ 450 metres) contains *D. protobifidus* graptolitic shales (Chewtonian 1, 476.68–475.44 Ma) near its base, cherts, andesitic breccias and graded and slumped tuffs with abundant clear volcanic quartz detritus. The Tourmakeady Formation (~850 metres) contains a lower sub-volcanic to volcanic rhyo-dacitic body (500–750 metres) overlain by fossiliferous limestones, limestone breccias and tuffs of Castlemaine 1–3 age (475.44–472.36 Ma). A graptolitic shale (Darriwillian 1, 470.54–469.57 Ma) marks the base of the overlying volcaniclastics of the Srah Formation (>130 metres). This group is interpreted as andesitic-dacitic-rhyolitic submarine volcano that developed in deep water with background shale sedimentation with fringing reefs being formed as the structure reached the photic zone (Graham et al. 1989).

Volcanism within the overlying formations of the southern limb succession comprise tuff and ignimbrite bands generally believed to be derived from the south or the east (Fig. 13.4a). All formations contain some primary volcanic detritus (Dewey and Mange 1999; Clift et al. 2009; McConnell et al. 2009). Two several-metre-thick andesitic ignimbrite bands occur within the Rosroe Formation (Archer 1977). Five rhyolitic ignimbrite bands occur within the Mweelrea Formation (Dewey 1963), which range in age from Darriwillian 3, 467.94–463.04 Ma (Skevington and Archer 1971) to Sandbian (Harper et al. 2010), which is equivalent to Gisbornian 1 (460.86–456.35 Ma). Ignimbrite Band 1 is dated at 464.4 ± 3.9 Ma (a concordant U–Pb age on an acicular zircon by Dr Stephen Noble personally communicated to Dewey and Mange (1999)).

The Bohaun Volcanic Group (>1,000 m) of the northern limb succession (Figs. 13.3 and 13.4a) is of unknown age and comprises spilitized massive pillow lavas with jasper lenses and pillow breccias. It is of higher metamorphic grade than other volcanic groups (albite-oligoclase, epidote and chlorite) and bedding is locally inverted. The pillows are interbedded with minor nodular green cherts, jaspers and calcareous shales. It is a probable correlative of the Bencorragh Formation (Clift and Ryan 1994).

The Derrymore to Glenummera Formations of the north limb succession contain 22 tuff bands which are laterally continuous for tens of kilometres and have been derived from the south and east (Stanton 1960; Dewey 1963). These exhibit a variety of textures and many may have had an origin as sea-bed ash flow deposits (Dewey 1963). These tuffs commonly contain angular quartz, albite, calcic oligoclase, and broken glass shards set in a matrix of sericite and volcanic dust. They have been subject to low-grade regional latest Silurian – earliest Devonian (Caledonian) regional metamorphism and are cleaved. The Mweelrea Formation in the northern limb of the syncline also contains five to six silicic ignimbrite bands (bands 3 and 4 anastomose eastwards) which are correlated with those on the southern limb. Tuff bands in the Derrylea Formation may correlate with those in the Rosroe Formation (Archer 1977) . Available palaeontological data suggest that the Tourmakeady Volcanic

Group was broadly synchronous with tuff bands within the lower and middle portions of the Sheeffry Formation (Graham et al. 1989).

In summary, whilst tuff bands higher in the succession are correlated on an individual basis, such precision is not possible for those nearer the base. However, the major eruptive centre at Tourmakeady is coeval with tuff bands within the Sheeffry Formation, the lowest of which, tuff band 2, is over 50 metres in thickness. The correlation between the Lough Nafooey Group and the Bohaun Volcanic Group is based on petrochemical considerations (Clift and Ryan 1994). The volcanism broadly develops from basalt to andesite to rhyolite up section in both successions and the available outcrop on the southern limb suggests that, volumetrically, basalt comprises 59% (range 48–70%), andesite 23% (range 31–15%) and rhyolite-dacite 18% (range 21–15%) of the total primary eruptive deposits (Fig. 13.4c), values comparable with those for the western Pacific intra-oceanic arcs rather than the continental (Andean) arcs (Thorpe 1982). This is consistent with interpretations based on South Mayo geochemistry that the pre-collisional Lough Nafooey Arc was strictly intra-oceanic before approaching the Laurentian margin.

13.5.2.2 Volcanic Geochemistry

The geochemical evolution of the volcanic rocks within the South Mayo Trough is well described in the recent literature (Clift and Ryan 1994; Draut and Clift 2001; Draut et al. 2002, 2004, and Ryan and Williams 2007). This account will briefly review the main findings and seek to integrate results from these various studies, particularly those from the volcanic complexes of the south limb with the tuff bands of the north limb succession. The various plots presented below are intended to complement, not duplicate, those within these publications.

There is a general increase in silica and decrease in Mg and Ti up section (Clift and Ryan 1994; Figs. 13.8a, c) with initial basaltic products being replaced by andesites then dacites and rhyolites. However this is not a simple linear trend and a detailed stratigraphic analysis (Clift and Ryan 1994) shows several cycles with an overall upwards increase. The geochemical affinities for the finer-grained tuffs can be further tested to avoid metamorphic alteration effects (Hastie et al. 2007) using the Th versus Co diagram (Fig. 13.8b), which shows a similar result to that of the total alkalis versus silica (TAS; Fig. 13.8a) plot (Verma et al. 2002). The Tourmakeady Volcanic Group shows a wide range in silica composition similar to that of the broadly coeval tuffs within the Sheeffry Formation although the latter tend to show alkali enrichment (Fig. 13.8a). The succeeding tuffs of the Derrylea and Rosroe Formations are generally andesitic to dacitic in composition. The ignimbrites of the Mweelrea Formations range from a dacitic to rhyolitic composition. The Bohaun Formation pillows show higher average and a more restricted range of magnesium numbers (molar Mg/ molar MgO) and lower TiO2 wt% than those of the Lough Nafooey Group (Fig. 13.8c). Syn-collision volcanic products tend to intermediate magnesium numbers whilst those post-collision have intermediate to low such values (Fig. 13.8c).

Early erupted basalts of both the Bohaun Volcanic Formation and the Lough Nafooey Group show tholeiitic affinities evolving to calc-alkaline affinities up section (Clift and Ryan 1994) (Fig. 13.9a). In the Lough Nafooey Group this change is associated with the eruption of andesites (Ryan et al. 1980). Volcanic rocks with greater than 57% silica (the divide between basaltic andesite and andesite in the TAS diagram, Fig. 13.8a) are of calc-alkaline affinities on the Zr/Y versus Th/Yb plot (Ross and Bedard 2009) (Fig. 13.9b).

All volcanic rocks show the characteristic enrichment in large-ion-lithophile elements and depletion of high-field-strength elements associated with subduction zone volcanism (Fig. 13.10). Tectonic discrimination diagrams for basaltic rocks (Ryan et al. 1980; Clift and Ryan 1994 and Fig. 13.9a) suggest eruption in an island arc setting. The Bohaun Volcanic Formation lavas show depletion in immobile trace elements with respect to the Lough Nafooey Group (Figs. 13.10a and 13.11a); such low levels of immobile trace elements are reminiscent of boninitic chemistries, although these basalts do not have a true boninitic composition. The depleted chemistry and apparently short-lived volcanism with no equivalent to the Finny and Knock Kilbride Formations of the Lough Nafooey Group being preserved, argue for their eruption in a fore-arc setting during the onset of subduction (Clift and Ryan 1994). The syn- and post-collisional felsic and silicic volcanic rocks generally fall within

the volcanic arc field (Fig. 13.12a) of the Rb versus Y+Nb diagram (Pearce et al. 1984) and the active continental margin fields (Fig. 13.12b) of the Yb versus Th/Ta discriminant of Gorton and Schandl (2000) and the Hf–Rb–Ta diagram of Pearce et al. (1984) [Fig. 13.3 in Ryan and Williams (2007)]. The major and trace element geochemistry is, therefore, consistent with volcanism initiating in an oceanic island arc setting and evolving to an active continental margin setting.

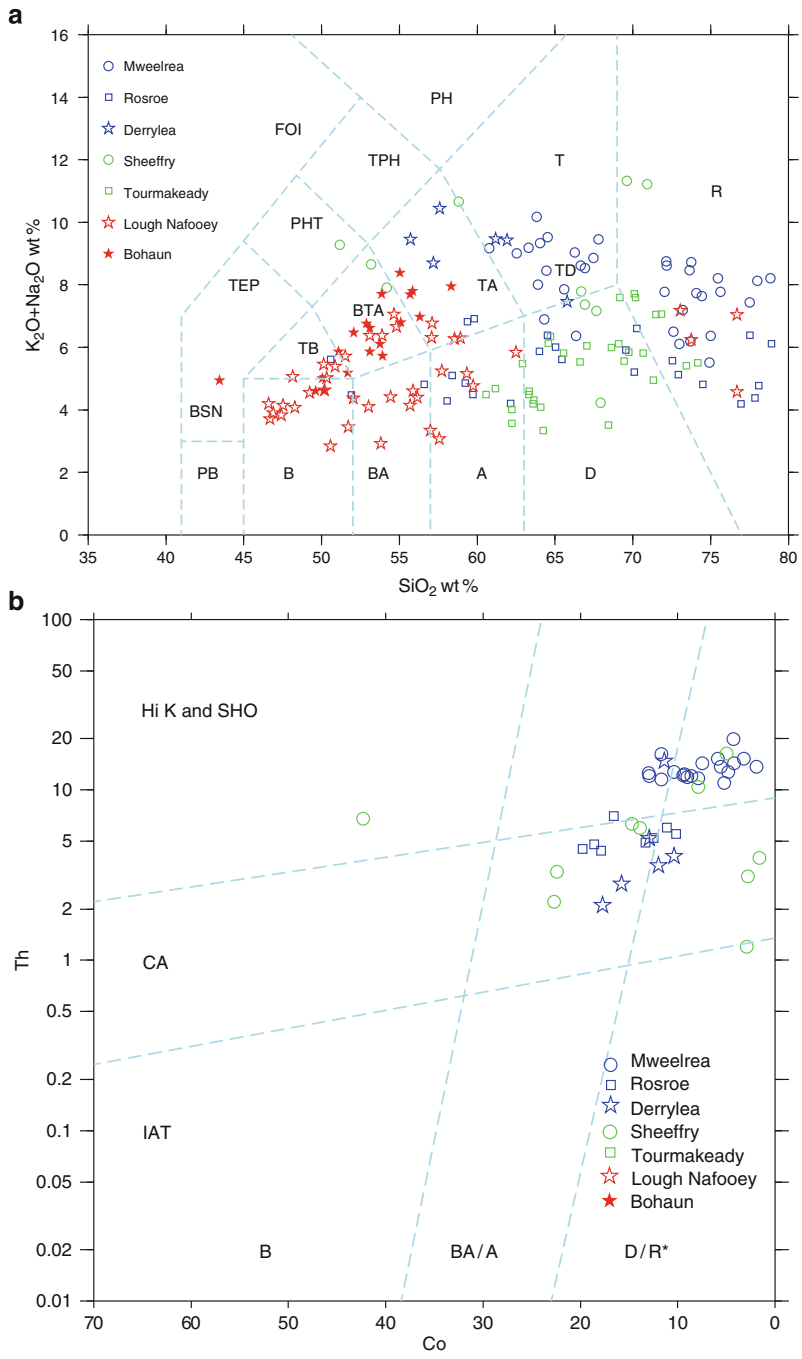

Fig. 13.8 (continued)

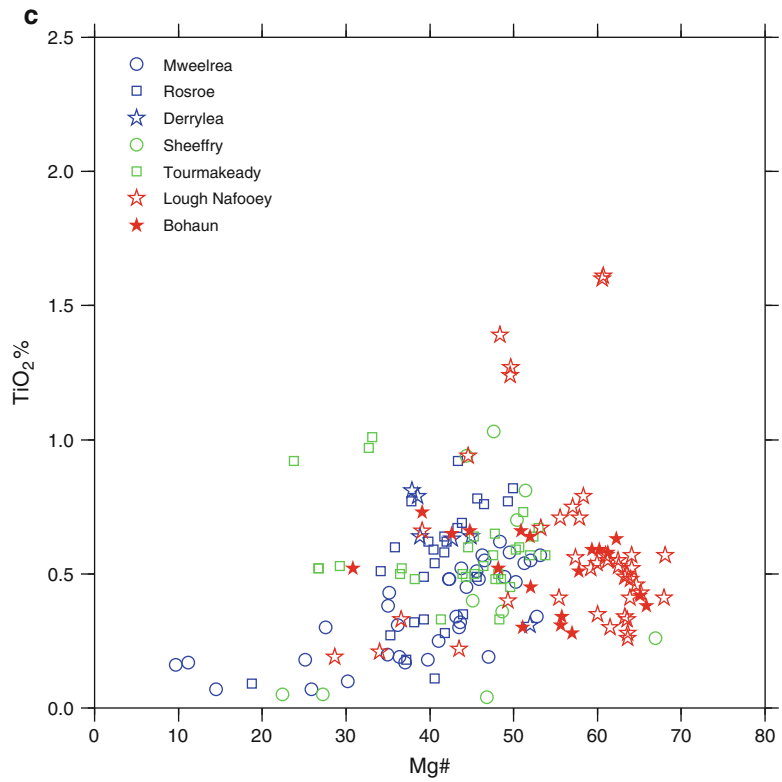

Fig. 13.8 (continued) Discriminant plots showing the variation in composition and affinity for all eruptive products from the Ordovician of the South Mayo Trough. (**a**) Total alkalis versus silica diagram. The fields are after Verma et al. (2002). The following abbreviations are used: *A* Andesite, *B* Basalt, *BA* Basaltic andesite, *BSN* Basanite, *BTA* Basaltic trachyandesite, *D* Dacite, *FOI* Foidite, *PB* Picrobasalt, *PH* Phonolite, *PHT* Phonotephrite, *R* Rhyolite, *T* Trachyte, *TA* Trachyandesite, *TB* Trachybasalt, *TD* Trachydacite, *TEP* Tephrite, *TPH* Tephriphonolite. (**b**) Co versus Th diagram (Hastie et al. 2007). The following abbreviations are used: *A* andesite, *B* basalt, *BA* basaltic-andesite, *CA* Calk-alkaline, *D* dacite, *IAT* Island Arc Tholeiite, *H-K* High K calc-alkaline; R, *SHO* Shoshenite. (**c**) Mg number (molar Mg/Molar MgO) versus TiO2 plot.

Draut and Clift (2001) report that lavas at the base of the Lough Nafooey have a positive $E_{nd(t)}$ consistent with an intra-oceanic arc origin. $E_{Nd(t)}$ values decrease and become negative upwards as light-rare-earth elements (REEs) become more enriched (Fig. 13.11). The Tourmakeady Volcanic Group is also light REE enriched (Fig. 13.11b) and has strongly negative $E_{Nd(t)}$, whilst the Rosroe and Mweelrea Formations show wide scatter of La/Sm and Nb/Zr values, suggesting mixed mantle sources (Fig. 13.2 in Draut and Clift 2001). Chew et al. 2007 report a $E_{Nd(490)}$ value of +0.41 for a plagiogranite boulder probably sourced from the Finny Formation of the Lough Nafooey Group suggesting that old continental crust had begun to be assimilated by this time. Draut and Clift (2001) attribute the decrease in $E_{Nd(t)}$ in the upper portion of the Lough Nafooey Group to Laurentian-derived sediment entering the subduction channel. In a subsequent study, Draut et al. 2004, estimate the proportions of Laurentian-derived melt to be: <1% at the base of the Lough Nafooey Group rising to 2.3–4.7% in the Knock Kilbride Formation and 7.1–21.7% in the Derry Bay Formation; from 25.0 to 28.8% in the Tourmakeady Volcanic Group; and to approximately 14–39% in the Rosroe and Mweelrea Formations. Draut et al. (2004) attribute this to the onset of a "soft" collision during Lough Nafooey times leading to a "hard" collision during the eruption of the Tourmakeady Volcanic Group followed by orogenic collapse and subduction flip resulting in a steady

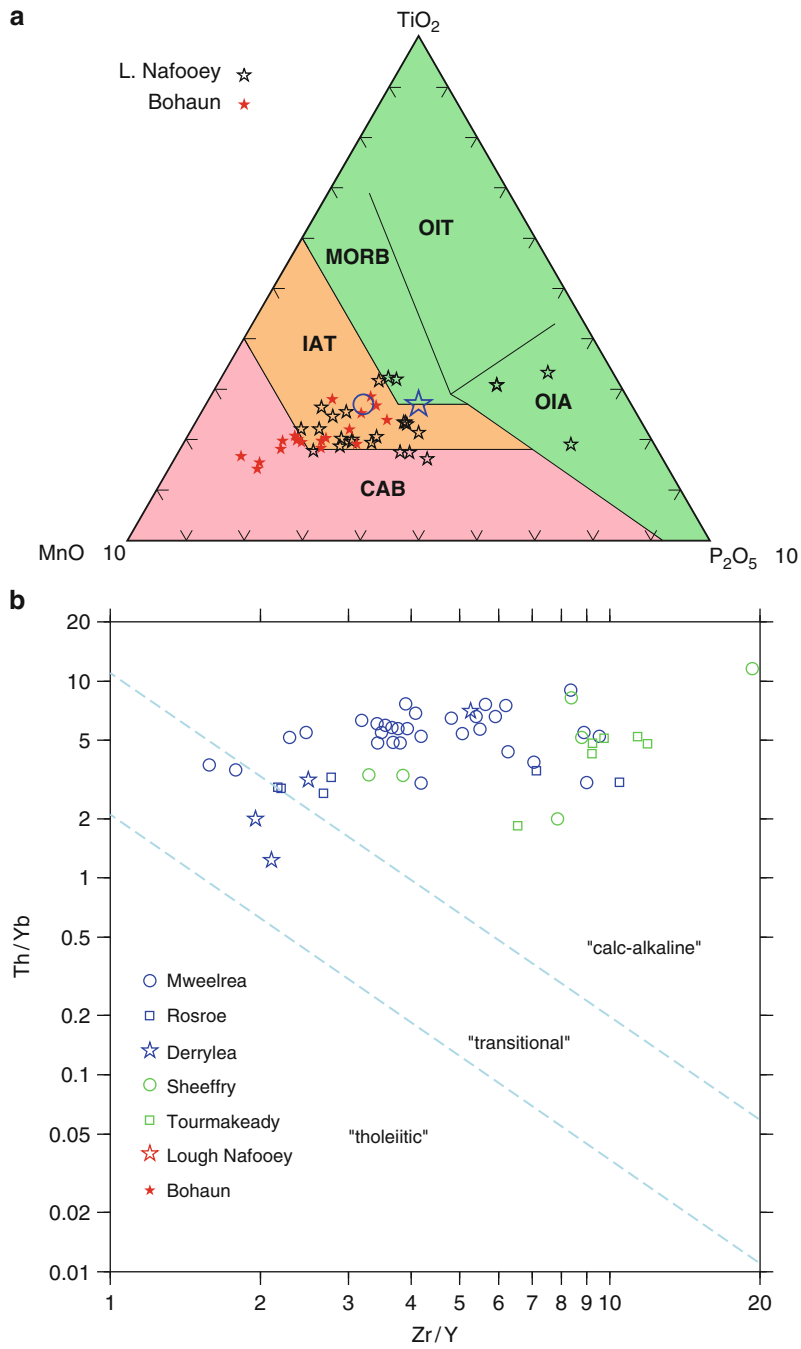

Fig. 13.9 Plots showing the petrological affinities for eruptive products from the Ordovician of the South Mayo Trough. (**a**) Mn-P_2O_5-TiO_2 plot after Mullen (1983) for all basalts (<57% SiO_2): *CA* calk-alkaline basalts, *IAT* island arc tholeiites, *MORB* mid ocean ridge basalt, *OIA* ocean island alkaline basalts, *OIT* ocean island tholeiites. The *large blue circle* represents the mean value for 12 basalts from the Bencorragh Formation and the *blue star* the mean value for 14 basalts from the Knock Kilbride Formation (Ryan et al. 1980). (**b**) Zr/Y versus Th/Yb plot after (Ross and Bedard 2009) for all eruptive products with ≥57% SiO_2.

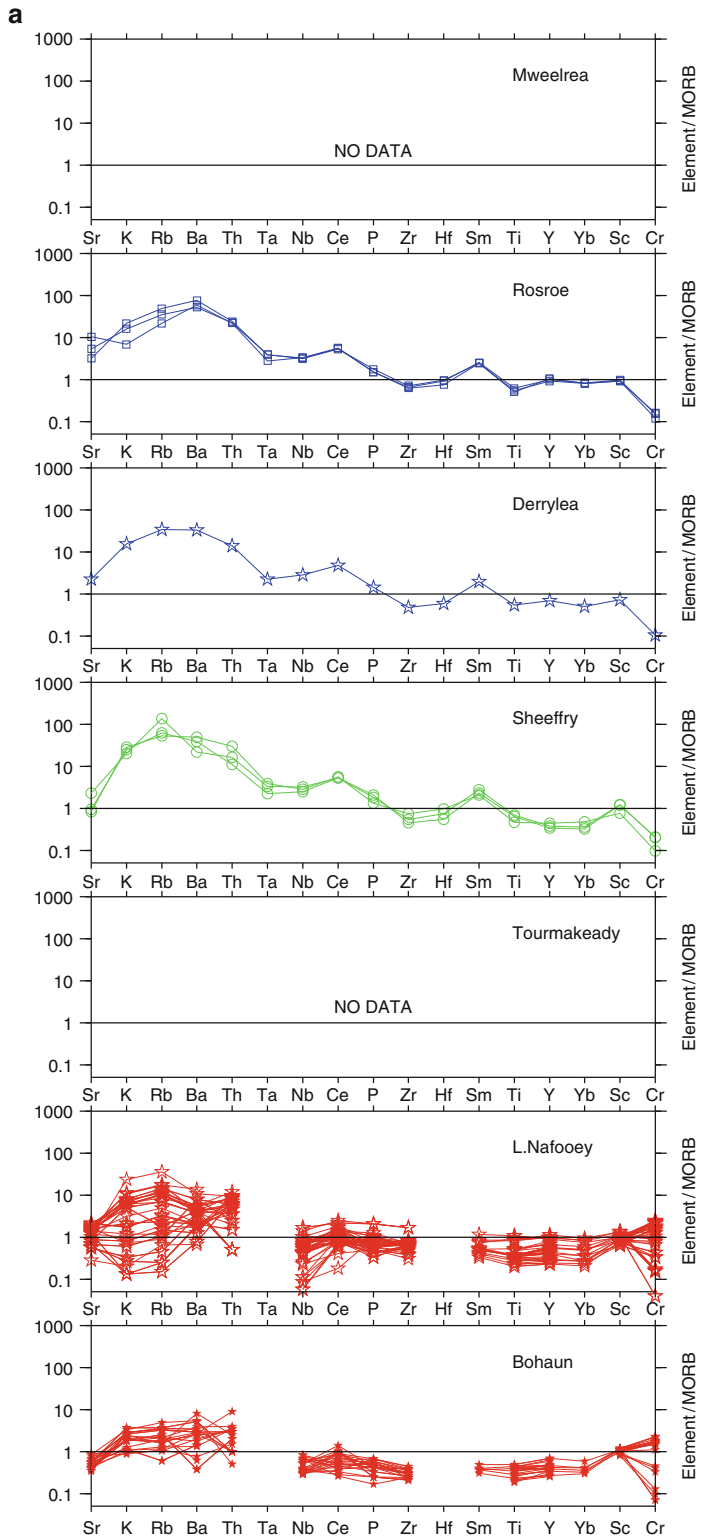

Fig. 13.10 (continued)

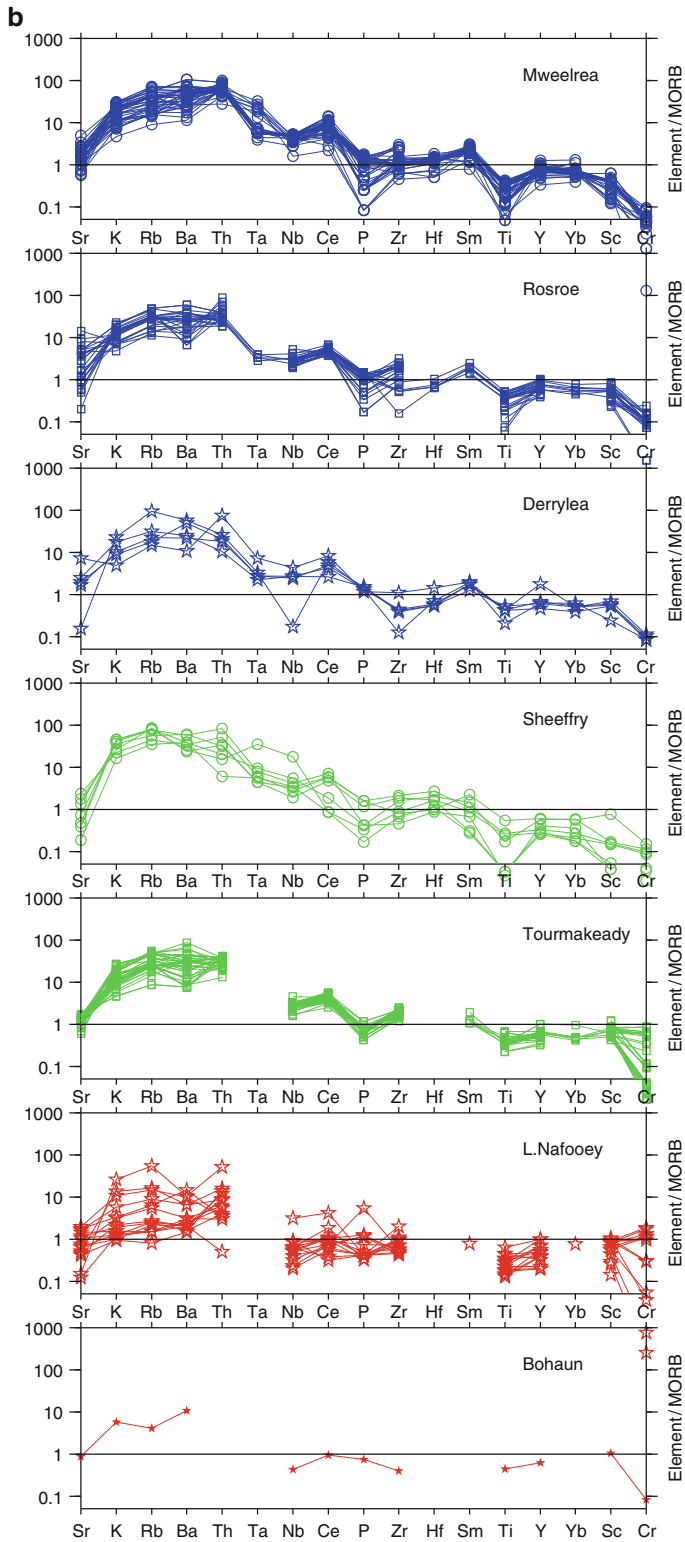

Fig. 13.10 Multi-element variation diagrams after (Pearce et al. 1984) for eruptive products from the Ordovician of the South Mayo Trough. (**a**) Rocks with <57% SiO_2 and (**b**) rocks with ≥57% SiO_2.

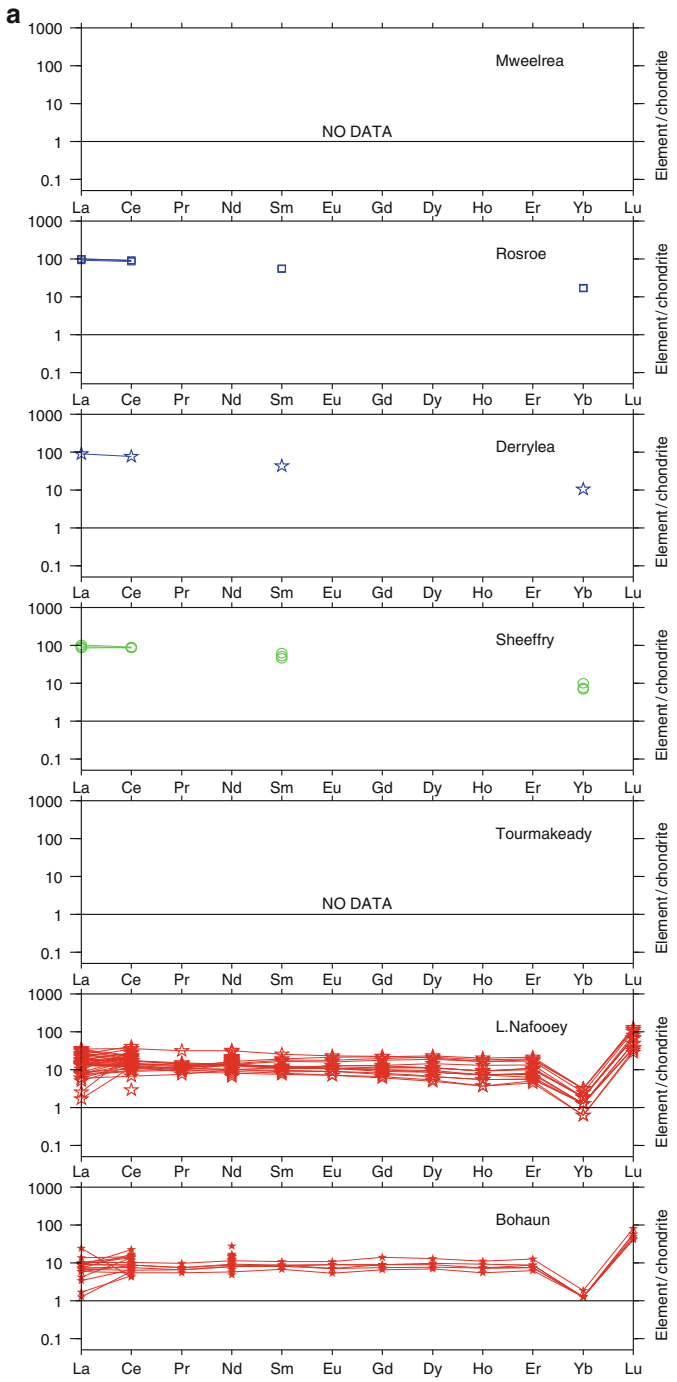

Fig. 13.11 (continued)

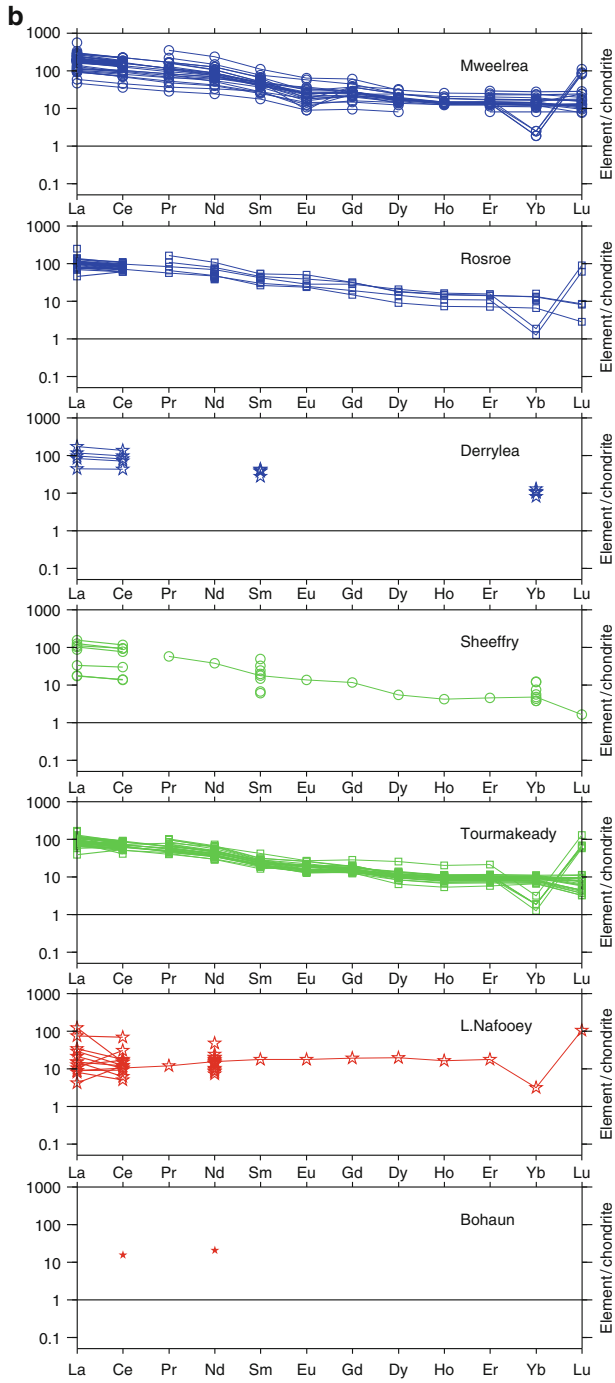

Fig. 13.11 Chondrite normalised rare earth element (REE) plots using the values of McDonough and Sun (1995) for eruptive products from the Ordovician of the South Mayo Trough. (**a**) rocks with <57% SiO_2 and (**b**) rocks with ≥57% SiO_2.

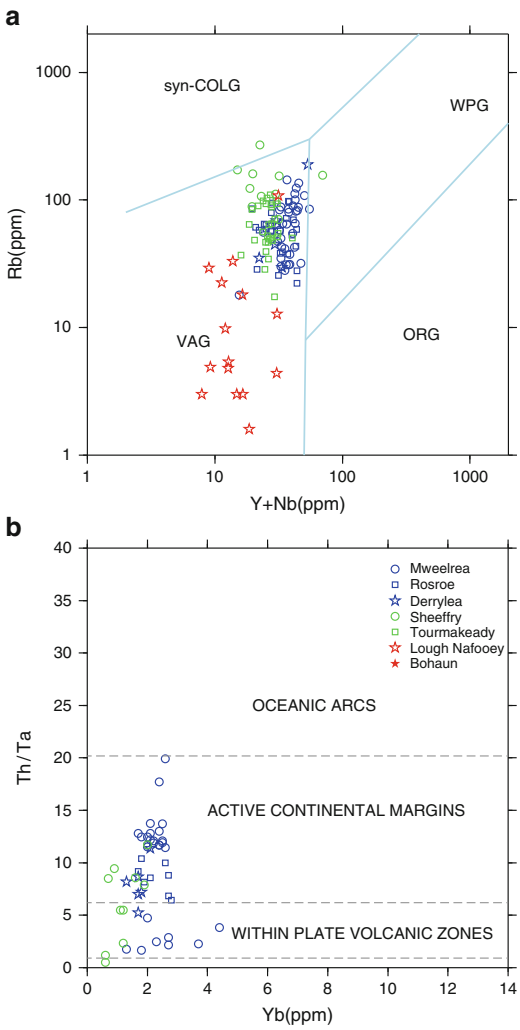

Fig. 13.12 Tectonic discriminant diagrams for eruptive rocks with ≥57% SiO_2. (**a**) Y+Nb versus Rb (Pearce et al. 1984). The following abbreviations are used: *ORG* orogenic granites, *syn-COLG* syn-collision granites, *WPG* within-plate granites, *VAG* volcanic arc granites. (**b**) Yb versus Th/Ta discriminant of Gorton and Schandl (2000). The following abbreviation is used: *WPVZ* within-plate volcanic zones.

state addition of Laurentian-enriched mantled-derived melts to the new active continental margin by Mweelrea (Sandbian) times.

13.6 The Timing and Nature of Events on the Upper and Lower Plates

The detailed structural and metamorphic evolution of Connemara and its relationship to the stratigraphy of South Mayo has been recently reviewed (Clift et al. 2004; Dewey 2005). In summary, The Lough Nafooey Group was erupted within an island arc setting with Dalradian sedimentation still taking place on the Laurentian passive margin situated on the plate that was subducting beneath this arc. The deposition of the Sheeffry Formation was coincident with the eruption of the Tourmakeady Volcanic Group lavas, with their increased components of continentally-derived melt. This was synchronous with the onset of north-verging D1-2 nappes, development of garnet and kyanite , and the development of peak metamorphic pressures (0.6 GPa, Yardley et al. 1987) within Connemara, which is interpreted as the onset of hard collision with the Laurentian margin entering the subduction channel. The Rosroe and Derrylea Formations whose upper levels record the first influx of juvenile metamorphic detritus are coincident with late D2 – early D3 mafic intrusions, peak metamorphic temperatures producing sillimanite, and the onset of exhumation in Connemara, which is attributed to detachment due to buoyancy forces of the subducting slab attached to the Laurentian margin and the onset of subduction flip (Clift et al. 2004). Extensional collapse of the Grampian orogeny would have been facilitated by extension in the newly-formed back-arc. The Mweelrea Formation coincided with D4 uplift in Connemara and is believed to mark the erosional denudation of the Grampian Orogen, which then lay on an active continental margin with South Mayo in the back-arc. Magmatism within Connemara and South Mayo at this time both show high levels of light-rare-earth enrichment indicating a similar mixed mantle source (Draut et al. 2002). Late southwards motion on the Mannin Thrust occurred at about the same time (Sandbian) at the end of sedimentation in South Mayo and may have marked deformation moving into the back-arc.

The relationship between the timing of events in Connemara and South Mayo are shown in Fig. 13.5. Stratigraphic horizons within the South Mayo Trough have been assigned absolute ages by first mapping biostratigraphically-dated horizons to the scale of Sadler et al. (2009) and then assuming a constant rate of deposition for each formation to assign the formation boundaries between dated horizons. Errors in the age assignment are estimated by using maximum and minimum ages for each graptolite zone. Sedimentation rates derived from this analysis are: Sheeffry Formation 0.5 mm/yr (range 0.3–2.6 mm/yr); Rosroe/Derrylea Formations 1.7 mm/yr (lower bound 0.3 mm/yr, upper bound cannot be estimated as this Formation occupies

a single graptolite zone); and Mweelrea Formation 0.3 mm/yr (range 0.07–0.7 mm/yr). The estimated rates for the Sheeffry, Rosroe and Derrylea Formations are not dissimilar with those recorded from around Taiwan within the past few 1,000 years. Huang et al. (2005) report 1.5–9 mm/yr in the Okinawa Trough, rates adjacent to the east coast are 2.8 mm/yr (Gwo and Yu-Chia 1994) and 0.8–2.0 mm/yr (Lee et al. 1993) and up to 10 mm/yr is recorded in the Gaoping Canyon (Huh et al. 2009). This analysis suggests that the Rosroe and Derrylea Formations, although some 1,700 m in thickness, may have been deposited between 469 and 468 Ma. implying, perhaps, that subduction polarity reversal took place over a similar time interval.

In spite of there currently being a high level of consensus for the above model, two problems still remain. First, the timing and sense of emplacement of the docking of Connemara with the South Mayo Trough is difficult to determine. Previous workers have proposed a late Ordovician docking associated with sinistral displacement (Hutton 1987). However, much of this sinistral motion is now attributed to later events (see Dewey and Mange 1999). Recent evidence (McConnell et al. 2009) that southerly-derived high level granite clasts and detrital zircons in the Mweelrea Formation were sourced from Connemara imply that Connemara was outboard of, and supplied coarse detritus to, South Mayo by at least 464 Ma. This is consistent with: the <10 myr. lag-time recorded in detrital micas within the Rosroe, Derrylea and Maumtrasma Formations (Idleman et al. 2004); the ~5 myr. lag-time in zircons from the Maumtrasma Formation (Clift et al. 2009); the fact that Connemara was back-thrust by ~460 Ma over arc rocks which were the same age and composition of those of the Tourmakeady Group (Draut and Clift 2002); and the remarkable coincidence of timing between events in Connemara and South Mayo (Dewey 2005). The marked increase in sedimentation rate during the deposition of the Rosroe, Derrylea and, by implication, the Maumtrasma Formations (Fig. 13.5) and the sudden appearance of relatively high-grade metamorphic detritus (garnet and staurolite) in upper levels of the Rosroe, Derrylea and Maumtrasma Formations (Dewey and Mange 1999) all argue that a rapidly-exhuming metamorphic source area capable of supplying large volumes of coarse detritus lay to the east or south of South Mayo by 468 Ma. This is consistent with the sedimentology of the Rosroe Formation comprising proximal, base of slope submarine fans sourced from the south or east (Archer 1977) and containing significant sand injectites (Archer 1984). Zircon U–Pb provenance studies (Clift et al. 2002, 2009) indicate that Laurentian-derived sediment, mostly sourced from the north and east was being deposited in the South Mayo Trough by Rosroe, Derrylea, Maumtrasma times (~469–468 Ma). Modern Taiwan provides a useful analogy to explain the provenance data. The North Luzon Trough fore-arc basin receives material from the Luzon arc, the Taiwan Orogen and mass-wasting of the accretionary prism (Yen and Lundberg 2006). Perhaps the rapidly exhuming Connemara lay to the east and was supplying sediment into the South Mayo fore-arc via submarine canyon systems by 468 Ma and then docked by Mweelrea times (464 Ma). This would suggest dextral emplacement during the Darriwillian, a conclusion supported by structural analysis (Power et al. 2001).

The second outstanding problem, which is related to the wider issue of arc–continent collision, is the short duration of the Grampian Orogeny (Dewey 2005) which makes it difficult to explain the origin for the heat required to produce the observed Barrovian assemblages, not just in Connemara but over the whole Grampian terrane. Assuming that the main stratigraphic sequence in Connemara, the Argyll Group, were rift phase sediments lying in a thermally mature continental rifts (Harris et al. 1978), it is likely that, prior to deformation, it was buried to between 3 and 5 km . The maximum D2 pressures (0.6 GPa, Yardley et al. 1987) require further burial by about 16 km to 18 km in a period that post-dates the Lough Nafooey Group and lasts until the emplacement of the Connemara gabbros, a maximum of 8 myr. (Fig. 13.5). There would be insufficient time for the crustal thickening model of metamorphic heating (England and Thompson 1984) to achieve the required temperatures (600–800°C, Yardley et al. 1987). Vertical pure shear would require extremely high strain rates (6×10^{-15} s^{-1}–8×10^{-15} s^{-1} for initial burial depths of 5 km and 3 km respectively), it would also produce blueschist facies rather than Barrovian metamorphism (Ryan 2001). Three other possible, and not necessarily mutually exclusive, mechanisms exist: first, that the heat was advected by the mafic intrusions; secondly, that a phase of extension during overall convergence moved colder upper plate rocks onto hotter lower plate rocks along zones generating shear

heat (Viete et al. 2006); and thirdly that the Laurentian margin was buried under a hot ophiolite-arc nappe (Dewey and Shackleton 1984). The first mechanism, although it explains the high temperatures south of the Clifden Steep Belt, cannot explain the 400–620°C temperatures encountered in North Mayo (Yardley et al. 1987), which was not invaded by large volumes of mafic magma. It is difficult to reconcile the extensional model with pre-D2 heating as this involved crustal burial, although it might have contributed significantly to heating during the rapid D3 exhumation. There is geological support for the third model. Connemara was thrust southwards, prior to D4 folding, over the Delaney Dome Formation (Leake et al. 1983) which is of the same age (474.6 ± 5.5 Ma) and chemistry as the Tourmakeady Group (Draut and Clift 2002). This implies that a nappe containing an arc complex lay structural above Connemara prior to D4. Emplacement of an ophiolite-arc nappe would explain rapid initial burial. If the base thrust dipped at 5° and the motion on the thrust was 20 mm/yr, the footwall would have been buried by15 km in 8.6 myr., assuming there was no erosion. If the dip was 15°, such burial would have taken place in 2.9 myr. We, therefore, suggest that Barrovian metamorphism in the Grampian terrains of Ireland was primarily a result of the emplacement of a hot ophiolite-arc nappe; we are currently investigating the thermal consequences of such a model.

13.7 The Topographic Record of Arc–Continent Collision

Perhaps the most remarkable aspect of the geology of South Mayo is the suppression of topography and continued sedimentation in the fore-arc basin during and after arc–continent collision that allowed the South Mayo Trough to record this process and to be subsequently preserved. Many factors could contribute to this. Firstly, the arc could bulldoze its way into the continental margin, but a concave, not a convex (Mac Niocaill et al. 1998) orocline (Fig. 13.1a) would be expected. Secondly, the high density of the subducting slab, if it were a volcanic margin, would have depressed topography during arc–continent collision by approximately the observed amount (Ryan 2008). Thirdly, the high density of an obducting ophiolite-arc nappe would have depressed topography. Indeed, even some of the sediments in the South Mayo Trough with their high serpentine and chromite contents have densities above 3,000 kg m^{-3}. Fourthly, the rapid reversal of subduction polarity, possible in as little as 1 myr. (see above), would have provided a free face to the south of the system which would have facilitated extensional collapse and, therefore, the preservation of structurally higher part of the system (Clift et al. 2004). Fifthly, mid-Ordovician sea-levels for Laurentia were between 250 m (Haq et al. 1987) and 500 m (Wyatt 1995) above present levels , this would have required between 10 and 20% greater positive buoyancy forces to elevate the crust to sea level approximately 2.90–3.15 km, rather than the 2.65 km required at present, above the level of the asthenosphere at the mid oceanic ridges. Finally, loading of the lithosphere by a thickening arc can cause subsidence in arc-related basins (Waltham et al. 2008). The elastic thickness of the continental margin will control this effect during collision. There is no record of a Grampian foreland basin in Ireland, suggesting a low effective elastic thickness for the Laurentian lithosphere in this region (Ryan 2008); this would facilitate the preservation of a narrow, deep basin with relatively dense fill such as the South Mayo Trough.

13.8 Concluding Remarks

Brown and Huang (2009) argue that ancient sites permit study of the third and fourth dimensions of arc-continent orogens which can aid our understanding of how plate tectonics works, the process of crustal growth and the formation of mineral wealth. The Ordovician of western Ireland is a good example. The time constraints are good (typically to about one graptolite zone or ±1.0 Ma), coeval processes in the upper and lower plates can be studied and there is excellent field access. Ancient collision zones such as western Ireland allow access to sampling the middle and (if available) lower crust in a way that dredging/sampling from ships at modern active arcs does not. Perhaps the most powerful illustration of the value of fossil terrains is the fact that the influx of abundant juvenile metamorphic detritus is detected on a single bedding plane in both north and south limb successions of the South Mayo Trough (Dewey and Mange

1999). Such precision would be impossible in geophysically imaged sections in modern environments.

Acknowledgements We would like to thank Maria A. Mange for help with drafting Fig. 13.6. and Amy E. Draut and Peter D. Clift for supplying original geochemical data files used in preparing Figs. 13.10 and 13.11.

References

Alsop GI, Hutton DHW (1993) Caledonian extension in the north Irish Dalradian: implications for the timing and activation of gravity collapse. J Geol Soc 150(1):33–36

Archer JB (1977) Llanvirn stratigraphy of the Galway-Mayo border area, western Ireland. Geol J 12:77–98

Archer JB (1984) Clastic intrusions in deep-sea fan deposits of the Rosroe Formation, Lower Ordovician, western Ireland. J Sediment Petrol 54:1197–1205

Brown D, Huang CY (2009) Arc-continent collision. Tectonophysics 479(1–2):1–3

Brown C, Whelan J (1995) Terrane boundaries in Ireland inferred from the Irish Magnetotelluric Profile and other geophysical data. J Geol Soc 152(3):523–534

Chew DM (2003) Structural and stratigraphic relationships across the continuation of the Highland Boundary Fault in western Ireland. Geol Mag 140(1):73–85

Chew DM, Daly JS, Page LM, Kennedy MJ (2003) Grampian orogenesis and the development of blueschist-facies metamorphism in western Ireland. J Geol Soc 160(6):911–924

Chew DM, Graham JR, Whitehouse MJ (2007) U-Pb zircon geochronology of plagiogranites from the Lough Nafooey (= Midland Valley) arc in western Ireland: constraints on the onset of the Grampian orogeny. J Geol Soc 164(4):747–750

Clift PD, Ryan PD (1994) Geochemical evolution of an Ordovician island arc, South Mayo, Ireland. J Geol Soc 151(2):329–342

Clift PD, Dewey JF, Draut AE, Chew DM, Mange M, Ryan PD (2004) Rapid tectonic exhumation, detachment faulting and orogenic collapse in the Caledonides of western Ireland. Tectonophysics 384:91–113

Clift PD, Carter A, Draut AE, Long HV, Chew DM, Schouten HA (2009) Detrital U/Pb zircon dating of lower Ordovician syn-arc-continent collision conglomerates in the Irish Caledonides. In: Brown D, Huang CY (eds) Tectonophysics 479: 165–174

Condon DJ, Prave AR (2000) Two from Donegal: Neoproterozoic glacial episodes on the northeast margin of Laurentia. Geology 28(10):951–954

Cooper MJ, Crowley QG, Rushton AWA (2008) New age constraints for the Ordovician Tyrone Volcanic Group, Northern Ireland. J Geol Soc 165(1):333–339

Cox W (2005) Finding gold in Ireland: past, present and future. Extractive industry in Ireland, Newsletter 146:1–3

Daly JS (1996) Pre-Caledonian history of the Annagh gneiss complex, north-western Ireland, and correlation with Laurentia-Baltica. Ir J Earth Sci 15:5–18

Daly JS (2001) The Precambrian. In: Holland G (ed) The geology of Ireland, 2nd edn. Scottish Academic Press, Edinburgh, pp 7–44

Daly JS, Flowerdew MJ (2005) Grampian and late Grenville events recorded by mineral geochronology near a basement-cover contact in north Mayo, Ireland. J Geol Soc 162(1): 163–174

Dewey JF (1963) The lower Palaeozoic stratigraphy of central Murrisk, County Mayo, Ireland, and the evolution of the south Mayo Trough. Q J Geol Soc Lond 119:313–344

Dewey JF (2005) Orogeny can be very short. Proc Natl Acad Sci USA 102(43):15286–15293

Dewey J, Mange M (1999) Petrography of Ordovician and Silurian sediments in the western Irish Caledonides: tracers of a short-lived Ordovician continent-arc collision orogeny and the evolution of the Laurentian Appalachian-Caledonian margin. In: MacNiocaill C, Ryan PD (eds) Continental tectonics, vol 164. Geological Society London Special Publications, London, pp 55–107

Dewey JF, Ryan PD (1990) The Ordovician evolution of the South Mayo Trough, western Ireland. Tectonics 9(4): 887–901

Dewey JF, Shackleton RM (1984) A model for the evolution of the Grampian tract in the early Caledonides and Appalachians. Nature (Lond) 312:115–121

Dewey JF, McKerrow WS, Moorbath S (1970a) The relationship between isotopic ages, uplift and sedimentation during Ordovician times in western Ireland. Scot J Geol 6(2): 133–145

Dewey JF, Rickards RB, Skevington D (1970b) New light on the age of Dalradian deformation and metamorphism in western Ireland. Norsk Geologisk Tidsskrift. Supplement 50(1):19–44

Draut AE, Clift PD (2001) Geochemical evolution of arc magmatism during arc-continent collision, South Mayo, Ireland. Geology 29(6):543–546

Draut AE, Clift PD (2002) The origin and significance of the Delaney Dome Formation, Connemara, Ireland. J Geol Soc 159(1):95–103

Draut AE, Clift PD, Hannigan RE, Layne G, Shimizu N (2002) A model for continental crust genesis by arc accretion; rare earth element evidence from the Irish Caledonides. Earth Planet Sci Lett 203(3–4):861–877

Draut AE, Clift PD, Chew DM, Cooper MJ, Taylor RN, Hannigan RE (2004) Laurentian crustal recycling in the Ordovician Grampian Orogeny: Nd isotopic evidence from western Ireland. Geol Mag 141(2):195–207

Draut AE, Clift PD, Amato JM, Blusztajn J, Schouten H (2009) Arc-continent collision and the formation of continental crust – a new geochemical and isotopic record from the Ordovician Tyrone Igneous Complex, Ireland. J Geol Soc Lond 166:485–500

England PC, Thompson AB (1984) Pressure-temperature-time paths of regional metamorphism, I. Heat transfer during the evolution of regions of thickened continental crust. J Petrol 25(4):894–928

Ffrench GD, Williams DM (1984) The sedimentology of the South Connemara Group, western Ireland; a possible Ordovician trench-fill sequence. Geol Mag 121(5):505–514

Flowerdew MJ, Daly JS, Whitehouse MJ (2005) 470 Ma granitoid magmatism associated with the Grampian Orogeny in the Slishwood Division, NW Ireland. J Geol Soc Lond 162: 563–575

Flowerdew MJ, Chew DM, Daly JS, Millar IL (2009) Hidden Archaean and Palaeoproterozoic crust in NW Ireland?

Evidence from zircon Hf isotopic data from granitoid intrusions. Geol Mag 146(6):903–916
Friedrich AM (1998) 40Ar/39Ar and U-Pb geochronological constraints on the thermal and tectonic evolution of the Connemara Caledonides, Doctoral Thesis. Department of Earth, Atmospheric and Planetary Sciences, Massachusetts Institute of Technology
Friedrich AM, Bowring SA, Martin MW, Hodges KV (1999a) Short-lived continental magmatic arc at Connemara, western Irish Caledonides: implications for the age of the Grampian orogeny. Geology 27:27–30
Friedrich AM, Hodges KV, Bowring SA, Martin MW (1999b) Geochronological constraints on the magmatic, metamorphic and thermal evolution of the Connemara Caledonides, western Ireland. J Geol Soc 156(6):1217–1230
Gorton MP, Schandl ES (2000) From continents to island arcs: a geochemical index of tectonic setting for arc-related and within-plate felsic to intermediate volcanic rocks. Can Mineralog 38(5):1065–1073
Graham JR, Leake BE, Ryan PD (1989) The geology of South Mayo, western Ireland. Scottish Academic Press, Edinburgh
Graham JR, Wrafter JP, Daly JS, Menuge JF (1991) A local source for the Ordovician Derryveeny Formation, western Ireland; implications for the Connemara Dalradian. In: Morton AC, Todd SP, Haughton PDW (eds) vol 57. Geological Society Special Publications, pp 199–213
Gray JR, Yardley B (1979) A Caledonian blueschist from the Irish Dalradian. Nature 278:736–737
Gromet LP, Dymek RF, Haskin LA, Korotev RL (1984) The "North American shale composite"; its compilation, major and trace element characteristics. Geochim Cosmochim Acta 48(12):2469–2482
Gwo W, Yu-Chia C (1994) Sedimentation rates on the continental slope off eastern Taiwan. Mar Geol 119(1–2):99–109
Haq B, Hardenbol J, Vail P (1987) "Chronology of fluctuating sea levels since the Triassic". Science 235(4793):1156–1167
Harkin J, Williams DM, Menuge JF, Daly JS (1996) Turbidites from the Clew Bay Complex, Ireland; provenance based on petrography, geochemistry and crustal residence values. Geol J 31(4):379–388
Harper DAT, Parkes MA (2000) Terranes in the British and Irish Ordovician: a revised correlation of Ordovician Rocks in the British Isles. Geol Soc Lond Spec Rep 24:30–40
Harper DAT, Parkes MA, McConnell BJ (2010) Late Ordovician (Sandbian) brachiopods from the Mweelrea Formation, South Mayo, western Ireland: stratigraphic and tectonic implication. Geol J 45(4):445–450
Harris AL, Baldwin CT, Bradbury HJ, Johnson HD, Smith RA (1978) Ensialic basin sedimentation: the Dalradian Supergroup. In: Bowes DR, Leake BE (eds) Crustal evolution in northwest Britain and adjacent regions. Special Issue Geological Journal, 10:115–138
Harris DHM (1995) Caledonian transpressional terrane accretion along the Laurentian margin in Co. Mayo, Ireland. J Geol Soc 152(5):797–806
Hastie AR, Kerr AC, Pearce JA, Mitchell SF (2007) Classification of altered volcanic island arc rocks using immobile trace elements: development of the Th Co discrimination diagram. J Petrol 48(12):2341
Huang C-Y, Chiu Y-L, Meixum Z (2005) Core description and a preliminarily sedimentology study of site 1202D, Leg 195, in the southern Okinawa Trough. Terr Atmos Oceanic Sci 16(1):19–44
Huh C, Lin H, Lin S, Huang Y (2009) Modern accumulation rates and a budget of sediment off the Gaoping (Kaoping) River, SW Taiwan: a tidal and flood depositional environment around a submarine canyon. J Mar Syst 76(4):405–416
Hutton DHW (1987) Strike-slip terranes and a model for the evolution of the British and Irish Caledonides. Geol Mag 124(5):405–425
Idleman BD, Dewey JF, Mange MA, Anonymous (2004) Single-crystal 40 Ar/ 39 Ar geochronology of detrital muscovite from the south Mayo Trough, western Ireland. Abstr Programs – Geol Soc Am 36(5):504
Kay SM, Godoy E, Kurtz A (2005) Episodic arc migration, crustal thickening, subduction erosion, and magmatism in the south-central Andes. Geol Soc Am Bull 117(1–2):67–88
Klemperer SL, Ryan PD, Snyder DB (1991) A deep seismic reflection transect across the Irish Caledonides. J Geol Soc 148(1):149–164
Leake BE (1986) The geology of SW Connemara, Ireland: a fold and thrust Dalradian and metagabbroic-gneiss complex. J Geol Soc 143(2):221–236
Leake BE (1989) The metagabbros, orthogneisses and paragneisses of the Connemara complex, western Ireland. J Geol Soc 146(4):575–596
Leake BE, Tanner PWG, Singh D, Halliday AN (1983) Major southward thrusting of the Dalradian rocks of Connemara, western Ireland. Nature (Lond) 305(5931):210–213
Lee T, You C, Liu T (1993) Model-dependent ^{10}Be sedimentation rates for the Taiwan Strait and their tectonic significance. Geology 21(5):423–426
Liu Z, Shouting T, Colin C, Liu JT, Huang C, Selvaraj K, Chen CA, Yulong Z, Siringan FP, Boulay S, Zhong C (2008) Detrital fine-grained sediment contribution from Taiwan to the northern South China Sea and its relation to regional ocean circulation. Mar Geol 255(3–4):149–155
Lowe C, Jacob AWB (1989) A north-south seismic profile across the Caledonian suture zone in Ireland. Tectonophysics 168(4):297–318
Mac Niocaill C, Smethurst MA, Ryan PD (1998) Oroclinal bending in the Caledonides of western Ireland: a mid-Palaeozoic feature controlled by a pre-existing structural grain. In: Morris A, Anderson MW (eds) Tectonophysics 299(1–3): 31–47
Max MD, Riddihough RP (1975) Continuation of the Highland Boundary fault in Ireland. Geology 3(4):206–210
Max MD, Ryan PD, Inamdar DD (1983) A magnetic deep structural geology interpretation of Ireland. Tectonics 2(5): 431–451
McConnell B, Riggs N, Crowley QG (2009) Detrital zircon provenance and Ordovician terrane amalgamation, western Ireland. J Geol Soc 166(3):473–484
McDonough WF, Sun S-S (1995) The composition of the earth. Chem Geol 120:223–253
McManus J (1972) The stratigraphy and structure of the lower Palaeozoic rocks of eastern Murrisk, County Mayo. Proc R Ir Acad B 72:307–333
Menuge JF, Williams DM, O'Connor PD (1995) Silurian turbidites used to reconstruct a volcanic terrain and its Mesoproterozoic basement in the Irish Caledonides. J Geol Soc 152(2):269–278

Mitchell A, McKerrow WS (1975) Analogous evolution of the Burma Orogen and the Scottish Caledonides. Geol Soc Am Bull 86(3):305–315

Mullen ED (1983) MnO/TiO2/P2O5: a minor element discriminant for basaltic rocks of oceanic environments and its implications for petrogenesis. Earth Planet Sci Lett 62:53–62

Murphy FC, Anderson TB, Daly JS, Gallagher V, Graham JR, Harper DAT, Johnston JD, Kennan PS, Kennedy MJ, Long CB, Morris JH, O'Keeffe WG, Parkes M, Ryan PD, Sloan RJ (1991) An appraisal of Caledonian suspect terranes in Ireland. Ir J Earth Sci 11:11–41

Parnell J, Earls G, Wilkinson JJ, Hutton DHW, Boyce AJ, Fallick AE, Ellam RM, Gleeson SA, Moles NR, Carey PF, Legg I, Carey PF (2000) Regional fluid flow and gold mineralization in the Dalradian of the Sperrin Mountains, northern Ireland. Econ Geol 95(7):1389–1416

Paskevicius J (2007) Correlation of the Ordovician regional stages of the Baltic palaeobasin with new global stages. Geologija – Vilniaus Universitetas 57:30–36

Pearce JA, Harris NBW, Tindle AG (1984) Trace element discrimination diagrams for the tectonic interpretation of granitic rocks. J Petrol 25(4):956–983

Power SE, Ryan PD, Feely M (2001) Fluid inclusion studies on the late structural history of the Connemara Dalradian, western Ireland. Abstr Programs Geol Soc Am 33(6):448

Pudsey CJ (1984a) Ordovician stratigraphy and sedimentology of the South Mayo Inlier. J Earth Sci (Dublin) 6(1):15–45

Pudsey CJ (1984b) Fluvial to marine transition in the Ordovician of Ireland; a humid-region fan-delta? Geol J 19(2): 143–172

Rice AHN, Williams DM (2010) Caledonian strike-slip terrane accretion in W. Ireland: insights from very low-grade metamorphism (illite-chlorite crystallinity and b0 parameter). Geol Mag 147(2):281–298

Roser BP, Korsch RJ (1988) Provenance signatures of sandstone-mudstone suites determined using discriminant function analysis of major-element data. Chem Geol 67:119–139

Ross PS, Bedard JH (2009) Magmatic affinity of modern and ancient subalkaline volcanic rocks determined from trace-element discriminant diagrams. Can J Earth Sci 46:823–839

Ryan PD (2001) The role of deep basement during continent-continent collision; a review. In: Miller JA, Holdsworth RE, Buick IS, Hand M (eds) vol 184. Geological Society Special Publications, pp 39–55

Ryan KM, Williams DM (2007) Testing the reliability of discrimination diagrams for determining the tectonic depositional environment of ancient sedimentary basins. Chem Geol 242(1–2):103–125

Ryan PD (2008) Preservation of fore-arc basins during island arc-continent collision; some insights from the Ordovician of western Ireland. In: Draut AE, Clift PD, Scholl DW (eds) vol 36. Geological Society of America Special Paper, pp 1–9

Ryan PD, Archer JB (1978) The Lough Nafooey fault: a Taconic structure in western Ireland. Geol Surv Ireland Bull 2:255–264

Ryan PD, Dewey JF (1991) A geological and tectonic cross-section of the Caledonides of western Ireland. J Geol Soc 148(1):173–180

Ryan PD, Dewey JF (2004) The South Connemara Group reinterpreted; a subduction-accretion complex in the Caledonides of Galway Bay, western Ireland. J Geodyn 37(3–5): 513–529

Ryan PD, Floyd PA, Archer JB (1980) The stratigraphy and petrochemistry of the Lough Nafooey Group (Tremadocian), western Ireland. J Geol Soc 137(4):443–458

Ryan PD, Max MD, Kelly T (1983a) The petrochemistry of the basic volcanic rocks of the South Connemara Group (Ordovician), western Ireland. Geol Mag 120(2):141–152

Ryan PD, Sawal VK, Rowlands AS (1983b) Ophiolitic melange separates ortho- and para-tectonic Caledonides in western Ireland. Nature (Lond) 302(5903):50–52

Ryan PD, Stillman CJ, Allen M, Pow S (1995) Terrane geochemistry contrasts across the Iapetus Suture in Ireland. Geol Mag 132(5):581–597

Sadler PM, Cooper RA, Melchin M (2009) High-resolution, early Paleozoic (Ordovician-Silurian) time scales. Geol Soc Am Bull 121(5–6):887–906

Skevington D, Archer JB (1971) A review of the Ordovician graptolite faunas of the west of Ireland. Ir Nat J 17(3):70–78

Soper NJ, Ryan PD, Dewey JF (1999) Age of the Grampian orogeny in Scotland and Ireland. J Geol Soc 156(6): 1231–1236

Stanton WI (1960) The lower Palaeozoic rocks of south-west Murrisk, Ireland. Q J Geol Soc Lond 116:269–296

Strachan RA, Holdsworth RE (2000) Late Neoproterozoic (<750 Ma) to Early Ordovician passive margin sedimentation along the Laurentian margin of Iapetus. In: Woodcock NH, Strachan RA (eds) Geological history of Britain and Ireland. Blackwell, London, pp 73–87

Thorpe RS (ed) (1982) Andesites; orogenic andesites and related rocks. Wiley, Chichester, UK, p 724

van Staal CR, Dewey JF, Mac Niocaill C, McKerrow WS (1998) The Cambrian-Silurian tectonic evolution of the Northern Appalachians and British Caledonides; history of a complex, west and southwest Pacific-type segment of Iapetus. In: Blundell DJ, Scott AC (eds) vol 199. Geological Society Special Publications, pp 199–242

Verma SP, Torres-Alvarado IS, Sotelo-Rodriguez ZT (2002) SINCLAS; standard igneous norm and volcanic rock classification system. Comput Geosci 28:711–715

Viete DR, Richards SW, Lister GS, Anonymous (2006) Timescales and heat sources for Barrovian regional metamorphism. Geochim Cosmochim Acta 70(185): A672

Waltham D, Hall R, Smyth HR, Ebinger CJ (2008) Basin formation by volcanic arc loading. In: Draut AE, Clift PD, Scholl DW (eds) vol 436. Geological Society of America Special Paper, pp 11–26

Williams DM, Harper DAT (1991) End-Silurian modifications of Ordovician terranes in western Ireland. J Geol Soc 148 (1):165–171

Williams SH, Harper D (1994) Late Tremadoc Graptolites from the Lough Nafooey Group, South Mayo, Western Ireland. Ir J Earth Sci 13:107–111

Williams DM, O'Connor PJ, Menuge JF (1992) Silurian turbidite provenance and the closure of Iapetus. J Geol Soc 149 (Part 3):349–357

Williams DM, Harkin J, Higgs AK (1996) Implications of new microfloral evidence from the Clew Bay Complex for Silurian relationships in the western Irish Caledonides. J Geol Soc 153(5):771–777

Wrafter JP, Graham JR (1989) Short Paper: Ophiolitic detritus in the Ordovician sediments of South Mayo, Ireland. J Geol Soc 146(2):213–215

Wyatt AR (1995) Late Ordovician extinctions and sea-level change. J Geol Soc 152(6):899–902

Yardley BWD (1976) Deformation and metamorphism of Dalradian rocks and the evolution of the Connemara Cordillera. J Geol Soc 132(5):521–542

Yardley BWD, Barber JP, Gray JR (1987) The metamorphism of the Dalradian rocks of western Ireland and its relation to tectonic setting. In: Oxburgh ER, Yardley BWD, England PC (eds) Philosophical Transactions of the Royal Society of London, Series A: Mathematical and Physical Sciences 321(1557): 243–270

Yen JY, Lundberg N (2006) Sediment compositions in offshore southern Taiwan and their relations to the source rocks in modern arc-continent collision zone. Mar Geol 225(1–4):247–263

Chapter 14
Multiple Arc Development in the Paleoproterozoic Wopmay Orogen, Northwest Canada

F.A. Cook

14.1 Introduction

14.1.1 General

The Paleoproterozoic Wopmay orogen is located in the northwestern Canadian Shield between the western boundary of the Archean Slave craton and the easternmost overlapping Paleozoic rocks of the Western Canada Sedimentary basin (Figs. 14.1 and 14.2). As is common in modern orogens, and particularly those that form between arcs and continents, the lithotectonic belts of the Wopmay Orogen exhibit a linear arrangement that is parallel, or subparallel, to the ancient continental margin upon which it was built. In this case, the exposed part of the orogen strikes north–south for a distance of ~500 km and has an east–west width of ~250 km. However, as noted in a number of studies and described further below, the Wopmay Orogen extends westward and southward beneath the Phanerozoic strata of the Western Canada Sedimentary Basin where it can be tracked by distinctive signatures on potential field maps supplemented by drill hole data. The regional belt-like domains are illustrated in Fig. 14.1. As a result, the orogen is believed to have a geographic extent of at least 1,000 km north–south and 500 km east–west.

The Wopmay Orogen formed between 1.89 and 1.84 Ga and is interpreted to have evolved from the accretion of island arcs to a passive margin (Coronation margin, formerly the Coronation geoscyncline) on the western side of the Slave craton. Most of the deformation and metamorphism took place during the Calderian orogeny between about 1.88 and 1.87 Ga (e.g., Hildebrand et al. 2010). The products of these events have most of the geological earmarks of arc collisions observed in the modern world and were therefore interpreted by Hoffman (1980) to have been the result of plate tectonic processes. Since then, a great deal of research has refined the timing, stratigraphic relationships, structural variations, and lithospheric geometry of various components of the orogen, nearly all of which have strengthened the basic notion that the Wopmay Orogen is a product of lithospheric plate interactions that were analogous to, if not identical to, the processes that are operating on the Earth today.

Accordingly, the characteristics of the arc–margin and arc–arc interactions that are observed in the orogen provide a window into processes that were active during the Paleoproterozoic. Additionally, the similarity of the products between the Wopmay Orogen and modern orogens may be used as a predictive tool for enhancing or extending uncertain structural and or stratigraphic trends, for interpreting missing (e.g., eroded) regions, and perhaps even for predicting optimal regions for mineral enrichment. The purpose of this paper is thus to illustrate some of these possibilities by analyzing key features of the Wopmay Orogen, particularly arc development, to relate features in the exposed portion of the orogen to regional geophysical studies that link the surface to large-scale lithospheric structures, and to compare and contrast the tectonic evolution of the orogen with modern orogens that formed by plate tectonism.

F.A. Cook
Department of Geoscience, University of Calgary, Calgary, AB, Canada T2N1N4,
e-mail: fcook@ucalgary.ca

D. Brown and P.D. Ryan (eds.), *Arc-Continent Collision*, Frontiers in Earth Sciences,
DOI 10.1007/978-3-540-88558-0_14,

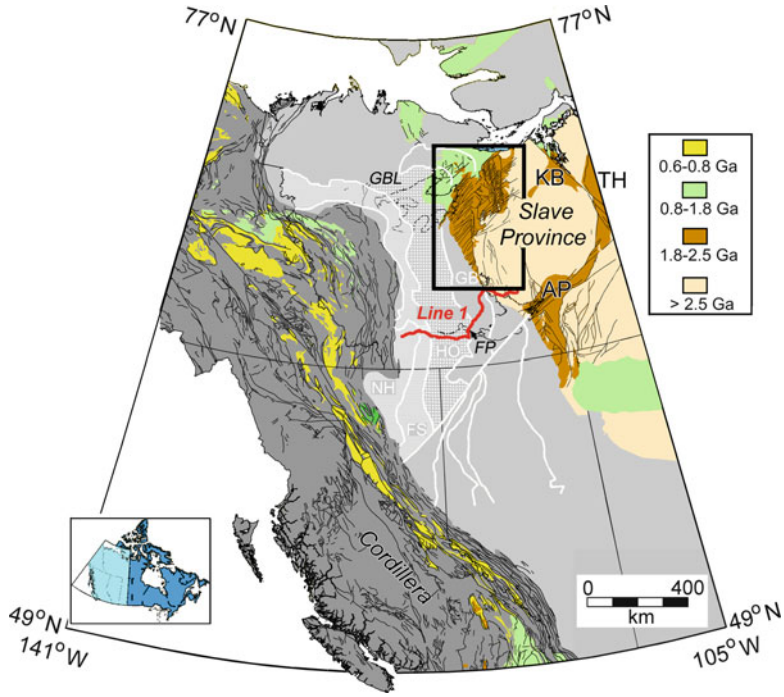

Fig. 14.1 Map of western Canada illustrating the locations of exposed Precambrian rocks (colors). The *boxed area* is the exposed portion of the Wopmay Orogen (Fig. 14.2), and the *white lines* and *labels* are the locations of belts that are composed of Paleoproterozoic rocks related to the Wopmay Orogen that lie beneath the Western Canada Sedimentary Basin. The *red lines* are the locations of the Lithoprobe SNORCLE seismic surveys. *Dark gray* = Cordillera; *light gray* = Phanerozoic rocks of platform and Western Canada Sedimentary Basin. The Muskwa Assemblage mentioned in the text is the exposure of 0.8–1.8 Ga strata (*green*) about 100 km southwest of the NH label. Labels are: *AP* Athapuscow basin, *FP* Fort Providence, *FS* Fort Simpson arc, *GB* Great Bear magmatic zone, *GBL* Great Bear lake, *HO* Hottah terrane, *KB* Kilohigok basin, *NH* Nahanni domain, *TH* Thelon orogen.

14.1.2 Regional Geology of the Wopmay Orogen

14.1.2.1 General Features

The regional structures of the Wopmay Orogen strike north–south and the exposed rocks of the orogen are bounded by the Archean Slave Province to the east, the Mesoproterozoic Coppermine Homocline to the north, and the Phanerozoic Western Canada Sedimentary Basin to the west and south (Fig. 14.2). It is uncertain how far north Wopmay structures project in the subsurface because many of the potential field (gravity and magnetic) anomalies that have proven so crucial for projecting Wopmay structures elsewhere (e.g., Coles et al. 1976; Hoffman 1987; Cook et al. 1999) are dominated by igneous rocks of the younger Coppermine Homocline in this region (Baragar and Donaldson 1973).

Nevertheless, the trends that are mapped in exposed Wopmay structures are easily followed on gravity and magnetic maps to the west and south, at least as far south as the northeast–southwest striking Great Slave Lake shear zone, a ~1.9 Ga dextral strike-slip fault that probably accommodated the convergence of the Archean Slave craton with the Archean Rae Province (Fig. 14.2; Coles et al. 1976; Hoffman 1987). Confirmation of the projections is provided by numerous petroleum industry drill holes that penetrate through the Phanerozoic sedimentary cover and provide evidence that Wopmay-age rocks are present (Villeneuve et al. 1991; Cook et al. 1999; Ross et al. 2000; Cook, in press).

Taken together, therefore, the exposed Wopmay structures and the projections beneath the Western Canada Sedimentary Basin indicate that the orogen covers at least may be as much as five times the

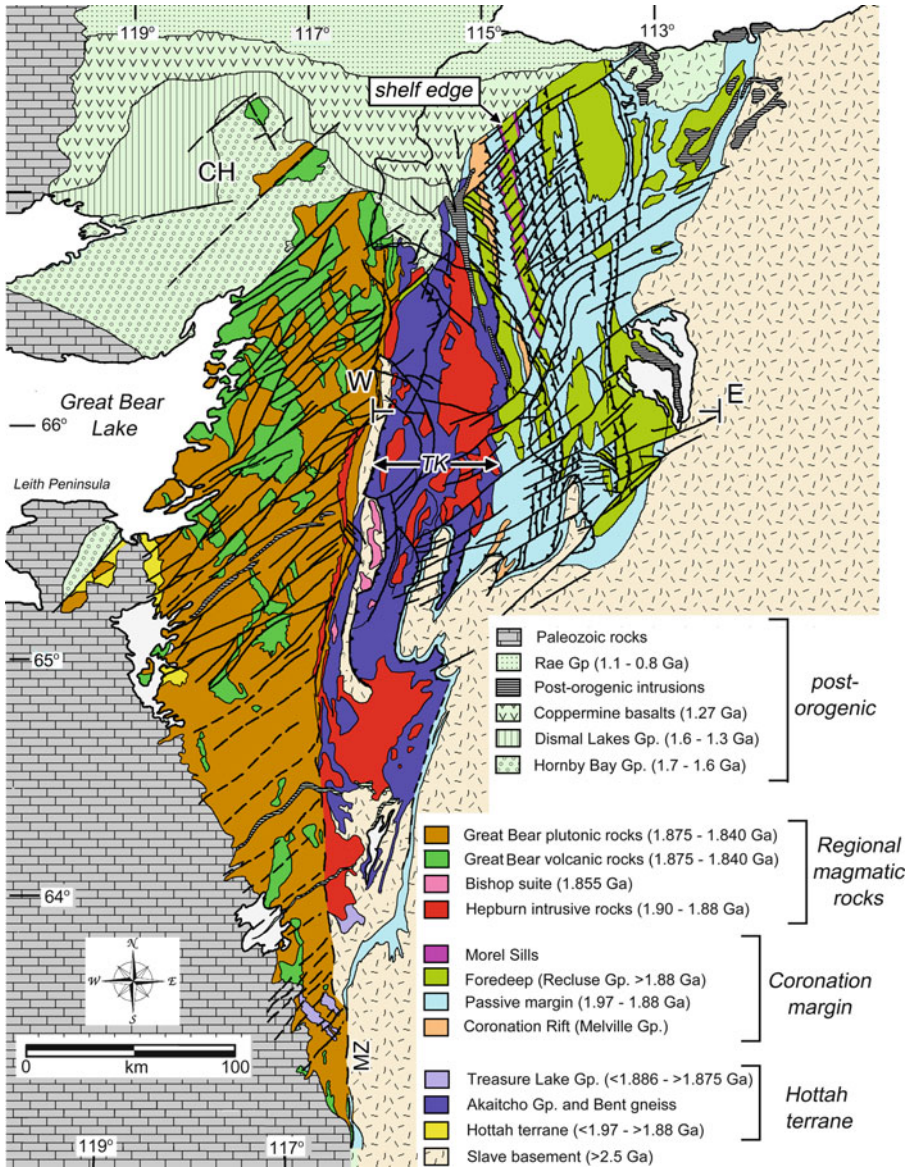

Fig. 14.2 Geological map of the Wopmay Orogen compiled from Hoffman and Bowring (1984), Hoffman et al. (1988), Gandhi et al. (2001), Jackson (2008) Jackson and Ootes (2010). W–E is the approximate location of the cross section in Fig. 14.4. *CH* Coppermine Homocline, *MZ* the north-striking Medial zone.

exposed area (Fig. 14.1). Following is a description of the major geological features across the orogen from east to west.

14.1.2.2 The Coronation Margin

In the east the foreland region (shown in cross section in Fig. 14.4) consists of generally deformed sedimentary rocks of the pre-orogenic Coronation margin that were deposited nonconformably on the Slave craton, along with unconformably overlying syn-orogenic flysch deposits (Recluse Group; see Figure 2 of Hildebrand et al. 2010) that were deposited on the Coronation margin strata during and after contraction of the Coronation margin strata. Initiation of deposition of the Coronation strata was initially thought to have been at about 1.90 Ga based upon U–Pb ages of zircons in ash

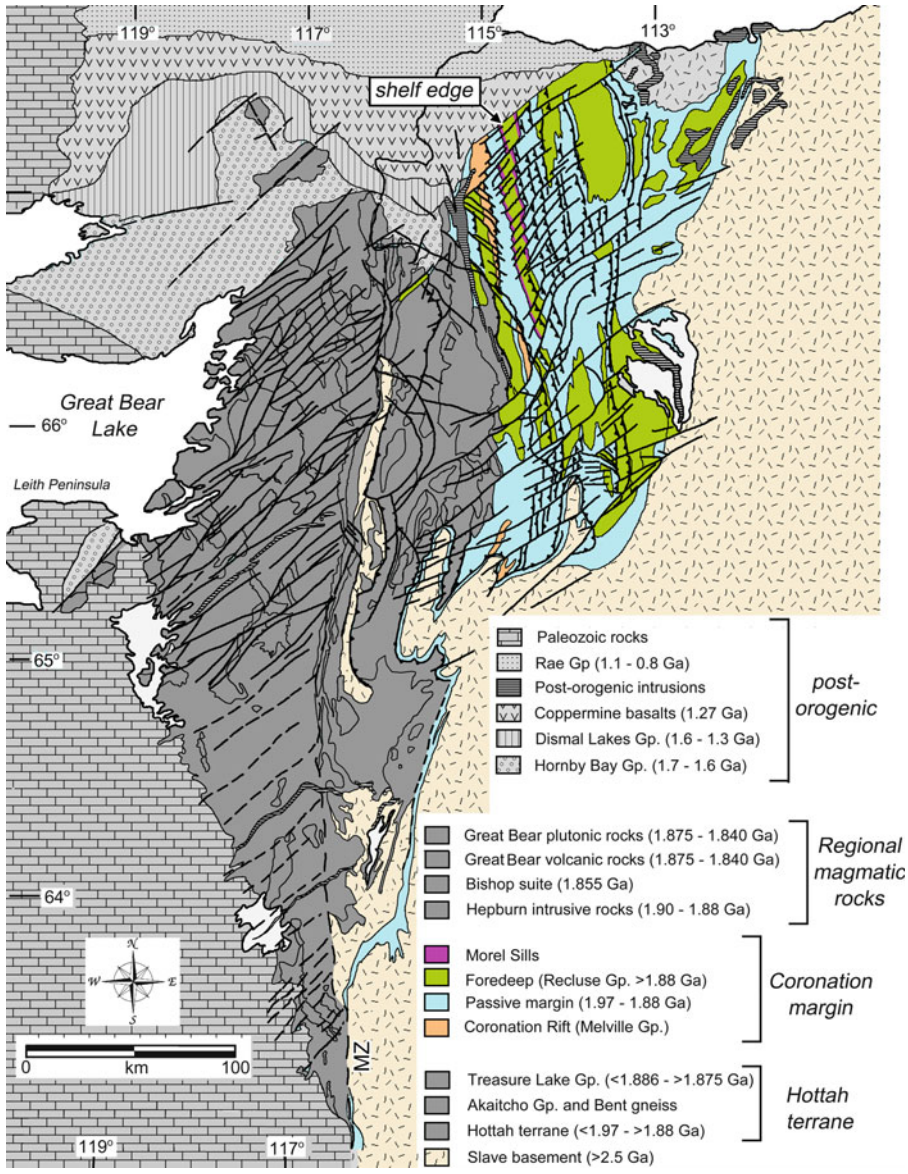

Fig. 14.3 Same map as in Fig. 14.2 with the rocks of the Coronation margin (autochthon and Asiak thrust and fold belt) and the foreland deposits of the Recluse Group highlighted. Melville Group rocks are considered part of the Coronation margin (Bowring and Grotzinger 1992; Hildebrand et al. 2010).

deposits and the assumption that the presumed earliest strata (Akaitcho Group) were deposited on the Slave basement (Hoffman and Bowring 1984). However, subsequent studies have led to an reinterpretation that these strata were deposited on or adjacent to the basement of an accreted terrane (Hottah terrane) and thus do not represent the early stages of margin development (Hildebrand et al. 1991, 2010; Bowring and Grotzinger 1992). According to these authors, early rift-stage deposits (e.g., Melville Group; Hoffman and Pelletier 1982) may be at least as old as 1.97 Ga (Bowring and Grotzinger 1992). Cessation of sedimentation on the Coronation margin preceded the early deposition of the flysch deposits at 1.882 Ga (Bowring and Grotzinger 1992).

Asiak thrust and fold belt structures were generally confined to supracrustal strata (i.e., the fold-thrust belt is of the "thin-skin" type; Rodgers 1949) during the

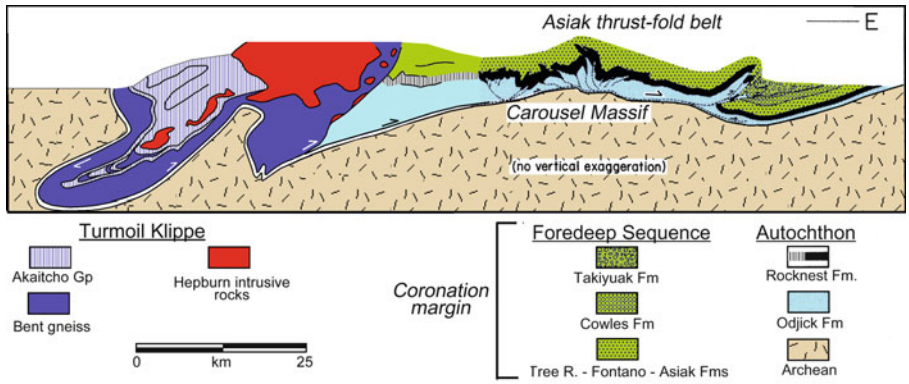

Fig. 14.4 Composite cross section of the eastern Wopmay Orogen from the autochthonous Coronation margin strata on the east to the Medial zone on the west based on plunge projections (modified from Hoffman et al. 1988 and Hildebrand et al. 2010). The position of the Asiak thrust and fold belt and Rocknest Formation shelf edge are indicated. Note that the basal décollement is deformed in above basement uplifts (e.g., Carousel massif).

Calderian orogeny (ca 1.89–1.88 Ga; Hildebrand et al. 2010) but were later deformed into broad open folds due to large-scale basement deformation (Fig. 14.4; Hoffman et al. 1988; Hildebrand et al. 2010). It is uncertain, however, whether these basement folds are cored by deep intra-basement thrust faults, such as those in the Wyoming province of the western United States (e.g., Hoffman et al. 1988).

14.1.2.3 The Coronation Margin: Original Configuration

The original configuration of the Coronation margin and its underlying Archean basement have been interpreted, at least in the northern Wopmay Orogen, from reconstructing deformed strata to their pre-orogenic position, combining this information with isotopic evidence of crust-formation ages of the magma/melt region observed in late- to post-orogenic arc magmas, and by incorporating these results with subsurface structures and properties delineated on regional geophysical surveys. In the southern Wopmay Orogen, south of about 64°N, only scattered remnants of the margin appear to be preserved at the erosion surface. This appears to be largely due to differential uplift and exhumation of as much as 15 km in the southern Wopmay relative to the north (e.g., King 1986).

Between about 64°N and 67°N the deformed strata of the Coronation margin are well preserved, thus allowing cross-section reconstructions to estimate the amount of contractional displacement and thus the original configuration. The minimum amount of eastward-directed contraction is estimated to be ~60 km within the Asiak fold and thrust belt (e.g., Tirrul 1984, 1992; Hoffman et al. 1988). This places the retrodeformed western limit of exposed Coronation strata near the present position of a north-striking Medial zone (formerly "Wopmay fault zone"; Hoffman 1984; Hildebrand et al. 1990, 2010), a narrow zone of north – striking narrow zone of intense folding and faulting.

Isotopic characteristics of syn- to post-orogenic igneous rocks provide evidence bearing on relative amounts of contamination by Archean basement rocks (i.e., Slave craton). In the northern Wopmay Orogen, analyses of lead (Housh et al. 1989) and neodymium (Bowring and Podosek 1989) isotopes have been interpreted to indicate that the rocks west of the Medial zone are generally devoid of signatures that could be related to Archean Slave rocks, and thus that the Slave basement projects in the subsurface to the vicinity the this structure.

Remote sensing geophysical data provide support for the interpretation that Slave basement is present in the subsurface as far west as the Medial zone, but also indicate that it may project at least 20 km farther west than the surface position of the fault (Cook et al. 1999; Spratt et al. 2009; Cook, in press). In the images provided by Cook et al. (1999), Spratt et al. (2009), and discussed in Sect. 14.3, the top of the Archean Slave basement appears to dip westward and form a westward tapering wedge in the middle and lower crust. The geometry suggests that the lower part of

the westernmost Slave craton and any lithosphere attached to it became detached and sank into the sub-lithospheric mantle (Hildebrand and Bowring 1999). If this interpretation is correct, the Slave lithosphere, and overlying Coronation margin, may have projected substantially farther west prior to collision and orogenic contraction during the Calderian orogeny (ca. 1.88–1.87 Ga), than it does today.

The original southern extent of the Coronation margin is uncertain. At the present time, scattered remnants of it are present to ~64°N (Fig. 14.2), but whether it continues southward beneath the Phanerozoic strata of the Western Canada Sedimentary Basin is not known. According to St-Onge and King (1987), contrasts in metamorphic assemblages between the southern and northern Wopmay Orogen are indicative of ~15 km of differential exhumation along strike; such differential exhumation may also account for substantially deeper levels of erosion in the south.

14.1.2.4 The Hepburn Metamorphic and Plutonic Belt and Turmoil Klippe

The Hepburn metamorphic and plutonic belt (now "Turmoil klippe"; Hildebrand et al. 1991, 2010; Figs. 14.2 and 14.5) consists of metamorphosed supracrustal rocks of the allochthonous Akaitcho Group and Bent gneiss that are separated from underlying Coronation Supergroup strata and Slave basement by the penetratively deformed mylonitic straight gneiss (Hildebrand et al. 1991, 2010), syn- to post-orogenic intrusive rocks of the Hepburn (ca. 1.90–1.88 Ga; Bowring 1984) and Bishop (ca. 1.855 Ga) plutonic suites, and minor amounts of the late- to post-orogenic Great Bear magmatic zone (Hildebrand et al. 1987; Lalonde 1989; Housh et al. 1989). The Akaitcho Group strata were originally thought to be part of the initial rift deposits of the Coronation margin (e.g., Hoffman and Bowring 1984), but these rocks are now considered to have been deposited either on or adjacent to the accreted Hottah terrane, perhaps in a forearc setting (e.g., Bowring and Grotzinger 1992; Hildebrand et al. 2010). Accordingly, the Turmoil klippe represents possible fore-arc rocks and their basement (Bent gneiss) that were subjected to substantial burial (to as much as 15 km), metamorphism, intrusion and subsequent uplift and exhumation (St-Onge and King 1987) as a result of collision between the Hottah terrane that the Coronation margin (Hildebrand et al. 2010).

The Hepburn and Bishop intrusive suites represent pre- and post-orogenic (post Calderian) intrusions respectively. Analyses of the chemical and isotopic signatures in these rocks illustrate key differences between them that have been interpreted in the context of the evolving orogen. For example, both suites are represented by a range of compositions from gabbro to granite (Lalonde 1989). However, the older Hepburn intrusive suite includes granites that assimilated substantial amounts of metasedimentary material during intrusion, are foliated to migmatitic, and were intruded into the Akaitcho Group strata that were subsequently incorporated into the Turmoil klippe that was emplaced during Calderian deformation. In contrast, the younger Bishop suite granites are commonly more hornblende-muscovite bearing, are more massive (less foliated), and intruded the Archean Slave basement (Lalonde 1989; Housh et al. 1989) and the Turmoil klippe after its emplacement (Hildebrand et al. 2010). The Bishop suite plutonic rocks represent the waning stages of calc-alkaline arc development in the Great Bear magmatic zone (Lalonde 1989).

Isotopic analyses affirm some of these differences and further serve to distinguish the origins of Bishop and Hepburn magmas. Specifically, the Hepburn intrusive suite, as well as the Great Bear magmatic rocks to the west (Fig. 14.2), display Pb and Nd isotopic compositions that are inconsistent with significant involvement of or contamination by Archean Slave basement rocks and are thus interpreted to represent magmas derived from and intruded through early Paleoproterozoic (ca. 2.0–2.4 Ga) basement (Housh et al. 1989; Bowring and Podosek 1989). Conversely, granites in the Bishop suite display substantially lower $^{206}Pb/^{204}Pb$ ratios, indicating much less radiogenic lead, consistent with the observation that they intruded into, and interacted with, less radiogenic Archean basement (Housh et al. 1989; Bowring and Podosek 1989).

The proximity of the Hepburn and Bishop suites (Fig. 14.2), coupled with their ~30 My difference in ages, contrasting isotopic signatures and deformational characteristics, has been interpreted to indicate that the Hepburn intrusive suite intruded at ~1.89–1.88 Ga west of Archean Slave basement and was transported eastward during the Calderian deformation to its location along with the Turmoil klippe

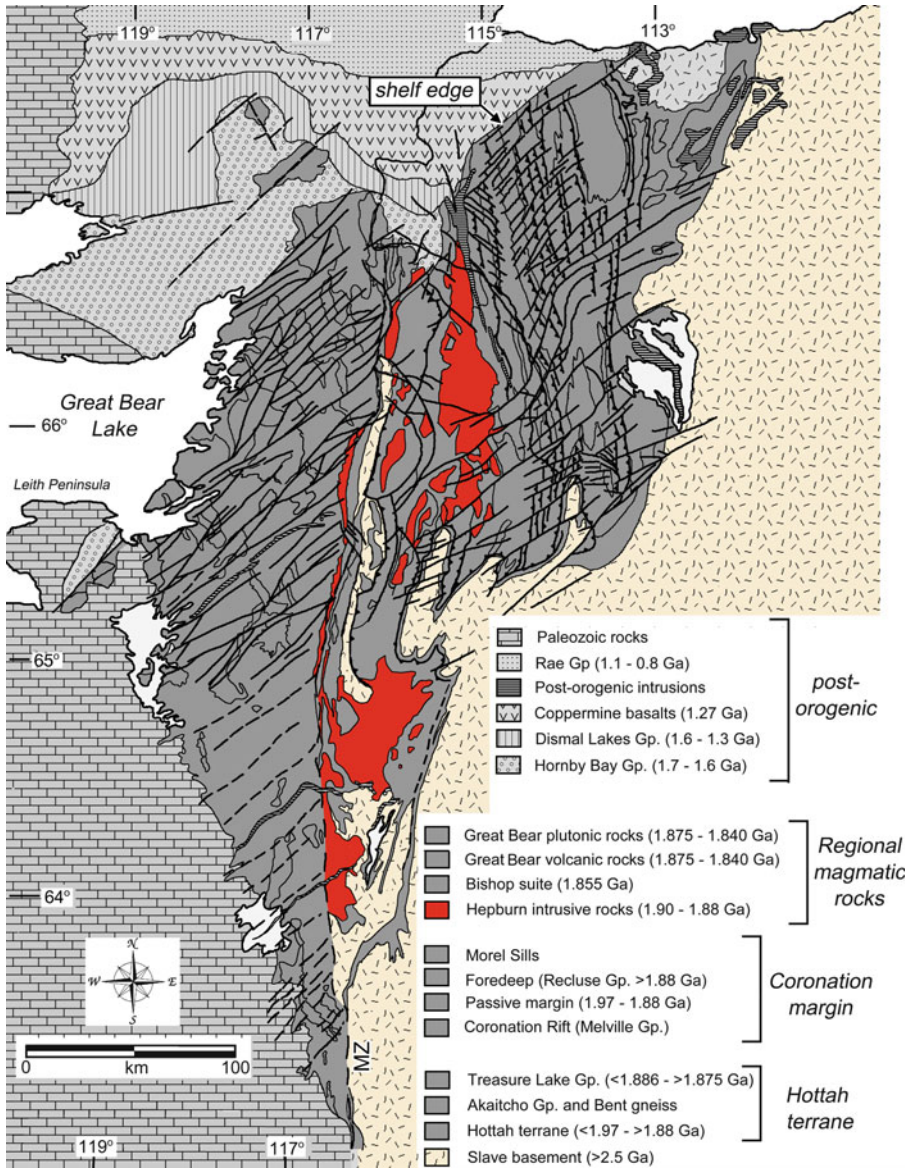

Fig. 14.5 Same map as in Fig. 14.2 with the rocks of the Hepburn intrusive suite highlighted.

overlying the Slave craton. Subsequently, the Bishop suite was emplaced farther to the west and intruded through the Archean basement, as well as the previously deformed and metamorphosed Hepburn rocks.

14.1.2.5 The Hottah Arc Terrane

Rock assemblages in the Leith Peninsula region south of Great Bear Lake were described by Hildebrand (1981) and Hildebrand and Roots (1985) as exotic to those occurring in the eastern part of the Wopmay Orogen. Because interpretations of terranes in Proterozoic regions do not benefit from many of the analyses available in Phanerozoic orogens, such as detailed paleomagnetic differences and paleontological comparisons, such interpretations are less firm than they are in Phanerozoic orogens. Nevertheless, key elements to the interpretation of the Hottah sequences as an exotic terrane are the following.

According to Hildebrand and Roots (1985) and Bowring and Grotzinger (1992), Hottah terrane

consists of amphibolite grade metasedimentary and intermediate volcanic rocks that were intruded by 1.94–1.89 Ga calc-alkaline plutonic rocks (Hottah arc). Isotopic and zircon data are interpreted to indicate that these rocks were built on an older (2.0–2.4 Ga) basement. Overlying these rocks, supracrustal basin deposits include sedimentary and volcanic rocks that are lithologically distinct from Coronation margin strata. For example, the exposed Bell Island Bay Group includes rift-basin clastics and submarine volcanic rocks (pillow basalts) that are similar to calc-alkaline arc sequences observed today (Reichenbach 1991; Hildebrand et al. 2010) and that have been dated at ~1.90–1.88 Ga (Hildebrand and Roots 1985; Reichenbach 1991; Bowring and Grotzinger 1992). All of the magmas associated with the Hottah arc, including the Bell Island Bay Group, the Akaitcho Group (~1.9 Ga; Bowring and Grotzinger 1992) in the Turmoil klippe and the Hepburn intrusive suite (1.90–1.88 Ga; Bowring 1984) are calc-alkaline to tholeiitic and are interpreted to have been formed as mantle-derived magmas interacted with continental crust (Hildebrand et al. 2010).

In the southern Wopmay Orogen, rocks of the Treasure Lake Group include platformal clastic and carbonate rocks west of the Medial zone (Fig. 14.2). These rocks are intruded by Great Bear magmas (Gandhi and van Breemen 2005; Jackson et al. 2010) and have been interpreted to be correlative with the Snare group east of the Medial zone and to the Akaitcho Group strata in the Turmoil klippe (Gandhi and van Breemen 2005). Treasure Lake Group strata include detrital zircons that range in age from Archean (3.12 Ga) to Paleoproterozoic (~1.884 Ga) (Gandhi and van Breemen 2005; Jackson et al. 2010).

Isotopic characteristics described by Housh et al. (1989) and Bowring and Podosek (1989) establish that the igneous rocks of the Hottah exhibit distinctly different signatures than those of the eastern Wopmay. Most notably, the Nd signatures provide strong evidence that the lower crust and upper mantle of the on which the Hottah rocks were deposited was Paleoproterozoic with no evidence for Archean (e.g., Slave) basement. Furthermore, the cross-strike transition from rocks with Archean signatures to those with Paleoproterozoic (2.1–2.4 Ga) signatures occurs in the vicinity of the Medial zone. The significance of this is discussed further in Sect. 14.3.1.

14.1.2.6 Great Bear Magmatic Zone: Stitching Hottah Terrane to Slave Craton

The Great Bear magmatic zone (Fig. 14.6) was active from ~1.878 to ~1.840 Ga (Bowring 1984; Hildebrand et al. 1987, 2010). The earliest volcanic and plutonic rocks of the arc were slightly deformed in the latter stages of the Calderian orogeny, whereas the youngest magmas post-dated regional deformation and metamorphism (Hildebrand et al. 1987). The metamorphism of the Great Bear arc was generally low grade (sub-greenschist to greenschist facies), but the deformation produced broad folding that has resulted in 10 km of exposed section (e.g., Hoffman and McGlynn 1977; Hildebrand et al. 1987).

Great Bear magmatism predominantly occurred in two episodes between ~1.878 and 1.860 Ga that pre-dated major regional Calderian folding, and at ~1.85–1.84 Ga that post-dated it. The entire region was subsequently subjected to major episode of regional northeast and northwest striking transcurrent faulting (Fig. 14.2) and broad open folds (Hildebrand et al. 2010).

Early Great Bear magmatism was dominated by calc-alkaline volcanic rocks that range in composition from basalt to rhyolite and that have a composite thickness exceeding 10 km (Hildebrand 1981). These extrusive sequences were subsequently intruded by related biotite-hornblende plutonic rocks. The post-folding magmatic rocks are dominantly intrusive, with compositions including biotite syenogranites, hornblende-bearing diorites, quartz diorites and monzodiorites (Hildebrand et al. 1987). The Bishop suite described previously is part of these late intrusives and represents the easternmost, and some of the youngest, remnants of the Great Bear arc magmatism.

Trace element analyses of the Great Bear extrusive rocks illustrate comparable patterns to those of continental arc magmas today (Hildebrand 1981; Fig. 14.7). In addition to the overall enrichment of light rare earth elements, a distinctive Eu anomaly is observed that may indicate substantial fractionation (i.e., formation of a residual magma following removal of an earlier plagioclase-bearing differentiate; Raymond 2002). Such anomalies are common in continental calc-alkaline arc magmas (Fig. 14.8), as is the relatively flat heavy rare earth element pattern (e.g., Kay 1977; Atherton et al. 1979).

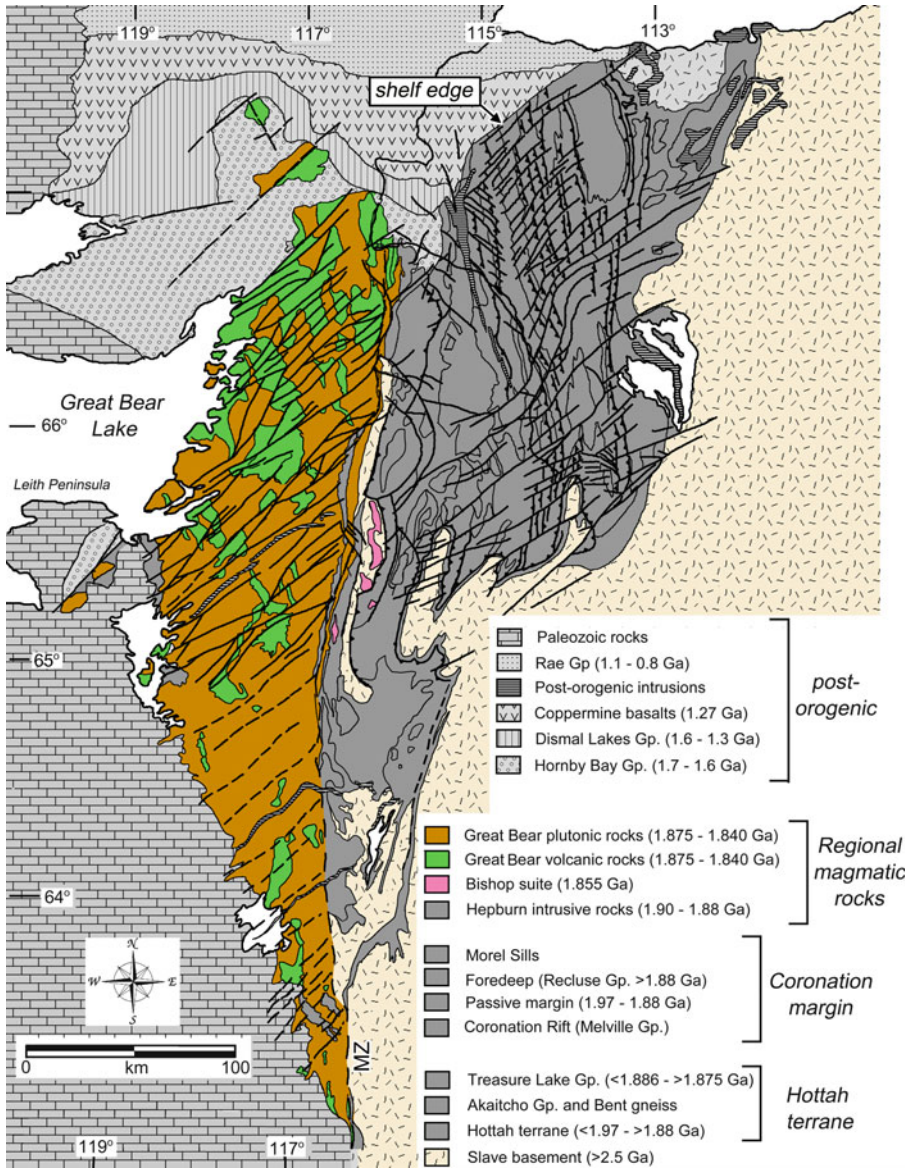

Fig. 14.6 Same map as in Fig. 14.2 with the rocks of the Great Bear magmatic zone (including the Bishop intrusive suite rocks) highlighted. Note that the Great Bear magmatic rocks are in contact with both Archean Slave basement and the Hottah terrane and thus stitches them together by the time Great Bear magmatism took place.

14.1.2.7 The Cryptic Fort Simpson/Nahanni Arc Terrane

Although the exposed rocks of the Wopmay Orogen exhibit temporally and chemically distinctive magmatic arcs (the allochthonous Hepburn suite east of the Medial zone, the exotic Hottah island arc in the west, and the Great Bear magmatic zone and Bishop suite that straddle both the Hottah terrane and the western Slave province), it is likely that at least one additional arc existed outboard (west) of the Great Bear magmatic zone during the latter stages of Great Bear magmatism. The term "Fort Simpson" was first applied by Hoffman (1987) and Hildebrand et al. (1987) to a prominent north-striking residual magnetic anomaly trend (a series of magnetic highs and lows; Cook et al. 1992) that corresponds generally to a similar linear trend of gravity anomalies. Subsequently,

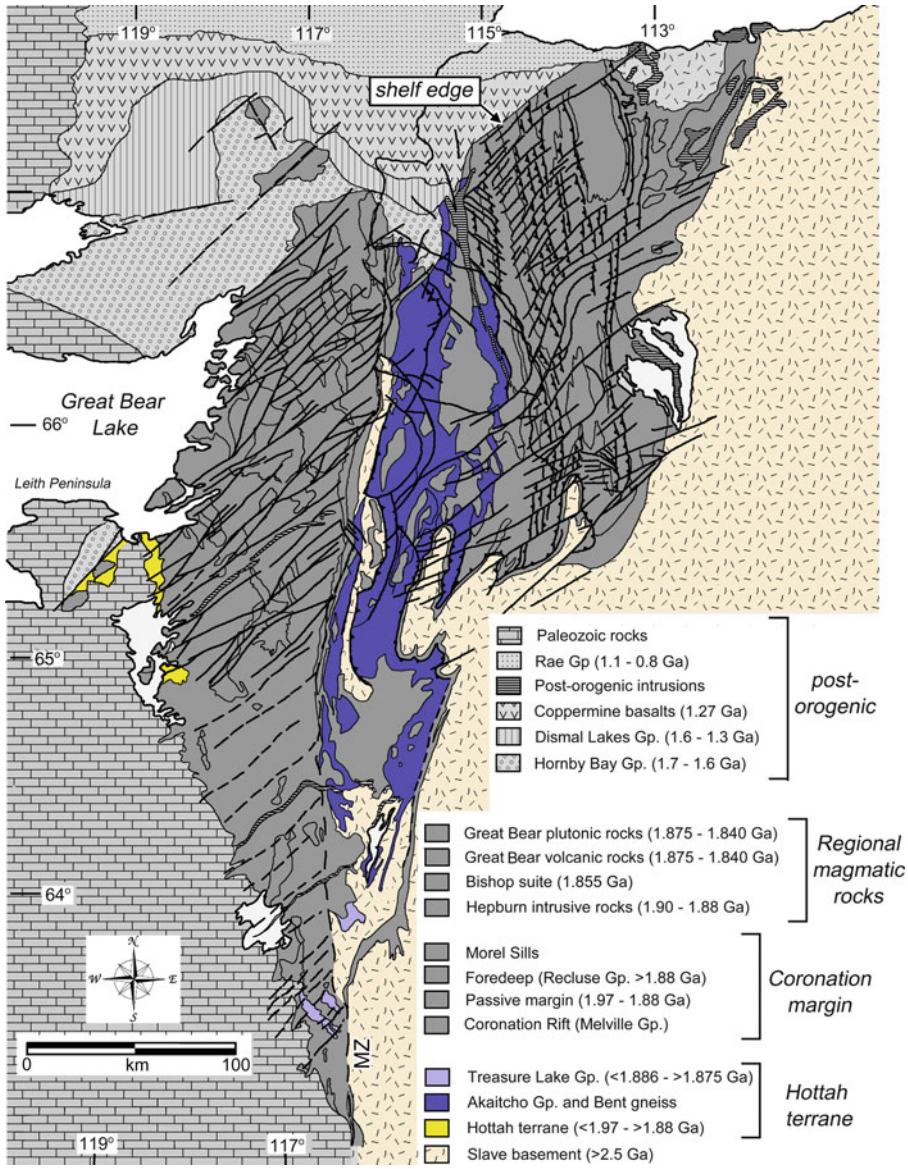

Fig. 14.7 Same map as in Fig. 14.2 with the rocks of the Hottah terrane highlighted. The Akaitcho Group – Bent gneiss are also highlighted as well as it these are considered to have been part of the Hottah terrane prior to the Calderian orogeny (Hildebrand et al. 1991; Bowring and Grotzinger 1992; Hildebrand et al. 2010).

Villeneuve et al. (1991) referred to a cryptic terrane that included the Fort Simpson magmatic arc as the "Nahanni terrane". Here, as in Cook (in review), I use the moniker "Fort Simpson/Nahanni terrane" to clarify that they are not considered to have been separate lithospheric plates.

Nevertheless, the evidence for the Fort Simpson/Nahanni terrane is substantially less firm than for terranes in Phanerozoic orogens or even for the Hottah terrane discussed previously. The interpretation is essentially based on three key observations. First, and the original reason for proposing a terrane outboard of the Hottah terrane, is that the entire exposed Wopmay Orogen, including the Hottah terrane and the Great Bear arc, was subjected to regional transcurrent faulting and broad folding that appears to require deformation at the lithospheric scale throughout the orogen prior to the deposition of the latest intrusives of

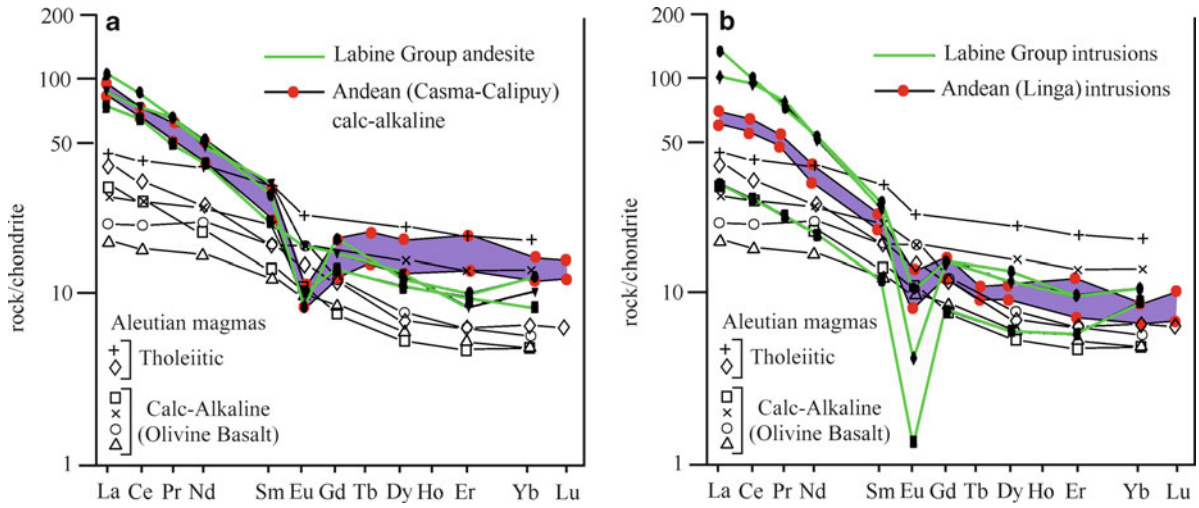

Fig. 14.8 Rare earth element (REE) signatures of (**a**) andesite (Labine Group) and (**b**) intrusive units of the GB magmatic arc (*heavy black lines*; from Hildebrand 1981). Also shown are patterns from the Andean magmatic arc from Atherton et al. (1979). Values are normalized to chondrites (Hildebrand 1981). Note the similar general decreasing abundance with decreasing ionic radius and the distinct Eu anomalies, features that are typical for continental magmatic arcs formed above subduction zones. Also shown for comparison purposes are some typical patterns with LIL enrichment from the Aleutian arc (Kay 1977).

the Great Bear magmatic zone (e.g., Tirrul 1984, 1992; Hildebrand et al. 1987, 2010). Second, gravity and magnetic anomalies have regionally extensive, linear highs (Bulmer Lake high of Hornal et al. 1970; Fort Simpson highs of Hoffman 1987; Fort Simpson trend of Cook et al. 1992) that could be interpreted as a suture (Johnny Hoe suture of Hildebrand et al. 1987 and Hoffman 1987). Third, samples from drill holes that penetrate to Precambrian granitic rocks beneath the Western Canada Sedimentary Basin along the Fort Simpson trend were dated by Villeneuve et al. (1991) and Ross et al. (2000) to be ca. 1.844–1.854 Ga. While these ages overlap temporally with the youngest ages of the Great Bear magmas, their position far to the west appears to preclude a direct magmatic and/or tectonic connection to the Great Bear. Finally, mapping the deep structure throughout the region established the presence of lithosphere-penetrating boundaries that may be relict subduction zones associated with these arcs (Cook et al. 1998, 1999).

14.1.2.8 Post-orogenic Deformation

Lithospheric deformation that post-dates the Calderian Orogeny is of three types (1) large-scale dextral transcurrent faulting as noted above, (2) broad, differential uplift and erosion, and (3) regional extension. The dextral transcurrent faulting (Tirrul 1984) resulted in a series of northeast- and northwest-striking faults that displaced virtually all features formed during the Calderian Orogeny. Accordingly, the transcurrent faulting must post-date the youngest Great Bear magmas, and is therefore estimated to have occurred at ~1.84 Ga and to have been a product of the accretion of the Fort Simpson/Nahanni terrane (e.g., Hildebrand et al. 1987).

The regional uplift from ~1.880 to 1.870 Ga preceded the formation of deep late Paleoproterozoic to Mesoproterozoic extensional basins age to the west. In the Coppermine Homocline (Fig. 14.2) more than 4 km of sedimentary rocks were deposited in the westward thickening the Hornby Bay and Dismal Lakes groups (Ross and Kerans 1989) For example, in the Wernecke Mountains of the central Yukon, thick (>15 km; Delaney 1981) deposits of Early Proterozoic sediments (Wernicke Supergroup) were deposited prior to ~1.76 Ga (Thorkelson et al. 2005). Additional deposits approximately 500 km southeast of the Wernecke Mountains in the Canadian Cordillera have a wide range of detrital zircons with ages varying from 3.075 to 1.766 Ga, although there is a distinct concentration near 1.850 Ga (Muskwa Assemblage on Fig. 14.1; Ross et al. 2001). These ages are typical of

rocks in the Canadian Shield and the 1.850 Ga zircons are virtually the same age as the magmatic rocks of the adjacent Fort Simpson arc as well as the youngest Great Bear magmas. Snyder et al. (2002) and Cook et al. (2004) proposed that these strata represent syn- to post-orogenic deposits derived from the exhumed Wopmay Orogen to the east.

The geometry of the post-orogenic extensional basins is further exemplified by the Fort Simpson basin on the west side of the Fort Simpson geophysical trend. The low gravity and magnetic values that characterize this region were interpreted at one point to be representative of the "Nahanni terrane" (e.g., Villeneuve et al. 1991), but they have since been shown to be associated with thick (>20 km) basin deposits of the Fort Simpson basin (Cook and van der Velden 1993; Cook et al. 1999). The ages of the basin deposits are not known in detail, but as some of them have been correlated with the aforementioned Muskwa assemblage, it appears likely that some are older than 1.760 Ga, but post-date the Wopmay orogenic activity. The Fort Simpson basin is visible on the western end of the SNORCLE seismic cross section east of the Cordillera (Fig. 14.9b).

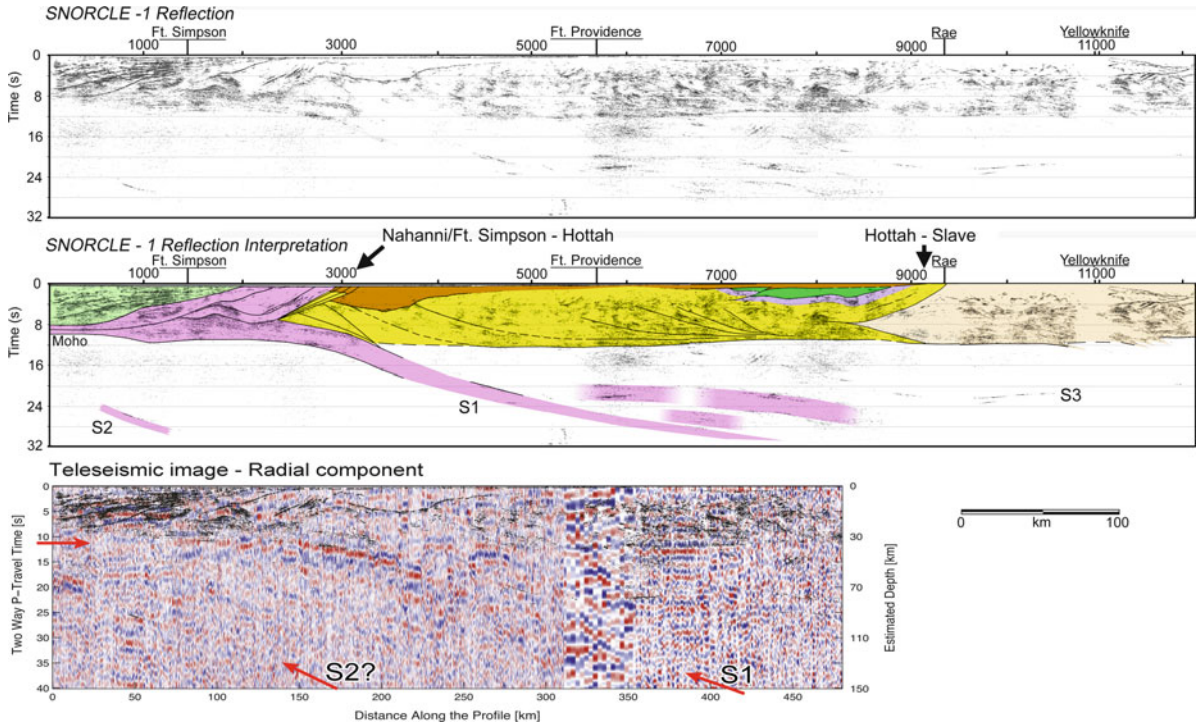

Fig. 14.9 (**a**) (upper) Lithoprobe seismic reflection profile along SNORCLE line 1 (modified from Cook et al. 1999). Data are plotted to 32 s, or about 110 km. (**b**) (middle) Interpretation of data along SNORCLE line 1 (modified from Cook et al. 1999). Boundaries between different colored regions are determined by correlating surface information (outcrops, potential field anomalies, drill hole information) to the reflection geometry. In most cases, these are taken from Cook et al. 1999; some modification has been made in the vicinity of the Hottah – Slave transition to accommodate new results from electromagnetic studies (Spratt et al. 2009). The color scheme is the same as that used for Fig. 14.2 with the addition of the *pink* color for the Fort Simpson/Nahanni terrane and elements of it that project into the mantle and the *light green* color for the post-orogenic extensional Fort Simpson basin on the far west. Note the dipping boundaries S1, S2 and S3 as described in the text. The approximate positions of the Hottah-Slave and Nahanni/Ft. Simpson – Hottah sutures are labeled with the *large arrows*. (**c**) (lower) Cross section along the lower portion of SNORCLE Line 1 calculated from teleseismic arrivals (Mercier et al. 2008). The *black lines* are reflections from SNORCLE reflection line 1 (**a**). The Moho is near 30 km depth (*upper arrow*), and two prominent dipping zones are observed in the mantle. Zone S1 corresponds to S1 on Fig. 14.13c and zone S2 corresponds to zone S2 in (**b**). A key point is that, although S2 appears as only a limited reflection on SNORCLE Line 1 (**b**), it appears as a substantially more prominent zone here. This supports the interpretation that S2 is a major boundary, perhaps associated with the formation of the Fort Simpson arc (Cook et al. 1999).

14.2 The Structure of the Lithosphere Today

14.2.1 General

Ever since imaging techniques such as seismic refraction and reflection profiling have been applied to mapping the subsurface structure of the crust and lithosphere, a primary objective has been to delineate and map the detailed characteristics of lithospheric-scale structures such as sutures and subduction zones. In the Canadian Lithoprobe project, acquisition of more than 15,000 km each of refraction and reflection data, as well as a substantial quantity of regional magnetotelluric data, provided opportunities to map such features at scales and resolutions that were previously not possible (e.g., Van der Velden and Cook 2005; Hammer et al. 2010).

Throughout this database across northern North America, some of the most prominent and deeply penetrating boundaries were imaged along the SNORCLE (**S**lave **NOR**thern **C**ordillera **L**ithospheric **E**volution) transect that traverses from the Archean Slave province, westward across the Wopmay Orogen where it projects beneath the Western Canada Sedimentary Basin (Fig. 14.1), across the northern Canadian Cordillera, and ends near the Pacific Ocean (e.g., Cook and Erdmer 2005). The portion of the seismic reflection and refraction surveys that are relevant to the Wopmay Orogen along with an interpretation is presented in Fig. 14.10 (based largely on Cook et al. 1999).

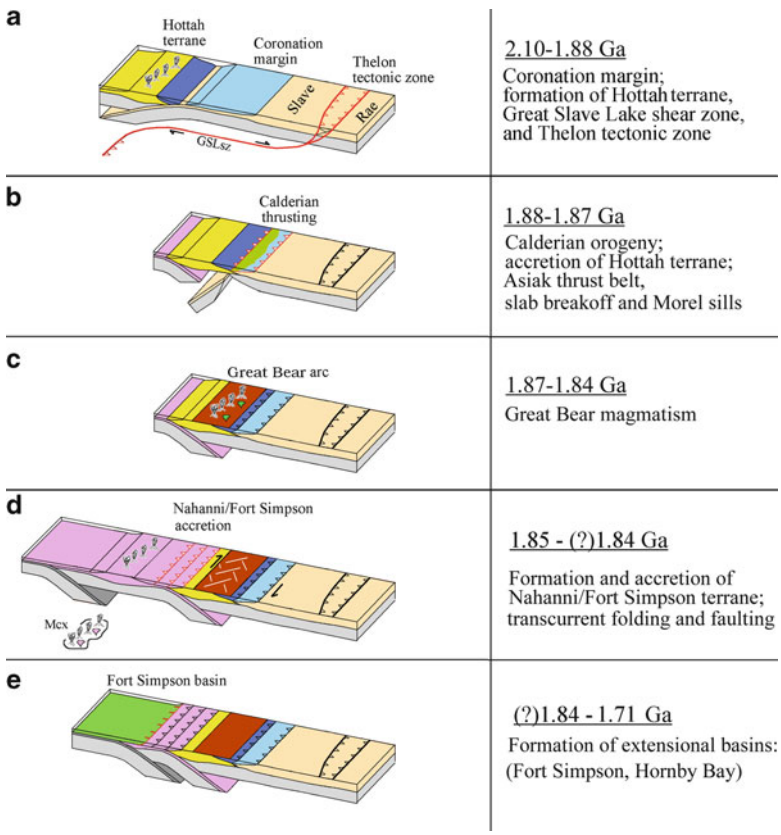

Fig. 14.10 Series of schematic evolutionary diagrams of the Wopmay Orogen from ~2.10 to 1.71 Ga. Details are described in the text. *Green color* in (**b**) represents the Recluse Group foreland deposits. GSLsz is the Great Slave Lake shear zone. Mcx in panel (**d**) is the Monashee complex in the Cordillera of southern British Columbia where rocks with ages similar to those of the Hottah terrane (2.08 Ga) and Nahanni/Fort Simpson terrane (~1.845–1.848 Ga; Crowley 1999) are exposed. *Arrows* in (**d**) represent oblique deformation resulting from non-orthogonal convergence between the Nahanni/Ft. Simpson terrane and the previously accreted Hottah terrane. Modified from Hildebrand et al. (1987), Cook et al. (1999) and Cook (in press).

14.2.2 Sutures

Sutures are the surface and subsurface manifestations of zones along which oceanic lithospheres were totally subducted (Dewey 1977). Two such zones have been proposed for the Wopmay Orogen. They are:

1. The suture between the Hottah terrane and the Slave Province (~1.88–1.87 Ga).
2. The suture between the Fort Simpson/Nahanni terrane and the western side of the Hottah terrane (~1.840 Ga).

The approximate surface location of the Hottah – Slave suture is determined from mapping and analyses in the northern Wopmay. There, retrodeformation of the deformed Coronation strata in the Asiak thrust and fold belt establish that the position of the shelf edge of the margin was located near the present location of the Medial (e.g., Tirrul 1984, 1992; Hoffman et al. 1988; Hildebrand and Bowring 1999). In addition, as noted the Pb and Nd isotopic signatures have been interpreted to delineate a crustal transition from Archean to Paleoproterozoic basement, also near the Medial zone (Housh et al. 1989; Bowring and Podosek 1989). The approximate location of the Hottah – Slave suture based on surface geology is labeled on Fig. 14.9. However, it surface position is only approximate due masking by the Great Bear magmas and Paleozoic sedimentary rocks.

As noted previously, the position of the Fort Simpson/Nahanni – Hottah suture is less well defined from surface relationships. Hildebrand et al. (1987) and Hoffman (1987) proposed that it is associated with the eastern side of the Fort Simpson geophysical trend. This position is also labeled on Fig. 14.9. In contrast to the Hottah terrane – Slave Province suture, this proposed suture appears to be well defined seismically as a series of west-dipping reflections that penetrate to the lower crust (Cook et al. 1999; Fig. 14.9).

Detailed examination of the subsurface geometry in the vicinities of these transitions helps to delineate the subsurface geometry and thus to illustrate some of the complexities associated with these sutures (Fig. 14.10). In the subsurface a dominantly east-dipping surface (yellow–blue transition) may be the east edge of the Hottah terrane. This structure is overlain by metasedimentary rocks (e.g., Akaitcho group) that were likely deposited in the fore-arc basin separating the Hottah terrane from the Coronation margin (Bowring and Grotzinger 1992).

The subsurface geometry in the vicinity of the Fort Simpson/Nahanni – Hottah terrane suture has many of the geometric earmarks of a trench – accretionary wedge – arc complex. Specifically, in the lower crust and upper mantle, east-dipping layers (S1 on Fig. 14.9) appear to be similar to reflections generated by subducted oceanic crust and these are overlain by oppositely verging (west-dipping) structures (labeled "Nahanni/Fort Simpson – Hottah" on Fig. 14.9b) that can be followed to subcrop beneath the Phanerozoic strata of the Western Canada sedimentary basin. These have a geometry that is similar to landward-vergent thrust faults in accretionary prisms (e.g., Seely 1977). Together these features outline a geometric wedge between the Fort Simpson (purple) and the Hottah (yellow) terranes (Fig. 14.9b).

Above the westernmost Hottah terrane is an upper crustal zone that is virtually devoid of reflections (brown on Fig. 14.9b), and a lower crustal zone that includes dominantly east-dipping surfaces (in the toe of the Hottah wedge on Fig. 14.9b). The upper crustal zone appears to have a geometry that is similar to an upper slope basin in a modern accretionary complex, although drill holes into the upper portions of it have penetrated igneous rocks (Ross et al. 2001; Cook, in press). The lower crustal zone has a series of east-dipping reflectors (faults?) that increase in dip eastward, as is commonly observed in modern accretionary prisms where thrust faults display progressively increasing dip away from the trench (Karig and Sharman 1975).

14.2.3 Deep Lithospheric Structures

14.2.3.1 Deep Structure of the Hottah: Slave Transition

The intra-lithospheric structures observed along this profile provide some of the most detailed deep lithosphere geometries yet observed. In the vicinity of the Hottah – Slave transition, the reflection Moho is relatively flat at ~35 km and deep crustal structures either flatten into it or are truncated at it (Cook 2002; Cook and Vasudevan 2003). Although there is some evidence for sub-Moho boundaries, none appears to cross the Moho and connect to crustal structures in the vicinity

of the transition. Hence there is no clear evidence for lithosphere-penetrating boundary that may be the subsurface projection of the Hottah – Slave suture.

The lack of clear evidence for an intra-lithospheric boundary below the Moho in this region where there is evidence for such a boundary within the crust, coupled with the Moho configuration and the geometric relationship between lower crustal structures and the Moho, leads to the following alternative interpretations. In one scenario, it is possible that the Moho is younger than the Hottah – Slave collision. In this case, the seismic transition identified as the Moho could be produced by a thermal effect that essentially overprinted older structures, and reflectivity of such older structures below the Moho would be attenuated (e.g., Cook 2002; Van der Velden and Cook 2005). Alternatively, the Moho may be an old feature that, due to substantial contrast in material properties across it, may have localized deformation and acted as a zone of detachment after the Hottah – Slave collision. In this case crustal structures could be displaced from correlative structures in the mantle (e.g., Cook et al. 1999).

14.2.3.2 Deep Structures of the Fort Simpson/ Nahanni: Hottah Transition

Reflector S1 can be followed from the lower crust, across the Moho, and into the mantle to a depth of ~80–100 km (Fig. 14.9b, c). In the deep part of the section, it appears to flatten, but this may in part be due to a change in the orientation of the profile (Eaton et al. 2008). The geometry of this boundary, its correlation and connection to crustal structures near the Nahanni/ Fort Simpson – Hottah suture, and its position nearly 100 km vertically beneath the Great Bear magmatic zone, lead to an interpretation that it represents reflections from the subduction zone responsible for the Great Bear magmatic zone (Cook et al. 1998, 1999).

14.3 The Wopmay Orogenic Puzzle Through Time: Tectonic Evolution

14.3.1 General: Similarities to Modern Orogens

Since 1980 (Hoffman 1980), most interpretations of the Wopmay Orogen have resembled lithospheric plate–margin interactions comparable to those that are observed today. Key elements that lead to this view are the following.

The regional belt-like structural arrangement of the orogen is more or less parallel to the original configuration of the Coronation margin and the western margin of the Slave province (Figs. 14.1 and 14.2). Orogen (and margin) parallel variations are relatively small, whereas cross-strike variations are often dramatic in terms of lithology, metamorphic conditions and structural characteristics.

The cross-orogen variations are similar to the types of variations observed in Phanerozoic orogens. In the east, and overlying a pre-orogenic basement, supracrustal rocks that were deposited on the basement are deformed into a thrust and fold belt principally by thin-skinned style of thrusting (Asiak thrust and fold belt). The fold-thrust belt gives way westwards to the Hepburn metamorphic and plutonic belt, just as the southern Appalachains have the Blue Ridge and Piedmont and the Canadian Cordillera has the Omineca and Intermontane regions. The exotic Hottah terrane is analogous to, and in an identical tectonic position to, the various exotic terranes in modern orogens.

Magmatism in the Great Bear magmatic zone is similar in several key ways to the modern Andean (continental) arc. First its position and geometry are identical to subduction-related continental arcs. It was extruded onto and intruded into deformed rocks that were adjacent to the Coronation margin, and it strikes parallel to the margin. Both its major element (calc-alkaline) and trace element (LIL-enriched) characteristics are essentially identical to modern arcs.

Finally, regional geophysical imaging has detected crustal and lithospheric mantle structures that could be easily taken for modern subduction-style features. The depth, geometry, location, and correlations to surface transitions are all analogous to what are observed in modern plate-boundary orogens.

Nevertheless, the Wopmay Orogen, as presently understood, does not have some key characteristics that some authors (e.g., Stern 2005) suggest are necessary hallmarks for identifying the products of plate tectonism in the modern style. Such characteristics include ophiolites (as defined in Anonymous 1972), blueschist/paired metamorphic belts and ultra high pressure belts (Stern 2005). The view presented here

and elsewhere (e.g., Hoffman 1980, 2006; Hildebrand et al. 1987; Cook, in press) is that such features may be diagnostic when found, but are not necessary for interpreting modern-style plate tectonism.

As noted in Van der Velden and Cook (1999) and Cook (in review), seismic images of structures within subduction assemblages in Phanerozoic orogens appear to be similar to lithospheric-scale structures in Paleoproterozoic orogens (and even the Neoarchean; Van der Velden et al. 2006), the primary differences being related to the amount of subduction overthrusting, the level of erosion and the amount of subsequent preservation. It is the author's view that variations in such processes are likely greater from one orogen to another, or even along strike in a single orogen, than they are between modern orogens and Paleoproterozoic orogens.

With these considerations, evolutionary models that are based on lithospheric plate–margin interactions have been proposed, and modified, since 1980. A recent, and recently modified, incarnation that includes results from lithospheric geophysical imaging is illustrated in Fig. 14.10 (Cook, in press).

14.3.2 The Hottah Arc Configuration

The size and original position of the Hottah arc (e.g., distance from the Slave craton) are poorly known. Based on paleomagnetic data, it appears that the Slave craton was in an equatorial region (0°–20° latitude; Evans and Hoye 1981), and probably the southern hemisphere (Hildebrand 1988) at about 1.9 Ga, but, as there are no data concerning the paleomagnetic relationship between the Hottah and the Coronation margin prior to convergence, their geographic relationship has been interpreted on the basis of geochronology (Hoffman and Bowring 1984) and sedimentological characteristics (Hildebrand 1988).

Early arguments centered on the geochronological relationships of the Akaitcho group (ca. 1.90 Ga), presumed to be early strata in the Coronation passive margin, and the initial stages of the Calderian orogeny (ca. 1.88–1.87 Ga). The remarkably short (~10–15 Ma) time difference led to interpretations of either rapid plate movement to accommodate closure of an ocean basin (Hoffman and Bowring 1984) or closure of a much smaller back-arc basin (Lalonde 1989; Hildebrand 1988).

Subsequent correlations and geochronological measurements, however, led to an interpretation of the Akaitcho Group as strata that were located at the leading edge of the approaching Hottah terrane, and thus not part of the Coronation margin (Bowring and Grotzinger 1992). In this scenario the time between passive margin development in the Coronation Supergroup and the onset of Calderian deformation is uncertain, but may be as much as 90 Ma (Bowring and Grotzinger 1992), thus allowing time for substantial basin development. In any case, 1.882 Ga zircons in the lower Recluse Group strata indicate that Calderian deformation was underway by that time and that detritus was being shed eastward onto the foreland (Bowring and Grotzinger 1992).

The orientation of subduction that was responsible for the Hottah arc is uncertain, but likely dipped westward (Fig. 14.10a). If, for example, the Recluse Group is indeed a foreland basin sequence (Hoffman and Bowring 1984; Hildebrand et al. 2010), then the continental margin was loaded from the west and subduction was likely west-dipping. Furthermore, if the Hottah-Coronation basin were small, it is conceivable that it could have closed by east-dipping subduction, but there are no obvious products of such subduction that are visible on the Coronation margin. Intrusion of the syn-orogenic Morel sills (Fig. 14.2) is interpreted to be associated with slab breakoff (Hildebrand and Bowring 1999; Fig. 14.10b)

14.3.3 The Great Bear Magmatic Zone Configuration

The Great Bear magmatic zone (Fig. 14.10c) in part straddles the boundary between the Hottah terrane and the deformed Coronation margin and thus provides a tectonic and geochronological link between them following suturing. Specifically, convergence of the Hottah terrane and the Coronation margin ended prior to the onset of Great Bear magmatism at ca. 1.87 Ga, and later deformation produced folding and uplift of some Great Bear volcanic and sedimentary rocks prior to the termination of magmatism ca. 1.845 Ga (e.g., Hildebrand et al. 1987; Bowring and Grotzinger 1992). It is likely

that the subduction responsible for Great Bear magmatism dipped eastward (Hildebrand et al. 1987), and is now visible on the geophysical images (Cook et al. 1999; Fernandez-Viejo and Clowes 2003; Mercier et al. 2008; Fig. 14.11c). This is a strong indication that subduction flipped from west-dipping (Fig. 14.10b) to east-dipping (Fig. 14.10c) as is common in modern arc–continent collisions.

If correct, this means that the time from the ~1.88 Ga onset of Calderian contraction (convergence of the Hottah terrane with the Coronation margin via west-dipping subduction; Fig. 14.11b) to the ~1.87 Ga onset of Great Bear magmatism due to east dipping subduction (Fig. 14.11c) represents a subduction flip that took place in less than ten million years.

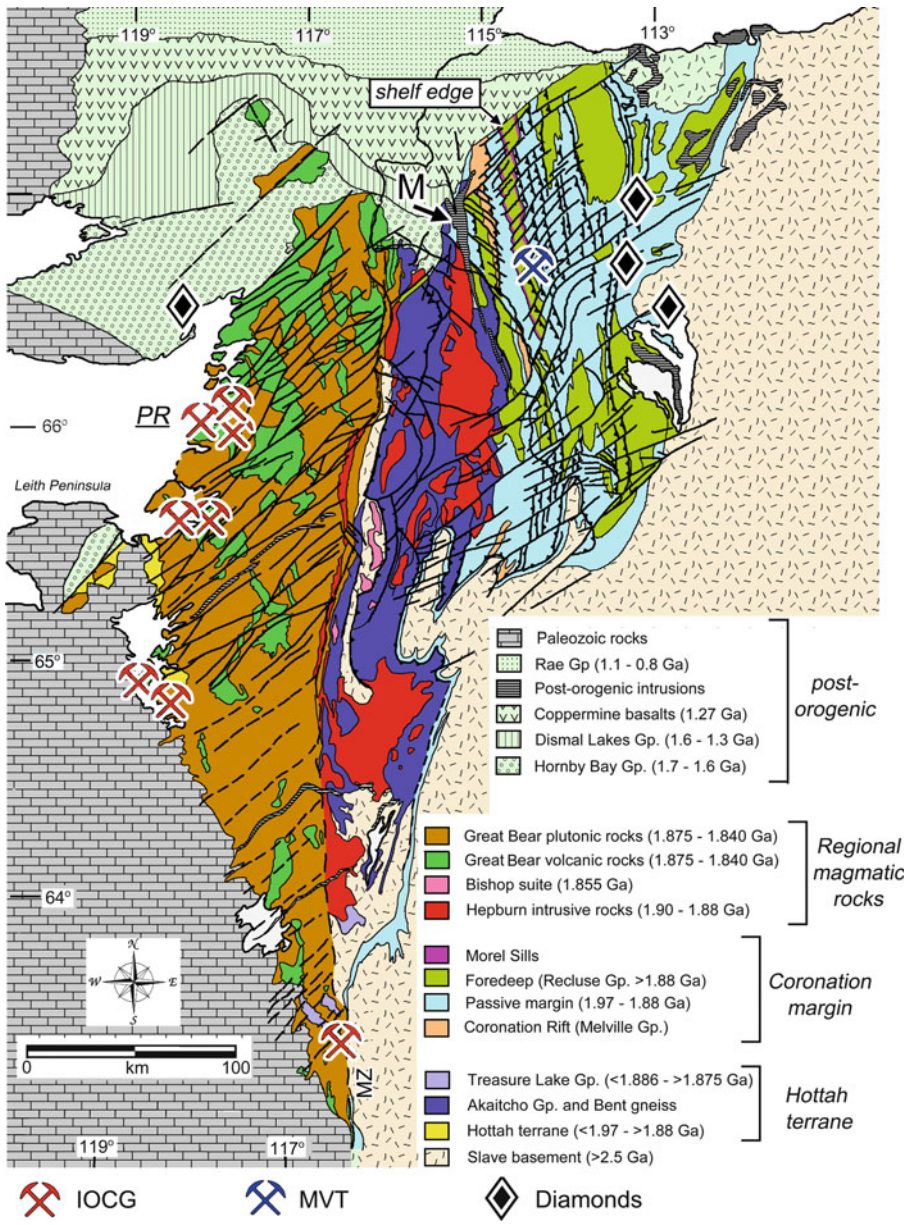

Fig. 14.11 Geological map from Fig. 14.2 illustrating the locations of some key mineral deposits (Alston 2001; Boyd 2001; Robins 2001; Ewing 2001; Paradis et al. 2007; Corriveau 2007). M, Muskox intrusion.

14.3.4 The Nahanni: Fort Simpson Configuration

The original geographical position and the regional extent of the Nahanni-Fort Simpson terrane are unknown. The only direct evidence for the terrane are a series of drill holes that penetrate into ~1.845–1.854 Ga felsic intrusive rocks, and the configuration of the potential field anomalies associated with them (Hoffman 1987; Villeneuve et al. 1991; Cook et al. 1992, 2005; Fig. 14.1). Furthermore it is likely that the post-orogenic extensional Fort Simpson and Wernecke basins dismembered the terrane outboard (west) of the Fort Simpson magmatic arc so that it rifted away and is now on another continent (e.g., Snyder et al. 2002).

Although the subduction orientation for the Great Bear arc magmas was most likely east-dipping as described previously, the subduction orientation that was responsible for the Fort Simpson magmas is uncertain. However, it seems likely that it was also east-dipping because there is no obvious disruption of the Great Bear subduction zone on the subsurface images (Fig. 14.9). Images of an east-dipping boundary in the mantle beneath the Fort Simpson arc appear independently on different seismic data sets (Cook et al. 1999; Fernandez-Viejo et al. 1999; Fernandez-Viejo and Clowes 2003; Mercier et al. 2008; Cook, in review). It is visible on seismic reflection data (Fig. 14.9a, b) between 60 and 75 km depth approximately 25–50 km west of the Fort Simpson arc (Cook et al. 1999). It also appears as a more extensive feature on teleseismic data (S2 on Fig. 14.9c) where it can be seen dipping east between ~44 km depth approximately 175 km west of the arc to ~100 km depth beneath the arc (Mercier et al. 2008; Cook, in press). An attractive interpretation is that this reflection represents a remnant of the subduction zone for the Fort Simpson magmas (Fig. 14.10d).

14.3.5 Implications for the Evolution of the Continental Lithosphere

Island arcs and continental arc magmas have commonly been cited as possible candidates for progressive additions to and thus growth of continental crust (e.g., Taylor and White 1965; McLennan 1988). While models of continental growth since the Archean vary considerably from substantial growth (e.g., Taylor and White 1965) to virtually no growth (e.g., Armstrong 1991), most workers favor some compromise of continuous, but decreasing rates, of continental growth due to internal global cooling and slowing of the convection in the mantle.

An important uncertainty in any model for continental evolution is the way in which terranes are accreted to each other and to the margins of the continents. The results from the Wopmay Orogen are relevant to this discussion in two key ways. First, the crustal geometry near the Hottah-Slave convergence as well as the Fort Simpson-Hottah convergence appears to be indicative of tectonic wedging and delamination of upper and middle crustal rocks from the lower crust and upper mantle (Cook et al. 1998). Thus, the bulk of the lithospheres beneath the terranes appears to be subducted and recycled, with only a relatively small residual component left at and near the surface. This type of geometry, with detached upper and middle crustal sheets and recycled lower crust and upper mantle lithosphere, is common in Phanerozoic orogens (e.g., Cook et al. 1979, 1980, 2004; Snyder et al. 2002).

Second, the recycling of crustal and upper mantle material appears to take place in at least two ways. The subduction process, by definition, carries crustal material, whether oceanic or detached arc, into the mantle. However, complex structures in the uppermost mantle with a flat, or nearly flat, Moho, can be interpreted as crustal material of Wopmay age (possibly related to Hottah terrane convergence) that was heated such that felsic magmas were removed and a mafic, or even ultramafic, restite remained. This process could have caused a Moho that was originally deepened when the crust thickened by convergence to be overprinted (in a petrologic and thus geophysical sense) at a shallower level above the mafic-ultramafic restite (Hynes and Snyder 1995; Cook 2002; Cook and Vasudevan 2003).

The result is that there is little evidence for the formation and addition of "new" continental material to the margin of the Slave craton during the development of the Wopmay Orogen. Rather, the process of recycling, whether by subduction or by restite formation or both, appears to be significant.

Following Wopmay orogenesis, the region was subjected to post-orogenic extension that formed the

Fort Simpson basin (Fig. 14.9e) and the Hornby Bay basin (Fig. 14.2). The Fort Simpson basin sedimentary rocks can be followed on seismic profiles beneath the Cordillera and comprise a large fraction of the crust upon which the Cordillera was constructed (Snyder et al. 2002, 2009; Cook et al. 2004). The tectonic cause(s) of the extension that formed these basins is uncertain. For example, a younger collision that followed the accretion of the Fort Simpson/Nahanni terrane may have occurred and then been separated from western Laurentia during formation of the Fort Simpson and Hornby Bay basins. However, as no evidence for such a collision has been observed, this seems unlikely. In the absence of such evidence, perhaps a more likely scenario might be that plate velocity changes caused the active continental margin to be fragmented due to buoyancy of the mantle wedge, which in turn promoted trench retreat, gravitational collapse and the ultimate breakup of the margin (e.g., Rey and Muller 2010).

14.4 Mineral Deposits of the Wopmay Orogen

Mineral deposits of the Wopmay Orogen are of the following different types (Fig. 14.11) (1) syn- to late orogenic Mississippi Valley type (MVT) carbonate-hosted Pb–Zn deposits, (2) syn- to post orogenic Iron Oxide – Copper – Gold (IOCG) deposits, and (3) post-orogenic, kimberlite-hosted diamond deposits.

Probably the best known MVT deposit in the Wopmay Orogen is the Esker deposit that occurs in the Rocknest formation of the Coronation Supergroup. The Esker deposit occurs as Pb–Zn enrichment in zones up to 10 m thick as showings over hundreds of square km (Gummer et al. 1996; Paradis et al. 2007). The age of mineralization is uncertain, but silicification near the sulphides is interpreted to be late-depositional or immediately post-depositional age (Paradis et al. 2007). If mineralization is found to be post-depositional, it may indicate that fluid migration was related to orogenic uplift and development of the foreland fold-thrust belt at the orogen margin as has been suggested for MVT deposits elsewhere (e.g., Oliver 1986).

Perhaps the most actively prospected minerals in the Wopmay orogen are associated with IOCG deposits that can be related to the Great Bear arc (e.g., Corriveau 2007). However, whether the mineralization was associated with arc magmatism or whether it occurred at some later date (or a combination) is uncertain. Perhaps the most famous of these deposits are the Port Radium radioactive mineral deposits along the eastern margin of Great Bear Lake that were discovered in 1930 and produced uranium oxide for nuclear purposes until 1960. Jory (1964) proposed that the host granitic rocks near Port Radium were intruded at about 1.820 $\pm$ 0.030 Ga (now thought to be 1.85–1.87 Ga; Mumin et al. 2008). Early geochronological results were interpreted to indicate that the mineralized veins could have been substantially younger, near 1.445 Ga or even younger (e.g., Jory 1964). However, more recent mapping supports an interpretation of the alteration and mineralization as syn-magmatic (Mumin et al. 2008).

The past production of the Port Radium – Echo bay district along the western margin of Great Bear Lake includes ~15 $\times$ 10^6 kg of U_3O_8 and ~32 $\times$ 10^6 of Ag (Corriveau 2007; Corriveau and Mumin 2007). Hence many of the IOCG deposits in the region are associated with radioactive minerals. Radioactivity of the region is high and is concentrated in the Great Bear arc, particularly in the region east and northeast of Great Bear Lake (Fig. 14.12). Little surface radioactivity is observed in the foreland region of the orogen. Mapping the distribution of surface radioactivity provides a tool for expanding the exploration away from known deposits and even into post-orogenic strata that overlie the Great Bear arc (e.g., Ootes et al. 2007).

Post orogenic mineral deposits (other than possible MVT fluid activity or post-orogenic vein deposits) include layered mafic intrusive rocks of the Muskox intrusion complex and kimberlite-hosted diamonds. The Muskox intrusion (Fig. 14.2) is a generally funnel shaped post-orogenic, mafic to ultra-mafic intrusion that is part of the Mackenzie Large Igneous Province (ca 1.27 Ga; LeCheminant and Heaman 1989) that also includes the Coppermine basalts of the Coppermine Homocline, the continent -scale Mackenzie dyke swarm and the Muskox intrusion. The Muskox intrusion, which is ~50–60 km long and up to ~12 km wide, was emplaced into rocks of the Coronation passive margin, Recluse Group foredeep and Akaitcho accreted complex (Fig. 14.2). The intrusion is ~50–60 km long and ~12 km wide at its widest point. The intrusion plunges gently northward such that the

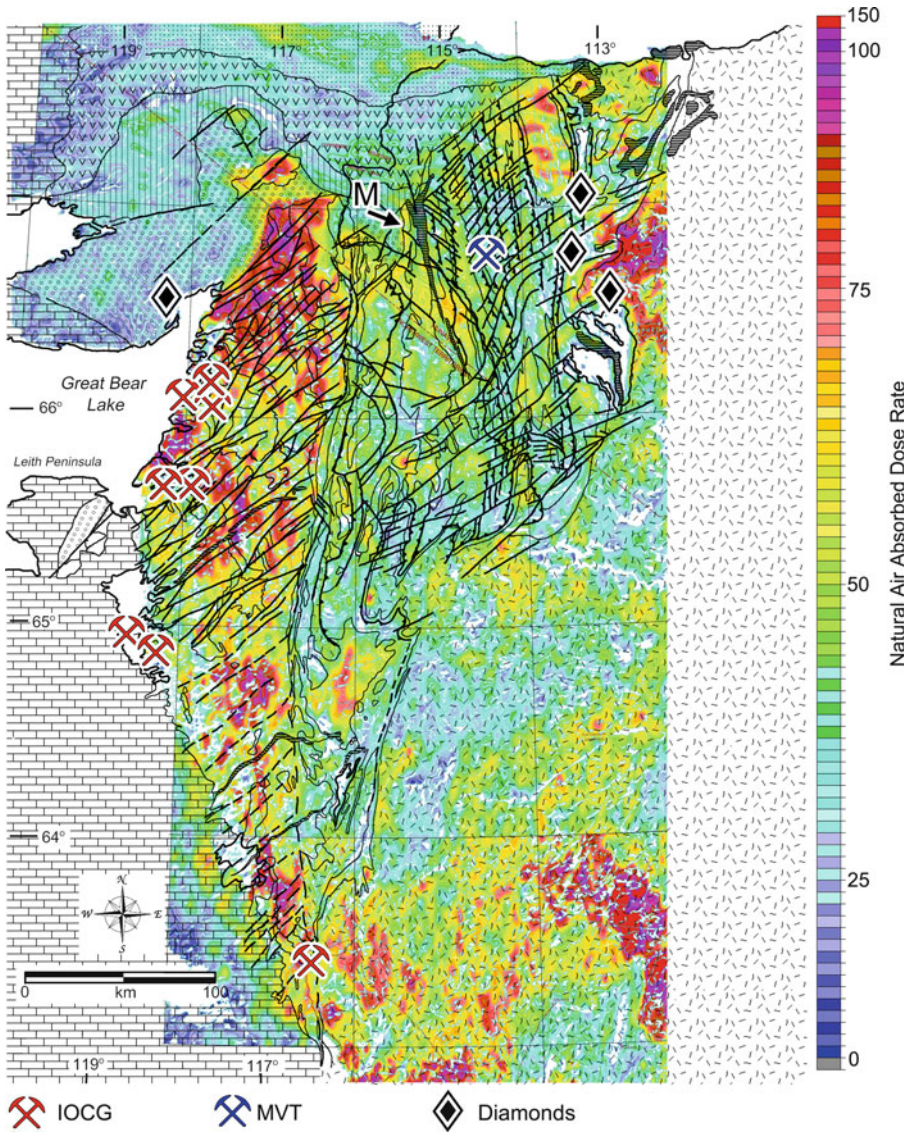

Fig. 14.12 Map of surface radioactivity (Carson et al. 2001) with an outline of the geological map of the Wopmay orogen superimposed. Note the large concentrations of high radioactivity (indicative of radioactive minerals) in the vicinity of eastern Great Bear Lake (e.g., Port Radium).

deep levels, including the feeder zone, are exposed to the south. Crystal settling within the magma chamber resulted in the northern upper portion of the intrusion being dominantly gabbroic, and the southern middle and lower parts of the intrusion being dominantly dunite and peridotite. Accordingly, it exhibits prominent gravity and magnetic signatures, is tantalizingly similar to large mafic- ultramafic intrusion deposits such as Noril'sk in Russia, and is thus being actively explored for Ni, Cu and platinum group elements.

While not specifically related to the arc development during the formation of the Wopmay Orogen, some kimberlite deposits are associated with thickened Archean lithosphere of the Slave craton. In this area, cratonic basement of the Slave Province projects westward to at least the Medial zone, and perhaps somewhat farther (Cook, in press; see also Fig. 14.9b). Diamondiferous kimberlites have been found in the eastern Asiak thrust and fold belt (Alston 2001; Boyd 2001; Robins 2001; Ewing 2001), autochthonous

Coronation margin strata (Fig. 14.11) and the adjacent Slave Province. Recently, diamonds have been discovered in kimberlite near the northeast corner of Great Bear Lake in the Hornby Bay basin (Fig. 14.11) and in Darnley Bay, about 400 km farther northwest (Gochnauer et al. 2010). Although Slave basement crust probably projects in the subsurface to the west of the medial zone (Fig. 14.9b; Cook et al. 1999; Spratt et al. 2009; Cook, in press), it seems unlikely that it projects as far as Great Bear Lake or even farther. Hence, the relationship between the diamonds near Great Bear Lake and Darnley Bay to Slave craton is presently unknown.

14.5 Seismic Risk

The seismic risk of the Wopmay Orogen may seem moot as the arc-related tectonism has been dormant for ~1.85 Ga. However, the structures that developed as a result of the formation of the orogen are key factors in focusing modern seismic activity in the region. In the exposed portion of the orogen, only two small earthquakes have been observed between 1965 and 1991 (Fig. 14.13). These were small, and probably shallow. It is likely they were associated with structures in the Asiak thrust and fold belt or mine blasts at nearby mines.

More importantly, a series of earthquakes with magnitudes ranging from very small to nearly 7.0 has been observed in the vicinity of the Mackenzie Mountains (Fig. 14.13). While these are clearly related to modern tectonism, most likely as a result of collision along the Pacific margin (Mazzotti and Hyndman 2002), the seismic activity along the eastern margin of the Mackenzie Mountains is localized along, or near, the eastern limit of the Fort Simpson basin, which is, in turn, characterized by a prominent (~20 km) west-facing ramp in the basement at the position of the Fort Simpson/Nahanni magmatic arc (Fig. 14.9; Cook et al. 2005). Hence the position and deep structure of the arc, though formed at approximately 1.85 Ga, is an important factor in localizing substantial modern seismicity, some of which would be potentially damaging in more populated areas.

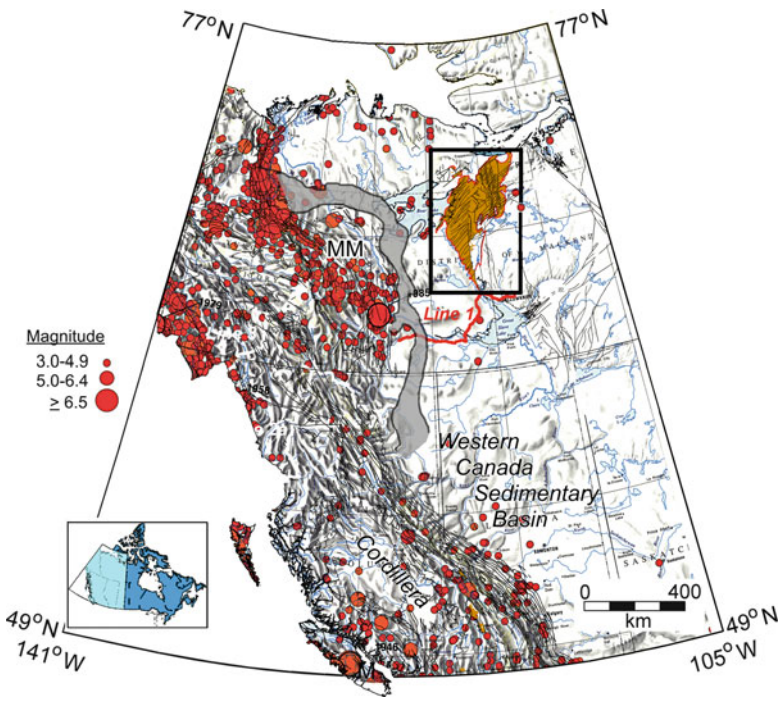

Fig. 14.13 Map of the seismicity of western Canada (Anglin et al. 1990). Note that, although the Wopmay orogen is generally seismically quiet, the position of the Fort Simpson arc and associated ramp (shown by *gray coloring*; Cook et al. 1992, 1999, 2005) displays a significant concentration of seismic activity at the eastern front of the Mackenzie Mountains (MM), some of which produces quite large ($M > 6.5$) earthquakes.

14.6 Conclusions

Arc development in the Paleoproterozoic Wopmay orogen was of two types – continental margin (e.g., Hepburn intrusive rocks, Great Bear magmatic zone and Bishop intrusive suite) and arc terranes that were formed offshore and subsequently accreted to the margin as a result of subduction (Hottah and Nahanni/Fort Simpson terranes). The Great Bear magmatic zone (and Bishop intrusive suite) was also formed by subduction, but was emplaced onto the margin following accretion of the Hottah arc terrane to the Coronation margin, thus stitching the terrane to the margin. The different types of arcs are distinguished by intrusive and stratigraphic relationships, ages (accreted arcs may predate orogeny on the continental margin), and isotopic signatures more readily than by rock types, which may be similar.

The evidence for the oldest two arcs, the Hottah arc terrane (~2.10–1.90 Ga) and the Great Bear magmatic zone (~1.87–1.84 Ga) appears to be reasonably well established, although the geographic extent of the Hottah terrane is unknown due to the fact that it is largely covered by Phanerozoic rocks of the Western Canada Sedimentary Basin. Collision of the Hottah terrane with the Slave craton took place by west-dipping subduction which terminated and was followed by east-dipping subduction that was responsible for the Great Bear magmatism. Evidence for the youngest arc, the Fort Simpson arc, is less certain. It probably formed as a magmatic arc outboard of the accreted Hottah terrane and more or less coeval with the later stages of the Great Bear magmatism. As with the Hottah terrane, the geographic extent of the Fort Simpson arc is uncertain beyond the limits of the potential field signatures that outline it because it is entirely covered by Phanerozoic strata of the Western Canada Sedimentary Basin.

In summary, arcs of the Wopmay Orogen appear to be geologically, geochemically, and geometrically similar to modern arcs. They are integral parts of the tectonic development of the Wopmay Orogen and they, along with the foreland fold-thrust belt, display large-scale geometric characteristics that are similar to the plate tectonically induced margin-parallel characteristics of Phanerozoic orogens.

Acknowledgments This research was supported by the Natural Sciences and Engineering Research Council of Canada (Grant 2623-2005) and the Geological Survey of Canada. Seismic data were processed at the Lithoprobe Seismic Processing Facility at the University of Calgary. The manuscript benefited from reviews by T. Rivers and an anonymous reviewer.

References

Alston GR (2001) Rhonda Announces Completion of 2001 Spring Core drill Program, Rhonda Corporation news release of July 12, 2001

Anglin FM, Wetmiller RJ, Horner RB, Rogers GC, Drysdale JA (1990) Seismicity map of Canada, Geological Survey of Canada, Canadian Geophysical Atlas Map 15. Scale 1:1,000,000

Anonymous (1972) Penrose field conference on ophiolites. Geotimes 17:24–25

Armstrong RA (1991) The persistent myth of crustal growth. Australian Journal of Earth Sciences 38:613–630

Atherton MP, McCourt WJ, Sanderson LM, Taylor WP (1979) The geochemical character of the segmented Peruvian Coastal Batholith and associated volcanics. In: Atherton MP, Tarney J (eds). Origin of Granite Batholiths. Shiva Publishing Ltd., Orpington 45–64

Baragar WRA, Donaldson JA (1973) Coppermine and Dismal lakes map-areas 86 O and 86 N. Geological Survey of Canada Paper 71-39, p 20

Bowring SA (1984) U-Pd zircon geochronology of early Proterozoic Wopmay Orogen, N.W.T., Canada: an example of rapid crustal evolution. PhD. Thesis, University of Kansas, Lawrence, Kansas

Bowring SA, Grotzinger JP (1992) Implications of new chronostratrigraphy for tectonic evolution of the Wopmay orogen, northwest Canadian shield. Am J Sci 292:1–20

Bowring SA, Podosek FA (1989) Nd isotopic evidence for 2.0-2.4 Ga crust in western North America. Earth Planet Sci Lett 94:217–230

Boyd R (2001) Artemisia Kimberlite Sample Highly Diamondiferous, Ashton Mining of Canada Inc. news release of November 1, 2001

Carson JM, Holman PB, Ford KL, Grant JA, Shives RBK (2001) Airborne gamma-ray spectrometry compilation series, Great Bear River, Northwest Territories-Nunavut, Geological Survey of Canada Open File 4113. Scale 1:1,000,000

Coles RA, Haines GV, Hannaford W (1976) Large scale magnetic anomalies over western Canada and the arctic: a discussion. Can J Earth Sci 13:790–802

Cook FA in press. Paleoproterozoic assembly of the Wopmay orogen lithosphere. In: Percival J, Cook F, Clowes R Geological Association of Canada Special Paper

Cook FA (2002) Fine structure of the continental reflection Moho. Geological Society of America Bulletin 114:64–79

Cook FA, Erdmer P (2005) An 1800 km cross section of the lithosphere through the northwestern North American plate:

lessons from 4.0 billion years of Earth's history. Can J Earth Sci 42:1295–1311

Cook FA, van der Velden AJ (1993) Proterozoic crustal transition beneath the Western Canada Sedimentary basin. Geology 21:785–788

Cook FA, Albaugh D, Brown LD, Kaufman S, Oliver JE, Hatcher R Jr. (1979) Thin-skinned tectonics in the crystalline southern Appalachians: COCORP seismic reflection profiling of the Blue Ridge and Piedmont: Geology 7: 653–657

Cook FA, Vasudevan K (2003) Are there relict crustal fragments beneath the Moho? Tectonics 22:1026, 10-1 to 10-12

Cook F, Dredge M, Clark EA (1992) The Proterozoic Fort Simpson structural trend in northwestern Canada. Geol Soc Am Bull 104:1121–1137

Cook FA, van der Velden A, Hall KW, Roberts B (1998) Tectonic delamination and subcrustal imbrication of the Precambrian lithosphere in northwestern Canada mapped by Lithoprobe. Geology 26:839–842

Cook FA, van der Velden A, Hall KW, Roberts B (1999) Frozen subduction in Canada's Northwest Territories: lithoprobe deep lithospheric reflection profiling of the western Canadian Shield. Tectonics 18:1–24

Cook FA, Clowes RM, Snyder DB, van der Velden AJ, Hall KW, Erdmer P, Evenchick CA (2004) Precambrian crust beneath the Mesozoic northern Canadian Cordillera discovered by Lithoprobe seismic reflection profiling. Tectonics 23:TC2010. doi:10.1029/2002TC001412

Cook FA, Hall KW, Lynn CE (2005) The edge of northwestern North America in the Mesoproterozoic. Can J Earth Sci 42:983–997

Corriveau L (2007) Iron oxide copper-gold deposits: a Canadian perspective. In: Goodfellow WD (ed) Mineral deposits of Canada: a synthesis of major deposit-types, district metallogeny, the evolution of geological provinces, and exploration methods. Geological Association of Canada, Mineral Deposits Division, Special Publication 5, pp 307–328

Corriveau L, Mumin H (2007) Geoscience and exploration tools for multiple discoveries within the extraordinary range of IOCG polymetallic mineral deposits, 35th Annual Yellowknife Geoscience Forum Abstracts of Talks and Posters November 20–22, 2007, p 10

Crowley JL (1999) U-Pb geochronologic constraints on Paleoproterozoic tectonism in the Monashee complex, Canadian Cordillera. Elucidating an overprinted geologic history. Geological Society of America Bulletin 111:560–577

Delaney GD (1981) The mid-Proterozoic Wernecke Supergroup, Wernecke Mountains, Yukon Territory. In: Campbell FHA (ed) Proterozoic basins of Canada. Geological Survey of Canada Paper 81-10, pp 1–23

Dewey JF (1977) Suture zone complexities: A review. Tectonophysics, 40:53–67

Eaton DWS, Vasudevan K, Cook FA (2008) Application of skeletonization-migration in deep crustal reflection seismic profiling. In:13th international symposium on deep crustal profiling of the continents and their margins. Saariselka, Finland, p 15

Evans ME, Hoye GS (1981) Paleomagnetic results from the lower Proterozoic rocks of Great Slave Lake and Bathurst Inlet areas, Northwest Territories. In: Campbell FHA (ed) Proterozoic basins of Canada, Geological Survey of Canada Paper 81-10, pp 191–202

Ewing G (2001) Further significant diamond results from Tahera's Anuri East Kimberlite, Tahera Corporation news release of December 11, 2001

Fernandez-Viejo G, Clowes RM (2003) Lithospheric structure beneath the Archean Slave Province and Proterozoic Wopmay Orogen, northwest Canada, from a Lithoprobe refraction/wide-angle reflection survey. Geophys J Int 153(1–19):2003

Fernandez-Viejo G, Clowes RM, Amor JR (1999) Imaging the lithospheric mantle in northwestern Canada with seismic wide-angle reflections. Geophys Res Lett 26:2809–2812

Gandhi SS, van Breemen O (2005) SHRIMP U-Pb geochronology of detrital zircons from the Treasure Lake Group – New evidence for Paleoproterozoic collisional tectonics in the southern Hottah terrane, northwestern Canadian Shield. Can J Earth Sci 42:833–884

Gandhi SS, Mortensen JK, Prassad N, van Breeman O (2001) Magmatic evolution of the southern Great Bear continental arc, northwestern Canadian Shield. Can J Earth Sci 38: 767–785

Gochnauer K, Falck H, Irwin D (2010) 2009 Northwest Territories mineral exploration overview. Northwest Territories Geoscience Office, p 22

Gummer PK, Plint HE, Rainbird RH (1996) The Esker Lake prospect: stratabound Pb-Zn-Cu-Ag in emergent inner shelf carbonates, Rocknest Formation, Coronation Supergroup, Northwest Territories: 3, in 1996 Exploration Overview: Department of Indian and Northern Development Canada, pp 18–19

Hammer PTC, Clowes RM, van der Velden AJ, Cook FA, Vasudevan K (2010) The LITHOPROBE trans-continental lithospheric cross-sections: imaging the internal structure of the North American continent. Can J Earth Sci 47(5): 821–857

Hildebrand RS (1981) Early Proterozoic LaBine Group of Wopmay orogen: remnant of continental volcanic arc developed during oblique convergence. In: Campbell FHA (ed) Proterozoic Basins of Canada. Geological Survey of Canada Paper 81-10, pp 133–156

Hildebrand RS (1988) Implications of ash dispersal for tectonic models with an example from Wopmay orogen. Geology 16:1089–1091

Hildebrand RS, Bowring SA (1999) Crustal recycling by slab failure. Geology 27:11–14

Hildebrand RS, Roots CF (1985) Geology of the Rivière Grandin map area (Hottah terrane and western Great Bear Magmatic Zone), District of Mackenzie, in Current Research, Part A. Geological Survey of Canada Paper 85-1 A, pp 373–383

Hildebrand RS, Hoffman PF, Bowring SA (1987) Tectonomagmatic evolution of the 1.9 Ga Great Bear magmatic zone, Wopmay orogen, northwestern Canada. J Volcanol Geoth Res 32:99–118

Hildebrand RS, Bowring SA, Housh T (1990) The medial zone of Wopmay orogen. Geological Survey of Canada Paper 90-1C, pp 167–176

Hildebrand RS, Paul D, Pietekainen P, Hoffman P, Bowring SA, Housh T (1991) New geological developments in the internal zone of Wopmay Orogen. Geological Survey of Canada Paper 91-1C, pp 157–164

Hildebrand RS, Hoffman PF, Bowring SA (2010) The Calderian orogeny in Wopmay orogen (1.9 Ga), northwest Canadian Shield. Geol Soc Am Bull 122:794–814

Hoffman PF (1980) Wopmay Orogen: a Wilson cycle of Early Proterozoic age in the northwest of the Canadian Shield. In: Strangway DW (ed) The continental crust and its mineral deposits. Geological Association of Canada Special Paper 20,pp 523–549

Hoffman P.F, Pelletier K.S. (1982) Cloos nappe in Wopmay orogen: significance for stratigraphy and structure of the Akaitch Group, and implications for opening and closing of an early Protoerozoic continental margin. Geological Survey of Canada Paper 82-1A:109–115

Hoffman PF (1984) Wopmay fault zone and its role in evolution of Wopmay orogen. Geological Association of Canada Program and Abstracts 9, p 74

Hoffman PF (1987) Continental transform tectonics: Great Slave Lake shear zone (ca. 1.9 Ga), northwest Canada. Geology 15:785–788

Hoffman PF (2006) Evidence from ophiolites, blueschists, and ultrahigh-pressure metamorphic terranes that the modern episode of subduction tectonics began in Neoproterozoic time: Comment and Reply: COMMENT. Geological Society of America Online Forum. doi: 10.1130/G22300.1

Hoffman PF, Bowring SA (1984) Short-lived 1.9 Ga continental margin and its destruction, Wopmay Orogen, northwest Canada. Geology 12:68–72

Hoffman PF, McGlynn JC (1977) Great Bear batholith: a volcano-plutonic depression. In: Baragar WRA, Coleman LC, Hall JM (eds) Volcanic regimes in Canada. Geological Association of Canada Special Paper 16, pp 170–192

Hoffman Pf, Tirrul R, Grotzinger JP, Lucas SB, Eriksson KA (1984) The externides of the Wopmay orogen, Takijuq Lake and Kikerk Lake map areas, District of Mackenzie. Geological Survey of Canada Paper 84-1A, pp 383–395

Hoffman PF, Tirrul R, King JE, St-Onge MR, Lucas SB (1988) Axial projections and modes of crustal thickening, eastern Wopmay Orogen, northwest Canadian Shield. In: Clark SP Jr, Burchfiel BC, Suppe J (eds) Processes in continental lithospheric deformation. Geological Society of America Special Paper 218, pp 1–29

Hornal RW, Sobczak LW, Burke WEF, Stephens LE (1970) Preliminary results of gravity surveys over the Mackenzie Basin and Beaufort Sea: Energy, Mines and Resources Canada, Earth Physics Branch, Gravity Map Series, Maps 117, 118, 119

Housh T, Bowring SA, Villeneuve M (1989) Lead isotope study of Early Proterozoic Wopmay orogen, NW Canada: role of continental crust in arc magmatism. J Geol 97:735–747

Hynes A, Snyder DB (1995) Deep-crustal mineral assemblages and potential for crustal rocks below the Moho in the Scottish Caledonides. Geophys J Int 123:323–339

Jackson VA (2008) Preliminary Geologic Map of the southern Wopmay Orogen. Northwest Territories Open Report 2008–007. Scale 1:100,000

Jackson VA, Ootes L (2010) Preliminary geologic map of the south-central Wopmay Orogen (parts of NTS 86B, 86C, and 86D); results from 2009, Northwest Territories Geoscience Office, NWT open report 2010–004. Scale 1:100,000

Jackson VA, Bennett V, van Breemen O, Ootes L, Bleeker W, Davis W (2010) Geochronology of the south-central Paleoproterozoic Wopmay Orogen, northwest Canadian Shield. Geological Association of Canada Abstracts with Program, Abstract no. 312

Jory LT (1964) Mineralogical and isotopic relations in the Port Radium pitchblende deposit, Great Bear Lake, Canada. Ph D Thesis, California Institute of Technology, p 275

Karig DE, Sharman G (1975) Subduction and accretion in trenches, Geological Society of America Bulletin 86:377–389

Kay RW (1977) Geochemical constraints on the origin of Aleutian arc magmas. In: Talwani M, Pitman WC III (eds) Island Arcs, Deep Sea Trenches and Back – Arc Basins. American Geophysical Union Maurice Ewing Series I, pp 229–242

King JE (1986) The metamorphic internal zone of Wopmay orogen (Early Proterozoic), Canada: 30 km of structural relief in a composite section based on plunge projection. Tectonics 5:973–994

Lalonde AE (1989) Hepburn intrusive suite: peraluminous plutonism within a closing back-arc basin, Wopmay orogen, Canada. Geology 17:261–264

LeCheminant AN, Heaman LM (1989) Mackenzie igneous events, Canada: middle Proterozoic hotspot magmatism associated with ocean opening. Earth Planet Sci Lett 96: 38–48

McLennan SM (1988) Recycling of the continental crust. Pure and Applied Geophysics 128:683–724

Mazzotti S, Hyndman RD (2002) Yakutat collision and strain transfer across the northern Canadian Cordillera. Geology 30:495–498

Mercier J-P, Bostock MG, Audet P, Gaherty JB, Garnero EJ, Revenaugh J (2008) The teleseismic signature of fossil subduction: northwestern Canada. J Geophys Res 113:B04308. doi:10.1029/2007JB005127

Mumin AH, Corriveau L, Somarin AK, Ootes L (2008) Iron oxide copper-gold-type polymetallic mineralization in the Contact Lake belt, Great Bear magmatic zone, Northwest Territories, Canada. Explor Min Geol 16:187–208

Oliver J (1986) Fluids expelled tectonically from orogenic belts: Their role in hydrocarbon migration and other geologic phenomena. Geology 14:99–102

Ootes L, Goff S, Corriveau L, Harris J, Jackson V (2007) Uranium metallogeny in the Great Bear magmatic zone (Wopmay orogen) Aand adjacent terranes, 35th Annual Yellowknife Geoscience Forum Abstracts of Talks and Posters November 20–22, 2007, pp 10–11

Paradis S, Hannigan P, Dewing K (2007) Mississippi Valley-type lead-zinc deposits. In: Goodfellow WD (ed) Mineral deposits of Canada: a synthesis of major deposit-types, district metallogeny, the evolution of geological provinces, and exploration methods. Geological Association of Canada, Mineral Deposits Division, Special Publication No. 5, pp 185–203

Raymond L (2002) Petrology, the Study of Igneous, Sedimentary and Metamorphic Rocks. McGraw-Hill Higher Education Co., New York, 720 pp

Reichenbach IG (1991) The Bell Island Bay group, Remnant of an Early Proterozoic ensialic marginal basin in Wopmay Orogen. Geological Survey of Canada Paper 88-28, p 43

Rey PF, Muller RD (2010) Fragmentation of active continental plate margins owing to the buoyancy of the mantle wedge. Nat Geosci 3:257–260

Robins J (2001) Kimberlite Discovered on Kikerk Lake Property, Northern Empire Minerals Ltd. News release of September 6, 2001

Rodgers J (1949) Evolution of thought on structure of middle and southern Appalachians. Am Assoc Pet Geol 33:1643–1654

Ross GM, Kerans C (1989) Hornby Bay and Dismal Lakes Groups, Coppermine Homocline, Northwest Territories. Geological Survey of Canada, Map 1663A. Scale 1:250,000

Ross GM, Annell HC, Hamilton MA (2000) Lithology and geochronology of shallow basement along the SNORCLE line, southwest Northwest Territories: a preliminary report. In: Cook FA, Erdmer P (eds) Lithoprobe Slave-Northern Cordillera Lithospheric Evolution (SNORCLE) and Cordilleran Tectonics Workshop, Lithoprobe report 72, pp 76–80

Ross GM, Villeneuve ME, Theriault RJ (2001) Isotopic provenance of the lower Muskwa assemblage (Mesoproterozoic, Rocky Mountains, British Columbia): new clues to correlation and source areas. Precambrian Res 111:57–77

Seely DR (1977) The significance of landward vergence and oblique structural trends on trench inner slopes. In: Talwani M, Pitman WC III (eds) Island arcs, deep sea trenches and back – arc basins. American Geophysical Union Maurice Ewing Series I, pp 187–198

Snyder DB, Clowes RM, Cook FA, Erdmer P, Evenchick CA, van der Velden AJ, Hall KW (2002) Proterozoic prism arrests suspect terranes: insights into the ancient Cordilleran margin from seismic reflection data. GSA Today 12:4–10

Snyder DB, Pilkington M, Clowes RM, Cook F (2009) The underestimated Proterozoic component of the Canadian Cordillera accretionary margin. Geol Soc Lond Spec Publ 318:257–271. doi:10.1144/SP318.9

Spratt JE, Jones AG, Jackson V, Collins L, Avdeeva A (2009) Lithospheric geometry of the Wopmay Orogen from a Slave craton to Bear Province magnetotelluric transect. J Geophys Res. 114: B01101 doi:10.1029/2007JB005326

Stern RJ (2005) Evidence from ophiolites, blueschists, and ultrahigh-pressure metamorphic terranes that the modern episode of subduction tectonics began in Neoproterozoic time. Geology 33:557–560

St-Onge MR, King JE (1987) Evolution of regional metamorphism during back-arc stretching and subsequent crustal shortening in the 1.9 Ga Wopmay orogen, Canada. Philos Trans R Soc Lond A321:199–218

Taylor SR, White AJR (1965) Geochemistry of andesites and the growth of continents. Nature 208:271–273

Thorkelson DJ, Abbott JG, Mortensen JK, Creaser RA, Villeneuve ME, McNicholl VJ, Layer PW (2005) Early and Middle Proterozoic evolution of Yukon, Canada. Can J Earth Sci 42:1045–1071

Tirrul R (1984) Regional pure shear deformation by conjugate transcurrent faulting, externides of Wopmay orogen, NWT. In: Geological Association of Canada Abstracts with Programs, 9, p 111

Tirrul R (1992) Geology and Structural Restoration of the east-central part of Asiak thrust-fold Belt, Wopmay. Orogen, Northwest Territories. Geological Survey of Canada, Map 1654A. Scale 1:50,000

Van der Velden A, Cook F (1999) Proterozoic and Cenozoic subduction complexes: a comparison of geometric features. Tectonics 18:575–581

Van der Velden AJ, Cook FA (2005) Relict subduction zones in Canada. J Geophys Res 110:B08403. doi:1029/2004JB003333

van der Velden AJ, Cook FA, Drummond BJ, Goleby BR (2006) Reflections of the Neoarchean: A global perspective. American Geophysical Union Geophysical Monograph 164: 255–265

Villeneuve ME, Theriault RJ, Ross GM (1991) U-Pb ages and Sm-Nd signature of two subsurface granites from the Fort Simpson magnetic high. Can J Earth Sci 28:1003–1008

Part III
Models of Arc–Continent Collision Processes

Chapter 15
The Origin of Obducted Large-Slab Ophiolite Complexes

J.F. Dewey and J.F. Casey

15.1 Introduction

Ophiolites (sensu lato) are widespread but intermittent, along and across strike, in orogens and island arcs, and along rifted continental margins. Commonly, it is not easy to discern the origin of a sliver of serpentinite, gabbro, dolerite, or basalt caught up in an orogenic deformation zone. Some may even be flattened/sheared Alaskan-type sub-volcanic ultramafic plugs (Taylor and Noble 1960). Nine rock suites that have been termed ophiolites (Dewey 2003) are:

1. The oceanic crust and mantle of intra-arc/back-arcs. Spreading would be expected to be roughly arc-normal and dykes roughly parallel with arc trend. They could be obducted "hot" with subjacent granitic melt sheets. Some Klamath ophiolites (Boudier et al. 1989), Sarmiento (Stern and De Wit 2003), and Karmoy, Solund, and Leka (Furnes et al. 1988) may be of this type. Subduction can be partitioned into arc-parallel and arc-normal components. Obduction is likely to be difficult/limited, especially onto rifted continental margins. A variant is illustrated by the Andaman Sea where arc-parallel motion allows a pull-apart back-arc basin with arc-normal dykes. It is not obvious how these could be obducted as thin sheets onto continental margins.
2. Narrow Red Sea type oceans. Dykes are expected to be parallel with rift trend. They could be obducted young and "hot" with subjacent granitic melt sheets but will not be boninitic. The Vourinos, Othrys, and Balkan-trend Jurassic ophiolites (Phillips-Lander and Dilek 2009; Robertson et al. 2009) may be of this origin.
3. Narrow pull-apart oceans, such as the Cayman Trough and the Gulf of California, in transtensional segments of major strike-slip faults with dykes normal to the overall trend of the margin (Casey and Dewey 1984).
4. Alpine-type; sub-continental mantle pulled up beneath continental extensional detachments at rifted margins (Boillot et al. 1995; Dewey 2003). These lack sheeted complexes and, typically have an association of lherzolite intruded by gabbro and dolerite with pillow basalt. The classic Steinmann Trinity (spilite, serpentinite, and chert) is typical of this tectonic environment (Dewey 2003). The Galician margin, the Highland Boundary Fault Zone ultramafic/mafic association, the Platta/Malenco/Finero/Ivrea/Aosta ultramafic complexes, and the Sestri-Voltaggio complexes probably represent this origin. Such complexes may pass laterally into oceanic crust and mantle generated by organized sea-floor-spreading where continental stretching/rifting advances from continental stretching to separation.
5. Oceanic crust and mantle clipped, as thin sheets, from oceanic ridge crests where they enter subduction zones at ridge/trench/trench triple junctions (Van den Beukel and Wortel 1992). Possible examples are Taitao (Bourgois et al. 1993) and Nicoya (Berrange and Thorpe 1988). Such complexes are likely to be rotated thin flakes. This is the only obvious way in which obduction can occur from

J.F. Dewey
University College Oxford, Oxford, UK
Department of Geosciences, University of Houston, Houston, TX, USA
Department of Geology, UC Davis, Davis, CA, USA

J.F. Casey
Department of Geosciences, University of Houston, Houston, TX, USA

D. Brown and P.D. Ryan (eds.), *Arc-Continent Collision*, Frontiers in Earth Sciences,
DOI 10.1007/978-3-540-88558-0_15,

oceanic ridges that are not associated with arcs and is likely to be on a small scale.

6. Transforms exactly at continental margins that uplift complexes such as the late Jurassic, MORB thin crust, Masirah Complex (Shackleton and Ries 1990).
7. The local, very rare, possibility of the steady-state, diachronous conversion from ridge to trench or transpressive transform, such as the Macquarie Ridge (Varne et al. 1969, 2000; Dijkstra et al. 2010 and references therein), near or at a pole of rotation or by a change in pole of rotation position (Dewey 1975).
8. Mafic and ultramafic scraps, shreds and slivers scraped and clipped off subducting plates from whole seamounts to fragments of oceanic plateaux and fracture zones, such as those of the Franciscan, Ankara, and Malaita mélanges (Dewey 2003).
9. The subject of this paper; big flat obducted slabs with the full "1972" sequence (Coleman 1977), up to 12 km of, from base to top, harzburgite, dunite, layered gabbro, isotropic or weakly-layered gabbro with trondjemites at the top, mafic sheeted dike complex, pillow basalt, and sediment . For several years in the early 1970s, they were generally regarded, and are regarded by some subsequently and today, as fragments of the oceanic crust and mantle of the main oceanic spreading ridges (Casey et al. 1981; Coleman 1977; Dewey and Kidd 1977; Moores and Vine 1971; Nicolas 1989). They contain minuscule amounts of silicic igneous rocks apart from trondjemite. In places, garnet/phlogopite/kaersutite lherzolites (ariegites) form a basal unit to the harzburgite. Commonly, a mafic protolith, two-pyroxene granulite/garnet amphibolite up to 20 m thick forms a basal sole or aureole (Church and Stevens 1971; Dewey 1974, 1976; Gartzos et al. 2009). Troodos (Gass 1968; Moores and Vine 1971); Semail Complex Oman, (Nicolas 1989) Papua-New Guinea, (Davies 1971) Bay of Islands, (Casey et al. 1981) and New Caledonia (Nicolas 1989) are examples. Boninite (high Si and Mg high T/low P "wet" andesite, extremely depleted in incompatible heavy REE non-fluid-mobile trace elements but enriched in fluid-mobile elements (Rb, Ba, K), a primitive andesite derived from metasomatized mantle) are common in the pillow lavas of type 9 ophiolites (Coish 1989; Harper 2003; Hickey and Frey 1982; McCullough and Cameron 1983; Pearce et al. 1984; Schroetter et al. 2003; Taylor et al. 1992; Taylor and Nesbitt 1992) especially towards the top following earlier tholeiites. Boninites occur in the fore-arcs of oceanic arcs and are extant at several ridge/trench intersections (Deschamps and Lallemand 2003). Layer 1 andesite turbidite fans, sometimes with mafic/intermediate volcanics and sills (e.g., Snooks Arm; Upadhuay et al. 1971) with interstratified basalt/andesite sequences are common and suggest a close regional relationship with arc assemblages. We recognize that the Snooks Arm sequence, with its basal Betts Cove Ophiolite Complex, is not obviously a thin-sheet obducted ophiolite but we believe that all the western Newfoundland ophiolites, excluding the Annieopsquotch Ophiolite Complex belong to a single obducted fore-arc ophiolite sheet. Sheeted dykes are, commonly, normal to fore-arc trend (Casey et al. 1981; Dewey 2002; Lissenburg et al. 2004, 2005). Basal aureoles are about the same age or slightly younger than the ophiolite (Dewey 1976). They have a patchy/intermittent occurrence along orogenic margins although they are of roughly the same age in any orogenic belt, and are obducted during arc/continent collision. They are intimately associated with, commonly, mafic/ultramafic rock suites that have complex polyphase relationships among structural and mafic igneous events that can be best-explained as originating in transforms/fracture zones (e.g., Coastal Complex, Karson and Dewey 1978; Suhr and Cawood 2001; Arakapas Zone, Allerton and Vine 1992).

There are very great variations in types of "ophiolite" along-strike at the margins of and within orogens. All types occur in the Appalachian/Caledonian chain and the Alpine System. We draw our data and ideas, principally, from the ophiolites of Newfoundland, Shetland, the Lizard, Troodos, Oman, New Caledonia, and the Dinarides.

15.2 Previous Models

Previous models for the origin of type-9 ophiolite complexes include:

1. The nucleation of a subduction zone on an oceanic transform/fracture zone (Casey and Dewey 1984; Cawood and Suhr 1992). This was a useful step in

understanding the origin of subduction zones and the common association between large-slab ophiolites and rock assemblages that must have originated in transforms/fracture zones, and in placing ophiolites in fore-arcs. It can explain only transform assemblages that predate the ophiolite, can explain arc-normal dike trends but cannot account for boninites.

2. Arc-normal spreading in the fore-arc, by subduction roll-back, either at the infant arc stage immediately following the origin of a subduction zone (Pearce 2003; Hawkins 2003) or later with an RTT triple junction and oblique fore-arc spreading (Stern and Bloomer 1995). It does not explain the arc-normal dyke trend. Also, where old oceanic lithosphere is subducted and subduction roll-back is likely occurring, it is expressed by extension and intra-arc splitting of the overriding plate to form intra to back-arc basins (Karig 1982) not by magmatism between the overriding and subducting plates. It is not clear why a juvenile subduction zone should behave differently.
3. Deschamps and Lallemand (2003) have pointed out the association of boninites with RTF triple junctions in the region of the Fiji Islands and suggest this as a location for ophiolite genesis. Such a triple junction can generate only a short length of ophiolite because, as the triple junction evolves, it changes to an RFF junction, which gets further and further from the boninite subduction factory.
4. Dewey (2002) suggested an origin in fore-arc/arc pull-apart basins along transforms resulting from the partitioning of oblique subduction. This would account for boninites, arc-normal dyke trends with inside or outside corners ridge/transform intersections, and contacts that exhibit intrusive relationships between ophiolites, arcs, and transform/fracture zone assemblages. The principal drawback is that partitioned oblique subduction (Fitch 1972) mostly generates transforms along the arc axis (Dewey 1980) not in the fore-arc. Also, there is no obvious sign of the earlier fore-arc basement into which the ophiolite was intruded.
5. An origin in back/intra-arcs (Karig 1982; Bird et al. 1971; Dewey and Bird 1971). This would, usually, generate arc-parallel dyke trends and cannot explain boninites. Arc-normal dykes could result from the development of pull-apart basins in arc transforms resulting from the partitioning of oblique subduction. A particular problem with this model is how to obduct such a complex onto a rifted continental margin because there would always be an arc blocking the obduction route onto the rifted continental margin.
6. Moores et al. (2000) suggested a solution to the ophiolite conundrum/paradox/enigma based upon the principle of historical contingency. They argued that calc-alkaline material can be subducted from arcs into the mantle, to be cycled into the magma–genesis zones of ridges and thus generate calc-alkaline magmas in oceanic ridges, which may then become obducted . Sturm et al. (2000) demonstrated that such "contamination" of the mantle is possible. Our principal criticism of this model are that such contamination is likely to be too patchy and minor to coincide precisely with ophiolite geographic and temporal occurrences. Also, it is difficult to account, mechanically, for the obduction of substantial ophiolite nappes from oceanic ridges onto rifted continental margins.

15.3 Evidence from the Philippine Sea Plate

As others (Hawkins 2003; Pearce 2003; Stern and Bloomer 1995) have realized, the Cenozoic tectonic history of the Philippine Sea Plate is a critical key in unlocking the mode of ophiolite genesis. The Philippine Sea Plate (Fig. 15.1) consists of six tectonic elements, from west to east (1) The West Philippine Sea Basin was generated by sea-floor-spreading from the Late Cretaceous to 32 Ma (Early Oligocene). From 54 Ma to about 43 Ma, the spreading direction was roughly NNE (present co-ordinates). At 43 Ma, the spreading direction changed to roughly NS, which we attribute to a plate reorganization caused by the India/Asia collision, (2) The Palau-Kyushu Ridge, which, we suggest (Casey and Dewey 1984), was the site of conversion of a transform/fracture zone to a trench at about 54 Ma. This "trapped" the West Philippine Sea Basin behind an east-facing arc. From 54 to 32 Ma, an RTT triple junction was synchronous with the generation of the West Philippine Sea Basin and fore-arc boninites that now comprise much of element 6, (3) The Parece-Vela Basin, a back arc basin that split the arc, from 29 to 16 Ma, to leave the Palau-Kyushu Ridge as a remnant

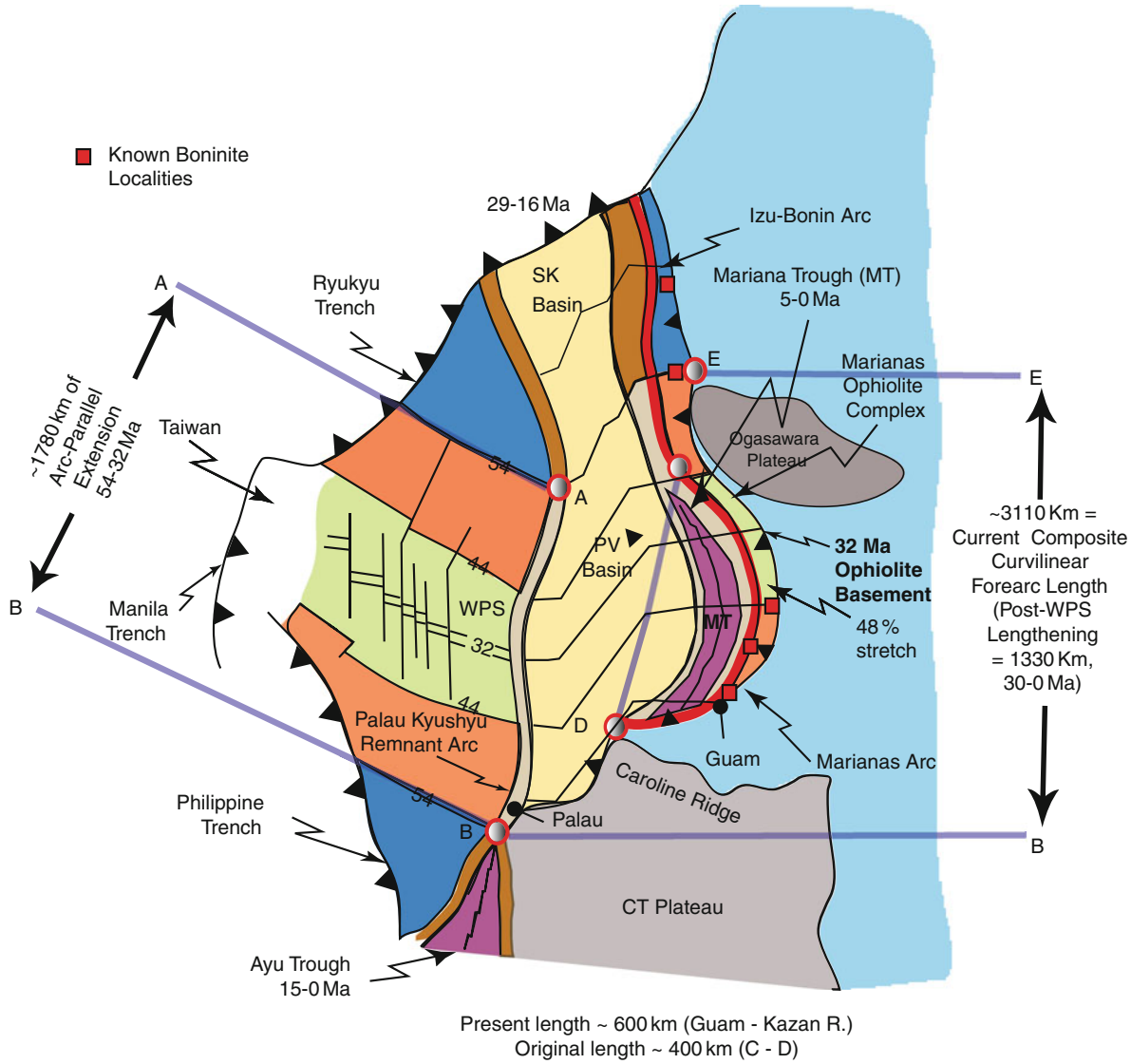

Fig. 15.1 Summary tectonic map of Philippine Sea Plate. Palau/Kyushu ridge denotes initiation of subduction, end of RTT, and beginning of back-arc basin sequence and arc splitting. *CT* Caroline-Truk Plateau, *MT* Marianas Trough, *PV* Parece Vela Basin, *SK*-, *WPS* West Philippine Sea.

arc, (4) The Marianas Trough, a Miocene back-arc basin that accompanied eastward bowing of the arc pinned at its northern and southern end by oceanic plateaux/seamounts, (5) The Izu-Bonin-Marianas Arc, (6) The Izu-Bonin-Marianas fore-arc, characterized by Eocene to early Oligocene boninites and extensive serpentinite diapirism. Restoring, by closing the Marianas Trough and the Parece Vela Basin, and taking out the 48% stretch of, and straightening, the Marianas Arc, places the element 6 boninitic fore-arc against the Palau-Kyushu Ridge. Thus, point E is brought against point A and point D against point B, which places, temporally and spatially, the boninitic fore-arc and the synchronous spreading at the east-west back-arc ridge axis. Therefore, the back-arc spreading was synchronous with the boninitic fore-arc, which implies an RTT triple junction for about 22 Ma during the Eocene and early Oligocene. We suggest that this indicates that the fore-arc was generated by arc elongation to generate a fore-arc ophiolite over about 22 Ma. Hall's (2002) reconstructions for the Eocene period, shows several places where a "back-arc" ridge strikes normal to an arc/trench, in which the

ridge terminates before it intersects the trench, a non-viable plate tectonic solution unless arc-parallel transforms take up the spreading vector. We continue the ridge to an RTT triple junction at the trench, the basis for our model.

15.4 The Model

Our model was conceived and developed from aspects of Hall's (2002) tectonic evolution model of southeast Asia, our analysis, above, of the geology and tectonic evolution of the Philippine Sea Plate, our model for the conversion of a transform/fracture zone into a subduction zone (Casey and Dewey 1984), and our ongoing global synthesis of obducted large-slab ophiolites. The model (Fig. 15.2) involves a ridge/trench/trench triple junction with the ridge between the upper plates. Plate separation, parallel with the arc strike, generates and elongates an oceanic (ophiolite) fore-arc. We suggest that such a plate geometry is developed by the conversion, probably by plate reorganization, of a transform/fracture zone to a subduction zone (Fig. 15.3). Two RTT triple junctions originate (Fig. 15.3) such that one ridge is on the upper plate, hanging wall side of the subduction zone whereas the other ridge is subducted. The petrology and chemistry of pillow basalts along the hanging-wall ridge is likely to change from MORB well behind the newly-established arc, through arc-tholeiite where the ridge crosses the arc, to boninite in the forearc.

Boninites are hydrous low-pressure/high-temperature, high silica and high magnesium andesites that are characteristic of the fore-arcs of oceanic arcs (Pearce 2003). Modern boninites occur at RFT/RTT triple junctions (north Lau, south-west Fiji, Deschamps and Lallemand 2003) and in Cenozoic and late Cretaceous and early Ordovician fore-arcs (Bonin/Guam/Saipan, Late Eocene to early Oligocene, Stern and Bloomer 1995; Papua New Guinea, Palaeocene; Troodos/Oman, Cretaceous; Balkans, early Jurassic; Setouchi sanukitoids, Miocene; Baja bajaites, Miocene; New Caledonia, Cretaceous; Shetland/Ballantrae/Bay of Islands/Betts Cove, early Ordovician (Coish 1989). Their likely origin is by partial melting of the mantle wedge beneath the fore-arc ridge axis, the water being supplied by dehydration of the mafic upper oceanic crust of the subducting slab. Type 9 ophiolites pillow lava sequences are, commonly, more tholeiitic below (earlier) and more boninitic above (later). This is accounted for by our model; water from the dehydrating slab will progressively permeate and saturate the sub-ridge melt zone for any segment of the newly-generated

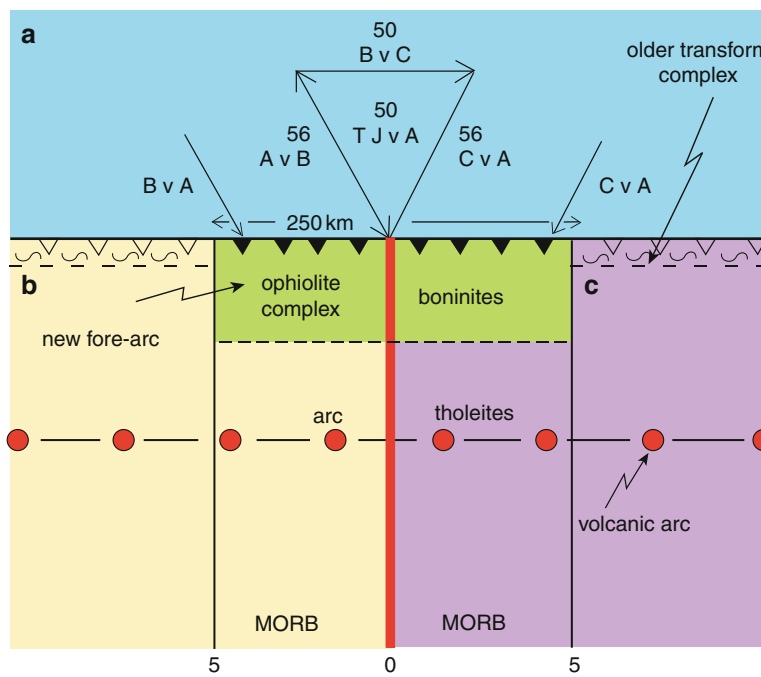

Fig. 15.2 Plan and block diagram of new model. Explanation in text.

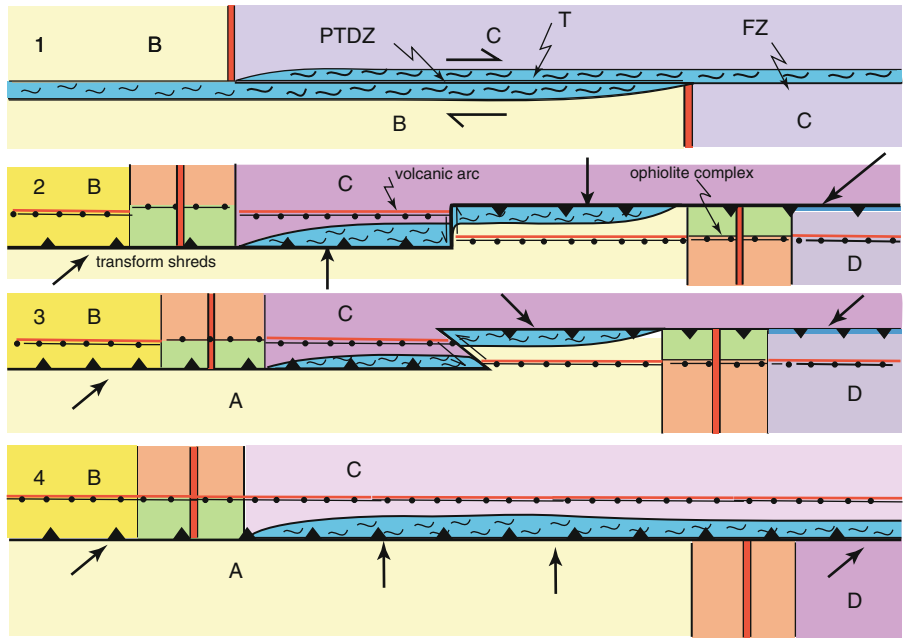

Fig. 15.3 Conversion of a ridge/transform/fracture zone/ridge system to a ridge/subduction zone/ridge complex. Explanation in text. *FZ* fracture zone, *PDTZ* principal transform displacement zone, *T* transform.

fore-arc segment so that an earlier drier tholeiite melt is expected to be followed by a wetter boninite melt.

The model shows that an ophiolite with an arc-parallel length of 250 km can be generated in only 5 million years with the modest spreading rate of 50 mm/a (Fig. 15.2). A particular problem with our model is that there is not an obvious along-arc-strike change in boninite age in the Marianas arc.

Central questions are, how commonly and where, does an RTT triple junction originate and develop to generate an ophiolite complex. Casey and Dewey (1984) developed a model for the nucleation of a subduction zone on a transform/fracture zone complex (weak zone), which they proposed to be the principal origin of intra-oceanic arcs, and the reason for "trapped" rear-arc basins with magnetic anomalies orthogonal to the arc, such as the Bering Sea and the West Philippine Basin (Fig. 15.1). There are several possible geometries, which produce quite different results from the starting configuration illustrated in Figs. 15.3 and 15.1. First (Figs. 15.3 and 15.2), if older, thicker, colder, and deeper lithosphere is subducted beneath thinner, younger, warmer, shallower lithosphere, both offset ridges are on the hanging wall of the subduction zone and an elongating trench/trench transform is needed to connect the two trenches/arcs with different polarities. The subduction slip direction must change at each triple junction, from oblique to orthogonal with an orthogonal transform (2) or between different oblique senses with an oblique transform (3). Thirdly, if the trench develops with a constant polarity (Figs. 15.3 and 15.4), one of the ridges is on the hanging wall of the subduction zone, the other on the subducting footwall, which leads to ridge subduction; we suggest that this is the way that the Marianas arc system and most, if not all, intra-oceanic arc systems develop. We cannot account for the pattern of the intermittent/patchy distribution of RTT triple junctions inherent in our model, that is typical of the intermittent distribution of ophiolite complexes in orogens, beyond the necessary conversion of continental margin-parallel transform fracture zones and margin-normal ridges that seems to be common at certain times in the history of Earth at the margins of oceans. However, such triple junctions have been a common feature of southeast Asia during the Cenozoic (Hall 2002).

The reason for the conversion of transform/fracture zone systems to trenches may be a combination of the gravitational instability of old, thick, lithosphere adjacent to long ridge to ridge transforms combined with regional or global plate boundary reorganizations. For

example, the Eocene origin of the Marianas Trench along the eastern margin of the Palau-Kyushu Ridge may have been a consequence of the India/Asia collision (Dewey et al. 1989). The rough synchroneity of early Ordovician and of mid-Cretaceous ophiolites around Earth was likely a result of global plate reorganizations associated with periods of accelerated plate motion rates, higher sea level, and blue-schist metamorphism (Dewey 2003).

The subduction slip direction must be oblique towards, and be in the opposite sense on each side of, the triple junction (Fig. 15.2), which has implications for structures in sole amphibolites/granulites discussed below. Furthermore, subduction cannot partition into trench-orthogonal and parallel components, because partitioning would prevent the ridge meeting the trench at the triple junction, would generate two transforms with opposite senses of displacement, and generate a uniform slip-direction along a single trench. Such a geometry is possible but is not a consequence of an RTT triple junction. Although it is generally likely that the generation of an RTT triple junction will involve ridge-orthogonal transforms (Figs. 15.4 and 15.1a), any configuration of an RTT or RFT triple junction will remain as or evolve to an RTT junction in

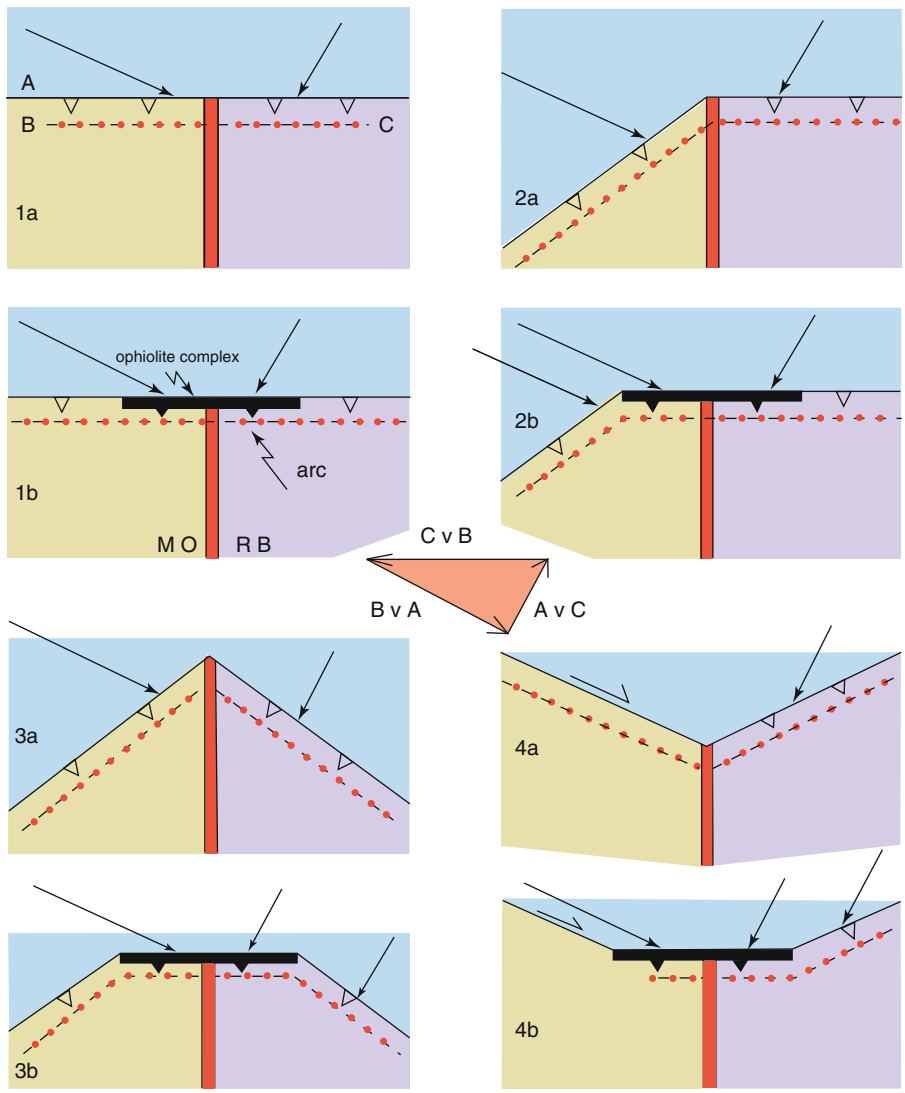

Fig. 15.4 Plan view variation of RTT triple junctions, their orientation and consequences. Note that, whatever the initial configuration, all evolve to an RTT triple junction with oblque subduction slip.

which the arc and fore-arc elongate parallel with the arc (Fig. 15.4).

The model implies and predicts distinctive diachronous stratigraphical sequences in the fore-arc. As the fore-arc ophiolite is generated, older ophiolite basement bears older stratigraphical sequences from ridge-flanking carbonates/cherts to arc-derived air-fall tuffs and andesitic turbidites with mafic sills and flows (e.g., Snooks Arm Sequence, Newfoundland; Upadhuay et al. 1971).

The oblique slip vector at the two subduction zones may have an influence in rotating simple extensional stress field near the ridge and in generating finite rotations along the fore-arc, especially near the triple junction. Ophiolite dykes may become oblique (Harper 2003; MacLeod and Rothery 1992) and block rotations may occur, clock-wise on one side of the ridge and anti-clockwise on the other (Fig. 15.2).

In Fig. 15.5, we have reconstructed the Marianas arc at 35 Ma based upon Hall's (2002) palaeo-tectonic maps and our model. At an average spreading rate of 85 mm/a (well-constrained by the anomaly sequence of the west Philippine Sea Basin), the 1,780 km-long Eocene-Oligocene ophiolite fore-arc would have been generated in 19 my, from 54 to 35 Ma. We acknowledge that the data does not indicate, clearly, an age progression along the Marianas fore-arc. The model predicts that substantial fore-arc lengths of ophiolite complex can be generated rapidly. The length is determined by how long an RTT triple junction can exist. The development of ophiolite complexes in the Appalachian/Caledonian and Tethyan systems suggests that a strike length of individual ophiolite complexes of about 500 km is typical. At a spreading rate of 50 mm/a, a 500 km ophiolite is generated in 10 my. The data suggests that the length of ophiolite varies from about 500 to 1,700 km and that RTT triple junctions can last up to about 20 my. The consequent arc/subduction zone

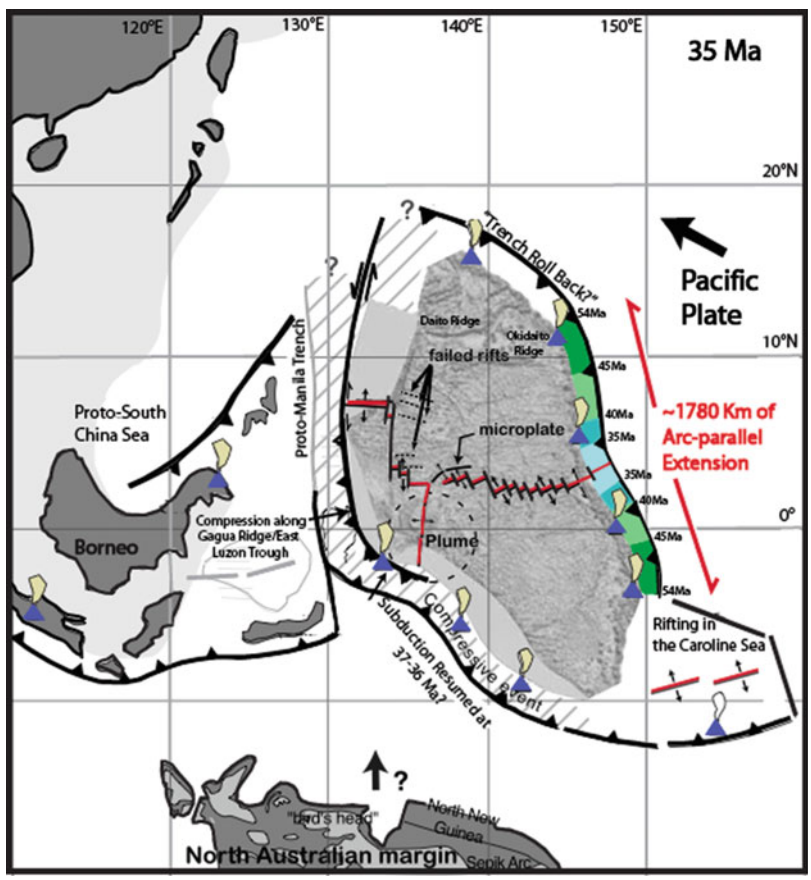

Fig. 15.5 Eocene evolution of the Marianas fore-arc based upon the Hall (2002) model. Explanation in text.

lengthening has interesting plate tectonic consequences. Lengthening can be accommodated by termination subduction, by migrating triple junctions, and/or by bowing/bending of the arc, especially if its terminations are pinned and subduction roll-back enhances the bowing.

The length of time during which the ophiolite fore-arc exists before it collides with another arc or rifted continental margin is critical in determining whether or not thin sheet ophiolite obduction occurs and in determining the structural/metamorphic style of the collisional zone. At the triple junction, there is no overriding slab, the subducting plate is beneath 1,300° mantle almost at the surface. As the fore-arc lithosphere moves away from the triple junction and thickens, its thickness is buffered by the upper surface of the subducting slab (Fig. 15.6) beyond which it cannot thicken

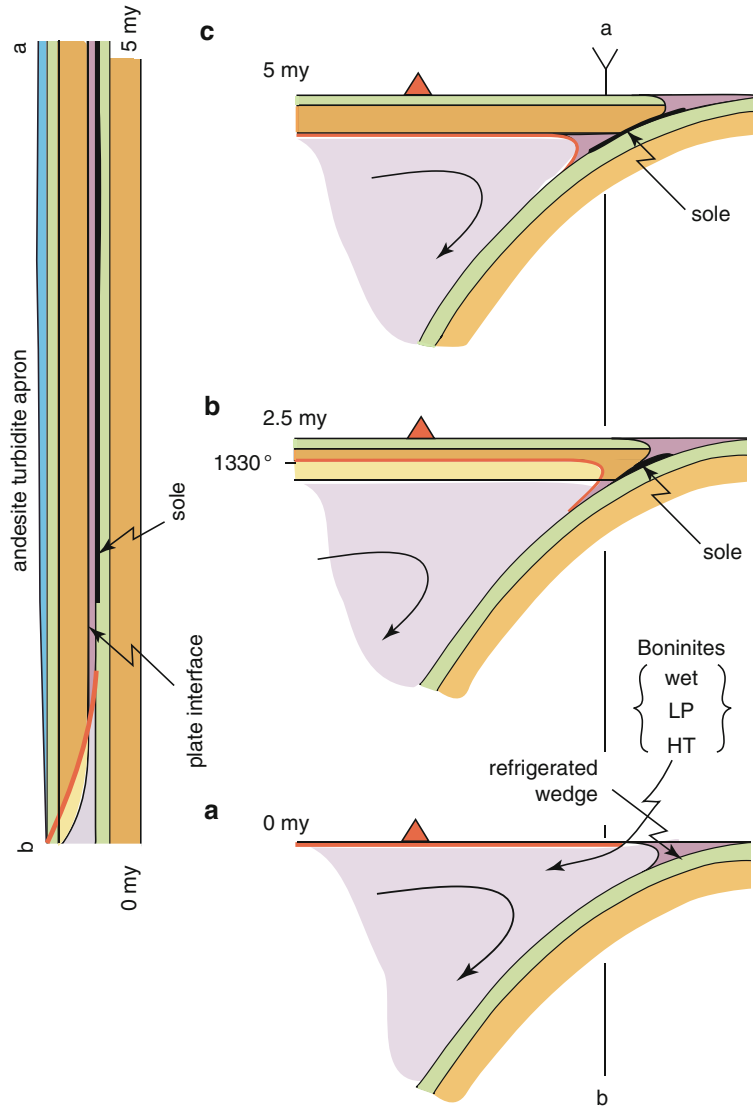

Fig. 15.6 Cross and longitudinal sections of RTT relationships showing lithospheric thickness, ophiolite structure and position and age of sole metamorphism/detachment. *HT* high temperature, *LP* low pressure. **A** – cross-section exactly at the triple junction; along this section, the subducting slab is sliding beneath asthenosphere not beneath an over-riding plate. As the over-riding plates thicken as they move away from the ridge, a longer and longer interface develops between over-riding and subducting plates with increasing shear traction and diminishing temperature. The ophiolite sole aureole is developed in the subducting mafic oceanic crust at temperatures of 900–1,000°C and then detached from the subducting slab to be attached to the base of the fore-arc ophiolite so that the highest aureole temperatures are recorded closest to the aureole with later subcreted additions at lower metamorphic grades. Further explanation and discussion in text.

and subside to its age-depth whatever its age. For lithospheric thicknesses of up to about 15 km, the typical maximum thickness of ophiolite complexes, obduction of a thin sheet is possible. Beyond a lithospheric thickness of about 15 km, obduction becomes progressively less likely; the thick fore-arc lithosphere is more likely to bulldoze the arc or continental margin with which it collides and generate a more upright orogenic style.

Clearly, even at the triple junction, there must be a "refrigerated corner" above the subducting slab which widens and thickens with time as the fore-arc lithosphere thickens and subsides. The refrigerated corner results from asthenosphere freezing against the cold subducting slab just as it does for general corner flow along the length of the fore-arc (Fig. 15.6). Thus, the ridge per se does not make it all the way to the trench but, probably, terminates in a complex extensional/transtensional region of rotational flaking of ultramafic and mafic rocks in the immediate hanging wall to the trench. Yet, substantial volumes of asthenosphere and its derivative partial melt must pass through and from the corner flow region. In the region around the triple junction, there is likely to be an interference between the monoclinic flow patterns of corner flow and sub-ridge to generate oblique triclinic patterns. Some of the complex peridotite fabric patterns of the Oman Ophiolite may be a result of this interference. Understanding the geology of the refrigerated corner will come from mapping the distal parts of obducted ophiolites.

If our model for the nucleation of subduction zones on transform/fracture zones and the development of RTT triple junctions is viable, the frontal zone of obducted ophiolites, between the offset ridges, is likely to preserve the complex polyphase deformation and igneous geology of the transforms and fracture zones upon which nucleation occurred (Fig. 15.3) and which should not be confused with any deformation that occurs in the subduction zone or fore-arc (Karson and Dewey 1978; Dewey 2002).

15.5 Ophiolite Basal Aureoles

Our model provides a new basis for understanding the mafic protolith (garnet amphibolite/two pyroxene granulite) sole aureoles that characterize most obducted large-slab ophiolite sheets. We suggest that the aureoles are generated in subduction zones as the fore-arc ophiolite is generated, not during obduction. As the ophiolite lithosphere thickens (Fig. 15.6), its thickness is buffered by the position of the upper surface of the subducting slab. When 12 km of ophiolite lithosphere is generated after about 5 my, the basaltic rocks in the oceanic crust of the subducting slab are sliding against a harzbugite/lherzolite hanging wall at about 900–1,000°C. At these temperatures, the aureoles could be generated, detached after dehydration, and attached to the base of the ophiolite. It might be expected that the mafic protolith should be derived from uppermost pillow basalts and dyke complex. Some amphibolite soles clearly have a basalt/diabase protolith but, commonly, two-pyroxene granulite soles have a gabbroic protolith. This could have one or both of two explanations. First, the modern oceanic crust exposes gabbros drawn up beneath extensional detachments and, secondly, shortly after the conversion of a fracture zone/transform to a subduction zone, rocks from the base of the gabbro section to the top of the oceanic crust in the newly-subducting slab will slide along the subduction interface with the developing fore-arc ophiolite. Thus, we see the sole aureole as generated in the subducting slab, then detached from the subducting slab and attached to the base of the hanging wall ophiolite above the subducting slab (Fig. 15.6). The lineation direction in the sole must be oblique to the trench if it is parallel with the slip direction (Fig. 15.2) (Gomez Barreiro et al. 2010; Savci 1988; Cawood and Suhr 1992; Suhr and Cawood 1993). The sole aureole is obducted later with the ophiolite. Where mafic and silicic protoliths both exist in same aureole complex, the hotter mafic granulites/amphibolites predate and are above the colder silicic (Church and Stevens 1971). The subjacent silicic complex is derived from rocks of the continental margin and is commonly in the blueschist facies. Interdigitation of the sole mafic aureole rocks and high-pressure silicics may occur during upward flow in the subduction channel. Ridge subduction, a consequence of the model (Fig. 15.3), was probably responsible for the mafic dykes that cut the sole aureole of the Pozanti-Karsanti ophiolite complex in Turkey (Polat et al. 1996).

Clearly, some ophiolites were hot when obducted. Melted granite sheets back-vein obducted ultramafics in the Lizard (Kennack Gneiss, Fanos Granite, Pearce 1989), and the Solund Ophiolite (Sogneskollen Granite, Skjerlie et al. 2000). This suggests direct

obduction of a hot ophiolite possibly from a back-arc basin or narrow rift ocean. Some ophiolites do not have immediately subjacent aureoles. For example, the Coast Range Ophiolite of California defines the basement and the upturned western margin of the Great Valley (Shervais and Kimbrough 1985). It forms the post-Nevadan, subduction-flip backstop to the blueschist/jadeite-lawsonite Cretaceous assemblage of the Franciscan.

15.6 Arc–Continent Collision and Ophiolite Emplacement

Ophiolite obduction results from arc–continent collision but not all collisions involve ophiolite obduction. Arc–continent collision takes many forms and generates a wide spectrum of structural styles and geometries, and metamorphic consequences. These variations result from both the great variation in the structure of arcs and the rifted continental margins and other oceanic and continental arcs with which they collide. Rifted margins may be sharp and abrupt or stretched and thinned with rapid lateral variations. Obduction of the ophiolite fore-arc and the arc as a thin sheet will be easier in the former and lead to flat structural styles whereas the latter may lead to obstructive "bull-dozing" with steeper structural styles. The history of the ophiolite fore-arc is also critical. As the ophiolite ages, its lithosphere thickens and subsides. Young thin hot fore-arc lithosphere is easy to obduct but old thick cold lithosphere may simply "bull-doze" its colliding margin. Therefore, if a fore-arc ophiolite is to be obducted, the arc must collide with a margin before the fore-arc lithosphere is too old and thick. The typical thickness of obducted ophiolite sheets is about 12 km and sole aureoles were generated at about 900–1,000°C. This means that arc-margin collision must occur within 10–15 my. of ophiolite generation. However, if the fore-arc ultramafics were to become completely serpentinized (serpentinite diapirism occurs in boninitic fore-arcs), their density would approximate that of continental rocks and the age constraint would not apply. We suggest that this is generally unlikely; most ultramafic rocks in ophiolite complexes are only lightly serpentinized, have densities above 3.0, and serpentinization is mainly post-obduction. Finally, another tectonic mechanism is a possibility, the likely thinning of the fore-arc mantle wedge (Casey and Dewey 1984) by shallowing of the subduction zone dip during arc/continent collision. This would allow metamorphosed mafic crust from the subducting slab from higher-pressure deeper levels to rise with the slab to become attached to the base of the ophiolite as a sole and sliced from the subducting slab. However, only the asthenosphere and that portion of the ophiolite above 900°C (olivine plastic-slip-activation temperature) can be thinned so that the age constraint would still apply.

The Bay of Islands and Semail complexes were emplaced cold, with their metamorphic soles, onto foreland basins. The Semail Complex developed a blue-schist shear carpet. If the fore-arc ages and develops a thick lithosphere, it may bull-doze the margin for a while but then be overridden by the thin hot arc so that the arc comes to lie directly upon the margin along a new subduction zone with the thick fore-arc being subducted. Regional Barrovian metamorphism such as that of the Grampian Orogen in western Ireland may have been developed by obducting a hot arc across the Laurentian continental margin (Paul Ryan, verb. comm.). Fore-arc ophiolites, according to our model, should be intermittent along strike because they develop from RTT triple junctions, which, by definition, cannot generate an ophiolitic fore-arc that is continuous along fore-arc strike. We have not explored, more than in this broad and general way, the range of implications of these and other variations for the structure and history of arc/continent collision zones but the structural and metamorphic consequences are profound in that there is no simple model that explains all arc–continent collisions and their structure, metamorphism, and history.

15.7 Summary and Conclusions

Large-slab obducted ophiolite complexes such as the Bay of Islands and Semail Complexes were generated in the fore-arcs of oceanic island arcs as shown by the common boninitic petrology of the upper part of their pillow lava sequences. We suggest that such ophiolites originated where an arc-normal and arc-cutting spreading ridge joined a trench at an RTT triple junction. Boninites are characteristic components of Cenozoic extant fore-arcs especially at RTT and RTF triple

junctions in the western and southwestern Pacific Ocean. Arc-parallel spreading, and lithospheric cooling and thickening, generates an ophiolitic fore-arc with arc-normal dykes. At a spreading rate of 50 mm/a, a 250 km long ophiolite complex can be generated in only 5 my. Therefore, subduction takes place beneath a newly-created fore-arc. Subduction must always be oblique with an opposite sense on either side of the triple junction; partitioning cannot occur because it would cancel relative motion at the triple junction.

The RTT triple junction originates as a result of the conversion of a ridge/transform/ridge system to a subduction zone. If the polarity of subduction is constant, two RTT triple junctions develop, one with an upper plate ridge (the site of ophiolite generation) the other with a lower plate ridge that is progressively subducted. Along-strike from the newly-generated ophiolite, the hanging wall will contain rocks generated in a transform/fracture zone; these rocks will comprise assemblages with complicated polyphase structural/igneous histories, such as those in the Coastal Complex of Newfoundland (Karson and Dewey 1978; Suhr and Cawood, 2002).

The basal (sole) two-pyroxene garnet-granulite to garnet-amphibolite, mafic protolith aureole is developed not during ophiolite obduction but in the sub-fore-arc subduction channel as a natural consequence of the dynamothermal metamorphism of the subducting oceanic crust below the sub ridge asthenosphere of the fore-arc. As the ophiolitic lithosphere thickens, its thickness is buffered by the position of the subducting slab; a lengthening shear interface develops whose pressure increases downwards along the slab and whose temperature varies from 0 to about 1,300°C. At temperatures ranging from about 700 to 900°C, the sole aureole is developed in the subducting mafic oceanic crust and sliced from the subducting slab to be attached to the base of the fore-arc ophiolite. Linear fabrics in the aureole will be oblique to the trend of the arc and "point" to the triple junction. Ridge subduction is a likely consequence of the conversion of a ridge/transform/ridge/fracture zone system to a subduction zone, which could lead to post-sole mafic magmatism.

A fore-arc origin for large-slab ophiolites is preferred because of their boninites but also because a juvenile fore-arc is, mechanically a more likely site from which to obduct a 10–15 km-thick ophiolite sheet onto a rifted continental margin, the commonest ophiolite location. Intra and back-arc basin oceanic crust and mantle is more likely to be thrust against/onto an adjacent volcanic arc. It is also difficult to see how large ophiolite sheets could be obducted onto rifted continental margins from the ridges of main ocean basins. The age of an ophiolite fore-arc is critical in determining the style of arc–continental collision. Large-slab ophiolites are obducted, typically, very soon after generation. Hence, 10–15 km thin hot ophiolite nappes are thrust onto continental margins with their high-temperature aureoles but still hot enough to cause low-amphibolite to greenschist dynamothermal metamorphism of continental margin siliceous rocks, which become attached to the obducting sole. As the ophiolite fore-arc ages, it thickens to the point, perhaps about 20 km after which it becomes mechanically difficult to obduct an ophiolite slab. Beyond this point, the fore-arc lithosphere thickens to a bull-dozing ram that telescopes the continental margin. Alternatively, it is possible that the subduction zone transfers to the arc/fore-arc boundary so that the hot arc overrides the fore-arc onto the continental margin and the thick fore-arc is subducted; this may have occurred to provide the downwards transfer of heat to generate the Barrovian metamorphism of the Dalradian rocks of western Ireland. In general, early high-temperature sole formation in the subduction channel from a mafic protolith is progressively followed by colder accretion of siliceous continental margin facies to the base of the sole during obduction. In places, blueschist assemblages are developed beneath the obducted ophiolite.

Large-slab obducted ophiolite complexes are not uniformly distributed in time. They are mainly restricted to the Phanerozoic, principally three periods of associated high sea-level, carbonate platforms and oceanic black shales, and blueschist metamorphism. These are early Ordovician, mid- Jurassic, and mid-Cretaceous and may be a result of major plate boundary re-organizations and conversions associated with periods of increased rates of relative plate motion. The origin of the Marianas fore-arc coincides with the Eocene Himalayan continental collision.

Acknowledgements We acknowledge the substantial importance of Robert Hall's (2002) paper on our thinking. Robert Stern's work and ideas on the Marianas fore-arc influenced us greatly. We thank NSF, NERC, BP-Amoco, Exxon, and Shell for financial and logistic support over many years.

References

Allerton S, Vine FJ (1992) Deformation styles adjacent to transform faults: evidence from the Troodos Ophiolite, Cyprus. Geol Soc Lond Spec Publ 60:251–261

Berrange JP, Thorpe R (1988) The geology, geochemistry and emplacement of the Cretaceous-Tertiary ophiolitic Nicoya Complex of the Osa Peninsula, southern Costa Rica. Tectonophysics 147:193–220

Bird JM, Dewey JF, Kidd WSF (1971) Appalachian/Caledonian ophiolites: early Palaeozoic oceanic crust and mantle. Nature (Lond) 281:28–31

Boillot G, Besler MO, Krawkczyk CM, Rappin D, Reston TJ (1995) The formation of passive margins: constraints from the crustal structure of the and segmentation of the deep Galicia margin, Spain. Geol Soc Lond Spec Publ 90:71–91

Boudier F, Le Sueur E, Nicolas A (1989) Structure of an atypical ophiolite: the Trinity complex, eastern Klamath Mountains, California. Geol Soc Am Bull 101:820–833

Bourgois J, Lagabrielle Y, Moigne JL, Urbina O, Janin M-Ch, Beuzart P (1993) Preliminary results of a field study of the Taitao ophiolite (Southern Chile). Ofioliti 18(2):112–129

Casey JF, Dewey JF (1984) Initiation of subduction zones along transform and accreting plate boundaries, triple junction evolution and spreading centres – implications for ophiolite geology and obduction. In: Gass IG, Lippard SJ, Shelton AW (eds) Ophiolites and oceanic lithosphere, vol 13. Geological Society of London Special Publication, London, pp 269–290

Casey JF, Dewey JF, Fox PJ, Karson JA, Rosencrantz E (1981) Heterogeneous nature of oceanic crust and upper mantle: a perspective from the Bay of Islands Ophiolite Complex. In: Cesare E (ed) The sea, vol 5. Wiley, New York, pp 305–338

Cawood PA, Suhr G (1992) Generation and obduction of ophiolites: constraints from the Bay of Islands Complex, western Newfoundland. Tectonics 11:884–897

Church WR, Stevens RK (1971) Early Paleozoic ophiolite complexes of the Newfoundland Appalachiansas mantle-oceanic crustal sequences. J Geophys Res 76:1460–1466

Coish RA (1989) Boninitic lavas in Appalachian ophiolites: a review. In: Crawford AJ (ed) Boninites and related rocks. Unwin Hyman, London, pp 264–287

Coleman RG (1977) Ophiolites. Springer, Berlin, p 229

Davies HL (1971) Peridotite-gabbro-basalt complex in eastern Papua: an overthrust plate of oceanic crust and mantle. Aust Bur Miner Resour Bull 128:48

Deschamps A, Lallemand S (2003) Geodynamic setting of Izu-Bonin-Mariana boninites. Geol Soc Lond Spec Publ 219: 163–185

Dewey JF (1974) Continental margins and ophiolite obduction: Appalachian/Caledonian system. In: Burk CA, Drake CL (eds) Continental margins. Springer, New York, pp 933–952

Dewey JF (1975) Finite plate evolution: some implications for the evolution of rock masses in plate boundary zones. Am J Sci 275-A:260–284

Dewey JF (1976) Ophiolite obduction. Tectonophysics 31: 93–120

Dewey JF (1980) Episodicity, sequence and style at convergent plate boundaries. Geol Assoc Can Spec Pap 20:553–573

Dewey JF (2002) Transtension in arcs and orogens. Int Geol Rev 44:402–438

Dewey JF (2003) Ophiolites and lost oceans: rifts, ridges, arcs, and/or scrapings. Geol Soc Am Spec Pap 373:153–158

Dewey JF, Bird JM (1971) The origin and emplacement of the ophiolite suite: Appalachian ophiolites in Newfoundland. J Geophys Res 76:3179–3206

Dewey JF, Kidd WSF (1977) Geometry of plate accretion. Geol Soc Am Bull 88:960–968

Dewey JF, Cande SC, Pitman WC III (1989) Tectonic evolution of the India-Eurasia convergent zone. Eclog Geol Helv 82:717–734

Dijkstra AH, Sergeev D, Spandler CA, Meisel T, Cawood PA (2010) Ultra-refractory peridotites and enriched-type oceanic crust on MacquarieIsland: the case for anciently-depleted domains in the Earth's mantle. J Petrol 51:469–493

Fitch TJ (1972) Plate convergence, transcurrent faults, and internal deformation adjacent to southeast Asia and the western Pacific. J Geophys Res 77:4432–4461

Furnes H, Pederson RB, Stillman CJ (1988) The Leka Ophiolite Complex, central Norwegian Caledonides: field characteristics and geotectonic significance. Geol Soc Lond J 145: 401–412

Gartzos E, Dietrich VJ, Migiros G, Serelis K, Lymperopoulos Th (2009) The origin of amphibolites from metamorphic soles beneath the ultramafic ophiolites in Evia and Lesvos (Greece) and their geotectonic implication. Lithos 106:224–242

Gass IG (1968) Is the Troodos Massif of Cyprus a fragment of Mesozoic ocean floor. Nature 220:39–42

Gomez Barreiro J, Martinez Catalan JR, Prior D, Wenk HR, Vogel S, Diaz Garcia F, Arenas R, Sanchez Martinez S, Lonardelli I (2010) Fabric development in a Middle Devonian Introceanic Subduction Regime: The Careon Ophiolite (Northwest Spain). J Geol 118:163–186

Hall R (2002) Cenozoic geological and plate tectonic evolution of SE Asia and the SW Pacific. J Asian Earth Sci 20:353–431

Harper GD (2003) Tectonic implications of boninite, arc tholeiite, and MORB magma types in the Josephine Ophiolite, California-Oregon. Geol Soc Lond Spec Publ 218:207–230

Hawkins JW (2003) Geology of supra-subduction zones-implications for the origin of ophiolites. Geol Soc Am Spec Pap 373:227–268

Hickey RL, Frey FA (1982) Geochemical characteristics of boninite series volvanics: implications for their source. Geochim Cosmochim Acta 46:2099–2115

Karig DE (1982) Initiation of subduction zones: implications for arc evolution and ophiolite development. Geol Soc Lond Spec Publ 19:563–576

Karson J, Dewey JF (1978) The Coastal Complex, western Newfoundland: an early Ordovician fracture zone. Geol Soc Am Bull 89:1037–1049

Lissenburg CJ, Bedard JH, van Staal CR (2004) The structure and geochemistry of the gabbro zone of the Annieopsquotch ophiolite, Newfoundland: implications for lower crustal accretion at spreading ridges. Earth Planet Sci Lett 229:105–123

Lissenburg CJ, van Staal CR, Bedard JH, Zagorevski A (2005) Geochemical constraints on the origin of the Annieopsquotch ophiolite belt, Newfoundland Appalachians. Geol Soc Am Bull 117:1413–1426

MacLeod CJ, Rothery DA (1992) Ridge axial segmentation in the Oman Ophiolite: evidence from along-strike variations

in the sheeted dyke complex. Geol Soc Lond Spec Publ 60:39–63

McCullough MT, Cameron WE (1983) Nd-Sr isotopic study of primitive lavas from the Troodos ophiolite, Cyprus: evidence for a subduction-related setting. Geology 11:727–731

Moores EM, Vine FJ (1971) The Troodos Massif, Cyprus,and other ophiolites as oceanic crust: Evaluation and implications. Roy Soc Lond Phil Trans 286-A:443–466

Moores EM, Kellogg LH, Dilek Y (2000) Tethyan ophiolites, mantle convection, and tectonic "historical contingency": a resolution of the "ophiolite conundrum". Geol Soc Am Spec Pap 349:3–12

Nicolas A (1989) Structures of ophiolites and dynamics of oceanic lithosphere. Kluwer, Dordrecht, p 367

Pearce JA (1989) High T/P metamorphism and granite genesis beneath ophiolite thrust sheets. Ofioliti 14(3):195–211

Pearce JA (2003) Supra-subduction-zone ophiolites: the search for modern analogues. Geol Soc Am Spec Pap 373:269–293

Pearce JA, Lippard SJ, Roberts S (1984) Characteristics and tectonic significance of supra-subduction ophiolites. Geol Soc Lond Spec Publ 16:77–94

Phillips-Lander CM, Dilek Y (2009) Structural architecture of the sheeted dike complex and extensional tectonics of the Jurassic Mirdita ophiolite, Albania. Lithos 106:192–206

Polat A, Casey JF, Kerrich R (1996) Geochemical characteristics of accreted material beneath the Pozanti-Karsanti ophiolite, Turkey: intra-oceanic detachment, assembly, and obduction. Tectonophysics 263:249–276

Robertson A, Karamata S, Saric K (2009) Overview of ophiolites and related units in the Late Palaeozoic-Early Cenozoic magmatic and tectonic development of Tethys in the northern part of the Balkan region. Lithos 106:1–36

Savci G (1988) Structural and metamorphic geology of the subophiolitic dynamothermalmetamorphic sole andperidotite tectonites, Blow-Me-Down Massif, Newfoundland, Canada: tectonic implications for subduction and obduction: Ph. D. dissertation, University of Houston

Schroetter J-M, Page P, Bedard JH, Tremblay A, Becu V (2003) Fore-arc extension and sea-floor spreading in the Thetford Mines Ophiolite Complex. Geol Soc Lond Spec Publ 218: 231–251

Shackleton RM, Ries AC (1990) Tectonics of the Masirah Fault Zone and eastern Oman. Geol Soc Lond Spec Publ 49: 715–724

Shervais JW, Kimbrough DL (1985) Geochemical evidence for the Coast Range ophiolite: a composite island arc-ocean crust terrane in western California. Geology 13:35–38

Skjerlie KP, Pederson RB, Wennberg OP, De La Rosa J (2000) Volatile phase fluxed anatexis of metasediments during late Caledonian ophiolite obduction: evidence from the Sognes-kollen Granitic Complex, west Norway. Geol Soc Lond J 157:1199–1213

Stern RJ, Bloomer SH (1995) Subduction zone infancy; examples from the Eocene Izu-Bonin-Marianas and Jurassic California Arcs. Geol Soc Am Bull 104:1621–1636

Stern C, De Wit MJ (2003) Rocas Verdes ophiolites, southernmost South America: a remnant of oceanic-type crust in a continental marginal back-arc basin. Geol Soc Lond Spec Publ 218:665–683

Sturm ME, Klein EM, Karsten JL, Karson JA (2000) Evidence for subduction-related contamination of the mantle beneath the southern Chile Ridge: implications for ambiguous ophiolite compositions. Geol Soc Am Spec Pap 349:13–20

Suhr G, Cawood PA (1993) Structural styles and kinematics of ophiolite detachment, Bay of Islands Complex, Newfoundland. Geol Soc Am Bull 105:399–410

Suhr G, Cawood PA (2001) Southeastern Lewis Hills (Bay of Islands Complex): geology of a deeply-eroded, inside-corner, ridge-transform intersection. Geol Soc Am Bull 113: 1025–1038

Taylor RN, Nesbitt RW (1992) A geochemical transect of the Izu-Bonin aec-trench system. Ofioliti 17(1):57–71

Taylor HP, Noble JA (1960) Origin of the ultramafic complexes in southeastern Alalska. In: Report of 21st International Geological Congress, vol 13. pp 175–187

Taylor RN, Murton BJ, Nesbitt RW (1992) Chemical transects across intra-oceanic arcs: implications for the tectonic setting of ophiolites. Geol Soc Lond Spec Publ 60: 117–132

Upadhuay HD, Dewey JF, Neale ERW (1971) Betts Cove ophiolite Complex, Newfoundland: Appalachian oceanic crust and mantle. Proc Geol Assoc Can 24:27–34, June

Van den Beukel J, Wortel R (1992) Ridge-trench interaction: a possible mechanism for ophiolite emplacement. Ofioliti 17(1):141–154

Varne R, Gee RD, Quilty PGJ (1969) Macquarie Island and the cause of linear magnetic anomalies. Science 166: 230–233

Varne R, Brown AV, Falloon T (2000) Macquarie Island; its geology, structural history, and the timing and tectonic setting of the N-MORB to E-MORB magmatism. Geol Soc Am Spec Pap 349:301–320

Chapter 16
Physical Modeling of Arc–Continent Collision: A Review of 2D, 3D, Purely Mechanical and Thermo-Mechanical Experimental Models

D. Boutelier and A. Chemenda

16.1 Introduction

Geological data provide the foundation for investigating lithospheric processes such as arc–continent collisions. However these data are generally limited and only give partial insights into the mechanics of these processes characterized by very large spatial and time scales. Therefore geodynamic modeling, using either physical/experimental or numerical techniques, is now routinely used to make up the lack of data and to better understand the evolution of the processes taking into account, as much as possible, its thermo-mechanical and 3D nature. The physical modeling technique appears to be particularly efficient to gain insights into such a complex phenomenon as continental subduction/collision. In this work, we review the modeling results obtained using the method developed by A. Chemenda and based on the use of temperature-sensitive elasto-plastic hydrocarbon materials to model the various layers of the lithosphere. This method and its thermo-mechanical evolution have provided numerous insights into the physics of oceanic and continental subduction, arc–continent collision, and the exhumation of ultra-high pressure/low temperature rocks, which have been presented in multiple publications (Shemenda 1992, 1993, 1994; Shemenda and Grocholsky 1992 Chemenda et al. 1995, 1996, 1997a, b, 2000a, b, 2001a, b; Boutelier et al. 2002, 2003, 2004; Boutelier 2004; Boutelier and Chemenda 2008). In this chapter we attempt to form, out of these numerous results, a coherent whole in order to provide geologists with a robust mechanical framework of arc–continent collision. We present the employed modeling technique and detail the key modeling results as well as some of their applications to active or fossil arc–continent collision zones.

D. Boutelier
Helmholtz Zentrum Potsdam, Deutsches GeoForschuns Zentrum, Telegrafenberg, 14471 Potsdam, Germany
e-mail: david@gfz-potsdam.de

A. Chemenda
Géoazur, Université de Nice-Sophia Antipolis, CNRS, 250 av. A. Einstein, 06560 Valbonne, France

16.2 Modeling Technique

16.2.1 General Modeling Scheme

The principal difficulties in physical modeling are the creation of analogue materials and experimental conditions allowing the physics of the investigated process to be conveniently reproduced in a small-scale experiment. A considerable progress in this direction was achieved using the method developed by A. Chemenda and based on the use of specially designed temperature-sensitive elasto-plastic hydrocarbon compositional systems to model the various layers of the lithosphere (Shemenda 1992, 1993, 1994; Shemenda and Grocholsky 1992). The general modeling scheme of this technique is presented below.

The lithosphere may be defined as the superficial shell of the Earth capable of undergoing large quasi-rigid horizontal displacements with strain-rates far lower than those experienced by the underlying asthenosphere. This definition provides the general framework for our modeling. Since the mechanical strength of the asthenosphere is low and its viscosity is far lower (several orders of magnitude) than the effective viscosity of the lithosphere, one can consider

D. Brown and P.D. Ryan (eds.), *Arc-Continent Collision*, Frontiers in Earth Sciences,
DOI 10.1007/978-3-540-88558-0_16,

that the asthenosphere exerts a small shear traction on the base of the lithosphere. This traction can thus be neglected if we focus our interest on the solid interaction of the plates in the subduction zone because the action of such small shear traction on a limited area such as the subduction zone is small. However, integrated over the very large surface area of the base of the entire lithospheric plate, this shear traction can become very important and must be taken into account (Funiciello et al. 2003a, b, 2004, 2006; Schellart 2004a, b). Therefore, we can neglect the shear traction exerted by the asthenosphere on the lithosphere in the subduction zone and replace its large scale effect as a driving/resisting force of plate motion by a piston producing the constant-rate convergence of the lithospheric plates. Consequently we can model the asthenosphere with a low-viscosity fluid whose unique role is to provide hydrostatic equilibrium below the lithosphere.

If it is rather clear that the asthenosphere can be represented by a low-viscosity fluid, the mechanical behavior of the lithosphere is more complicated. Natural observations (Jeffreys 1970) and laboratory measurements of rock strength extrapolated to the conditions of pressure, temperature and strain-rates characteristic of plate tectonics (Goetze and Evans 1979; Brace and Kohlstedt 1980; Molnar 1992; Kohlstedt et al. 1995; Jackson 2002) led to the development of the Brace–Goetze strength profile for the rheological stratification of the lithosphere. It appears clear that the mechanical behavior of the lithosphere is brittle near the surface and is mainly controlled by frictional sliding (Byerlee 1978). However at greater depth the lithospheric properties become less well constrained. The lithosphere becomes stronger but also more ductile, and with further increase of temperature and pressure, the lithospheric behavior becomes more viscous (Ranalli and Murphy 1987). One could then represent the oceanic lithosphere with a three-layers model in which the uppermost layer is elasto-plastic with high brittleness, the second layer is more ductile (elastic-plastic with no brittleness) and the bottom layer is elasto-visco-plastic. In this simplified view, the middle layer would be the strongest. In this study, the oceanic lithosphere is simplified and represented by one unique elasto-plastic and ductile layer. In the case of the continental lithosphere, the more complex rheological stratification, due to the different composition, density and strength of the crust and the lithospheric mantle, requires that at least two different materials are employed to model these layers.

Finally, since we are interested in the large deformation of the lithosphere we must also consider the material strain softening behavior, required in order to produce and maintain lithospheric-scale shear zones. In the brittle layers of the lithosphere the localization seems to be natural and an unavoidable consequence of the deformation mechanism, although there is much debate in the material mechanics literature about how exactly this process occurs. The materials with ductile constitutive response were also shown to be able to localize deformation in narrow bands, which results from a constitutive instability. The deformation bifurcation induced by this instability can occur even at positive hardening modulus (Rudnicki and Rice 1975; Chemenda 2007), i.e., during strengthening of the material (before reaching the stress peak on stress-strain diagrams) and especially when the dilatancy factor is negative (Chemenda 2009). On the other hand, to develop large shear deformation without considerable increase of the shear zone width, the material should start to soften at some point anyway.

Localization in the ductile regime, which appears to depend strongly on the water content in the lithosphere (Regenauer-Lieb 2006), may be promoted by strain softening mechanisms such as dynamic recrystallization and shear heating (Poirier 1980; White et al. 1980; Kirby 1985; Montési and Zuber 2002; Hartz and Podladchikov 2008; Regenauer-Lieb et al. 2008). However, the softening functions associated with these mechanisms are still debated (Rutter 1999; De Bresser et al. 2001; Montési and Hirth 2003). An equivalent efficient strain localization process (up to 50% softening) is obtained in our model lithosphere using specially designed strain-softening elasto-plastic materials. These materials are alloys of solid hydrocarbons (paraffin and ceresin waxes), mineral oils, finely ground powders, with surface-active substances (Shemenda 1992, 1993, 1994; Shemenda and Grocholsky 1992). Microscopically, they are thixotropic dispersions of solid hydrocarbons and powders in oil possessing macroscopic elasto-visco-plastic properties that are strongly dependent on temperature. Like real rocks, the analogue materials exhibit various rheological behaviors for various temperatures and strain-rates, from linear viscous to non-linear viscous to plastic and brittle-dilatant properties. Both the temperature of the model lithosphere and strain rate were chosen such that

the materials can be considered purely elasto-plastic (i.e., not sensitive to strain-rate) with softening and satisfy the scaling or similarity criteria presented below in Sect. 16.2.3.

16.2.2 Experimental Setups

Multiple experimental setups have been employed for 2D and 3D, mechanical and thermo-mechanical experiments of oceanic or continental subduction and arc–continent collision. However, these various types of experiments shared the same general layout described here for the arc–continent collision experiments.

The experimental setup comprises a tank filled with water representing the low-viscosity asthenosphere, on which two lithospheric plates are placed. The overriding plate is oceanic and generally made of one single lithospheric mantle layer. This plate can be thinned under the magmatic arc and under the back-arc basin (Fig. 16.1) as suggested by petrologic, geothermal and seismic data (Furukawa 1993; Zhao et al. 1994, 1997; Schmidt and Poli 1998). The subducting plate comprises two parts. One part is oceanic and made of one single layer of mantle lithosphere material. The second part is continental and made of at least two layers: the continental crust, and the lithospheric mantle. In between the continental and oceanic domains is a continental passive margin where the thicknesses of the crust and lithospheric mantle reduce progressively towards the ocean (Fig. 16.1).

In the purely mechanical experiments, both the temperature of the asthenosphere T_a and of the model surface T_s are controlled and maintained at 40°C. This task is performed using two thermal probes located at the model surface and under the lithosphere, two electrical heaters placed at the bottom of the experimental tank and above the model surface (see Fig. 16.1) as well as an auto-adaptive temperature controller. At this temperature, the strength of the employed analogue materials satisfies the similarity criteria required for the scaling (see Sect. 16.2.3). The convergence of the two lithospheric plates is imposed at a constant rate during the experiment using a motor. The setup of the 3D purely mechanical experiments of arc–continent collision (Chemenda et al. 1997b, 2000b, 2001b) is similar to that employed for the 2D experiments, but the model lithospheric plates are considerably larger and the interplate surface is not planar.

The setup of the 2D thermo-mechanical experiments of continental subduction and arc–continent collision is similar to that in Fig. 16.1. The difference with 2D purely mechanical experiments is that the temperature at the model surface T_s is lowered (37–38°C) and the temperature of the asthenosphere T_a is increased (~42°C), which leads to a conductive

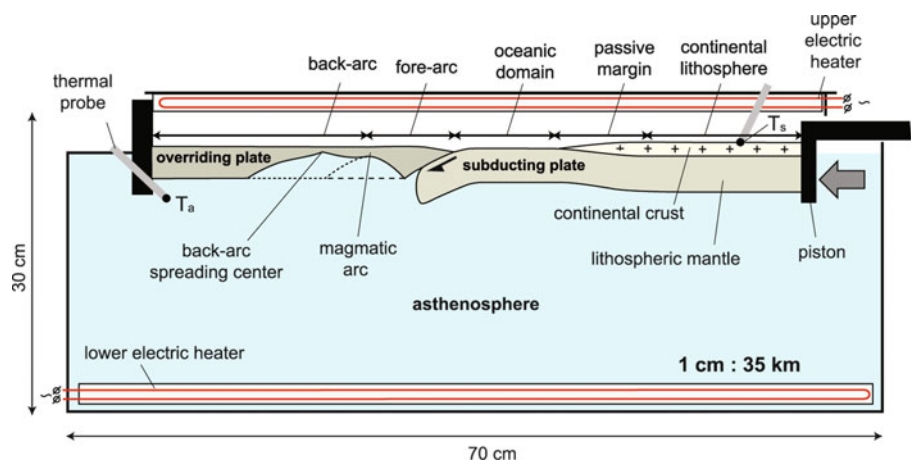

Fig. 16.1 Scheme of the experimental setup. The lithospheric layers are made of temperature-sensitive elasto-plastic with softening hydrocarbon compositional systems (Shemenda 1992, 1994). The asthenosphere is modeled by water. Temperature T_s and T_a are controlled and maintained at the model surface and the asthenosphere using thermal probes, electric heaters and an auto-adaptive thermo-regulator. The convergence is imposed by a piston moving at a constant rate during the experiment. The *dashed lines* show possible geometries of the base of the overriding plate depending on whether the thinning of this plate in the arc area and in the back-arc domain are implemented or not.

temperature gradient in the lithosphere prior to subduction and a smooth rheological stratification. Both the temperature gradient and the model materials were chosen to satisfy the scaling or similarity criteria (see Sect. 16.2.3) using the strengths of the materials averaged over the layers thicknesses. Since the employed materials possess elasto-plastic properties, they are almost insensitive to strain-rate (Shemenda 1992, 1993, 1994; Shemenda and Grocholsky 1992) and the imposed convergence rate can be adjusted to allow proper scaling of the heating rate during subduction and thus the weakening of the materials during this process (Chemenda et al. 2000a).

16.2.3 Scaling

The production of a physical model of a natural process cannot be reduced to producing a model that is only geometrically similar to the real studied object. Its mechanical or thermo-mechanical behavior must also be reproduced, at a smaller and more convenient scale. To ensure that the mechanics is similar in the model and nature, one must employ similarity criteria, which are non-dimensional ratios of the parameters controlling the studied phenomena. These non-dimensional ratios must be equal in the model and in nature in order to guarantee that the mechanics of the process is properly scaled (Buckingham 1914; Hubbert 1937; Ramberg 1967; Shemenda 1994). The similarity criteria can either be deduced from an analysis of the dimensions of the controlling parameters (Buckingham 1914) or they can be deduced directly from the mathematical equations governing the phenomena when these equations are known (Shemenda 1994).

The thermo-mechanical modeling of arc–continent collision within the framework described above with a simple three-layers continental lithosphere should satisfy the following criteria:

$\sigma_c/\rho_c g H_c = \text{const}$, $\sigma_l/\rho_l g H_l = \text{const}$, $H_c/H_l = \text{const}$, $\rho_c/\rho_l = \text{const}$, $\rho_l/\rho_a = \text{const}$, $VH/\kappa = \text{const}$, and $Vt/H = \text{const}$

Where σ_c and σ_l are the yield stress of the crust and lithospheric mantle; ρ_c, ρ_l and ρ_a are the densities of the crust, lithospheric mantle and the asthenosphere, respectively; H_c and H_l are the thicknesses of the crust and lithospheric mantle, g is the gravitational acceleration, V is the plate velocity, κ is the thermal diffusivity, H is the thickness of the lithosphere and t is the time. The small elastic strain before onset of plasticity is approximately scaled using the ratio of the elastic modulus E to the lithostatic pressure $\rho g H$. The employed analogue materials have an elastic modulus of ~1,000 Pa which scales appropriately to $\sim 1 \times 10^{11}$ Pa in nature. The ranges of values for other parameters are provided in Table 16.1.

16.3 Mechanical Essentials of Subduction

16.3.1 Oceanic Subduction

The regime of oceanic subduction prior to arc–continent collision strongly influences the scenario of the collision and therefore must be taken into account. Furthermore, oceanic subduction experiments best illustrate the effects of the bending strength of the subducting lithosphere and the force due to the

Table 16.1 Ranges of parameter value used in the experiment and scaled to nature

Parameter	Symbol (unit)	Model (M)	Nature (N)	Scaling factor (M/N)
Averaged yield limit of the continental crust	σ_c (Pa)	18–43	$2.05–5.7 \times 10^8$	8.79×10^{-8}
Averaged yield limit of the continental lithospheric mantle	σ_l (Pa)	27–43	$3.07–5.7 \times 10^8$	8.79×10^{-8}
Young's modulus	E (Pa)	$\sim 2 \times 10^3$	$\sim 1 \times 10^{11}$	8.79×10^{-8}
Density of the upper crust	ρ_c (kg.m^{-3})	860	2795	3.08×10^{-1}
Density of the continental lithospheric mantle	ρ_l (kg.m^{-3})	1,000–1,030	3,250–3,350	3.08×10^{-1}
Density of the asthenosphere	ρ_a (kg.m^{-3})	1,000	3,250	3.08×10^{-1}
Thickness of the upper crust	H_c (m)	8×10^{-3}	2.1×10^4	2.86×10^{-7}
Thickness of the continental lithospheric mantle	H_l (m)	1.5×10^{-2}	8.75×10^4	2.86×10^{-7}
Convergence rate	V (m.s^{-1})	3×10^{-5}	1.28×10^{-13}	9.80×10^4
Thermal diffusivity of the lithosphere	κ (m^2.s^{-1})	8×10^{-8}	1.0×10^{-6}	2.8×10^{-2}
Time	t (s)	6.0×10^2	2.06×10^{14}	2.92×10^{-12}

Scaling factors are the ratios of the values in the model over the values assumed for nature

negative buoyancy of the subducted lithosphere, on the distribution of stresses along the interplate zone. Both these effects play an essential role during an arc–continent collision.

The stress state of the lithosphere is defined by its mechanical structure and the conditions along its boundaries. In subduction zones, the stress and tectonic regime in the overriding plate are generally controlled by the stresses along the interplate zone. These are the normal and tangential stresses generated by the subduction process. Since the interplate friction appears generally small for oceanic subduction zones (Tichelaar and Ruff 1993; Peacock 1996; Hassani et al. 1997), the normal stress (interplate pressure) is the main parameter controlling the stress state of the upper plate during oceanic subduction.

Purely mechanical laboratory experiments of oceanic subduction revealed the existence of two end-member regimes of this process defined by the interplate pressure which can either be higher or lower than hydrostatic pressure depending on whether the non-hydrostatic component of the normal stress (σ_n) is compressive or tensile (Shemenda 1993, 1994). The two regimes of oceanic subduction are associated respectively with compressive or tensile tectonic regimes in the arc/back-arc area. Both the magnitude and sign of σ_n, and hence, the subduction regime are mostly controlled by the bending strength (flexural rigidity) of the downgoing plate and its buoyancy. Viscous interaction between the subducting lithosphere and surrounding mantle, however, also affects the stress conditions at the plate boundary. Flow in the mantle may be resisting or assisting slab subduction. Depending on the flow pattern, it can cause σ_n to be compressive or tensile (Shemenda 1994; Boutelier and Cruden 2008). Nevertheless, laboratory experiments suggest that the stress state of the lithosphere in subduction zones is generally controlled by the buoyancy (negative or positive) of the subducted slab (Boutelier and Cruden 2008).

16.3.1.1 Oceanic Subduction in the Compressive Regime

The strength of the subducted lithosphere, which resists bending during subduction, causes a compressive non-hydrostatic normal stress σ_n whose magnitude increases with depth along the interplate zone (Fig. 16.2a, c). If the effect of the plate bending is not counterbalanced by any other forces, a compressive subduction regime is obtained (Shemenda 1993; Hassani et al. 1997). The integration of the non-hydrostatic interplate pressure over the plate boundary yields the tectonic pressure force F_p. The compressive horizontal component of F_p defines the compressive tectonic regime in the arc/back-arc area (Fig. 16.2a, c), while the vertical component drives the non-isostatic uplift of the fore-arc area (Fig. 16.2c).

16.3.1.2 Oceanic Subduction in the Tensile Regime

When the density of the subducted lithosphere is significantly larger than that of the surrounding mantle, the negative buoyancy of the subducted slab generates a downward pull force F_{sp}, which results in a tensile non-hydrostatic normal stress σ_n on the interplate zone. The magnitude of this stress increases with depth (Fig. 16.2b, d) and adds to the stress generated by the bending of the subducting plate. The integration of the total interplate pressure now gives a resultant pressure force oriented downward and toward the subducting plate. The vertical component of F_p now causes non-isostatic subsidence of the fore-arc, while the horizontal component generates horizontal extension of the arc/back-arc area (Fig. 16.2d). The action of the slab pull force thus naturally leads to the opening of a back-arc basin through rifting of the magmatic arc followed by spreading (Fig. 16.2b). However, when the length of the subducted slab reaches a certain critical value, the slab pull force becomes sufficient to cause slab break-off, after which oceanic subduction switches to the compression regime (see Shemenda 1994, Fig. 4.5).

16.3.2 Continental Subduction

Two principal regimes of continental subduction, characterized by high or low interplate pressure and associated with high or low-compression tectonic regime, are also obtained in the purely mechanical laboratory experiments of this process (Chemenda et al. 1995, 1996). As for oceanic subduction, the regime of continental subduction is mainly controlled

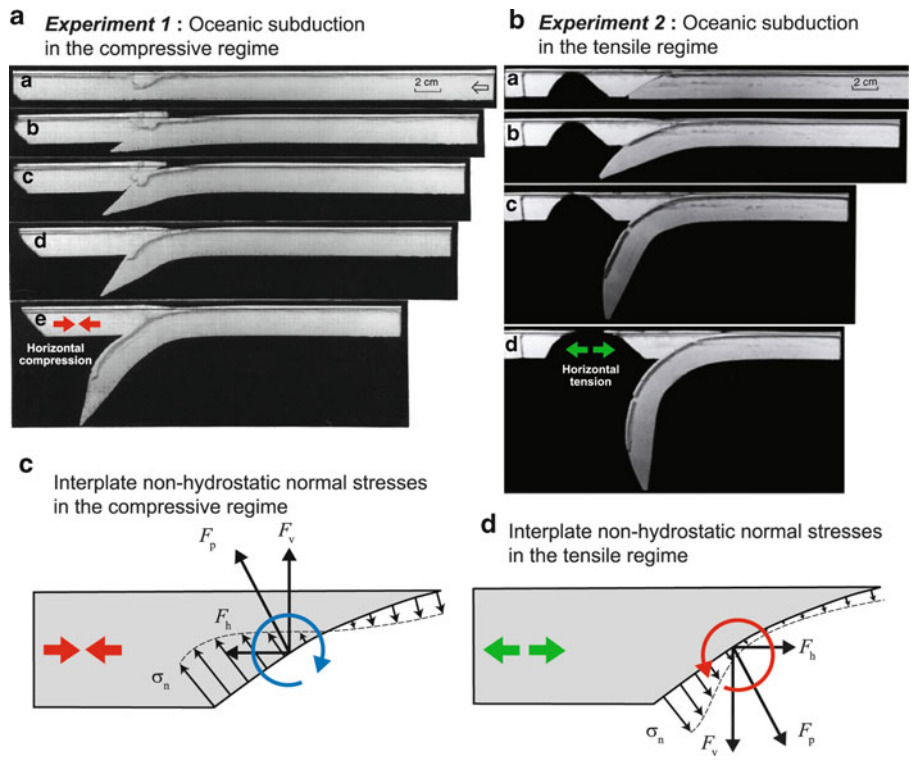

Fig. 16.2 Purely mechanical experiments of oceanic subduction in the compressive (**a**, **c**) and extensive (**b**, **d**) regimes (Shemenda 1993). (**a**) Experiment 1. The compressive regime is due to the flexural rigidity of the subducting plate, which induces a generally compressive non-hydrostatic normal stress on the interplate zone (**c**). In this experiment the density of the subducted lithosphere equals the density of the surrounding asthenosphere ($\rho_l = \rho_a$). (**b**) Experiment 2. The tensile regime of oceanic subduction with slab roll back and opening of a back-arc basin is obtained when the subducting lithosphere is ~4% denser than the asthenosphere ($\rho_l > \rho_a$). The generated pull force counterbalances the compressive stress due to the flexural rigidity of the subduction plate and even induces a tensile non-hydrostatic stress along the interplate zone (**d**).

by the slab-pull force due to the negative buoyancy of the subducted lithospheric mantle and the bending strength (flexural rigidity) of the lower plate. However, because of the high buoyancy of the subducting continental crust, continental subduction is always associated with horizontal compression that can either be high or low.

16.3.2.1 Continental Subduction in the High Compression Regime

The high compression regime of continental subduction is obtained in laboratory experiments when the density of the continental lithospheric mantle layer and oceanic lithosphere subducted prior to collision equals the density of the asthenosphere ($\rho_l = \rho_a$). In this case, both the flexural rigidity of the subducting lithosphere and the buoyancy of the subducted continental crust produce a strong compressive non-hydrostatic normal stress σ_n in the interplate zone and thus generate a strong horizontal compression of the plates. In purely mechanical experiments of continental subduction in the high compression regime (Chemenda et al. 1995), the subducted continental crust reaches a critical depth (~200 km) proportional to the plate strength and then the crust fails in front of the subduction zone, forming a major thrust (Fig. 16.3a, b). Buoyancy-driven uplift and exhumation of the subducted crust is then only possible with erosion of forming relief (Fig. 16.3c), which sets a maximum limit to the exhumation rate of about 10 mm/year (Burbank 2002).

16.3.2.2 Continental Subduction in the Low Compression Regime

The low compression regime of continental subduction is obtained in laboratory experiments when the density of the lithospheric mantle of the subducting plate is

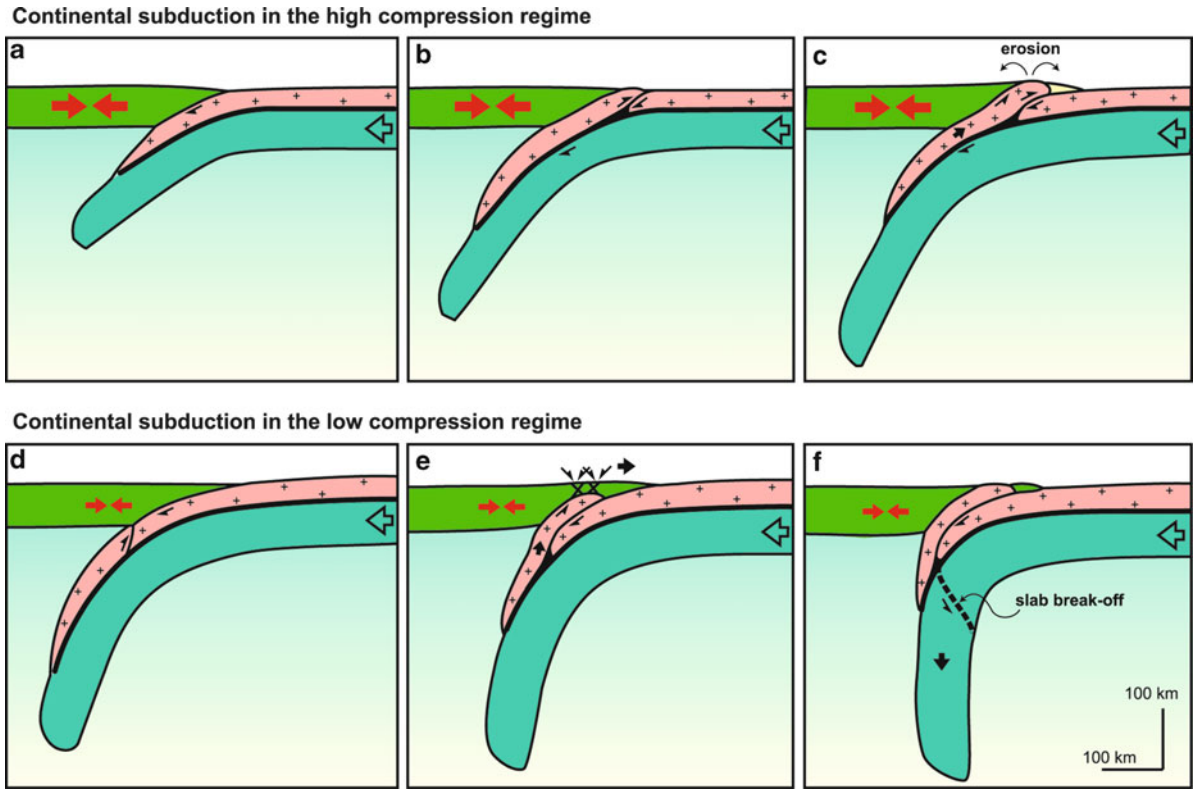

Fig. 16.3 Two principal regimes of continental subduction obtained in purely mechanical experiments of this process (Chemenda et al. 1995, 1996). (**a**–**c**) Experiment 3. The continental lithospheric mantle and the oceanic lithosphere subducted prior to continental subduction have the same density as the asthenosphere ($\rho_l = \rho_a$). A strong horizontal compression is generated in the plates (**a**). The continental crust then fails in front of the subduction zone and the buoyancy-driven exhumation is obtained due the erosion of the topography (**b**, **c**). (**d**–**f**) Experiment 4. The continental lithospheric mantle and the oceanic lithosphere subducted prior to continental subduction are denser (~4%) than the asthenosphere ($\rho_l > \rho_a$), which result in a low horizontal compression of the plates (**d**). The failure of the crust occurs in this case near the bottom of the interplate zone (**d**) forming a large crustal unit that detaches from the subducting lithosphere and rises up in between the plates driven by the buoyancy force (**e**, **f**). Continental subduction can switch from the low compression regime (**d**–**f**) to the high compression regime (**a**–**c**) when the negative buoyancy of the subducted lithospheric mantle results in the slab break-off (**f**).

significantly greater than the density of the asthenosphere ($\rho_l > \rho_a$). The non-hydrostatic interplate normal stress is small in this case but remains compressive generating only a weak horizontal compression in the plates. As for continental subduction in the high compression regime, the continental crust reaches a critical depth and fails (Fig. 16.3d). However, this time the failure of the crust occurs under the base of the overriding plate and is followed by the spontaneous buoyancy driven uplift (exhumation) of the subducted crust between the plates (Fig. 16.3e). This process can be interrupted by slab break-off (Fig. 16.3f), which triggers a rapid switch to the high compression regime of continental subduction (Chemenda et al. 1996).

16.4 Deformation of the Overriding Plate

Subduction of the continental margin thus generates an increasing horizontal tectonic compression of the overriding lithosphere. Physical experiments of arc-continent collision showed that when the overriding plate contains a major weak zone associated with the magmatic arc or a back-arc spreading center, the increasing horizontal compressive stress can result in failure of this plate in the weakest zone and formation of a new subduction zone where plate convergence can be temporarily accommodated.

16.4.1 Failure of the Overriding Plate in the Arc Area

The magmatic arc carried by the overriding plate constitutes a major lithospheric-scale zone of weakness. Petrology and geochemistry of arc magmas indicate magma temperatures of at least 1,200–1,300°C in the source regions at ~100 km-depth under the arc (Tatsumi et al. 1983; Schmidt and Poli 1998; Ulmer 2001; Kelemen et al. 2003; Peacock 2003). High temperatures in the sub-arc mantle are also supported by high surface heat flow (Lewis et al. 1988; Furukawa 1993; Currie et al. 2004; Currie and Hyndman 2006), low seismic velocities and high seismic attenuation (Zhao et al. 1994, 1997; Zhao 2001; Schurr et al. 2003, 2006). Such high temperatures in the sub-arc mantle have been produced in a variety of thermal and thermo-mechanical models of oceanic subduction where convection induced in the mantle wedge (corner flow) leads to thermo-mechanical erosion of the overriding plate under the magmatic arc (Furukawa 1993; Peacock 1996; Kincaid and Sacks 1997; Eberle et al. 2002; Arcay et al. 2006). Furthermore, petrologic experimental data attest that fluids released by the dehydrating slab in the asthenospheric wedge reduce its effective viscosity, which enhances the intensity of the induced convection and the thinning of the overriding plate (Billen and Gurnis 2001; Honda et al. 2002; Honda and Saito 2003; Arcay et al. 2005, 2006 Honda and Yoshida 2005). Other mechanisms have also been proposed for the thinning of the overriding lithosphere in the arc area. These include drip or delamination of the mantle lithosphere weakened by the wet rheology (Kay and Mahlburg Kay 1993; Sobolev and Babeyko 2005; Gögüs and Pysklywec 2008).

In the laboratory experiments of arc–continent collision, the overriding lithosphere is therefore thinned in the magmatic arc area to account for ongoing thermal erosion/drip of the mantle lithosphere beneath the arc (Fig. 16.1). Furthermore, if the oceanic subduction prior to the collision was in the extension regime (Fig. 16.2b), the magmatic arc may have been split and a back-arc basin may have been opened. In the newly created basin, the oceanic lithosphere is very young and therefore thin. Such thinning of the back-arc lithosphere is implemented in experiments specially designed to model an arc–continent collision following oceanic subduction in the extensional regime (Fig. 16.1).

16.4.1.1 Subduction of the Fore-Arc Block

In the case of failure of the overriding plate in the magmatic arc area, the dipping direction of the fault zone mainly depends on the sum of two opposite torques acting on the fore-arc block and caused by the distribution of stresses along the interplate zone (Tang and Chemenda 2000; Chemenda et al. 2001a).

The flexural rigidity of the subducting plate produces a generally compressive non-hydrostatic normal stress σ_n on the interplate zone whose magnitude increases with depth (Fig. 16.2c) and therefore produces a clockwise (arbitrarily we always place the overriding plate on the left side) torque on the fore-arc block. Similarly, interplate friction drags the fore-arc block towards the arc and down and therefore also generates a clockwise torque. On the other hand, during the subduction of the passive margin the distribution of σ_n changes such that it becomes larger at shallow depths due to the increasing thickness of the subducting buoyant crust (Fig. 16.4). Therefore the torque in this case is counter-clockwise. It follows that narrow continental passive margin (i.e., high gradient of crustal thickness perpendicular to the margin), low flexural rigidity of the lower plate and low interplate friction tend to produce a counter-clockwise resultant torque and hence failure of the arc lithosphere along an ocean-dipping fault zone.

In Experiment 5 (Fig. 16.4), the arc–continent collision occurs in the high compression regime. The collision follows oceanic subduction in the compressional regime and the force due to the negative buoyancy of the subducted oceanic or continental lithospheric mantle is very low ($\rho_l = \rho_a$). Subduction of the continental passive margin generates a large horizontal compression of the overriding plate resulting in the formation in the arc area of two deformation zones (incipient faults) with opposite dipping-directions (Fig. 16.4a, b). In this case, the resultant torque is counter-clockwise, which causes the final failure of the arc lithosphere to occur along the ocean-dipping localization zone (Fig. 16.4a, b). The failure is followed by subduction of the fore-arc block (Fig. 16.4c, d). During this process, displacement along the main subduction thrust is almost entirely stopped: convergence is mostly

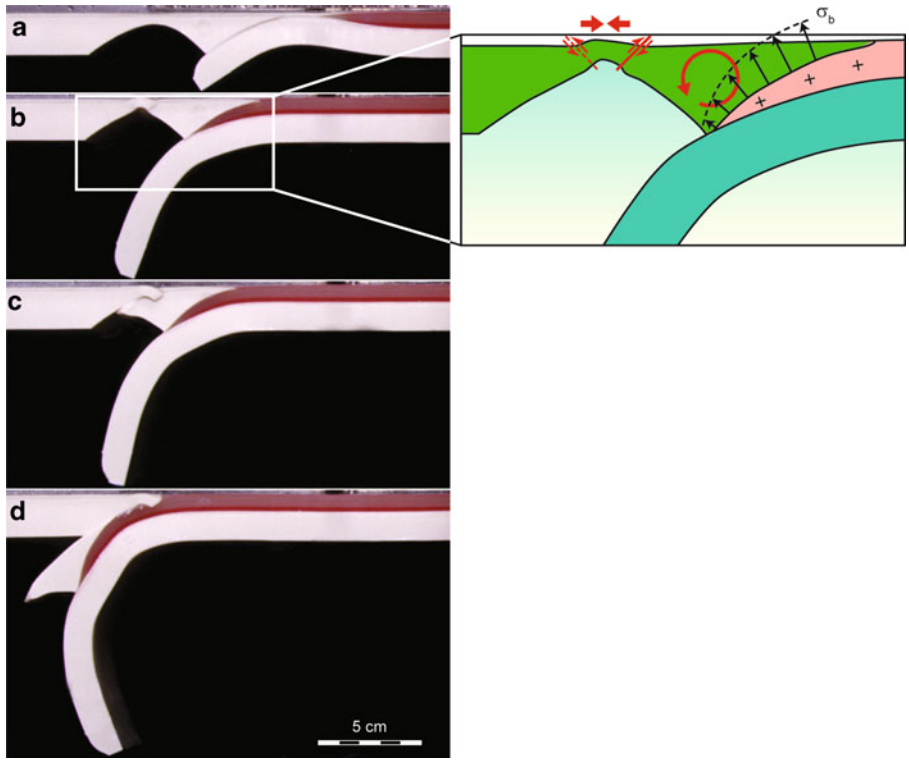

Fig. 16.4 Experiment 5; Purely mechanical model of arc–continent collision with failure of the overriding plate in the arc area during subduction of the continental passive margin (**a**, **b**), followed by subduction of the fore-arc block (**c**, **d**). The failure of the overriding plate occurs because the subduction of the continental passive margin generates a strong horizontal compression. The density of the subducted lithospheric mantle (oceanic and continental) equals the density of the asthenosphere ($\rho_l = \rho_a$) and continental subduction is therefore in the high compression regime (see Fig. 16.3). The distribution of the non-hydrostatic stress σ_b, due to the buoyancy of the subducted continental crust, along the interplate zone produces a counter-clockwise torque that lifts the upper part of this zone and leads to fore-arc block subduction. This figure is simplified after Chemenda et al. 2001a. Other model parameters and scaling are further detailed in the original paper.

accommodated by the deformation in the arc (see the position of the tip of the passive margin with respect to bottom of fore-arc block in Fig. 16.4). The passive margin can then be subducted to great depth (~150–200 km), maintaining relatively low temperatures because it is shielded from the asthenosphere by the subducting fore-arc block. The purely mechanical experiments of arc–continent collision in the high compression regime with subduction of the fore-arc block suggest that this process allows reaching ultra-high pressure and low temperature (UHP/LT) conditions in the deeply subducted crust.

16.4.1.2 Subduction Reversal

Failure of the overriding plate in the arc area may also occur along a continent-dipping fault zone, which leads to the subduction reversal. Such a scenario is presented in Fig. 16.5. This experiment was specifically designed to investigate how the scenario of subduction reversal evolves when the two subducted slabs meet at depth (Chemenda et al. 2001b). The overriding plate is thus pre-cut in the arc area along a fault zone dipping toward the continent. The subduction of the main oceanic plate under the magmatic arc occurs simultaneously with the subduction of the passive margin (Fig. 16.5a–c). The collision of the slabs at depth is initially accommodated by deformation of the new subducted slab. However, this deformation eventually stops and the first subducted slab is cut by the new subducting slab (Fig. 16.5d, e). The new subduction then becomes stable.

This scenario of subduction reversal corresponds to the Cenozoic evolution of the magmatic arc in Kamchatka (Konstantinovskaia 2000, 2011) and probably to the present situation in Timor (Silver et al.

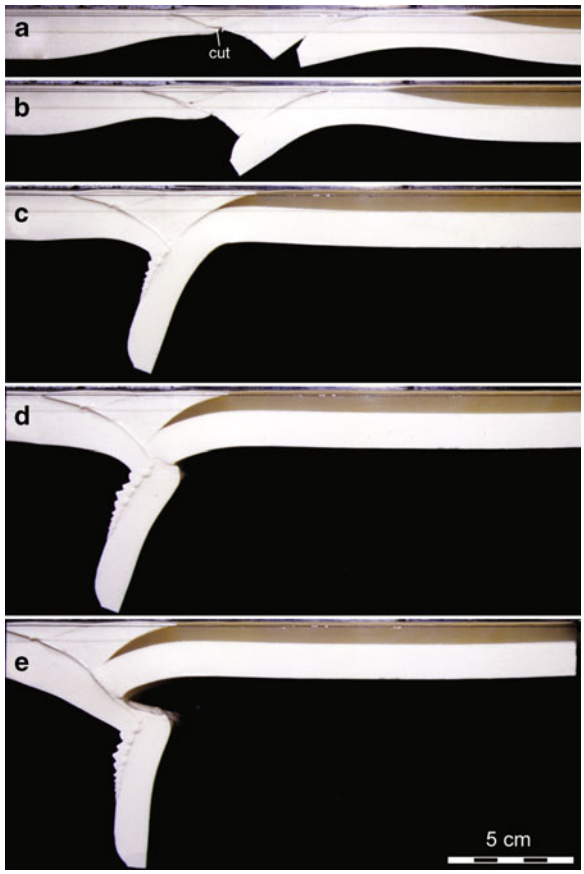

Fig. 16.5 Experiment 6; Purely mechanical model of arc–continentcollision producing a subduction reversal. As in Experiment 5 (Fig. 16.4), continental subduction is in the high compression regime ($\rho_l = \rho_a$) and generates a strong horizontal compression of the overriding lithosphere. A cut dipping towards the continental plate was made in the overriding lithosphere in the arc area to investigate the evolution of the subduction reversal scenario (**a**). Subduction of the continental margin leads to the development of the new subduction zone with an inverted polarity (**b**, **c**). The newly subducting slab cuts the older one (**d**). This figure is simplified after Chemenda et al. 2001b. Model parameters and scaling are detailed in the original paper.

1983; Snyder et al. 1996; Bock et al. 2003; Harris 2011). Subduction reversal is also proposed for the Ordivician arc–continent collision in Western Ireland (Ryan and Dewey 2011).

16.4.1.3 Evolutionary Scenario for the Arc–Continent Collision in Taiwan

The presented 2D experimental results including failure of the overriding plate in the arc area followed by subduction of the fore-arc block (Experiment 5: Fig. 16.4) or subduction reversal (Experiment 6: Fig. 16.5) have been employed together with 3D experimental results to produce a possible evolutionary scenario of the arc–continent collision in Taiwan (Chemenda et al. 1997b, 2001b). This scenario based on the experimental results and geological data includes:

- Thrusting and thickening of the subducting crust of the Chinese continental margin under the frontal part of the Philippine Sea Plate since 6–7 Ma (Fig. 16.6a, b).
- Uplift and exhumation of the subducted crustal slice of the Chinese margin and initiation of the Central Range 5 Ma ago (Fig. 16.6b).
- Flexural buckling and subsidence of the Luzon arc/fore-arc under strong horizontal compression and sedimentary infilling of this area by the material shed from the growing and exhuming Central Range (Fig. 16.6b).
- Failure of the Philippine Sea Plate along the west-vergent Longitudinal Valley Fault dipping beneath the arc and subduction of the fore-arc block (Fig. 16.6c).
- Subduction reversal and stoppage of continental subduction, which has already occurred in northern Taiwan and propagates to the south (Fig. 16.6d).

Multiple evidences for a subducted fore-arc mantle bloc beneath the Luzon arc in Central Taiwan have recently been obtained using seismic tomography. The studies showed an east-dipping promontory of low seismic attenuation, high V_p, V_s and Poisson's ratio beneath the Luzon arc (Coastal Range) at ~25 km-depth that approximately aligns with the Longitudinal valley fault at the surface (Kim et al. 2005; Wu et al. 2007; Cheng 2009; Lee et al. 2010; Wang et al. 2010). Together these geophysical characteristics indicate that this promontory is composed of mafic and/or ultramafic rocks and therefore must be the subducted fore-arc mantle bloc (Cheng 2009). The failure of the Philippine Sea plate along an east-verging fault located in the back of the Luzon arc in northern and central Taiwan is evidenced by the rapid uplift of marine terraces and geodetic data, which can be fitted with an offshore fault in the back of the Luzon arc (Huang et al. 2010; Wang and Burnett 1990; Hsieh et al. 2004). The geology of Taiwan is further detailed in Chap. 8 (Byrne et al. 2011), and the three-dimensional interaction between

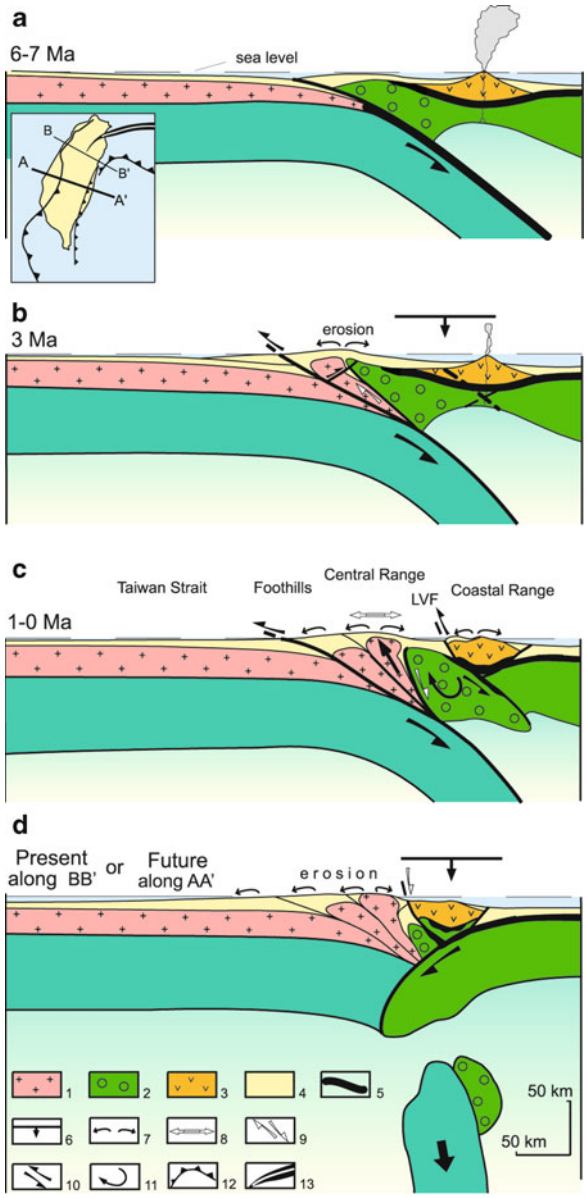

Fig. 16.6 Evolutionary scenario for the arc–continent collision in Taiwan based on experimental modeling results (after Chemenda et al. 2001b). (1) continental crust, (2) core part of the overriding wedge of the Philippines Sea plate corresponding to the fore-arc block, (3) volcanics of the Luzon arc, (4) sediments, (5) oceanic crust, (6) subsidence, (7) uplift and erosion, (8) direction of extension, (9) normal faulting; over/underthrust, (11) block rotation, (12) subduction (*inset*); Okinawa rift (*inset*). *LVF* Longitudinal Valley Fault.

the arc–continent collision in Taiwan and the Ryukyu oceanic subduction to the north is described in Sect. 16.5.

16.4.1.4 Evolutionary Scenario for the Arc–Continent Collision in the Ural Mountains

The presented 2D experimental results of arc–continent collision including failure of the overriding plate in the arc area followed by subduction of the fore-arc block (Experiment 5: Fig. 16.4) have also been combined with earlier experimental results on continental subduction and exhumation of subducted crust (Experiment 4: Fig. 16.3d–f) in an evolutionary scenario for the arc–continent collision in the Ural Mountains (Chemenda et al. 1997a). There, the fore-arc block appears to be missing and high-pressure rocks from the subducted continental lithosphere have been exhumed. The proposed evolutionary scenario includes:

- Closure of the western Uralian Ocean by intra-oceanic subduction associated with the Magnitogorsk island arc (MIA) (Fig. 16.7a).
- Subduction of the European continental margin causing failure of the overriding lithosphere in the arc area along an eastward-dipping fault (Main Uralian fault) under the arc (Fig. 16.7b).
- Subduction of the fore-arc block together with the underlying continental crust and a part of its sedimentary cover as in experiment 5 (Fig. 16.4). Fragments of the sedimentary cover, the crust as well as mantle fragments of the fore-arc block are scrapped off and accreted in front of and under the arc. At least a part of the fore-arc basin sediments remained on top of the hanging wall and together with the magmatic arc were obducted onto the European continental lithosphere. The continental crust, shielded from the hot mantle by the fore-arc block, subducts to depths of more than 150 km and remains at a relatively low temperature. The crust then fails near the base of overriding plate (Fig. 16.7c).
- The subducted crustal slice starts to rapidly rise and intrude the interplate zone, as in experiment 4 (Fig. 16.3d–f), scraping and pushing the sediments and slivers of the fore-arc block previously dragged down to various depths (Fig. 16.7d).
- Finally, erosion-driven exhumation of the rising high-pressure/low temperature rocks within the Uraltau dome (UD), separating the subduction accretionary complex from the Magnitogorsk arc and fore-arc basin sediments (Fig. 16.7e).

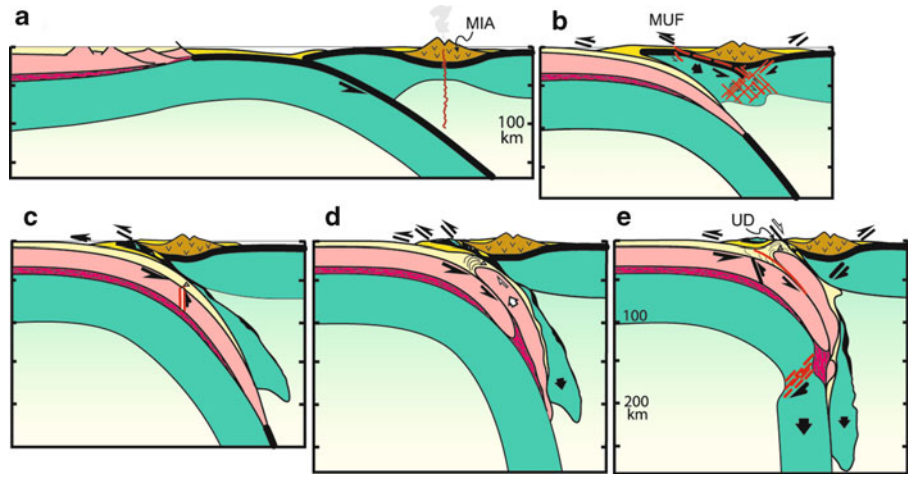

Fig. 16.7 Evolutionary scenario for the arc–continent collision in the Urals resulting in the subduction of the fore-arc block and exhumation of high-pressure/low temperature material from the subducted continental crust (after Chemenda et al. 1997). The hatching under the magmatic arc (**b**) represents deformation of the mantle lithosphere prior to formation of one through-going fault allowing the subduction of the fore-arc mantle block. The Main Uralian Fault (MUF), interpreted as the fault in the arc area allowing subduction of the fore-arc block may have reached the surface in the fore-arc basin near the backstop of the accretionary wedge. At least a part of the fore-arc basin may then have been sitting on the hanging wall and was not subducted with the mantle basement block. *MIA* Magnitogorsk Island Arc, *MUF* Main Uralian Fault, *UD* Uraltau Dome.

This evolutionary model rests on the recognition of the Main Uralian fault (MUF) as a fault separating the volcanic arc complex (including some fore-arc basin sediments and ultramafic rocks) from the accretionary complex. According to this interpretation, the fore-arc block is almost entirely missing and the most likely explanation is that it has been subducted. However, an alternative scenario without fore-arc block subduction was proposed based on the recognition of undeformed fore-arc sediments between the Main Uralian Fault and the Magnitogorsk arc. The MUF is then interpreted to be the backstop of the accretionary prism (Brown et al. 1998, 2006; Brown and Spadea 1999). Figure 16.7 presents a modified version of the original scenario published by Chemenda and co-workers in 1997, showing that the failure of the arc lithosphere obtained in laboratory experiments may also reach the surface near the backstop of the accretionary wedge and therefore at least a part of the fore-arc basin may be preserved at the surface. The location of the fault zone is controlled by the poorly constrained shape of the lithospheric mantle thinning below the magmatic arc and the internal structure of the fore-arc block, which is very variable (Stern 2002; Boutelier et al. 2003). Therefore it is not possible, from the modeling results, to precisely locate the position of the fault within the fore-arc basin. However, if this fault zone reaches the surface near the backstop or even in the middle of the fore-arc basin, at least a part of this basin must then sit on top of the hanging wall and therefore was not subducted. P and S-wave tomographic models in southern Urals reveal a small change in velocity from the European margin to the Magnitogorsk arc but the mantle does not show any velocity structure (Carbonell et al. 2000; Brown 2009). High-velocity mafic/ultramafic fore-arc mantle basement cannot be observed and the fore-arc sediments and arc crust could be resting over the Paleozoic continental crust as presented in our model (higher velocities are only observed in the lower crust at 40–45 km-depth). However, care must be taken when interpreting these tomographic data since the lack of a deep (>45–50 km) crustal root suggests that post-collisional processes (equilibration) have certainly already affected the deep structure of the collision zone. The geology of the Urals is further detailed in Chap. 11 (Brown et al. 2011).

16.4.2 Failure of the Overriding Plate in the Back-Arc Basin and Subduction of the Entire Arc Plate

Subduction of a continental margin can follow oceanic subduction in either of the two regimes (Fig. 16.2). In both cases it results in increasing horizontal compression of the overriding plate and eventually failure of this plate in its weakest place. When the arc–continent collision is preceded with oceanic subduction in the extension regime, the overriding plate may include a young back-arc basin where the newly created oceanic lithosphere is very thin. Subduction of the continental margin generates horizontal compression which stops the extension in the back-arc basin and causes its closure in a new subduction zone located near the back-arc basin spreading center. In this case, the failure zone is located far from the interplate surface. Therefore the failure direction is less sensitive to the stress conditions along this surface and is largely controlled by the trench/back-arc spreading center distance (Tang and Chemenda 2000; Tang et al. 2002). However, multiple poorly controlled factors, such as pre-existing faults at shallow depth, can also intervene and affect the failure direction. It is therefore not possible to predict the fault zone dipping direction from the modeling results. A failure along a fault zone dipping towards the continent results in the subduction reversal similar to what was obtained in Experiment 6 (Fig. 16.5). A failure along a fault zone dipping towards the ocean leads to subduction of the entire arc plate (Fig. 16.8). Plate convergence is then accommodated simultaneously on both the original main thrust (where the passive margin is subducted) and the new subduction zone in the closing back-arc basin (Fig. 16.8c, d).

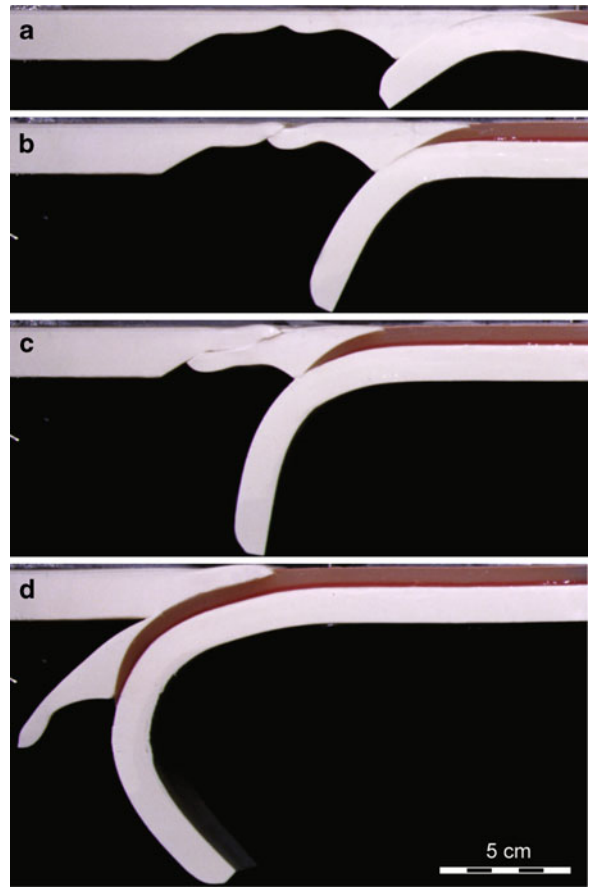

Fig. 16.8 Experiment 7; Purely mechanical model of arc–continent collision producing failure of the overriding plate near the back-arc basin spreading center (**a**, **b**) and subduction of the arc plate (**b**–**d**). This figure is simplified after Chemenda et al. 2001a. Arc–continent collision follows oceanic subduction in the tensile regime which resulted in the formation of a back-arc basin. In this experiment, continental subduction is in the high compression regime because the density of the subducted lithospheric mantle (oceanic and continental) equals the density of the asthenosphere ($\rho_l = \rho_a$). Other model parameters and scaling are detailed in the original paper.

16.4.2.1 Evolutionary Scenario of the Arc–Continent Collision in the Oman

The complete disappearance of the arc plate obtained in Experiment 7 (Fig. 16.8) led to an evolutionary scenario of arc–continent collision resulting in the emplacement of the young Oman ophiolite onto the Arabian continental lithosphere (Chemenda et al. 2001a). This scenario based on experimental results and geological data includes:

- Formation of the Oman ophiolite in a rifted immature intra-oceanic volcanic arc (in the active back-are basin context) 100 Ma ago (Fig. 16.9a).
- The extension regime of the oceanic subduction changed to compression by 94 Ma (Boudier et al. 1988; Hacker et al. 1996).
- Compression caused the overriding lithosphere to fail along a NE-dipping fault in the vicinity of the back-arc spreading ridge (Fig. 16.9a).
- Underthrusting of the arc plate occurred simultaneously with the main subduction under the arc

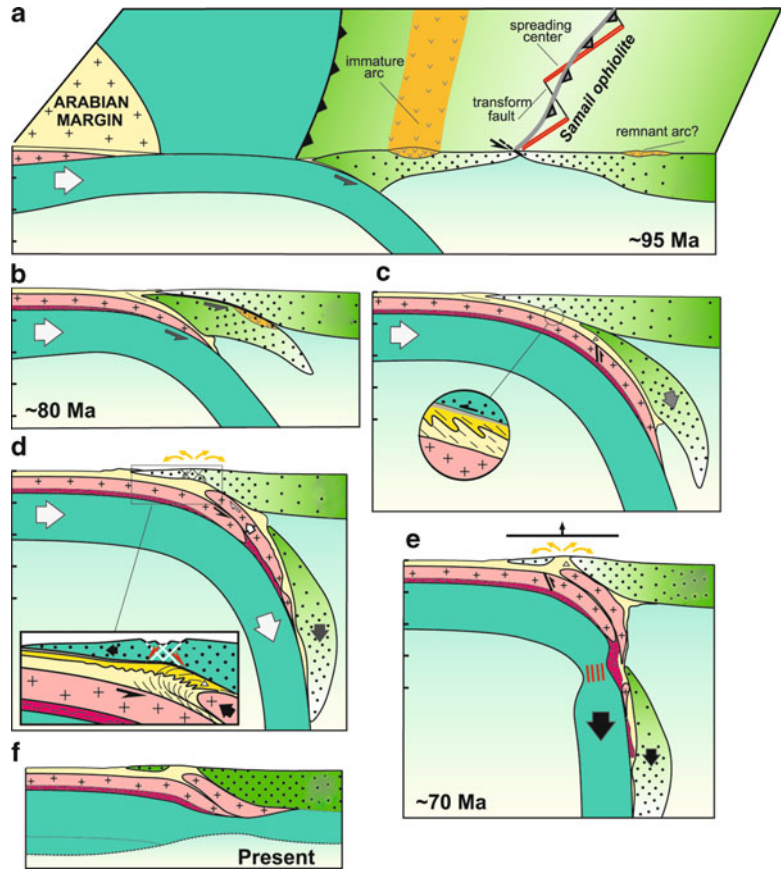

Fig. 16.9 Evolutionary scenario for the arc–continent collision in the Oman Mountains resulting in the subduction of the whole arc plate including an immature volcanic arc and resulting in the obduction of the Oman ophiolite on the Arabian continental lithosphere (after Chemenda et al. 2000a).

plate as in experiment 7 (Fig. 16.8), and then was blocked until the arrival of the Arabian continental passive margin in the main subduction zone at 88 Ma (Fig. 16.9b).

- Subduction of the passive margin resulted in progressive increase of horizontal compression of the overriding lithosphere. Overthrusting of the Oman ophiolite was then reactivated and the entire arc plate, including the immature volcanic arc, was subducted (Fig. 16.9c, d).
- The deeply subducted continental crust of the Arabian margin failed and a slice of deeply subducted continental crust started rapidly rising in between the plates. During this rapid exhumation the HP rocks reached a few tens of kilometers depth (Fig. 16.9d).
- The subsequent slower exhumation occurred between 80 and 68 Ma due to erosion of the ophiolite shield (Fig. 16.9e).
- The break-off of the dense lithospheric mantle caused a reduction of the pull force and a rapid isostatic uplift of the orogen resulting in almost complete emergence of the ophiolite above sea level at 72–65 Ma (Fig. 16.9e, f).

The geological constrains for this evolutionary model are detailed in Chemenda et al. (2001a) and references therein.

16.5 Three-Dimensional Physical Modeling of Arc–Continent Collision

Three-dimensional physical modeling experiments have been produced with the presented modeling technique in order to gain insights into the mechanics of

the arc–continent collision in Taiwan (Chemenda et al. 1997b, 2001b). Two important questions could be raised from the earlier 2D modeling results that could not have been answered with 2D experiments of arc–continent collision: What is the interaction between the westward subduction in the Ryukyu and the eastward subduction in northern Taiwan? How does the oblique arc–continent collision in Taiwan propagate southwards?

16.5.1 Interaction Between Two Opposite Facing Subduction Zones in Northern Taiwan

The first 3D models of arc–continent collision (Chemenda et al. 1997b) showed that the junction between the opposite facing subduction zones undergoes continuing failure of the subducting lithospheric plates (i.e., slab tears) resulting in the growth of a transform fault zone in between the subduction zones (Fig. 16.10). In Experiment 8 (Fig. 16.10) the model Philippine Sea plate suffered considerable plastic shortening along this fault zone, corresponding roughly to the position of the northern termination of the Luzon magmatic arc. This shortening, manifested by fractures at the model surface, attests that this area is submitted to a very high compressive stress. However, this stress is not sufficient to cause complete failure of the thick and strong plate which did not include the thinning and weakening of the overriding plate in the magmatic arc area. This thinning and weakening was first introduced in simpler 2D experiments (Figs. 16.4, 16.6, and 16.7) which have demonstrated that it plays a fundamental role in the scenario of arc–continent collision. Only then was the thinning and weakening of the arc lithosphere introduced in 3D models (Chemenda et al. 2001b). Experiment 9 (Fig. 16.11) shows that, with the thinning of the arc lithosphere, the northernmost part of the Luzon arc, which belongs to the model Philippines Sea plate, also underwent large plastic shortening but now the compressive stress is sufficient to cause complete failure of the arc lithosphere in multiple locations. Failure first occurred along the western side (front) of the Luzon arc, leading to the subduction of the fore-arc block, and then along the eastern side of the volcanic arc (back), leading to the subduction reversal scenario (Fig. 16.6).

16.5.2 Southward Propagation of the Arc–Continent Collision in Taiwan

Due to the oblique orientation of the Luzon arc and Eurasia passive continental margin, the collision is propagating southwards. The collision is more advanced in northern Taiwan while it is only in its initial stages near the southern tip of the Island. The propagation of the collision in Taiwan was proposed to be stationary (Suppe 1981, 1984). Three-dimensional experiments of this process do confirm the southward propagation, but show that it is not stationary (Chemenda et al. 1997b, 2001b). The analysis of the spatial distribution of seismicity and gravity field in the area (Tang and Chemenda 2000) supports this conclusion. This analysis suggests that the southern tip of the Philippine Sea plate failure in the western foot of the magmatic arc is currently located to the south of Taiwan near 21°30′N. However, at this latitude, the continental subduction is just starting, while in central Taiwan the upper plate failed (forming the Longitudinal Valley fault) after a relatively long period of continental subduction (~4 Ma). Therefore, it appears that the southward propagation of the east-dipping fault under the Luzon arc was more rapid than the southward propagation of the continental subduction. In other words, if the process of fore-arc block subduction has affected a large part of the orogen, it may have started in various locations for different amount of continental subduction and therefore the propagation is non-stationary.

16.6 Thermo-mechanical Physical Modeling

Although the presented modeling results correspond quite well to the available geological data, they are purely mechanical and do not consider any change in the mechanical properties of the subducting materials. In nature, however, both pressure and temperature increase during subduction, causing the strength of the subducting crust and mantle to generally reduce (although at low temperature, the growth of pressure induces increase in the strength). Experimental studies of coesite aggregates show that the strength of the crustal rocks reduces from >100 MPa at mid-crustal

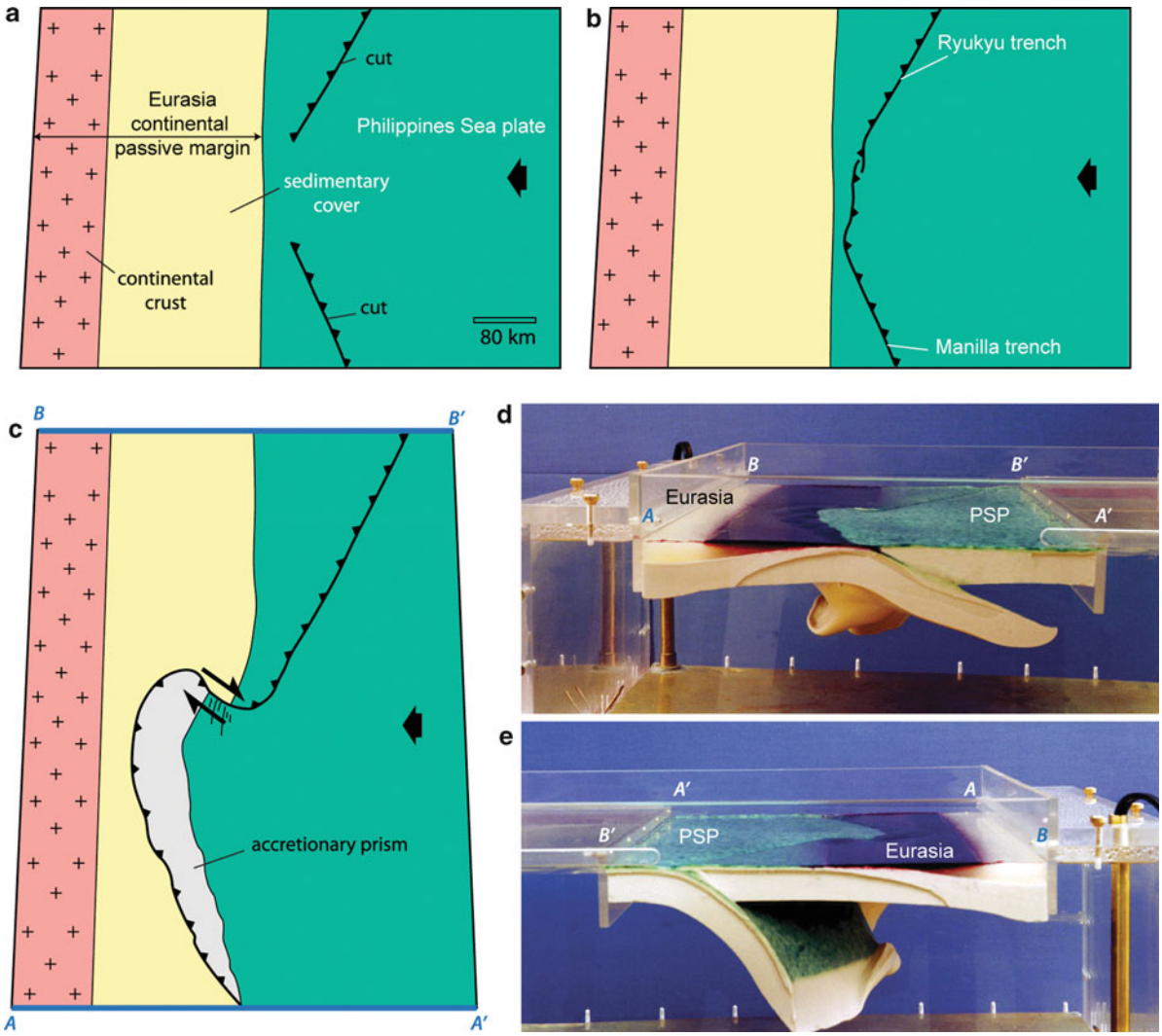

Fig. 16.10 Experiment 8; Drawings of the model surface (**a**–**c**) and general views (**d**, **e**) of the 3D purely mechanical model of arc–continent collision in the high compression regime ($\rho_l = \rho_a$), showing the interaction of two opposite-dipping slabs associated with the Manillas and Ryukyu subduction zones in northern Taiwan (Chemenda et al. 2001b). In this experiment, the thinning and weakening of the overriding plate in the area was not included. Imposed convergence results in the formation of a transform fault connecting the two subduction zones with opposite polarities. The upper plate is shortened near the transform fault zone in the location corresponding to the magmatic arc. However, the compressive stress is not sufficient to cause the complete failure of this plate.

depth (Ranalli and Murphy 1987) to about 10 MPa (Stockert and Renner 1998; Renner et al. 2001) at a temperature of 750 ± 150°C and pressure of 3 GPa corresponding to ca. 100 km-depth. Such strong change in the mechanical properties must affect the continental subduction and exhumation processes, which therefore must be addressed by thermo-mechanical modeling.

16.6.1 Low Compression Regime of Continental Subduction

The initially horizontal lithosphere is now subjected to a constant vertical temperature gradient. The continental lithosphere contains three layers: the very weak sedimentary layer, the crust made of a stronger material

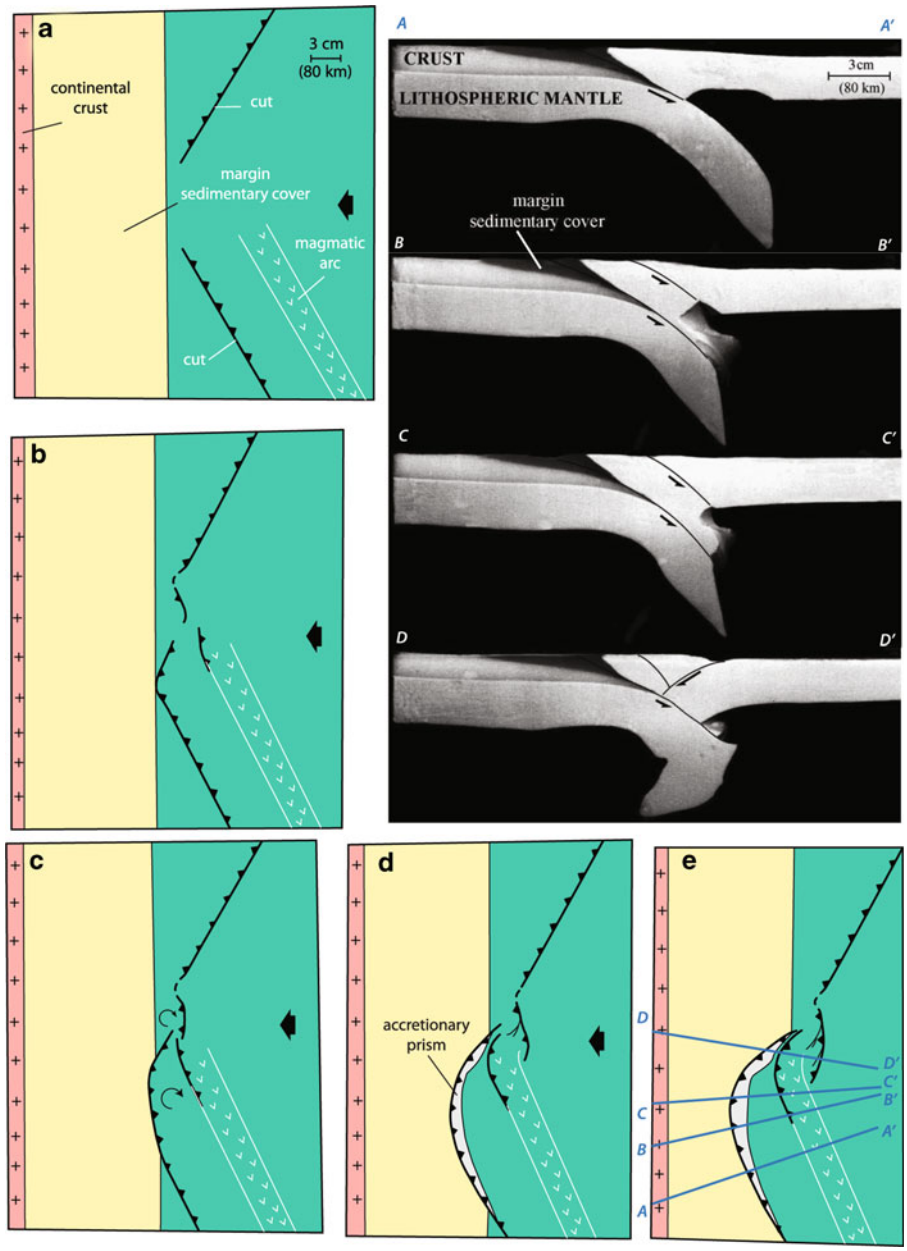

Fig. 16.11 Experiment 9; Drawings of the model surface (**a**–**e**) and cross-sections of the 3D purely mechanical model of arc–continent collision in the high compression regime ($\rho_l = \rho_a$), showing the interaction of two opposite-dipping slabs when the thinning of the arc lithosphere is implemented (Chemenda et al. 2001b). This experiment is similar to that presented in Fig. 16.10 except that the mantle lithosphere is thinned under the Luzon magmatic arc (see section AA'). The thinned arc lithosphere now fails near the junction between the two subduction zones. The first failure occurs in the western foot of the magmatic arc and results in the subduction of the fore-arc block (see panels **b** and **c** as well as sections BB' and CC'). The second failure occurs along the eastern foot of the arc and leads to subduction of the Philippine Sea plate under the Luzon magmatic arc (see panels **d** and **e** and section DD'). This new subduction zone is connected to the Ryukyu subduction zone to the north.

but whose strength reduces with depth due to the temperature increase, and the lithospheric mantle, made of a still stronger material with strength also reducing with depth. During subduction, the temperature of all layers increases, causing reduction of their strength and limiting the depth of crustal subduction

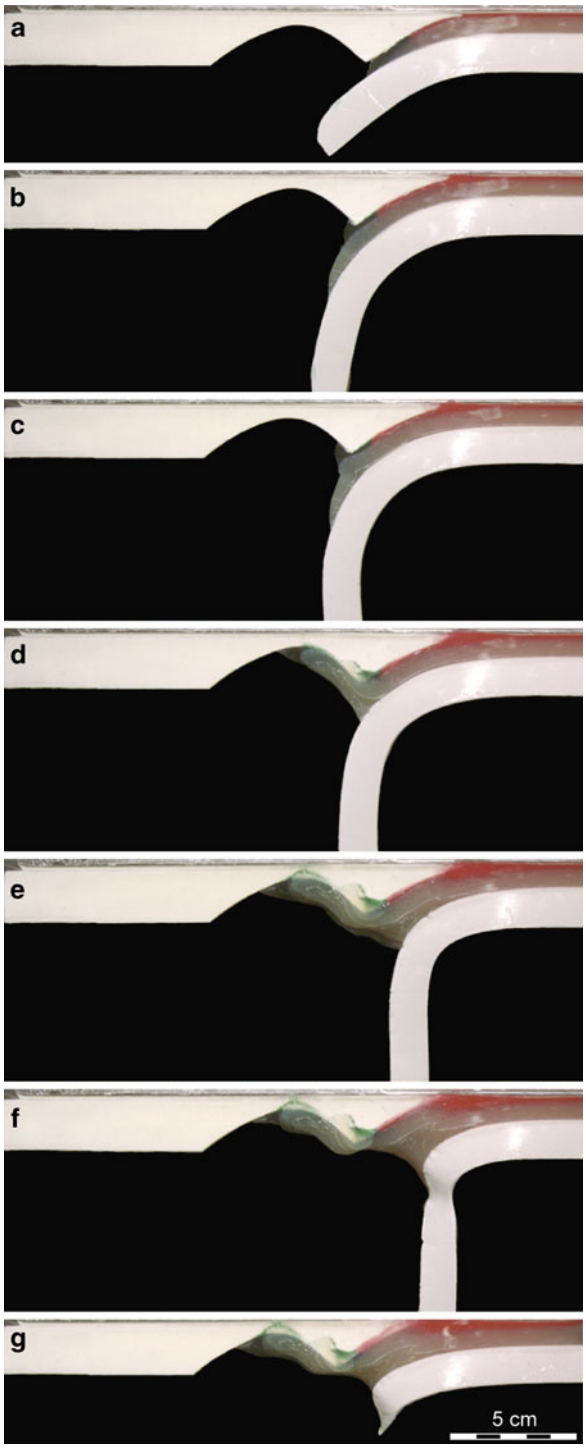

Fig. 16.12 Experiment 10; Thermo-mechanical model of arc–continent collision with continental subduction in the low compression regime. The continental lithospheric mantle and oceanic lithosphere are slightly denser than the asthenosphere ($\rho_l > \rho_a$). Subduction of the continental passive margin does not produce the failure of the overriding plate in the thin, hot and weak arc area. The continental crust is subducted in the asthenosphere to ~120 km-depth becoming hot and weak. It detaches and flows upward to be finally underplated under the overriding plate. The segment of continental crust gripped between the plates undergoes failure at few tens of kilometer-depth and rises up in between the plates in a manner similar to that obtained in purely mechanical experiments of continental subduction in the low compression regime (Experiment 4, Fig. 16.3). This exhumation is accompanied by the upward propagating delamination of the crust and the mantle lithosphere. Both delamination and exhumation are stopped by the slab break-off. This figure is simplified after Boutelier et al. 2002. Model parameters and scaling are detailed in the original paper.

(Fig. 16.12a–c). The crust subducts to 130 km-depth and then undergoes large and complex deformation including the upward ductile flow of the deeply subducted portions (Fig. 16.12d) and a localized failure of the upper crust at depth of only a few tens of kilometers (Fig. 16.12e). This deformation is accompanied by the delamination of crustal and mantle layers (Fig. 16.12e, f), which can be stopped by the break-off of the subducted continental lithospheric mantle and the previously subducted oceanic lithosphere (Fig. 16.12f, g). In experiments where the convergence was continued after the slab break-off, we observed a significant shortening of the formed orogen due to the increased horizontal compression produced by the removal of the pull force (the system switched to the high compression regime of continental subduction).

One can recognize in Experiment 10 presented in Fig. 16.12 the evolution of the continental subduction and exhumation corresponding to the low-compression regime obtained in the purely mechanical experiments (Experiment 4, Fig. 16.3d–f). As in previous experiments, starting from some critical depth of continental subduction, the continental crust undergoes failure and buoyancy driven uplift along the interplate zone followed by the mantle layer break-off. The thermo-mechanical model, however, provide new important insights into this process. Crustal failure and following uplift are closely related to the delamination of the crust and mantle, which is caused by the pull force generated by the subducted oceanic lithosphere and the continental mantle, both denser that the asthenosphere. Delamination occurs due to the large ductile deformation of the subducted (heated) crust and notably of its lower hotter part. These strongly weakened units flow up under the upper crust segment

located between the plates due to the buoyancy force. The upper crust segment gripped between the plates undergoes much smaller internal deformation. In the presented experiment (Fig. 16.12), this upper crust segment fails at ~40 km-depth forming one coherent rising unit which reaches ~20 km-depth. In other similar experiments, the delamination propagated further upward, leading to the formation of a second rising unit (Boutelier et al. 2004). A new result obtained from the thermo-mechanical experiments is that the rising crustal units are not deeply rooted in the asthenosphere as in previous purely mechanical experiments (Fig. 16.3). The reason is that the deep portion of the subducted continental crust flows upward and is underplated under the base of the overriding plate. The thermo-mechanical experiments reveal short rising crustal units and the uplift of the continental crust-asthenosphere interface in the interplate zone. Such uplift of the hot asthenosphere must provide heating of the surrounding crustal and mantle material, leading to magmatism and high-temperature metamorphism (Davies and von Blanckenburg 1995; Von Blanckenburg and Davies 1995).

The thermo-mechanical experiments of arc–continent collision in the low-compression regime (Boutelier et al. 2002, 2004) also reveal an interesting burial/exhumation evolution of the sedimentary cover of the passive margin. The sediments are subducted to the overriding plate base, and then partially accreted at the lower part of the interplate zone and partially flow under the overriding plate base (Fig. 16.12b–d). The sediments underplated in the interplate zone remain there until the delamination of the crust and mantle and the formation of the rising crustal unit. During delamination, the crust is not pulled down anymore by the dense mantle layer. Therefore the pressure between the crust and overriding plate increases along the interplate zone, starting from the bottom of this zone as the delamination propagates upwards. The increasing pressure squeezes the underplated sediments upward. They are extruded upward and even overtake the rising crustal slice. This mechanism allows the very rapid exhumation of small volumes of sedimentary materials.

Thus, the thermo-mechanical experiments of arc–continent collision with continental subduction in the low-compression regime on the one hand confirm the results of previous purely mechanical experiments of this process and on the other hand, reveal new effects. The exhumation depth in the thermo-mechanical experiments is limited by the overriding plate thickness (i.e., ~60–70 km). In nature, crustal rocks from the subducted passive margin can reach depths of more than 150 km and maintain relatively low temperature (750–900°C) at these depths (Ernst and Liou 2000; Chopin 2003). In the presented experiments it is impossible to obtain not only the exhumation from such depths, but simply the formation of the UHP/LT material since when it reaches ~100 km-depth the crust becomes too hot and weak and cannot be dragged deeper. To deliver the continental passive margin to >150 km-depth, it appears necessary that continental subduction triggers the failure of the overriding plate and the subduction of the fore-arc block/arc plate (e.g., Figs. 16.4 and 16.8) as this unit would shield the subducted passive margin from the hot asthenosphere. However, such deformation of the overriding plate is not obtained when continental subduction is in the low-compression regime: the horizontal compressive stress of the lithosphere in this regime is not sufficient to cause the failure of the overriding plate and make its frontal part subduct. The high horizontal compression and resulting large deformation and failure of the overriding plate is only obtained in the experimental models of arc–continent collision when the subducted oceanic lithosphere and continental lithospheric mantle do not exert a large pull force (i.e., continental subduction is in the high compression regime).

16.6.2 High Compression Regime of Continental Subduction

16.6.2.1 Subduction of the Fore-Arc Block

Thermo-mechanical experiments of arc–continent collision with continental subduction in the high compression regime results in almost the same scenario as that obtained in purely mechanical experiments. When the overriding plate does not contain a young back-arc basin, the weakest part of this plate is the magmatic arc area, where the lithosphere is hot and thin. Subduction of a continental margin may result in the failure of the overriding plate in this area. The lithospheric-scale fault can dip under the arc in either of two possible directions. In Experiment 11 (Fig. 16.13), the fault dips towards the ocean (Fig. 16.13b). The fault

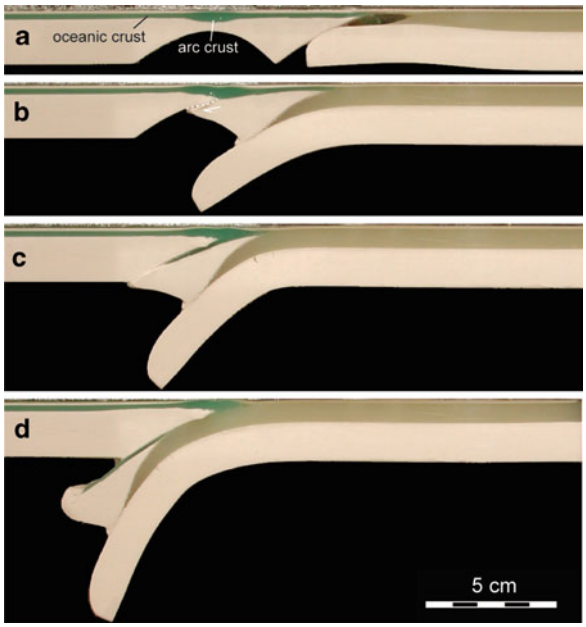

Fig. 16.13 Experiment 11; Thermo-mechanical model of arc–continent collision with continental subduction in the high compression regime ($\rho_l = \rho_a$) producing failure of the overriding plate in the arc area and subduction of the fore-arc block. This figure is simplified after Boutelier et al. 2003. Model parameters and scaling are detailed in the original paper.

formation is followed by nearly complete subduction of the fore-arc block (Fig. 16.13c). This experiment was part of a series of experiments conducted to investigate the evolution of deformation of the arc and oceanic crust during the processes of fore-arc block or arc-plate subduction (Boutelier et al. 2003). Both the arc crust and the oceanic crust were thus implemented in the overriding plate model. The fore-arc block (including its crustal part) is subducted under the magmatic arc, while the arc crust remained at the surface (Fig. 16.13a–c) and is obducted on the continental lithosphere (Fig. 16.13d).

As a consequence of the fore-arc block subduction, the continental crust is deeply subducted, remaining relatively cold. Indeed, the temperature measured with micro-thermal probes during the experiments at the surface of the crust subducted to the equivalent depth of ~150 km corresponds to ~900°C (Boutelier et al. 2004). The subducted fore-arc block thus does play the role of a thermal shield protecting the crust from being overheated by the asthenosphere. Furthermore, despite the relatively low temperature in the deeply subducted continental passive margin, this unit becomes very weak at depth, but does not flow upward as in Experiment 10 (Fig. 16.12). This is because the subducted fore-arc block also plays the role of a rigid guide preventing the buoyancy driven upward flow of the weak subducted crust in the asthenosphere, and thus allowing deeper crustal subduction. In this model the UHP/LT conditions are therefore achieved in the subducted passive margin, but this unit is not exhumed; this model shows no exhumation at all. The reason is that the crust in the interplate zone is blocked between rigid units (the overriding plate and the subducting lithospheric mantle) because of the high interplate pressure. To obtain the exhumation of the UHP/LT rocks in a scenario similar to that presented in Fig. 16.7, a reduction of the interplate pressure appears necessary.

16.6.2.2 Subduction of the Arc Plate with Accretion of the Magmatic Arc

As discussed in Sect. 16.4.2, arc–continent collision may follow oceanic subduction in the tensile regime with the opening of a back-arc basin. In this case, the subduction of the continental margin can cause failure of the lithosphere near the back-arc spreading center. The thermo-mechanical modeling of this process result in basically the same scenarios as those obtained from purely mechanical experiments (Fig. 16.8). However, the behavior of the magmatic arc crust during the subduction of the arc plate was shown to strongly depend on the arc composition and structure (notably on the thickness of both crustal and lithospheric mantle layers) (Boutelier et al. 2003).

Experiment 12 (Fig. 16.14) shows the failure of the overriding plate near the back-arc spreading center during the subduction of a continental passive margin (Fig. 16.14a) in the thermo-mechanical experiment. In this experiment, the magmatic arc crust is weak (made of continental crust material) and undergoes large deformation. A small part of the arc crust is dragged into subduction, but the main part is accreted at shallow depth. Relatively small volumes of the back-arc and fore-arc oceanic crust are also accreted to the overriding plate and obducted onto the continental lithosphere. During the subduction of the arc plate, the subduction of the continental crust under the arc plate continues at a very low rate. As in the previous experiment (Fig. 16.13), the continental passive margin can

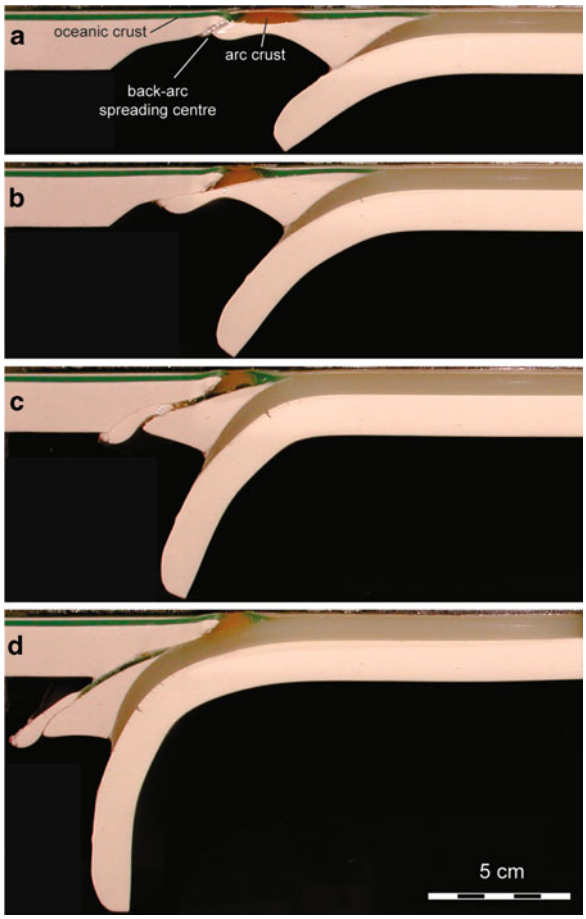

Fig. 16.14 Experiment 12; Thermo-mechanical model of arc–continent collision with continental subduction in the high compression regime ($\rho_l = \rho_a$) producing failure of the overriding plate near the back-arc basin spreading center and subduction of the arc-plate. The volcanic arc crust made of the same material as the continental crust is scrapped-off the arc-plate and obducted onto the continental lithosphere. This figure is simplified after Boutelier et al. 2003. Model parameters and scaling are detailed in the original paper.

be deeply subducted and preserved at low temperature because the subducted arc plate shields the crust from the asthenosphere. UHP/LT conditions are therefore achieved in the subducted passive margin but this unit is not exhumed. The same scenario of subduction of the arc plate with accretion of the magmatic arc crust is also obtained if the magmatic arc is strong but thick (>20 km). The reason is that the temperature at the bottom of the magmatic arc is larger for a thick arc than for a thin one. Consequently, the strength at the bottom of the arc crust is lower for a thick arc than for a thin one, and a thick arc is accreted, while a thin one can be subducted (Boutelier et al. 2003).

The scenario of thick/weak volcanic arc crust accretion and subduction of the rest of the arc plate corresponds to the situation in the western Himalayas. The collision between India and Asia was preceded by a long-lived intra-oceanic subduction that produced the Kohistan and Ladakh magmatic arcs (Tahirkheli et al. 1979; Bard et al. 1980; Coward et al. 1986), which are now accreted in the suture zone (Burg 2011). However, instead of the fore-arc and back-arc lithospheres there are only small remnants of the oceanic crust and sedimentary units. The solution consisting of subduction of the arc plate with arc accretion is then logical.

Calc-alkaline volcanic and volcanoclastic rocks in the southern-Tibetan part of the suture zone indicate that an intra-oceanic subduction also existed to the east of the Kohistan-Ladakh arc and was active in the Cretaceous. This intra-oceanic arc was almost entirely disappeared (Aitchison et al. 2000; Davis et al. 2002; McDermid et al. 2002). Since the arc could not have been erased by erosion (Fielding 2000), the most plausible mechanism for its disappearance is its subduction with the arc plate.

16.6.2.3 Subduction of the Arc Plate Including the Entire Magmatic Arc

Experiment 13 (Fig. 16.15) shows failure of the overriding plate near the back-arc spreading center during the subduction of a continental passive margin (Fig. 16.15a, b), followed by the complete subduction of the arc plate, including the arc crust (Fig. 16.15c, d). Such behavior is only obtained when the arc crust was strong, homogeneous (i.e., no weak zone was present within the arc crust) and thin (<20 km). The threshold arc crust thickness that controls the transition between accretion and subduction of the arc crust obviously cannot be precisely quantified from the modeling results.

This scenario of complete or almost complete arc subduction can be applied to orogens where the arc is missing. The alternative solution is that there was no arc at all because the intra-oceanic subduction was too short. However, when not only the arc is absent but also the fore-arc and back- arc basins, such a solution is no longer valid. The subduction of the whole arc

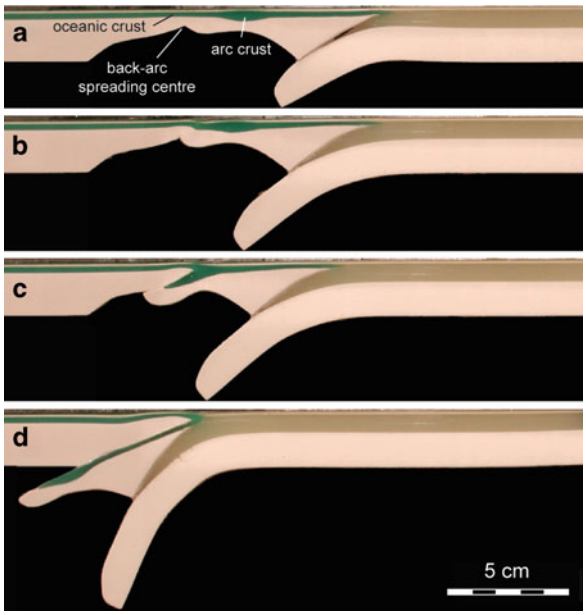

Fig. 16.15 Experiment 13; Thermo-mechanical model of arc–continent collision with continental subduction in the high compression regime ($\rho_l = \rho_a$) producing failure of the overriding plate near the back-arc basin spreading center and subduction of the arc-plate. The volcanic arc crust is thin and strong. It is entirely subducted with the arc plate and leaves few traces at the surface. This figure is simplified after Boutelier et al. 2003. Model parameters and scaling are detailed in the original paper.

plate including the arc crust is a more plausible scenario, which fits well the history and structure of the Oman Mountains (Chemenda et al. 2001a), the Himalayas in southern Tibet (Boutelier et al. 2003), and the French Variscan Belt in Massif Central and Massif Armoricain (Faure et al. 2008).

16.6.2.4 Subduction of the Arc Plate and Closing the Back-Arc Basin

Experiment 14 (Fig. 16.16) shows failure of the overriding lithosphere near the back-arc basin spreading centre during subduction of the passive margin. In this case, the fault zone dips towards the continent and therefore should lead to a scenario of subduction reversal as already presented in Experiment 7 (Fig. 16.8). However, as the oceanic lithosphere of the back-arc basin is subducting, a second fault zone is created in the arc area (Fig. 16.16b). This fault also dips toward the continent and therefore the subduction reversal scenario is in play, but the location of subduction has

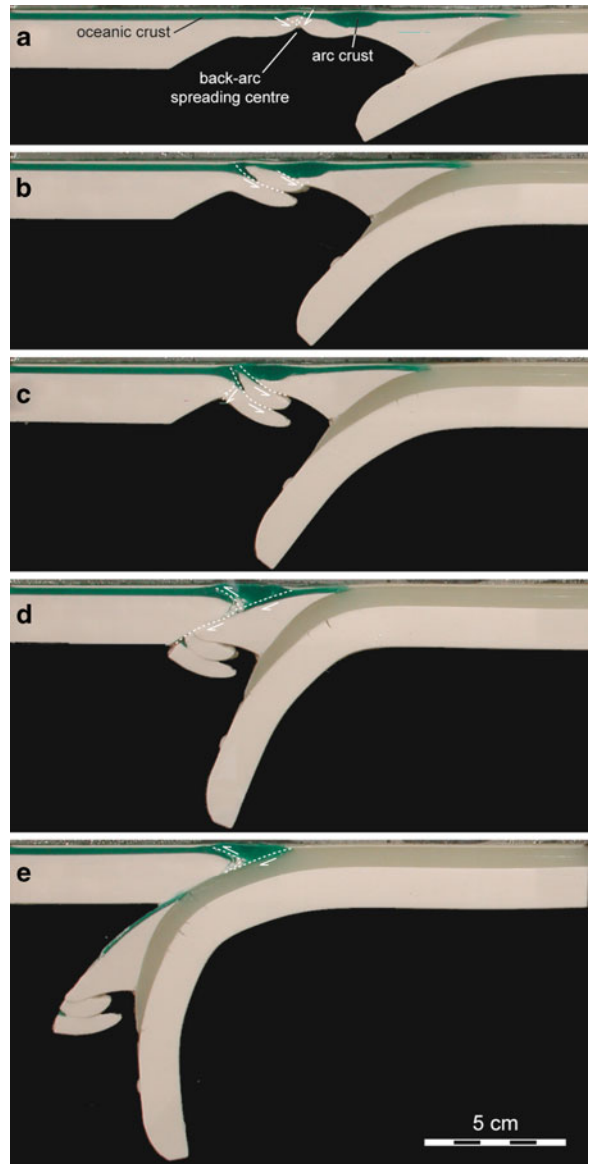

Fig. 16.16 Experiment 14; Thermo-mechanical model of arc–continent collision with continental subduction in the high compression regime ($\rho_l = \rho_a$) producing multiple failures of the overriding plate near the back-arc basin spreading center, the arc area and finally within the back-arc basin. This experiment shows that deformation of the overriding plate can initiate with subduction reversal and change to subduction of the fore-arc block. The volcanic arc crust is obducted onto the continental lithosphere, but both the fore-arc block and entire back-arc basin are missing. This figure is simplified after Boutelier 2004. Model parameters and scaling are detailed in the original paper.

jumped closer to the arc. Then, a third fault zone is created through the oceanic lithosphere of the back-arc basin. This fault zone dips towards the ocean and

therefore allows the subduction of not only the arc plate but also the part of the overriding plate corresponding to the young oceanic lithosphere of the back-arc basin (Fig. 16.16c–e). During this process the arc crust is accreted and obducted onto the continental lithosphere but the fore-arc and entire back-arc are missing.

In this experiment as well as in the Experiments 11 (Fig. 16.13), 12 (Fig. 16.14) and 13 (Fig. 16.15), the passive margin can be subducted to great depth (>150 km) and maintained at low temperature, which allows the formation of the UHP/LT rocks. However, no exhumation of the deeply subducted crust was observed in the experiments with subduction of the fore-arc block or arc plate that occur only in the high compression regime, i.e., when the interplate pressure is high. On the other hand, exhumation of the subducted crust appears possible only when this pressure is low, i.e., in the low compression regime. It is thus necessary that the continental subduction initiates in the high compression regime to create the UHP/LT rocks and then the regime must switch to the low compression, thereby allowing the buoyancy-driven exhumation of UHP/LT rocks from the deeply subducted continental margin.

The interplate pressure can be rapidly increased because of slab break-off and continental subduction then switches from the low compression to the high compression regime. The opposite, a decrease of the interplate pressure, is more difficult to imagine in a 2D configuration. However, this becomes possible locally in specific 3D situations.

16.7 Exhumation of UHP/LT Rocks Due to the Local Reduction of the Interplate Pressure

Spatial distribution of UHP/LT terrains in different regions suggests that exhumation of UHP/LT rocks is essentially a 3D process that does not occur all along convergent plate boundaries, but only in specific places characterized by geometrical or structural complexities (e.g., western Alps virgation, western syntaxis in the Himalayas, Tan-Lu transform fault in Dabie Shan-Sulu). Can these and/or other 3D complexities cause a local reduction of the interplate pressure that would allow the exhumation of the UHP/LT rocks within a generally high compression subduction regime?

Using 3D thermo-mechanical modeling technique, we investigated one situation where, following the deep subduction of the continental passive margin and the fore-arc block (Fig. 16.17a–c), the frontal part of the overriding plate is subjected to an extension parallel to the plate boundary with activation of a pre-existing strike-slip/transform fault oblique to the interplate zone (Fig. 16.17d). The displacement along this fault results in a local reduction of the interplate pressure at its intersection with the interplate zone. The lateral extension is artificially imposed in this model (Boutelier and Chemenda 2008) but in reality it may result from the obliquity of the convergence (Ave Lallemant and Guth 1990; McCaffrey 1992, 1996), the curvilinear geometry of the plate boundary (Boutelier 2004; Boutelier and Cruden 2007; Bonnardot et al. 2008; Boutelier and Oncken 2010), or other structural/cinematic complexities.

The produced local reduction of interplate pressure results in a complex local exhumation of the model crustal and sedimentary material subjected to UHP/LT conditions (Fig. 16.17e–g). In the 3D models, the exhumed units stem from equivalent depths between ~175–150 km for the crustal unit, and ~200–100 km for the sediments but the temperature in the subducted crust does not exceed ~900°C. The obtained extreme P/T conditions are consistent with those recorded in the Kokchetav massif (Kazakstan), >4.3 GPa/950°C (Hermann et al. 2001), the Western Gneiss of Norway, 3.2 ± 0.26 GPa/805 ± 40°C (Van Roermund and Drury 1998), or to some extend in the Rhodope massif in Greece, 3.1–3.9 GPa/600–900°C (Mposkos and Kostopoulos 2001). Other UHP/LT massifs show less high P conditions that can also be achieved in the model when the rising sheet detaches at shallower depth.

The finite deformation of the exhumed unit in Fig. 16.17 includes transport-parallel extension and top-to-the-subducting-plate (i.e., thrusting) shearing (Boutelier and Chemenda 2008) that corresponds to the first order deformation observed in the Tso Morari in Western Himalaya (Steck et al. 1998; Treolar et al. 2003), Dora Maira in Western Alps (Wheeler 1991; Avigad et al. 2003), or the Western Gneiss of Norway (Labrousse et al. 2002).

The evolution of the deformation during exhumation also matches the natural observations. The rising unit does not undergo significant deformation while being very deep but is more strongly

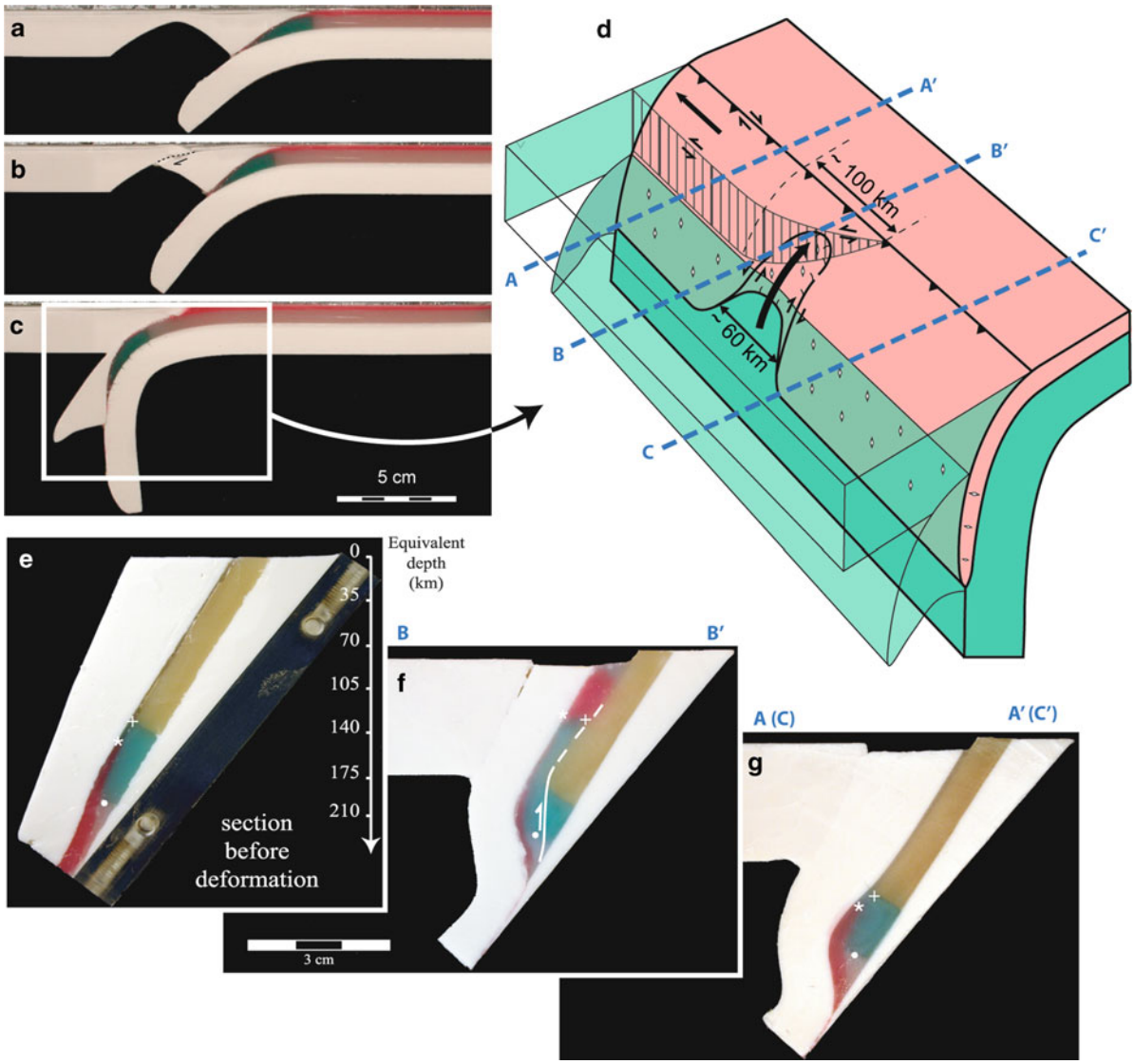

Fig. 16.17 Experiment 15; 3D thermo-mechanical model of exhumation of UHP/LT rocks due to the lateral extension in the overriding plate. The 3D modeling starts with the situation obtained in 2D thermo-mechanical experiments of arc–continent when the continental passive margin is deeply subducted and shielded from the asthenosphere by the subducted fore-arc block (**a**–**c**). The continental crust and sedimentary cover of the passive margin are thus deeply subducted and undergo UHP/LT conditions but cannot rise upward because of the high interplate pressure (**c**). (**d**) 3D sketch of the local exhumation obtained in the 3D thermo-mechanical laboratory experiments of exhumation of UHP/LT rocks due to the lateral extension of the overriding plate. In some specific situations the overriding plate may be submitted to trench-parallel tension which produces trench-parallel displacement of the overriding plate frontal tip and the local retreat of this frontal tip near the intersection with the subduction zone. This local retreat produces a local reduction of the interplate pressure which allows the buoyancy driven exhumation of the deeply subducted passive margin. Details of the implementation of this lateral extension and of the setup of this modeling are presented in Boutelier and Chemenda 2008. (**e**–**g**) Sections of the 3D thermo-mechanical model. (**e**) Model section before extension. (**f**) Model section in the area of decreased interplate pressure corresponding to profile B-B' of the 3D sketch. (**f**) Model section outside the area of decreased interplate pressure corresponding to profiles A-A' or C-C' of the 3D sketch.

sheared and stretched through a narrow passage at shallower depth. This may correspond to the observed lack of significant deformation associated with the ultra-high pressure event, while deformation during eclogite to amphibolite facies metamorphism is common (Tilton et al. 1997; Stockert and

Renner 1998; Renner et al. 2001; Treolar et al. 2003).

Finally, the exhumation process starts in our experiments with a fast equivalent rate of ca. 3 cm/yr and then slows down. This result is in agreement with geochronological data in the western Alps massifs of Dora Maira (~3.4 cm/yr) (Rubatto and Hermann 2001) and Zermatt-Saas-Fee (1.0–2.6 cm/yr) (Amato et al. 1999), the Kokchetav massif (~2.0 cm/yr) (Hermann et al. 2001) and the western Gneiss of Norway (~1.2 cm/yr) (Terry et al. 2000). Most UHP/LT units show a decrease of the exhumation rate to a few mm/yr before reaching the crustal level (Duchêne et al. 1997; Terry et al. 2000) as is also observed in our models.

16.8 Conclusions

Laboratory modeling of arc–continent collision have provided numerous insights into the mechanics of this process. Our experiments showed that the basic subduction scheme can be considerably modified at the beginning of continental subduction when the burial of the buoyant continental crust of the passive margin and its sedimentary cover generates a high horizontal compression of the overriding lithosphere. The compression can result in the failure of this plate in its weakest place, which can be the magmatic arc area or the back-arc spreading center. A new subduction zone can be created in the overriding plate and during a few million years two active subduction zones can coexist. Failure of the upper plate in the arc or back-arc basin spreading centre areas along a fault dipping towards the continent leads to subduction reversal. This scenario corresponds to the Cenozoic evolution of the magmatic arc in Kamchatka and probably to the present situation in Timor.

Failure of the overriding plate in the arc area along a fault dipping in the same direction as the principal subduction, leads to the subduction of the fore-arc block. This scenario corresponds well to the active arc–continent collision in Taiwan and may as well correspond to the fossil arc–continent collision in the Urals. Finally the failure may occur in the back-arc spreading centre and dip towards the ocean. This leads to the subduction of the arc plate, with either accretion or subduction of the volcanic arc, depending on its size and strength. This process provides an explanation for the absence of the intra-oceanic volcanic arc in the central Himalayas and the French Variscan Belt in Massif Central and Massif Armoricain.

The arc–continent collision plays a fundamental role in the fabrication of the UHP/LT rocks during deep continental subduction. The subducting fore-arc block or/and arc plates play the role of a thermal shield protecting the deeply subducting continental crust from heating by the asthenosphere. The exhumation of the UHP/LT rocks is rare and can occur only in specific 3D situations allowing a local reduction of the interplate pressure necessary for exhumation of UHP/LT rocks.

Acknowledgments Constructive comments by reviewers R. Glen and F. Rossetti as well as the editors improved the manuscript. Funding was provided by a Humboldt research grant to DB.

References

Aitchison J, Davis A, Liu J, Luo H, Malpas J, McDermid I, Wu H, Ziabrev S, Zhou M (2000) Remnants of a Cretaceous intra-oceanic subduction system within the Yarlung–Zangbo suture (southern Tibet). Earth Planet Sci Lett 183(1–2): 231–244

Amato J, Johnson C, Baumgartner L, Beard B (1999) Rapid exhumation of the Zermatt–Saas ophiolite deduced from high-precision Sm–Nd and Rb–Sr geochronology. Earth Planet Sci Lett 171:425–438

Arcay D, Tric E, Doin M (2005) Numerical simulations of subduction zones effect of slab dehydration on the mantle wedge dynamics. Phys Earth Planet Inter 149(1–2):133–153

Arcay D, Doin M, Tric E, Bousquet R, De Capitani C (2006) Overriding plate thinning in subduction zones: localized convection induced by slab dehydration. Geochem Geophys Geosyst 7(2):Q02007

Ave Lallemant H, Guth L (1990) Role of extensional tectonics in exhumation of eclogites and blueschists in an oblique subduction setting: Northeastern Venezuela. Geology 18(10):950

Avigad D, Chopin C, Le Bayon R (2003) Thrusting and extension in the southern Dora-Maira ultra-high-pressure massif (Western Alps): view from below the coesite-bearing unit. J Geol 111(1):57–70

Bard J, Maluski H, Matte P, Proust F (1980) The Kohistan sequence: crust and mantle of an obducted island arc. Geol Bull Univ Peshawar 11:87–94

Billen M, Gurnis M (2001) A low viscosity wedge in subduction zones. Earth Planet Sci Lett 193(1–2):227–236

Bock Y, Prawirodirdjo L, Genrich J, Stevens C, McCaffrey R, Subarya C, Puntodewo S, Calais E (2003) Crustal motion in Indonesia from global positioning system measurements. J Geophys Res 108:2367

Bonnardot M, Hassani R, Tric E, Ruellan E, Régnier M (2008) Effect of margin curvature on plate deformation in a 3-D numerical model of subduction zones. Geophys J Int 173(3): 1084–1094

Boudier F, Ceuleneer G, Nicolas A (1988) Shear zones, thrusts and related magmatism in the Oman ophiolite: initiation of thrusting on an oceanic ridge. Tectonophysics 151(1–4): 275–296

Boutelier D (2004) La modélisation expérimentale tridimensionnelle thermomécanique de la subduction continentale et l'exhumation des roches de ultra haute pression/basse température. Ph.D Thesis, Université de Nice – Sophia Antipolis, Nice, p 250

Boutelier D, Chemenda A (2008) Exhumation of UHP/LT rocks due to the local reduction of the interplate pressure: thermo-mechanical physical modelling. Earth Planet Sci Lett 271(1–4):226–232

Boutelier D, Cruden A (2007) Influence of plate boundary geometry on the stress regime in an arc/back-arc setting. Eos Trans AGU, 88, Fall Meet Supl, pp. Abstract T31A-0285

Boutelier D, Cruden A (2008) Impact of regional mantle flow on subducting plate geometry and interplate stress: insights from physical modelling. Geophys J Int 174(2):719–732

Boutelier D, Oncken O (2010) The role of the plate margin curvature in the plateau build-up: consequences for the Central Andes. J Geophys Res 115(B04402):1–17

Boutelier D, Chemenda A, Jorand C (2002) Thermo-mechanical laboratory modelling of continental subduction: first experiments. J Virtual Explor 6:61–65

Boutelier D, Chemenda A, Burg J (2003) Subduction versus accretion of intra-oceanic volcanic arcs: insight from thermo-mechanical analogue experiments. Earth Planet Sci Lett 212(1–2):31–45

Boutelier D, Chemenda A, Jorand C (2004) Continental subduction and exhumation of high-pressure rocks: insights from thermo-mechanical laboratory modelling. Earth Planet Sci Lett 222(1):209–216

Brace W, Kohlstedt D (1980) Limits on lithospheric stress imposed by laboratory experiments. J Geophys Res 85: 6248–6252

Brown D (2009) The growth and destruction of continental crust during arc-continent collision in the Southern Urals. Tectonophysics 479(1–2):185–196

Brown D, Spadea P (1999) Processes of forearc and accretionary complex formation during arc-continent collision in the southern Ural Mountains. Geology 27(7):649

Brown D, Juhlin C, Alvarez-Marron J, Perez-Estaun A, Oslianski A (1998) Crustal-scale structure and evolution of an arc-continent collision zone in the southern Urals, Russia. Tectonics 17(2):158–171

Brown D, Spadea P, Puchkov V, Alvarez-Marron J, Herrington R, Willner A, Hetzel R, Gorozhanina Y, Juhlin C (2006) Arc–continent collision in the Southern Urals. Earth Sci Rev 79(3–4):261–287

Brown D, Herrington R, Alvarev-Marron J (2011) Processes of arc-continent collision in the Uralides. In: Brown D, Ryan P (eds) Arc-continent collision: the making of an orogen, Frontiers in earth sciences. Springer, Heidelberg, 309–338

Buckingham E (1914) On physically similar systems; illustrations of the use of dimensional equations. Phys Rev 4(4): 345–376

Burbank D (2002) Rates of erosion and their implications for exhumation. Mineralog Mag 66(1):25

Burg J-P (2011) The Asia-Kohistan-India collision. Review and discussion. In: Brown D, Ryan P (eds) Arc-continent collision: the making of an orogen, Frontiers in earth sciences. Springer, Heidelberg, 471–487

Byerlee J (1978) Friction of rocks. Pure Appl Geophys 116(4): 615–626

Byrne T, Chan Y-C, Rau R-J, Lu C-Y, Lee Y-H, Wang Y-J (2011) The arc-continent collision in Taiwan. In: Brown D, Ryan P (eds) Arc-continent collision: the making of an orogen, Frontiers in earth sciences. Springer, Heidelberg, 211–243

Carbonell R, Gallart J, Perez-Estaun A, Diaz J, Kashubin S, Mechie J, Wenzel F, Knapp J (2000) Seismic wide-angle constraints on the crust of the southern Urals. J Geophys Res 105(B6):13755

Chemenda A (2007) The formation of shear-band/fracture networks from a constitutive instability: theory and numerical experiment. J Geophys Res 112(B11):B11404

Chemenda A (2009) The formation of tabular compaction-band arrays: theoretical and numerical analysis. J Mech Phys Solids 57(5):851–868

Chemenda A, Mattauer M, Malavieille J, Bokun A (1995) A mechanism for syn-collisional rock exhumation and associated normal faulting: results from physical modelling. Earth Planet Sci Lett 132(1–4):225–232

Chemenda A, Mattauer M, Bokun A (1996) Continental subduction and a mechanism for exhumation of high-pressure metamorphic rocks: new modelling and field data from Oman. Earth Planet Sci Lett 143(1–4):173–182

Chemenda A, Matte P, Sokolov V (1997a) A model of Palaeozoic obduction and exhumation of high-pressure/low-temperature rocks in the southern Urals. Tectonophysics 276(1–4):217–227

Chemenda A, Yang R, Hsieh C, Groholsky A (1997b) Evolutionary model for the Taiwan collision based on physical modelling. Tectonophysics 274(1–3):253–274

Chemenda A, Burg J, Mattauer M (2000a) Evolutionary model of the Himalaya–Tibet system: geopoem based on new modelling, geological and geophysical data. Earth Planet Sci Lett 174(3–4):397–409

Chemenda A, Lallemand S, Bokun A (2000b) Strain partitioning and interplate friction in oblique subduction zones: constraints provided by experimental modeling. J Geophys Res 105:5567–5582

Chemenda A, Hurpin D, Tang J, Stephan J, Buffet G (2001a) Impact of arc-continent collision on the conditions of burial and exhumation of UHP/LT rocks: experimental and numerical modelling. Tectonophysics 342(1–2): 137–161

Chemenda A, Yang R, Stephan J, Konstantinovskaya E, Ivanov G (2001b) New results from physical modelling of arc–continent collision in Taiwan: evolutionary model. Tectonophysics 333(1–2):159–178

Cheng W (2009) Tomographic imaging of the convergent zone in Eastern Taiwan – a subducting forearc sliver revealed? Tectonophysics 466(3–4):170–183

Chopin C (2003) Ultrahigh-pressure metamorphism: tracing continental crust into the mantle. Earth Planet Sci Lett 212(1–2):1–14

Coward M, Rex D, Khan M, Windley B, Broughton R, Luff I, Petterson M, Pudsey C (1986) Collision tectonics in the NW Himalayas. Geol Soc Lond Spec Publ 19(1):203

Currie C, Hyndman R (2006) The thermal structure of subduction zone back arcs. J Geophys Res 111:B08404

Currie C, Wang K, Hyndman R, He J (2004) The thermal effects of steady-state slab-driven mantle flow above a subducting plate: the Cascadia subduction zone and backarc. Earth Planet Sci Lett 223(1–2):35–48

Davies JH, von Blanckenburg F (1995) Slab breakoff: a model of lithosphere detachment and its test in the magmatism and deformation of collisional orogens. Earth Planet Sci Lett 129(1–4):85–102

Davis A, Aitchison J, Luo H, Zyabrev S (2002) Paleogene island arc collision-related conglomerates, Yarlung–Tsangpo suture zone, Tibet. Sed Geol 150(3–4):247–273

De Bresser J, Ter Heege J, Spiers C (2001) Grain size reduction by dynamic recrystallization: can it result in major rheological weakening? Int J Earth Sci 90(1):28–45

Duchêne S, Lardeaux J, Albarède F (1997) Exhumation of eclogites: insights from depth-time path analysis. Tectonophysics 280(1–2):125–140

Eberle M, Grasset O, Sotin C (2002) A numerical study of the interaction between the mantle wedge, subducting slab, and overriding plate. Phys Earth Planet Inter 134:191–202

Ernst W, Liou J (2000) Overview of UHP metamorphism and tectonics in well-studied collisional orogens. Ultrahigh-pressure metamorphism and geodynamics in collision-type orogenic belts: Final Report of the Task Group III-6 (1994–1998) of the International Lithosphere Project: 3

Faure M, Be Mezeme E, Cocherie A, Rossi P, Chemenda A, Boutelier D (2008) Devonian geodynamic evolution of the Variscan Belt, insights from the French Massif Central and Massif Armoricain. Tectonics 27(TC2005):1–19

Fielding E (2000) Morphotectonic evolution of the Himalayas and Tibetan Plateau. In: Summerfield M (ed) Geomorphology and global tectonics. Wiley, Chichester, pp 201–222

Funiciello F, Faccenna C, Giardini D, Regenauer-Lieb K (2003a) Dynamics of retreating slabs: 2. Insights from three-dimensional laboratory experiments. J Geophys Res 108(B4):2207

Funiciello F, Morra G, Regenauer-Lieb K, Giardini D (2003b) Dynamics of retreating slabs: 1. Insights from two-dimensional numerical experiments. J Geophys Res 108:2206

Funiciello F, Faccenna C, Giardini D (2004) Role of lateral mantle flow in the evolution of subduction systems: insights from laboratory experiments. Geophys J Int 157(3):1393–1406

Funiciello F, Moroni M, Piromallo C, Faccenna C, Cenedese A, Bui H (2006) Mapping mantle flow during retreating subduction: laboratory models analyzed by feature tracking. J Geophys Res 111(B3):B03402

Furukawa Y (1993) Magmatic processes under arcs and formation of the volcanic front. J Geophys Res 98(B5):8309–8319

Goetze C, Evans B (1979) Stress and temperature in the bending lithosphere as constrained by experimental rock mechanics. Geophys J R Astron Soc 59(3):463–478

Gögüs O, Pysklywec R (2008) Near-surface diagnostics of dripping or delaminating lithosphere. J Geophys Res 113: B11404

Hacker B, Mosenfelder J, Gnos E (1996) Rapid emplacement of the Oman ophiolite: thermal and geochronologic constraints. Tectonics 15(6):1230–1247

Harris R (2011) The nature of the Banda arc-continent collision in the Timor region. In: Brown D, Ryan P (eds) Arc-continent collision: the making of an orogen, Frontiers in earth sciences. Springer, Heidelberg, 163–210

Hartz E, Podladchikov Y (2008) Toasting the jelly sandwich: the effect of shear heating on lithospheric geotherms and strength. Geology 36(4):331

Hassani R, Jongmans D, Chéry J (1997) Study of plate deformation and stress in subduction processes using two-dimensional numerical models. J Geophys Res 102:17951–17965

Hermann J, Rubatto D, Korsakov A, Shatsky V (2001) Multiple zircon growth during fast exhumation of diamondiferous, deeply subducted continental crust (Kokchetav Massif, Kazakhstan). Contrib Mineral Petrol 141(1):66–82

Honda S, Saito M (2003) Small-scale convection under the back-arc occurring in the low viscosity wedge. Earth Planet Sci Lett 216(4):703–715

Honda S, Yoshida T (2005) Application of the model of small-scale convection under the island arc to the NE Honshu subduction zone. Geochem Geophys Geosyst 6(1):Q01002

Honda S, Saito M, Nakakuki T (2002) Possible existence of small-scale convection under the back arc. Geophys Res Lett 29(21):2043

Hsieh M, Liew P, Hsu M (2004) Holocene tectonic uplift on the Hua-tung coast, eastern Taiwan. Quatern Int 115:47–70

Huang W, Johnson K, Fukuda J, Yu S (2010) Insights into active tectonics of eastern Taiwan from analyses of geodetic and geologic data. J Geophys Res Solid Earth 115(B14): 03413

Hubbert M (1937) Theory of scale models as applied to the study of geologic structures. Geol Soc Am Bull 48(10): 1459

Jackson J (2002) Strength of the continental lithosphere: time to abandon the jelly sandwich? GSA Today 12(9):4–9

Jeffreys H (1970) The Earth. Cambridge University Press, Cambridge, p 300

Kay R, Mahlburg Kay S (1993) Delamination and delamination magmatism. Tectonophysics 219(1–3):177–189

Kelemen P, Rilling J, Parmentier E, Mehl L, Hacker B (2003) Thermal structure due to solid-state flow in the mantle wedge beneath arcs. AGU Monogr 138:293–311

Kim K, Chiu J, Pujol J, Chen K, Huang B, Yeh Y, Shen P (2005) Three-dimensional VP and VS structural models associated with the active subduction and collision tectonics in the Taiwan region. Geophys J Int 162(1):204–220

Kincaid C, Sacks I (1997) Thermal and dynamical evolution of the upper mantle in subduction zones. J Geophys Res 102:12,295–12,315

Kirby S (1985) Rock mechanics observations pertinent to the rheology of the continental lithosphere and the localization of strain along shear zones. Tectonophysics 119(1–4):1–27

Kohlstedt D, Evans B, Mackwell S (1995) Strength of the lithosphere: constraints imposed by laboratory experiments. J Geophys Res 100(17):587–17

Konstantinovskaia E (2000) Geodynamics of an Early Eocene arc-continent collision reconstructed from the Kamchatka Orogenic Belt, NE Russia. Tectonophysics 325(1–2):87–105

Konstantinovskaya E (2011) Early Eocene arc-continent collision in Kamchatka, Russia: structural evolution and geodynamic model. In: Brown D, Ryan P (eds) Arc-continent collision: the making of an orogen, Frontiers in earth sciences. Springer, Heidelberg, 245–275

Labrousse L, Jolivet L, Agard P, Hébert R, Andersen T (2002) Crustal-scale boudinage and migmatization of gneiss during their exhumation in the UHP Province of Western Norway. Terra Nova 14(4):263–270

Lee C, Hirata N, Huang B, Huang W, Tsai Y (2010) Evidence of a highly attenuative aseismic zone in the active collision orogen of Taiwan. Tectonophysics 489:128–138

Lewis T, Bentkowski W, Davis E, Hyndman R, Souther J, Wright J (1988) Subduction of the Juan de Fuca plate: thermal consequences. J Geophys Res 93:15207–15225

McCaffrey R (1992) Oblique plate convergence, slip vectors, and forearc deformation. J Geophys Res 97(B6): 8905–8915

McCaffrey R (1996) Slip partitioning at convergent plate boundaries of SE Asia. Geol Soc Lond Spec Publ 106(1):3

McDermid I, Aitchison J, Davis A, Harrison T, Grove M (2002) The Zedong terrane: a Late Jurassic intra-oceanic magmatic arc within the Yarlung–Tsangpo suture zone, southeastern Tibet. Chem Geol 187(3–4):267–277

Molnar P (1992) Brace-Goetze strength profiles, the partitioning of strike-slip and thrust faulting at zones of oblique convergence, and the stress-heat flow paradox of the San Andreas fault. Int Geophys 51:435–459

Montési L, Hirth G (2003) Grain size evolution and the rheology of ductile shear zones: from laboratory experiments to post-seismic creep. Earth Planet Sci Lett 211(1–2):97–110

Montési L, Zuber M (2002) A unified description of localization for application to large-scale tectonics. J Geophys Res 107(3): 2045. doi: 10.1029/2001JB000465

Mposkos E, Kostopoulos D (2001) Diamond, former coesite and supersilicic garnet in metasedimentary rocks from the Greek Rhodope: a new ultrahigh-pressure metamorphic province established. Earth Planet Sci Lett 192(4):497–506

Peacock S (1996) Thermal and petrologic structure of subduction zones. Geophys monogr 96:119–133

Peacock S (2003) Thermal structure and metamorphic evolution of subducting slabs. AGU Monogr 138:7–22

Poirier J (1980) Shear localization and shear instability in materials in the ductile field. J Struct Geol 2(1–2):135–142

Ramberg H (1967) Gravity, deformation and the earth's crust: as studied by centrifuged models. Academic, London

Ranalli G, Murphy D (1987) Rheological stratification of the lithosphere. Tectonophysics 132(4):281–295

Regenauer-Lieb K (2006) Water and geodynamics. Rev Mineral Geochem 62(1):451

Regenauer-Lieb K, Rosenbaum G, Weinberg R (2008) Strain localisation and weakening of the lithosphere during extension. Tectonophysics 458(1–4):96–104

Renner J, Stockert B, Zerbian A, Röller K, Rummel F (2001) An experimental study into the rheology of synthetic polycristalline coesite aggregates. J Geophys Res 106: 19411–19429

Rubatto D, Hermann J (2001) Exhumation as fast as subduction? Geology 29(1):3

Rudnicki J, Rice J (1975) Conditions for the localization of deformation in pressure-sensitive dilatant materials. J Mech Phys Solids 23(6):371–394

Rutter E (1999) On the relationship between the formation of shear zones and the form of the flow law for rocks undergoing dynamic recrystallization. Tectonophysics 303(1–4): 147–158

Ryan PD, Dewey JF (2011) Arc-continent collision in the Ordovician of western Ireland: stratigraphic, structural, and metamorphic evolution. In: Brown D, Ryan P (eds) Arc-continent collision: the making of an orogen, Frontiers in earth sciences. Springer, Heidelberg, 369–396

Schellart W (2004a) Kinematics of subduction and subduction-induced flow in the upper mantle. J Geophys Res 109(B7): B07401

Schellart W (2004b) Quantifying the net slab pull force as a driving mechanism for plate tectonics. Geophys Res Lett 31(7):L07611

Schmidt M, Poli S (1998) Experimentally based water budgets for dehydrating slabs and consequences for arc magma generation. Earth Planet Sci Lett 163(1–4):361–379

Schurr B, Asch G, Rietbrock A, Trumbull R, Haberland C (2003) Complex patterns of fluid and melt transport in the central Andean subduction zone revealed by attenuation tomography. Earth Planet Sci Lett 215(1–2):105–119

Schurr B, Rietbrock A, Asch G, Kind R, Oncken O (2006) Evidence for lithospheric detachment in the central Andes from local earthquake tomography. Tectonophysics 415(1–4): 203–223

Shemenda A (1992) Horizontal lithosphere compression and subduction: constraints provided by physical modeling. J Geophys Res 97(B7):11097–11116

Shemenda A (1993) Subduction of the lithosphere and back arc dynamics: insights from physical modeling. J Geophys Res 98(B9):16167–16185

Shemenda A (1994) Subduction: insights from physical modeling. Kluwer, Dordrecht

Shemenda A, Grocholsky A (1992) Physical modelling of lithosphere subduction in collision zones. Tectonophysics 216(3–4):273–290

Silver E, Reed D, McCaffrey R, Joyodiwiryo Y (1983) Back arc thrusting in the eastern Sunda arc, Indonesia: a consequence of arc-continent collision. J Geophys Res 88(B9):7429–7448

Snyder D, Prasetyo H, Blundell D, Pigram C, Barber A, Richardson A, Tjokosaproetro S (1996) A dual doubly vergent orogen in the Banda Arc continent-arc collision zone as observed on deep seismic reflection profiles. Tectonics 15(1):34–53

Sobolev S, Babeyko A (2005) What drives orogeny in the Andes? Geology 33(8):617

Steck A, Epard J, Vannay J, Hunziker J, Girard M, Morard A, Robyr M (1998) Geological transect across the Tso Morari and Spiti areas: the nappe structures of the Tethys Himalaya. Eclogae Geol Helv 91:103–122

Stern R (2002) Subduction zones. Rev Geophys 40(4):1012

Stockert B, Renner J (1998) Rheology of crustal rocks at ultrahigh pressure. In: Hacker B, Liou J (eds) When continents collide: geodynamics and geochemistry of ultrahigh-pressure rocks. Kluwer, Dordrecht, pp 57–95

Suppe J (1981) Mechanics of mountain building and metamorphism in Taiwan. Mem Geol Soc China 4:67–89

Suppe J (1984) Kinematics of arc-continent collision, flipping of subduction, and back-arc spreading near Taiwan. Mem Geol Soc China 6:21–33

Tahirkheli R, Mattauer M, Proust F, Tapponnier P (1979) The India Eurasia suture zone in northern Pakistan: synthesis and interpretation of recent data at plate scale. In: Farah A, De Jong KA (eds) Geodynamics of Pakistan. Geological Survey of Pakistan, Quetta, pp 125–130

Tang J, Chemenda A (2000) Numerical modelling of arc–continent collision: application to Taiwan. Tectonophysics 325(1–2):23–42

Tang J, Chemenda A, Chéry J, Lallemand S, Hassani R (2002) Compressional subduction regime and initial arc-continent collision: numerical modeling. Geology and geophysics of an arc-continent collision, Taiwan, p 177

Tatsumi Y, Sakuyama M, Fukuyama H, Kushiro I (1983) Generation of arc basalt magmas and thermal structure of the mantle wedge in subduction zones. J Geophys Res 88(B7):5815–5825

Terry M, Robinson P, Hamilton M, Jercinovic M (2000) Monazite geochronology of UHP and HP metamorphism, deformation, and exhumation, Nordoyane, Western Gneiss Region, Norway. Am Mineralog 85(11–12):1651

Tichelaar B, Ruff L (1993) Depth of seismic coupling along subduction zones. J Geophys Res 98(B2):2017–2037

Tilton G, Ames L, Schertl H, Schreyer W (1997) Reconnaissance isotopic investigations on rocks of an undeformed granite contact within the coesite-bearing unit of the Dora Maira Massif. Lithos 41(1–3):25–36

Treolar P, O'Brien P, Parrish R, Khan M (2003) Exhumation of early Tertiary, coesite-bearing eclogites from the Pakistan Himalaya. J Geol Soc Lond 160:367–376

Ulmer P (2001) Partial melting in the mantle wedge-the role of H2O in the genesis of mantle-derived arc-related magmas. Phys Earth Planet Inter 127(1):215–232

Van Roermund H, Drury M (1998) Ultra-high pressure (P > 6 GPa) garnet peridotites in Western Norway: exhumation of mantle rocks from> 185 km depth. Terra Nova 10: 295–301

Von Blanckenburg F, Davies JH (1995) Slab breakoff: a model for syncollisional magmatism and tectonics in the Alps. Tectonics 14:120–120

Wang C, Burnett W (1990) Holocene mean uplift rates across an active plate-collision boundary in Taiwan. Science 248 (4952):204

Wang Y, Ma K, Mouthereau F, Eberhart-Phillips D (2010) Three-dimensional Qp-and Qs-tomography beneath Taiwan orogenic belt: implications for tectonic and thermal structure. Geophys J Int 180(2):891–910

Wheeler J (1991) Structural evolution of a subducted continental sliver: the northern Dora Maira massif, Italian Alps. J Geol Soc Lond 148(6):1101

White S, Burrows S, Carreras J, Shaw N, Humphreys F (1980) On mylonites in ductile shear zones. J Struct Geol 2(1–2):175–187

Wu Y, Chang C, Zhao L, Shyu J, Chen Y, Sieh K, Avouac J (2007) Seismic tomography of Taiwan: improved constraints from a dense network of strong motion stations. J Geophys Res 112:B08312

Zhao D (2001) Seismological structure of subduction zones and its implications for arc magmatism and dynamics. Phys Earth Planet Inter 127(1):197–214

Zhao D, Hasegawa A, Kanamori H (1994) Deep structure of Japan subduction zone as derived from local, regional, and teleseismic events. J Geophys Res 99:22–22

Zhao D, Xu Y, Wiens D, Dorman L, Hildebrand J, Webb S (1997) Depth extent of the Lau back-arc spreading center and its relation to subduction processes. Science 278(5336):254

Part IV
Putting it All Together

Chapter 17
Arc–Continent Collision: The Making of an Orogen

D. Brown, P.D. Ryan, J.C. Afonso, D. Boutelier, J.P. Burg, T. Byrne, A. Calvert, F. Cook, S. DeBari, J.F. Dewey, T.V. Gerya, R. Harris, R. Herrington, E. Konstantinovskaya, T. Reston, and A. Zagorevski

17.1 Introduction

There is no one model, no paradigm, that uniquely defines arc–continent collision. Natural examples and modelling of arc–continent collision show that there is a large degree of, and variation in, complexity that depend on a number of key first-order parameters and the nature of the main players; the continental margin and the arc–trench complex (the arc–trench complex includes the arc and the subduction zone). Although modelling techniques can be used to gain insights into these, they cannot and do not aim at reproducing the

D. Brown
Instituto de Ciencias de la Tierra "Jaume Almera", CSIC, c/Lluís Solé i Sabarís s/n, 08028 Barcelona, Spain
e-mail: dbrown@ija.csic.es

P.D. Ryan
Earth and Ocean Sciences, National University of Ireland Galway, Galway, Ireland
e-mail: paul.ryan@nuigalway.ie

J.C. Afonso
Department of Earth and Planetary Sciences, GEMOC ARC Key Centre for Geochemical Evolution and Metallogeny of Continents, Macquarie University, North Ryde 2109, Sydney, NSW, Australia
e-mail: juan.afonso@mq.edu.au

D. Boutelier
Helmholtz Zentrum Potsdam, Deutsches GeoForschunsZentrum, telegrafenberg, 14471 Potsdam, Germany
e-mail: david@gfz-potsdam.de

J.P. Burg
Department of Earth sciences, ETH- and University Zurich, Sonneggstrasse 5, CH 8092 Zurich, Switzerland
e-mail: jean-pierre.burg@erdw.ethz.ch

T. Byrne
Center for Integrative Geosciences, University of Connecticut, Beach Hall, U-2045, 354 Mansfield Rd, Storrs, CT 06269, USA
e-mail: timothybyrne@earthlink.net

A. Calvert
Department of Earth Science, Simon Fraser University, 8888 University Drive, Burnaby, BC V5A 1S6, Canada
e-mail: acalvert@sfu.ca

F. Cook
Department of Geoscience, University of Calgary, Calgary, AB T2N1N4, Canada
e-mail: fcook@ucalgary.ca

S. DeBari
Department of Geology, Western Washington University, Bellingham, WA 98225, USA
e-mail: debari@geol.wwu.edu

J.F. Dewey
Department of Geology, UC Davis, One Shields Avenue, Davis, CA 95616, USA
e-mail: jfdewey@ucdavis.edu

T.V. Gerya
Geophysical Fluid Dynamics Group, Institute of Geophysics, Department of Earth Sciences, Swiss Federal Institute of Technology (ETH-Zurich), Sonneggstrasse, 5, 8092 Zurich, Switzerland
e-mail: taras.gerya@erdw.ethz.ch

R. Harris
Brigham Young University, Provo, UT, USA
e-mail: ramelau@gmail.com

R. Herrington
Department of Mineralogy, Natural History Museum, Cromwell Road, London SW7 5BD, England, UK
e-mail: r.herrington@nhm.ac.uk

E. Konstantinovskaya
Institut national de la recherche scientifique, Centre Eau, Terre et Environnement (INRS-ETE), 490 de la Couronne, Quebec, QC G1K 9A9, Canada
e-mail: ekonst@sympatico.ca

T. Reston
Earth and Environmental Sciences, University of Birmingham, School of Geography, Birmingham, UK
e-mail: t.j.reston@bham.ac.uk

A. Zagorevski
Geological Survey of Canada, 601 Booth St, Ottawa, ON K1A 0E8, Canada
e-mail: Alex.Zagorevski@NRCan-RNCan.gc.ca

D. Brown and P.D. Ryan (eds.), *Arc-Continent Collision*, Frontiers in Earth Sciences,
DOI 10.1007/978-3-540-88558-0_17,

messiness of nature. In natural examples, identifying the nature of the main players involved, such as the age, physical properties, and pre-existing structure of the margin and the arc is just a beginning. Once this is done, parameters such as time, convergence velocity and vector need to be taken into account when determining the tectonic processes that were operative in any one arc–continent collision. In active examples, such as those in the southwest Pacific, some of these first-order parameters can be readily determined, and the nature of the main players easily assessed. Fossil arc–continent collisions, however, have commonly undergone post-collision deformation, erosion, and possibly partial dispersion to be left outcropping in the middle of a forest, with many of the key ingredients missing or hidden. This leaves the geologist to resort to comparison with other natural examples and with models that are mechanically constrained and simplified reproductions of the process to reconstruct and explain what may have been there and, importantly, what processes may have been operating and when. We attempt to show that this is not an easy task that can be put into one simple model. In this chapter we do not present a model for arc–continent collision. Instead, we begin with the main players involved, highlighting the characteristics of each that likely have a major influence on an arc–continent collision. Then, we investigate a range of possible processes that could take place once an intra-oceanic volcanic arc collides with a continental margin.

17.2 Processes of Arc–Continent Collision

The two main players involved in an arc–continent collision are a continental margin, and an intra-oceanic volcanic arc–trench complex. To illustrate the possible complexities of the margins and the arc–trench complexes that could be involved in an arc–continent collision, in Fig. 17.1 we have juxtaposed, at the same scale and map projection, the Izu-Bonin-Mariana arc–trench complex and the eastern Atlantic margin from south of the Iberian Peninsula to the Faroe Islands in the north. To further reinforce this point, in Fig. 17.2 we show in cross section a range of continental margin (from Reston and Manatschal 2011) and arc–trench complex (from Calvert 2011) structural architectures that could collide with each other. As with any convergent margin, a wide range of convergence vectors and rates is possible, including the

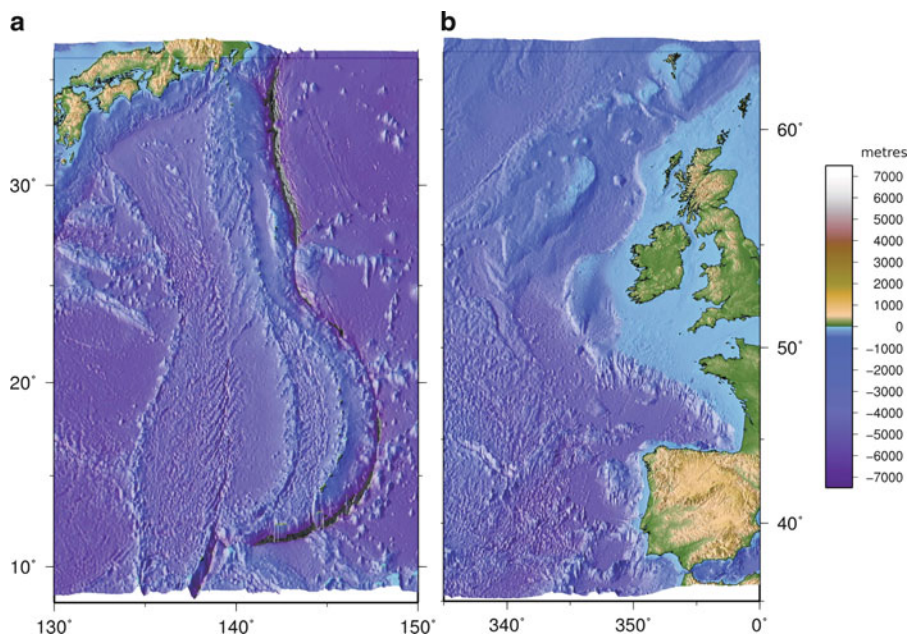

Fig. 17.1 Obliquely illuminated digital elevation models for; (**a**) the Izu-Bonin-Marianas arc and, (**b**) the Atlantic passive margin from the Faeroes to Gibraltar. Both images use a UTM projection and have the same scale at the centre of the projection. Topographic data was taken from the ETOPO1 bedrock Global Relief Model (Amante and Eakins 2009) and plotted using Generic Mapping Tools (Wessel and Smith 1991).

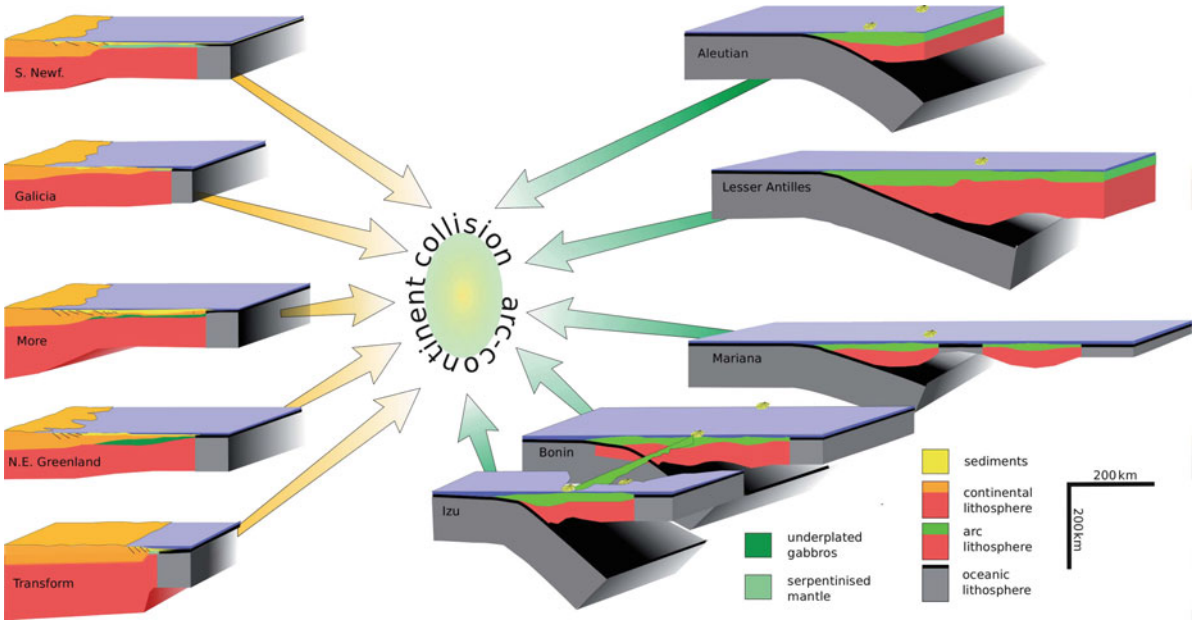

Fig. 17.2 Crustal cross-section of some modern arcs and continental margins drawn to the same scale. Oceanic lithosphere thickness is based upon age. Abbreviations used: S. Newf. = southern Newfoundland.

possibility that these may, and most likely would, change along strike and with time as arc–continent collision advances. An extreme possibility is that an arc could converge end-on with an active margin along a completely different subduction system than that responsible for the arc formation, similar to the relationship between the Izu-Bonin arc and the margin of Japan today.

17.2.1 The Continental Margin

Non-volcanic (magma-poor) rifted continental margins are wide zones (typically between 150 and 400 km) of thinned continental and transitional crust overlain by a several kilometer thick carapace of sediments and possibly underplated by a layer of serpentinised mantle (Keen and Dehler 1997; Sayers et al. 2001; Bauer et al. 2000; Funck et al. 2004; Reston 2009; Reston and Manatschal 2011) (Fig. 17.2). There are exceptions to this, such as the current margin of Ghana, which is much narrower (Edwards et al. 1997). Rifted volcanic (magma-rich) margins, such as that in Namibia (Fernàndez et al. 2010), are generally much narrower and thicker, with a different overall crustal composition and physical properties (Reston and Manatschal 2011). The differences between the two types of margin will have a significant effect on their subductability (Afonso and Zlotnik 2011). Furthermore, the different shapes of the passive margins lead to different distributions of tectonic (non-hydrostatic) stresses along the plate boundary and different deformation-style in the magmatic arc (Boutelier and Chemenda 2011). Common to all rifted continental margins are rift-related, sediment-filled basins (Reston 2009; Reston and Manatschal 2011). These basins can vary significantly in depth, thickness of sedimentary fill, structural style, and orientation and linkage of the basin-bounding faults relative to the margin edge. In some extreme cases, such as the Rockall Trough or the Porcupine Basin on the northwestern Irish margin (Fig. 17.1b), a thick sedimentary fill may directly overlie either an extremely thinned continental crust or serpentinised mantle (Reston 2009). Continental margins also display significant along-strike changes in thickness, width, and composition (Reston 2009; Reston and Manatschal 2011; Byrne et al. 2011). A margin may be relatively straight over long distances, or it may have one or more salients and re-entrants (Fig. 17.1b). All of these variables are important in how an arc–continent collision proceeds and how the continental margin reacts once it enters a subduction zone and, subsequently, to the collision of an arc.

With the arrival of the leading edge of the continental crust at the subduction zone the sedimentary cover of the slope and rise can be scraped off the downgoing slab and thrust over the incoming margin. In the Uralides, for example, the forearc ultramafic and ophiolite allochthons currently sit on top of this type of sediment, suggesting that the two were obducted together at an early stage of the collision (Brown et al. 2006, 2011). In Taiwan, slope-derived sediments were thrust over the margin to form the so-called "slate belt" of the western part of the Central Range. Parts of the crust may be subducted to shallow or even very deep levels before returning to the surface as low to ultra-high pressure metamorphic rocks that form part of the growing arc–continent collision orogen (e.g., Hetzel et al. 1998; Hetzel 1999; Ye et al. 2000; Liou et al. 2000a; Chopin 2003; Chemenda et al. 2001; Boutelier et al. 2003, 2004; Baldwin et al. 2004; Boutelier and Chemenda 2011; Brown et al. 2006; Escuder-Viruete and Pérez-Estaún 2006; Afonso and Zlotnik 2011; Konstantinovskaya 2011). Around this time, the developing orogen, which, in most cases includes the imbricating continental margin and the arc complex, begins to rise above sea level and can quickly form high topography. Taiwan, for example, has more than 100 peaks that have reached over 3,000 m in height, with the highest reaching nearly 4,000 m, in the c. 3 My since it rose above sea level. Calculations of uplift rates in eastern Taiwan (up to 20 mm per year), Papua New Guinea (up to 10 mm per year), and Timor (up to 3–5 mm per year) provide some indication of just how fast the development of high topography can take place (De Smet et al. 1990; Abbott et al. 1997; Shyu et al. 2006; Hsieh and Rau 2009; Roosmawati and Harris 2009; Harris 2011). As it rises above sea level, the orogen starts to erode. In active arc–continent collisions, erosion rates determined by apatite fission track data range from an average of 2.3 mm per year in Taiwan (Fuller et al. 2006), and up to 2 mm per year in Timor (Harris et al. 2000), although these rates can be locally higher or lower.

The eroding orogen provides sediments to a foreland basin that develops along the continent side of the orogen, and to basins that form across the developing suture zone and the accreting arc (Jahn et al. 1986; Audley-Charles 1986; De Smet et al. 1990; Abbott et al. 1997; Huang et al. 2000; Brown et al. 2006, 2011; Iturralde-Vinent et al. 2008; Byrne et al. 2011; Konstantinovskaya 2011; Zagorevski and van Staal 2011; Cook 2011). Initially, these basins may be submarine, but they often become subaerial as the basin fills during the advanced stage of collision. Accurate dating of the sediments in these basins, and a detailed analyses of their heavy mineral component, can provide critical information on the timing of a number of processes that were taking place during this stage of the arc–continent collision (e.g., Dewey and Mange 1999; Willner et al. 2002; Brown et al. 2006, 2011; Ryan and Dewey 2011; Cook 2011). As convergence continues, these sediments become involved in the deformation; those of the foreland basin commonly form large thrust sheets that can accommodate considerable displacement. Significant forearc and arc uplift may also take place, providing volcanic clasts to the basins (De Smet et al. 1990; Dewey 2003; Abbott et al. 1994; Dewey and Mange 1999; Huang et al. 2000; Byrne et al. 2011). In the Papua New Guinea, Timor, and the Uralides, uplift and subaerial exposure of the imbricated continental crust and forearc has been interpreted to mark the arrival of the full thickness of the continental crust at the subduction zone (De Smet et al. 1990; Abbott et al. 1994; Brown and Spadea 1999; Brown et al. 2006; Harris 2011). In the Uralides, high- to ultrahigh-pressure rocks were exhumed to the surface at this time and provided clasts to the "suture" forearc basin (Beane et al. 1995; Brown et al. 1998, 2006, 2011; Hetzel et al. 1998; Willner et al. 2002). The sediments deposited in the foreland and "suture" forearc basins can display widespread synsedimentary deformation (Brown et al. 2000; Malavieille et al. 2002; McIntosh et al. 2005; Konstantinovskaya 2011; Zagorevski and van Staal 2011) that is possibly related to seismicly-induced instability in the basins. These "seismites", which can become important at a certain stratigraphic level in a basin, possibly recording increased seismicity associated with the arrival of the full thickness of the continental crust at the subduction zone.

There is a large degree of variability in how the continental margin platform deforms once the full thickness of the continental crust arrives at the subduction zone. How the deformation proceeds results from a number of factors, including: across and along-strike architecture (including the orientation of pre-existing structures such as basin-bounding faults, basement highs, salients and re-entrants), rheology; the convergence angle, and the convergence rate (e.g., Harris

2011; Byrne et al. 2011). It will also depend on the nature of the colliding arc (see below). Figures 17.1 and 17.2 provide examples a range of highly-complex arc–trench complexes that could collide with an equally complex range of continental margins. In general, the sedimentary carapace of the platform appears to become detached from the underlying crystalline basement (basement is defined as any pre-rift rocks whether crystalline or not) to form a thrust belt that verges continent-ward (e.g., Byrne et al. 2011; Brown et al. 2011; Harris 2011). At the rear of the thrust belt, an arc-verging thrust can develop. These thrust belts can range from less than 100 km (e.g., Brown et al. 2006, 2011; Harris 2006; Alsleben et al. 2008; Cook 2011) to several hundred kilometers in width (e.g., Papua New-Guinea; Hill (1991)) and have varying amounts of shortening. The forearc region acts as a backstop to the thrust belt and can be strongly deformed (or even partly subducted or obducted) to form a wide damage zone along the location of the subduction zone (Brown et al. 2001). In many cases the crystalline basement can also become involved in the thrusting at some stage in the development of the orogen, and at any position within the thrust belt. For example, parts of the Central Range of Taiwan involve Mesozoic crystalline basement that is currently being thrust over slope-derived sediments to the west (Byrne et al. 2011; Huang et al. 1997, 2000). Furthermore, seismicity in Taiwan indicates that basement is involved in the deformation beneath the entire thrust belt, to depths of at least 30–35 km and perhaps more (e.g., Wu et al. 1997, 2004; Wu et al. 2007; Gourley et al. 2007). Basement involvement in the thrusting during arc–continent collision is commonly the result of reactivation of pre-existing structures and rift-related basin faults. How these become reactivated, whether as thrusts, strike-slip faults, or transpressive structures, and the resultant structural architecture, depends largely on their orientation relative to the margin edge and the resolution of the stress axes relative to the convergence vector of the colliding arc (see Harris 2011). An extreme case of the re-use of margin faults could occur in places like the Rockall Trough (Fig. 17.1b), for example, where nearly whole crustal imbrication could take place. Re-entrants and salients along the margin could also add a high degree of complexity to the architecture of the thrust belt. For example, an along strike comparison of the mid-Ordovician Taconic (Zagorevski and Van Staal 2011) and Grampian (Ryan and Dewey 2011) orogenic tracts exhibits such complexity. The Taconic portion had a complex arc system and was dominated by re-entrants. It likely had a relatively stronger rheology and, therefore, developed an associated foreland basin. The part of the margin affected by the Grampian orogeny had a simpler arc system and may have lain on a salient that was likely of volcanic origin (Ryan 2008). Its rheology may have been weaker and, therefore, it did not develop and/or preserve a significant foreland basin.

17.2.2 The Volcanic Arc

Like continental margins, intra-oceanic arcs display significant across and along-strike structural and compositional complexity (Holbrook et al. 1999; Stern 2002; Tatsumi et al. 2008; Kodaira et al. 2007; Calvert et al. 2008; Calvert 2011; DeBari et al. 2011) that influence the outcome of any arc–continent collision in which they are involved. Geophysical data, in particular seismic velocities, show that the across-strike crustal thickness of intra-oceanic arcs ranges from up to 35 km in the case of the Aleutian arc system to as little as 10 km in parts of the Izu-Bonin arc (Holbrook et al. 1999; Kodaira et al. 2007; Calvert 2011). In both these arc systems, there are also large along-strike changes in crustal thickness, with variations of up to 25 km in the Izu-Bonin-Mariana system, and perhaps as much as 10 km in the Aleutian system (Calvert 2011). The overall crustal composition of arcs derived from the inversion of seismic velocity data indicates a fairly uniform composition of the upper, middle, and lower crust between different arc systems, even though these intervals could be very different in thickness. This first-order similarity in composition derived from seismic velocities in active arcs is confirmed by natural examples of exposed fossil arcs (DeBari et al. 2011). However, the composition of the arc lower crust, or "basement", depends on the type of crust the arc was built on, whether it be a continental crustal fragment or oceanic crust. The variation in the thickness of the different crustal levels of the arc has important implications for its rheology and consequently how it behaves during arc–continent collision. Finally, most arc–trench complexes that are active today are non-accreting (Stern 2002; Leat and Larter 2003; Calvert

2011; Gerya 2011), so very little, if any, of the sediment that sits on top of the subducting oceanic plate can be expected in arc–continent collision orogens.

The complex across- and along-strike structure of an arc–trench system could result in a complicated final structural architecture of an arc–continent collision. For example, intra-arc rifting and basin development can take place within the intra-oceanic setting. A possible extreme consequence of this could be arc splitting, with a new spreading center developing and new oceanic crust formation, as in the case of the Mariana arc (e.g., Takahashi et al. 2007; Calvert 2011, and references therein) (Figs. 17.1a and 17.2). This process also seems to have been active in the Paleozoic development of arcs currently found in the Appalachians arcs of Newfoundland (e.g., Zagorevski et al. 2009). Collision of a rifted arc, or an arc that has split into two, with a continental margin could lead to imbrication of the arc (e.g., Burg 2011) or detachment of the arc's lower crust from the upper crust (Zagorevski et al. 2009). If seafloor spreading has occurred, then a new subduction zone could form (see Sect. 17.2.3) and it may appear that two arcs have collided with the possible obduction of an ophiolite. This senario may go some way toward explaining what appears to be multiple arc collisions in such places as the Appalachians of Newfoundland (Zagorevski et al. 2009; Zagorevski and van Staal 2011; van Staal et al. 2009), or the Uralides of Russia (Brown et al. 2006, 2011). In the case of the Uralides, syncollisional rifting of the Magnitogorsk arc appears to have taken place, and can be directly correlated with the widespread development of volcanogenic massive sulphide deposits in the Karamalytash Formation (Herrington et al. 2002, 2005; Herrington and Brown 2011).

The forearc can vary in width, thickness, composition, structure, and rheology, depending on whether it is accretionary or tectonically eroded (e.g., Stern and Smoot 1998; Stern 2002; Calvert 2011). In some cases, a thick wedge of sediment can build up as the forearc approaches the continent (e.g., Taiwan, Huang et al. 1997). It can also have an arc-parallel fault system (Lallemand et al. 1999; Chemenda et al. 2000), or be strongly affected by the infiltration of fluids (e.g., Stern 2002), both of which will affect its rheology and therefore how it deforms or gets obducted once collision starts. On the basis of physical modelling, it has been suggested that the entire forearc, or the whole arc, could be subducted during arc–continent collision (Chemenda et al. 1997a, b; Boutelier et al. 2003, 2004; Boutelier and Chemenda 2011). In some orogens, such as the Appalachians of Newfoundland (Zagorevski et al. 2009; Zagorevski and van Staal 2011; van Staal et al. 2009), Grampians of Ireland (Ryan and Dewey 2011), the Talkeetna arc of Alaska (DeBari et al. 2011), or the Kohistan arc of India (Burg 2011), there is evidence for subduction of at least some parts of the forearc, but with some fragments being preserved as ophiolites or ultramafic massifs. Fragmentation and, possibly, the subduction of parts of a forearc may be related to inversion of the trench-parallel faults commonly developed in this region of volcanic arcs (e.g., Lallemand et al. 1999; Chemenda et al. 2000). High-pressure rocks found in many arc–continent collision zones commonly represent fragments of forearc that were subducted in the intra-oceanic phase of the arc–trench complex, and that were subsequently exhumed along the subduction channel (Brown et al. 2000; Escuder-Viruete and Pérez-Estaún 2006; García-Casco et al. 2006). If several high- or ultrahigh-pressure units occur along the same subduction zone, they may provide information about the physical, chemical and fluid conditions, as well on the flux of material through the subduction channel (e.g., Brown et al. 2000; Escuder-Viruete and Pérez-Estaún 2006; Lázaro et al. 2009). An interesting caveat on the occurrence of high-pressure rocks is proposed by Dewey and Casey (2011) in which the high metamorphic grade aureole found at the base of some ophiolites were also generated in the subduction zone, juxtaposed against the base of the ophiolite, and then obducted along with it. Nevertheless, it is clear from outcropping geology in a number of other orogens that the subduction of the entire forearc is a simplification due to the necessary simplicity of the experimental models from which this concept derives and does not always take place. For example, Chemenda et al. (1997a) suggested that the whole of the Magnitogorsk forearc in the Uralides was subducted, yet geological mapping and the geochemistry of the volcanic rocks demonstrate, very clearly, that this is not the case and at least a large portion of the forearc is still in place (Spadea et al. 1998, 2002; Brown and Spadea 1999; Brown et al. 2001, 2006, 2011). An exception to this may be taking place in Taiwan where, on the basis of seismic velocities and analog modelling, Malavieille and Trullenque (2009) interpret that a portion of the Luzon forearc underthrusts the Central

Range of Taiwan, splitting the continental crust along the brittle to ductile transition. Note that there has not been any obduction of ophiolites or ultramafic rocks on the Taiwan orogen (Byrne et al. 2011). In recent years it has been demonstrated that the forearc is the source of much of the ophiolitic material obducted onto a continental margin during arc–continent collision (García-Casco et al. 2006; Dewey and Casey 2011 and references therein). The obduction of forearc ophiolites should, then, be taken into account when making a balance of the forearc material in a particular orogen and proposing such processes as forearc subduction. In fossil orogens, post arc–continent collision processes should also be considered, because dismemberment of the arc by closure of the ocean basin outboard of the collision and subsequent continent–continent collision might mean that the forearc region is not recognised, or is simply buried or otherwise removed. We, therefore, recommend that care be taken when interpreting the absence of part or whole of a forearc to mean that it was subducted.

Fossil arc–continent collisions, unlike those that are active today, can provide important information on processes that take place at different levels of the arc during collision. The outcropping Magnitogorsk arc of the Uralides, for example, did not undergo any metamorphism and, with the exception of intra-arc rifiting, only very minor deformation (Brown et al. 2001) during its collision with the margin of Laurussia. Today, the Magnitogorsk arc provides a snapshot of a Devonian sea floor complete with sulphide chimneys containing fossilised vent fauna assemblages (Zaykov et al. 1996; Herrington et al. 1998; Little et al. 1997). In comparison with this, in the Appalachians of Newfoundland, strong imbrication of the arc with, locally, intense deformation and high grade metamorphism took place (van Staal et al. 2009; Zagorevski et al. 2009; Zagorevski and van Staal 2011). For example, in the Annieopsquotch accretionary track, there appears to have been detachment of the arc and backarc sequences at a mid-crustal level followed by emplacement of the upper part of the arc onto the continental margin under relatively low metamorphic grade conditions (Zagorevski et al. 2009). However, the shear zones along which the Annieopsquotch accretionary track was emplaced appear to have developed under much higher metamorphic grade conditions than those that affected the rest of the arc crust (Lissenberg et al. 2006; Zagorevski et al 2009). When comparing collisional processes at different levels of the crust the difference in the rates at which processes take place can be important. For example, surface uplift (see above), erosion, and sediment deposition can occur very quickly, whereas deeper level processes appear to be much slower (see van Staal et al. 2009; Zagorevski et al. 2009; Zagorevski and van Staal 2011). In part, this might result from the resolution of the different techniques used to measure them.

17.2.3 The Subduction Zone

Intra-oceanic subduction zones are perhaps the most complex part of an arc–continent collision to assess, especially in fossil orogens. As pointed out by Stern (2002), "subduction zones are the three-dimensional manifestation of convective downwelling, convergent plate margins are the surficial manifestations of downwelling, and arcs are the surficial and crustal manifestations of a subduction zone that is operating beneath it." In arc–continent collision, therefore, understanding the subduction zone can give important information about such parameters as plate convergence vectors and velocity. Nevertheless, it is the evolution, structure, and composition of the intra-oceanic arc that provides direct information on the subduction zone dynamics, and the processes that take place within and above it (Stern 2002; Leat and Larter 2003; Gerya 2011; DeBari et al. 2011). Therefore, the arc is the most important and direct record of the intra-ocean stage of the subduction zone that is recorded in an arc– continent collision.

Subduction zone dynamics, as well as the physical and chemical conditions within the subduction channel and the arc–trench complex, begin to change once the leading edge of the continental crust begins to subduct (van den Beukel 1992; Chemenda et al. 2001; Stern 2002; Draut et al. 2002, 2009; Boutelier et al. 2003, 2004; Boutelier and Chemenda 2011; Elburg et al. 2005; Afonso and Zlotnik 2011; Herrington et al. 2011; Harris 2011). Although calculations by Ryan (2001) show that thermally mature continental crust with a thickness of up to 10 km can be subducted without significantly influencing the dynamics of the subduction zone, with an increasing thickness of less dense continental crust entering the subduction zone,

the build up of positively buoyant material tends to decrease convergence velocities and, if the crust has enough strength, stall subduction (Afonso and Zlotnik 2011). Nevertheless, the occurrence of high- and ultra-high-pressure rocks derived from continental crust provides first-order evidence that it can be deeply subducted, and parts of it subsequently be returned to the surface (Ye et al. 2000; Liou et al. 2000a; Chopin 2003; Hetzel et al. 1998; Escuder-Viruete and Pérez-Estaún 2006). These high- and ultra-high pressure rocks therefore make up an important component of an arc–continent collision orogen since they too can provide key evidence for the physical, chemical, and fluid conditions in and along the subduction channel during collision (Ernst et al. 1994; Shreve and Cloos 1986; Brown et al. 2000, 2006; García-Casco et al. 2006; Gerya 2011). The deep subduction of continental crust is also predicted by modelling (van den Beukel 1992; Ranalli et al. 2000; Boutelier et al. 2003; Massone et al. 2007; Afonso and Zlotnik 2011). Indeed, the results of the fully dynamic thermomechanical models of Afonso and Zlotnik (2011) suggest that, with a strong rheology, there is no limit to the depth to which continental crust can be subducted, since at depths greater than 250–300 km it can become denser than the surrounding mantle and will continue on down the subduction zone. Their modelling also suggests that at depths less than this, continental crust remains positively buoyant and can be returned to the surface along the subduction channel as ultrahigh-pressure rocks. Afonso and Zlotnik (2011) suggest, then, that the 250–300 km depth range appears to be "a point of no return" for subducted continental crust, in agreement with estimations from laboratory experiments (e.g., Dobrzhinetskaya and Green 2007). Note that this "point of no return" coincides with the so-called "forbidden zone", or supposed limit to the depth to which continental crust can be subducted (Liou et al. 2000a). Subduction appears to stall in an arc–continent collision once the downgoing slab contains a sufficient amount of positively buoyant continental crust to slow and eventually stop it, although the build up of positively buoyant material in turn depends on factors such as the chemical composition and the strength of the crustal material (Afonso and Zlotnik 2011). A final consequence of the subduction might be some form of slab break-off (Afonso and Zlotnik 2011; Boutelier and Chemenda 2011) which could result in an increase in uplift rate and the formation of topography (Duretz et al. 2010).

It has been proposed that during the late stages of an arc–continent collision a polarity reversal (or flip) in the subduction zone can take place in which a new subduction zone develops with a continent-ward dip (e.g., Stern 2004; Dewey 2005, and references therein). However, it is not clear from natural examples that such a subduction reversal takes place during every arc–continent collision (see below). Therefore, the question must be asked whether or not subduction zone reversal is an inherent part of arc–continent collision? Before beginning to answer this question we must first define what we mean by subduction zone reversal following arc–continent collision. To be considered an inherent part of the arc–continent collision process a subduction zone reversal must take place during the late stages of, or immediately following, the collision of an intra-oceanic arc with a continental margin, and it must have a continent-ward polarity (Fig. 17.3a). An older subduction zone sweeping through, such as is happening today in Taiwan, or the development of a new subduction zone along the margin much later on cannot be inherent to the arc–continent collision and must be considered as being separate from it. We suggest, therefore, that there are a number of possible ways in which subduction can act following arc–continent collision; (1) there is a polarity reversal and a new, continent-ward dipping subduction zone forms, (2) the subduction zone can simply stop and nothing more happens until much later, possibly with the arrival of a new plate margin (Fig. 17.3b), (3) there is transference of the subduction to a new site, away from the arc–continent collision altogether (Fig. 17.3c).

In the first case, with continued convergence a new subduction zone may be induced in the thermally elevated, thin and weak crust of the back-arc region (e.g., Stern 2004). To some degree this senario depends on the composition, age, and thermal maturity of the crust that the arc is built on. The Wetar and Flores thrusts of the Banda Orogen (see Harris 2011) may represent the initiation of such a spontaneously induced subduction zone polarity reversal. However, the amount of displacement along these thrusts, although poorly constrained, appears to be limited (an estimate of 50 km on the Wetar thrust is based solely on the size of the thrust belt) and there is no associated volcanism, so they cannot be considered subduction zones *sensu stricto*. The recognition of

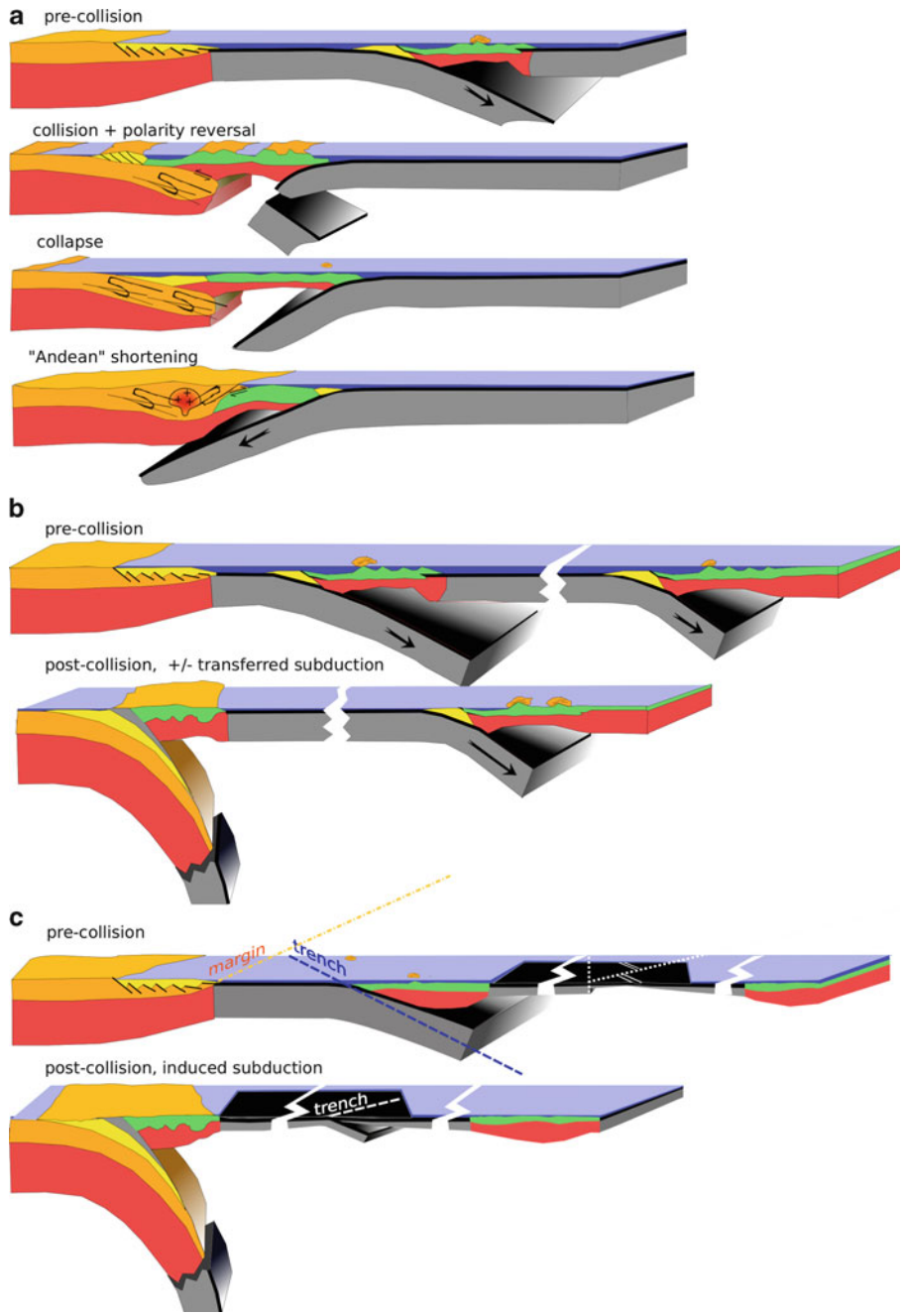

Fig. 17.3 Tectonic models for arc–continent collision and its immediate aftermath. (**a**) Collision is followed by subduction "flip" (see text for definition). The "flip" or polarity reversal is followed by collapse and then an Andean shortening phase. Based on a model for the Ordovician Grampian Orogeny in Ireland (Dewey 2005; Ryan and Dewey 2011). (**b**) Collision is associated with continuing subduction of the continental margin but not with the development of a new subduction zone outboard of the system. Convergence may also be accommodated on pre-existing subduction zones within the system. Based on models for the late-Devonian to early-Carboniferous evolution of the southern Urals (Brown et al. 2011). (**c**) Collision involving an arc with extensive back-arc spreading. If the collision is oblique then transforms within the back-arc basin will be sub-parallel to the convergence zone and provide a site for subduction initiation (Stern 2004). The sense of the subduction will depend upon the relative offset of the transform. In this case the transform offset is such that the relatively older marginal basin lithosphere lies on the side of the arc–continent collision initiating subduction in the same sense as that which led to this collision. A different back-arc basin geometry would lead to different subduction polarity.

subduction reversal in fossil arc–continent orogens is mostly based on the presence of slightly younger subduction-related rocks cutting the accreted arc (e.g., Dewey 2005 and references therein; Ryan and Dewey 2011; Cook 2011; Zagorevski and van Staal 2011; Konstantinovskaya 2011). In these cases a reversal in subduction zone polarity seems like a reasonable explanation for the age, composition, and cross-cutting relationships of the younger volcanic rocks that are present.

In the second case, the upper plate on which the arc is built is rheologically strong and there is less work required to deform the continental margin than to spontaneously induce subduction in the back-arc region (c.f., Stern 2004). This is also indicated in the thermomechanical models of Afonso and Zlotnik (2011), where the passive margin units and continental crust in the lower plate accommodates most of the deformation during subduction without any apparent effect in the back-arc region. The arc–continent collision that took place in the South Urals might be an example of this type, since the age and geochemistry of the arc rocks, together with the crustal structure, strongly suggest that there was no subduction zone reversal following the collision of the Magnitogorsk arc with the margin of Laurussia (Brown and Spadea 1999; Brown et al. 2006, 2011). Also, in Taiwan there is no indication of a polarity reversal in the subduction zone along which the Luzon arc is colliding with the margin of Eurasia. The current impingement of the Ryukyu subduction zone on the Taiwan arc–continent collision has been considered to be a polarity reversal (Suppe 1984; Clift et al. 2003, 2009a) yet, when taking into account the plate reconstructions of Hall (1996, 1998, 2002), it is difficult to argue that the Ryukyu subduction zone is in any way directly related to the Taiwan arc–continent collision.

In the third case, if convergence continues the subduction zone is transferred away from the arc–continent collision to begin elsewhere. This may involve rupturing of the oceanic lithosphere and the formation of a new subduction zone (Stern 2004; Gerya 2011). Transform margins, such as the Cayman Trough, which developed following the Late Cretaceous accretion of the Caribbean arc with the margin of North America, may be an ideal site for rupture to take place and subduction to begin anew (e.g., Casey and Dewey 1984; Stern 2004; Dewey and Casey 2011; Gerya 2011).

Regardless of whether subduction reversal takes place or not, once arc–continent collision stops, the structure, composition, physical properties, and rheology of the new continental margin will have changed significantly from those of the old margin. Instead of being a wide, thinned zone of continental crust, it will be a thick, dense margin that will have a very different role to play in any subsequent collisional event, be it with another arc or with a continent.

17.3 Arc–Continent Collision: Short-Lived Orogeny?

It has been suggested that arc–continent collision, in comparison with continent–continent collisions, can be a short-lived orogenic event (Dewey 2005). In fossil orogens, such as the Wopmay (Cook 2011), the Taconic of the Appalachians (Zagorevski et al. 2009; Zagorevski and van Staal 2011), the Grampian (Dewey 2005; Ryan and Dewey2011), the Uralides (Brown et al. 2006, 2011), Kohistan (Burg 2011), and Kamchatka (Konstantinovskaya 2011) arc–continent collision appears to have lasted between to 20 to >50 My (Fig. 17.4). In active arc–continent collision zones such as Timor (Silver et al. 1983; Harris 2011), Taiwan (Huang et al. 2000; Byrne et al. 2011), or Papua New Guinea (Abers and McCaffrey 1994), seismicity indicates that continental crust continues to underthrust the arc some 3–15 My after its entry into the subduction zone. In a more extreme example, the collision of the Greater Caribbean arc with the margin of North America began during the Late Paleocene in Cuba and continues to be active today in Hispaniola, more than 55–60 My later (Mann et al. 1991).

However, there are a number of difficulties in determining exactly when the continental crust entered the subduction zone, particularly in fossil orogens. The isotope geochemistry of the volcanic rocks has, in a number of cases (e.g., Draut et al. 2002, 2009; Elburg et al. 2005; Herrington et al. 2011), provided clear evidence for the arrival of either sediments derived from, or the arrival of, the leading edge of the continental margin at the subduction zone. Other indicators, such as high-pressure rocks that can be shown to have been derived from the continental

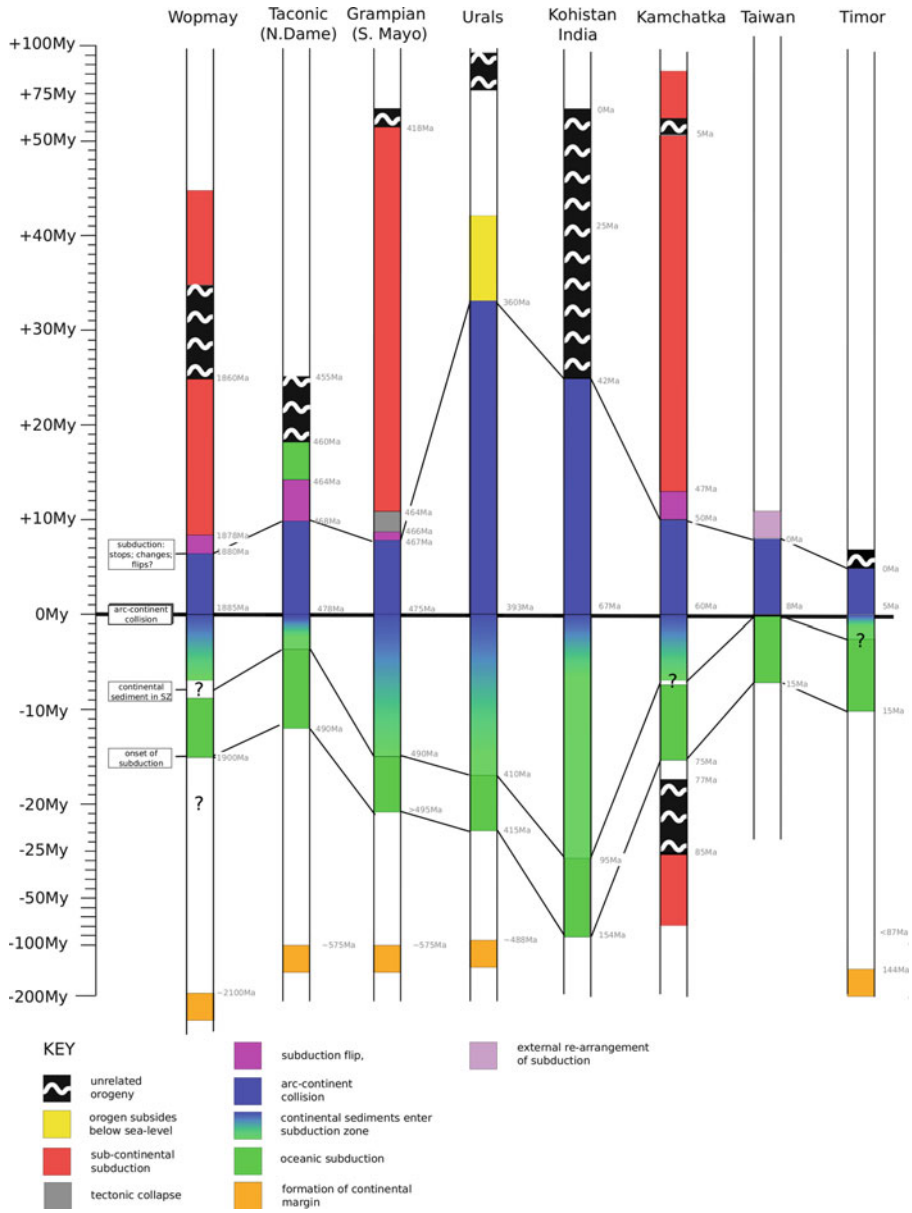

Fig. 17.4 Duration of several arc–continent orogens reviewed in this book. The orogens are arranged from left to right in order of decreasing geological age. Zero on the relative time scale (abscissa) coincides with the arrival of the continental margin at the subduction zone. Abbreviations used: S. Mayo = South Mayo; N. Dame = Notre Dame. Sources used: Wopmay (Cook 2011); Taconic (Notre Dame) (Zagorevski and van Staal 2011); Grampian (South Mayo) (Ryan and Dewey 2011; Dewey 2005); Kamchatka (Konstantinovskaya 2011); Urals (Brown et al. 2006, 2011); Timor (Standley and Harris 2009; Roosmawati and Harris 2009; Harris 2011); Kohistan (Burg 2011); and Taiwan (Byrne et al. 2011; Huang et al. 2006).

crust (e.g., Hetzel et al. 1998; Brown et al. 2006), or sediments derived from the orogen once it has risen to above sea level (e.g., Ryan and Dewey 2011; Brown et al 2011; Burg 2011; Harris 2011) can provide information about the early stages of arc–continent collision. In general, however, it may be difficult to

determine exactly when the leading edge of the continental margin entered into the subduction zone and arc–continent collision *sensu stricto* began. Nevertheless, in the examples given in this book it appears that arc–continent collision orogeny lasts between approximately 20–50 My.

17.4 The Growth and Destruction of the Continental Crust During Arc–Continent Collision

There is general agreement that the accretion of intra-oceanic volcanic arcs to a continental margin during arc–continent collision is one of the major processes in which new material has been added to the continental crust throughout geological time (Rudnick 1995; Rudnick and Fountain 1995). With the addition of the accreted arc and subduction of the extended continental crust, its age and composition will also have changed. There are various proposals for how the continental crust is recycled back into the mantle. Tectonic erosion of the continents and subduction of the resultant sediments along active margins has been shown to be an important mechanism by which large volumes of continental crust can be recycled back into the mantle (e.g., Von Huene and Scholl 1991; Clift and Vannucchi 2004; Clift et al. 2009a, b). Evidence from the geochemistry of volcanic rocks erupted above subduction zones suggests that at least part of this material is recycled back into the volcanic arc rocks (Draut and Clift 2001; Draut et al. 2002; Gao et al. 2004, 2008; Elburg et al. 2005; Herrington et al. 2005; Wang et al. 2006; Clift et al. 2009b). In areas of thickened crust, delamination (or crustal foundering) and sinking of the lower crust into the mantle has also been proposed as a way to remove and/or recycle the lower continental crust (Arndt and Goldstein 1989; Kay and Mahlburg-Kay 1991; Hawkesworth and Kemp 2006) and should, therefore, act as a recycling mechanism (e.g., Gao et al. 2008). However, the increasing number of seismic reflection images of relict subduction zones within the upper mantle in fossil collisional orogens (Calvert et al. 1995; Warner et al. 1996; Cook et al. 1999; White et al. 2003; van der Velden and Cook 2005; Cook 2011) suggest that crustal delamination may not have occurred in these orogens (e.g., van der Velden and Cook 2005) and that this process may not be as widespread as first thought.

There is now ample evidence from high-pressure rocks that provide first-order evidence for the deep subduction of the continental crust. This is supported by seismic tomography and seismic reflection profiling across active arc–continent collision orogens (e.g., Wu et al. 2009; Wang et al. 2006a, b; Snyder et al. 1996; Cook 2011) and by both analog and numerical modelling (van den Beukel 1992; Ranalli et al. 2000; Boutelier et al. 2003; Boutelier and Chemenda 2011; Massone et al. 2007; Afonso and Zlotnik 2011). Having established that continental crust can be deeply subducted, then its subsequent fate must be considered. This can involve either being brought back to the surface to form (ultra) high-pressure massifs (e.g., Liou et al. 2000a; Chopin 2003), being recycled back into magmatic rocks via melting processes (e.g., Draut et al. 2009; Gao et al. 2004; Harris 2011), or to reside in the mantle as the metamorphic products of the original lithologies (e.g., Hynes and Snyder 1995; Cook 2002; Gao et al. 2008). It seems that all of these processes take place on a number of scales and are as equally important in the growth and destruction (or recycling) of the continental crust as the accretion of intra-oceanic arcs.

Brown (2009), Brown et al. (2011) suggest that about 280,000 km^3 of continental crust could have been lost to the present day mantle following the collision of the Magnitogorsk arc with the margin of Laurussia, whereas approximately 800,000 km^3 of new material was accreted to the margin. This rough calculation suggests that a net volume of around 520,000 km^3 of material was added to the Laurussia margin during its collision with the Magnitogrsk arc. Zagorevski et al. (2009) estimate that c. 64,500 km^3 of new material was added to the Laurentian margin along the c. 250 km length of the Annieopsquotch accretionary track, although they do not provide an estimate of the amount of continental crust lost via subduction of the margin. Also, Cook (2011) suggests that there was very little addition of new continental material to the Slave Craton during the Wopmay orogeny, but that there appears to have been a significant amount of recycling of material. Whatever its fate, it is clear that the subduction of continental crust must be taken into account in the global calculation of the growth of the continents over geological time.

17.5 Mineral Deposits in Arc–Continent Collision Orogens

Zones of arc–continent collision are producers of much of the worlds mineral wealth, especially porphyry Cu–Mo–Au, epithermal Au–Ag and volcanic hosted massive sulfide (VMS) deposits, and are primary targets for exploration companies involved in the search for base and precious metals. While models for the location and geochemical development of volcanic-hosted massive sulfide deposits in island arcs are very evolved, it is only recently that researchers have begun to place these deposits in a geodynamic context (e.g., Kerrich et al. 2005; Herrington et al. 2002, 2005). As pointed out by Herrington and Brown (2011), the majority of mineral deposits found in fossil arc–continent collision zones were formed in intra-oceanic subduction settings and were subsequently preserved as a result of arc accretion. Nevertheless, other deposits appear to form either during the collision event (e.g., some deposits in the Urals and Wetar; Herrington and Brown 2011; Herrington et al. 2011) or following it as the subduction zone changes polarity (e.g., gold deposits in the Grampian orogen of western Ireland, Ryan and Dewey 2011) or jumps to a new position.

References

Abbott LD, Silver EA, Galewsky J (1994) Structural evolution of a modern arc-continent collision in Papua New Guinea. Tectonics 13:1007–1034

Abbott LD, Silver EA, Anderson RS, Smith R, Ingle JC, Kling SA, Haig D, Small E, Galewsky J, Sliter W (1997) Measurement of tectonic surface uplift rate in a young collisional mountain belt. Nature 385:501–507

Abers GA, McCaffrey R (1994) Active arc-continent collision: earthquakes, gravity anomalies, and fault kinematics in the Huon-Finisterre collision zone, Papua New Guinea. Tectonics 13:227–245

Afonso JC, Zlotnik S (2011) The subductability of continental lithosphere: the before and after story. In: Brown D, Ryan P (eds) Arc-continent collision: the making of an orogen, Frontiers in earth sciences. Springer, Heidelberg

Alsleben H, Wetmore PH, Schmidt KL, Paterson SR, Melis EA (2008) Complex deformation during arc-continent collision: quantifying finite strain in the accreted Alisitos arc, Peninsular Ranges batholith, Baja California. J Struct Geol 30:220–236

Amante C, Eakins BW (2009) ETOPO1, 1 Arc-minute global relief model: procedures, data sources and analysis. NOAA Technical Memorandum NESDIS NGDC-24, 19 pp

Arndt NT, Goldstein SL (1989) An open boundary between lower continental crust and mantle: its role in crust formation and crustal recycling. Tectonophysics 161:201–212

Audley-Charles MG (1986) Timor-Tanimbar trough: the foreland basin of the evolving Banda orogen; In: Allen PA, Homewood P (eds) Foreland basins, vol 8. International Association of Sedimentology, Special Publication, pp 91–104

Baldwin SL, Monteleone BD, Webb LE, Fitzgerald PG, Grove M, Hill J (2004) Pliocene eclogite exhumation at plate tectonic rates in eastern Papua New Guinea. Nature 431: 263–267

Bauer K, Neben S, Schreckenberger B, Emmermann R, Hinz K, Fecher N, Gohl K, Schulze A, Rumbull RB, Weber K (2000) Deep structure of the Namibia continental margin as derived from integrated geophysial studies. J Geophys Res 105: 25829–25853

Beane RJ, Liou JG, Coleman RG, Leech ML (1995) Petrology and retrograde P-T path for eclogites of the Maksyutov Complex, southern Urals Mountains, Russia. The Island Arc 4:254–266

Boutelier D, Chemenda A (2011) Physical modeling of arc-continent collision: A review of 2-D, 3-D, purely mechanical and thermo-mechanical experimental models. In: Brown D, Ryan P (eds) Arc-continent collision: the making of an orogen, Frontiers in earth sciences. Springer, Heidelberg

Boutelier D, Chemenda A, Burg J-P (2003) Subduction versus accretion of intra-oceanic volcanic arcs: insight from thermo-mechanical analogue experiments. Earth Planet Sci Lett 212:31–45

Boutelier D, Chemenda A, Jorand C (2004) Continental subduction and exhumation of high-pressure rocks: insights from thermo-mechanical laboratory modeling. Earth Planet Sci Lett 222:209–216

Brown D (2009) The growth and destruction of the continental crust during arc-continent collision in the southern Urals. Tectonophysics 479:185–196

Brown D, Spadea P (1999) Processes of forearc and accretionary complex formation during arc-continent collision in the Southern Ural Mountains. Geology 27:649–652

Brown D, Juhlin C, Alvarez-Marron J, Perez-Estaun A, Oslianski A (1998) Crustal-scale structure and evolution of an arc-continent collision zone in the southern Urals, Russia. Tectonics 17:158–171

Brown D, Hetzel R, Scarrow JH (2000) Tracking arc-continent collision subduction zone processes from high-pressure rocks in the southern Urals. J Geol Soc 157:901–904

Brown D, Alvarez-Marron J, Perez-Estaun A, Puchkov V, Ayarza P, Gorozhanina Y (2001) Structure and evolution of the Magnitogorsk forearc basin: identifying upper crustal processes during arc-continent collision in the Southern Urals. Tectonics 20:364–375

Brown D, Spadea P, Puchkov V, Alvarez-Marron J, Herrington R, Willner AP, Hetzel R, Gorozhanina Y (2006) Arc-continent collision in the Southern Urals. Earth Sci Rev 79:261–287

Brown D, Herrington R, Alvarev-Marron J (2011) Processes of arc-continet collision in the Uralides. In: Brown D, Ryan P (eds) Arc-continent collision: the making of an orogen, Frontiers in earth sciences. Springer, Heidelberg

Burg JP (2011) The Asia-Kohistan-India collision. Review and discussion. In: Brown D, Ryan P (eds) Arc-continent collision: the making of an orogen, Frontiers in earth sciences. Springer, Heidelberg

Byrne T, Chan Y-C, Rau R-J, Lu C-Y, Lee Y-H, Wang Y-J (2011) The arc-continent collision in Taiwan. In: Brown D, Ryan P (eds) Arc-continent collision: the making of an orogen, Frontiers in earth sciences. Springer, Heidelberg

Calvert AJ (2011) The seismic structure of island arc crust. In: Brown D, Ryan P (eds) Arc-continent collision: the making of an orogen, Frontiers in earth sciences. Springer, Heidelberg

Calvert AJ, Sawyer EW, Davis WJ, Ludden JH (1995) Archean subduction inferred from seismic images of a mantle suture in the Superior Province. Nature 375:670–674

Calvert AJ, Klemperer SL, Takahashi N, Keer B (2008) Three-dimensional crustal structure of the Mariana island arc from seismic tomography. J Geophys Res 113 doi: 10.1029/2007JB004939

Casey JF, Dewey JF (1984) Initiation of subduction zones along transform and accreting plate boundaries, triple junction evolution and spreading centres – implications for ophiolite geology and obduction. In: Gass IG, Lippard SJ, Shelton AW (eds) Ophiolites and oceanic lithosphere, vol 13. Geological Society, London, pp 269–290

Chemenda A, Matte P, Sokolov V (1997a) A model of Palaeozoic obduction and exhumation of high-pressure/low-temperature rocks in the southern Urals. Tectonophysics 276:217–227

Chemenda A, Yang R, Hsieh C, Groholsky A (1997b) Evolutionary model for the Taiwan collision based on physical modelling. Tectonophysics 274:253–274

Chemenda A, Lallemand S, Bokun A (2000) Strain partitioning and intraplate friction in oblique subduction zones: constraints provided by experimental modeling. J Geophys Res 105:5567–5582

Chemenda A, Hurpin D, Tang J-C, Stefan J-F, Buffet G (2001) Impact of arc-continent collision on the conditions of burial and exhumation of UHP/LT rocks: experimental and numerical modeling. Tectonophysics 342:137–161

Chopin C (2003) Ultrahigh-pressure metamorphism: tracing continental crust into the mantle. Earth Planet Sci Lett 212:1–14

Clift P, Vannucchi P (2004)Controls on tectonic accretion versus erosion in subduction zones; implications for the origin and recycling of the continental crust. Rev Geophys 42, doi: 8755-1209/04/2003RG000127

Clift PD, Schouten H, Draut AE (2003) A general model of arc-continent collision and subduction polarity reversal from Taiwan and the Irish Caledonides. In: Larter RD, Leat PT (eds) Intra-oceanic subduction systems; tectonic and magmatic processes, vol 219. Geological Society of London, special publication, London, pp 81–98

Clift P, Vannucchi P, Phipps Morgan J (2009a) Crustal redistribution, crust-mantle recycling and Phanerozoic evolution of the continental crust. Earth Sci Rev 97:80–104

Clift P, Schouten H, Vannucchi P (2009b) Arc-continent collisions, sediment recycling and the maintenance of the continental crust. In: Cawood P, Kroener A (eds) Accretionary orogens in space and time, vol 318. Geological Society of London, Special Publication, London, pp 75–103

Cook FA (2002) Fine structure of the continental Moho. Geol Soc Am Bull 114:64–79

Cook F (2011) Multiple arc development in the Paleoproterozoic Wopmay Orogen, northwest Canada. In: Brown D, Ryan P (eds) Arc-continent collision: the making of an orogen, Frontiers in earth sciences. Springer, Heidelberg

Cook FA, van der Velden AJ, Hall KW, Roberts BJ (1999) Frozen subduction in Canada's Northwest Territories: lithoprobe deep lithosphereic reflection rofiling of the western Canadian Shield. Tectonics 18:1–24

De Smet MEM, Fortuin AR, Troelstra SR, Van Mrale LJ, Karmini M, Tjokosaproetro S, Hadiwasastra S (1990) Detection of collision-related vertical movements in the Outer Banda Arc (Timor, Indonesia), using micropaleontological data. J Southeast Asian Earth Sci 4:337–356

DeBari SM, Greene A, Johnson M (2011) Vertical stratification of composition, density, and inferred magmatic processes in exposed arc crustal sections. In: Brown D, Ryan P (eds) Arc-continent collision: the making of an orogen, Frontiers in earth sciences. Springer, Heidelberg

Dewey JF (2003) Ophiolites and lost oceans, vol 373, Geological Society of America, Special Paper., pp 153–158

Dewey JF (2005) Orogeny can be very short. Proc Am Acad Sci 102:15286–15293

Dewey JF, Casey JF (2011) The origin of obducted large-slab ophiolite complexes. In: Brown D, Ryan P (eds) Arc-continent collision: the making of an orogen, Frontiers in earth sciences. Springer, Heidelberg

Dewey JF, Mange M (1999) Petrography of Ordovician and Silurian sediments in the western Irish Caledonides; tracers of a short-lived Ordovician arc-continent collision orogeny and the evolution of the Laurentian Appalachian-Caledonian margin. In: MacNiocaill C, Ryan PD (eds) Continental tectonics, vol 164. Geological Society of London, Special Publication, London, pp 55–108

Dobrzhinetskaya LF, Green HW (2007) Experimental studies of mineralogical assemblages of metasedimentary rocks at Earth's mantle transition zone conditions. Journal of Metamorphic Geology 25:83–96

Draut A, Clift PD (2001) Geochemical evolution of arc magmatism during arc-continent collision, South Mayo, Ireland. Geology 29:543–546

Draut A, Clift PD, Hannigan RE, Layne G, Shimizu N (2002) A model for continental crust genesis by arc accretion: rare earth element evidence from the Irish Caledonides. Earth Planet Sci Lett 203:861–877

Draut A, Clift PD, Amato JM, Blusztajn J, Schouten H (2009) Arc-continent collision and the formation of continental crust: a new geochemical and isotopic record from the Ordovician Tyrone Complex, Ireland. J Geol Soc 166:485–500

Duretz T, Gerya TV, May DA (2010) Numerical modelling of spontaneous slab breakoff and subsequent topographic response. Tectonophysics doi: 10.1016/j.tecto.2010.05.024

Edwards RA, Whitmarsh RB, Scrutton RA (1997) The crustal structure across the transform continental margin off Ghana, eastern equatorial Atlantic. J Geophys Res 102:747–772

Elburg MA, Foden JD, van Bergen MJ, Zulkarnain I (2005) Australia and Indonesia in collision: geochemical sources of magmatism. J Volcanol Geoth Res 140:25–47

Ernst WG, Liou JG, Hacker BR (1994) Petrotectonic significance of high- and ultrahigh-pressure metamorphic belts:

inferences for subduction-zone histories. Int Geol Rev 36:213–237
Escuder-Viruete J, Pérez-Estaún A (2006) Subduction-related P-T path for eclogites and garnet glaucophanites from the Samaná Peninsula basement complex, northern Hispaniola. Int J Earth Sci 95:995–1017
Fernàndez M, Afonso JC, Ranalli G (2010) The deep lithospheric structure of the Namibian volvanic margin. Tectonophysics 481:68–81
Fuller CW, Willett SD, Fisher D, Lu CY (2006) A thermomechanical wedge model of Taiwan constrained by fission-track thermochronometry. Tectonophysics 425:1–24
Funck T, Jackson HR, Louden KE, Dehler SA, Wu Y (2004) Crustal structure of the northern Nova Scotia rifted continental margin (eastern Canada). J Geophys Res 109 doi: 10.1029/2004JB003008
Gao S, Rudnick RL, Yuan HL, Liu XM, Liu YS, Xu WL, Ling WL, Ayers J, Wang XC, Wang QH (2004) Recycling lower continental crust in the North china craton. Nature 432:892–897
Gao S, Rudnick RL, Xu W-L, Yuan H-L, Liu Y-S, Walker RJ, Puchtel IS, Liu X, Huang H, Wang X-R, Yang J (2008) Recycling deep cratonic lithosphere and generation of intraplate magmatism in the North China Craton. Earth Planet Sci Lett 270:41–53
García-Casco A, Torres-Roldán RL, Iturralde-Vinent M, Millán G, Nuñuez Cambra K, Lázaro Calisalvo C, Rodríguez Vega A (2006) High pressure metamorphism of ophiolites in Cuba. Geologica Acta 4:63–88
Gerya TV (2011) Intra-oceanic subduction zones. In: Brown D, Ryan P (eds) Arc-continent collision: the making of an orogen, Frontiers in earth sciences. Springer, Heidelberg
Gourley JR, Byrne T, Chan Y-C, Wu F, Rau RJ (2007) Fault geometries illuminated from seismicity in central Taiwan: implications for crustal scale structural boundaries in the northern Centrl Range. Tectonophysics 445:168–185
Hall R (1996) Reconstructing Cenozoic SE Asia. In: Hall R, Blundell D (eds) Tectonic evolution of Southeast Asia, vol 106. Geological Society of London, Special Publication, London, pp 153–184
Hall R (1998) The plate tectonics of Cenozoic SE Asia and the distribution of land and sea. In: Hall R, Holloway JD (eds) Biogeography and geological evolution of SE Asia. Backbuys, Leiden, pp 99–131
Hall R (2002) Cenozoic geological and plate tectonic evolution of SE Asia and the SW Pacific: computer-based reconstructions and animations. J Asian Earth Sci 20:353–434
Harris R (2006) Rise and fall of the eastern Great Indonesian arc recorded by the assembly, dispersion and accretion of the Banda Terran, Timor. Gondwana Res 10:207–231
Harris R (2011) The nature of the Banda arc-continent collision in the Timor region. In: Brown D, Ryan P (eds) Arc-continent collision: the making of an orogen, Frontiers in earth sciences. Springer, Heidelberg
Harris R, Kaiser J, Hurford AJ, Carter A (2000) Thermal history of Australian passive margin cover sequences accreted to Timor during Late Neogene arc-continent collision, Indonesia. J Asian Earth Sci 18:47–69
Hawkesworth CJ, Kemp AIS (2006) Evolution of the continental crust. Nature 443:811–817
Herrington RJ, Brown D (2011) The generation and preservation of mineral deposits in arc-continent collision environments. In: Brown D, Ryan P (eds) Arc-continent collision: the making of an orogen, Frontiers in earth sciences. Springer, Heidelberg
Herrington RJ, Maslennikov VV, Spiro B, Zaykov VV, Little CTS (1998) Ancient vent chimney structures in the Silurian massive sulphides of the Urals. In: Mills RA, Harrison K (eds) Modern ocean floor processes and the geological record, vol 148. Geological Society of London, Special Publications, London, pp 241–257
Herrington RJ, Armstrong RN, Zaykov VV, Maslennikov VV, Tessalina SG, Orgeval J-J, Taylor RNA, (2002) Massive sulfide deposits in the South Urals: geological setting within the framework of the Uralide Orogen. In: Brown D, Juhlin C, Puchkov V (eds) Mountain building in the Uralides: pangea to present, vol 132. American Geophysical Union, Geophysical Monograph, pp 155–182
Herrington R, Zaykov V, Maslennikov V, Brown D, Puchkov V (2005) Mineral deposits of the Urals and links to geodynamic evolution. In: Hedenquist JW, Thompson JFH, Goldfarb RJ, Richards JP (eds) Economic Geology. 100 Anniversary Volume, pp 1069–1095
Herrington RJ, Scotney PM, Roberts S, Boyce AJ, Harrison D (2011) Temporal association of arrested subduction, progressive magma contamination in arc volcanism and formation of gold-rich massive sulphide deposits on Wetar Island (Banda Arc). Gondwana Res 19(3):583–593
Hetzel R (1999) Geology and geodynamic evolution of the high-P/low-T Maksyutov Complex, Southern Urals, Russia. Geol Rundsch 87:577–588
Hetzel R, Echtler HP, Seifert W, Schulte BA, Ivanov KS (1998) Subduction- and exhumation-related fabrics in the Paleozoic high-pressure–low-temperature Maksyutov Complex, Antingan area, Southern Urals, Russia. Geol Soc Am Bull 110: 916–930
Hill K (1991) Structure of the Papuan fold belt, Papua new Guinea. Am Assoc Petrol Geol 75:857–872
Holbrook WS, Lizarralde D, McGreary S, Bangs N, Diebold J (1999) Structure and composition of the Aleutian island arc and implications for continental crustal growth. Geology 27: 31–34
Hsieh ML, Rau RJ (2009) Late Holocene coseismic uplift on the Hua-tung coast, eastern Taiwan: evidence from mass mortality of intertidal organisms. Tectonophysics 474: 595–609
Huang C-Y, Wu W-Y, Chang C-P, Tsao S, Yuan PB, Lin CW, Kuan-Yuan X (1997) Tectonic evolution of an accretionary prism in the arc-continent collision terrane of Taiwan. Tectonophysics 281:31–51
Huang C-Y, Yuan PB, Lin C-W, Wang TK, Chang C-P (2000) Geodynamic processes of Taiwan arc-continent collision and comparison with analogs in Timor, Papua New Guinea, Urals and Corsica. Tectonophysics 325:1–22
Huang C-Y, Yuan PB, Tsao S-J (2006) Temporal and spatial records of active arc-continent collision in Taiwan: a synthesis. Geol Soc Am Bull 118:274–288
Hynes A, Snyder DB (1995) Deep-crustal mineral assemblages and potential for crustal rocks below the Moho in the Scottish Caledonides. Geophys J Int 123:323–339

Iturralde-Vinent MA, Díaz-Otero A, van Hinsbergen DJJ (2008) Peleogene foredeep basin deposits of north-central Cuba: a record of arc-continent collision between the Caribbean and North American plates. Int Geol Rev 50:868–884

Jahn BM, Martineau F, Peucat JJ, Cornichet J (1986) Geochronology of the Tananao schist complex, Taiwan, and its regional tectonic significance. Tectonophysics 125:103–124

Kay RW, Mahlburg-Kay S (1991) Creation and destruction of the lower continental crust. Geol Rundsch 80:259–278

Keen CE, Dehler SA (1997) Extensional styles and gravity anomalies at rifted continental margins: some North Atlantic examples. Tectonics 16:744–754

Kerrich R, Goldfarb R, Richards J (2005) Metallogenic provinces in an evolving geodynamic framework. In: Hedenquist JW, Thompson JFH, Goldfarb RJ, Richards JP (eds) Economic geology. 100 Anniversary Volume. pp 1097–1136

Kodaira S, Sato T, Takahashi N, Ito N, Tamura Y, Tatsumi Y, Kaneda Y (2007) Seismological evidences for variation of continental growth along the Izu intra-oceanic arc and its implication for arc volcanism. J Geophys Res 112 doi: 10.1029/2006JB004593

Konstantinovskaya E (2011) Early Eocene arc-continent collision in Kamchatka, Russia: structural evolution and geodynamic model. In: Brown D, Ryan P (eds) Arc-continent collision: the making of an orogen, Frontiers in earth sciences. Springer, Heidelberg

Lallemand S, Liu C-S, Dominguez S, Schnurle P, Malavieille J, The ACT Scientific Crew (1999) Trench-parallel stretching and folding of forearc basin and lateral migration of the accretionary wedge in the southern Ryukyu: a case of strain partition caused by oblique convergence. Tectonics 18:231–247

Lázaro C, García-Casco A, Rojas Agramonte Y, Kröner A, Newbauer F, Iturralde-Vinent M (2009) Fifty-five-million-year history of oceanic subduction and exhumation at the northern edge of the Caribbean plate (Sierra del Convento mélange, Cuba). J Metamorph Geol 27:19–40

Leat PT, Larter RD (2003) Intra-oceanic subduction systems. In: Larter RD, Leat PT (eds) Intra-oceanic subduction systems: tectonic and magmatic processes, vol 219. Geological Society of London, Special Publication, London, pp 1–17

Liou JG, Hacker BR, Zhang RY (2000a) Into the forbidden zone. Science 287:1215–1216

Lissenberg CJ, McNicoll VJ, van Staal CR (2006) The origin of mafic-ultramafic bodies within the northern Dashwoods Subzone, Newfoundland Appalachians. Atl Geol 42:1–12

Little CTS, Herrington RJ, Maslennikov VV, Morris NJ, Zaykov VV (1997) Silurian hydrothermal-vent community from the southern Urals, Russia. Nature 385:146–148

Malavieille J, Trullenque G (2009) Consequences of continental subduction on forearc basin and accretionary wedge deformation in SE Taiwan: insights from analogue modeling. Tectonophysics 466:377–394

Malavieille J, Lallemand SE, Dominguez S, Deschamps A, Lu CY, Liu CS, Schnürle P, ACT Scientific Crew (2002) Arc-continent collision in Taiwan. New marine observations and tectonic evolution. In: Bryne TB, Liu CS (eds) Geology and geophysics of an arc-continent collision, Taiwan, vol 358, Geological Society of America, Special Paper., pp 187–211

Mann P, Draper G, Lewis JF (1991) Geologic and tectonic development of the North America-Caribbean plate boundary in Hispañola, vol 262. Geological Society of America Special Paper. 401 pp

Massone H-J, Willner AP, Gerya T (2007) Densities of metapelitic rocks at high to ultrahigh pressure conditions: what are the geodynamic consequences. Earth Planet Sci Lett 256:12–27

McIntosh K, Nakamura Y, Wang TK, Shih RC, Chen A, Liu CS (2005) Crustal-scale seismic profiles across Taiwan and the western Philippine Sea. Tectonophysics 401:23–54

Ranalli G, Pellegrini R, D'Offizi S (2000) Time dependence of negative bouyancy and the subduction of continental lithosphere. J Geodyn 30:539–555

Reston TJ (2009) The structure, evolution and symmetry of the magma-poor rifted margins of the North and Central Atlantic: a synthesis. Tectonophysics 468:6–27

Reston T, Manatschal G (2011) Rifted margins: building blocks of later collision. In: Brown D, Ryan P (eds) Arc-continent collision: the making of an orogen, Frontiers in earth sciences. Springer, Heidelberg

Roosmawati N, Harris R (2009) Surface uplift history of the incipient Banda arc-continent collision: geology and synorogenic foraminifera of Rote and Savu islands, Indonesia. Tectonophysics 479:95–110

Rudnick RL (1995) Making continental crust. Nature 378: 571–578

Rudnick RL, Fountain DM (1995) Nature and composition of the continental crust: a lower crustal perspective. Rev Geophys 33:267–309

Ryan PD (2001) The role of deep basement during continent-continent collision: a review. In: Miller JA, Holdsworth RE, Buik IS, Hand M (eds) Continental reactivation and reworking, vol 184. Geological Society of London, Special Publication, London, pp 39–55

Ryan PD (2008) Preservation of fore-arc basins during island arc-continent collision; some insights from the Ordovician of western Ireland. In: Draut AE, Clift PD, Scholl DW (eds) Sedimentation in arc collision settings, vol 436, Geological Society of America, Special Paper., pp 1–9

Ryan PD, Dewey JF (2011) Arc-continent collision in the Ordovician of western Ireland: Stratigraphic, structural, and metamorphic evolution. In: Brown D, Ryan P (eds) Arc-continent collision: the making of an orogen, Frontiers in earth sciences. Springer, Heidelberg

Sayers J, Symonds PA, Direen NG, Bernardel G (2001) Nature of the continent-ocean transition on the non-volcanic rifted margin of the central Great Australian Bight. In: Wilson RCL, Whitmarsh RB, Taylor B, Froitzheim N (eds) Non-volcanic rifting of continental margins: a comparison of evidence from land and sea, vol 187. Geological Society of London, Special Publication, London, pp 51–76

Shreve RL, Cloos M (1986) Dynamics of sediment subduction, mélange formation, and prism accretion. J Geophys Res 91:10229–10245

Shyu JBH, Sieh K, Avouac JP, Chen WS, Chen YG (2006) Millennial slip rate of the Longitudinal Valley fault from river terraces: implications for convergence across the active suture of eastern Taiwan. J Geophys Res 111 doi: 10.1029/2005JB003971

Silver EA, Reed D, McCaffrey R, Joyodiwiryo Y (1983) Back arc thrusting in the eastern Sunda Arc, Indonesia: a consequence of arc-continent collision. J Geophys Res 88:7429–7448

Snyder DB, Prasetyo H, Blundell DJ, Pigram CJ, Barber AJ, Richardson A, Tjokosaproetro S (1996) A dual doubly vergent orogen in the Banda Arc continent-arc collision zone as observed on deep seismic reflection profiles. Tectonics 15:34–53

Spadea P, Kabanova LY, Scarrow JH (1998) Petrology, geochemistry and geodynamic significance of Mid-Devonian boninitic rocks from the Baimak-Buribai area (Magnitogorsk Zone, southern Urals). Ofioliti 23:17–36

Spadea P, D'Antonio M, Kosarev A, Gorozhanina Y, Brown D (2002) Arc-continent collision in the Southern Urals: petrogenetic aspects of the forearc complex. In: Brown D, Brown D, Juhlin C, Puchkov V (eds) Mountain building in the uralides: pangea to present, American Geophysical Union, Geophysical Monograph., pp 101–134

Standley CE, Harris R (2009) Tectonic evolution of forearc nappes of the active Banda arc-continent collision: origin, age, metamorphic history and structure of the Lolotoi Complex, East Timor. Tectonophysics 479:66–94

Stern RJ (2002) Subduction zones. Rev Geophys 40 doi: 10.1029/2001RG000108

Stern RJ (2004) Subduction initiation: spontaneous and induced. Earth Planet Sci Lett 226:275–292

Stern RJ, Smoot NC (1998) A bathymetric overview of the Mariana forearc. Island Arc 7:525–540

Suppe J (1984) Kinematics of arc-continent collision, flipping of subduction, and back-arc spreading near Taiwan, vol 6. Memoir of the Geological Society of China. pp 21–33

Takahashi N, Kodaira S, Klemperer S et al (2007) Crustal structure and evolution of the Mariana intra-oceanic island arc. Geology 35:203–206

Tatsumi Y, Shukuno H, Tani K, takahashi N, Kodaira S, Kogiso T (2008) Structure and growth of the Izu-Bonin-Mariana arc crust: 2. Role of crust-mantle transformation and the transparent Moho in arc crust. J Geophys Res 13 doi: 10.1029/2007JB005121

van den Beukel J (1992) Some thermomechanical aspects of the subduction of continental lithosphere. Tectonics 11:316–329

Van der Velden AJ, Cook FA (2005) Relict subduction zones in Canada. J Geophys Res 110 doi: 10.1029/2004JB003333

van Staal CR, Whalen JB, Valverde-Vaquero P, Zagorevski A, Rogers N (2009) Pre-Carboniferous, episodic accretion-related orogenesis along the Laurentian margin of the northern Appalachians. In: Murphy JB, Keppie JP, Hynes AJ (eds) Ancient orogens and modern analogues, vol 327. Geological Society of London, Special Publication, London, pp 271–316

Von Huene R, Scholl DW (1991) Observations at convergent margins concerning sediment subduction, subduction erosion, and the growth of continental crust. Rev Geophys 29:279–316

Wang Q, Wyman DA, Xu J, Dong Y, Vasconcelos PM, Pearson N, Wan Y, Dong H, Li C, Yu Y, Zhu T, Feng X, Zhang Q, Zi F, Chu Z (2006a) Eocene melting of subducted continental crust and early uplifting of central Tibet: evidence from central-western Qiangtang high-K calc-alkaline andesites, dacites, and rhyolites. Earth Planet Sci Lett 272:158–171

Wang Z, Zhao D, Wang J, Kao H (2006) Tomographic evidence for the Eurasian lithosphere beneath Taiwan. Geophys Res Lett 33 doi: 10.1029/2006GL027166

Warner MR, Morgan J, Barton P, Morgan P, Price C, Jones K (1996) Seismic reflections from the mantle represent relict subduction zones within the continental lithosphere. Geology 24:39–42

Wessel P, Smith WHF (1991) Free software helps map and display data. EOS Transactions, AGU 72:441

White DJ, Musacchio G, Helmstaedt HH, Harrap RM, Thurston PC, van der Velden A, Hall K (2003) Images of a lower-crustal oceanic slab: direct evidence for tectonic accretion in the Archean western Superior province. Geology 31:997–1000

Willner AP, Ermolaeva T, Gorozhanina YN, Puchkov VN, Arzhavitina M, Pazukhin VN, Kramm U, Walter R (2002) Surface signals of an arc-continent collision: the detritus of the Upper Devonian Zilair Formation in the Southern Urals, Russia. In: Brown D, Juhlin C, Puchkov V (eds) Mountain building in the uralides: pangea to present, vol 132, American Geophysical Union, Geophysical Monograph., pp 183–210

Wu FT, Rau RJ, Salzberg D (1997) Taiwan orogeny: thin-skinned or lithospheric collision? Tectonophysics 274: 191–220

Wu F, Chang C-S, Wu YM (2004) Precisely relocated hypocentres, focal mechamisms and active orogeny in Central Taiwan. In: Malpas J, Fletcher CJN, Ali JR, Aitchison JC (eds) Aspects of the tectonic evolution of China, vol 226. Geological Society of London, Special Publication, London, pp 333–354

Wu YH, Chang CH, Zhao L, Shyu BH, Chen YG, Sich K, Avouac JP (2007) Seismic tomography of Taiwan: Improved constraints from a dense network of strong motion stations. J Geophys Res 112 doi: 10.1029/2007JB004983

Wu YM, Zhao L, Chang CH, Hsiao NC, Chen YG, Hsu SK (2009) Relocation of the 2006 Pingtung Earthquake sequence and seismotectonics in Southern Taiwan. Tectonophysics 479:19–27

Ye K, Cong B, Ye D (2000) The possible subduction of continental material to depths greater than 200 km. Nature 407:734–736

Zagorevski A, van Staal CR (2011) The record of Ordovician arc-arc and arc-continent collisions in the Canadian Appalachians during the closure of Iapetus. In: Brown D, Ryan P (eds) Arc-continent collision: the making of an orogen, Frontiers in earth sciences. Springer, Heidelberg

Zagorevski A, Lissenberg CJ, van Staal CR (2009) Dynamics of accretion of arc and backarc crust to continental margins: inferences from the Anniopsquotch accretionary tract, Newfoundland Appalachians. Tectonophysics 479: 150–164

Zaykov VV, Maslennikov VV, Zaykova EV, Herrington RJ (1996) Hydrothermal activity and segmentation in the Magnitogotsk-west Mugodjarian zone on the margins of the Urals palaeo-ocean. In: MacLeod CJ, Tyler PA, Walker CL (eds) Tectonic, magmatic, hydrothermal and biological segmentation of mid-ocean ridges, vol 118. Geological Society of London, Special Publication, London, pp 199–210